Jurnal Ilmu Pertanian Indonesia (JIPI), April 2022
ISSN 0853-4217
EISSN 2443-3462

Vol. 27 (2) 226–236
http://journal.ipb.ac.id/index.php/JIPI
DOI: 10.18343/jipi.27.2.226

Deteksi Alih Fungsi Lahan Padi Sawah Menggunakan Sentinel-2 dan *Google Earth Engine* di Kota Serang, Provinsi Banten

(Rice Fields Change Detection Using Sentinel-2 and *Google Earth Engine* In Serang City, Banten Province)

Tian Mulyaqin[1]*, Kardiyono[1], Ismatul Hidayah[1], Fadhlullah Ramadhani[2], Muchamad Yusron[3]

(Diterima Juni 2021/Disetujui Maret 2022)

ABSTRAK

Lahan merupakan salah satu faktor utama dalam produksi padi, tetapi alih fungsi lahan pertanian ke sektor lain terus berlanjut dan menjadi tantangan dalam penyediaan pangan di Indonesia. Kota Serang merupakan salah satu daerah penghasil beras di Provinsi Banten. Kajian ini bertujuan menganalisis perubahan alih fungsi lahan sawah ke sektor lain dengan memetakan tutupan lahan sawah menggunakan citra satelit Sentinel-2 tahun 2021 dibandingkan tahun 2019 dengan metode *Random Forest* dengan mendayagunakan aplikasi *Google Earth Engine* (GEE) dan dukungan komputasi awan (*cloud computing*). Hasil kajian menunjukkan bahwa tutupan lahan sawah di Kota Serang pada tahun 2021 berkurang 602,87 ha (–7,20%) dibandingkan tahun 2019 dari total tutupan lahan; tutupan lahan berupa vegetasi lain juga berkurang 242 ha (–2,45%), sementara tutupan lahan wilayah perkotaan pada tahun 2021 meningkat 781,82 ha (10,89%). Kajian ini menunjukkan telah terjadi perubahan alih fungsi lahan di Kota Serang akibat ekspansi perkotaan dalam rentang waktu 3 tahun, sekaligus juga bahwa penggunaan GEE dapat mengefisienkan pemantauan perubahan alih fungsi lahan dan tutupan penggunaan lahan.

Kata kunci: *Google Earth Engine*, padi, Sentinel-2

ABSTRACT

Land availability is one of the main factors in rice production. However, the agricultural land-use change to other sectors continues and becomes a challenge in the food supply in Indonesia. Serang City is one of the rice-producing areas in Banten Province. This study aims to analyze changes in the land use of rice field functions to other sectors by mapping rice field cover using Sentinel-2 satellite imagery in 2021 compared to 2019 with the Random Forest method by using Google Earth Engine (GEE) applications and cloud computing approach. The study results showed that the cover of rice fields in Serang City in 2021 decreased by 602.87 ha (–7.20%) compared to 2019 from the total land cover. Land cover in other vegetation was also reduced by 242 ha (–2.45%), while urban land cover in 2021 increased by 781.82 ha (10.89%). This study shows that there has been a change in land transfer in Serang City due to urban expansion in 3 years, as well as that the use of GEE can streamline monitoring of land-use change and land use cover.

Keywords: Google Earth Engine, rice field, Sentinel-2

PENDAHULUAN

Produksi padi di Indonesia khususnya Provinsi Banten merupakan salah satu kunci ketahanan pangan di Indonesia. Kota Serang sebagai ibukota Provinsi Banten juga mengalami kontraksi produksi. Walaupun berstatus kota, Serang masih merupakan kontributor produksi padi bagi Banten. BPS Banten mencatat produksi padi Kota Serang pada tahun 2019 mencapai 67,34 ribu ton atau 4,48% dari total produksi padi Banten (BPS Banten 2021). Konsumsi beras sebagai bahan makanan pokok akan seiring dengan jumlah penduduk yang ada di Kota Serang, yaitu 688.603 jiwa dengan tingkat kepadatan penduduk 2582 jiwa/km^2 dan laju pertumbuhan penduduk 1,59% pada tahun 2019 (BPS Kota Serang 2020). Lahan pertanian untuk produksi beras harus bersaing juga dengan kebutuhan lahan untuk pemukiman dan sektor lain yang juga semakin tinggi. Peningkatan jumlah penduduk dan peningkatan aktivitas ekonomi dari sektor lainnya menyebabkan upaya mencapai ketahanan pangan di masa mendatang menjadi semakin berat. Peningkatan tersebut menyebabkan meningkatnya kebutuhan lahan termasuk mengakibatkan alih fungsi lahan pertanian menjadi permukiman, pembangunan infrastruktur (jalan, bendungan, dan sebagainya), atau industri. Pembangunan yang terus dilaksanakan menyebabkan banyak lahan pertanian yang harus beralih fungsi menjadi non-pertanian. Harga lahan yang cukup tinggi menjadi salah satu faktor pemicu para petani untuk melepas kepemilikan lahannya ke

[1] Balai Pengkajian Teknologi Pertanian Provinsi Banten Jl. Ciptayasa KM 01 Ciruas Serang Banten 42182
[2] Balai Penelitian Agroklimat dan Hidrologi, Jl. Tentara Pelajar No. 1A Bogor 16114
[3] Balai Besar Pengkajian dan Pengembangan Teknologi Pertanian, Jl. Tentara Pelajar No. 10 Bogor 16114
* Penulis Korespondensi:
E-mail: tianmulyaqin@pertanian.go.id

investor untuk dialihfungsikan. Artinya, motif ekonomi menjadi salah satu penyebab utama dari alih fungsi lahan (Ridwan 2016; Janah *et al*. 2017). Selain itu, pendapatan petani, luas kepemilikkan lahan, sistem waris, pengaruh tetangga yang mengalihfungsikan lahannya, pengaruh pengusaha/investor, keadaan lingkungan, kebijakan pemerintah dan pendidikan petani juga ikut berperan dalam pengambilan keputusan untuk mengalihfungsikan lahan (Martunisa & Noor 2018).

Alih fungsi lahan semakin masif terjadi di wilayah perkotaan dan kadang terjadi gejala penjalaran kota yang tidak teratur atau sering disebut dengan *urban sprawl*. Gejala ini terjadi dalam bentuk pembangunan kota dengan kepadatan rendah atau tersebar tidak teratur dan sering kali juga berimbas pada terjadinya alih fungsi lahan dari sektor pertanian ke pemukiman atau bangunan untuk pemanfaatan sektor lain (Prasetyo 2017). Untuk mengatasi penjalaran kota yang tidak teratur, pemerintah menerbitkan Undang-Undang No. 26 Tahun 2007 tentang Penataan Ruang yang telah mengamanatkan asas penyelenggaraan penataan ruang, yaitu keterpaduan, keserasian, keselarasan dan keseimbangan, keberlanjutan, keberdayagunaan dan keberhasilgunaan, keterbukaan, kebersamaan dan kemitraan, perlindungan kepentingan umum, kepastian hukum dan keadilan, serta akuntabilitas. Asas tersebut tentunya ditetapkan demi mencapai dan mewujudkan harmonisasi antara lingkungan alam dan buatan, keterpaduan dalam penggunaan sumber daya alam dan sumber daya buatan dengan memperhatikan sumber daya manusia, serta perlindungan fungsi ruang dan pencegahan dampak negatif pada lingkungan akibat pemanfaatan ruang. Hal ini sesuai dengan tujuan penyelenggaraan penataan ruang, yaitu mewujudkan ruang wilayah nasional yang aman, nyaman, produktif, dan berkelanjutan berlandaskan wawasan nusantara dan ketahanan nasional.

Diharapkan penataan ruang di daerah selaras juga dengan Undang-undang No. 41 Tahun 2009 tentang Perlindungan Lahan Pertanian Pangan Berkelanjutan untuk mewujudkan ketahanan, kemandirian dan kedaulatan pangan. Agar cita-cita tersebut terwujud, diperlukan lahan pertanian eksisting dan tidak dialihfungsikan untuk keperluan di luar pertanian pangan. Ekspansi perkotaan sudah berlangsung cukup lama dan tidak terelakkan, sehingga pemerintah daerah perlu memantau kondisi eksisting lahan sawah untuk melihat status ketahanan pangan di daerahnya secara cepat dan akurat.

Salah satu metode yang yang dapat digunakan untuk mendeteksi perubahan tutupan lahan untuk penggunaan tanaman padi sawah dan ekspansi perkotaan dengan cepat ialah menggunakan penginderaan jauh. Satelit-satelit yang membawa sensor optik dan radar telah diluncurkan oleh berbagai badan antariksa di dunia seperti NASA-Amerika Serikat dan ESA-Eropa. Satelit Sentinel-2 adalah bagian dari program *Copernicus* dari *European Commission* (EC), *European Space Agency* (ESA) yang telah mengembangkan dan mengoperasikan misi Sentinel-2 untuk memperoleh citra optik resolusi spasial tinggi. Sentinel-2 merupakan misi pencitraan multispektral lebar, resolusi tinggi dengan konstelasi dua satelit yaitu Sentinel-2A dan Sentinel-2B yang diluncurkan tahun 2015 dan 2017. Konstelasi satelit ini memungkinkan dengan frekuensi kunjungan ulang 5 hari di skala global. Instrumen Multispektral S2 (MSI) mengambil sampel 13 *band spectral* (Tabel 1): *visible* (terlihat), dan NIR (*near infrared*) dengan ketinggian 10, *Red Edge* (tepi merah), dan SWIR (*Short Wave Infrared*) pada ketinggian 20 m, dan pita atmosfer pada resolusi spasial 60 m. Fitur tersebut memberikan data yang sesuai untuk menilai keadaan dan perubahan vegetasi, tanah, dan tutupan air (Gascon *et al.* 2016).

Era *big data* saat ini memungkinkan tutupan lahan sawah dapat dideteksi dengan sangat mudah dan terbuka. Salah satu *platform open source* yang sudah memanfaatkan *big data* berupa data citra satelit dan sudah sering dimanfaatkan untuk memetakan dan memantau tutupan lahan, vegetasi, ekspansi perkotaan, dan kepentingan lainnya ialah aplikasi *Google Earth Engine* (GEE) (Mutanga & Kumar 2019). Aplikasi GEE ini merupakan platform komputasi awan yang dirancang untuk menyimpan dan memproses kumpulan data yang sangat besar (pada skala *petabyte*) untuk analisis dan pengambilan keputusan akhir. Selain itu juga GEE dilengkapi bahasa pemrograman yang memungkinkan pengguna menginvestigasi perubahan lahan secara cepat dan akurat.

Google Earth Engine (GEE)

Koleksi data penginderaan jauh geospasial yang disediakan di GEE telah banyak dimanfaatkan dalam berbagai studi mengenai stadia tanaman padi (Ramadhani *et al.* 2020), perkebunan kelapa sawit (Shaharum *et al.* 2020), deteksi perubahan (Miettinen *et al*. 2019), klasifikasi perkotaan (Nguyen 2020), bahkan digunakan untuk mengkaji kondisi sosial ekonomi di suatu wilayah (Jean *et al.* 2016). Platform GEE merupakan platform *open-source*, tidak berbayar, dan menggunakan *Application Programming Interface* (API) atau *Interactive Development Environtment* (IDE) berbasis web (Gambar 1). Pengguna dapat mendaftar dan login melalui tautan https://earthengine.google.com dan mengakses antarmuka pengguna, serta panduan penggunaan, bahkan menyediakan kurikulum pendidikannya. Katalog data publik *Earth Engine* adalah kumpulan multi-*petabyte*, yakni kumpulan data geospasial yang banyak digunakan. Sebagian besar katalog terdiri atas citra penginderaan jauh pengamatan bumi, termasuk seluruh arsip Landsat serta arsip lengkap data dari Sentinel-1 dan Sentinel-2, bahkan mencakup prakiraan iklim, data tutupan lahan, dan lainnya (Gorelick *et al.* 2017).

Kajian ini mendeteksi dan memetakan tutupan penggunaan lahan dan alih fungsi lahan padi sawah menggunakan koleksi citra satelit Sentinel-2 pada

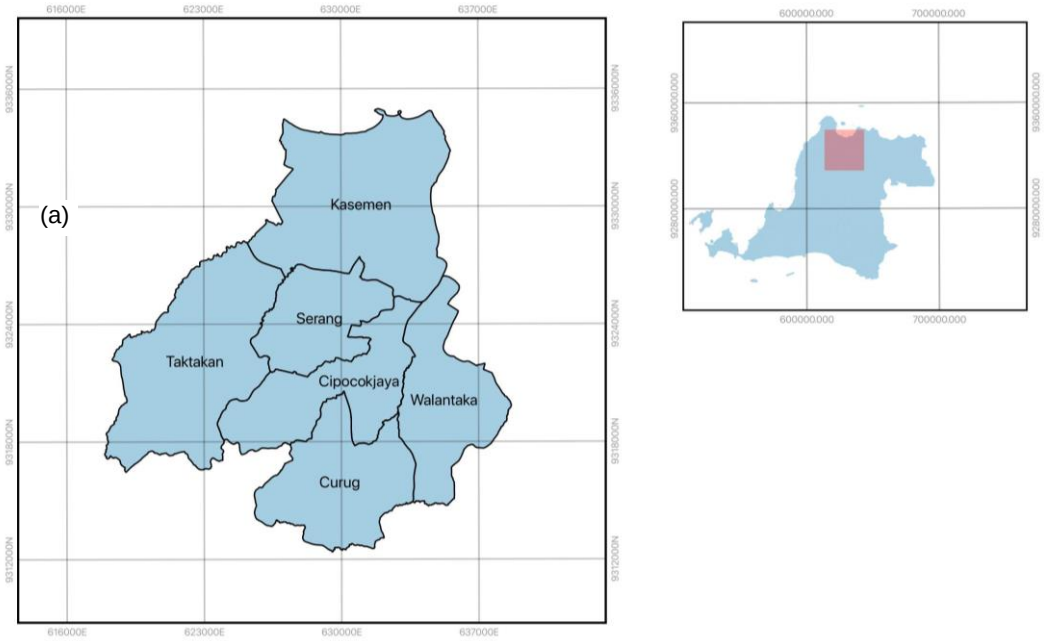
aplikasi GEE di Kota Serang pada tahun 2019 dan tahun 2021 guna mendukung pemantauan ketahanan pangan di Provinsi Banten.

METODE PENELITIAN

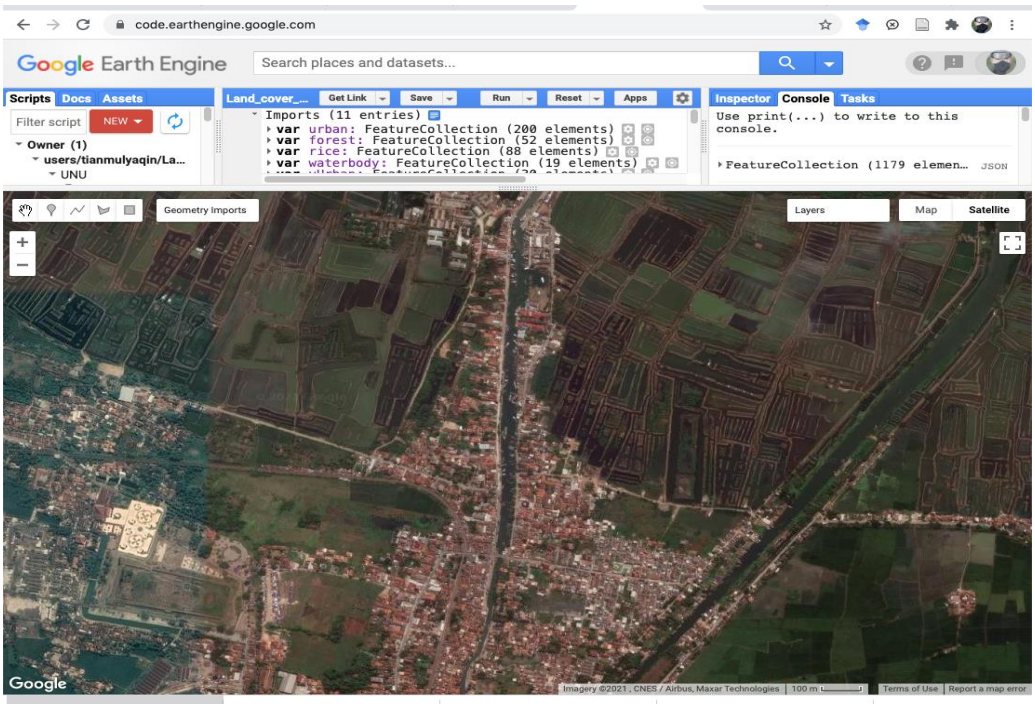
Lokasi Penelitian

Kota Serang terletak di sebelah utara Provinsi Banten; di sebelah utara berbatasan dengan Laut Jawa, dan sebelah timur, selatan, serta barat berbatasan dengan Kabupaten Serang. Secara astronomis, kota ini terletak pada 5°99'–6°22' Lintang Selatan dan 106°07'–106°25' Bujur Timur (Gambar 2). Luasnya 266,74 km^2 atau 26674 ha dan sebagian besar wilayahnya terletak di dataran rendah dengan ketinggian kurang dari 500 mdpl (BPS Kota Serang 2020).

Kota Serang memiliki potensi lahan sawah 8.474 ha (4,26%) dari total luas baku sawah Provinsi Banten, yaitu 198.520 ha. Sawah di Kota Serang yang luasnya 4.945 ha (53,04%) merupakan sawah irigasi dan sisanya, 3.979 ha (46,94%), merupakan sawah tadah hujan. Hal ini akan memengaruhi frekuensi tanam padi sebab di sawah irigasi padi



Gambar 1 Lokasi penelitian: (a) Kota Serang Provinsi Banten dan (b) Letak Kota Serang di Provinsi Banten.



Gambar 2 Tampilan platform *Google Earth Engine* (GEE) berbasis web.

dapat ditanam sedikitnya dua kali dalam setahun, sementara sawah tadah hujan dapat ditanami padi tidak lebih dari dua kali dali dalam setahun (BPS Banten 2020).

Metode

Penelitian ini sepenuhnya menggunakan aplikasi GEE (koleksi dan analisis data) dan aplikasi ArcMap 10.4 untuk membantu membuat *layout* peta. Data yang digunakan dalam penelitian ini ialah dataset Sentinel-2A pada rentang waktu 1 Januari 2019 sampai 31 Desember 2019 dibandingkan dengan dataset Sentinel-2A pada rentang waktu 1 Januari 2021 sampai 31 Desember 2021 untuk menghasilkan peta tutupan lahan di Kota Serang. Untuk mengetahui alih fungsi lahan sawah ke sektor lain sebagai akibat ekspansi perkotaan dilakukan analisis lanjutan dengan menumpang-susun (*overlay*) peta tutupan lahan wilayah perkotaan dengan lahan baku sawah Kota Serang tahun 2019 dan citra satelit *Google Earth* resolusi tinggi.

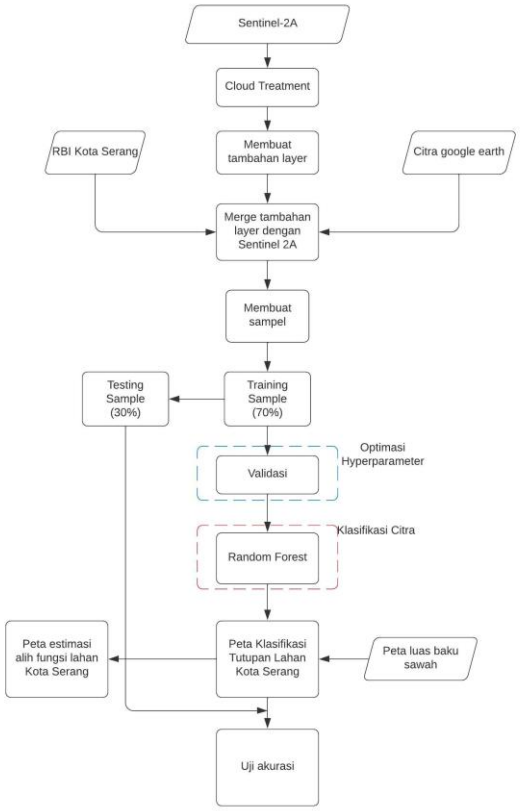
Pada tahap pertama, dipilih citra Sentinel-2 yang bebas awan pada rentang waktu studi, kemudian dibuat *region of interest* (ROI) dengan menumpang-susun citra Sentinel-2 dengan Peta Rupa Bumi Indonesia (RBI) Kota Serang, membuat titik sampel analisis dengan melihat citra satelit resolusi tinggi *Google Earth*, dan menganalisis titik sampel menggunakan algoritma mesin pembelajaran (*machine learning*) Random Forest (RF) pada aplikasi GEE. Klasifikasi menggunakan RF sudah digunakan untuk mengklasifikasi tanaman skala luas (Shelestov *et al.* 2017), tutupan lahan tanaman sawit (Descals *et al.* 2019), dan deteksi penebangan-habis hutan (Johansen *et al*. 2015).

Klasifikasi tutupan lahan pada kajian ini dibagi menjadi empat kelas, yaitu sawah, urban (pemukiman, lahan terbangun, jalan dan atau wilayah perkotaan), vegetasi lain, dan air (sungai, kolam, empang, rawa, tambak). Kerangka kerja penelitian diberikan pada Gambar 3.

Data untuk Klasifikasi

Studi ini memanfaatkan data katalog dari Sentinel-2A dan B melalui aplikasi GEE. Data yang digunakan merupakan data Sentinel-2A Bottom of Atmosphere (BOA) yang sudah dilakukan *cloud treatment*. Sentinel-2 sangat baik digunakan untuk memantau, mengklasifikasi, atau mendeteksi perubahan ter-utama untuk kegiatan pertanian (Zhang *et al.* 2017; Van der Werff & Van der Meer 2016).

Citra satelit Sentinel-2 untuk mengklasifikasi lahan memanfaatkan data 13 pita yang ada pada citra tersebut (Tabel 1). Namun, dari 13 pita, kajian ini hanya memanfaatkan tiga jenis pita, yaitu NIR, *Red,* dan *Green*. Selain itu juga digunakan data beberapa indeks untuk mengklasifikasi tutupan lahan, yaitu menggunakan *Normalised Difference Vegetation Index* (NDVI), *Normalised Difference Water Index* (NDWI), dan *Soil Adjusted Vegetation Index* (SAVI). Data pita ini dimaksudkan untuk menghasilkan data tambahan (Tabel 2). Sejumlah persamaan digunakan untuk menghasilkan data tambahan yang digunakan pada tahap klasifikasi citra. Lapisan pada Tabel 2 ditumpang-susun bersama dengan pita Sentinel-2 (Tabel 1) untuk digunakan dalam proses klasifikasi. Lapisan tambahan ini mampu mengekstraksi informasi tertentu dengan cara yang lebih efisien.



Gambar 3 Kerangka kerja penelitian.

Sampel

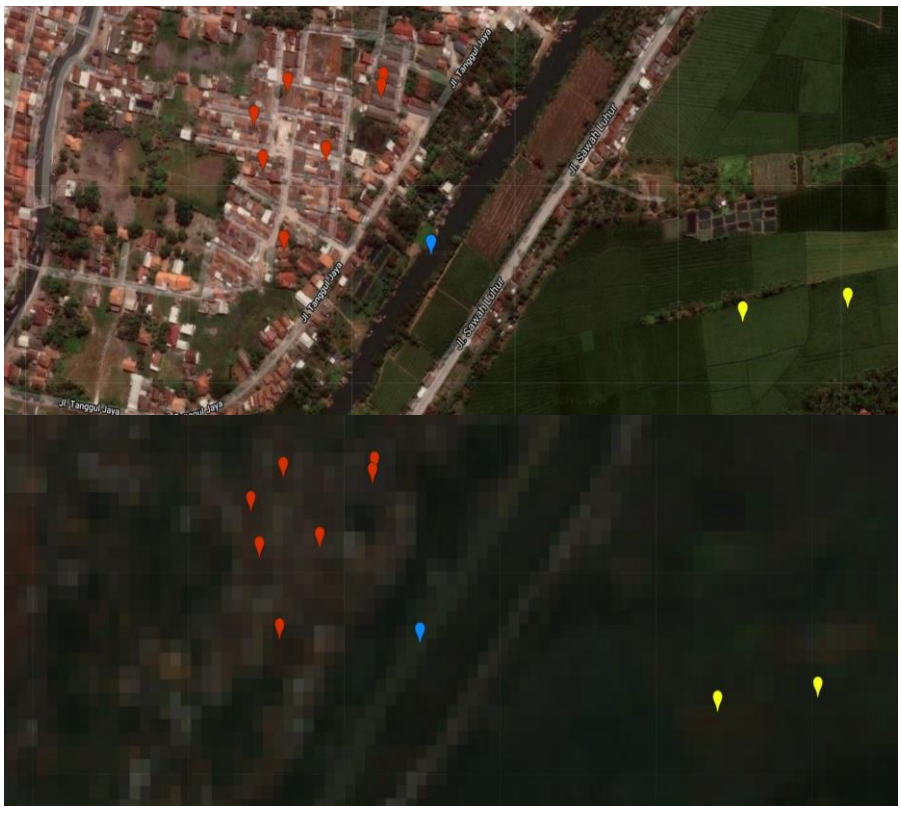
Sampel dibuat pada platform GEE dengan total 4 kelas diidentifikasi: sawah, urban, vegetasi lain, dan air. Sampel dibuat menggunakan format poin yang tersebar di wilayah administrasi Kota Serang, dengan bantuan peta RBI dari Badan Informasi Geospasial guna menentukan batas lokasi penelitian dan citra Google Earth resolusi tinggi dibandingkan dengan citra Sentinel-2 seperti yang ditunjukkan pada Gambar 4. Sampel kemudian dibagi menjadi dua komponen: pelatihan (*training*) dan validasi. *Training* terdiri atas 70% dari semua sampel yang dibuat (510 titik), yang terdiri atas sawah (200 titik), urban (200 titik), vegetasi lain (60 titik), dan air (50 titik), yang digunakan untuk mengklasifikasikan citra Sentinel 2-A. Sementara validasi merupakan 30% dari semua sampel (153 buah poligon), yang terdiri atas sawah (60 buah), urban (60 buah), vegetasi lain (20 buah), dan air (15 buah) untuk divalidasi dan dinilai akurasinya menggunakan RF. Semua sampel ini menjadi hiperparameter yang dipakai oleh mesin pembelajaran dalam pengklasifikasian. Hiperparameter adalah parameter yang nilainya mengendalikan proses pembelajaran dan menen-tukan nilai parameter model yang akhirnya dipelajari oleh algoritma pembelajaran. Awalan *'hiper_*' menunjukkan parameter 'tingkat atas' yang

Tabel 1 Informasi Pita pada Sentinel- 2

Nama pita	Deskripsi	Ukuran piksel (m)	Panjang gelombang (nm)
Pita 1	Aerosols	60	443,9 nm (S2A)/442,3 nm (S2B)
Pita 2	Blue	10	496,6 nm (S2A)/492,1 nm (S2B)
Pita 3	Green	10	560 nm (S2A)/559 nm (S2B)
Pita 4	Red	10	664,5 nm (S2A)/665 nm (S2B)
Pita 5	Red Edge 1	20	703,9 nm (S2A)/703,8 nm (S2B)
Pita 6	Red Edge 2	20	740,2 nm (S2A)/739,1 nm (S2B)
Pita 7	Red Edge 3	20	782,5 nm (S2A)/779,7 nm (S2B)
Pita 8	NIR	10	835,1 nm (S2A)/833 nm (S2B)
Pita 8A	Red Edge 4	20	864,8 nm (S2A)/864 nm (S2B)
Pita 9	Water vapor	60	945 nm (S2A)/943,2 nm (S2B)
Pita 11	SWIR 1	20	1613,7 nm (S2A)/1610,4 nm (S2B)
Pita 12	SWIR 2	20	2202,4 nm (S2A)/2185,7 nm (S2B)

Tabel 2 Lapisan tambahan yang digunakan untuk klasifikasi tutupan lahan

Lapisan	Rumus	Sumber
NDVI	$NDVI = \frac{NIR - Red}{NIR + Red}$	(Piragnolo *et al.* 2018)
NDWI	$NDWI = \frac{Green - NIR}{Green + NIR}$	
SAVI	$SAVI = \frac{NIR - Red}{NIR + Red + 0.5} * (0.5 + 1)$	



Gambar 4 (a) Citra satelit Google Earth resolusi tinggi, (b) Citra satelit Sentinel-2: titik kuning menunjukkan sampe sawah, titik merah menunjukkan sampel urban (terbangun), dan titik biru menunjukkan sampel air.

mengendalikan proses pembelajaran dan parameter model yang dihasilkannya. Klasifikasi dan validasi dilakukan pada aplikasi GEE dan penilaian akurasi dihitung menggunakan metode matriks konfusi.

Uji Akurasi

Pengujian akurasi bertujuan menilai galat klasifikasi sehingga dapat diketahui persentase ketepatannya (akurasi). Akurasi hasil klasifikasi diuji dengan cara membuat matriks kontingensi yang sering disebut dengan matriks galat *(error matrix*) atau matriks konfusi (*confusion matrix*). Matriks ini dihitung menggunakan fungsi matriks konfusi pada pengkodean di GEE. Dari matriks ini, akurasi suatu klasifikasi dapat dihitung dari akurasi keseluruhan (*overall accuracy*), pembuat akurasi (*producer's accuracy*), akurasi pengguna (*user's accuracy*), dan akurasi kappa (*kappa accuracy*) (Tabel 3). Semakin tinggi nilai akurasinya semakin tinggi pula tingkat kebenaran citra hasil klasifikasi. Pedoman pengolahan data satelit multispektral secara *digital supervised* untuk klasifikasi menetapkan akurasi klasifikasi tutupan lahan adalah rata-rata di atas 75% (LAPAN 2015).

Tingkat akurasi suatu klasifikasi dapat dinilai dari akurasi keseluruhan, pembuat akurasi, dan akurasi pengguna. Menurut (Jensen 2015) untuk mencari nilai ketiga-tiganya digunakan formula sebagai berikut:

Akurasi keseluruhan (OA) merupakan jumlah nilai akurasi keseluruhan dari klasifikasi, yang merupakan perbandingan jumlah total area (piksel) yang diklasifikasikan dengan benar terhadap total area (piksel) observasi; ini menunjukkan tingkat kebenaran citra hasil klasifikasi:

$$\text{Akurasi keseluruhan} = D/N \times 100\% \quad .....(1)$$

Keterangan:
D = Total nilai baris yang benar yang telah ditambah secara diagonal
N = Total nilai yang benar di dalam matriks galat

Nilai akurasi pembuat (PA) menunjukkan persentase peluang rata-rata suatu piksel akan diklasifikasikan dengan benar dan secara rata-rata menunjukkan seberapa baik setiap kelas di lapangan telah diklasifikasi. Semakin tinggi nilai PA semakin tinggi pula piksel dari kelas tersebut tidak masuk ke kelas yang lain:

$$\text{Akurasi pembuat} = x_{ii} / x_{+i} \times 100\% \quad .....(2)$$

Keterangan:
x_{ii} = Total nilai sel yang benar di dalam kelas
x_{+i} = Jumlah nilai sel di dalam baris

Nilai Akurasi Pengguna (UA) mengindikasikan persentase peluang rata-rata suatu piksel dari citra yang telah terklasifikasi secara aktual mewakili kelas-kelas tersebut di lapangan. Apabila semua kelas mempunyai nilai akurasi pengguna 100%, ini menunjukkan bahwa pada kelas-kelas tersebut tidak terjadi galat klasifikasi dengan tidak mengambil piksel dari kelas lain:

$$\text{Akurasi pengguna} = x_{ii}/x_{i+} \times 100\% \quad ....(3)$$

Keterangan:
x_{ii} = Total nilai sel yang benar di dalam kelas
x_{i+} = Jumlah nilai sel di dalam baris

HASIL DAN PEMBAHASAN

Klasifikasi Tutupan Lahan

Dalam kajian ini tutupan lahan kota Serang berhasil dibagi menjadi 4 kelas yaitu sawah, urban, vegetasi lain, dan air. Namun, tujuan utama kajian ini ialah untuk mendeteksi perubahan sebaran lahan yang digunakan untuk padi sawah yang ada di Kota Serang pada tahun 2019 dan tahun 2021. Kelas lahan sawah mengklasifikasikan tutupan lahan yang selalu atau sering digunakan untuk budi daya padi sawah. Kelas urban mengklasifikasikan tutupan lahan berupa bangunan, perumahan, jalan, dan lahan non-pertanian. Adapun kelas vegetasi lain mengklasifikasikan tutupan lahan berupa vegetasi lain selain padi berupa vegetasi besar seperti pohon atau wilayah dapat berupa kebun atau hutan yang terdapat banyak pohon. Kelas air merupakan tutupan lahan yang diklasifikasikan sebagai air seperti kolam/empang, sungai, atau tambak. Seperti diketahui, Kota Serang berbatasan langsung dengan Laut Jawa; masyarakat di sekitar pantai utara banyak membudidayakan ikan pada tambak. Hasil klasifikasi tutupan lahan yang dihasilkan oleh GEE ditunjukkan pada Tabel 4 dan Gambar 5.

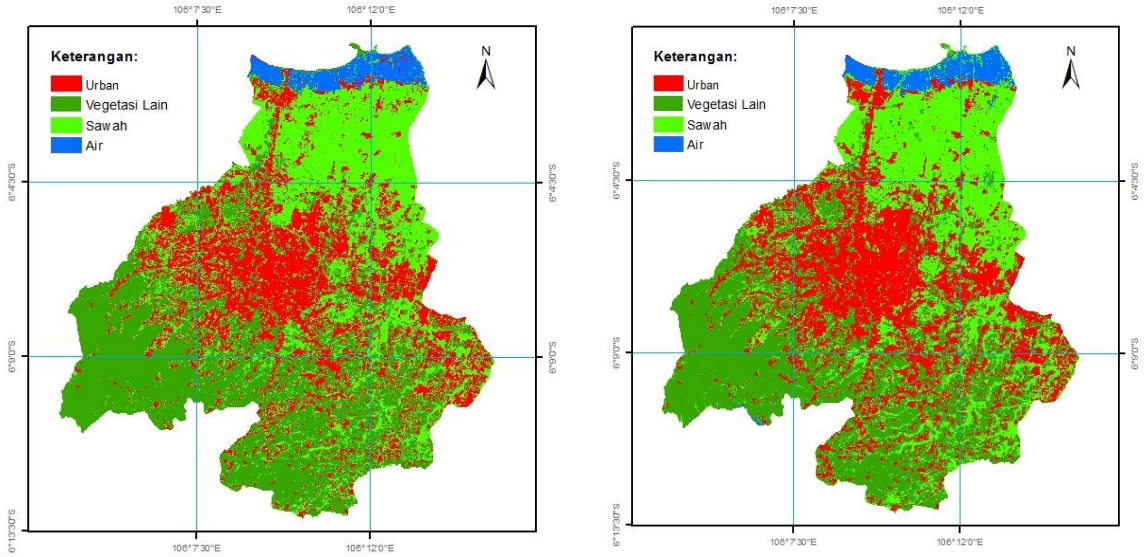
Hasil klasifikasi tutupan lahan menggunakan data Sentinel-2A pada aplikasi GEE menunjukkan bahwa tutupan lahan di Kota Serang didominasi oleh kelas vegetasi lain 9.899,39 ha (37,65%) pada tahun 2019 dan seluas 9.657,22 ha (36,73%) pada tahun 2021.

Tabel 3 Hasil uji akurasi klasifikasi tutupan lahan di Kota Serang

Uraian	Tahun 2019			Tahun 2021		
	Akurasi Pembuat (%)	Akurasi Pengguna (%)	Akurasi Keseluruhan (%)	Akurasi Pembuat (%)	Akurasi Pengguna (%)	Akurasi Keseluruhan
Urban	93,36	94,69	96,56	98,39	91,40	95,59
Vegetasi Lain	100,00	99,60		99,73	97,23	
Sawah	94,88	93,68		88,30	96,79	
Air	96,41	98,17		92,81	98,10	

Tabel 4 Luas tutupan lahan berdasarkan klasifikasi di Kota Serang

Kelas	Tahun 2019		Tahun 2021		Selisih	
	Luas (ha)	%	Luas (ha)	%	Luas (ha)	%
Urban	7.180,63	27,31	7.962,45	30,28	781,82	10,89
Vegetasi Lain	9.899,39	37,65	9.657,22	36,73	–242,17	–2,45
Sawah	8.376,36	31,86	7.773,49	29,56	–602,87	–7,20
Air	838,34	3,19	901,56	3,43	63,22	7,54
Total	26.294,72	100,00	26.294,72	100,00		



Gambar 5 Hasil klasifikasi tutupan lahan oleh *Google Earth Engine* (GEE) di Kota Serang (a) tahun 2019 dan (b) tahun 2021.

Vegetasi lain ini dapat berupa tanaman atau pohon di hutan dan atau di kebun, semak, dan lainnya selain tanaman padi. Tutupan lahan kedua didominasi oleh sawah seluas 8.376,36 ha (31,86%) pada tahun 2019, tetapi pada tahun 2021 urutan kedua didominasi oleh kelas urban 7.962,45 ha (30,28%). Data ini memperlihatkan perubahan alih fungsi lahan sawah ke sektor lain berupa kelas urban. Tutupan lahan ketiga, pada tahun 2019 didominasi oleh kelas urban 7.189,63 ha (27,31%), sementara pada tahun 2021 didominasi oleh kelas sawah 7.773,49 ha (29,56%). Tutupan lahan keempat, pada tahun 2019 dan 2021 sama-sama didominasi oleh tutupan lahan berupa kelas air, berturut-turut 838,34 ha (3,19%) dan 901,56 ha (3,43%) dari total tutupan lahan (Gambar 6).

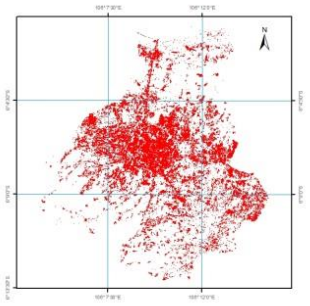
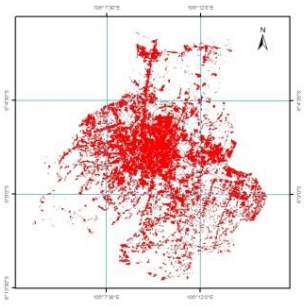
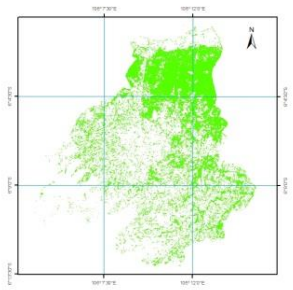
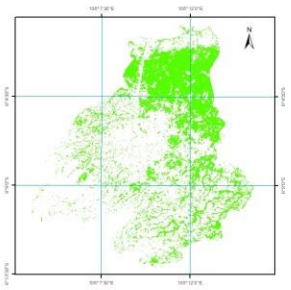
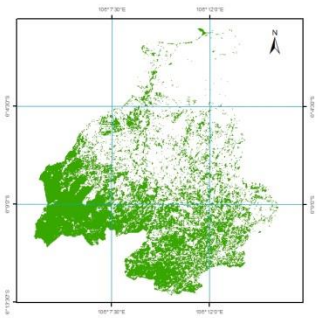
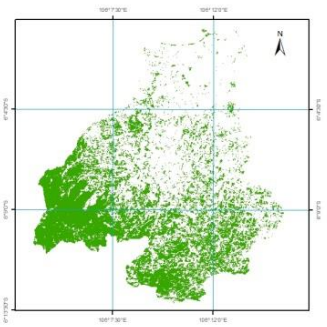
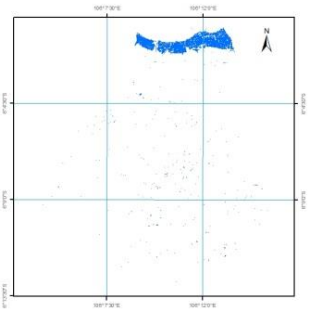
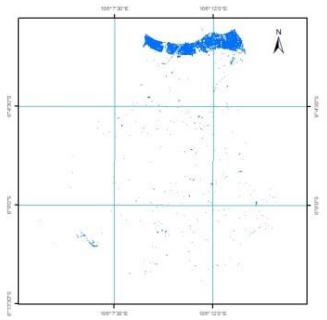
Hasil Uji Akurasi

Tingkat akurasi klasifikasi dan pemetaan lahan sawah menggunakan GEE dapat dinilai dari nilai akurasi keseluruhan, akurasi pembuat, dan akurasi pengguna yang dihasilkan dari matriks konfusi pada aplikasi GEE (Tabel 4). Perhitungan matriks dan hasil analisis GEE menunjukkan akurasi keseluruhan dari citra yang diklasifikasikan ke dalam 4 kelas memiliki tingkat akurasi keseluruhan 96,56% (tahun 2019) dan 95,59% (tahun 2021). Nilai akurasi pembuat dan akurasi pengguna pada klasifikasi kajian ini pun menunjukkan akurasi yang baik, dengan nilai di atas 90% untuk semua kelas baik untuk tahun 2019, kecuali untuk kelas sawah sebesar 88,30% pada tahun 2021.

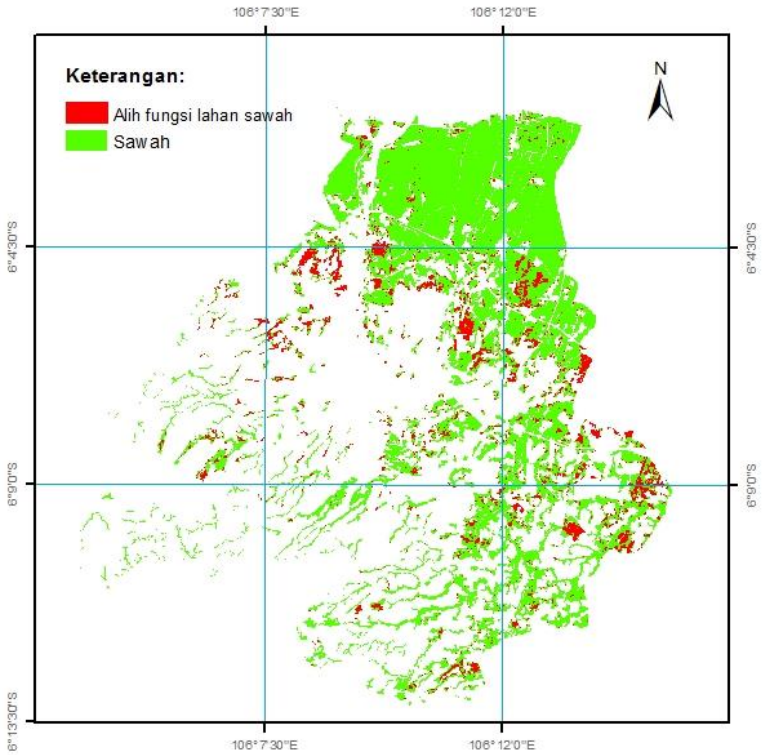
Estimasi Alih Fungsi Lahan Sawah

Hasil klasifikasi tutupan lahan menggunakan data Sentinel-2A pada aplikasi GEE (Tabel 4) juga menunjukkan bahwa tutupan lahan sawah menurun 7,20% (602,87 ha) pada tahun 2021 dibandingkan tahun 2019. Hal sama juga terjadi pada tutupan lahan untuk vegetasi lain, menurun 2,45% (242,17 ha). Penurunan ini diduga karena ekspansi dari tutupan lahan berupa kelas lain, yaitu urban dan atau tutupan lahan berupa air. Hal ini dibuktikan dengan meningkatnya tutupan lahan untuk kelas urban 10,89% (781,82 ha) pada tahun 2021 dibandingkan tahun 2019. Selain itu, tutupan lahan untuk kelas air juga meningkat 7,54% (63,22 ha).

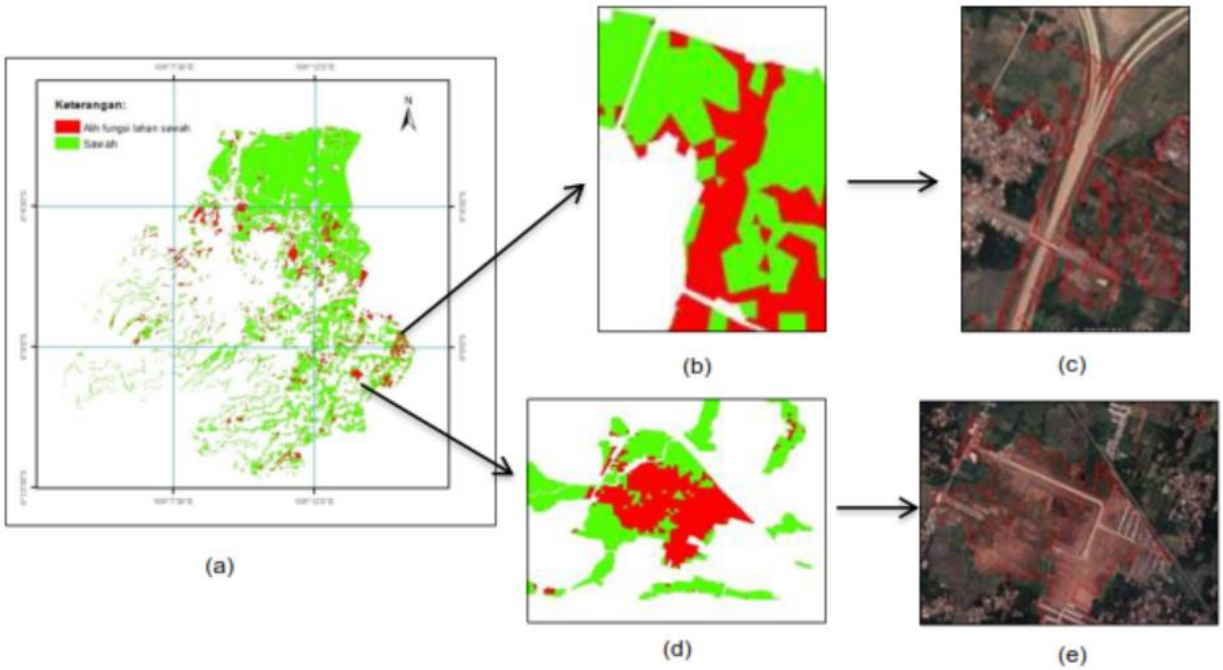
Berdasarkan kajian ini, lokasi atau titik yang mengalami alih fungsi lahan sawah ke sektor lain dideteksi dengan menganalisis peta lebih lanjut. Peta dianalisis lebih lanjut dengan menumpang-susun peta hasil klasifikasi kelas urban dengan luas baku sawah dan citra satelit *Google Earth* yang beresolusi tinggi. Hasil estimasi ekspansi urban ke lahan sawah dapat dilihat pada peta estimasi alih fungsi lahan (Gambar 7). Ekspansi urban terjadi hampir di seluruh wilayah Kota Serang. Dengan membandingkan peta hasil estimasi alih fungsi lahan dengan citra satelit resolusi tinggi *Google Earth*, diduga beberapa jenis ekspansi perkotaan yang terjadi dapat berupa perumahan/pemukiman, jalan, dan lahan kosong

Tahun 2019	Tahun 2021
	
(a)	
	
(b)	
	
(c)	
	
(d)	

Gambar 6 Peta hasil klasifikasi citra Sentinel-2 menggunakan GEE pada tahun 2019 dan tahun 2021 (a) Peta tutupan lahan berupa urban area; (b) Peta tutupan lahan berupa sawah; (c) Peta tutupan lahan berupa vegetasi lain; (d) Peta tutupan lahan berupa air.



Gambar 7 Peta estimasi alih fungsi lahan sawah pada tahun 2021 dibandingkan tahun 2019.



Gambar 8 Deteksi alih fungsi lahan sawah sentinel-2 divalidasi dengan citra google earth (a) Peta estimasi alih fungsi lahan sawah; (b) titik diduga lokasi alih fungsi lahan sawah; (c) terjadi alih fungsi lahan sawah ke jalan dan lainnya; (d) titik diduga lokasi allih fungsi lahan sawah; (e) terjadi alih fungsi lahan sawah menjadi perumahan atau pemukiman

untuk kegiatan sektor lain. Kelebihan dari Sentinel-2 adalah resolusi yang tinggi sehingga memungkinkan lokasi dan bentuk perubahan lahan pertanian ke non-pertanian secara akurat dapat diketahui. Gambar 8 memperlihatkan hasil deteksi alih fungsi lahan sawah divalidasi dengan citra satelit *Google Earth* sehingga terlihat bahwa di Kota Serang terjadi perubahan lahan sawah ke perumahan atau pemukiman, jalan tol, dan sektor lain.

Peta hasil estimasi alih fungsi lahan sawah ini dapat dimanfaatkan oleh pemangku kepentingan untuk memantau dan mendeteksi dini ekspansi

perkotaan yang tidak teratur atau tidak sesuai dengan Rencana Tata Ruang Wilayah di Kota Serang. Perhatian ditujukan terutama berkaitan dengan alih fungsi lahan sawah, sebab sawah merupakan salah satu faktor utama dalam penyediaan pangan di Kota Serang.

KESIMPULAN

Pemanfaatan citra satelit Sentinel-2 menggunakan aplikasi *Google Earth Engine* dapat memetakan tutupan lahan sawah dan mendeteksi perubahan alih fungsi lahan sawah ke sektor lain. Kota Serang memiliki tutupan lahan berupa sawah seluas 29,56% (7.773,49 ha) dari total luas Kota Serang pada tahun 2021. Perubahan alih fungsi lahan terdeteksi mencapai 7,20% (602,87 ha) pada tahun 2021 dibandingkan tahun 2019. Alih fungsi lahan sawah ke sektor lain diakibatkan oleh ekspansi perkotaan berupa pembangunan perumahan atau pemukiman, jalan tol, serta perubahan ke sektor lainnya. Tutupan lahan menggunakan citra satelit Sentinel-2 dan aplikasi GEE dapat dipetakan dengan cepat dan cukup akurat, sebagaimana ditunjukkan dengan tingkat akurasi keseluruhan yang melebihi 90%. Informasi tutupan lahan berupa lahan sawah akan sangat bermanfaat bagi para pemangku kepentingan untuk menentukan kebijakan yang berkaitan dengan produksi pangan dan status ketahanan pangan di wilayahnya.

DAFTAR PUSTAKA

[BPS] Badan Pusat Statistik Banten. 2020. *Luas Lahan Menurut Penggunaanya Provinsi Banten Tahun 2020*. Serang (ID): BPS Provinsi Banten.

[BPS] Badan Pusat Statistik Banten. 2021. *Provinsi Banten Dalam Angka 2020*. Serang (ID): BPS Provinsi Banten.

[BPS] Badan Pusat Statistik Kota Serang. 2020. *Kota Serang Dalam Angka 2020*. Serang (ID): BPS Kota Serang.

Descals A, Szantoi Z, Meijaard E, Sutikno H, Rindanata G, Wich S. 2019. “Oil Palm (Elaeis Guineensis) Mapping with Details: Smallholder versus Industrial Plantations and Their Extent in Riau, Sumatra.” *Remote Sensing* 11(21). https://doi.org/10.3390/rs11212590

Gascon F, Thépaut O, Jung M, Francesconi B, Louis J, Lonjou V, Lafrance B, Massera S, Vacaresse AG, Languille F, Alhammoud B, Viallefont F, Pflug B, Vieniarz J, Clerc S, Pessiot L, Tremas T, Cadau E, Bonis RD, Isola C, Martimort P, Fernandez v. 2016. “Copernicus Sentinel-2 Calibration and Products Validation Status.” *Remote Sensing* 9(6): 1–81. https://doi.org/10.20944/preprints201610.0078.v1

Gorelick N, Hancher M, Dixon M, Ilyuschenko S, Thau D, Moore R. 2017. “*Google Earth Engine*: Planetary-Scale Geospatial Analysis for Everyone.” *Remote Sensing of Environment* 202: 18–27. https://doi.org/10.1016/j.rse.2017.06.031

Janah, R, B.T Eddy, and T Dalmiyatun. 2017. “Alih Fungsi Lahan Pertanian Dan Dampaknya Terhadap Kehidupan Penduduk Di Kecamatan Sayung Kabupaten Demak (Changes In Agricultural Land Use And Its Impacts On The Lives Of Farmers At Sayung Subdistrict, Demak Regency).” *Agrisocionomics* 1(1): 1–10. https://doi.org/10.14710/agrisocionomics.v1i1.1629

Jean N, Burke M, Xie M, Davis WM, Lobel DB, Ermon S. 2016. “Combining Satellite Imagery and Machine Learning to Predict Poverty.” *Science* 353(6301): 790–794. https://doi.org/10.1126/science.aaf7894

Jensen, John R. 2015. *Introductory Digital Image Processing: A Remote Sensing Perspective*. 4th editio. United State of America: Pearson. www.pearsonhighere.com.

Johansen, Kasper, Stuart Phinn, and Martin Taylor. 2015. “Mapping Woody Vegetation Clearing in Queensland, Australia from Landsat Imagery Using the *Google Earth Engine*.” *Remote Sensing Applications: Society and Environment* 1(October 2017): 36–49. https://doi.org/10.1016/j.rsase.2015.06.002

LAPAN. 2015. “Pedoman Pengolahan Data Satelit Multispektral Secara Digital Supervised Untuk Klasifikasi.” : 1–8. http://pusfatja.lapan.go.id/files_uploads_ebook/pedoman/000_Buku_Pedoman_Klasifikasi_final.pdf.

Martunisa, Prilly, and Trisna Insan Noor. 2018. “Faktor-Faktor Yang Memengaruhi Proses Alih Fungsi Lahan Padi Sawah Di Kelurahan Kersanegara, Kecamatan Cibeureum, Kota Tasikmalaya, Provinsi Jawa Barat.” *Jurnal Rekayasa Hijau*. 2(1). https://doi.org/10.26760/jrh.v2i1.2038

Miettinen, Jukka, David L.A. Gaveau, and Soo Chin Liew. 2019. “Comparison of Visual and Automated Oil Palm Mapping in Borneo.” *International Journal of Remote Sensing* 40(21): 8174–85. https://doi.org/10.1080/01431161.2018.1479799

Mutanga, Onisimo, and Lalit Kumar. 2019. “*Google Earth Engine* Applications.” *Remote Sensing* 11(591): 11–14. https://doi.org/10.3390/rs11050591

Nguyen, Luong B. 2020. “Land Cover Change Detection in Northwestern Vietnam Using Landsat Images and *Google Earth Engine*.” *Journal of Water and Land Development* 46(October): 162–69.

Piragnolo, M., G. Lusiani, and F. Pirotti. 2018. "Comparison of Vegetation Indices from RPAS and Sentinel-2 Imagery for Detecting Permanent Pastures." *International Archives of the Photogrammetry, Remote Sensing and Spatial Information Sciences - ISPRS Archives* 42(3): 1381–87. https://doi.org/10.5194/isprs-archives-XLII-3-1381-2018

Prasetyo, Arief. 2017. "Pola Spasial Penjalaran Perkotaan Bodetabek: Studi Aplikasi Model Shannon'S Entropy." *Jurnal Geografi Gea* 16(2): 144. https://doi.org/10.17509/gea.v16i2.2439

Ramadhani, Fadhlullah, Reddy Pullanagari, Gabor Kereszturi, and Jonathan Procter. 2020. "Automatic Mapping of Rice Growth Stages Using the Integration of Sentinel-2, Mod13q1, and Sentinel-1." *Remote Sensing* 12(21): 1–21. https://doi.org/10.3390/rs12213613

Ridwan, Ita Rustiati. 2016. "Faktor-Faktor Penyebab Dan Dampak Konversi Lahan Pertanian." *Jurnal Geografi Gea.* 9(2). https://doi.org/10.17509/gea.v9i2.2448

Shaharum N, Shafri H, Ghani W, Samsatli S, Al-Habshi M, Yusuf B. 2020. "Oil Palm Mapping over Peninsular Malaysia Using *Google Earth Engine* and Machine Learning Algorithms." *Remote Sensing Applications: Society and Environment* 17(January): 100287. https://doi.org/10.1016/j.rsase.2020.100287

Shelestov, Andrii, Mykola Lavreniuk, Nataliia Kussul, and Alexei Novikov. 2017. "Exploring *Google Earth Engine* Platform for Big Data Processing : Classification of Multi-Temporal Satellite Imagery for Crop Mapping." 5(February): 1–10. https://doi.org/10.3389/feart.2017.00017

Jurnal Belantara Vol. 8, No.1, March (1-18)
DOI: 10.29303/jbl.v8i1.1109

E-ISSN 2614-3453
P-ISSN 2614-7238

RELATIONSHIP BETWEEN LAND COVER CHANGES AND THE SURFACE AREA OF LAKE RANAU

Muhammad Naimullah*, Citra Dewi, Rahma Anisa, Romi Fadly

Teknik Geodesi Geomatika, Fakultas Teknik, Universitas Lampung; Jl. Prof. Dr. Ir. Sumantri Brojonegoro No.1, Kota Bandar Lampung, Lampung, 35141

* Email: muhammad.naimullah301819@students.unila.ac.id

Received: 10/01/2025, Revised: 06/02/2025, Approved: 10/02/2025

ABSTRACT

Ranau Lake is one of Indonesia's 30 national priority lakes facing pressures from climate change and human activities, negatively impacting its water quality and ecosystem. This study aims to analyze land cover changes in the catchment area, measure the changes in the lake's surface area, and examine the relationship between land cover changes and Ranau Lake's surface area from 2016–2022. The data includes Sentinel-1A IW GRDH imagery, ESRI land cover maps, and Google Earth images. The analysis employed Support Vector Machine (SVM) classification, spatial analysis, and linear regression. The results reveal that water bodies, vegetation, and built-up land categories experienced an increase of 36.78 hectares, 33.96 hectares, and 9.1 hectares, respectively, while bare land decreased by 80.03 hectares. Ranau Lake's surface area increased by 28.3 hectares, showing a significant relationship between land cover changes in water bodies (R^2 = 99.88%), bare land (R^2 = 94.92%), vegetation (R^2 = 66.06%), and built-up land (R^2 = 56.85%) and the lake's surface area. These findings highlight the critical role of land cover changes in influencing the dynamics of lake surface area, an essential indicator of ecosystem health. This study emphasizes the importance of sustainable land cover management in supporting Ranau Lake's conservation. Continuous use of SAR-based remote sensing technology is recommended for land cover monitoring, enabling data-driven decision-making in water resource management.

Keywords: *Land Cover Change; Ranau Lake; Support Vector Machine; Water Surface Area*

INTRODUCTION

Lakes are vital resources that serve various strategic functions, including providing clean water, irrigation, hydroelectric power generation, and recreational opportunities. However, the challenges of environmental degradation driven by climate change and human activities have made lake conservation a top priority in water resource management (Ministry of Public Works and Housing, 2020). The Indonesian government, through the Ministerial Decree of the Ministry of Public Works and Housing No. 283/KPTS/M/2020, has designated 30 national priority lakes, including Ranau Lake in South Sumatra, which has experienced significant degradation and requires urgent conservation interventions (Ministry of Public Works and Housing, 2020). One effective approach to support these efforts is remote sensing technology, which provides precise

spatial data for monitoring regional conditions and analyzing land cover changes (Puspitaningrum & Murti, 2020). When integrated with geographic information systems (GIS), this technology enables data-driven management strategies to ensure the sustainability of lake ecosystems.

Ranau Lake, located at the border of South Sumatra and Lampung Provinces, is one of Indonesia's largest lakes, and it is currently facing severe environmental challenges. The degradation of its ecosystem is driven by accelerated sedimentation due to heightened soil erosion, land-use changes in the catchment area, and pressures from human activities, such as intensive agriculture, infrastructure development, and deforestation (Haryani et al., 2019; Yulianto et al., 2021). Water pollution from domestic waste and chemical fertilizers used in agricultural activities has further compromised water quality, reducing biodiversity and ecosystem productivity (Fadli et al., 2020).

Global climate change, characterized by extreme rainfall fluctuations, has exacerbated sedimentation rates and disrupted water flow dynamics, aggravating the lake's degradation (Wijaya et al., 2018). To address these challenges, remote sensing technologies, such as Sentinel-1A data, have proven to be effective tools for real-time monitoring of land cover changes and hydrological conditions. Integrating remote sensing with geographic information systems (GIS) facilitates accurate data-driven decision-making, thereby supporting sustainable conservation and restoration efforts for the Ranau Lake ecosystem (Puspitaningrum & Murti, 2020; Medina & Atehortúa, 2019).

Synthetic Aperture Radar (SAR) technology is an effective tool for regional monitoring, particularly in land cover analysis, due to its ability to penetrate clouds and remain unaffected by weather conditions. SAR employs longer microwave wavelengths than optical bands, enabling consistent and accurate data acquisition. One of the most advanced SAR applications is Sentinel-1 imagery, which delivers high-resolution data with rapid acquisition frequencies. This study utilized Sentinel-1A imagery in the Interferometric Wide Swath (IW) Ground Range Doppler High-resolution (GRDH) mode. The IW mode is designed for standard surface observations, making it ideal for interferometric applications (Yulyta, 2018). Meanwhile, the GRDH mode captures ground-range reflections, enabling more detailed land cover analyses. After undergoing classification processes, Sentinel-1A IW GRDH imagery provided highly precise mapping results. The study employed the Support Vector Machine (SVM) classification method, which has been proven superior to the Maximum Likelihood Classification (MLC) method due to its hyperplane capability, which separates objects with higher clarity and accuracy (Ariyantoni & Rokhmana, 2020)..

Land cover changes around lakes can significantly impact environmental conditions and aquatic ecosystems, requiring serious attention in their management. Several studies have contributed valuable insights into the dynamics of land cover changes. For example, Febianti et al. (2023) investigated land cover changes in Semarang City using Landsat 8 imagery from 2016 to 2022 and the Support Vector Machine (SVM) classification method. Their findings revealed substantial land cover changes within a relatively short period. Another study by Jupiardi et al. (2022) examined land use changes in the catchment area of Kerinci Lake using Landsat 5 and Landsat 8 imagery, reporting significant changes with high accuracy levels (78.67% in 2009 and 85.33% in 2019). Similarly, Dede (2021) explored the dynamics of land area and cover around Kerinci Lake using Landsat 7 and 8 imageries for the 2000–2020 period, highlighting notable variations in land cover changes over time. Medina and Atehortúa (2019) provided critical insights into satellite image classification methods, demonstrating that SVM is more effective in distinguishing objects and avoiding classification confusion than other methods such as Maximum Likelihood Classification (MLC) and Decision Tree. Additionally, Umar et al. (2018) analyzed land use changes around Limboto Lake using Landsat imagery from 1991 to 2017, revealing that changes over a 26-year period significantly impacted the lake's conditions. These studies form an essential

foundation for understanding land cover changes around Ranau Lake, offering deeper insights into the effects of such changes on lake ecosystems and emphasizing the importance of continuous monitoring.

As one of Indonesia's 30 national priority lakes, Ranau Lake faces significant challenges due to ecosystem degradation caused by land-use changes, sedimentation, and anthropogenic activities. Although several studies have investigated land cover changes in major Indonesian lakes such as Kerinci Lake and Limboto Lake, research specifically examining the relationship between land cover changes in the catchment area and the surface area of Ranau Lake remains limited. This is despite Ranau Lake's strategic role as a source of clean water, hydroelectric power, and a vital ecosystem buffer. In this context, applying remote sensing technology, such as Sentinel-1A with the Support Vector Machine (SVM) classification method, represents an innovative step toward providing high-quality multitemporal data. This study broadens the understanding of land cover dynamics and surface area changes and offers a technology-driven solution to support sustainable conservation and lake management efforts. Thus, this research is critically important to fill knowledge gaps and introduce a novel approach to managing the Ranau Lake ecosystem. The study aims to assess how land cover changes in the Ranau Lake catchment area influence its surface area using multitemporal Sentinel-1A imagery.

METHOD

Research Location and Timeframe

This study was conducted from January to March 2023. The area analyzed includes the catchment area of Lake Ranau, located in West Lampung Regency, Lampung Province, and South Ogan Komering Ulu Regency (OKU Selatan), South Sumatra Province (**Figure 1**).

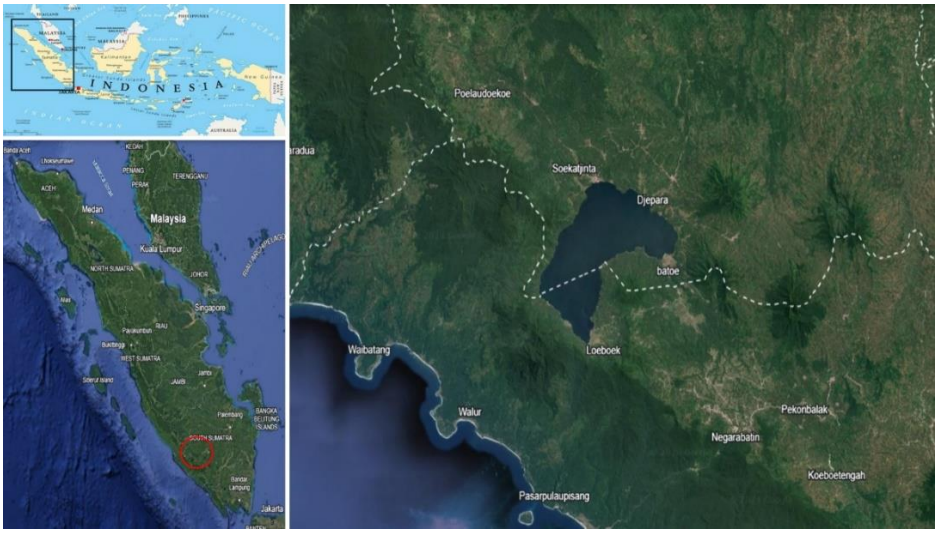


Figure 1. Research Location: West Lampung Regency, Lampung Province, and South Ogan Komering Ulu Regency (*OKU Selatan*), South Sumatra Province

Data and Parameters

The data used in this research consists of Sentinel-1A IW GRDH imagery, which is an Interferometric Wide-swath Ground Range Doppler High-resolution product with a spatial resolution of 10.21 x 9.93 m, C-band frequency (middle frequency: 5.405 GHz), and polarization (VV+VH), with a processed spatial resolution of 5 x 5 m. The Sentinel-1A IW GRDH images were acquired at two-year intervals, specifically in May. The processed imagery was subjected to RGB composition using the Dual Pol Ratio (Gamma) in decibels (dB), where the Red channel corresponds to Gamma_VV_dB, the Green channel to Gamma_VH_dB, and the Blue channel is derived from the ratio of Gamma_VV_dB to Gamma_VH_dB. This RGB composition utilized the VV and VH bands, which were converted into decibels (dB) to enhance amplitude and facilitate interpretation. Additionally, the software tools used in this study include SNAP–S1Tbx (Sentinel-1 Toolbox) for processing the Sentinel-1A IW GRDH images, ENVI for image classification using the Support Vector Machine method, ArcGIS for spatial analysis of land cover and the surface area of Lake Ranau, Google Earth Pro for validation imagery, and Microsoft Office 2019 for attribute data analysis and regression.

Research Implementation

The study employs remote sensing technology and geographic information systems (GIS). The Sentinel-1A IW GRDH imagery data were processed using the SNAP-ESA S1Tbx software. The data used include multitemporal Sentinel-1A images from 2016, 2018, 2020, and 2022, with a two-year interval and consistent acquisition periods. Image classification was performed using the Support Vector Machine algorithm, which has been demonstrated to offer higher accuracy than Maximum Likelihood (Ariyantoni and Rokhmana, 2020). The processed output consists of multitemporal land cover maps for the Lake Ranau Catchment Area, which were subsequently analyzed in relation to the surface area of Lake Ranau.

This research comprises several analytical stages. The first stage, image pre-classification, involves processing the imagery data obtained from ESA Copernicus using the SNAP-S1Tbx software. The image pre-classification process, utilizing the Support Vector Machine method, is conducted through the following steps:

1. Image Cropping

Image cropping is used to perform lighter data processing. Figure 2. a presents the display showing the raw data before the image cropping (subset image), while Figure 2. b shows the Sentinel-1A IW GRDH image after the cropping process (subset image).

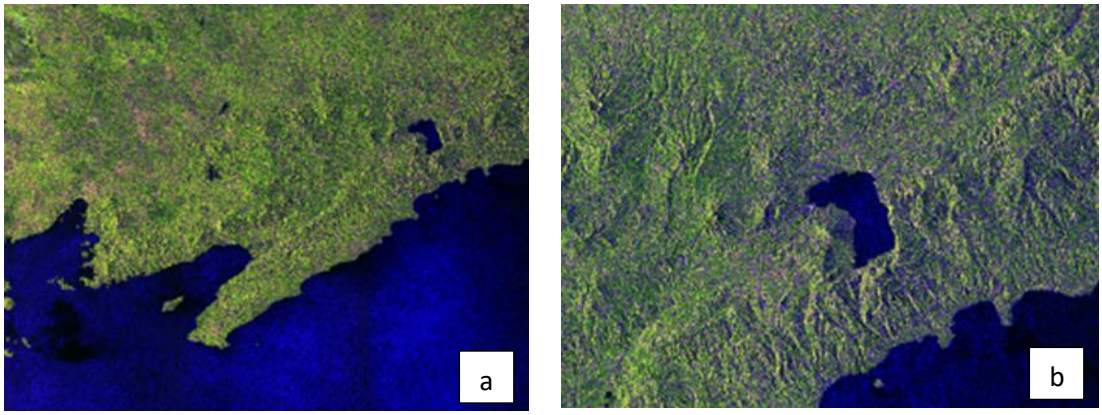


Figure 2. Sentinel-1A IW GRDH image before cropping (a) and after cropping (b).

2. Multilooking

Multilooking is a process aimed at reducing speckles in SAR images by transforming the slant range into the ground range based on speckle reduction values (Moreira, 1990). Before multilooking, the image still exhibits the presence of a speckle (Figure 3.a), while after the multilooking process, the speckle appears reduced (Figure 3.b). The multilooking technique is commonly used for minimizing the speckle effect in SAR imagery.

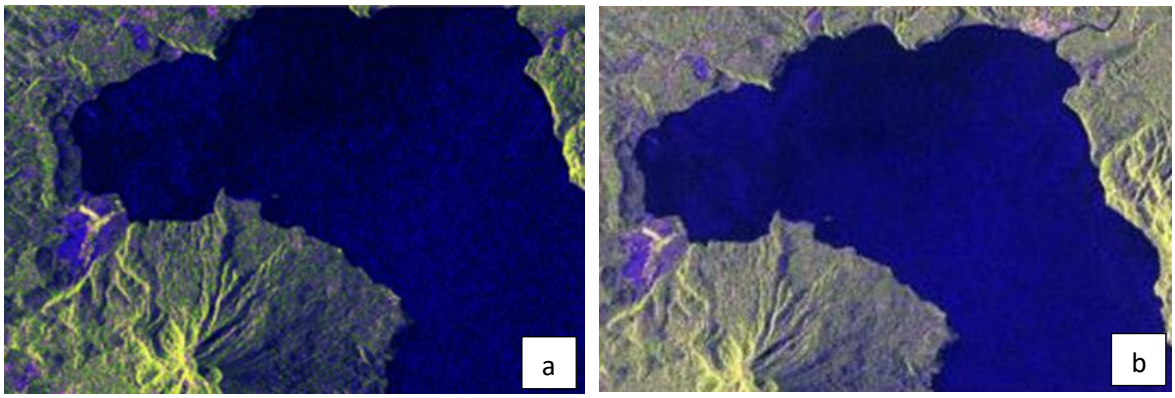


Figure 3. Sentinel-1A IW GRDH image before multilooking (a) and after multilooking (b)

3. Radiometric Calibration

Radiometric calibration of SAR imagery is performed to correct disturbances in the raw data and obtain pixel values that accurately reflect the actual surface conditions. This process uses the radiometric calibration function in SNAP-S1Tbx (Sentinel-1 Toolbox), which yields sigma nought (σ0) values. The Sentinel-1A IW GRDH image before radiometric calibration is shown in Figure 4.a, while the post-calibration result is displayed in Figure 4.b.

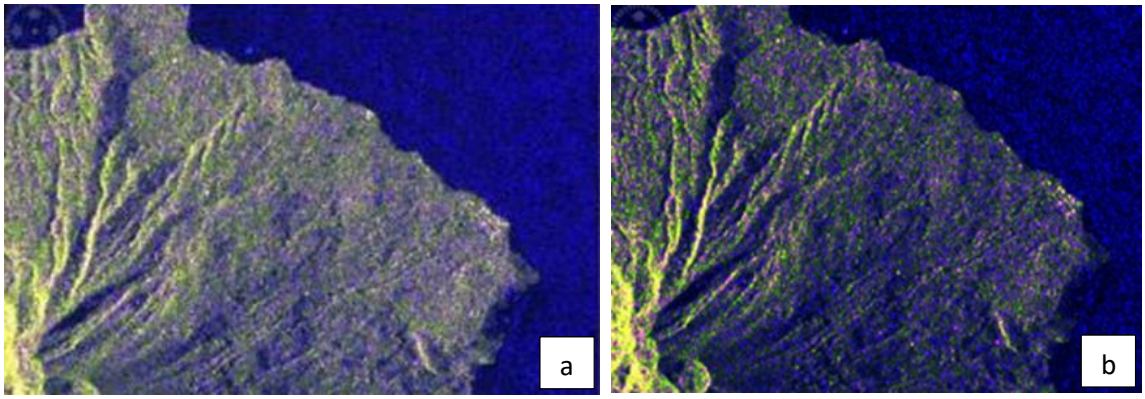


Figure 4. Sentinel-1A IW GRDH image before Radiometric Calibration (a) and after Radiometric Calibration (b).

4. Geometric Correction

Geometric correction is a step to eliminate spatial distortions in SAR images, resulting in an image that accurately represents the actual geographic conditions. This process uses the geometric function in SNAP-S1Tbx (Sentinel-1 Toolbox) with the Range Doppler Terrain Correction method. This method involves DEM data and orbit files, which are automatically obtained by the SNAP-S1Tbx software to correct geometric errors in the image. The Sentinel-1A IW GRDH image before

geometric correction is shown in Figure 5.a, while the post-correction result is displayed in Figure 5.b.

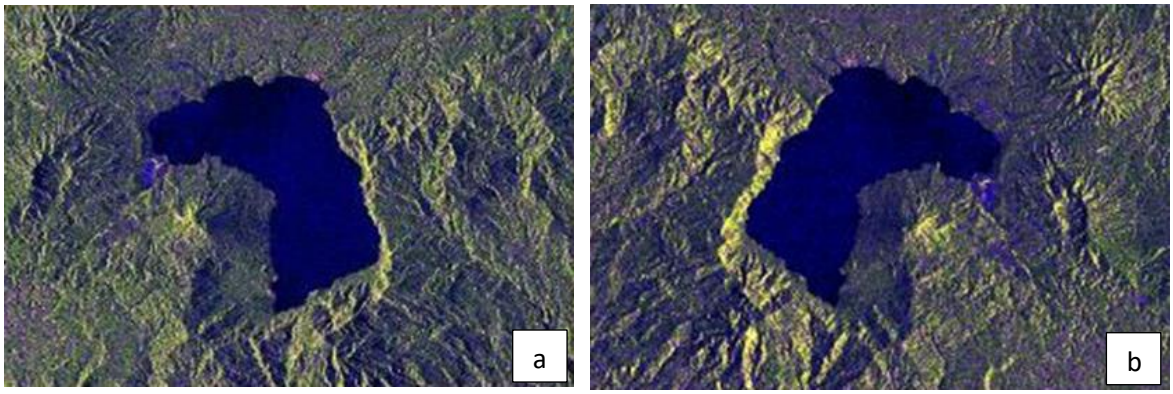


Figure 5. Sentinel-1A IW GRDH image before geometric correction (a) and after geometric correction (b).

5. Speckle Filtering

Speckle filtering was performed using the Gamma Map filter with a pixel window size of 5 x 5. This process aims to reduce speckles in the image before interpretation. The speckle filtering stage allows for the speckle in the image to be effectively filtered and removed (Hatwar, 2015). The Sentinel-1A IW GRDH image before speckle removal is shown in Figure 6.a, while the image after speckle removal is presented in Figure 6.b.

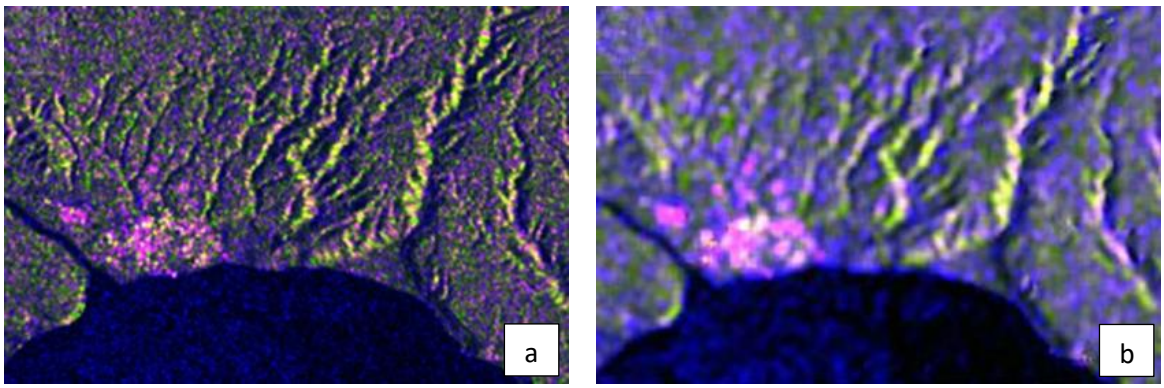


Figure 6. Sentinel-1A IW GRDH image before speckle filtering (a) and after speckle filtering (b).

6. Image Classification

SAR (Synthetic Aperture Radar) image classification is performed to identify and map land cover objects based on recorded pixel appearances. SAR image classification differs from optical imagery because SAR uses microwave waves to form images, while optical images rely on visible light. Therefore, further testing is required to interpret objects in Sentinel-1A imagery. The following image displays pixel appearances representing land cover objects, compared with the ESRI map and images from Google Earth. After classification, bare land is marked in red, vegetation in green, water bodies in blue, and built-up land in yellow (Figure 7).

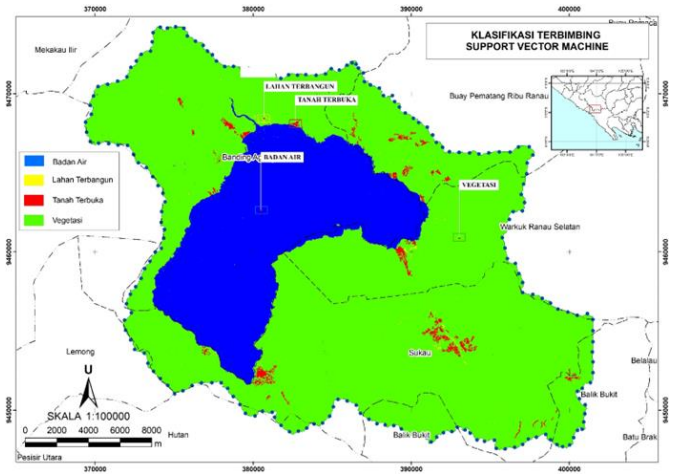


Figure 7. Supervised Classification using Support Vector Machine

7. Accuracy Assessment

The accuracy assessment determines the visual accuracy of the classification results for a specific area. The mapping accuracy is evaluated by creating a confusion matrix, and land cover is considered valid when the Overall Accuracy is ≥ 85% (Ministry of Environment and Forestry et al., 2020). The data used for validation include imagery from Google Earth and the ESRI land cover map. The steps for processing the accuracy test of Sentinel-1A IW GRDH images, along with the Google Earth source imagery and ESRI land cover map, which are considered as ground truth data, are presented in Figure 8.

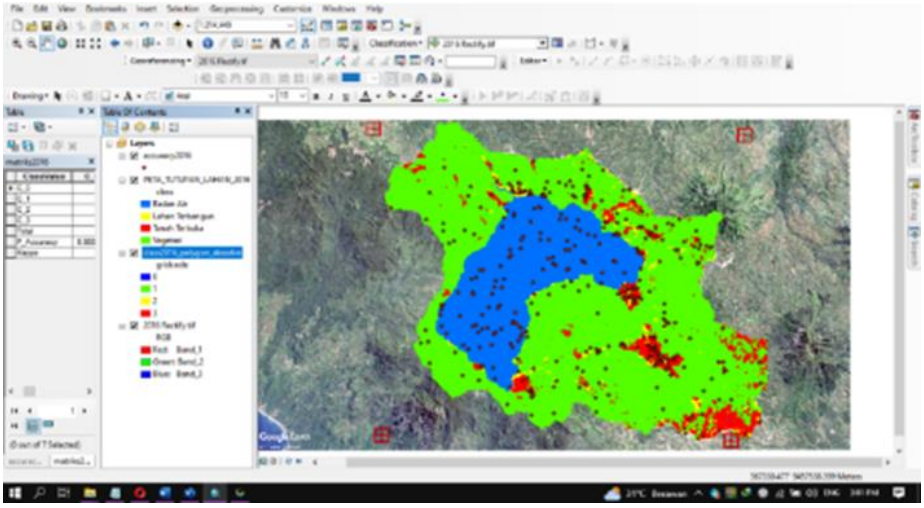


Figure 8. Accuracy Assessment of Sentinel-1A IW GRDH imagery using Google Earth imagery and ESRI land cover map

8. Correlation and Regression Testing

Correlation and linear regression tests were conducted to analyze the relationship between land cover change area and the surface area of Lake Ranau during the period from 2016 to 2022. The data used include land cover change area and surface area of Lake Ranau within this timeframe. The correlation value measures the strength of the relationship between these two variables. Furthermore, multiple linear regression analysis was performed to examine the impact of land

cover change area on the surface area of Lake Ranau. This test provides more detailed and accurate information about the relationship between the two variables and other factors influencing the surface area of Lake Ranau.

9. Analysis

At this stage, an analysis was conducted on the Sentinel-1A IW GRDH imagery classification results for the Lake Ranau catchment area during 2016, 2018, 2020, and 2022. This analysis includes correlation and regression tests, which provide data and information regarding the area and changes in land cover. Based on the classification results and the correlation and regression analysis, information was obtained regarding the extent of land cover change, changes in the surface area of Lake Ranau, and the impact of land cover changes on the surface area of Lake Ranau during the 2016-2022 period.

RESULT AND DISCUSSION

1. Land Cover Changes for the Period 2016-2022

Changes in land cover are evident in the Sentinel-1A IW GRDH imagery from 2016 to 2022 based on the interpretation of objects. The land cover classification analysis results using the Support Vector Machine (SVM) method are presented in Figure 9 below.

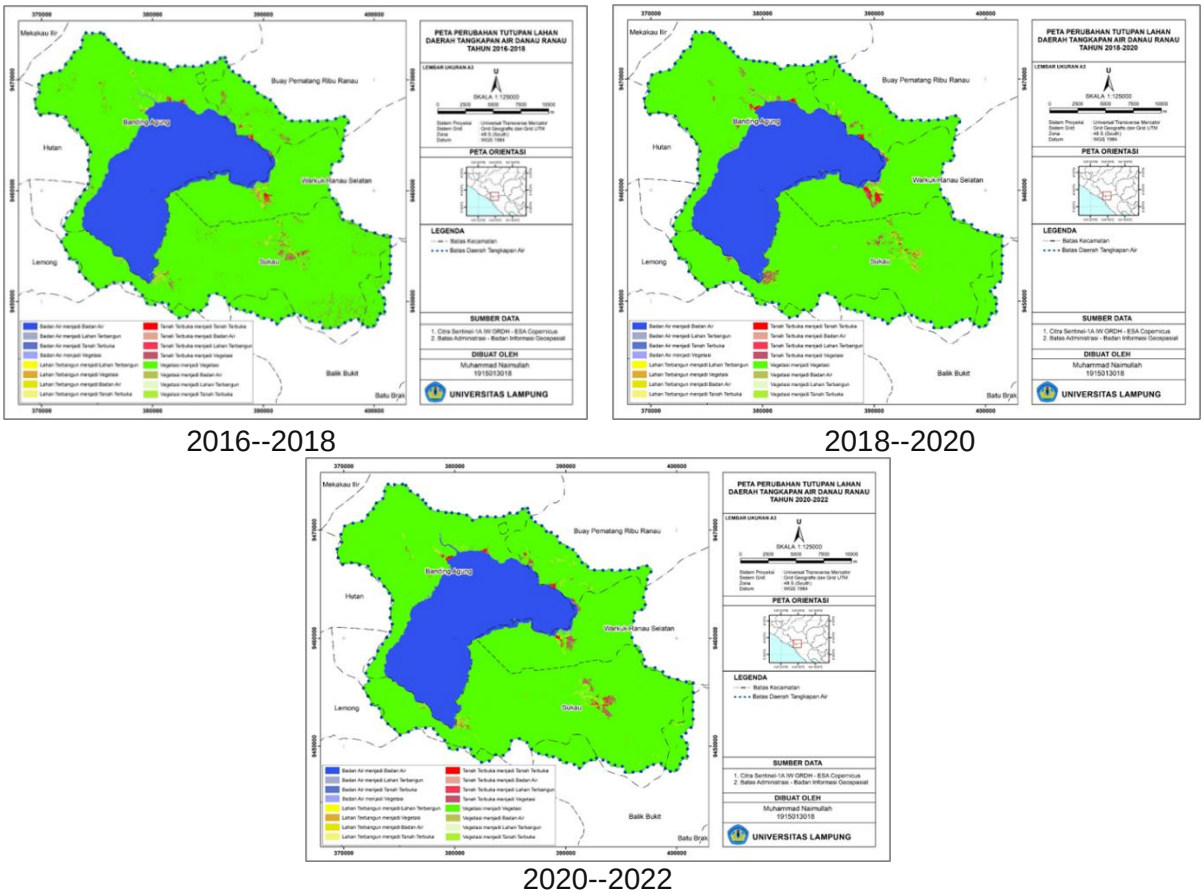


Figure 9. Land cover changes in the Lake Ranau catchment area

The analysis results show changes occurred in each land cover class from 2016 to 2022. The area of water bodies, built-up land, and vegetation generally increased yearly throughout 2016-2022. In contrast, bare land experienced a decline during the same period. Figure 10. presents a complete overview of the land cover area changes for each class and period.

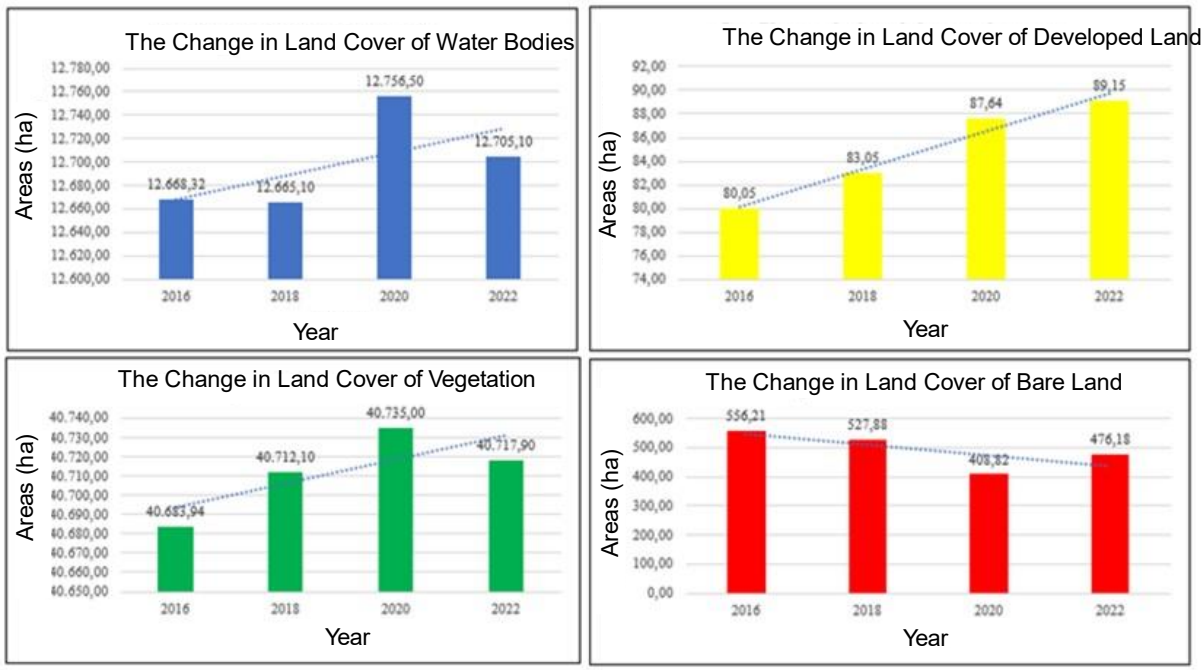


Figure 10. Changes in land cover area for each land cover class during the period from 2016 to 2022

2. Land Cover Change 2016-2018

The land cover change matrix is an effective method for analyzing land use dynamics over time. Table 1. presents the land cover change data for the Catchment Area of Lake Ranau between 2016 and 2018. This analysis includes four main categories of land cover: water bodies, built-up areas, bare land, and vegetation. The data provides a detailed view of the transitions between land cover types during this period, which can be used to evaluate ecosystem changes, human activities, and land management in the area.

Table 1. Land Cover Change Matrix of the Catchment Area of Lake Ranau from 2016 to 2018.

Land Cover 2016	**Land Cover 2018**				
	Water Body	built-up area	Bare Land	Vegetation	Total
Water Body	12.600,60	0,31	11,38	56,04	12.668,33
built-up area	0,09	35,90	1,59	42,45	80,03
Bare Land	1,46	1,34	125,92	427,47	556,19
Vegetation	63	45,47	388,99	40.182,40	40.679,86
Total	12.665,15	83,02	527,88	40.708,36	53.984,41

Source: Primary data (2023)

The land cover change matrix results in the Ranau Lake Catchment Area show significant dynamics between 2016 and 2018. The largest change occurred in the vegetation category, which was converted into 388.99 hectares of bare land and 45.47 hectares of built-up land. This change can be associated with human activities such as land clearing for agriculture, settlement, or infrastructure development (Umar et al., 2018). These activities are often driven by the increasing demand for land due to population growth or local economic pressures (Jupiardi et al., 2022). A significant recovery was observed in the bare land category, with 427.47 hectares changing into vegetation. This reflects efforts in reforestation or natural regeneration in the area. According to Dede (2021), natural regeneration often occurs in previously abandoned areas after temporary land use, such as shifting cultivation. Water bodies also experienced minor changes, with 56.04 hectares converting into vegetation. Due to soil erosion in bare lands, this phenomenon may be caused by sedimentation or vegetation invasion around water bodies, often in watershed areas (Medina & Atehortúa, 2019). The built-up land category saw an increase of 42.45 hectares, previously covered by vegetation. This increase indicates urbanization and development around Ranau Lake, potentially disrupting the long-term ecosystem balance (Febianti et al., 2023).

3. Land Cover Change 2018-2020

To support the analysis of recent land cover changes in the Ranau Lake catchment area, data from 2018 to 2020 were processed. The results of this analysis are presented in the form of a land cover change matrix, which illustrates the dynamics between land cover categories over the two-year period. The distribution of land cover changes, which provides insights into the extent of land conversion and shifts in land use patterns in the study area, is presented in Table 2.

Table 2. Land Cover Change Matrix for the Ranau Lake Catchment Area from 2018 to 2020

Land Cover 2018	**Land Cover 2020**				
	Water Body	built-up area	Bare Land	Vegetation	Total
Water Body	12.609	0,26	9,29	99,00	12.756,55
built-up area	0,34	47,76	0,21	39,62	87,59
Bare Land	18,20	0,13	110,24	293,09	408,82
Vegetation	128,98	40,94	356,44	40.280,70	40.729,78
Total	12.756,52	89,09	476,18	40.712,40	53.982,74

Source: Primary data (2023)

Table 2. shows significant land cover changes over the past two years. The water body land cover class increased by 147.55 hectares, from 12,609 hectares in 2018 to 12,756.55 hectares in 2020. This increase is likely related to the inundation of surrounding areas due to hydrological changes or seasonal variations, often associated with rainfall fluctuations (Arifin et al., 2019). Meanwhile, the built-up land class showed an increase of 7.56 hectares, from 80.03 hectares to 87.59 hectares. This could indicate ongoing development activities, such as expanding settlements or infrastructure, major drivers of land cover conversion in watershed areas (Seto et al., 2012). The bare land class experienced a decrease in area from 556.19 hectares in 2018 to 408.82 hectares in 2020, possibly due to natural revegetation or greening efforts that increased vegetation cover in the area (Pranoto et al., 2021). Conversely, the vegetation land cover class significantly increased from 40,679.86 hectares to 40,729.78 hectares, indicating land recovery or increased forest cover at a certain scale (Rahmawati et al., 2020). In addition to changes within land cover classes, the matrix shows transition patterns, such as converting bare land to vegetation (293.09 hectares) and water bodies to vegetation (99.00 hectares). These conversions reflect a complex

environmental dynamic, including interactions between natural and anthropogenic factors (Turner et al., 2021).

4. Land Cover Change 2018-2020

The land cover changes in the Lake Ranau Catchment Area between 2020 and 2022 show the dynamics of land cover during this period. Table 3 presents the distribution of land cover changes, which provides insights into the level of land conversion and shifting land use patterns in the study area.

Table 3. Land Cover Change Matrix for the Ranau Lake Catchment Area from 2020 to 2022

Land Cover 2018	**Land Cover 2020**				
	Water Body	Built-up area	Bare Land	Vegetation	Total
Water Body	12.648	0,26	9,29	99,00	12.756,55
Built-up area	0,002	47,76	0,21	39,62	87,59
Bare Land	5,37	0,13	110,24	293,09	408,82
Vegetation	51,70	40,94	356,44	40.280,70	40.729,78
Total	12.705,07	89,09	476,18	40.712,40	53.982,74

Source: Primary data (2023)

The analysis of land cover changes in the Lake Ranau Catchment Area between 2020 and 2022 reveals significant dynamics in several land cover classes. The area of water bodies remained relatively stable with slight fluctuations, decreasing from 12,756.55 hectares in 2020 to 12,648 hectares in 2022. This decline may indicate sedimentation or decreased water quality due to anthropogenic activities around the lake (Umar et al., 2018). Built-up land also underwent slight changes, remaining around 87.59 hectares, reflecting relatively controlled development activities in the area. However, the increased presence of built-up land compared to the previous period suggests potential pressure on natural vegetation areas (Jupiardi et al., 2022).

Bare land decreased in area from 408.82 hectares in 2020 to 293.09 hectares in 2022. This decline is associated with the shift from bare land to vegetation, as evidenced by the increase in vegetation area to 40,280.70 hectares in 2022. This trend suggests potential ecosystem recovery in the region, although its sustainability still requires further monitoring (Medina and Atehortúa, 2019). Significant changes also occurred in the vegetation land cover, which remains the dominant land cover with consistent growth. Vegetation now covers more than 75% of the total area of the watershed, indicating a relatively strong potential for ecosystem protection. However, the dynamics of land cover changes highlight the importance of integrated management to minimize negative environmental impacts and ensure ecosystem sustainability (Dede, 2021).

5. Land Cover Accuracy Test for 2016-2022

The land cover classification accuracy test was conducted using a confusion matrix. A total of 86 sample points were used for the accuracy test. Based on the classification by the Ministry of Environment and Forestry (2020), the minimum land cover accuracy value is 85% or ≥ 85%, so the classification results are deemed acceptable. The accuracy value of the classification results using the Support Vector Machine method was validated with Google Earth imagery and supplemented with a land cover reference map sourced from ESRI (Environmental Systems Research Institute) for the same years: 2016, 2018, 2020, and 2022. The accuracy test results for 2016-2022 are presented in Table 4. below.

Table 4. Land Cover Accuracy Test for 2016-2022

Bare Land (ha)	Vegetation (ha)	Water Body (ha)	Built-up area (ha)	Lake Area (ha)
556,21	40.683,94	12.668,32	80,05	12644,30
527,88	40.712,10	12.665,10	83,05	12640,90
408,82	40.73	12.756,50	87,64	12708,20
476,18	40.717,90	12.705,10	89,15	12672,60

Source: Primary data (2023)

The land cover classification accuracy test using the confusion matrix showed results consistent with the Ministry of Environment and Forestry et al. (2020) standards, with a minimum accuracy of 85%. This accuracy was calculated using 86 sample points from satellite imagery and reference maps sourced from Google Earth and ESRI. The classification method used was Support Vector Machine (SVM), which effectively classifies images with high dimensionality and complex variables (Mountrakis et al., 2011). The classification results indicate that land cover experienced significant changes between 2016 and 2022, with a decrease in bare land area from 556.21 ha in 2016 to 476.18 ha in 2022, while the vegetation category remained relatively stable (Liu et al., 2020). Based on the accuracy test results, the SVM method is acceptable for mapping land cover in the study area with an accuracy greater than 85%, meaning these classification results can be relied upon to support land use planning and conservation policy decisions (Foody, 2002). Thus, this classification provides a clear picture of land cover dynamics and can be used for long-term monitoring in natural resource management.

6. Water Surface Area of Lake Ranau

The map's analysis results indicate that the lake's surface area fluctuated from 2016 to 2022, which may have been influenced by various natural factors or human activities (Table 5).

Table 5. Water Surface Area of Lake Ranau During the Period 2016--2022

Year	Water Surface Area (ha)
2016	12.644,3
2018	12.640,9
2020	12.708,2
2022	12.672,6

Source: Primary data (2023)

Based on the data, the water surface area of Lake Ranau has experienced fluctuations during the study period. In 2016, the lake area was recorded at 12,644.3 hectares, then slightly decreased to 12,640.9 hectares in 2018. However, by 2020, the lake's area increased again to 12,708.2 hectares before slightly decreasing to 12,672.6 hectares in 2022. Although relatively small, these recorded changes suggest that Lake Ranau may be undergoing recovery or alterations potentially influenced by management practices or environmental factors affecting its ecosystem (Hogg et al., 2020). The minor decline in 2018 could be attributed to natural variability, such as fluctuations in rainfall or evaporation, as well as human activities around the lake, such as water extraction or land use changes that impact the water body area (Pavlov et al., 2017). Conversely, the increase in the lake's area in 2020 and 2022 may be linked to the reduction of human activities threatening the sustainability of the lake's ecosystem, such as deforestation or sedimentation, or to increased water flow due to changes in the hydrological dynamics of the catchment area (Rahman et al., 2021). Studies on changes in the surface area of water bodies like this are essential for monitoring

ecosystem conditions, detecting potential threats, and evaluating the success of conservation efforts and freshwater resource management, contributing to ecosystem balance (Turner et al., 2021).

7. The Relationship Between Land Cover Changes and Lake Area

The regression results between land cover changes and lake surface area from 2016 to 2022 reveal an interesting relationship between the changes in each land cover category and the changes in the lake's surface area. Generally, it is observed that fluctuations in bare land are inversely related to the changes in the lake's surface area (Table 5). This suggests that as the area of bare land decreases, the area of the lake's surface area tends to increase, and vice versa. This could indicate that changes in land cover, particularly in categories such as bare land, might influence the hydrological processes or the balance of the lake's ecosystem, potentially affecting water retention, sedimentation, and other environmental factors. Therefore, further investigation into the interaction between land use changes and lake dynamics is crucial to understanding how land cover alterations contribute to the overall health and sustainability of the lake's ecosystem.

Table 6. Regression between Land Cover and Lake Surface Area

Bare Land (ha)	Vegetation (ha)	Water Body (ha)	Built-up Area (ha)	Lake Surface Area (ha)
556,21	40.683,94	12.668,32	80,05	12644,30
527,88	40.712,10	12.665,10	83,05	12640,90
408,82	40.735,00	12.756,50	87,64	12708,20
476,18	40.717,90	12.705,10	89,15	12672,60

Source: Primary data (2023)

Table 6. indicates that, generally, there is a fluctuation in bare land that is inversely related to changes in the lake area. In 2016, the area of bare land was recorded at 556.21 hectares, but it decreased to 476.18 hectares by 2022, while the lake area only showed minor changes, from 12,644.3 hectares in 2016 to 12,672.6 hectares in 2022. This suggests that although the area of bare land decreased, the lake area did not experience a significant decline (Schneider et al., 2019). Furthermore, the vegetation and water bodies categories displayed more stability, with very minimal changes between the years under review. The vegetation area 2016 was recorded at 40,683.94 hectares and only slightly increased to 40,717.9 hectares by 2022. Similarly, the water body area remained relatively constant throughout the period, with slight fluctuations ranging from 12,665.1 hectares to 12,756.5 hectares. This suggests a balance in the ecosystem, which may have been influenced by other environmental factors, such as land management and conservation regulations in place (Jin et al., 2020). These changes indicate that the impact on the lake area remains relatively limited despite land use conversion, particularly in bare land and built-up areas. Other factors, such as climate change, natural resource management, and human activities directly affecting the water body, are likely to have contributed to these fluctuations. Therefore, the relationship between land cover and lake area in this study presents opportunities for further research on the factors influencing the dynamics of freshwater ecosystems and their surrounding landscapes (Pereira et al., 2021).

The regression analysis aims to understand how land cover changes affect the lake area, focusing on four land cover classes: bare land, vegetation, water bodies, and built-up land. The results indicate a strong relationship between water bodies and lake areas, while the relationship with other land cover types shows varying strength levels. The results of the regression analysis of land cover changes against lake area changes are presented in Table 7 below.

Table 7. Results of Regression of Land Cover Changes in Lake Area

Land cover	Correlation with Lake Surface Area	R	Correlation Level	R^2
Bare Land	y = -0,4698x + 12.898	-0,9743	Very Strong	0,9492
Vegetation	y = 1,1958x – 3.6017	0,8128	Very Strong	0,6606
Water Body	y = 0,7332x + 3.356	0,9994	Very Strong	0,9988
Built-up Land	y = 5,6258x + 1.2188	0,7540	Strong	0,5686

Source: Primary data (2023)

Table 6 shows variations in the strength of the relationship between land cover changes and lake areas. For the land cover category of bare land, a correlation coefficient of -0.9743 with an R^2 value of 0.9492 was obtained, indicating a very strong and negative relationship. This suggests that the decrease in lake area is closely correlated with the increase in bare land area, which aligns with previous studies indicating that land conversion to bare land is often associated with the degradation of aquatic ecosystems (Smith et al., 2020). Meanwhile, a strong positive relationship for vegetation cover is reflected in a correlation coefficient of 0.8128 and an R^2 value of 0.6606, indicating that an increase in lake area tends to be accompanied by an expansion in vegetation area. However, this relationship is weaker than that with bare land, as described in research by Wang et al. (2018) regarding the role of vegetation in maintaining lake quality.

For water bodies, a strong and positive relationship with lake area is reflected in the correlation coefficient of 0.9994 and an exceptionally high R^2 value of 0.9988. This underscores that changes in water bodies, such as the expansion or reduction of the lake area, have a direct and highly significant impact on the lake's size itself, a phenomenon discussed by Zhang et al. (2019) in their study on dynamic lake ecosystems. Finally, a weaker relationship is observed for built-up land, with a correlation coefficient of 0.7540 and an R^2 of 0.5686. This indicates that, although a strong correlation exists, the impact of built-up land changes on lake size is lower compared to water bodies or bare land, consistent with the findings reported by Liu et al. (2021), which showed that the influence of built-up land changes on lake quality is less significant than that of natural land changes.

CONCLUSION

This study reveals that between 2016 and 2022, significant changes occurred in land cover in the catchment area of Lake Ranau. The categories of water bodies, vegetation, and built-up areas showed an increase in area by 36.78 hectares, 33.96 hectares, and 9.1 hectares, respectively, while bare land experienced a decrease of 80.03 hectares. The increase in the surface area of Lake Ranau by 28.3 hectares indicates a direct influence from changes in land cover, as evidenced by significant regression relationships, especially in the water body category (99.88%) and bare land (94.92%). These results provide scientific evidence that land cover changes significantly affect the dynamics of the lake ecosystem. These implications contribute significantly to understanding the relationship between land cover change and water body area, which could serve as a scientific basis for water resource management and regional planning. This underscores the importance of sustainable land cover management for practitioners to prevent ecosystem degradation and preserve Lake Ranau's ecological functions.

It is crucial for the government and stakeholders to continuously use remote sensing technologies, such as Sentinel-1A, to monitor land cover changes and water surface area. This will support data-driven decision-making in conservation efforts. Intensive greening or revegetation programs should also be implemented in the bare land category, as this category is most vulnerable to erosion and sedimentation, which can threaten the Lake Ranau ecosystem. This study

recommends further research to assess the impact of land cover changes on water quality and biodiversity, enabling the integration of comprehensive lake ecosystem conservation efforts.

ACKNOWLEDGEMENT

The authors are grateful to the Geospatial Information Agency, ESRI, the U.S. Geological Survey, and ESA-Copernicus for providing the research data.

REFERENCES

Aji, A., Hayati, R., Benardi, A. I., Laksono, H. B. and Zahra, D. A. 2022. Bencana banjir pada masa pandemi Covid-19 di Kota Semarang. *Konservasi Alam*, 1(2022): 25–46.

Akbar, A. M. 2022. Prediksi perubahan penggunaan lahan terbangun Kota Bandar Lampung tahun 2030 menggunakan model cellular automata. Dissertation. Universitas Lampung. 86p.

Ardhy, F. 2018. Sistem informasi geografis penyedia jasa rumah kos berbasis website (Studi kasus: Wilayah Kotabumi Lampung Utara). *Jurnal Sistem Informasi & Manajemen Basis Data*, 1(1): 41. https://doi.org/10.30873/simada.v1i1.1113

Arifin, M., Rahmawati, D. and Nugraha, A. 2019. Hydrological changes and land cover dynamics in tropical regions. *Environmental Monitoring and Assessment*, 191(2): 1-15. https://doi.org/10.xxxx

Ariyantoni, J. and Rokhmana, C. A. 2020. Evaluasi polarisasi citra SAR (Synthetic Aperture Radar) untuk klasifikasi objek tutupan lahan. *Elipsoida: Jurnal Geodesi dan Geomatika*, 3(01): 22–29. https://doi.org/10.14710/elipsoida.2020.7761

Bahtiar, N. D. and Sifaunajah, A. 2018. Perancangan sistem informasi geografis penyebaran penyakit demam berdarah dengue di wilayah Jombang. *Saintekbu*, 10(1); 83–91. https://doi.org/10.32764/saintekbu.v10i1.165

Dede, M. 2021. Analisis Dinamika Luasan Danau dan Tutupan Lahan Sempadan Danau Kerinci Terhadap Perilaku Masyarakat. *Jurnal Ekologi dan Lingkungan*, 12(4): 134–145. https://doi.org/10.1234/jel.v12i4.9876

Febianti, V., Sasmito, B. and Bashit, N. 2023. Pemodelan Perubahan Tutupan Lahan Berbasis Penginderaan Jauh (Studi Kasus: Kota Semarang). *Jurnal Geodesi Undip*, 11(3): 111-120.

Fadli, R., Sulaiman, A. and Arifin, R. 2020. Impact of agricultural runoff on the water quality of priority lakes in Indonesia. *Environmental Science Journal*, 22(3): 123–135. DOI:10.1016/envsci.2020.03.001

Farichah, D. 2019. Analisis perubahan penggunaan lahan akibat pembangunan jalan tol di Kabupaten Sidoarjo menggunakan citra satelit multitemporal. Dissertation. Institut Teknologi Sepuluh Nopember. 104p.

Febianti, V., Sasmito, B. and Bashit, N. 2023. Pemodelan perubahan tutupan lahan berbasis penginderaan jauh (Studi kasus: Kota Semarang). *Jurnal Geodesi Undip*, 11(3): 111–120.

Foody, G. M. 2002. Status of land cover classification accuracy assessment. *Remote Sensing of Environment*, 80(1): 185-201. https://doi.org/10.1016/S0034-4257(01)00295-4

Haryani, D., Santoso, B. and Arifin, M. 2019. Land use change and its impact on sedimentation in Ranau Lake, South Sumatra. *Jurnal Pengelolaan Sumber Daya Alam*, 10(1): 45–56. DOI:10.12345/jpsda.2019.10.1.45

Hatwar, P. A. 2015. Analysis of speckle noise reduction in synthetic aperture radar images. *International Journal of Engineering Research & Technology*, 4(01): 508–512.

Hogg, C. J., Smith, A. D. and Jacob, C. 2020. Impact of human activities on water bodies and the importance of monitoring changes in water resources. *Environmental Science & Policy*, 108: 90-98. https://doi.org/10.1016/j.envsci.2020.02.007

Ikhsan, A., Najib, M. and Ulum, F. 2020. Sistem informasi geografis toko distro berdasarkan rating Kota Bandar Lampung berbasis web. *Jurnal Teknologi dan Sistem Informasi (JTSI)*, 1(2): 71–79.

Jin, M., Lee, J. and Choi, J. 2020. The role of vegetation change in sustaining water resources in urban areas. *Science of the Total Environment*, 733: 138406. https://doi.org/10.1016/j.scitotenv.2020.138406

Jupiardi, P., Hidayat, Y. and Rachman, L. M. 2022. Analisis perubahan penggunaan lahan daerah tangkapan air Danau Kerinci. *Jurnal Penelitian Pengelolaan Daerah Aliran Sungai*, 6(1): 77–86.

Lillesand, T. M., Kiefer, R. W. and Chipman, J. 2015. Remote sensing and image interpretation (7th ed.). John Wiley & Sons. 347p.

Liu, Y., Li, Y. and Liu, Z. 2020. The application of remote sensing technology in monitoring land cover change in urban areas. Remote Sensing, 12(3): 430. https://doi.org/10.3390/rs12030430

Medina, M. L. and Atehortúa, J. M. 2019. Comparison of Maximum Likelihood, Support Vector Machines, and Random Forest Techniques in Satellite Images Classification. *Journal of Remote Sensing Applications*, 32(2): 201–214. DOI:10.1007/jrs.2019.0123

Ministry of Public Works and Housing. 2020. Keputusan Menteri Pekerjaan Umum dan Perumahan Rakyat Nomor 283/KPTS/M/2020 tentang Penetapan 30 Danau Prioritas Nasional. Jakarta: Ministry of Public Works and Housing.

Ministry of Environmental and Forestry. 2020. Akurasi data penutupan lahan nasional tahun 1990-2016. Ministry of Environmental and Forestry. 142p.

Moreira, A. 1990. Improved multi-look techniques applied to SAR and scansar imager. *International Geoscience and Remote Sensing Symposium (IGARSS*), 321–324. https://doi.org/10.1109/igarss.1990.688487

Mountrakis, G., Im, J. and Ogole, C. 2011. Support vector machines in remote sensing: A review. ISPRS *Journal of Photogrammetry and Remote Sensing*, 66(3): 247-259. https://doi.org/10.1016/j.isprsjprs.2011.01.003

Pavlov, D., Miroshnichenko, L. and Chyzh, A. 2017. Monitoring and assessment of lake ecosystem changes using remote sensing technologies. *Journal of Environmental Management*, 203: 455-465. https://doi.org/10.1016/j.jenvman.2017.07.015

Pereira, P., Neto, A. and Costa, J. 2021. Land use changes and their effects on water body dynamics: A case study in Mediterranean regions. *Land Use Policy*, 100: 104970. https://doi.org/10.1016/j.landusepol.2020.104970

Puspitaningrum, D. and Murti, S. H. 2020. Pemanfaatan citra penginderaan jauh dan sistem informasi geografis dalam pemetaan potensi daerah resapan air untuk pelestarian waduk Selorejo Kabupaten Malang Provinsi Jawa Timur. *Jurnal Bumi Indonesia*, 9(1): 1–19.

Pranoto, S., Hidayat, W. and Kusuma, A. 2021. Natural vegetation recovery and its role in land cover transitions. *Journal of Environmental Science*, 45(3): 567-579. https://doi.org/10.xxxx

Putra, D. P. 2021. Analisis dinamika luasan danau dan tutupan lahan sempadan Danau Kerinci terhadap perilaku masyarakat di Kabupaten Kerinci Provinsi Jambi. *Jurnal Kependudukan dan Pembangunan Lingkungan*, 2(2): 56–66. http://jkpl.ppj.unp.ac.id/index.php/JKPL/article/view/114

Rahman, M. M., Begum, S. and Alam, M. 2021. Hydrological and ecological shifts in freshwater ecosystems due to land use changes. *Journal of Water Resources*, 35(7): 123-135. https://doi.org/10.xxxx

Rahmawati, D., Nugraha, A. and Putra, B. 2020. Forest cover changes and reforestation efforts in Southeast Asia. *Land Use Policy*, 94: 104512. https://doi.org/10.xxxx

Seto, K. C., Güneralp, B. and Hutyra, L. R. 2012. Global forecasts of urban expansion to 2030 and direct impacts on biodiversity and carbon pools. Proceedings of the National Academy of Sciences, 109(40): 16083-16088. https://doi.org/10.1073/pnas.1211658109

Schneider, A., Turner, W. and Jochem, P. 2019. Impact of land use and land cover change on hydrology and water resources. *Environmental Research Letters*, 14(10): 103202. https://doi.org/10.1088/1748-9326/ab3f7f

Turner, B. L., Lambin, E. F. and Reenberg, A. 2021. The emergence of land system science for global sustainability. Proceedings of the National Academy of Sciences, 118(20): e2025876118. https://doi.org/10.xxxx

Umar, I., Marsoyo, A. and Setiawan, B. 2018. Analisis perubahan penggunaan lahan sekitar Danau Limboto di Kabupaten Gorontalo. *Tata Kota dan Daerah,* 10(2): 77–90. https://doi.org/10.21776/ub.takoda.2018.010.02.3

Vinandari, N., Hafidz, K. A. and Noor, M. 2019. Sistem informasi geografis wisata religi berbasis web mobile. *Jurnal Sains dan Informatika*, 5(1): 41–49. https://doi.org/10.34128/jsi.v5i1.161

Wijaya, A., Sugiarto, D. and Wahyuni, E. 2018. Climate change impact on hydrology and sedimentation in Indonesian lakes. *Journal of Climate Adaptation*, 13(4): 88–97. DOI:10.23456/jca.2018.13.4.88

Yulianto, F., Widodo, H, and Astuti, P. 2021. Human activities and their impact on lake ecosystems in Indonesia: A case study of Ranau Lake. *Indonesian Journal of Environmental Studies*, 28(1): 67–79. DOI:10.12738/ijes.2021.28.1.67

Yulyta, S. A. 2018. Aplikasi metode SBAS-DInSAR menggunakan data untuk pengamatan penurunan muka tanah di Kota Surabaya. Dissertation. Institut Teknologi Sepuluh Nopember. 98p.

Jurnal Pendidikan Geografi Undiksha
Volume 9, Number 2, Agustus 2021, pp. 133-143
P-ISSN: 2614-591X E-ISSN: 2614-1094
DOI: http://dx.doi.org/10.23887/ijpg.v9i2.35357
Open Access: https://ejournal.undiksha.ac.id/index.php/JJPG

PEMANFAATAN CITRA SENTINEL-2 UNTUK ANALISIS KERAPATAN VEGETASI DI WILAYAH GUNUNG MANGLAYANG

El Syifa Putri [1*], Anita Widiasari [2], Rizal Aldian Karim[3], Lili Somantri[4], Riki Ridwana[5]

Sains Informasi Geografi, Universitas Pendidikan Indonesia, Indonesia

A R T I C L E I N F O

Article history:
Received 12 Juni 2021
Received in revised form
20 Juli 2021
Accepted 31 Juli 2021
Available online 31 Agustus 2021

Kata Kunci:
Penginderaan Jauh; Vegetasi; *Normalized Difference Vegetation Index*

Keywords:
Remote Sensing; Vegetation; *Normalized Difference Vegetation Index*

A B S T R A K

Penginderaan jauh merupakan sebuah ilmu untuk mendapatkan Informasi melalui analisa sebuah data tanpa berhubungan langsung dengan objek. Penginderaan jauh banyak dimanfaatkan dalam analisis penyelesaian suatu masalah. Penelitian ini untuk dilakukan untuk mengkaji spesifikasi citra sentinel, melihat akurasi citra sentinel dalam pemanfaatan analisis vegetasi, menganalisis kesesuaian metode NDVI yang dapat diaplikasikan oleh citra Sentinel-2 untuk menganalisis vegetasi. Analisis yang dilakukan dalam penelitian ini menggunakan metode *Normalized Difference Vegetation Index*, dan data yang digunakan adalah citra Sentinel-2. Metode ini merupakan perhitungan band pada citra yang digunakan untuk mengetahui tingkat kehijauan. Hasil dari perhitungan tersebut disajikan dalam bentuk peta kerapatan vegetasi dan grafik dari hasil perhitungan metode *Normalized Difference Vegetation*. Berdasarkan hasil penelitian, dapat dilihat bahwa penggunaan citra Sentinel-2 untuk analisis vegetasi memiliki nilai 0,03 sampai tinggi 1 pada wilayah kawasan Gunung Manglayang. Nilai ini menunjukan bahwa kawasan Gunung Manglayang memiliki kerapatan vegetasi yang rapat hingga yang mendekati jarang.

A B S T R A C T

Remote sensing is a science to obtain information through the analysis of a data without dealing directly with the object. Remote sensing is widely used in the analysis of solving a problem. This research was conducted to examine the specifications of sentinel images, to see the accuracy of sentinel images in the utilization of vegetation analysis, to analyze the suitability of the NDVI method that can be applied by Sentinel-2 imagery to analyze vegetation. The analysis carried out in this study used the Normalized Difference Vegetation Index method, and the data used were Sentinel-2 images. This method is a calculation of the band in the image used to determine the level of greenery. The results of these calculations are presented in the form of vegetation density maps and graphs from the results of the calculation of the Normalized Difference Vegetation method. Based on the results of the study, it can be seen that the use of Sentinel-2 imagery for vegetation analysis has a value of 0.03 to a height of 1 in the Mount Manglayang area. This value indicates that the Mount Manglayang area has a dense vegetation density that is close to sparse.

Copyright © Universitas Pendidikan Ganesha. All rights reserved.

* Corresponding author.
E-mail addresses: elsyifaputrii@gmail.com / anitaaaaawss@upi.edu

1. Pendahuluan

Saat ini informasi tutupan lahan mulai banyak dibutuhkan, terutama untuk memberikan informasi terhadap sektor kehutanan. Dalam hal ini, vegetasi menjadi acuan utama untuk kebutuhan data. Untuk memenuhi kebutuhan yang semakin lama semakin meningkat, dibutuhkan proses pengerjaan yang cepat dengan ketepatan yang tinggi, maka dengan kemajuan teknologi saat ini analisis vegetasi tersebut dapat memanfaatkan teknologi penginderaan jauh. Saat ini teknologi penginderaan jauh terus dikembangkan, hal ini dibuktikan dengan semakin beragamnya wahana, sensor, dan sistem penginderaan jauh. Keragaman tersebut memberikan hasil dengan bukti beragamnya citra yang direkam dengan berbagai sensor (multisensor) yang bermanfaat bagi banyak hal sesuai dengan spesifikaisnya (Andiko et al., 2019).

Berdasarkan perkembangan teknologi tersebut tidak hanya beragam citra dan sensor yang muncul, namun juga resolusi spasial pada citra tersebut. Dengan semakin meningkatnya resolusi spasial pada citra, maka analisis tekstur semakin memiliki peranan penting dalam menganalisis dan mengilah citra, klasifikasi citra, dan interpretasi citra penginderaan jauh (He dan Wang, 1990 dalam (Chulafak et al., 2018)). Setiap citra digital yang dihasilkan oleh setiap sensor pada citra memiliki sifat khas pada setiap datanya. Sifat khas tersebut dihasilkan dari sifat orbit satelit, sifat dan kepekaan sensor penginderaan jauh terhadap panjang gelombang elektromagnetik, jalur transmisi yang yang digunakan, sifat sasaran objek, dan sifat sumber tenaga radiasinya (Firmansyah et al., 2021).

Penginderaan jauh makin banyak dimanfaatkan karena memiliki banyak manfaat diantaranya dengan menggunakan penginderaan jauh obyek di prmukaan bumi dapat tergambarkan sesuai dengan wujud dan letak obyek sama dengan keadaan aktualnya, selain itu gambar yang terdapat pada citra penginderaan jauh juga dapat memberi efek tiga dimenasi jika dilihat menggunakan stereoskop (Nurmalasari & Santosa, 2016).

Berdasarkan hal tersebut maka citra yang dihasilkan oleh penginderaan jauh ini dapat diaplikasikan untuk berbagai kebutuhan sesuai dengan fungsi dan spesifikasinya sehingga dapat digunakan untuk membantu pekerjaan manusia, seperti penggunaan teknologi penginderaan jauh saat ini yang sudah banyak digunakan untuk menganalisis vegetasi. Hal ini dikarenakan, kemampuan citra saat ini yang memiliki banyak keuntungan seperti memiliki resolusi temporal yang baik dan dapat digunakan untuk cakupan wilayah yang luas dalam waktu yang singkat. Terdapat banyak citra yang dapat digunakan untuk membantu analisis vegetasi, namun hal tersebut disesuaikan dengan kebutuhan.

Terdapat banyak citra yang dapat digunakan untuk menganalisis vegetasi, diantaranya citra yang dapat digunakan untuk menganalisis vegetasi adalah citra sentinel. Citra Sentinel-2 merupakan salah satu citra satelit yang memiliki 13 band, 4 band beresolusi 10 m, 6 band beresolusi 20 m, dan 3 band beresolusi spasial 60 m dengan area sapuan 290 km. Sentinel-2 dapat digunakan untuk kepentingan monitoring lahan, data dasar untuk penggunaan lahan yang dapat digunakan untuk berbagai aplikasi monitoring dan perencanaan lingkungan (Kawamuna, dkk., 2017 dalam (Awaliyan & Sulistyoadi, 2018)).

Penelitian ini dilakukan dengan menggunakan metode NDVI (Normalized Difference Vegetation Index). NDVI merupakan perhitungan band pada citra yang digunakan untuk mengetahui tingkat kehijauan, kemudian dilakukan analisis untuk mengetahui sebaran kerapatan vegetasi. Nilai NDVI ini merupakan nilai yang digunakan untuk mengetahui tingkat kehijauan pada daun dengan panjang gelombang inframerah (Awaliyan & Sulistyoadi, 2018).

Vegetasi memiliki berbagai tipe yang dapat terlihat dalam hasil perekaman citra yang merepresentasikan perbedaan dari jenis vegetasi. Perbedaan ini akan menghasilkan biomassa yang berbeda. Hal ini dikarenakan perbedaan kepadatan volume antar jenis begetaasi yang berbeda (Hendry et al., 2015).

Dalam ekologi istilah vegetesi untuk keseluruhan komunitas tetumbuhan. Vegetasi merupakan bagian hidup yang tersusun dari tetumbuhan yang menempati suatu ekosistem. Beraneka tipe hutan, kebun, padang rumput, dan tundra merupakan contoh-contoh vegetasi. Analisis vegetasi adalah cara mempelajari susunan (komposisi jenis) dan bentuk (struktur) vegetasi atau masyarakat tumbuh-tumbuhan Dalam ekologi hutan satuan yang diselidiki adalah suatu tegakan, yang merupakan asosiasi konkrit (Rohman dan Sumberartha, 2001 dalam (Andini et al., 2018)).

Berdasarkan kamus besar bahasa Indonesia, vegetasi didefinisikan sebagai suatu bentuk kehidupan yang berhubungan dengan tumbuh-tumbuhan atau tanam-tanaman. Istilah vegetasi dalam ekologi adalah istilah yang digunakan untuk menyebut komunitas tumbuh-tumbuhan yang hidup di dalam suatu ekosistem. Vegetasi yang ada di suatu tempat dapat berubah seiring dengan berjalannya waktu dan perubahan iklim dan aktivitas manusia.

Sifat optik klorofil yaitu menyerap spektrum merah dan memantulkan dengan kuat spektrum inframerah. Metode NDVI dapat menunjukkan parameter yang berhubungan dengan parameter vegetasi, antara lain biomassa dedaunan hijau, dan daerah dedaunan hijau yang nilainya dapat diperkirakan untuk analsisi vegetasi. NDVI pada dasarnya menghitung seberapa besar penyerapan radiasi matahari oleh tanaman terutama bagian daun (Freddy dkk., 2015 dalam (Awaliyan & Sulistyoadi, 2018)).

Penentuan kerapatan vegetasi dengan menggunakan metode NDVI menggunakan nilai indeks dengan nilai antara (-1) hingga (+1), dengan ketentuan nilai sama dengan atau lebih kecil dari 0 menunjukan awan, badan air, atau selain vegetasi (Hendry et al., 2015).

Indeks vegetasi NDVI didasarkan pada pengamatan bahwa permukaan yang berbeda-beda merefleksikan berbagai jenis gelombang cahaya yang berbeda-beda. Vegetasi yang aktif melakukan fotosintesis akan menyerap sebagian besar gelombang merah sinar matahari dan mencerminkan gelombang inframerah dekat lebih tinggi. Vegetasi yang sudah mati atau kurang sehat lebih banyak mencerminkan gelombang merah dan lebih sedikit pada gelombang inframerah dekat (Wulandari, 2020).

Penelitian kali ini dilakukan pada wilayan kawasan Gunung Manglayang. Gunung ini masih memiliki tuuhan yang cukup banyak (Tri et al., 2014). Analisis dilakukan untuk mengetahui struktur dan komposisi hutan. Hasil dari penelitian ini dapat memberi gambaran mengenai kondisi vegetasi dan menggambarkan kondisi hutan pada kawasan Gunung Manglayang.

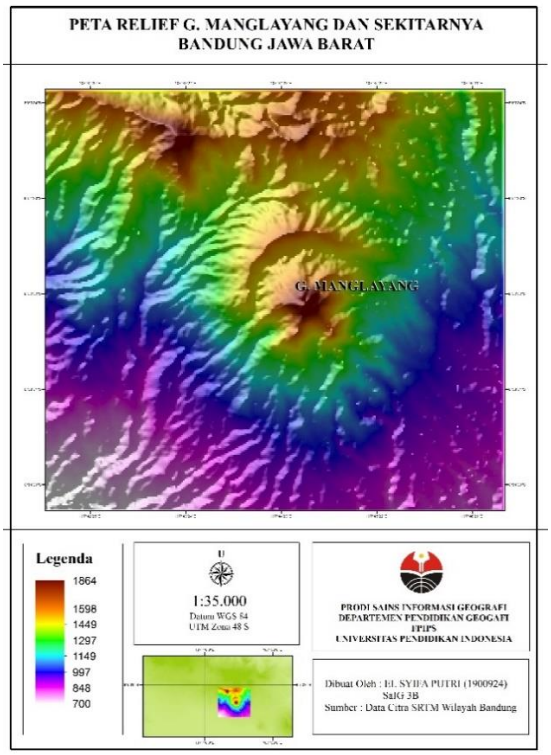
Adapun tujuan dari adanya penelitian ini untuk: (1) mengkaji spesifikasi citra sentinel, (2) menganalisis hasil akurasi citra sentinel dalam pemanfaatan analisis vegetasi, (3) menganalisis kesesuaian metode NDVI yang dapat diaplikasikan oleh citra sentinel untuk menganalisis vegetasi.

Kemudian manfaat yang dihasilkan dari penelitian ini adalah : (1) mengetahui spesifikasi citra sentinel, (2) mengetahui tingkat akurasi citra sentinel untuk pemanfaatan analisis vegetasi, (3) mengetahui keefektifan metode NDVI yang dapat digunakan oleh citra sentinel dalam analisis vegetasi.

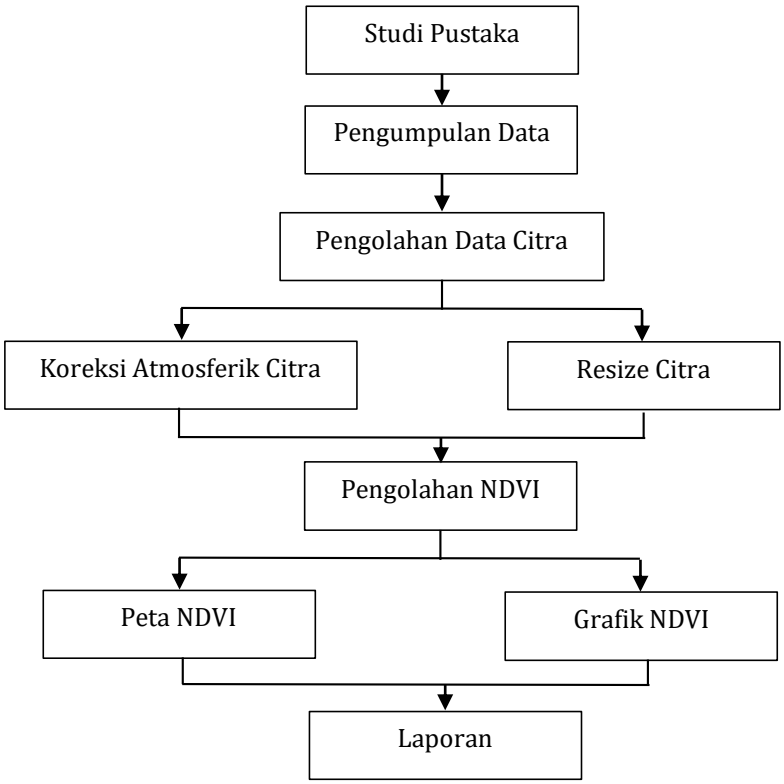
2. Metode

Penelitian ini berada di Gunung Manglayang yang terletak di sela Kabupaten Sumedang dan Bandung, Jawa Barat, Indonesia. Titik koordinat berada di 6°52'27"S dan 107°44'38"E. Gunung manglayang berbatasan dengan rangkaian gunung – gunung yaitu Burangrang, Tangkuban Perahu, dan Bukit Tunggul. Ketinggian dari gunung manglayang sekitar 1600 mdpl dan menjadi gunung yang terendah dari rangkaian gunung tersebut.

(Muttaqien, 2005 dalam (Tri et al., 2014)) mengatakan bahwa secara umum Gunung Manglayang memiliki tiga tipe vegetasi, yaitu hutan pinus, lahan terbuka dan hutan alam. Hutan pinus umumnya terdapat pada ketinggian berkisar antara 1.000─1.375 meter di atas permukaan laut (dpl) dan lahan terbuka umumnya hasil perubahan bentuk dari habitat hutan pinus ataupun dari habitat hutan alam. Hutan alam umumnya terdapat pada ketinggian >1.250 meter di atas permukaan laut (dpl) serta dominan pada ketinggian >1.375 m dpl, dan vegetasi hutan alam di Gunung Manglayang merata pada ketinggian >1.500 meter di atas permukaan laut (dpl). Vegetasi hutan alam juga terdapat pada daerah yang terjal dengan kemiringan lereng lebih dari 40°. Berikut adalah tampilan relief dari Gunung Manglayang.



Gambar 1. Peta relief gunung manglayang



Gambar 2. Bagan alur penelitian

Pada penelitian kali ini, data yang digunakan adalah data citra satelit sentinel-2. Data citra ini dipilih karena citra ini baik untuk melakukan analisis vegetasi karena memiliki resolusi yang tinggi. Data yang digunakan dalam penelitian ini menggunakan Citra Sentinal-2 tahun 2019. Adapun citra sentinel-2 memiliki 12 band seperti yang tertera pada tabel di bawah ini:

Tabel 1.
Spesifikasi citra Sentinel-2

Sentinel-2 Band	Cetra Wavelength	Resolution
Band 1 - Coastal aerosol	0,443	60
Band 2 - Blue	0,49	10
Band 3 - Green	0,56	10
Band 4 - Red	0,665	10
Band 5 - Vegetation Red Edge	0,705	20
Band 6 - Vegetation Red Edge	0,74	20
Band 7 - Vegetation Red Edge	0,783	20
Band 8 - NIR	0,842	10
Band 8A - Vegetation Red Edge	0,865	20
Band 9 - Water vapour	0,945	60
Band 10 -SWIR - Cirrus	1,375	60
Band 11 - SWIR	1,61	20
Band 12 - SWIR	2,19	20

Manfaat dari citra sentinel ini adalah untuk menyajikan data dalam rangka memenuhi kebutuhan beberapa hal, diantaranya monitoring lahan, dan dapat dijadikan sebagai data dasar yang dapat diaplikasikan dalam berbagai hal, seperti pertanian hingga perhutana, juga monitoring lingkungan, hingga perencanaan perkotaan. Selain itu dapat juga digunakna untuk deteksi tutupan lahan, penggunaan lahan, pemetaan bencana, dan aplikasi lainnya (Kawamuna et al., 2017). Untuk melakukan analisis vegetasi menggunakan metode NDVI, komposit band yang dibutuhkan ialah band 8 sebagai NIR dan band 4 sebagai RED pada citra sentinel-2.

Perangkat lunak yang digunakan yaitu ArcMap 10.8 dan Qgis. Tahapan pengolahan dan analisis citra mencakup tahapan sebagai berikut:

a. Koreksi atmosferik menggunakan software Qgis.
b. Cropping citra, dan hasil cropping citra terbaru yang kualitasnya terbaik karena digunakan untuk disegmentasi
c. Segmentasi digital citra untuk mencari kombinasi nilai parameter band yang digunakan untuk melakukan proses pengolahan NDVI
d. Analisis terhadap hasil segmentasi.
e. Hasil analisis kemudian dibagi menjadi 5 klasifikasi sesuai dengan parameter kelas pada NDVI.

Sebelum melakukan pemrosesan citra dengan menggunakan metode NDVI, terdapat beberapa langkah yang harus dilakukan pada citra untuk menghasilkan hasil yang optimal, yaitu koreksi atmosferik, resize citra, lalu pemrosesan citra.

Koreksi atmosferik ini dilakukan untuk memperjelas kenampakan obyek pada citra, sehingga citra dapat lebih baik dibaca saat melakukan pemrosesan NDVI oleh software. Pengolahan koreksi atmosferik ini dilakukan dengan menggunakan tools plugin yang berada pada software QGis, dimana nilai reflektansi yang tidak sesuai akibat adanya pengaruh penyerapan, hamburan, dan pantulan atmosfer dikoreksi dengan pengolahan data original dari citra Sentinel-2.

Proses resizing merupakan perubahan Pada proses resizing ini besar ukuran piksel citra akan dirubah dan dibuat menjadi sama antara satu citra dengan citra lainnya dengan menggunakan fungsi imresize. Besar ukuran piksel citra ditentukan dengan mencoba satu persatu besar ukuran yang sesuai agar citra terhindar dari *blurring*.

Interpretasi citra Sentinel-2 dengan menghitung indeks kerapatan vegetasi atau *Normalized Difference Vegetation Index* diperoleh dengan melakukan perhitungan gelombang *near infrared* dengan gelombang red yang dipantulkan oleh tumbuhan (Wahrudin et al., 2019). Metode NDVI ini mampu melakukan identifikasi terhadap tutupan tanaman melalui komputasi citra yang diolah (Purboyo et al., 2018). Pada citra Sentinel-2 citra yang digunakan untuk melakukan pengolahan NDVI adalah Band 4 dengan gelombang *Red*, dan Band 8 dengan gelombang *Near Infrared* (NIR).

NDVI = (NIR – Red) / (NIR+Red) (1)

Keterangan :

NIR = kanal radiasi inframerah dekat dari piksel,

Red = kanal radiasi cahaya merah dari piksel,

Nilai NDVI berkisar dari -1 (lahan tidak bervegetasi) sampai +1 (vegetasi lebat dan rapat). Terdapat 5 kelas pada NDVI, yaitu :

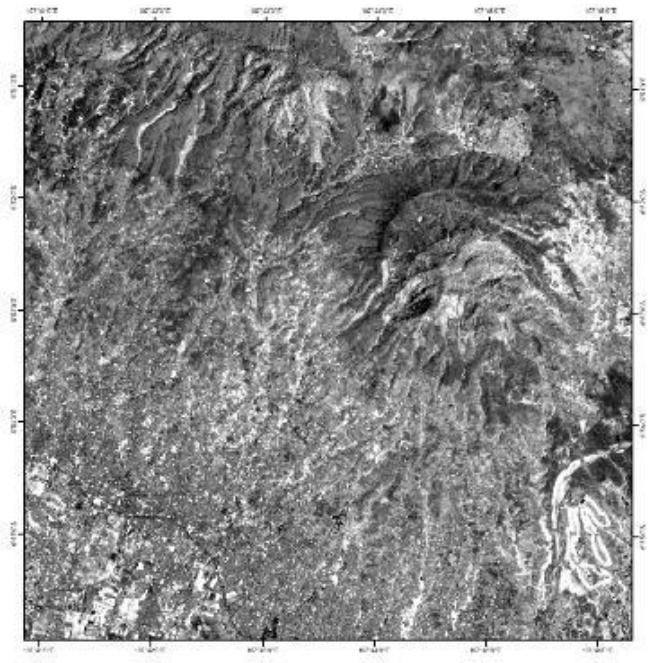
Tabel 2.
Nilai NDVI

Kelas	NDVI	Keterangan
1	-1 s/d -0,03	Lahan Tidak Bervegetasi
2	-0,04 s/d 0,15	Kehijauan Sangat Rendah
3	0,16 s/d 0,25	Kehijauan Rendah
4	0,26 s/d 0,35	Kehijauan Sedang
5	0,36 s/d 1,00	Kehijauan Tinggi

(Sumber : Peraturan Menteri Kehutanan RI nomor P.12/Menhut-II/2012 dalam (Fadlillah et al., 2018))

3. Hasil dan Pembahasan

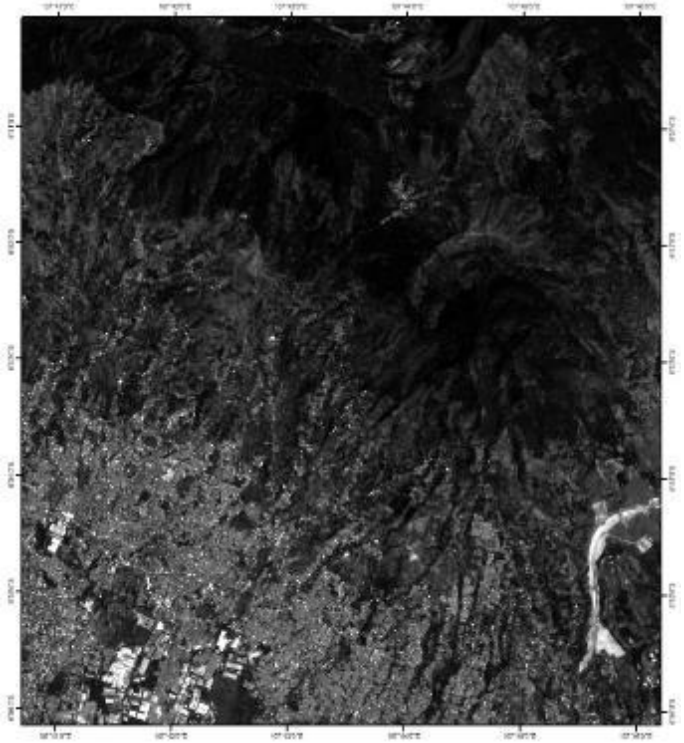
Koreksi atmosferik dilakukan dengan pertimbangan berbagai parameter atmosfer dalam proses koreksi. Parameter tersebut yaitu faktor musim, dan kondisi iklim di lokasi pada saat perekaman citra. Kelebikan dari koreksi atmosferik ini adalah kemampuannya untuk memperbaiki berbagi gangguan yang terdapat pada atmosfer seperti kabut tipis, asap, dan lain-lain (Lilik et al., 2016).



Gambar 3. Citra Sentinel-2 band 8 sebelum koreksi atmosferik



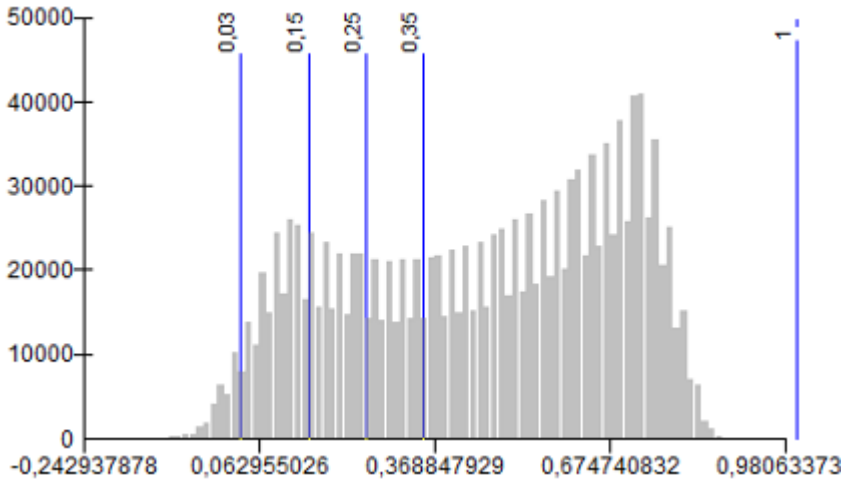
Gambar 4. Citra Sentinel-2 band 4 sebelum koreksi atmosferik



Gambar 5. Citra Sentinel-2 hasil koreksi atmosferik band 4 dan 8

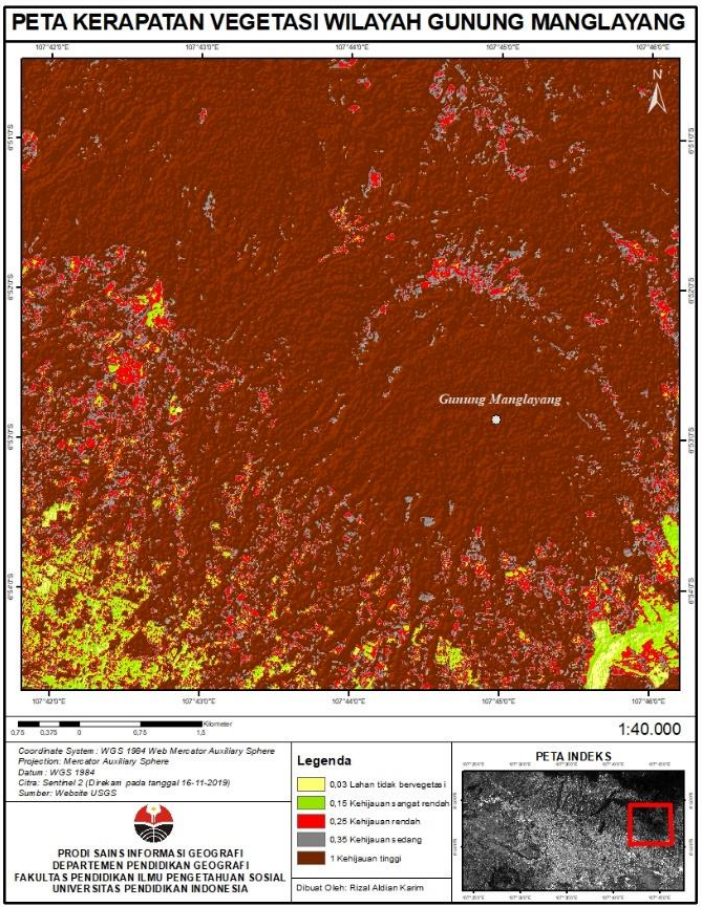
Hasil dari koreksi atmosferik citra Sentinel-2 pada gabungan band 4 dan 8 ini adalah berkurangnya gangguan yang disebabkan oleh berbagai parameter atmosferik. Koreksi ini menjadikan citra lebih jelas terlihat kenampakan objeknya.

Setelah melakukan pengolahan terhadap citra sentinel wilayah Gunung Manglayang dengan menggunakan metode NDVI, diperoleh hasilnya mulai dari tingkat rendah yaitu 0,03 sampai tinggi 1. Dalam rentang sebesar itu bisa dibilang wilayah gunung manglayang kondisi vegetasinya masih sehat dan mendominasi. Apabila dilihat dari citra secara segmentasi maka akan terlihat kerapatan vegetasi di gunung manglayang sangatlah tinggi. Adapun grafik intervalnya seperti di bawah ini:



Gambar 6. Grafik interval hasil NDVI

Dalam tahap analisis ndvi, penuis mengkategorikan menjadi lima kelas, yaitu kelas lahan tidak bervegetasi, kehijauan sangat rendah, kehijauan rendah, kehijauan sedang dan kehijauan tinggi. Hasil NDVI dapat dilihat pada **gambar 5**.



Gambar 5. Hasil pengolahan NDVI

Setelah berhasil menemukan nilai rentang NDVI nya, maka dilakukannya perhitungan luas tiap kelasnya masing-masing seperti yang tercantum dalam tabel berikut.

Tabel 3.
Kelas Klasifikasi Hasil NDVI

Nama Kelas	Luas (Ha)
Lahan tidak bervegetasi	290
Kehijauan sangat rendah	1.822
Kehijauan rendah	1.559
Kehijauan sedang	1.405
Kehijauan tinggi	9.345
Total	**14.421**



Gambar 5. Kenampakan citra Sentinel-2 *true color* Gunung Manglayang

Berdasarkan tabel tersebut dapat dilihat bahwa pada kelas lahan tidak bervegetasi memiliki luas 290 ha. Kelas ini menjadi kelas dengan luas terendah jika dibandingnkan dengan kelas yang lain. Kelas ini tersebar di daerah sekitaran gunung manglayang tepatnya di bawah atau selatannya. Kelas ini menunjukan bangunan pada citra. Pada daerah tersebut terdapat pemukiman warga.

Pada kelas kehijauan sangat rendah memiliki luasan yaitu 1.822 ha. Kelas ini tersebar pada daerah selatan gunung manglayang pada citra. Kelas ini meliputi permukiman dan lahan kosong.

Kelas Kehijauan rendah memiliki luas 1.559 ha. Persebarannya di sisi selatan dan sebagian barat dan timur sekitaran gununug manglayang. Kehijuan sedang memiliki luas wilayah 14.05 Kelas ini tersebar sekitarana sisi-sisi gunung manglayang.

Kelas kehijauan tinggi mempunyai luas 9.345 ha dan menjadi kelas yang paling besar luas areanya dibandingkan dengan luas wilayah.kelas ini tersebar secara merata pada peta NDVI dan didapati kawsan gunung manglayang diselimuti oleh kelas ini yang artinya kondisi vegetasi disana masih tergolong sehat dan baik.

Sebelumnya terdapat penelitian mengenai vegetasi di gunung manglayang. Yakni penelitian yang dilakukan yaitu meneliti mengenai indeks keberagaman vegetasi di wilayah gunung manglayang. Hasil penelitianya yaitu ditemukannya 11 jenis pohon yang masuk ke 7 suku dengan jumlah sebanyak 75 individu. Selain itu juga terdapat penelitian yang meneliti mengenai keanekaragaman tumbuhan di wilayah Gunung Manglayang. Dari hasil penelitiannya yaitu terdapat indeks keberagaman sebesar 1,64 untuk anak pohon. Hal tersebut bisa dikategorikan bahwa keanekaragaman di gunung manglayang masuk ke dalam spesies sedang. Sedangkan untuk tempat yang ditelitinya mendapatkan indeks sebesar 0,48. Hal tersebut memberitahukan bahwa nilai keseragaman jenis pada hutan alam gunung manglayang tergolong ke dalam kategori rendah.

Lalu terdapat penelitian serupa yang mendapatkan nilai indeks keanekaragaman sebesar 2,00 untuk pohon yang masuk ke kategori spesies sedang. kemudian indeks keseragaman pohon di tempat penelitian bernilai 0,53 yang termasuk kategori tinggi oleh (Tri et al., 2014). Namun kebanyakan penelitian terdahulu belum ada yang fokus mengkaji mengenai indeks kerapatan vegetasi di wilayah Gunung Manglayang. Hal tersebut mengindikasikan pada penelitian ini untuk mengkaji mengenai kerapatan vegetasinya.

4. Simpulan dan Saran

Beradasarkan hasil penelitian dapat dilihat bahwa teknologi penginderaan jauh dapat digunakan untuk membantu pekerjaan manusia, diantaranya untuk menganalisis. Analisis ini dapat dilakukan oleh berbagai citra diantaranya oleh citra Sentinel-2. Berdasarkan hasil yang telah dibuat, citra ini menghasilkan hasil analisis vegetasi dengan cukup baik. Untuk hasil nilai vegetasi yang didapat setelah melakukan pemrosesan yaitu sebesar 0,03 hingga 1. Nilai ini menunjukan bahwa vegetasi yang berada kawasan Gunung Manglayang memiliki kerapatan yang tinggi karena memiliki nilai 1 dan juga kawasan ini memiliki vegetasi dengan kerapatan yang kurang karena hasil dari peta memiliki nilai 0,03.

Diharakan untuk masyarakat khususnya yang tinggal di wilayah kawasan Gunung manglayang untuk menjaga lingkungan semaksimal mungkin, an melakukan pembangunan tanpa merusak lingkungan karena lambat laun pemukiman akan semakin bertambah dan tidak menutup kemungkinan untuk merambah ke area gunung sehingga vegetasi akan semakin hilang dan akan menimbulkan banyak dampak bagi semua makhluk hidup.

Daftar Rujukan

Andiko, J. A., . D., & Darmawan, A. (2019). Efisiensi Penggunaan Citra Multisensor untuk Pemetaan Tutupan Lahan. *Jurnal Sylva Lestari*, *7*(3), 342. https://doi.org/10.23960/jsl37342-349

Andini, S. W., Prasetyo, Y., & Sukmono, A. (2018). Analisis Sebaran Vegetasi Dengan Citra Satelit Sentinel Menggunakan Metode Ndvi Dan Segmentasi. *Jurnal Geodesi Undip*, *7*(1), 14–24.

Awaliyan, R., & Sulistyoadi, Y. B. (2018). Klasifikasi Penutupan Lahan Pada Citra Satelit Sentinel-2a Dengan Metode Tree Algorithm. *ULIN: Jurnal Hutan Tropis*, *2*(2), 98–104. https://doi.org/10.32522/ujht.v2i2.1363

Chulafak, G. A., Kushardono, D., & Zylshal, N. (2018). Optimasi Parameter Dalam Klasifikasi Spasial Penutup Penggunaan Lahan Menggunakan Data Sentinel Sar (Parameters Optimization in Spatial Land Use Land Cover Classification Using Sentinel Sar Data). *Jurnal Penginderaan Jauh Dan Pengolahan Data Citra Digital*, *14*(2), 111–130. https://doi.org/10.30536/j.pjpdcd.1017.v14.a2746

Fadlillah, M. F., Hadiani, R., & Solichin. (2018). *Analisis Kekeringan Hidrologi Berdasarkan Metode Normalized Difference Vegetation Index (NDVI) Di Daerah Aliran Sungai Alang Kabupaten Wonogiri*. *September*, 34–44.

Firmansyah, A., Triana, E., Arifin, N., Nurfalah, I., & Ridwana, R. (2021). *Pemanfaatan Citra Satelit Landsat 8 Dan Sentinel 2A Dalam Identifikasi Lahan Kritis Mangrove Di Wilayah Kecamatan Ciemas Kabupaten Sukabumi*. *6*(1), 21–34.

Hendry, F., Hartono, & Retnadi, J. H. (2015). *Komparasi Indeks Vegetasi Untuk Estimasi Stok Karbon*

Hutan Mangrove Kawasan Segoro Anak Pada Kawasan Taman Nasional Alas Purwo Banyuwangi , Jawa Timur (Comparison of Vegetation Indices for Mangrove Carbon Stock Estimation. 113–123.

Kawamuna, A., Suprayogi, A., & Wijaya, A. P. (2017). *Jurnal Geodesi Undip Januari 2017 ANALISIS KESEHATAN HUTAN MANGROVE BERDASARKAN Jurnal Geodesi Undip Januari 2017*. *6*, 277–284.

Lilik, K., Arwan, P. W., & Abdi, S. (2016). Analisis Pengaruh Koreksi Atmosfer Terhadap Estimasi Kandungan Klorofil-A Menggunakan Citra Landsat 8. *Jurnal Geodesi Undip*, *5*(4), 254–262.

Nurmalasari, I., & Santosa, S. H. M. B. (2016). *Pemanfaatan Citra Sentinel-2A untuk Estimasi Produksi Pucuk Teh di Sebagian Kabupaten Karanganyar*. *4*(4), 1–11.

Purboyo, A. A., Ramadhan, A. H., Safitri, E., Ridwana, R., & Himayah, S. (2018). Jurnal sains informasi geografi [jsig]. *Jurnal Sains Informasi Geografi [JSIG]*, *I*(November), 40–43.

Tri, C., Destiana, C., & Tony, S. (2014). Analisis Vegetasi Pohon Hutan Alam Gunung Manglayang Kabupaten Bandung. *Tetrahedron Letters*, *55*(2), 3909.

Wahrudin, U., Atikah, S., Habibah, A. Al, Paramita, Q. P., Tampubolon, H., Sugandi, D., & Ridwana, R. (2019). Pemanfaatan Citra Landsat 8 Untuk Identifikasi Sebaran Kerapatan Vegetasi di Pangandaran. *Geodika: Jurnal Kajian Ilmu Dan Pendidikan Geografi*, *3*(2), 90. https://doi.org/10.29408/geodika.v3i2.1790

Wulandari, N. (2020). *Penggunaan Metode Ndvi (Normalized Difference Vegetation Index) Dan Savi (Soil Adjusted Vegetation Index) Untuk Mengetahui Ketersediaan Ruang Terbuka Hijau Terhadap Pemenuhan Kebutuhan Oksigen (Studi Kasus : Kota Yogyakarta)*. http://eprints.itn.ac.id/4597/

JPIG (Jurnal Pendidikan dan Ilmu Geografi)
Vol. 9, No. 2, September 2024
Halaman: 120-129
Online: http://ejournal.unikama.ac.id/index.php/JPIG/



Analisis Perubahan Penggunaan Lahan Menggunakan Citra Sentinel-2 Di Kecamatan Percut Sei Tuan Tahun 2018 - 2022

Immanuel Sinabang[1*], Klarita Dwijayanti Waruwu[2], Adesiana Sihombing[3], Adeline[4], Eni Yuniastuti[5]
[1,2,3,4,5]Jurusan Pendidikan Geografi, Fakultas Ilmu Sosial, Universitas Negeri Medan
Email: [*]imanuelsinabang@gmail.com, klarytadwijayanti@gmail.com, adesianasihombing2020@gmail.com, stplalin@gmail.com, enigeografi2023@gmail.com

Dikirim: 22 Juni 2024; Revisi:9 September 2024; Diterima: 17 September 2024

Abstrak: Pertumbuhan penduduk merupakan pendorong utama perubahan tutupan/penggunaan lahan secara umum karena mengarah pada pembangunan ekonomi, yang pada gilirannya membutuhkan ketersediaan lahan untuk penggunaan lahan lainnya, termasuk infrastruktur, jasa, industri, dan permukiman. Menggunakan simbolisme satelit penginderaan jauh untuk merencanakan penggunaan lahan di wilayah yang luas adalah salah satu pendekatan yang dapat dilakukan. Penelitian ini bertujuan untuk menganalisis perubahan penggunaan lahan di Kecamatan Percut Sei Tuan, Kabupaten Deli Serdang, Sumatera Utara pada periode 2018-2022 menggunakan citra satelit Sentinel-2. Metode yang digunakan adalah interpretasi visual citra satelit dengan bantuan perangkat lunak ArcGIS dan analisis perbandingan data spasial multi-temporal. Hasil penelitian menunjukkan terdapat 8 kelas penggunaan lahan yaitu badan air, hutan, sawah, perkebunan, lahan terbangun, tanah terbuka, awan, dan semak belukar. Perubahan penggunaan lahan yang signifikan terjadi pada lahan terbangun yang mengalami penambahan sebesar 627 hektar (dari 34% menjadi 37% total luas wilayah), sementara luas hutan berkurang 521 hektar (dari 8% menjadi 5%). Perubahan ini mengindikasikan adanya konversi lahan dari area hutan dan lahan produktif lainnya menjadi kawasan terbangun, yang didorong oleh pertumbuhan penduduk dan kebutuhan infrastruktur. Penelitian ini menyimpulkan bahwa monitoring perubahan penggunaan lahan secara berkala sangat diperlukan untuk mendukung perencanaan tata ruang dan pengelolaan sumber daya lahan yang berkelanjutan.
Kata kunci: Citra Satelit, Penggunaan Lahan, Perubahan Penggunaan Lahan

Abstract: Population growth is a major driver of land cover/use change in general as it leads to economic development, which in turn requires land availability for other land uses, including infrastructure, services, industry and settlements. Using the symbolism of remote sensing satellites to plan land use over large areas is one approach that can be taken. This study aims to analyze land use change in Percut Sei Tuan District, Deli Serdang Regency, North Sumatra in the 2018-2022 period using Sentinel-2 satellite imagery. The method used is visual interpretation of satellite images with the help of ArcGIS software and multi-temporal spatial data comparison analysis. The results showed that there were 8 land use classes, namely water bodies, forests, rice fields, plantations, developed land, open land, clouds, and shrubs. Significant land use change occurred in built-up land which increased by 627 hectares (from 34% to 37% of the total area), while forest area decreased by 521 hectares (from 8% to 5%). These changes indicate land conversion from forest areas and other productive lands to built-up areas, driven by population growth and infrastructure needs. This study concludes that regular monitoring of land use change is necessary to support spatial planning and sustainable land resource management.
Keywords: Satellite Imagery, Land Use, Land Use Change

This is an open access article under the CC–BY license.

https://doi.org/ 10.21067/jpig.v9i2.10348

Pendahuluan

Kecamatan Percut Sei Tuan merupakan salah satu wilayah di Kabupaten Deli Serdang, Sumatera Utara yang mengalami perkembangan pesat dalam beberapa tahun terakhir. Diduga penggunaan lahan di daerah ini telah berubah sebagai akibat dari pertumbuhan penduduk, pembangunan perumahan, kawasan industri, dan infrastruktur. Pemantauan perubahan penggunaan lahan secara berkala sangat diperlukan untuk mengevaluasi pola perubahan yang terjadi dan menentukan arahan kebijakan tata ruang wilayah yang tepat.

Lahan adalah suatu wilayah pada lapisan terluar bumi yang sifat-sifatnya (kualitas) menggabungkan setiap sifat yang sangat mantap atau yang dapat dianggap berulang dari biosfer, iklim, tanah, geografi, hidrologi, tumbuhan, dan populasi makhluk hidup serta efek samping dari latihan manusia sebelumnya. terlebih lagi, saat ini, selama pengidentifikasi ini secara mendasar memengaruhi penggunaan lahan di masa sekarang dan di kemudian hari.(Indah et al., 2019). Perubahan lahan dicirikan sebagai pergeseran penggunaan seluruh atau sebagian lahan dari penggunaan semula menjadi penggunaan yang berdampak negatif terhadap lingkungan dan potensi lahan (Miswar et al., 2020). Menurut Suban & Sunimbar (2021) menyatakan bahwa alih fungsi lahan mengakibatkan perubahan penggunaan lahan. Sementara itu menurut Kubangun (dalam Akbar et al., 2022) menyatakan bahwa pertumbuhan penduduk merupakan pendorong utama perubahan tutupan/penggunaan lahan secara umum karena mengarah pada pembangunan ekonomi, yang pada gilirannya membutuhkan ketersediaan lahan untuk penggunaan lahan lainnya, termasuk infrastruktur, jasa, industri, dan permukiman.

Mengetahui perubahan penggunaan berfungsi untuk mengidentifikasi potensi perubahan lingkungan yang berhubungan dengan tingkat perpindahan penduduk, alih fungsi hutan, dan perluasan lahan pertanian. Ketersediaan alat analisis serta data dan informasi sering menjadi kendala di lapangan. Menggunakan simbolisme satelit penginderaan jauh untuk merencanakan penggunaan lahan di wilayah yang luas adalah salah satu pendekatan yang dapat dilakukan (Fadlin et al., 2022). Akuisisi data mengenai suatu fenomena tanpa bersentuhan langsung dengannya merupakan pengertian dari penginderaan jauh. Proses ini mengandalkan deteksi dan kuantifikasi variasi yang terpancar dari target, yang dipengaruhi oleh keadaan optik di sekelilingnya, mencakup aspek-aspek seperti gelombang elektromagnetik, bunyi, serta medan gaya (Suni et al., 2023).

Satelit pencitraan optik Eropa, Sentinel-2 diluncurkan pada tanggal 23 Juni 2015, sebagai bagian dari program Copernicus dari Organisasi Antariksa Eropa. Sentinel-2 adalah salah satu satelit yang digunakan untuk membuat gambar satelit dari tutupan lahan di Bumi saat ini. Berdasarkan asal cahaya, pita-pita ini dikategorikan ke dalam daerah panjang gelombang. Pita merah, biru, hijau, dan inframerah dekat Sentinel-2 memiliki resolusi spasial masing-masing 10meter, 20 meter, dan 60 meter. Tujuan utama Sentinel-2 adalah mengumpulkan data persepsi sebanyak mungkin selama sepuluh hari dengan satu satelit dan lima hari lagi dengan dua satelit (Miranda & Aryuni, 2021). Pemanfaatan simbolisme satelit dalam penemuan tutupan lahan telah banyak digunakan mengingat fakta bahwa memiliki tujuan dan inklusi duniawi yang besar wilayah yang luas. Sentinel-2 dapat digunakan untuk memeriksa tanah dan menyediakan data penggunaan lahan dasar yang berfungsi sebagai skenario pemeriksaan dan kondisi iklim (Awaliyan & Sulistyoadi, 2018).

Hasil penelitian yang dilakukan oleh Ridwan (2023) menunjukkan Hasil penelitian Ridwan (2023) menunjukkan bahwa luas lahan kawasan terbangun (built area) meningkat sebesar 43% dari tahun 2017 hingga 2021, dengan total luas perubahan tutupan lahan

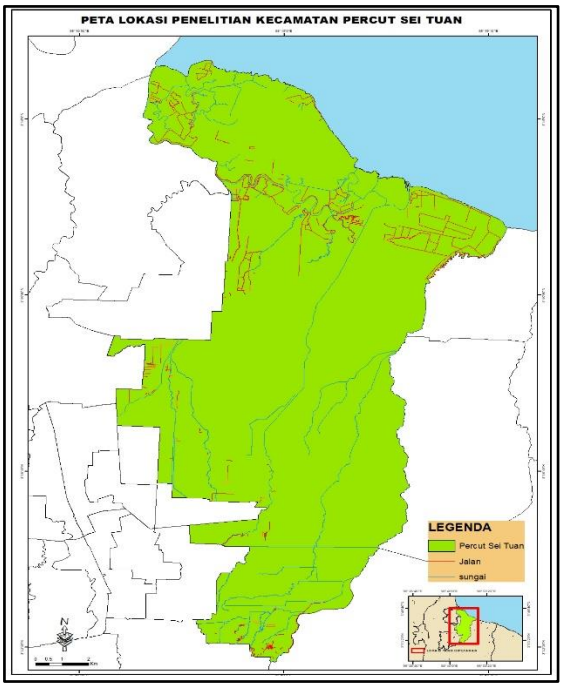
233,6105564 ha. Fungsi rangeland mengkonversi paling banyak lahan sebesar 56%, dan fungsi tutupan lahan mengkonversi paling banyak lahan sebesar 50,52001167 ha.

Hasil penelitian yang dilakukan oleh Fardilla et al (2023) berdasarkan temuan tersebut, terjadi perubahan tutupan lahan di Kota Padang dari tahun 2018 hingga 2022. Secara khusus, terjadi penurunan tutupan hutan seluas 342 ha dan peningkatan tutupan lahan permukiman (717 ha), ruang terbuka (568 ha), dan lahan pertanian (151 ha). Di Kota Padang, sejumlah faktor, termasuk pertambahan penduduk, perubahan tutupan lahan antropogenik, bencana alam, dan suksesi, dapat memberikan dampak.

Berdasarkan uraian tersebut penelitian ini bertujuan untuk mengetahui luasan, menganalisis perubahan penggunaan lahan dan perbandingan perubahan lahan yang terjadi di Kecamatan Percut Sei Tuan dengan intepretasi citra satelit Sentinel 2 pada tahun 2018 dan 2022.

Metode Penelitian

Penelitian ini dilakukan di Kecamatan Percut Sei Tuan, Kabupaten Deli Serdang, Provinsi Sumatera Utara. Kecamatan Percut Sei Tuan dipilih karena merupakan salah satu wilayah yang mengalami pertumbuhan dan perkembangan yang pesat dalam beberapa tahun terakhir.



Gambar 1. Lokasi Penelitian (Sumber: Hasil Olah Data, 2022)

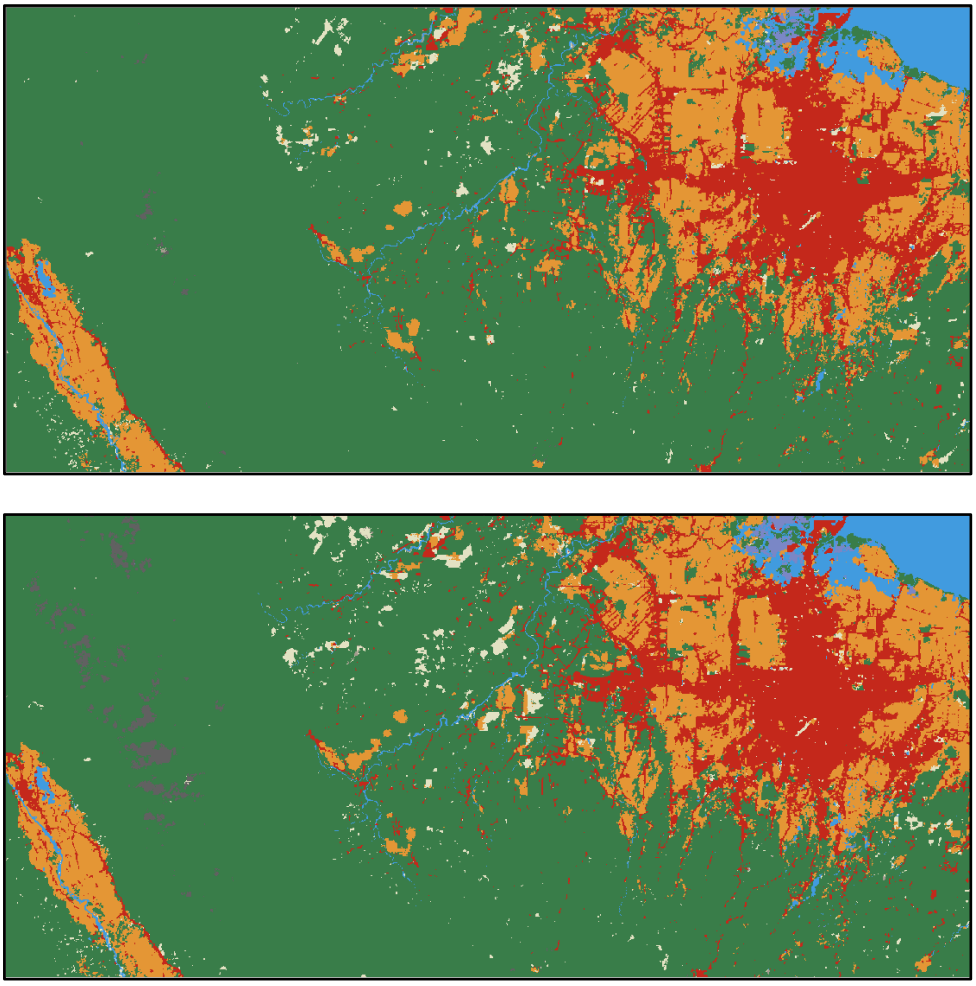
Pengumpulan data penelitian ini menggunakan studi literatur. Peneliti mengumpulkan data dari website ESRI untuk mendapatkan hasil citra Sentinel-2 perekaman tahun 2018 dan 2022 yang mencakup wilayah Kecamatan Percut Sei Tuan. Data lainnya seperti peta administrasi diperoleh dari website Badan Indonesia Geospasial (BIG)., serta artikel yang berkaitan dengan topik penelitian. Data dianalisis secara kuantitatif dan kualitatif. Analisis deskriptif kualitatif menjelaskan jenis-jenis perubahan dan penggunaan lahan. Sementara analisis kuantitatif digunakan untuk menghitung luasan dan besaran perubahan penggunaan

lahan yang terjadi antara tahun 2018 dan 2022. Hasil akhir berupa peta perubahan penggunaan lahan di Kecamatan Percut Sei Tuan tahun 2018-2022.

Hasil Penelitian

Pengolahan Citra

Data visualisasi penggunaan lahan dengan berbagai rona warna dihasilkan dari pengolahan data citra satelit Sentinel 2 dengan ArcGIS. Variasi rona warna menunjukkan variasi tutupan lahan dan juga variasi pantulan spektral di permukaan. Perangkat lunak ArcGIS dan foto satelit resolusi tinggi kemudian digunakan untuk mengkaji perbedaan rona warna tersebut untuk menentukan klasifikasi penggunaan lahan di lokasi penelitian Kecamatan Percut Sei Tun. Gambar 2 menunjukkan hasil pengolahan citra satelit Sentinel 2 dengan ArcGIS.

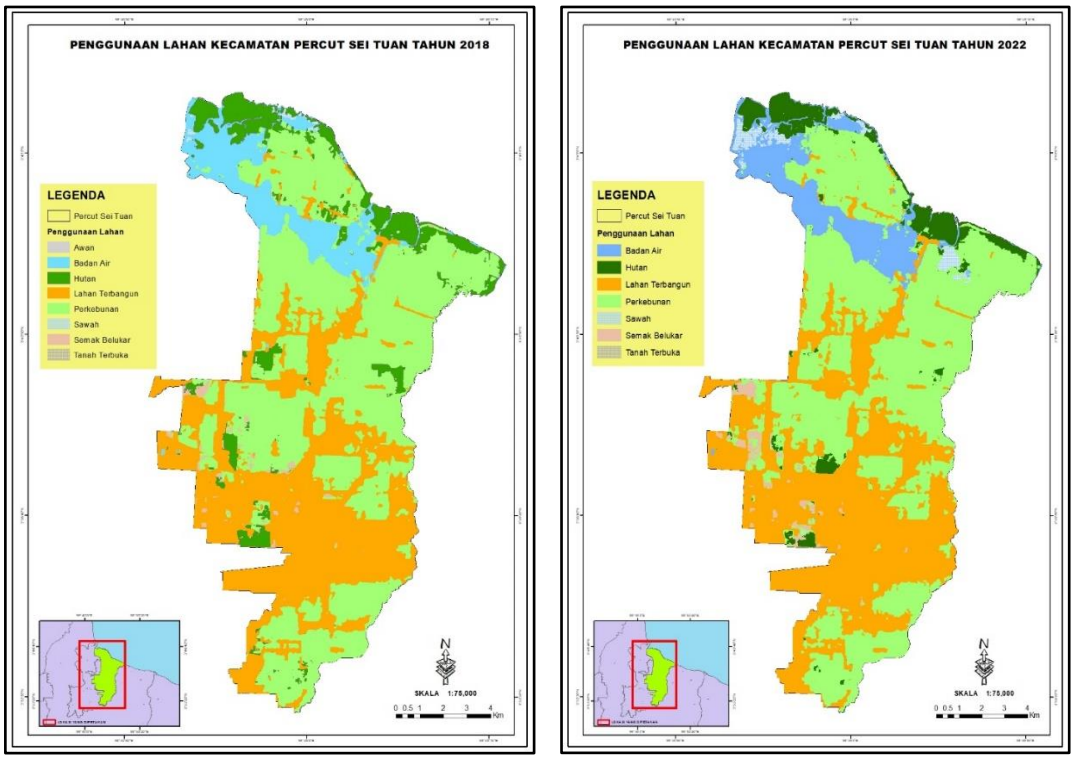


Gambar 2. Citra Satelit Sentinel 2 Tahun 2018 dan 2022
(Sumber: Hasil Olah Data, 2022)

Klasifikasi Penggunaan Lahan

Delapan kelas dihasilkan dari analisis perangkat lunak ArcGIS terhadap data citra Sentinel 2, yaitu: awan, badan air, hutan, lahan terbangun, perkebunan, sawah, semak belukar,

dan lahan terbuka. Kualitas kenampakan visual dalam proses interpretasi dijelaskan sebagai berikut.

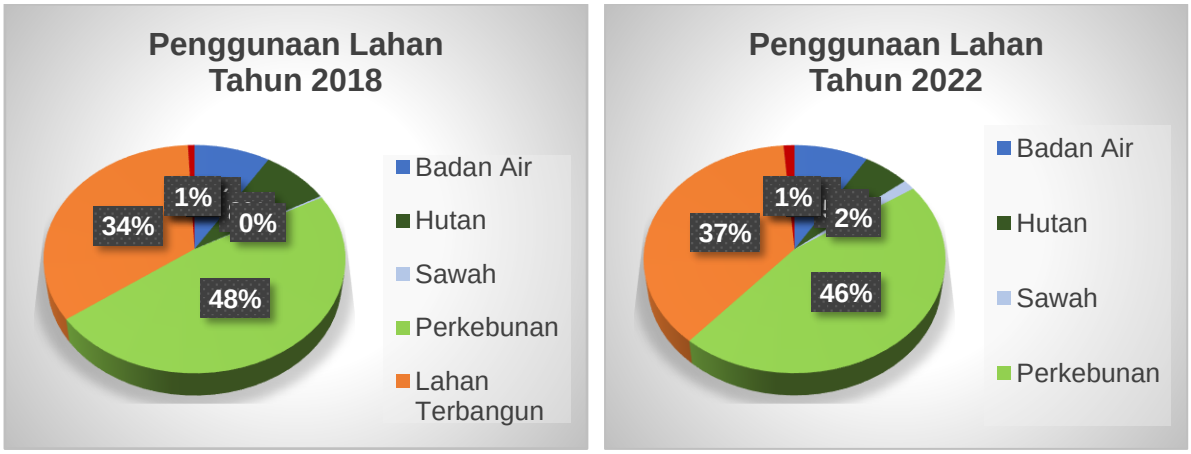


Gambar 3. Peta Penggunaan Lahan Kecamatan Percut Sei Tuan Tahun 2018 dan 2022 (Sumber: Hasil Olah Data, 2022)

1) Peta menunjukkan warna biru tua dan coklat muda pada badan air. Untuk badan air, warnanya berwarna coklat karena perekaman citra yang terjadi selama musim hujan, yang menyebabkan sedimentasi yang lebih tinggi di permukaan. Dalam penelitian ini, badan air yang dimaksud adalah sungai, irigasi, danau, rawa, embung, dan tambak ikan.
2) Hutan pada peta berwarna hijau gelap memiliki tekstur yang kasar karena menunjukkan variasi pepohonan yang tinggi atau kepadatan yang jarang.
3) Dalam peta, lahan yang terbangun tampak memiliki pola teratur, tekstur kasar, warna cerah, dan bentuk persegi atau limas. Dalam penelitian ini, lahan terbangun yang dimaksud adalah permukiman seperti perumahan atau tempat tinggal, pabrik, sekolah, dan bangunan lainnya.
4) Perkebunan memiliki kenampakan berwarna hijau muda dengan tekstur yang halus. Perkebunan yang dimaksud berupa jagung, kelapa sawit, dan padi.
5) Sawah, Sawah dalam gambar memiliki tekstur yang cerah, halus, bentuk yang tidak rata, dan warna biru muda. Ini adalah sawah dengan pematang dan padi yang tumbuh di atasnya.
6) Semak Belukar, kenampakan semak belukar berwarna violet dengan tekstur kasar dan bentuk petak-petak. Semak belukar yang dimaksud adalah rerumputan, sabana, dan semak.
7) Tanah Terbuka, kenampakan tanah terbuka berwarna abu tua dengan tekstur halus. Tanah terbuka yang dimaksud seperti lahan kosong.
8) Awan pada citra berwarna abu muda dengan tekstur yang kasar. Tanah Terbuka, kenampakan tanah terbuka berwarna abu tua dengan tekstur halus. Tanah terbuka yang dimaksud seperti lahan kosong.

Analisis Perubahan Penggunaan Lahan

Analisis perubahan penggunaan lahan dilakukan dengan membandingkan peta penggunaan lahan dari tahun 2018 dengan peta penggunaan lahan dari tahun 2022. Melalui perbandingan ini, diperoleh gambaran umum mengenai perubahan luas lahan dan penyebabnya. Perbandingan luas penggunaan lahan antara tahun 2018 dan 2022 ditampilkan dalam bentuk diagram pada Diagram 1. Diagram ini menggambarkan perubahan penggunaan lahan dari satu kelas ke kelas lainnya dan memberikan informasi mengenai persentase luasan dari tahun 2018 ke tahun 2022.



Gambar 4. Diagram Penggunaan Lahan Kecamatan Percut Sei Tuan Tahun 2018 dan 2022 (Sumber: Hasil Olah Data, 2022)

Tabel 1. Penggunaan Lahan Kecamatan Percut Sei Tun 2018-2022

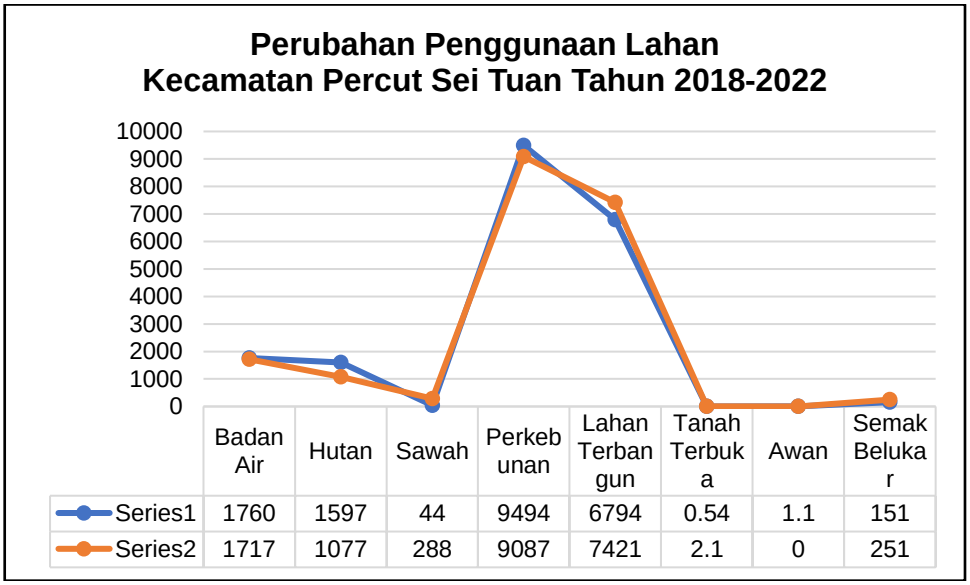
Penggunaan Lahan	Luas (Ha)	
	2018	2022
Badan Air	1760	1717
Hutan	1597	1077
Sawah	44	288
Perkebunan	9494	9087
Lahan Terbangun	6794	7421
Tanah Terbuka	0.54	2.1
Awan	1.1	0
Semak Belukar	151	251
Jumlah	19842	19843

(Sumber: Hasil Olah Data, 2018)

Pada tabel 1 disajikan luas penggunaan Lahan di Kecamatan Percut Sei Tuan pada tahun 2018 yaitu 19842 Hektar sedangkan pada tahun 2022 yaitu 19843 Hektar. Pada tahun 2018 Badan air memiliki luas 1760 ha atau 9% dari luas wilayah Kecamatan Percut Sei Tuan. Hutan memiliki luas 1597 ha atau 8% dari wilayah luas kecamatan Percut Sei Tuan. Sawah memiliki luas 44 ha atau 0% dari wilayah luas kecamatan Percut Sei Tuan. Perkebunan memiliki luas 9494 ha atau 48% dari wilayah luas kecamatan Percut Sei Tuan. Lahan terbangun memiliki luas 6794 ha atau 34% dari wilayah luas kecamatan Percut Sei Tuan. Tanah terbuka memiliki luas 0,54 ha atau 0% dari wilayah luas kecamatan Percut Sei Tuan. Awan memiliki luas 1,1 ha atau

0% dari wilayah luas Kecamatan Percut Sei Tuan. Semak belukar memiliki luas 151 ha atau 1% dari wilayah luas kecamatan Percut Sei Tuan.

Pada tahun 2022 Badan air memiliki luas 1717 ha atau 9% dari luas wilayah Kecamatan Percut Sei Tuan. Hutan memiliki luas 1077 ha atau 5% dari wilayah luas kecamatan Percut Sei Tuan. Sawah memiliki luas 288 ha atau 2% dari wilayah luas kecamatan Percut Sei Tuan. Perkebunan memiliki luas 9087 ha atau 46% dari wilayah luas kecamatan Percut Sei Tuan. Lahan terbangun memiliki luas 7421 ha atau 37% dari wilayah luas kecamatan Percut Sei Tuan. Tanah terbuka memiliki lus 2,1 ha atau 0% dari wilayah luas kecamatan Percut Sei Tuan. Semak belukar memiliki luas 251 ha atau 1% dari wilayah luas kecamatan Percut Sei Tuan.



	Badan Air	Hutan	Sawah	Perkebunan	Lahan Terbangun	Tanah Terbuka	Awan	Semak Belukar
Series1	1760	1597	44	9494	6794	0.54	1.1	151
Series2	1717	1077	288	9087	7421	2.1	0	251

Grafik 1. Perubahan Penggunaan Lahan Kecamatan Percut Sei Tun 2018-2022 (Sumber: Hasil Olah Data, 2022)

Pada luas perubahan lahan di Kecamatan Percut Sei Tuan disajikan pada grafik 1. Pada tahun 2018 Badan air memiliki luas 1760 ha atau 9%. Pada tahun 2022 Badan air berkurang 43 ha menjadi 1717 ha atau sekitar 9%. Pada tahun 2018 Hutan memiliki luas 1597 ha atau 8%. Pada tahun 2022 hutan berkurang 521 ha menjadi 1077 ha atau sekitar 5%. Pada tahun 2018 sawah memiliki luas 44 ha atau 0%. Pada tahun 2022 sawah bertambah 243 ha menjadi 288 ha atau 2%. Pada tahun 2018 perkebunan memiliki luas 9494 ha atau 48%. Pada tahun 2022 perkebunan berkurang 407 ha menjadi 9087 ha atau 46%. Pada tahun 2018 lahan terbangun memiliki luas 6794 ha atau 34%. Pada tahun lahan terbangun bertambah 627 ha menjadi 7421 ha atau 37%. Pada tahun 2018 tanah terbuka memiliki luas 0,54 ha atau 0%. Pada tahun 2022 tanah terbuka bertambah 1,54 ha menjadi 2,1 ha atau 0%. Pada tahun 2018 semak belukar memiliki luas 151 ha atau 1%. Pada tahun 2022 semak belukar bertambah 100 ha menjadi 251 ha atau 1%. Pada tahun 2018 awan memiliki luas 1.1 ha atau 0% sedangkan tahun 2022 awan sudah tidak ada lagi atau berubah menjadi lahan lainnya.

Pembahasan

Penelitian ini memanfaatkan citra satelit Sentinel-2 untuk menganalisis perubahan penggunaan lahan di Kecamatan Percut Sei Tuan. Pengolahan citra dilakukan dengan bantuan perangkat lunak ArcGIS. Citra Sentinel-2 memiliki kemampuan resolusi spasial yang baik,

dengan pita merah, biru, hijau, dan inframerah dekat yang masing-masing memiliki resolusi 10meter, 20 meter, dan 60 meter. Kemampuan ini memungkinkan interpretasi visual yang akurat untuk mengidentifikasi perbedaan rona warna dan tekstur, yang selanjutnya digunakan untuk klasifikasi penggunaan lahan.

Melalui pengolahan dengan ArcGIS, peneliti mampu menghasilkan peta penggunaan lahan yang menampilkan variasi warna dan tekstur sesuai dengan jenis penutupan lahan di wilayah studi. Perbedaan rona warna pada citra, misalnya biru tua untuk badan air, hijau gelap untuk hutan, dan warna cerah untuk lahan terbangun, memberikan informasi yang cukup jelas untuk interpretasi visual oleh peneliti. Selain itu, fitur-fitur ArcGIS seperti digitasi on-screen, komposisi band, dan analisis spasial membantu dalam proses klasifikasi penggunaan lahan secara akurat.

Klasifikasi Penggunaan Lahan

Berdasarkan hasil interpretasi visual citra Sentinel-2 dengan bantuan ArcGIS, peneliti berhasil mengidentifikasi delapan kelas penggunaan lahan di Kecamatan Percut Sei Tuan, yaitu: badan air, hutan, sawah, perkebunan, lahan terbangun, tanah terbuka, awan, dan semak belukar. Setiap kelas penggunaan lahan memiliki karakteristik visual yang khas, yang memudahkan proses klasifikasi. Misalnya, badan air terlihat berwarna biru tua dan coklat muda, hutan berwarna hijau gelap dengan tekstur kasar, lahan terbangun memiliki pola yang teratur dengan warna cerah, serta perkebunan dan sawah masing-masing memiliki warna dan tekstur yang khas. Pengenalan terhadap karakteristik visual ini menjadi dasar yang solid bagi peneliti untuk melakukan klasifikasi penggunaan lahan secara akurat.

Selain itu, peneliti juga memanfaatkan sumber data penunjang lainnya, seperti citra resolusi tinggi dan informasi geospasial, untuk memvalidasi hasil klasifikasi dan memastikan keakuratan identifikasi jenis penggunaan lahan di lapangan. Proses ini sangat penting untuk memperoleh data penggunaan lahan yang valid dan dapat digunakan untuk analisis lebih lanjut.

Analisis Perubahan Penggunaan Lahan

Setelah mengidentifikasi kelas-kelas penggunaan lahan pada citra Sentinel-2 tahun 2018 dan 2022, peneliti melakukan analisis perbandingan untuk mengetahui perubahan yang terjadi selama periode tersebut. Analisis perubahan penggunaan lahan merupakan bagian penting dari penelitian ini, sebagai upaya untuk memahami dinamika pemanfaatan lahan di Kecamatan Percut Sei Tuan.

Hasil analisis menunjukkan beberapa temuan signifikan terkait perubahan penggunaan lahan, antara lain:

1. Peningkatan luas lahan terbangun sebesar 627 hektar, dari 34% menjadi 37% dari total luas wilayah. Hal ini mengindikasikan adanya konversi lahan dari area hutan dan lahan produktif lainnya menjadi kawasan permukiman, industri, dan infrastruktur.
2. Penurunan luas hutan sebesar 521 hektar, dari 8% menjadi 5% dari total luas wilayah. Konversi lahan dari hutan menjadi lahan terbangun dan peruntukan lainnya menunjukkan adanya tekanan terhadap sumber daya hutan di wilayah ini.
3. Peningkatan luas sawah sebesar 243 hektar, dari 0% menjadi 2% dari total luas wilayah, sementara luas perkebunan berkurang 407 hektar, dari 48% menjadi 46%. Perubahan ini mengindikasikan adanya konversi lahan dari perkebunan menjadi sawah atau lahan pertanian lainnya.
4. Peningkatan luas lahan terbuka dan semak belukar, meskipun dengan persentase yang relatif kecil, yang dapat disebabkan oleh berbagai faktor seperti alih fungsi lahan, pembukaan lahan, atau suksesi alami vegetasi.

Perubahan penggunaan lahan yang terjadi di Kecamatan Percut Sei Tuan dapat memberikan berbagai dampak, baik positif maupun negatif, terhadap aspek lingkungan, sosial, dan ekonomi. Monitoring perubahan penggunaan lahan secara berkala sangat diperlukan untuk mendukung perencanaan tata ruang dan pengelolaan sumber daya lahan yang berkelanjutan.

Kesimpulan

Di wilayah Kecamatan Percut Sei Tuan, penggunaan lahan berubah secara signifikan antara tahun 2018 dan 2022. Kelas lahan terbangun meningkat sebesar 627 ha, atau 37%, sementara penggunaan lahan hutan menurun sebesar 521 ha, atau 5%. Hal ini disebabkan oleh kebutuhan infrastruktur masyarakat yang terus meningkat dan pada akhirnya menekan lahan-lahan produktif menjadi tidak produktif lagi. Harapan penulis agar penelitian selanjutnya dapat fokus pada mengkaji dampak dari perubahan penggunaan lahan terhadap aspek lingkungan, sosial, dan ekonomi. Hal ini penting untuk memahami konsekuensi dari dinamika pemanfaatan lahan dan menyusun langkah-langkah mitigasi atau adaptasi yang tepat.

Ucapan Terimakasih

Penulis ucapkan terima kasih yang sebesar–besarnya atas segala bantuan yang telah diberikan oleh kedua orang tua, dosen pengampu serta teman tim yang telah membantu selama pelaksanaan proses penelitian ini. Akhirnya penulis berharap semoga hasil penelitian ini dapat memberikan manfaat bagi kita semua. Saran dan kritikan yang membangun juga penulis harapkan demi menyempurnakan hasil penelitian ini.

Referensi

Akbar, W., Soma, A. S., & Arsyad, U. (2022). *Analisis Perubahan Penutupan Lahan di Daerah Aliran Sungai Kelara Menggunakan Citra Sentinel 2*. *14*(2), 73–87. https://doi.org/10.24259/jhm.v14i2.24107

Awaliyan, R., & Sulistyoadi, Y. B. (2018). Klasifikasi Penutupan Lahan Pada Citra Satelit Sentinel-2a Dengan Metode Tree Algorithm. *ULIN: Jurnal Hutan Tropis*, *2*(2), 98–104. https://doi.org/10.32522/u-jht.v2i2.1363

Fadlin, F., Thaha, M. A., Maricar, F., & Hatta, M. P. (2022). Monitoring Perubahan Penggunaan Lahan Menggunakan Citra Satelit Sentinel 1 di DAS Wanggu Kota Kendari. *Jurnal Teknik Sumber Daya Air*, *1*(2), 77–88. https://doi.org/10.56860/jtsda.v1i2.5

Fardilla, A., Septiavi, R., T, R. J., Arba, R. M., Sefmaliza, R., Fanbudy, A. R., Afdhal, T., & Novarino, W. (2023). *MENGGUNAKAN CITRA SATELIT Analysis of Land Cover Changes in Padang City using Satellite Imagery*. *10*(2), 353–367. https://doi.org/10.21776/ub.jtsl.2023.010.2.19

Indah, P., Mokodompit, S., Kindangen, J. I., & Tarore, R. C. (2019). Perubahan Lahan Pertanian Basah Di Kota Kotamobagu. *Jurnal Perencanaan Wilayah Dan Kota*, *6*(3), 792–799.

Miranda, E., & Aryuni, M. (2021). Klasifikasi Tutupan Lahan Menggunakan Convolutional Neural Network pada Citra Satelit Sentinel-2. *Sistemasi*, *10*(2), 323. https://doi.org/10.32520/stmsi.v10i2.1226

Miswar, D., Sugiyanta, I. G., Yarmaidi, & Yasta, R. D. (2020). Analisis Geospasial Perubahan Penggunaan Lahan Sawah Berbasis LP2B Kecamatan Pagelaran Utara. *Media Komunikasi Geografi*, *21*(2), 130–143.

Ridwan, V. F. (2023). *Analisis Perubahan Kawasan Terbangun Kota Parepare dengan Citra Satelit Sentinel-2 (2017-*. *3*(2).

Suban, I., & Sunimbar, A. (2021). *Analisis Perubahan Penggunaan Lahan Kota Kupang Nusa Tenggara Timur Tahun 2010-2018 (Studi Kasus di Kecamatan Kelapa Lima , Oebobo , dan Kota Lama)*. *2*, 36–52.

Suni, M. A., Borman, A. K., & Fahrul, M. (2023). *PEMETAAN PENGGUNAAN LAHAN DI KOTA PALU MENGGUNAKAN CITRA SENTINEL 2-A*. *1*(4), 384–391.

CROP TYPE MAPPING USING MACHINE LEARNING-BASED APPROACH AND SENTINEL-2: STUDY IN LUMAJANG, EAST JAVA, INDONESIA
/
PEMETAAN JENIS TANAMAN MENGGUNAKAN PENDEKATAN MACHINE LEARNING DAN SENTINEL-2: STUDI DI LUMAJANG, JAWA TIMUR, INDONESIA

Irsyam MAHRUS [1)], Indarto INDARTO *[1)], Khristianto WHENY [1)], Kurnianto FAHMI [1)]
[1)] Research Group of Agroindustrial and Food Safety (Keris Dimas KPPI), Research Centre (LP2M), University of Jember / Indonesia;
Tel: +62 813-4444-5615; E-mail: indarto.ftp@unej.ac.id
DOI: https://doi.org/10.35633/inmateh-72-12

Keywords: *Crop-type mapping, Sentinel-2, Random Forest, Lumajang*

ABSTRACT
In general, sentinel-2 imagery can be used for crop mapping. Crop types mapping aims to develop future strategies for sustainable agricultural systems. This study used Sentinel-2 from June 25 to July 6, 2023, with 10% cloud cover. The research was conducted in Pasrujambe and Candipuro sub-districts (± 242.23 km^2). The image is processed using a random forest on the GEE platform. Accuracy was generated using a confusion matrix with an overall accuracy of 85.82% and a kappa of 71.19%. Five main types of land use/cover were produced, namely: paddy (17.31%), sugarcane (0.93%), vegetation (69.74%), sand (7.4%) and built-up land (4.59%).

ABSTRAK
Secara umum, citra sentinel-2 dapat digunakan untuk pemetaan tanaman. Pemetaan jenis tanaman bertujuan untuk mengembangkan strategi masa depan untuk sistem pertanian berkelanjutan. Penelitian ini menggunakan Sentinel-2 pada tanggal 25 Juni hingga 6 Juli 2023 dengan tutupan awan 10%. Penelitian dilakukan di Kecamatan Pasrujambe dan Candipuro (± 242,23 km2). Gambar diproses menggunakan random forest pada platform GEE. Akurasi dihasilkan menggunakan matriks konfusi dengan akurasi keseluruhan sebesar 85,82% dan kappa sebesar 71,19%. Lima jenis penggunaan/tutupan lahan utama yang dihasilkan, yaitu: padi (17,31%), tebu (0,93%), vegetasi (69,74%), pasir (7,4%) dan lahan terbangun (4,59%).

INTRODUCTION

Crop Type Mapping indicates the intensity of land use in an area to develop sustainable future policy strategies in agriculture, plantations, and the like, both economically and ecologically *(Blickensdörfer et al., 2022).* In the agricultural sector, up-to-date information can be obtained by mapping crop types for planning and recognizing food security threats and their sustainability *(Hegarty-Craver et al., 2020).* Crop identification concerning the field of plant phenology, including the growth stage, has been carried out using remote sensing data *(Erdanaev et al., 2022a).* Remote sensing is a technique that has been proven effective in producing specific information on land cover and plant species *(Sun et al., 2020)*, both for its application in narrow *(Salas et al., 2020)* and large areas *(Griffiths et al., 2019).*

The Sentinel 2 platform is a remote sensing data widely used to map crop types in an area because of its multispectral sensor capabilities with 10 m, 20 m, and 60 m resolution and has an ideal wavelength *(Prins & Van Niekerk, 2021).* Several studies related to the mapping of crop types have been carried out, such as using sentinel 2 for crop type identification in small-plot agriculture land, which has a high accuracy value *(Gumma et al., 2022).* Xie and Niculescu 2022 *(Xie & Niculescu, 2022)* evaluated the Sentinel 2 image to map winter crops in the growing season. Furthermore, depending on the high precipitation frequency in their study location, they use Sentinel-1 C-band SAR data to monitor crop phenology. Sentinel-2 time series data for land cover mapping can reduce misclassification in its application to precision farming activities. It can also identify land cover features with small coverage, such as small fields, roads, and rivers *(Liu et al., 2020; Tran et al., 2022).* Different classification approaches and methods followed by pixel-based and object-based classifications were performed and evaluated using the Google Earth Engine (GEE) platform. No research can be found on mapping crop types using sentinel 2 in the Pasrujambe and Candipuro District of Lumajang.

Crop-type maps can be generated using a machine-learning approach applied to satellite images. Many studies on crop-type mapping used various machine-learning algorithms and Sentinel-2 data *(Alami Machichi et al., 2023; Luo et al., 2023).*

Machine Learning (ML) is a machine developed based on artificial intelligence (AI) to collect data independently using designed algorithms to imitate how humans learn (source). Machine learning has more features, such as simple operation, swiftness of operations, and the ability to process different data types (source). The use of machine learning for remote sensing, including Random Forests (RF), Neural Networks (NN), Support Vector Machines (SVM), and other processing methods, have proliferated with a high degree of accuracy *(Feng et al., 2019).* In several studies of various algorithms of machine learning for crop type identification, the random forest was recognized as one of the most efficient and accurate algorithms *(Akbari et al., 2020; Kpienbaareh et al., 2021; Wei et al., 2023).*

The objectives of this study are (1) to generate crop-type maps using 10 m Sentinel 2 of Pasrujambe and Candipuro District, Lumajang, and (2) to evaluate the random forest algorithm used to generate crop-type maps in the study area. The accuracy of the classification result is assessed using a confusion matrix derived from field data collection. Crop types have been widely mapped in large areas, and plant varieties have been uniform. This research was conducted in a limited area with various field sizes and plant varieties.

MATERIALS AND METHODS

Study Area

Two study areas were selected for crop type mapping, including Candipuro and Pasrujambe District, located in Lumajang Regency (Figure 1) and covering an area of 242.23 km2. Pasrujambe district, specifically, is located approximately 23 km south of the center of Lumajang city, with an average altitude of 75-2500 meters above sea level, and has an average rainfall of 952 mm with rainy days for 220 days within a year. Most of the Pasrujambe area is the mountainous area of Mount Semeru, and nearly 50% of its land cover is dense vegetation. Meanwhile, Candipuro District is 322 meters above sea level with a 2018 mm/year of rainfall.

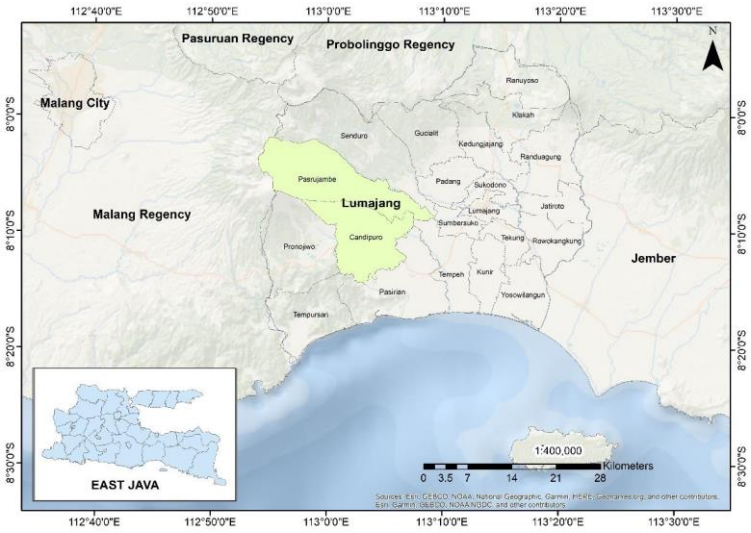


Fig. 1 - Study area in Candipuro and Pasrujambe District, Lumajang Regency

Input Data

Satellite Data

Spectral information from sentinel-2 imagery recorded in 2023 was used in this study. Sentinel-2 is a multispectral imaging mission based on a constellation of two high-resolution satellites launched in the sun-synchronous orbit *(Agency, 2015).* This study used time series data of Sentinel-2 from June 25 to July 6, 2023, with a minimum cloud cover of 10%. Due to the topography and climate conditions in the study area, the recorded images have a heavy cloud cover, and it is not easy to obtain satellite imagery with clear cloud cover.

Field Data Collection and Sampling

Field data on crop types were identified and collected from June to July 2023. The coordinates were recorded on each field using a GPS device at the center of the field boundaries. Crop types in each field were collected using a photo camera. One hundred sixty (160) ground truth samples from different crop types were collected, including paddy, built-up area, river, sugarcane, and dense vegetation (forest area, pine, teak plantations, and sengon trees). Field data collection is adjusted to the actual condition of vegetation cover in the field.



Fig. 2 - Example of field data in the study area captured using a digital camera and drone

Field data is used as a reference for making training areas. To improve the creation of training samples, Google Earth imagery was used to identify other types of land cover that are difficult to reach in the field data collection process. The training sample was divided into 70% training data and 30% validation data, as described by *(Adam et al., 2014)*. 70% of training data (31896 pixels) is used as input for classification, and 30% (13726 pixels) is used to validate the algorithm and assess the accuracy *(Shaharum et al., 2020).* The training data was used for training of the random forest classifier, while the validation data was used for accuracy assessment *(Adam et al., 2014)*. Optimization of the random forest parameters was done by repeated k-fold cross-validation using only the training sample *(Duro et al., 2012).*

Five (5) classes were identified and created using GEE, including built-up areas, sand, vegetation, paddy, and sugarcane. Samples were created using a polygon format. Table 1 illustrates the classes and number of each sample.

Table 1

Summary of the number of samples and the classes

Class	Number of samples (pixel)	Percentage (%)
Built-up Area	1229	3.27
Sand	11109	29.53
Vegetation	23062	61.31
Paddy	1184	3.15
Sugarcane	1032	2.74

Image Processing

The image processing was performed using the Google Earth Engine (GEE) platform. GEE provides a set of pixel-based classifiers to map crop types *(Shelestov et al., 2017).* GEE is used to collect a set of Sentinel-2 time series data, vegetation index transformation, and create a crop classification raster by performing a random forest classifier. A random forest classifier was used to produce crop-type maps and combine multiple vegetation indices to improve accuracy. The proposed workflow of the methodology of this study is shown in Figure 3.

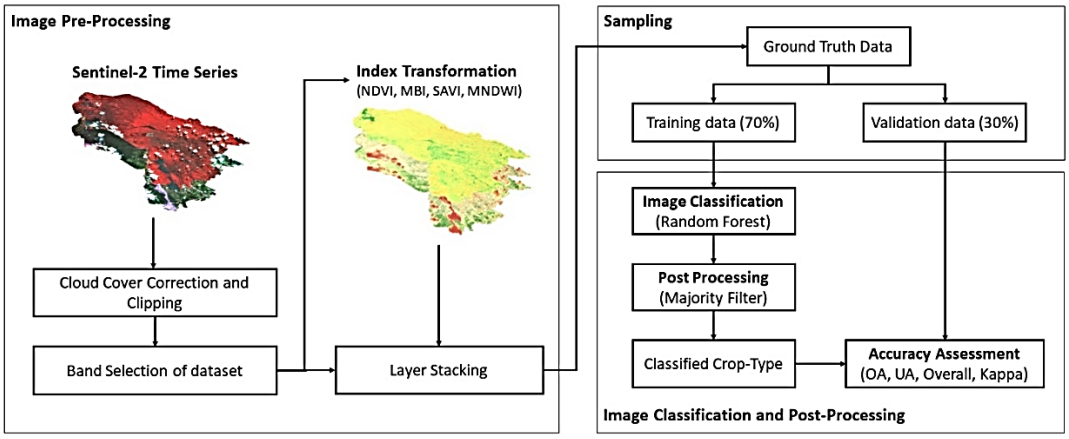


Fig. 3 - The workflow of this study was conducted in GEE to produce a crop-type map

a. Vegetation indices

Multiple vegetation indices were calculated as classification input data, including the Normalised Difference Vegetation Index (NDVI), Modified Bare Soil Index (MBI), Soil Adjusted Vegetation Index (SAVI), and Modified Normalised Difference Water Index (MNDWI). Each vegetation indices equation is shown in Table 2.

Table 2

Vegetation indices and the equation used in this study

Index	Formula	References
NDVI	(NIR – Red) / (NIR + Red)	*(Nouri et al., 2017)*
MBI	((SWIR1 – SWIR2 – NIR) / (SWIR1 + SWIR2 + NIR) + f))	*(Nguyen et al., 2021)*
SAVI	((NIR – Red) / (NIR + Red + L)(1 + L))	*(Huete et al., 1992)*
MNDWI	(Green – SWIR) / (Green + SWIR)	*(Xu, 2006)*

NDVI is an index widely used to produce crop-type classification maps *(Erdanaev et al., 2022b; HAO et al., 2020; Tariq et al., 2022)* by comparing the differences in the reflectance values of the red band (Red) and the near-infrared (NIR) band. NDVI values ranged from -1 to 1 *(Nouri et al., 2017)* and were calculated using the equation in Table 3.

MBI is used to distinguish between agricultural and non-agricultural fields. Specifically, it can identify bare soil and fallow land *(Nguyen et al., 2021).* The MBI value ranges from -0.5 to +1.5, where a higher MBI value indicates vacant land while a lower value indicates a body of water or vegetation. In MBI, an additional factor f is used with a value of 0.5 and is calculated using the equation in Table 3.

SAVI is a vegetation index aimed at minimizing the influence of soil on the calculation of vegetation values by using the L value as a soil adjustment factor. It has a value ranging from -1 to 1. The L value differs for each vegetation cover type, specifically 0 or 0.25 for dense vegetation, 1 for sparse vegetation, and 0.5 for moderate vegetation cover.

MNDWI is a modified form of NDWI *(McFeeters, 1996),* which computes using the SWIR band. This index is needed to delineate water bodies against other land covers.

b. Random Forest

Random Forest (RF) is a non-parametric supervised machine learning classification method. RF is a collection of decision trees combined to reduce variance and make data predictions more accurate. It can be used for classification and regression analysis *(Shaharum et al., 2020).* The random forest was selected because it is widely used and performs well for crop-type mapping.

RESULTS

Accuracy Assessment

The accuracy assessment was performed using the AcATaMa plugin provided by QGIS software. For sampling, response planning, and estimating in a framework for design-based inference, the AcATaMa plugin is a feature that offers thorough support *(Llano, 2019).* The crop type classification thematic map was evaluated using a confusion matrix (Table 3).

Table 3

Accuracy assessment of crop-type map

Class	Built-Up Area	Sand	Vegetation	Paddy	Sugarcane	Total	User Accuracy
Built-Up Area	36	3	0	6	1	46	78.26
Sand	1	48	9	18	1	77	62
Vegetation	3	3	665	60	8	739	89.99
Paddy	11	5	10	144	5	175	82.29
Sugarcane	0	0	1	3	3	7	43
Total	51	59	685	231	18	1044	
Producer Accuracy	70.59	81	97.08	62.34	17		
Overall Accuracy = 85.82%, Kappa Accuracy = 71.19%							

Table 4 - shows the accuracy of thematic maps, including PA, UA, OA, and Kappa. In general, crop type classification with NDVI, MBI, SAVI, and MNDWI index combination using RF classifier produced the accuracy derived from the confusion matrix shows good value where the Kappa of 71.19% and OA of 85.82%. In this study, paddy and sugarcane are the crop types that can be recognized. However, UA and PA of the sugarcane class showed the smallest value. The sugarcane class has a UA of 43% and a PA of 17%.

Identifying the crop type in Candipuro and Pasrujambe, Lumajang Regency is challenging due to the climatological and geographical conditions. The study area is a hillside area of Mount Semeru with relatively high rainfall, causing the image used as input for classification not to be free from cloud cover. On the other hand, the agricultural conditions in the study area are heterogeneous, and many farmers plant crops using an intercropping system. Due to the condition, the classification result is ambiguous.

This research uses limited sentinel-2 images and training samples illustrated in Table 2, recorded from June 25 to July 6, 2023. The classification accuracy can be improved using crop type label data in several years as training and test data. The experiment by Zhi et al. *(Zhi et al., 2022)* shows that classification accuracy will be low if only using data on plant species in one year. However, the accuracy can be increased when the coupling crop label from several years is used to classify crops, especially paddy and maize.

Thematic Maps of Crop Type Classification

This study used sentinel-2 level 2-A time series data computed by the GEE platform. The images were processed using an RF Classifier provided by GEE. The crop-type classification map identified using Sentinel-2 imagery obtained five (5) classes consisting of (1) built-up area, (2) sand, (3) vegetation, (4) paddy, and (5) sugarcane presented in Figure 3. The types of plant cover are identified using field data collection.

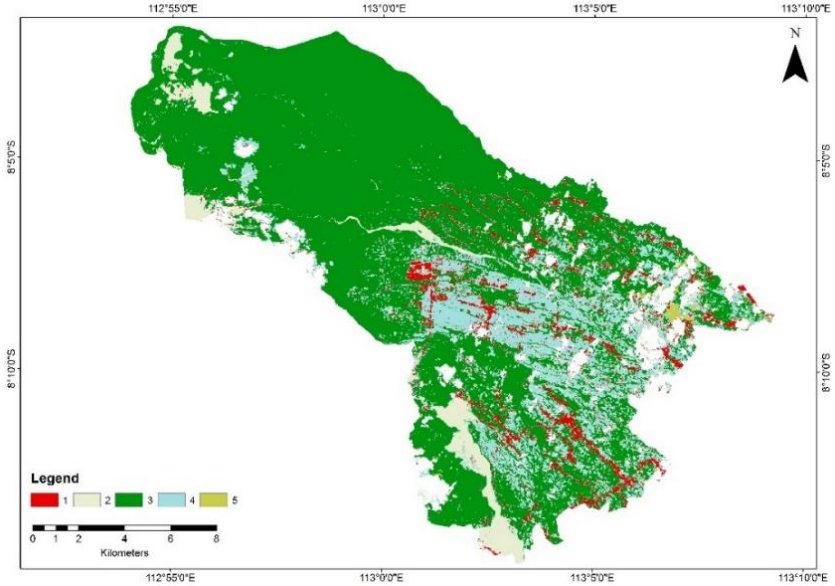


Fig. 3 - Thematic map of crop type classification of Candipuro and Pasrujambe, Lumajang Regency

Table 5- shows the area of each class, where two dominant food crops identified in the study area are paddy and sugarcane. In the study area, primary forests, pines, teak plantations, and sengon trees comprise most vegetation cover. Respectively, the classification results show that the paddy area is 46.22 ha (17.31%) and sugarcane is 2.49% (0.93%). In our study area, vegetation accounted for 69.74% of the total estimated area, so its effect on overall accuracy was relatively significant. Furthermore, the Built-Up Area shows an estimated area of 12.25 ha or approximately 4.59%, and sand of 19.87 ha or 7.44% of the study area.

Table 4

Summary of per-class estimated area

Class	Area (ha)	Percentage (%)
Built-Up Area	12.25	4.59
Sand	19.87	7.44
Vegetation	186.26	69.74
Paddy	46.22	17.31
Sugarcane	2.49	0.93
Total	267.09	100

DISCUSSION

Crop-type mapping is essential for various applications, especially in agriculture. However, mapping crop types in Candipuro and Pasrujambe Districts is challenging because this region is a heterogeneous environment with climatological and geographical conditions and temporal and spatial resolution of images. After all, the region has a tropical climate. Another challenge faced was the availability of cloud-free and shadow-free data, making it difficult to find optimal solutions for cloud-free temporal and composite resolution, leading to a lot of data loss. The solution offered for further studies is using Sentinel-1 images and a fusion of Sentinel-1 and Sentinel-2 images. Sentinel-1 uses a microwave sensor and operates day and night without any weather barriers, thus offering cloud-free data. The experiments conducted by Guo et al. and Kpeinbaareh et al. *(Guo et al., 2018; Kpienbaareh et al., 2021)* showed that fusing Sentinel-1 and Sentinel-2 data could improve the classification results of plant species in Northern Germany and Northern Malawi. In this research, the focus was on the uses of Sentinel-2 images combined with several vegetation indices (i.e., NDVI, MBI, SAVI, MNDWI) processed on the GEE cloud platform using an RF classifier to produce a thematic crop type map in Candipuro and Pasrujambe District, Lumajang Regency.

Random forest is an algorithm widely used in various studies and proved more accurate *(Dakir et al., 2023; Hudait & Patel, 2022).* Our result showed that the RF classifier can distinguish crop types in this study area in terms of overall accuracy (Table 4-). The overall accuracy obtained was 85.82%, and the kappa value of 71.19%. The causal factor that affects the accuracy is the occurrence of misclassification. For example, in this study, misclassification occurred due to similarities in pixel value between paddy (Band 02 = 0.1288, Band 03 = 0.1479, and Band 04 = 0.126) and vegetation (Band 02 =0.1238, Band 03 = 0.1385, Band 04 = 0.1206). Figure 4a shows how the paddy is classified as vegetation. A comparison of similarities between rice and vegetation in Sentinel-2 imagery is shown in Figure 4.



(a) (b) (c)

Fig. 4 - Comparison of the classified map, Sentinel-2 dataset, and Google image

This study uses the GEE cloud computing as a data processing platform. GEE is a geospatial analysis platform that provides multiple processing algorithms, an extensive database, and computing power and facilitates large amounts of high-resolution imagery to map crop types *(Liu et al., 2020).* Data processing by conventional methods (without cloud computing) will take quite a long time. With GEE, processing can be completed in just a few seconds, allowing for fast decision-making *(Shelestov et al., 2017).*

CONCLUSIONS

Crop-type maps in Candipuro and Pasrujambe Districts are generated using a machine learning approach provided by the Google Earth Engine (GEE) cloud computing platform. This study used Sentinel-2 time series data provided in large and free by GEE. The image was processed using a random forest classifier and showed an overall accuracy of about 85.82% and a kappa value of 71.19%. However, because of the climatological and geographical characteristics, identifying the crop type in the research area is difficult. The research region is a hillside area of Mount Semeru with relatively high rainfall, resulting in cloud cover in the photograph utilized as input for classification. On the other hand, the agricultural conditions in the research area are varied, and many farmers produce crops using an intercropping technique.

ACKNOWLEDGEMENT

The authors thank Hibah Internal Universitas Jember Skim Penelitian Produktivitas Guru Besar (PRGB) Tahun 2023 SK. Rektor Universitas Jember Nomor: 7575/UN25/KP/2023, all field personnel, and all parties involved in the research.

REFERENCES

[1] Adam, E., Mutanga, O., Odindi, J., & Abdel-Rahman, E. M. (2014). Land-use/cover classification in a heterogeneous coastal landscape using RapidEye imagery: evaluating the performance of random forest and support vector machines classifiers. *International Journal of Remote Sensing*, *35*(10), 3440–3458. https://doi.org/10.1080/01431161.2014.903435

[2] Agency, E. S. (2015). *SENTINEL-2 User Handbook Sentinel-2 User Handbook SENTINEL-2 User Handbook*. *1*, 1–64.

[3] Akbari, E., Boloorani, A. D., Samany, N. N., Hamzeh, S., Soufizadeh, S., & Pignatti, S. (2020). Crop Mapping Using Random and Particle Swarm Optimization based on Multi-Temporal Sentinel-2. *Remote Sensing*, *12*(9), 1–21. https://doi.org/10.3390/rs12091449

[4] Alami Machichi, M., mansouri, loubna El, imani, yasmina, Bourja, O., Lahlou, O., Zennayi, Y., Bourzeix, F., Hanadé Houmma, I., & Hadria, R. (2023). Crop mapping using supervised machine learning and deep learning: a systematic literature review. *International Journal of Remote Sensing*, *44*(8), 2717–2753. https://doi.org/10.1080/01431161.2023.2205984

[5] Blickensdörfer, L., Schwieder, M., Pflugmacher, D., Nendel, C., Erasmi, S., & Hostert, P. (2022). Mapping of crop types and crop sequences with combined time series of Sentinel-1, Sentinel-2 and Landsat 8 data for Germany. *Remote Sensing of Environment*, *269*(January), 112831. https://doi.org/10.1016/j.rse.2021.112831

[6] Dakir, A., Barramou, F., & Alami, O. B. (2023). Towards a Machine Learning-based Model for Automated Crop Type Mapping. *International Journal of Advanced Computer Science and Applications*. https://doi.org/10.14569/IJACSA.2023.0140185

[7] Duro, D. C., Franklin, S. E., & Dubé, M. G. (2012). A comparison of pixel-based and object-based image analysis with selected machine learning algorithms for the classification of agricultural landscapes using SPOT-5 HRG imagery. *Remote Sensing of Environment*, *118*, 259–272. https://doi.org/10.1016/j.rse.2011.11.020

[8] Erdanaev, E., Kappas, M., & Wyss, D. (2022a). Irrigated Crop Types Mapping in Tashkent Province of Uzbekistan with Remote Sensing-Based Classification Methods. *Sensors*. https://doi.org/10.3390/s22155683

[9] Erdanaev, E., Kappas, M., & Wyss, D. (2022b). The Identification of Irrigated Crop Types Using Support Vector Machine, Random Forest and Maximum Likelihood Classification Methods with Sentinel-2 Data in 2018: Tashkent Province, Uzbekistan. *International Journal of Geoinformatics*. https://doi.org/10.52939/ijg.v18i2.2151

[10] Feng, S., Zhao, J., Liu, T., Zhang, H., Zhang, Z., & Guo, X. (2019). Crop Type Identification and Mapping Using Machine Learning Algorithms and Sentinel-2 Time Series Data. *IEEE Journal of Selected Topics in Applied Earth Observations and Remote Sensing*, *12*(9), 3295–3306. https://doi.org/10.1109/JSTARS.2019.2922469

[11] Griffiths, P., Nendel, C., & Hostert, P. (2019). Intra-annual reflectance composites from Sentinel-2 and Landsat for national-scale crop and land cover mapping. *Remote Sensing of Environment*. https://doi.org/10.1016/j.rse.2018.10.031

[12] Gumma, M. K., Tummala, K., Dixit, S., Collivignarelli, F., Holecz, F., Kolli, R. N., & Whitbread, A. M. (2022). Crop type identification and spatial mapping using Sentinel-2 satellite data with focus on field-level information. *Geocarto International*. https://doi.org/10.1080/10106049.2020.1805029

[13] Guo, J., Wei, P.-L., Liu, J., Jin, B., Su, B.-F., & Zhou, Z.-S. (2018). Crop Classification Based on Differential Characteristics of H/α Scattering Parameters for Multitemporal Quad- and Dual-Polarization SAR Images. *IEEE Transactions on Geoscience and Remote Sensing*. https://doi.org/10.1109/tgrs.2018.2832054

[14] HAO, P. yu, TANG, H. jun, CHEN, Z. xin, MENG, Q. yan, & KANG, Y. peng. (2020). Early-season crop type mapping using 30-m reference time series. *Journal of Integrative Agriculture*. https://doi.org/10.1016/S2095-3119(19)62812-1

[15] Hegarty-Craver, M., Polly, J., O'Neil, M., Ujeneza, N., Rineer, J., Beach, R. H., Lapidus, D., & Temple, D. S. (2020). Remote crop mapping at scale: Using satellite imagery and UAV-acquired data as ground truth. *Remote Sensing*. https://doi.org/10.3390/rs12121984

[16] Hudait, M., & Patel, P. P. (2022). Crop-type mapping and acreage estimation in smallholding plots using Sentinel-2 images and machine learning algorithms: Some comparisons. *Egyptian Journal of Remote Sensing and Space Science*. https://doi.org/10.1016/j.ejrs.2022.01.004

[17] Huete, A. R., Hua, G., Qi, J., Chehbouni, A., & van Leeuwen, W. J. D. (1992). Normalization of multidirectional red and NIR reflectances with the SAVI. *Remote Sensing of Environment*. https://doi.org/10.1016/0034-4257(92)90074-T

[18] Kpienbaareh, D., Sun, X., Wang, J., Luginaah, I., Bezner Kerr, R., Lupafya, E., & Dakishoni, L. (2021). Crop Type and Land Cover Mapping in Northern Malawi Using the Integration of Sentinel-1, Sentinel-2, and PlanetScope Satellite Data. *Remote Sensing*, *13*(4), 700. https://doi.org/10.3390/rs13040700

[19] Liu, L., Xiao, X., Qin, Y., Wang, J., Xu, X., Hu, Y., & Qiao, Z. (2020). Mapping cropping intensity in China using time series Landsat and Sentinel-2 images and Google Earth Engine. *Remote Sensing of Environment*, *239*, 111624. https://doi.org/10.1016/j.rse.2019.111624

[20] Llano, X. C. (2019). *AcATaMa - QGIS plugin for Accuracy Assessment of Thematic Maps*. https://plugins.qgis.org/plugins/AcATaMa/

[21] Luo, K., Lu, L., Xie, Y., Chen, F., Yin, F., & Li, Q. (2023). Crop type mapping in the central part of the North China Plain using Sentinel-2 time series and machine learning. *Computers and Electronics in Agriculture*, *205*, 107577. https://doi.org/10.1016/j.compag.2022.107577

[22] McFeeters, S. K. (1996). The use of the Normalized Difference Water Index (NDWI) in the delineation of open water features. *International Journal of Remote Sensing*. https://doi.org/10.1080/01431169608948714

[23] Nguyen, C. T., Chidthaisong, A., Kieu Diem, P., & Huo, L.-Z. (2021). A Modified Bare Soil Index to Identify Bare Land Features during Agricultural Fallow-Period in Southeast Asia Using Landsat 8. *Land*, *10*(3), 231. https://doi.org/10.3390/land10030231

[24] Nouri, H., Anderson, S., Sutton, P., Beecham, S., Nagler, P., Jarchow, C. J., & Roberts, D. A. (2017). NDVI, scale invariance and the modifiable areal unit problem: An assessment of vegetation in the Adelaide Parklands. *Science of The Total Environment*, *584–585*, 11–18. https://doi.org/https://doi.org/10.1016/j.scitotenv.2017.01.130

[25] Prins, A. J., & Van Niekerk, A. (2021). Crop type mapping using LiDAR, Sentinel-2 and aerial imagery with machine learning algorithms. *Geo-Spatial Information Science*, *24*(2), 215–227. https://doi.org/10.1080/10095020.2020.1782776

[26] Salas, E. A. L., Subburayalu, S. K., Slater, B., Zhao, K., Bhattacharya, B., Tripathy, R., Das, A., Nigam, R., Dave, R., & Parekh, P. (2020). Mapping crop types in fragmented arable landscapes using AVIRIS-NG imagery and limited field data. *International Journal of Image and Data Fusion*. https://doi.org/10.1080/19479832.2019.1706646

[27] Shaharum, N. S. N., Shafri, H. Z. M., Ghani, W. A. W. A. K., Samsatli, S., Al-Habshi, M. M. A., & Yusuf, B. (2020). Oil palm mapping over Peninsular Malaysia using Google Earth Engine and machine learning algorithms. *Remote Sensing Applications: Society and Environment*. https://doi.org/10.1016/j.rsase.2020.100287

[28] Shelestov, A., Lavreniuk, M., Kussul, N., Novikov, A., & Skakun, S. (2017). Exploring Google Earth Engine Platform for Big Data Processing: Classification of Multi-Temporal Satellite Imagery for Crop Mapping. *Frontiers in Earth Science*, *5*. https://doi.org/10.3389/feart.2017.00017

[29] Sun, L., Chen, J., Guo, S., Deng, X., & Han, Y. (2020). Integration of time series sentinel-1 and sentinel-2 imagery for crop type mapping over oasis agricultural areas. *Remote Sensing*. https://doi.org/10.3390/RS12010158

[30] Tariq, A., Yan, J., Gagnon, A. S., Riaz Khan, M., & Mumtaz, F. (2022). Mapping of cropland, cropping patterns and crop types by combining optical remote sensing images with decision tree classifier and random forest. *Geo-Spatial Information Science*. https://doi.org/10.1080/10095020.2022.2100287

[31] Tran, K. H., Zhang, H. K., McMaine, J. T., Zhang, X., & Luo, D. (2022). 10 m crop type mapping using Sentinel-2 reflectance and 30 m cropland data layer product. *International Journal of Applied Earth Observation and Geoinformation*, *107*, 102692. https://doi.org/10.1016/j.jag.2022.102692

[32] Wei, P., Ye, H., Qiao, S., Liu, R., Nie, C., Zhang, B., Song, L., & Huang, S. (2023). Early Crop Mapping Based on Sentinel-2 Time-Series Data and the Random Forest Algorithm. *Remote Sensing*, *15*(13), 3212. https://doi.org/10.3390/rs15133212

[33] Xie, G., & Niculescu, S. (2022). Mapping Crop Types Using Sentinel-2 Data Machine Learning and Monitoring Crop Phenology with Sentinel-1 Backscatter Time Series in Pays de Brest, Brittany, France. *Remote Sensing*, *14*(18), 4437. https://doi.org/10.3390/rs14184437

[34] Xu, H. (2006). Modification of normalised difference water index (NDWI) to enhance open water features in remotely sensed imagery. *International Journal of Remote Sensing*. https://doi.org/10.1080/01431160600589179

[35] Zhi, F., Dong, Z., Guga, S., Bao, Y., Han, A., Zhang, J., & Bao, Y. (2022). Rapid and Automated Mapping of Crop Type in Jilin Province Using Historical Crop Labels and the Google Earth Engine. *Remote Sensing*. https://doi.org/10.3390/rs14164028

Jurnal Pengabdian Kolaborasi dan Inovasi IPTEKS
Volume 1, No 4 – Agustus 2023
e-ISSN : 29863104

PEMETAAN PENGGUNAAN LAHAN DI KOTA PALU MENGGUNAKAN CITRA SENTINEL 2-A

Muhammad Adam Suni[1*], Andre Kurniawan Borman[2], Mohammad Fahrul Himalaya Umar[2], Agung Dwi Kurniawan[3],
[1] Balai Besar Taman Nasional Lore Lindu, Palu
[2,3] Fakultas Kehutanan, Universitas Tadulako, Palu

muhammadadamsuni@gmail.com*

Received: 12-08- 2023	Revised: 20-08-2023	Approved: 25-08-2023

ABSTRAK

Pembuatan peta dalam pengabdian masyarakat ini dilatarbelakangi kebutuhan data akan luas areal penggunaan lahan oleh berbagai pihak baik dari instansi pemerintah, kebutuhan penelitian dan pendidikan, maupun instansi non pemerintah. Kebutuhan data ini cukup tinggi sementara ketersediaan data terbatas dan tidak ada pembaharuan data setiap tahun. Sementara perubahan luasan areal penggunaan sangat dinamis. Untuk mengetahui luas areal penggunaan lahan secara efektif dan efisien, dapat dilakukan pemetaan dengan menggunakan penginderaan jauh. Tujuan pengabdian Masyarakat ini adalah untuk mengetahui luas dan kelas penggunaan lahan di Kota Palu. Pengabdian ini merupakan penelitian secara deskriptif. Luas penggunaan lahan didapatkan melalui penginderaan jauh dengan metode digitasi visualisasi (on screen) menggunakan citra sentinel 2-A dan survey langsung dilapangan. Kombinasi band yang digunakan pada citra sentinel 2-A adalah kombinasi band 4-3-2. Hasil pengabdian masyarakat menunjukkan bahwa terdapat 12 (dua belas) kelas penggunaan lahan di Kota Palu yang didominasi oleh kelas tutupan lahan semak belukar 14.185,91 Ha (37,36%), hutan 6.669,53 Ha (17,57%) dan pemukiman6.431,04 Ha (16,94%).

Kata Kunci : *Pemetaan, Citra Sentinel 2A, Sistem Informasi Geografis*

PENDAHULUAN

Kota Palu dengan wilayah seluas 395,06 Km^2 adalah Ibu Kota Provinsi Sulawesi Tengah. Terdiri atas 8 kecamatan pada tahun 2018. Wilayah ini terbentang dari Palu Selatan (Kecamatan paling selatan) sampai di tawaeli (Kecamatan paling utara. Kecamatan yang terluas adalah Kecamatan Mantikulore yaitu 206,8 Km^2 dan yang terkecil adalah Kecamatan Palu Timur yaitu sebesar 7,7 Km^2. Implikasi pertumbuhan penduduk berdapak pada kebutuhan lahan antara lain: pertanian, pemukiman, jasa dan sarana transportasi. Desakan lahan terpakai akan berdampak pada penggunaan lahan yang menimbulkan terjadinya konversi lahan. Di sisi lain, penggunaan lahan adalah aktivitas manusia yang dilakukan di atas lahan untuk memenuhi tujuan tertentu. Tutupan dan penggunaan lahan dalam beberapa kasus dapat memiliki sebutan yang sama (Van Noordwijk *et al*. 2008).

Permasalahan lahan di perkotaan secara umum berkisar pada persoalan kepemilikan, alih fungsi lahan bervegetasi menjadi kawasan terbangun, kerusakan

lahan akibat kegiatan penambangan sumberdaya alam secara terbuka dan merusak lingkungan yang dapat mengakibatkan bencana alam seperti banjir dan tanah longsor. Tutupan lahan yang tergerus merupakan persoalan serius yang terdapat pada pengelolaan lahan perkotaan yang terus mengalami perubahan signifikan dari tahun ke tahun. Perubahan penggunaan lahan terutama terjadi pada alih fungsi lahan pertanian sawah dan bukan sawah yang mengalami penurunan serta peningkatan lahan yang dibangun (Hidayat dan Noor, 2020). Kepadatan penduduk dapat mempengaruhi kualitas hidup penduduknya. Pada daerah dengan kepadatan yang tinggi, usaha peningkatan kualitas penduduk akan lebih sulit dilakukan. Hal ini menimbulkan permasalahan sosial ekonomi, kesejahteraan, Keamanan, ketersediaan lahan, air bersih dan kebutuhan pangan (Suni *et al,* 2023).

Penginderaan jauh didefinisikan sebagai perolehan informasi suatu objek tanpa adanya kontak fisik dengan objek tersebut. Informasi dalam penginderan jauh diperoleh dengan mendeteksi dan mengukur perubahan dari objek yang digeneralisasikan dengan kondisi optic disekitarnya, meliputi elektromagnetik, akustik dan potensial. Medan Elektromagnetik yang dipancarkan lalu dipantulkan oleh objek, gelombang akustik dipantulkan atau dihamburkan oleh objek (Rahmatsyah, Juliani, dan Tampubolon, 2020). Satelit Sentinel 2 MSI adalah satelit milik *Europe Space Agency* (ESA) yang diluncurkan pada 23 Juni 2015. Sentinel 2 MSI memiliki sudut inklinasi 98,62^{o} dengan periode rotasi selama 40 menit dan merekam permukaan bumi pada 10:30 pagi waktu setempat dengan tujuan untuk memperoleh hasil dengan tutupan awan minimal serta penyinaran matahari yang sesuai (Suhet, 2014).

Perkembangan perubahan tutupan lahan suatu wilayah dapat dianalisis dengan memanfaatkan data penginderaan jauh (remote sensing) berupa citra satelit multitemporal. Pemanfaatan teknologi penginderaan jauh merupakan salah satu cara untuk mengetahui secara cepat alih fungsi lahan. Alih fungsi lahan juga dapat diartikan sebagai perubahan untuk penggunaan lain disebabkan oleh faktor–faktor yang secara garis besar meliputi keperluan untuk memenuhi kebutuhan penduduk yang makin bertambah jumlahnya dan meningkatnya tuntutan akan mutu kehidupan yang lebih baik (Suni, dan Baharuddin, 2023).

Perkembangan perubahan tutupan lahan suatu wilayah dapat dianalisis dengan memanfaatkan data penginderaan jauh (*remote sensing*) berupa citra satelit *multitemporal*. Pemanfaatan teknologi penginderaan jauh merupakan salah satu cara untuk mengetahui secara cepat alih fungsi lahan. (Suni *et al,* 2023). Citra penginderaan jauh, dapat memberikan gambaran keruangan dan ukuran yang merupakan data yang bermanfaat dalam mempelajari fenomena atau kenampakan muka bumi, yang selanjutnya dapat digunakan sebagai dasar rencana dan pemanfaatan praktis (Feri, 2007).

Penginderaan jauh dapat memberikan informasi mengenai karakteristik tutupan vegetasi suatu hutan yang di teliti. Maullana dan Darmawan (2014) mengungkapkan bahwa penginderaan jauh adalah suatu metode untuk mengidentifikasi objek di permukaan bumi tanpa kontak langsung dengan objek. Klasifikasi *supervised* melibatkan interaksi analis secara intensif, dimana analis menuntun proses klasifikasi dengan identifikasi objek pada citra (training area). Sehingga pengambilan sampel perlu dilakukan dengan mempertimbangkan pola spektral pada setiap panjang gelombang tertentu, sehingga diperoleh daerah acuan

yang baik untuk mewakili suatu objek tertentu. Metode *supervised* (dengan bimbingan), pada metode ini, analis terlebih dahulu menentukan beberapa training area (daerah contoh) pada citra sebagai kelas kenampakan objek tertentu. Penetapan ini berdasarkan pengetahuan analis terhadap wilayah dalam citra mengenai daerah-daerah tutupan lahan. Nilai-nilai piksel dalam daerah contoh kemudian digunakan oleh perangkat lunak komputer sebagai kunci untuk mengenali piksel lain. Daerah yang memiliki nilai-nilai piksel sejenis akan dimasukkan ke dalam kelas yang telah ditentukan sebelumnya.

Suni *et al* (2023) melakukan penelitian dengan menggunakan citra satelit Landsat 8 OLI untuk mengetahui kelas dan perubahan luasan tutupan lahan pada sub DAS Toili di Kabupaten Banggai. Hasil penelitian menunjukan bahwa terdapat 9 (Sembilan) kelas tutupan lahan yaitu, hutan lahan kering sekunder, pemukiman, perkebunan, pertanian lahan kering, sawah, semak belukar, tanah terbuka, tubuh air, dan awan yang didominasi oleh kelas tutupan lahan perkebunan, pertanian lahan kering, sawah dan semak belukar. Terjadi perubahan luasan terbesar terdapat pada kelas tutupan lahan perkebunan yang mengalami perubahan luasan di tahun 2022 menjadi 6.342,54 Ha atau bertambah luasannya sebanyak 2.392,35 Ha. Sedangkan perubahan tutupan lahan terkecil terdapat pada kelas tutupan lahan berupa tutupan lahan berupa hutan lahan kering sekunder mengalami perubahan luasan di tahun 2022 menjadi 255,07 Ha atau berkurang luasannya sebanyak 103,48 Ha.

Tablaseray, Pairin, Fakdawer, dan Hamuna, (2018) melakukan penelitian dengan menggunakan citra satelit Landsat 8 OLI untuk mengetahui kerapatan dan sebaran mangrove di pesisir Pulau Biak, Papua. Pada penelitian tersebut dilakukan analisis kerapatan mangrove dengan menggunakan formula Normalized Differece Vegetation Index (NDVI). Hasil penelitian menunjukan bahwa luasan mangrove di wilayah pesisir timur Pulau Biak sebesar 144,81 ha, dimana kerapatan jarang 89,64 ha, kerapatan sedang 26,19 ha dan kerapatan padat 28,98 ha. Rendahnya luasan mangrove umumnya diakibatkan oleh faktor antropogenik seperti penebangan, perubahan alih fungsi mangrove dan akibat tsunami yang terjadi pada tahun 1996.

Gifari, Kusrini, dan Yuana, (2023) Melakukan penelitian dengan hasil identifikasi jenis tutupan lahan di Kota Samarinda menggunakan metode terbimbing MLC pada tahun 1994 menghasilkan luasan tutupan lahan vegetasi alami dengan persentase 53,81% seluas 38.868 ha, vegetasi sekunder dengan persentase 32,66% seluas 23.591 ha, pemukiman dengan persentase 10,24% seluas 7401 ha, water body dengan persentase 3,29% seluas 2368 ha. Sedangkan pada tahun 2022 menghasilkan luasan tutupan lahan vegetasi alami dengan persentase 47,43% seluas 34.077 ha, vegetasi sekunder dengan persentase 27,14% seluas 19.503 ha, pemukiman dengan persentase 19,75% seluas 14.172 ha, water body dengan persentase 5,68% seluas 4086 ha.

Hasil penelitian Dimyati, Somantri, dan Sugito, (2022) menunjukan tingkat perubahan Penggunaan lahan yang terjadi di Kecamatan Parongpong pada kurun waktu dua tahun yaitu dimulai pada tahun 2017 sampai dengan tahun 2019 memiliki laju perubahan pada rentang nilai antara -0,21% sampai dengan 0,17 %. Pengurangan penggunaan lahan terbesar pada semak Belukar dan lahan kosong berkurang sebesar 8,9 Ha dan penambahan terbesar pada penggunaan lahan

Pemukiman dan Tempat Kegiatan Sebesar 7,27 Ha. Pola Perubahan yang terjadi hanya pada empat jenis Penggunaan lahan Hutan, Semak Belukar, ladang dan pemukiman.

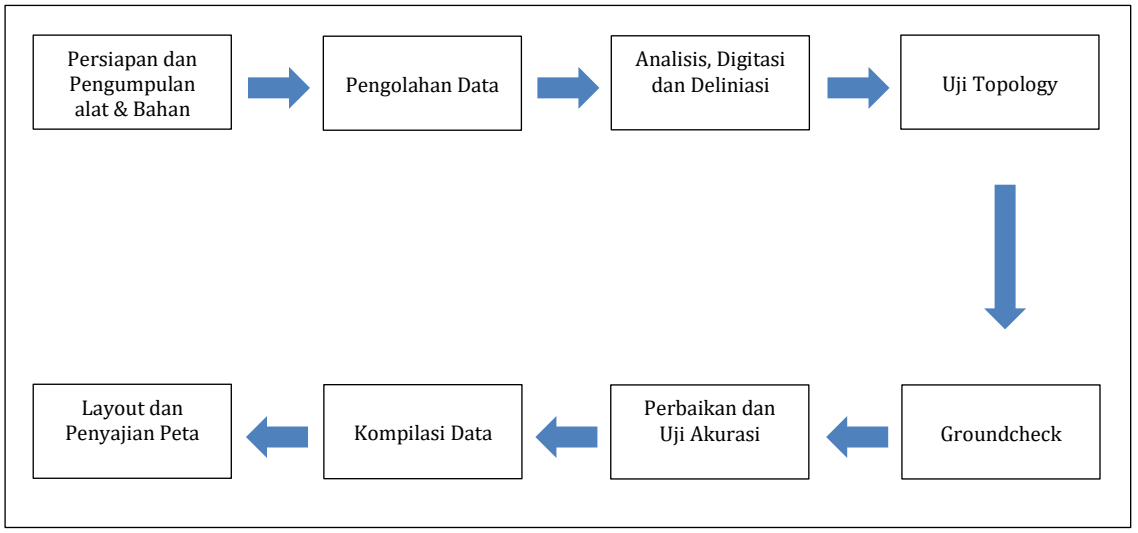
Salah satu upaya untuk mengetahui kelas penggunaan lahan dan luasan terkini adalah dengan sistem penginderaan jauh. Teknologi penginderaan jauh adalah teknologi yang mudah, murah, dan cepat sebagai alternatif yang cukup baik untuk melakukan pemetaan ekosistem mangrove. Citra yang sering digunakan dalam penginderaan jauh diantaranya foto udara menggunakan drone, citra SPOT, Landsat, Google Earth, Sentinel, dan lainnya.

Melalui sistem penginderaan jauh dapat mempermudah penyajian informasi spasial khususnya yang terkait dengan kondisi lahan serta dapat menganalisis dan memperoleh informasi terbaru kondisi suatu lingkup wilayah tertentu. Mengingat pentingnya data luasan dan areal kelas penggunaan lahan di Kota Palu, perlu dilakukan pengabdian masyarakat yang merupakan hilirisasi penelitian pemetaan areal penggunaan lahan dengan metode penginderaan jauh menggunakan citra satelit yang memiliki resolusi cukup baik dan mudah didapatkan. Pengabdian masyakat ini bertujuan untuk mengetahui kondisi terkini penggunaan lahan dan luas areal di kota Palu. Batasan masalah dalam pengabdian masyarakat ini adalah :

1) Daerah pelaksanaan ini berada di wilayah administrasi Kota Palu Provinsi Sulawesi Tengah yang secara geografis terletak di koordinat 119°45 - 121°15 BT dan 0°36 - 0°56 LS.
2) Data spasial yang digunakan adalah citra sentinel level 2-A liputan bulan 28 Juli 2021 dan 18 Juni 2022, citra satelit google earth, dan peta rupa bumi Indonesia.

METODE KEGIATAN

Pengabdian masyarakat ini dilaksanakan pada bulan Oktober sampai Desember 2022 yang meliputi studi literatur, pengumpulan dan pengolahan data, pengecekan lapangan, analisis data, dan penyusunan naskah. Lokasi pengabdian masyarakat berada di Kota Palu. Bahan yang digunakan adalah data sekunder berupa citra sentinel 2-A liputan tanggal 28 Juli 2021 dan 18 Juni 2022, citra satelit google earth, peta Rupa Bumi Indonesia skala 1: 50.000 tahun 2019. Alat yang digunakan adalah laptop dengan spesifikasi RAM 8 Gb, Software ArcGIS 10.8, Software SAS Planet, dan Google Chrome. Peta penggunaan lahan didapatkan dengan metode *digitasi on screen* mengunakan citra satelit google earth dan citra sentinel level 2A dengan kombinasi band 4-3-2. Sesuai SNI 7645-2010 *Klasifikasi Penutup Lahan*, luas dinyatakan dalam bilangan bulat dengan satuan hektar. Kelas penutupan lahan ditentukan dengan interpretasi berdasarkan kenampakan visual pada citra satelit. Tahapan pelaksanaan pengabdian masyarakat pembuatan peta mangrove iniadalah sebagai berikut:



Gambar 1.
Diagram alur pelaksanaan pengabdian masyarakat

(a) Persiapan dan pengumpulan alat bahan
Komputer yang digunakan diinstal aplikasi ArcGIS 10.8.1 dan SAS Planet. Buka software SAS Planet dan buat polygon pada kota Palu Provinsi Sulawesi Tengah, kemudian unduh citra dengan resolusi pada *zoom* 19. Buka website https://scihub.copernicus.eu/pada lalu buat akun dan unduh citra sentinel level 2-A pada lokasi kota Palu Provinsi Sulawesi Tengah. Buka website https://tanahair.indonesia.go.id/ lalu buat akun dan unduh peta Rupa Bumi Indonesia kota Palu Provinsi Sulawesi Tengah. Buka software ArcGIS 10.8.1 kemudian buat shapefile polygon baru dan tambahkan atribut kelas lahan, luas, keterangan. Simpan semua data yang akan digunakan pada lokasi penyimpanan yang sama.

(b) Pengolahan data
Buka aplikasi ArcGIS 10.8.1, sambungkan folder lokasi penyimpanan data spasial yang digunakan. Tambahkan data *shapefile* wilayah administrasi seluruh kota, gabungkan dengan perintah *Union* atau *Intersect* pada tab *Geoprocessing*. Tambahkan data citra sentinel 2-A, buka Composit Band pada *ArcToolbox* lalu *composite* semua citra sentinel 2-A yang ada. Simpan hasil *Composit Band* pada lokasi penyimpanan yang sama.

(c) Proses analisis, digitasi dan deliniasi
Ubah sistem koordinat pada layer menjadi *Universal Transverse Mercator* Zona 50 S. Tambahkan shapefile polygon, citra satelit google earth, citra sentinel 2-A ke layer ArcGIS. Lakukan tumpang susun (overlay) data-data tersebut. Ubah band (pita) pada citra sentinel 2-A menjadi 4-3-2 untuk memudahkan proses analisis. Aktifkan editor, digitasi dan deliniasi pada lokasi kota Palu. Tentukan kelas penggunaan lahan berdasarkan kenampakan visual dan tuliskan kategori kelas pada *attribute table*. Hitung luas dengan *calculate geometry*. Tambahkan *shapefile* administrasi yang telah di *union* kemudian *overlay* dengan *shapefile* penggunaan lahan yang telah dibuat.

(d) Uji topology dan perbaikan data

Lakukan *uji topology* pada *shapefile* batas admistrasi dan penggunaan lahan yang telah digabungkan untuk melihat *polygon* yang tumpang tindih dan terdapat celah diantara polygon yang ada. Perbaiki apabila *terdapat topology error*. Periksa *atribute table* dan isi atribut pada kolom yang masih kosong dengan disesuaikan pada *polygon* terdekat.

(e) Penentuan lokasi dan *Groundcheck*
Lokasi pengecekan lapangan ditentukan dengan mempertimbangkan akses menuju lokasi dan diutamakan pada lokasi yang yang terdapat keraguan saat interpretasi citra. Dokumentasikan kondisi lokasi pengecekan lapangan. Catat koordinat, dan catatan lain apabila terdapat informasi penting lainnya.

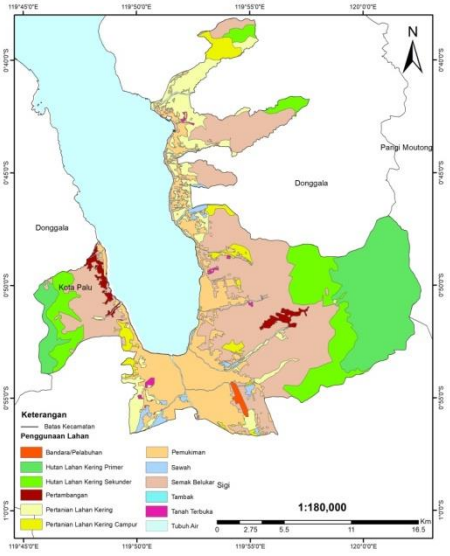
(f) Uji Akurasi
Perbaiki peta pada lokasi yang tidak sesuai antara kondisi lapangan dengan hasil analisis peta. Uji akurasi hasil pengolahan citra diperlukan untuk menghasilkan informasi yang sesuai dengan kondisi yang seharusnya.

(g) Kompilasi Data
Kompilasi data digunakan untuk menghitung jumlah kategori kelas penggunaan lahan dan seluruh luasan dari hasil akhir.

(h) *Layout* dan Penyajian peta
Buat layout pada ukuran kertas A4 dan cetak peta menggunakan skala 1:180.000.

HASIL DAN PEMBAHASAN

Hasil pengolahan dan analisis data dari pengabdian masyarakat didapatkan kelas dan luas penggunaan lahan di Kota Palu tahun 2022 diperoleh dari hasil *digitasi on screen* menggunakan citra satelit *google earth* dan citra Sentinel level 2A. Dari hasil analisis ini, diperoleh 12 (dua belas) tipe/kelas penggunaan lahan di Kota Palu dapat dilihat pada gambar 2.



Gambar 2.
Peta Penggunaan Lahan Kota Palu

Dari hasil pengolahan data citra Sentinel 2A tahun 2022 menunjukan bahwa

kawasan hutan lahan kering primer memiliki luas 6.669,53 Ha atau (17,57%), hutan lahan kering sekunder memiliki luas 4.842,32 Ha atau (12,75%), permukiman memiliki luas 6.431,04 Ha atau (16,94%), pertambangan memiliki luas 543,48 Ha atau (1,43%), pertanian lahan kering memiliki luas 3.024,21 Ha atau (7,96%), pertanian lahan kering campuran memiliki luas 1.187,57 Ha atau (3,13), sawah memiliki luas 396,17 Ha atau (1,04%), semak belukar memiliki 14.185,91 Ha atau (37,36%), tambak memiliki luas 7,48 Ha atau (0,02%) tanah terbuka memiliki luas 192,41 Ha atau (0,51%), tubuh air memiliki luas 250,94 Ha atau (0,66%) dan bandara/pelabuhan memiliki luas 239,18 Ha atau (0,63%) dari luas total. Pada tabel tersebut diketahui penggunaan lahan terluas yaitu semak belukar seluas 14.185,91 Ha, sedangkan penggunaan lahan terendah yaitu bandara/Pelabuhan dengan luas 7,48 Ha, dapat dilihat pada tabel 1.

Tabel 1. Kelas dan Luas Penggunaan Lahan Kota Palu tahun 2022

Penggunaan Lahan 2022	Luas (Ha)	Persen (%)
Hutan lahan kering primer	6.669,53	17,57
Hutan lahan kering sekunder	4.842,32	12,75
Permukiman	6.431,04	16,94
Pertambangan	543,48	1,43
Pertanian Lahan Kering	3.024,21	7,96
Pertanian Lahan Kering Campuran	1.187,57	3,13
Sawah	396,17	1,04
Semak Belukar	14.185,91	37,36
Tambak	7,48	0,02
Tanah Tebuka	192,41	0,51
Tubuh Air	250,94	0,66
Bandara/Pelabuhan	239,18	0,63
Jumlah	**37.970,26**	**100**

KESIMPULAN

Berdasarkan hasil pengabdian kepada masyarakat yang telah dilakukan, dapat diperoleh kesimpulan terdapat 12 (dua belas) tipe/kelas penggunaan lahan di Kota Palu yaitu, hutan lahan kering primer, hutan lahan kering sekunder, pemukiman, pertambangan, pertanian lahan kering, pertanian lahan kering campuran, sawah, semak belukar, tambak, tanah terbuka, tubuh air, dan bandara yang didominasi oleh kelas tutupan lahan semak belukar 14.185,91 Ha (37,36%), hutan 6.669,53 Ha (17,57%) dan pemukiman6.431,04 Ha (16,94%).

DAFTAR PUSTAKA

Dimyati, A. E. F., Somantri, L., dan Sugito, N. T. (2022). Klasifikasi Berbasis Objek Citra Satelit Sentinel 2 untuk Pemetaan Perubahan Lahan di Kecamatan Parongpong Kabupaten Bandung Barat. Jurnal Geografi: Media Informasi Pengembangan dan Profesi Kegeografian, 19(1), 24-28.

Feri, T. 2007. Analisis Perubahan Penggunaan Lahan dan Keterkaitannya Dengan Fluktuasi Debit Sungai Di DAS Antokan Provinsi Sumatera Barat. Tesis. Institut Pertanian Bogor. Bogor. 124.

Gifari, O. I., Kusrini, K., dan Yuana, K. A. (2023). Analisis Perubahan Tutupan Lahan Menggunakan Metode Klasifikasi Terbimbing Pada Data Citra Penginderaan

Jauh Kota Samarinda-Kalimantan Timur. Informatika Mulawarman: Jurnal Ilmiah Ilmu Komputer, 18(2), 71-77. http://dx.doi.org/10.30872/jim.v18i2.5716

Hidayat, M. A., dan Noor, A. (2020). Pengaruh pertumbuhan ekonomi terhadap alih fungsi lahan di kota samarinda. Inovasi, 16(2), 299-308. https://doi.org/10.30872/jinv.v16i2.8256

Maullana, D. A., dan Darmawan, A. (2014). Perubahan penutupan lahan di taman nasional way kambas. Jurnal Sylva Lestari, 2(1), 87-94.

Rahmatsyah, M. S., Juliani, R., dan Tampubolon, T. (2020). Fisika Kelautan. Media Sains Indonesia.

Suhet. (2014). Sentinel-2 User Handbook. Paris. ESA Standard Document : European Space Agency.

Suni, M. A., Muis, H., Arianingsih, I., Misra, M., dan Baharuddin, R. F. (2023). Analisis dan Permodelan Spasial Perubahan Tutupan Lahan Di Hutan Produksi Terbatas Kecamatan Kulawi Kabupaten Sigi. Jurnal Tanah dan Sumberdaya Lahan, 10(2), 273-284. https://doi.org/10.21776/ub.jtsl.2023.010.2.11

Suni, M. A., Asa, S., Umar, F. H., dan Baharuddin, R. F. (2023). Analisis Perubahan Tutupan Lahan Di Sub DAS Toili Kabupaten Banggai. Nusantara Hasana Journal, 2(10), 28-37.

Suni, M. A., dan Baharuddin, R. F. (2023). Analisis Perubahan Tutupan Lahan di Hutan Produksi Terbatas Kecamatan Kulawi Kabupaten Sigi. BULLET: Jurnal Multidisiplin Ilmu, 2(1), 77-84.

Tablaseray, V.E., Pairin, M., Fakdawer, N., dan Hamuna, B. (2018). Pemetaan Sebaran dan Kerapatan Mangrove di Pesisir Timur Pulau Biak, Papua Menggunakan Citra Satelit Landsat 8. Jurnal Perikanan dan Kelautan Universitas Cenderawasih, Vol.VIII, hlm. 31-39.

Van Noordwijk, M., Mulyoutami, E., Sakuntaladewi, N. and Agus, F. 2008. Swiddens in transition: shifted perceptions on shifting cultivators in Indonesia. Occasional Paper no.9. World Agroforestry Centre. Bogor. 49 p.

www.czasopisma.pan.pl PAN www.journals.pan.pl
POLSKA AKADEMIA NAUK



JOURNAL OF WATER AND LAND DEVELOPMENT
e-ISSN 2083-4535

Polish Academy of Sciences (PAN), Committee on Agronomic Sciences
Section of Land Reclamation and Environmental Engineering in Agriculture
Institute of Technology and Life Sciences (ITP)

JOURNAL OF WATER AND LAND DEVELOPMENT
2020, No. 47 (X–XII): 89–95
https://doi.org/10.24425/jwld.2020.135035

Available (PDF): http://www.itp.edu.pl/wydawnictwo/journal; http://journals.pan.pl/jwld

Received 01.03.2020
Reviewed 10.05.2020
Accepted 25.05.2020

Using Sentinel-2A to identify the change in dry marginal agricultural land occupation

Indarto INDARTO ✉, **Bayu T.W. PUTRA**, **Marga MANDALA**

University of Jember, Faculty of Agricultural Technology, Jl kalimantan No. 37 Kampus Tegalboto, 68121, Jember, Jawa Timur, Indonesia

For citation: Indarto I., Putra B.T.W., Mandala M. 2020. Using Sentinel-2A to identify the change in dry marginal agricultural land occupation. Journal of Water and Land Development. No. 47 (X–XII) p. 89–95. DOI: 10.24425/jwld.2020.135035.

Abstract

Dry marginal agricultural land (DryMAL) potentially use as an alternative resource for crop production. DryMAL defined as land having low natural fertility due to its intrinsic properties and forming environmental factors. This study uses Sentinel-2A imagery to map the spatial extent, compare the result of the classification, and identify the change in DryMAL occupation. The area of study (461.9 km^2) is part of Situbondo Regency and is located at the eastern part of East Java, Indonesia. Sentinel-2A image captured in dry-season of 2018 use for this study. Then, supervised image classification using a maximum likelihood algorithm use for image treatment and processing. Furthermore, 450 ground control points for training areas collected during the field surveys. Five bands use in the classification process. The maps produced from the classification process were then compared to the land-use map from the year 2000. The change in DryMAL occupation from 2000 to 2018 was calculated by comparing the classified and land-use map. Supervised classification yielded an overall accuracy of 95.8% and a kappa accuracy of 93.2%. The classification produced six (6) classes of land use: (1) forest, (2) pavement or built-up area, (3) irrigated paddy field, (4) non-irrigated rural area, (5) dry marginal land and (6) water body. Globally, during the last two decades, regional development led by the Regency occupied more DryMAL area for developing plantation. The effort reduces the amount of non-irrigated and converting to the plantation, pavement areas, and irrigated paddy-field.

Keywords: *agricultural, change, land, mapping, marginal, Sentinel-2A*

INTRODUCTION

According to ELBERSEN *et al.* [2018] and VON COSSEL *et al.* [2019], Marginal agricultural land defined as limitation lands which are severe for sustained application and sensitive to land degradation. Inappropriate human intervention, contaminated and potentially contaminated sites can cause land degradation. Marginal agricultural land (MAL) exists in many parts of Indonesia. According to MILBRANDT and OVEREND [2008], the Indonesian total land area covering 1,847,033 km^2. The marginal land occupied about 37,123 km^2 (2% of total area). The biomass resource potential on marginal lands estimated at 15,494,000 t·y^{-1}.

These lands are abandoned and rarely used, especially for agricultural activities. However, this land type can be used as an alternative resource for crop production, both food and energy services. MAL use for the production of industrial crops to serve biomass and energy demand [GERWIN *et al.* 2018; LONGATO *et al.* 2019; VON COSSEL *et al.* 2019].

Dry marginal agricultural land (DryMAL) in this study is the specifics form of MAL. DryMAL defined as land having low natural fertility due to its intrinsic properties and forming environmental factors [MULYANI, SARWANI 2013]. An illustration of DryMAL discussed in this study is shown in Photo 1. DryMAL usually has a lower crop-growing capacity than average fertile land. This condition is probably due to the soil's lack of organic content, the limited availability of water, and other intrinsic factors that are constrained by the nature of this environment [MULYANI, SARWANI 2013].

Usually, farmers will often choose to apply more fertilizer, pesticide, and herbicide in a bid to grow their crops. Inappropriate choices of the types of crops plant in their fields have added to the complexity of the problem. The majority of farmers will usually carry out crop planting on a massive scale, as other farmers do. This massive planting

© 2020. The Authors. Published by Polish Academy of Sciences (PAN) and Institute of Technology and Life Sciences (ITP).
This is an open access article under the CC BY-NC-ND license (https://creativecommons.org/licenses/by-nc-nd/3.0/).



Photo 1. Example of dry marginal agricultural land (phot. *I. Indarto*)

results in over-supply during the peak season and a rapid decrease in crop prices, meaning farmers' total revenues will fall below their expected values. This cycle is repeated every time, with only a few farmers able to escape it and survive [INDARTO, MANDALA 2019].

The limited amounts of land owned by farmers on which to grow their crops is also a constraint factor. The system of smallholder farming [NYAMBO *et al*. 2019] on narrow areas of land tends to increase input-cost and a reduction in net revenue. Besides the issue explained above, many farmers in these marginal areas use their land resources to grow crops solely for their own everyday consumption (i.e. not to sell) [INDARTO, MANDALA 2019]. These typical problems of smallholder farmers as described above, also found in many parts of the world [DONATTI *et al.* 2019].

Various efforts have been initiated by the government of Situbondo, University of Jember and other stakeholders. There have been many activities aimed at strengthening the capacity building of farmer organizations, to increase land productivity, increase farmer revenue, and increase the social welfare of the society. Over the last fifteen years, the government introduced several deep pumping stations to distributing water from groundwater resources for consumptive use and irrigation. However, the pumping of water from deep groundwater sources for agricultural practices continues to be both expensive and inefficient. The operational and high servicing costs of a pump system remain out of reach for farmers [INDARTO, MANDALA 2019].



Photo 2. Example of mango trees planted in dry marginal agricultural land on the area of study (phot. *I. Indarto*)

The government has made other efforts, however, through the introduction of certain varieties of mango. Some farmers in these areas have opted to plant mango trees as an alternative to a secondary income (Photo 2). Mango trees favour the long dry period and lower rainfall. To this end, mangoes have been successfully planted and developed in the region, and today, more investors are planting mango in these regions. However, the added value from mango circulation is captured mostly by distributors, investors, buyers and re-sellers. Again, the farmer remains stuck in a poverty cycle [PAYNE 2005].

Despite this, however, there are mango plantations on only a few areas of this marginal land. The abundant DryMAL resources are still unusable during the peak dry season, which means limitations on the usability of these land resources for agricultural practice remain a barrier. Contrary to the view of sustainable development goals, this type of farming practice will create more marginal populations [INDARTO, MANDALA 2019].

The duration of the dry season in this area most likely benefits the production of grain seed. There have been many efforts initiated to increase productivity and reduce barriers. One such measure has involved the introduction of a public-private partnership (PPP), and the region is now positively supporting grain seed production. The advantage for grain seed posed by the length of the dry season in the region has enabled it to become established as a grain seed production area by leveraging the existing DryMAL resources [INDARTO, MANDALA 2019].

Optimizing the productivity of these land resources will benefit the society through the addition of marginal income from seed production and therefore bolster the incomes of the farmers. At the initial stage of its implementation, the PPP involved focus group discussions, field surveys, mapping, and setting-up of demo-plots. There is an urgent need to conduct mapping to calculate the spatial extent of these marginal lands [INDARTO, MANDALA 2019].

This study aims to employ Sentinel-2A image to map the spatial extent of DryMAL, to compare the classification result and to detect the change in DryMAL occupation over the last two decades.

Sentinel-2A has provided fine-resolution imagery that is available for free download. The data can be downloaded from the United States Geological Survey website [USGS 2019] or by using the Sentinel hub [ESA 2013; Sentinel Hub undated]. This remote sensing satellite system has global coverage and provides imagery at a global level. Furthermore, Sentinel-2A provide the spatial, spectral and temporal resolution that may appropriate for the identification and mapping of DryMAL in this study.

The use of satellite imagery for mapping agricultural areas is a widely known method and employed by many researchers around the world. There are many studies containing examples of the use of Sentinel-2 imagery for the identification and mapping of agricultural-related issues [ABDI 2019; FORKUOR *et al.* 2018; GOGA *et al.* 2019; MANSARAY *et al.* 2019; RUJOIU-MARE *et al.* 2017]. These studies illustrate the potential applicability of Sentinel-2A for mapping land use and land cover or other phenomena related to the agriculture field.

Pixel-based image classification is a widely known method to recognize and to map objects based on the digital number contained in the pixel. There are two well-known types of classification methods, i.e., supervised and unsupervised [SCHOWENGERDT 2007]. Supervised classification explores any available algorithms, and the critical thing to be considered is the type and number of training areas and selected band combinations used. Unsupervised classification uses any clustering algorithms to classify the pixels based solely on the similarity of their DN values [RICHARDS 2013].

METHODS

STUDY AREA AND INPUT DATA

Situbondo Regency (Fig. 1) is located in the eastern part of East Java and covers a total area of 1649.80 km^2. The region has a tropical climate, yet is relatively dry compared with other sub-areas. Its annual rainfall ranges from 500 to 1500 mm·y^{-1}, which is less than the average annual rainfall amounts received in other regions of East Java (1500–3500 mm·y^{-1}) [INDARTO 2013].

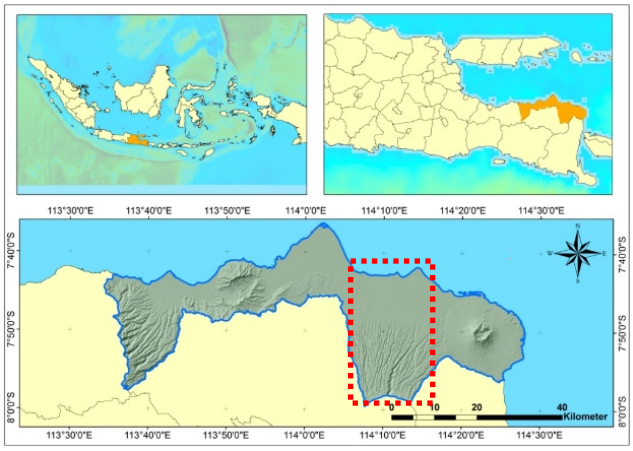


Fig. 1. Situbondo Regency and a subset of the study area; source: BIG 2019

DryMAL makes up around 60% of the total agricultural areas in Situbondo Regency. The area of study covers three districts in the eastern part of Situbondo (Fig. 1). The total area of around 461.69 km^2. The dry season in this region varies in length, from between seven to nine months per year. The dry season begins in May/June and lasts until November/December. There is also very less monthly rainfall. Rainfall amounts greater than 100 mm per month fall only from January to April (four months) [INDARTO 2013].

The ground in the region is characterized by a thin layer of soil comprising only shallow solum and relatively small amounts of organic matter. Many places in the study area have gravel in the upper soil layers (Photo 3). This stony soil layer is typical of the study area and tends to have a slight to moderate slope.

Moreover, the soil layer contains macropores that increase the rate at which runoff infiltrates and percolates to the deep soil layer. As such, only a few intermittent rivers flow in this region. The shallow soil layer in stepped terrain drainage combined with the presence of macropores and intermittent rivers means the groundwater resources are continuously recharged. Groundwater is the primary water source in this region. Similar DryMAL areas also found in central and western areas of the Regency [INDARTO, MANDALA 2019].



Photo 3. Example of the soil in the region (phot. *I. Indarto*)

The input data for this study is Sentinel Image of the location of interest. The image was selected based on the minimum of cloud coverage. The image capture on 20 July 2018, cloud cover 0.68%, tile number = T49MHM, orbit number 46, and orbit direction = descending (Fig. 2).



Fig. 2. Raw image input data; source: USGS EarthExplorer

The existing map is known as RBI (Rupa Bumi Indonesia) digital map. This map is called "RBI (Rupa Bumi Indonesia) format shp" in vector layer format and can be downloaded free of charge from the Indonesian Geospatial Agency (Ind. the Badan Informasi Geospatial – BIG) official site [BIG 2019]. RBI map presents the land use and land cover map of all Indonesian region. The map of this area was created between the years 1999 and 2000. The change in DryMAL occupation interpreted by comparing the map created from sentinel and this RBI map.

TOOL USED

In this study, a Multispec© package [BIEHL 2018] use as a tool for an image processing task. In this study, the QGIS [QGIS 2019] serve for atmospheric correction and visualisation. The Global Positioning System (GPS) and camera used to obtain and to capture the Ground Control Points (GCPs).

PROCEDURE

The image treatment consists of atmospheric correction, image composite, supervised classification, accuracy assessment, and image interpretation (Fig. 3).

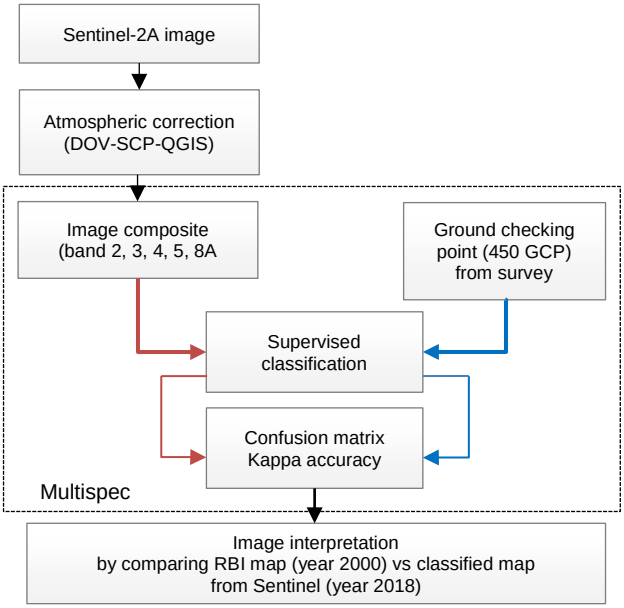


Fig. 3. Procedure of image treatment; source: own elaboration

A Dark Object Subtraction (DOS) algorithm was employed to conduct atmospheric correction by using the Semi-automatic classification (SCP) plug-in on the QGIS platform [CONGEDO 2017]. Five bands of Sentinel-2A (i.e. bands 2, 3, 4, 5 and 8A) are explored to produce image composite.

The classification procedure followed the existing tutorials [BIEHL 2018]. Supervised classification conducted using maximum-likelihood algorithms and collected GCP for training areas. Field surveys conducted between May and October 2019 to collect the 450 GCPs, identify the real conditions in the field and take photographs from the region of interest. Table 1 summarized the statistics of GCPs for each class.

Table 1. Statistics of collected Ground Control Points (GCPs)

Class	Number of the training area	Area (ha)			
		total	min	max	median
Forest-plantation	90	1 238	1.7	41.7	14.0
Built-up area	104	1 067	1.2	44.3	7.3
Irrigated paddy field	86	2 394	16.7	71.4	27.6
Non-irrigated rural area	70	1 648	2.6	39.0	24.9
DryMAL	75	1 423	3.0	37.6	19.2
Waterbody	25	309	11.3	29.4	13.4
Total	450	8 079			

Explanation: DryMAL = dry marginal agricultural land.
Source: own elaboration.

Then, the image clipped with a polygon covering the boundary of the three districts (Arjasa, Asembagus and Jangkar). Figure 4 shows the study area, collected GCPs and photos taken during the field survey. Interpretation conducted by comparing and analysing the change visualised on the Sentinel and existing digital maps.

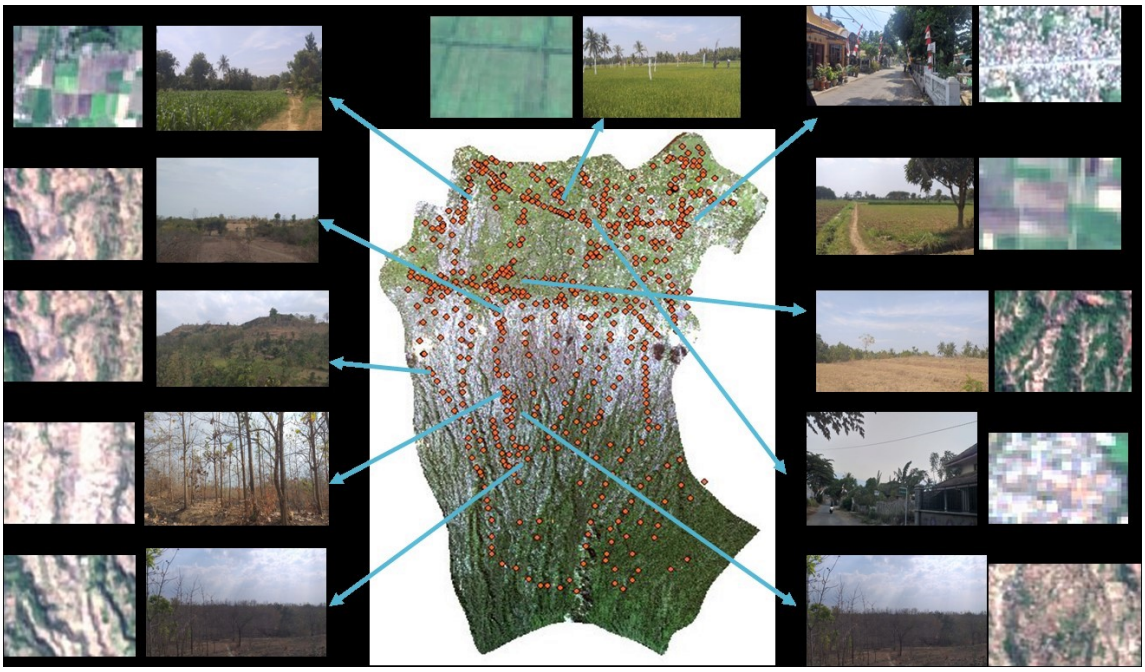


Fig. 4. Collected ground control points; source: own elaboration

Table 2. Confusion matrix

Class type	Irrigated	Dryland	Waterbody	Non-irrigated	Forest	Pavement	Total
Irrigated	13 521	476	5	149	72	252	14 475
DryMAL	500	25 270	38	118	34	218	26 178
Water body	7	3	1 802	6	0	56	1 874
Non-irrigated	441	133	3	7 017	1	66	7 661
Forest	1 608	354	4	9	67 668	251	69 894
Pavement	111	129	33	62	0	2 258	2 593
Total	16 188	26 365	1 885	7 361	67 775	3 101	122 675

Source: own study.

RESULTS AND DISCUSSION

CLASSIFICATION RESULT

The supervised classification enabled separation of six types of land use, i.e. irrigated paddy (24.78%), DryMAL (26.22%), waterbody (0.89%), non-irrigated area (4.98%), forest (35.51%) and pavement area (7.62%). The classification achieved an overall accuracy = 95.8% and a kappa accuracy = 93.2%. The confusion matrix is presented in Table 2. The map (Fig. 5) shows the result obtained from the supervised classification.

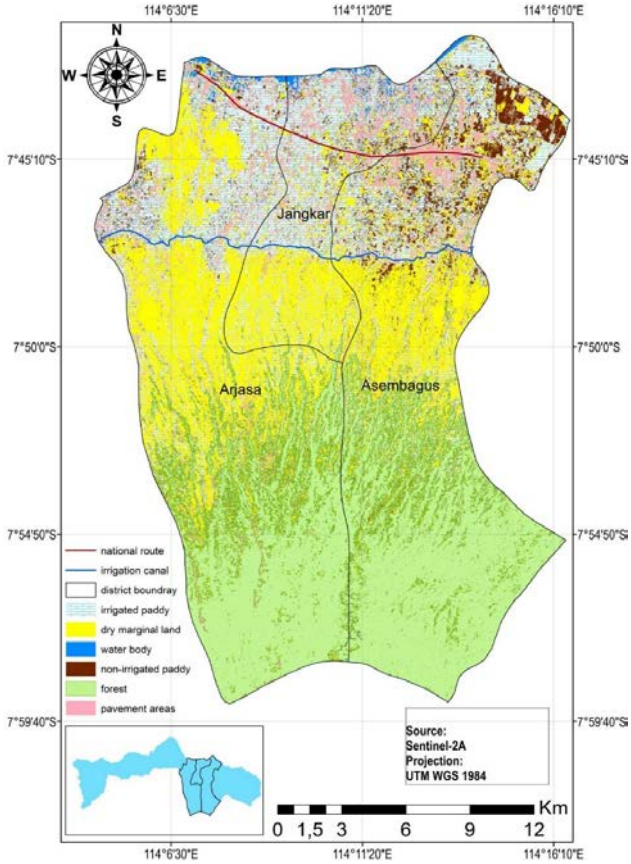


Fig. 5. Classification result; source: own study

The DryMAL, as investigated in this study, appears mostly in the middle area of Figure 5. Moreover, an area of DryMAL also located in the upper-left of the study areas (in the district Arjasa). The upland area of this map composed of forest and plantation, which confirms the existing reality.

Additionally, according to this map, the total area of the three districts is 461.69 km^2. The land in this region is composed of DryMAL (34.3%), irrigated paddy fields (22.0%), non-irrigated areas (13.8%), pavement (3.5%), forests and plantations (26.30%) and water bodies (0.10%). It is confirmed with the reality on the terrain. Figure 6 presents the clipped RBI map of the region of interest. This official digital map uses to compare the classification result.

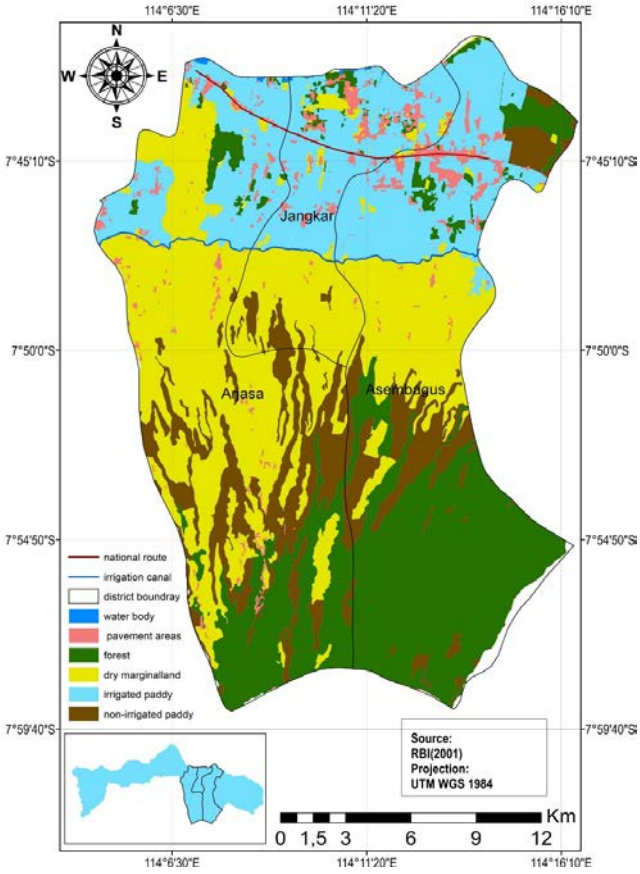


Fig. 6. RBI map; source: own study

INTERPRETATION

Table 3 presents the class type in (km^2) and (%) of the total area mapped using supervised classification method and compared to the RBI digital maps. In the RBI map (Tab. 3, Fig. 6), the pavement area covers only 3.5% of the total area, while between 2000 and 2018, this appears to have increased to 7.62% of the total area mapped. The increase is due to population increase and development in the villages.

Table 3. Comparison of maps

Class	Supervised		RBI map	
	km^2	%	km^2	%
Pavement area	35.17	**7.62**	16.0	**3.5**
DryMAL	121.04	**26.22**	158.4	**34.3**
Irrigated paddy	114.41	**24.78**	101.4	**22.0**
Forest and plantation	163.94	**35.51**	121.4	**26.3**
Non-irrigated paddy	23.01	**4.98**	63.9	**13.8**
Water body	4.12	**0.89**	0.6	**0.1**
Total	461.69	100	461.7	100

Source: own study.

The supervised classification enables better identification of water bodies. The waterbody area increased by 0.79%. The increase is due to the development of aquaculture sites to culture shrimp and harvest salt, located along the region's coastline (the northern part of the map). The Sentinel-2A band enables better identification of these sites. Part of the economic development in the regions supported by this type of industry. It noted that parallel to the coastal area, we see the national route (appearing as a continuous red line) that links Sumatra, Java and Bali Islands.

The irrigated-paddy-field class is a land-use type that mapped consistently using both the supervised and RBI. This region characterized by the constant development of irrigated areas over the past twenty years. The primary irrigation canal passes across the maps and noticeably divides the region into two distinct land-use types. The RBI map (Fig. 6) shows that below the irrigation canal, we find the irrigated area (irrigated paddy denoted as a light-blue colour). This area accounts for around 22% of the total area on the map. The government built the canal between 1980 and 1985. The region of interest is the driest area in East Java. Water flows to this area through an irrigation canal from the Sampean Reservoir located ±40 km from the region. This region is the last downstream area covered by the canal; as such, there is only minimal water available for irrigation. In the two maps above, we see slightly different totals calculated for irrigated paddy, i.e. 24.78% (in the supervised map) and 22% (in the RBI map). The difference is 2.78%. It noted that the region received more rainfall in the year 2018, and therefore more agricultural areas (in both irrigated and non-irrigated areas) were planted with paddy. These were monitored via the Sentinel imagery and classified using the supervised method as additions to the irrigated area. Agricultural fields have also been converted to pavement areas in the area below the canal.

The shift in land occupation in the region observed using three classes of land-use type, i.e., DryMAL, forest and plantation (forest), and non-irrigated area. The original land resources for these three classes in this region were similar, i.e. DryMAL. The total area occupied by these three classes in the RBI map = (34.30 + 26.30 + 13.80) = 74.40%, while on the supervised map, the total area = (26.22 + 35.51 + 4.98) = 66.71%. The illustration above demonstrates the potential for DryMAL resources in this region.

Globally, regional development led by local government during the last two decades has changed the land use by reducing the amount of DryMAL area, increasing forest plantation and reducing the amount of non-irrigated areas. DryMAL and non-irrigated areas are the land resources should be optimised for further agricultural activities. In summary, the Sentinel-2A sufficiently appropriate for the identification and mapping of principal DryMAL occupation in this region.

CONCLUSIONS

This study demonstrates the application of Sentinel-2A imagery to map the change of DryMAL occupation from periods of 2000 to 2018. Three districts in the eastern part of Situbondo Regency (i.e. Arjasa, Jangkar, and Asembagus, that cover an area of 461 km^2) used as a sample of DryMAL region investigated. Supervised classification using a maximum likelihood algorithm and conducted on the platform of Multispec can successfully classify Sentinel-2A pixels into six classes of land-occupations. The pavement or build area occupied only 7.62% of the total area mapped. Then, the DryMAL cover about 26.22%, followed by irrigated paddy-field (24.78%), forest and plantation (35.51%), non-irrigated area (4.98%) and water body (0.89%). The comparison of the classified and RBI maps shows how DryMAL occupation has changed. The spatial, spectral and temporal resolution of the imagery obtained by Sentinel-2A sufficiently appropriate for the identification and mapping of primary DryMAL occupation in this region. The map will benefit for the government agency, local stakeholders and the university for further action related to DryMAL optimization and development.

FUNDING

This study forms part of a DRPM RISTEK DIKTI Research Grant, with Contract-ID No7/E/KPT/2019, followed by subcontract No 175/SP2H/LT/DRPM/2019, with entitle "Peningkatan Produktivitas Lahan Sub-optimal di Wilayah Kabupaten Situbondo Jawa Timur" or "Optimalisation of Dry Marginal Agricultural Land (DryMAL) productivity in the Situbondo Regency in East Java".

REFERENCES

ABDI A. M. 2019. Land cover and land use classification performance of machine learning algorithms in a boreal landscape using Sentinel-2 data. GIScience & Remote Sensing. Vol. 57. Iss. 1 p. 1–20. DOI 10.1080/15481603. 2019.1650447.

BIEHL L. 2018. Intro to remote sensing using MultiSpec [online]. In: NEXUS Remote Sensing Workshop. 6.08.2018. [Access 15.12.2019]. Available at: https://engineering.purdue.edu/~biehl/MultiSpec/tutorials/20180806_Nexus_Remote_Sensing_Exercise_English.pdf

BIG 2019. Ina-Geoportal. Geo-spatial untuk Negri [Indonesia Geospatial Portal] [online]. [Access 15.12.2019]. Available at: http://tanahair.indonesia.go.id/portal-web

CONGEDO L. 2017. Semi-automatic classification plugin semi-automatic classification plugin documentation. Technical Report pp. 198. DOI 10.13140/RG.2.2.29474.02242/1.

DONATTI C.I., HARVEY C.A., MARTINEZ-RODRIGUEZ M., VIGNOLA R., RODRIGUEZ C.M. 2019. The vulnerability of smallholder farmers to climate change in Central America and Mexico: Current knowledge and research gaps. Climate and Develop-

ment. Vol. 11(3) p. 264–286. DOI 10.1080/17565529.2018.1442796.

ELBERSEN B., VAN VERZANDVOORT M., BOOGAARD S., MUCHER S., CICARELLI T., ELBERSEN W., MANTEL S., BAI Z., MCALLUM I., IQBAL Y. 2018. Deliverable 2.1 Definition and classification of marginal lands suitable for industrial crops in Europe. EU Horizon 2020; MAGIC; GANo.: 727698. Wageningen, The Netherlands. University and Research pp. 60.

ESA 2013. Sentinel-2 user handbook. Iss. 1. Rev. 1. European Space Agency pp. 64.

FORKUOR G., FORKUOR G., DIMOBE K., SERME I., TONDOH J.E. 2018. Landsat-8 vs. Sentinel-2: Examining the added value of Sentinel-2's red-edge bands to land-use and land-cover mapping in Burkina Faso. GIScience & Remote Sensing. Vol. 55. Iss. 3p. 331–354. DOI 10.1080/15481603.2017.1370169.

GERWIN W., REPMANN F., GALATSIDAS S., VLACHAKI D., GOUNARIS N., BAUMGARTEN W., VOLKMANN C., KERAMITZIS D., KIOURTSIS F., FREESE D. 2018. Assessment and quantification of marginal lands for biomass production in Europe using soil-quality indicators. Soil. 4(4) p. 267–290. DOI 10.5194/soil-4-267-2018.

GOGA T., FERANEC J., BUCHA T., RUSNÁK M., SAČKOV I., BARKA I., KOPECKÁ M., PAPČO J., OŤAHEĽ J., SZATMÁRI D., PAZÚR R., SEDLIAK M., PAJTÍK J., VLADOVIČ J. 2019. A review of the application of remote sensing data for abandoned agricultural land identification with focus on Central and Eastern Europe. Remote Sensing. DOI 10.3390/rs11232759.

INDARTO I. 2013. Variabilitas spasial hujan harian di Jawa Timur [Spatial variability of number rainy-day in East Java] [online]. Jurnal Teknik Sipil. Vol. 20. No. 2 p. 107–120. [Access 15.10.2019]. Available at: http://journals.itb.ac.id/index.php/jts

INDARTO I., MANDALA M. 2019. Final Report (Lap. Akhir) – Internal Research Grant (Hibah Keris) – Inventory and mapping of Marginal agricultural land in Situbondo Regency (Inventarisasi dan Pemetaan Lahan Sub-Optimal di Wilayah Situbondo). LP2M-Univertity of Jember. Jember.

LONGATO D., GAGLIOC M., BOSCHETTI M., GISSI E. 2019. Bioenergy and ecosystem services trade-offs and synergies in marginal agricultural lands: A remote-sensing-based assessment method. Journal of Cleaner Production. Vol. 237, 117672. DOI 10.1016/j.jclepro.2019.117672.

MANSARAY L.R., WANG F., HUANG J., YANG L., KANU A.S. 2019. Accuracies of support vector machine and random forest in rice mapping with Sentinel-1A, Landsat-8 and Sentinel-2A datasets. Geocarto International. Vol. 35. Iss. 10 p. 1088–1108. DOI 10.1080/10106049.2019.1568586.

MILBRANDT A., OVEREND R.P. 2008. Assessment of biomass resources from marginal lands in APEC Economies, August 2009 [online]. [Access. 5.04.2020]. Available at: https://www.nrel.gov

MULYANI A., SARWANI M. 2013. Karakteristik dan Potensi Lahan Sub-Optimal untuk Pengembangan Pertanian di Indonesia. [The Characteristic and Potential of Sub Optimal Land for Agricultural Development in Indonesia] [online]. Jurnal Sumberdaya Lahan Vol. 7(1) p. 47–55. [Access 26.11.2019]. Available at: http://ejurnal.litbang.pertanian.go.id/index.php/jsl/article/view/6429 DOI 10.21082/jsdl.v7n1.2013.%25p.

NYAMBO D.G., LUHANGA E.T., YONAH Z.Q. 2019. A review of characterization approaches for smallholder farmers: Towards predictive farm typologies. The Scientific World Journal. Vol. 2019. Art. ID 6121467 pp. 9. DOI 10.1155/2019/6121467.

PAYNE R. 2005. A framework for understanding poverty. 4th ed. Highland, TX. aha! Process Inc. ISBN 9781929229482 pp. 199.

QGIS 2019. QGIS Geographic Information System. Open Source Geospatial Foundation Project [online]. QGIS Development Team. [Access 2.12.2019]. Available at: http://qgis.osgeo.org

RICHARDS J.A. 2013. Remote sensing digital image analysis: An introduction, Remote Sensing Digital Image Analysis: An Introduction. Berlin–Heidelberg. Springer-Verl. DOI 10.1007/978-3-642-30062-2.

RUJOIU-MARE M.R., MARINA R., OLARIU B., MIHAI B., NISTOR C., SĂVULESCU I. 2017. Land cover classification in Romanian Carpathians and Subcarpathians using multi-date Sentinel-2 remote sensing imagery. European Journal of Remote Sensing. Vol. 50(1) p. 496–508. DOI 10.1080/22797254.2017.1365570.

SCHOWENGERDT R.A. 2007. Thematic classification. In: Remote sensing: Models and methods for image processing. 3rd ed. Academic Press, Elsevier p. 387–456. DOI 10.1016/B978-012369407-2/50012-7.

USGS 2019. Landsat levels of processing [online]. US Geological Survey. [Access 15.11.2019]. Available at: https://www.usgs.gov/land-resources/nli/landsat/landsat-levels-processing

VON COSSEL M., LEWANDOWSKI I., ELBERSEN B., STARITSKY I., VAN EUPEN M., IQBAL Y., …, ALEXOPOULOU E. 2019. Marginal agricultural land low-input systems for biomass production. Energies. Vol. 12(16), 3123. DOI 10.3390/ en12163123.

Pak. j. sci. ind. res. Ser. A: phys. sci. 2021 **64A**(3) 265-274

A Comparative Study of Support Vector Machine and Maximum Likelihood Classification to Extract Land Cover of Lahore District, Punjab, Pakistan

Fatima Mushtaq[a], Khalid Mahmood[bd]*, Mohammad Hamid Chaudhry[a], Rahat Tufail[c]
[a]Center for Geographical Information System, University of the Punjab, Lahore-54590, Pakistan
[b]Department of Space Science, University of the Punjab, Lahore-54590, Pakistan
[c]College of Earth and Environmental Science, University of the Punjab, Lahore-54590, Pakistan
[d]Remote Sensing, GIS and Climatic Research Laboratory, University of the Punjab, Lahore-54590, Pakistan

(received December 2, 2019; revised June 9, 2020; accepted July 13, 2020)

Abstract. The advent of technological era, the scientists and researchers develop machine learning classification techniques to classify land cover accurately. Researches prove that these classification techniques perform better than previous traditional techniques. In this research main objective is to identify suitable land cover classification method to extract land cover information of Lahore district. Two supervised classification techniques i.e., Maximum Likelihood Classifier (MLC) (based on neighbourhood function) and Support Vector Machine (SVM) (based on optimal hyper-plane function) are compared by using Sentinel-2 data. For this optimization, four land cover classes have been selected. Field based training samples have been collected and prepared through a survey of the study area at four spatial levels. Accuracy for each of the classifier has been assessed using error matrix and kappa statistics. Results show that SVM performs better than MLC. Overall accuracies of SVM and MLC are 95.20% and 88.80% whereas their kappa co-efficient are 0.93 and 0.84 respectively.

Keywords: maximum likelihood classification, support vector machine, land cover, accuracy assessment, kappa statistics

Introduction

Land cover and land use. Land is a basic necessity for living beings and its utility varies from purpose to purpose. Generally, it is described as a space on the surface of the earth at which living beings perform their activities. It is multi-resource base for mankind as it provides shelter, forestry, fruits, vegetables, water, and clothes. Nation's economy and growth mainly depends upon the land of that region (Chiemelu and Onwumere, 2013). Usually land cover and land use is misunderstood and think of alternate of each other but in reality it's the opposite. Land cover represents the physical material at the earth's surface like urban buildings, forests, meadows, snow, lakes, mountains, whereas land use is described as how this physical material is used by human beings like residential, commercial, and recreational (Brar, 2013). Lahore is the metropolitan city in Punjab Province of Pakistan and recent infrastructure change in the land cover expands the urban area (Riaz *et al*., 2014).

*Author for correspondence; E-mail: khalid.spsc@pu.edu.pk
khalid.m270@yahoo.com

Role of remote sensing and GIS in land cover. Land cover directly impacts the diversity of living beings, water cycle of region and quality of environment. Important information of the land cover is now easily monitor and directly record with the help of remote sensing instruments (Abdi, 2020; Ngo *et al*., 2020; Cui, 2019). Advancement in remote sensing (RS) and geographical information system (GIS) techniques provides remarkable applications which helps in understanding the complex dynamics of environment. In this regard spatial analysis like mapping of land cover, land cover change detection and land cover classification are playing vital role in providing important land cover information not only at local but also at global level (Gupta and Srivastava, 2010). With the help of appropriate correlation tools of remote sensing and GIS, land cover information can be handled accurately and can be mapped timely with limited labour. In remote sensing satellite data application, accuracy of land cover classification is highly preferable (Wulder *et al*., 2018; Hutt *et al*., 2016).

Parametric and non-parametric classifiers. Parametric and non-parametric classifiers are the most generalized

terms in classification techniques. Parametric classifiers consider that the data distribution for each individual class is normal. The most popular, conventional and widely used parametric classifier is Maximum Likelihood Classification (MLC). Based upon the mean and covariance of the data this classifier generates decision surfaces (Srivastava *et al*., 2012). Non-parametric classifier is not based upon the normal distribution of the data and assumption about statistical nature of the data is negligible. One of the non-parametric classifiers is the support vector machine which consists of various machine learning algorithms and is used for classification purpose (Varma *et al*., 2016). In 1971, SVM theory is proposed as a binary classification method by Vapnik and Chervonenkis and details of SVM was discussed by Vapnik in 2000. SVM being an artificial intelligence machine learning algorithm have been used in diverse applications of remote sensing (Varma *et al*., 2016; Taati *et al*., 2015; Ustuner *et al*., 2015).

Current problems and challenges. Satellite remote sensing is the most advance technology of this era and provides timely and accurate geospatial information of land cover of any region all around the world (Puletti *et al*., 2018; Olmanson and Bauer, 2017). Researchers and scientists reviewed numerous image classification techniques to extract and map land cover information (Thanh and Kappas, 2018). Today, various satellites have been launched and data availability is not the issue anymore but the real problem lies when it comes to its processing. Classification of these satellite data and extraction of important information without compromising its accuracy is the real challenge. Conventional classification methods have their limitations in processing high dimension image data in large amount, as this data also contains diverse spectral characteristics and spatial distribution of objects on the surface of the earth. Also, it is difficult and sometimes not possible to obtain complete sample sets and priori knowledge. So, common methods fail to overcome these challenges as they lack the ability of self-learning process (Abdi, 2020; Ngo *et al*., 2020; Cui, 2019).

To overcome these limitations machine learning techniques are playing vital role as they self-learn through the mechanism. Many researches have been conducted to find the best technique for land cover classification but to know the most suitable technique more comparative studies are required. Nitze *et al*. (2012) has compared three such machine learning classifiers with the conventional technique to classify different crop types. With the help of rapideye (5m resolution) data SVM significantly gave better performance. The overall accuracy obtained by SVM method was 68.6 %. Similarly, Thanh and Kappas, 2018, compared and examined the performances of three classifiers using sentinel-2 (10 m resolution) satellite data which are random, k-nearest neighbour, and support vector machine. Classification results show high overall accuracy in between 90-95 %. But SVM showed the highest overall accuracy in comparison with the other classifiers.

The study in hand has tended to compare and evaluate two of the supervised classifiers, one is Support Vector Machine (SVM) and the other is Maximum Likelihood Classification (MLCC). The suitable method is identified using remote sensing satellite data of Sentinel-2 by comparing the classification accuracy in the Lahore district, Punjab Pakistan.

Materials and Methods

Study area. Lahore is the capital of Punjab province and a rapidly growing metropolitan has been chosen as the study area in this research. Associations of the study area are shown in Fig. 1. Lahore is one of the developed districts in Punjab Pakistan. In terms of population and urban sprawl, Lahore is the second largest city in Pakistan after Karachi. It stretches over an area of 1772 km^2 (Riaz *et al*., 2014) and population is about 11.13 million (Census, 2017). It is located in the north-eastern part of the Punjab province and lies on the left bank of Ravi river. Its geographical extension lies within latitude from 31°15' N to 31°44'2" N and longitude from 74°1'1"E to 74°38'10"E. Because of the river, its land is composed of fertile alluvial plain with a slope towards south east. Its underground water table is about 35 – 40 km deep (non-drinkable) and range of height above the sea level is between 680 to 700 feet with 1 feet slope gradient after every 5 to 10 km. The water used for drinking purpose is available at the depth of 125-150 m (Riaz *et al*., 2014). It is located in subtropical climatic zone and its temperature and rainfall varies. The only precipitation source of this area is monsoon season (Sajjad *et al*., 2015). Soil and climate of this region is suitable for every type of crops (Riaz *et al*., 2014).

Data sets. The Sentinel-2A datasets used in this study are acquired from Copernicus open access hub which is operated by European space agency (ESA) on 29th March 2018, with no cloud covering the area. Study area does not lie in one grid that's why two images

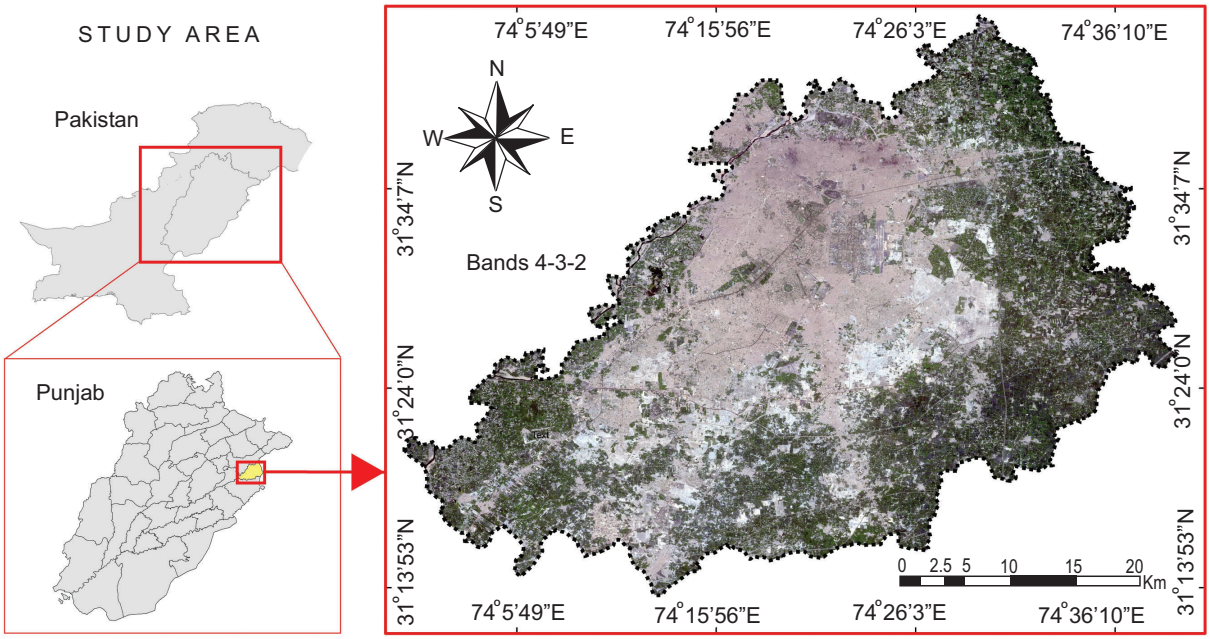


Fig. 1. Map of study area.

were used from MSI sensor with reference numbers of T43SDR and T43RDQ under the reference grid system of Sentinel-2. To minimize the seasonal effect, both images were selected with similar calendar date. The total 10 bands (optical, near infrared and short wave infrared bands) of sentinel-2A dataset were selected for image classification. Spectral and spatial ranges of these 10 bands can be seen in Table 1. In order to minimise the computational time a subset of images according to vector district boundary was considered in the study. Four different sets of representative training polygons were created using stratified random sampling technique. Map of 400 training samples can be seen in Fig. 2. In addition, 250 reference points were also collected through surveying the study area for accuracy assessment or validation (Fig. 3).

Table 1. Spectral and spatial information of sentinel-2

Spectral bands	Wavelength description	Wavelengths (im)	Resolution (m)
2	Blue	0.490	10
3	Green	0.560	10
4	Red	0.665	10
5	Vegetation red edge	0.705	20
6	Vegetation red edge	0.740	20
7	Vegetation red edge	0.783	20
8	NIR	0.842	10
9	Narrow NIR	0.865	20
12	SWIR	1.610	20
13	SWIR	2.190	20

Satellite image interpretation. Atmospheric corrections are not always required for image classification when the acquisition date of satellite image is same specifically when desired classes are computed from spectral signature but it is very important when one wants to do change detection (Chrysoulakis *et.al*., 2010). According to Vanonckelen *et al*. (2013), atmospheric corrections are necessary when more than one image is used at different temporal level. The Sentinel-2A imagery had already been corrected atmospherically and geometrically,

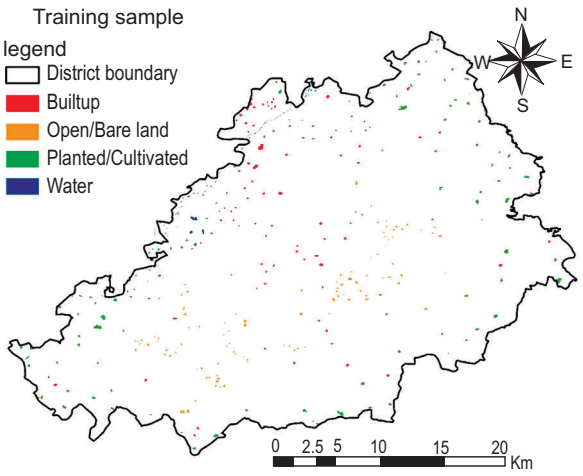


Fig. 2. Spatial distribution of training samples.

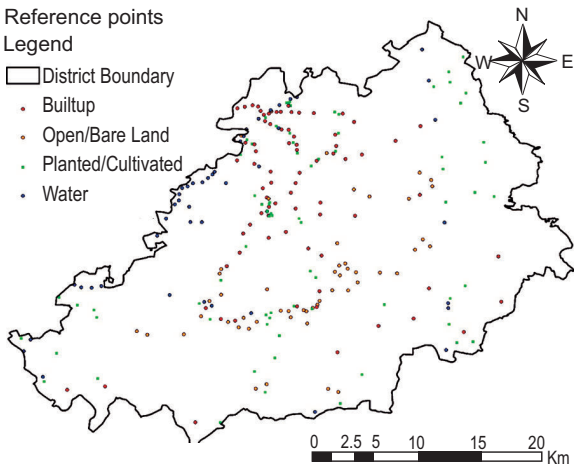


Fig. 3. Spatial distribution of reference/validation data.

and ortho-rectified. The Sentienl-2A imagery was imported into Erdas Imagine 2014 software and geo-referencing of the image was initially checked with a vector data layer of the area. The layers were stacked together and the output image file was ready to be used. The swath width of these satellite images was 290 km by 290 km so the images were subset to study area in order to get a small portion of the image from large data file. In this way unnecessary imagery data cut off from the image and better analysis could be performed at the study area.

Sub-setting of the data also speeds up the processing time of the image especially in the case of SVM image

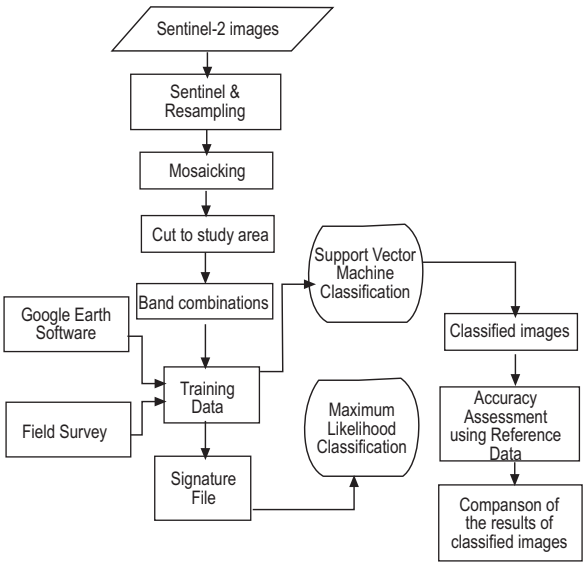


Fig. 4. Flow chart of methodology.

classification. Same number of bands is used and orderly stacked (Band 2, 3, 4, 5, 6, 7, 8, 9, 11, 12) to minimize the biasness which is usually caused by using different band combination. In this research sampling of the training area and reference data is generated using polygon and point vector design respectively, for each land cover type. Erdas Imagine and R software is used for classification in this research. For the selection of land cover types, expert opinion, Google Earth imagery and different band combinations were applied. Four land cover classes were determined from Sentinel-2A satellite imagery in the year of 2018.

Maximum likelihood classification (MLC). The MLC method examines statistical data like covariance and variances of the selected class signatures when assigning values to the unknown pixels from represented class signature file. This method is based upon Bayes' theorem of decision making in which the distribution of the data in multidimensional space is linear or normal. With this assumption of linear distribution, covariance matrix and mean vector specifies a class. These two parameters are given to each pixel value. In order to compute the cell relevance to the class, statistical probability is calculated for each class. With prior specification of weightage each pixel has been identified to be a member of landcover class to which it has highest similarity under the rules (Srivastava *et al*., 2012). Likelihood of unknown value from known class value is calculated by the following Bayesian equation (1) (Otukei and Blaschke, (2010).

$$D = \ln(a_c) - [0.5\ln(|cov_c|)] - [0.5(X - M_c)\, T(cov_c - 1)(X - M_c)] \quad \text{..... (1)}$$

where;

D = likelihood/ weighted distance; ac = probability percentage that any candidate pixel is a member of class c (is entered from a priori knowledge or default to 1.0); c = specific class; X= measurement candidate pixel; cov_c = covariance matrix of the pixels in the sample of class c; Mc = mean vector of the sample class c; $|cov_c|$ = determinant of covariance matrix; cov_c-1 = inverse of covariance matrix; ln = natural logarithm function; T = transposition function

Support vector machine (SVM) classification. SVM uses kernel functions defined by users in order to map the non-separable decision boundaries from an original dataset into separable decision boundaries of feature

space or higher multi-dimensional space. SVMs are non-parametric supervised learning algorithms based on statistics. The algorithm finds an Optimal Separating Hyper-plane (OSH) between each pair of classes. This OSH is obtained by using training data from the study area. Therefore, the main purpose of SVM is to find out the OSH among all other separating hyper-planes which is achieved through an optimization problem by using quadratic programming methods and Lagrange multipliers (Szuster *et al*., 2011). All hyper-planes separate two classes but OSH minimizes the generalization error in classification by maximizing the margins (distance) between the two classes. The support vectors are that data points which lie at the edge of each class hyper-plane in higher multi-dimensional space and are very close to the OSH (Szuster *et al*., 2011). Suppose training dataset with n number of samples, represented as:

$\{xi, yi\}, i = 1, 2, …., n$

where;

xi = Lm (m-dimensional vector); yi = {-1, +1}, (1 represents each class label)

If a vector W and scalar b can satisfy the following two inequality equations (equation (2) and equation (3)) then training dataset can be linearly separated. Equation (4) represents the constraint that must be satisfied in order to achieve a completely and linearly separable hyper-plane between two classes.

$W. xi – b = 1$ for all $y = +1$ ..... (2)

$W. xi – b = 1$ for all $y = –1$ ..... (3)

$yi (W . xi – b) = 1$ ..... (4)

Compared to traditional approaches researches shows that SVM algorithms produce results of higher accuracies and depends on following three parameters i.e. the kernel, its parameters and algorithm of SVM.

Scheme of classification. Keeping in view the scope and the spatial (10m) resolution of the image following scheme was developed Fig. 4. and Table 2.

- **Built-up area:** land use area consists of construction material i.e., commercial, industrial, road network and residential
- **Planted/cultivated area:** this area includes land under various crops, parks and green belts
- **Water bodies:** contains river, lakes, ponds and lakes
- **Open/ bare area:** consists of undeveloped land and open spaces

Table 2. Land cover classification scheme and training points

Classes	Actual land cover type (satellite image)	Training polygons	Validation pixels
Built up area	Residential, commercial, industrial, road network and educational area	25 50 75 100	78
Planted/ cultivated area	Parks, cultivated and non-cultivated lands	25 50 75 100	75
Water bodies	Open water land	25 50 75 100	45
Open/ bare area	Barren land, sand, recreational and undeveloped land	25 50 75 100	52

To overcome the noise problem, polygon based approach is used. MLC is performed in Erdas imagine 2014 software while SVM is performed in R software.

Accuracy assessment. Accuracy assessment of the classifiers is evaluated with the help of reference datasets. Error matrix or confusion matrix measures the accuracy of the classification result by comparing it with validation data. Kappa co-efficient is a well-known parameter in accuracy assessment and was computed by the following equation 5:

$$K = \frac{N\Sigma^{r}_{i=1} X_{ii} - \Sigma^{r}_{i=1}(x_{i+})(x_{+i})}{N^2 - \Sigma^{r}_{i=1}(x_{i+})(x_{+i})} \quad \text{..... (5)}$$

where;

N = number of observations; r = number of rows in matrix; X_{ii} = number of observation in ith row and column; X_{+i} = marginal total of r row; X_{i+} = marginal total of ith column.

Overall accuracy measures ratio of the correctly classified pixels to number of reference pixels, whereas producer's accuracy is the count of accurate pixels, among total pixels of same category. While the user's accuracy measures overall accuracy, not class specific. The

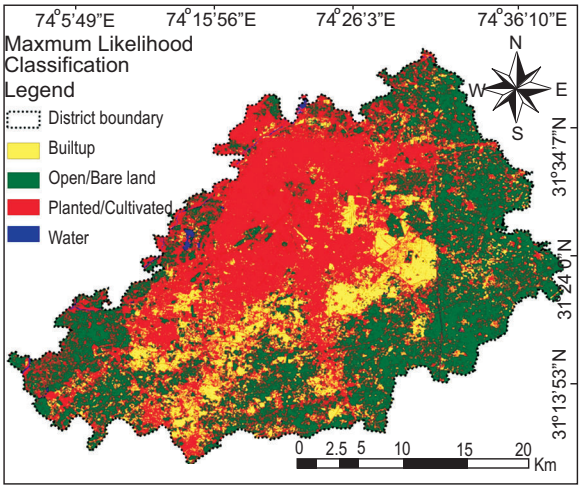


Fig. 5. Land cover map produced using MLC of Sentinel-2 for year 2018

producer's accuracy and user's category measurements are actually related to error of omission and error of commission respectively (Gupta and Sirivasstava, 2010).

Results and Discussion

MLC results. Land cover classification maps for 10-m resolution Sentinel-2 image were produced using MLC method. Four different training sample size were used i.e. 100, 200, 300 and 400 in order to know the effect of training dataset size. These datasets show different percentages of overall accuracy (Fig. 5).

An increase in the number of training samples size decreases the overall accuracy in MLC. It is due to the fact that in MLC decision boundaries are produced with the help of likelihood pixels not from learning algorithm and an increase in the number of training pixels' size, mean and median parameter of the dataset changes and mixed pixel problem generates. Accuracy of MLC is highly dependent on training samples. Abrupt trend can be seen in Fig. 6, as accuracy is not directly and inversely proportional to the size of training sample but general trend shows inverse relation. The highest overall accuracy of MLC (88.80 %) was computed using 100 training polygon sizes while lowest overall accuracy was 80.80 % using 400 dataset size (Fig. 6). Overall accuracy and kappa statistics of MLC with various dataset sizes can be seen in Table 3.

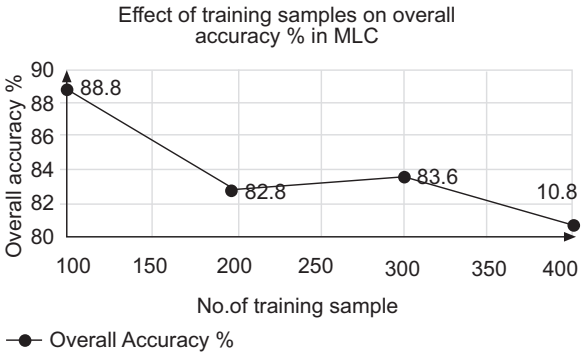


Fig. 6. Effect of training samples on overall accuracy in MLC.

SVM results. SVM classification also performed on same datasets i.e. Sentinel-2 and four different training data size. Overall accuracy of SVM increases as the number of training dataset increase but the effect of sample size is minor (Fig. 7).

SVM is a machine learning technique and when training sample size increases, algorithm has more data to find support vectors that achieve larger margin and as a result

Table 3. Overall Accuracy and Kappa statistics of MLC and SVM in tabular form

No of training datasets	MLC		SVM	
	Overall accuracy %	Kappa statistics	Overall accuracy %	Kappa statistics
100	88.80	0.8462	94.00	0.9188
200	82.80	0.7662	94.40	0.9241
300	83.60	0.7782	94.80	0.9294
400	80.80	0.7375	95.20	0.9348

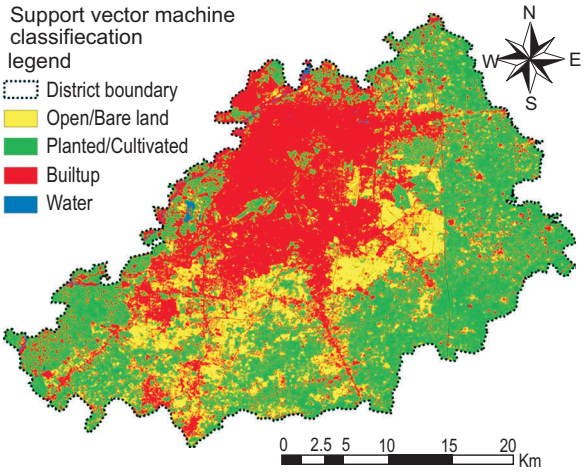


Fig. 7. Land cover map produced using SVM of Sentinel-2 for year 2018.

generalization error become minimum. The highest overall accuracy using SVM algorithm is 95.00 % and the number of training dataset (400) is also maximum (Fig. 8). Table 3 shows the kappa statistics and overall accuracy of SVM using different sizes of training datasets.

Comparison of MLC and SVM. Highest overall accuracy results from both of the classification techniques were selected for the comparison. Number of training samples for each classification method is different i.e. 100 for MLC and 400 for SVM. Error matrices for each classification method were produced in order to analyse land cover class separation performance for each method with overall accuracies. Difference is obvious between two methods:

The accuracy of land cover classification in SVM method is not dependent upon size of the training samples and results are almost same with smaller or larger number of training sample. In contrast to it, accuracy of land cover classification in MLC method is highly dependent upon the size of the training sample (Fig. 9). While selecting the size, a researcher has to be very careful.

Also SVM method shows more spatially cohesive map than that of MLC. Built-up areas are also more delineated with SVM method, and accuracy values reflect these differences. The MLC method produced the lower overall accuracy of 88.80 % as expected. MLC separates the planted/cultivated land and open/bare land effectively while it is less effective in case of water and built-up. Out of 45 water pixels, it only classifies 30 pixels correctly.

It is due to the mixed pixel problem. As water pixels are mixed with built-up and planted/cultivated pixels. Similarly, built-up pixels are mixed with open/bare land and out of 78 pixels 76 pixels are classified correctly through MLC method. Of this overall accuracy, the water cover class yielded the lowest producer's accuracy

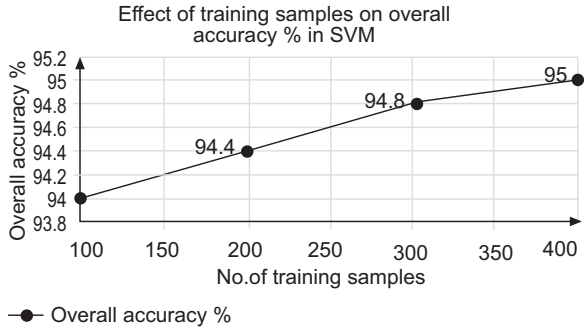


Fig. 8. Effect of training samples on overall accuracy in SVM.

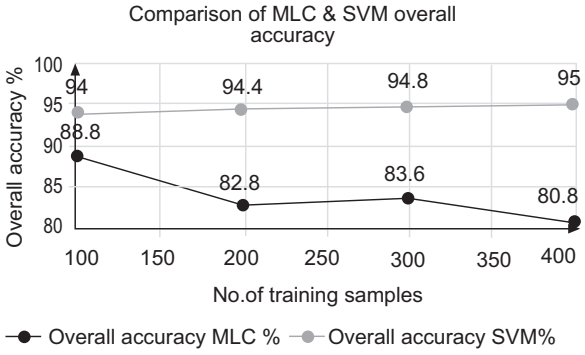


Fig. 9. Overall accuracy comparison between MLC and SVM.

of only 66.67 %. The other three classes were fair, with the producer's accuracy of 97.44 % for the built-up area class, 93.33 % for the planted/cultivated class and 88.46 % for the open/bare class Table 4.

The SVM method produced a higher accuracy, with an overall accuracy of 95.20 %. This method also provided higher user's accuracy for each land cover class. It behaves differently in respect to separate every class and provides significant separating hyper-plane for each class than the decision boundaries in MLC. Built-up land had the greatest increase from 80.00 % using MLC method to 90.24 % with the SVM method. Open/bare class had increase of 5 % in accuracy using SVM approach. Planted/cultivated class increased only moderately with a 2 % increase while water accuracy remains the same (Table 4). Although both the classifiers have resulted into good accuracy and reliability but SVM is found relatively better than MLC. A similar result for this comparison has been reported by Szuster *et al*. (2011) for Thailand. He has used ASTER data with spatial resolution of 15 m and have successfully obtained accuracy of 94.15% and 93.9% for SVM and MLC respectively. The use of better spatial and spectral resolutions in the current study has improved this accuracy to 95.20% for SVM. This comparison is clearly indicating supremacy of higher spatial resolution. Another difference found by current study is the accuracy gap between both the classifiers which is higher than shown by Szuster *et al*. (2011) and is surely controlled by spatial resolution of the used data.

Kappa statistics. Highest Kappa coefficients of both the classification techniques were compared. It is interesting to note that kappa coefficient of water class in both classification is 1 because the number of total classified pixels and the number of total correct classified

Table 4. Land cover classification accuracy (%) of two classifiers.

		SVM			
Classes name	Built up	Open/ Bare land	Planted/ Cultivated land	Water	Total
Classified totals	82	49	74	45	250
Reference totals	78	52	75	45	250
No of correct points	74	48	71	45	238
Producers accuracy (%)	94.87	92.31	94.67	100.00	….
Users accuracy (%)	90.24	97.96	95.95	100.00	….
Overall accuracy	95.20 %				
		MLC			
Classes name	Built up	Open/ Bare land	Planted/ Cultivated land	Water	Total
Classified totals	95	50	75	30	250
Reference totals	78	52	75	45	250
Number of correct points	76	46	70	30	222
Producers accuracy (%)	97.44	88.46	93.33	66.67	…
Users accuracy (%)	80.00	92.00	93.33	100.00	…
Overall accuracy	88.80 %				

pixels are same in both methods (45 in SVM and 30 in MLC) but the number of misclassified pixels are large in MLC than SVM. Other three classes also show remarkable accuracy in SVM method. Kappa accuracy increases 0.15 in built-up land cover from 0.70 in MLC to 0.85 in SVM, 0.04 in planted/cultivated land cover from 0.90 in MLC to 0.94 in SVM and 0.08 in open/bare land cover from 0.89 in MLC to 0.97 in SVM. Therefore, SVM shows overall kappa accuracy of 0.93 and MLC shows 0.84 (Table 5).

Srivastava *et al*. (2012) recorded Kappa accuracy of SVM as 0.74 higher than MLC which is 0.71. The difference is less because number of bands used in this study was four (Landsat TM), while bands used in this research are ten (Sentinel-2). Besides this the total numbers of correct classification pixels were 236 out of 250 in SVM and 202 out of 250 in MLC. Range of kappa coefficient is from -1 to 1. 0 indicates that classification is no better than a random classification. -1 indicates that classification is worse than the random classification while values close and equal to 1 indicate that classification is remarkably better than the random classification.

Areal statistics of MLC and SVM. Area from built-up land cover from MLC and SVM methods are 779.43 km^2 and 670.96 km^2 respectively. The complete areal statistics of each land cover class using SVM and MLC methods is shown in Table 6.

With the help of MLC and SVM results, spatial similarity of each land cover class has been calculated. About 277.22 km^2 area is computed as dissimilar spatial area

Table 5. Kappa statistics

Classes name	Built up	Open/ bare land	Planted/ cultivated land	Water	Overall kappa statistic
MLC	0.70	0.89	0.90	1.00	0.84
SVM	0.85	0.97	0.94	1.00	0.93

while, 1483.83 km^2 area is computed as spatially similar. Thus, the unmatched and matched areas correspond to 15.74 % and 84.17 respectively. Figure 10 shows the matched and unmatched spatial similarity of the both classification results.

Conclusion and recommendation. Mapping a heterogeneous land cover types is always a task for researchers. The findings of this study suggests that with the help of medium scale imagery (10-m Sentinel-2), support vector machine classifier can outstands its performance in comparing with the other classifier and can be used as a suitable land cover classification tool with an overall accuracy of 95.20 % and kappa coefficient of 0.93. Also, SVM performed better in higher dimensional data and classify the mixed classes over the Lahore district. Whereas the other compared technique of maximum likelihood classifier has resulted into an overall accuracy of 88.80 % with kappa coefficient of 0.84. The sample data taken to check accuracy of the classifiers is Sentinal-2A, so it may be concluded here that SVM performs better than MLC for spectral ranges and resolution of Sentinel-2A images and may varies if used with other datasets having different spectral ranges. As the accuracy of SVM is very good, it is recommended to use for hyper-

Table 6. Areal statistics of MLC and SVM

land classes		Built up	Open/ Bare land	Planted/ Cultivated land	Water	Total
MLC	Area (km^2)	557.68	392.23	806.10	7.87	1762.74
	Area (%)	31.63	22.27	45.72	0.44	100
SVM	Area (km^2)	715.17	294.07	743.10	12.40	1762.74
	Area (%)	40.57	16.70	42.15	0.72	100

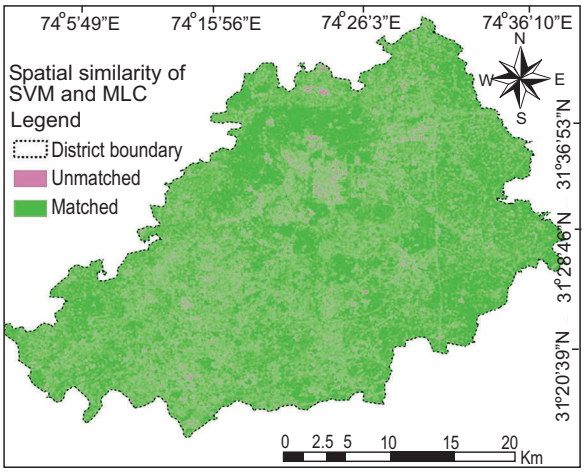


Fig. 10. Spatial similarity of SVM and MLC.

spectral imageries. Accuracy of SVM is based upon the kernel and parameter. So a sensitivity analysis of different kernels can be performed to extract the land cover information. More classes can be added to cultivated/agricultural land cover in order to extract detailed information about crop types in the specific area and built-up area can be further divided into dense, moderate, low density areas so that population density can be estimated precisely. High resolution satellites are recommended for classification purposes because they serve the diverse needs and various applications of urban and agricultural development, risk assessment and planning and policy making. In this regard, Pakistan has launched its first high resolution remote sensing satellite (PRSS) and its data availability will be very useful to classify different land cover of Pakistan accurately.

Conflict of Interest. The authors declare no conflict of interest.

References

Abdi, A.M. 2020. Land cover and land use classification performance of machine learning algorithms in a boreal landscape using Sentinel-2 data. *GIScience & Remote Sensing*, **57:** 1-20. (https://doi.org/10.1080/15481603.2019.1650447)

Brar, G.S. 2013. Detection of land use and land cover change with Remote sensing and GIS: A case study of Punjab Siwaliks. *International Journal of Geomatics and Geosciences*, **4:** 296-304. (https://www.semanticscholar.org/paper/Detection-of-land-use-and-land-cover-change-with-A-Brar/1667abddcd5cb786cbb68543c26580f2d3555f20)

Census. 2017. Provisional summary results of 6th population and housing census-2017. Pakistan bureau of statistics. (http://www.pbs.gov.pk/content/provisional-summary-results-6th-population-and-housing-census-2017-0)

Chiemelu, N.E., Onwumere, V.O. 2013. Land information systems for efficient land administration and revenue generation: a case study of tans-amadi industrial layout. Port Harcourt, Nigeria, *Journal of Information Engineering and Application*, **3:** 13-23. (https://www.iiste.org/Journals/index.php/JIEA/article/view/8920)

Chrysoulakis, N., Abrams, M., Feidas, H., Arai, K. 2010. Comparison of atmospheric correction methods using ASTER data for the area of Crete, Greece. *International Journal of Remote Sensing*, **31:** 6347-6385. (https://www.researchgate.net/publication/253497600)

Cui, H.S. 2019. Sub-urban land classification using GF-2 images and support vector machine method. In: *Proceedings of International Conference on Advances in Civil and Ecological Engineering Research*, pp. 351 012028, Kaohsiung, Taiwan. (https://iopscience.iop.org/article/10.1088/1755-1315/351/1/012028/meta)

Gupta, M., Srivastava, P.K. 2010. Integrating GIS and remote sensing for identification of groundwater potential zones in the hilly terrain of Pavagarh, Gujarat, India. *Water International*, **35:** 233-245. (https://www.tandfonline.com/doi/full/10.1080/0

2508061003664419)

Hütt, C., Koppe, W., Miao, Y., Bareth, G. 2016. Best accuracy land use/land cover (LULC) classification to derive crop types using multi-temporal, multi-sensor, and multi-polarization SAR satellite images. *Remote Sensing*, **8:** 684. (https://doi.org/10.3390/rs8080684)

Ngo, K.D., Lechner, A.M., Vu, T.T. 2020. Land cover mapping of the Mekong delta to support natural resource management with multi-temporal Sentinel-1A synthetic aperture radar imagery. Remote Sensing Applications: *Society and Environment*, **17:** 100272. (https://doi.org/10.1016/j.rsase.2019.100272)

Nitze, I., Schulthess, U., Asche, H. 2012. Comparison of machine learning algorithms random forest, artificial neural network and support vector machine to maximum likelihood for supervised crop type classification. In: *Proceedings of 4th GEOBIA,* pp. 35, Rio de Janeiro - Brazil. (https://www.researchgate.net/profile/Ingmar_Nitze/publication/275641579)

Olmanson, L.G., Bauer, M.E. 2017. Land cover classification of the lake of the woods/rainy river Basin by object-based image analysis of Landsat and lidar data. *Lake and Reservoir Management*, **33:** 335-346. (https://doi.org/10.1080/10402381.2017.1373171)

Otukei, J.R., Blaschke, T. 2010. Land cover change assessment using decision trees, support vector machines and maximum likelihood classification algorithms. *International Journal of Applied Earth Observation and Geoinformation*, **12:** S27–S31. (https://doi.org/10.1016/j.jag.2009.11.002)

Puletti, N., Chianucci, F., Castaldi, C. 2018. Use of Sentinel-2 for forest classification in Mediterranean environments. *Annals of Silvicultural Research*, **42:** 32-38. (http://dx.doi.org/10.12899/asr-1463)

Riaz, O., Ghaffar, A., Butt, I. 2014. Modelling land use patterns of Lahore (Pakistan) using remote sensing and GIS. *Global Journal of Science Frontier Research*. *Environment & Earth Science*, **14:** 24-30. (https://www.researchgate.net/profile/Omar_Riaz/publication/281741257)

Sajjad, S.H., Batool, R., Qadri, S.T., Shirazi, S.A., Shakrullah, K. 2015. The long-term variability in minimum and maximum temperature trends and heat island of Lahore city, Pakistan. *Science International*, **27:** 1321-1325. (https://www.researchgate.net/profile/Sm_Talha_Qadri/publication/280802787)

Srivastava, P.K., Kiran, G., Gupta, M., Sharma, N., Prasad, K. 2012. A study on distribution of heavy metal contamination in the vegetables using GIS and analytical technique. *International Journal of Ecology & Development*, **21:** 89-99. (http://www.ceserp.com/cp-jour/index.php/ijed/article/view/3936)

Szuster, B.W., Chen, Q. Borger, M.A. 2011.comparison of classification techniques to support land cover and land use analysis in tropical coastal zones. *Applied Geography*, **31:** 525-532. (https://doi.org/10.1016/j.apgeog.2010.11.007)

Taati, A., Sarmadian, F., Mousavi, A., Pour, C.T.H., Shahir, A.H.E. 2015. Land use classification using support vector machine and maximum likelihood algorithms by Landsat 5 TM images. *Walailak Journal of Science and Technology*, **12:** 681-687. (https://doi.nrct.go.th//ListDoi/listDetail?Resolve_DOI=10.14456/wjst.2015.33)

Thanh N.P., Kappas, M. 2018. Comparison of random forest, k-nearest neighbor, and support vector machine classifiers for land cover classification using Sentinel-2 imagery. *Sensors*, **18:**18. (https://doi.org/10.3390/s18010018)

Ustuner, M., Sanli, F.B., Dixon, B. 2015. Application of support vector machines for landuse classification using high-resolution RapidEye images: a sensitivity analysis. *European Journal of Remote Sensing*, **48:** 403-422. (https://doi.org/10.5721/EuJRS20154823)

Vanonckelen, S., Lhermitte, S., Rompaey, A.V. 2013. The effect of atmospheric and topographic correction methods on land cover classification accuracy. *International Journal of Applied Earth Observation and Geoinformation*, **24:** 9-21. (https://doi.org/10.1016/j.jag.2013.02.003)

Varma, M.K.S., Rao, N.K.K., Raju, K.K., Varma, G.P.S. 2016. Pixel-based classification using support vector machine classifier. In: *Proceedings of IEEE 6th International Conference on Advanced Computing*, pp. 51-55, Bhimavaram, India (https://ieeexplore.ieee.org/abstract/document/7544809)

Wulder, M.A., Coops, N.C., Roy, D.P., White, J.C., Hermosilla, T. 2018. Land cover 2.0. *International Journal of Remote Sensing*, **39:** 4254-4284. (https://doi.org/10.1080/01431161.2018.1452075)

JPIG (Jurnal Pendidikan dan Ilmu Geografi)
Vol. 9, No. 2, September 2024
Halaman: 120-129
Online: http://ejournal.unikama.ac.id/index.php/JPIG/



Analisis Perubahan Penggunaan Lahan Menggunakan Citra Sentinel-2 Di Kecamatan Percut Sei Tuan Tahun 2018 - 2022

Immanuel Sinabang[1*], Klarita Dwijayanti Waruwu[2], Adesiana Sihombing[3], Adeline[4], Eni Yuniastuti[5]
[1,2,3,4,5]Jurusan Pendidikan Geografi, Fakultas Ilmu Sosial, Universitas Negeri Medan
Email: [*]imanuelsinabang@gmail.com, klarytadwijayanti@gmail.com, adesianasihombing2020@gmail.com, stplalin@gmail.com, enigeografi2023@gmail.com

Dikirim: 22 Juni 2024; Revisi:9 September 2024; Diterima: 17 September 2024

Abstrak: Pertumbuhan penduduk merupakan pendorong utama perubahan tutupan/penggunaan lahan secara umum karena mengarah pada pembangunan ekonomi, yang pada gilirannya membutuhkan ketersediaan lahan untuk penggunaan lahan lainnya, termasuk infrastruktur, jasa, industri, dan permukiman. Menggunakan simbolisme satelit penginderaan jauh untuk merencanakan penggunaan lahan di wilayah yang luas adalah salah satu pendekatan yang dapat dilakukan. Penelitian ini bertujuan untuk menganalisis perubahan penggunaan lahan di Kecamatan Percut Sei Tuan, Kabupaten Deli Serdang, Sumatera Utara pada periode 2018-2022 menggunakan citra satelit Sentinel-2. Metode yang digunakan adalah interpretasi visual citra satelit dengan bantuan perangkat lunak ArcGIS dan analisis perbandingan data spasial multi-temporal. Hasil penelitian menunjukkan terdapat 8 kelas penggunaan lahan yaitu badan air, hutan, sawah, perkebunan, lahan terbangun, tanah terbuka, awan, dan semak belukar. Perubahan penggunaan lahan yang signifikan terjadi pada lahan terbangun yang mengalami penambahan sebesar 627 hektar (dari 34% menjadi 37% total luas wilayah), sementara luas hutan berkurang 521 hektar (dari 8% menjadi 5%). Perubahan ini mengindikasikan adanya konversi lahan dari area hutan dan lahan produktif lainnya menjadi kawasan terbangun, yang didorong oleh pertumbuhan penduduk dan kebutuhan infrastruktur. Penelitian ini menyimpulkan bahwa monitoring perubahan penggunaan lahan secara berkala sangat diperlukan untuk mendukung perencanaan tata ruang dan pengelolaan sumber daya lahan yang berkelanjutan.
Kata kunci: Citra Satelit, Penggunaan Lahan, Perubahan Penggunaan Lahan

Abstract: Population growth is a major driver of land cover/use change in general as it leads to economic development, which in turn requires land availability for other land uses, including infrastructure, services, industry and settlements. Using the symbolism of remote sensing satellites to plan land use over large areas is one approach that can be taken. This study aims to analyze land use change in Percut Sei Tuan District, Deli Serdang Regency, North Sumatra in the 2018-2022 period using Sentinel-2 satellite imagery. The method used is visual interpretation of satellite images with the help of ArcGIS software and multi-temporal spatial data comparison analysis. The results showed that there were 8 land use classes, namely water bodies, forests, rice fields, plantations, developed land, open land, clouds, and shrubs. Significant land use change occurred in built-up land which increased by 627 hectares (from 34% to 37% of the total area), while forest area decreased by 521 hectares (from 8% to 5%). These changes indicate land conversion from forest areas and other productive lands to built-up areas, driven by population growth and infrastructure needs. This study concludes that regular monitoring of land use change is necessary to support spatial planning and sustainable land resource management.
Keywords: Satellite Imagery, Land Use, Land Use Change

This is an open access article under the CC–BY license.

https://doi.org/ 10.21067/jpig.v9i2.10348

Pendahuluan

Kecamatan Percut Sei Tuan merupakan salah satu wilayah di Kabupaten Deli Serdang, Sumatera Utara yang mengalami perkembangan pesat dalam beberapa tahun terakhir. Diduga penggunaan lahan di daerah ini telah berubah sebagai akibat dari pertumbuhan penduduk, pembangunan perumahan, kawasan industri, dan infrastruktur. Pemantauan perubahan penggunaan lahan secara berkala sangat diperlukan untuk mengevaluasi pola perubahan yang terjadi dan menentukan arahan kebijakan tata ruang wilayah yang tepat.

Lahan adalah suatu wilayah pada lapisan terluar bumi yang sifat-sifatnya (kualitas) menggabungkan setiap sifat yang sangat mantap atau yang dapat dianggap berulang dari biosfer, iklim, tanah, geografi, hidrologi, tumbuhan, dan populasi makhluk hidup serta efek samping dari latihan manusia sebelumnya. terlebih lagi, saat ini, selama pengidentifikasi ini secara mendasar memengaruhi penggunaan lahan di masa sekarang dan di kemudian hari.(Indah et al., 2019). Perubahan lahan dicirikan sebagai pergeseran penggunaan seluruh atau sebagian lahan dari penggunaan semula menjadi penggunaan yang berdampak negatif terhadap lingkungan dan potensi lahan (Miswar et al., 2020). Menurut Suban & Sunimbar (2021) menyatakan bahwa alih fungsi lahan mengakibatkan perubahan penggunaan lahan. Sementara itu menurut Kubangun (dalam Akbar et al., 2022) menyatakan bahwa pertumbuhan penduduk merupakan pendorong utama perubahan tutupan/penggunaan lahan secara umum karena mengarah pada pembangunan ekonomi, yang pada gilirannya membutuhkan ketersediaan lahan untuk penggunaan lahan lainnya, termasuk infrastruktur, jasa, industri, dan permukiman.

Mengetahui perubahan penggunaan berfungsi untuk mengidentifikasi potensi perubahan lingkungan yang berhubungan dengan tingkat perpindahan penduduk, alih fungsi hutan, dan perluasan lahan pertanian. Ketersediaan alat analisis serta data dan informasi sering menjadi kendala di lapangan. Menggunakan simbolisme satelit penginderaan jauh untuk merencanakan penggunaan lahan di wilayah yang luas adalah salah satu pendekatan yang dapat dilakukan (Fadlin et al., 2022). Akuisisi data mengenai suatu fenomena tanpa bersentuhan langsung dengannya merupakan pengertian dari penginderaan jauh. Proses ini mengandalkan deteksi dan kuantifikasi variasi yang terpancar dari target, yang dipengaruhi oleh keadaan optik di sekelilingnya, mencakup aspek-aspek seperti gelombang elektromagnetik, bunyi, serta medan gaya (Suni et al., 2023).

Satelit pencitraan optik Eropa, Sentinel-2 diluncurkan pada tanggal 23 Juni 2015, sebagai bagian dari program Copernicus dari Organisasi Antariksa Eropa. Sentinel-2 adalah salah satu satelit yang digunakan untuk membuat gambar satelit dari tutupan lahan di Bumi saat ini. Berdasarkan asal cahaya, pita-pita ini dikategorikan ke dalam daerah panjang gelombang. Pita merah, biru, hijau, dan inframerah dekat Sentinel-2 memiliki resolusi spasial masing-masing 10meter, 20 meter, dan 60 meter. Tujuan utama Sentinel-2 adalah mengumpulkan data persepsi sebanyak mungkin selama sepuluh hari dengan satu satelit dan lima hari lagi dengan dua satelit (Miranda & Aryuni, 2021). Pemanfaatan simbolisme satelit dalam penemuan tutupan lahan telah banyak digunakan mengingat fakta bahwa memiliki tujuan dan inklusi duniawi yang besar wilayah yang luas. Sentinel-2 dapat digunakan untuk memeriksa tanah dan menyediakan data penggunaan lahan dasar yang berfungsi sebagai skenario pemeriksaan dan kondisi iklim (Awaliyan & Sulistyoadi, 2018).

Hasil penelitian yang dilakukan oleh Ridwan (2023) menunjukkan Hasil penelitian Ridwan (2023) menunjukkan bahwa luas lahan kawasan terbangun (built area) meningkat sebesar 43% dari tahun 2017 hingga 2021, dengan total luas perubahan tutupan lahan

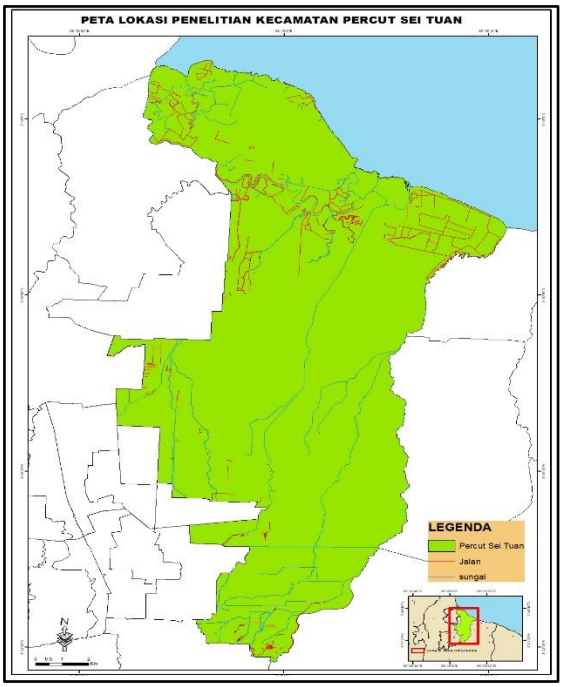
233,6105564 ha. Fungsi rangeland mengkonversi paling banyak lahan sebesar 56%, dan fungsi tutupan lahan mengkonversi paling banyak lahan sebesar 50,52001167 ha.

Hasil penelitian yang dilakukan oleh Fardilla et al (2023) berdasarkan temuan tersebut, terjadi perubahan tutupan lahan di Kota Padang dari tahun 2018 hingga 2022. Secara khusus, terjadi penurunan tutupan hutan seluas 342 ha dan peningkatan tutupan lahan permukiman (717 ha), ruang terbuka (568 ha), dan lahan pertanian (151 ha). Di Kota Padang, sejumlah faktor, termasuk pertambahan penduduk, perubahan tutupan lahan antropogenik, bencana alam, dan suksesi, dapat memberikan dampak.

Berdasarkan uraian tersebut penelitian ini bertujuan untuk mengetahui luasan, menganalisis perubahan penggunaan lahan dan perbandingan perubahan lahan yang terjadi di Kecamatan Percut Sei Tuan dengan intepretasi citra satelit Sentinel 2 pada tahun 2018 dan 2022.

Metode Penelitian

Penelitian ini dilakukan di Kecamatan Percut Sei Tuan, Kabupaten Deli Serdang, Provinsi Sumatera Utara. Kecamatan Percut Sei Tuan dipilih karena merupakan salah satu wilayah yang mengalami pertumbuhan dan perkembangan yang pesat dalam beberapa tahun terakhir.



Gambar 1. Lokasi Penelitian (Sumber: Hasil Olah Data, 2022)

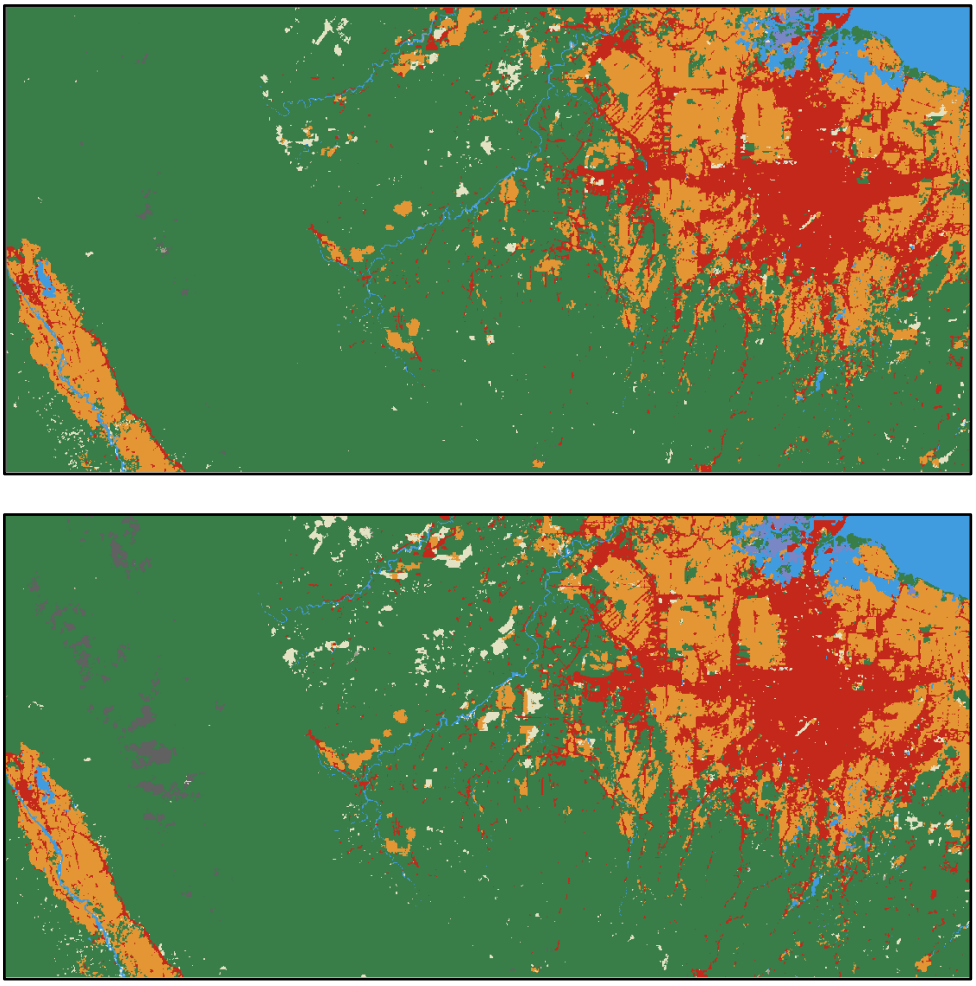
Pengumpulan data penelitian ini menggunakan studi literatur. Peneliti mengumpulkan data dari website ESRI untuk mendapatkan hasil citra Sentinel-2 perekaman tahun 2018 dan 2022 yang mencakup wilayah Kecamatan Percut Sei Tuan. Data lainnya seperti peta administrasi diperoleh dari website Badan Indonesia Geospasial (BIG)., serta artikel yang berkaitan dengan topik penelitian. Data dianalisis secara kuantitatif dan kualitatif. Analisis deskriptif kualitatif menjelaskan jenis-jenis perubahan dan penggunaan lahan. Sementara analisis kuantitatif digunakan untuk menghitung luasan dan besaran perubahan penggunaan

lahan yang terjadi antara tahun 2018 dan 2022. Hasil akhir berupa peta perubahan penggunaan lahan di Kecamatan Percut Sei Tuan tahun 2018-2022.

Hasil Penelitian

Pengolahan Citra

Data visualisasi penggunaan lahan dengan berbagai rona warna dihasilkan dari pengolahan data citra satelit Sentinel 2 dengan ArcGIS. Variasi rona warna menunjukkan variasi tutupan lahan dan juga variasi pantulan spektral di permukaan. Perangkat lunak ArcGIS dan foto satelit resolusi tinggi kemudian digunakan untuk mengkaji perbedaan rona warna tersebut untuk menentukan klasifikasi penggunaan lahan di lokasi penelitian Kecamatan Percut Sei Tun. Gambar 2 menunjukkan hasil pengolahan citra satelit Sentinel 2 dengan ArcGIS.

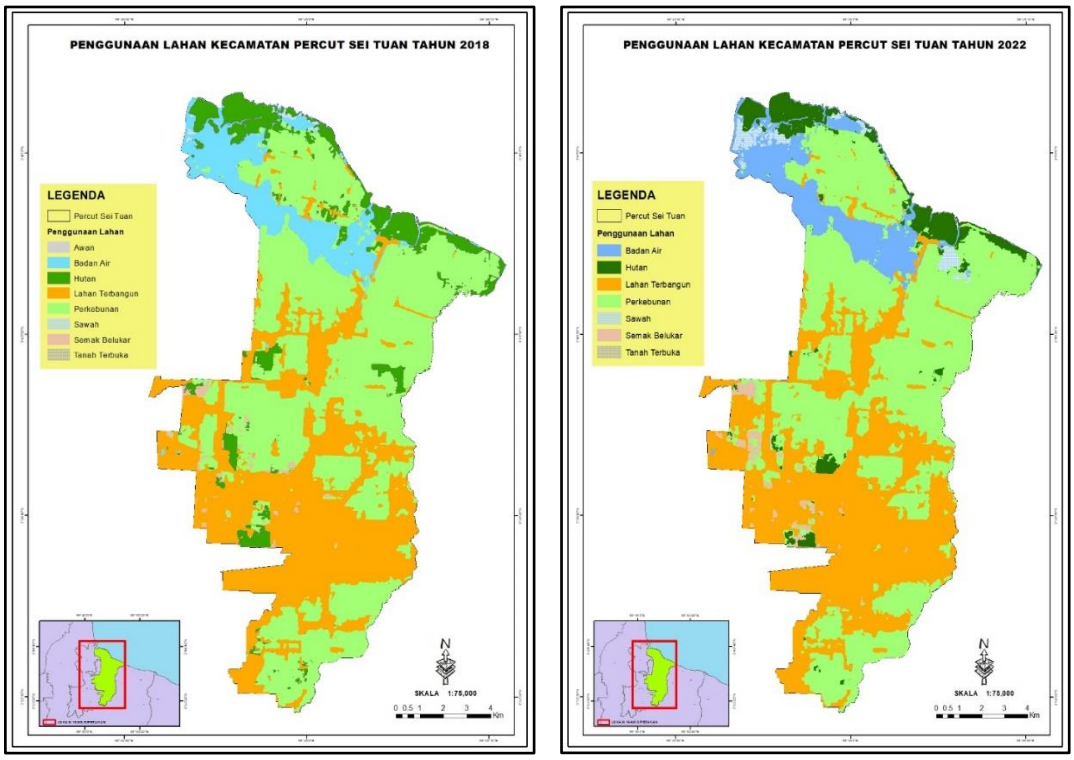


Gambar 2. Citra Satelit Sentinel 2 Tahun 2018 dan 2022
(Sumber: Hasil Olah Data, 2022)

Klasifikasi Penggunaan Lahan

Delapan kelas dihasilkan dari analisis perangkat lunak ArcGIS terhadap data citra Sentinel 2, yaitu: awan, badan air, hutan, lahan terbangun, perkebunan, sawah, semak belukar,

dan lahan terbuka. Kualitas kenampakan visual dalam proses interpretasi dijelaskan sebagai berikut.

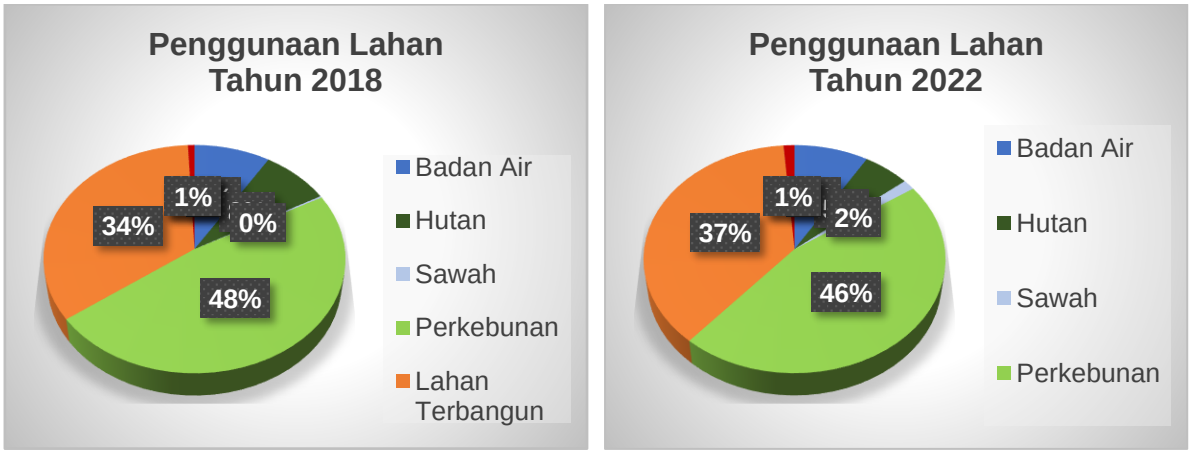


Gambar 3. Peta Penggunaan Lahan Kecamatan Percut Sei Tuan Tahun 2018 dan 2022 (Sumber: Hasil Olah Data, 2022)

1) Peta menunjukkan warna biru tua dan coklat muda pada badan air. Untuk badan air, warnanya berwarna coklat karena perekaman citra yang terjadi selama musim hujan, yang menyebabkan sedimentasi yang lebih tinggi di permukaan. Dalam penelitian ini, badan air yang dimaksud adalah sungai, irigasi, danau, rawa, embung, dan tambak ikan.
2) Hutan pada peta berwarna hijau gelap memiliki tekstur yang kasar karena menunjukkan variasi pepohonan yang tinggi atau kepadatan yang jarang.
3) Dalam peta, lahan yang terbangun tampak memiliki pola teratur, tekstur kasar, warna cerah, dan bentuk persegi atau limas. Dalam penelitian ini, lahan terbangun yang dimaksud adalah permukiman seperti perumahan atau tempat tinggal, pabrik, sekolah, dan bangunan lainnya.
4) Perkebunan memiliki kenampakan berwarna hijau muda dengan tekstur yang halus. Perkebunan yang dimaksud berupa jagung, kelapa sawit, dan padi.
5) Sawah, Sawah dalam gambar memiliki tekstur yang cerah, halus, bentuk yang tidak rata, dan warna biru muda. Ini adalah sawah dengan pematang dan padi yang tumbuh di atasnya.
6) Semak Belukar, kenampakan semak belukar berwarna violet dengan tekstur kasar dan bentuk petak-petak. Semak belukar yang dimaksud adalah rerumputan, sabana, dan semak.
7) Tanah Terbuka, kenampakan tanah terbuka berwarna abu tua dengan tekstur halus. Tanah terbuka yang dimaksud seperti lahan kosong.
8) Awan pada citra berwarna abu muda dengan tekstur yang kasar. Tanah Terbuka, kenampakan tanah terbuka berwarna abu tua dengan tekstur halus. Tanah terbuka yang dimaksud seperti lahan kosong.

Analisis Perubahan Penggunaan Lahan

Analisis perubahan penggunaan lahan dilakukan dengan membandingkan peta penggunaan lahan dari tahun 2018 dengan peta penggunaan lahan dari tahun 2022. Melalui perbandingan ini, diperoleh gambaran umum mengenai perubahan luas lahan dan penyebabnya. Perbandingan luas penggunaan lahan antara tahun 2018 dan 2022 ditampilkan dalam bentuk diagram pada Diagram 1. Diagram ini menggambarkan perubahan penggunaan lahan dari satu kelas ke kelas lainnya dan memberikan informasi mengenai persentase luasan dari tahun 2018 ke tahun 2022.



Gambar 4. Diagram Penggunaan Lahan Kecamatan Percut Sei Tuan Tahun 2018 dan 2022 (Sumber: Hasil Olah Data, 2022)

Tabel 1. Penggunaan Lahan Kecamatan Percut Sei Tun 2018-2022

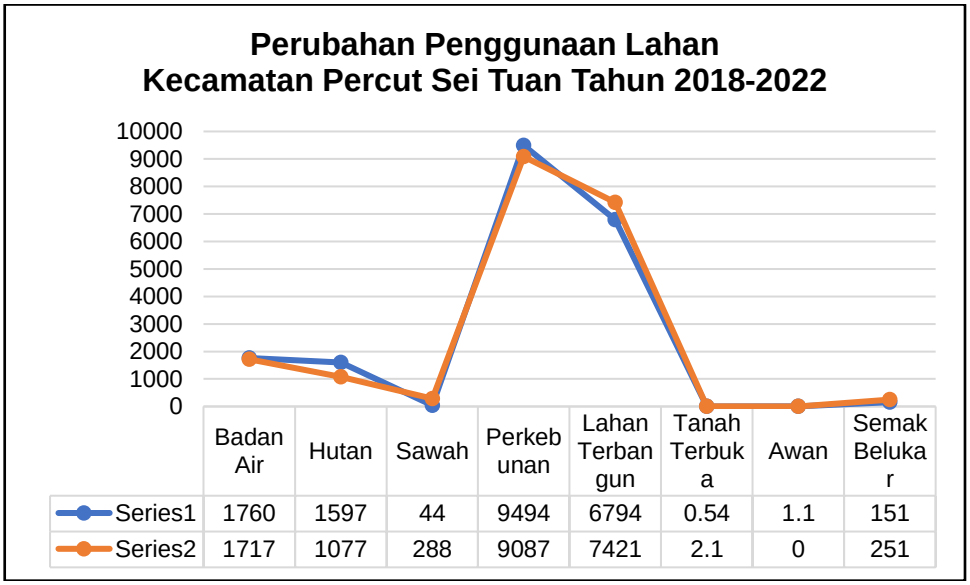
Penggunaan Lahan	Luas (Ha)	
	2018	2022
Badan Air	1760	1717
Hutan	1597	1077
Sawah	44	288
Perkebunan	9494	9087
Lahan Terbangun	6794	7421
Tanah Terbuka	0.54	2.1
Awan	1.1	0
Semak Belukar	151	251
Jumlah	19842	19843

(Sumber: Hasil Olah Data, 2018)

Pada tabel 1 disajikan luas penggunaan Lahan di Kecamatan Percut Sei Tuan pada tahun 2018 yaitu 19842 Hektar sedangkan pada tahun 2022 yaitu 19843 Hektar. Pada tahun 2018 Badan air memiliki luas 1760 ha atau 9% dari luas wilayah Kecamatan Percut Sei Tuan. Hutan memiliki luas 1597 ha atau 8% dari wilayah luas kecamatan Percut Sei Tuan. Sawah memiliki luas 44 ha atau 0% dari wilayah luas kecamatan Percut Sei Tuan. Perkebunan memiliki luas 9494 ha atau 48% dari wilayah luas kecamatan Percut Sei Tuan. Lahan terbangun memiliki luas 6794 ha atau 34% dari wilayah luas kecamatan Percut Sei Tuan. Tanah terbuka memiliki luas 0,54 ha atau 0% dari wilayah luas kecamatan Percut Sei Tuan. Awan memiliki luas 1,1 ha atau

0% dari wilayah luas Kecamatan Percut Sei Tuan. Semak belukar memiliki luas 151 ha atau 1% dari wilayah luas kecamatan Percut Sei Tuan.

Pada tahun 2022 Badan air memiliki luas 1717 ha atau 9% dari luas wilayah Kecamatan Percut Sei Tuan. Hutan memiliki luas 1077 ha atau 5% dari wilayah luas kecamatan Percut Sei Tuan. Sawah memiliki luas 288 ha atau 2% dari wilayah luas kecamatan Percut Sei Tuan. Perkebunan memiliki luas 9087 ha atau 46% dari wilayah luas kecamatan Percut Sei Tuan. Lahan terbangun memiliki luas 7421 ha atau 37% dari wilayah luas kecamatan Percut Sei Tuan. Tanah terbuka memiliki lus 2,1 ha atau 0% dari wilayah luas kecamatan Percut Sei Tuan. Semak belukar memiliki luas 251 ha atau 1% dari wilayah luas kecamatan Percut Sei Tuan.



	Badan Air	Hutan	Sawah	Perkebunan	Lahan Terbangun	Tanah Terbuka	Awan	Semak Belukar
Series1	1760	1597	44	9494	6794	0.54	1.1	151
Series2	1717	1077	288	9087	7421	2.1	0	251

Grafik 1. Perubahan Penggunaan Lahan Kecamatan Percut Sei Tun 2018-2022 (Sumber: Hasil Olah Data, 2022)

Pada luas perubahan lahan di Kecamatan Percut Sei Tuan disajikan pada grafik 1. Pada tahun 2018 Badan air memiliki luas 1760 ha atau 9%. Pada tahun 2022 Badan air berkurang 43 ha menjadi 1717 ha atau sekitar 9%. Pada tahun 2018 Hutan memiliki luas 1597 ha atau 8%. Pada tahun 2022 hutan berkurang 521 ha menjadi 1077 ha atau sekitar 5%. Pada tahun 2018 sawah memiliki luas 44 ha atau 0%. Pada tahun 2022 sawah bertambah 243 ha menjadi 288 ha atau 2%. Pada tahun 2018 perkebunan memiliki luas 9494 ha atau 48%. Pada tahun 2022 perkebunan berkurang 407 ha menjadi 9087 ha atau 46%. Pada tahun 2018 lahan terbangun memiliki luas 6794 ha atau 34%. Pada tahun lahan terbangun bertambah 627 ha menjadi 7421 ha atau 37%. Pada tahun 2018 tanah terbuka memiliki luas 0,54 ha atau 0%. Pada tahun 2022 tanah terbuka bertambah 1,54 ha menjadi 2,1 ha atau 0%. Pada tahun 2018 semak belukar memiliki luas 151 ha atau 1%. Pada tahun 2022 semak belukar bertambah 100 ha menjadi 251 ha atau 1%. Pada tahun 2018 awan memiliki luas 1.1 ha atau 0% sedangkan tahun 2022 awan sudah tidak ada lagi atau berubah menjadi lahan lainnya.

Pembahasan

Penelitian ini memanfaatkan citra satelit Sentinel-2 untuk menganalisis perubahan penggunaan lahan di Kecamatan Percut Sei Tuan. Pengolahan citra dilakukan dengan bantuan perangkat lunak ArcGIS. Citra Sentinel-2 memiliki kemampuan resolusi spasial yang baik,

dengan pita merah, biru, hijau, dan inframerah dekat yang masing-masing memiliki resolusi 10meter, 20 meter, dan 60 meter. Kemampuan ini memungkinkan interpretasi visual yang akurat untuk mengidentifikasi perbedaan rona warna dan tekstur, yang selanjutnya digunakan untuk klasifikasi penggunaan lahan.

Melalui pengolahan dengan ArcGIS, peneliti mampu menghasilkan peta penggunaan lahan yang menampilkan variasi warna dan tekstur sesuai dengan jenis penutupan lahan di wilayah studi. Perbedaan rona warna pada citra, misalnya biru tua untuk badan air, hijau gelap untuk hutan, dan warna cerah untuk lahan terbangun, memberikan informasi yang cukup jelas untuk interpretasi visual oleh peneliti. Selain itu, fitur-fitur ArcGIS seperti digitasi on-screen, komposisi band, dan analisis spasial membantu dalam proses klasifikasi penggunaan lahan secara akurat.

Klasifikasi Penggunaan Lahan

Berdasarkan hasil interpretasi visual citra Sentinel-2 dengan bantuan ArcGIS, peneliti berhasil mengidentifikasi delapan kelas penggunaan lahan di Kecamatan Percut Sei Tuan, yaitu: badan air, hutan, sawah, perkebunan, lahan terbangun, tanah terbuka, awan, dan semak belukar. Setiap kelas penggunaan lahan memiliki karakteristik visual yang khas, yang memudahkan proses klasifikasi. Misalnya, badan air terlihat berwarna biru tua dan coklat muda, hutan berwarna hijau gelap dengan tekstur kasar, lahan terbangun memiliki pola yang teratur dengan warna cerah, serta perkebunan dan sawah masing-masing memiliki warna dan tekstur yang khas. Pengenalan terhadap karakteristik visual ini menjadi dasar yang solid bagi peneliti untuk melakukan klasifikasi penggunaan lahan secara akurat.

Selain itu, peneliti juga memanfaatkan sumber data penunjang lainnya, seperti citra resolusi tinggi dan informasi geospasial, untuk memvalidasi hasil klasifikasi dan memastikan keakuratan identifikasi jenis penggunaan lahan di lapangan. Proses ini sangat penting untuk memperoleh data penggunaan lahan yang valid dan dapat digunakan untuk analisis lebih lanjut.

Analisis Perubahan Penggunaan Lahan

Setelah mengidentifikasi kelas-kelas penggunaan lahan pada citra Sentinel-2 tahun 2018 dan 2022, peneliti melakukan analisis perbandingan untuk mengetahui perubahan yang terjadi selama periode tersebut. Analisis perubahan penggunaan lahan merupakan bagian penting dari penelitian ini, sebagai upaya untuk memahami dinamika pemanfaatan lahan di Kecamatan Percut Sei Tuan.

Hasil analisis menunjukkan beberapa temuan signifikan terkait perubahan penggunaan lahan, antara lain:

1. Peningkatan luas lahan terbangun sebesar 627 hektar, dari 34% menjadi 37% dari total luas wilayah. Hal ini mengindikasikan adanya konversi lahan dari area hutan dan lahan produktif lainnya menjadi kawasan permukiman, industri, dan infrastruktur.
2. Penurunan luas hutan sebesar 521 hektar, dari 8% menjadi 5% dari total luas wilayah. Konversi lahan dari hutan menjadi lahan terbangun dan peruntukan lainnya menunjukkan adanya tekanan terhadap sumber daya hutan di wilayah ini.
3. Peningkatan luas sawah sebesar 243 hektar, dari 0% menjadi 2% dari total luas wilayah, sementara luas perkebunan berkurang 407 hektar, dari 48% menjadi 46%. Perubahan ini mengindikasikan adanya konversi lahan dari perkebunan menjadi sawah atau lahan pertanian lainnya.
4. Peningkatan luas lahan terbuka dan semak belukar, meskipun dengan persentase yang relatif kecil, yang dapat disebabkan oleh berbagai faktor seperti alih fungsi lahan, pembukaan lahan, atau suksesi alami vegetasi.

Perubahan penggunaan lahan yang terjadi di Kecamatan Percut Sei Tuan dapat memberikan berbagai dampak, baik positif maupun negatif, terhadap aspek lingkungan, sosial, dan ekonomi. Monitoring perubahan penggunaan lahan secara berkala sangat diperlukan untuk mendukung perencanaan tata ruang dan pengelolaan sumber daya lahan yang berkelanjutan.

Kesimpulan

Di wilayah Kecamatan Percut Sei Tuan, penggunaan lahan berubah secara signifikan antara tahun 2018 dan 2022. Kelas lahan terbangun meningkat sebesar 627 ha, atau 37%, sementara penggunaan lahan hutan menurun sebesar 521 ha, atau 5%. Hal ini disebabkan oleh kebutuhan infrastruktur masyarakat yang terus meningkat dan pada akhirnya menekan lahan-lahan produktif menjadi tidak produktif lagi. Harapan penulis agar penelitian selanjutnya dapat fokus pada mengkaji dampak dari perubahan penggunaan lahan terhadap aspek lingkungan, sosial, dan ekonomi. Hal ini penting untuk memahami konsekuensi dari dinamika pemanfaatan lahan dan menyusun langkah-langkah mitigasi atau adaptasi yang tepat.

Ucapan Terimakasih

Penulis ucapkan terima kasih yang sebesar–besarnya atas segala bantuan yang telah diberikan oleh kedua orang tua, dosen pengampu serta teman tim yang telah membantu selama pelaksanaan proses penelitian ini. Akhirnya penulis berharap semoga hasil penelitian ini dapat memberikan manfaat bagi kita semua. Saran dan kritikan yang membangun juga penulis harapkan demi menyempurnakan hasil penelitian ini.

Referensi

Akbar, W., Soma, A. S., & Arsyad, U. (2022). *Analisis Perubahan Penutupan Lahan di Daerah Aliran Sungai Kelara Menggunakan Citra Sentinel 2*. *14*(2), 73–87. https://doi.org/10.24259/jhm.v14i2.24107

Awaliyan, R., & Sulistyoadi, Y. B. (2018). Klasifikasi Penutupan Lahan Pada Citra Satelit Sentinel-2a Dengan Metode Tree Algorithm. *ULIN: Jurnal Hutan Tropis*, *2*(2), 98–104. https://doi.org/10.32522/u-jht.v2i2.1363

Fadlin, F., Thaha, M. A., Maricar, F., & Hatta, M. P. (2022). Monitoring Perubahan Penggunaan Lahan Menggunakan Citra Satelit Sentinel 1 di DAS Wanggu Kota Kendari. *Jurnal Teknik Sumber Daya Air*, *1*(2), 77–88. https://doi.org/10.56860/jtsda.v1i2.5

Fardilla, A., Septiavi, R., T, R. J., Arba, R. M., Sefmaliza, R., Fanbudy, A. R., Afdhal, T., & Novarino, W. (2023). *MENGGUNAKAN CITRA SATELIT Analysis of Land Cover Changes in Padang City using Satellite Imagery*. *10*(2), 353–367. https://doi.org/10.21776/ub.jtsl.2023.010.2.19

Indah, P., Mokodompit, S., Kindangen, J. I., & Tarore, R. C. (2019). Perubahan Lahan Pertanian Basah Di Kota Kotamobagu. *Jurnal Perencanaan Wilayah Dan Kota*, *6*(3), 792–799.

Miranda, E., & Aryuni, M. (2021). Klasifikasi Tutupan Lahan Menggunakan Convolutional Neural Network pada Citra Satelit Sentinel-2. *Sistemasi*, *10*(2), 323. https://doi.org/10.32520/stmsi.v10i2.1226

Miswar, D., Sugiyanta, I. G., Yarmaidi, & Yasta, R. D. (2020). Analisis Geospasial Perubahan Penggunaan Lahan Sawah Berbasis LP2B Kecamatan Pagelaran Utara. *Media Komunikasi Geografi*, *21*(2), 130–143.

Ridwan, V. F. (2023). *Analisis Perubahan Kawasan Terbangun Kota Parepare dengan Citra Satelit Sentinel-2 (2017-*. *3*(2).

Suban, I., & Sunimbar, A. (2021). *Analisis Perubahan Penggunaan Lahan Kota Kupang Nusa Tenggara Timur Tahun 2010-2018 (Studi Kasus di Kecamatan Kelapa Lima , Oebobo , dan Kota Lama)*. *2*, 36–52.

Suni, M. A., Borman, A. K., & Fahrul, M. (2023). *PEMETAAN PENGGUNAAN LAHAN DI KOTA PALU MENGGUNAKAN CITRA SENTINEL 2-A*. *1*(4), 384–391.

ISSN 2621-9883
Elipsoida : Jurnal Geodesi dan Geomatika
Vol 05 No 01, (2022)

ANALISIS PENGARUH CURAH HUJAN TERHADAP ESTIMASI PRODUKTIVITAS PADI BERBASIS PEMROSESAN CITRA SENTINEL 2A PADA SUBROUND I DAN II TAHUN 2018-2021 (STUDI KASUS : KECAMATAN WINONG, KABUPATEN PATI)

Riska Amirotul Qudriyah[1*], Yudo Prasetyo[1], Muhammad Adnan Yusuf[1]
[1]Departemen Teknik Geodesi-Fakultas Teknik Universitas Diponegoro, Jawa Tengah Indonesia
Jl. Prof Soedarto, SH, Tembalang, Semarang, Indonesia-75123Telp./Faks: (024) 736834
e-mail: riskaamirotul@gmail.com*

(Diterima 12 April 2022, Disetujui 4 Juni 2022)

ABSTRAK

Padi adalah salah satu tanaman terpenting yang menyediakan sumber makanan pokok bagi hampir separuh penduduk dunia. Akan tetapi, permasalahan yang dihadapi di Indonesia adalah penurunan nilai produksi padi akibat dari berkurangnya lahan pertanian dan nilai produktivitas padi. Penurunan nilai produksi dialami di Kecamatan Winong, puncaknya pada masa panen kedua tahun 2019 akibat adanya penurunan curah hujan di lokasi penelitian. Tujuan penelitian ini adalah untuk mengetahui pengaruh curah hujan terhadap estimasi produktivitas padi pada subround I dan II Tahun 2018-2021 di Kecamatan Winong. Algoritma NDRE (*Normalized Difference Red-Edge Index*) digunakan dalam pembuatan model produktivitas. Citra CHIRPS dimanfaatkan untuk mendapatkan data curah hujan. Hasil estimasi produktivitas padi pada subround I tahun 2018 sebesar 64,568 kuintal/hektar, subround II tahun 2018 sebesar 56,219 kuintal/hektar, subround I tahun 2019 sebesar 65,290 kuintal/hektar, subround II tahun 2019 sebesar 31,496 kuintal/hektar, subround II tahun 2020 sebesar 54,005 kuintal/hektar, dan subround II tahun 2021 sebesar 52,546 kuintal/hektar. Hubungan curah hujan dan estimasi produktivitas menunjukkan 4 masa tanam memiliki kesesuaian dengan peningkatan maupun penurunan hasil produktivitas dan 2 masa tanam tidak memiliki hubungan kesesuaian. Hasil uji korelasi menunjukkan adanya hubungan yang sangat kuat antara curah hujan dan produktivitas. Curah hujan memberikan sumbangan efektif sebesar 66,8% terhadap hasil produktivitas padi, sedangkan 23,2% berasal dari faktor-faktor lain yang tidak diteliti dalam penelitian ini.

Kata Kunci: Curah Hujan, Fase Tumbuh Padi, NDRE, Produktivitas Padi, Sentinel-2A

ABSTRACT

Rice is one of the most important crops that provides a staple food source for nearly half of the world's population. However, the problem faced in Indonesia is the decline in the value of rice production due to the reduction in agricultural land and the value of rice productivity. The decline in production value was experienced in Winong District, the peak during the second harvest period in 2019 due to a decrease in rainfall at the research site. The purpose of this study was to determine the effect of rainfall on the estimated rice productivity in subrounds I and II of 2018-2021 in Winong District. The NDRE (Normalized Difference Red-Edge Index) algorithm is used in the determination of rice growing phases and the creation of productivity models. CHIRPS images are utilized to obtain rainfall data. The results of the estimated rice productivity in subround I in 2018 were 64,568 quintals/hectare, subround II in 2018 was 56,219 hectare/ quintals, subround I in 2019 was 65,290 quintals/quintals, subround II in 2019 was 31,496 quintals/quintals, subround II in 2020 was 54,005 hectare/quintals, and subround II in 2021 was 52,546 hectare/quintals. The relationship between rainfall and productivity estimates shows that 4 planting periods have compatibility with increases or decreases in productivity yields and 2 planting periods have no conformity relationship. The results of the correlation test show a very strong relationship between rainfall and productivity. Rainfall contributed 66,8% to rice productivity, while 23,2% came from other factors not disclosed in the study.

Keywords: NDRE, Rainfall, Rice Growing Phase, Rice Productivity, Sentinel-2A

1. PENDAHULUAN

Padi dengan nama latin *Oryza sativa* adalah salah satu tanaman terpenting yang menyediakan sumber makanan pokok bagi hampir separuh penduduk dunia (FAO, 2008) dan menjadi makanan pokok masyarakat Indonesia. Indonesia memiliki luas lahan produksi padi sebesar 10,41 juta hektar pada tahun 2021. Jumlah tersebut turun 2,3% dibandingkan tahun sebelumnya. Penurunan luas lahan pertanian mengakibatkan penurunan nilai produksi Gabah Kering Giling (GKG) sebesar 54,42 juta ton (BPS, 2022). Salah satu penyebabnya adalah karena iklim.

Variabilitas iklim erat kaitannya dengan permasalahan sektor pertanian, terutama dengan variabilitas curah hujan. Curah hujan memiliki dampak yang besar terhadap keberhasilan pertanian di sawah tadah hujan. Sawah di Kecamatan Winong terdiri dari 3 kategori yaitu 45% sawah tadah hujan, 39% sawah irigasi setengah teknis, dan sisanya irigasi sederhana. Oleh karena itu, curah hujan sangat berpengaruh terhadap produktivitas di lokasi penenlitian. Pada masa panen kedua tahun 2019, Kecamatan Winong mengalami kemarau panjang yang mengakibatkan puso dan produktivitas padi menurun sampai 31,82% atau sekitar 7.629 ton (DISPERTAN, 2020).

Informasi jumlah panen tersebut dibutuhkan Kementerian Pertanian guna mengetahui cadangan pangan untuk menentukan kebijakan impor ekspor serta menentukan harga pasar. Informasi tersebut bisa didapat dengan melakukan estimasi produksi, salah satunya dengan teknologi penginderaan jauh. Model penginderaan jauh yang menghubungkan data reflektansi citra satelit dengan parameter tanaman padi akan sangat berguna untuk memantau pertumbuhan biomassa dan memprediksi produktivitas hasil tanaman (*crop yield*) secara lebih cepat dan efisien. Berdasarkan penelitian (Saadi & Wijayanto, 2021), Sentinel-2 menunjukkan hasil prediksi yang lebih baik dari Landsat 8 dari segi kinerja dan representasi yang lebih baik dalam mendeteksi daerah produksi padi. Identifikasi fase pertumbuhan padi menggunakan data Sentinel-2 dengan algoritma EVI dan NDRE telah diuji dan didapatkan hasil NDRE yang lebih baik dalam mengidentifikasi fase pertumbuhan padi (Shabrina, dkk., 2020). Pola yang dihasilkan dari indeks vegetasi tersebut, kemudian dilakukan perhitungan regresi linear untuk menentukan produktivitas padi yang dihasilkan.

Berdasarkan masalah dan fakta diatas, maka perlu adanya penelitian untuk menganalisis hubungan pola pertumbuhan padi dengan jumlah produktivitas yang dihasilkan serta melakukan estimasi produktivitas padi secara temporal di wilayah Kecamatan Winong. Estimasi produktivitas padi pada subround I dan II dapat digunakan untuk memprediksi persediaan beras sebelum panen, sehingga dapat menjadi bahan pertimbangan untuk melakukan impor beras. Selain itu, adanya analisis pengaruh curah hujan dapat memberikan informasi mengenai faktor yang mempengaruhi produktivitas padi. Hal ini bertujuan untuk membantu memaksimalkan dan menaikkan hasil produktivitas padi lewat perencanaan spasial yang tepat serta dapat menjadi solusi untuk mencapai ketahanan pangan nasional sesuai dengan *Sustainable Development Goals* (SDGs) butir kedua.

2. METODE PENELITIAN

Penelitian diawali dengan melakukan studi literatur, kemudian mempersiapkan data. Data yang digunakan dalam penelitian ini sebagai berikut :

1. Citra Sentinel-2A sebanyak 24 bulan karena setiap masa tanam sampai panen membutuhkan 4 bulan.
2. Citra CHIRPS sebanyak 24 buah sesuai dengan masa tanam padi.
3. Citra SPOT 6 dan 7 tahun 2021.
4. Batas administrasi sawah Kecamatan Winong
5. Data produktivitas padi yang berasal dari hasil wawancara dengan petani.
6. Data panen padi Kecamatan Winong pada Tahun 2018-2021.

Setelah data diperoleh dapat dilakukan pengolahan citra Sentinel-2A yang meliputi *cloud masking, resampling*, uji geometrik, pemotongan citra, dan transformasi indeks vegetasi NDRE. *Cloud masking* dilakukan untuk menghilangkan awan, kemudiana dilakukan penambalan (*overlaping*) citra berawan dengan citra yang tidak berawan. *Resampling* dilakukan untuk membuat resolusi spasial *band* menjadi seragam dan agar dapat dilakukan penggabungan (*mosaic*) citra. Uji geometrik digunakan untuk mengetahui nilai ketelitian citra satelit yang telah mengalami orthorektifikasi. Pemotongan (*clipping*) citra sesuai batas sawah bertujuan untuk mempersempit daerah penelitian.

Proses selanjutnya yaitu melakukan transformasi indeks vegetasi NDRE. Indeks vegetasi NDRE memanfaatkan perbedaan reflektansi antara panjang gelombang tepi merah (*red edge*) dan inframerah dekat (NIR) dengan panjang gelombang sekitar 700 nm untuk mengukur kepadatan dan kondisi vegetasi (Thompson, 2019). NDVI dan NDRE memiliki dasar penentuan indeks vegetasi yang mirip, namun pada NDRE memanfaatkan saluran *red edge* untuk mengukur kepadatan dan kondisi vegetasi, serta mampu melewati daun jauh lebih dalam karena adanya saluran *red edge* daripada saluran *red* dalam proses NDVI. Rentang nilai indeks vegetasi NDRE yaitu

antara -1 sampai +1. Rumus algoritma NDRE ditunjukkan pada persamaan 1.

$$\text{NDRE} = \frac{\text{NIR} - \text{Red edge}}{\text{NIR} + \text{Red edge}} \quad (1)$$

keterangan :

NIR = nilai *near infrared* yang terletak pada *band* 8

Red edge = nilai *red edge* saluran tepi *infrared* yang terletak *band* 5

Selanjutnya dilakukan pengolahan citra *Climate Hazards Group InfraRed Precipitation with Station* (CHIRPS). CHIRPS menyediakan daa curah hujan dengan resolusi spasial spasial 0,05˚ x 0,05˚ atau 5 km x 5 km dan menyediakan data dalam periode bulanan. Proses yang dilakukan berupa *georeferencing* atau pemberian sistem koordinat dan *clipping* sesuai batas penelitian.

Perhitungan estimasi produktivitas padi yang diperoleh dari persamaan regresi antara data produktivitas yang diambil saat wawancara dengan petani dan nilai NDRE di lokasi sampel. Wawancara dilakukan kepada 20 responden dengan persebaran merata dan kondisi sumber air yang beragam. Pemilihan sampel didasarkan pada teori Roscoe dalam Soegiono (2015) yaitu jumlah minimal sampel yang dibutuhkan dalam analisis korelasi atau regresi adalah 10 kali dari variabel yang digunakan. Penelitian ini menggunakan 2 variabel yaitu NDRE maksimum dan produktivitas wawancara, sehingga minimum sampel yang dibutuhkan sebanyak 20. Data yang diperoleh dari hasil wawancara berupa data Gabah Kering Panen (GKP) yang kemudian dikonversi kedalam Gabah Kering Giling (GKG). Nilai GKG merupakan 86% dari produktivitas GKP.

Setelah pengolahan citra selesai dilakukan, kemudian dilakukan uji statistika yang meliputi uji normalitas, uji korelasi, uji *Paired T test*, perhitungan Sumbangan Efektif (SE), *Root Mean Square Error* (RMSE), dan *Linear Error* (LE).

2.1 Uji Normalitas

Uji normalitas adalah pengujian data dalam model regresi yang bertujuan untuk menentukan sampel yang telah diambil dari populasi yang normal atau tidak (Ghozali, 2013). Uji normalitas dapat dilakukan dengan analisis grafik dengan cara dengan melihat persebaran data (titik) pada sumbu diagonal dari grafik atau melihat histogram dari residualnya dan analisis statistik dengan syarat residual berdistribusi normal apabila nilai signifikansi lebih besar dari 5% atau 0,05.

2.2 Uji Korelasi

Korelasi bertujuan untuk mengetahui hubungan antara 2 variabel yang berskala interval atau rasio. Rumus perhitungan korelasi pearson seperti pada Rumus 2.

$$r_{x\,y} = \frac{n\sum X_i Y - (\sum X_i)(\sum Y_i)}{\sqrt{\{n\,Xi^2 - (\Sigma X_i)^2\}\{\sum Y_i^2 - (\sum Y_i)^2\}}} \quad (2)$$

keterangan :

r_{xy} = koefisien korelasi r pearson

n = jumlah sampel

x = variabel bebas

y = variabel terikat

2.3 Uji *Paired T Test*

Tujuan dari uji-t berpasangan adalah untuk mengetahui apakah ada hubungan antara dua data yang digunakan sebagai variabel. *Paired t test* ditunjukkan pada Rumus 3.

$$\boldsymbol{t} = \frac{\overline{x_1} - \overline{x_2}}{\sqrt{\frac{s_1^2}{n_1} + \frac{s_2^2}{n_2} - 2r\left(\frac{s_1}{\sqrt{n_1}}\right)\left(\frac{s_2}{\sqrt{n_2}}\right)}} \quad (3)$$

keterangan :

$\overline{x_1}$ = rata-rata sampel 1

$\overline{x_2}$ = rata-rata sampel 2

s_1 = simpangan baku sampel 1

s_2 = simpangan baku sampel 2

s_1^2 = variansi sampel 1

s_2^2 = variansi sampel 2

r = korelasi antara dua sampel

2.4 Sumbangan Efektif (SE)

Sumbangan efektif adalah persentase sumbangan dalam analisis regresi dari satu variabel independen terhadap variabel dependen dengan tetap memperhitungkan variabel independen lain yang tidak diperhitungkan (Hadi, 2004). Penjumlahan dari SE seluruh variabel independen sama dengan jumlah nilai koefisien determinasi(R^2). Rumus sumbangan efektif seperti pada Rumus 4.

$$\boldsymbol{SE(X)\% = Beta_X\, x\, r_{xy}\, x100\%} \quad (4)$$

keterangan :

SE(X)% = sumbangan efektif dari satu prediktor

Beta x = koefisien regresi

rxy = koefisien korelasi

2.5 *Root Mean Square Error* (RMSE)

RMSE adalah besarnya tingkat kesalahan hasil prediksi atau akar kuadrat dari rata-rata kuadrat selisih antara nilai koordinat data dan nilai koordinat dari sumber independen yang akurasinya lebih tinggi (BIG, 2014). Persamaan RMSE seperti pada Rumus 5.

$$\boldsymbol{RMSE} = \sqrt{\frac{\sum_{i-1}^{N}(x_i - xi)^2}{-N}} \quad (5)$$

keterangan :

x_i = nilai data aktual

$\hat{x}_i$ = nilai hasil peramalan
N = banyaknya data

2.6 *Linear Error* (LE)

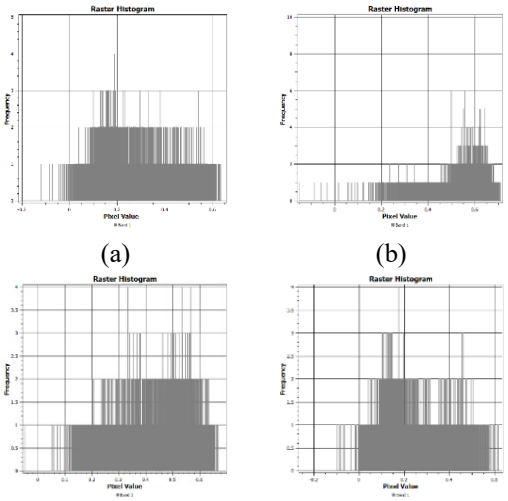
LE adalah penyimpangan data dari garis lurus tertentu pada rentang yang diinginkan (Regtien dan Dertien, 2018). LE yang dipilih yaitu sebesar 90% sesuai dengan Peraturan Kepala Badan Informasi Geospasial Nomor 15 Tahun 2014 bahwasanya LE90 dapat digunakan untuk pembuatan peta dasar seperti Peta Rupabumi Indonesia (RBI). Penggunaan LE90 dalam distribusi normal seperti pada Rumus 6.

$$LE90 = 1,6499\ x\ RMSE \quad (6)$$

3. HASIL DAN PEMBAHASAN

3.1 Hasil Interpretasi NDRE

Hasil pengolahan algoritma NDRE pada citra Sentinel-2A secara multitemporal menunjukkan adanya perubahan warna citra. Hal ini sesuai dengan adanya perubahan nilai spektral citra seperti pada **Gambar 1**.



(a) (b) (c) (d)

Gambar 1. Histogram NDRE (a) November 2017 (b) Desember 2017 (c) Januari 2018 (d) Februari 2018

Perubahan pada pola spektral tersebut menunjukkan fase tumbuh padi. Nilai spektral yang tinggi menunjukkan padi pada reproduktif, sedangkan nilai spektral rendah menunjukkan tinggi tanaman masih rendah atau sawah dalam kondisi kosong. Hasil ekstraksi NDRE akan digunakan untuk membuat pemodelan produktivitas bersama dengan produktivitas hasil wawancara adalah nilai NDRE maksimum atau pada fase reproduktif untuk mengurangi kemungkinan gagal panen padi.

3.2 Hasil Pengolahan Produktivitas Padi

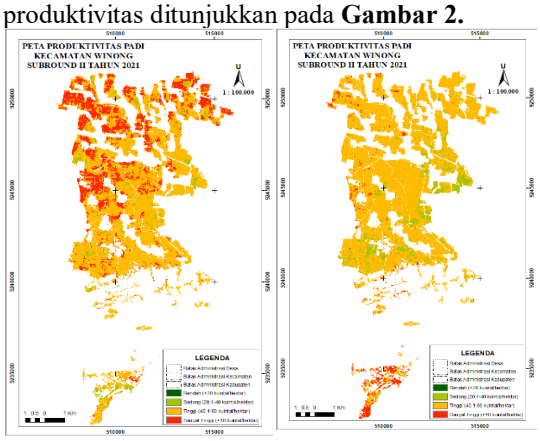
3.2.1 Hasil Pemodelan Produktivitas Padi

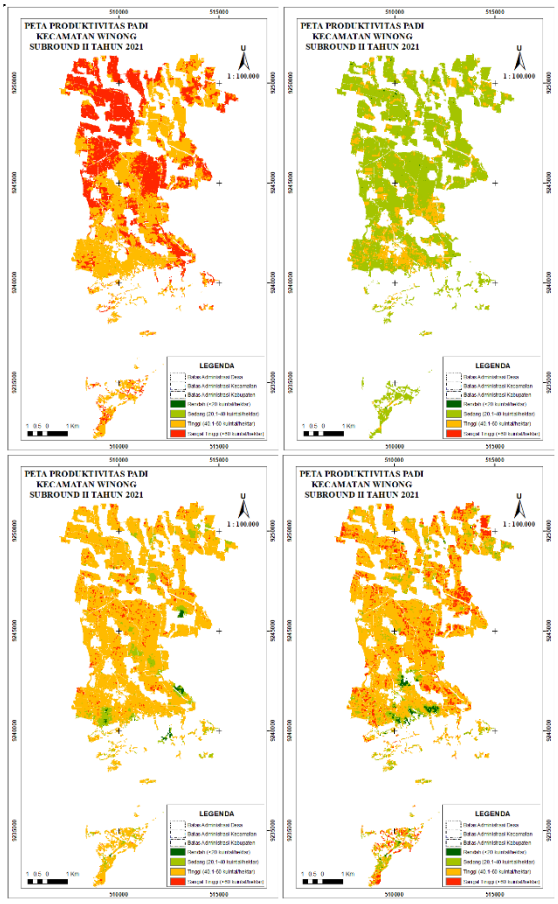
Pemodelan produktivitas padi menggunakan regresi linier dengan menghubungkan antara variabel produktivitas padi hasil wawancara sebagai variabel terikat dengan nilai transformasi NDRE maksimum sebagai variabel bebasnya.

Tabel 1. Estimasi Produktivitas Padi

Tahun	SR	Persamaan	Estimasi Produktivitas (kuintal/ha)
2018	I	y =70,795x+23,039	64,568
	II	y = 55,338x+27,698	56,219
2019	I	y = 42,219x+43,123	65,290
	II	y = 15,938x+22,636	31,496
2020	II	y = 63,077x+15,583	54,005
2021	II	y = 80,322x+9,0655	52,546

Nilai produktivitas yang diperoleh pada **Tabel 1** adalah produktivitas Gabah Kering Giling (GKG). Produktivitas tertinggi terdapat pada subround I tahun 2019 dan terendah pada subround II tahun 2019. Berdasarkan Peraturan Pemerintah Nomor 1 Tahun 2011 hasil estimasi produktivitas padi termasuk 3 kategori yaitu sangat tinggi pada subround I tahun 2018 dan 2019, tinggi pada subround II tahun 2018, 2020, dan 2021. Sedangkan pada subround II tahun 2019 termasuk kategori sedang. Sehingga dapat disimpulkan bahwa hasil produktivitas pada subround I lebih tinggi dari pada subround II. Hal ini dikarenakan penurunan curah hujan pada subround II yang menghambat produktivitas padi. sementara itu, peta persebaran produktivitas ditunjukkan pada **Gambar 2.**





Gambar 2. Peta Produktivitas Padi

3.2.2 Hasil Uji Akurasi Model Estimasi Produktivitas

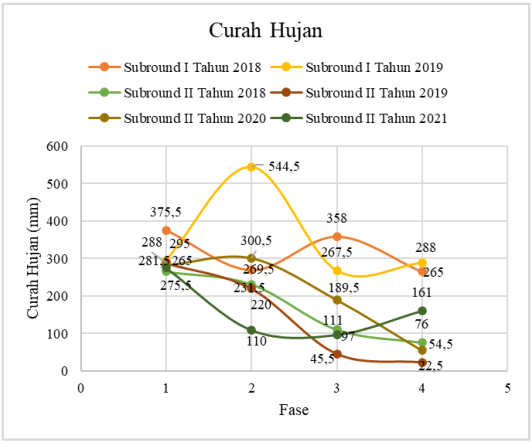
Uji akurasi dilakukan pada 3 titik sampel. Dari nilai estimasi produktivitas akan dihitung selisih (*error*) dengan nilai produktivitas hasil wawancara untuk memperoleh nilai RMSE dan LE. Hasil pengolahan produktivitas seperti pada **Tabel 2**. Dari **Tabel 2** diperoleh nilai *error*, RMSE, dan LE90. Nilai RMSE yang diperoleh sebesar 1,383 kuintal/hektar dan LE90 sebesar 2,281 kuintal/hektar. Sehingga dapat disimpulkan bahwa akurasi hasil estimasi produktivitas dengan produktivitas wawancara sebesar 2,281 kuintal/hektar.

Tabel 2. Hasil Uji Akurasi Produktivitas

Titik	Tahun	SR	Estimasi Produktivitas (kuintal/hektar)	Produktivitas Wawancara (kuintal/hekta)	*Error* (kuintal / hektar)	*Error*^{2} (kuintal/hektar)
1	2018	I	57,786	58,919	-1,132	1,282
		II	43,822	44,778	-0,957	0,915
	2019	I	68,572	65,989	2,583	6,674
		II	48,573	47,135	1,438	2,068
	2020	II	57,017	54,205	2,812	7,909
	2021	II	49,084	49,492	-0,408	0,166
2	2018	I	55,156	56,034	-0,878	0,771
		II	45,963	44,827	1,136	1,291
	2019	I	65,917	63,505	2,411	5,815
		II	49,466	48,563	0,903	0,816
	2020	II	57,017	56,034	0,984	0,967
	2021	II	49,761	48,563	1,199	1,437
3	2018	I	61,113	61,271	-0,158	0,025
		II	57,525	57,045	0,480	0,230
	2019	I	59,421	59,158	0,263	0,069
		II	22,884	21,128	1,757	3,086
	2020	II	54,542	54,932	-0,390	0,152
	2021	II	57,923	57,045	0,878	0,771
			Jumlah			20,767
			RMSE			1,383
			LE90			2,281

3.3 Hasil dan Analisis Curah Hujan

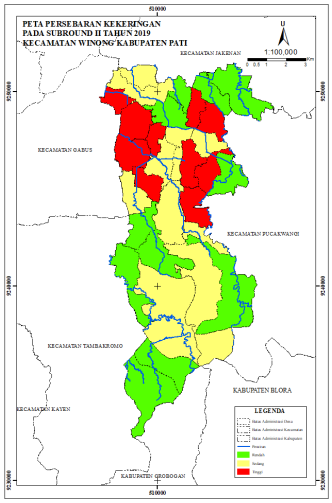
Data curah hujan dari citra CHRIPS berupa nilai curah hujan bulanan. Pada setiap subround terdapat 4 citra CHIRPS yang digunakan. Data curah hujan tersebut ditunjukkan pada **Gambar 3**.



Gambar 3. Grafik curah hujan

Fase tumbuh padi dimulai dari persemaian benih padi atau fase vegetatif awal, fase ini membutuhkan air untuk mempermudah proses perkecambahan dan pertunasan benih padi. Hal tersebut sesuai dengan data curah hujan pada tahun 2018-2021 yang memiliki intensitas curah hujan tinggi. Curah hujan pada fase ini berkisar antara 265-375,5 mm/bulan. Selanjutnya pada fase pembentukan anakan sampai menjelang masa keluarnya malai atau fase vegetatif. Curah hujan dibutuhkan agar tanaman padi dapat beranak dengan maksimal. Curah hujan pada fase ini berkisar antara 110-544,5 mm/bulan. Intensitas hujan rata-rata melebihi 263 mm/bulan bisa menyebabkan banjir di daerah persawahan yang tidak dekat pantai (Estiningtyas, Analisis Hubungan Curah Hujan dengan Kejadian Banjir dan Kekeringan Pada Wilayah dengan Sistem Usahatani Padi di Provinsi Jawa Barat, 2009). Berdasarkan wawancara dengan petani, berlebihnya air hujan pada awal fase padi tidak mengakibatkan banjir pada lahan sawah di Kecamatan Winong karena air tersebut dapat dibuang.

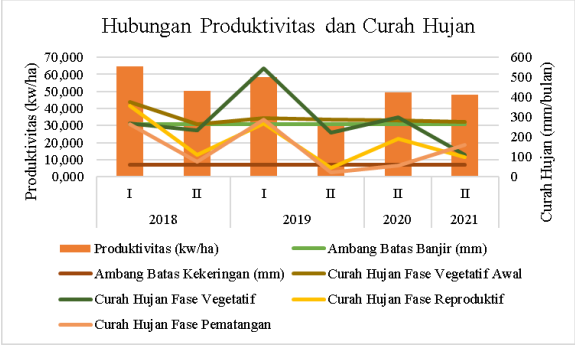
Tanaman padi pada kondisi keluar malai sampai pengisian bulir padi atau fase reproduktif, tanaman padi membutuhkan air untuk fotosintesis agar pengisian bulir dapat berjalan dengan baik. Curah hujan fase 3 ini berkisar antara 45,5-358 mm/bulan atau dengan intensitas rendah sampai tinggi. Curah hujan cukup akurat digunakan sebagai indikator untuk deteksi dini kekeringan agronomis tanaman padi pada sawah tadah hujan dan sawah irigasi. Nilai ambang curah hujan pada sawah tadah hujan adalah 60-70 mm, sedangkan untuk sawah irigasi adalah 20 mm (Surmaini, 2014).



Gambar 4. Persebaran kekeringan pada subround II 2019

Curah hujan pada subround II Tahun 2019 fase ke-3 sebesar 45,5 mm yang berada dibawah ambang batas kekeringan tanaman padi. Hal tersebut sesuai dengan wawancara langsung dengan petani dan data persebaran perairan (sungai dan irigasi) yang diperoleh dari DPUPR Kabupaten Pati.

Dari 30 desa yang ada di Kecamatan Winong dibagi menjadi 3 kategori yaitu rendah, sedang, dan tinggi. Pembagian kategori tersebut didasarkan pada pasokan air yang diterima desa tersebut. Kategori rendah apabila pasokan air merata pada seluruh area persawahan tersebut dan berdasarkan wawancara produktivitas yang dihasilkan normal. Kategori sedang apabila pasokan air dapat diterima lebih dari setengah dari total lahan sawah dan berdasarkan wawancara terjadi penurunan produktivitas atau tidak. Kategori tinggi apabila aliran air tidak merata dan berdasarkan wawancara mengalami puso. Berdasarkan **Gambar 4**, terdapat 10 desa yang termasuk kategori rendah,10 desa termasuk kategori sedang, dan 10 desa termasuk dalam kategori tinggi.



Gambar 5. Hubungan produktivitas padi dan curah hujan

Grafik pada **Gambar 5** menunjukkan hubungan curah hujan yang sesuai dengan peningkatan maupun penurunan hasil produksi padi terdapat pada subround II Tahun 2018-2021 yaitu sebesar 66,7% atau 4 dari 6 masa tanam. Sedangkan 33,3% atau 2 masa tanam pada subround I tidak sesuai karena menurut penelitian (Estiningtyas, Boer, & Buono, 2009) dianggap melebihi ambang batas banjir. Namun kenyataan di lapangan hujan yang berlebih tidak menyebabkan banjir dan produktivitas padi normal.

3.4 Hasil dan Analisis Uji Statistika

3.4.1 Hasil dan Analisis Uji Normalitas

Uji normalitas data dilakukan sebelum membuat pemodelan produktivitas padi. Hasilnya didapatkan nilai signifikansi sebesar 0,153. Hal

tersebut memenuhi syarat data penelitian berdistribusi normal karena nilai > 0,05.

3.4.2 Hasil dan Analisis Uji Korelasi

Uji korelasi dilakukan terhadap 2 variabel yaitu NDRE terhadap produktivitas padi hasil wawancara.

Tabel 3. Hasil Uji Korelasi

Tahun	Subround	r	Signifikansi
2018	I	0,864	0,000
	II	0,791	0,002
2019	I	0,782	0,003
	II	0,186	0,564
2020	II	0,857	0,000
2021	II	0,903	0,000

Tabel 3 menunjukkan nilai koefisien korelasi (r) positif pada keseluruhan subround yang berarti apabila nilai NDRE naik, maka nilai produktivitas juga naik. Sedangkan besarnya angka menunjukkan hubungan antara NDRE dengan produktivitas padi. Pada subround I tahun 2018, subround II tahun 2020, dan subround II tahun 2021 menunjukkan terdapat hubungan yang sangat kuat. Hasil uji korelasi pada subround II tahun 2018 dan subround I tahun 2019 menunjukkan terdapat hubungan yang kuat antara dua variabel. Sedangkan hasil uji korelasi pada Subround II tahun 2019 menunjukkan tidak terdapat hubungan antara 2 variabel tersebut dengan tingkat keeratan hubungan yang sangat lemah di antara keduanya. Hal ini disebabkan adanya penurunan produktivitas padi pada beberapa wilayah akibat kekeringan.

Koefisien korelasi tertinggi yang dihasilkan pada penelitian ini adalah sebesar 0,903. Dapat disimpulkan proporsi keeratan hubungan variabel NDRE terhadap tingkat produktivitas padi sebesar 90,3%. Sedangkan sisanya sebesar 9,7% dipengaruhi oleh variabel lain yang tidak ada dalam model regresi yang dikerjakan pada penelitian ini.

3.4.3 Hasil dan Analisis Uji T

Uji T yang digunakan adalah *Paired T Test* yang bertujuan untuk mengetahui adanya perbedaan antara 2 variabel yang berpasangan. Syarat dapat dilakukannya uji T adalah data berdistribusi normal.

Tabel 4. Hasil *Paired T Test*

Tahun	Subround	Signifikansi *Paired T Test*
2018	I	0,000000001 x10^3
	II	0,000000032 x10^3
2019	I	0,000000300 x10^3
	II	0,553999657 x10^3
2020	II	0,000006782 x10^3
2021	II	0,000019923 x10^3

Hasil pada **Tabel 4** diperoleh nilai signifikansi <0,05 yang berarti terdapat perbedaan yang signifikan antara NDRE dengan produktivitas padi.

3.4.4 Hasil dan Analisis Sumbangan Efektif (SE)

Sumbangan efektif digunakan untuk mengetahui besarnya sumbangan variabel independent (curah hujan) terhadap variabel dependen (produktivitas). Nilai SE pada penelitian ini sama dengan nilai R^2 dari model regresinya dikarenakan hanya menggunakan satu variabel independen. Dari hasil perhitungan SE didapatkan nilai 0,664 yang berarti bahwa curah hujan memberikan sumbangan efektif sebesar 66,8% terhadap produktivitas padi, sedangkan sisanya sebesar 23,2% disumbang oleh variabel lain yang tidak diteliti pada penelitian ini.

4. KESIMPULAN DAN SARAN

4.1 Kesimpulan

Berdasarkan hasil penelitian yang sudah dilakukan terdapat kesimpulan dari penelitian sebagai berikut :

1. Estimasi produktivitas didapatkan dari persamaan regresi antara data produktivitas yang didapat saat wawancara dengan petani dengan nilai NDRE pada lokasi sampel. Nilai produktivitas yang didapat adalah produktivitas Gabah Kering Panen (GKP) yang kemudian dikonversi ke dalam Gabah Kering Giling (GKG). Berdasarkan hasil pengolahan didapatkan produktivitas tertinggi pada subround I Tahun 2019 yaitu 65,290 kuintal/hektar dan terendah pada subround II Tahun 2019 yaitu sebesar 31,496 kuintal/hektar. Berdasarkan Peraturan Pemerintah Nomor 1 Tahun 2011 hasil produktivitas padi di Kecamatan Winong termasuk dalam 3 kategori yaitu sangat tinggi pada subround I tahun 2018 dan 2019, sedang pada subround II Tahun 2019, dan tinggi pada fase yang lainnya.
2. Berdasarkan hubungan data curah hujan yang didapatkan dari citra CHIRPS dengan hasil produktivitas menunjukkan 4 dari 6 masa tanam memiliki kesesuaian dengan peningkatan maupun penurunan hasil produktivitas dan 2

masa tanam tidak memiliki hubungan kesesuaian. Hasil uji korelasi menunjukkan adanya hubungan yang sangat kuat antara curah hujan dan produktivitas. Curah hujan memberikan sumbangan efektif sebesar 66,8% terhadap hasil produktivitas padi, sedangkan 23,2% berasal dari faktor-faktor lain yang tidak diungkapkan dalam penelitian ini. Pada subround II Tahun 2019 terjadi kekeringan pada 10 desa yang mengakibatkan puso. Sedangkan 10 desa mengalami penurunan produktivitas padi dan 10 desa memiliki produktivitas normal. Hal tersebut mengakibatkan produktivitas padi pada subround II Tahun 2019 mengalami penurunan.

4.2 Saran

Berdasarkan hasil penelitian yang telah dilaksanakan terdapat saran yang dapat digunakan pada penelitian selanjutnya, antara lain :

1. Penggunaan data berbasis citra radar agar terbebas dari awan. Apabila menggunakan citra pasif untuk mengestimasi produksi padi, sebaiknya menggunakan subround II maupun III untuk meminimalisir keberadaan awan yang terlalu banyak pada lokasi penelitian.
2. Wilayah penelitian yang digunakan mencakup satu kabupaten agar mempermudah dalam mendapatkan data karena umumnya data di instansi menggunakan unit terkecil kabupaten.
3. Penambahan parameter yang menyebabkan fluktuasi nilai produksi padi dalam suatu wilayah seperti hama, jenis tanah, kondisi irigasi, nutrisi, dan serta varietas dari padi.

DAFTAR PUSTAKA

BIG. (2014). *Peraturan Kepala Badan Informasi Geospasial Nomor 15 Tahun 2014.* Cibinong: BIG.

BPS. (2022). *Produksi Padi Tahun 2021 Turun 0,43 persen (Angka Tetap).* Jakarta: Badan Pusat Statistika.

Climate Hazards Center. (2022, April 12). *CHIRPS: Rainfall Estimates from Rain Gauge and Satellite Observations*. Retrieved from https://www.chc.ucsb.edu/data/chirps

DISPERTAN. (2020). *Data Luas Sawah, Produktivitas, dan Produksi Padi Kecamatan Winong Kabupaten Pati Tahun 2019-2020.* Pati.

Estiningtyas, W., Boer, R., & Buono, A. (2009). Analisis Hubungan Curah Hujan dengan Kejadian Banjir dan Kekeringan Pada Wilayah dengan Sistem Usahatani Padi di Provinsi Jawa Barat. *J.Agromet 23 (1)*, 11-19.

FAO, F. a. (2008). *FAO and Sustainable Intensification of Rice Production for Food Security.* . Rome, Italy: FAO.

Ghozali, I. (2013). *Aplikasi Analisis Multivariate dengan Program SPSS.* Semarang: Universitas Diponegoro.

Hadi, S. (2004). Metodologi Research Jilid III. Jogjakarta: Penerbit Andi.

Saadi, T. D., & Wijayanto, A. W. (2021). Machine Learning Applied to Sentinel-2 and Landsat-8 Multispectral And Medium-Resolution Satellite Imagery For The Detection Of Rice Production Areas In Nganjuk, East Java, Indonesia. *International Journal of Remote Sensing and Earth Sciences Vol. 18 No.1* , 19-32.

Surmaini, E. (2014). Penentuan Nilai Ambang Curah Hujan untuk Deteksi Dini Kekeringan pada Tanaman Padi Sawah: Studi Kasus Provinsi Jawa Barat dan Sulawesi Selatan. *ISSN 1410-7244*, 79-87.

Thompson, C. N. (2019). *Using normalized difference red edge index to assess maturity in cotton.* Crop Science, 59(5), 2167-2177.

Pustaka dari Wawancara :

Rohim, Abdul., Muntamah., Rofiatun., Sarkasi, Harun., Sunari., Masri., Karni., Wardi., Susanto, Mad., Supriyati., Suparyati., Supardi. 2022. "Produktivitas dan kekeringan pada Lahan Sawah Kecamatan Winong". Hasil Wawancara Pribadi: 10-11 September 2022. Petani di Kecamatan Winong.

DOI: 10.24114/jg.v12i02.16970
e-ISSN: 2549–7057 | p-ISSN: 2085–8167

APLIKASI CITRA SENTINEL-2 UNTUK PEMETAAN TUTUPAN DAN PERUNTUKAN LAHAN PADA TINGKAT DESA

Marga Mandala[1], Indarto Indarto*[1], Fery Febrian Arifin[2], Farid Lukman Hakim[2]
[1]Keris P-LSO (Pengembangan Lahan Sub-Optimal), Universitas Jember
[2]PS Teknik Pertanian, Fakultas Teknologi Pertanian, Universitas Jember
Jalan Kalimantan No 37, Kampus Bumi Tegalboto, Krajan Timur, Kecamatan Sumbersari, Kabupaten Jember, Jawa Timut, 68121, Indonesia
e-mail: indarto.ftp@unej.ac.id

Diterima: 05 Februari 2020, Direvisi: 18 Juni 2020, Disetujui: 22 Juni 2020

Abstrak

Sentinel-2 menjanjikan citra yang gratis, pada ketelitian spasial sedang dan ketelitian spektral tinggi. Data citra ini mungkin dapat digunakan sebagai dasar pemetaan tutupan lahan (land cover) dan pruntukan lahan (land use) sampai dengan level Desa. Artikel ini bertujuan untuk membandingkan dan mengevaluasi peta tematik yang dihasilkan dari: (1) Klasifikasi dari citra Sentinel-2A, (b) digitasi manual dari Google Earth Image, (c) dan peta RBI (Rupa Bumi Indonesia). Citra Sentinel-2A, citra google earth dan peta RBI digital digunakan sebagai input utama. Pengolahan citra Sentinel-2A mencakup: atmosferic correction, image composite, klasifikasi terbimbing, koleksi training area, dan uji-akurasi. Selanjutnya, ke tiga jenis peta tematik yang dihasilkan digunakan untuk membandingkan luasan per jenis tutupan lahan yang dipetakan dan interpretasi perubahan peruntukan lahan yang terjadi. Selanjutnya, wilayah empat desa digunakan sebagai sampel pengukuran. Penelitian menghasilkan peta tematik tutupan dan peruntukan lahan pada level Desa. Perbandingan peta tematik menunjukkan bahwa citra Sentinel mampu untuk menangkap fitur tutupan lahan yang utama (yaitu: Lahan-sub-optimal kering, lahan irigasi, lahan non-irigasi, area terbangun, hutan-perkebunan, dan badan air) pada level desa. Lebih lanjut peta yang dihasilkan dari citra Sentinel dapat digunakan untuk memperbaharui, perencanaan dan evaluasi kegiatan pembangunan di Desa.

Kata Kunci: *Sentinel-2A, Pemetaan, Tutupan Lahan, peruntukan lahan, desa.*

Abstract

Sentinel-2 provide a free of cost imagery in medium spatial and high spectral resolutions. These data promise a rapid, low-cost and easy to apply imagery for the end-user. These free data may produce a rationale thematic land cover and land use (LCLU) map at the village level. This paper aims to compare and to evaluate the thematics maps created by (a) Sentinel-2, (b) digitalisation from Google Earth and (c) RBI (Rupa Bumi Indonesia) Digital Map. Sentinel-2 image, google earth image, and RBI digital map used as the primary input. The treatment of sentinel 2A imagery consists of atmospheric correction, image composite, supervised classification, collecting training areas, and accuracy assessment. The three types of maps use to compare area extent mapped for each type of land cover (LC), and the interpretation of land-use change occurred. Four villages used as samples of measurement. The research produces thematic LCLU maps at the village level. Comparison of maps shows that Sentinel capable of capturing major LC (i.e., Dry-marginal land, non-irrigated area, irrigated area, pavement areas, forest - plantation, and water

DOI: 10.24114/jg.v12i02.16970
e-ISSN: 2549–7057 | p-ISSN: 2085–8167

body) at the village level. Moreover, Sentinel-2A produce more detail of land cover type. Finally, the maps derived from Sentinel data provide data for up-dating, planning and evaluation of village development.

Keywords : *Sentinel-2A, mapping, land cover, land use, village.*

PENDAHULUAN

Pada tulisan ini definisi tutupan lahan atau *Land cover (LC)* dan peruntukan lahan atau *Land use (LU)* mengacu pada publikasi oleh EUROSTAT (2001) sebagai berikut : tutupan lahan (LC) menyatakan deskripsi fisik dari suatu ruang di permukaan bumi kita dan dengan deskripsi ini memungkinkan berbagai macam kategori sifat bio-fisik dapat dibedakan. Pengamatan tutupan lahan dapat dilakukan melalui berbagai metode, mencakup: pengamatan langsung, fotografi udara dan sensor satelit.

Peruntukan lahan atau *land use (LU)* mengacu pada dimensi fungsi dari suatu luasan terkait dengan tujuan ekonomi (misal: luasan untuk pemukiman, industri, pusat komersial, pertanian atau hutan, tempat rekreasi atau konservasi alam (EUROSTAT, 2001). Selanjutnya, (Parece and Campbell, 2015) mengadopsi definisi yang sama dan menyatakan bahwa pada prakteknya istilah tutupan-lahan *(LC)* dan peruntukan-lahan *(LU)* dapat saling dipertukarkan. Citra satelit menawarkan alternatif solusi untuk berbagai malasah terkait dengan perubahan *LCLU* dan dampaknya terhadap masyarakat dan lingkungan.

Ketersedian data citra yang gratis dengan ketelitian spasial sedang dan ketelitian spektral tinggi, seperti citra satelit Sentinel-2, menawarkan metode pemetaan yang cepat, murah dan mudah untuk diterapkan. Peta tematik yang dihasilkan dari citra Sentinel-2 dapat menyediakan informasi yang lebih terbaharui. Informasi tersebut selanjutnya dapat digunakan sebagai dasar perencanaan dan aplikasi peta lainya.

Sentinel-2 merupakan salah satu satelit penginderaan jauh dengan sensor pasif. Sentinel-2 memiliki 13-band spektral yaitu band 2,3,4 dan 8 dengan ketelitian spasial 10 m, band 5,6,7, 8a, 11 dan 12 mempunyai ketelitian spasial 20 m dan band 1, 9, dan 10 memiliki ketelitian spasial 60 m (Esa, 2013). Citra sentinel-2 banyak digunakan untuk identifikasi dan analisis permasalahan terkait dengan lingkungan, perencanaan perkotaan, deteksi perubahan tutupan lahan, pemetaan resiko bencana dan beragam aplikasi lainnya (Clerici, Valbuena Calderón & Posada, 2017; Tavares *et al.*, 2019; Lopes *et al.*, 2020).

Peta tematik *LCLU* dapat dihasilkan dari peta konvensional yang ada atau diturunkan melalui citra satelit. Ke dua jenis peta tersebut dapat digunakan untuk mempelajari *LCLU* dan perubahannya, seperti pada penelitian yang dilakukan oleh (Eremiasova & Skokanova 2009) dan (Ptak & Ławniczak, 2012).

Selanjutnya Lambin *et al.* (2001); Martínez & Mollicone (2012); Efroymson *et al.* (2016); dan Song *et al.* (2018) memberi contoh bagaimana eksplorasi lebih lanjut hubungan sebab-akibat antara perubahan *LCLU* dan kosenkuensinya terhadap masyarakat dan lingkungan. Pada kasus yang lain, beberapa penelitian mencoba mengintegrasikan berbagai macam data citra melalui teknik fusi citra *(image fusion)* untuk mempelajari fenomena *LCLU* dengan lebih komprehensif (Moran, 2010; Li, Lu, Moran, Dutra, & Batistella, 2012; Wężyk, Hawryło, Szostak, Pierzchalski, & Kok, 2016; Tavares *et al.*, 2019).

Penggunaan citra Sentinel-2A untuk interpretasi *LCLU*, perubahan dan konsekuensinya telah menjadi subjek penelitian yang cukup populer pada 5 tahun terakhir. Beberapa contoh aplikasi citra Sentinel-2A untuk identifikasi dan pemetaan pada bidang terkait dengan

DOI: 10.24114/jg.v12i02.16970
e-ISSN: 2549–7057 | p-ISSN: 2085–8167

pertanian, misalnya dijumpai dalam tulisan (Rujoiu-Mare *et al.*, 2017; Tavares *et al.*, 2019 ; Abdi, 2019). Penelitian tersebut menunjukkan potensi aplikasi citra sentinel-2A untuk pemetaan *LCLU* dan fenomena terkait.

Interval waktu pemotretan dengan frekuensi yang cukup tinggi, yang ditawarkan oleh Landsat-8 (Operational Land Imager) dan citra Sentinel 2A atau 2B MSI (*Multi Spekctral imaging*) memberikan peluang baru untuk memetakan dan mengidentifikasi karakteristik dinamika perubahan permu-kaan bumi kita dari waktu ke waktu dengan mengkombinasikan ke dua citra tersebut (Bolton *et al.*, 2020). Memetakan menggunakan citra satelit pada prinsipnya adalah mengklasifikasikan piksel menjadi sekelompok piksel berdasar-kan logika tertentu, sehingga objek atau fitur yang ada di alam dapat digambarkan semirip mungkin. Hal ini dapat dilakukan dengan berbagai metode, misalnya: klasifikasi, segmentasi, *machine-learning* atau algoritma yang lain.

Metode klasifikasi sudah sangat umum digunakan. Khorram *et al.*, (2013) menyatakan bahwa kebanyakan metode klasifikasi citra didasarkan pada "*hard-logic*", menggunakan baik infomasi spektral dan pola temporal-spasial. Klasifikasi berbasis "*hard-logic*" ini secara umum dibedakan menjadi dua, yaitu klasifikasi terbimbing *(supervised classification)* dan klasifikasi tidak terbimbing *(un-supervised classification)*.

Secara prinsip ke dua jenis teknik klasifi-kasi tersebut dapat menggunakan berbagai macam algoritma yang ada. Pada klasifikasi terbimbing, titik kritis metode ada pada jenis dan jumlah training area yang digunakan untuk proses klasifikasi. Kombinasi kanal yang dipilih juga akan menentukan hasil klasifikasi (Richards, 2013).

Klasifikasi tidak terbimbing dapat menggunakan berbagai algoritma pengelom-pokan *(clustering-algorithm)*. Klasifikasi tidak terbimbing menggabungkan piksel hanya berdasarkan kemiripan karaktertisik piksel dan dilambangkan oleh nilai digital (DN value)(Richards, 2013). Lebih lanjut, Khorram *et al.* (2013) menyatakan bahwa algoritma yang paling umum digunakan pada proses klasifikasi terbimbing adalah *Maximum Likelihood Classification (MLC).*

Ketelitian hasil klasifikasi dapat diukur dengan berbagai metode (Foody, 2002, 2004). Metode yang paling umum digunakan untuk mengukur ketelitian hasil kaslifikasi adalah matrik kesalahan atau *confusion-matrix* (Foody, 2004). Konsep matrik kesalahan umumnya telah ditulis pada buku teks tentang penginderaan jauh (Lillesand, Kiefer & Chipman, 2008; Campbell & Wynne, 2011).

Ada perbedaan tingkat penerimaan dari hasil matrik kesalahan. USGS, (2019) menyatakan minimal 85% tingkat kesalahan cukup untuk menyatakan hasil klasifikasi yang baik. Sementara, LAPAN (2015) mensyaratkan tingkat ketelitian lebih dari 75% untuk menyatakan bahwa hasil klasifikasi memadai. Selanjutnya Foody (2008) merekomendasikan tingkat ketelitian 89% ± 5% interval konfidensi untuk menyatakan hasil klasifikasi yang baik.

Di Indonesia, sumber utama untuk interpretasi *LCLU* pada wilayah pedesaan adalah Peta Rupa bumi Indonesia (RBI). Peta ini dapat didownload secara gratis untuk semua wilayah NKRI, melalui laman resmi portal BIG. Peta RBI dapat didownload dalam format raster (*.Jpeg) dari hasil scan lembar peta atau dalam format shapefile (*.shp) (format vektor)(BIG, 2019).

Pada kebanyakan wilayah pedesaan di Indonesia, peta RBI yang tersedia adalah peta RBI produksi tahun 1999 sd 2001. Artinya peta RBI yang ada menggambarkan tutupan dan peruntukan lahan wilayah pada sekitar tahun 2000 (atau 20 tahun yang lalu). Dan pada kebanyakan wilayah peta RBI yang ada masih belum terbaharui. Tetapi pada kenyataannya, peta RBI juga masih digunakan sebagai dasar kajian dan

DOI: 10.24114/jg.v12i02.16970
e-ISSN: 2549–7057 | p-ISSN: 2085–8167

interpretasi (Riadi & Makmuriyanto, 2014; Susetyo, 2015).

Pada beberapa kasus peta RBI masih dapat dan layak digunakan. Pada kasus dimana fenomena yang akan dibahas adalah masalah terkait kekinian, peta detail perkotaan, maka peta RBI perlu diperbaharui dengan interpretasi citra satelit yang memiliki ketelitian spasial tinggi, hasil survei, foto udara atau drone (Hakim, Riqqi & Harto, 2014; Riadi & Rachma, 2017; Sudarman, Sadikin & Prijatna, 2020).

Salah satu cara sederhana membuat peta adalah dengan digitasi manual dari peta Google Earth. Namun demikian, proses digitasi manual tidak disarankan untuk wilayah yang luas, karena beresiko pada banyak-nya kesalahan digitasi yang mungkin dilakukan, disamping proses lebih lama, hasil kurang teliti dan biaya mahal. Alternatif lain adalah menggunakan Citra satelit resolusi tinggi, *Unmanned Aerial Vehicle (UAV)* atau drone. Drone sangat bagus untuk digunakan pada wilayah yang relatif sempit dan membutuhkan ketelitian yang cukup tinggi. Namun demikian, penggunaan citra resolusi tinggi dan drone untuk pemetaan wilayah yang luas, akan membutuhkan banyak biaya, proses rendering, penggabungan *(mozaick)* dan interpretasi menjadi lebih lama, dan membutuhkan teknologi hardware dan software dengan kapasitas memadai.

Ketersediaan data citra Sentinel yang gratis dan mencakup setiap wilayah di permukaan bumi kita, menjanjikan alternatif solusi bagi proses pemetaan yang cukup akurat, biaya murah, dan mudah diterapkan.

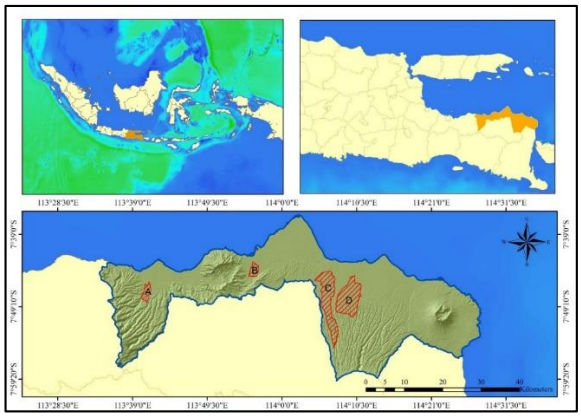
Penelitian ini bertujuan untuk: (1) menghasilkan peta tematik *LCLU* dari interpretasi Sentinel, (2) membandingkan peta tematik yang dihasilkan dari interpretasi citra sentinel, digitasi manual dan peta RBI, (3) menginterpretasikan peta tutupan dan peruntukan lahan pada level desa. Desa merupakan wilayah administrasi paling kecil. Perencanaan wilayah, perubahan *LCLU* dan aspek pembangunan lainnya dimulai dari level Desa, sehingga pemetaan status dan perubahan *LCLU* pada level desa sangat pentin untuk dilakukan. Apa jenis LCLU utama pada level desa yang dapat dideteksi melaluai Sentinel? Apakah hasil pemetaan rasional dan dapat dibandingkan dengan RBI, dan dengan digitasi manual.

METODE PENELITIAN

Lokasi Penelitian

Kabupaten Situbondo (Gambar 1) terletak di bagian timur wilayah Jawa Timur memiliki luas wilayah total = 1651,33 km^2. Jumlah penduduk per Kabupaten = 691622 orang. Kepadatan populasi = 422 per km^2 dan pertumbuhan penduduk tahunan dihitung selama periode 2018–2019 is 0,46 (%)(BPS, 2019).

Wilayah kabupaten situbondo relatif kering dibanding wilayah lain di Jawa Timur. Hujan tahunan rerata berkisar antara 500 sd 1500 mm/tahun. Umumnya di Jawa timur hujan tahunan berkisar antara 1000 sd 3500 mm/tahun. Bulan kering (hujan < 100mm/bln) , lamanya antara 7 sd 9 bulan per tahun. Penelitian ini dilaksanakan antara bulan Maret sampai November 2019.



Gambar 1. Lokasi Penelitian

Alat dan Bahan

1. Perangkat lunak *multispec Versi* 9 (Landgrebe, 2005) digunakan untuk klasifikasi dan interpretasi citra sentinel-2A.

DOI: 10.24114/jg.v12i02.16970
e-ISSN: 2549–7057 | p-ISSN: 2085–8167

2. Q-GIS 3.2.0 diunduh dari website https://qgis.org (QGIS Development Team, 2019) dan digunakan untuk *reclass dan koreksi atmosferik.*
4. GPS digunakan untuk mengambil titik GCP *(Ground check point)* dan *Google earth* image (digunakan untuk melihat kecocokan keadaan yang ada dilapang.
5. Camera untuk mengambil gambar GCp.

Input Data

1. Input utama pada penelitin ini adalah citra Sentinel-2A yang mencakup seluas wilayah Kabupaten Situbondo. Citra diunduh dengan kriteria penutupan awan *(cloud coverage)* yang paling minimal. Citra didownload dari web site USGS (USGS, 2019). Karena fokus penelitian ini adalah pemetaan jenis *LCLU* maka citra yang paling baik untuk diunduh adalah citra dengan tutupan awan yang minimal. Dua scene citra dari tanggal 25 bulan Juni 2019 diunduh dan digabung.

Tabel 1. *Raw image metadata*

Cloud cover(%)	Data type	orbit
0,0179	S2A_MSIL1C	Descending
0,1016	S2A_MSIL1C	Descending

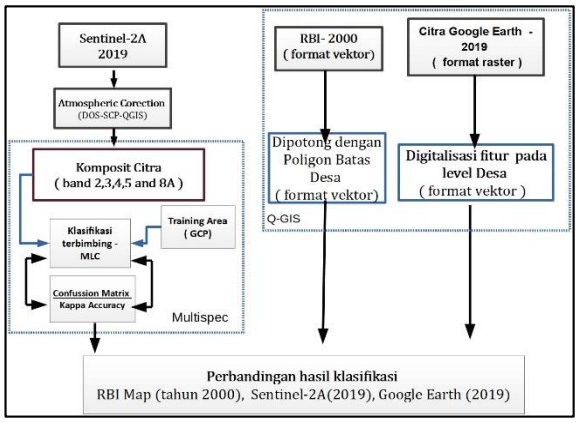
Sumber: Pemrosesan Data, 2019

2. Peta RBI diunduh dari laman resmi website BIG (BIG, 2019). Peta RBI skala 1:25000 (skala sedang) diunduh seluas wilayah Kab. Situbondo. Peta RBI selanjutnya di potong seluas wilayah 4 desa sebagai sampel evaluasi.
3. Google Earth image diunduh hanya seluas 4 wilayah desa yang dijadikan sample. Baik RBI maupun google erath image dignakan sebagai pembanding dapam penelitian ini.

Prosedur Pemrosesan Data

Gambar (2) menampilkan prosedur penelitian. Blok kiri merinci urutan langkah pengolahan citra sentinel-2A, yang mencakup: koreksi atmosferik *(atmospheric correction),* komposit citra, klasifikasi terbimbing, survey lapang, dan *accuracy assessment*.

Koreksi atmospheric menggunakan algo-ritma DOS *(Dark Object Sub-traction)* yang ada pada tool SCP *(semi automatic plugin)* dan mengikuti prosedur yang telah dipubikasi oleh (Congedo, 2016). Koreksi atmosferik dilakukan menggunakan QGIS. Citra Sentinel-2A yang tersedia adalah Level-1C artinya telah terkoreksi secara geometrik. Komposit citra dibuat dengan kombinasi 5 kanal yaitu (kanal 2,3,4,5 dan 8A).



Gambar 2. Prosedur Pemrosesan Data

Beberapa kali kegiatan survey lapang dilakukan antar bulan Mei sd November 2019 untuk mengoleksi GCP dan memotret wilayah kajian. Sejumlah 771 GCP dibuat untuk membantu proses klasifikasi terbimbing (Tabel 2).

Tabel 2. Ringkasan GCP

LCLU class	Jumlah GCP	Luas ukuran GCP (ha)		
		Total	Min	Mak
Water body	40	553,9	1,23	54,3
Forest-plantation	184	12.366,5	1,78	209
DryMAL	165	4.280,2	1,21	93,5
Non-Irrigated	92	2.169,5	1,40	46,8
Built- up area	140	3.425,6	2,38	56,7
Irrigated paddy field	150	3.222,6	1,14	56,8
Total	771	26.018,3		

Sumber: Pemrosesan Data, 2019

DOI: 10.24114/jg.v12i02.16970
e-ISSN: 2549–7057 | p-ISSN: 2085–8167

Klasifikasi dilakukan dengan algoritma *maximul likelihood classification (MLC) (Landgrebe and Biehl, 2011)*. *MLC* dijalankan dengan menggunakan lima kanal untuk komposit citra dan 771 GCP. Proses kasifikasi mengikuti prosedur pada tutorial (Landgrebe, 2015).

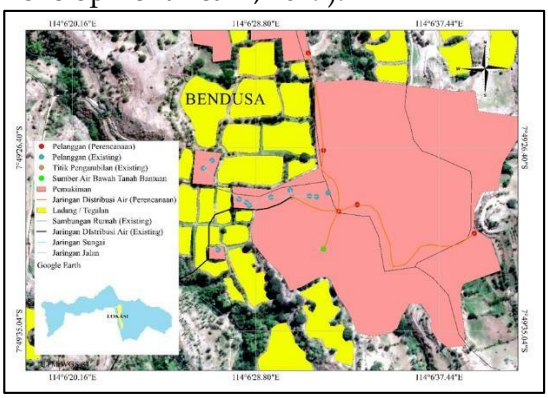
Selanjutnya digunakan, matrik kesalahan berbasis indek *overall* dan *kappa accuracy*, untuk menilai kualitas hasil klasifikasi. Kriteria ketelitian menggunakan 89% (Foody, 2008).

Langkah berikutnya, Empat (4) wilayah Desa digunakan sebagai sampel untuk mengevaluasi hasil klasifikasi, yaitu desa: Jatisari, Sopet, Kendit, dan Jatibanteng. Pemilihan desa berdasarkan lokasi dan karakteristik LCLU yang ada pada tiap desa. Selanjutnya peta tematik hasil klasifikasi dipotong *(clip)* seluas batas Desa untuk dibandingkan dengan peta RBI dan hasil digitasi manual.

Peta RBI yang diunduh dari laman BIG, se batas wilayah kabupaten Situbondo (dalam format vector), selanjutnya dipotong dengan poligon batas desa (Blok tengah dari gambar 2). Hasilnya berupa peta LCLU desa versi RBI tahun 2000, sebagai bahan perbandingan. Proses dilakukan pada software QGIS.

Selanjutnya, pada blok kanan, google earth image diunduh dengan Easy Google Map downloader dan digabung seluas batas Desa. Selanjutnya , citra *Google Earth* (dalam format raster) tersebut, dijadikan sebagai background map-file untuk proses digitalisasi. Hasil digitalisasi adalah peta raster.

Selanjutnya, (1) peta RBI dan (2) peta hasil digitasi manual dari Google Earth digunakan untuk Evaluasi. Peta RBI dipotong *(clip)* sebatas desa Jatisari dan dihitung luas tiap jenis peruntukan lahan. Kemudian, Citra Google Earth di mosaick dan dipotong dengan batas Desa Jatisari. Selanjutnya, dilakukan pembuatan peta LCLU desa secara manual dengan melakukan digitalisasi. Dalam hal ini citra google tidak diolah, tetapi hanya digunakan sebagai back- ground map file untuk melakukan digitalisasi (gambar 3). Metode ini sudah sangat umum dipraktekkan. Proses digitalisasi dilakukan menggunakan QGIS (QGIS Development Team, 2019).



Gambar 3. Ilustrasi Proses Digitasi

Selanjutnya, evaluasi dilakukan dengan membandingkan jenis fitur yang dapat dipetakan dan prosentase luas. Interpretasi dilakukan dengan membandingkan ke tiga peta tematik *LCLU*, yaitu: (1) dari RBI, (2) hasil klasifikasi terbimbing metode *MLC*, (3) Digitasi dari google earth. Interpretasi juga dilakukan dengan membandingkan kenya-taan yang ada di Lapang.

HASIL DAN PEMBAHASAN

Interpretasi Umum

Klasifikasi terbimbing menggunakan *MLC* menghasilkan indek overall dan kappa accuracy = 95,6% dan 93%. Menurut Foody (2008) hasil ini cukup memadai dan memenuhi kriteria standar klasifikasi. Tabel 3 menampilkan perbandingan hasil klasifi-kasi dengan peta RBI tahun 2000.

Table 3. Perbandingan RBI dan Sentinel

LULC Class	RBI-2000		Sentinel - 2019	
	km²	%	km²	%
Area terbangun	90	5,45	174	10,53
LSO-kering	859	52,0	439,1	26,6
Lahan irigasi	207	12,5	170,9	10,35
Lahan non-irigasi	109	6,6	33,4	2,02
Hutan-perkebunan	363,3	22,0	821,7	49,8
Badan air	23,0	1,39	12,18	0,74
Total	1651,3	100	1651,3	100

Sumber: Pengolahan Data, 2019

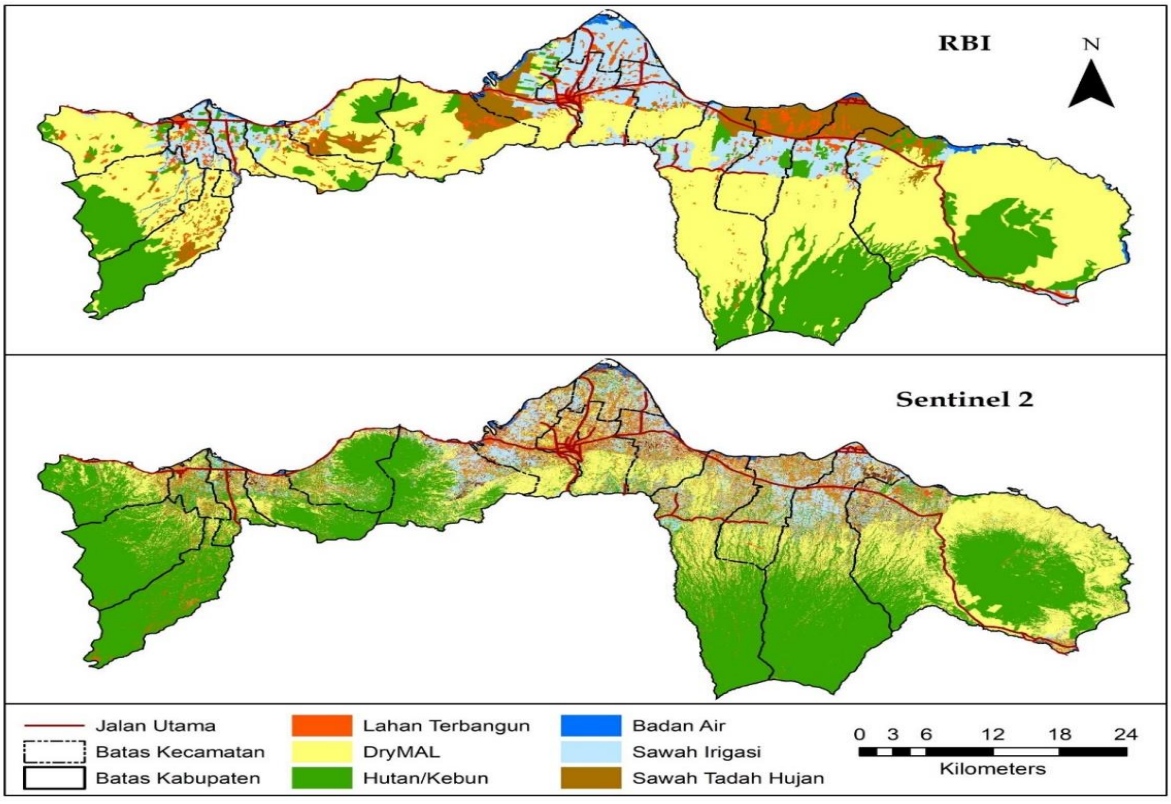
DOI: 10.24114/jg.v12i02.16970
e-ISSN: 2549–7057 | p-ISSN: 2085–8167

Gambar (4) menampilkan peta hasil klasifikasi Sentinel dibandingkan dengan peta RBI. RBI dibuat pada tahun 2000-an, sementara sentinel berdasarkan citra tahun 2019. Perubahan *LCLU* dapat diamati dengan membandingkan 3 kelas, yaitu: LSO-kering, kebun-hutan, dan lahan non-irigasi. Asal dari ke tiga kelas ini pada hakekatnya sama yaitu Lahan Sub-optimal kering (LSO-Kering). Definisi LSO-kering merujuk pada publikasi (Mulyani & Sarwani, (2013) ; Mulyani, Priyono & Agus, (2013).

Luas total ke tiga kelas pada RBI = (859 + 109 + 363,3) = 1331,3 km^2 = 80,62% dari total luas wilayah Situbondo. Sedangkan pada citra Sentinel luas total = 439,1 + 33,4 + 821,7 1294,2 km^2= 78.37%. Hal ini menunjukan telah terjadi perubahan peruntukan lahan (LU) dari LSO-kering menjadi peruntukan lainnya. LSO-kering berkurang karena dimanfaatkan untuk peruntukan lainnya, menjadi hutan dan sebagian besar LSO-Kering telah dimanfaatkan untuk kebun, pemukiman dan sawah atau ladang.

Peruntukan lahan untuk area terbangun (berupa pemukiman warga, infrastruktur jalan, kawan pertokoan, dll) telah meningkat secara signifikan selama dua dekade. Pada peta RBI (tahun 2000) luas total area terbangun = 90 km^2 , hanya mencakup 5,45% dari luas total wilayah Kabupaten Situbondo. Pada tahun 2019 (sentinel), area terbangun sudah mencapai = 174 km^2 = 10,53% luas total wilayah. Jadi dari tahun 2000 sd 2019 telah terjadi peningkatan luas pemukiman di Kabupaten Situbondo menjadi 2x lipat.

Perubahan terjadi dan dapat disebabkan karena urbanisasi dan peningkatan jumlah penduduk di wilayah perkotaan Situbondo. Misalnya terjadi di kecamatan Besuki, Bungatan, Panarukan, Mangaran, Situbondo, Panji, Kapongan, Jangkar, Arjasa dan Asembagus. Umumnya wilayah kecamatan yang berada di sepanjang Pantai utara Jawa. Perkembangan industri dan lokasi wisata di sepanjang pantai Situbondo juga meningkatkan konversi lahan ke pemukiman dan fasilitas perkotaan terkait.



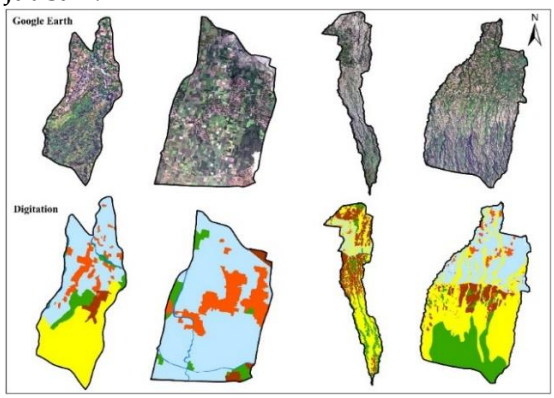
Gambar 4. Perbandingan hasil klasifikasi dengan peta RBI.

DOI: 10.24114/jg.v12i02.16970
e-ISSN: 2549–7057 | p-ISSN: 2085–8167

Konversi lahan sawah dan tegalan menjadi pemukiman (lahan terbangun) juga terjadi. Fenomena ini teramati pada wilayah perkotaan (bagian tengah dari Peta), di kecamatan Mangaran, Situbondo, Panarukan, Panji, dan Kapongan. Lahan Irigasi di wilayah tersebut telah terkonversi sebagian menjadi area-terbangun untuk pemukiman atau fasilitas kota lainnya (infrastruktur jalan, mall, dll). Lahan irigasi pada peta RBI tampak sebagai blok-luasan berwarna biru-muda, dan telah berubah menjadi lahan campuran yang terdiri dari pemukiman dan lahan sawah (terlihat pada peta hasil klasifikasi Sentinel).

Peta Hasil Digitalisasi

Gambar (5) menampilkan perbandingan antara citra Google Earth dan hasil digitalisasi pada ke empat (4) desa sampel. Ketelitian proses digitalisasi sangat tergantung pada konsistenti dan ketelitian operator dalam melakukan digitasi. Terlihat bahwa hasil digitalisasi yang baik dan paling detail adalah desa Jatisari.



Gambar 5. Peta Hasil Digitasi

Luas wilayah ke empat desa juga berbeda, yaitu : Jatibanteng (6.78 km²), Kendit (6.45 km²), Jatisari (45.97 km²), and Sopet (43.51 km²).

Pada wilayah desa Jatibanteng, Kendit dan Sopet relatif hanya fitur utama yang didigitasi. Artinya, seharusnya pada penelitian ini, peta hasil digitasi dari Google Earth dapat menjadi acuan utama, tetapi faktor operator dapat menyebabkan hasil digitasi atau perhitungan luas menjadi kurang tepat, sehingga digitasi menjadi pertimbangan dalam interpretasi tetapi tidak dapat menjadi tolok ukur utama.

Interpretasi LCLU Desa Jatisari

Tabel (4) menampilkan perbandingan *LCLU* di desa Jatisari (45.97 km²). Luasan yang sama dipetakan dengan cara yang berbeda akan menghasilkan detail yang berbeda.

Table 4. Perbandingan LCLU Jatisari

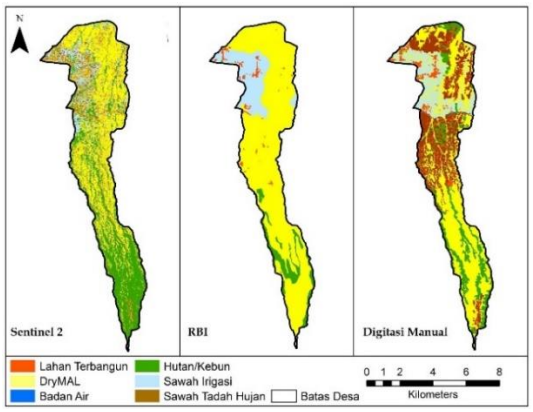
Kelas LCLU	RBI-2000		Google Earth - 2019		Sentinel 2A-2019	
	km²	%	km²	%	km²	%
Area terbangun	1,03	2,24	1,79	3,90	1,83	3,99
LSO-kering	34,9	76,0	23,3	50,6	23,7	51,6
Lahan irigasi	6,57	14,3	6,89	15,0	4,65	10,1
Lahan non-irigasi	0,00	0,00	8,12	17,7	0,49	1,08
Hutan-kebun	3,42	7,44	5,83	12,6	15,3	33,2
Badan air	0,00	0,00	0,05	0,12	0,00	0,01
Luas total	45,9	100	45,9	100	45,9	100

Sumber: Pengolahan Data, 2019

Area terbangun yang pada tahun 2000 hanya seluas 1,03 km² atau (2,24%) dari luas Desa Jatisari. Pada tahun 2019 telah berkembang menjadi hampir 2x lipat (1,83 km²) atau (±3,90%) pada tahun 2019. Hasil klasifikasi relatif identik dengan hasil digitasi manual. Perbedaan hanya sekitar = 1.83 – 1.79 = 0.04 km².

Kemiripan hasil juga terlihat untuk kelas LSO-kering. Sentinel dapat memisahkan dengan jelas pemukiman dan LSO. Proses digitasi sawah irigasi lebih luas dari yang seharusnya, karena mungkin ada lahan non-irigasi yang dianggap sebagai lahan irigasi. Pada citra Google Earth kenampakan ke dua-nya hampir mirip. Lahan irigasi pada wilayah Jatisari relatif tidak bertambah, sejak dibangun-nya Jaringan Irigasi. Daerah irigasi (warna biru muda) hanya ada diujung sebelah kiri atas dari peta RBI (Gambar 6).

DOI: 10.24114/jg.v12i02.16970
e-ISSN: 2549–7057 | p-ISSN: 2085–8167



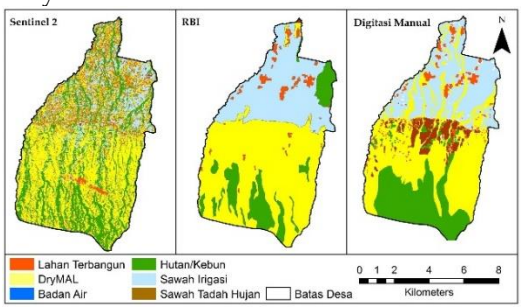
Gambar 6. LCLU Desa Jatisari

Pada proses digitasi, karena dilakukan secara manual, maka lahan non-irigasi dapat dipisahkan dari Kebun. Proses digitasi mengindentifikasi kebun mangga warga dengan baik. Dimana area berpohon dianggap kebun, sedangkan area kosong didigit lahan non-irigasi. Pada Sentinel tutupan lahan (LC) dipisahkan menjadi 2, area yang tidak bervegatasi dimasukan sebagai LSO (ladang/tegalan) dan area berpohon (termasuk tanah kosong di sekitar kebun atau tanaman) diklasifikan sebagai hutan-kebun. Dalam hal ini, sentinel melihat hutan dan kebun sama sebagai kelas tanaman tahunan. Pohon besar yang hijau sepanjang tahun. Sementara, RBI mengidentifikasi lahan berbasis land use (fungsi kebun dan fungsi hutan).

Lahan irigasi yang pada peta RBI digambarkan sebagai blok-area (*Land-use*) berwarna biru muda, telah berubah karena sebagian dikonversi untuk pemukiman warga. Sehingga, tampak di peta Sentinel sebagai campuran warna biru-merah-kuning yang menunjukan kondisi tutupan lahan *(LC)* yang lebih terfragmentasi berupa campuran antara pemukiman vegetasi dan lahan irigasi.

LCLU Desa Sopet

Peruntukan lahan (LU) di peta RBI terbagi ke dalam : area-terbangun, lahan-irigasi, LSO-kering, hutan dan perkebunan (gambar 7). Saluran irigasi Sampeanbaru melintas dari Barat ke Timur dan membagi wilayah Sopet menjadi dua bagian yang kontras (Gambar 7). Di bawah saluran adalah lahan irigasi. Pada peta RBI, lahan irigasi berupa blok-area berwarna biru-muda, mencakup ± 30% wilayah desa dan terletak di sebelah utara saluran. Sebagian lahan irigasi telah terkonversi menjadi pemukiman. Di atas saluran adalah LSO-kering, perkebunan dan hutan mencakup seluas ±30 km² atau 67,7% dari total wilayah desa.



Gambar 7. LCLU Desa Sopet

Proses digitasi dilakukan dengan mengikuti fitur utama dari google earth sehingga hasilnya menyerupai RBI. Sentinel dapat mengklasifikasikan konsidi *penutupan lahan (LC)* di Sopet dengan lebih detail. Dimana terlihat bahwa area yang awalnya diperuntukan untuk lahan irigasi, telah terkonversi sebagian menjadi area terbangun dan vegetasi tahunan. Demikian juga di bagian selatan dari saluran. LSO-kering (pada RBI 2000) diklasifikasikan menjadi LSO-kering dan vegatsi tahunan (hutan –perkebunan) dalam bentuk yang lebih terfragmentasi. Hal ini karena sentinel mengelompokan pixel ke dalam kelas berdasarkan penutupan lahan (*land cover*).

Table 5. LCLU desa Sopet

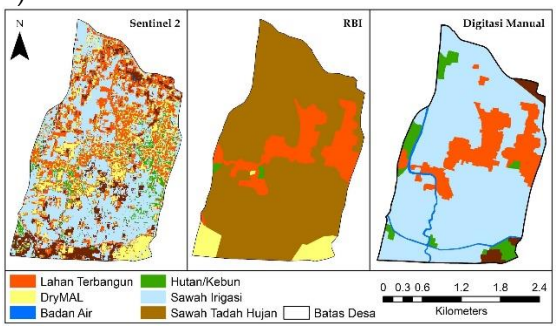
Kelas LCLU	RBI 2000		Google Earth- 2019		Sentinel 2A - 2019	
	km²	%	km²	%	km²	%
Area terbangun	1,15	2,64	1,42	3,3	5,6	12,9
LSO-kering	23,5	54,1	17,42	40,1	18,7	43,0
Lahan irigasi	12,9	29,7	11,09	25,5	6,31	14,5
Lahan non irigasi	0,04	0,09	3,07	7,07	0,54	1,24
Hutan - perkebunan	5,9	13,5	9,11	20,9	12,3	28,4
Badan air	0,00	0,00	1,39	3,19	0,00	0,00
Total	43,5	0,00	43,51	100	43,5	100

DOI: 10.24114/jg.v12i02.16970
e-ISSN: 2549–7057 | p-ISSN: 2085–8167

Selama 19 tahun, area terbangun meningkat 4,86 kali lebih luas. LSO-kering berkurang – 20% dari luas sebelumnya. Lahan irigasi telah berkurang hampir 50%. Luas area untuk perkebunan dan hutan menjadi 2 kali lipat (Tabel 5).

LCLU Desa Kendit

Desa kendit terletak di wilayah bawah, dekat dengan pantai dan pada topografi yang relatif datar. Pada tahun 2000 (peta RBI), hampir 80% wilayah di Kendit adalah lahan non-irigasi atau sawah tadah hujan. Pengembangan jaringan irigasi (dalam hal ini, saluran Induk Panarukan) telah mampu mengairi lahan tersebut menjadi sawah irigasi. Saluran irigasi pada proses digitalisasi digambarkan sebagai badan air (Gambar 8).



Gambar 8. LCLU Desa Kendit

Lahan irigasi didigitasi seluas 75%. Selama 19 tahun, area terbangun hanya bertambah = 1,07 – 0,99 = 0,08 km², sesuatu yang sulit untuk dipahami untuk suatu wilayah perkotaan. Hal ini karena proses digitasi dilakukan hanya mengambil secara umum (berupa zona). Ini salah satu kelemahan dari operator dalam proses digitasi. Dalam hal ini, Sentinel dapat menggambarkan proses perubahan dari lahan non-irigasi ke lahan-irigasi, area terbangun dan vegetasi tahunan dengan lebih baik. Luas area terbangun selama 19 tahun telah meningkat menjadi 1,6 x dari sebelumnya (tabel 6). Lahan irigasi tinggal 45% dari luas total. Lahan non-irigasi (tegalan/ladang) seluas 10% berada di utara saluran dan merupakan wilayah yang lebih tinggi dari saluran induk, sehingga tidak terairi. Hutan-perkebunan seluas 4,34% hakekat-nya adalah tanaman tahunan, seperti pohon mangga, tanaman di sekitar jalan atau pohon di sekitar pekarangan rumah.

Table 6. LCLU at Kendit

Kelas LCLU	RBI 2000		Google Earth - 2019		Sentinel 2A - 2019	
	km²	%	km²	%	km²	%
Area terbangun	0,99	15,4	1,07	16,6	1,58	24,5
LSO-kering	0,34	5,26	0,00	0,00	0,96	14,9
Lahan irigasi	0,00	0,00	4,81	74,6	2,92	45,2
Lahan non-irigasi	5,07	78,6	0,15	2,33	0,70	10,9
Hutan - perkebunan	0,04	0,69	0,31	4,75	0,28	4,34
Badan air	0,00	0,00	0,11	1,72	0,01	0,12
Total	6,45	100	6,45	100	6,45	100

Sumber: Pengolahan Data, 2019

LULC Desa JatiBanteng

Desa Jatibanteng merupakan pusat dari Kecamatan Jatibanteng. Dalam hal ini area terbangun relatif tidak berubah selama 19 tahun. LSO-kering berkurang dai 36% menjadi 24% (Tabel 7).

Tabel 7. LCLU Jatibanteng

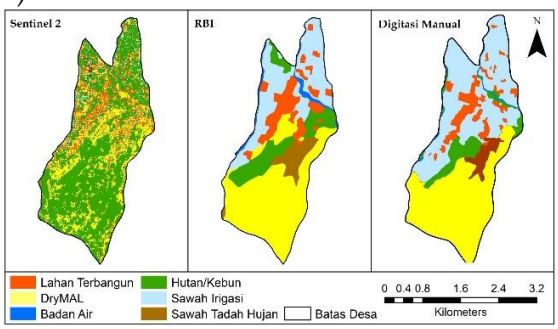
LCLU class	RBI 2000		Google Earth- 2019		Sentinel 2019	
	km²	%	km²	%	km²	%
Area terbangun	0,79	11,7	0,59	8,7	0,80	11,9
LSO-kering	2,43	35,9	2,69	39,6	1,60	23,6
Lahan irigasi	1,72	25,4	2,70	39,9	0,27	4,0
Lahan non-irigasi	0,41	6,00	0,25	3,68	0,06	0,88
Hutan-perkebunan	1,18	17,4	0,49	7,17	4,05	59,7
Badan air	0,24	3,57	0,07	1,00	0,00	0,00
Total	6,78	100	6,78	100	6,78	100

Sumber: Pengolahan Data, 2019

Sebaliknya wilayah hutan-perkebunan digambarkan oleh Sentinel lebih besar. Hal ini karena, citra yang digunakan adalah hasil pemotretan pada akhir musim penghujan (juni 2019). Lahan di wilayah Jati Banteng masih banyak tertutup oleh vegetasi. Vegetasi yang dominan, diklasifikasikan lebih ke

DOI: 10.24114/jg.v12i02.16970
e-ISSN: 2549–7057 | p-ISSN: 2085–8167

dalam kelas hutan-perkebunan (Gambar 9).



Gambar 9. LCLU Desa Jatibanteng

KESIMPULAN

Artikel ini membahas perbandingan peta hasil klasifikasi dari citra-Sentinel 2A, peta hasil digitasi manual dari Google Earth dan peta RBI Digital untuk menggambarkan tutupan dan peruntukan lahan (*LCLU*) pada level desa. Perbandingan hasil klasifikasi, dengan digitasi manual dan RBI dapat digunakan sebagai dasar interpretasi *LCLU* di wilayah empat desa tersebut dan identifikasi perubahan *LCLU* yang utama selama 19 tahun terakhir.

Hasil evaluasi juga menunjukan kemampuan Sentinel 2A untuk memetakan tutupan lahan sampai dengan level desa. Digitasi secara manual dari goole earth beresiko pada terjadinya kesalahan interpre-tasi. Secara umum citra sentinel dapat digunakan untuk mengambarkan fitur utama *LCLU* suatu Desa. Citra juga dapat digunakan untuk memperbaharuai peta RBI dan perencanaan pembangunan di tingkat Desa

UCAPAN TERIMA KASIH

Penelitian dan publikasi terkait LSO di wilayah Jatisari merupakan bagian dari skema Hibah Pendamping IDB LP2M UNEJ tahun anggaran 2019, No SK rektor: 13455/UN25/LT/2019 (Tanggal 9 Agustus 2019) dan contract no: 3200 /UN25.3.1/LT/2019 (tanggal 16 Agustus 2019). A.n Indarto, berjudul : "Pengembangan Jaringan Distribusi Air dan Desain Irigasi Mikro Berbasis Sumur Tanah dalam pada Lahan Sub-Optimal di Desa Jatisari, Kec Arjasa, Kab Situbondo", di bawah koordinasi keris LSO. Kepada LP2M UNEJ, pemkab Situbondo dan semua pihak yang telah membantu kelancaran proses penelitian ini disampaikan banyak terima kasih.

DAFTAR PUSTAKA

Abdi, A. M. (2019) 'Land cover and land use classification performance of machine learning algorithms in a boreal landscape using Sentinel-2 data', *GIScience & Remote Sensing*. Taylor & Francis, pp. 1–20. doi: 10.1080/15481603.2019.1650447.

BIG (2019) *Indonesia Geospatial Portal*. Available at: http://tanahair.indonesia.go.id/portal-web (Accessed: 15 December 2019).

Bolton, D. K. *et al.* (2020) 'Continental-scale land surface phenology from harmonized Landsat 8 and Sentinel-2 imagery', *Remote Sensing of Environment*. Elsevier Inc., 240. doi: 10.1016/j.rse.2020.111685.

BPS, S. (2019) *Kabupaten Situbondo dalam angka tahun 2019 (Regency Situbondo in number)*. Situbondo. Available at: https://situbondokab.bps.go.id/publication/2019/12/26/ee20f467bae2040464413b80/statistik-daerah-kabupaten-situbondo-2019.html (Accessed: 25 May 2020).

Campbell, J. B. and Wynne, R. H. (2011) *Introduction to remote sensing*. Guilford Press.

Clerici, N., Valbuena Calderón, C. A. and Posada, J. M. (2017) 'Fusion of sentinel-1a and sentinel-2A data for land cover mapping: A case study in the lower Magdalena region, Colombia', *Journal of Maps*. doi: 10.1080/17445647.2017.1372316.

Congedo, L. (2016) *Semi-Automatic Classification Plugin Documentation*. doi: 10.13140/RG.2.2.29474.02242/1.

Efroymson, R. A. *et al.* (2016) 'A causal analysis framework for land-use change and the potential role of bioenergy

policy', *Land Use Policy*. Elsevier Ltd, 59, pp. 516–527. doi: 10.1016/j.landusepol.2016.09.009.

Eremiášová, R. and Skokanová, H. (2009) 'Land Use Changes (Recorded in Old Maps) and Delimitation of the Most Stable Areas from the Perspective of Land Use in the Kašperské Hory Region', *Journal of Landscape Ecology*. Berlin: Sciendo, 2(1), pp. 20–34. doi: https://doi.org/10.2478/v10285-012-0012-5.

Esa (2013) *SENTINEL-2 User Handbook Sentinel-2 User Handbook SENTINEL-2 User Handbook Title Sentinel-2 User Handbook Issue 1 Revision 1 SENTINEL-2 User Handbook*.

EUROSTAT (2001) *Manual of concepts on land cover and land use information systems*. Available at: http://europa.eu.int (Accessed: 17 May 2020).

Foody, G. (2008) 'Harshness in image classification accuracy assessment', *International Journal of Remote Sensing*. Taylor and Francis Ltd., 29(11), pp. 3137–3158. doi: 10.1080/01431160701442120.

Foody, G. M. (2002) 'Status of land cover classification accuracy assessment', *Remote Sensing of Environment*. Elsevier Inc., pp. 185–201. doi: 10.1016/S0034-4257(01)00295-4.

Foody, G. M. (2004) 'Thematic map comparison: Evaluating the statistical significance of differences in classification accuracy', *Photogrammetric Engineering and Remote Sensing*. American Society for Photogrammetry and Remote Sensing, pp. 627–633. doi: 10.14358/PERS.70.5.627.

Hakim, Y. F., Riqqi, A. and Harto, A. B. (2014) 'Kontrol Kualitas Dalam Alur Produksi Kartografi Peta RBI di Badan Informasi Geospasial', *GEOMATIKA*, 20(1).

Hariyono, M. I. (no date) 'Kajian Perubahan Penutup Lahan Peta Rupabumi pada Skala yang Berbeda'.

Khorram, S. *et al.* (2013) 'Digital Image Acquisition: Preprocessing and Data Reduction BT - Handbook of Satellite Applications', in Pelton, J. N., Madry, S., and Camacho-Lara, S. (eds). New York, NY: Springer New York, pp. 809–837. doi: 10.1007/978-1-4419-7671-0_46.

Lambin, E. F. *et al.* (2001) 'The causes of land-use and land-cover change: Moving beyond the myths', *Global Environmental Change*. Elsevier Ltd, pp. 261–269. doi: 10.1016/S0959-3780(01)00007-3.

Landgrebe, D. (2015) *MultiSpec Tutorial: Supervised Classification-Select Training Fields*. Available at: https://engineering.purdue.edu/~biehl/MultiSpec/documentation.html (Accessed: 26 November 2019).

LAPAN (2015) 'LAPAN Pedoman Pengolahan Data Penginderaan Jauh Landsat 8 untuk MPT'. Available at: file:///F:/BISMILLAH/Ris/000_Buku_Pedoman_TSM_final.pdf.

Li, G. *et al.* (2012) 'A comparative analysis of ALOS PALSAR L-band and RADARSAT-2 C-band data for land-cover classification in a tropical moist region', *ISPRS Journal of Photogrammetry and Remote Sensing*, 70, pp. 26–38. doi: 10.1016/j.isprsjprs.2012.03.010.

Lillesand, T. M., Kiefer, R. W. and Chipman, J. W. (2008) *Remote Sensing and Image Interpretation*. 6th edn. New Jersey.

Lopes, M. *et al.* (2020) 'Combining optical and radar satellite image time series to map natural vegetation: savannas as an example', *Remote Sensing in Ecology and Conservation*. Wiley-Blackwell. doi: 10.1002/rse2.139.

Martínez, S. and Mollicone, D. (2012) 'From Land Cover to Land Use: A Methodology to Assess Land Use from Remote Sensing Data', *Remote Sensing*. MDPI AG, 4(4), pp. 1024–1045. doi: 10.3390/rs4041024.

Moran, E. F. (2010) 'Land Cover Classification in a Complex Urban-Rural Landscape with Quickbird Imagery', *Photogrammetric engineering and remote sensing*. NIH Public Access, 76(10), p. 1159.

DOI: 10.24114/jg.v12i02.16970
e-ISSN: 2549–7057 | p-ISSN: 2085–8167

Mulyani, A., Priyono, A. and Agus, F. (2013) 'Semiarid Soils of Eastern Indonesia: Soil Classification and Land Uses', in, pp. 449–466. doi: 10.1007/978-94-007-5332-7_24.

Mulyani, A. and Sarwani, M. (2013) 'Karakteristik dan Potensi Lahan Sub Optimal untuk Pengembangan Pertanian di Indonesia | Mulyani | Jurnal Sumberdaya Lahan', *Jurnal Sumberdaya Lahan*, 7(1), pp. 47–55. Available at: http://ejurnal.litbang.pertanian.go.id/index.php/jsl/article/view/6429 (Accessed: 26 November 2019).

Parece, T. E. and Campbell, J. B. (2015) 'Land use/land cover monitoring and geospatial technologies: An overview', in *Handbook of Environmental Chemistry*. Springer Verlag, pp. 1–32. doi: 10.1007/978-3-319-14212-8_1.

Ptak, M. and Ławniczak, A. E. (2012) 'Changes in land use in the buffer zone of lake of the Mała Wełna catchment', *Limnological Review*. Berlin: Sciendo, 12(1), pp. 35–44. doi: https://doi.org/10.2478/v10194-011-0043-z.

Putri Abdi. Sudarsono, Bambang., D. R. S. (2018) 'Analisis Kombinasi Citra Sentinel-1a Dan Citra Sentinel-2a Untuk Klasifikasi Tutupan Lahan (Studi Kasus: Kabupaten Demak, Jawa Tengah)', *Jurnal Geodesi Undip*, 7(2), pp. 85–96. doi: 10.1016/j.cirp.2008.03.009.

Riadi, B. and Makmuriyanto, A. (2014) 'Kajian Percepatan Penetapan dan Penegasan Batas Kecamatan/Distrik, Desa/Kelurahan Secara Kartometris', *Majalah Ilmiah Globe*, 16(2).

Riadi, B. and Rachma, T. R. N. (2017) 'Kajian Prototipe Peta Desa Menggunakan Citra Satelit Resolusi Tinggi', *Majalah Ilmiah Globe*, 19(2), pp. 147–156.

Richards, J. A. (2013) *Remote Sensing Digital Image Analysis*. 5th edn. Heidelberg: Springer-Verlag. Available at: file:///D:/KULIAH/SKRIPSI/05_Jurnal Penunjang/Remote_Sensing_Digital_Image_Analysis_www.GISman.ir.pdf.

Rujoiu-Mare, M.-R. *et al.* (2017) 'Land cover classification in Romanian Carpathians and Subcarpathians using multi-date Sentinel-2 remote sensing imagery', *European Journal of Remote Sensing*. Taylor & Francis, 50(1), pp. 496–508. doi: 10.1080/22797254.2017.1365570.

Song, X. P. *et al.* (2018) 'Global land change from 1982 to 2016', *Nature*. Nature Publishing Group, 560(7720), pp. 639–643. doi: 10.1038/s41586-018-0411-9.

Sudarman, S., Sadikin, H. and Prijatna, K. (2020) 'Desain Alternatif Lembar Peta Rupabumi Indonesia (RBI) Skala Besar', *GEOMATIKA*, 26(1), pp. 35–44.

Susetyo, D. B. (2015) 'Generalisasi kartografis pada peta Rupabumi Indonesia (RBI) skala 1: 25.000 menjadi 1: 50.000', *Proceeding of Simposium Sains Geoinformasi*, pp. 217–225.

Tavares, P. A. *et al.* (2019) 'Integration of sentinel-1 and sentinel-2 for classification and LULC mapping in the urban area of Belém, eastern Brazilian Amazon', *Sensors (Switzerland)*. MDPI AG, 19(5). doi: 10.3390/s19051140.

USGS (2019) 'EarthExplorer - Home', *U.S. Geological Survey*. Available at: https://earthexplorer.usgs.gov/ (Accessed: 15 December 2019).

USGS, U. S. G. (2019) 'Landsat 8 (L8) Data Users Hanbook Version 4.0', *Department of the Interior, U.S. Geological Survey*, 4(April), p. 106. Available at: https://prd-wret.s3-us-west-2.amazonaws.com/assets/palladium/production/atoms/files/LSDS-1574_L8_Data_Users_Handbook_v4.0.pdf.

Wężyk, P. *et al.* (2016) 'Using Geobia and Data Fusion Approach for Land use and Land Cover Mapping', *Quaestiones Geographicae*. Berlin: Sciendo, 35(1), pp. 93–104. doi: https://doi.org/10.1515/quageo-2016-0009.

MONITORING MODEL OF LAND COVER CHANGE FOR THE INDICATION OF DEVEGETATION AND REVEGETATION USING SENTINEL-2

Samsul Arifin[1]*,Tatik Kartika[1], Dede Dirgahayu[1], and Gatot Nugroho[1]
[1]Remote Sensing Applications Center – National Institute of Aeronautics and Space (LAPAN)
*e-mail: samsul_lapan@yahoo.com
Received: 11 August 2020; Revised: 17 December 2020; Approved: 21 December 2020

Abstract. Information on land cover change is very important for various purposes, including the monitoring of changes for environmental sustainability. The objective of this study is to create a monitoring model of land cover change for the indication of devegetation and revegetation using data from Sentinel-2 from 2017 to 2018 of the Brantas watershed. This is one of the priority watersheds in Indonesia, so it is necessary to observe changes in its environment, including land cover change. Such change can be detected using remote sensing data. The method used is a hybrid between Normalized Difference Vegetation Index (NDVI) and Normalized Burn Ratio (NBR) which aims to detect land changes with a focus on devegetation and revegetation by determining the threshold value for vegetation index (ΔNDVI) and open land index (ΔNBR). The study found that the best thresholds to detect revegetation were Δ NDVI > 0.0309 and Δ NBR < 0.0176 and to detect devegetation Δ NDVI < - 0.0206 and Δ NBR > 0.0314. It is concluded that Sentinel-2 data can be used to monitor land changes indicating devegetation and revegetation with established NDVI and NBR threshold conditions.

Keywords*: Model, Monitoring. Land Cover, Sentinel-2, devegetation, revegetation*

1 INTRODUCTION

Geobiophysics is one of the parameters for determining the phenomenon of land surface change. It has been applied by several researchers using the vegetation index and open/burned land index from optical satellite data. The vegetation index describes the level of greenness of plants, using a mathematical combination of the red band and NIR (Near-Infrared) band (Lillesand & Kiefe, 1997). According to Ryan (1997), the calculation of the Normalized Difference Vegetation Index (NDVI) is based on the principle that green plants grow very effectively by absorbing radiation in the red spectrum region of Photosynthetic Active Radiation (PAR), and strongly reflect sunlight from the infrared region close to the range value indices -1 to 1. The vegetation index has been used in numerous studies on a global scale of vegetation and to map drought, devegetation and deforestation (Horning **,** Juli. Robinson, Eleanor Sterling, Turner, and Spector, 2010; Kartika et al., 2018). Determination of the extraction of forest identification geobiophysical parameters can be made using the NDVI model with a threshold value with SATELIT LAPAN -3 data (Arifin, S., Kartika, T., & Carolita, I., 2019).

In general, NDVI with a combination of red and infrared specimens is an index that is widely used to identify signs of burning land (Chuvieco, E., Martin, M.P., & Palacios, A ., 2002., 2002). In addition, there have been many developments in the method of identifying burnt land/forests through the single band method (Near IR, Mid IR, Spectral thermal temperature Brightness) and the ratio band vegetation index. Research on the detection of burnt land has been widely conducted globally

http://dx.doi.org/10.30536/j.ijreses.2020.v17.a3385 @National Institute of Aeronautics and Space of Indonesia (LAPAN)

using low to medium resolution remote sensing satellite data, such as that from MODIS (Martín M.P., & Díaz-Delgado R., 2002; Roy, D.P, Boschettm, L., & Triffm, S.N., 2002; Chuvieco et al., 2005); from NOAA-AVHRR (Barbosa, P.M., Pereira, J.M.C., & Grégoire, J. M., 1998); Nielsen, T.T., Mbow, C., & Kane R., 2002);; Nielsen et al., 2002); and from SPOT VEGETATION (Silva, J.M.N, Cadima, J.F.C.L., Pereira, J.M.C. M. Grégoire., 2004). This study aims to map mangrove density in Arakan village and to determine the best NDVI results from the band combination used (Philiani, I, Saputra, L, Harvianto, L., & Muzaki, A.A., 2016). However, it should be noted that low and medium resolution data cannot detect burnt areas of less than 25 ha well (Miettinen, 2007). NDVI, the Normalized Burn Ratio (NBR), Soil-adjusted Vegetation Index (SAVI), Modified Soil-Adjusted Vegetation Index (MSAVI), and multivariate component (Principle Component Analysis, Tasseled Cap-greenness, Tasseled Cap-wetness) (Escuin, 2007) will be compared by the calculation of field data using the Composite Burn Index (CBI) method. The results show that the NBR index using the Near Infrared (NIR) and Shortwave Infrared (SWIR) spectral has a high correlation with the field data (CBI), especially in forest vegetation, in comparison to other indices. NIR and SWIR radiation spectral are exceptionally good at separating burnt and unburned land. Decreases in the tree canopy and water content after changes due to fire can be represented well by the SWIR spectrum, which has increased reflection (Key & Benson 1999; Escuin et al., 2007).NBR can be used to identify burned areas using SPOT-4 (Parwati et al., 2012). According to the index theory, NBR would be optimal in quantifying fire severity. Although previous studies have reported a high correlation between fire severity as measured in the field and satellite-derived NBR, our results provide no evidence for this (Roy et al., 2006). The formula is similar to a NDVI, except that it uses NIR and SWIR portions of the electromagnetic spectrum (Key & Benson, 1999). The TIRS band has a 100-metre spatial resolution but can be resampled to 30 metres for it to be used to identify burned scar areas. SWIR bands (TM bands 5 and 7 in Landsat 5 and 7 systems) as an NBR composite can be used to detect and map burnt areas. The Thermal Infrared Sensor (TIRS) algorithm which was used to detect fires and SWIR, which was used to detect water stress in vegetation and burned vegetation, will be seen in green, and both will become darker when burning takes place. This method modifies the dNBR (pre-NBR-post-NBR) composite (Indratmoko & Rizqihandar, 2019).

Based on several examples of studies on the utilization of NDVI and NBR geobiophysical information extracts, it is necessary to use this geobiophysical combination as a requirement for the devegetation and revegetation of land.

The objective of this study is to create a monitoring model of land cover change for the indication of devegetation and revegetation using Sentinel-2 data from 2017 to 2018. The definition of devegetation used is when there is a decrease in the appearance of the green level in the image (Aldrian & Sucahyono, 2013), while revegetation is shown by an increase in the appearance of the green level in the image at a certain location compared to the previous time.

2 MATERIALS AND METHODOLOGY

The Sentinel-2 satellite uses remote sensing technology that is easily obtained for analysis of spatial information. The satellite is a medium resolution type and has a temporal resolution of 5 days. Sentinel-2 is faster than Landsat, which has temporal resolution of 16 days. The data can be used to monitor land and

coastal cover. The Sentinel-2 Multi-spectral Instrument (MSI) has 13 spectral bands: four bands (Bands 2, 3, 4 and 8) with a resolution of 10m; six (Bands 5, 6, 7, 8a, 11 and 12) with a spatial resolution of 20m; and three (Bands 1, 9 and 10) with a spatial resolution of 60m. Sentinel-2 is complements Landsat-7 and 8 and can also be used for other themes, such as spatial planning, agro/environmental monitoring, water resources, forests and vegetation, carbon resources, and global agricultural products (The European Spance Agency, 2015)

The research location was the Brantas watershed in East Java Province (Figure 2-1). The data used in the study were Sentinel-2A multi-temporal data for 2017 and 2018 (Figure 2-2).

2.3 Sentinel Characteristics

Sentinel-2 is a European wide-swath, high-resolution, multi-spectral imaging mission. The full mission specification of the twin satellites, flying in the same orbit but phased at 180°, is designed to give a high revisit frequency of 5 days at the Equator and with orbital swath width is 290 km.

2.3.1 Sentinel-2 MSI

The Sentinel-2 Multi-spectral Instrument (MSI) measures the earth's reflected radiance in 13 spectral bands consisting of three levels of spatial resolution: four bands at 10 meters , six bands at 20 meters and three bands at 60 meters. Sentinel-2 is supporting Copernicus land monitoring studies with an imaging mission to monitor vegetation, soil and water cover, as well as to observe inland waterways and coastal areas. The data is designed to be modified and adapted by users interested in areas such as spatial planning and the monitoring of the agro-environment, water, forests and vegetation, land carbon and natural resources, and global crops.

The spatial resolution of Sentinel-2 depends on the spectral band, as shown in Table 2.1.

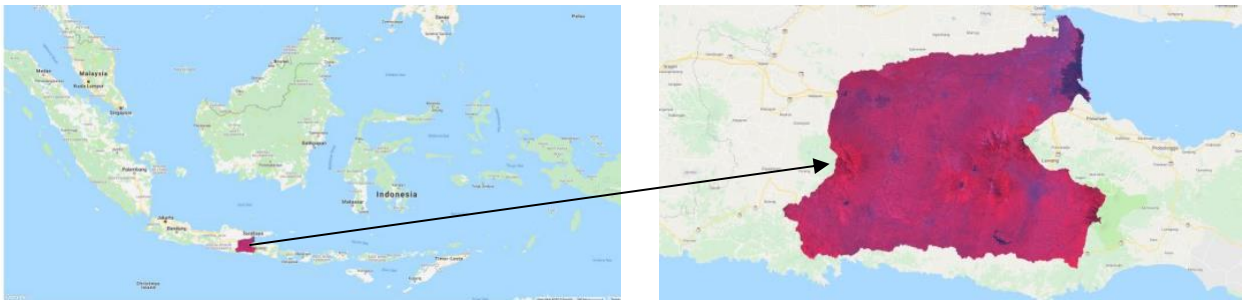


Figure 2-1: Research location: the Brantas Watershed in East Java



Figure 2-2: Sentinel-2 Data 2017-2018

Table 2-1. Spatial Resolution of Sentinel-2

Sentinel-2 Bands	Central Wavelength (μ)	Resolution (m)
Band 1: Coastal Aerosol	0.443	60
Band 2: Blue	0.490	10
Band 3: Green	0.560	10
Band 4: Red	0.665	10
Band 5: Vegetation Red Edge	0.705	20
Band 6: Vegetation Red Edge	0.740	20
Band 7: Vegetation Red Edge	0.783	20
Band 8: NIR	0.842	10
Band 8A: Vegetation Red Edge	0.865	20
Band 9: Water Vapour	0.945	60
Band 10: SWIR-Cirrus	1.375	60
Band 11: SWIR	1.610	20
Band 12: SWIR	2.190	20

2.3.3 Normalized Difference Vegetation Index (NDVI)

The NDVI quantifies vegetation by measuring the difference between near-infrared (which vegetation strongly reflects) and red light (which vegetation absorbs). As shown below, NDVI uses the NIR and red channels in its formula:

$$NDVI = \frac{NIR - Red}{NIR + Red} \quad (2\text{-}1)$$

Healthy vegetation (chlorophyll) reflects more near-infrared (NIR) and green light compared to other wavelengths, but absorbs more red and blue light. Therefore, we see vegetation as green. If it were possible to see near-infrared, this would also show strong vegetation. The satellite sensors of Sentinel-2 both have the necessary NIR and red bands. The result of this formula generates a value between -1 and +1.

$$\Delta NDVI = NDVI_{t1} - NDVI_{t2} \quad (2\text{-}2)$$

where $NDVI_{t1}$ is NDVI at the initial time and $NDVI_{t2}$ is NDVI at the final time.

2.3.4 Normalized Burn Ratio (NBR)

The NBR is used to identify burned areas. The formula is similar to a NDVI, except that it uses near-infrared (NIR) and shortwave-infrared (SWIR) portions of the electromagnetic spectrum (Key & Benson, 1999).

$$NBR = \frac{NIR - SWI}{NIR + SWIR} \quad (2\text{-}3)$$

$$\Delta NBR = NBR_{t1} - NBR_{t2} \quad (2\text{-}4)$$

where NBR_{t1} is NBR at the initial time and NBR_{t2} is NBR at the final time.

The NIR and SWIR parts of the electromagnetic spectrum are a powerful combination of bands for the index to use, given that vegetation is reflected strongly in the NIR region of the electromagnetic spectrum and weakly in the SWIR (see Figure 2-3).

Plants are reflected very strongly on the NIR spectrum, but weak on the SWIR spectrum, the combination of the NIR and SWIR spectra is excellent for identifying areas of burned land (wood / bark burnt) and soil / earth US Forest Service

The NBR index was originally developed for use with Landsat TM and ETM+ bands 4 and 7, but it will work with any multi-spectral sensor with an NIR band between 760-900 nm and a SWIR band between 2080-2350 nm. Therefore, this index can be used with both Landsat-8, MODIS and other multi (and hyper) spectral sensors.

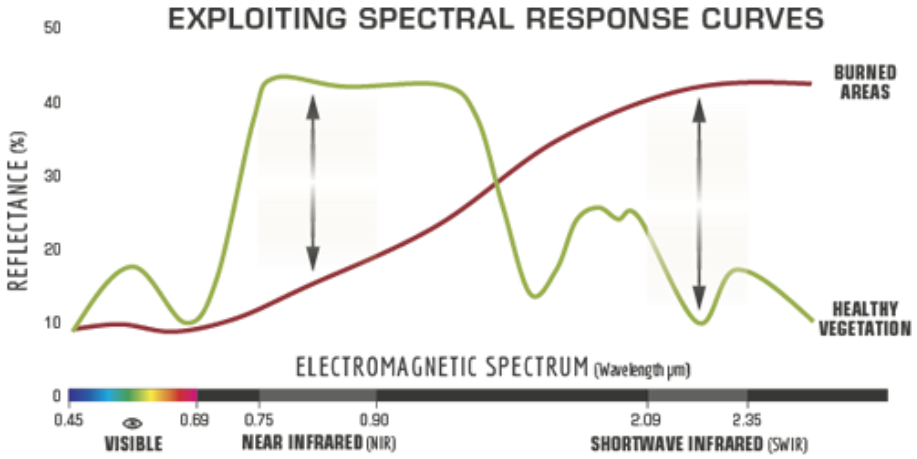


Figure 2-3: Exploiting Spectral Response Curves of Burned Areas with Healthy Vegetation
Source: US Forest Service, 2017

Based on the USGS, NBR succeeded to level 2 derived from Landsat from Landsat 4–5 (TM)), Landsat 7 (ETM +), and Landsat 8 (OLI) / (TIRS), so that it became a Level-2 Surface Reflectance product.

It is calculated as a ratio between the NIR and SWIR values in a traditional fashion (NIR - SWIR) / (NIR + SWIR). In Landsat 4-7, NBR = (Band 4 – Band 7) / (Band 4 + Band 7). In Landsat 8, NBR = (Band 5 – Band 7) / (Band 5 + Band 7).

NBR is delivered as a single band product, specified as shown in the Table 2-2.

Table 2-2: Landsat Surface Reflectance-derived Normalized Burn Ratio (NBR) Specifications

Attribute	Value
Long Name	Normalized Burn Ratio
Short Name	LC8NBR, LE7NBR, LT5NBR, or LT4NBR
File Name	*_sr_nbr.tif
Data Type	Signed 16-bit Integer
Units	Spectral Index (Band Ratio)
Valid Range	-10,000 — 10,000
Fill Value	-9999
Saturate Value	20,000
Scale Factor	*0.0001

Source : USGS Earth Resources Observation and Science (EROS) Center Science Processing Architecture (ESPA) On Demand Interface (ESPA).

2.3.5 Determination of the Threshold

In previous example, the threshold of NDVI and NBR single data was ascertained visually by comparison between 2017 and 2018 using the trial and error

In previous studies that correlated between LAPAN, KLHK and WRI, the NDVI and NBR single data threshold was visually confirmed by comparison between 2017 and 2018 using trial and error. method. However, this research was conducted by observing changes in the vegetation index (NDVI) and in the open land index (NBR). Differences between NDVI and NBR between 2017 and 2018 were minimal as a threshold to identify indications of changes in land cover. This was determined by sampling the difference between the NDVI and NBR points.

To detect revegetation and devegetation, the threshold requirements of each index were used. Revegetation can be expressed using equation 5 and devegetation by equation 6.

$$If\ (NDVI > n\ and\ NBR < m),\ then\ class\ 1 \quad (2\text{-}5)$$

$$If\ (NDVI < n\ and\ NBR > m),\ then\ class\ 2 \quad (2\text{-}6)$$

where n is the NDVI threshold, m is the NBR threshold. The revegetation area (class 1) is based on the result of equation 2-5, and the revegetation area (class 2) is based on the result of equation 2-6.

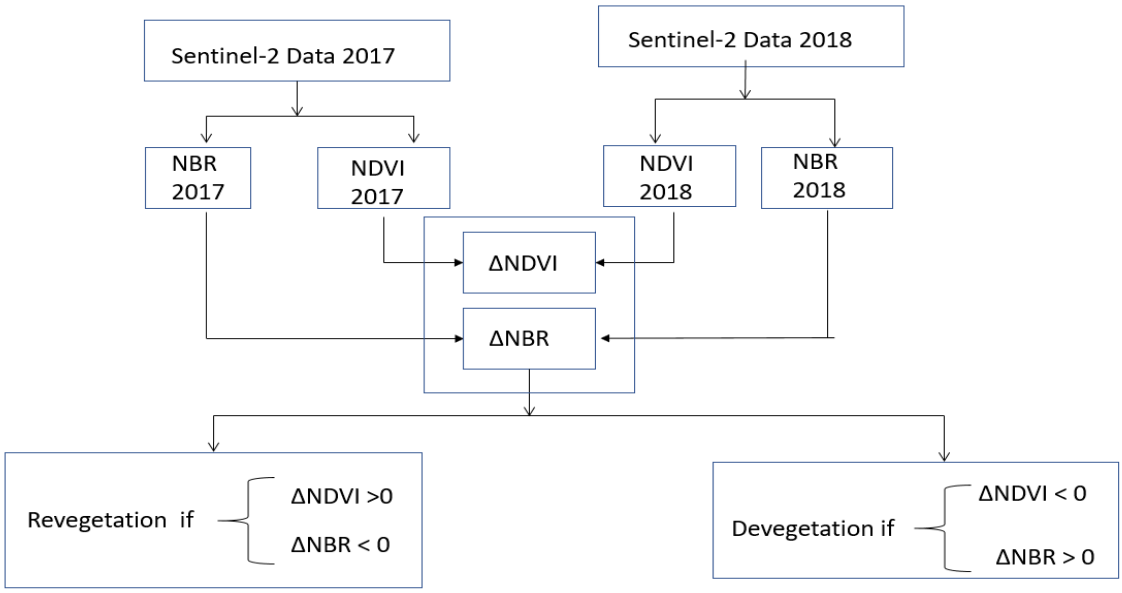


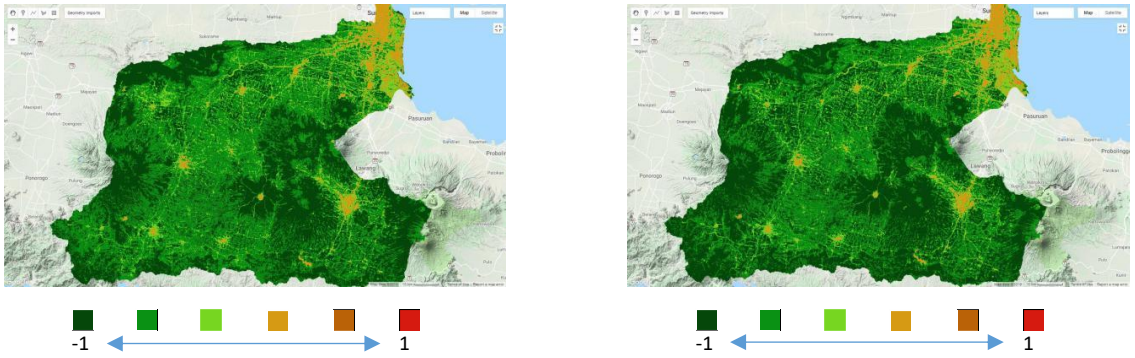
Figure 2-4: Flow diagram of the research development.

3 RESULTS AND DISCUSSION

The results from equations 1 and 3 are shown in Figures 3.1 and 3.2. Figure 3.1(a) shows the annual mean NDVI images for 2017, while 3.1(b) shows those for 2018 for the Brantas watershed. Figure 3.2(a) shows the annual mean NBR images for 2017 and 3.2(b) those for 2018. Visually, the NDVI and NBR imagery from 2017 and 2018 shows no changes in land cover. However, a digital assessment shows there is a change in land cover, indicated by a change in the NDVI and NBR values from 2017 to 2018. If the NDVI in 2018 is lower than that of 2017 and the NBR in 2018 is higher than that of 2017, then land cover is indicated to be devegetated; the sample data are shown in Figure 3.3. Conversely, if the value of NDVI in 2018 is higher than that of 2017 and if the NBR in 2018 is lower than that of 2017, then this indicates land cover revegetation, as shown in Figure 3-4. Figure 3-1 shows images of NDVI in 2017 and 2018, with an index value of -1 to 1. This value is depicted by the gradation of colour from light to dark, namely yellow, green and dark green, which shows the level of green of the vegetation.

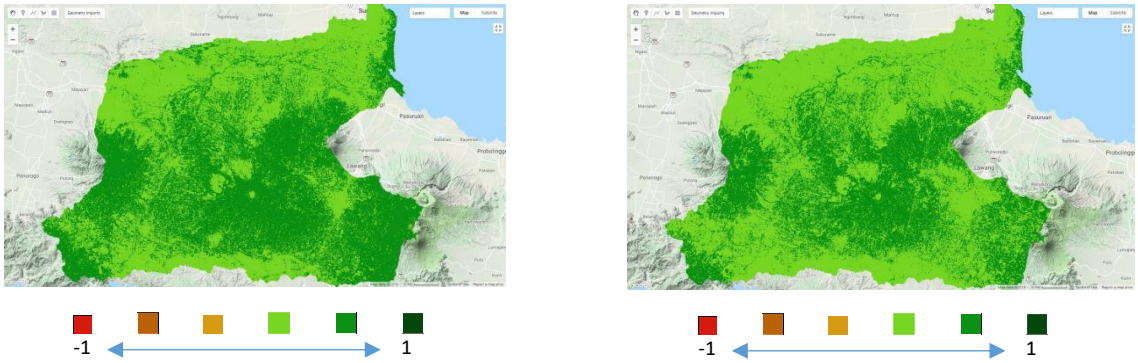
Figure 3-2 shows NBR images from 2017 and 2018, with the NBR index value from -1 to 1, which shows the level of land openness. The light green colour indicates a greater level of land openness than that shown in dark green. Figure 3-3(a) shows an image of the results of the 2017 and 2018 NDVI change analysis. The level of vegetation change is divided into three classes based on the ΔNDVI value interval, as shown in Table 3.2. Figure 3-3(b) shows an image of the results of the analysis of NBR changes in 2017 and 2018. The level of vegetation change is also divided into three classes based on the ΔNBR value interval, as shown in Table 3.3.

http://dx.doi.org/10.30536/j.ijreses.2020.v17.a3385
@National Institute of Aeronautics and Space of Indonesia (LAPAN)



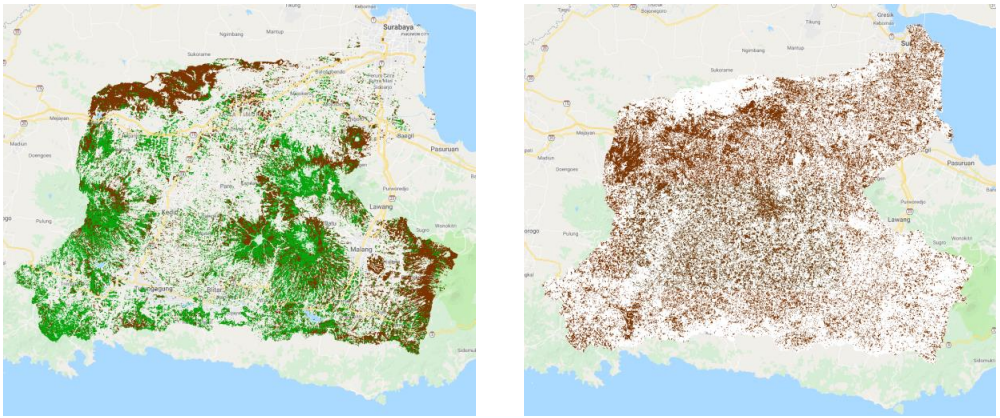
(a) NDVI 2017 (b) NDVI 2018

Figure 3-1: NDVI 2017-2018



NBR 2017 NBR 2018

Figure 3-2: NBR 2017-2018



(a) Change in vegetation in 2017-2018 (b) Change in open land in 2017-2018

Figure 3-3: Change in vegetation and open land 2017-2018.

Table 3-2. NDVI 2017-2018 Changes

No	ΔNDVI (2017-2018)	NDVI Change	Colour
1	>-1	No Change	
2	-1 to 0	Small Change	
3	0 to 1	Large Change	

Table 3-3. NBR 2017-2018 Changes

No	ΔNBR (2017-2018)	NBR Change	Colour
1	>-1	No Change	
2	-1 to 0	Small Change	
3	0 to 1	Large Change	

http://dx.doi.org/10.30536/j.ijreses.2020.v17.a3385
@National Institute of Aeronautics and Space of Indonesia (LAPAN)

Revegetation and devegetation areas were determined by application of the threshold of Δ NDVI and Δ NDVI, obtained from several sample points which were visually experiencing changes, as shown in figures 3-3, 3-4 and 3-5 Example Revegetation and devegetation. The results of the sample points obtained by the threshold for identifying indications of revegetation and devegetation are shown in Figure 3-6.

The threshold obtained to determine the existence of revegetation was ΔNDVI= 0.0309 and ΔNBR= -0.0176, while ΔNDVI= -0.0206 and ΔNBR= 0.0314 was the threshold for devegetation. Based on these calculations, the spatial information of revegetation and devegetation obtained is shown in Figure 3-6.

Spatial revegetation locations can be determined using the equation 5 algorithm, namely if Δ NDVI > 0.0309 and Δ NBR < 0.0176; and the spatial location of devegetation can also be determined using the equation 5 algorithm, namely if Δ NDVI < - 0.0206 and Δ NBR > 0.0314.

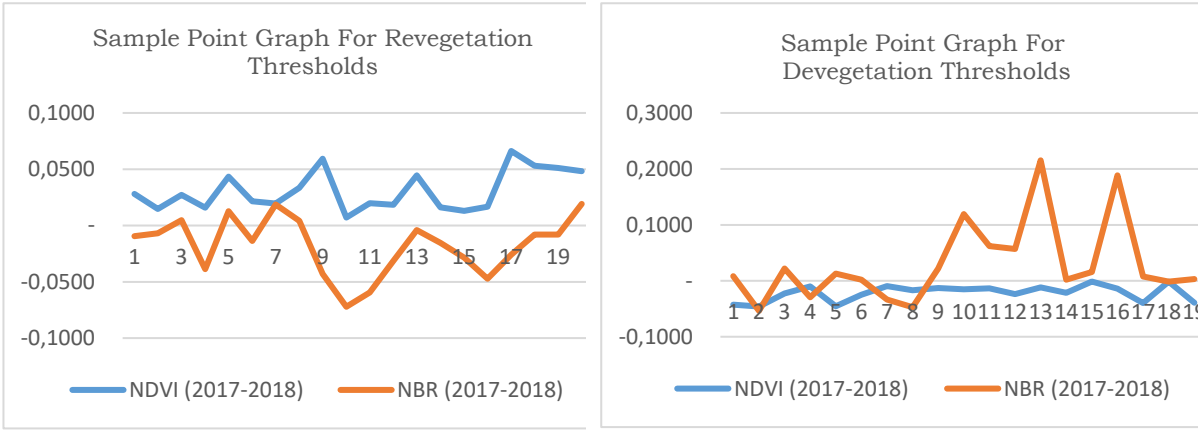
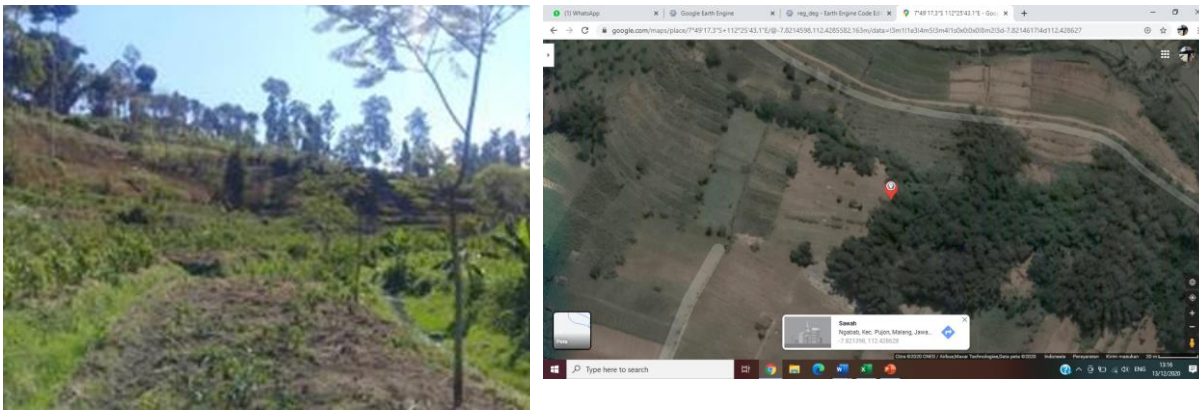
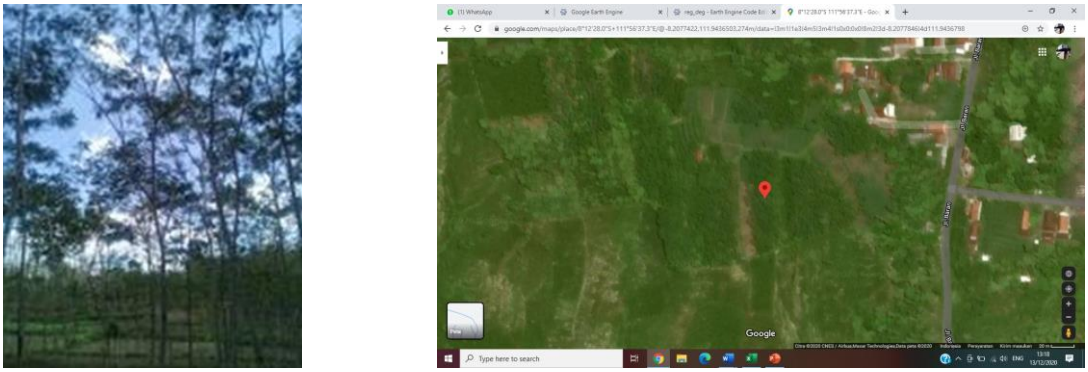


Figure 3-4: Graph of sample points for threshold determination



Devegetation, Malang,Pujon,Ngabab
-7.8214617,112.428627

http://dx.doi.org/10.30536/j.ijreses.2020.v17.a3385
@National Institute of Aeronautics and Space of Indonesia (LAPAN)



Revegetation Tulungagung,Kalidawir,Banyuurip
-8.2077846,111.9436798

Figure 3-5: Revegetation and devegetation spatial information

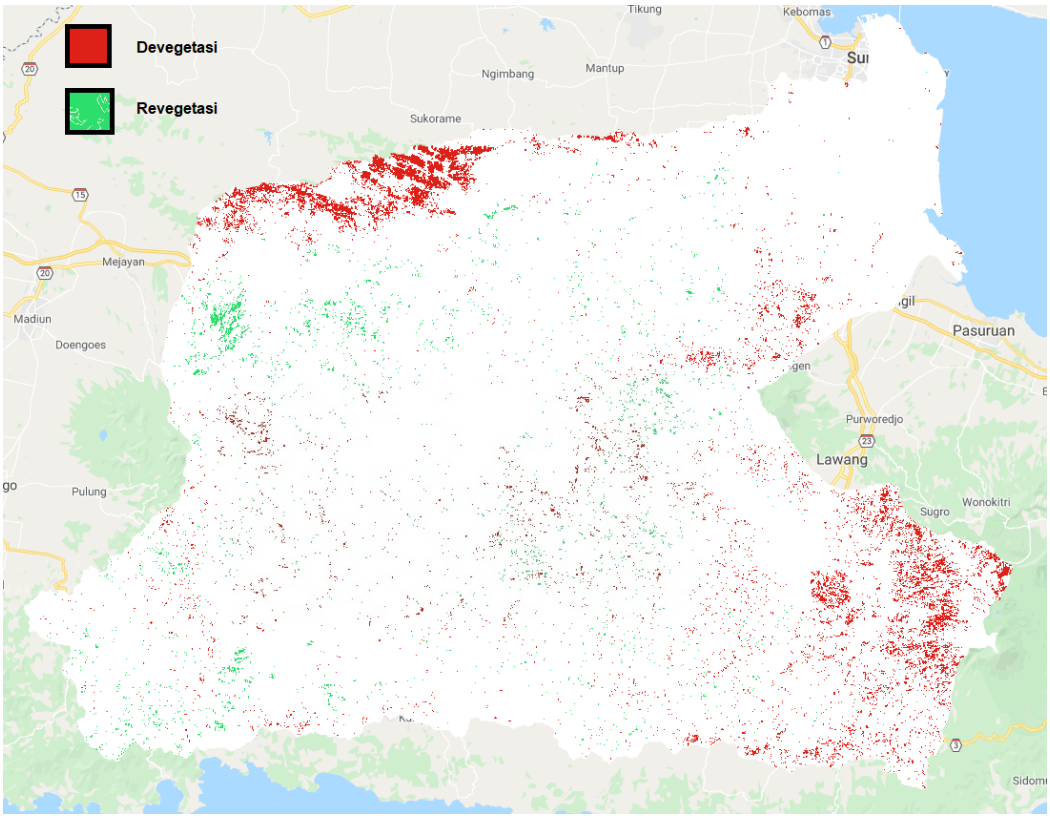


Figure 3-6: Revegetation and devegetation spatial information

In the study area, not all land-cover experienced revegetation or devegetation changes, as it includes cultivation and natural land. For example, rice fields are not considered to be devegated or revegetated due to the growth of the rice plant phase, or changes in teak forests can be due to changes between the rainy season and dry season, so such change in land cannot be said to be devegetation or revegetation.

4 CONCLUSION

Sentinel-2 MSI data with multi-temporal mosaic data can be used for monitoring changes in land cover dynamics, especially for tree cover loss. The results showed that revegetation can be determined by if Δ NDVI > 0.0309 and Δ NBR < 0.0176, and devegetation if Δ NDVI < - 0.0206 and Δ NBR > 0.0314. Based on the NDVI and NBR threshold requirements set in this study, it is shown that devegetation is more widespread

than revegetation. Devegetation generally occurs in the barren highlands and revegetation in the low and high lands/mountains, which often experience rain. The weakness of using the Sentinel satellite is that the method cannot detect land that is narrow or steep.

ACKNOWLEDGMENTS

This research was able to be carried out because of the collaboration of several parties. We would like to thank the INSINAS 2019 Program, the Ministry of Research and Technology/National Agency for Research and Technology and national research program 2020 LPDP for funding the research. Thanks also to the Remote Sensing Application Center and Remote Sensing Technology and Data LAPAN which provided us with facilities and input, as well as suggestions for the research.

AUTHOR CONTRIBUTIONS

The main authors of the scientific work of this research are Samsul Arifin and Tatik Kartika, while Dede Dirgahayu and Gatot Nugroho are contributing members.

REFERENCES

Aldrian and Sucahyono. (2013). Dictionary of climate change terms. BMKG

Arifin, S., Kartika, T., & Carolita, I. (2019) Application of geobiophysics NDVI model for forest identification in Lapan-A3 Satellite data. *Jurnal Penginderaan Jauh dan Pengolahan Data Citra Digital 16*(2), 91-100 http://dx.doi.org/10.30536/j.pjpdcd.2018 .v0.a3109

Barbosa, P.M., Pereira, J.M.C., & Grégoire, J. M. (1998). Compositing criteria for burned area assessment using multi-temporal low resolution satellite data, *Remote Sensing of Environment 65*(1), 38-49.

Chuvieco, E., Martin, M.P., & Palacios A. (2002). Assessment of different spectral indices in the red-near infrared spectral domain for burned land discrimination, *International Journal of Remote Sensing 23*, 5103–5110.

Escuin, S., Navarro, R.M., & Fernandez, P. (2008). Fire severity assessment by using NBR (Normalized Burn Ratio) and NDVI (Normalized Difference Vegetation Index) derived from LANDSAT TM/ETM images. *International Journal of Remote Sensing*, *29*(4), 1053–1073. DOI:10.1080/01431160701281072.

ESA-Sentinel-2. (2015) Mission Sentinel-2, https://sentinel.esa.int/web/sentinel/missions/sentinel-2, Europe.

Garcia, M.J.L., & Caselles, V. (1991). Mapping burns and natural reforestation using Thematic Mapper data. *Geocarto International*, *6*(1), 31–37.

Horning, N., Robinson, J.A., Sterling E.J., Turning, W., Spector, S. (2010). *Remote Sensing for Ecology and Conservation*. New York: Oxford University Press.

Indratmoko S., & Rizqihandar N. (2019). Burn area detection using Landsat 8 OLI TIRS. *Southeast Asian Geography Association (SEAGA) 13th Conference IOP Conf. Series: Earth and Environmental Science* 338 012035 IOP Publishing doi:10.1088/1755-1315/338/1/012035 1 of Geography, Faculty of Mathematic and Natural Science Universitas Indonesia Depok, Indonesia

Kartika, T., Arifin S., Sari I.L., Tosiani, A., Firmansyah, R., Kustiyo, Carolita, I., Adi, K., Daryanto, F., Said, Z. (2018), Analysis of vegetation indices using metric landsat-8 data to identify tree cover change in Riau Province**.** *Earth and Environmental Science 280*, 1-8. doi:10.1088/1755-1315/280/1/ 012013

Key, C.H., & Benson N. (1999). *Measuring and remote sensing of burn severity: the CBI and NBR*. https://www.researchgate.net

Lillesand, T.M., Kiefer R.W., & Chipman J.W. (2008). *Remote sensing and image interpretation* (Sixth Edition). New York: John Wiley & Sons, Inc.

Martín M.P., & Díaz-Delgado R. (2002). Burnedland mapping using NOAA-AVHRR

and TERRA-MODIS. In: Viegas (Ed.). *Conference proceedings: Forest fire research & wildland fire safety*. Millpress, Rotterdam.

Miettinen, J. (2007). *Burnt area mapping in insular Southeast Asia using* medium resolution satellite imagery. Academic dissertation. Department of Forest Resource Management Faculty of Agriculture and Forestry University of Helsinki.

Nielsen, T.T., Mbow, C., & Kane R. (2002). A statistical methodology for burned area estimation using multi-temporal AVHRR data. *International Journal of Remote Sensing 23*(6), 1181-1196.

Parwati, Zubaidah, A., Vetrita, Y., Yulianto, F., Ayu, K. DS, Khomarudin, M.R. (2012), Usage of Spot-4, Normalized Burn Ratio (NBR) and Normalized Difference Vegetation Index (NDVI) to identify burnt area. *Jurnal Ilmiah Geomatika 18*(1), 29-41.

Philiani, I, Saputra, L, Harvianto, L., & Muzaki, A.A. (2016). Mapping of mangrove forest vegetation using method Normalized Difference Vegetation Index (NDVI). *Surya Octagon Interdisciplinary Journal of Technology*, *1*(2), 211-222.

Roy, D.P., Lewis, P.E., & Justice C.O. (2002). Burned area mapping using Multi-temporal moderate spatial resolution data - a bi-directional reflectance model-based expectation approach. *Remote Sensing and Environment 83*, 263- 286.

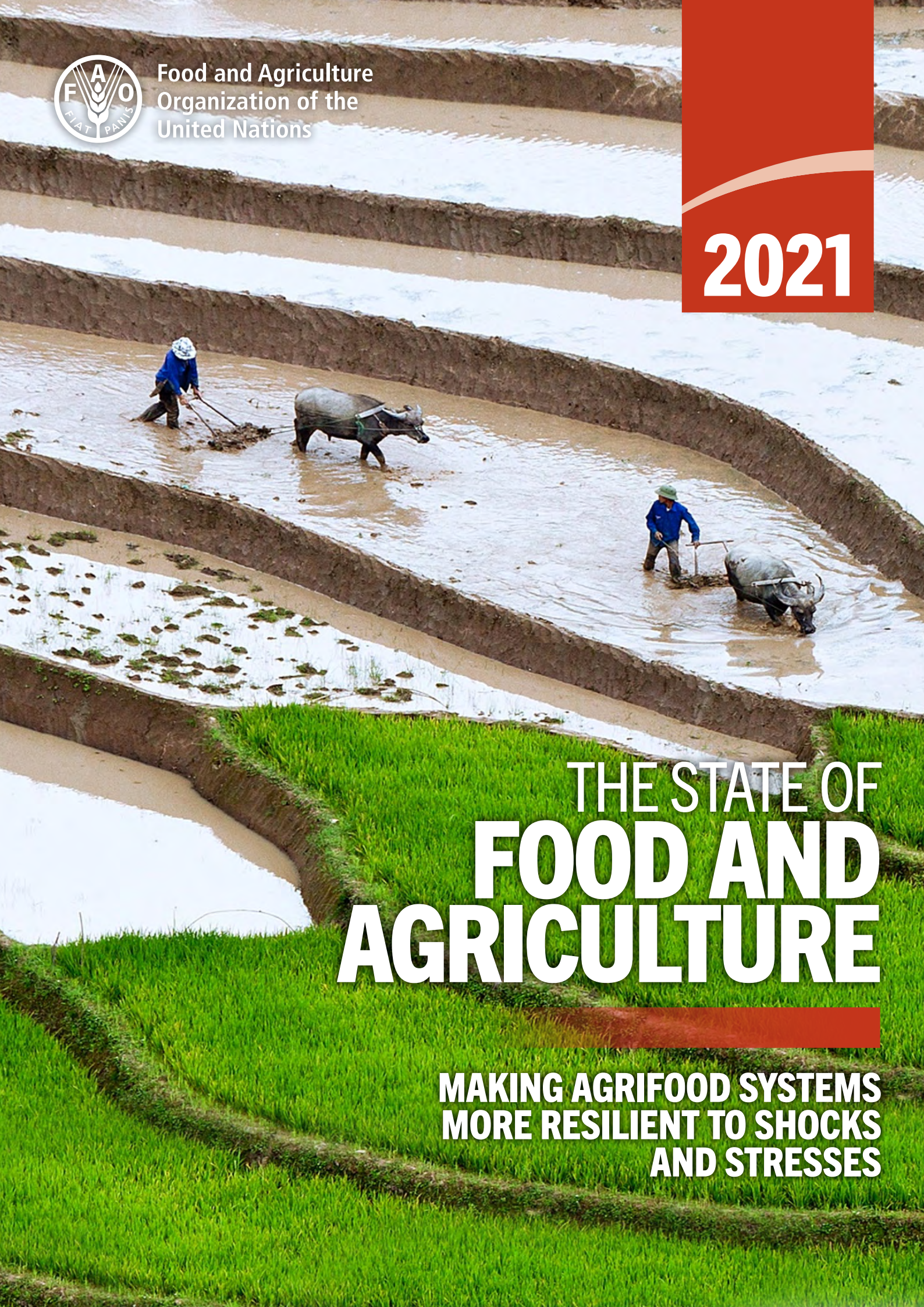
Roy, D.P, Boschettm, L., & Triffm, S.N. (2006). Remote sensing of fire severity: assessing the performance of the normalized burn ratio. *IEEE Geoscience and Remote Sensing Letters, 3*(1), 112-116.

Ryan, L. (1997). Creating a Normalized Difference Vegetation Index (NDVI) image using multispectral. University of New Hampshire.

Silva, J.M.N, Cadima, J.F.C.L., Pereira, J.M.C. M. Grégoire. (2004), Assessing the feasibility of a global model for multi-temporal burned area mapping using SPOT-VEGETATION data. *International Journal of Remote Sensing 25*(22), 4889-4913. DOI: 10.1080/01431160412331291251.

USGS-EROS. (2017). Comparison-Sentinel-2-And-Landsat, https://www.usgs.gov /centers/eros/science/.

Weier, J, Herring, D, (2000), Measuring Vegetation (NDVI and EVI), NASA, https://earthobservatory.nasa.gov/features.



Food and Agriculture Organization of the United Nations

2021

THE STATE OF FOOD AND AGRICULTURE

MAKING AGRIFOOD SYSTEMS MORE RESILIENT TO SHOCKS AND STRESSES

This flagship publication is part of **The State of the World** series of the Food and Agriculture Organization of the United Nations.

Required citation:
FAO. 2021. *The State of Food and Agriculture 2021. Making agrifood systems more resilient to shocks and stresses*. Rome, FAO. https://doi.org/10.4060/cb4476en

The designations employed and the presentation of material in this information product do not imply the expression of any opinion whatsoever on the part of the Food and Agriculture Organization of the United Nations (FAO) concerning the legal or development status of any country, territory, city or area or of its authorities, or concerning the delimitation of its frontiers or boundaries. The mention of specific companies or products of manufacturers, whether or not these have been patented, does not imply that these have been endorsed or recommended by FAO in preference to others of a similar nature that are not mentioned.

The designations employed and the presentation of material in the maps do not imply the expression of any opinion whatsoever on the part of FAO concerning the legal or constitutional status of any country, territory or sea area, or concerning the delimitation of frontiers. Dashed lines on maps represent approximate border lines for which there may not yet be full agreement.

ISSN 0081-4539 (print)
ISSN 1564-3352 (online)
ISBN 978-92-5-134329-6
© FAO 2021

Some rights reserved. This work is made available under the Creative Commons Attribution-NonCommercial-ShareAlike 3.0 IGO licence (CC BY-NC-SA 3.0 IGO; https://creativecommons.org/licenses/by-nc-sa/3.0/igo).

Under the terms of this licence, this work may be copied, redistributed and adapted for non-commercial purposes, provided that the work is appropriately cited. In any use of this work, there should be no suggestion that FAO endorses any specific organization, products or services. The use of the FAO logo is not permitted. If the work is adapted, then it must be licensed under the same or equivalent Creative Commons licence. If a translation of this work is created, it must include the following disclaimer along with the required citation: "This translation was not created by the Food and Agriculture Organization of the United Nations (FAO). FAO is not responsible for the content or accuracy of this translation. The original English edition shall be the authoritative edition."

Any mediation relating to disputes arising under the licence shall be conducted in accordance with the Arbitration Rules of the United Nations Commission on International Trade Law (UNCITRAL) as at present in force.

Third-party materials. Users wishing to reuse material from this work that is attributed to a third party, such as tables, figures or images, are responsible for determining whether permission is needed for that reuse and for obtaining permission from the copyright holder. The risk of claims resulting from infringement of any third-party-owned component in the work rests solely with the user.

Sales, rights and licensing. FAO information products are available on the FAO website (www.fao.org/publications) and can be purchased through publications-sales@fao.org.
Requests for commercial use should be submitted via: www.fao.org/contact-us/licence-request.
Queries regarding rights and licensing should be submitted to: copyright@fao.org.

COVER PHOTOGRAPH ©123RF/bvh2228

VIET NAM. Farmers working in terraced rice fields in Mu Cang Chai, Yen Bai.

ISSN 0081-4539

2021

THE STATE OF FOOD AND AGRICULTURE

MAKING AGRIFOOD SYSTEMS MORE RESILIENT TO SHOCKS AND STRESSES

Food and Agriculture Organization of the United Nations
Rome, 2021

CONTENTS

FOREWORD v
METHODOLOGY viii
ACKNOWLEDGEMENTS ix
ACRONYMS AND ABBREVIATIONS xi
GLOSSARY xii
CORE MESSAGES xv
EXECUTIVE SUMMARY xvi

CHAPTER 1
AGRIFOOD SYSTEMS' RESILIENCE: WHAT IT IS 1
Key messages 1
The need for more resilient agrifood systems 4
Understanding resilience in agrifood systems 5
How shocks and stresses disrupt agrifood systems 7
Agrifood systems' resilience in changing contexts 12
Building agrifood systems' resilience – a framework 13
Laying out the scope of this report 18

CHAPTER 2
AGRIFOOD SYSTEMS' RESILIENCE AT NATIONAL AND SUBNATIONAL LEVELS 21
Key messages 21
Resilience of agrifood systems' functions 22
Absorbing shocks in the primary production sector 22
Guaranteeing availability of nutritious food 28
Ensuring physical access to food at subnational level – the domestic food transport network 32
Ensuring economic access to food 40
Conclusions 45

CHAPTER 3
RESILIENCE OF FOOD SUPPLY CHAINS 47
Key messages 47
Setting the stage – a supply chain perspective of resilience 48
Managing food supply chain resilience 55
Conclusions 60

CHAPTER 4
ENHANCING THE RESILIENCE OF RURAL LIVELIHOODS 63
Key messages 63
Determinants of resilience of rural livelihoods 64
Small-scale agricultural producers bear a double burden 68
Potential solutions for resilient rural livelihoods 70
Conclusions 76

CHAPTER 5
BUILDING RESILIENT AGRIFOOD SYSTEMS: GUIDING PRINCIPLES 79
Key messages 79
Means of enhancing national agrifood systems' resilience: structural characteristics 82
Policy measures that enhance food supply chain resilience 85
Enhancing the resilience capacities of small-scale producers and vulnerable households 90
Planning for the future – broader policy areas and priorities 92
Conclusions 94

ANNEXES 97

ANNEX 1
Description, data and methodology of the indicators in Chapter 2 98

ANNEX 2
Additional figures to Chapter 2 107

ANNEX 3
Statistical tables 110

ANNEX 4
Additional tables to Chapter 4 133

REFERENCES 134

TABLES

1 Indicators of resilience and vulnerability of food transport networks for selected countries 38

2 Indicators of unaffordability of healthy diets 43

3 Summary of COVID-19 impacts on food supply chains in three countries and subsequent adaptations 55

4 Drivers of rural household resilience and policy implications 68

5 Entry points to manage agrifood systems' risk and uncertainty 95

A3.1 Primary production flexibility index (PPFI) for protein, 2016–2018 110

A3.2 Dietary sourcing flexibility index (DSFI) for kilocalories and for tonnes of fruits and vegetables, 2016–2018 115

A3.3 Dietary sourcing flexibility index (DSFI) for protein and for fat, 2016–2018 120

A3.4 Indicators of resilience and vulnerability of food transport networks 125

A3.5 Affordability of energy-sufficient and healthy diets in 2019 128

A4.1 List of countries in the FAO-RIMA data set 133

A4.2 List of countries in the MICS data set 133

FIGURES

1 Agrifood systems' resilience and the six dimensions of food security 7

2 Conceptual framework for agrifood systems' resilience analysis 16

3 PPFI for protein, 2016–2018 25

4 DSFI for kilocalories, 2016–2018 31

5 Proximity-based resilience as a function of the average transport time of food in selected countries 37

6 Placement of selected countries based on the level of economic access to a healthy diet and DSFI for tonnes of fruits and vegetables, 2016–2019 44

7 Schematic representation of a food supply chain and its connection to input and service supply chains 49

8 A simplified illustration of three types of food supply chains regarding vulnerability to shocks and stresses and their resilience capacities 53

9 RIMA resilience pillars by country profile 67

10 Agrifood systems' components and contextual factors 81

A1.1 Pathways to produce agricultural output and sell it in domestic and export markets, for value 99

A1.2 Pathways to source food from stocks, domestic production or imports, for kilocalories 101

A1.3 Pathways to source primary commodities as inputs to produce processed foods and sell them in domestic and export markets, for value 104

A2.1 Dietary sourcing flexibility index (DSFI) for protein, 2016–2018 107

A2.2 Dietary sourcing flexibility index (DSFI) for fat, 2016–2018 108

A2.3 Dietary sourcing flexibility index (DSFI) for tonnes of fruits and vegetables, 2016–2018 109

BOXES

1 Defining agrifood systems in relation to food systems 2

2 FAO's Anticipatory Action approach 11

3 The PPFI in a nutshell 23

4 The PPFI in value terms, including non-food products 27

CONTENTS

5 The DSFI in a nutshell 29

6 Comparing the DSFI with the PPFI and identifying the hidden middle 33

7 Methodology to examine the resilience of domestic food transport networks 35

8 Simulating the impact of floods on food transport networks in Nigeria and Pakistan 39

9 The contribution of forestry to the livelihoods of small-scale producers 41

10 Calculating the share of population at risk of not being able to afford a healthy diet 41

11 Many cannot afford – or are at risk of not being able to afford – an energy-sufficient diet 43

12 The impact of the COVID-19 pandemic on SMAEs 51

13 RIMA in brief 66

14 The climate resilience of pastoralists and agropastoralists in sub-Saharan Africa 70

15 Synergies between productivity, resilience and sustainability: the Mountain Partnership Products initiative 73

16 Direct and indirect impacts of social protection programmes on household resilience to multiple shocks 75

17 Putting the DSFI and PPFI to use 84

18 Logistics Centre in Kemin, Kyrgyzstan 89

FOREWORD

The novel coronavirus disease (COVID-19) pandemic has had profound impacts on all our lives and we continue to struggle with it. Border closures and curfews to contain the spread of the SARS-CoV-2 virus stopped international travel, shut down countless businesses and left millions of people unemployed. Restrictions on the movement of people and goods, particularly in the initial stages of the pandemic, impeded the flow of inputs to farmers and of their produce to markets. Where harvesting and transport were blocked, huge quantities of fresh fruits and vegetables were left to decay in farmers' fields.

Restrictions have harmed not only agrifood trade, agrifood supply chains and agrifood markets, but also people's lives, livelihoods and nutrition. After initial disruptions and uncertainty, many supply chains showed a remarkable degree of resilience in absorbing and adapting to the shock caused by the pandemic; however, lack of access to adequate food for millions of people emerged as a huge and persistent problem. Many rural people were unable to travel for seasonal work – an important source of income in poor communities. Immobilized by lockdowns, low-income urban households saw their incomes and spending on food fall sharply.

Even before the COVID-19 pandemic, the world was not on track to meet the shared commitment to end global hunger and malnutrition in all its forms by 2030, but the pandemic has sent us even further off track. This year's *State of Food Security and Nutrition in the World* estimates that between 720 and 811 million people were affected by hunger in 2020, up to 161 million more than in 2019, with the increase largely propelled by the COVID-19 crisis. Tragically, women and children have often borne the brunt of the crisis. According to the *Sustainable Development Goals Report 2020*, the disruption of health services and access to adequate food has added to the toll of under-five and maternal deaths. The United Nations' *Policy Brief: The Impact of COVID-19 on Food Security and Nutrition* suggests that 370 million children have been denied school meals owing to school closures. There is no doubt that the impact of the pandemic on food security and nutrition will be felt for many years.

Agrifood production and supply chains have historically been vulnerable to shocks – from droughts and floods to armed conflict and food price hikes – and are under growing pressure from longer-term stresses, including the climate crisis and environmental degradation. But the COVID-19 pandemic is exceptional in that it has shown how a shock of global proportions can occur suddenly, spread rapidly and compromise the food security, nutrition status and livelihoods of billions of people to an unprecedented degree and over a long period.

The COVID-19 pandemic has left the fragilities of national agrifood systems widely exposed. An obvious reason to address these fragilities is, of course, the unwelcome increase in food insecurity and malnutrition. However, agrifood systems are too large for us to believe that their fragilities, if left unaddressed, will impede only the goal of achieving Zero Hunger by 2030, however crucial this objective may be. The implications go further. Agrifood systems produce 11 billion tonnes of food a year, employing 4 billion people directly or indirectly. The agrifood sector, including forestry and fisheries, also accounts for one-third of the anthropogenic greenhouse gas emissions driving climate change and occupies 37 percent of the Earth's land area. Agrifood systems have, therefore, an essential role to play in realizing other Sustainable Development Goals (SDGs) related to poverty, resource and energy efficiency, cleaner economies, and healthy aquatic and terrestrial ecosystems, among others.

International consensus has grown around the idea that transforming agrifood systems – towards greater efficiency, resilience, inclusiveness and sustainability – is an essential condition for realizing the 2030 Agenda for

FOREWORD

Sustainable Development. Momentum for change led to the first ever United Nations Food Systems Summit in September 2021, which agreed on innovative solutions and strategies to transform agrifood systems and leverage those changes to deliver progress across all the SDGs. The Summit's call to action focused on five objectives, one of which is building resilience to vulnerabilities, shocks and stresses to ensure the continued functioning of healthy, sustainable agrifood systems.

The theme of this year's report responds to the United Nations Food Systems Summit's call to bring forward a series of concrete actions that people from all over the world can take to support transformation of the world's agrifood systems. More specifically, the report provides evidence and guidance on actions that can help actors in agrifood systems manage their vulnerability to shocks and stresses, and strengthen the capacity of these systems to support livelihoods and sustainably provide continuous access to sufficient, safe and nutritious food to all in the face of disruptions.

To this end, the Food and Agriculture Organization of the United Nations (FAO) has developed a suite of resilience indicators designed to measure the robustness of primary production, the extent of food availability, and the degree of people's physical and economic access to adequate food in countries worldwide. These indicators can help assess the capacity of national agrifood systems to absorb the impact of any shock, which is a key aspect of resilience. Analysis shows that a country's primary production sector is more resilient when it produces a diverse mix of food and non-food products and sells them to a wide range of markets, both domestic and international, a configuration mainly seen in higher-income countries or those with a large agrifood base. In terms of food availability, however, analysis of multiple sourcing pathways for crop, fish and livestock commodities shows that lower-income countries have a diversity that is comparable to that of larger, higher-income countries.

Another important aspect underscored by this report is that low-income countries face much bigger challenges in ensuring physical access to food through transport networks, key to keeping agrifood supply chains active. Analysis of data from 90 countries shows that if main transport routes were disrupted, many low-income countries in particular would have limited capacity to decentralize food distribution or use alternative delivery routes. For nearly half the countries analysed, the closure of critical network links would increase local transport time by 20 percent or more, thereby increasing costs and food prices for consumers.

Taking an agrifood systems approach, the report also notes that risks associated with economic access to food are even more worrisome. Globally, we already know that around 3 billion people cannot afford a healthy diet to protect against malnutrition. Since low-income households spend most of their income on food, any significant loss of purchasing power – from food price hikes, crop failures or loss of income – poses a threat to their food security and nutrition. In fact, this report finds that an additional 1 billion people are at risk as they would not be able to afford a healthy diet if a shock were to reduce their incomes by one-third. The burden of this shock would fall mostly on middle-income countries, but the report also notes that, in the event of such an income shock, proportionately many more people in low-income countries would be unable to afford even an energy-sufficient diet. These risks are unacceptable in a world that produces enough food to feed its entire population.

The report finds that diverse, redundant and well-connected agrifood supply chains are needed to increase resilience, as they provide multiple pathways for producing, sourcing and distributing food. However, some actors in these agrifood supply chains are more vulnerable than others. The vulnerability of small and medium agrifood enterprises (SMAEs) is critical, as well as the fact that the resilience capacity of rural households – especially those involved in small-scale agricultural production – is increasingly put to the test in the face of adverse climatic events and depletion of natural resources.

Based on the evidence of this report, FAO is in a strong position to recommend that governments make resilience in agrifood systems a strategic part of national and global responses to ongoing and future challenges. A guiding principle is diversity – input sources, production mixes, output markets and supply chains – because diversity creates multiple pathways for absorbing shocks. Connectivity multiplies benefits: well-connected agrifood networks overcome disruptions faster by shifting sources of supply and channels for transport, marketing, inputs and labour.

Governments should encourage better coordination and organization of SMAEs within agrifood supply chains through, for example, forming consortia, which increase their scale, visibility and influence. Similarly, small-scale food producers can stay competitive and resilient by integrating into supply chains through producer associations and cooperatives, and by adopting resource-conserving practices. Social protection programmes may be needed to improve rural households' resilience in the event of shocks. Policies should also address issues beyond agrifood systems, including the need for better health and education services, gender equality and women's participation, and must recognize agrifood's role as a steward of the natural environment.

FAO stands firmly committed to taking advantage of the opportunity offered by events such as the United Nations Food Systems Summit and others to move from commitments to action in order to transform agrifood systems to make them more efficient, more inclusive, more resilient and more sustainable for better production, better nutrition, a better environment and a better life for all, leaving no one behind. This report offers evidence and guidance to take concrete steps in this important direction.



Qu Dongyu
FAO Director-General

METHODOLOGY

The preparation of *The State of Food and Agriculture 2021* began with a workshop that was held virtually on 26–30 October 2020 and attended by FAO specialists and external experts to discuss the outline of the report. Following the workshop, an advisory group representing all relevant FAO technical units was formed and, together with a panel of external experts, it assisted the research and writing team. The preparation of the report was informed by four background papers and original empirical analysis prepared by FAO and external experts. The advisory group met virtually to discuss the research on 26 January 2021 and commented on the first draft of Chapter 1 in February 2021. Drafts of the chapters were presented to the advisory group and panel of external experts in advance of a workshop held virtually on 10–16 March 2021 and chaired by the Deputy Director of FAO's Agrifood Economics Division. With guidance from that workshop and a follow-on advisory group meeting, the report was revised and presented to the management team of FAO's Economic and Social Development stream. The revised draft was sent for comments to other FAO streams and to the FAO regional offices for Africa, Asia and the Pacific, Europe and Central Asia, Latin America and the Caribbean, and the Near East and North Africa. Comments were incorporated in the final draft, which was reviewed by the Deputy Director of FAO's Agrifood Economics Division, the FAO Chief Economist and the Office of the Director-General.

ACKNOWLEDGEMENTS

The State of Food and Agriculture 2021 was prepared by a multidisciplinary team from the Food and Agriculture Organization of the United Nations (FAO), under the direction of Marco V. Sánchez Cantillo, Deputy Director of FAO's Agrifood Economics Division, and Andrea Cattaneo, Senior Economist and Editor of the publication. Overall guidance was provided by Máximo Torero Cullen, FAO Chief Economist, and by the management team of the Economic and Social Development stream.

RESEARCH AND WRITING TEAM
Theresa McMenomy, Fergus Mulligan (consulting editor), Ahmad Sadiddin, Jakob Skøt, Graeme Thomas (consulting editor) and Sara Vaz.

BACKGROUND PAPERS AND DATA ANALYSIS
Imran Ali (CQUniversity), Mark Brussel (University of Twente), Mark Constas (Cornell University), Ellestina Jumbe (FAO), Rolf de By (University of Twente), Marco d'Errico (FAO), Serkan Girgin (University of Twente), Vu Minh Hien (FAO), John Hoddinott (Cornell University), Hong Anh Luu (FAO), Andy Nelson (University of Twente), Robert Ohuru (University of Twente), Rebecca Pietrelli (FAO), Jeanne Pinay (FAO), Thomas Reardon (Michigan State University), Alessandro Tavoni (University of Bologna), Tom Thomas (University of Twente), Valentijn Venus (University of Twente) and David Zilberman (University of California, Berkeley).

ADDITIONAL FAO INPUTS
Abram Bicksler, Adriana Ignaciuk, Giorgo Grussu, Yuka Makino, Dario Lucantoni, Anne Mottet, Beate Scherf and Antonio Scognamillo.

FAO ADVISORY GROUP
Fenton Beed, Dubravka Bojic, Ben Davis, Marco d'Errico, Ana Paula de la O Campos, Kim Friedman, Stepanka Gallatova, Giorgo Grussu, Panagiotis Karfakis, Michelle Kendrick, Preetmoninder Lidder, Yuka Makino, Roman Malec, Erdgin Mane, Zitouni Oulddada, Rebecca Pietrelli, Pilar Santacoloma, Guido Santini, Nick Sitko, Beate Scherf, Josef Schmidhuber, Kostas Stamoulis, Salar Tayyib, Jim Tefft, José Valls Bedeau and Sylvie Wabbes Candotti.

ACKNOWLEDGEMENTS

PANEL OF EXTERNAL EXPERTS

Imran Ali (Central Queensland University Melbourne), Mark Constas (Cornell University), Ika Darnhofer (University of Natural Resources and Life Sciences, Vienna), Rolf de By (University of Twente), Paolo D'Odorico (University of California, Berkeley), John Hoddinott (Cornell University), Helena Kahiluoto (LUT University), Matti Kummu (Aalto University), Andy Nelson (University of Twente), Mohan Rao (University of Massachusetts Amherst), Thomas Reardon (Michigan State University), Donato Romano (University of Florence), David Seekell (Umeå University), Jamie Stone (Biotechnology and Biological Sciences Research Council), Alessandro Tavoni (University of Bologna), Paul Winters (University of Notre Dame) and David Zilberman (University of California, Berkeley).

ANNEXES

The annexes were prepared by Ahmad Sadiddin and Sara Vaz.

ADMINISTRATIVE SUPPORT

Liliana Maldonado provided administrative support.

Translations were delivered by the Language Branch (CSGL) of the FAO Governing Bodies Servicing Division (CSG).

The Publications Branch (OCCP) in FAO's Office of Communications (OCC) provided editorial support, design and layout, as well as production coordination, for editions in all six official languages.

ACRONYMS AND ABBREVIATIONS

AA	Anticipatory Action
BFA	biodiversity for food and agriculture
CSA	climate-smart agriculture
COVID-19	novel coronavirus disease
DSFI	dietary sourcing flexibility index
FAO	Food and Agriculture Organization of the United Nations
GHG	greenhouse gas
HLPE	High Level Panel of Experts
ICT	information and communications technology
LLDC	landlocked developing country
MFI	midstream flexibility index
MICS	multiple indicator cluster surveys
MPP	Mountain Partnership Products
NGO	non-governmental organization
PPFI	primary production flexibility index
R&D	research and development
RCI	resilience capacity index
RIMA	resilience index measurement and analysis
SDGs	Sustainable Development Goals
SIDS	small island developing States
SMAE	small and medium agrifood enterprise
TAPE	tool for agroecology performance evaluation
UN	United Nations
WASH	water, sanitation and hygiene
WHO	World Health Organization

GLOSSARY

Agricultural household. A household that derives any income, however minimal, from agriculture or contributes some labour input to agricultural production.[1]

Agricultural innovation. The process whereby individuals or organizations bring new or existing products, processes or ways of organization into use for the first time in a specific context in order to increase effectiveness, competitiveness, resilience to shocks or environmental sustainability and thereby contribute to food security and nutrition, economic development or sustainable natural resource management.[2]

Agrifood systems. Encompass the entire range of actors, and their interlinked value-adding activities, engaged in the primary production of food and non-food agricultural products, as well as in storage, aggregation, post-harvest handling, transportation, processing, distribution, marketing, disposal and consumption of all food products including those of non-agricultural origin.

- **Food systems.** Comprise all food products that originate from crop and livestock production, forestry, fisheries and aquaculture, and from other sources such as synthetic biology that are meant for human consumption.

Agrifood systems' resilience. The capacity over time of agrifood systems, in the face of any disruption, to sustainably ensure availability of and access to sufficient, safe, and nutritious food for all, and sustain the livelihoods of agrifood systems' actors.[a]

Agroecology. An integrated approach that simultaneously applies ecological and social concepts and principles to optimize interactions between plants, animals, humans and the environment while addressing social aspects to achieve sustainable and fair agrifood systems.[4]

Biodiversity for food and agriculture (BFA). The variety and variability of animals, plants and micro-organisms at the genetic, species and ecosystem levels that sustain ecosystem structures, functions and processes in and around production systems and provide food and non-food agricultural products.[5]

Climate-smart agriculture (CSA). An approach to guide actions to transform and reorient agricultural systems to effectively support development and ensure food security under a changing climate through: sustainably increasing agricultural productivity and incomes; adapting and building resilience to climate change; and mitigating greenhouse gas emissions.[6]

Covariate shock. An event that directly affects groups of households, communities, regions or even entire countries.[7]

Event. The manifestation of threats and hazards or disturbances, or a combination thereof, in a particular place and in a specific period of time.[8, 9]

Exposure. The situation of people, infrastructure, housing, production capacities and other tangible human assets located in hazard-prone areas.[8]

Food safety. The assurance that food will not cause adverse health effects to the consumer when prepared or eaten according to its intended use.[10]

Food security. The situation that exists when all people, at all times, have physical, social, and economic access to sufficient, safe, and nutritious food that meets their dietary needs and food preferences for an active and healthy life. Four traditional dimensions can be identified (food availability, economic and physical access to food, and food utilization), as well as the two additional dimensions of agency and sustainability that are proposed by the High Level Panel of Experts (HLPE) of the Committee on World Food Security (CFS) but are not formally agreed upon by FAO or other bodies, nor is there an agreed language on the definition.[11, 12]

Food supply chain. Consists of a connected series of activities encompassing the primary production of food from crops, livestock, forestry, fisheries and aquaculture; and the value-adding activities of storage, transportation, processing; wholesale

a This definition is adapted from Tendall *et al.* (2015).[3]

and retail distribution. This definition differs from that of "food value chains" as proposed by FAO (2014) by excluding food consumption and disposal.[13]

- **Traditional food supply chains.** Spatially short involving a small number of small-scale producers, intermediaries and micro to small enterprises using labour-intensive technology and relying on spot markets. They handle locally produced food with basic processing, storage, logistics and other post-farm activities.
- **Transitional food supply chains.** Spatially long, with many small-scale producers and small to medium enterprises and intermediaries, such as processors, wholesalers and retailers who are fragmented; product diversification and value-addition are relatively high; contracts are used although spot market relations still prevail.
- **Modern food supply chains.** Serve large urban populations; spatially short, long or very long (including transnational); dominated by supermarkets and large processors; technology is largely capital-intensive where cold storage, packaging and private quality standards are very common; contracts dominate but spot markets are used for perishables.

Hazard. A process, phenomenon or human activity that may cause loss of life, injury or other health impacts, property damage, social and economic disruption, or environmental degradation.[9]

Household. A group of people, related or not, living together in the same dwelling, amenable to the same household head, and sharing food, food expenses, income and other household assets.

Idiosyncratic shock. An event that affects individuals or households.[7]

Net food consumer. Individual whose total sales of food to the market are less than purchases of food from the market.[14]

Net food producer. Individual whose total sales of food to the market exceed total purchases of food from the market.[14]

Redundancy. The duplication of critical components or functions of a system that increase its reliability. Often refers to backup systems or processes such that, if one part fails, the system as a whole will still be able to function. Examples of relevance for agrifood systems include spare inventory capacity at the firm level, alternative transport routes between stages or backup infrastructure at supply chain level and strategic food stocks at national level. Incorporating redundancy within a system typically entails a cost that needs to be weighed against how much it improves system performance.[15–17]

Resilience. The ability of individuals, households, communities, cities, institutions, systems and societies to prevent, anticipate, absorb, adapt and transform positively, efficiently and effectively when faced with a wide range of risks, while maintaining an acceptable level of functioning, without compromising long-term prospects for sustainable development, peace and security, human rights and well-being for all.[18]

Resilience capacities. Systems, institutions and people are considered resilient when they have at their disposal the following distinct capacities, many of which overlap. They are crucial to manage multiple risks and to withstand, cope with and recover from adverse events.[8]

- **Preventive capacity.** The ability to take measures to reduce exposure and vulnerability to shocks and stresses, i.e. to reduce existing risks and avoid creating new ones.[9]
- **Anticipative capacity.** The ability to take early action in anticipation of a threat to reduce its potential negative impacts, through early warning, early action or forecast-based financing.[19]
- **Absorptive capacity.** The ability to withstand shocks and stresses and bounce back afterwards using predetermined responses to preserve and restore essential basic structures and functions.[20–22]
- **Adaptive capacity.** The ability to make incremental adjustments and changes to the structure and actions of a system, to preserve its core functions without major changes in functional or structural identity.[21–24]

GLOSSARY

- **Transformative capacity.** The ability to create fundamentally new systems when ecological, economic or social structures make the existing ones untenable.[23, 25] Transformative capacity is required when the change needed goes beyond systems' anticipatory, preventive, absorptive and adaptive capacities and when there is recognition that ecological, economic or social structures trap people in a vicious circle of poverty, disasters and conflict, making current systems unsustainable.[26]

Risk. The potential of shocks and stresses to negatively affect systems, communities, households, or individuals. Risk is a function of hazard, exposure, vulnerability and capacity and accounts for the probability of direct and indirect social, economic and environmental costs of shocks and stresses.[9, 27]

Rural livelihood. The capabilities, assets and activities that rural people need to make a living.[28]

Shocks. Short-term deviations from long-term trends that have substantial negative effects on a system, people's state of well-being, assets, livelihoods, safety and ability to withstand future shocks.[8, 29] Shocks impacting on food systems include disasters, extreme climate events, biological and technological events, surges in plant and animal diseases and pests, socio-economic crises and conflicts. Shocks may be covariate or idiosyncratic.

Small and medium agrifood enterprises (SMAEs). These are independent post-harvest agrifood businesses (e.g. food processing, storage, transport or distribution) whose revenues, assets and number of employees are below a certain threshold. They are seen as more vulnerable and require special attention from both policy and research perspectives.[30, 31]

Small-scale producers. They comprise households running small-scale agricultural businesses of crops, livestock, fisheries, aquaculture, pastoralism or forestry, operating under greater constraints due to limited access to markets and resources such as land and water, information, technology, capital, assets and institutions.[32]

Stresses. Long-term trends or pressures that undermine the stability of a system and increase vulnerability within it. Stresses can result from natural resource degradation, urbanization, demographic pressure, climate variability, political instability or economic decline.[33]

Sustainable agrifood systems. Systems that deliver food security and nutrition for all, while sustaining the livelihoods of agrifood systems' actors, without compromising the economic, social, and environmental bases for the food security and nutrition of future generations. Systems must be sustainable economically (i.e. profitable and equitable), socially (having broad-based benefits for society) and environmentally (with positive or neutral impact on the natural environment).[34]

Sustainable development. The management of economic, social and environmental resources and technological and institutional change, to attain and continue to meet the human needs of present and future generations.[35]

Uncertainty. Refers to a situation where no probability can be assigned to outcomes of shocks and stresses, either because relevant information and data are missing (i.e. the outcomes cannot be measured or inferred based on past information and modelling), or the outcome is completely unforeseeable because it results from an unpredictable shock.

Vulnerability. The conditions determined by physical, social, economic and environmental factors or processes that increase the susceptibility of an individual, a community, assets or systems to the adverse impacts of shocks and stresses.[9]

CORE MESSAGES

1 To preserve their functionality and ensure the food security, nutrition and livelihoods of millions of people, agrifood systems must become more resilient to increasing shocks and stresses of diverse origins, both biophysical and socio-economic.

2 Because agrifood systems are complex – including primary production, food supply chains, domestic transport networks and households – and involve many interlinked actors, a shock in any component can spread rapidly throughout systems.

3 The fragility of agrifood systems can affect large numbers of people: already 3 billion people cannot afford a healthy diet and an additional 1 billion would join their ranks if a shock reduced their income by one-third. Food costs could increase for up to 845 million people if a disruption to critical transport links were to occur.

4 Of the five distinct resilience capacities agrifood systems must have – to prevent, anticipate, absorb, adapt and transform – absorptive capacity is critical in confronting unforeseen shocks and is complementary to risk management of shocks that can be anticipated.

5 Key to building the absorptive capacity of agrifood systems is diversity in food sources (domestic production, imports or existing stocks), diversity of actors in food supply chains, redundant and robust transport networks, and affordability of a healthy diet for all households, particularly the poorest and most vulnerable.

6 Risk management strategies for shocks such as droughts, floods and pests – including multi-risk assessments, timely forecasts, early warning systems and early action plans – are key to help all agrifood systems' actors prevent and anticipate major disruptions to systems and avoid human suffering and costly recovery interventions.

7 Enhancing the resilience of food supply chains requires government support to develop small and medium agrifood enterprises, cooperatives, consortia and clusters, as well as social protection programmes.

8 Resilience capacities of rural low-income households, in particular small-scale producers whose livelihoods are increasingly vulnerable to climate shocks and depletion of natural resources, can be significantly strengthened through education, non-farm employment and cash transfers.

9 Ensuring economic access to sufficient food for a healthy diet at all times is a key dimension of agrifood systems' resilience. Policies and investments that reduce poverty, generate decent employment and expand access to education and basic services, as well as social protection programmes when needed, are essential building blocks of resilience.

10 Building resilient agrifood systems should be a key policy objective and must ensure that all agrifood systems' components function well over time. This requires mainstreaming resilience in agrifood policies and greater coordination across all relevant sectors and layers of government institutions to ensure policy coherence.

EXECUTIVE SUMMARY

RESILIENT AGRIFOOD SYSTEMS ARE A STRATEGIC PART OF THE WORLD'S RESPONSE TO ONGOING AND FUTURE CHALLENGES

Agrifood systems encompass primary agricultural production of food and non-food products (from crops, livestock, fisheries, forestry and aquaculture), the production of food of non-agricultural origin (e.g. synthetic meat), the food supply chain from producer to consumer and the final consumer of food. Globally, these systems produce some 11 billion tonnes of food each year and form the backbone of many economies. In an ideal world, agrifood systems would be resilient, inclusive and sustainable, producing sufficient, safe and nutritious food for all, and generating livelihoods that guarantee people's economic access to that food. Today, however, agrifood systems fail to keep about 10 percent of the world's population free from hunger.

Increasingly, food supply chains and the livelihoods of agrifood systems' actors are disrupted by shocks – from droughts and floods to armed conflict and food price hikes – and long-term stresses, including climate change and environmental degradation. Risk and uncertainty are inherent in agrifood systems, affecting both primary production and their middle and downstream food supply components, as well as all actors at all stages. The vulnerability of agrifood systems became starkly clear in 2020, when measures to contain the novel coronavirus disease (COVID-19) pandemic disrupted global and national supply chains and caused economic downturns in many countries. Loss of purchasing power harmed the food security and nutrition of billions of people, particularly in low-income countries and among the poorest.

Truly resilient agrifood systems address all dimensions of food security

This report examines the challenge of building more resilient agrifood systems. Drawing on the *UN Common Guidance on Helping Build Resilient Societies*, it defines agrifood systems' resilience as "the capacity over time of agrifood systems, in the face of any disruption, to sustainably ensure availability of and access to sufficient, safe and nutritious food for all, and sustain the livelihoods of agrifood systems' actors".

Whether traditional, modern or transitioning between the two, agrifood systems have three main components: (i) primary production; (ii) food distribution, linking production to consumption through food supply chains and transport networks; and (iii) household consumption, including intra-household food distribution. Key actors are: primary producers; those providing input supply, post-harvest, storage, transport and food processing services; food distributors, wholesalers and retailers; and households and individuals as final consumers.

Truly resilient agrifood systems must have a robust capacity to prevent, anticipate, absorb, adapt and transform in the face of any disruption, with the functional goal of ensuring food security and nutrition for all and decent livelihoods and incomes for agrifood systems' actors. Such resilience addresses all dimensions of food security, but focuses specifically on stability of access and sustainability, which ensure food security in both the short and the long term. Another dimension of food security – agency – is deeply connected to human rights, including the right to food, and underscores the need for inclusiveness in systems.

Shocks have immediate impact, while stresses gradually undermine systems' coping capacity

Compared to other economic sectors, agriculture is disproportionately exposed and vulnerable to adverse natural hazards, especially those climate related. Climate change drives short-term shocks, such as extreme weather events, and generates slow-onset stresses, such as higher temperatures and loss of biodiversity. Shocks have immediate impact, while stresses are slow processes that gradually undermine the capacity of systems to cope with change and which render them more vulnerable. Agrifood systems' components and actors are exposed to shocks and stresses of various types and intensity and, because components are interlinked, disruption in any of them can spread quickly throughout systems. The same shock or stress may have different impacts on different systems' components and actors. Among producers, shocks are most likely to affect the livelihoods of low-income, small-scale operators; among food consumers, the poorest will be the most affected by rising food prices.

Risk management strategies that reduce exposure and vulnerability to a known, specific shock – such as drought preparedness – help build agrifood systems' resilience. However, the COVID-19 crisis has shown that some shocks are unpredictable in terms of timing and extent. Agrifood systems must have the capacity to continue functioning in the presence of shocks that are not foreseeable. Building resilience is, therefore, more than risk management: resilient agrifood systems are a strategic component of the world's response to ongoing and future challenges.

The ability to withstand shocks and stresses and bounce back is key in an uncertain environment

A key focus of the report is building the capacity of agrifood systems to absorb the impacts of shocks and stresses. Absorptive capacity refers to the ability to withstand shocks and stresses and bounce back in the aftermath, using predetermined responses to preserve and restore essential basic structures and functions. It is particularly important to address unforeseeable shocks.

Shocks and stresses can be very different in nature and origin. The magnitude of their impact is shaped by the specific vulnerabilities and resilience capacity of agrifood systems' components and actors, as well as the surrounding context (including climatic, environmental, socio-economic and political dimensions) and external sectors, such as energy and health. Complex, bidirectional linkages between the different systems' components mean that disruptions to food production eventually impact on household food security, while shocks affecting food consumption can ripple back to affect producers; this in turn will affect the environment.

In low-income countries, agricultural households with limited access to farm insurance and credit often rely on crop diversification and crop–livestock integration to mitigate the risks associated with climate variability and market volatility. However, diversification foregoes specialization, a strategy that allows households to accumulate experience. This raises the issue of the potential trade-off between building resilience through diversification, on the one hand, and efficiency, on the other. Another effective resilience strategy is redundancy, which reinforces the capacity of agrifood systems to absorb shocks by duplicating critical components and functions. However, this same redundancy can be costly to society and is particularly challenging when resources are limited.

UNDERSTANDING SYSTEMS' FUNCTIONS AND VULNERABILITIES

The report analyses the absorptive capacity of agrifood systems at the national level using a series of indicators linked to four key

systems' functions, that is, to ensure: (i) robust primary production; (ii) availability of food; (iii) physical access to food; and (iv) economic access to food. Each national system is unique, comprising numerous components and actors, operating on several interlinked levels, and often including international trade. Some components may be more resilient than others and the impacts of shocks may be component or actor specific. Policymakers need to understand systems' functioning and be aware of potential vulnerabilities. A participatory, inclusive and collaborative process may then help engage systems' participants in a more coordinated response to challenges.

Diversity in production and trade partners can help minimize risk

To measure the capacity of primary producers to absorb shocks, FAO developed a primary production flexibility index (PPFI) for this report, covering 181 countries, to measure the extent of diversity in production across crop and livestock commodities and the potential to produce for domestic and export markets. A high PPFI value indicates multiple potential pathways for generating agricultural value and for finding final outlets for primary food production. For more than 80 percent of countries, the PPFI is driven by domestic market diversity, and countries with the lowest diversity values are strongly skewed towards the domestic market. Most are low-income countries, with little external trade, where primary production is vulnerable to shocks that affect key commodities or reduce consumers' incomes. Greater diversification in primary production is found in high-income countries or in those with a large agricultural base. These countries rely on a mix of comparative advantage in producing and exporting agricultural products, openness to international trade, and a sizeable domestic demand for marketing their products.

Not all agricultural powerhouses are exempt from vulnerabilities: even countries with a sizeable agricultural base and export demand may reveal a low capacity to absorb shocks if the number of trading partners is limited. If those partners suffer a shock, the country is left with limited options. It can also be indicative of specialization in very few export commodities, which increases vulnerability to commodity-specific domestic shocks, such as pests, and to international shocks, such as sharp price declines due to oversupply.

An important function of agrifood systems is to make available a diverse range of foods that provide the nutrients essential for human health. To measure their capacity to absorb shocks and ensure the availability of food necessary for a nutritious diet, FAO also developed the dietary sourcing flexibility index (DSFI) for this report, computed with data for 153 countries. The indicator captures the multiple sourcing pathways of crop, fish and livestock commodities available from domestic production, food imports and available stocks. What emerges is that countries diversify their sources of food in different ways and effectiveness in diversifying does not depend on country size or income level. Where income does matter is in diversifying sources of fruits and vegetables, which is limited in low-income countries due to logistical constraints associated with transporting and storing perishables.

Countries with a sizeable agricultural base that rely more on domestic production may have the same absorptive capacity as countries that diversify more through imports. Those importing from multiple trade partners and across multiple commodities attain among the highest DSFI scores by buffering any supply shocks over many partners and commodities. Conversely, countries dependent on food imports from only a few major sources are vulnerable to shocks that hit their trading partners. In this case, diversifying import baskets and international trade partners, and possibly investing in domestic stocks, would be prudent.

Ensuring physical and economic access to food is a key aspect of agrifood systems' resilience

An efficient, flexible transport network with optimal redundancy guarantees physical access to food at subnational level. To capture the structural vulnerabilities of food transport networks around the world, FAO analysed their resilience in 90 countries, by examining how transport networks connect food demand nodes to where food is produced. The analysis measured food systems' capacity to respond locally to disruptions, the availability of alternative routes, and systems' sensitivity to the closure of critical links owing to shocks or stresses. While several very large countries had long distribution networks, food production and distribution in others could be adjusted to more locally based systems, if needed.

Low-income countries face the biggest challenges in applying system-wide resilience measures to their food transport networks. They have limited capacity to adjust to local systems and lack reliable alternative routes during disruptions. Since proximity-based resilience depends on how production is distributed relative to demand, some large, high-income countries are also vulnerable. For nearly half the countries analysed, the closure of critical network links would increase local travel time by 20 percent or more, increasing food costs.

Providing physical access to food is not enough to ensure food security. Well-functioning agrifood systems must also ensure people's economic access to food. Globally, some 3 billion people cannot afford a healthy diet, one that protects against malnutrition in all its forms. Since the share of household expenditure on food is highest in low-income households, any significant loss of purchasing power – caused by disruptions such as food price spikes, crop failures and loss of assets – poses a threat to their food security and nutrition. Based on data for 143 countries, FAO also developed an indicator for this report revealing that, if a shock reduced their income by one-third, a healthy diet would be beyond the financial reach of an additional 1 billion people. The burden of this additional challenge would fall mostly on middle-income countries: out of the 1 billion people at risk of not being able to afford a healthy diet, 95 percent live in lower- and upper-middle-income countries. In low-income countries – where already a large majority cannot afford a healthy diet – the challenge is that, in the face of the same one-third cut in income, many more people risk not being able to afford even an energy-sufficient diet, consisting mainly of starchy staples that provide the energy needed for a day's work.

When incomes are affected by a shock, truly resilient, inclusive and sustainable agrifood systems must aim at ensuring the affordability of a healthy diet. To achieve that, either the cost of food must come down, or the incomes of the vulnerable population must increase or be supported through, for example, social protection programmes – or, ideally, both.

DIVERSE, REDUNDANT, WELL-CONNECTED FOOD SUPPLY CHAINS UNDERPIN RESILIENCE

Labour shortages during COVID-19 lockdowns exposed the vulnerability of small and medium agrifood enterprises

The smooth functioning of food supply chains underpins the resilience of national agrifood systems. A food supply chain is composed of interconnected activities performed by various actors – farmers, processors, wholesalers and retailers – who, in turn, draw on lateral chains that supply inputs and logistic services. The capacity of a food supply chain to absorb shocks depends on the resilience of each of its segments. Diverse, redundant and well-connected food supply chains enhance agrifood systems' resilience by providing multiple pathways

for producing, sourcing and distributing food. This resilience is necessary not only for safeguarding and enhancing the livelihoods of farmers and businesses, but also for ensuring the physical availability of food to all.

The vulnerabilities and resilience capacities of food supply chains are shaped largely by their structural characteristics and product attributes. Traditional chains are spatially short, involve a small number of local intermediaries, but lack product diversification, quality and safety standards, and economies of scale. Transitional supply chains are spatially longer, with many small and medium agrifood enterprises (SMAEs) handling midstream processing and distribution. Modern chains, which supply large urban populations mainly with horticultural and animal products, are dominated by multinationals in their midstream and downstream segments.

Understanding how shocks and stresses are likely to affect a given food supply chain is the key to developing resilience capacities that mitigate damage and provide recovery options. Large-scale modern food supply chains proved resilient to COVID-19 lockdowns because they operate on a global scale, with the capacity to adjust to disruptions geographically and temporally. Transitional supply chains, with their multitude of SMAEs and heavy reliance on labour, were more vulnerable to labour and transport disruptions. There is also evidence that some traditional supply chains filled gaps left by modern and transitional chains disrupted by lockdowns. Many proved to be nimble in their responses, especially in high-income countries. However, traditional supply chains are usually more vulnerable because, as they are often highly informal, they are invisible in national statistics, and government support and social protection programmes do not reach them.

Resilience-building strategies may involve trade-offs with efficiency and inclusiveness

Agrifood businesses are heterogeneous in terms of economic scale, input composition, technology use and outputs, which range from bulk food commodities to niche items and differentiated products. They have different capacities to bear risk and make resilience-building investments. Businesses may adopt diversification or redundancy strategies, or both. For example, the world's biggest rice milling firm has built two ports upriver from its primary port in Thailand to guarantee shipping movements in the event of a typhoon; this is a representative case of the trade-off between efficiency and resilience. To reduce such trade-offs, businesses may seek partnerships with other, complementary companies. But this may not be feasible for SMAEs, which face the double challenge of being resilient to shocks while also remaining competitive with larger enterprises. What they gain in resilience and agility, they may lose in access to lucrative markets.

Essential to all these strategies is public infrastructure – roads, culverts, power lines, running water, irrigation schemes and ports – that helps to avert or buffer shocks. Producers and food chain actors located in agricultural territories with well-developed infrastructure will have greater absorptive capacity. Increasingly, public infrastructure is complemented by private infrastructure, such as collection stations, road hauliers and temperature-controlled warehouses. Businesses with the capacity to make the necessary investments and bear the risks will survive and outcompete those with less capacity, adding momentum to the competitive forces that are concentrating the off-farm segments of food supply chains in fewer hands. Agrifood businesses, farmers and agricultural territories that are excluded in this way lose their crucial link to urban and export markets

and find themselves in a poverty trap, where the confluence of market and climate changes makes them especially vulnerable. The social cost of unemployment and lost livelihoods incurred as SMAEs are driven out of business may outweigh gains from the increased resilience of large-scale firms.

The limited resources available to small-scale producers and SMAEs in food supply chains often make recovery following a disruption more difficult. Improving public infrastructure, along with easier access to credit and information, can create synergies between efficiency and resilience that accelerate recovery. Governments can also support better coordination and organization of SMAEs within food supply chains. One approach is to form consortia, which increase the scale, visibility and influence of small businesses and facilitate access to private and government funding. Nurturing inter-organizational relationships in networks or strategic alliances can generate relational, structural and cognitive capital, promote more robust and effective risk management through resource pooling, and improve access to modern technologies and know-how. Another way of encouraging coordination and enhancing relational capital among SMAEs is through territorial development tools such as clusters. In countries where credit markets are imperfect or underdeveloped, enhancing industrial clusters can contribute to easing credit constraints. Consortia and clusters are also excellent facilitators of human development programmes and the diffusion of digital technologies.

ROBUST RURAL LIVELIHOODS STRENGTHEN ENTIRE SYSTEMS

The resilience capacities of all households are important for the functioning of agrifood systems. All households have a role to play in agrifood systems, whether as food producers and suppliers or as consumers. The resilience capacities of rural households – especially low-income small-scale farm families – are particularly and increasingly put to the test in the new normal of climate change and depletion of natural resources. While they often engage in non-farm activities, many rural people depend mainly on agriculture for their livelihoods. The impacts of shocks and stresses on those livelihoods, and consequently on people's food security and nutrition, play out essentially within households. Hundreds of millions of farming households contribute to agrifood systems, through primary food production and small-scale agrifood businesses. Rural households that engage in diverse and multiple activities are generally better able to cope with, and recover from, stresses and shocks.

Households that are net food producers are more vulnerable to shocks and stresses that affect agricultural and food production, such as pests and diseases, drought, and disruptions to input and food marketing chains. On the other hand, households that are net food consumers – practising farming as a part-time activity and relying on employment mainly in the non-farm economy – are more prone to shocks such as price spikes that affect their purchasing power. Households running small-scale agrifood businesses operate under greater constraints than their larger competitors due to more limited access to information, technology, capital, assets and institutions. They bear a double burden of vulnerability to risks and shocks: while facing those intrinsic to agriculture, they also risk being excluded from productive assets and lucrative markets in the accelerating modernization of food supply chains in developing countries.

Education, non-farm work and cash transfers help rural households cope better with shocks and stresses

Rural households have developed a variety of strategies to help navigate foreseen and unforeseen disruptions and strengthen their capacity to prevent, anticipate, absorb, adapt and transform. At farm level, households respond to the unpredictable interplay between

natural, technological and social factors by reconfiguring and using available resources in novel ways. To reduce risks and mitigate the impacts of shocks before they occur, they diversify production mixes, adjust planting dates to cope with rainfall variability, and invest in risk reduction by improving irrigation, drainage and pest control and adapting land use practices to reduce soil erosion. They diversify their sources of income through part-time employment in the rural non-farm economy. Households also have coping mechanisms for the aftermath of shocks: they cover their losses and smooth out their consumption by liquidating assets, taking out loans or drawing on savings and informal insurance based on community networks. However, coping strategies that reduce household assets run the risk of aggravating vulnerability by undermining future income-generating capacity.

FAO's resilience index measurement and analysis (RIMA) model was used to identify the main factors underpinning resilience in rural households in 35 countries. Findings from 23 countries indicate that education, income diversification and cash transfers mainly drove gradual improvements in resilience capacity. Analysis of another 12 countries showed that in more than half of cases, the most important pillar of resilience was access to productive and non-productive assets. Also important to household resilience was adaptive capacity, which depended critically on education and human capacity development within the household. Access to basic services, such as improved sanitation and safe drinking water, and primary services, especially schools, hospitals and agricultural markets, provided important support to household resilience, particularly in very arid zones and in pastoralist households.

The RIMA analysis also showed that rural households comprising mainly women pay the heaviest toll during and after shocks. Women tend to have much less access than men to land and other assets that are crucial for resilience. Children are particularly vulnerable to shocks and stresses. Studies show that widespread shocks increase the rates of stunting and underweight among children under two years of age. Since child nutrition status is associated with performance in cognitive tests, school attainment and labour market outcomes later in life, shocks may generate substantial, long-term economic costs to both individuals and society.

Small-scale producers need organization, sustainable practices and social protection

To stay competitive and protect their livelihoods, small-scale agricultural producers need to be well integrated in supply chains for food, inputs and services. One means of achieving this integration is producer associations and cooperatives, which reinforce livelihoods by allowing the pooling of resources to achieve scale, facilitating access to productive resources such as machinery, equipment and credit, and enhancing marketing power. Coordination with other actors in the food supply chain is also key to managing market risks. Mutual benefits can be achieved, for example, through forward contracts: farmers receive guaranteed prices for their outputs regardless of market conditions, while processors and distributors receive products of a desired quality.

Another resilience-enhancing strategy that small-scale farming households use increasingly is the adoption of more sustainable production practices. One option is agroecology, an approach that applies ecological and social principles to the design and management of agrifood systems. An important element of agroecology is food and agricultural biodiversity, which boosts resilience to shocks and stresses, facilitates adaptation, maintains stability and supports recovery from disturbances. Another option is climate-smart

agriculture, which enhances food security and healthy livelihoods while promoting climate change adaptation and mitigation. These concepts recognize that conventional mainstream agriculture cannot feed the growing world population sustainably because it degrades the natural resource base.

Social protection programmes, which emerged in developing countries in the 1980s and early 1990s, now extend beyond welfare concerns, with increasing emphasis on reducing risks and the harmful effects of shocks on vulnerable livelihoods. Social protection supports low-income farming households in adopting more profitable, but also riskier, economic activities and provides an alternative to negative coping strategies. Programmes that provide social protection and productive support are highly complementary and their implementation is increasing in rural areas.

GUIDING PRINCIPLE FOR POLICYMAKERS: PREPARE FOR DISRUPTION

Diversity in food sources and output markets creates multiple pathways for absorbing shocks

In a multi-risk environment, some disruptions are predictable and some not. Preparing for the unknown requires careful assessment of the structural characteristics of systems, including the absorptive capacity provided by their diversity of pathways and connectivity. Policies and investments need to recognize the distinction between risk and uncertainty. Managing risk typically involves reducing exposure and vulnerability to a specific adverse event. Managing uncertainty, on the other hand, requires that systems have sufficient diversity of actors and responses to maintain their core functions should an unforeseen shock materialize. Both approaches are needed and are complementary.

Key to building the absorptive capacity of agrifood systems is diversity in all its forms. Agrifood systems – and related food supply chains – with access to more diversified sources of food and output markets are less vulnerable. Knowing the multiple pathways through which a shock can be absorbed is crucial for policymakers to devise strategies to deal with a crisis. While sourcing through international trade makes agrifood systems less vulnerable to domestic shocks and stresses, a high dependency on imports from only a few partners may make them vulnerable to external shocks. Importing diversified foods from different countries with heterogeneous socio-economic and climatic profiles helps diversify the risks and reduce vulnerability to external shocks. International efforts to overcome trade barriers between countries may be needed for such flexible sourcing of food. In countries where the capacity to absorb shocks mostly stems from what is produced and traded domestically, diversifying domestic production and imports, as well as stocks, will be an essential part of food security and nutrition strategies, especially where many cannot afford or are at risk of not being able to afford a healthy diet.

Well-connected agrifood systems overcome disturbances faster by shifting sources of supply and channels for transporting and marketing of food products, inputs and labour, as well as transmission channels for knowledge and financial resources. Connectivity and diversification contribute to absorptive capacity and being prepared for disruption: they do not target a specific event but provide options once a disruptive event occurs. However, connectivity and diversification should be complemented with risk management. For example, disasters and crises can significantly impact on infrastructure and services, such as roads, transport or food storage. It is very important, therefore, to assess, protect and risk-proof infrastructure and to develop new risk-sensitive and climate-resilient infrastructure.

To ensure climate resilience, it is essential to assess and address the infrastructure's physical vulnerabilities.

The heterogeneity of farms and businesses must be recognized

Policies and interventions should facilitate a mix of traditional, transitional and modern food supply chains, which can buffer shocks and stresses of different types. Policymakers should acknowledge the heterogeneity of farms and businesses along the urban–rural continuum and address vulnerabilities at different scales. Improvements in risk management and early warning capacity may be needed to help predict shocks and their impacts. To enhance decision-making, government at various levels should work with academia, research centres, civil society and the private sector and make data available and accessible for analysis throughout systems. Inclusive governance and institutions will promote better risk management capable of rapid responses during crises. Subnational and local multi-risk management strategies may be needed to address underlying vulnerabilities and risk drivers.

Existing disaster and risk management tools in national laws, policies and regulations could be tailored to food supply chains to help stakeholders function more effectively and collaboratively within and across sectors. Policies also need to help producers and agribusinesses adopt resilience-enhancing business tools, including business literacy, expanded access to the Internet, credit and insurance, and funding for research and agricultural extension services. An environment that supports individual agrifood systems' actors will include leveraging information and communications technologies for logistics. Central and local governments, along with the private sector, non-governmental organizations and international development agencies, have an important role to play in supporting their adoption.

Risk management, crop insurance and social protection enhance household resilience

Resilient livelihoods are the basis of resilient agrifood systems because they ensure access to food even in the face of shocks. Among vulnerable rural households, those involved in small-scale agriculture and other primary agrifood production will benefit most from the logistical support, production innovations and inclusive governance of food supply chains. In framing policies to build the resilience capacities of small-scale producers and vulnerable households, policymakers should seek to facilitate risk management and enable household resilience capacities. As extreme climatic events become more frequent and more pronounced, producers will need access to agroclimatic disaster risk and early warning systems. Increasing their access to crop and weather insurance will enhance their ability to take out production loans and participate in more risky, higher-return farming activities.

Social protection programmes may be needed to improve household resilience in the event of a shock. Risk-informed and shock-responsive social protection systems are designed to provide support not only to routine beneficiaries, such as pensioners, but also at-risk and crisis-prone populations before, during and after disruptions. They can expand the provision of benefits according to the emerging needs of potential beneficiaries and enable them to invest and engage in productive activities. If well designed, social protection enables synergies with productive support programmes and investments, which strengthen both the resilience and the sustainability of small-scale producers' livelihoods.

Policies will need to address issues beyond agrifood systems. Key policy areas that have a clear impact on household resilience include strong, inclusive health insurance and medical services. Education and training are also important for strengthening long-term

household resilience. Broader policies aimed at promoting gender equality will significantly improve resilience thanks to the increased participation of women in all components. Policies aimed at boosting employment can also strengthen livelihoods and incomes, with positive impacts on agrifood systems.

Ensuring the sustainability of agrifood systems is an integral part of building resilience. Policies can promote systems' sustainability by recognizing its role in stewardship of the natural environment. Rather than aggravating climate change and natural resource degradation, agrifood systems need to adopt agroecological farming and other resource-conserving practices.

It is important to recognize that policymaking can have unintended consequences. To avoid implementing restrictions that hurt agrifood systems' actors, policymakers must understand how systems function and interact. Policy coherence is essential. A significant issue requiring policy coherence is that of subsidies, such as agricultural price support. Subsidies can provide immediate and short-term relief to agricultural producers, but may also reduce their capacity to adapt to shocks when they occur. At the same time, subsidies, as well as any other policies supporting agrifood systems' resilience, will need to be fiscally sustainable. To meet the challenge of policy coherence, government institutions across all relevant sectors and different layers must be involved. ■



KENYA
A refugee grows vegetables as a source of food and income by using collected water near Kakuma refugee camp in Kalobeyei.
©FAO/Luis Tato

CHAPTER 1
AGRIFOOD SYSTEMS' RESILIENCE: WHAT IT IS

KEY MESSAGES

➔ The COVID-19 pandemic's unprecedented impact on livelihoods and food security is a wake-up call to address the weaknesses, vulnerabilities and multiple risks in agrifood systems and safeguard their functions in the face of disruptions.

➔ Enhancing the resilience of agrifood systems means strengthening their capacities and those of their actors to prevent, anticipate, absorb, adapt and transform when struck by shocks and stresses.

➔ Agrifood systems are increasingly threatened by long-term stresses, such as climate change, deforestation, natural resource degradation and other protracted crises.

➔ Stresses aggravate vulnerabilities to multiple shocks, such as extreme weather events, conflicts, pandemics and socio-economic crises, which can strike anywhere in agrifood systems and spread through them and beyond.

➔ Building resilience in agrifood systems contributes in a fundamental way to their sustainability by enhancing their capacities to manage the risks posed by multiple shocks and stresses.

➔ Building agrifood systems' resilience begins by identifying systems' characteristics, their components and actors, understanding the linkages and interactions between them and broader economic, social and environmental contexts, to assess specific risks, vulnerabilities and responsive capacities.

➔ Key elements of building resilience are diversification (e.g. in production and sources of supply) and redundancy (i.e. duplication of agrifood systems' components). These may require managing trade-offs with efficiency and sometimes with equity.

The world's agrifood systems comprise a gargantuan global enterprise that each year produces approximately 11 billion tonnes of food[1] and a multitude of non-food products, including 32 million tonnes of natural fibres[2] and 4 billion m^3 of wood.[3] The estimated gross value of agricultural output in 2018 was USD 3.5 trillion.[4] Primary production alone provides about one-quarter of all employment globally, more than half in sub-Saharan Africa and almost 60 percent in low-income countries.[5] Including middle and downstream segments – from food storage and processing to transportation, retailing and consumption – agrifood systems are the backbone of many economies. Even in the European Union, the food and beverage industry employs more people than any other manufacturing sector.[6]

In an ideal world, all agrifood systems would be resilient, inclusive and sustainable, producing sufficient safe and nutritious food to meet the needs of all for an active and healthy life – without compromising the food security, health and nutrition of future generations. They would be underpinned by biological systems allowing them to be abundant providers of food and to sustain livelihoods. By generating livelihoods and prosperity, agrifood systems would guarantee billions of people economic access to food, a key pillar of food security.

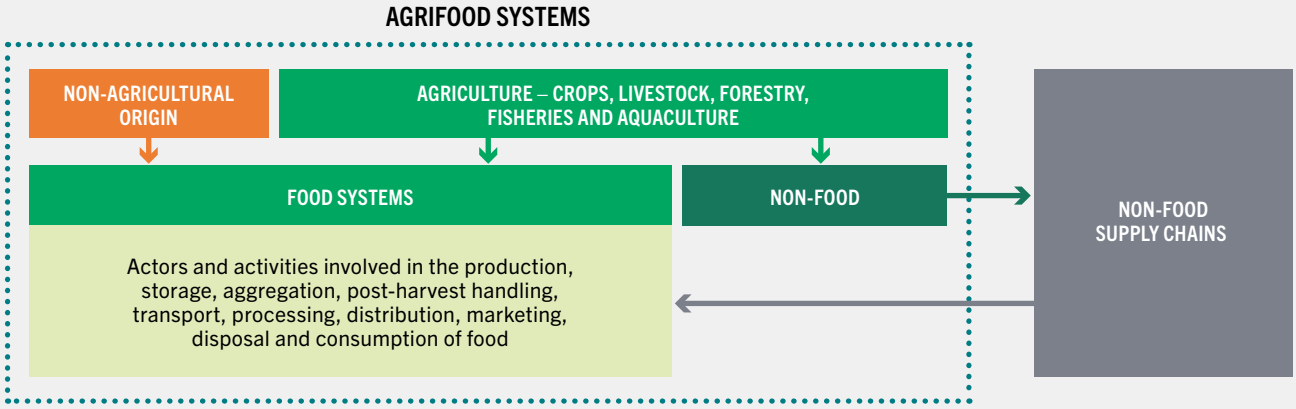
Then there is reality. In 2020, an estimated 768 million people, or 9.9 percent of the global population, suffered from hunger, an increase of nearly 118 million compared to 2019 and 153 million compared to 2015.[7] Even as the world faces extreme pressure to produce more food, shocks ranging from droughts and floods to armed conflict and price instability, aggravated by longer-term stresses such as economic inequalities

BOX 1 DEFINING AGRIFOOD SYSTEMS IN RELATION TO FOOD SYSTEMS

As illustrated in the figure in this box, **agrifood systems** encompass the entire range of actors and their interlinked value-adding activities in the primary production of food and non-food agricultural products, as well as in food storage, aggregation, post-harvest handling, transportation, processing, distribution, marketing, disposal and consumption. Within agrifood systems, **food systems** comprise all food products that originate from crop and livestock production, forestry, fisheries and aquaculture, and from other sources such as synthetic biology, and that are intended for human consumption. While non-agricultural food products, such as synthetic meat, are currently negligible, they are likely to grow and could have a major impact on the resilience of agrifood systems. They may limit risks linked to climatic events and pests, but could have potentially negative impacts as well, especially in terms of loss of jobs and livelihoods for people working in agricultural food production.

Agrifood systems interact with non-food supply chains through the purchase of inputs such as fertilizer, pesticide, and farm and fishing equipment, and the provision of intermediate inputs for the production of non-food commodities (e.g. maize for biofuel production or cotton for textiles). Broader economic, social and natural environments shape and influence agrifood systems and their diverse production systems.

FIGURE A CONCEPTUAL FRAMEWORK FOR AGRIFOOD SYSTEMS



NOTE: Food of non-agricultural origin includes meat analogues produced through synthetic biology.
SOURCE: FAO elaboration for this report.

and climate variability, threaten both agricultural production and other vital segments of agrifood systems. Multiple risks and uncertainties have a disproportionate effect on the world's most vulnerable and food-insecure populations, who are on the front line facing multiple shocks and stresses. Even before the novel coronavirus disease (COVID-19) pandemic, nearly 3 billion people could not afford a healthy diet, one that protects against malnutrition in all its forms.

Shocks and stresses impair agrifood systems by disrupting the operations of related institutions, supply chains and actors.[8] Box 1 shows how agrifood systems encompass food systems, including the entire range of actors and their interlinked value-adding activities, and the primary production of non-food products in the crop, livestock, forestry, fisheries and aquaculture sectors. Shocks and stresses can emerge from the surrounding socio-economic

and environmental context and spread both within and outside systems: the most recent major example is the COVID-19 pandemic. Physical, social, economic and environmental conditions determine the level of *vulnerability* of individuals, communities, institutions, assets, infrastructures or systems to the negative impacts of shocks and stresses.[9] Understanding differences in vulnerability to various shocks and stresses and the resilience capacities of agrifood systems is necessary to identify specific measures that build resilience in the face of disturbances.[10]

Being heavily dependent on climatic, biological, physical and chemical processes, agrifood systems face multiple potential shocks and stresses, including climate change, extreme weather events, pest and disease upsurges, water scarcities and deteriorating natural resources. FAO estimates that between 2008 and 2018, the agriculture sector in low-income and lower-middle-income countries – without considering their broader agrifood systems – absorbed 26 percent of all economic damage and losses caused by medium- to large-scale disasters.[11] For small-scale producers and other agrifood systems' actors in those countries, stresses can be particularly pervasive and chronic. They amplify the effects of existing structural deficiencies, such as inadequate road, power, irrigation, clean water, processing, storage and marketing infrastructures. Those deficiencies condemn millions of farmers and other rural people to geographic and economic isolation, limited opportunities to develop businesses, poor access to services and high dependence on local weather conditions.

The consequences can be highly adverse: factors of production are underused, productivity is low, food and non-food agricultural output is lost, and access to lucrative markets is blocked. Amplifying agrifood systems' vulnerability to multiple shocks and stresses undermines the capacities of actors to prevent, anticipate, absorb, adapt and transform. Once resilience capacities are compromised, the likelihood of acute and chronic food insecurity and malnutrition increases.

The international community has recognized the urgent need for action to strengthen food systems, the part of agrifood systems that encompass producing, processing, transporting and consuming food (Box 1). The United Nations (UN) Food Systems Summit, held in September 2021, launched bold new actions to accelerate progress towards all the Sustainable Development Goals (SDGs), each of which relies to some degree on healthier, more sustainable and equitable food systems. Building *resilience* is essential to implement the SDGs and the overall 2030 Agenda for Sustainable Development. Agrifood systems' resilience is directly aligned with achieving SDG 2, Zero Hunger, and key to progress towards several other SDGs with a socio-economic focus (SDG 1, No poverty; SDG 5, Gender equality; SDG 8, Decent work and economic growth; SDG 10, Reduced inequalities; SDG 11, Sustainable cities and communities) and those relating to environmental sustainability (SDG 6, Clean water; SDG 12, Responsible consumption and production; SDG 13, Climate action; SDGs 14 and 15, Life below water and on land). By creating peace and prosperity for all people on the planet by 2030 (in line with SDG 16, Peace, justice and strong institutions), achievement of the SDGs will prevent many disturbances, or at least strongly mitigate their impact.

This report addresses the following questions: What characterizes resilient agrifood systems? How can agrifood systems' actors manage their vulnerability to shocks and stresses? How can households – especially the poor and most vulnerable – meet their food needs when disruptions to agrifood systems reduce production and incomes, force price increases or create food shortages? How can we ensure that agrifood systems support livelihoods and sustainably provide continuous access to sufficient, safe and nutritious food to all in the face of disruptions? In short, how do we improve the resilience of our agrifood systems? ■

THE NEED FOR MORE RESILIENT AGRIFOOD SYSTEMS

Building agrifood systems' resilience becomes all the more urgent given the persistence of hunger and malnutrition. Hunger is increasing, and more so in countries affected by conflict, climate extremes and economic downturns, and with high income inequality.[12] The magnitude and severity of food crises also worsened in 2020 as protracted conflict, the economic fallout of the COVID-19 pandemic and weather extremes exacerbated pre-existing fragilities.[13] Economic downturns in 2020, including those resulting from COVID-19 restrictions, delivered the hardest blow in decades to those suffering from hunger, increasing the number of undernourished people by 118 million in 2020 alone[12] and illustrating the devastating impact of a shock that occurs alongside existing vulnerabilities. There is little evidence of reduced food supply (beyond initial disruptions due to panic buying),[8] which may be attributable to government exemptions for the agrifood sector. However, lockdowns and other mobility restrictions drastically reduced the movement of people and goods, impacting on livelihoods. Loss of income and purchasing power sharply reduced the food security and nutrition of billions of people, particularly in low-income and middle-income countries. Families were forced to shift consumption to cheaper, less nutritious foods[8] at a time when they needed to protect and strengthen their immune system.[14] Reduced access to nutritious food and a shift to low-quality and energy-dense diets triggered by the economic impacts of the COVID-19 pandemic, also risk increasing the levels of overweight and obesity in almost all regions of the world. Adult obesity is on the rise with no reversal in the trend at global or regional level for more than 15 years, increasing the non-communicable diseases associated with those forms of malnutrition.[12]

The ability of agrifood systems to ensure food security and nutrition for all will depend not only on their own capacities, but also on the functioning of other interconnected socio-economic and environmental systems such as transport, education, health, water, soil and energy, as well as social protection mechanisms. The negative impact of the shock triggered by the pandemic on infant and young child morbidity could be exacerbated by reduced healthcare to prevent and treat malaria, diarrhoea and other infectious diseases. School closures may lead to missed meals and nutrition education provided through school food and nutrition programmes.[8] A compelling body of evidence shows that the adverse impacts of such shocks and related stresses on preschool children's nutritional status are not only immediate but persist into adulthood.[15]

Demographic and environmental pressures make agrifood systems' resilience ever more imperative as a rapidly growing global population drives increased demand for food. At the same time, shocks and stresses, including more frequent and intense extreme and slow-onset events due to climate change, threaten both agricultural production – crops, livestock, aquaculture, fisheries and forestry – and the middle and downstream stages of agrifood systems. But as agrifood systems are affected by climate shocks and stresses, they are themselves a major driver of climate change. To feed a world population forecast to reach 9.7 billion in 2050,[16] agriculture may need to produce 40–54 percent more food, feed and biofuel feedstock than in 2012,[17] depending on the scenario. This is a daunting task that could place unsustainable pressures on the Earth's natural resources. Moving towards more sustainable agriculture and food production is needed. Central to this are the three priorities of: protecting nature; restoring and rehabilitating natural environments; and sustainably managing food production systems.[18] Significant reductions in food loss and waste,[19] better resource-use efficiency and trade have an important role, as imports may be needed to fill domestic deficits where there are natural resource constraints.

Another approach is agroecology, which encompasses three dimensions: science, a set of practices, and a social movement. There is increasing evidence to show how agroecology benefits the environment, biodiversity and farmers' incomes, as well as helping farmers adapt to and mitigate climate change and build

resilience to multiple shocks and stresses. Climate-smart agriculture (CSA), another resilience-enhancing approach, emerged in response to climate change[20] and other stresses, including environmental degradation and demographic pressures, as further shown in this report.

Also required is far-reaching adjustment to current dietary trends. Urbanization and greater affluence are shifting diets in many low-income and middle-income countries towards increased consumption of more resource-intensive animal source and processed food.[17] If those trends continue, by 2030, diet-related health costs linked to non-communicable diseases will exceed USD 1.3 trillion a year, while the annual cost of associated greenhouse gas (GHG) emissions will exceed USD 1.7 trillion.[7]

Given these and future challenges, agrifood systems must not only find ways to cope with adverse changes but strive towards achieving the SDGs by transforming current business-as-usual approaches. Agrifood systems need to focus on providing nutritious food for all and using resources efficiently, while becoming more inclusive, sustainable and resilient. Producing more with less, and at the same time protecting and enhancing the livelihoods of small-scale agricultural producers and other agrifood actors, are global challenges. The COVID-19 pandemic, along with lessons from other shocks in recent decades, shows clearly that some degree of risk and uncertainty is inherent in agrifood systems. Therefore, risk management strategies that reduce exposure and vulnerability to a specific shock – such as drought preparedness in drought-prone areas – will be a key measure to build resilience. The sudden appearance of the COVID-19 pandemic, however, shows that some shocks may be unknown in terms of timing and extent of their impacts until they actually happen. Resilience building is, therefore, broader than risk management. Risk management is key to help agrifood systems' actors anticipate and prevent major disruptions; however, to be resilient, agrifood systems must have all of the five resilience capacities – prevent, anticipate, absorb, adapt and transform – in order to continue functioning in the presence of shocks that are not completely predictable.

Investments in risk-informed and shock-responsive social protection and insurance programmes, diversified supply chains and farming systems, and flexible logistics are examples of essential interventions to build or enhance these capacities. ■

UNDERSTANDING RESILIENCE IN AGRIFOOD SYSTEMS

The concept of resilience originated in the study of ecosystems[21] and has evolved over 50 years into an object of study across an array of disciplines, including engineering, agriculture, economics and psychology. Although there is little agreement today as to a precise definition across disciplines, broadly speaking, *resilience* can be defined as the dynamic capacity to continue to achieve goals despite disturbances.[22]

In a call for cross-sectoral collaboration to prevent, anticipate, absorb, adapt and transform in the face of shocks and stresses across all sectors of society, the UN has developed and adopted the *UN Common Guidance on Helping Build Resilient Societies*.[9] Since there is a wide variety of risks relating to understanding *resilience*, the UN offers the following definition:

> the ability of individuals, households, communities, cities, institutions, systems and societies to prevent, anticipate, absorb, adapt, and transform positively, efficiently and effectively when faced with a wide range of risks, while maintaining an acceptable level of functioning and without compromising long-term prospects for sustainable development, peace and security, human rights and well-being for all.

This definition underscores the fact that shocks and stresses can have detrimental effects in the short and the long term. Resilience entails recognizing their dynamic and intertemporal nature. For agrifood systems to overcome shocks and stresses,[9, 23] they require five distinct resilience capacities – to prevent, anticipate, absorb, adapt and transform in the

face of multiple evolving, overlapping and even colliding events.

This report focuses mainly on the absorptive capacity of resilience and how it should be combined with risk management, such as preventive and anticipatory actions, to enable positive adaptation and inclusive and sustainable agrifood systems' transformation. Absorptive capacity refers to the ability to withstand shocks and stresses and bounce back after a shock, using predetermined responses to preserve and restore essential basic structures and functions. Building absorptive capacity requires designing and investing in diversified responses to preserve and restore essential structures and functions. Absorptive capacity is in part also determined by systems' structural characteristics, such as the number and diversity of stakeholders involved, the institutions that coordinate them and the robustness of the infrastructure on which they rely. The structural nature of absorptive capacity is central in this report, guiding the development of indicators and shaping new insights on how to improve the resilience of agrifood systems.

The report applies the UN definition of resilience specifically to food and agriculture, defining agrifood systems' resilience as the objectives of ensuring food security and nutrition for all and decent livelihoods and incomes for agrifood systems' actors. Building resilient agrifood systems calls for linking the concept of resilience to all dimensions of food security, not only food availability, economic and physical access to food, food utilization and stability over time, but also the dimensions of agency and sustainability, recently proposed by the High Level Panel of Experts (HLPE) of the Committee on World Food Security. These two dimensions are not formally agreed upon by FAO or other bodies, nor is there an agreed language on the definition. However, due to their relevance in the context of this report, they are included here. The HLPE defines *agency* as the capacity of individuals or groups to make their own informed decisions about which foods they eat and produce, how food is produced, processed and distributed within food systems, and their ability to engage in shaping food systems' policies and governance. *Sustainability* refers to the long-term ability of food systems to provide food security and nutrition in a way that does not compromise the economic, social and environmental bases that can generate food security for future generations.[24]

Agrifood systems' resilience focuses on all six dimensions of food security and nutrition, but more specifically on stability of access and sustainability, to ensure short- and long-term food security and nutrition. Agrifood systems' resilience is a dynamic process defined as:

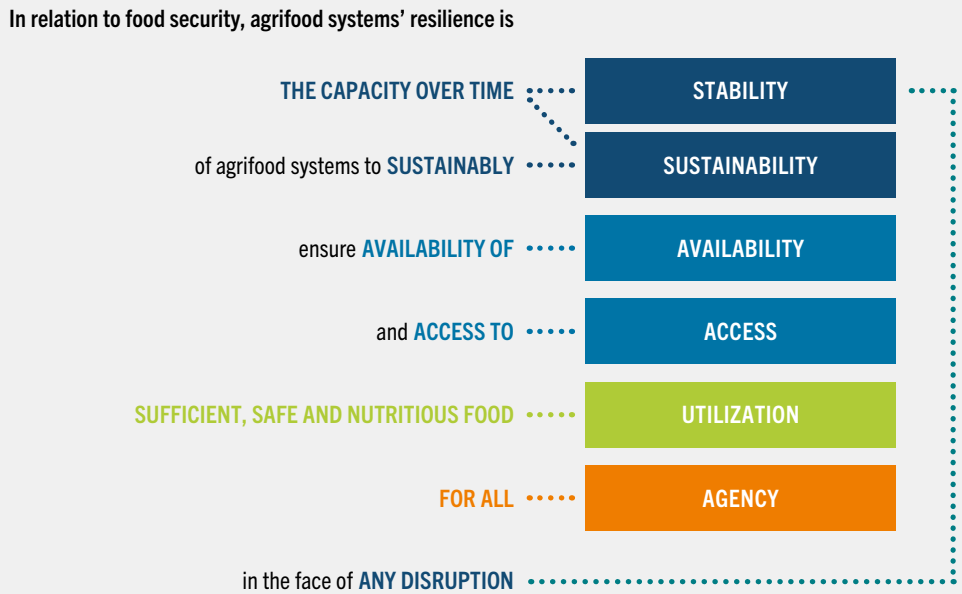
> the capacity over time of agrifood systems, in the face of any disruption, to sustainably ensure availability of and access to sufficient, safe and nutritious food for all, and sustain the livelihoods of agrifood systems' actors.[b]

Figure 1 illustrates how the definition of agrifood systems' resilience supports each of the six dimensions of food security.

Agency, a key dimension of food security, is deeply connected to human rights, including the right to food, and emphasizes the need for inclusiveness in agrifood systems. As indicated in the HLPE's 2020 report, historically disadvantaged individuals and communities, such as women and small-scale agricultural producers, often lack agency with respect to food security and food systems, and frequently experience high levels of food insecurity.[24] Their disempowerment manifests itself in, for example: income and gender inequalities affecting choices; uneven local and global power dynamics regarding individual and community decisions on agrifood systems; weak and fragmented governance of agrifood systems; and the failure of States to uphold the right to food. When agency is upheld, all people and groups can make choices and use their voice to shape agrifood systems and the livelihood opportunities they provide. ■

b This definition is based on Tendall *et al.* (2015).[22]

FIGURE 1 AGRIFOOD SYSTEMS' RESILIENCE AND THE SIX DIMENSIONS OF FOOD SECURITY



SOURCE: FAO elaboration based on HLPE. 2020, Figure 1.[24]

HOW SHOCKS AND STRESSES DISRUPT AGRIFOOD SYSTEMS

As societies develop and transform, they also transform the surrounding environment, the vulnerabilities, embedded risks, and the set of stresses and shocks with which they must deal. While some shocks and stresses depend on factors at supranational or global level, many are the result of specific geographical or local conditions. In either case, the risk of negative impacts will depend on how shocks and stresses manifest themselves, interact with and affect the vulnerabilities and capacities of each component of agrifood systems and their actors. Understanding these processes is essential to design effective interventions to manage multiple risks and build the resilience of agrifood systems by strengthening their capacities to prevent, anticipate, absorb, adapt and transform.

Agrifood systems are very diverse. They depend on agricultural and natural ecosystems and encompass numerous actors along several interlinked components, from production to consumption. For this reason, a shock or stress, impacting on any component, will not only affect the actors in it but will spread throughout systems upstream or downstream, eventually impacting on many if not all other actors and components. The magnitude of the impacts of a shock or stress will depend on the type of event, the vulnerabilities of the components and systems as a whole, and the resilience of each component, including individuals and groups of actors. It will also depend on the degree and direction of interdependence between them. For example, the current global

spread of fusarium wilt on bananas is a threat to production and to the livelihoods of those depending on the value chain,[25] with potential impacts on household nutrition should scarcities lead to higher prices. A comprehensive approach that accounts for multiple risks to agrifood systems and their internal interactions – and potential interactions with other systems – is key to understanding and analysing systems' resilience and addressing its associated challenges.[22]

Characteristics of agrifood systems shape the impact of disturbances

Broadly speaking, agrifood systems can be classified into three types: traditional, mostly located in rural and coastal areas and serving local populations; modern, focused on serving urban populations from diversified sources, including global markets; and transitional, in a phase of transition from the former towards the latter, possibly co-existing with them.[26] Classifying agrifood systems into discrete types should not, however, hide the huge diversity within each type. Multiple agrifood systems co-exist simultaneously in any given country but may differ substantially in terms of their structure or access to markets and services, or interactions with other systems. The key actors in agrifood systems are producers, input providers, those providing post-harvest services, such as storage, transportation, food processing, food distribution and marketing (wholesaling and retailing), and the final consumers.

The characteristics of agrifood systems will determine their ability to prevent, anticipate, absorb, adapt and transform rapidly in the face of shocks and stresses. Traditional agrifood systems are usually found in specific regions and are vulnerable to delimited shocks, while local agrifood systems may be transitional or modern. Traditional systems typically have inadequate infrastructure and lack access to inputs, markets and services such as credit, with higher vulnerability to weather conditions. When a shock such as a flood occurs, whole systems, including the actors, may be severely affected, with negative short- to long-term implications for food security and livelihoods.

Modern and transitional agrifood systems, on the other hand, may be affected by the same event in different ways, depending on their scale of operations, the structure and contracting process between actors, the level of risk proofing of infrastructure and capacities, and their access to inputs and services such as climate risk insurance. Becoming increasingly interconnected and interdependent with other agrifood systems, they may be more vulnerable to shocks transmitted from elsewhere. Modernization has contributed to agricultural specialization and intensification, leading to declining crop diversity and deforestation in many parts of the world with a loss of diverse agricultural landscapes and ecosystems, undermining the biological base of agrifood systems.

In building agrifood systems' resilience, the first tasks are to identify the type of system and its components and actors, understand the linkages and interactions between them, and assess the specific vulnerabilities, threats and capacities that shape the multiple risks facing each one.

In this report, agrifood systems' components refer to three main types of agrifood systems' functions. Their nature and characteristics, and how they affect livelihoods, may vary widely across and within countries.

i. **Primary production** includes food from agricultural and non-agricultural origins, as well as non-food agricultural products that serve as inputs to other industries. Agriculture here means all subsectors: crops, livestock, pastoralism, fisheries, aquaculture and forestry. Food may be produced by a mix of large-scale producers and business enterprises – typical in modern agrifood systems – and small-scale producers and small and medium agrifood enterprises (SMAEs), operating in a range of traditional, transitional and modern systems. Small-scale producers account for around one-third of the world's food and contribute significantly to food security and nutrition.[27]
ii. **Food distribution** links production to consumption through food supply chains and domestic food transport networks. **Food supply chains** include all actors and activities involved in post-harvest

handling, storage, aggregation, transport, processing, distribution and marketing of food. They range from modern, highly integrated and very long chains with plenty of sourcing options, including international trade, to very short chains, mainly serving local urban, peri-urban or rural populations. Similarly, **domestic food transport networks** range from those with well-developed infrastructure linking producers to consumers efficiently (including through trade), to those relying on fragile infrastructure and services that are easily exposed to disruptions resulting in bottlenecks and inefficiencies.

iii. **Consumption** is the downstream outcome of functioning agrifood systems, subject to varying degrees of demand shocks, such as loss of income, depending on the proportion of vulnerable groups in the population. The higher this proportion, the more difficult it is to protect food security and nutrition from shocks. Examples of vulnerable households include small-scale farmers, fishers and pastoralists, landless agricultural workers, poorer population groups, and those that suffer greater inequality and marginalization, such as Indigenous Peoples. The level of agrifood systems' resilience is a crucial determinant of adequate and stable access to food.

The different characteristics, risk environments, and inherent vulnerabilities and capacities of these components determine their susceptibility to various adverse shocks and stresses. The same shock or stress may have different impacts across different components. For example, given its reliance on natural processes, the agriculture sector is disproportionately exposed and vulnerable to adverse climate-related events, especially droughts, floods and storms. Over half of all shocks to crop production are the result of extreme weather events, reinforcing concern about the vulnerability of arable systems to climatic and meteorological volatility.[28] Drought is the single greatest cause of agricultural production losses, with 82 percent of its impact on agriculture.[11] In aquatic systems, there are well-established linkages between harvesting of fish, ocean productivity and global meteorology. Global climate plays a major role in fluctuating fishery productivity.[29, 30]

Actors within the same agrifood systems' component may be affected differently. The livelihoods of small-scale agricultural producers are more likely to be adversely affected by a shock owing to their limited access to resources compared to large-scale producers. Likewise, actors in formal markets will be less affected than those in informal markets, thanks to regulation, government programmes, access to safety nets, finance, insurance, and other risk and impact mitigation mechanisms.

Components of agrifood systems are interlinked, and their characteristics will determine how each is affected as the impact of a shock or stress propagates through systems. Shocks affecting **household consumption** are a case in point. Households who rely on agrifood systems – as agricultural producers or supply chain actors – will be negatively affected by any shock to their business or their employer. The poorest will be the most affected by rising food prices because food represents a larger share of their household budget and they have limited capacity to access credit and savings or to liquidate assets to cover deficits.[31] When faced with a shock, they are more likely to reduce their spending on food by shifting towards cheaper, less nutritious items and in a downward spiral become more vulnerable to food insecurity and malnutrition.

The higher the proportion of vulnerable households, the greater the likelihood that demand responses to shocks (such as reduced demand for certain foods) will disturb or disrupt other agrifood systems' components, ultimately affecting the flow of produce and, in the medium and longer term, even the structure of entire systems. Just as vulnerable households are the most affected by income shocks, small-scale producers and SMAEs in **agricultural production** are possibly more exposed to this ripple effect as well as to longer-term stresses, including climate change. Their vulnerability is often accentuated by their limited assets and access to credit and insurance, which may constrain their ability to adapt and transform.

The degree of diversity and connectivity of **food distribution networks** also shapes the impacts of shock events. Producers and SMAEs who are well connected to supply chains, have various sources and deal in diverse food products, are likely to overcome supply shortages and recover from disturbances more quickly. Connecting to international trade is one of several strategies that distribution networks use to buffer against agrifood systems' disruptions caused by domestic production failure or domestic variability in food supply. However, there is a flip side: the same links can become a channel for transmission of policy-induced shocks, as evidenced by the impact of COVID-19 lockdowns, closure of ports and export restrictions that disrupted food supply chains and international trade. The development level of domestic logistics and infrastructure matters; they can be either an additional bottleneck or a facilitator of fast recovery.

Various shocks and stresses affect agrifood systems differently

Agrifood systems are exposed to shocks and stresses of various types that differ in nature and intensity. Some, such as technological innovation and social pressure for more inclusiveness and equality, can have a positive impact. However, given the theme of building agrifood systems' resilience, this report focuses on negative shocks and stresses that can disrupt systems' functions. Such a focus is crucial to inform the range of strategies and investments required to prevent, anticipate, absorb, adapt and transform.

While shocks have an immediate impact, stresses are slow processes that gradually alter the internal nature of agrifood systems, undermining their capacities to cope with change and rendering them more vulnerable. Shocks and stresses are also different in terms of their predictability. A stress represents a continuous pressure, often observable and predictable – at least in theory – though with various degrees of precision. For example, agricultural intensification, a characteristic of modern high-productivity food systems, may threaten environmental sustainability and, eventually, production outcomes.[32] Since this process can be observed and measured and its consequences projected over time, action is possible to prevent, adapt and even transform, so as to reduce risks and negative impacts. Shocks, on the other hand, are sudden disruptions, which are at best predictable based on levels of probability and previous experience. Identifying and investing in risk assessment and appropriate measures will be needed to reduce vulnerability and risk.

Shocks and stresses can have many sources originating from various domains, for example: biophysical and environmental; demographic and socio-economic; biological; and socio-political and legal. Examples of biophysical and environmental shocks include adverse weather and geophysical phenomena such as earthquakes and tsunamis, while significant stresses are associated with climate change and its effects, loss of biodiversity, and natural resource degradation. Demographic and socio-economic shocks may include economic crises, while examples of stresses are socio-economic inequality or high levels of population growth. Pandemics like COVID-19 and food safety breaches represent typical examples of biological shocks, while stresses may be the emergence of antimicrobial resistance or the persistence of food safety issues. In the socio-political domain, examples of shocks include crises involving civil unrest and population displacement or the erection of trade barriers by individual countries. Examples of socio-political stresses are distress migration or endemic corruption.

Shocks and stresses can directly affect either agrifood supply or demand, or both. However, as sustainable agrifood livelihoods are fundamental to food security, the impacts of shocks or stresses on agrifood supply and food demand are closely connected. Where agrifood suppliers are negatively affected, the incomes and purchasing power of the actors will decline, which can then affect demand for food and non-food products.

Developing options to deal with threats to agrifood systems requires an understanding of the types of shocks and stresses that strike systems, the mechanisms that affect »

BOX 2 FAO'S ANTICIPATORY ACTION APPROACH

Working with national governments and humanitarian, development and scientific partners, FAO's Anticipatory Action (AA) approach monitors risk information systems and translates warnings into anticipatory actions to reduce the impact of disasters. A key enabling factor for anticipatory action is the development of pre-agreed plans – ideally developed jointly by multiple actors – which provide details on early warning information, the risk monitoring process, triggers, predefined funding sources, and a decision-making protocol. Multilevel early warning information is analysed to identify and prioritize the greatest risks to agricultural livelihoods and food security. Then, where needed, FAO's Special Fund for Emergency and Rehabilitation Activities can rapidly release funds from its anticipatory action window (SFERA-AA).

Anticipatory actions are varied and flexible; they include cash transfers for fishing communities to safely store their nets ahead of an impending cyclone, livestock feed and treatments for herders before the peak of a drought, and waterproof storage equipment for farmers before a forecast flood. They may also include agricultural inputs and technical skills to boost food production ahead of potential food crises.

Since 2016, FAO has implemented AA projects across high-risk countries in Africa, Asia and Latin America to protect the livelihoods of vulnerable farming and herding households. These communities were at the forefront of droughts, floods, socio-economic crises (e.g. due to the COVID-19 pandemic), transboundary animal diseases, and crop pests, often combined with conflict, displacement and forced migration.

The table in this box summarizes the results of impact assessments of FAO anticipatory action interventions in various countries. Depending on the context, the shocks addressed and the socio-economic characteristics of targeted vulnerable households, AA interventions have resulted in relatively high to very high returns on investments in terms of avoided disaster impacts and additional benefits. The table, and the results of impact assessments conducted in the targeted countries, show that even with small funds, well-designed and timely interventions can lead to very positive results in terms of protecting vulnerable livelihoods and empowering households to cope with shocks.

However, these assessments shed light on the enormous challenges that governments and international agencies face to scale up these interventions to the level of national agrifood systems. The growing intensity and increasing frequency of climate-driven disasters and conflicts mean that different priorities will compete for limited resources. When resources are limited, anticipatory action should target the most vulnerable – typically those living in extreme poverty and facing multiple risks – combined with efforts to strengthen the absorptive capacity of agrifood systems. Additional efforts are needed to fully mainstream this approach into disaster risk management frameworks, leading to a decisive shift from a reactive to a preventive approach to food crises.

TABLE SUMMARY OF SELECTED FAO ANTICIPATORY ACTION INTERVENTIONS – FUNDS SPENT, NUMBER OF BENEFICIARIES AND RETURN ON INVESTMENTS

Country	Type of action	Amount of dedicated funds (USD)	Beneficiary households	Return on investment (per USD spent)
Bangladesh	Protect farming families from impending floods	500 000	18 700	0.8
Colombia	Curb the impact of drought and migration crisis	955 000	1 003	2.6
Kenya	Protect pastoralist livelihoods ahead of drought	400 000	1 493	3.5
Madagascar	Protect farming livelihoods ahead of drought	400 000	8 400	2.5
Mongolia	Protect livelihoods of herders from a very harsh winter	290 000	1 008	7.1
Philippines	Protect farming communities from El Niño-induced drought	400 000	1 500	4.4
Sudan	Protect pastoralist livelihoods ahead of drought	400 000	5 000	6.7

SOURCES: FAO. 2018,[33,34] FAO. 2019,[35–37] FAO. 2020,[38] and FAO. 2021.[39]

» them, and their specific vulnerabilities. For example, drought, export restrictions, transport bottlenecks and climate variations can all reduce food supply but do so in very different ways and through different channels, impacting on countries and people differently. The impact of the same shock or stress can vary widely, depending on the vulnerabilities of agrifood systems, the components impacted and their capacities to prevent, anticipate, absorb, adapt and transform. The impact of a shock such as severe drought may be mitigated by preventative and anticipative investments in irrigation; however, the drought may still have devastating effects if the surface water or groundwater is already overexploited.

Building absorptive capacities within agrifood systems – the focus of this report – is complementary to and should go hand in hand with risk management, especially actions focused on anticipation and prevention. The importance of building absorptive capacity is linked to the cost and often limited potential of early action initiatives despite their high returns, given the resources required to scale up anticipatory actions geared to identifiable risks (Box 2). In addition, absorptive capacity is critical to confront shocks that are unknown in terms of their timing and extent until they actually happen and cannot therefore be addressed through risk management strategies that reduce exposure and vulnerability to anticipated shocks. ■

AGRIFOOD SYSTEMS' RESILIENCE IN CHANGING CONTEXTS

Growing concern over the resilience of agrifood systems is driven by increases in the frequency and intensity of adverse shocks, from climate-related disasters, and animal and crop diseases, to sudden price hikes. Cottrell *et al.* (2019) associate this with a rising number of conflicts exacerbated by climate change and depleted natural resources.[40] Conflicts appear to be a key driver of higher levels of hunger in recent years.[41] In particular, the incidence of hunger has grown in the Near East and North Africa since 2012, mainly because of increasing conflict and instability.[42]

Climate change also impacts on agrifood systems, food supply chains and food security through short-term shocks, such as extreme weather events, and slow-onset stresses, such as increasing temperatures, desertification, salinization and loss of biodiversity.[43] Climate change is also associated with shifts in the geographic occurrence, prevalence and intensity of transboundary animal and plant pests and diseases, and changes in patterns of pathogens, mycotoxins, marine biotoxins and heavy metal contamination, all of which threaten food safety.[31, 44, 45] Yet agrifood systems themselves are a major driver of climate change. Innovative mechanisms to reduce climate-related risks, widespread adoption of climate-smart production techniques, and the conservation and rehabilitation of natural environments can strengthen the sustainability and resilience of agrifood systems against increased climate variability and extremes.[12]

Globalization has altered the set of risks agrifood systems face. On the one hand, it smooths disruptions in supply due to domestic shocks thanks to international trade, but on the other, it facilitates transmission of unpredictable shocks originating far away. For example, after the 2008–2009 global financial crisis, Mexico's economy shrank by almost 7 percent in 2009, poorer households reduced their spending on food and the number of severely food-insecure individuals grew from 9.8 million in 2008 to 12.2 million in 2010.[46]

More recently – a prime example of how crises from other systems can affect agrifood systems – the COVID-19 health crisis disrupted global and national food supply chains as governments sought to contain the spread of the virus by imposing lockdowns. The resulting bottlenecks in labour availability, import and distribution of farm inputs, and transport and logistics networks disrupted food supply chains, especially those of perishable high-value products such as fruits and vegetables, raising concerns over food security and nutrition.[47, 48]

Many food supply chains demonstrated remarkable resilience, supported by government declarations that food was an essential sector. It also helped that when the pandemic began, global food markets were well supplied and stable and most supermarket shelves remained stocked. Countries learned from the 2008–2009 crisis and adopted measures to reduce vulnerability to future food shortages. Most countries in the Near East and North Africa, highly dependent on food imports, used a mix of policies to encourage domestic food production, diversify import sources and build national food stocks. The pandemic also sparked changes in many countries' output markets, such as a switch from reliance on exports to serving domestic markets, as was the case with Kenya's coffee industry.[49]

A study by Béné *et al.* (2021) finds that despite disruptions caused by initial panic buying, there is no clear evidence that food availability was universally affected during the pandemic.[50] In fact, the biggest threat to food security and nutrition during the COVID-19 pandemic has come not from disruptions to food availability but from the often severe limitations on households' physical and economic access to food, particularly in urban areas and in low-income and middle-income countries.[50] The pandemic caused dramatic reductions in the purchasing power of many households, as lockdowns and other restrictions led to shrinking incomes and job losses. The services sector, which employs the largest share of the population in most countries, has been hard hit, pushing many vulnerable households into poverty and food insecurity. Millions of households have been forced to reduce spending on food, with high risk of lowering overall calorie intake and dietary quality.

The adverse impacts of these past and ongoing crises reveal that current agrifood systems are fragile and not taking due consideration of issues like equity, access, resilience and sustainability. They fail to provide sufficient and nutritious food for all and are the principal driver of biodiversity loss, land degradation and freshwater depletion. They interfere heavily with global nitrogen and phosphorus cycles and are a major source of the GHG emissions driving climate change.[51] The COVID-19 pandemic has also heightened concern over the threat of zoonotic diseases in agrifood systems.[52]

By becoming more inclusive, resilient and sustainable, agrifood systems can ensure access to food – not only physical, but also economic access. One way to achieve this is through the agricultural production of food and non-food products to generate income and livelihoods for the estimated 3.4 billion people worldwide who live in rural areas.[53] Resilience is one means of achieving sustainability, especially during times of disruption[54, 55] and is thus essential to enable sustainability.[56, 57] Part of the challenge of making agrifood systems more sustainable is to reduce their inherent vulnerabilities and enhance their capacities to manage risks posed by multiple shocks and stresses. ■

BUILDING AGRIFOOD SYSTEMS' RESILIENCE – A FRAMEWORK

The global crisis triggered by the COVID-19 pandemic and its impacts on food security and livelihoods adds a new sense of purpose to investigating the weaknesses of agrifood systems, the risks they face and why they fail to deliver desired outcomes. Exploring these issues will help to strengthen agrifood systems' resilience as an essential element in efforts to build back better and achieve the SDGs. Rendering agrifood systems resilient means enhancing their capacity to prevent, anticipate, absorb, adapt and transform in the face of risks to particular shocks and stresses and to safeguard their specific functional goal: sustaining the livelihoods of agrifood systems' actors and ensuring food security and nutrition for all.

A tangible framework for agrifood systems' resilience analysis

Building on the discussion so far, Figure 2 presents a conceptual framework for analysing agrifood systems' resilience. It frames the analysis around three fundamental questions: *Resilience to* what? *Resilience of* what? and *Resilience for* what? Broadly speaking, the overall objective »



ITALY
Syrian farmers learning how Robiola cheese is made during a visit to Amaltea farm in the village of Roccaverano. ©FAO/Alessandra Benedetti

» is to build the resilience of agrifood systems to shocks and stresses so that all actors and stakeholders – producers, intermediaries and consumers – can prosper while sustainably contributing to, and benefiting from, food and nutrition security.

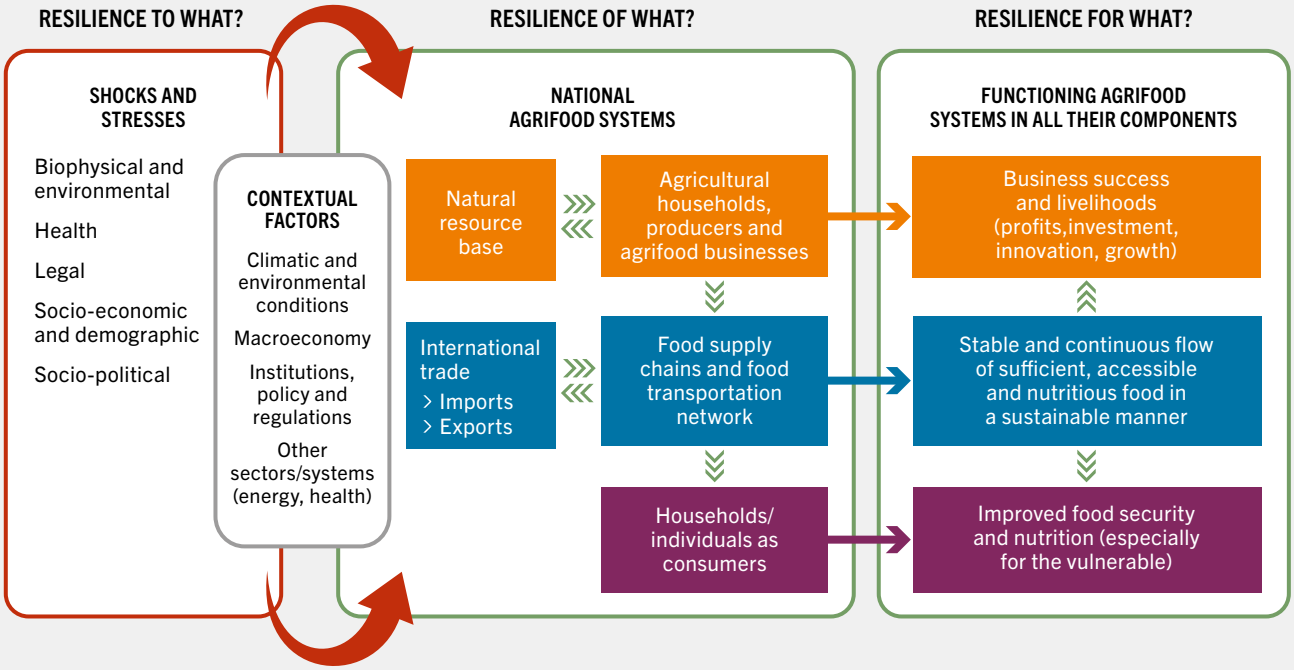
As illustrated in column 1 of Figure 2 (Resilience to what?), shocks and stresses can vary greatly and have different origins. The nature and magnitude of their impacts will depend not only on the shocks and stresses themselves but also on the specific vulnerabilities and resilience capacity of each of the components and actors in agrifood systems and the overall context (column 2, Contextual factors). These factors include the climatic, environmental, social, economic and political dimensions that influence and shape agrifood systems' activities. Other contextual factors are systems and sectors (such as energy and health) that are external but linked to agrifood systems. The COVID-19 pandemic is a prime example of the interaction between the food and health systems.
The energy sector is another: energy is required to grow, process and distribute food, while crops are grown to produce biofuel energy. In addition, non-food agricultural crops – essential to the livelihoods of many agricultural producers – compete with food production for limited resources. Resilient and sustainable agrifood systems need to balance their dual objectives of providing food for all and generating income through non-food production, while preserving the natural resource base. The framework highlights these interactions as they contribute to agrifood systems' functioning and to their final outcomes.

How shocks and stresses impact on agrifood systems depends also on the characteristics of their components. Column 3 (Resilience of what?) presents national agrifood systems, in which food and non-food agricultural products are produced by agricultural households (see Glossary), producers and businesses reliant on the natural resource base and services provided by ecosystems. Food is then processed, stored, transported and distributed by agrifood businesses through food supply chains and domestic transport networks to households and individual consumers. It is worth noting the crucial role of food supply chains and domestic food transport networks to connect production and consumption. Whether domestically produced or imported, food must go through these channels to reach households and individual consumers. Agricultural households living in rural areas – namely as small-scale producers – are both consumers and producers of food. The impact of shocks on the food security and nutrition of agricultural households depends also on the extent of their engagement in agriculture and food production (Chapter 4).

Building agrifood systems' resilience requires action that addresses all the components that constitute national agrifood systems, from producers to consumers, including international trade. It also requires maintaining or restoring ecosystem services and biodiversity to preserve the natural resource base on which agriculture depends.

Column 4 (Resilience for what?) illustrates the outcomes or desired objectives of agrifood systems' resilience. Agricultural households, producers and other food supply chain actors produce, process and supply food using resources, innovations and technology to their own advantage. Their private objective is to maximize profits, improve livelihoods and reduce risks. They need to be resilient to remain economically viable in the face of shocks and stresses. Actors need to be aware they are part of a broader socio-environmental system and must ensure the sustainable management and use of natural resources for the benefit of present and future generations. Resilient food supply chains and domestic food transport networks essentially provide the public goods and coordination necessary to ensure a continuous, sustainable and stable flow of goods through systems. This is essential for the success of both farmers and agrifood enterprises so that safe and nutritious food is physically and economically available to all to ensure food security of households and individual members as final consumers. In this report, the focus is on households; indeed, if a household is food insecure no one in the household is food secure. However, due to intra-household distributional issues, even within food-secure households, individuals, particularly women of reproductive

FIGURE 2 CONCEPTUAL FRAMEWORK FOR AGRIFOOD SYSTEMS' RESILIENCE ANALYSIS



SOURCE: FAO elaboration for this report.

age, adolescent girls and young children, may be food insecure. Attention to intra-household variability is needed to effectively target the most vulnerable.

It is important to emphasize the complexity of the linkages between different parts of the analytical framework in Figure 2, as well as their bidirectional nature. Shocks directly affecting food production or food imports are transmitted through forward market linkages and eventually affect households and consumers, worsening their food security. At the same time, external shocks that affect food consumption or other systems' parts can also ripple back and affect primary producers. For example, policy changes that adversely affect productive activities and incomes in other economic sectors can impact on agrifood systems by reducing demand for both food and non-food products. Lifting subsidies on fuel directly affects the energy-intensive stages of the food supply chain, such as processing and transport, triggering a series of further impacts affecting both primary producers and consumers.

The proposed conceptual framework suggests five vantage points for analysis of agrifood systems' resilience that shape this report:

i. **Agricultural households and producers and agrifood businesses**, including small-scale producers and SMAEs, aiming to maximize their livelihoods and business success. Agriculture (crop and livestock production, aquaculture, fisheries and forestry) transforms land and other natural resources, capital and labour into food and non-food products. Agrifood enterprises are involved in food processing, manufacturing, packaging and distribution.
ii. **Food supply chains**, whose effectiveness, resilience and capacity – ranging from local to global level – depend on the agrifood market

structure and are influenced by network infrastructure and logistics.

iii. **Domestic food networks** that span the rural–urban continuum. Connectivity within agrifood systems is highly influenced by transport infrastructure and logistics, critical for how systems deal with shocks to the network.

iv. **Households**, including individuals within households, representing the level of final demand for food. Analysis here focuses on the food security and nutrition of vulnerable rural households, and the role played by various factors in achieving it, including access to basic services such as education and sanitation.

v. **National agrifood systems**, aggregating all subsystems – economic, social and environmental – including the full range of actors, networks and food supply chains that contribute to food security and nutrition and impact on the environment. Agrifood systems encompass climatic and environmental conditions, along with macroeconomic factors, institutions, policies and regulations and the role of international trade in balancing supply and demand.

Managing trade-offs when building resilience

In the framework proposed in Figure 2, a shock occurring at one point in agrifood systems can propagate through systems and affect all the other components. In response to that shock, all agrifood systems' actors will want options to absorb the impact and adapt. One possibility for food supply chains is to diversify sourcing of food products through expanded international trade. A country whose agrifood systems are highly connected into global and regional markets can more easily respond to domestic shocks by sourcing what it needs through international trade. However, the country may become more exposed to outside shocks, in particular policy-induced shocks such as trade restrictions, and face a trade-off: greater exposure to internal or to external shocks. This trade-off raises the important question of how to manage multiple risks originating from various sources. In the case of high reliance on food imports, managing international trade connectivity is critical to reduce exposure to external shocks. A country can balance domestic sourcing of food with diversified imports and international trade partners with different socio-economic and climatic profiles to manage multiple risks from various sources.

Diversification is a common resilience strategy among agricultural households in low-income countries. In the absence of well-functioning crop and livestock insurance and credit markets, crop diversification and integration with livestock production help to mitigate risks associated with climate variability and market volatility. Agricultural households also diversify into the non-farm economy to counter the seasonality of agricultural income and cope with shocks that affect farm output. Beyond the farm, households engaged in the informal economy diversify livelihoods and income sources to cope with the uncertainties of informal employment. Diversification can thus be a strong resilience tool providing sizeable benefits when a shock occurs.

However, diversification is not without costs: it foregoes the specialization that allows households to accumulate experience. This raises the question of a potential trade-off between building resilience through diversification on the one hand and efficiency on the other. Until recently, the balance has been in favour of the greater efficiency provided by specialization, to the detriment of diversification.[58, 59] However, it has become increasingly evident that improved efficiency through specialization requires stable conditions. In a world increasingly facing unexpected shocks, on top of long-term stresses, specialization might actually reduce efficiency when shocks occur. The trade-off between efficiency and resilience is a short-term concern, where building resilience may weaken efficiency in the short term but improve it in the long term.

The question then becomes: what kind of diversification is needed and at what level should it be applied to maximize the benefits of increased diversity? Developing a diverse set of responses to specific challenges, rather than diversity for its own sake, can be the guiding

principle of a strategy in which diversification facilitates synergies between efficiency and resilience.[59] Countries with limited agricultural resources, such as most of the Near East and North Africa, may have little scope to meet their food needs by expanding and diversifying agricultural production. Given limited land and water resources, they may need to maximize efficiency by specializing in products for which they have comparative advantages, while engaging in international trade to source other products. This would mean greater reliance on imports for essential food items they cannot produce locally in sufficient quantities. The risks of high import dependency can be mitigated by diversifying import sources from countries and regions with different climatic profiles, combined with building food stocks to deal with supply uncertainties in times of crisis.

Redundancy – the duplication of critical systems' components or functions to increase their reliability – is another effective resilience strategy. It reinforces the capacity of agrifood systems to absorb shocks by assigning the same function to multiple actors. However, incorporating redundancy into agrifood systems can be costly to society and is particularly challenging when resources are limited. More redundancy in one systems' component may weaken resilience in another. For example, the option of importing food or increasing commercial food production in a new region may expose small-scale agricultural producers to unsustainable competition if there is a new shock.

While it is widely acknowledged that redundancy and diversification improve resilience, there can be trade-offs with efficiency and even equity. Decisions on optimal levels of redundancy and diversification, and the parts of systems where they should be applied, remain very much context-specific and depend on understanding multiple risks and their potential impacts as well as available alternatives. Diversification through integrating crop and livestock production may create synergies between resilience and efficiency by using crop residues as cattle feed, and livestock manure to maintain soil health. At the same time, the existence of an efficient crop and livestock insurance system may encourage producers to limit crop/livestock diversification and integration to the level necessary for productivity growth (e.g. crop rotation) rather than risk reduction. The final choice will depend on the balance between costs, in terms of efficiency losses, and the benefits of increased resilience. Minimizing costs, maximizing benefits, and reducing damage and losses requires identification of optimal combinations that create synergies and balance trade-offs, so that redundancy and diversification increase long-term efficiency without eroding specialization gains. Although sustainability considerations can provide guidance, the exercise can be very challenging owing to huge uncertainties surrounding future shocks, stresses and cascading crises. ■

LAYING OUT THE SCOPE OF THIS REPORT

This chapter has argued for the urgency of building more resilient agrifood systems to ensure food security and nutrition for all, now and in the future. It stresses the close relationship between resilience and sustainability, with its social, economic and environmental dimensions. Within the economic and social dimensions, special attention needs to be given to decent livelihoods and incomes for small-scale producers and other vulnerable people with agrifood livelihoods. It highlights the complexity and diversity of agrifood systems, as well as the wide spectrum of stresses and shocks they endure. Owing to these multiple factors, building more resilient agrifood systems is no simple task; it requires urgent and converging collective and individual actions on the part of a multitude of public, private and community actors. To this end, the chapter presents a conceptual framework to understand risks, vulnerabilities and capacities of agrifood systems, focusing on the capacity to absorb, as well as five vantage points for analysing their resilience: agricultural households and producers and agrifood businesses, food supply chains, domestic food networks, households, and national agrifood systems.

These vantage points will shape the discussion in the following four chapters. Chapter 2 examines the absorptive capacity of agrifood systems through four indicators that measure the robustness of primary production, the availability of food, physical access to food and economic access to food. Chapter 3 focuses on the resilience of individual food supply chains and agrifood businesses. Chapter 4 addresses the resilience of rural livelihoods, especially the most vulnerable. Based on that analysis, the concluding Chapter 5 discusses policy and investment priorities for building resilient agrifood systems at multiple levels.

This report follows the UN Food Systems Summit's call to bring forward a series of concrete actions that support a transformation of agrifood systems for realizing the 2030 Agenda for Sustainable Development. The Summit's call to action focused on five objectives, one of which is building resilience to vulnerabilities, shocks and stresses to ensure the continued functionality of healthy and sustainable food systems. This report provides evidence and guidance for actions that can help agrifood systems' actors manage vulnerability to shocks and stresses, and strengthen the capacity of agrifood systems to support livelihoods and sustainably provide continuous access to sufficient, safe and nutritious food to all in the face of disruptions. ■



PERU
Workers from the port of Pucusana loading boxes of pota (giant squid) onto a refrigerated truck.
©FAO/Jordi Vaque

CHAPTER 2
AGRIFOOD SYSTEMS' RESILIENCE AT NATIONAL AND SUBNATIONAL LEVELS

KEY MESSAGES

➔ The agriculture sector can better absorb disturbances when it has access to diversified domestic and international markets and produces a diversified mix of food and non-food products. This occurs mostly in high-income countries or those with a large agricultural base.

➔ Combined with stocks and imports, diversified domestic production ensures food is available even during disruptions. Yet, due to logistical constraints, stocks and imports on their own may not guarantee the diversity of fruits, vegetables and other perishables needed for a healthy diet.

➔ A robust transport network supports agrifood systems' resilience to shocks and stresses and guarantees physical access to food at local level. Yet, for half of the 90 countries analysed, the closure of a critical transport route could increase travel time by 20 percent or more for food diverted from the disrupted route, potentially affecting food costs for 845 million people.

➔ A key characteristic of agrifood systems' resilience is its capacity to ensure access to sufficient nutritious food. Around 3 billion people cannot afford a diet that will protect against malnutrition and an additional 1 billion would join their ranks if a shock reduced their income by one-third in the 143 analysed countries.

➔ Low-income countries are the ones unlikely to be able to afford a healthy diet. However, the threat from shocks and stresses for those who normally can afford such a diet, in 95 percent of cases, affects people in lower- and upper-middle-income countries. In low-income countries many more people may be unable to even afford an energy-sufficient diet if incomes are reduced by one-third.

Building on the conceptual framework in Chapter 1, this chapter uses national indicators as proxies to assess the vulnerability of agrifood systems to shocks and stresses. It analyses one of the five main resilience capacities: that of agrifood systems to absorb any disturbance that affects them, from natural hazards to pests to financial shocks, using the multiple pathways that protect food security and sustain the livelihoods of agrifood systems' actors. Exploring these pathways is important to understand how to improve agrifood systems' resilience. Absorptive capacity is essential to maintain agrifood systems' functions, ensuring food is available and accessible and generating incomes.

The analysis considers four key agrifood systems' dimensions: (i) the robustness of primary production; (ii) food availability; (iii) physical access to food; and (iv) economic access to food. These are relevant to food security, nutrition and sustainable livelihoods. The resilience of agrifood systems depends on many factors and some – for example, social and environmental dimensions – do not appear among these indicators. Because the chapter considers resilience at the system level, the absorptive capacity of individuals is also not discussed. ■

RESILIENCE OF AGRIFOOD SYSTEMS' FUNCTIONS

Assessing the resilience of national agrifood systems is challenging because each one has many components and actors, at several interlinked levels from production to consumption, including international trade. Some components and actors may be more resilient than others, and some shocks and stresses may be specific to one or more component or actor. Assessing resilience should consider the full range of actors and levels involved. The first step is to understand how those levels function and identify vulnerabilities. A participatory and inclusive process may help engage systems' actors in a more coordinated response to shocks and stresses.[1]

While agrifood systems differ substantially in their structure and access to markets and services, key actors are invariably agricultural producers, processors, distributors and consumers. Building on the conceptual framework in Figure 2, the resilience of national agrifood systems is a function of:

i. the existing domestic agricultural production system;
ii. the availability of food for consumers through domestic production, stocks and imports;
iii. the efficiency and flexibility of food transport systems to facilitate domestic trade and provide physical access to food; and
iv. people's economic access to food.

Any shock or stress affecting one dimension is likely to impact on others, with consequences for food security as well as the livelihoods of actors, particularly those most vulnerable. Shocks can also spread through trade channels, financial markets, remittances, etc. During large-scale disruptions, such as the 2008–2009 financial crisis and early in the COVID-19 pandemic, export restrictions affected food supply.[2–4] Diversifying international trade partners is crucial to buffer against external shocks. This requires considering a number of factors that influence choice of trading partners, from price and proximity, to the degree of integration in the global economy. Diversifying trade partners depends on a balance between costs and the benefits of increased resilience.

Managing the diversity of food production for the domestic market, and of stocks and exports is also essential for food security, nutrition and health. It allows agrifood systems to maintain food availability despite shocks, such as pests or sudden demand shifts as occurred during the COVID-19 pandemic. Exports are important to generate livelihoods. They are also a resource that can be leveraged to absorb supply and demand shocks as they express the breadth of the agricultural base of a country. ■

ABSORBING SHOCKS IN THE PRIMARY PRODUCTION SECTOR

In the course of a farming season, agricultural producers need to make decisions in the face of uncertainties about weather, prices, logistics, pests, diseases and other factors. Their resilience depends on the right decisions regarding, for example, farm or income diversification strategies, and on contextual factors such as the natural resource base, access to credit, markets and infrastructure, and the viability of production practices.

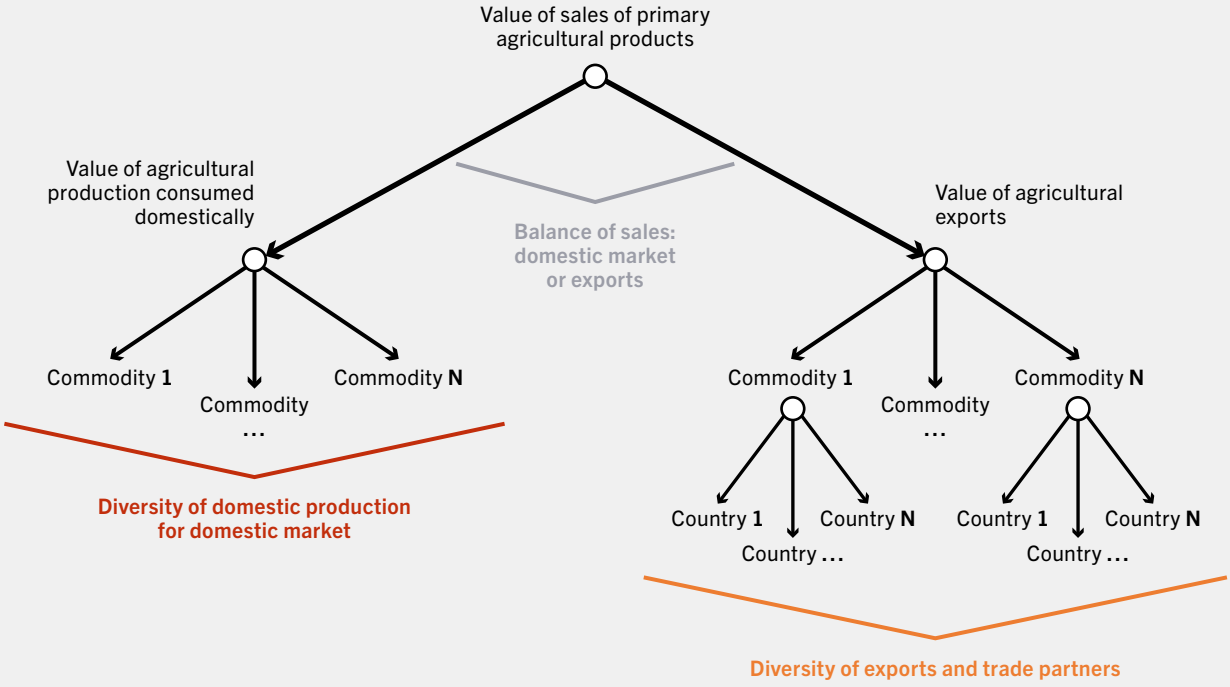
Aggregating those characteristics into a national indicator is challenging. Put simply, the capacity of a country's primary production sector to absorb a shock depends to a large extent on two factors: (i) the diversity of commodities produced; and (ii) the diversity of output markets as regards trading partners and the domestic demand for those commodities. These underpin the primary production flexibility index (PPFI), developed for this report to measure the extent of diversity across commodities and the potential to produce for domestic or export markets. A high value of this index indicates multiple potential paths for generating agricultural value and finding final outlets for primary production (i.e. redundancy of demand channels) and thus a higher capacity to absorb shocks. Box 3 describes the methodology underpinning the PPFI. »

BOX 3 THE PPFI IN A NUTSHELL

The PPFI uses FAO's extensive production and trade data to examine the pathways to generate agricultural value and find outlets for primary production. A production sector with wider options to produce and market agricultural products is better able to absorb covariate risks that affect groups, regions or entire countries. Covariate risks include pest attacks, floods and droughts that reduce supply, as well as demand shocks to domestic and export markets. The primary production sector can increase its absorptive capacity through, *inter alia*, product and income diversification and, in the case of demand shocks, by being able to switch from export to domestic markets and vice versa. An example of the latter is coffee, typically exported with limited domestic demand in many producing countries, except Brazil and Ethiopia. Higher domestic consumption in countries such as Kenya helped producers weather the storm during the COVID-19 pandemic, as logjams at ports and a sharp drop in global demand devastated exports.[5] National agrifood systems that provide some latitude to producers in terms of production options (agroecological zones and climate) and markets (logistics, certification and institutions) will be more resilient and maintain production.

The figure in this box illustrates potential pathways as a tree. A unit of agricultural product value is marketed through either domestic or export channels (top branches) and then distributed across a range of commodities and importing countries if exported. Domestic sales may be as finished products or intermediate inputs into processing. The indicator does not track whether the processed product is consumed domestically or exported. The more channels, the easier it is to absorb a demand shock, unless all domestic and export channels are affected simultaneously, or a shock occurs to a specific commodity. See Annex 1 for a more comprehensive description of the PPFI.

FIGURE PATHWAYS TO PRODUCE AGRICULTURAL OUTPUT AND SELL IT IN DOMESTIC OR EXPORT MARKETS, FOR VALUE



SOURCE: FAO elaboration for this report.

BOX 3 (CONTINUED)

Limited producer commodity price data impeded calculation of the indicator for value terms. It is calculated for protein terms instead, as the two were found to be closely correlated in countries for which price data were available. This implies excluding non-food primary commodities (e.g. wood), which cannot be converted into nutrients, despite their importance in generating income and livelihoods.

Interpreting the PPFI – The PPFI shows how the structure of production can facilitate or hamper absorption of a production shock to a specific commodity or a demand shock. Low values reflect low absorptive capacity, high values indicate high capacity. The total value of the PPFI can be further divided into three parts: (i) the balance between exports and domestic sales (grey branches in the figure); (ii) diversity of domestic production for domestic market (red); and (iii) diversity of exports and trade partners (orange).

For producers, if all agricultural production goes to the domestic market without the option to export, the value of the PPFI is equal to the contribution of domestic demand (red in the figure). Exports add two types of producer flexibility: the relative balance between exports and domestic sales (grey in the figure); and the diversity of exports and trade partners (orange in the figure).

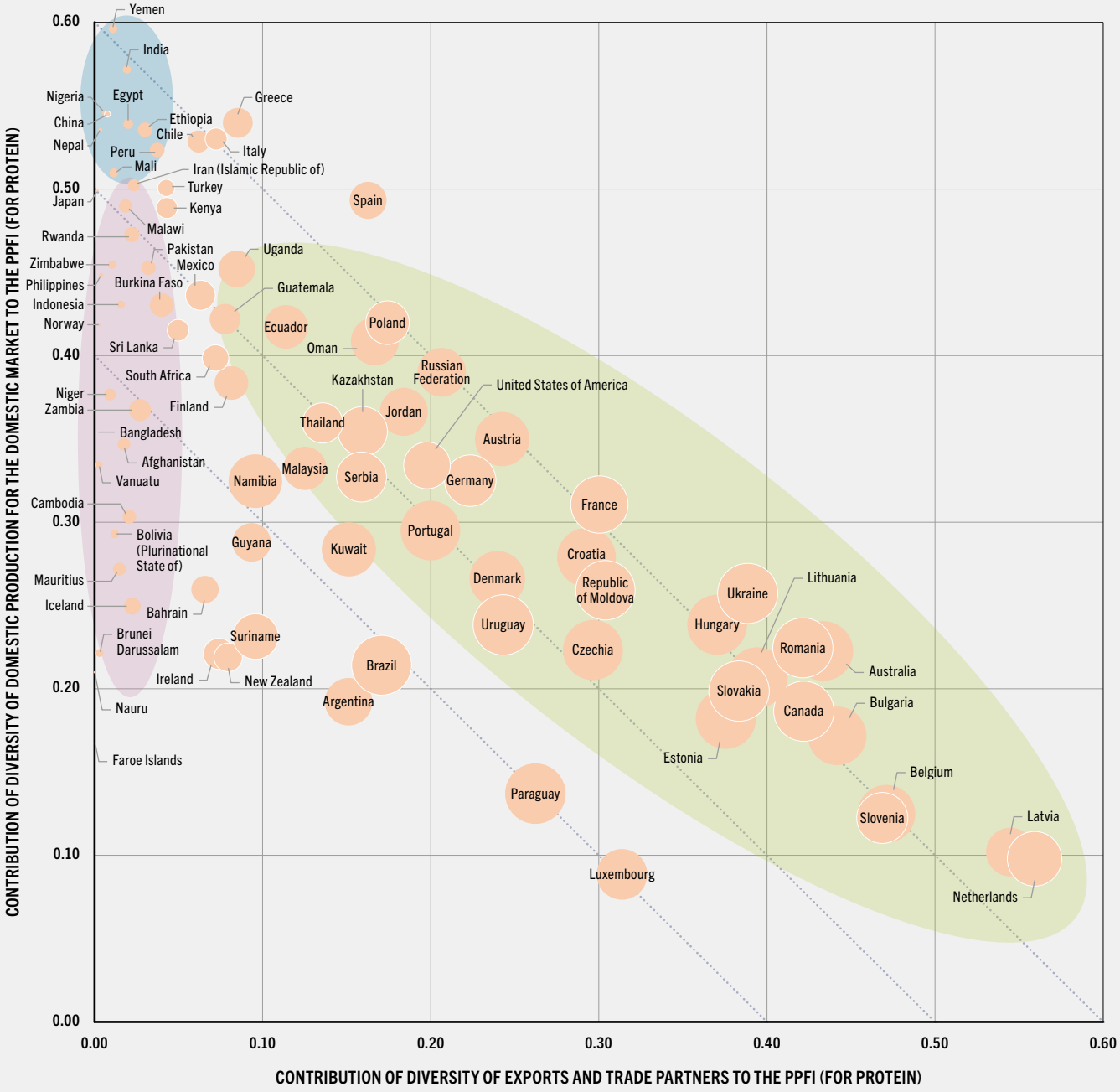
Higher values across all three types of diversity indicate a greater capacity to absorb a shock to the primary production sector. If a reduction in global commodity prices affects exporters, a high PPFI value indicates there is a broad domestic market and they may be able to redirect their products to it. For instance, due to the COVID-19 pandemic, some Chinese exporters turned to the domestic market to sell their outputs.[6] Similarly, producers may reabsorb a shock in domestic demand if there are export channels open to them. Looking at these diversities – or PPFI contributors – can also help identify specific weaknesses in systems' absorptive capacity. By way of illustration, if export sales are significant but the diversity of exports and international trade partners is limited and the primary sector diversifies very little between domestic sales and exports, this could make it vulnerable if, for example, a shock hits the main export commodity on the production or demand side.

Caveats – The PPFI is a systemic measure of how agricultural producers may be susceptible to shocks. However, it does not mean that individual producers can switch from one form of production to another or one market to another. The PPFI does not differentiate between sales to processors (intermediate demand) and consumers (final demand). Without this, it cannot capture the diversity of exports of processed goods because producers' primary commodity sales to processors are registered as domestic sales. Similarly, it does not differentiate between primary commodities sold as food, feed or biofuel, despite potentially significant competition between the three. The PPFI will therefore need additional information on the resilience of the midstream (see Annex 1). Information on unequal access to resources (credit, information, technology, land and water, etc.) across primary producers would be useful, because they shape capacities to shift between different production mixes and markets.

» Diversifying trade partners and commodities may come at a cost. Producers make decisions based on input and output prices and resource constraints, affecting a country's comparative advantage in agricultural exports. A country may need to overcome trade barriers, such as limited infrastructure or meeting phytosanitary measures, and make decisions based on historical relationships with other countries or political orientation. Trade openness, avoiding export restrictions, which exacerbates market volatility, and limiting commodity subsidies are examples of best practices to increase production flexibility.

Figure 3 presents the three dimensions of the PPFI for protein – valid proxy for value given scarce producer price data – as a 2016–2018 average for all crop and livestock products. The contribution of the diversity of exports and trade partners is in the horizontal axis, while that of the diversity »

FIGURE 3 PPFI FOR PROTEIN, 2016–2018



NOTES: The graph plots the contribution of diversity of exports and trade partners against the contribution of diversity of domestic production for the domestic market, both to the total value of the PPFI, for protein terms. The size of the orange bubbles represents the balance between the two (i.e. the balance between what is exported and what goes to the domestic market). Countries placed in the same diagonal line report the same value for export and domestic diversity – 0.4, 0.5 and 0.6, respectively. Results include all crop and livestock commodities for which FAOSTAT production and trade data were available. Fisheries and aquaculture are excluded due to the lack of trade partner data and protein conversion factors for fish species. Due to limited producer price data, non-food agricultural commodities are also excluded and the protein content of food commodities is a proxy for agricultural value. Protein conversion factors are calculated based on FAOSTAT data and then used to convert tonnes of food into tonnes of protein. To simplify graphic presentation, 90 countries that overlapped in the graph were dropped. Results are the three-year average of 2016, 2017 and 2018. Results for the full set of countries are in **Annex 3**. See **Annex 1** for methodology and data sources.
SOURCE: FAO elaboration for this report.

» of production for the domestic market is in the vertical axis. The size of the bubble indicates the contribution of the balance between the two (domestic sales or exports). Diagonal lines are the sum of export and domestic market diversity where countries along the same line report the same diversity level.

The results indicate that countries have several possible options to diversify production and to market agricultural products domestically and abroad. These are driven by a combination of country-specific factors. First, a country's comparative advantage, or lack thereof, in producing and exporting agricultural products, depends on the resource base, infrastructure, input cost and a business-enabling environment. Second, where there is openness to international trade, producers can export easily without restrictions or trade barriers by importers. And third, the size of domestic demand relative to domestic markets may partly determine the importance of exports. In China, India and Nigeria, for example, the low contribution of exports to diversification (blue oval in Figure 3) can be partly explained by their large agricultural base and diverse domestic demand. This, however, increases vulnerability to domestic economic downturns, indicated by the small orange bubbles which pinpoint domestic market orientation.

High-income countries with open trade policies, such as Australia, or part of large trading blocs like the European Union, have some of the highest PPFI values (see green oval in Figure 3), combining diversity of domestic and export markets. However, openness to trade and comparative advantage do not necessarily increase production flexibility. In Argentina and Brazil, more than 70 percent of protein value is from two commodities: soybean and maize. Specializing in a few export commodities with limited domestic demand increases vulnerability to international shocks, such as sharp price declines due to excess supply from other exporting countries.

For more than 80 percent of countries, the PPFI is driven by domestic market diversity. This is especially true for those with low PPFI values, mostly in the low-income group with little external trade and most production consumed locally (purple oval in Figure 3).[7] Consequently, the primary production sector is particularly vulnerable to domestic income shocks,[c] even for populous countries like Bangladesh and Indonesia where domestic demand is strong but commodity diversity is lower than in countries like China and India. High-income countries with a protected agriculture sector and limited comparative advantage in agriculture, such as Japan and Norway, also exhibit low diversity in exports and domestic markets, indicating low production flexibility. A low PPFI can also be due to having few trading partners, even if exports are significant. Brazil is again a case in point, having 60 percent of export value coming from one trading partner. Relying on a limited number of significant trading partners leaves a country with fewer options if a shock hits a partner country.

Small countries, such as Latvia or Slovenia, despite having a small agriculture sector, report a PPFI value almost as high as those with a much broader agricultural base, such as Canada or France, even in export diversity. This highlights the fact that the indicator does not measure magnitude but the primary sector's absorptive capacity through diversity of domestic production and marketing.

These findings can help policymakers determine which elements of production and trade add to the absorptive capacity of their country's primary sector and which contribute to its vulnerability. The analysis, however, excludes non-food primary commodities (e.g. tobacco and wool) due to lack of producer price information for all commodities and because these cannot be converted into nutrients. Their contribution to a primary sector's absorptive capacity is therefore not captured, although they generate important potential economic value for primary producer livelihoods. Box 4 discusses this issue, comparing the PPFI for value and protein terms for selected countries with sufficient information on prices of food and non-food primary commodities. As seen in Box 4, the PPFI is generally higher when measured in value terms, due to the addition of non-food

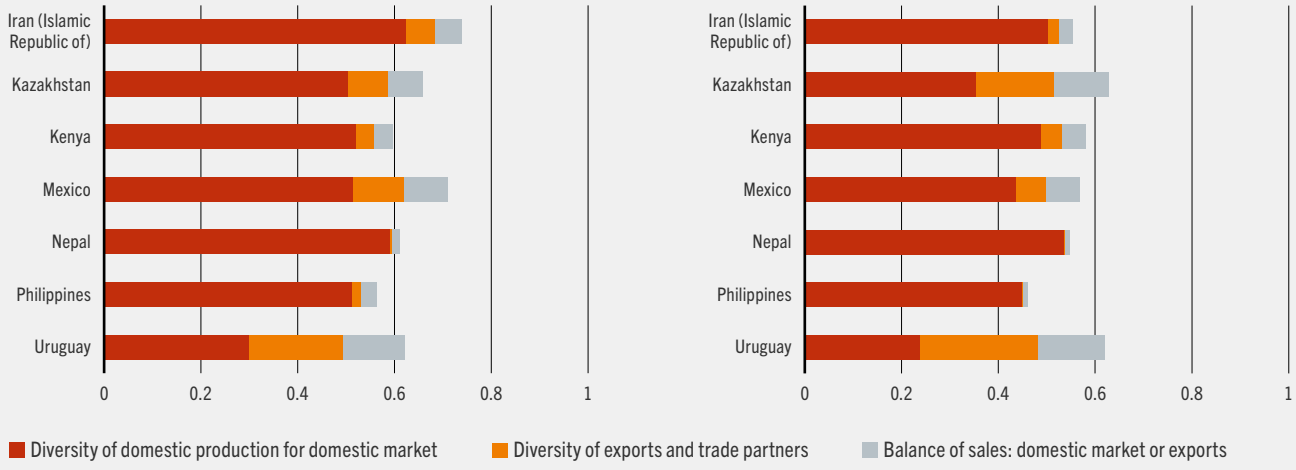
c These shocks are of particular concern in low-income countries where the share of household expenditure on food is higher and therefore an income shock may lead to a sharper reduction in food purchases.

BOX 4 THE PPFI IN VALUE TERMS, INCLUDING NON-FOOD PRODUCTS

During the COVID-19 pandemic and other major crises affecting agrifood systems in the past, timely and reliable food price information has been important to monitor food security and inform policies to build agrifood systems' resilience. Food price information also supports humanitarian aid decisions, especially in low-income countries and regions susceptible to food insecurity and malnutrition. Unfortunately, it is precisely in these areas that timely and accurate data are most often unavailable. For this reason, the PPFI is measured for protein terms, given the high correlation between protein and value. Using protein instead of value conceals a vital part of agrifood systems: non-food primary commodities, such as some types of feed and biofuel, fuelwood, fibre, skins, hides and construction materials.

The non-food agriculture sector is an important source of livelihoods for primary producers. For this reason, the figure in this box compares the PPFI for value terms (left) with that for protein terms (right) for countries where food and non-food prices were available for items representing more than 70 percent of food production. The flexibility of primary production is always higher when measured in value terms, except for Uruguay where the values are practically identical. This is explained by the inclusion of non-food items, such as tobacco and wool, and the fact some food items may be high in value but low in protein content. The contribution of domestic demand has also increased for virtually every country.

FIGURE PPFI FOR VALUE (LEFT) AND PROTEIN (RIGHT) FOR SELECTED COUNTRIES, 2016–2018



NOTES: The two bar graphs represent the total value of the PPFI, for value (left) and protein terms (right) for selected countries as a 2016–2018 average. The different stacked bars represent the relative contribution of export and domestic diversity, and the balance between the two, to the total value of the PPFI. Price data were taken from FAOSTAT. Due to the lack of protein content, non-food agricultural commodities are excluded from the PPFI for protein terms (right) but included when measured for value (left). See **Annex 1** for methodology and data sources.
SOURCE: FAO elaboration for this report.

items representing new pathways to generate value for primary producers. The analysis does not distinguish between commodities sold as food, feed or biofuel. Future analysis should take this into consideration, as growing crops for feed or biofuel may reduce food production.[8] These results highlight the need for a more thorough understanding of the issues, through more and better data and improved, expanded analysis.

In summary, results from the PPFI have shown that the primary sector can better absorb disturbances when it produces a diversified mix of products, and when it has access to diversified domestic and international markets. This occurs mostly in high-income countries or in those with a large agricultural base. ■

GUARANTEEING AVAILABILITY OF NUTRITIOUS FOOD

Species diversity in crop and livestock production, forestry, fisheries and aquaculture stimulates productivity, stability and ecosystem services.[9–11] Aquaculture, in particular, has shown to be one of the world's most diverse farming practices in terms of species, farming methods and environments used. Findings indicate that, in the future, the number of farmed species in the world will oscillate around 428, of which 29 dominant and 116 relevant, that is, responsible for 99 percent of annual production.[12] Diversifying aquatic farmed species can be of importance for long-term performance and viability of the sector with respect to sustaining food production under changing conditions. Indeed, countries with high species diversity are usually associated with higher production, with Asian countries – particularly China – producing the most diverse collection of species.[13]

Just as diversity helps ensure the capacity of agricultural production to absorb disturbances, diversity in food availability strengthens consumer resilience, providing the nutrients essential for health. Beyond producing more food to meet a growing demand from a growing and increasingly affluent population, agrifood systems must provide diverse foods of high nutritional quality.[7, 14] There is evidence pointing to declining diversity of national food supplies[15] and this trend is likely to continue as farm sizes increase,[14] raising concerns about global nutritional diversity. Maintaining diversity of food supplies needs to happen in a context where specialization and intensification of agrifood systems lead to loss of resilience in agricultural landscapes, evidenced by a decline in crop diversity, landscape multifunctionality and regulating ecosystem services.[16]

In most low-income countries where international trade is generally limited, consumption diversity requires a wide range of agricultural goods produced domestically, as seen in the PPFI results. Diversifying production is thus essential to ensure food security and nutrition. Conversely, countries with specialized production of a small basket of commodities can enhance food supply by importing a range of food products from a similarly broad range of trading partners. This is particularly important for countries with a narrow agricultural base, where climate or lack of land or water limits diversification, as in small island developing States (SIDS) and landlocked developing countries (LLDCs). Countries with broad-based agriculture can achieve food diversity more easily by combining diversified national production and international trade; production and supply diversity are not strongly interdependent.

International trade is one of the many strategies for buffering against shocks and stresses and increasing food supply diversity. It allows countries and regions to maintain food security and overcome growth limitations.[17, 18] Trade can reduce pressures on natural resources such as water,[17, 18] help keep prices down[3] and provide seasonal goods throughout the year.[4] Through trade, agrifood systems are becoming increasingly interconnected and interdependent. Data for 1992–2009 show global wheat and rice trade connections doubled while trade flows increased by 42 percent for wheat and 90 percent for rice.[19] Fish and fishery products are some of the most traded food commodities. In 2018, 67 million tonnes, or 38 percent of total fisheries and aquaculture production, were traded internationally.[20] However, although it buffers against domestic shocks, international trade increases exposure to external shocks and can itself become a channel of shock transmission.[19, 21, 22]

Studies of resilience often focus on the response to a shock, such as a trade shock, without looking at resilience capacities ranging from prevention, anticipation and absorption of

BOX 5 THE DSFI IN A NUTSHELL

The DSFI uses FAO's food balance sheets and trade data to plot the pathways through which a unit of food is available to consumers with external stock data complementing FAO data. It is assumed food availability can be linked to the share of food produced domestically, stocked from previous years or imported, and to the food's diversity. Agrifood systems that draw on food from many different sources have greater capacity to absorb supply shocks.

The three possible pathways a unit of food, measured for kilocalories, can reach a consumer are represented as a tree in the figure as follows: (i) food produced domestically; (ii) imported food; and (iii) stocks carried over from the previous year (imports or domestic production, public and private).

Since stocks and production are within a country, policymakers can exercise through them more direct control over food self-sufficiency, represented in the figure by the Stocks in kilocalories and Kilocalories domestically available branches. The latter is further disaggregated by destination (local market or export) and subsequently by commodity produced. If a supply shock occurs, exports may be redirected by producers to the domestic market through price signals or policy interventions – of last resort – to ensure food availability. Imports are represented on the right side of the figure as Imports in kilocalories, also further disaggregated into trading partners and import diversity. The balance between imports and what is produced or stocked domestically measures the role of trade in supplying food and sourcing diversity. A country with balanced production relative to imports may still be vulnerable if it imports from only a few trading partners and holds limited food stocks, restricting the possibility to redirect surplus food to the domestic market. Increasing buffer stocks or diversifying international trade partners before the shock hits can enhance absorptive capacity. This will help policymakers identify the weaknesses in their food systems' absorptive capacity for different supply shocks.

shocks to adapting and transforming systems. Policymakers make decisions in a multi-risk environment, where the next disruption may be domestic. Building on Kummu *et al.* (2020),[17] FAO developed a dietary sourcing flexibility index (DSFI) for this report to assess the role of diversification in domestic production, stocks and imports, so as to ensure the food that makes up a healthy diet is available to a country's population. The index captures multiple sourcing pathways of a unit of food (for nutritional outcomes, such as kilocalories) based on a country's domestic production, food imports, and public and private stocks. A high value indicates multiple possible sourcing pathways for a unit of food (i.e. redundancy of sources). The DSFI thus measures flexibility in sourcing a specific food unit. National agrifood systems supplying food from different sources are more flexible and capable of absorbing supply shocks. See Box 5 for a more detailed description of the indicator, and Annex 1 for the full methodology. This index complements the PPFI by extending the focus beyond domestic agriculture to imports and food stocks in order to capture the multiple pathways through which a unit of food can reach the consumer. In short, the DSFI measures the capacity of agrifood systems to absorb shocks and ensure food availability to consumers, while the PPFI focuses on ensuring livelihoods for primary producers.

Figure 4 illustrates the DSFI for kilocalories for all crop, fish and livestock commodities for available FAOSTAT new food balance sheets and trade data, as a 2016–2018 average. To provide for healthy diets, countries also need to source a variety of other nutrients.[23] The report expands the analysis to cover another three nutritional components: fruits and vegetables, fat, and protein, included in Annex 2. Other nutrients, such as vitamins and iron, are also required for a healthy diet, yet data are lacking in FAO's food balance sheets.

Aside from nutritional components, the DSFI can also be divided into different elements that »

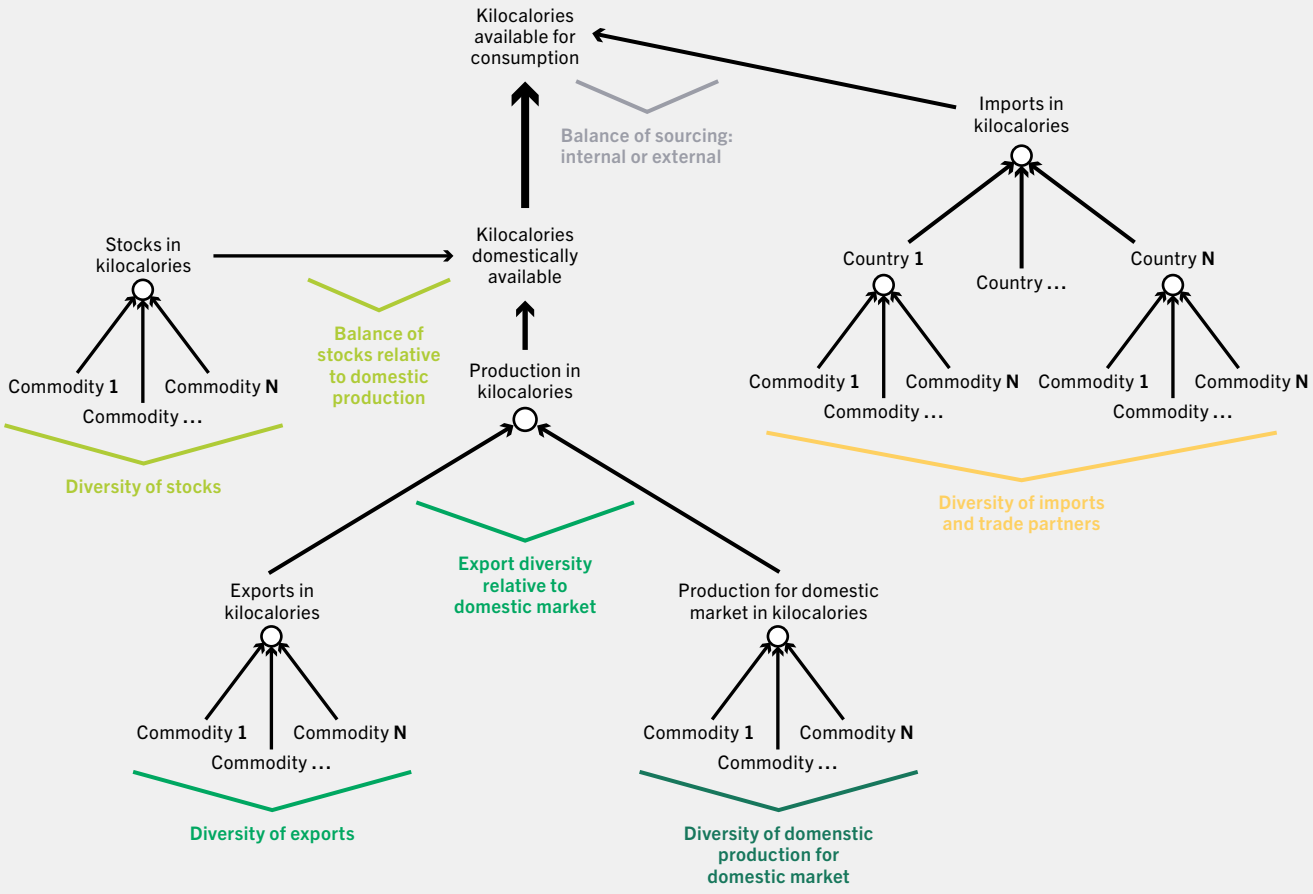
BOX 5 (CONTINUED)

The DSFI captures these multiple pathways as a snapshot in time. Over time, its different contributions may interact (e.g. imports may become stocks in the following year or stocks may become exports).

Interpreting the DSFI – The DSFI measures the redundancy of sources by capturing multiple pathways for sourcing a food unit. It is particularly useful in understanding how production, trade and stocks can help agrifood systems absorb supply shocks. The tree in the figure shows how flexible sourcing is built into agrifood systems. For households as consumers, in a situation of economic autarchy, the value of the DSFI equals the contribution of production diversity for the domestic market (dark green in the figure). If there are exports, systems have greater flexibility because this surplus can be directed to domestic markets in times of crisis. This increases the value of the DSFI by diversity of sourcing and commodities exported, generated by adding in those exports (mid green in the figure). Buffer stocks and imports also add flexibility to food systems. As for the PPFI (Box 3), a high DSFI value reflects high absorptive capacity.

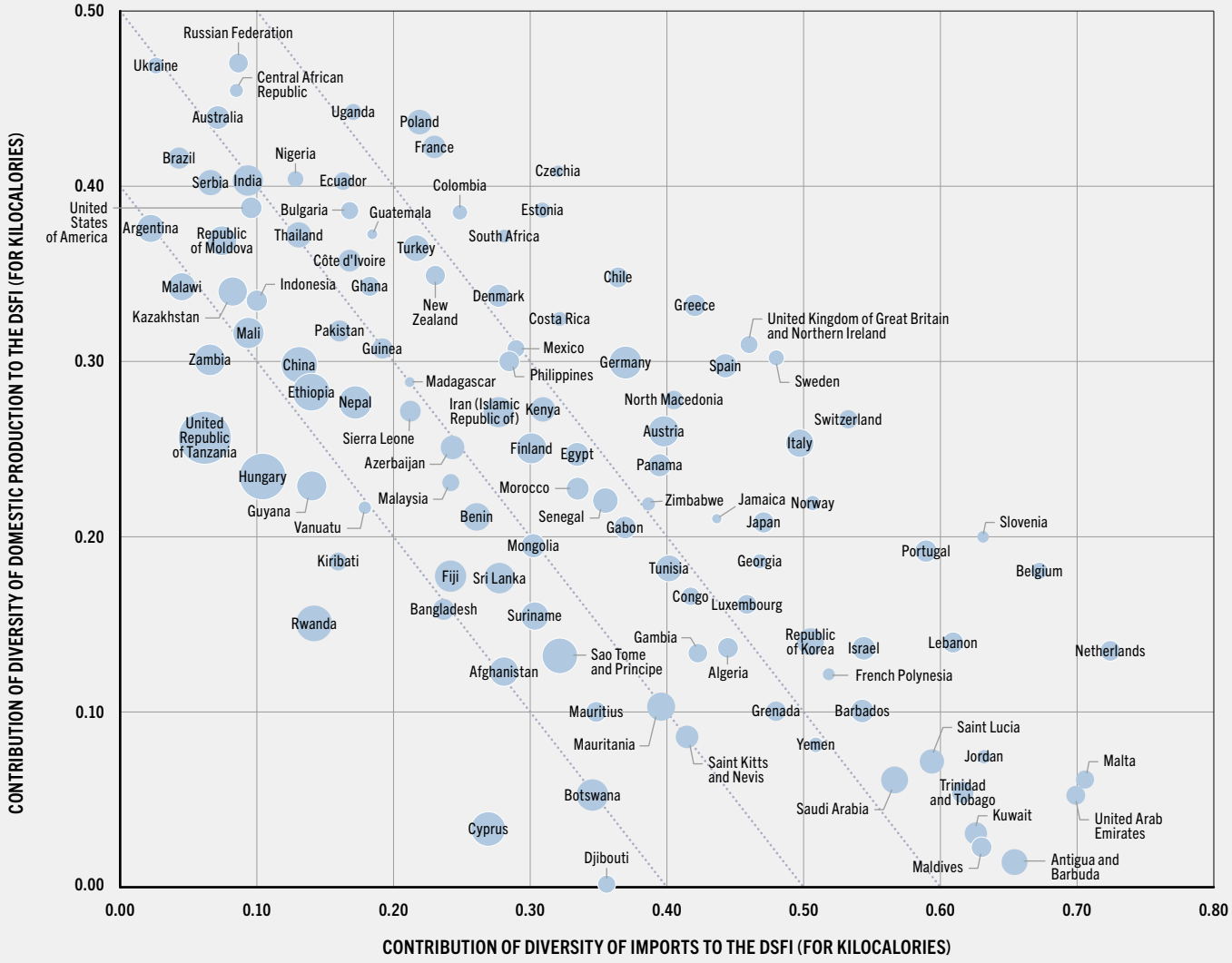
Caveats – The DSFI needs to be complemented with information on a country's size and level of development and those of its trading partners that influence agrifood systems' vulnerability. Shocks such as a flood will affect entire agrifood systems in a small country but have less impact in a larger country with different agroclimatic zones. A country's development level is also important where redundant and robust infrastructure is essential to absorb shocks.

FIGURE PATHWAYS TO SOURCE FOOD FROM STOCKS, DOMESTIC PRODUCTION OR IMPORTS, FOR KILOCALORIES



SOURCE: FAO elaboration for this report.

FIGURE 4 DSFI FOR KILOCALORIES, 2016–2018



NOTES: The graph plots the contribution of the diversity of imports (i.e. diversity of imports and trade partners plus balance of sourcing: internal or external) against the contribution of the diversity of domestic production (for both domestic market or exports), both to the total value of the DSFI, for kilocalories. The size of the blue bubbles represents the contribution of the diversity of stocks to the DSFI. Countries placed in the same diagonal line report the same value for production and import diversity – 0.4, 0.5 and 0.6, respectively. Results include all crop, fish and livestock commodities for which FAOSTAT new food balance sheets and trade data were available. Kilocalorie conversion factors are based on FAOSTAT data and then used to convert tonnes of food into kilocalories. To simplify graphic presentation, 40 countries that overlapped in the graph were dropped. Results are the three-year average of 2016, 2017 and 2018. Results for the full set of countries disaggregated by DSFI contributions are available in **Annex 3**. See **Annex 1** for methodology and data sources.
SOURCE: FAO elaboration for this report.

» provide diversity of sourcing food: domestic production, imports and stocks. The bubble chart in Figure 4 illustrates these three value dimensions of the DSFI for kilocalories: the horizontal axis is the contribution of imports and their diversity across trade partners with multiple commodities; the vertical axis is the contribution of commodities produced domestically; and the size of the bubble is the contribution of estimated stocks.[d] It is important to note that import diversity (horizontal axis) also includes the balance between imports and what is domestically available. This balance represents a country's reliance on a mix of both domestic

d Stock data are notoriously difficult to estimate accurately, therefore this contribution to domestically available food is separated from other components contributing to diversity.

production and imports. Similarly, the balance between exports and production for the domestic market – representing a country's agricultural base and capacity to produce a surplus – is incorporated under domestic production diversity.

Two results emerge clearly from Figure 4: first, countries diversify their food sources in different ways; second, the effectiveness of diversification does not depend on country size or income level. The latter is illustrated by countries with different income levels appearing on the same diagonal lines, where the sum of import and production diversity levels is the same.

A similar DSFI value can be attained by countries with a sizeable agricultural base that rely more on domestic production (e.g. India, Nigeria, Russian Federation and United States of America) and by those that diversify more through imports (e.g. Turkey, Senegal and Tunisia). Given the diversity of import options, some countries that rely on imports do so with high diversity across trade partners and multiple commodities, attaining some of the highest DSFI scores by buffering supply shocks over many partners and commodities (e.g. Japan, Jordan, Norway, Republic of Korea and United Arab Emirates). Except for France and Poland, European Union countries with free circulation of goods across borders tend to have significant diversification through imports, especially Belgium and the Netherlands.

Although reliable and consistent stock data are rarely available, results indicate stocks tend to matter more for countries with lower DSFI values (below the central diagonal line), that rely more on domestic production with relatively low import diversification. As seen in the PPFI results, unsurprisingly, low-income countries, such as in sub-Saharan Africa, are among those with the lowest import diversity (see Box 6 for a comparison between the DSFI and PPFI methodology and results), partly explained by limited trading of some staples, such as millet, sorghum and fonio. In these countries, food systems' flexibility is mostly driven by production for the domestic market. Thus, when a shock occurs, policymakers are constrained by managing production diversity to absorb it or rely on existing stocks.

Having a mix of domestic and imported food is important to minimize risk, especially for smaller countries. For countries that depend heavily on imports due to scarcity of domestic natural resources, such as countries in the Near East as well as SIDS and LLDCs, it is crucial they diversify import baskets and international trade partners, while investing in domestic stocks.

Unlike for calories, the DSFI for fruits and vegetables, which are key to a healthy diet, has a clear association with a country's income because of logistical constraints in perishable transport and storage. High-income countries in Europe, Northern America and the Persian Gulf have noticeably higher DSFI values, with some exceptions (see Annex 2). Countries with higher DSFI values for overall kilocalories than for tonnes of fruits and vegetables, such as China, Ethiopia and Uganda, probably have greater absorptive capacity for shocks affecting staple foods than for shocks affecting fruits and vegetables. ■

ENSURING PHYSICAL ACCESS TO FOOD AT SUBNATIONAL LEVEL – THE DOMESTIC FOOD TRANSPORT NETWORK

The robustness of agrifood systems depends on a confluence of factors. Guaranteeing production, availability and economic access to food will capture part of what makes it resilient. Country logistics also play a fundamental role in ensuring physical access to food and producing non-food agricultural output. Agrifood systems are supported by a network across the rural–urban continuum and how it responds to shocks will depend on connectivity within that network. During regional weather anomalies and yield losses, food supply chains can rely on the same or compensatory products from other regions in the country or combine imports with domestic purchases to ensure affordable food remains available. These alternative pathways help ensure food supply chains maintain their

BOX 6 COMPARING THE DSFI WITH THE PPFI AND IDENTIFYING THE HIDDEN MIDDLE

The PPFI and the DSFI differ in several aspects. Capturing multiple pathways through which a unit of food reaches the consumer, the DSFI measures the capacity of countries' agrifood systems to absorb a shock while ensuring food availability. The PPFI captures possible pathways by which agricultural producers can generate value, a measure of the capacity of domestic agriculture to absorb shocks and create livelihoods for primary producers. (If data were available, the PPFI could also capture the potential contribution of non-food primary commodities, such as cotton, tobacco and timber, to the primary sector's capacity to absorb shocks – see Box 4.)

In addition to the diversity of domestic production, the DSFI also captures a country's mix of imports, the diversity of trade partners, and the diversity of stockholding, which can act as a buffer during a crisis. A further difference is that the DSFI is based on various nutritional units (e.g. kilocalories, protein, fat), while the PPFI is based on production value (quantity multiplied by unit price) or on protein terms if price data are missing.

The PPFI overlaps with the part of the DSFI that captures production diversity. However, even though the rationale is the same for both, there are important differences. First, the PPFI captures not only export diversity but also the diversity of importing countries. Second, since the PPFI focuses on agricultural value, it considers crops and primary livestock products, but excludes anything processed (e.g. flour from wheat), unlike the DSFI which focuses on both processed and unprocessed. The DSFI considers any crop or animal product processed in a country to be produced in that country, even if the raw input was imported. For these reasons, the share of production diversity in the DSFI and the total value of the PPFI differ.

It is important to note that neither indicator casts light on the midstream components of agrifood systems – for example, they provide no information on whether primary producers are selling to consumers or to processors and whether processed food remains on the domestic market or is exported. Knowing more about the midstream in food supply chains matters because systems are only as resilient as their weakest link. For a more complete picture of the resilience of agrifood systems, the degree of flexibility in options for midstream actors also needs to be measured. Issues to address include access to primary inputs from domestic and imported sources, the level of diversification in processed foods, and options to sell those foods on the domestic or export markets. A midstream flexibility index (MFI) could combine these three elements to measure the diversification of the processing sector in terms of sourcing its primary inputs (domestic or imports), the types of goods it produces and market outlets. National food systems in which processors offer more latitude in food production give the option to produce for domestic and export markets, and to use diverse input sources; systems thus become more resilient and maintain productive capacity in food processing.

The report proposed the theoretical underpinning of this indicator but did not compute it as it requires data not readily available. Enhancing data collection and measuring capability will then be key to complete the set of indicators proposed in this report. For more details on how the MFI can be calculated and its data requirement, see Annex 1.

core functions. Well-functioning transport networks of non-food agricultural commodities, such as wood, reduce costs of production, labour, materials and energy. This, in turn, improves profitability and generates income for non-food agricultural producers.

Connectivity builds resilience to shocks throughout the network. Network theory, as applied to food supply chains,[24–27] provides insights into how certain aspects of agrifood systems' resilience can be measured and suggests entry points for an analysis of domestic food transport networks, for example, the criticality of transport links and the redundancy of some routes if a link is broken.[e] Such an approach can

e A link is any part of the road, rail or water transport network that forms part of the route where food transport occurs between supply and demand locations.

be useful to understand how additional network links affect agrifood systems – an important question because network density will typically increase over time.[25]

This section analyses the resilience of food transport networks in 90 countries representing 7 billion people (92 percent of the global population) in 2017. Based on these data, three national indicators are computed to capture the vulnerability of transport networks around the world (see Box 7 for the methodology). Due to lack of data, the analysis is limited to crops (except oil crops) and does not include transport of other agricultural commodities, including non-food commodities. Hence, the analysis is limited to the food component of agrifood systems, and more specifically to crops. Some food commodities considered may go to agro-industrial processing, feed or biofuel instead of consumers. The analyses do not differentiate between these destinations.

The vertical axis in Figure 5 is the proximity-based resilience indicator for 43 countries, colour-coded for country income. The horizontal axis measures the average time to transport food. Proximity-based resilience levels (vertical axis) equal to 1 indicate that production can meet demand in its specific catchment area, implying each catchment could revert to self-contained city-region agrifood systems if needed. However, no country approaches that limit, given that the complete collapse of its transport network is extremely unlikely. There is considerable variation across countries, where those with shorter average transport time (horizontal axis) generally have higher proximity-based resilience (vertical axis).

This is not surprising, as lower transport time means food is delivered close to where it is produced. This is the case for France, the Republic of Korea and Turkey. At the other extreme are much larger countries with longer distribution networks, such as Australia, Brazil and Canada. However, some large countries, such as China and Nigeria, have made their food production and distribution more compatible with short supply chains and if transport costs increase, they can easily readjust. Proximity-based resilience also seems uncorrelated with country income. These results also have sustainability implications, as shorter transport networks imply not only lower transportation and possibly network maintenance costs but possibly lower environmental costs as well, such as lower energy use and pollution. Figure 5 captures the flexibility of transport networks going local but does not consider the likelihood of a disruption, nor its location or impact on producers and suppliers.

The second indicator, route redundancy, examines the availability of alternative routes when road links are broken. The third, the relative detour cost indicator, examines the impact of disruptions to critical links. To estimate detour costs, the extra cost from closed critical links is calculated by determining the shortest routes and the difference in travel time before and after disruption. When divided by travel time, this difference captures systems' sensitivity to closed links. By this measure, for 47 countries out of 90 analysed, the closure of a critical transport route could increase travel time by 20 percent or more for food diverted from the disrupted route, potentially affecting food costs for 845 million people.[f] The effects are more local in some countries than in others: the share of population potentially affected ranges from 25 percent in Nigeria to 78 percent in South Africa.

Table 1 places the three indicators side by side. Countries with colour-coded green cells score very highly on resilience for that specific indicator, while those in dark orange have low scores. The indicators are uncorrelated with one another but deliver a more comprehensive picture of transport network resilience and its vulnerabilities when analysed together. China has the capacity to adjust to more proximity-based food systems with high redundancy (green cells under Proximity-based resilience and Route redundancy), reducing the probability of systems having to go local. If a critical link is disrupted, average travel time also does not increase by a significant amount (green cells under Relative detour cost [local »

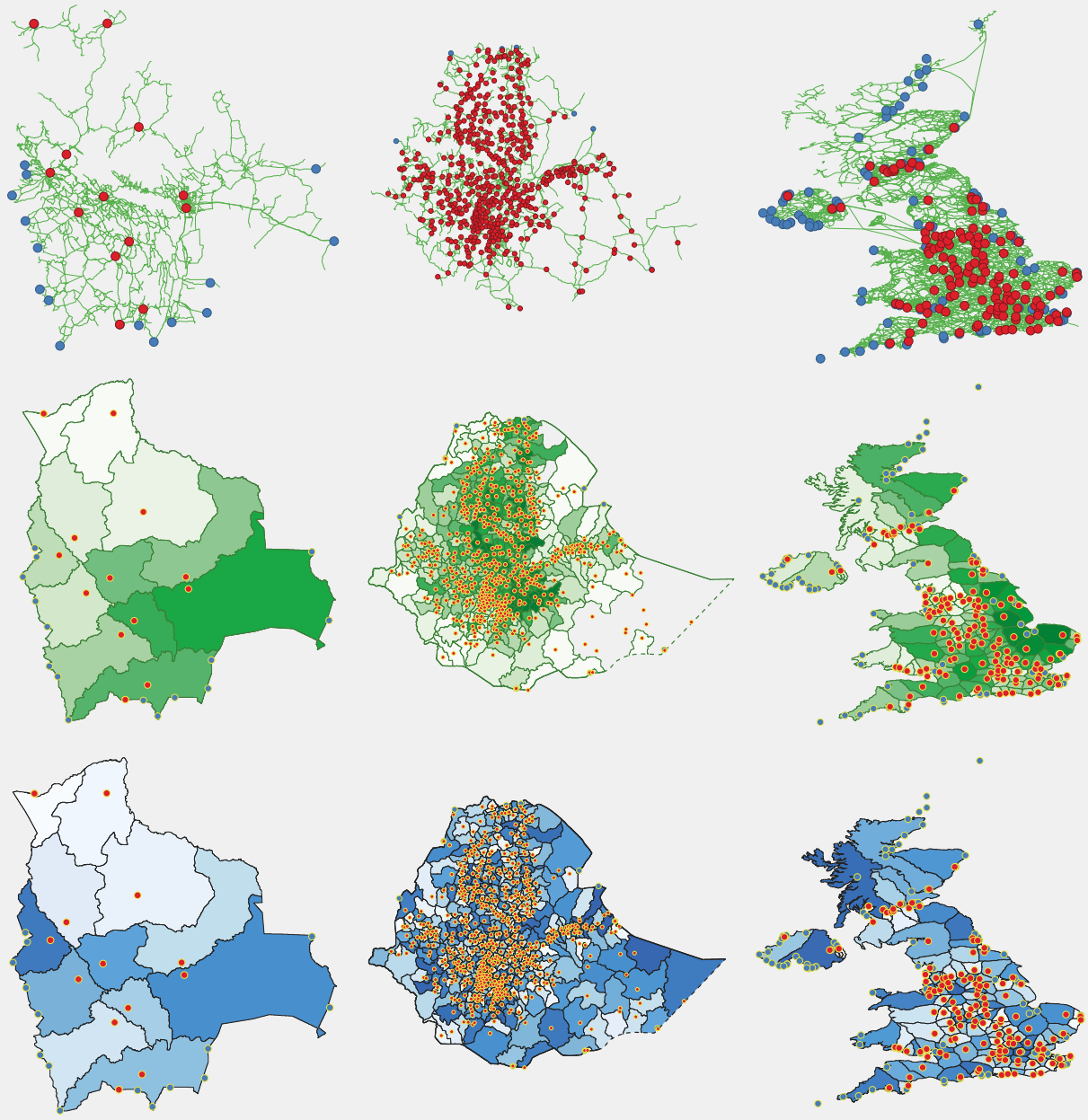
f Some of the larger countries that experience a 20 percent or more increase in travel time are Bangladesh, Ethiopia, Nigeria, the Philippines and the Russian Federation. See Annex 3 for the full list.

BOX 7 METHODOLOGY TO EXAMINE THE RESILIENCE OF DOMESTIC FOOD TRANSPORT NETWORKS

To represent food transport networks, both cities and transport modes (roads, railways, waterways and ports) are analysed. Crops were selected based on the quantity, diversity and nutritional value needed to achieve a nutritionally adequate diet. The selected crops represent, globally, 66 percent of food supply, 60 percent of calories and 58 percent of protein. Beverages, animal products and oil crops are excluded due to data constraints.

Production and demand were spatially represented to analyse transport network resilience. Spatial data for production and population are combined with tabular data for: (i) food production, spatially allocated to production zones in each country; (ii) food supply, spatially allocated based on population distribution, with per capita supply varying by commodity but remaining constant within countries; and (iii) exports and imports, allocated to trade locations based on the most likely mode of transport (ports or land border crossings).

FIGURE FOOD DISTRIBUTION NETWORKS IN BOLIVIA (PLURINATIONAL STATE OF), ETHIOPIA AND THE UNITED KINGDOM OF GREAT BRITAIN AND NORTHERN IRELAND



Bolivia (Plurinational State of) | Ethiopia | United Kingdom of Great Britain and Northern Ireland

NOTE: Spatial zones in the middle and bottom row are catchment areas around cities. See **Annex 1** for methodology and data sources.
SOURCE: Nelson *et al.* (forthcoming).[28]

BOX 7 (CONTINUED)

The figure in this box illustrates the domestic food distribution network in three countries: Bolivia (Plurinational State of), Ethiopia and the United Kingdom of Great Britain and Northern Ireland. The top row presents the transport network, with cities in red and trading nodes in blue. The middle row presents production volumes for each country's main crop, respectively, fruits, pulses and wheat, and is obtained by superimposing production over the cities and trading nodes in the top row. The bottom row presents the final supply map for those crops. Together, the maps show how food transport networks connect production to demand. A darker shade means greater production (green in middle row) or greater demand (blue in bottom row). Overlaying urban centres and their rural catchment areas with the transport network provides a topological representation of the internal agrifood systems' distribution network.

Based on the above, there are three national indicators to capture the structural vulnerability to disruptions to food systems' transport network:

i. The **proximity-based resilience** indicator connects food production to supply to measure how food systems respond to disruptions. Systems are less vulnerable to network disruptions if food is produced locally, as it is not transported over long distances.
ii. The **route redundancy** indicator measures availability of alternative routes by calculating the percentage of tonnes over links for which there are other routes. Most countries have alternative routes for virtually every link, but exceptions exist.
iii. The **relative detour cost** indicator measures systems' sensitivity to closure of critical transport links due to shocks or stresses (e.g. floods or political instability). It calculates the extra travel time when a critical link between origin and destination closes.

» and aggregate impact]), suggesting that China has a resilient transport network. At the other extreme, in a country like Somalia, where food systems are not set up to go local and route redundancy is low (see dark orange and orange cells), disruptions to critical links may still force food systems to go local for a time, which can be challenging.

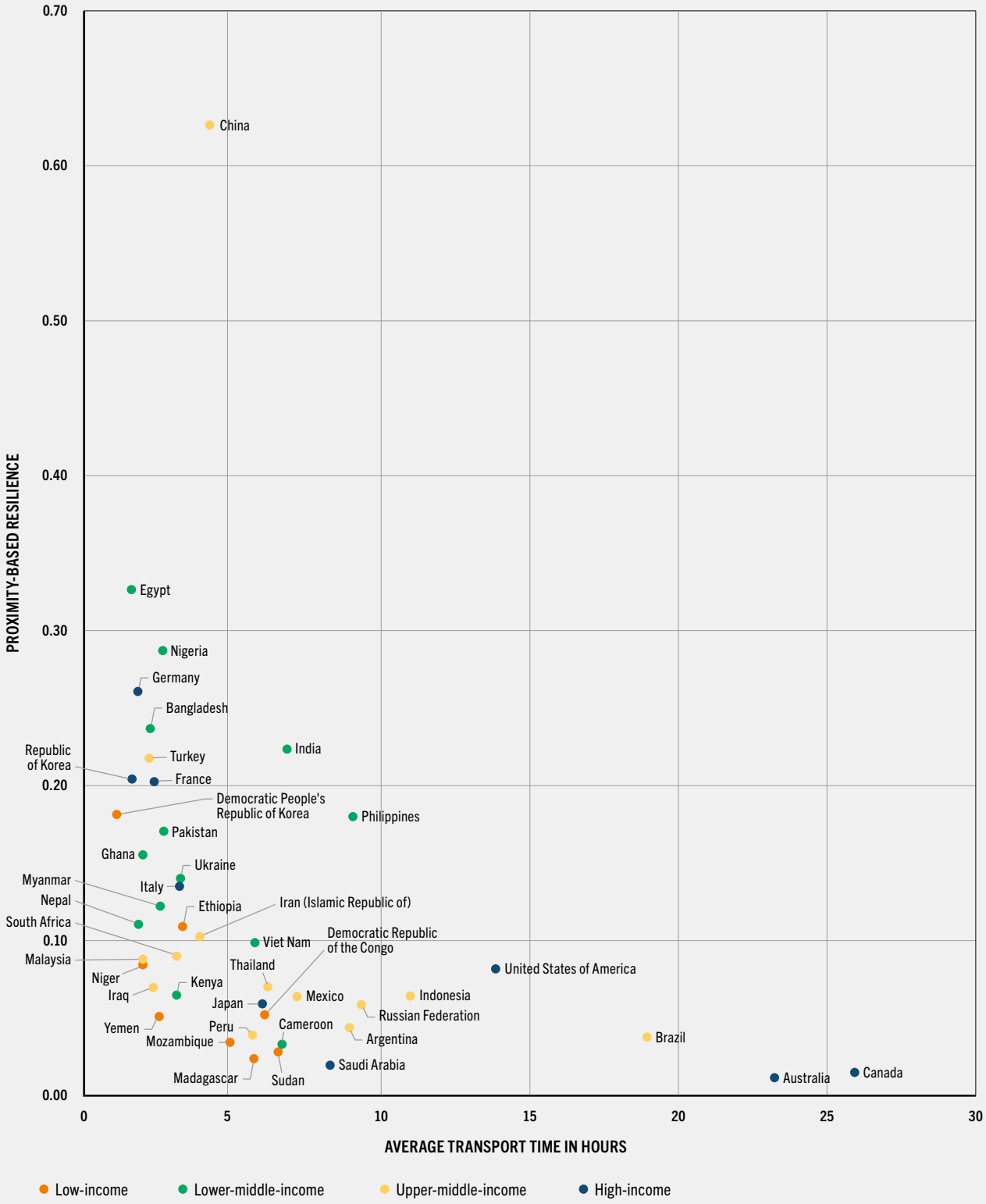
Limited redundancy does not affect only low-income countries (see Chile, Indonesia and Papua New Guinea in Table 1). Yet, it is low-income countries that face the greatest challenges in system-wide resilience measures regarding food transport networks, with a combination of low capacity to adjust to proximity-based systems, and a high number of links without practicable alternative routes in case of disruption. High-income countries like France and the United States of America are at the other end of the spectrum, although exceptions exist since proximity-based resilience depends on how production is distributed relative to demand. Australia, Canada and Chile are vulnerable in this respect.

The relative detour cost (right column) highlights how, for some countries, closure of critical links can be incredibly costly. For countries like Bangladesh, Brazil, the Democratic Republic of the Congo, Haiti, Madagascar, Niger, the Philippines, Senegal and the Sudan, travel time increases by, on average, 30 percent or more, increasing the cost of food. For some, like the Philippines and the Sudan, the impact of critical link closures is felt nationally, not just locally.

Table 1 reports only the average effect of random disruption to critical links. However, it is possible to examine the relative detour cost of specific disruptions. Box 8 analyses specific disruption scenarios in flood-prone regions of Nigeria and Pakistan.

Overall, this analysis highlights the critical importance of a robust transport network in supporting resilience of food systems to shocks and stresses and guaranteeing physical access to food at local level. A robust transport network would prevent increases in travel time with the knock-on effect on food costs, in the event of the closure of a critical transport route. ■

FIGURE 5 PROXIMITY-BASED RESILIENCE AS A FUNCTION OF THE AVERAGE TRANSPORT TIME OF FOOD IN SELECTED COUNTRIES



NOTES: Countries were selected based on population (more than 20 million). For comparability across countries, proximity-based resilience is corrected for tonnage (i.e. multiplied by the square root of the total tonnage of transported crops) to correct for the artificial effects between country size and the resilience metric. The corrected metric is considered the more appropriate system-wide estimate of the resilience of a country's food transport network because it takes into account the size of the country. The uncorrected measure would tend to overestimate resilience of small countries, where distances and volumes transported are limited, and underestimate that of large ones. See **Annex 1** for methodology and **Annex 3** for the proximity-based resilience results for the full set of countries.
SOURCE: Nelson *et al.* (forthcoming).[28]

TABLE 1 INDICATORS OF RESILIENCE AND VULNERABILITY OF FOOD TRANSPORT NETWORKS FOR SELECTED COUNTRIES

	COUNTRY	SYSTEM-WIDE MEASURES		LOCALIZED DISRUPTION	
		Proximity-based resilience	Route redundancy	Relative detour cost (local impact)	Relative detour cost (aggregate impact)
Low-income	Democratic Republic of the Congo				
	Haiti				
	Madagascar				
	Mali				
	Niger				
	Somalia				
	South Sudan				
	Sudan				
Lower-middle-income	Bangladesh				
	India				
	Myanmar				
	Nigeria				
	Pakistan				
	Papua New Guinea				
	Philippines				
	Senegal				
	Zambia				
Upper-middle-income	Brazil				
	China				
	Indonesia				
	Russian Federation				
	South Africa				
	Thailand				
High-income	Australia				
	Canada				
	Chile				
	France				
	United States of America				

Food transport network resilience

Low
Medium
High
Very high

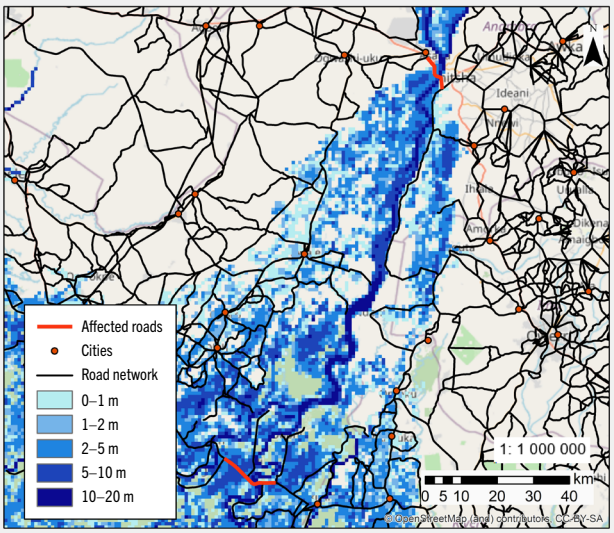
NOTE: Proximity-based resilience is measured as follows: low when values are less than or equal to 0.02; medium when values range between 0.02 and 0.05; high for between 0.05 and 0.2; and very high when it surpasses 0.2. Route redundancy is measured as follows: low when values are less than or equal to 70; medium when values range between 70 and 80; high for between 80 and 90; and very high when it surpasses 90. Relative detour cost (local impact) is measured as follows: low (resilience) when values surpass 30; medium when values range between 15 and 30; high for between 5 and 15; and very high when values are less than or equal to 5. Finally, relative detour cost (aggregate impact) is measured as follows: low (resilience) when values surpass 10; medium when values range between 5 and 10; high for between 2 and 5; and very high when values are less than or equal to 2. Proximity-based resilience is corrected for tonnage. Countries were selected based on population (more than 5 million), income group and region, so as to capture as much differentiation as possible. See **Annex 1** for methodology and **Annex 3** for the results for the full set of countries.
SOURCE: Nelson *et al.* (forthcoming).[28]

BOX 8 SIMULATING THE IMPACT OF FLOODS ON FOOD TRANSPORT NETWORKS IN NIGERIA AND PAKISTAN

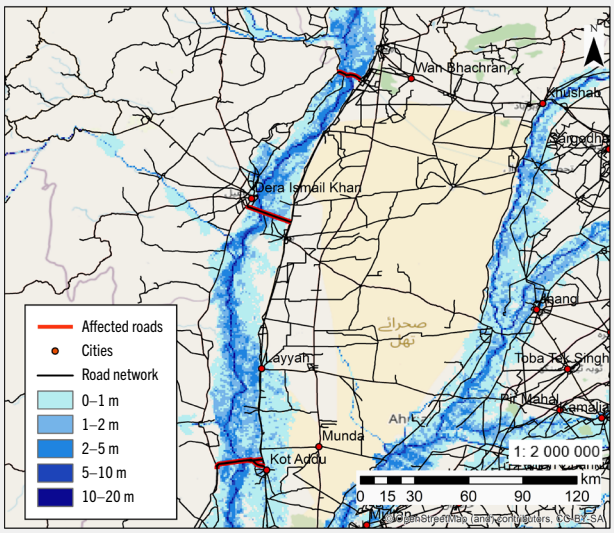
Flooding, from flash floods to longer-duration stagnant waters, reduces the connectivity of transport networks. Roads may become impassable, bridges too dangerous to cross or even washed away. Once the flood subsides, direct infrastructure impacts may be short-lived if there is no material damage, but there can be long-lasting effects if repairs are delayed, often the case in less developed countries. Floods can also affect a larger area for a longer time, with traffic delays and congestion on alternative routes, increased journey distances/durations, and higher fuel consumption and GHG emissions.[29]

Nelson *et al.* (forthcoming) simulate the impact of localized flooding in Nigeria and Pakistan, considering loss of network connectivity from flooding when links become impassable. The scenarios shown in the figure are based on 1-in-10-year flood events, considering plausible losses of network connectivity due to flooding based on network links becoming impassable. Travel time for trips that rely on the damaged links would increase by 108 percent and 32 percent in the Niger River delta and Indus plain, respectively. At national level (aggregate impact), travel time would increase by 4.7 percent and 1.2 percent in Nigeria and Pakistan, respectively. These results indicate how impacts depend on the interaction between the disruption location, how food is transported, and the exposure and vulnerability of transport.

FIGURE FLOOD SCENARIOS AFFECTING CRITICAL TRANSPORT INFRASTRUCTURE IN THE NIGER RIVER DELTA IN NIGERIA (A) AND THE INDUS PLAIN IN PAKISTAN (B)



(A) Nigeria flood scenario



(B) Pakistan flood scenario

SOURCE: Nelson *et al.* (forthcoming).[28]

ENSURING ECONOMIC ACCESS TO FOOD

The goal of building resilient agrifood systems is to ensure food security, and continuous access to sufficient, safe and nutritious food for all (see Resilience for what? in Figure 2). There is little to gain from food being available if people cannot access it. This section focuses on whether food available through domestic production and international trade is *economically* accessible to all of a country's population. If there is a strong supply and diversity of food capacity in a country but the demand is vulnerable, agrifood systems are also vulnerable. Having access to food is mainly an issue of prices and income. Not having a reliable and substantial income limits households' options during shocks, such as food price spikes, crop failures or loss of assets.[30] On the supply side, factors such as low levels of agricultural productivity, insufficient diversification, inadequate food storage and poor road infrastructure all drive up the cost of healthy diets. Beyond the direct impact of agrifood systems on the cost of diets, other interconnected systems, including health, environment and social protection systems also influence access to nutritious foods. Coherence between food systems and these other systems is thus needed, as further explained in the report.[31]

Agrifood systems' resilience and food security and nutrition will be higher in countries where the greatest percentage of the population has sufficient income to ensure food security following a shock to their livelihoods. Although the focus of this report is on the food pillar of agrifood systems, non-food agricultural production also plays a key role in generating livelihoods for small-scale producers and the agro-industrial sector, enhancing economic access to food. Box 9 summarizes the benefits that people derive from forests in terms of livelihoods.

Seekell *et al.* (2017) verify the extent to which per capita income of the poor is sufficient to access food by calculating the ratio of the income of the lowest quintile of the population of each country and the average cost of food.[34] They find that lower socio-economic groups still lack access to food in many countries. But what level of reliable income does a household need to absorb shocks and ensure food security? Following the approach of *The State of Food Security and Nutrition in the World 2021*,[31] we set the target of a healthy diet that includes foods from several groups with greater diversity within food groups to help prevent malnutrition in all its forms. However, this diet – also called cheapest healthy diet – is still largely unaffordable to approximately 3 billion people.

We estimate for each country the share of the population unable to afford this healthy diet after a reduction of one-third in real incomes (see Box 10 for a description of the approach). The choice of threshold is based on recent evidence of the impact of the COVID-19 pandemic on incomes. In Cambodia, more than 60 percent of people affected suffered income loss of one-third or more, while 90 percent suffered one-fifth or more.[35] Another nine-country study found that income loss is common across study sites, with 51 percent of respondents in Myanmar and 79 percent in Liberia reporting their income "reduced a lot" or "completely stopped".[36] A study of Brazilian doctors found that, of those whose income was affected, 31 percent experienced a reduction of 25–50 percent and about 60 percent, a reduction of over 50 percent.[37] These estimates indicate the thresholds assumed here are on the low end in terms of income reduction for those affected by a shock. This means the number of people we estimate to be at risk of being unable to afford a healthy diet after a shock is likely a lower bound.

FAO *et al.* (2021) estimates about 3 billion people, around 40 percent of the world's population, cannot afford a healthy diet.[31] According to this report, almost another 1 billion people will be at risk if a shock reduces their income by one-third in the 143 countries analysed (Table 2). Of these, most live in lower- and upper-middle-income countries, comprising 16 percent and 17 percent of the population, respectively. This share is much smaller in low-income countries, where already 88 percent cannot afford a healthy diet, let alone an income buffer of 50 percent when a shock reduces their income by one-third. In these countries, the challenge is having many more people unable

BOX 9 THE CONTRIBUTION OF FORESTRY TO THE LIVELIHOODS OF SMALL-SCALE PRODUCERS

Much of human society has at least some interaction with forests and their biodiversity. In low-income countries, about 1.2 billion people rely on agroforestry farming systems.[32] There, wood and non-wood forest products provide around 20 percent of income for rural households. More than 40 million people produce commercial fuelwood and charcoal for urban centres, with the production of fuelwood generating USD 33 billion globally in 2011. Taking into account direct and indirect employment, the formal forest sector provides an estimated 45 million jobs globally and labour income of USD 580 billion per year. Small and medium forest enterprises employ around 20 million people, generating USD 130 billion per year. The informal forest sector generated an estimated USD 124 billion in 2011, providing employment for an estimated 41 million additional people. The sustainability of forests and the biodiversity they contain is extremely important to people's livelihoods.

SOURCE: FAO. 2020.[33]

BOX 10 CALCULATING THE SHARE OF POPULATION AT RISK OF NOT BEING ABLE TO AFFORD A HEALTHY DIET

The percentage of people who cannot afford a reference healthy diet in 2019 was computed using the consumer price index-inflated cost of their diet as per FAO *et al*. (2021),[31] as well as the reference year of 2019 income distribution available from the World Bank PovcalNet database.[38] Percentages are then multiplied by the 2019 population in each country using the World Development Indicators of the World Bank to calculate the number of people who cannot afford a reference healthy diet this year.[39]

A healthy diet is considered unaffordable when its cost exceeds 63 percent of a person's income. Since people do not spend all their income on food, the 63 percent accounts for a portion that can be credibly reserved for food, based on observations that the poorest in low-income countries spend, on average, that amount of their income on food.[40]

The percentage of people who cannot afford a healthy diet is obtained based on this threshold and comparing the cost of their diet with country income distributions.

An additional buffer of 50 percent was added, representing the extra income needed for a healthy diet and all basic non-food expenditures after a shock reduces income, to estimate the share of people at risk of unaffordability. To illustrate, if the cost of a healthy diet is USD 3 per day, to meet food and non-food needs, an individual needs a daily minimum of USD 4.76 (USD 3 divided by 63 percent). To continue meeting those needs if a shock reduces income by one-third, a person's starting income needs to be USD 7.14. This affordability indicator is computed for 143 countries in 2019 as follows:

$$(1+\text{Buffer}) \times \frac{\text{Cost of the diet}}{0.63}$$

to even afford a basic energy-sufficient diet meeting calorie needs if incomes are reduced by one-third (Box 11). The incidence of similar vulnerability to shocks is only 1 percent in high-income countries.

Most people at risk of not being able to afford a healthy diet after an income shock live in Eastern and South-eastern Asia (398 million), Southern Asia (303 million), Latin America and the Caribbean (85 million) and sub-Saharan Africa

(81 million). The remainder live in Northern Africa and Western Asia (60 million).

Economic access to a healthy diet is most interesting when considered at national level. Figure 6 brings together measures of economic access to a healthy diet and the DSFI for fruits and vegetables (in tonnes). The horizontal axis shows the share of the population that cannot afford a healthy diet and the vertical access those at risk of not being able to afford it if incomes drop by one-third. The size of the bubbles represents the DSFI value for tonnes of fruits and vegetables. Including the DSFI for fruits and vegetables is informative because they are essential to a healthy diet and, if availability is limited, they are likely to have an impact on the affordability of a healthy diet.

Countries are distributed along an inverted U, and in many (especially in sub-Saharan Africa), more than 80 percent of the population cannot access a healthy diet and are in dire need of greater affordability (orange oval). This challenge is compounded by limited variety of fruits and vegetables (the bubble is quite small), key to a healthy diet. As well as a large share of the population who cannot afford a healthy diet, many countries have large sectors at risk of not being able to afford one if their income drops by one-third (yellow oval). This is a particular concern in Asian countries: Bangladesh, India, Indonesia, Pakistan and the Philippines.

Other countries, mostly high-income, are better able to guarantee economic access to healthy diets (green oval). Unexpectedly, in some countries, mostly middle-income, where two-thirds or more of the population can afford a healthy diet in normal times, a large share of the population is at risk of not being able to afford one after an income drop of one-third (blue oval). This is particularly the case for Latin America and the Caribbean where it is alarming that over half of the region's workers are in the informal sector, resulting in lower-quality and more vulnerable jobs. As they lack labour contracts or access to unemployment insurance and rely on day-to-day work that cannot be carried out from home, these workers are especially vulnerable to income fluctuations following shocks, such as with the COVID-19 pandemic.[41]

These results can deliver a more comprehensive picture of the resilience of national food systems, indicating that the DSFI and buffering capacity of household incomes are complementary measures of absorptive capacity. Countries with high absorptive capacity in both are mostly high-income countries. These are less likely to put in place emergency measures to guarantee a healthy diet. Countries with low values in both are prone to major disruptions in times of crisis, especially if food prices increase. Intermediate situations warrant revisiting the strengths and weaknesses of food systems to tailor interventions.

A broad share of the world's population is vulnerable to food insecurity and malnutrition when confronted with an income shock – another strong reason to build resilient agrifood systems on the supply and demand sides. Such vulnerability is due to limited incomes, combined with the cost of a healthy diet and its unaffordability. While the problem of limited incomes for many people is not due only to what happens in agrifood systems, on the other hand, the cost drivers of a healthy diet are evident throughout the food supply chain, within the food environment and in the political economy that shapes trade, public expenditure and investment policies.

Tackling these cost drivers will require major transformations in agrifood systems, trade-offs and synergies for different countries with no one-size-fits-all solution.[42] For nutrition knowledge and behaviour change to effectively influence choices, price and income constraints must be addressed.[42] Many countries need to rebalance their agricultural and nutrition-sensitive social protection policies for efficiencies at all stages of the food supply chain and to make healthier diets more affordable for vulnerable populations. This, in turn, would help them address the problem of limited incomes which, as mentioned, is not due only to agrifood systems. The effect of these policies and programmes in increasing affordability will depend, *inter alia*, on effective targeting, adequate transfer amounts and modalities, and integration of nutrition-specific components. ■

TABLE 2 INDICATORS OF UNAFFORDABILITY OF HEALTHY DIETS

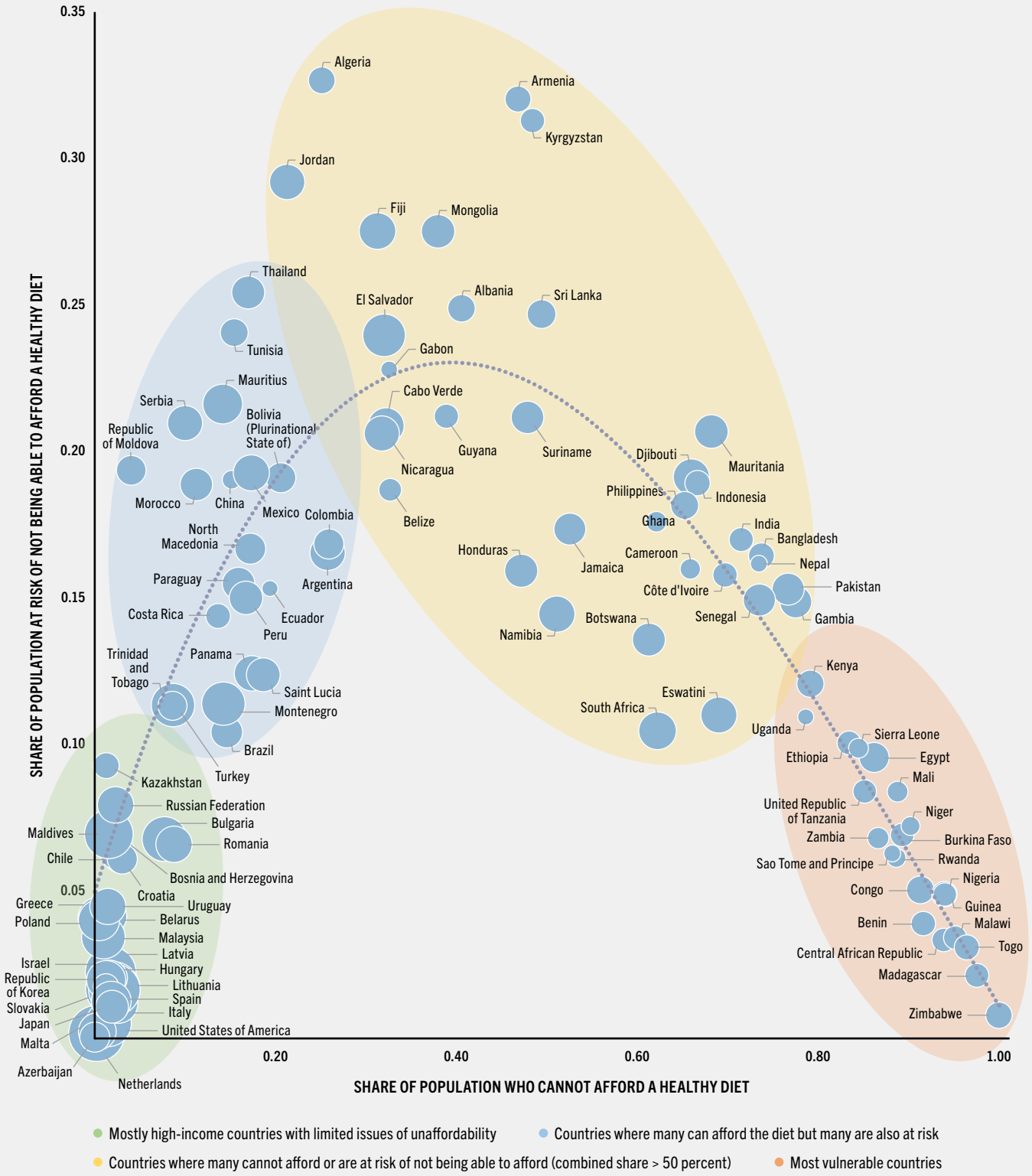
	Number of people unable to afford a healthy diet in 2019		Number of people at risk of unaffordability of a healthy diet if incomes are reduced by one-third	
	Percent	Total number (millions)	Percent	Total number (millions)
WORLD	**41.9**	**3 000.5**	**13.4**	**956.4**
Central Asia	16.9	5.8	18.1	6.2
Eastern and South-eastern Asia	23.9	530.0	18.0	398.0
Europe	1.7	12.0	3.1	22.0
Latin America and the Caribbean	19.3	113.0	14.5	85.0
Northern Africa and Western Asia	45.0	178.0	15.1	60.0
Northern America	1.4	5.1	0.5	1.7
Oceania	1.8	0.5	0.9	0.2
Southern Asia	71.3	1 282.0	16.8	303.0
Sub-Saharan Africa	84.7	875.0	7.8	81.0
COUNTRY INCOME GROUPS				
Low-income	87.6	463.0	6.9	37.0
Lower-middle-income	69.6	1 953.0	15.9	447.0
Upper-middle-income	21.1	568.0	17.1	460.0
High-income	1.4	16.0	1.1	12.0

NOTES: The table shows the number and share of people who cannot afford a healthy diet, or who are at risk of not being able to afford one if a shock reduces their income by one-third, by region and income group in 2019. The 2019 cost of a healthy diet is taken from FAO *et al.* (2021).[31] See **Annex 1** for methodology and data sources and **Annex 3** for the results for the full set of countries.
SOURCE: FAO elaboration for this report.

BOX 11 MANY CANNOT AFFORD – OR ARE AT RISK OF NOT BEING ABLE TO AFFORD – AN ENERGY-SUFFICIENT DIET

In times of crisis, it may be challenging for many to be able to afford an energy-sufficient diet, consisting mainly of starchy staples that provide adequate energy for a day's work. This diet is considerably cheaper because it does not provide all the essential nutrients of a healthy diet; yet, many cannot afford it or are at risk of not being able to afford it. The cost of the energy-sufficient diet was used to calculate its affordability, following the same approach as for the affordability of a healthy diet. Globally, about 177 million people cannot meet basic dietary energy requirements, with an additional 265 million at risk of not being able to afford as well if their incomes fall by one-third. Vulnerability to income shocks for meeting basic dietary energy requirements is concentrated in low-income countries, although not exclusively. In both South Africa (lower-middle-income) and Zambia (lower-middle-income), 14 percent of the population is at risk if their income drops by one-third (see Annex 3), on top of the 18 percent and 31 percent, respectively, who cannot afford such a diet even in normal conditions. When even the cheapest diet is beyond reach for many, increasing incomes of the vulnerable population is critical.

FIGURE 6 PLACEMENT OF SELECTED COUNTRIES BASED ON THE LEVEL OF ECONOMIC ACCESS TO A HEALTHY DIET AND DSFI FOR TONNES OF FRUITS AND VEGETABLES, 2016–2019



NOTES: The horizontal axis represents the share of population who cannot afford a healthy diet, while the vertical axis is the share of population at risk of not being able to afford one if a shock reduces their income by one-third or more. The size of each country's bubble indicates the value of the DSFI (see Box 5) for tonnes of fruits and vegetables. To simplify graphic presentation, 20 high-income countries with very low levels of unaffordability (up to 1 percent) were dropped. The DSFI refers to 2016–2018 averaged data and the economic access indicator refers to 2019 data. See **Annex 1** for methodology and data sources and **Annex 3** for the results for the full set of countries.
SOURCE: FAO elaboration for this report.

CONCLUSIONS

This chapter introduced a set of national resilience indicators that express the vulnerabilities and risks to agrifood systems' functions. It assessed four dimensions that are key for agrifood systems in dealing with a disturbance: (i) the robustness of primary production; (ii) the availability of food; (iii) physical access to food; and (iv) economic access to food.

Findings indicate that, while a large part of the world population lives in countries where food can be sourced and made available quite flexibly, there is substantial scope in many countries for improving economic access to healthy diets, especially when incomes are affected by a shock. This type of challenge has been very evident among households affected by large systemic shocks, such as the COVID-19 pandemic.[42] Many governments and donors were concerned that the pandemic would force a shutdown of supply chains and national agrifood systems more generally, requiring action to step in and replace the market. Considering the massive scale of the market and food demand, this would have been neither possible nor necessary in many cases, given the steps agrifood systems' actors took to adapt and build resilience.[43] Instead, the major impact of the pandemic on agrifood systems' actors and their food security has been on incomes and associated purchasing power.[1] In many cases, the cost of a healthy diet is higher than the international poverty line, established at USD 1.90 purchasing power parity (PPP) per day. This puts economic access to sufficient, safe and nutritious food beyond the reach of many living below or just above the official poverty line, especially in low-income and lower-middle income countries.

The availability of food in general appears far less vulnerable to shocks than consumers' economic access to food. Thus, for agrifood systems to become more resilient, the factors driving up the cost of food must be addressed. In terms of which types of diversity matter most for a country's dietary flexibility, there is considerable variation in: the mix of domestic production; the balance between imports, domestic production and stocks; and the number of trading partners. Examining the DSFI indicator, this chapter offered areas of intervention to strengthen resilience in food supply and ensure multiple pathways exist to make nutritious food available.

In terms of the capacity of the primary production sector to absorb demand shocks affecting domestic and export markets, findings indicate a significant contribution from domestic market diversity to countries' overall absorptive capacity. Countries whose agrifood systems include a significant share of exports are mostly high-income countries with a strong agricultural base. There is also a correlation between a country's primary flexibility and income and its agricultural base. However, exceptions exist, indicating other factors play a role.

Much work on the indicators remains to be done to improve our understanding of what makes agrifood systems resilient. The indicators are neutral when it comes to the resilience of midstream agrifood supply chains (see Annex 1) and do not capture the role of non-food components in determining resilience. Fisheries and aquaculture are also excluded from the production flexibility and transportation network indices due to data constraints, despite being some of the world's most diverse farming practices in terms of number of species. More work is also needed to represent other capacities that make agrifood systems resilient, namely the ability to prevent, anticipate, adapt and transform. The indicators presented in this chapter provide important new insights into the ability of national agrifood systems to absorb environmental, social and economic shocks.

At national level, resilience is, in part, understood as maintaining systems' functions during a disturbance. Since systems are typically composed of, *inter alia*, a multitude of farms, business enterprises, value chains and institutions, national agrifood systems' resilience does not necessarily reflect the resilience of individuals. How value chain actors react to shocks and stresses is a critical aspect of resilience in agrifood systems and the focus of the next chapter. ■



EGYPT
Labourers unloading a truck of tomatoes for distribution to retail.
©FAO/Heba Khamis

CHAPTER 3
RESILIENCE OF FOOD SUPPLY CHAINS

KEY MESSAGES

➔ The continuous functioning of food supply chains – as well as the input and service supply chains connected to them – is essential to ensure a smooth, stable and sustainable flow of food to all.

➔ The impacts of shocks and stresses vary by type of food supply chain. Transitional chains tend to be long with many small and medium agrifood enterprises (SMAEs) particularly vulnerable to shocks from various sources and limited resilience capacities.

➔ Diverse, redundant and well-connected food supply chains enhance agrifood systems' resilience by providing multiple pathways for producing, sourcing and distributing food.

➔ Building resilience in food supply chains requires costly investments and will entail trade-offs with efficiency and with inclusiveness; mostly large companies with sufficient investment capacities can overcome the trade-offs with efficiency while many SMAEs risk being pushed out of business as they lack these capacities.

➔ Improved food supply chain coordination and organization, through consortia and agri-territorial tools, can enable SMAEs to overcome size constraints and create synergies between resilience, inclusiveness and efficiency.

➔ Government support is key to create an enabling environment for improved coordination in food supply chains and to overcome trade-offs, for example, through public investments in infrastructure and research as well as developing mechanisms to connect an upgraded research and education system to the agrifood sector.

Chapter 2 took stock of agrifood systems' resilience at national and subnational levels. It analysed key factors that help determine the vulnerabilities of national agrifood systems: (i) the diversity of primary agricultural production and its marketing channels; (ii) the diversity of available food, including from imports and stocks; (iii) transport networks that ensure physical availability of food locally; and (iv) people's economic access to food. It concluded that diversification, in terms of trade partners and foods produced domestically, stocked and imported, coupled with robust food transportation networks, gives national agrifood systems a certain degree of latitude and overall capacity to absorb shocks.

The resilience of national agrifood systems also depends on how supply chains function. This chapter focuses on food supply chains because of their prominence in agrifood systems and because non-food agricultural products, which are also part of agrifood systems (see Chapter 1), are viewed as exiting that system once they enter non-food supply chains. The food component of agrifood systems is far larger than the non-food part: in 2018, primary food products accounted for more than 97 percent of total primary agricultural production value, excluding forestry.[1] The primary sector also only generates a small part of the total food

value reaching consumers. Using data from 61 countries, over 2005–2015 and covering 90 percent of the world economy, a recent study finds that only 16–38 percent (27 percent as a global average) of the value of home-consumed foods goes to agricultural producers.[2] This is in line with a previous estimate suggesting that, in Asia and Africa, the value of primary food production is only 40 percent, while midstream and downstream segments capture 40 percent and 20 percent, respectively.[3, 4]

Diverse and well-connected food supply chains are better able to absorb and recover from shocks and stresses, contributing to more resilient agrifood systems. Resilient food supply chains also enhance growth opportunities for farmers and businesses and guarantee a stable and continuous flow of food to all (see Figure 2).

Being one of the main components of agrifood systems, this chapter's focus is on food supply chains. Building on a simplified framework, it describes its main constituent elements and the interactions within. It outlines how farms and agrifood businesses, such as processors and wholesalers, source inputs and sell their outputs, and whether they are connected to consumers in ways that allow consumer preferences to be expressed and met. It also identifies the main drivers of change in food supply chains – such as credit, consumer demand, prices, logistics, risk perception, technology, policy developments and disturbances hitting systems. While the resilience of *food* supply chains is the explicit focus, it must be recognized that shocks and stresses affecting *non-food* primary production can also propagate through, and impact on, sectors of the economy that rely on primary non-food products as inputs.

Acknowledging there are different types of food supply chains around the world – classified as traditional, transitional and modern – and within them businesses of varying scales, the chapter describes business strategies and priority action areas that facilitate adjustment during a shock and contribute to resilience. It presents practical examples from around the world, with recommended policy directions and interventions that build and strengthen food supply chain resilience. ■

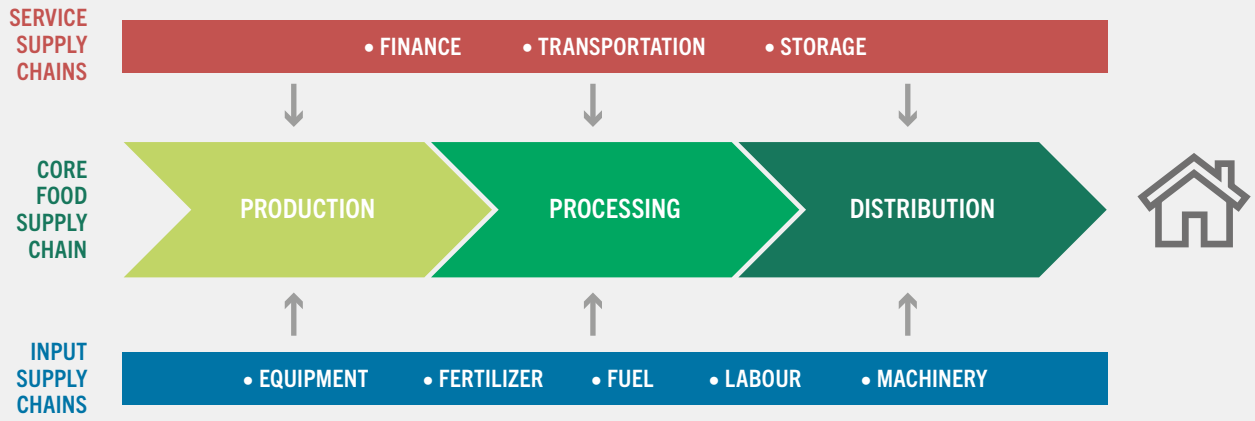
SETTING THE STAGE – A SUPPLY CHAIN PERSPECTIVE OF RESILIENCE

The importance of resilience in food supply chains is gaining increasing attention with the rise in the intensity and frequency of shocks[5] and longer, more sophisticated and potentially more vulnerable chains serving rapidly growing cities. Building resilient food supply chains is necessary to face disturbances and safeguard the livelihoods of those involved in supply chains as well as people's food security and nutrition, the ultimate goals of resilient agrifood systems.

A key point is that a food supply chain comprises interconnected activities performed by various actors within and outside the chain. All are vulnerable to diverse risks, shocks and stresses. As well as being connected along the food supply chain, farmers, processors and distributors depend on actors in lateral chains to supply inputs and logistics and transport services outside agrifood systems. These are exposed to shocks and stresses, whose impacts can disrupt food supply chains.

Primary producers and other food supply chain actors produce, process and distribute food using resources, innovations and technology for their own benefit. Their objective is to improve their well-being, subject to credit constraints and risks they face. To remain economically viable, they need to use resources efficiently but also be resilient in the face of shocks and stresses. However, the interconnection of food supply chains actors implies that resilience at any stage of a supply chain depends on the overall performance along the chain. The decisions made by one group of actors have implications for the others. A shock to any segment in the supply chain rarely stays within that segment but will probably spread to and affect other segments upstream and downstream. During the COVID-19 pandemic, lockdowns led to reductions in consumer incomes and food demand, negatively affecting supply chain

FIGURE 7 SCHEMATIC REPRESENTATION OF A FOOD SUPPLY CHAIN AND ITS CONNECTION TO INPUT AND SERVICE SUPPLY CHAINS



SOURCE: FAO elaboration based on FAO. 2017;[7] Reardon & Zilberman. 2021.[8]

actors upstream, from vendors to wholesalers and eventually to producers. Food supply chains are thus complex socio-economic systems with interactions at different levels, distances and times, all of which must be considered when addressing resilience.[6]

Since food supply chains are connected to supply chains for inputs and for services, all three must be resilient to shocks and stresses if agrifood systems are to function efficiently and deliver sufficient, safe and nutritious food. The structures of supply chains will affect how shocks and stresses impact on them and how they react to them.

Figure 7 is a schematic representation of the three supply chains. It shows how agricultural commodities are produced at upstream farm level, then supplied to the midstream agrifood businesses that process them for subsequent shipment to downstream retailers. These three main functions, crucial to almost any food supply chain, use inputs and services from input and service supply chains. A shock to any part of these interconnected supply chains can have negative impacts on the performance of the food supply chain. The responses of suppliers to disruptions are decisive for the overall functioning of the food supply chain. Resilient suppliers recover more quickly and enhance overall food supply chain resilience.

Input and service supply chains interact with food supply chains at every stage. Input supply chains provide variable inputs, such as seed, fertilizer, fuel and labour, and quasi-fixed inputs, such as farm machinery, milling machines and coolers for perishables. Service supply chains include actors and activities for movement of inputs, outputs and factors such as transport and storage operators, connecting production to consumption. For example, in Nigeria, a chain of third-party logistics providers transports 75 percent of the maize harvest almost 1 000 km from farmers in the north to wholesalers in the south. Similarly, almost all wholesalers rely on the same providers for storage.[8]

Even labour and credit can be viewed as supply chains and not just production factors, because a chain of decisions and actions beyond the

control of the direct providers can influence their availability. Labour availability can depend on mobility of people over long distances and recruitment practices. This makes its availability vulnerable to various disruptions affecting, for example, transportation, recruiters or mobility as with the COVID-19 pandemic.[8] Formal and informal credit services are a function of socio-economic conditions, and availability can be affected by financial shocks and other crises, in addition to government monetary and fiscal policies.

Most research and policy debate on agrifood systems' resilience has focused on input supply chains for the farm segment.[4] However, this segment constitutes only a small part of the food economy, ranging from 16 percent to 37 percent,[2] the rest being post-harvest, processing and distribution segments.[3, 4] Each midstream segment also relies on input supply chains for labour, water, physical inputs and equipment.[3, 4]

The fact that disruptions to any of these lateral chains can have devastating impacts on food supply chains, as well as on non-food agriculture, illustrates how agrifood systems can be negatively affected by disruptions to other systems such as transport and industry. The energy sector is a clear example: a shock that stops oil freighter traffic can reduce fuel supply and bring food supply chain operations to a grinding halt. The COVID-19 pandemic provides further examples: restrictions on labour mobility in the early weeks severely affected fruit harvesting in many countries; classifying wood production as non-essential in some countries hampered fruit supplies by stopping crate production; and the decision by many governments to declare wholesale markets essential but much of the logistics supply chains non-essential caused major disruption to food supply chains.[9]

Types of food supply chains

Food is produced, processed and distributed by supply chains that are in continuous transformation, driven by changes in the socio-economic, biophysical and technological spheres. Technological innovation, demographic changes and economic development, for example, spur the creation of new food supply chains or the transformation of existing ones. They determine the conditions that shape the three broad types of agrifood systems outlined in Chapter 1: traditional, transitional and modern.

This categorization can help policymakers identify broad priority areas for action within different food supply chains, as these have distinct levels of vulnerability to shocks and stresses. Indeed, the vulnerabilities and the resilience capacities of food supply chains are largely shaped by their structural characteristics and product attributes, with supply chains relying on SMAEs experiencing shocks differently from those dominated by large-scale enterprises. Fresh produce supply chains are more susceptible to short-term market fluctuations compared to, for example, those specializing in cereals, especially if cold storage is not available. The most appropriate resilience strategy will depend on the vulnerabilities of each food supply chain to different risks.[10] Before discussing how shocks and stresses affect food supply chains, it is useful to recall the key characteristics of each one.

Traditional supply chains

Traditional food supply chains are spatially short with a small number of intermediaries. They handle seasonally produced food, mainly from local small-scale producers, marketed locally. The share of staples is high, while that of value-added produce in post-harvest segments is low. Only basic processing, such as fruit drying, flour milling or dairy processing, takes place, usually in the home. Wholesale and logistics supply chains are small-scale, since food does not move long distances and micro and small agro-processing enterprises (the smallest of the SMAEs) dominate. Food processing falls disproportionately on women: in many African countries, women spend on average four hours per day pounding grain.[11] A lack of product diversification, quality and safety standards, and economies of scale constrain traditional systems. Technology is labour-intensive, spot market relations dominate and contracts are rare. Concentration of supply chains usually only occurs when governments subsidize cereal production through parastatals to supply staples to growing urban populations.[8]

BOX 12 THE IMPACT OF THE COVID-19 PANDEMIC ON SMAEs

The resilience of SMAEs requires special attention, given their critical role in agrifood systems and food supply chains, particularly those serving vulnerable, low-income populations in low-income and middle-income countries. They connect farmers to markets, add value to local agricultural produce and create employment opportunities for women and young people. Rough estimates suggest that domestic supply chains account for 75 percent to 90 percent of food consumed in Southern Asia and sub-Saharan Africa, with around 80 percent supplied through SMAE-dominated chains and the rest through large-scale enterprises.[10]

SMAEs tend to be labour-intensive with limited capacity to manage risks associated with product perishability and seasonality.[12] Being heavily interdependent,[13, 14] disruption anywhere in the supply chain can produce a harmful cascading effect. SMAEs also have a unique strength: embedded in local communities, they are better able to adapt services, such as transport, food processing and distribution, to local needs,[15] making important grassroots investments in rural areas.

The demand- and supply-side shocks caused by the COVID-19 pandemic had devastating consequences for SMAEs, as millions of supply chain workers lost their jobs and livelihoods.[16] Labour shortages and transport interruptions had strongly negative impacts on SMAEs because of their unique characteristics, such as labour-intensive operations, resource scarcity, perishable products, seasonal production systems and greater vulnerability to weather.[12] The impacts varied for different products. For example, lockdowns in Pakistan caused the most serious disruptions in the fresh produce value chain. With harvesting and transport blocked, huge quantities of fresh fruits and vegetables were left to rot in the fields.[17]

Demand-side risks also materialized owing to gaps between a firm's projected and actual customer demand, leading to costly shortages and lost sales and market shares. In a recent survey of 363 SMAEs in 17 countries, more than 90 percent reported reduced sales, and difficulties accessing inputs and paying staff.[18] Furthermore, due to their informality, many SMAEs were excluded from government stimulus and recovery plans that favoured larger enterprises.[19, 20]

Transitional supply chains

Transitional supply chains are longer, with many midstream intermediaries such as processors, wholesalers and retailers, who add value and move food across rural and urban areas. Short supply chains still dominate in highly perishable product markets, such as dairy and leafy vegetables. The share of value-added products in post-harvest segments (wholesale, processing, logistics and retail) is moderately large, but heavily dominated by SMAEs. Processed food, mainly produced and retailed by SMAEs, is also important in diets as the opportunity cost of women's time has increased with out-of-home employment. Home processing, such as hand pounding of grain found in the traditional phase, has given way to milling SMAEs, alongside a few emerging large-scale companies.[8] SMAEs co-exist with microenterprises, mostly large numbers of street vendors selling prepared dishes;[11] these were particularly affected by mobility restrictions during the COVID-19 pandemic (Box 12).

Fragmentation is a key characteristic of transitional supply chains, which rely on a multitude of small-scale primary producers and SMAEs. Thanks to low labour costs, they use labour-intensive technologies, although machines are also used. Customized harvest and other agronomic and trading services support small-scale producers of food and non-food products to access intensification technologies, skilled labour and services – for

example, traders providing sprayers for mango producers in Indonesia, or mobile teams providing combine harvesting for rice farmers in China.[21, 22] Spot market relations dominate, but contracts are beginning to emerge in domestic and export supply chains.

Cereals and other staples are a much smaller share of the total food economy because, as incomes increase, people consume fewer starchy staples and more nutrient-dense, processed and expensive foods. Food production diversification, particularly into animal and horticultural products, is therefore higher. These products have relatively long supply chains, with more rigorous transport and cold storage requirements, increasing their vulnerability to disruptions. Longer supply chains of perishables make food safety an urgent issue, as quality standards are often difficult to enforce.

Modern supply chains

Modern supply chains serve large urban populations. They can be long or short depending on the primary production to meet households' food demands. As demand for staples declines, they provide mainly perishables, such as horticultural and animal products. These may be sourced locally, but can also be produced far from cities and shipped frozen or chilled. As demand for animal products increases, there is also an increase in the vulnerability of the food supply to animal diseases, antimicrobial resistance and food safety issues.

Supermarkets and large processors transact directly among themselves and, in some cases, buy directly from producers or wholesale markets which are less important than in the transitional stage. Cold storage, packaging and private quality standards applied to suppliers are also much more common. The supply chain is highly concentrated and multinationals dominate. SMAEs can remain competitive if they diversify production or if high transaction costs discourage large companies from operating in remote or less developed areas. Technology is largely capital-intensive, and information-based tools such as global positioning system (GPS) and drones are more common. Spot market relations are found in the fruit and vegetable sector, but contracts dominate elsewhere. Downstream of modern chains is the food service sector comprising formal restaurants and fast-food chains.

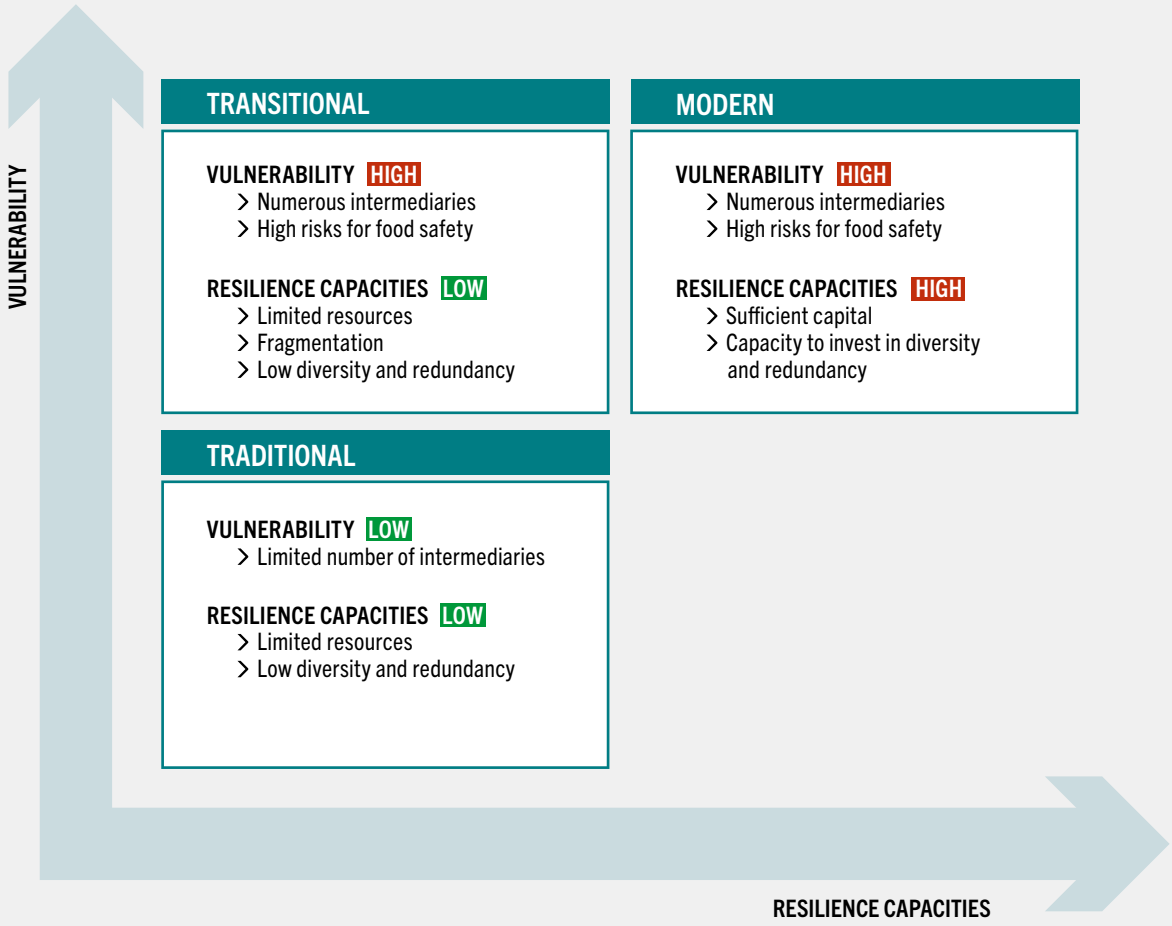
Modern supply chains have emerged, albeit unevenly, in low-income regions over the past three decades. Southern Africa, Eastern and South-eastern Asia and Latin America have seen extensive penetration by food industry multinationals and large supermarkets, although they are still only emerging in the rest of sub-Saharan Africa and in Southern Asia. Modern supply chains also dominate in international trade.

Different food supply chains are affected by, and cope with, shocks differently

Agrifood systems and their food supply chains experience various shocks and stresses. They stem from different sources in the socio-economic and natural environments and can be natural or human-made. Understanding which ones are more likely to strike a food supply chain is the key to developing resilience capacities that can mitigate impacts and help the supply chain recover.

The marked differences between the three types of food supply chains – traditional, transitional and modern – imply that the same shock or stress can have very different impacts. The vulnerability and the resilience capacities of any food supply chain will be shaped, at least partially, by its characteristics. Figure 8 illustrates, in a very simplified way, the overall levels of vulnerability and resilience to shocks for food supply chains. The impacts of shocks and stresses will be determined by the vulnerability–resilience combination of any supply chain in addition to the nature of the shock itself. For example, restrictive government policies to contain the spread of COVID-19 affected labour mobility and the supply of labour to farmers, processors and distributors along food supply chains as well as their linked input and service supply chains (see Figure 7). However, the impacts are varied among the three types of supply chains. Being short, traditional supply chains may be

FIGURE 8 **A SIMPLIFIED ILLUSTRATION OF THREE TYPES OF FOOD SUPPLY CHAINS REGARDING VULNERABILITY TO SHOCKS AND STRESSES AND THEIR RESILIENCE CAPACITIES**



SOURCE: FAO elaboration for this report.

least affected because they do not require much mobility. They are also less exposed to shocks caused by disruptions to midstream input and service supply and tend to rely on only a few, mostly local, intermediaries.

The recent literature on food supply chains provides interesting examples on how COVID-19 disruptions have enabled traditional supply chains to provide alternatives to long, modern and transitional chains experiencing disruptions.[23-28] With closed borders and movement restrictions within and between countries, many consumers had no alternative to traditional food sectors, which are less dependent on large-scale processing units and bulk transport and rely mostly on local labour.[29] Despite limited financial capacities, many supply chains proved to be nimble in their responses, especially in high-income countries, where capacities are higher and infrastructure is robust.[24, 25, 28]

Compared to traditional chains, transitional and modern supply chains can be seriously affected by shocks to midstream operations, which may be numerous between primary

food production and its final delivery to consumers. There are also differences between transitional and modern supply chains that can determine the impact of shocks and stresses. Modern supply chains comprise mainly large-scale businesses with easier access to capital than SMAEs in transitional supply chains. Since large-scale operators are generally capital-intensive, they can more easily switch between markets and increase their capital–labour ratios to reduce dependence on hired labour.[10, 30] For this reason, modern food supply chains were more resilient than transitional ones to COVID-19 shocks – mostly labour mobility and trade restrictions – because they operate globally and can adjust to disruptions geographically and temporally and, to some extent, can adapt product composition.[10] However, their intensive use of energy for cold storage and mechanization makes them highly vulnerable to shocks that hit the energy sector.

The fragmented nature of transitional food supply chains, with their multitude of SMAEs and heavy reliance on labour, makes them especially vulnerable to labour supply shocks. Case studies in Australia, Egypt, Pakistan and the United Republic of Tanzania show this was evident in the restrictions early in the COVID-19 pandemic.[17, 20] The impact on SMAEs was uneven according to their products, diversity of destination markets and overall capacity to deal with shocks. Transport risks can potentially disrupt all SMAEs, although case studies from Australia[12] and Egypt[20] show that those dealing with perishable foods were disproportionately affected. In Egypt, fresh fruit SMAEs in domestic and multiple export markets perceived less risk from the pandemic because they could move their products from one export market to another or redirect them to the domestic market.[20]

Climate risks and shocks, highly relevant for the agrifood sector, also affect food supply chains differently. The heavy reliance of traditional food supply chains on local sourcing of inputs and local markets for produce make them the most vulnerable to climate shocks. Smaller enterprises and small-scale producers comprising traditional supply chains, lack the cost advantages of large companies. Without economies of scale, traditional supply chains incur higher production costs, making them less competitive and exposing them to exogenous supply and demand shocks, a risk that also affects transitional supply chains.[27]

Transitional and modern supply chains are less vulnerable to local shocks because they have access to more diversified input sources and output markets. Modern supply chains are generally less vulnerable to climate and environmental shocks than transitional ones, because large-scale firms can more easily impose protective measures such as biosecurity on primary suppliers.

Policy and socio-economic conditions matter for risks, and vulnerabilities and resilience capacities of food supply chains, and they vary considerably between countries. A study on the impacts of the COVID-19 pandemic in Australia, Pakistan and the United Republic of Tanzania found that, while food processing SMAEs in all three countries experienced increases in input prices, loss of buyers and shortage of skilled labour, Pakistani and Tanzanian SMAEs also suffered extreme financial pressure and difficulties accessing credit, which was not the case in Australia. As a result, many small processing plants closed in Pakistan and the United Republic of Tanzania, but not in Australia, where government support targeted the food sector and was critical to the survival of many SMAEs. The same study points to significant differences in adaptive capacity among SMAEs. Those in the United Republic of Tanzania and Pakistan continued conventional business practices due to lack of knowledge of alternatives, while most Australian SMAEs switched to e-commerce and omnichannel retailing, quickly adopting COVID-19 health measures such as social distancing and mask wearing. The capacities of Australian SMAEs, thanks in part to public support, allowed them to recover quickly from the initial shock, maintain and diversify their business, and invest in innovations. Table 3 indicates these options were very limited in Pakistan and the United Republic of Tanzania.[17]

TABLE 3 SUMMARY OF COVID-19 IMPACTS ON FOOD SUPPLY CHAINS IN THREE COUNTRIES AND SUBSEQUENT ADAPTATIONS

		Australia	Pakistan	United Republic of Tanzania
Impacts	Input price increase	x	x	x
	Labour shortages	x	x	x
	Shutdown of some SMAEs		x	x
	Loss of buyers	x	x	x
Adaptation measures	COVID-19-related safety measures	x		
	Switch to e-commerce	x		
	Business diversification	x		x
	Investment in innovations	x		

SOURCE: Ali. 2021.[17]

Traditional and transitional food supply chains are also more vulnerable because they comprise highly informal businesses. Small-scale, informal or semi-formal businesses are mostly family based and serve as the main source of revenues and incomes for many vulnerable segments of their societies, including owners and employees. They are thus unlikely to disappear, even when illegal or state-oppressed.[31] They are, however, at high risk of being hit by shocks, as seen during the COVID-19 closures. Informality also makes many actors in traditional chains invisible in national statistics, which means the impacts of shocks may go unrecorded, while crucial social protection programmes remain out of reach.[32] Although there are no official statistics on the degree of business informality in food supply chains, some estimates suggest it can be a serious challenge in low-income countries, where it is estimated that about 90 percent of food supply chain actors, including primary producers, operate informally. Informality is less common in middle-income countries, but still relatively high, at about 50 percent.[32] ■

MANAGING FOOD SUPPLY CHAIN RESILIENCE

When examining the resilience of food supply chains, it is important to note that a chain is not simply the sum of its actors or activities. Rather, it is a dynamic network of actors and activities under regular transformation, driven by factors like innovation and new technologies, demographic and income changes, and contractual and market relations. The socio-economic characteristics of agrifood firms and the way they interact with these transformations largely determine their capacities to prevent, anticipate, absorb, adapt and transform in the face of shocks and stresses. Transformation will always entail winners and losers. Similarly, shocks and stresses may have disastrous impacts on some actors in the supply chain while creating opportunities for others to transform and improve. A resilient food supply chain does not require all its actors to be resilient. One that continues to function and deliver its products in the face of disruptions can be considered resilient, regardless of what happens to individual actors.[8]

It is not enough to manage food supply chains with only business growth and optimization objectives in mind and to apply conventional risk

management tools. To build effective resilience, it is necessary to: recognize that shocks, stresses and their impacts on food supply chains can be highly unpredictable; and keep pathways to adapt and transform open. Transformative capacity is particularly important, albeit not the focus of the report; it provides a new lens to explore opportunities during a crisis, reveal ways to overcome hurdles, move forward and become even more resilient in the face of future challenges.[33, 34]

Building food supply chain resilience among agrifood businesses poses dilemmas in the design of policies and interventions. First, it often entails costly investments which may require trade-offs between resilience and efficiency. These are more problematic for smaller-scale producers and SMAEs, given their limited access to credit. A second trade-off is between resilience and inclusiveness: the resilience of some supply chain actors may involve putting others out of business. The rest of this chapter addresses these strategic issues, examining the incentives for resilience building within food supply chains and how resilience investment decisions are made, taking trade-offs into consideration. It also discusses government policies and interventions that may condition the capacity of food supply chains to implement these strategies, with a focus on the role of public policies.

Resilience-building strategies may imply trade-offs between efficiency and inclusiveness

Operating in all food supply chains, agrifood businesses are heterogeneous in terms of economic scale, input composition, technology use and outputs. The goods they produce range from bulk commodities to local niche items and differentiated products. They also have different capacities to bear risk and make important resilience-building investments. These capacities depend on the level of human capital, access to information and credit, and retained earnings, all typically a function of scale.[35] Firms draw on these capacities to diversify (e.g. inputs, logistics and downstream markets) or introduce redundancy as strategies to build resilience, depending on their operations.

Businesses producing differentiated products, competing on characteristics such as quality rather than cost, are more constrained when diversifying input sources than firms sourcing bulk and undifferentiated commodities. This is because producing quality products requires sophisticated technology and specific assets, for example, high-cost machinery that can only be used for a specific product or investments that have little relevance when shifting to different products.[36] This reduces the overall flexibility of the business, as moving to a new product may involve new costly investments. Companies producing quality products need to induce their input suppliers to make the required asset-specific investments, locking in suppliers through incentives and co-investments, so they comply with the company's standards and accept monitoring.

Given the constraints to diversifying input sources, companies may explore diversification in suppliers and sourcing from different zones, while investing in redundancy. An example of this would be an agrifood business establishing a network of suppliers in secondary and tertiary zones to serve as backups if those in the primary supply zone experienced a climate shock. This entails the expense of incentivizing suppliers to make asset-specific investments and organize supply chain infrastructure in each zone. The Charoen Pokphand Group in Thailand, the world's largest rice miller, has taken this approach, building two ports upriver from its primary facility to guarantee shipping access in the event of a typhoon. Only the largest businesses can afford this level of diversity and redundancy, unlike SMAEs, especially those in fragmented supply chains, which trade off efficiency and resilience. These SMAEs face financial and logistical constraints to such investments and yet remain efficient and competitive. However, their reliance on sourcing from fewer and closer zones exposes them to ripple effects if a shock hits their suppliers.

To reduce the trade-off, businesses may seek investment partnerships with other, complementary companies, such as intermediaries, but again, this is not feasible for all. For example, in a national market for

tomatoes, a business might source produce through specialized wholesalers with systematic relationships with suppliers in low-risk, high-capacity zones[37] and contractual relations with suppliers in zones with low transaction costs.[38] Investments may include search costs, setting up sourcing or input networks (including social capital investments), outlays on durable goods such as warehouses and ship berths, and market fees. These costs are a problem for most SMAEs who face the double challenge of needing to be resilient to shocks while also being competitive with larger enterprises.

Another way firms can diversify exemplifies a trade-off between resilience and inclusiveness. Large food processing companies may diversify their production mixes to include midstream supply inputs and other factors or increase their primary production to reduce reliance on small-scale producers who are vulnerable to shocks (e.g. climate or plant disease risks). This shift happened in Kenya and Zimbabwe during the 1990s, when vegetable exporters sourced half their produce from their own plantations and half from other large farms.[39] This is a trade-off between the exporters' resilience and economic inclusiveness, since small-scale producers are deprived of access to lucrative markets while large-scale firms gain agility.

Food supply chain businesses can diversify their logistics to avoid shocks such as the closure of ports and hurricane damage to transit areas. This entails, again, investment in private infrastructure or procuring space in public infrastructure (e.g. dedicated sections in shipyards, fuelling stations and ports), as well as investment in vehicles and containers, deemed too costly for most SMAEs.

Businesses may also need to address shocks that occur downstream in the food supply chain. During the COVID-19 pandemic, when food suppliers faced a sudden drop in customers shopping in stores or dining in restaurants, many diversified through e-commerce, using delivery companies who quickly adapted to the demand for home deliveries. While this was already a trend in many countries before COVID-19, the pandemic accelerated it,[10] although the pace varied according to infrastructure, managerial capacity and human capital.[17]

Essential to all these strategies is public infrastructure, such as roads, culverts, power lines, running water, irrigation schemes and ports. These are key to avert or buffer shocks, depending on the configuration and levels of robustness and redundancy. Upstream of the food supply chain, the capacity of agricultural producers to withstand shocks from climate change is at least in part determined by infrastructure availability and quality. Those in territories with well-developed infrastructure have greater capacity to bear shocks, especially when combined with farm-level access to irrigation, technology and information.

If primary food producers or agricultural territories are resilient to shocks, but partners in the food, input and service supply chains are not, the ripple effect of a shock, amplified by food supply chain connectivity and actors' interdependence, could lead to disruption to farmer livelihoods. This underscores the importance of resilience along all segments of food supply chains and their connected input and service supply chains. Public infrastructure, roads, power lines and irrigation networks need to be complemented by private or collective infrastructure provided by actors and companies in the lateral input and service supply chains, such as collection stations, large trucks and temperature-controlled warehouses. Businesses better able to make the investments and bear risks will more likely survive and outcompete those with less capacity, while those that fail to invest may be forced out of the market. The higher frequency of climate change or health shocks, such as the COVID-19 pandemic, will add further impetus to the competitive forces already leading to rapid concentration in the off-farm segments of food supply chains. Traditional and transitional chains, dominated by SMAEs and microenterprises, risk losing further ground to more advanced chains dominated by large-scale enterprises. This is a central issue when making trade-offs between resilience and inclusiveness:

the social cost of increased unemployment and lost livelihoods incurred as SMAEs are driven out of business may outweigh gains from the increased resilience of individual large-scale businesses.

Agrifood businesses, farmers and agricultural territories that are excluded lose a crucial link to urban and export markets – the main markets for their products. They find themselves in a poverty trap, where the confluence of market and climate changes can render resource-poor and infrastructure-poor territories especially vulnerable. When resilience falters, government support, including credit access, is necessary to address infrastructure failures and ease the constraints vulnerable businesses and farms face, not only to making investments to build resilience, but also to surviving in times of crisis.

The trade-offs in this section matter because efficiency and inclusiveness are both important elements of resilient agrifood systems, where the goal is to ensure food security and nutrition for all and sustain and improve the livelihoods of agrifood systems' actors. Careful consideration of trade-offs is necessary to minimize them or even, to the fullest extent possible, turn them into synergies through an enabling environment, investments and policies.

Enabling synergies between resilience, efficiency and inclusiveness for SMAEs and small-scale producers

Economic size is a key determinant of the resilience capacity of actors in the food supply chain. The limited resources of SMAEs and small-scale producers will often make their recovery more arduous when disrupted by shocks. Timely support, including access to credit, will be essential not only to help them survive in times of crisis, but to invest in interventions that address their vulnerabilities and build systematic resilience. In low-income countries, where traditional and transitional food supply chains dominate agrifood systems, better public infrastructure, and access to credit and information can create synergies between efficiency and resilience for SMAEs and small-scale producers.

Well-configured, robust and redundant public infrastructure is essential to avert or soften the impacts of shocks. For example, the installation of concrete dikes and culverts can help farmers overcome drought. But this infrastructure can also be important for resilience to extreme weather events, such as hurricanes and storms, by preventing floods from washing out roads and blocking food movements along the food supply chain.[40] While improved infrastructure enhances connectivity and reduces transaction costs, it also enhances resilience along and across food supply chains by alleviating climate shocks and enhancing the absorptive capacity of agrifood businesses.

Along with investments in physical infrastructure, large investments in strengthening institutions and in human capital are often essential. For example, during the bovine spongiform encephalopathy ("mad cow disease") crisis, which provoked a massive consumer shift towards chicken and pork in various high-income countries, beef businesses in the United States of America that could show traceable supply chains and differentiate their beef products had better chances of survival.[41] During the COVID-19 pandemic, phytosanitary institutions in South Africa, in collaboration with the private sector, were crucial in the citrus industry's response to the sudden additional biosecurity requirements of their main market in Europe.[42] Managerial capacity was also important during the pandemic for a rapid shift to e-commerce and digital tools to diversify market outlets.[17] Digital infrastructure, technology research and development, and a business enabling environment are also key areas for support.

Enhancing the resilience of food supply chains requires governments to address their high informality, especially in low-income countries. Despite their importance to rural economies, informal food enterprises – mostly micro-entities and often family based – are at risk of being left behind owing to limited resources and assets and lack of access to credit and social protection. It is assumed

small-scale entrepreneurs earning a basic livelihood have no aspiration to grow nor the resources to reinvest in their businesses.[43] The policy response to the informal sector is often ambiguous and inconsistent, leading to various forms of support, repression and neglect that fluctuate over time.[44] However, survey evidence from Rwanda, Senegal and South Africa shows these businesses are held back solely by institutional barriers and lack of resources – equally true for male and female owners, who reported nearly the same level of aspiration.[43]

Governments can facilitate coordination and organization within food supply chains to allow actors to enhance their resilience capacities. One approach is to form consortia, in which SMAEs pool resources and overcome scale-related constraints, to respond better to climate risks and other shocks. While climate risks cannot be totally avoided, social capital through inter-organizational relationships in networks or strategic alliances among SMAEs could mitigate their negative effects. Such interactions among consortia can generate relational, structural and cognitive capital, promoting more robust and effective risk management through resource pooling.[45]

Access to modern technologies, know-how and equipment may be out of reach of individual SMAEs but facilitated through collective action and resource pooling. Policies to enhance SMAE resilience should encourage resource sharing and trust building to create the synergies that improve efficiency, avoid duplication of efforts and increase access to additional resources.

One way to encourage coordination and enhance relational capital is through territorial development tools.[46, 47] A study on the impact of the pandemic on SMAEs in China finds that rural counties with higher concentrations of industrial clusters were less adversely affected by the shock of COVID-19 lockdowns, as measured by the entry of new enterprises and the performance of incumbents. In these dense areas, incumbents shared risks and helped one another overcome barriers for new entrants from their home towns.[48]

Consortia or other forms of cooperation and coordination can increase the scale, visibility and influence of a small business, which may improve access to private and government funding. In countries where credit markets are imperfect or underdeveloped, enhancing industrial clusters can ease credit constraints for SMAEs.[48] The benefits of relational capital can also facilitate access for SMAEs to international markets, opening up new business horizons.[45] This can encourage marketing diversification, a valuable source of resilience in times of crisis. A study of the performance of SMAEs in Egypt found that heavy dependence on just a few destination markets left them vulnerable during rapid changes and sudden shocks. It recommended that national policy for building SMAE resilience focus on strengthening their role in national markets while also promoting export market diversification and creating an institutional and regulatory framework that supports SMAE competitiveness in global markets.[20] In this regard, as suggested in Chapter 2, establishing new free trade areas and expanding the coverage of existing ones will facilitate market diversification also for SMAEs.

Consortia and clusters are excellent facilitators for training and human development programmes and facilitate the exchange of information about the risks and remedies for dealing with calamities.[45, 48] They also function as accelerators for adopting digital technologies. Knowledge about such technologies and their operational benefits is often limited among managers, especially in low-income countries.[17] Their adoption would enable SMAEs to conduct instant data exchange before and after a crisis and help open new marketing channels. However, given the difficulties facing SMAEs in adopting innovations and new technologies, policymakers will need to develop strategies that support SMAE efforts to become more competitive and resilient.[49, 50] ■

CONCLUSIONS

Food is produced, processed and distributed by various types of supply chains that differ in composition, technology and products. The changes taking place today in food supply chains reflect changes in socio-economic conditions and technology, as well as biophysical and environmental conditions.[51] New discoveries in biology and information technology, along with demographic change and socio-economic development, are continuously transforming supply chains and driving the emergence of new chains, new products and new risks.

Although most innovations originate in more advanced economies, globalization accelerates their adoption across the world. Supermarkets, refrigeration, mobile phones, computers and e-commerce have all been essential in transforming agrifood systems. Food supply chains will continue to generate more differentiated products, as the result also of demographic, income, climatic and sociocultural changes. As modernization and globalization advance, differentiation may create new vulnerabilities and capacities in the face of systemic disturbances, such as climate change, biodiversity loss or pandemics. Food supply chain actors need to adapt and transform to remain economically viable and actively engage in agrifood systems. At the same time, governments should act to create enabling conditions for these transformations to be environmentally sustainable and socially inclusive.

The process of innovation in food and information technologies is enhancing human capital and local capacity to manage multiple risks and adapt to changing realities. An upgraded research and education system has a key role to play, helping to develop capacities to capture value within supply chains and risk-proof them. The linkage between academia and industry needs to be strengthened to foster entrepreneurship as well as capacities for prevention, anticipation, absorption, adaptation and transformation. Equally important is promoting institutional, social and financial innovations in value chains, market access and delivery.

The interaction between different actors within and across supply chains will be key regarding how agrifood systems respond to shocks and stresses. Agricultural producers are highly vulnerable to shocks affecting the sector directly as well as those affecting suppliers and customers. Primary agricultural producers and consumers will be affected by the adaptation of intermediaries to shocks, and all actors along the food supply chain will be impacted by how shocks hit lateral input and service supply chains. Although the shocks and stresses may threaten their viability, they can also favour the emergence of better adapted, more resilient supply chains. Because of the importance of interactions within and across supply chains, improving their overall capacity to deal with shocks calls for integrated approaches. Central to this is applying existing global policy frameworks, such as the Sendai Framework for Disaster Risk Reduction 2015–2030[52] and the related UN Common Guidance on Resilience,[53] valid across and within sectors.

The COVID-19 pandemic has illustrated the high cost of coping and adapting once a shock occurs. While global supply chains coped and adapted quite well, the overall cost of absorbing and responding to the crisis was immense in terms of loss of life and livelihoods and damage to the economy. Low-income countries often paid the highest price. This underscores the urgency of investing in risk management and building resilience capacities, especially against disruptions caused by climate change, future pandemics and economic crises, in ways that minimize the trade-offs and make the most of potential synergies.

Planning and investments are needed to ensure resilience of food supply chains with all their five main capacities: to prevent, anticipate, absorb, adapt and transform in the face of shocks and stresses. Investments in infrastructure (roads, storage and emergency systems) and economic support mechanisms are essential. In some cases, long-term shocks may lead to relocating farm production and SMAEs. Developing plans that take into account the

choices and interests of multiple players within supply chains, as well as the capacity of the public and private sectors to manage multiple risks, should be major priorities.

Households, the focus of Chapter 4, are at the end of food supply chains and exposed to varying degrees of shocks that affect their demand for food and consequently their food security and nutrition. The most vulnerable consumers are in households who work within food systems as small-scale farmers, fishers, pastoralists and landless agricultural workers, along with the urban poor and populations that suffer greater inequality and marginalization, such as women and Indigenous Peoples. In any society, the extent and stability of such households' food security is a crucial determinant of agrifood systems' resilience. The following chapter analyses the livelihoods of these households and how they shape their access to sufficient and nutritious food. ■



PHILIPPINES
Beneficiaries of FAO's livelihood restoration efforts apply their knowledge and skills to improve rice patty productivity and to better cope with shocks.
©FAO/M. Navales

CHAPTER 4
ENHANCING THE RESILIENCE OF RURAL LIVELIHOODS

KEY MESSAGES

➔ Building resilience of rural households is an objective in its own right – it helps improve their livelihoods, but it also renders agrifood systems more resilient.

➔ Rural households experience shocks and stresses differently based on their socio-economic characteristics, social protection and other support programmes, and whether they primarily sell or buy food. Predominantly female households are worst affected by shocks and stresses, due, in most part, to lack of access to land and other assets.

➔ Damage to infants and young children may be irreversible and has long-term economic costs to individuals and society; social safety programmes with limited resources should give priority to infants and children to prevent malnutrition impacts such as childhood stunting and wasting.

➔ Education and income diversification are powerful factors in enhancing the resilience of rural livelihoods in low-income countries. For those living in harsh conditions, such as pastoral households, access to basic services like clean water and sanitation is key.

➔ Creating or strengthening producer associations and cooperatives and adopting more sustainable production practices – including agroecology, climate-smart agriculture and biodiversity conservation – are important to enhance resilience.

➔ By easing restraints on credit, savings and liquidity, risk-informed and shock-responsive social protection helps vulnerable households avoid negative coping strategies and reduces their vulnerability to shocks.

➔ Policies must build on agricultural households' own resilience to ensure inclusive and sustainable livelihoods, combining regular social protection with productive support.

Chapter 1 presented a framework for analysing agrifood systems' resilience and Chapter 2 analysed agrifood systems' resilience at national and subnational levels. Chapter 3 then analysed the resilience of food supply chains and agrifood businesses. This chapter complements the analysis so far by focusing on rural livelihoods and household resilience capacities. Rural livelihoods are the capabilities, assets and activities that rural people require to make a living[1] and may include farm and non-farm activities, although agriculture is crucial to most of them.

The impacts of shocks and stresses on livelihoods, food security and nutrition play out essentially within households, making them a key focus of resilience analysis. Many rural households play an important role as producers

in agrifood systems – either in agriculture or running small agrifood businesses. Hundreds of millions of family farms of different sizes, as well as the fishers and pastoralists whose livelihoods depend on primary production, form the backbone of agriculture in most countries. Rural households that engage in diverse and multiple activities to improve their livelihoods can better cope with and recover from stresses and shocks, thus rendering agrifood systems more resilient. By maintaining or enhancing capabilities and assets without undermining the natural resource base, rural livelihoods also contribute to more sustainable agrifood systems.

This chapter focuses on the livelihoods of rural households and the higher incidence of poverty in rural areas. The most recent estimate of multidimensional poverty finds that, of the 1.3 billion people who are multidimensionally poor worldwide, 84.2 percent live in rural areas.[2] Thus, the majority of the 3 billion people who cannot afford a healthy diet, together with the other 1 billion people at risk of joining their ranks if their incomes fall by one-third (see Chapter 2), are likely to be in rural areas and depend to a large extent – directly or indirectly – on agriculture for their livelihoods. For this reason, given the central role of agriculture in reducing poverty and ensuring food security and nutrition, the focus of the chapter extends also to agricultural households in rural areas (see Glossary). In fact, billions of people around the world are linked to agrifood systems in one way or another through their livelihoods. A nuanced understanding of household-level vulnerabilities, and the various ways households are linked to agrifood systems through their livelihoods, will help in developing policies that positively influence food security and nutrition outcomes for millions of people in the face of shocks and stresses.

Based on empirical analysis, the chapter starts with a discussion of the resilience determinants of rural livelihoods to shocks and stresses. It then focuses on the constraints faced by agricultural households in rural areas and small-scale producers in managing risks and building capacities to cope with shocks and stresses. The chapter then proposes solutions to address the needs of vulnerable households and enhance synergies between household resilience, efficiency and sustainability.

Because the impacts of shocks on households are among the main drivers of poverty and food insecurity, the ability to cope with them has been the subject of intense research and policy debate. Shocks that affect households may be *idiosyncratic*, that is, affecting only one individual or household in the case of illness or death, or they may be *covariate*, that is, the shock is widespread and affects many (e.g. droughts, floods, conflicts, or pest and disease outbreaks) (see Glossary).[3–5] Households' coping strategies differ according to the type of shock. Preparation for idiosyncratic shocks can be ensured at household and community levels, while coping with covariate shocks may require risk-pooling across larger areas and populations.[6] However, regardless of whether shocks are idiosyncratic or covariate, household capacities to prevent, anticipate, absorb, adapt and transform – in short, their resilience capacities – are strongly linked to their socio-economic status (e.g. income level) and social and support networks, and to social protection and productive support programmes. ■

DETERMINANTS OF RESILIENCE OF RURAL LIVELIHOODS

Rural livelihoods depend to a large extent on agriculture and agrifood activities. They are exposed not only to shocks caused by price fluctuations and disruptions in input and food supply chains (see Chapter 3), but also to adverse events such as floods, droughts, soil erosion and pests.[4] According to the 2014 *Human Development Report* of the United Nations Development Programme (UNDP), between 2000 and 2012, more than 200 million people, most of them in low-income countries, were hit every year by environmental disasters, especially floods and droughts.[7] A drought can reduce the local food supply and increase market prices, hurting especially households that predominantly buy, rather than sell, food in the market.[8] In Malawi,

a recent study found that weather shocks such as drought and floods during an agricultural season can reduce household food consumption by 9 percent. Stresses such as poor infrastructure can aggravate the negative impacts of weather shocks. The same study finds that the combined impact of extreme weather events and poor infrastructure caused a 17 percent drop in food consumption.[3] Even in countries that are not low-income, shocks can have a major impact on livelihoods. A study using panel data from 1994–2004 showed that more than 50 percent of Russian households were hit by shocks that forced them to make rapid and large adjustments in their food spending. The most affected were rural households which had less access to income-smoothing mechanisms such as credit and insurance.[9]

A recent global FAO study finds that the economic loss associated with all disasters – climatological, hydrological, biological and geophysical – averaged roughly USD 170 billion a year over the past decade. Data from 71 post-disaster needs assessments conducted between 2008 and 2018 showed that agriculture, including crops, livestock, forestry, fisheries and aquaculture, absorbed 26 percent of the overall impact of medium- to large-scale disasters in low-income and lower-middle-income countries and 63 percent of damage and loss in the combined agriculture, industry, commerce and tourism sectors.[10]

In response to this risky environment, rural agricultural households, especially in low-income countries, use a set of strategies to manage risks *ex ante* and cope with shocks *ex post*. They can diversify income either by on-farm crops or livestock diversification or by engaging in the rural non-farm economy. They manage their agricultural risks by investing in risk reduction strategies such as irrigation, drainage management and pest control. They adapt their agricultural land-use practices to reduce soil erosion and landslides, and change cropping mixes and planting dates in response to adverse climatic conditions. When shocks occur, they use savings, liquidate assets and borrow to cope. Some rural households use insurance via formal insurance providers or informal inter-household insurance based on community networks.[11]

Households differ in their ability to use any, or a combination, of these strategies. Resilience is a dynamic process, meaning it is important that strategies to reduce risks or cope with shocks do not diminish the household's overall ability to deal with subsequent shocks. Decisions on how to manage risks and cope with shocks depend, to a large extent, on the household's socio-economic well-being and support programmes. Findings from India's national household survey indicate that non-poor households actively anticipate shocks by strengthening their safety nets as a precautionary measure. They are also more likely to draw on support from informal credit sources. These options are more limited for poor households, especially extremely poor households who face high food insecurity.

To explore the resilience capacities of rural households, FAO's resilience index measurement and analysis (RIMA) model was applied (Box 13) to data from 46 household surveys covering 23 countries (two surveys per country) from the United Nations Children's Fund (UNICEF) multiple indicator cluster surveys (MICS) (see Annex 4 for the list of countries). Despite being in rural areas, some households may not be involved in agriculture, deriving livelihoods exclusively from non-farm activities. The findings indicate that it was mostly education, income diversification and transfers (both formal and informal) that drove improvements over time in rural household resilience capacities. For agropastoralist households, the most important drivers of resilience capacity were greater access to basic services such as schools, health and sanitation. Shocks, especially of high intensity, lead to a reduction in resilience capacity over time. Price shocks seem to have the greatest detrimental effect on household resilience, producing a greater impact than more frequent shocks such as health and environmental shocks.[12]

The RIMA model was also applied to agricultural households (i.e. engaged in farming, pastoralism or agropastoralism), covering another 12 countries and 17 additional surveys (see Annex 4 for the full list). Despite all households being agricultural, some rely partly on the rural non-farm economy for their livelihoods. Figure 9 summarizes results for 12 countries using four

BOX 13 RIMA IN BRIEF

In 2008, FAO pioneered the RIMA model, a quantitative approach to a rigorous analysis of how households cope with shocks and stresses. An enhanced version of the model, RIMA-II, directly measures resilience through its resilience capacity index (RCI). RIMA builds on four pillars of resilience, listed in the table, which determine the food security resilience of households as measured by the RCI.

TABLE RIMA PILLARS OF RESILIENCE

Pillars of resilience	Definition
Adaptive capacity	The ability of a household to adapt to a new situation and develop new livelihood strategies.
Social safety nets	The ability of a household to seek help from relatives and friends, support from government, and timely and reliable assistance from international agencies, charities and non-governmental organizations (NGOs).
Assets	*Productive assets* are key livelihood elements, enabling households to produce consumable or tradable goods (e.g. land, livestock and durables). Context-specific sets of productive assets that determine household income are evaluated. *Non-productive* assets such as a house, vehicle or household amenities reflect living standards and wealth.
Access to basic services	The ability of a household to meet basic needs, and to access and make effective use of basic services (e.g. schools, health facilities, infrastructure and markets).

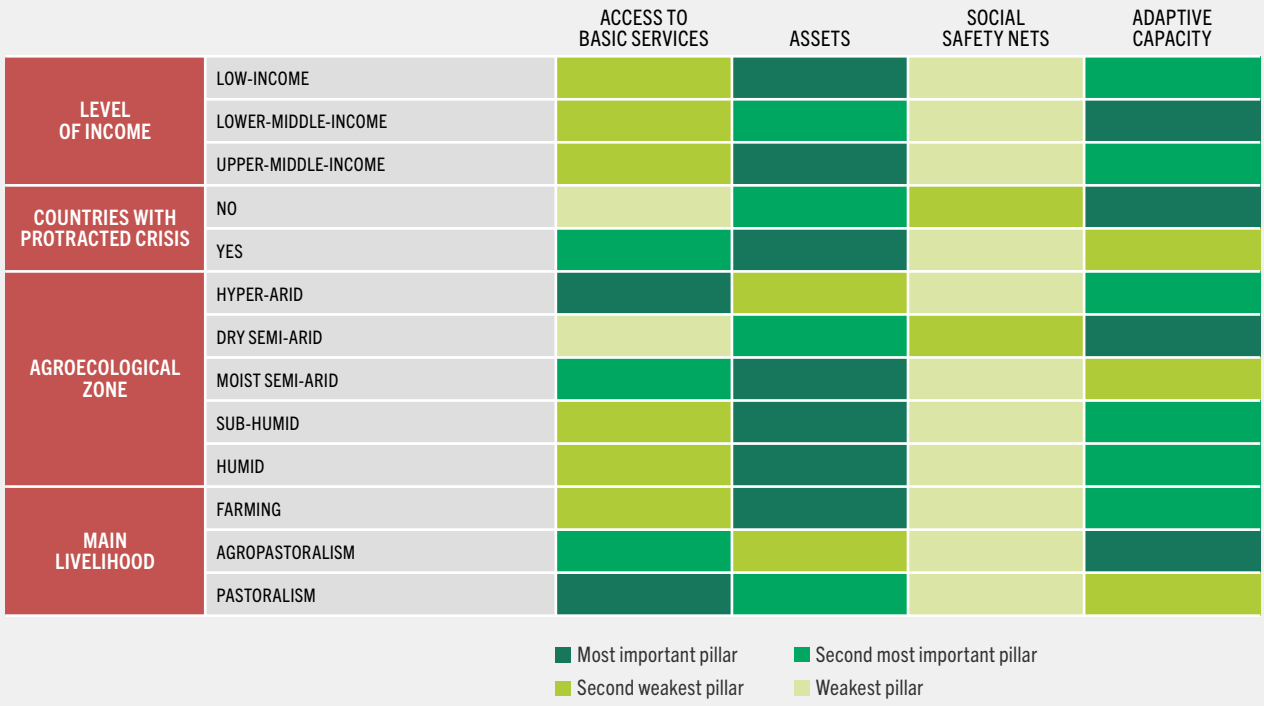
SOURCE: d'Errico *et al.* 2021.[12]

pillars of household resilience – access to basic services, assets, social safety nets and adaptive capacity – to identify the most important factors for the resilience of agricultural households (see Box 13 for a description of the RIMA model and the four pillars). The findings are presented for different profiles: country level of income, whether a country is affected by a protracted crisis, agroecological zone, and the main household livelihood source. The colour coding from dark to light green illustrates the importance of each pillar in determining the resilience of agricultural households, the darkest being the most important, the lightest the least important.

In just over half of Figure 9 classifications, assets (productive and non-productive) is the most important pillar to ensure households' capacity to bounce back after a shock. At any time, asset ownership plays an important role in sustaining household livelihoods and generating income. During a crisis, it is essential to their coping strategies of last resort, allowing them to buffer against shocks by selling off productive and non-productive assets. However, this strategy can lead some households, especially the poorest, into a poverty trap if they are left with too few assets.

Figure 9 shows that the adaptive capacity of households is also a significant pillar of their resilience. A household's capacity to adapt is closely linked to the education level within the household and to human capacity building, which give the members more value on the labour market. Access to basic services such as improved sanitation and sources of water and to primary services, in particular schools, hospitals and agricultural markets, is crucial to support their resilience, particularly in hyper-arid zones and for pastoralist households.

FIGURE 9 RIMA RESILIENCE PILLARS BY COUNTRY PROFILE



NOTE: Protracted crises are contexts in which a significant proportion of the population is acutely vulnerable to hunger, disease and disruptions to livelihoods over prolonged periods.[13]
SOURCE: d'Errico *et al.* 2021.[12]

Table 4 summarizes the drivers of household resilience across the 35 countries covered by the two sets of data (MICS covering 23 countries and RIMA covering 12 countries; see Annex 4) and the main policy implications for building the resilience of rural households.

The RIMA analysis also shows that rural households comprising mainly women suffer the most during and after shocks. Women tend to have much less access than men to land and other assets – important drivers of resilience. Their main coping strategy is often to sell their assets; this is risky in the long term as it reduces income-generating capacity. Providing women with greater access to social protection and assets could counterbalance this. Access to productive assets will allow women to restock and bounce back after a shock without any threat to their food security. Education plays a key role in strengthening women's resilience capacity, underscoring the importance of expanding access to education for all, especially girls. Women with more education have wider access to the labour market and can expand their available options for income-generating activities.[12]

Children are also vulnerable to shocks and stresses. In terms of nutrition, infants and young children bear the brunt of shocks. A recent review found that covariate shocks have a permanent effect on child growth in low-income countries, with most studies showing that widespread shocks increase the prevalence of stunting and underweight among children under two years of age.[14] Evidence of

TABLE 4 DRIVERS OF RURAL HOUSEHOLD RESILIENCE AND POLICY IMPLICATIONS

Indicators of resilience	Role in enhancing resilience	Policy implications
Productive and non-productive assets (e.g. agricultural tools, land, livestock)	Asset ownership is key to ensuring households' capacity to bounce back after a shock. It plays an important role not only in sustaining households' livelihoods, but also as a buffer in case of shocks – selling productive and/or non-productive assets is a common coping strategy.	Interventions should expand access to productive and non-productive assets, and support the diversification of income sources, especially for the poorest households. It is important to help households avoid negative coping strategies, which can lead to a low level of asset holdings and, ultimately, a poverty trap.
Access to education	When combined with income-generating activities and diversification strategies, household members with a higher level of education can improve their livelihoods as they are more valued on the labour market. When a shock negatively affects households' livelihoods, they can adapt more easily if they can rely (temporarily or not) on another source of income.	Policies supported by investments are needed to expand access to education and post-education capacity-building programmes, especially for women.
Access to basic WASH services (e.g. improved sanitation and sources of water) **and primary services** (e.g. schools, hospitals and agricultural markets)	The harsher the environment in which the household lives (e.g. arid agroecological zone, a country affected by a protracted crisis, or low-income country), the more resilience depends on access to basic services.	Long-term policies to improve the availability and quality of infrastructure can sustainably increase household resilience. Large infrastructure projects to expand primary services are especially needed for households located, for example, in countries in the Sahel region.

NOTE: WASH: water, sanitation and hygiene.
SOURCE: d'Errico *et al.* 2021.[12]

the effects on acute undernutrition (standardized weight-for-height or wasting status) is much less consistent – probably because it can be reversed with weight gain after the shock and therefore is not captured by studies unless measured immediately. The effects of stunting are largely irreversible: children simply cannot recover height in the same way they can gain weight. Evidence of the effect of shocks on micronutrient deficiency is quite limited and merits further research. Child nutrition status is associated with performance in cognitive tests, school attainment and labour market outcomes later in life,[15, 16] suggesting that shocks may generate substantial, long-term economic costs to both individuals and society.[14] ■

SMALL-SCALE AGRICULTURAL PRODUCERS BEAR A DOUBLE BURDEN

Agricultural production – crops and livestock, aquaculture, fisheries and forestry – is a risky business. All agricultural sectors depend on natural processes and limited natural resources and are more exposed to natural hazards than food processing and trade. Agriculture increasingly faces new shocks, stresses and risk drivers from a variety of sources, including: more frequent and extreme climatic events, biodiversity erosion, new diseases, climate change, natural resource degradation, an ageing farm population, seasonal labour shortages, food safety scares and commodity price volatility.[17]

However, the capacities of rural households to handle risks are not equal. Those running small-scale businesses operate under greater

constraints due to more limited access to land and water, resources, information, technology, capital and assets.[18, 19] They bear a double burden of vulnerability to risks and shocks: in addition to risks intrinsic to agriculture, they also face the risk of being excluded from productive assets and lucrative markets in the transformation process of food supply chains (see Chapter 3).[20]

The impact of shocks on the food security and nutrition of agricultural households depends also on the extent of their engagement in agriculture and food production. Shocks and stresses that hit agricultural and food production, such as pests, diseases, drought and disruptions to food supply chains, impact more on households which are net food producers (see Glossary). On the other hand, net food consumer households rely more on the non-farm economy, and for them farming is a part-time activity; they are more prone to shocks that affect their purchasing power as consumers, such as price spikes and general economic crises.

Regardless of how agricultural households are categorized, there is clearly no single strategy to build their resilience against shocks. Most agricultural risk management tools are not available to agricultural households – especially those operating small-scale businesses – owing to a lack of multi-risk governance and related policies and investments, market failures, and the absence or underdevelopment of markets. In an ideal world, small-scale agricultural households could use risk-sharing tools, such as credit, crop and livestock insurance, and forwards, options and futures, to transfer their risks to the wider economy and operate more efficiently. However, tools such as agricultural insurance need active government support – not yet feasible in all countries – while others (e.g. futures and options) are practised in limited cases, even in high-income countries, as they require specific skills not available to the majority of agricultural households.

Risk management schemes are particularly underdeveloped in aquaculture and fisheries compared to other food producing sectors.[21] Although aquaculture provided 52 percent of fish for human consumption in 2018,[22] the sector is still inherently more risky than other food production activities, owing to higher variability in yields and revenues and sensitivity to multiple biological hazards (disease and food safety events).[23–25] As a result, in low-income countries, the livelihoods of 20.5 million people, most of them small-scale aquaculture workers engaged full-time, part-time or occasionally, may be in jeopardy if a shock occurs.[22] Similar conditions apply to small-scale fishing households in low-income countries disproportionately affected in times of shock or crisis; they are least prepared due to low rates of savings and inadequate credit or insurance facilities.[26] Their unpredictable earnings (dependant on whether they catch fish or not) and lack of assets for use as collateral make their access to favourable credit or insurance schemes extremely difficult.[27]

Due to the range of market failures involving risk-sharing tools, agricultural households employ other strategies to manage the multiple challenges they face. They diversify production mixes to reduce risks and mitigate the impacts of shocks before they occur. They also accumulate savings and assets as coping mechanisms in the aftermath of shocks. At farm level, agricultural households respond to the unpredictable interplay between natural, technological and social factors by reconfiguring and using available resources in novel ways.[28] This process helps them navigate foreseen and unforeseen change,[28] strengthening their capacity to prevent, anticipate, absorb, adapt and transform.

With climate change and greater frequency of disasters the new normal, the resilience capacities of agricultural households are increasingly put to the test. An assessment of the climate resilience of pastoralists and agropastoralists in sub-Saharan Africa found that while their capacities and knowledge helped them cope with unexpected shocks and climate variability, there is much need for improvement (Box 14). The most vulnerable bear the true burden of climate change and disasters disproportionately.[10] During the COVID-19 pandemic, small-scale producers have experienced reduced access to inputs, labour and farmland, resulting in production losses, lower household incomes and declining nutrition levels. The severity of the damage caused depends on multiple factors, such as the timing of the spread of COVID-19 and how containment measures disrupted the agricultural calendar, input prices and demand.[29–31] ■

BOX 14 THE CLIMATE RESILIENCE OF PASTORALISTS AND AGROPASTORALISTS IN SUB-SAHARAN AFRICA

Climate-related shocks cause crop, animal and asset losses, displacement, and water scarcities, all of which affect the livelihoods of pastoralists and agropastoralists in sub-Saharan Africa. As the intensity of these shocks increases, the impacts include a deterioration in food security, affecting the most vulnerable households disproportionately.

A recent FAO assessment looked at the degree of resilience to climate change among small-scale pastoralists and agropastoralists in Angola, Burkina Faso, Burundi, the Gambia, Kenya, Mozambique, Niger, South Sudan and Uganda.[32] The survey reached 1 466 household heads, of whom 20 percent were female.

The study finds that while resilience to climate change is low, both strengths and weaknesses exist. Social factors, including trust and cooperation, as well as household composition and types of production, scored highly as drivers of resilience. Other factors are identified as being at risk, such as savings – half the respondents have some savings but two-thirds reported having fewer savings than five years earlier. The study highlights the reduced capacity to rely on both financial assets and physical assets (e.g. seed and livestock) in the case of unexpected shocks. The assessment also uncovered weaknesses in other areas – for example, agronomic and production practices, animal disease control, access to veterinary services and livestock husbandry practices – indicating the need for improved animal breeding, breed diversity, animal safety mechanisms and better livestock nutrition.

SOURCE: Hernandez Lagana & Savino. 2018.[32]

POTENTIAL SOLUTIONS FOR RESILIENT RURAL LIVELIHOODS

The ultimate goal of agrifood systems' resilience is to ensure sufficient, safe and nutritious food for all in the face of any disruption, and to sustain the livelihoods of agrifood systems' actors. The rest of this chapter focuses on potential solutions that can guide policy and interventions to strengthen the livelihood resilience of rural households. The solutions can be grouped into three main categories: institutional solutions, technical solutions and cross-cutting policy interventions.

Institutions for improved resilience

The resilience capacity of rural households depends on contextual factors and local circumstances. The economic impact of drought depends on a host of local factors: soil quality, cropping patterns, irrigation infrastructure, and the flexibility of credit providers and supply chain partners.[33] Access to products, inputs and credit – which shape resilience capacities – largely depends on physical distance to urban centres and markets. Rural households are embedded in local networks and interact formally and informally with other actors in specific agroecological, socio-economic and territorial contexts. These interactions constitute their production and livelihood systems.[17, 34] Livelihoods and resilience also depend on how they interact with their surroundings. Social networks are crucial for resilience of poor households, providing access to informal credit and saving mechanisms to help face emergencies and shocks. However, covariate shocks will affect most households and social networks may fail to provide support. Policies and strategies to enhance the resilience of the vulnerable rural poor should build on existing informal safety nets and address their weaknesses, for example, by encouraging the formalization of social networks and linking them to productive enterprises and financial services.[27]

The integration of producers into food supply chains and lateral input and service supply chains varies (see Chapter 3). While consumption of produced food is the main objective of subsistence farmers, it is less important in agricultural households that are well connected with agribusinesses for sourcing inputs, securing credit and selling outputs. Large-scale farmers may even provide jobs and informal credit. Small-scale agricultural households have weaker linkages to food supply chains and rely heavily on their community networks for informal credit, information, technology and marketing. This marginalized position and their exclusion from access to more lucrative markets leaves small-scale producers more exposed to risks and shocks and unable to operate efficiently and productively. Small-scale agricultural households face constraints that weaken their livelihoods and narrow their opportunities for growth, thus undermining their resilience and that of agrifood systems; their three weaknesses – small scale, limited access to resources, and weak market power – may create a vicious circle.

Policies that create or strengthen producer associations and cooperatives can contribute to breaking this cycle and improving livelihoods by: pooling resources to achieve scale; providing access to productive resources such as machinery, equipment and credit; and enhancing market power. By purchasing inputs and selling outputs as a group, small-scale producers protect themselves from market fluctuations and obtain better input and higher output prices. FAO's Dimitra Clubs are community-based groups, often established in remote or conflict-affected areas, which come together on a voluntary basis to discuss common challenges and organize forms of collective action to improve the livelihoods of rural communities and empower rural people, especially women.[35]

Coordination with other actors in the food supply chain is also key to managing market risks in order to enable trust, networking, cooperation and information exchange between small-scale producers and other value chain actors. This can lead to mutual benefits through mechanisms such as contract farming[36] where small-scale agricultural producers involved in crops, livestock and aquaculture receive guaranteed prices for their outputs, while processors and distributors receive produce of the desired quality.[37]

Enhancing resilience through agroecology and adaptation to climate change

Adopting more sustainable production practices is another important resilience-enhancing strategy for agricultural households. The proposed practices are highly relevant to agricultural households running small-scale businesses. They create synergies between enhancing resilience and improving productivity, sustainably, in addition to being accessible to small-scale producers because they do not entail large risky investments. Agroecology is one approach that can help small-scale producers adapt to and mitigate climate change. There is increasing evidence of its benefits for the environment, biodiversity, farmers' incomes, adaptation to climate change, and resilience to multiple shocks and stresses. However, this evidence remains fragmented across case studies, isolated experiences and field observations, based on heterogeneous methods and data, as well as different scales and time frames.[38]

To overcome the lack of systematic data, FAO and a large number of partners have developed the tool for agroecology performance evaluation (TAPE), an innovative framework that consolidates global evidence on how agroecology supports the transformation to more sustainable and resilient agrifood systems.[39] Resilience is one of the elements explicitly measured, using the following descriptive scales:

- overall diversification of the production system – diversity of crops, animals, trees and economic activities;
- economic resilience – stability of production and income and the capacity to recover from disturbances;
- social resilience – social mechanisms to reduce vulnerability; and
- environmental resilience – the capacity of the agroecosystem to adapt to climate change.

Across the 25 countries in five continents where TAPE has been applied, there is a strong link between agroecology and biological and economic diversity: more advanced agroecological

farms are more diverse in terms of crops, trees and animals, but also in terms of economic activities, leading to enhanced economic and environmental resilience. Improved resilience has often translated into better diets and food security. Animals in particular have a key role in enhancing resilience[40] – TAPE's results show that more advanced agroecological farms have more diverse species and breeds of well-adapted, healthy animals, associated with higher biodiversity and improved soil health, which in turn contribute to better ecological resilience and enhanced ecosystem services.

A TAPE evaluation in Mali showed that more advanced agroecological farms have higher net revenues than conventional farms using high levels of chemical inputs. Indeed, agroecological farms incur much lower costs because they rely more on biological synergies that substitute for external inputs.[41, 42] Examples include using manure as fertilizer and crop residues as livestock feed. At the same time, greater biodiversity in agroecological farms leads to greater capacity to resist pest and disease attacks.[43]

Beyond its benefits to agricultural producers, agroecology, if widely adopted, can help reverse trends of biodiversity loss and enhance biodiversity for food and agriculture (BFA). Dominant production systems have contributed to biodiversity loss through habitat destruction, monocropping, excessive use of inputs such as fertilizers and chemicals, and replacement of diverse crop and livestock genetic resources with a narrow range of species, breeds and varieties.[44]

Based on BFA, agroecology can create various synergies that lead to resilient livelihoods while enhancing environmental sustainability. It helps stabilize and increase yields, fosters growth of local crops and animal breeds, enhances income and diversifies household diets.[45] BFA also contributes to building resilient rural livelihoods indirectly by providing rural people with wild foods and other resources such as wood for fuel. Box 15 contains examples of how approaches aligned with agroecology and biodiversity can generate resilient livelihoods for rural mountain populations.

Climate-smart agriculture (CSA) is another resilience-enhancing approach, which aims to promote food security, resilient livelihoods and climate-resilient agriculture.[48, 49] The concept recognizes that conventional mainstream agriculture cannot feed the growing world population sustainably, because it degrades the environment and depletes scarce natural resources.[50] A review of the applications of CSA in Africa shows that it provides multiple benefits. It has helped small-scale agricultural producers implement sustainable land management, slowed desertification and improved resistance to drought, while achieving higher productivity and income. It has also enhanced the capacity of agricultural households – especially those that are female-headed – to adapt to climate change.[51]

One successful example of CSA implementation comes from the Kodroka Forest Reserve in the Northern State of the Sudan. Much of the forest has been severely degraded by a combination of factors, including desert expansion, climate change and inefficient water management. Many of the farmers had already begun adapting to climate change by adjusting planting and harvest times to longer summers and unpredictable rainfall. FAO worked with the communities around the forest to plant rows of crops and trees (e.g. acacia and eucalyptus) on the degraded land. Within a few harvest cycles, the area became verdant and productive again. The trees act as a buffer against the expanding desert, crops improve farmers' livelihoods and careful harvesting of the trees at appropriate intervals generates additional income.[52]

Social protection – an important tool to enhance rural household resilience

The precarious condition of many rural livelihoods means they are more vulnerable to shocks, which may further undermine their asset base as well as their capacity to manage future shocks effectively.[53] Hundreds of millions of rural families are trapped in a cycle of hunger, poverty and low productivity, causing unnecessary suffering and impeding agricultural development and broader economic growth. Breaking this cycle requires action in two complementary domains: social protection and the productive sectors of the economy. In many developing

BOX 15 SYNERGIES BETWEEN PRODUCTIVITY, RESILIENCE AND SUSTAINABILITY: THE MOUNTAIN PARTNERSHIP PRODUCTS INITIATIVE

The Mountain Partnership Products initiative (MPP initiative) provides concrete examples of how aligning agricultural practices with agroecology and BFA can lead to synergies between improved productivity, environmental sustainability and resilient livelihoods. The MPP initiative aims to strengthen the resilience of mountain peoples, their economies and ecosystems. It is a certification and labelling scheme that promotes local and short supply chains while ensuring transparency and trust between producers and consumers, fair returns for primary producers, conservation of agrobiodiversity and preservation of ancient techniques. Currently, the initiative operates in eight countries and includes 20 products.

A prominent product example is Jumla mixed beans, produced using agroecological practices in the Sinja Valley in Nepal at an altitude of 2 300 metres. Due to the product's high nutritional and cultural value, the producers were able to increase the price of the beans by more than 25 percent and they now sell in national supermarkets; there has been a major increase in sales with production scaled up four times in three years. Another example is Melipona honey, produced by stingless bees and harvested by six honeybee associations in Bolivia's Serranía del Iñao National Park, at the foot of the Eastern Cordillera. Perfectly adapted to the local environment, these bees are crucial pollinators; their loss would lead to a decrease in biodiversity in Bolivian forests. The producers were able to increase their sales price by more than 80 percent.

In both cases, there has been a significant improvement in food security and nutrition in the local community, with benefits for women, who have been increasingly engaged in farming, but also for many young people who have been able to resume education.

SOURCE: FAO. 2018;[46] Li, El Solh & Siddique. 2019.[47]

countries, most of the poor live in rural areas and agriculture is the most important productive sector. Linking social protection with agricultural development is, therefore, a potentially powerful means of breaking the cycle of rural poverty.[54]

Social protection policies in developing countries emerged initially to help groups of people harmed by structural adjustment programmes in the 1980s and early 1990s. They now extend beyond welfare concerns, with increasing emphasis on reducing risks and the harmful effects of shocks on vulnerable livelihoods, as well as supporting economic and productive inclusion.[55] When designed to be gender-, nutrition- and risk-sensitive, as well as shock-responsive, social protection policies help raise incomes and make up for consumption shortfalls of poor households, allowing them to invest and engage in productive activities.

The role of social protection combined with adopting climate-smart approaches in climate risk management strategies is particularly interesting (see the FAO studies summarized in Box 16).

There is substantial evidence to show that social safety nets can be effective in protecting well-being, assets and food security.[56–58] When guaranteed at regular, predictable intervals, they also have productive impacts, providing some degree of insurance and liquidity, and allowing households to take advantage of economic opportunities. Furthermore, social protection may have positive multiplier effects on local communities and economies.[59]

Social protection has evolved to encompass both public and private initiatives to support communities, households and individuals in

managing risk. It has three components: (i) social assistance (such as cash or in-kind transfers and public works programmes); (ii) social insurance; and (iii) labour market programmes.[64] Social protection relief facilitates recovery after a shock by enhancing incomes and overall household capabilities.[55] Where they are already established, they can, in relatively short time, deliver additional social assistance to beneficiaries and expand services to newly vulnerable households.[65]

Evidence on the use of social protection during the COVID-19 pandemic indicates that countries have responded in part by increasing the generosity of existing programmes and reaching new participants. The number of new programmes has become significant, such that 63 percent of the cash transfer responses to the pandemic are newly introduced schemes.[66] The adequacy of these responses in terms of speed, coverage, generosity and duration of the social protection varied across regions and countries. On average, responses lasted for only three months, far less than the duration of the crisis, while roughly 40 percent of programmes were one-off payments.[66] Countries with more developed social protection systems were better prepared to protect people's incomes, underscoring the importance of investing in strengthening social protection systems in normal times, so as to expand them easily in response to the needs of the vulnerable in times of crisis.[67]

Social protection can support small-scale agricultural households to adopt more profitable livelihood strategies otherwise beyond their reach due to the additional risks involved.[54] It provides poor rural households, reliant mostly on agriculture, with an alternative to negative coping strategies, such as drawing down assets, which aggravate their vulnerability and undermine future income-generating capacity. By alleviating constraints to credit, savings and liquidity and providing cash and in-kind support, it reduces the vulnerability of rural households. Regular and predictable social protection instruments enable households to better manage risks and to engage in more profitable livelihood and agricultural activities. If well designed, social protection can establish synergies with productive activities and investments, which strengthen both the resilience and sustainability of small-scale producers' livelihoods.[68]

Programmes that provide social protection and productive support are highly complementary and their implementation is increasing in rural areas. An FAO review of enabling policies in the period 2007–2018 found that these programmes have contributed to combating rural poverty.[64] It identified ways of creating further synergies, specifically:

- Globally, unconditional cash transfers and school feeding programmes were the most widely used social assistance programmes. However, few focused on rural communities, where needs are greatest. National programmes should include components that are specifically designed to address the challenges of rural poverty.
- Most social assistance programmes with an agricultural support component involved public procurement schemes, mainly for school feeding programmes and food subsidies. But there is still scope to improve links between social protection and public procurement.
- Apart from public procurement programmes, social assistance components in productive support programmes are still rare. Linkages between cash transfers and programmes related to production factors (e.g. inputs, credit and irrigation) should be strengthened.
- There is a growing trend towards agricultural insurance programmes; acceleration is crucial, considering their potential to boost production and reduce poverty and vulnerability in rural areas.

The focus of existing programmes needs to be refined to address the unique challenges of rural poverty and harness the potential links between social protection and productive support programmes. Social protection should be linked to good agricultural approaches and practices, such as agroecology and CSA, to create synergy gains and enhance the impacts of both types of support, as illustrated by a case study in Zambia.[69] Risk-informed and shock-responsive social protection programmes can create synergies with public spending on agricultural and rural development, leading to greater inclusiveness for both types of support. Targeted programmes have had positive outcomes, particularly in health,

BOX 16 DIRECT AND INDIRECT IMPACTS OF SOCIAL PROTECTION PROGRAMMES ON HOUSEHOLD RESILIENCE TO MULTIPLE SHOCKS

Social protection programmes are increasingly seen as a mechanism to reduce household vulnerability to multiple shocks, including food shortages and climate shocks. Through transfer of cash or in-kind resources, they directly support vulnerable households facing food insecurity. They can also encourage those receiving transfers to invest in economic activities. An FAO study of refugee communities in Uganda found that both cash and food transfers helped beneficiaries stabilize household food consumption and reduce reliance on negative coping strategies, such as asset liquidation or going into debt. Cash transfers also encouraged investment in agricultural activities, if the land plots were large enough to produce positive returns.[60]

Social protection programmes can also reduce vulnerability to shocks indirectly by enabling poor farmers to adopt strategies that reduce their sensitivity to rising temperatures, erratic rainfall and the spread of new pests and diseases. An FAO study in Malawi and Ethiopia showed that food aid provided to resource-poor farmers removed constraints to investing in improved, CSA practices.[61] Smallholders participating in the Malawi Social Action Fund, the country's major public works programme, were more likely to adopt CSA practices and technologies over multiple agricultural seasons, achieving greater productivity returns in the medium term.[62] In Ethiopia, households participating in the public works component of the Productive Safety Net Programme were less likely to suffer agricultural losses, food shortages and crop failure due to drought or other shocks.[63]

Such experiences demonstrate the effectiveness of social protection programmes in supporting households following shocks and during emergencies. However, these programmes are seldom complemented by explicit resilience-enhancing strategies. Breaking down silos and improving coordination and coherence between social protection and resilience-enhancing initiatives will contribute to a better use of resources and, at the same time, improve gains in productivity and food security.

nutrition and school attendance. Well-designed programmes can also help prevent the use of child labour, as families are more likely to keep their children in school. Expanding social protection to small-scale producers, including those in fisheries and aquaculture as well as informal workers, should be a top priority in efforts to enhance the resilience of vulnerable households in rural and urban areas.

Particular attention should be given to expanding social protection coverage to small-scale fishers and informal fishworkers. A comprehensive FAO review finds that these categories face multiple risks, against which they are inadequately protected or totally unprotected. They face unique economic vulnerabilities compared to other small-scale agricultural activities, and social vulnerabilities can be overwhelming. Therefore, innovative interventions are needed to provide protection across the specific set of challenges that these categories face in each national and local context.[70]

To enhance inclusiveness, social protection must be flexible enough for geographical and sectoral mobility, enabling households to seize opportunities emerging across sectors and spaces. This is especially crucial in countries and areas with rapid economic growth, where structural transformations may increase inequality and exclude more vulnerable and marginalized households.

The costs of such programmes cannot be sustained over a long period of time unless

accompanied by sustainable productivity and economic growth and increased government revenues. A balanced approach is required: agroterritorial investments and policies must aim to achieve growth and create employment, while tax and social protection must aim to reduce inequality and enhance inclusiveness, while also ensuring programme fiscal viability and sustainability.

Achieving long-term economic inclusion is contingent on a comprehensive social protection system that proposes a full range of preventive, protective, promotive and transformative measures to, not only address the wide range of vulnerabilities faced by the rural poor, but also support livelihoods. For example, national cash transfer programmes in sub-Saharan Africa have helped poor and marginalized agricultural households build assets, empower themselves and generate economically productive activities. This strengthens the case for social protection as an investment for better livelihoods. Features such as the level of transfers, the predictability and regularity of payments and the type of associated messaging are other critical factors for enhancing economic and productive impacts. Combining predictable and reliable social protection with agricultural support interventions – such as easing access to productive assets and training – can maximize the impacts and increase the likelihood of success for sustainable economic inclusion processes.[71]

Poverty and vulnerability have a territorial dimension; some areas risk isolation and impoverishment if they lose crucial links to urban and export markets. Such areas will benefit from investments in public and private infrastructure to stimulate value chain development. In the long run, facilitating access to credit, productive assets and technical training will be essential to boost rural livelihoods and increase productivity; otherwise, social protection programmes will become unsustainable. However, economic inclusion requires a more long-term and holistic approach, with gradual interventions to provide intensive support for a certain period with the objective of graduating progressively to sustainable livelihoods. The combination of social assistance and social insurance can play an important role in building resilience of rural livelihoods and ensuring gradual progress of the rural poor into economic inclusion pathways, reducing the need for social protection.[71] ■

CONCLUSIONS

This chapter analysed what drives the resilience of rural households. Empirical findings from 35 countries highlight assets (productive and non-productive), income diversification, and access to education and basic services such as sanitation as important determinants of household resilience. Expanding access to productive and non-productive assets and supporting the diversification of farm and non-farm income is therefore essential. Wider access to education also emerged as a fundamental intervention to enhance resilience, improving people's chances of engaging in stable, remunerative jobs. Access to water, sanitation and hygiene (WASH) services played a critical role in enhancing resilience for households, particularly those involved in pastoralism, generally located in a harsh environment. Interventions to improve the availability of quality infrastructure are highly recommended for pastoralist households.

The chapter also uncovered a wide range of experiences from the literature focused on building resilient livelihoods, with the aim of overcoming potential trade-offs and create synergies, improving efficiency and promoting the sustainability of small-scale agricultural production. The chapter underscored the role of collective action, strengthening networks and cooperation among small-scale producers and other value chain actors, such as producer associations and cooperatives, as a cornerstone of resilient rural livelihoods. Agroecology, climate-smart agriculture and biodiversity conservation can also contribute to building resilience to climate shocks and generating rural livelihoods, while improving environmental sustainability.

Regular and predictable risk-informed and shock-responsive social protection instruments, complemented by productive support

programmes, can enable households to better manage risks and engage in more profitable, sustainable agricultural activities. Insurance or emergency schemes can also provide critical supplies – such as seed for farmers and cattle for herders – after a disaster hits, to provide protection and kick-start their recovery.

Policies to safeguard food security and nutrition need to consider the segments of the population most vulnerable to shocks and stresses and who work informally; social protection programmes need to be inclusive. Ensuring the latter may require innovative measures to connect households with services and information and build their self-confidence. When a shock occurs, a comprehensive social protection system should offer the rural poor different types of interventions and schemes to enable them to engage in productive activities with decent employment and to prevent them from being pushed back into subsistence mode.

Households comprising mainly women and girls are among the most vulnerable and need greater attention when designing social protection and support programmes. Their marginalization from resources and productive assets is the major driver of their vulnerability, underscoring the need for empowerment programmes that build and enhance their resilience through access to resources and education. Infants and young children are uniquely vulnerable: their health can be irreversibly damaged by shocks that affect their food security and nutrition. When social safety nets have limited resources, priority should be given to infants and children to prevent childhood stunting, wasting and other forms of malnutrition.

Policies aimed at building resilient livelihoods should take account of the specific conditions and multiple risks surrounding targeted households.

Policy measures should not simply replace households' own resilience strategies, making them policy-dependent and thereby even more vulnerable if those policies are discontinued. For example, policies that cap food prices can render households dependent on that support and at risk of losing their resilience strategies. Policies that maintain macroeconomic stability, on the other hand, can enhance household resilience by facilitating self-insurance mechanisms such as savings.

Where agriculture dominates the economy, the development of the rural non-farm economy and other urban sectors is crucial to provide farmers and rural communities with more attractive and diversified income sources. Developing the non-farm economy is particularly important where agricultural households operate very small farms that are at risk of becoming economically unviable. There is a pressing need for major public involvement in technological development, if low-income farmers are to benefit from agricultural innovations. More attention must also be given to investments in public goods that reduce risks, such as irrigation and drainage systems and high-yielding, resistant crop varieties.

In conclusion, rural livelihood resilience depends on context-specific, often highly local, conditioning factors, ranging from socio-economic development to environmental and agroclimatic conditions. The success of household resilience strategies also depends on a wide range of interventions to improve risk management and resilience capacities at multiple levels of agrifood systems, including interventions directed at food supply chains, governance and institutions, as well as the infrastructure necessary to support them. These will be further discussed in the next, and final, chapter of the report. ■



DEMOCRATIC REPUBLIC OF CONGO
A woman carrying a load of Chinese cabbage through a field in Katanga province.
©FAO

CHAPTER 5
BUILDING RESILIENT AGRIFOOD SYSTEMS: GUIDING PRINCIPLES

KEY MESSAGES

➔ Building resilient agrifood systems should be a key policy objective in itself; it is a precondition for sustainable, functioning agrifood systems.

➔ The COVID-19 pandemic has taught us that resilient agrifood systems depend on factors beyond agrifood systems themselves; it has highlighted the close connections between human, animal and environmental health and the need for a holistic approach, for example, the One Health approach of the World Health Organization (WHO).

➔ The absorptive capacity of agrifood systems, key in confronting shocks and stresses, is strengthened by greater diversity of commodities, actors and sources of food, redundant and robust transport networks, and greater affordability of healthy diets.

➔ Risk management strategies – including multi-risk assessments, timely forecasts, early warning systems and early action plans – complement absorptive capacity by helping all agrifood systems' actors prevent and anticipate major disruptions.

➔ Traditional, transitional and modern food supply chains, long and short, play different roles within national agrifood systems, but all can act as buffers against different shocks and stresses.

➔ Rural households can be made more resilient through increased access to risk management tools – including early warning systems and insurance, social protection and social services, such as education and sanitation – as well as through income and asset diversification.

➔ Understanding the functioning of agrifood systems, including their resilience capacities and how they are affected by contextual factors, can inform the design of appropriate policies and help avoid unintended policy consequences.

Throughout history, agrifood systems have not been exempt from harm caused by different shocks and stresses. The COVID-19 pandemic delivered a massive shock to agrifood systems in many countries, with impacts felt most by the poor and vulnerable. Government lockdowns reduced their access to employment and income-earning opportunities, leading in turn to reductions in food spending. This, in turn, negatively affected the livelihoods of food supply chain actors, from vendors to wholesalers, processors and eventually, producers. Losses in income and purchasing power pushed as many as 118 million people into becoming undernourished.[1] The impact of the pandemic on food security has created both the demand and

the momentum for action to make the world's agrifood systems more resilient to shocks and stresses. This requires policies that strengthen agrifood systems' capacity to prevent, anticipate, absorb, adapt and transform. To put the policy priorities into context, it is useful to return briefly to Chapter 1's three essential questions:

- **Resilience to what?** Shocks and stresses, often unforeseen, arise within and outside agrifood systems and impair how they function by disrupting the operations of related institutions and actors.
- **Resilience of what?** The central focus is national agrifood systems, the entire range of actors and interlinked value-adding activities, in the production, storage, distribution and consumption of food.
- **Resilience for what?** Building resilience aims at sustainably ensuring availability of and access to sufficient, safe, nutritious food for all, in the face of any disturbance. It enhances the livelihoods of actors in agrifood systems – producers, intermediaries and consumers – and promotes sustainability.

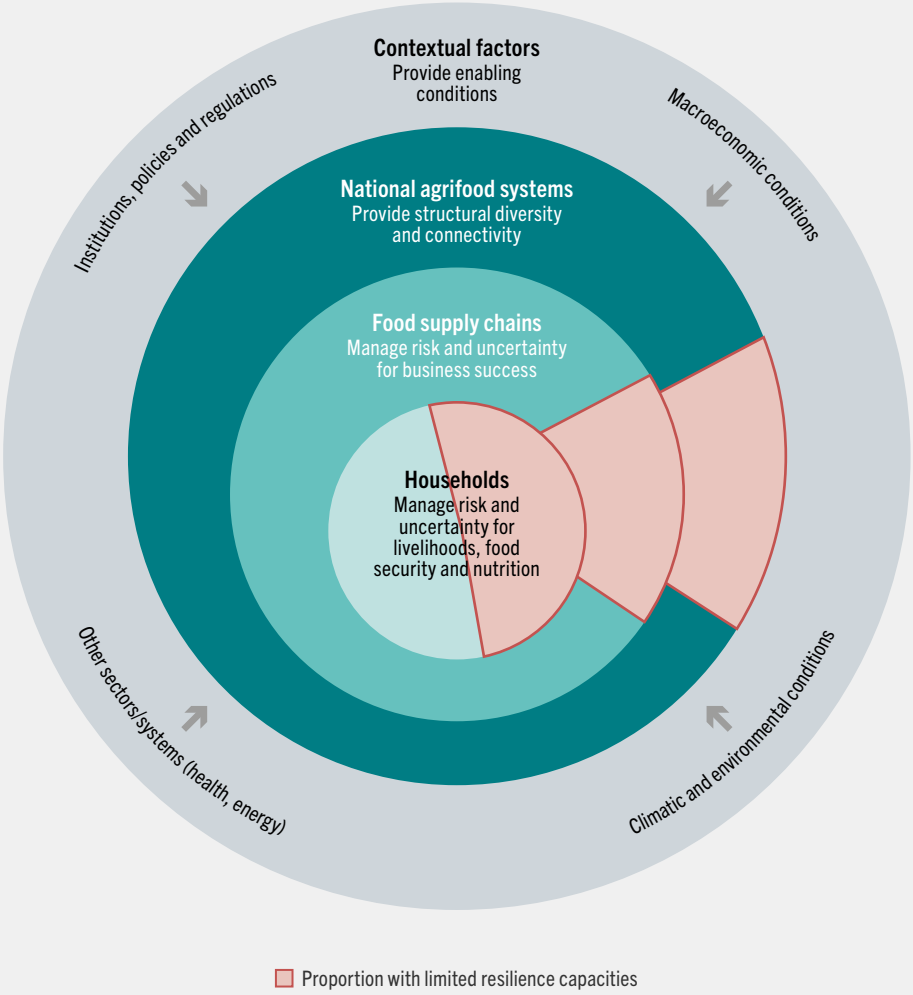
This chapter addresses the key question of ***How?*** A challenge to improve resilience is that any change to agrifood systems can generate unintended consequences and feedbacks, affecting systems' actors and activities, and may have positive or negative outcomes. Reconciling conflicting objectives will require policies (including strategies and budgets) that align the activities and decisions of different actors (public, private and civic) and promote innovative and sustainable practices that help to enhance resilience and address malnutrition, climate change and inclusion.[1, 2]

Figure 2 in Chapter 1 highlights the interlinkages between different levels and actors in agrifood systems. Policymakers need to be aware of these linkages well before a shock to a country's agrifood systems creates the need for corrective interventions or emergency measures. Overall systems' performance depends on these links and interactions between contextual factors, including institutions and regulations, and systems' components. The characteristics of the components determine not only their ability to adapt to shocks but the absorptive capacity of entire systems – the aspect of resilience that is the main focus of this report. For example, a food supply chain that reacts quickly to shocks by switching trading partners is more resilient and contributes to more resilient agrifood systems. Rapid, effective actions require collaboration between different supply chain actors. During the COVID-19 pandemic, many agrifood businesses switched to e-commerce through logistics firms that had not previously operated in the food sector.

Approaches to building resilience will need to be tailored to the wide range of shocks and stresses agrifood systems may face and to the different ways these spread through systems. The evidence in earlier chapters indicates that in order to build agrifood systems' resilience, it is important that policies, strategies and programmes adhere to **three guiding principles**:

1. **Resilience involves preparing for disruptions.** In a multi-risk environment, resilience includes preparing for both disruptions that are predictable and those that cannot be foreseen as they are surrounded by uncertainty. Preparing for the unknown requires assessing the structural characteristics of agrifood systems, including their absorptive capacity, provided by their diversity of pathways and connectivity (see Chapter 2), as well as their adaptive capacity, provided by a diversity of actors and responses (see Chapter 3). This allows systems to maintain their functions even in the presence of unforeseen disturbances.
2. **Resilience building is a system-wide multi-risk, multi-actor and multisectoral approach.** It therefore requires analysis of systems' components and the specific risks they face. This means focusing on food supply chains, small-scale producers and vulnerable households, and identifying risk-informed policies, practices and enabling conditions that improve their resilience. Mapping linkages is necessary for efficient agrifood systems' governance, optimal coordination among systems' components and their effective alignment with multiple objectives.
3. **Broader policy issues have important implications for resilience.** It is necessary

FIGURE 10 AGRIFOOD SYSTEMS' COMPONENTS AND CONTEXTUAL FACTORS



SOURCE: FAO elaboration for this report.

to consider the need for risk-informed policy measures beyond agrifood systems, promoting, for example, gender equality and women's inclusion, better and more inclusive health systems, more sustainable energy systems and sustainable use of natural resources in general. This requires comprehensive multi-risk assessments and coherent policies and practices within and across sectors and levels.

Figure 10 recalls the complexity of agrifood systems, which needs to be recognized when applying the principles and building resilience. Based on the conceptual framework of Chapter 1 (Figure 2), it represents agrifood systems and their linkages to contextual factors. The red–blue concentric circles illustrate the different components of agrifood systems discussed in Chapters 2–4 – national agrifood systems, food supply chains

and households – along with the main challenges they face with respect to building resilience. The shades of red illustrate the preparedness of agrifood systems to shocks and stresses, or rather the parts of the different agrifood systems' components and related actors (e.g. agricultural producers and SMAEs, households and the national agrifood systems in general) that lack the means to prepare for disruptions. The arrows in the outer circle indicate contextual factors outside agrifood systems – climatic and environmental, and macroeconomic conditions; as well as those in other sectors; in addition to institutions, policies and regulations – that have important implications for agrifood systems and their resilience.

Thus, with reference to the three guiding principles, the red shades in Figure 10 highlight the importance of preparing for disruptions (first principle) also for those agrifood systems' actors and parts of agrifood systems that currently do not possess the means to do so. The blue and red concentric circles illustrate the need to analyse the different components of agrifood systems and the linkages between them embedded in the second principle. The third principle, which draws attention to the importance of broader policy issues, is recalled by the contextual factors in the outer circle.

This chapter draws on the three principles to explore policies and investments that build the resilience of national agrifood systems, as well as individual food supply chains, activities and actors. The initial focus is on reducing risks and vulnerabilities of agrifood systems as a whole and safeguarding its various functions. Key concerns are the diversity of sources and supplies and the closely linked concept of connectivity to ensure a constant flow of goods in times of disturbance. The chapter then addresses the resilience of agricultural producers, agribusinesses, food supply chains and vulnerable households in terms of their capacities to prevent, anticipate, absorb, adapt and transform in the face of shocks and stresses. Resilience considerations within a broader policy environment and framework are then examined before the final conclusions are presented, summarizing the guidance provided in the chapter. ■

MEANS OF ENHANCING NATIONAL AGRIFOOD SYSTEMS' RESILIENCE: STRUCTURAL CHARACTERISTICS

Policies and investments aimed at improving the resilience of agrifood systems need to consider both risk and uncertainty. In the case of risk, a probability distribution can be assigned to possible outcomes; uncertainty, on the other hand, is characterized by an unknown probability of an outcome, either because of lack of information or because it is completely unforeseeable. Managing risk typically involves reducing exposure and vulnerability to a specific identifiable adverse event, such as through drought preparedness. By combining prevention, mitigation and preparedness actions, multi-risk management strategies also help agrifood systems become more resilient and better able to deal with the unforeseen.

Managing risk, however, must be complemented with the sufficient diversity of responses that make up absorptive capacity, as agrifood systems generally face simultaneous uncertainties and multiple risks originating from various sources. Building absorptive capacity is about guaranteeing diversity and being prepared for disruption in agrifood systems; it does not target a specific event, but provides options once a disruptive event occurs. Combining diversity with risk management will thus allow agrifood components and actors to adapt to unforeseen disruptions, while maintaining agrifood systems' core functions and potentially transforming towards a more sustainable and resilient status.

Ensuring diversity is a cornerstone of resilience

As mentioned throughout this report, and highlighted in Chapter 2, a diversity of actors and responses is essential to agrifood systems' resilience in the face of multiple risks and uncertainty. Diversity provides a network for

learning and transformation, for preventing risks and buffering shocks, and for ensuring agility in responses to varying needs and opportunities. Diversity in agrifood systems is characterized by the production of different commodities and reliance on different sources of supply and demand, both domestic and external. Food supply chains with access to more diversified input sources and output markets are less vulnerable. Likewise, reliance on multiple trading partners can enhance resilience by "importing" from different sources of supply or "exporting" to diverse demand outlets, thus diluting the impact that synchronous shocks in one place can have in other regions and sectors. In local civil society, diverse market channels – from cooperatives to community-supported and urban agriculture – can provide food security and nutrition to citizens.[3] Other buffering strategies include alternative food sources, such as food stocks.[4]

Chapter 2 provided a new perspective on the potential synergies and trade-offs generated by balancing food self-sufficiency with international trade. It highlighted the importance of incorporating redundancy in systems. On the one hand, agricultural producers benefit from redundancy in demand channels by producing for the domestic market or exporting to a diverse set of trading partners. On the other hand, consumers benefit from having food available on store shelves from various sources – domestic production, imports and food stocks.

While internal supply makes up a significant share of agrifood systems, having a mix of nutritious food available from both domestic and import sources is an important strategy to diversify risk, especially for smaller countries. For countries with a limited agricultural base, and thus higher reliance on food imports, managing trade connectivity by importing a diversified basket of nutritious foods from countries with heterogeneous socio-economic and climatic profiles is crucial to diversify the risks and reduce vulnerability to external shocks.

However, the dietary sourcing flexibility index (DSFI) presented in Chapter 2 illustrates how international trade is not neutral when it comes to sourcing nutritious foods: for many low-income countries, imports provide flexibility in sourcing kilocalories, but very little for fruits and vegetables – partly due to logistical constraints in transport and perishable storage. In these countries, policies and investments may be needed to facilitate international trade in nutritious foods to ensure their availability during disruptions.[1] Trade barriers also reduce flexibility in sourcing food. International efforts to establish new free trade areas and expand the commodity and product coverage of existing ones can provide mutual benefits to all participants and enhance resilience.

There is concern that diversification is less efficient than specialization and optimization (e.g. of transport logistics). However, diversification of the agrifood sector does not necessarily limit efficiency. Very often, different types of supply chains and stakeholders fill specific market niches and complement each other. Diversification in this broad sense does not mean that producers should not specialize. Instead, it means that at national level they should not *all* specialize in the *same* product, since this would increase systems' vulnerability to a shock affecting that specific product. If trade-offs exist, the appropriate choice of diversification will depend on the balance between the costs in terms of efficiency losses and the benefits of increased resilience in terms of higher revenues and reduced damage and losses from potential disruptions. It will also depend on the balance between short-term losses and the long-term – and potentially significant – gains from being more resilient and thus more able to manage unpredictable shocks.[5]

Choosing the most effective diversification strategy will enhance the gains from increased resilience. Building on information about exposure and vulnerability to disruptions contained in the set of flexibility indicators presented in Chapter 2 can help policymakers select an appropriate strategy, by allowing them to predict more accurately the vulnerabilities of each component and act upon it to improve systems' absorptive capacity (Box 17).

BOX 17 PUTTING THE DSFI AND PPFI TO USE

The flexibility indices for dietary sourcing (DSFI) and primary production (PPFI) presented in Chapter 2 (see Boxes 3 and 5 for a brief description of their methodology) measure the absorptive capacity of agrifood systems to shocks by capturing the multiple pathways to source food and generate value for primary producers. Covering more than 150 countries, the indicators do not capture, however, the level of exposure and vulnerability to disruptions of each pathway in each country. Rather, the approach is threat-agnostic. However, policymakers who have information on threats and their likelihood, as well as the pathways affected, may include this to derive a risk-adjusted set of indicators.

Since the indicators can be broken down into components representing a set of pathways (see the stacked bars in the figure in Box 4), this can be done by adding the probability of disruption to each component in the indicators' formula (see Annex 1 for a demonstration). The probabilities express, for each component, the likelihood that a set of pathways may not be available, and therefore cannot be relied upon when a disruption occurs. By way of illustration, if stocks in a given country are readily available when a shock occurs, then the probability would be zero, but if stocks cannot be used, the probability would take the value of 1. In reality, probabilities will fall somewhere in between. In the case of stocks, these may only be used if supply falls by a certain amount, in which case, the probability equals the likelihood that a shock does not cut supply by that amount.

Because it is unlikely that all pathways in a country are readily available during disruptions, the risk-adjusted set of indicators will be lower than the values presented in this report. How much lower depends on the (perceived) reliability of different pathways.

In complex systems, it is difficult to manage what one cannot measure. These indicators can help quantify the resilience of agrifood systems and provide important guidance on how to transform them to make them more resilient.

Connectivity is a cornerstone of diversity

In addition to being connected to international trade partners, agrifood systems rely on connectivity to physical and other infrastructures, such as communications and transport networks, crucial for ensuring supply diversity and rapid adaptation to shocks. Well-connected agrifood systems can overcome and recover from disturbances faster and more easily by shifting sources of supply and routes of transport and commercialization of food products, agricultural inputs and labour, as well as channels for knowledge and financial resources. Connectivity to international markets through infrastructure, as well as strong commercial relations, are part and parcel of this.

Developing and maintaining a robust and diversified domestic food transport network can facilitate physical access to food across a country's terrains and urban landscapes. Similarly, physical infrastructure that ensures international trade connectivity (ports, international railway systems, etc.) is important. During the COVID-19 pandemic, many governments provided support and adopted a coordinated approach to keep food shipments functioning. For example, the International Maritime Organization (IMO) called on governments to consider seafarers and marine personnel key workers providing an essential service and thus exempt them from movement restrictions, allowing them to join or leave ships and transit to an airport.[6] In Europe, private ports and terminals urged European Union Member States to consider ports as critical infrastructure and provide appropriate support to avoid disruption and prevent significant job losses.[7] China opened a green channel for fresh agricultural products and used e-delivery

platforms to resolve the logistical challenges connected to small-scale producers accessing urban communities, while minimizing the potential risk of infection from visiting crowded food markets.[8]

Guaranteeing connectivity is also about managing the risks that can disrupt it. Disasters and crises can significantly affect infrastructure and services, such as roads, transport or storage facilities, in agriculture and food supply chains. The result can be catastrophic damage and loss to people's livelihoods, the environment and the economy. It is important to assess, protect and risk-proof connectivity, and to plan, design and develop new risk-sensitive and climate-resilient infrastructure; achieving climate resilience requires assessing physical vulnerabilities. Land use planning should also be enhanced to prevent or reduce risks in the face of hazards.

Another important risk-related dimension of connectivity is the need for an effective and pervasive food safety management system that ensures food safety vigilance throughout agrifood systems. Assurance on meeting food safety standards greatly facilitates any shift in sourcing supplies in the case of shocks. The COVID-19 pandemic has underscored the close connections between human, animal and environmental health and the urgent need to address them in a holistic manner. Recent studies showed that the landscape of emerging and re-emerging infectious diseases is closely associated with changes in ecological factors, climate and human behaviours.[9–11] It is estimated that 75 percent of newly discovered or emerging infectious diseases are zoonotic (i.e. transmitted from animals to humans).[12]

Stronger international institutions and cooperation for contagious disease detection and containment and food security are needed.[13] WHO's One Health approach to programmes, policies, legislation and research to achieve better public health outcomes is a case in point.[14] It involves coordination across various sectors, from plant and animal health, food safety, nutrition and biodiversity, to climate change, forestry and environmental protection. It also requires embedding the principles of gender equality and economic and social responsibility into normative and operational capacity development. Legislation creates an enabling environment to promote and enforce such practices, with the regulatory basis to strengthen animal and plant health in agriculture and wildlife, as well as ensure food safety. It also contributes to safeguarding and restoring ecosystems by introducing mechanisms to prevent and control environmental contamination, biodiversity loss, degradation of forests and impacts of climate change.[15] ■

POLICY MEASURES THAT ENHANCE FOOD SUPPLY CHAIN RESILIENCE

As discussed in Chapter 3, the resilience of national agrifood systems is also strongly shaped by how diverse and well-connected food supply chains are, and how farms and agrifood businesses along those chains source inputs and sell outputs. This section identifies the main policy interventions that enhance the resilience of food supply chains. A resilient supply chain does not necessarily mean all its actors are resilient. Shocks and stresses may cause disastrous damage to some actors, but also create opportunities for others to transform and grow. Such dynamics will always entail winners and losers – some actors may grow and others may perish. The important point is that, when supply chains are resilient, shocks and stresses should lead to improvement in their functioning and delivery as a whole. Subsequent socio-economic costs should be minimized through measures such as social protection or use of existing food stocks.

An important consideration when assigning policy priorities is, therefore, the potential trade-offs in food supply chains between resilience on the one hand, and efficiency, inclusiveness and equity on the other. For example, trade-offs may be possible between incorporating some duplication and redundancy, which strengthen resilience, and

minimizing costs, which produces short-term efficiency benefits. Similarly, a food supply chain may be resilient, but not inclusive, if the enhanced resilience excludes vulnerable, small-scale agricultural producers. The challenge is to implement the right mix of policies and interventions that help build capacities to minimize trade-offs and create synergies that lead to resilient but also efficient and inclusive food supply chains.

Diversity is a source of resilience, but requires risk reduction measures

Maintaining diversity within and between food supply chains is important for ensuring agrifood systems' resilience. Chapter 3 categorized food supply chains into three broad types: traditional, transitional and modern, each with its own strengths and weaknesses when facing shocks and stresses. Policies and interventions to strengthen resilient food supply chains should do the following:

Allow for a mix of traditional, transitional and modern food supply chains. These supply chains play different roles within national agrifood systems, but all can act as buffers against shocks and stresses of different types. Transitional and modern supply chains, being long and serving wide geographical areas, can more easily respond to local shocks and ensure food availability in the directly affected areas. Large-scale agrifood companies, which dominate the modern food supply chains, have more access to capital and resources. Their financial strength enables them to buffer against shocks for long periods. In addition, they play a central role in international trade – key for diversifying food sourcing to enhance agrifood systems' resilience and buffer against domestic shocks.

However, traditional and local chains, particularly those based on small-scale producers and SMAEs, can play an important role in improving the resilience of food supply chains in the face of large-scale disruptions. For example, FAO found that, thanks to their close proximity to production areas and shorter supply chains, agrifood systems in small villages were more resilient to shocks than those serving larger urban areas over longer chains.[16] This was also evident during the COVID-19 pandemic, when many local supply chains proved to be quite nimble in their response to demand shifts.[17] SMAEs can also be sophisticated, efficient and resilient when they have access to adequate credit sources and infrastructure.

The COVID-19 pandemic created an opportunity to promote further interest in local food, made available by local supply chains.[17] With a small number of intermediaries and shorter distribution time, local food supply chains are often capable of providing consumers with fresher, more nutritious food, in addition to the perceived development and sustainability benefits of reduced fossil fuel consumption and increased support for the local economy.[17–19] Improved rural–urban infrastructure and building the capacities of actors within traditional food supply chains to use digital tools can create synergies between efficiency, inclusiveness and sustainability, while enhancing the diversity of overall agrifood systems. Home food delivery and other e-platforms, linking buyers and sellers through various digital tools, accelerated greatly during the pandemic to compensate for losses of traditional market outlets (see Chapter 3).

Modern, but short, food supply chains can also strengthen the diversity of food availability based on future foods such as micro-algae and cultured meat. Produced in closed environments, these foods provide various benefits in terms of resilience, namely: reducing exposure to biotic and abiotic risk factors; and providing nutritious foods through decentralized and local food supply chains. Although future food technologies require large-scale financial investments and new technical expertise, they can respond to local needs, providing an additional path for diversity in sourcing food – especially for countries with limited agricultural resources.[20]

Acknowledge the heterogeneity of farms and businesses along the urban–rural continuum. Addressing vulnerabilities and enhancing resilience at different scales requires a territorial perspective. For example, a recent worldwide FAO assessment showed that the shortage of labour in agriculture and food-related activities caused by COVID-19 mobility restrictions varied greatly by size of urban agglomeration.

In general, small towns between 5 000 and 25 000 inhabitants, where workers needed to travel shorter distances, were less affected, while cities of more than 5 million inhabitants were more vulnerable to disruptions.[16]

Diversity is also a trait of resilience at the producer level, and agriculture will most likely continue to comprise units of varying scales. Historically, agricultural producers have learned to cope with the impacts of multiple and simultaneous shocks which may be transient or lasting. Because producers' resilience capacities are strongly linked to farm characteristics and how they interact with their surroundings, policies and interventions need to focus on the regional context in which farming systems operate.[21] Enhancing producers' resilience needs to build on their strengths and address critical factors that constrain productivity growth, such as limited access to credit and markets. Policies should also avoid replacing producers' own strategies or making them policy dependent.

Account for context and heterogeneity. Different types of agricultural producers, agrifood enterprises and food supply chains have different degrees of exposure or vulnerability to shocks and stresses. Measures to reduce vulnerabilities, including livelihood diversification and alternatives, need to be adapted to the local context and take into account heterogeneity. Disaster risk reduction, good practices for climate change adaptation, technologies and innovations can all help reduce the underlying causes of vulnerability where exposure to disasters and climate-related shocks is highest. Climate-resilient practices and technologies at the level of the farm and/or business and the territory can help increase yields and support production sustainability, enhance diversification, and reduce risks of production failure caused by climate shocks and stresses.[22]

Practices that contribute to reducing vulnerabilities and risks in agrifood systems include the promotion of crop, livestock, tree and fish varieties that are more resilient to floods, droughts or saline conditions.[23] Soil and water practices, such as conservation agriculture, agroforestry, fodder conservation and improved seed storage are other examples of sound climate-resilient practices.[24, 25] According to a 2019 study of the benefit–cost ratio of good practices in disaster risk reduction, they generated, on average, benefits 2.2 times higher than did practices previously used by farmers under hazard conditions.[26]

Creating an enabling environment for food supply chains

The performance of any food supply chain is the outcome of numerous decisions taken by the various actors – also in connected input and services supply chains (see Chapter 3) – and how these decisions interact and change under diverse conditions. Designing and implementing strategies for resilient food supply chains requires an enabling environment for individual actors. Key enabling conditions that provide this infrastructure of supply chain resilience include the following:

Leveraging of information and communications technology (ICT) and digital tools for logistics. Central and local governments, together with the private sector, NGOs and international development agencies, have an important role to play in supporting ICT. Scale-appropriate ICT can provide tools for detecting early risk signals, making timely forecasts, adopting early warning strategies and realizing response diversification.[27] ICT and digital tools can also dramatically increase access to information in the agriculture sector, opening the way to substantially improve the effectiveness of agricultural extension, advisory services and learning.[28] They also contribute to informed decision-making regarding natural resources, cropping systems, pests, diseases, etc. Following the COVID-19 pandemic, there has been a global trend to create more online direct distribution links between farmers and consumers, such as e-commerce, which can improve access to fresh food, including fruits and vegetables.[29]

Improvements in risk management and early warning capacities. An integrated approach for agrifood systems' resilience can help predict the likelihood of shocks and how they impact on lives, livelihoods, food security and nutrition. This will include components such as

agroclimatic monitoring, disaster and crisis risk and vulnerability assessments (including pests and diseases), and agricultural damage and loss data.[30–32] To enhance risk- and crisis-informed decision-making, governments at various levels, in coordination with academia, research centres and the private sector, should make these data available for analysis throughout agrifood systems.[33] An early warning system combines monitoring and risk assessments with communication and preparedness systems and processes that enable anticipatory action to mitigate the effects of disasters and crises.[34] Public–private partnership is essential to put in place early warning systems to cope with multiple hazards occurring simultaneously or cumulatively over time, as well as any potential cascading impacts. Multi-risk early warning systems need to be coupled with actionable alerts which trigger immediate action and emergency response mechanisms. This implies connecting the early warning system to a range of government institutions and local stakeholders through clear anticipatory action and contingency plans with funding to take the necessary actions based on the warning system.

Inclusive governance and institutions for better risk management. Governance is the combination of processes through which public and private actors articulate their interests, frame and prioritize issues, and make, implement, monitor and enforce decisions.[35] Inclusive governance is at the core of preparedness that focuses on the knowledge and capacities to respond effectively to shocks and stresses. In combination with sound analysis of risks and potential crises and with early warning systems, governance is crucial to ensure quick and appropriate response and recovery, when needed.[34] Besides these national policy instruments, subnational and local multi-risk management strategies should also be developed to address underlying vulnerabilities and risk drivers, strengthening institutional capacities according to the local context. When several governing bodies on different levels work well together, they enable coordinated actions in the face of risks and uncertainty, and provide flexibility to deal with issues at the appropriate level.[36] One example is the city-region food systems approach, which recognizes the connection between urban centres and rural areas, while acknowledging the linkages between economic, environmental and social sustainability and the need to adopt a multisectoral view (see FAO. 2021).[37]

National disaster and risk management tools tailored to food supply chains. Envisaging these tools in national laws, policies, regulations and strategies for food supply chains will enable stakeholders to function effectively and collaboratively within and across sectors. Promoting diversity in sourcing food from multiple markets and regions (see Chapter 2), supporting a multisectoral approach to decision-making, and putting in place protocols that reduce specific risks (e.g. weather-related, biological) will enable stakeholders to reduce the risks and adverse impacts of multiple shocks and stresses. Diversifying sources of inputs and distribution networks also has the potential to improve the availability of food when disruptions occur. Government regulatory agencies also need to ensure that available products and services are of high quality and provided by a thriving and competitive private sector. WHO's One Health approach, explained above, is very relevant for resilience in food supply chains because it enhances productivity while reducing risks from biological threats along the food supply chain. The rationale is to integrate agrifood and health sectors for more efficient coordination of pest and disease emergencies through improved pest and disease prevention, early warning and management of national and global health risks, including appropriate use of antimicrobials to mitigate antimicrobial resistance.[25]

Innovation in distribution strategies and broad participation. To achieve the long-term objectives of agrifood systems' sustainability and resilience, the ability of food supply chains to consistently deliver food efficiently and effectively must be enhanced. Finding appropriately scaled market channels is particularly challenging for medium and small-scale producers and many SMAEs. They are often too small to distribute products economically through large, vertically integrated grocery chains, but their volumes are too great for direct-to-consumer channels, such as farmers' markets.[38] Creating an enabling environment and encouraging coordination along food supply

BOX 18 LOGISTICS CENTRE IN KEMIN, KYRGYZSTAN

The Logistics Centre in Kemin, Kyrgyzstan, an FAO pilot programme established in 2018, ensures schools have a sustainable supply of crops raised by local producers, thereby contributing to improved nutrition in school meals and increasing small farmers' income, as well as the economic development of the district. It supplies diverse and nutritious food from local producers to 29 schools in the Kemin district of Chui Province to improve the diet of 12 000 schoolchildren and provide a market for at least 50 small farmers. The Logistics Centre is a centralized procurement, storage and quality control facility; it has a capacity of 250 tonnes and a warehouse area of 270 m^2. It has equipment for cool storage and laboratory quality control of agricultural products. It also has a truck equipped with a thermobox, which maintains the quality of agricultural products delivered to schools in the most remote parts of the region.

The Logistics Centre is an example of successful unification within one programme of measures in the fields of agriculture, nutrition and social protection. A mid-term economic analysis found the Logistics Centre model could be sustainable with a return on investment in five years while charging a fee of 5 percent of the stored farm products in-kind to cover the cost of storage and distribution services. It improves resilience through greater connectivity and capacity to store stocks and provides a cost-efficient supply chain between local producers and schools, while respecting food quality standards.

SOURCE: Shuvaeva & Belova. 2019. [41]

chains can help them overcome scale-related constraints in accessing markets. Promoting the active participation of small-scale producers and SMAEs in producer associations, cooperatives, consortia and agro-industrial clusters, with policies that create an enabling environment to facilitate coordination, can help them access markets and adopt business strategies that improve resilience and efficiency.

Transporting food from rural and dispersed farming areas to distant urban demand centres is often too costly, especially for refrigerated or frozen goods. Most small-scale agricultural producers lack the expertise, capital or access to credit to acquire and use these logistics. Their distribution systems tend to be fragmented and less efficient than the centralized networks of modern food supply chains,[39] making regionally produced food more expensive. Efficiency-enhancing logistics best practices can bring down costs and increase consumers' access to food produced in regions lacking access to supermarkets. Improved logistics will be particularly important in helping small-scale producers and SMAEs to remain competitive once the COVID-19 pandemic is over, especially since many consumers have enjoyed the convenience of one-stop-shopping, home delivery and value-added products.[40] Logistics can be improved through optimized routing and scheduling and consolidation of delivery routes; development of logistic centres (Box 18); appropriate vehicle types and sizes to meet supply chain objectives; punctual and frequent deliveries; outsourced transportation; horizontal collaboration; and facility location (i.e. the optimum number and location of warehouses).[17]

Wider access to business tools that enhance agility and flexibility. Policies also need to focus on helping producers and agribusinesses adopt business tools that enhance resilience. Recommended measures include:

- *Enhancing business literacy* throughout the supply chain and developing and promoting business innovation and incubation services, as well as training on *ex ante* measures in preparation for short-term or long-term shocks.
- *Expanding access to and adoption of tools and resources* (e.g. internet, credit, insurance) to help producers and businesses build their capacities. Governments and development partners could support innovations in e-commerce by investing in hard and soft infrastructure and creating an enabling business and commercial environment for both large companies and SMAEs.
- *Funding research and development (R&D) and agricultural extension services* focused on agricultural adaptation strategies, including climate change adaptation and best agronomic practices, such as improved varieties, proper crop planting and harvesting periods and better nutrient management.[42–44] Participatory R&D builds on existing knowledge and responds to the needs of agricultural producers. ■

ENHANCING THE RESILIENCE CAPACITIES OF SMALL-SCALE PRODUCERS AND VULNERABLE HOUSEHOLDS

Resilient livelihoods are a key element of resilient agrifood systems as they ensure access to food even in the face of shocks. Among the households most vulnerable to shocks, those involved in small-scale primary production activities – such as crops, livestock, pastoralism, fisheries and aquaculture – will benefit most from the logistical support, production innovations and inclusive governance of food supply chains described in the previous section. Beyond support to those households, it is important to ensure physical and economic access to healthy diets for all. This report estimates that in addition to the nearly 3 billion people who cannot afford a healthy diet,[1] about another 1 billion are at risk of not being able to afford it if a shock reduces their income by one-third. Even in high-income countries, households can be hit by shocks that threaten their food security.[45]

However, households in low-income countries are disproportionately affected. The rural poor are among those who face the greatest challenges. They rely heavily on self-employment and family labour, as well as natural resource-based livelihoods. They are constrained by poorly functioning markets and lack of access to credit, insurance and adequate public services, such as health and education. This makes rural households highly vulnerable to shocks, such as: unexpected weather and environmental disasters; the effects of climate change; and financial and economic crises.[46] Such shocks affect their livelihoods and can undermine their asset base and their capacity to manage risks effectively.[47] In framing policies to build the resilience capacities of small-scale producers and vulnerable households, policymakers should seek to do the following:

Facilitate better risk management and enable household resilience capacities. This is particularly important for agricultural and rural households involved in small-scale farming, livestock, pastoralism, fisheries and aquaculture, as well as urban and rural households that earn their living in the informal food sector, for example as food processing workers or street food vendors. To be effective, policies should address the specific disadvantages of different agrifood systems' actors with a special focus on women, youth and Indigenous Peoples, and design targeted measures that build their capacities to prevent, anticipate, absorb, adapt and transform in the face of shocks.

Following the RIMA analysis in Chapter 4, other key interventions that can enhance the resilience of rural livelihoods include expanding access to productive and non-productive assets, supporting diversification of farm and non-farm income and improving access to social services (e.g. education and sanitation). The latter is highly relevant for households living in harsh

conditions, for example, those involved in pastoralism. Such interventions should be supplemented by actions to strengthen local institutions and traditional support networks, reinforcing local knowledge, improving infrastructure, and enabling services for inputs and market access. Enhancing rural advisory services will help meet small-scale producers' need for advice on how best to manage crops, soil, water, nutrients, pests and diseases.

Policies and interventions that target households comprising mainly women and girls are strongly encouraged because they pay the heaviest toll during and after shocks. Due to limited access to resources such as land and other assets, they are more likely to use negative coping mechanisms in times of shock, such as selling assets – a strategy which is risky and unsustainable in the long term. Empowering women and girls by expanding their access to productive assets and decent employment means they can absorb shocks and bounce back afterwards without undermining their food security status or depleting their assets. Education plays a key role in strengthening women's resilience capacity, underscoring the importance of expanding access to education for all, especially for girls. Women with more education have better access to the labour market and can expand their options for income generation.

When focusing on households involved in primary production, it is also important to distinguish between net sellers and net buyers of food. Net sellers need support that focuses on the commercial dimension of their activities as producers and promotes their inclusive integration into food supply chains. For net buyer households, policies need to enhance and guarantee their purchasing power and facilitate diversification of sources of income and livelihoods.

As extreme climatic events become more frequent and more pronounced, producers will face increasing risks. Expanding the access of small-scale producers to agroclimatic early warning systems for disaster risk reduction is important and may require training and subsidies to make them affordable. Increasing small-scale producers' access to insurance (e.g. crop and weather insurance) enhances their ability to take out production loans and participate in more risky, higher-return farming activities.

Design social protection policies that improve household resilience in the event of a shock. Social protection programmes help vulnerable households avoid negative coping strategies that are detrimental to their livelihoods and their capacity to face future risks and shocks. They are particularly relevant for vulnerable rural households, including those involved in small-scale fisheries and aquaculture activities, as well as informal workers and the urban poor. When designed to be sensitive to gender equality and improved nutrition, as well as responsive to multiple risks and shocks, social protection programmes can provide support not only to routine beneficiaries such as pensioners, but also to at-risk and crisis-prone populations before, during and after a shock. They can expand benefits according to the emerging needs of potential beneficiaries, help to fill poor households' consumption shortfalls, and enable them to invest and engage in productive activities. Social protection systems may also allow an increase in caseloads through contingency funds triggered by early warning systems as well as standard operating procedures.[48]

In this way, social protection policies can help safeguard food availability and access in the face of shocks and prevent ripple effects through food supply chains. In Ethiopia, for example, the Productive Safety Net Programme (PSNP) focuses on chronically food-insecure households, providing cash or food transfers on a predictable basis for five years, along with financial and technical support. The goal is to help these households build assets that can sustain them through future crises, while contributing to building rural infrastructure.[49] Results from the RIMA analysis in Chapter 4 show that access to timely social protection helped women and girls in particular cope with shocks, allowing them to avoid negative coping mechanisms. If well designed, social protection enables synergies with productive support programmes and investments, which strengthen both the resilience and sustainability of small-scale producers' livelihoods.[50] Efforts and policy reforms aimed at strengthening links between social protection and productive support programmes are highly encouraged. ■

PLANNING FOR THE FUTURE – BROADER POLICY AREAS AND PRIORITIES

A range of broader policy issues and priorities, some beyond the scope of agrifood systems, can have important implications for policies aimed at promoting agrifood systems' resilience:

Guaranteeing economic access to a healthy diet needs to be a priority not just in low-income countries. Chapter 2 outlined how a broad share of the world's population is unable to afford a healthy diet, or is at risk of not being able to afford it when confronted with an income shock, as further recalled above. Such vulnerability is the result of limited incomes combined with the cost of a healthy diet. Therefore, increasing incomes and transforming agrifood systems to make healthy diets more accessible are key. Figure 6 identified four broad country profiles: at one extreme are high-income countries with limited affordability issues; at the other are countries, especially low-income countries in Asia and sub-Saharan Africa, where more than 80 percent of the population cannot access a healthy diet and are in dire need of greater affordability independently of shocks. There are also numerous countries, mostly middle-income, where many who can afford a healthy diet are nevertheless at risk. Policy focus and the investments required will depend on where a country sits on this spectrum. Some countries may place more emphasis on addressing structural issues such as income levels and distribution, while others may focus more on risk management and diversification.

Policies must impact directly on the adaptive capacity of systems' actors, especially households. One important lesson of the COVID-19 pandemic is that the food security resilience of households depends on policies and measures beyond agrifood systems themselves. The importance of social safety nets to the rural and urban poor was mentioned in the previous section. Other key policy areas with a clear impact on household resilience include strong and inclusive health insurance and medical services. Education and training are also vital for strengthening household resilience in the long run. Broader policies aimed at promoting gender equality and women's inclusion will have significant impacts on resilience at household level and more broadly within agrifood systems, thanks to the increased participation of women in all sectors of agrifood systems. Policies aimed at boosting employment can sustain livelihoods and incomes, with positive impacts on entire agrifood systems.

Policies are needed to promote agrifood systems' sustainability through stewardship of the environment. With demographic and environmental pressures increasing and huge uncertainties surrounding future shocks and stresses, the resilience of agrifood systems has become a major international concern. Building the resilience of agrifood systems must be an integral part of ensuring sustainability, particularly in the long run. Rather than aggravating climate change and natural resource degradation, agrifood systems need to become stewards of the environment. Mainstreaming biodiversity in agrifood policies is essential to protect the health and diversity of ecosystems. It is key to reducing the adverse impacts of climate-related hazards, such as drought, floods and storms. Healthy and diverse ecosystems provide essential environmental services, such as fresh water, clean air, fertile soil and pollination, which contribute to food security and resilient livelihoods,[51] protecting against climate risks as well as geophysical and biological threats. Measures that aim to promote healthy and diverse ecosystems include nature-based solutions, which protect, sustainably manage and restore ecosystems, while addressing societal challenges.[52] Practices such as watershed management, landscape approaches, agro-ecological farming and climate-smart agriculture have an important role to play in win–win scenarios that not only ensure more resilient agrifood systems, but also promote high-yielding long-term investments.[53, 54]

Green infrastructure – bushes, orchards, hedgerows, grasslands, ponds, pools, wadis and wetlands – can also reduce vulnerabilities and

risks across and within agrifood systems while supporting environmental sustainability.[55] Given that Indigenous Peoples and local communities are often at the centre of natural resources management, thanks to their close links with and dependence on the environment and use of natural resources for their livelihoods, the resilience of these communities is indivisibly connected to the condition of the environment and management of its resources.[56]

Policies need to be coherent and coordinated in order to mainstream resilience in national planning across sectors. As in other domains, policy coherence is essential when addressing the needs of agrifood systems. The global impact of and response to the COVID-19 pandemic – a human health crisis thought to be caused by a virus passed from animals – highlights the fact that protecting health and preventing disruption to agrifood systems requires coordinated action across sectors relating to animals, people, plants and the environment: the One Health approach.[57]

It is also important to recognize that policymaking can have unintended consequences. To avoid implementing restrictions that hurt its agrifood systems' actors, policymakers must understand how agrifood systems function and how their actors interact. During the COVID-19 pandemic, for example, South Africa deemed the wood sector non-essential, which harmed fruit growers who rely on wooden crates to distribute their products. Conversely, in countries where agriculture was deemed essential, the sector remained relatively resilient. In Mexico, the agriculture sector was considered a priority activity and food prices remained relatively stable.[58]

Policy coherence is important with regard to subsidies and other instruments of agricultural support. While subsidies may provide immediate and short-term relief to agricultural producers, they can also reduce their capacity to adapt to shocks. Although individual producers may be protected in the short to medium term, this may be at the cost of making entire agrifood systems less resilient, with negative impacts reverting back to individual producers. This is what happened in the Syrian Arab Republic, where continuous government support for producer prices and irrigation-intensive crops (wheat and cotton) led to excessive use of groundwater and extreme depletion of the aquifers. This limited the adaptive capacity of Syrian farmers when severe drought struck the Near East in 2007–2008. Conditions worsened in 2008 when the Government lifted subsidies on diesel fuel – used in irrigation – triggering an overnight price increase of 300 percent.[59, 60] As a result, thousands of agricultural households abandoned their farms and migrated to cities. The United Nations estimated the crisis displaced more than 300 000 people in 2009, leaving 60–70 percent of villages in the regions of Hassakeh and Deir ez-Zor deserted.[61, 62] The fundamental lesson is that policies and interventions affecting agrifood systems need to be carefully assessed for their long-term sustainability and how they affect the resilience of individual actors and systems as a whole.

Another concern relates to the sustainability of social protection schemes, an essential component of resilient livelihoods among vulnerable populations. These programmes, alongside subsidies and any policies supporting agrifood systems' resilience, need to be fiscally sustainable.

To meet the challenge of policy coherence and coordination in building resilience, all sectors and layers of government institutions must be involved. More emphasis must be given to the need for vertical alignment of policies and actions at national and subnational levels. In particular, the role of local government in responding to shocks and building resilience is crucial. The FAO survey to assess the impact of the COVID-19 pandemic on urban food systems clearly highlighted the key role of local government in addressing impacts on food security and nutrition.[16] The empowerment of local government can make a big difference in preventing a food security crisis following a shock.

Many of these ideas are being mainstreamed into some countries' agricultural risk management policy frameworks, but they

are rarely considered as part of a holistic strategy to improve sectoral and cross-sectoral resilience. There is a need to mainstream resilience in agrifood policies and across sectors. Resilience should be a policy objective, not just a tool to achieve other objectives. Agriculture and government institutions should collaborate across sectors to better anticipate stresses, such as water depletion and emerging zoonotic diseases that may eventually disrupt systems. Specific case studies on resilience to drought in Australia, natural disasters in Canada, and animal and plant health risks in Italy and the Netherlands provide concrete examples of how countries are conceptualizing resilience.[63] ■

CONCLUSIONS

The COVID-19 pandemic has created space for new narratives about resilience in agrifood systems. The resilience perspective presented in this report implies the preparation for shocks and future challenges as yet unknown, by building agrifood systems' capacity to prevent, anticipate, absorb, adapt and transform in the face of any disruption. The overarching objective of this preparation is to manage stresses and shocks in a way that ensures continuous availability of and access to sufficient and nutritious food for all. Preparation is furthered by identifying the means and tools that strengthen agrifood systems' resilience capacity and facilitate systems' transformation towards sustainability and inclusiveness.

This chapter has revisited the holistic framework (presented in Chapter 1) for building resilient national agrifood systems, and has offered three guiding principles for policies, strategies and programmes. The principles call for preparation, cooperation, coordination, inclusiveness and equity. They aim to promote the mainstreaming of resilience objectives into policy frameworks and create incentives to dynamic change for the different components and actors of agrifood systems.

Table 5 summarizes different entry points to manage risk and uncertainty in agrifood systems, and the contextual factors to be considered. A distinction is made between entry points tailored to coping with uncertainty (Shocks difficult to foresee) and those adapted to managing specific risks (More predictable shocks).

The resilience capacity of agrifood systems can be enhanced by policies and interventions that: encourage diversity, connectivity and flexibility; promote dialogue, transparency and collective learning in food supply chains and networks; and ensure that vulnerable households have access to healthy diets, even when incomes are affected by a shock. Acknowledging that trade-offs can arise, this chapter recommended assessing the critical roles of diversity and trade in agrifood systems in response to shocks and stresses, to help actors tailor their strategies for managing resilience.

This chapter also identified the key interventions that can enhance the resilience of individual supply chain actors, upon which the resilience of national agrifood systems depends. They include framing innovative strategies for food transport and distribution, leveraging ICTs, maintaining diversity, and promoting inclusive governance and broad participation. Public policies also need to focus on helping small-scale producers, small and medium enterprises and vulnerable households gain access to business tools they need to enhance their resilience.

One of the objectives of this edition of *The State of Food and Agriculture* is to contribute to the dialogue and debate on how to build resilient agrifood systems in the wake of the UN Food Systems Summit. It aims to help guide action on the ground with regard to building resilient agrifood systems and thus make a concrete contribution to leveraging the power of these systems to deliver progress on all 17 Sustainable Development Goals (SDGs). Building resilience is a necessary condition and intrinsically linked with achieving the SDGs and the overall 2030 Agenda for Sustainable Development. Agrifood systems'

TABLE 5 ENTRY POINTS TO MANAGE AGRIFOOD SYSTEMS' RISK AND UNCERTAINTY

	SHOCKS DIFFICULT TO FORESEE → MORE PREDICTABLE SHOCKS		
	Ensuring diversity	Managing connectivity	Managing risks
CONTEXTUAL FACTORS	▸ Promote gender equality and support youth ▸ Pursue policies and regulation to protect the environment (water, land, biodiversity, fisheries and forests) ▸ Safeguard macroeconomic stability ▸ Ensure broad access to financial services ▸ Support indigenous knowledge systems	▸ Encourage and promote effective partnerships for sustainable development ▸ Promote an open, inclusive and equitable multilateral trading system	▸ Prepare and implement national adaptation plans for mitigating and adapting to climate change ▸ Ensure well-coordinated and coherent policies for long-term macroeconomic stability
NATIONAL AGRIFOOD SYSTEMS	▸ Ensure diversity of food production, market channels and trade partners (both domestic and external)	▸ Invest in robust and redundant food transport networks ▸ Invest in infrastructural connections to international markets (e.g. ports)	▸ Promote disaster risk reduction and disaster risk assessment ▸ Prepare national plans for drought management ▸ Invest in food safety management systems ▸ Carry out multi-risk assessments within and across sectors and levels ▸ Adopt a One Health approach
FOOD SUPPLY CHAINS AND ACTORS	▸ Allow for a mix of traditional, transitional, and modern food supply chains, including short, local food supply chains ▸ Promote inclusiveness for SMAEs	▸ Diversify sources of supply and output markets ▸ Enable and invest in stronger rural–urban linkages, especially for short supply chains ▸ Expand and improve access to ICT	▸ Ensure timely forecasts and tools for detecting early risk signals ▸ Establish and improve early warning systems
HOUSEHOLDS AND LIVELIHOODS (small-scale producers and vulnerable households)	▸ Support the diversification of on- and off-farm income sources ▸ Promote good agricultural approaches and practices ▸ Expand access to credit and insurance to the most vulnerable	▸ Expand access to ICT and agricultural extension services ▸ Support collective action by small producers to develop bargaining power	▸ Promote access to productive assets ▸ Expand access to social services and education ▸ Implement targeted and timely social protection assistance for all vulnerable groups, including small-scale producers and the urban poor ▸ Fund R&D relating to agricultural adaptation strategies (e.g. climate change)

SOURCE: FAO elaboration for this report.

resilience is directly aligned with the achievement of SDG 2, Zero Hunger, and is key to progress towards several other SDGs, both those with a socio-economic focus and others relating to environmental sustainability. Creating peace and prosperity for all people on the planet by 2030 (in line with SDG 16, Peace, Justice and Strong Institutions) will prevent many disturbances – or at least strongly mitigate their impact. This places resilience of agrifood systems in a much broader context. ■



MONGOLIA
A livestock herder, vulnerable to intensifying dzuds, pours a hot meal. FAO's interventions mitigate the impacts of climate change on Mongolia's poorest herders. ©FAO/Khangaikhuu Purevragchaa

ANNEXES

ANNEX 1
Description, data and methodology of the indicators in Chapter 2 98

ANNEX 2
Additional figures to Chapter 2 107

ANNEX 3
Statistical tables 110

ANNEX 4
Additional tables to Chapter 4 133

ANNEX 1
DESCRIPTION, DATA AND METHODOLOGY OF THE INDICATORS IN CHAPTER 2

PRIMARY PRODUCTION FLEXIBILITY INDEX (PPFI)

Description

The PPFI examines all the different pathways through which a country primary sector can generate value from agricultural output. If it has many different pathways, the primary sector will have greater capacity to absorb shocks. This depends on two main factors: (i) the level of diversification of the produced commodities; and (ii) access to markets for these commodities. The PPFI uses both factors to measure the diversity of production across commodities and the potential to produce for domestic or export markets based on the share of each commodity and its final destination (domestic or export). It indicates which commodity an average producer is likely to plant and whether it ends up in the domestic or export market. Higher values indicate multiple paths for generating agricultural value and for placing primary production in the markets (i.e. redundancy of demand channels) and thus a higher capacity to absorb shocks. The pathways are described in Figure A1.1.

The PPFI is, therefore, a combined measure of the possibility of choosing what to produce and the redundancy of demand channels to market it. Information entropy is used as a measure of uncertainty for what is produced and where it is sold. The expression of the PPFI can be derived from first principles following the standard measure for information, or the lack thereof, termed the Shannon Entropy,[1] defined below.

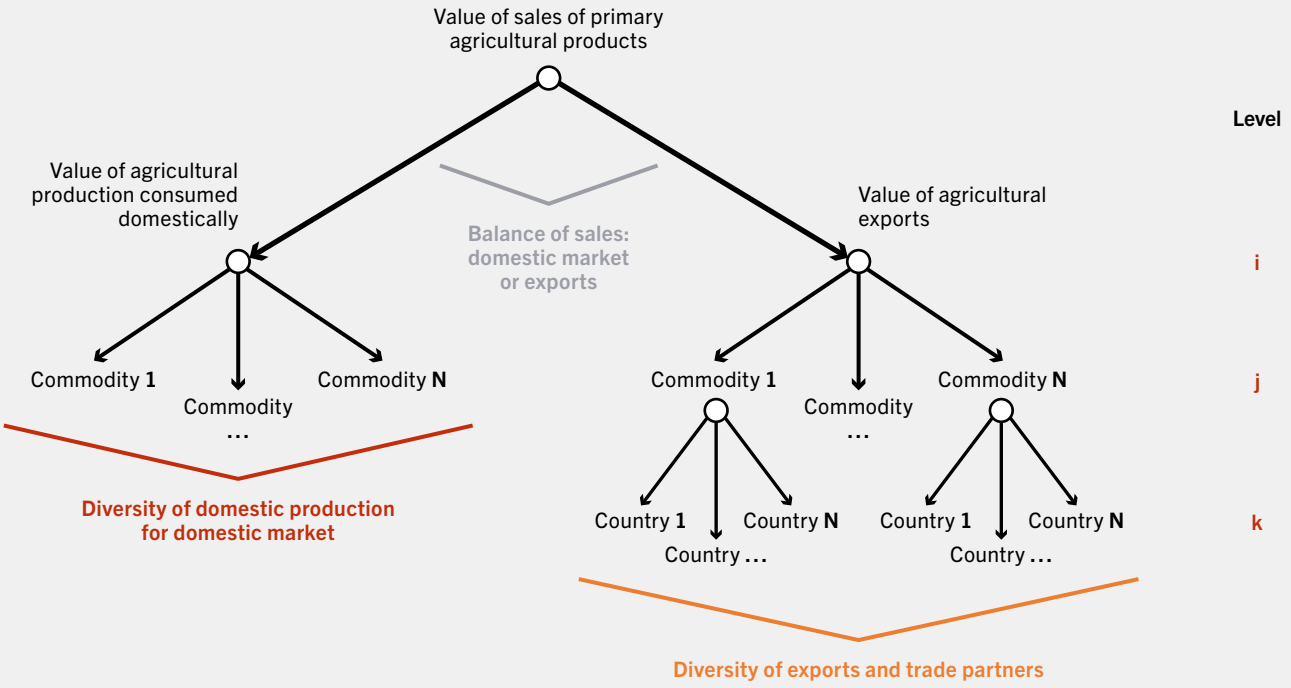
Let X be a discrete random variable taking a finite number of possible values $x_1, x_2, \ldots, x_n$ with probabilities $p_1, p_2, \ldots, p_n$ respectively, such that $p_i \geq 0, \sum_1^N p_i = 1$, then the information entropy associated with the uncertainty about the actual value taken on by x is:

$$H(p_1, p_2, \ldots, p_N) = -\sum_1^N p_i \cdot \log(p_i)$$

Information entropy can be interpreted as the information contained in a message that reveals the value taken on by the random variable. Information entropy has three important properties (see Shannon, 1948):[1]

i. Continuity – its value is continuous in probabilities;
ii. Monotonicity – if all p_i are equal ($p_i = 1/N$), then H is a monotonically increasing function of N; and
iii. Recursiveness – if a choice is broken down into two successive choices, the original H is the weighted sum of the individual values of H.

FIGURE A1.1 PATHWAYS TO PRODUCE AGRICULTURAL OUTPUT AND SELL IT IN DOMESTIC AND EXPORT MARKETS, FOR VALUE



SOURCE: FAO elaboration for this report.

Where p_i is the proportion (i/N) of pathways of one particular level in Figure A1.1 divided by the total number of pathways found (N), and H is the entropy of the set of probabilities.

Information entropy is the only function to satisfy all three properties. The third one is particularly important because it allows calculation of the information entropy for food units (in value terms) of different commodities for the domestic and exporting markets.

Take a country for which M commodities are produced domestically and assume that p_i is the probability that a unit value (USD) of sales comes from producing a specific commodity i. If the country has no food exports (only left branch of the tree in Figure A1.1) the information entropy associated with the diversity of domestic production for that country is:

$$H = -\sum_{i=1}^{M} p_i . log(p_i)$$

The information entropy increases if we assume that these M commodities can also be exported. How it increases can be derived according to the property of recursiveness, whereby information entropy is independent of the sequencing in Figure A1.1. The overall information entropy can be expressed as follows:

$$PPFI = \sum_{i=1}^{2} p_i \left[\sum_{j=1}^{N_i} p_{ij} \left[-\sum_{k=1}^{N_{ij}} p_{ijk} . log(p_{ijk}) \right] \right.$$

$$\left. - \sum_{j=1}^{N_i} p_{ij} . log(p_{ij}) \right] - \sum_{i=1}^{2} p_i . log(p_i)$$

Where p_i is the share of food value that goes to the domestic market (i=1) or is exported (i=2), p_{ij} is the share of value generated by commodity j if sold domestically (i=1; j=N_1) or exported (i=2; j=N_2), and p_{ijk} is the share of value from country k if exported (i=2; j=N_2; k=N_{2j}).

Note that p_i, p_{ij} and p_{ijk} each sum up to 1, as these are calculated as shares of food, in value, exported or sold locally, or from a certain commodity (within exports, and local market), or from a certain importing country. The PPFI equation can be further disaggregated into the different contributions depicted in Figure A1.1 as follows:

1. Contribution of diversity of domestic production for domestic market:

$$p_1\left[\sum_{j=1}^{N_1} p_{1j}\left[-\sum_{k=1}^{N_{1j}} p_{1jk}.log(p_{1jk})\right]-\sum_{ij=1}^{N_1} p_{1j}.log(p_{1j})\right]$$

2. Contribution of diversity of exports:

$$p_2\left[\sum_{j=1}^{N_2} p_{2j}\left[-\sum_{k=1}^{N_{2j}} p_{2jk}.log(p_{2jk})\right]-\right.$$

$$\left.-\sum_{j=1}^{N_2} p_{2j}.log(p_{2j})\right]$$

3. Contribution of balance of sales (domestic market or exports):

$$-\sum_{i=1}^{2} p_i.log(p_i)$$

In Figure 3 (Chapter 2), the values in the y-axis are expressed by diversity of exports, the bubbles by the balance of sales and the values in the x-axis by diversity of domestic production for the domestic market.

Data and methodology

Input data for the analysis are from FAOSTAT's production, producer prices and detailed trade matrix data.[2] The study covers 2016 to 2018. FAOSTAT's production data were converted from mass to value and protein (tonnes) using producer prices and product-, country- and year-specific protein conversion factors (based on FAOSTAT's food balance sheets), respectively. Where food balance sheets' protein contents were missing, the study uses subregional, regional, continental or global averages, depending on data availability. To account for short-term interannual fluctuation in the data, all PPFI values were averaged over the years 2016–2018. Data were also normalized between 0 and 1.

Since live animals were reported as head counts, the number of animals was transformed first to approximate weights, applying country-, animal- and year-specific yields per animal using livestock primary data, and then to value or tonnes of protein using food balance sheets' nutritional component contents for the parent product. The trade statistics do not specify the purpose of traded live animals which could be used for meat or milk production. The report assumes that once the animals are imported into a country, they will be slaughtered for food at the end of their life cycle, thus counting all imported live animals as meat.

DIETARY SOURCING FLEXIBILITY INDEX (DSFI)

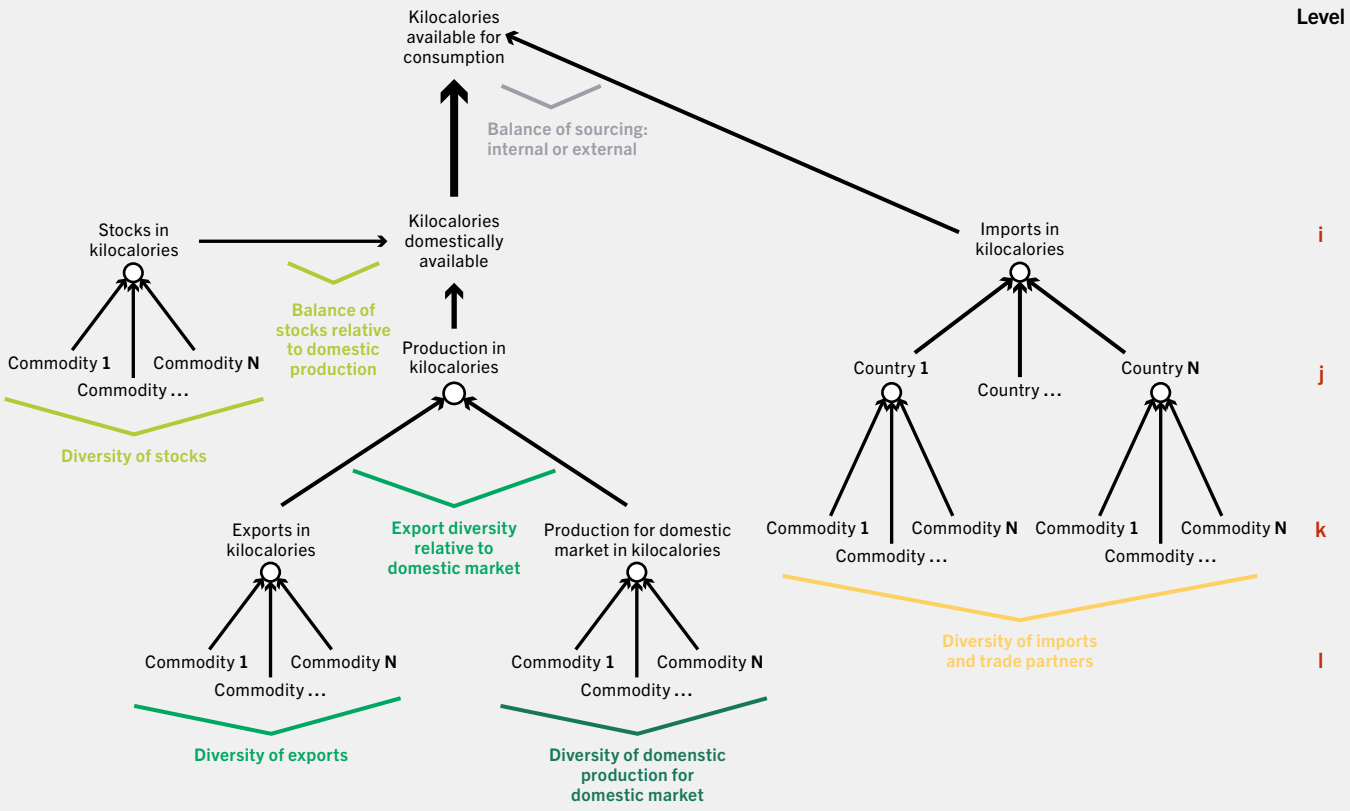
Description

The DSFI examines all the different pathways through which a unit of food (in nutritional outcomes) is available to a consumer. If it has many different origins, food systems will have greater capacity to absorb supply shocks.

The three possible pathways a unit of food, measured for kilocalories, can reach a consumer are represented as a tree in Figure A1.2 as follows: (i) food produced domestically; (ii) imported food; and (iii) reserves carried over from the previous year (imports or domestic production, public and private). Food produced domestically is further disaggregated by destination (local market or export) and subsequently by commodity. Imports are also further disaggregated into trading partners and import diversity. The balance between imports and what is produced or stocked domestically measures the role of trade in supplying food and sourcing diversity.

As for the PPFI, the expression of the DSFI can be derived from first principles following the standard measure for information, or the lack thereof, the Shannon Entropy.[1] It has the three

FIGURE A1.2 PATHWAYS TO SOURCE FOOD FROM STOCKS, DOMESTIC PRODUCTION OR IMPORTS, FOR KILOCALORIES



SOURCE: FAO elaboration for this report.

important properties of continuity, monotonicity and recursiveness.

Based on the above and on Figure A1.2, a basic entropy index of dietary sourcing flexibility is defined as:

$$DSFI = \sum_{i=1}^{2} p_i \left[\sum_{j=1}^{N_i} p_{ij} \left[\sum_{k=1}^{N_{ij}} p_{ijk} \left[-\sum_{l=1}^{N_{ijk}} p_{ijkl} \cdot \log\left(p_{ijkl}\right) \right] - \right. \right.$$

$$\left. \left. - \sum_{k=1}^{N_{ij}} p_{ijk} \cdot \log\left(p_{ijk}\right) \right] - \sum_{j=1}^{N_i} p_{ij} \cdot \log\left(p_{ij}\right) \right] - \sum_{i=1}^{2} p_i \cdot \log\left(p_i\right)$$

Where p_i is the share of food domestically available (i=1) or imported (i=2). p_{ij} is the probability that a unit of food will be produced internally (i=1; j=1) or sourced from buffer stocks (i=1; j=2) or sourced from country j if imported (i=2; j=N_2). p_{ijk} is the probability that a unit of food will go to the domestic market (i=1; j=1; k=1) or be exported (i=1; j=1; k=2); or that it will be sourced from commodity k if coming from buffer stocks (i=1; j=2; k=N_{12}) or from commodity k if coming from imports (i=2; j=N_2; k=N_{2j}). And p_{ijkl} is the probability that a unit of food will be sourced from commodity l once it is known whether it

goes to the domestic market (i=1; j=1; k=1; l=N_{111}) or is meant to be exported (i=1; j=1; k=1; l=N_{112}).

Note that p_i, p_{ij}, p_{ijk} and p_{ijkl} each sum up to 1, as these are calculated as shares of food, in nutritional components that are imported, sourced from stocks (if internally available), exported (if produced domestically), or from a certain commodity (within stocks, imports, exports and local market), or from a particular exporting country.

The DSFI equation can be further disaggregated into the different contributions depicted in Figure A1.2 as follows:

1. Contribution of diversity of domestic production for domestic market:

$$p_1\left[p_{11}\left[p_{111}\left[-\sum_{l=1}^{N_{111}} p_{111l}\cdot\log\left(p_{111l}\right)\right]\right]\right]$$

2. Contribution of diversity of exports:

$$p_1\left[p_{11}\left[p_{112}\left[-\sum_{l=1}^{N_{112}} p_{112l}\cdot\log(p_{112l})\right]-\right.\right.$$

$$\left.\left.-\sum_{k=1}^{N_{11}} p_{11k}\cdot\log(p_{11k})\right]\right]$$

3. Contribution of diversity of stocks:

$$p_1\left[p_{12}\left[-\sum_{k=1}^{N_{12}} p_{12k}\cdot\log\left(p_{12k}\right)\right]-\sum_{j=1}^{N_1} p_{1j}\cdot\log\left(p_{1j}\right)\right]$$

4. Contribution of diversity of imports and trade partners:

$$p_2\left[\sum_{j=1}^{N_2} p_{2j}\left[-\sum_{k=1}^{N_{2j}} p_{2jk}\cdot\log\left(p_{2jk}\right)\right]-\sum_{j=1}^{N_2} p_{2j}\cdot\log\left(p_{2j}\right)\right]$$

5. Contribution of balance of sourcing (internal or external):

$$-\sum_{i=1}^{2} p_i\cdot\log\left(p_i\right)$$

In Figure 4 (Chapter 2), the values on the y-axis are obtained by summing the contributions of expressions 1) and 2), while the values on the x-axis are obtained by summing the contributions of expressions 4) and 5). The sizes of the bubbles represent the contribution of diversity of stocks.

Data and methodology

Input data for the analysis are from FAOSTAT's food balance sheets and detailed trade matrix.[2] Data for buffer stocks were collected from FAOSTAT's supply utilization accounts;[2] the Agricultural Market Information System (AMIS);[3] FAO's Global Information and Early Warning System on Food and Agriculture (GIEWS);[4] and the Production, Supply and Distribution (PSD) database of the United States Department of Agriculture.[5] These data were used as follows: when FAOSTAT's supply utilization accounts were lacking, the study used the average of the remaining three data sources instead. Stock data are, however, notoriously difficult to estimate accurately. The study covers the years 2016 to 2018.

FAOSTAT's food balance sheet data were converted from mass to dietary energy (kilocalories), fat (tonnes), and protein (tonnes) using product-, country- and year-specific conversion factors (also based on food balance sheets). For fruits and vegetables, the weight (tonnes) of these two food item groups were used. Trade matrix data were also transformed to nutritional components using FAOSTAT's food balance sheet data for the given "parent" product. For example, the nutritional component contents for cattle meat were derived from "bovine meat" values for the reporting country. As the live animals were reported as head counts, the number of animals was first transformed to approximate weights applying country-, animal- and year-specific yields per animal and then to kilocalories, tonnes of protein and tonnes of fat using nutritional component contents for the corresponding parent product.

To account for the short-term interannual fluctuation in the data, all DSFI values were averaged over 2016–2018. Data were also normalized between 0 and 1. Spices, non-food items and alcohol were excluded from the analysis.

ADDING THE PROBABILITY OF DISRUPTION TO THE PPFI AND DSFI

Information on threats – whether objective or perceived – could be included to derive a risk-adjusted set of indicators. Since the PPFI and DSFI can be broken down into different components, information on the probability of disruptions to different pathways can be incorporated when available. The DSFI components are: (i) the contribution of diversity of imports and trade partners; (ii) the contribution of diversity of domestic production; and (iii) the diversity of stocks. It can therefore be expressed as:

(1) $\boldsymbol{DSFI}$ *= DSFI (imports)+DSFI (domestic production)+DSFI (stocks)*

If country-level information is available on the probability that the pathways contributing to these different contributions may fail, then it is possible to define a **risk-adjusted DSFI** as follows:

(2) $\boldsymbol{DSFI}_{risk}$ *=* $(1-p_{imp})\cdot$*DSFI(imports)+*$(1-p_{dom})\cdot$ *DSFI (domestic production)+*$(1-p_{stock})\cdot$*DSFI(stocks)*

Where the probabilities, p, express for each contribution the likelihood that a set of pathways may not be available and therefore cannot be relied on as alternatives when a disruption occurs.

Alternatively, these probabilities can be interpreted as the proportion of a contribution to diversity that cannot be relied upon. For example, if p_{stock} equals 0 it means stocks will be readily available and released in case of a supply shock. If, on the other hand, p_{stock} equals 1 then stocks cannot be used. In reality, the situation will be somewhere in between. For example, stocks may be released only if the supply shock exceeds a certain threshold. In such a case, the value of p_{stock} would be the probability that the supply shock does not meet the requirement to release stocks. The risk-adjusted DSFI would always be lower than the DSFI. How much lower depends on the reliability, or perceived reliability, of different pathways.

MIDSTREAM FLEXIBILITY INDEX (MFI)

Description

The MFI could be developed using the same rationale as for the PPFI and DSFI by measuring diversity of processed foods, sourcing (domestic or imported) and output markets (internal or external). Higher values indicate multiple paths to generate and sell processed food (in value terms). The MFI indicates which processed food an average food processor will likely produce, whether it ends up in the domestic or export market, and whether the inputs used to produce it were internal or external. It thus provides useful insights on the flexibility of the food processing sector. As for the PPFI and DSFI, information entropy can be used to measure this uncertainty.

Measurement challenges

As seen in Figure A1.3, the MFI is more complex than the PPFI (Figure A1.1) and the DSFI (Figure A1.2), as both input and output markets play a role. Another challenge is the lack of data, not least on the origin of inputs for food processing (internal or external) and prices. This means that many production pathways are unaccounted for, underestimating the indicator and thus the resilience of the processing sector.

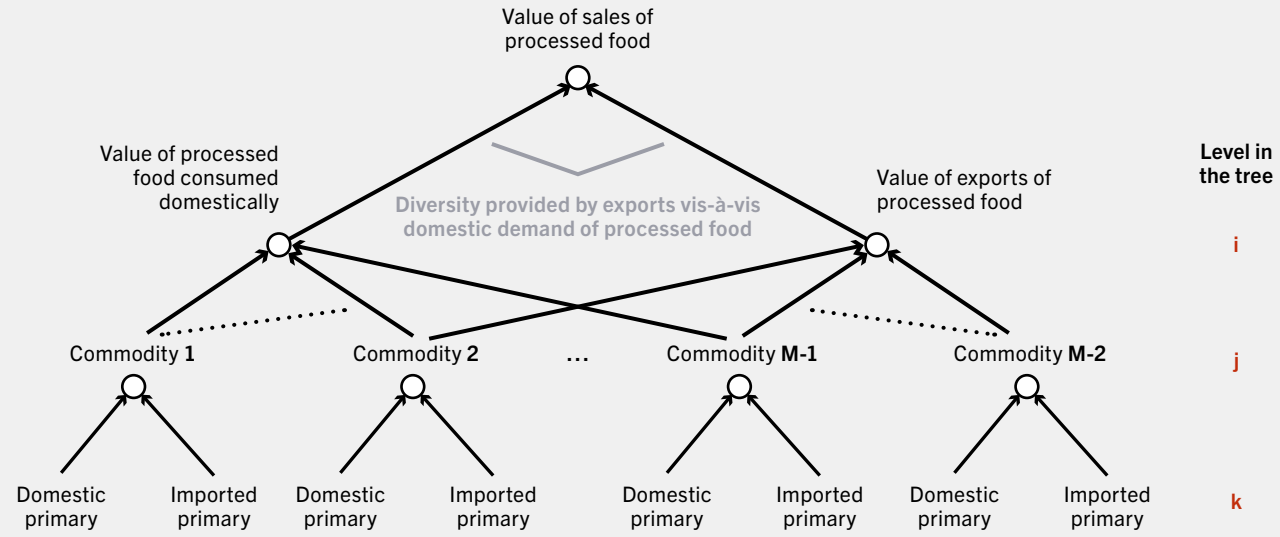
In this report, the analysis of the transport network resilience can be taken as a proxy for the broader concept of midstream resilience. However, estimating the midstream flexibility indicator will fill an important gap, highlighting the need for more and better data for an expanded analysis.

DATA AND METHODOLOGY FOR THE ECONOMIC ACCESS INDICATOR

A healthy diet provides not only adequate calories but also adequate levels of all essential nutrients for a healthy and active life. It ensures consumption of a wide variety of foods from different food groups. The cost of this diet is taken from the 2021 report on *The State of Food Security and Nutrition*.[6] For a full description of the cost methodology and data sources, see Annex 3 of FAO *et al.* (2020).[7]

To estimate the number of people at risk of not being able to afford a healthy diet if a shock reduces their income by one-third, we define

FIGURE A1.3 PATHWAYS TO SOURCE PRIMARY COMMODITIES AS INPUTS TO PRODUCE PROCESSED FOODS AND SELL THEM IN DOMESTIC AND EXPORT MARKETS, IN VALUE



SOURCE: FAO elaboration for this report.

income needed as that required for a healthy diet, other non-food needs (such as housing) plus a 50 percent income buffer in case of a shock. We compare this level of income with the estimated income distribution in a given country, using 2019 income distributions from the World Bank PovcalNet interface.[8] A diet is considered unaffordable when its cost (including the buffer) exceeds 63 percent of average income in a given country. The 63 percent accounts for a portion of the poverty line that can be credibly reserved for food, based on observations that the poorest people in low-income countries spend, on average, 63 percent of their incomes on food.[9–12] This affordability indicator is computed for 143 countries in 2019 as follows:

$(1+0.5) \times \textit{Cost of the diet}/0.63$

To illustrate, if the cost of a healthy diet in a given country is USD 3 per day, to be able to afford both food and non-food needs, an individual needs a daily minimum income of USD 4.76. To continue to meet those needs in the event of a shock that reduces income by one-third, the person's starting income needs to be USD 7.14.

This measure provides estimates of the share of people who cannot afford a healthy diet if a shock reduces their income by one-third. Percentages are then multiplied by the 2019 population in each country using the World Development Indicators of the World Bank to obtain the number of people who are at risk of not being able to afford such a diet.[13]

Figure 6 (Chapter 2) presents the results from this measure, that is, the share of people at risk of not being able to afford a healthy diet (vertical axis) crossed against the share of people who cannot afford a healthy diet without income reduction (horizontal axis).

DESCRIPTION OF THE INDICATORS OF TRANSPORT NETWORK RESILIENCE

Nelson *et al.* (forthcoming) developed three national indicators to capture the structural vulnerability to disruptions to food systems' transport networks: (i) proximity-based resilience; (ii) route redundancy; and (iii) relative detour cost.[14] These indicators are described in detail below.

Proximity-based resilience

Proximity-based resilience is an indicator of food transport network resilience and is related to the food matrix, that is, the way food is distributed from where it is produced to where it is consumed.[g] The food matrix estimates the tonnage of crops between origin zones (where crops are produced) and destination zones (where crops are consumed). The zones are catchment areas around all cities. The total attraction in the model is based on the total supply of crops (in tonnage, excluding exports). This total is distributed proportionally to the population of each zone. Specific crops are distinguished, as each crop may have different transport requirements. For example, highly perishable foods such as fruits may be transported over shorter distances than non-perishable foods like rice. The distribution function describes the propensity to transport food between A and B, irrespective of production and attraction, respectively, as follows:

$$f(c)=e^{-\beta c}$$

Where c is the travel cost between origin and destination and β is the slope of the distribution function.

Travel time is used as the best available option to express cost of transport. The coefficient β describes how fast the attractiveness drops with travel time (cost). In principle, it is most economic to supply food where it is produced. However, due to factors such as market mechanisms and consumer preferences, the distribution function can have a relatively small β.

Irrespective of β, systems will be more resilient when there is a balance between production and consumption. When production and consumption zones are the same, crops do not need to travel very far. Systems will thus be more resilient against network disturbances, as there is the possibility to supply locally. In contrast, if production occurs far from consumption, transportation time is longer even if β is large, increasing the vulnerability of the network to disturbances. In other words, when average travel time is greater than for the optimal situation of balanced production and consumption, systems are less resilient. The indicator for proximity-based resilience is the ratio of the average trip duration in the optimal situation of balanced production and consumption to the average trip duration in the actual situation where crops have to travel distances to reach consumers in various zones.

When analysing the results, there is a clear correlation between this resilience metric and country size. For example, the average trip length, and hence the proximity-based resilience, of a small country is high because of its size. Similarly, detours will on average be smaller for small countries, but relative detours will on average be larger. This is simply because there are (in general) more alternatives for longer trips. These patterns are not linked to the actual resilience of a transport network based on the investments made, but the geographical context. To adjust for this, proximity-based resilience is multiplied by the square root of the total tonnage of transported crops and divided by the average scale factor to keep the same order of magnitudes in both metrics. This is done to allow meaningful comparison of proximity-based resilience across countries.

Route redundancy

This indicator is the ratio of the tonnage that passes through links for which there is an alternative route over the total tonnage for all links:

$$\frac{T_{links\ with\ alternative\ route}}{T_{all\ links}}$$

It is thus a second route-based resilience metric. The higher the indicator, the more resilient the

g Although reference is made here to consumption nodes for convenience, it would be more accurate to refer to nodes where food is supplied, either for consumption or for export.

transport network is. For most countries, this value lies above 0.80 indicating that alternative routes are readily available. However, for Somalia, this value lies around 0.31; in other words, 69 percent of the tonnage is over links for which there are no alternative routes, indicating very low resilience.

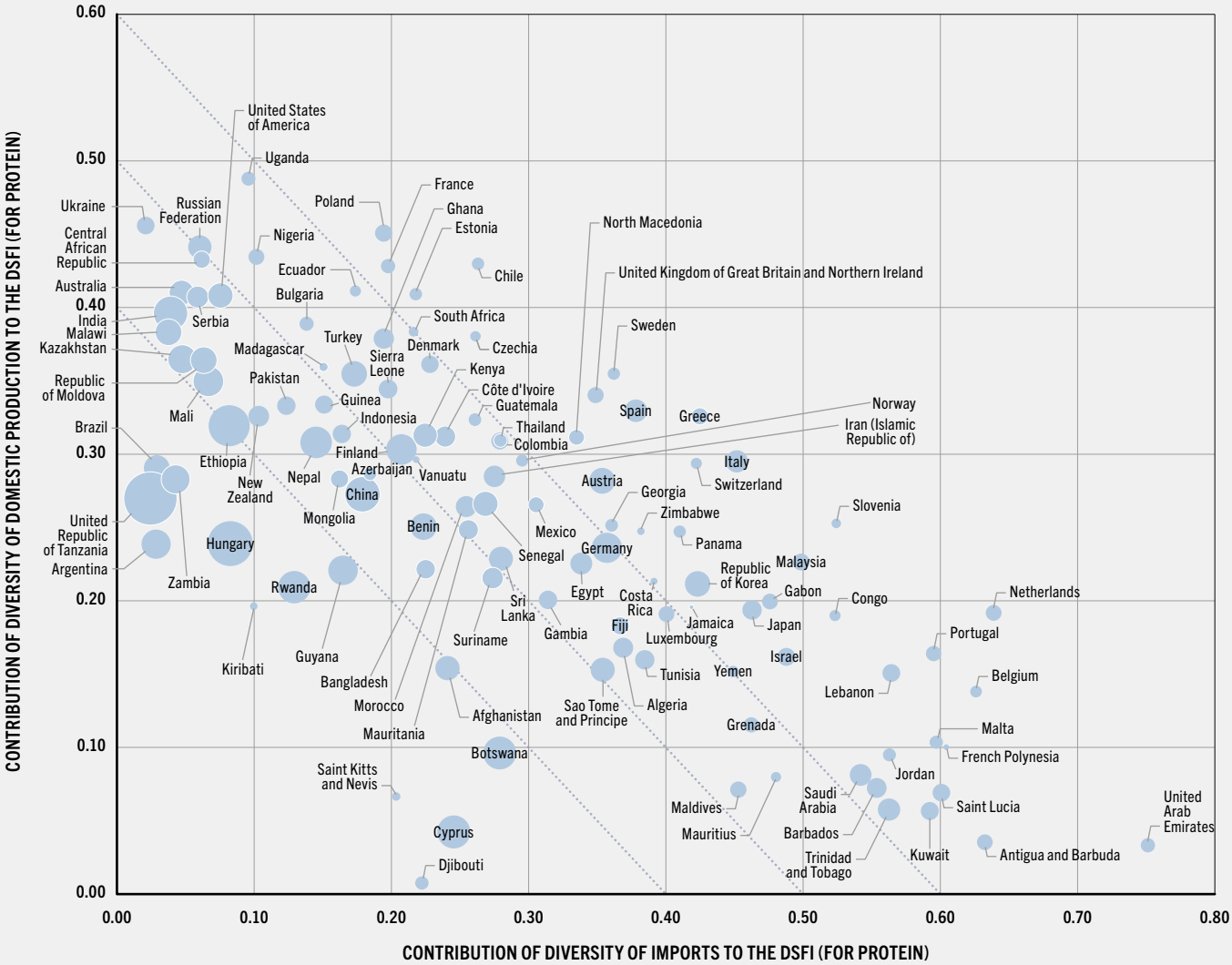
Relative detour cost

This indicator calculates how many extra tonnage-minutes result from closing 1 out of 20 important links. Selecting the most important links requires: (i) closing each link with traffic and calculating the travel time (cost) on the alternative route between the closed link's start and end node; and (ii) multiplying this travel time by the link's intensity. The higher this value, the higher the impact of the link removal. The links with the highest impact values are selected. However, one cannot simply select the 20 links with highest intensity, because to do so would possibly result in the selection of a number of links along the most important route, simulating a similar closure multiple times. Therefore, all origin–destination relations over the link with the highest impact value are selected. The exercise is repeated: disregarding transportations over already selected origin–destination relations from the previous iteration(s); and iterating back to the first step and repeating this procedure until 20 links are selected. This route-based resilience metric, called **relative detour cost**, is the average relative difference (in percentage) between the tonnage-minutes of the normal situation and the situation with one of the 20 high-intensity links removed.

The closure of high-intensity links (in the relative detour cost metric) will have an impact on the population that consumes travel-delayed food. The impact on the population purely in terms of people affected by the delay in food transport is estimated by considering each closed link in turn and determining which (origin–destination) pairs of nodes (i.e. catchments) are involved when the link is removed, and whether they are origin or destination catchments (it can be both if goods are moving both ways across the link). Then, without double counting, the average number of people in the destination catchments (consumers) affected across all link closures is computed, based on the known population per catchment. This metric does not consider the delayed food quantity, meaning that the number of people affected in a catchment is the same regardless of the quantity of food delayed.

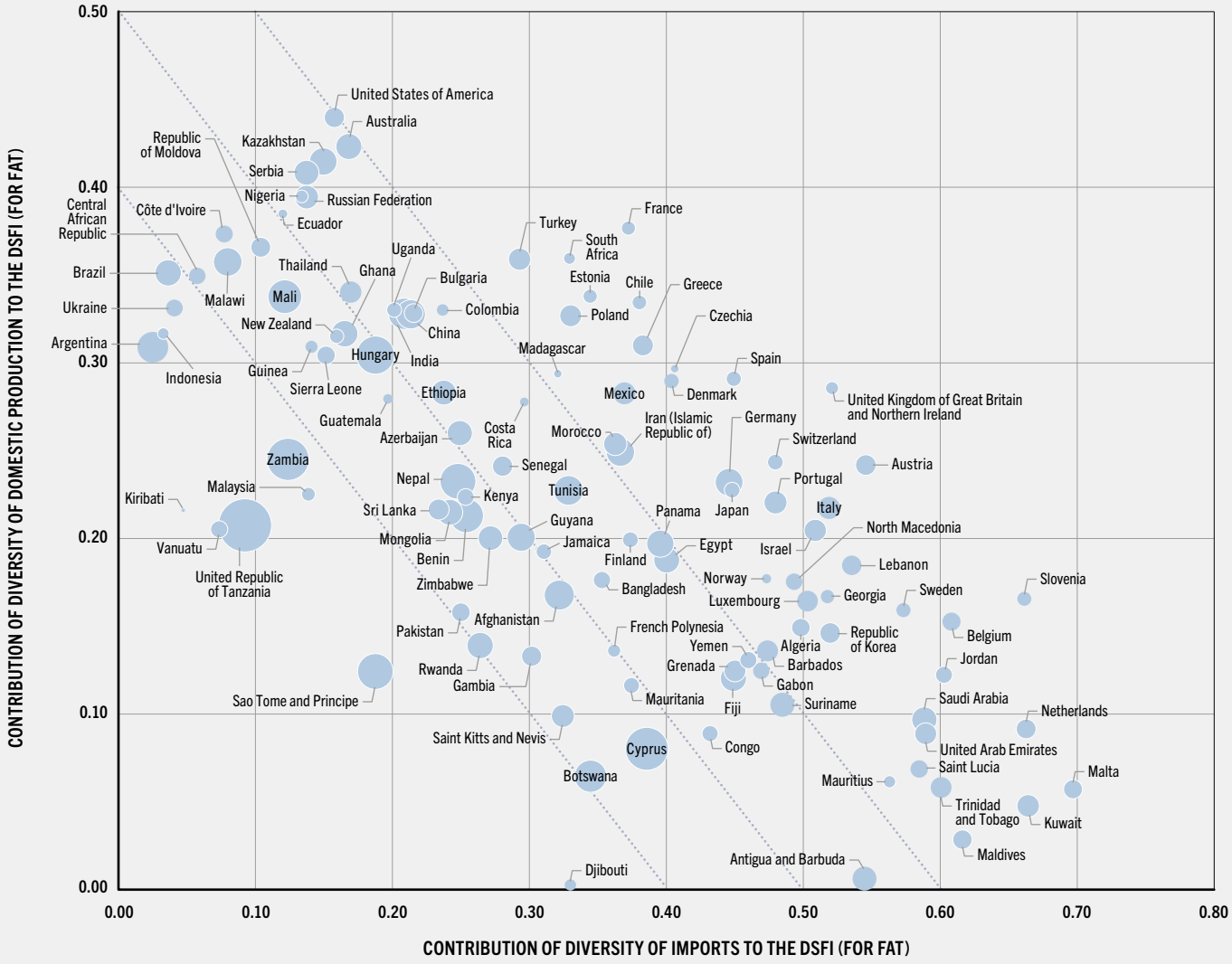
ANNEX 2
ADDITIONAL FIGURES TO CHAPTER 2

FIGURE A2.1 DIETARY SOURCING FLEXIBILITY INDEX (DSFI) FOR PROTEIN, 2016–2018



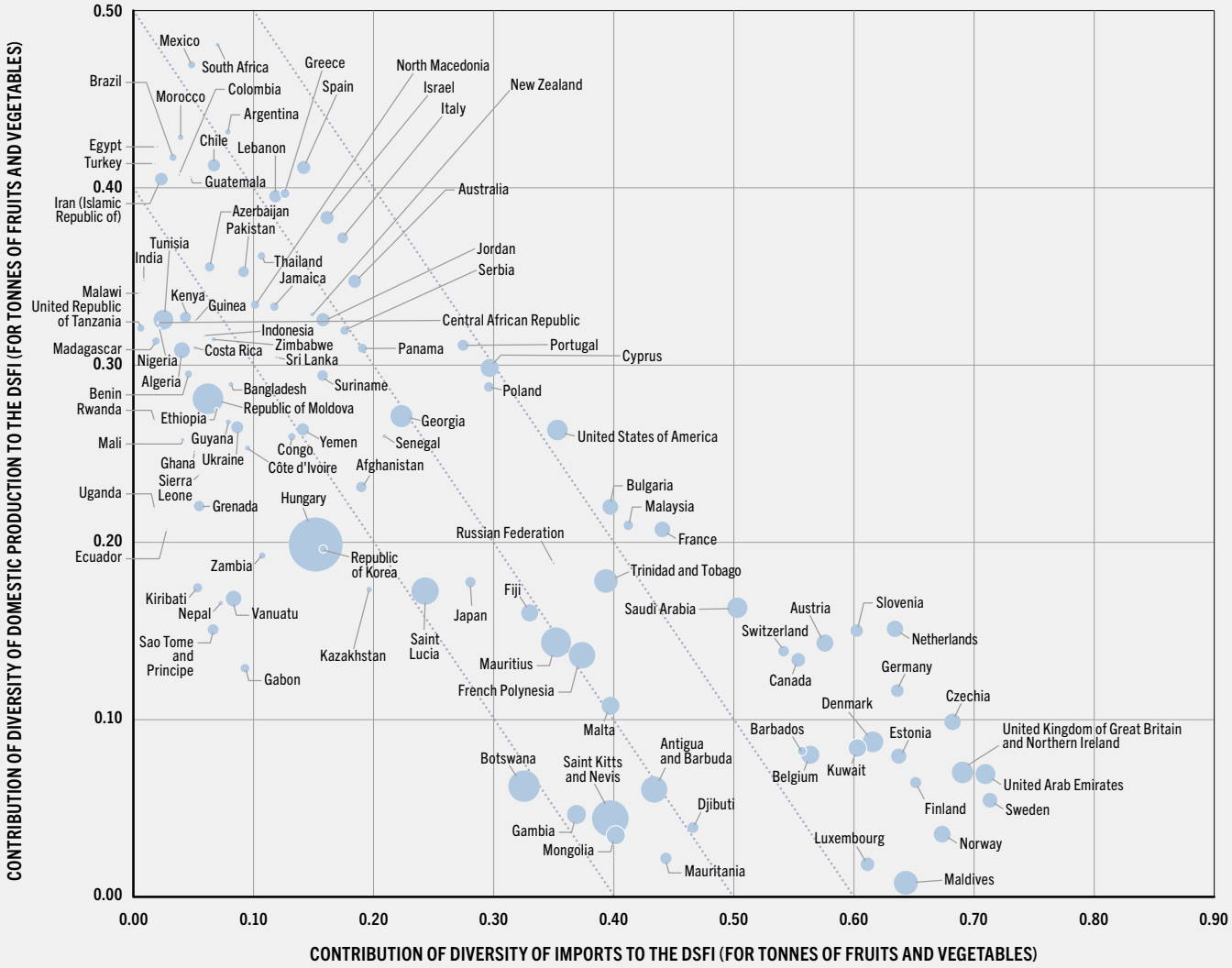
NOTES: The graph plots the contribution of the diversity of imports (i.e. diversity of imports and trade partners plus balance of sourcing: internal or external) against the contribution of the diversity of domestic production (for both domestic market or exports), both to the total value of the DSFI, for protein. The size of the blue bubbles represents the contribution of the diversity of stocks to the DSFI. Countries placed in the same diagonal line report the same value for production and import diversity – 0.4, 0.5 and 0.6, respectively. Results include all crop, fish and livestock commodities for which FAOSTAT new food balance sheets and trade data were available. Protein conversion factors are based on FAOSTAT data and then used to convert tonnes of food into protein. Results are the three-year average of 2016, 2017 and 2018. To simplify graphic presentation, 40 countries that overlapped in the graph were dropped. Results for the full set of countries disaggregated by DSFI contributions are available in **Annex 3**. See **Annex 1** for methodology and data sources.
SOURCE: FAO elaboration for this report.

FIGURE A2.2 DIETARY SOURCING FLEXIBILITY INDEX (DSFI) FOR FAT, 2016–2018



NOTES: The graph plots the contribution of the diversity of imports (i.e. diversity of imports and trade partners plus balance of sourcing: internal or external) against the contribution of the diversity of domestic production (for both domestic market or exports), both to the total value of the DSFI, for fat. The size of the blue bubbles represents the contribution of the diversity of stocks to the DSFI. Countries placed in the same diagonal line report the same value for production and import diversity – 0.4, 0.5 and 0.6, respectively. Results include all crop, fish and livestock commodities for which FAOSTAT new food balance sheets and trade data were available. Fat conversion factors are based on FAOSTAT data and then used to convert tonnes of food into fat. Results are the three-year average of 2016, 2017 and 2018. To simplify graphic presentation, 40 countries that overlapped in the graph were dropped. Results for the full set of countries disaggregated by DSFI contributions are available in **Annex 3**. See **Annex 1** for methodology and data sources.
SOURCE: FAO elaboration for this report.

FIGURE A2.3 DIETARY SOURCING FLEXIBILITY INDEX (DSFI) FOR TONNES OF FRUITS AND VEGETABLES, 2016–2018



NOTES: The graph plots the contribution of the diversity of imports (i.e. diversity of imports and trade partners plus balance of sourcing: internal or external) against the contribution of the diversity of domestic production (for both domestic market or exports), both to the total value of the DSFI, for tonnes of fruits and vegetables. The size of the blue bubbles represents the contribution of the diversity of stocks to the DSFI. Countries placed in the same diagonal line report the same value for production and import diversity – 0.4, 0.5 and 0.6, respectively. Results include all fruits and vegetables for which FAOSTAT new food balance sheets and trade data were available. To simplify graphic presentation, 40 countries that overlapped in the graph were dropped. Results are the three-year average of 2016, 2017 and 2018. Results for the full set of countries disaggregated by DSFI contributions are available in **Annex 3**. See **Annex 1** for methodology and data sources.
SOURCE: FAO elaboration for this report.

ANNEX 3
STATISTICAL TABLES

TABLE A3.1 PRIMARY PRODUCTION FLEXIBILITY INDEX (PPFI) FOR PROTEIN, 2016–2018

COUNTRY/TERRITORY	Contribution of different components to the PPFI (for protein)			
	Diversity of domestic production for domestic market	Diversity of exports and trade partners	Balance of sales (domestic market or exports)	Total PPFI value
WORLD				
AFRICA				
Northern Africa				
Algeria	0.54	0.00	0.00	0.54
Egypt	0.54	0.02	0.02	0.58
Libya	0.57	0.00	0.01	0.59
Morocco	0.48	0.01	0.02	0.51
Tunisia	0.55	0.02	0.02	0.59
Sub-Saharan Africa				
Eastern Africa				
Burundi	0.46	0.00	0.01	0.48
Comoros	0.42	0.02	0.03	0.47
Djibouti	0.17	0.29	0.13	0.59
Eritrea	0.53	0.00	0.00	0.53
Ethiopia	0.54	0.03	0.03	0.60
Kenya	0.49	0.04	0.05	0.58
Madagascar	0.42	0.02	0.03	0.46
Malawi	0.49	0.02	0.03	0.54
Mauritius	0.27	0.01	0.03	0.32
Rwanda	0.47	0.02	0.03	0.53
Réunion	0.28	0.00	0.00	0.28
Seychelles	0.39	0.00	0.02	0.40
Somalia	0.40	0.06	0.08	0.54
South Sudan	0.44	0.00	0.00	0.44
Uganda	0.45	0.08	0.08	0.62
United Republic of Tanzania	0.54	0.02	0.03	0.59
Zambia	0.37	0.03	0.05	0.44
Zimbabwe	0.45	0.01	0.02	0.48
Middle Africa				
Cameroon	0.55	0.01	0.02	0.59
Central African Republic	0.51	0.00	0.02	0.53
Congo	0.55	0.00	0.00	0.55
Democratic Republic of the Congo	0.46	0.00	0.00	0.47
Equatorial Guinea	0.35	0.00	0.01	0.37
Gabon	0.49	0.00	0.00	0.49
Sao Tome and Principe	0.39	0.04	0.08	0.51

TABLE A3.1 (CONTINUED)

COUNTRY/TERRITORY	Contribution of different components to the PPFI (for protein)			
	Diversity of domestic production for domestic market	Diversity of exports and trade partners	Balance of sales (domestic market or exports)	Total PPFI value
Southern Africa				
Botswana	0.39	0.01	0.03	0.43
Eswatini	0.30	0.02	0.05	0.37
Namibia	0.32	0.10	0.12	0.54
South Africa	0.40	0.07	0.06	0.53
Western Africa				
Benin	0.47	0.02	0.03	0.51
Burkina Faso	0.43	0.04	0.05	0.52
Cabo Verde	0.50	0.00	0.00	0.50
Côte d'Ivoire	0.42	0.11	0.10	0.63
Gambia	0.35	0.00	0.01	0.37
Ghana	0.49	0.04	0.05	0.58
Guinea	0.47	0.01	0.03	0.50
Mali	0.51	0.01	0.02	0.54
Mauritania	0.54	0.01	0.02	0.56
Niger	0.38	0.01	0.03	0.41
Nigeria	0.54	0.01	0.01	0.57
Senegal	0.42	0.01	0.02	0.45
Sierra Leone	0.45	0.00	0.02	0.47
Togo	0.41	0.03	0.04	0.48
AMERICA				
Latin America and the Caribbean				
Caribbean				
Antigua and Barbuda	0.39	0.00	0.01	0.40
Bahamas	0.43	0.01	0.04	0.49
Barbados	0.35	0.02	0.03	0.41
Cuba	0.57	0.00	0.00	0.57
Dominica	0.52	0.02	0.03	0.57
Grenada	0.54	0.03	0.04	0.61
Guadeloupe	0.26	0.00	0.00	0.26
Jamaica	0.50	0.01	0.01	0.52
Martinique	0.26	0.00	0.00	0.26
Puerto Rico	0.22	0.00	0.00	0.22
Saint Kitts and Nevis	0.42	0.00	0.01	0.43
Saint Lucia	0.48	0.05	0.08	0.60
Saint Vincent and the Grenadines	0.43	0.11	0.11	0.64
Trinidad and Tobago	0.31	0.01	0.02	0.34
Central America				
Belize	0.39	0.07	0.08	0.54
Costa Rica	0.33	0.19	0.12	0.64
El Salvador	0.37	0.02	0.06	0.44
Guatemala	0.42	0.08	0.07	0.57
Honduras	0.35	0.13	0.10	0.57
Mexico	0.44	0.06	0.07	0.57

TABLE A3.1 (CONTINUED)

COUNTRY/TERRITORY	Contribution of different components to the PPFI (for protein)			
	Diversity of domestic production for domestic market	Diversity of exports and trade partners	Balance of sales (domestic market or exports)	Total PPFI value
Nicaragua	0.43	0.08	0.08	0.59
Panama	0.42	0.03	0.05	0.51
South America				
Argentina	0.19	0.15	0.11	0.45
Bolivia (Plurinational State of)	0.29	0.01	0.02	0.32
Brazil	0.21	0.17	0.14	0.52
Chile	0.53	0.06	0.05	0.64
Colombia	0.48	0.02	0.03	0.53
Ecuador	0.42	0.10	0.08	0.61
French Guyana	0.25	0.00	0.00	0.25
Guyana	0.29	0.09	0.09	0.47
Paraguay	0.14	0.26	0.14	0.54
Peru	0.52	0.04	0.03	0.59
Suriname	0.23	0.10	0.10	0.43
Uruguay	0.24	0.24	0.14	0.62
Venezuela (Bolivarian Republic of)	0.54	0.00	0.00	0.54
Northern America				
Canada	0.19	0.42	0.14	0.75
United States of America	0.33	0.20	0.11	0.64
ASIA				
Central Asia				
Kazakhstan	0.35	0.16	0.11	0.63
Kyrgyzstan	0.49	0.02	0.04	0.55
Eastern Asia				
China	0.55	0.01	0.01	0.56
China, Hong Kong SAR	0.00	0.49	0.01	0.50
China, Macao SAR	0.22	0.05	0.07	0.34
China, mainland	0.59	0.01	0.01	0.60
Japan	0.50	0.00	0.00	0.51
Mongolia	0.39	0.02	0.06	0.46
Republic of Korea	0.51	0.00	0.01	0.52
Taiwan Province of China	0.53	0.01	0.01	0.55
South-eastern Asia				
Brunei Darussalam	0.22	0.00	0.02	0.24
Cambodia	0.30	0.02	0.03	0.36
Indonesia	0.43	0.02	0.02	0.46
Malaysia	0.33	0.13	0.10	0.56
Philippines	0.45	0.00	0.01	0.46
Singapore	0.03	0.61	0.11	0.76
Thailand	0.36	0.14	0.09	0.59
Southern Asia				
Afghanistan	0.35	0.02	0.03	0.39
Bangladesh	0.35	0.00	0.00	0.36
Bhutan	0.44	0.00	0.02	0.46
India	0.57	0.02	0.02	0.61

TABLE A3.1 (CONTINUED)

COUNTRY/TERRITORY	Contribution of different components to the PPFI (for protein)			
	Diversity of domestic production for domestic market	Diversity of exports and trade partners	Balance of sales (domestic market or exports)	Total PPFI value
Iran (Islamic Republic of)	0.50	0.02	0.03	0.55
Maldives	0.34	0.00	0.00	0.34
Nepal	0.54	0.00	0.01	0.55
Pakistan	0.45	0.03	0.03	0.52
Sri Lanka	0.42	0.05	0.05	0.51
Western Asia				
Armenia	0.49	0.01	0.02	0.51
Azerbaijan	0.42	0.01	0.01	0.44
Bahrain	0.26	0.07	0.06	0.39
Cyprus	0.46	0.03	0.04	0.54
Georgia	0.40	0.10	0.09	0.59
Israel	0.43	0.04	0.04	0.51
Jordan	0.37	0.18	0.11	0.66
Kuwait	0.28	0.15	0.12	0.56
Lebanon	0.52	0.06	0.05	0.64
Oman	0.41	0.17	0.11	0.69
Palestine	0.58	0.01	0.01	0.60
Qatar	0.42	0.02	0.06	0.51
Saudi Arabia	0.41	0.04	0.04	0.49
Syrian Arab Republic	0.52	0.02	0.02	0.57
Turkey	0.50	0.04	0.04	0.58
United Arab Emirates	0.12	0.67	0.11	0.90
Yemen	0.60	0.01	0.02	0.63
EUROPE				
Eastern Europe				
Belarus	0.47	0.03	0.04	0.54
Bulgaria	0.17	0.44	0.13	0.75
Czechia	0.22	0.30	0.14	0.66
Hungary	0.24	0.37	0.14	0.75
Poland	0.42	0.17	0.10	0.69
Republic of Moldova	0.26	0.30	0.14	0.70
Romania	0.22	0.42	0.14	0.78
Russian Federation	0.39	0.21	0.11	0.71
Slovakia	0.20	0.38	0.14	0.72
Ukraine	0.26	0.39	0.14	0.78
Northern Europe				
Denmark	0.27	0.24	0.13	0.63
Estonia	0.18	0.38	0.14	0.69
Faroe Islands	0.17	0.00	0.00	0.17
Finland	0.38	0.08	0.08	0.54
Iceland	0.25	0.02	0.04	0.31
Ireland	0.22	0.07	0.07	0.37
Latvia	0.10	0.54	0.11	0.76
Lithuania	0.21	0.39	0.14	0.74
Norway	0.42	0.00	0.01	0.43

TABLE A3.1 (CONTINUED)

COUNTRY/TERRITORY	Contribution of different components to the PPFI (for protein)			
	Diversity of domestic production for domestic market	Diversity of exports and trade partners	Balance of sales (domestic market or exports)	Total PPFI value
Sweden	0.37	0.14	0.10	0.61
United Kingdom of Great Britain and Northern Ireland	0.39	0.11	0.07	0.57
Southern Europe				
Albania	0.50	0.01	0.01	0.52
Bosnia and Herzegovina	0.41	0.05	0.06	0.52
Croatia	0.28	0.29	0.13	0.71
Greece	0.54	0.09	0.07	0.69
Italy	0.53	0.07	0.05	0.65
Malta	0.40	0.02	0.06	0.48
Montenegro	0.35	0.01	0.02	0.38
North Macedonia	0.48	0.05	0.05	0.58
Portugal	0.29	0.20	0.14	0.63
Serbia	0.33	0.16	0.11	0.60
Slovenia	0.12	0.47	0.12	0.71
Spain	0.49	0.16	0.08	0.74
Western Europe				
Austria	0.35	0.24	0.12	0.72
Belgium	0.12	0.47	0.13	0.73
France	0.31	0.30	0.13	0.74
Germany	0.32	0.22	0.12	0.67
Luxembourg	0.09	0.31	0.12	0.52
Netherlands	0.10	0.56	0.12	0.78
Switzerland	0.42	0.01	0.02	0.45
OCEANIA				
Australia and New Zealand				
Australia	0.22	0.43	0.14	0.79
New Zealand	0.22	0.08	0.07	0.36
Melanesia				
Fiji	0.48	0.02	0.02	0.52
New Caledonia	0.41	0.00	0.02	0.44
Papua New Guinea	0.48	0.04	0.05	0.57
Solomon Islands	0.42	0.00	0.04	0.46
Vanuatu	0.33	0.00	0.02	0.35
Micronesia				
Kiribati	0.17	0.00	0.00	0.17
Marshall Islands	0.00	0.00	0.00	0.00
Micronesia (Federated States of)	0.27	0.00	0.00	0.27
Nauru	0.21	0.00	0.01	0.22
Polynesia				
Cook Islands	0.39	0.00	0.00	0.39
French Polynesia	0.38	0.00	0.00	0.38
Niue	0.34	0.00	0.00	0.35
Tokelau	0.11	0.00	0.00	0.11
Tonga	0.47	0.01	0.04	0.52
Tuvalu	0.35	0.00	0.00	0.35

TABLE A3.2 DIETARY SOURCING FLEXIBILITY INDEX (DSFI) FOR KILOCALORIES AND FOR TONNES OF FRUITS AND VEGETABLES, 2016–2018

COUNTRY/ TERRITORY	Contribution of different components to the DSFI for:							
	Kilocalories				Fruits and vegetables			
	Diversity of domestic production	Diversity of imports	Diversity of food stocks	Total DSFI value	Diversity of domestic production	Diversity of imports	Diversity of food stocks	Total DSFI value
WORLD								
AFRICA								
Northern Africa								
Algeria	0.14	0.44	0.13	0.71	0.31	0.04	0.05	0.40
Egypt	0.25	0.33	0.15	0.73	0.42	0.02	0.01	0.45
Morocco	0.23	0.33	0.15	0.71	0.43	0.04	0.02	0.49
Tunisia	0.18	0.40	0.17	0.75	0.33	0.03	0.07	0.42
Sub-Saharan Africa								
Eastern Africa								
Comoros	0.06	0.08	0.00	0.14				
Djibouti	0.00	0.36	0.11	0.47	0.04	0.47	0.04	0.54
Ethiopia	0.28	0.14	0.24	0.66	0.27	0.07	0.01	0.36
Kenya	0.27	0.31	0.15	0.74	0.33	0.04	0.04	0.41
Madagascar	0.29	0.21	0.06	0.56	0.31	0.02	0.02	0.36
Malawi	0.34	0.05	0.18	0.57	0.34	0.01	0.00	0.35
Mauritius	0.10	0.35	0.13	0.58	0.14	0.35	0.10	0.60
Rwanda	0.15	0.14	0.23	0.52	0.27	0.02	0.00	0.29
Seychelles	0.03	0.13	0.00	0.16				
Uganda	0.44	0.17	0.10	0.71	0.22	0.02	0.00	0.24
United Republic of Tanzania	0.26	0.06	0.34	0.65	0.32	0.01	0.02	0.35
Zambia	0.30	0.07	0.20	0.57	0.19	0.11	0.02	0.32
Zimbabwe	0.22	0.39	0.08	0.69	0.31	0.07	0.01	0.40
Middle Africa								
Cameroon	0.40	0.14	0.15	0.69	0.30	0.01	0.00	0.31
Central African Republic	0.45	0.09	0.09	0.63	0.32	0.02	0.01	0.35
Congo	0.17	0.42	0.12	0.70	0.26	0.13	0.02	0.42
Gabon	0.21	0.37	0.14	0.72	0.13	0.09	0.03	0.25
Sao Tome and Principe	0.13	0.32	0.23	0.68	0.15	0.07	0.04	0.25
Southern Africa								
Botswana	0.05	0.35	0.20	0.60	0.06	0.33	0.11	0.49
Eswatini	0.21	0.19	0.07	0.47	0.30	0.20	0.04	0.54
Namibia	0.16	0.42	0.18	0.75	0.17	0.25	0.12	0.54
South Africa	0.37	0.28	0.08	0.74	0.48	0.07	0.01	0.56
Western Africa								
Benin	0.21	0.26	0.17	0.65	0.29	0.05	0.02	0.36
Burkina Faso	0.29	0.18	0.18	0.64	0.17	0.16	0.02	0.35
Cabo Verde	0.07	0.56	0.13	0.76	0.16	0.30	0.09	0.54
Côte d'Ivoire	0.36	0.17	0.14	0.66	0.25	0.10	0.02	0.36
Gambia	0.13	0.42	0.12	0.68	0.05	0.37	0.06	0.48
Ghana	0.34	0.18	0.13	0.65	0.25	0.05	0.01	0.31
Guinea	0.31	0.19	0.13	0.63	0.33	0.05	0.00	0.38
Mali	0.32	0.09	0.20	0.61	0.26	0.04	0.01	0.31

TABLE A3.2 (CONTINUED)

COUNTRY/ TERRITORY	Contribution of different components to the DSFI for:							
	Kilocalories				Fruits and vegetables			
	Diversity of domestic production	Diversity of imports	Diversity of food stocks	Total DSFI value	Diversity of domestic production	Diversity of imports	Diversity of food stocks	Total DSFI value
Mauritania	0.10	0.40	0.18	0.68	0.02	0.44	0.04	0.50
Niger	0.30	0.11	0.11	0.52	0.25	0.02	0.01	0.28
Nigeria	0.40	0.13	0.10	0.63	0.32	0.02	0.01	0.35
Senegal	0.22	0.35	0.16	0.74	0.26	0.21	0.01	0.48
Sierra Leone	0.27	0.21	0.13	0.62	0.24	0.05	0.00	0.30
Togo	0.26	0.28	0.14	0.68	0.20	0.15	0.03	0.37
AMERICA								
Latin America and the Caribbean								
Caribbean								
Antigua and Barbuda	0.01	0.65	0.16	0.83	0.06	0.43	0.09	0.58
Bahamas	0.06	0.62	0.11	0.79	0.22	0.26	0.05	0.54
Barbados	0.10	0.54	0.15	0.79	0.08	0.56	0.03	0.67
Cuba	0.27	0.34	0.08	0.69	0.32	0.01	0.02	0.34
Dominica	0.20	0.31	0.20	0.71	0.31	0.05	0.01	0.37
Grenada	0.10	0.48	0.12	0.70	0.22	0.05	0.03	0.31
Jamaica	0.21	0.44	0.07	0.71	0.33	0.12	0.03	0.48
Saint Kitts and Nevis	0.09	0.41	0.14	0.64	0.04	0.40	0.12	0.56
Saint Lucia	0.07	0.59	0.15	0.82	0.17	0.24	0.09	0.51
Saint Vincent and the Grenadines	0.10	0.36	0.19	0.64	0.21	0.06	0.02	0.29
Trinidad and Tobago	0.05	0.62	0.14	0.81	0.18	0.39	0.08	0.65
Central America								
Belize	0.31	0.16	0.12	0.59	0.26	0.04	0.04	0.34
Costa Rica	0.32	0.32	0.09	0.73	0.31	0.05	0.01	0.37
El Salvador	0.24	0.35	0.10	0.68	0.14	0.46	0.04	0.64
Guatemala	0.37	0.18	0.07	0.63	0.41	0.05	0.00	0.46
Honduras	0.34	0.23	0.09	0.66	0.37	0.13	0.01	0.50
Mexico	0.31	0.29	0.11	0.71	0.47	0.05	0.02	0.54
Nicaragua	0.36	0.21	0.14	0.71	0.38	0.13	0.02	0.53
Panama	0.24	0.39	0.15	0.78	0.31	0.19	0.03	0.53
South America								
Argentina	0.38	0.02	0.18	0.58	0.43	0.08	0.02	0.53
Bolivia (Plurinational State of)	0.42	0.07	0.12	0.62	0.38	0.06	0.01	0.45
Brazil	0.42	0.04	0.13	0.59	0.42	0.03	0.02	0.47
Chile	0.35	0.36	0.13	0.84	0.41	0.07	0.04	0.52
Colombia	0.39	0.25	0.10	0.73	0.41	0.04	0.01	0.45
Ecuador	0.40	0.16	0.11	0.68	0.21	0.03	0.00	0.24
Guyana	0.23	0.14	0.19	0.56	0.27	0.08	0.02	0.36
Paraguay	0.37	0.02	0.13	0.52	0.33	0.15	0.01	0.49
Peru	0.35	0.27	0.12	0.74	0.47	0.02	0.01	0.50
Suriname	0.15	0.30	0.18	0.64	0.29	0.16	0.04	0.49
Uruguay	0.29	0.12	0.19	0.59	0.34	0.18	0.03	0.54

TABLE A3.2 (CONTINUED)

COUNTRY/ TERRITORY	Contribution of different components to the DSFI for:							
	Kilocalories				Fruits and vegetables			
	Diversity of domestic production	Diversity of imports	Diversity of food stocks	Total DSFI value	Diversity of domestic production	Diversity of imports	Diversity of food stocks	Total DSFI value
Venezuela (Bolivarian Republic of)	0.23	0.36	0.17	0.76	0.38	0.02	0.00	0.40
Northern America								
Canada	0.40	0.10	0.18	0.68	0.13	0.55	0.05	0.73
United States of America	0.39	0.10	0.14	0.62	0.26	0.35	0.07	0.69
ASIA								
Central Asia								
Kazakhstan	0.34	0.08	0.19	0.61	0.17	0.20	0.02	0.39
Kyrgyzstan	0.35	0.16	0.14	0.66	0.24	0.10	0.02	0.36
Eastern Asia								
China	0.30	0.13	0.23	0.66	0.26	0.02	0.00	0.28
China, Hong Kong SAR	0.02	0.90	0.06	0.98	0.00	0.59	0.03	0.63
China, Macao SAR	0.01	0.71	0.11	0.83	0.00	0.45	0.02	0.47
China, mainland	0.32	0.13	0.20	0.65	0.26	0.01	0.02	0.28
Japan	0.21	0.47	0.13	0.81	0.18	0.28	0.03	0.49
Mongolia	0.19	0.30	0.15	0.65	0.03	0.40	0.06	0.50
Republic of Korea	0.14	0.51	0.17	0.82	0.20	0.16	0.03	0.38
Taiwan Province of China	0.15	0.48	0.13	0.76	0.26	0.18	0.08	0.51
South-eastern Asia								
Cambodia	0.23	0.09	0.15	0.46	0.21	0.06	0.02	0.30
Indonesia	0.33	0.10	0.13	0.57	0.32	0.06	0.00	0.38
Malaysia	0.23	0.24	0.11	0.58	0.21	0.41	0.03	0.65
Philippines	0.30	0.28	0.13	0.72	0.36	0.05	0.01	0.42
Thailand	0.37	0.13	0.16	0.66	0.36	0.11	0.03	0.49
Southern Asia								
Afghanistan	0.12	0.28	0.19	0.59	0.23	0.19	0.04	0.46
Bangladesh	0.16	0.24	0.13	0.53	0.29	0.08	0.02	0.39
India	0.40	0.09	0.19	0.69	0.35	0.01	0.00	0.36
Iran (Islamic Republic of)	0.27	0.28	0.19	0.74	0.40	0.02	0.04	0.47
Maldives	0.02	0.63	0.13	0.78	0.01	0.64	0.08	0.73
Nepal	0.28	0.17	0.21	0.66	0.17	0.07	0.01	0.25
Pakistan	0.32	0.16	0.13	0.61	0.35	0.09	0.04	0.48
Sri Lanka	0.18	0.28	0.19	0.65	0.30	0.12	0.01	0.43
Western Asia								
Armenia	0.24	0.33	0.12	0.69	0.30	0.07	0.01	0.39
Azerbaijan	0.25	0.24	0.15	0.64	0.36	0.06	0.03	0.45
Cyprus	0.03	0.27	0.22	0.52	0.30	0.30	0.06	0.66
Georgia	0.19	0.47	0.10	0.75	0.27	0.22	0.07	0.57
Israel	0.14	0.54	0.15	0.83	0.38	0.16	0.04	0.59
Jordan	0.07	0.63	0.08	0.79	0.33	0.16	0.04	0.53

TABLE A3.2 (CONTINUED)

COUNTRY/ TERRITORY	Contribution of different components to the DSFI for:							
	Kilocalories				Fruits and vegetables			
	Diversity of domestic production	Diversity of imports	Diversity of food stocks	Total DSFI value	Diversity of domestic production	Diversity of imports	Diversity of food stocks	Total DSFI value
Kuwait	0.03	0.63	0.14	0.80	0.08	0.60	0.06	0.75
Lebanon	0.13	0.61	0.13	0.88	0.40	0.12	0.04	0.55
Oman	0.08	0.65	0.10	0.82	0.19	0.38	0.03	0.60
Saudi Arabia	0.06	0.57	0.17	0.80	0.16	0.50	0.07	0.73
Turkey	0.36	0.22	0.17	0.75	0.41	0.02	0.00	0.43
United Arab Emirates	0.05	0.70	0.12	0.87	0.07	0.71	0.07	0.85
Yemen	0.08	0.51	0.10	0.69	0.26	0.14	0.04	0.45
EUROPE								
Eastern Europe								
Belarus	0.40	0.14	0.19	0.73	0.21	0.37	0.06	0.64
Bulgaria	0.39	0.17	0.11	0.67	0.22	0.40	0.05	0.67
Czechia	0.41	0.32	0.07	0.80	0.10	0.68	0.06	0.84
Hungary	0.23	0.10	0.30	0.63	0.20	0.15	0.18	0.53
Poland	0.44	0.22	0.16	0.81	0.29	0.30	0.03	0.62
Republic of Moldova	0.37	0.07	0.19	0.63	0.28	0.06	0.10	0.45
Romania	0.39	0.17	0.12	0.68	0.24	0.27	0.04	0.54
Russian Federation	0.47	0.09	0.13	0.68	0.19	0.35	0.01	0.54
Slovakia	0.32	0.29	0.18	0.79	0.09	0.68	0.05	0.82
Ukraine	0.47	0.03	0.11	0.60	0.26	0.09	0.04	0.39
Northern Europe								
Denmark	0.34	0.28	0.15	0.76	0.09	0.62	0.07	0.77
Estonia	0.39	0.30	0.10	0.78	0.08	0.64	0.05	0.77
Finland	0.25	0.30	0.20	0.75	0.06	0.65	0.04	0.75
Iceland	0.27	0.36	0.07	0.69	0.01	0.78	0.05	0.83
Ireland	0.19	0.32	0.14	0.65	0.06	0.64	0.06	0.76
Latvia	0.26	0.32	0.12	0.70	0.11	0.60	0.06	0.76
Lithuania	0.37	0.24	0.14	0.75	0.10	0.64	0.03	0.77
Norway	0.22	0.51	0.10	0.82	0.04	0.67	0.06	0.77
Sweden	0.30	0.48	0.10	0.88	0.05	0.71	0.05	0.82
United Kingdom of Great Britain and Northern Ireland	0.31	0.46	0.11	0.88	0.07	0.69	0.07	0.83
Southern Europe								
Albania	0.30	0.27	0.11	0.69	0.34	0.07	0.00	0.41
Bosnia and Herzegovina	0.21	0.38	0.13	0.72	0.20	0.24	0.02	0.46
Croatia	0.34	0.28	0.16	0.78	0.13	0.22	0.10	0.45
Greece	0.33	0.42	0.14	0.90	0.40	0.13	0.03	0.56
Italy	0.25	0.50	0.18	0.93	0.37	0.17	0.04	0.58
Malta	0.06	0.71	0.11	0.88	0.11	0.40	0.06	0.56
Montenegro	0.08	0.61	0.07	0.76	0.17	0.44	0.04	0.65
North Macedonia	0.28	0.41	0.12	0.80	0.33	0.10	0.03	0.46
Portugal	0.19	0.59	0.14	0.92	0.31	0.27	0.04	0.62

TABLE A3.2 (CONTINUED)

COUNTRY/ TERRITORY	Contribution of different components to the DSFI for:							
	Kilocalories				Fruits and vegetables			
	Diversity of domestic production	Diversity of imports	Diversity of food stocks	Total DSFI value	Diversity of domestic production	Diversity of imports	Diversity of food stocks	Total DSFI value
Serbia	0.40	0.07	0.16	0.63	0.32	0.18	0.03	0.52
Slovenia	0.20	0.63	0.07	0.90	0.15	0.60	0.04	0.79
Spain	0.30	0.44	0.15	0.89	0.41	0.14	0.04	0.60
Western Europe								
Austria	0.26	0.40	0.20	0.85	0.14	0.58	0.06	0.78
Belgium	0.18	0.67	0.11	0.96	0.08	0.56	0.06	0.71
France	0.42	0.23	0.14	0.80	0.21	0.44	0.05	0.70
Germany	0.30	0.37	0.21	0.88	0.12	0.64	0.04	0.79
Luxembourg	0.16	0.46	0.13	0.75	0.02	0.61	0.05	0.68
Netherlands	0.13	0.72	0.13	0.99	0.15	0.63	0.05	0.84
Switzerland	0.27	0.53	0.12	0.92	0.14	0.54	0.04	0.72
OCEANIA								
Australia and New Zealand								
Australia	0.44	0.07	0.15	0.66	0.35	0.18	0.04	0.57
New Zealand	0.35	0.23	0.13	0.71	0.33	0.15	0.01	0.49
Melanesia								
Fiji	0.18	0.24	0.20	0.62	0.16	0.33	0.06	0.55
New Caledonia	0.07	0.58	0.11	0.77	0.12	0.35	0.08	0.54
Papua New Guinea	0.35	0.17	0.07	0.60	0.21	0.01	0.00	0.22
Solomon Islands	0.31	0.18	0.11	0.60	0.09	0.09	0.04	0.21
Vanuatu	0.22	0.18	0.09	0.48	0.17	0.08	0.05	0.30
Micronesia								
Kiribati	0.19	0.16	0.11	0.46	0.17	0.05	0.03	0.26
Polynesia								
French Polynesia	0.12	0.52	0.07	0.71	0.14	0.37	0.09	0.60

TABLE A3.3 DIETARY SOURCING FLEXIBILITY INDEX (DSFI) FOR PROTEIN AND FOR FAT, 2016–2018

COUNTRY/ TERRITORY	Contribution of different components to the DSFI for:							
	Protein				Fat			
	Diversity of domestic production	Diversity of imports	Diversity of food stocks	Total DSFI value	Diversity of domestic production	Diversity of imports	Diversity of food stocks	Total DSFI value
WORLD								
AFRICA								
Northern Africa								
Algeria	0.17	0.37	0.12	0.66	0.15	0.50	0.11	0.76
Egypt	0.23	0.34	0.13	0.70	0.19	0.40	0.15	0.74
Morocco	0.26	0.25	0.13	0.65	0.25	0.36	0.14	0.75
Tunisia	0.16	0.38	0.12	0.66	0.23	0.33	0.18	0.73
Sub-Saharan Africa								
Eastern Africa								
Comoros	0.07	0.08	0.00	0.15	0.05	0.08	0.00	0.13
Djibouti	0.01	0.22	0.08	0.31	0.00	0.33	0.07	0.40
Ethiopia	0.32	0.08	0.25	0.65	0.28	0.24	0.15	0.67
Kenya	0.31	0.22	0.15	0.68	0.22	0.25	0.10	0.58
Madagascar	0.36	0.15	0.06	0.57	0.29	0.32	0.05	0.66
Malawi	0.38	0.04	0.16	0.58	0.36	0.08	0.17	0.61
Mauritius	0.08	0.48	0.06	0.62	0.06	0.56	0.07	0.70
Rwanda	0.21	0.13	0.19	0.53	0.14	0.26	0.16	0.56
Seychelles	0.01	0.13	0.00	0.15	0.04	0.13	0.00	0.17
Uganda	0.49	0.10	0.08	0.67	0.33	0.20	0.09	0.62
United Republic of Tanzania	0.27	0.02	0.32	0.62	0.21	0.09	0.32	0.62
Zambia	0.28	0.04	0.17	0.50	0.25	0.12	0.25	0.62
Zimbabwe	0.25	0.38	0.04	0.67	0.20	0.27	0.15	0.62
Middle Africa								
Cameroon	0.38	0.14	0.17	0.68	0.39	0.08	0.13	0.60
Central African Republic	0.43	0.06	0.10	0.60	0.35	0.06	0.10	0.51
Congo	0.19	0.52	0.07	0.78	0.09	0.43	0.10	0.62
Gabon	0.20	0.48	0.10	0.77	0.12	0.47	0.10	0.69
Sao Tome and Principe	0.15	0.35	0.15	0.65	0.12	0.19	0.21	0.52
Southern Africa								
Botswana	0.10	0.28	0.20	0.57	0.06	0.34	0.19	0.60
Eswatini	0.18	0.33	0.07	0.58	0.16	0.41	0.11	0.68
Namibia	0.27	0.29	0.09	0.65	0.16	0.37	0.15	0.68
South Africa	0.38	0.22	0.06	0.66	0.36	0.33	0.07	0.76
Western Africa								
Benin	0.25	0.22	0.16	0.63	0.21	0.25	0.20	0.67
Burkina Faso	0.33	0.12	0.14	0.59	0.32	0.11	0.20	0.64
Cabo Verde	0.12	0.49	0.12	0.73	0.07	0.56	0.10	0.73
Côte d'Ivoire	0.31	0.24	0.13	0.68	0.37	0.08	0.10	0.55
Gambia	0.20	0.31	0.11	0.63	0.13	0.30	0.12	0.55
Ghana	0.38	0.19	0.12	0.70	0.32	0.17	0.16	0.64
Guinea	0.33	0.15	0.11	0.59	0.31	0.14	0.07	0.52
Mali	0.35	0.07	0.18	0.60	0.34	0.12	0.20	0.66
Mauritania	0.25	0.26	0.12	0.62	0.12	0.37	0.09	0.59

TABLE A3.3 (CONTINUED)

COUNTRY/ TERRITORY	Contribution of different components to the DSFI for:							
	Protein				Fat			
	Diversity of domestic production	Diversity of imports	Diversity of food stocks	Total DSFI value	Diversity of domestic production	Diversity of imports	Diversity of food stocks	Total DSFI value
Niger	0.30	0.05	0.10	0.45	0.31	0.14	0.11	0.56
Nigeria	0.43	0.10	0.10	0.63	0.39	0.13	0.08	0.60
Senegal	0.27	0.27	0.15	0.69	0.24	0.28	0.12	0.64
Sierra Leone	0.34	0.20	0.11	0.66	0.30	0.15	0.11	0.56
Togo	0.33	0.21	0.09	0.63	0.21	0.29	0.12	0.62
AMERICA								
Latin America and the Caribbean								
Caribbean								
Antigua and Barbuda	0.04	0.63	0.09	0.76	0.01	0.54	0.14	0.69
Bahamas	0.07	0.60	0.05	0.73	0.03	0.59	0.09	0.70
Barbados	0.07	0.55	0.12	0.75	0.14	0.47	0.12	0.73
Cuba	0.17	0.45	0.06	0.68	0.17	0.44	0.07	0.68
Dominica	0.19	0.34	0.15	0.69	0.12	0.33	0.13	0.58
Grenada	0.12	0.46	0.09	0.67	0.12	0.45	0.13	0.70
Jamaica	0.20	0.42	0.03	0.64	0.19	0.31	0.09	0.60
Saint Kitts and Nevis	0.07	0.20	0.05	0.32	0.10	0.32	0.14	0.56
Saint Lucia	0.07	0.60	0.11	0.78	0.07	0.58	0.10	0.76
Saint Vincent and the Grenadines	0.09	0.33	0.15	0.57	0.07	0.41	0.21	0.69
Trinidad and Tobago	0.06	0.56	0.13	0.75	0.06	0.60	0.12	0.78
Central America								
Belize	0.34	0.15	0.11	0.61	0.16	0.33	0.14	0.62
Costa Rica	0.21	0.39	0.04	0.65	0.28	0.30	0.05	0.63
El Salvador	0.22	0.33	0.10	0.65	0.16	0.48	0.08	0.71
Guatemala	0.32	0.26	0.08	0.66	0.28	0.20	0.06	0.53
Honduras	0.30	0.28	0.06	0.64	0.27	0.15	0.07	0.49
Mexico	0.27	0.31	0.10	0.67	0.28	0.37	0.13	0.78
Nicaragua	0.42	0.20	0.07	0.69	0.32	0.26	0.12	0.70
Panama	0.25	0.41	0.07	0.73	0.20	0.40	0.16	0.75
South America								
Argentina	0.24	0.03	0.18	0.44	0.31	0.03	0.18	0.52
Bolivia (Plurinational State of)	0.29	0.05	0.05	0.39	0.35	0.03	0.11	0.49
Brazil	0.29	0.03	0.16	0.48	0.35	0.04	0.16	0.54
Chile	0.43	0.26	0.08	0.77	0.33	0.38	0.09	0.80
Colombia	0.31	0.28	0.08	0.67	0.33	0.24	0.07	0.64
Ecuador	0.41	0.17	0.07	0.65	0.38	0.12	0.06	0.56
Guyana	0.22	0.16	0.18	0.56	0.20	0.29	0.17	0.66
Paraguay	0.29	0.01	0.08	0.38	0.32	0.02	0.12	0.45
Peru	0.35	0.24	0.07	0.66	0.34	0.28	0.07	0.69
Suriname	0.22	0.27	0.13	0.62	0.11	0.48	0.14	0.73
Uruguay	0.28	0.07	0.18	0.52	0.20	0.10	0.17	0.48

TABLE A3.3 (CONTINUED)

COUNTRY/ TERRITORY	Contribution of different components to the DSFI for:							
	Protein				Fat			
	Diversity of domestic production	Diversity of imports	Diversity of food stocks	Total DSFI value	Diversity of domestic production	Diversity of imports	Diversity of food stocks	Total DSFI value
Venezuela (Bolivarian Republic of)	0.25	0.35	0.11	0.70	0.26	0.30	0.12	0.68
Northern America								
Canada	0.37	0.06	0.18	0.61	0.35	0.10	0.15	0.60
United States of America	0.41	0.08	0.15	0.64	0.44	0.16	0.12	0.72
ASIA								
Central Asia								
Kazakhstan	0.36	0.05	0.17	0.59	0.41	0.15	0.16	0.73
Kyrgyzstan	0.40	0.10	0.12	0.61	0.28	0.26	0.14	0.68
Eastern Asia								
China	0.27	0.18	0.21	0.67	0.33	0.21	0.17	0.71
China, Hong Kong SAR	0.02	0.83	0.03	0.88	0.03	0.80	0.07	0.90
China, Macao SAR	0.02	0.70	0.06	0.78	0.02	0.66	0.10	0.78
China, mainland	0.30	0.18	0.17	0.65	0.37	0.22	0.12	0.71
Japan	0.19	0.46	0.12	0.77	0.23	0.45	0.09	0.77
Mongolia	0.28	0.16	0.11	0.56	0.21	0.24	0.15	0.61
Republic of Korea	0.21	0.42	0.15	0.79	0.15	0.52	0.12	0.79
Taiwan Province of China	0.12	0.43	0.10	0.65	0.18	0.42	0.08	0.69
South-eastern Asia								
Cambodia	0.28	0.05	0.14	0.47	0.36	0.16	0.16	0.68
Indonesia	0.31	0.16	0.11	0.59	0.32	0.03	0.07	0.42
Malaysia	0.23	0.50	0.10	0.83	0.23	0.14	0.08	0.45
Philippines	0.30	0.35	0.09	0.74	0.24	0.26	0.13	0.64
Thailand	0.31	0.28	0.10	0.69	0.34	0.17	0.13	0.64
Southern Asia								
Afghanistan	0.15	0.24	0.15	0.54	0.17	0.32	0.18	0.67
Bangladesh	0.22	0.22	0.12	0.56	0.18	0.35	0.10	0.63
India	0.40	0.04	0.21	0.64	0.33	0.21	0.19	0.72
Iran (Islamic Republic of)	0.28	0.28	0.13	0.69	0.25	0.37	0.17	0.78
Maldives	0.07	0.45	0.10	0.62	0.03	0.62	0.11	0.76
Nepal	0.31	0.15	0.19	0.64	0.23	0.25	0.21	0.69
Pakistan	0.33	0.12	0.11	0.57	0.16	0.25	0.11	0.52
Sri Lanka	0.23	0.28	0.14	0.65	0.22	0.23	0.12	0.57
Western Asia								
Armenia	0.30	0.24	0.09	0.63	0.20	0.42	0.07	0.70
Azerbaijan	0.29	0.18	0.08	0.55	0.26	0.25	0.15	0.66
Cyprus	0.04	0.25	0.20	0.49	0.08	0.39	0.25	0.72
Georgia	0.25	0.36	0.08	0.69	0.17	0.52	0.08	0.76
Israel	0.16	0.49	0.11	0.76	0.20	0.51	0.13	0.85
Jordan	0.09	0.56	0.08	0.74	0.12	0.60	0.10	0.83
Kuwait	0.06	0.59	0.11	0.76	0.05	0.66	0.13	0.85

TABLE A3.3 (CONTINUED)

COUNTRY/ TERRITORY	Contribution of different components to the DSFI for:							
	Protein				Fat			
	Diversity of domestic production	Diversity of imports	Diversity of food stocks	Total DSFI value	Diversity of domestic production	Diversity of imports	Diversity of food stocks	Total DSFI value
Lebanon	0.15	0.56	0.11	0.82	0.18	0.54	0.12	0.84
Oman	0.13	0.59	0.09	0.81	0.08	0.53	0.09	0.70
Saudi Arabia	0.08	0.54	0.13	0.75	0.10	0.59	0.15	0.84
Turkey	0.35	0.17	0.15	0.68	0.36	0.29	0.13	0.78
United Arab Emirates	0.03	0.75	0.09	0.87	0.09	0.59	0.13	0.81
Yemen	0.15	0.45	0.07	0.67	0.13	0.46	0.10	0.69
EUROPE								
Eastern Europe								
Belarus	0.36	0.10	0.18	0.65	0.30	0.17	0.19	0.66
Bulgaria	0.39	0.14	0.09	0.61	0.33	0.22	0.11	0.66
Czechia	0.38	0.26	0.06	0.70	0.30	0.41	0.04	0.75
Hungary	0.24	0.08	0.27	0.59	0.30	0.19	0.23	0.72
Poland	0.45	0.19	0.10	0.75	0.33	0.33	0.13	0.79
Republic of Moldova	0.36	0.06	0.16	0.59	0.37	0.10	0.12	0.59
Romania	0.40	0.15	0.10	0.65	0.41	0.19	0.13	0.72
Russian Federation	0.44	0.06	0.14	0.64	0.39	0.14	0.14	0.67
Slovakia	0.32	0.23	0.16	0.71	0.24	0.41	0.16	0.81
Ukraine	0.46	0.02	0.11	0.58	0.33	0.04	0.10	0.47
Northern Europe								
Denmark	0.36	0.23	0.11	0.69	0.29	0.40	0.09	0.78
Estonia	0.41	0.22	0.08	0.70	0.34	0.34	0.08	0.77
Finland	0.30	0.21	0.18	0.69	0.20	0.37	0.09	0.67
Iceland	0.25	0.17	0.03	0.44	0.29	0.25	0.04	0.59
Ireland	0.25	0.26	0.10	0.61	0.25	0.36	0.15	0.75
Latvia	0.30	0.27	0.10	0.66	0.29	0.39	0.10	0.77
Lithuania	0.40	0.17	0.12	0.68	0.31	0.42	0.09	0.82
Norway	0.30	0.30	0.07	0.66	0.18	0.47	0.05	0.70
Sweden	0.35	0.36	0.07	0.79	0.16	0.57	0.08	0.82
United Kingdom of Great Britain and Northern Ireland	0.34	0.35	0.10	0.79	0.29	0.52	0.08	0.88
Southern Europe								
Albania	0.32	0.21	0.08	0.61	0.28	0.28	0.10	0.65
Bosnia and Herzegovina	0.26	0.34	0.11	0.70	0.16	0.42	0.11	0.69
Croatia	0.40	0.23	0.11	0.75	0.30	0.38	0.16	0.85
Greece	0.33	0.42	0.10	0.85	0.31	0.38	0.12	0.82
Italy	0.30	0.45	0.13	0.88	0.22	0.52	0.13	0.87
Malta	0.10	0.60	0.08	0.78	0.06	0.70	0.11	0.87
Montenegro	0.11	0.55	0.06	0.72	0.06	0.59	0.07	0.72
North Macedonia	0.31	0.33	0.10	0.74	0.18	0.49	0.10	0.77
Portugal	0.16	0.60	0.09	0.85	0.22	0.48	0.14	0.84
Serbia	0.41	0.06	0.13	0.60	0.41	0.14	0.15	0.69
Slovenia	0.25	0.52	0.06	0.83	0.17	0.66	0.08	0.91
Spain	0.33	0.38	0.14	0.84	0.29	0.45	0.09	0.83

TABLE A3.3 (CONTINUED)

COUNTRY/ TERRITORY	Contribution of different components to the DSFI for:							
	Protein				Fat			
	Diversity of domestic production	Diversity of imports	Diversity of food stocks	Total DSFI value	Diversity of domestic production	Diversity of imports	Diversity of food stocks	Total DSFI value
Western Europe								
Austria	0.28	0.35	0.16	0.79	0.24	0.55	0.12	0.91
Belgium	0.14	0.63	0.07	0.84	0.15	0.61	0.11	0.87
France	0.43	0.20	0.09	0.71	0.38	0.37	0.08	0.83
Germany	0.24	0.36	0.18	0.78	0.23	0.45	0.17	0.84
Luxembourg	0.19	0.40	0.10	0.69	0.16	0.50	0.12	0.79
Netherlands	0.19	0.64	0.10	0.93	0.09	0.66	0.12	0.87
Switzerland	0.29	0.42	0.07	0.78	0.24	0.48	0.09	0.82
OCEANIA								
Australia and New Zealand								
Australia	0.41	0.05	0.15	0.61	0.42	0.17	0.15	0.75
New Zealand	0.33	0.10	0.12	0.55	0.32	0.16	0.09	0.56
Melanesia								
Fiji	0.18	0.37	0.11	0.66	0.12	0.45	0.16	0.73
New Caledonia	0.10	0.56	0.06	0.72	0.06	0.62	0.10	0.77
Papua New Guinea	0.32	0.22	0.07	0.61	0.27	0.08	0.02	0.37
Solomon Islands	0.31	0.21	0.08	0.60	0.31	0.07	0.07	0.45
Vanuatu	0.30	0.22	0.04	0.55	0.21	0.07	0.10	0.38
Micronesia								
Kiribati	0.20	0.10	0.05	0.34	0.22	0.05	0.02	0.28
Polynesia								
French Polynesia	0.10	0.60	0.03	0.74	0.14	0.36	0.08	0.58

TABLE A3.4 INDICATORS OF RESILIENCE AND VULNERABILITY OF FOOD TRANSPORT NETWORKS

COUNTRY/ TERRITORY	System-wide measures		Localized disruption			
	Proximity-based resilience	Route redundancy	Relative detour cost (local impact)	Relative detour cost (aggregate impact)	People affected (millions)	People affected (percent)
WORLD						
AFRICA						
Northern Africa						
Algeria	0.12	99.81	16.20	1.27	13.83	34.09
Egypt	0.33	93.97	12.96	1.03	36.87	39.03
Morocco	0.11	99.71	8.76	1.29	18.10	51.52
Sudan	0.03	54.74	93.57	20.60	15.89	39.88
Tunisia	0.13	99.43	16.79	1.73	6.42	56.82
Sub-Saharan Africa						
Eastern Africa						
Burundi	0.23	98.00	42.28	2.70	4.55	43.38
Ethiopia	0.11	73.72	26.07	1.88	77.63	74.92
Kenya	0.06	92.24	13.50	2.43	12.83	26.15
Madagascar	0.02	73.07	32.04	4.86	18.30	73.48
Malawi	0.09	97.05	13.81	2.23	6.60	38.38
Mozambique	0.03	71.86	25.43	5.63	15.22	54.65
Rwanda	0.11	100.00	21.31	2.73	5.73	49.11
Somalia	0.00	31.23	20.60	4.26	6.85	48.24
South Sudan	0.01	47.82	21.98	5.54	4.58	42.36
Uganda	0.11	94.59	26.84	2.57	14.26	35.93
United Republic of Tanzania	0.04	90.36	23.47	2.20	22.65	42.67
Zambia	0.03	87.93	58.97	12.08	9.60	58.69
Zimbabwe	0.05	81.81	32.42	4.63	4.00	28.49
Middle Africa						
Angola	0.04	93.37	36.44	4.38	10.45	36.22
Cameroon	0.03	95.19	13.44	2.46	7.35	30.72
Central African Republic	0.03	99.77	38.11	2.73	1.42	31.25
Chad	0.03	81.18	51.95	7.32	6.59	45.26
Congo	0.03	94.15	28.90	7.99	2.83	56.84
Democratic Republic of the Congo	0.05	70.78	41.06	4.29	42.55	53.99
Gabon	0.02	92.26	68.16	29.03	1.57	78.28
Southern Africa						
South Africa	0.09	72.28	16.11	1.44	30.71	54.64
Western Africa						
Benin	0.06	89.74	17.46	3.27	4.97	45.68
Burkina Faso	0.09	97.47	25.96	3.26	8.69	46.58
Côte d'Ivoire	0.11	97.68	18.43	2.37	6.68	28.04
Ghana	0.16	97.83	23.31	2.34	18.21	63.93
Guinea	0.08	83.85	40.24	3.81	5.81	49.44
Guinea-Bissau	0.03	89.03	31.06	12.09	0.80	44.65
Liberia	0.06	99.93	31.80	5.86	1.44	31.44
Mali	0.05	75.29	19.19	2.64	8.24	45.84
Niger	0.08	83.91	33.98	8.33	11.52	55.41
Nigeria	0.29	92.08	25.67	1.79	45.69	24.56

TABLE A3.4 (CONTINUED)

COUNTRY/ TERRITORY	System-wide measures		Localized disruption			
	Proximity-based resilience	Route redundancy	Relative detour cost (local impact)	Relative detour cost (aggregate impact)	People affected (millions)	People affected (percent)
Senegal	0.06	92.54	148.68	26.60	7.42	49.47
Sierra Leone	0.15	99.99	43.07	2.45	3.37	46.03
Togo	0.08	87.62	45.86	6.16	4.71	62.73
AMERICA						
Latin America and the Caribbean						
Caribbean						
Dominican Republic	0.11	84.81	18.16	3.16	9.22	88.63
Haiti	0.07	77.77	95.97	9.61	7.54	69.54
Jamaica	0.07	100.00	55.85	2.50	1.76	60.46
Central America						
Guatemala	0.07	66.68	24.84	4.82	7.54	47.62
Mexico	0.06	94.03	15.18	2.20	74.04	60.04
South America						
Argentina	0.04	84.09	9.92	1.13	16.69	38.30
Bolivia (Plurinational State of)	0.03	95.06	14.59	1.67	3.34	30.27
Brazil	0.04	83.46	14.02	1.28	149.62	72.58
Chile	0.02	71.11	4.57	0.66	11.12	61.06
Colombia	0.05	90.32	22.25	3.40	33.61	69.73
Ecuador	0.08	98.98	58.37	7.38	7.81	47.36
Peru	0.04	67.22	25.39	3.83	15.24	49.24
Venezuela (Bolivarian Republic of)	0.06	82.33	15.97	2.19	15.75	52.90
Northern America						
Canada	0.01	90.91	20.15	7.50	16.92	46.86
United States of America	0.08	97.18	4.97	0.34	123.55	38.27
ASIA						
Central Asia						
Kazakhstan	0.02	91.26	12.96	2.76	11.03	61.98
Uzbekistan	0.14	97.69	18.47	2.15	14.12	44.35
Eastern Asia						
China	0.63	97.73	4.50	0.16	920.71	66.78
Democratic People's Republic of Korea	0.18	99.80	33.33	2.39	7.87	31.09
Japan	0.06	99.09	4.56	0.72	101.73	80.12
Republic of Korea	0.20	100.00	8.44	0.94	11.17	21.81
South-eastern Asia						
Cambodia	0.10	99.11	28.02	3.26	9.00	57.06
Indonesia	0.06	77.38	5.49	0.47	179.79	68.75
Lao People's Democratic Republic	0.06	90.06	42.57	5.54	3.50	51.19
Malaysia	0.09	92.75	11.89	2.18	12.14	39.56
Myanmar	0.12	84.88	36.88	2.95	23.64	44.57
Philippines	0.18	78.39	55.04	17.39	63.80	61.55
Thailand	0.07	78.02	17.43	4.38	34.79	50.44
Viet Nam	0.10	95.40	3.95	0.80	57.20	61.09

TABLE A3.4 (CONTINUED)

COUNTRY/ TERRITORY	System-wide measures		Localized disruption			
	Proximity-based resilience	Route redundancy	Relative detour cost (local impact)	Relative detour cost (aggregate impact)	People affected (millions)	People affected (percent)
Southern Asia						
Afghanistan	0.08	88.74	28.11	3.28	16.92	47.85
Bangladesh	0.24	84.13	31.75	3.25	96.56	61.13
India	0.22	89.43	4.92	0.20	570.01	43.04
Iran (Islamic Republic of)	0.10	98.03	19.74	1.28	56.74	71.30
Nepal	0.11	90.13	23.07	3.08	11.12	40.74
Pakistan	0.17	94.92	10.81	0.74	92.04	45.20
Sri Lanka	0.13	100.00	10.98	1.19	5.63	26.56
Western Asia						
Azerbaijan	0.08	98.93	41.00	4.19	4.88	50.05
Iraq	0.07	92.09	11.15	1.49	23.93	65.43
Saudi Arabia	0.02	81.49	6.92	1.38	12.66	39.04
Syrian Arab Republic	0.07	99.21	10.96	2.35	4.74	27.07
Turkey	0.22	98.32	11.96	0.77	58.01	72.68
Yemen	0.05	68.86	25.62	2.83	11.04	40.62
EUROPE						
Eastern Europe						
Russian Federation	0.06	91.61	21.75	2.00	103.96	72.04
Ukraine	0.14	89.67	17.01	1.85	16.90	37.56
Northern Europe						
United Kingdom of Great Britain and Northern Ireland	0.20	98.87	10.31	0.72	17.84	27.20
Southern Europe						
Italy	0.14	93.92	20.25	2.01	30.67	50.59
Western Europe						
France	0.20	98.53	8.93	0.85	25.65	38.45
Germany	0.26	98.81	7.95	0.39	17.26	20.99
OCEANIA						
Australia and New Zealand						
Australia	0.01	57.47	15.90	2.50	8.15	33.68
Melanesia						
Papua New Guinea	0.01	37.63	9.69	2.29	3.42	41.32

TABLE A3.5 AFFORDABILITY OF ENERGY-SUFFICIENT AND HEALTHY DIETS IN 2019

COUNTRY/ TERRITORY	Population	People unable to afford a healthy diet	People at risk of not being able to afford a healthy diet if incomes are reduced by one-third	People able to afford a healthy diet even if incomes are reduced by one-third	People unable to afford an energy-sufficient diet	People at risk of not being able to afford an energy-sufficient diet if incomes are reduced by one-third	People able to afford an energy-sufficient diet even if incomes are reduced by one-third
	Thousands	Share	Share	Share	Share	Share	Share
WORLD							
AFRICA							
Northern Africa							
Algeria	43 053	0.25	0.33	0.42	0.00	0.00	1.00
Egypt	100 388	0.85	0.10	0.05	0.00	0.01	0.99
Morocco	36 472	0.11	0.19	0.70	0.00	0.00	1.00
Sudan	42 813	0.93	0.05	0.02	0.11	0.22	0.67
Tunisia	11 695	0.15	0.24	0.61	0.00	0.00	1.00
Sub-Saharan Africa							
Eastern Africa							
Burundi	11 531	0.97	0.02	0.01	0.31	0.27	0.41
Comoros	851	0.80	0.11	0.09	0.15	0.13	0.72
Djibouti	974	0.65	0.19	0.16	0.03	0.04	0.93
Ethiopia	112 079	0.83	0.10	0.07	0.01	0.06	0.92
Kenya	52 574	0.78	0.12	0.10	0.09	0.15	0.76
Madagascar	26 969	0.97	0.02	0.01	0.24	0.23	0.53
Malawi	18 629	0.94	0.03	0.02	0.02	0.06	0.93
Mauritius	1 266	0.14	0.22	0.64	0.00	0.00	1.00
Mozambique	30 366	0.93	0.03	0.04	0.08	0.12	0.80
Rwanda	12 627	0.88	0.06	0.06	0.02	0.08	0.90
Seychelles	98	0.06	0.08	0.86	0.00	0.00	1.00
Uganda	44 270	0.78	0.11	0.11	0.01	0.06	0.93
United Republic of Tanzania	58 005	0.84	0.08	0.07	0.05	0.16	0.80
Zambia	17 861	0.86	0.07	0.07	0.31	0.14	0.54
Zimbabwe	14 645	0.99	0.01	0.00	0.83	0.08	0.09
Middle Africa							
Angola	31 825	0.93	0.04	0.03	0.38	0.17	0.45
Cameroon	25 876	0.65	0.16	0.19	0.03	0.06	0.91
Central African Republic	4 745	0.93	0.03	0.04	0.36	0.19	0.45
Chad	15 947	0.80	0.11	0.09	0.08	0.10	0.82
Congo	5 381	0.90	0.05	0.05	0.41	0.19	0.40
Democratic Republic of the Congo	86 791	0.95	0.03	0.02	0.15	0.17	0.68
Gabon	2 173	0.32	0.23	0.45	0.01	0.03	0.97
Sao Tome and Principe	215	0.87	0.06	0.06	0.19	0.19	0.62
Southern Africa							
Botswana	2 304	0.61	0.14	0.26	0.01	0.02	0.98
Eswatini	1 148	0.68	0.11	0.21	0.13	0.15	0.72
Lesotho	2 125	0.78	0.12	0.10	0.07	0.09	0.84
Namibia	2 495	0.51	0.14	0.35	0.10	0.10	0.80
South Africa	58 558	0.62	0.10	0.28	0.18	0.14	0.68

TABLE A3.5 (CONTINUED)

COUNTRY/ TERRITORY	Population	People unable to afford a healthy diet	People at risk of not being able to afford a healthy diet if incomes are reduced by one-third	People able to afford a healthy diet even if incomes are reduced by one-third	People unable to afford an energy-sufficient diet	People at risk of not being able to afford an energy-sufficient diet if incomes are reduced by one-third	People able to afford an energy-sufficient diet even if incomes are reduced by one-third
	Thousands	Share	Share	Share	Share	Share	Share
Western Africa							
Benin	11 801	0.91	0.04	0.05	0.19	0.10	0.72
Burkina Faso	20 321	0.88	0.07	0.05	0.00	0.01	0.99
Cabo Verde	550	0.32	0.21	0.47	0.00	0.01	0.99
Côte d'Ivoire	25 717	0.69	0.16	0.15	0.03	0.06	0.91
Gambia	2 348	0.77	0.15	0.08	0.03	0.09	0.88
Ghana	30 418	0.61	0.18	0.21	0.05	0.05	0.90
Guinea	12 771	0.93	0.05	0.02	0.09	0.17	0.74
Guinea-Bissau	1 921	0.93	0.03	0.04	0.36	0.22	0.42
Liberia	4 937	1.00	0.00	0.00	0.47	0.25	0.28
Mali	19 658	0.88	0.08	0.04	0.03	0.13	0.84
Mauritania	4 526	0.67	0.21	0.12	0.02	0.04	0.94
Niger	23 311	0.89	0.07	0.03	0.01	0.04	0.95
Nigeria	200 964	0.93	0.05	0.02	0.23	0.23	0.54
Senegal	16 296	0.73	0.15	0.12	0.07	0.12	0.81
Sierra Leone	7 813	0.84	0.10	0.07	0.00	0.04	0.96
Togo	8 082	0.95	0.03	0.01	0.63	0.16	0.21
AMERICA							
Latin America and the Caribbean							
Caribbean							
Dominican Republic	10 739	0.15	0.20	0.65	0.00	0.01	0.99
Haiti	11 263	0.85	0.09	0.06	0.09	0.12	0.78
Jamaica	2 948	0.52	0.17	0.31	0.01	0.03	0.97
Saint Lucia	183	0.18	0.12	0.69	0.04	0.03	0.94
Trinidad and Tobago	1 395	0.09	0.11	0.80	0.00	0.00	1.00
Central America							
Belize	390	0.32	0.19	0.49	0.09	0.08	0.84
Costa Rica	5 048	0.13	0.14	0.72	0.01	0.01	0.99
El Salvador	6 454	0.32	0.24	0.44	0.02	0.04	0.94
Honduras	9 746	0.47	0.16	0.37	0.11	0.10	0.79
Mexico	127 576	0.17	0.19	0.64	0.00	0.01	0.99
Nicaragua	6 546	0.31	0.21	0.48	0.05	0.07	0.88
Panama	4 246	0.17	0.12	0.70	0.01	0.02	0.98
South America							
Argentina	44 939	0.25	0.17	0.58	0.01	0.01	0.98
Bolivia (Plurinational State of)	11 513	0.20	0.19	0.61	0.04	0.04	0.92
Brazil	211 050	0.14	0.10	0.75	0.02	0.02	0.96
Chile	18 952	0.02	0.06	0.91	0.00	0.00	1.00
Colombia	50 339	0.26	0.17	0.58	0.03	0.04	0.93
Ecuador	17 374	0.19	0.15	0.65	0.03	0.04	0.92
Guyana	783	0.38	0.21	0.40	0.04	0.02	0.95

TABLE A3.5 (CONTINUED)

COUNTRY/ TERRITORY	Population	People unable to afford a healthy diet	People at risk of not being able to afford a healthy diet if incomes are reduced by one-third	People able to afford a healthy diet even if incomes are reduced by one-third	People unable to afford an energy-sufficient diet	People at risk of not being able to afford an energy-sufficient diet if incomes are reduced by one-third	People able to afford an energy-sufficient diet even if incomes are reduced by one-third
	Thousands	Share	Share	Share	Share	Share	Share
Paraguay	7 045	0.16	0.16	0.69	0.00	0.01	0.99
Peru	32 510	0.17	0.15	0.68	0.00	0.01	0.99
Suriname	581	0.47	0.21	0.31	0.16	0.03	0.80
Uruguay	3 462	0.01	0.05	0.94	0.00	0.00	1.00
Northern America							
Canada	37 589	0.00	0.00	0.99	0.00	0.00	1.00
United States of America	328 240	0.01	0.00	0.98	0.01	0.00	0.99
ASIA							
Central Asia							
Kazakhstan	18 514	0.01	0.09	0.89	0.00	0.00	1.00
Kyrgyzstan	6 457	0.48	0.31	0.21	0.00	0.01	0.99
Tajikistan	9 321	0.27	0.26	0.47	0.00	0.02	0.98
Eastern Asia							
China	1 397 715	0.15	0.19	0.66	0.00	0.00	1.00
Japan	126 265	0.02	0.01	0.97	0.01	0.01	0.99
Mongolia	3 225	0.38	0.28	0.35	0.00	0.00	1.00
Republic of Korea	51 709	0.01	0.02	0.97	0.00	0.00	1.00
South-eastern Asia							
Indonesia	270 626	0.66	0.19	0.15	0.00	0.06	0.94
Lao People's Democratic Republic	7 169	0.81	0.11	0.08	0.00	0.04	0.96
Malaysia	31 950	0.01	0.03	0.96	0.00	0.00	1.00
Myanmar	54 045	0.52	0.28	0.20	0.00	0.01	0.99
Philippines	108 117	0.65	0.18	0.17	0.02	0.10	0.88
Thailand	69 626	0.17	0.25	0.58	0.00	0.00	1.00
Viet Nam	96 462	0.23	0.24	0.54	0.00	0.02	0.98
Southern Asia							
Bangladesh	163 046	0.73	0.16	0.11	0.00	0.01	0.99
Bhutan	763	0.45	0.22	0.33	0.00	0.02	0.98
India	1 366 418	0.71	0.17	0.12	0.00	0.04	0.95
Maldives	531	0.02	0.07	0.91	0.00	0.00	1.00
Nepal	28 609	0.73	0.16	0.11	0.01	0.06	0.93
Pakistan	216 565	0.76	0.15	0.09	0.00	0.02	0.98
Sri Lanka	21 803	0.49	0.25	0.26	0.00	0.01	0.99
Western Asia							
Armenia	2 958	0.46	0.32	0.22	0.00	0.02	0.98
Azerbaijan	10 023	0.00	0.00	1.00	0.00	0.00	1.00
Cyprus	1 199	0.00	0.00	1.00	0.00	0.00	1.00
Iraq	39 310	0.53	0.27	0.20	0.00	0.03	0.96
Israel	9 053	0.01	0.02	0.97	0.00	0.00	1.00
Jordan	10 102	0.21	0.29	0.50	0.00	0.00	1.00

TABLE A3.5 (CONTINUED)

COUNTRY/ TERRITORY	Population	People unable to afford a healthy diet	People at risk of not being able to afford a healthy diet if incomes are reduced by one-third	People able to afford a healthy diet even if incomes are reduced by one-third	People unable to afford an energy-sufficient diet	People at risk of not being able to afford an energy-sufficient diet if incomes are reduced by one-third	People able to afford an energy-sufficient diet even if incomes are reduced by one-third
	Thousands	Share	Share	Share	Share	Share	Share
Palestine	4 685	0.90					
Turkey	83 430	0.09	0.11	0.80	0.00	0.00	1.00
EUROPE							
Eastern Europe							
Belarus	9 467	0.01	0.04	0.95	0.00	0.00	1.00
Bulgaria	6 976	0.08	0.07	0.86	0.00	0.00	1.00
Czechia	10 670	0.00	0.00	1.00	0.00	0.00	1.00
Hungary	9 770	0.02	0.02	0.96	0.00	0.00	1.00
Poland	37 971	0.00	0.04	0.95	0.00	0.00	1.00
Republic of Moldova	2 658	0.04	0.19	0.77	0.00	0.00	1.00
Romania	19 357	0.09	0.07	0.85	0.00	0.01	0.99
Russian Federation	144 374	0.02	0.08	0.90	0.00	0.00	1.00
Slovakia	5 454	0.02	0.02	0.96	0.00	0.00	1.00
Northern Europe							
Denmark	5 819	0.00	0.00	1.00	0.00	0.00	1.00
Estonia	1 327	0.01	0.01	0.99	0.00	0.00	1.00
Finland	5 520	0.00	0.00	1.00	0.00	0.00	1.00
Iceland	361	0.00	0.00	1.00	0.00	0.00	1.00
Ireland	4 941	0.00	0.00	1.00	0.00	0.00	1.00
Latvia	1 913	0.02	0.02	0.96	0.00	0.00	1.00
Lithuania	2 787	0.02	0.02	0.96	0.00	0.00	1.00
Norway	5 348	0.00	0.00	0.99	0.00	0.00	1.00
Sweden	10 285	0.01	0.00	0.99	0.01	0.00	0.99
United Kingdom of Great Britain and Northern Ireland	66 834	0.00	0.00	0.99	0.00	0.00	1.00
Southern Europe							
Albania	2 854	0.40	0.25	0.35	0.00	0.00	1.00
Bosnia and Herzegovina	3 301	0.03	0.06	0.91	0.00	0.00	1.00
Croatia	4 068	0.03	0.06	0.91	0.00	0.00	1.00
Greece	10 716	0.01	0.04	0.94	0.00	0.00	1.00
Italy	60 297	0.03	0.01	0.96	0.01	0.00	0.99
Malta	503	0.00	0.00	0.99	0.00	0.00	1.00
Montenegro	622	0.14	0.11	0.74	0.01	0.00	0.99
North Macedonia	2 083	0.17	0.17	0.66	0.01	0.01	0.97
Portugal	10 269	0.01	0.01	0.98	0.00	0.00	1.00
Serbia	6 945	0.10	0.21	0.69	0.00	0.00	1.00
Slovenia	2 088	0.00	0.00	1.00	0.00	0.00	1.00
Spain	47 077	0.02	0.01	0.97	0.01	0.00	0.99
Western Europe							
Austria	8 877	0.01	0.00	0.99	0.00	0.00	1.00
Belgium	11 484	0.00	0.00	1.00	0.00	0.00	1.00

TABLE A3.5 (CONTINUED)

COUNTRY/ TERRITORY	Population	People unable to afford a healthy diet	People at risk of not being able to afford a healthy diet if incomes are reduced by one-third	People able to afford a healthy diet even if incomes are reduced by one-third	People unable to afford an energy-sufficient diet	People at risk of not being able to afford an energy-sufficient diet if incomes are reduced by one-third	People able to afford an energy-sufficient diet even if incomes are reduced by one-third
	Thousands	Share	Share	Share	Share	Share	Share
France	67 060	0.00	0.00	1.00	0.00	0.00	1.00
Germany	83 133	0.00	0.00	1.00	0.00	0.00	1.00
Luxembourg	620	0.00	0.00	0.99	0.00	0.00	1.00
Netherlands	17 333	0.00	0.00	1.00	0.00	0.00	1.00
Switzerland	8 575	0.00	0.01	0.99	0.00	0.00	1.00
OCEANIA							
Australia and New Zealand							
Australia	25 364	0.01	0.00	0.99	0.00	0.00	1.00
Melanesia							
Fiji	890	0.31	0.28	0.42	0.00	0.00	1.00

ANNEX 4
ADDITIONAL TABLES TO CHAPTER 4

TABLE A4.1 LIST OF COUNTRIES IN THE FAO-RIMA DATA SET

Country	Coverage	Year 1	Sample
Chad	National	2015	6 949
Democratic Republic of the Congo	Rutshuru (Nord-Kivu)	2017	1 719
Democratic Republic of the Congo	Rutshuru (Nord-Kivu)	2019	1 643
Mali	National	2014	3 804
Mauritania	National	2017	2 826
Myanmar	Rakhine State	2019	304
Niger	Maradi, Zinder	2018	2 300
Nigeria	Borno State	2018	2 049
Senegal	Matam	2015	414
Somalia	Jowhar district (Middle Shabelle)	2019	599
Somalia	Marka district (Lower Shabelle)	2019	622
South Sudan	Lakes State, Central Equatoria (Terekeka)	2019	777
Uganda	Karamoja	2016	1 965
Uganda	Karamoja	2019	1 965
Uganda	North	2017	3 034
Uganda	Southwest	2018	705
Venezuela (Bolivarian Republic of)	Portuguesa State	2020	839

TABLE A4.2 LIST OF COUNTRIES IN THE MICS DATA SET

Country	Coverage	Year 1	Year 2	Sample
Bangladesh	National	2012	2019	1 109
Democratic Republic of the Congo	National	2010	2017	748
Gambia	National	2010	2018	520
Ghana	National	2011	2017	430
Guinea-Bissau	National	2014	2018	527
Iraq	National	2011	2018	2 190
Kazakhstan	National	2010	2015	313
Kyrgyzstan	National	2014	2016	307
Lao People's Democratic Republic	National	2012	2017	1 186
Mali	National	2009	2015	885
Mauritania	National	2011	2015	543
Mongolia	National	2010	2018	252
Nepal	National	2014	2019	319
Nigeria	National	2011	2016	1 914
Pakistan	Punjab	2011	2017	3 728
Serbia	National	2010	2019	111
Sierra Leone	National	2010	2017	531
Sudan	National	2010	2014	878
Thailand	National	2012	2019	471
Togo	National	2010	2017	380
Tunisia	National	2011	2018	137
Viet Nam	National	2010	2013	255
Zimbabwe	National	2014	2019	490

REFERENCES

GLOSSARY

1. United Nations Economic Commission for Europe (UNECE), FAO, Organisation for Economic Co-operation and Development (OECD), World Bank & Statistical Office of the European Communities (Eurostat). 2007. *Rural households' livelihood and well-being. Statistics on rural development and agriculture household income*. New York, United Nations. 533 pp. (also available at http://www.fao.org/3/am085e/am085e.pdf).

2. FAO. 2019. *Proceedings of the International Symposium on Agricultural Innovation for Family Farmers - Unlocking the potential of agricultural innovation to achieve the Sustainable Development Goals*. J. Ruane, ed. Rome. 120 pp. (also available at http://www.fao.org/3/ca4781en/CA4781EN.pdf).

3. Tendall, D.M., Joerin, J., Kopainsky, B., Edwards, P., Shreck, A., Le, Q.B., Kruetli, P., Grant, M. & Six, J. 2015. Food system resilience: Defining the concept. *Global Food Security*, 6: 17–23.

4. FAO. 2021. Agroecology Knowledge Hub – Practices. In: *FAO* [online]. Rome. [Cited 7 April 2021]. http://www.fao.org/agroecology/knowledge/practices/en/

5. FAO. 2019. The State of the World's Biodiversity for Food and Agriculture 2019. In: *FAO* [online]. Rome. [Cited 17 June 2021]. http://www.fao.org/state-of-biodiversity-for-food-agriculture/en

6. FAO. 2021. Climate-Smart Agriculture. In: *FAO* [online]. Rome. [Cited 21 June 2021]. http://www.fao.org/climate-smart-agriculture/en/

7. FAO. (forthcoming). *Future of food and agriculture - Drivers and triggers of transformation*. Rome.

8. United Nations. 2020. *UN Common Guidance on Helping Build Resilient Societies. Draft*. New York. 64 pp. (also available at https://www.sparkblue.org/basic-page/un-common-guidance-helping-build-resilient-societies)

9. United Nations. 2016. *Report of the open-ended intergovernmental expert working group on indicators and terminology relating to disaster risk reduction*. New York. 41 pp. (also available at https://www.undrr.org/publication/report-open-ended-intergovernmental-expert-working-group-indicators-and-terminology).

10. CAC. 1969. *General Principles of Food Hygiene*. Rome. 35 pp. (also available at http://www.fao.org/fao-who-codexalimentarius/sh-proxy/en/?lnk=1&url=https%253A%252F%252Fworkspace.fao.org%252Fsites%252Fcodex%252FStandards%252FCXC%2B1-1969%252FCXC_001e.pdf).

11. HLPE. 2020. *Food security and nutrition: building a global narrative towards 2030.* A report by the High Level Panel of Experts on Food Security and Nutrition of the Committee on World Food Security. Rome. 91 pp. (also available at http://www.fao.org/3/ca9731en/ca9731en.pdf).

12. FAO, IFAD, UNICEF, WFP & WHO. 2021. *The State of Food Security and Nutrition in the World 2021. Transforming food systems for food security, improved nutrition and affordable healthy diets for all.* FAO. 240 pp. (also available at http://www.fao.org/documents/card/en/c/cb4474en).

13. FAO. 2014. *Developing sustainable food value chains – Guiding principles.* Rome. 75 pp. (also available at http://www.fao.org/3/i3953e/i3953e.pdf).

14. FAO. 2010. *Bioenergy and food security. The BEFS analytical framework*. Environment and Natural Resources Management Series No 16. Rome. 91 pp. (also available at http://www.fao.org/3/i1968e/i1968e.pdf).

15. Bahri, T., Vasconcellos, M., Welch, D.J., Johnson, J., Perry, R.I., Ma, X. & Sharma, R., eds. 2021. *Adaptive management of fisheries in response to climate change*. FAO Fisheries and Aquaculture Technical Paper No. 667. Rome, FAO. (also available at http://www.fao.org/documents/card/en/c/cb3095en/).

16. Low, B., Ostrom, E., Simon, C. & Wilson, J. 2002. Redundancy and diversity: do they influence optimal management? In F. Berkes, J. Colding & C. Folke, eds. *Navigating social-ecological systems: Building resilience for complexity and change*, pp. 83–114. Cambridge, Cambridge University Press.

17. Stone, J. & Rahimifard, S. 2018. Resilience in agri-food supply chains: a critical analysis of the literature and synthesis of a novel framework. *Supply Chain Management*, 23(3): 207–238.

18. United Nations. 2017. *Adopting an analytical framework on risk and resilience: a proposal for more proactive, coordinated and effective United Nations ACTION.* New York. 10 pp. (also available at https://unsceb.org/sites/default/files/imported_files/RnR_0.pdf).

19. Väänänen, E., Dale, L. & Dickson, B. 2017. *Anticipate, Absorb, Reshape: Current progress on three key capacities for climate resilience*. Briefing Paper. United Nations Climate Resilience Initiative: Anticipate, Absorb, Reshape – A2R. 12 pp. (also available at https://static1.squarespace.com/static/5651e0a2e4b0d031533efa3b/t/5911b65e725e256f43f30e18/1494333030141/A2R_infobrief_web_singlepages.pdf).

20. Cutter, S.L., Barnes, L., Berry, M., Burton, C., Evans, E., Tate, E. & Webb, J. 2008. A place-based model for understanding community resilience to natural disasters. *Global Environmental Change*, 18(4): 598–606.

21. Oxfam. 2017. *The future is a choice: The Oxfam framework and guidance for resilient development*. 43 pp. (also available at https://policy-practice.oxfam.org/resources/the-oxfam-framework-and-guidance-for-resilient-development-604990/).

22. Béné, C., Wood, R.G., Newsham, A. & Davies, M. 2012. *Resilience: New Utopia or New Tyranny? Reflection about the potentials and limits of the concept of resilience in relation to vulnerability reduction programmes*. IDS Working Paper 405. Brighton, Institute of Development Studies.

23. Organisation for Economic Co-operation and Development (OECD). 2014. *Guidelines for Resilience Systems Analysis: How to analyse risk and build a roadmap to resilience*. Paris, OECD Publishing. 47 pp.

24. Intergovernmental Panel on Climate Change (IPCC). 2012. *Managing the risks of extreme events and disasters to advance climate change adaption.* A Special Report of Working Groups I and II of the Intergovernmental Panel on Climate Change. New York, USA, and Cambridge, UK, Cambridge University Press. 582 pp.

25. Walker, B., Holling, C.S., Carpenter, S. & Kinzig, A. 2004. Resilience, adaptability and transformability in social–ecological systems. *Ecology and Society*, 9(2): 5.

26. ActionAid. 2016. *Resilience handbook – A guide to integrated resilience programming.* ActionAid International. 66 pp.

27. Gitz, V. & Meybeck, A. 2012. Risks, vulnerabilities and resilience in a context of climate change. *In* A. Maybeck, J. Lankoski, S. Redfern, N. Azzu & V. Gitz, eds. *Building resilience for adaptation to climate change in the agriculture sector. Proceedings of a Joint FAO/OECD Workshop*, pp. 19–36. Rome, FAO. (also available at http://www.fao.org/3/i3084e/i3084e.pdf).

28. FAO. 2003. *Enhancing Support for Sustainable Rural Livelihoods*. Committee on Agriculture, 17th Session. Rome. (also available at http://www.fao.org/3/Y8349e/Y8349e.htm).

29. Zseleczky, L. & Sivan, Y. 2014. *Are shocks really increasing? A selective review of the global frequency, severity, scope, and impact of five types of shocks*. 2020 Conference Paper No. 5. Washington, DC, IFPRI.

30. Montanari, S. & Kocollari, U. 2020. Defining the SME: A multi-perspective investigation. *In* A. Thrassou, D. Vrontis, Y. Weber, S.M.R. Shams & E. Tsoukatos, eds. *The changing role of SMEs in global business*, pp. 61–82. Palgrave Studies in Cross-disciplinary Business Research, in association with EuroMed Academy of Business. Palgrave Macmillan, Cham. (also available at https://doi.org/10.1007/978-3-030-45835-5_4).

31. Buculescu (Costică), M.-M. 2013. Harmonization process in defining small and medium-sized enterprises. Arguments for a quantitative definition versus a qualitative one. *Theoretical and Applied Economics*, 9(586): 103–114. (also available at https://ideas.repec.org/a/agr/journl/vxxy2013i9(586)p103-114.html).

32. Khalil, C.A., Conforti, P. & Gennari, P. 2017. *Defining smallholders to monitor target 2.3. of the 2030 Agenda for Sustainable Development*. FAO Statistics Working Paper Series. Rome, FAO. 43 pp. (also available at http://www.fao.org/publications/card/en/c/e7f3e6f7-59ee-42e7-9cce-36c18af2daea/).

33. Bujones, A., Jaskiewicz, K., Linakis, L. & McGirr, M. 2013. *A framework for analyzing resilience in fragile and conflict-affected situations*. Columbia University SIPA and USAID. 59 pp.

34. FAO. 2018. *Sustainable food systems: concept and framework*. [online]. Technical Brief. [Cited 1 August 2020]. www.fao.org/3/ca2079en/CA2079EN.pdf

35. FAO. 1989. *The State of Food and Agriculture 1989. World and regional reviews. Sustainable development and natural resource management.* Rome. 171 pp. (also available at http://www.fao.org/3/a-t0162e.pdf).

REFERENCES

CHAPTER 1

1. FAO. 2021. FAOSTAT. New Food Balance Sheets. In: *FAO* [online]. Rome. [Cited 12 July 2021]. http://www.fao.org/faostat/en/#data/FBS

2. Townsend, T. 2019. Natural fibres and the world economy. In: *Discover Natural Fibres Initiative* [online]. [Cited 12 July 2021]. https://dnfi.org/coir/natural-fibres-and-the-world-economy-july-2019_18043/

3. FAO. 2021. FAOSTAT. Forestry Production and Trade. In: *FAO* [online]. Rome. [Cited 12 July 2021]. http://www.fao.org/faostat/en/#data/FO

4. FAO. 2021. FAOSTAT. Value of Agricultural Production. In: *FAO* [online]. Rome. [Cited 12 July 2021]. http://www.fao.org/faostat/en/#data/QV

5. World Bank. 2021. Employment in agriculture (% of total employment) (modeled ILO estimate). In: *The World Bank* [online]. Washington, DC. [Cited 12 May 2021]. https://data.worldbank.org/indicator/SL.AGR.EMPL.ZS

6. Townsend, R., Benfica, R.M., Prasann, A., Lee, M. & Shah, P. 2017. *Future of food: shaping the food system to deliver jobs*. Washington, DC, World Bank Group. (also available at http://documents.worldbank.org/curated/en/406511492528621198/Future-of-food-shaping-the-food-system-to-deliver-jobs).

7. FAO, IFAD, UNICEF, WFP & WHO. 2020. *The State of Food Security and Nutrition in the World 2020. Transforming food systems for affordable healthy diets*. Rome, FAO. 320 pp. (also available at https://doi.org/10.4060/ca9692en).

8. Béné, C. 2020. Resilience of local food systems and links to food security – A review of some important concepts in the context of COVID-19 and other shocks. *Food Security*, 12(4): 805–822.

9. United Nations. 2020. *UN Common Guidance on Helping Build Resilient Societies. Draft*. New York. 64 pp. (also available at https://www.sparkblue.org/basic-page/un-common-guidance-helping-build-resilient-societies)

10. Béné, C., Wood, R.G., Newsham, A. & Davies, M. 2012. *Resilience: New Utopia or New Tyranny? Reflection about the potentials and limits of the concept of resilience in relation to vulnerability reduction programmes*. IDS Working Paper 405. Brighton, Institute of Development Studies.

11. FAO. 2021. *The impact of disasters and crises on agriculture and food security: 2021*. Rome. 211 pp. (also available at http://www.fao.org/documents/card/en/c/cb3673en).

12. FAO, IFAD, UNICEF, WFP & WHO. 2021. *The State of Food Security and Nutrition in the World 2021. Transforming food systems for food security, improved nutrition and affordable healthy diets for all*. Rome, FAO. 240 pp. (also available at http://www.fao.org/documents/card/en/c/cb4474en).

13. Food Security Information Network (FSIN) & Global Network Against Food Crises. 2021. *Global report on food crises: Joint analysis for better decisions*. Rome, FSIN. 304 pp. (also available at https://www.fsinplatform.org/sites/default/files/resources/files/GRFC%202021%20050521%20med.pdf).

14. Iddir, M., Brito, A., Dingeo, G., Fernandez Del Campo, S.S., Samouda, H., La Frano, M.R. & Bohn, T. 2020. Strengthening the immune system and reducing inflammation and oxidative stress through diet and nutrition: Considerations during the COVID-19 crisis. *Nutrients*, 12(6): 1562.

15. International Food Policy Research Institute (IFPRI). 2014. *Resilience for food and nutrition security*. Washington, DC. 211 pp. (also available at http://ebrary.ifpri.org/utils/getfile/collection/p15738coll2/id/128437/filename/128648.pdf).

16. United Nations. 2019. World population prospects 2019. In: *United Nations* [online]. New York. [Cited 12 July 2021]. https://population.un.org/wpp/

17. FAO. 2018. *The future of food and agriculture 2018 – Alternative pathways to 2050*. Rome. 224 pp. (also available at www.fao.org/3/I8429EN/i8429en.pdf).

18. Hodson, E., Niggli, U., Kaoru, K., Lal, R. & Sadoff, C. 2020. *Boost nature positive production at sufficient scale – A paper on Action Track 3*. United Nations Food Systems Summit 2021 Scientific Group. 16 pp. (also available at https://www.un.org/sites/un2.un.org/files/3-action_track_3_scientific_group_draft_paper_26-10-2020.pdf).

19. Springmann, M., Clark, M., Mason-D'Croz, D., Wiebe, K., Bodirsky, B.L., Lassaletta, L., de Vries, W. *et al.* 2018. Options for keeping the food system within environmental limits. *Nature*, 562: 519–525.

20. Capalbo, S.M., Seavert, C., Antle, J.M., Way, J. & Houston, L. 2018. Understanding tradeoffs in the context of farm-scale impacts: An application of decision-support tools for assessing climate smart agriculture. In L. Lipper, N. McCarthy, D. Zilberman, S. Asfaw & G. Branca, eds. *Climate smart agriculture*, pp. 173–197. Natural Resource Management and Policy, vol. 52. Springer International Publishing. (also available at http://link.springer.com/10.1007/978-3-319-61194-5_9).

21. Holling, C.S. 1973. Resilience and stability of ecological systems. *Annual Review of Ecology and Systematics*, 4: 1–23.

22. Tendall, D.M., Joerin, J., Kopainsky, B., Edwards, P., Shreck, A., Le, Q.B., Kruetli, P., Grant, M. & Six, J. 2015. Food system resilience: Defining the concept. *Global Food Security*, 6: 17–23.

23. Hertel, T., Elouafi, I., Ewert, F. & Tanticharoen, M. 2021. *Building resilience to vulnerabilities, shocks and stresses – Action Track 5*. United Nations Food Systems Summit 2021 Scientific Group. 20 pp. (also available at https://www.un.org/sites/un2.un.org/files/5-action_track-5_scientific_group_draft_paper_8-3-2021.pdf).

24. HLPE. 2020. *Food security and nutrition: building a global narrative towards 2030.* A report by the High Level Panel of Experts on Food Security and Nutrition of the Committee on World Food Security. Rome, FAO. 91 pp. (also available at http://www.fao.org/3/ca9731en/ca9731en.pdf).

25. FAO. 2016. *Combatting fusarium wilt disease of banana*. FCC-EMPRES Information Sheets No. 7. Rome. (also available at http://www.fao.org/3/i5874e/i5874e.pdf).

26. HLPE. 2017. *Nutrition and food systems*. A report by the High Level Panel of Experts on Food Security and Nutrition of the Committee on World Food Security. Rome, FAO. 151 pp. (also available at www.fao.org/3/a-i7846e.pdf).

27. Ricciardi, V., Ramankutty, N., Mehrabi, Z., Jarvis, L. & Chookolingo, B. 2018. How much of the world's food do smallholders produce? *Global Food Security*, 17: 64–72.

28. Dury, S., Bendjebbar, P., Hainzelin, E., Giordano, T. & Bricas, N., eds. 2019. *Food systems at risk. New trends and challenges*. Rome, FAO, CIRAD and European Commission. 132 pp. (also available at http://agritrop.cirad.fr/593617/).

29. Roxy, M.K., Modi, A., Murtugudde, R., Valsala, V., Panickal, S., Prasanna Kumar, S., Ravichandran, M., Vichi, M. & Lévy, M. 2015. A reduction in marine primary productivity driven by rapid warming over the tropical Indian Ocean. *Geophysical Research Letters*, 43(2): 826–833.

30. Kumar, P.S., Pillai, G.N. & Manjusha, U. 2014. El Nino Southern Oscillation (ENSO) impact on tuna fisheries in Indian Ocean. *SpringerPlus*, 3(1): 591.

31. FAO, IFAD, UNICEF, WFP & WHO. 2018. *The State of Food Security and Nutrition in the World 2018. Building climate resilience for food security and nutrition*. Rome, FAO. 183 pp. (also available at http://www.fao.org/3/i9553en/i9553en.pdf).

32. Darnhofer, I., Fairweather, J. & Moller, H. 2010. Assessing a farm's sustainability: insights from resilience thinking. *International Journal of Agricultural Sustainability*, 8(3): 186–198.

33. FAO. 2018. *Mongolia. Impact of Early Warning Early Action: Protecting the livelihoods of herders from a* dzud *winter*. Rome. 29 pp. (also available at http://www.fao.org/3/ca2181en/CA2181EN.pdf).

34. FAO. 2018. *Horn of Africa. Impact of Early Warning Early Action: Protecting pastoralist livelihoods ahead of drought*. Rome. 25 pp. (also available at http://www.fao.org/3/ca0227en/CA0227EN.pdf).

35. FAO. 2019. *The Sudan. Impact of Early Warning Early Action: Protecting agropastoralist livelihoods ahead of drought*. Rome. 7 pp. (also available at http://www.fao.org/3/ca4653en/ca4653en.pdf).

36. FAO. 2019. *Madagascar. Impact of Early Warning Early Action: Protecting farming livelihoods from drought and food insecurity*. Rome. 25 pp. (also available at http://www.fao.org/3/ca3933en/ca3933en.pdf).

37. FAO. 2019. *Colombia. Impact of Early Warning Early Action: Boosting food security and social cohesion on the frontline of the migration crisis*. Rome. 21 pp. (also available at http://www.fao.org/3/ca6818en/ca6818en.pdf).

REFERENCES

38. FAO. 2020. *The Philippines. Impact of Early Warning Early Action: Exploring the interplay between El Niño-induced drought, conflict and gender*. Rome. 25 pp. (also available at http://www.fao.org/3/ca9371en/ca9371en.pdf).

39. FAO. 2021. *Bangladesh. Impact of Anticipatory Action: Striking before the floods to protect agricultural livelihoods*. Rome. 31 pp. (also available at http://www.fao.org/3/cb4113en/cb4113en.pdf).

40. Cottrell, R.S., Nash, K.L., Halpern, B.S., Remenyi, T.A., Corney, S.P., Fleming, A., Fulton, E.A. *et al.* 2019. Food production shocks across land and sea. *Nature Sustainability*, 2: 130–137.

41. FAO, IFAD, UNICEF, WFP & WHO. 2017. *The State of Food Security and Nutrition in the World 2017. Building resilience for peace and food security*. Rome. 119 pp. (also available at http://www.fao.org/3/a-I7695e.pdf).

42. FAO. 2019. *Rural transformation – Key for sustainable development in the Near East and North Africa*. Overview of Food Security and Nutrition 2018. Rome. 85 pp. (also available at http://www.fao.org/documents/card/en/c/ca3817en/).

43. United Nations Framework Convention on Climate Change (UNFCCC). 2020. *Loss and damage. Online guide* [online]. New York. [Cited 12 July 2021]. https://unfccc.int/sites/default/files/resource/Online_Guide_feb_2020.pdf

44. FSIN & Global Network Against Food Crises. 2020. *2020 Global report on food crises: Joint analysis for better decisions*. Rome, FSIN. 240 pp. (also available at http://www.fao.org/publications/card/en/c/CA8786EN/).

45. FAO. 2020. *Climate change: Unpacking the burden on food safety*. Food Safety and Quality Series No. 8. Rome. 176 pp. (also available at http://www.fao.org/documents/card/en/c/ca8185en/).

46. Vilar-Compte, M., Sandoval-Olascoaga, S., Bernal-Stuart, A., Shimoga, S. & Vargas-Bustamante, A. 2014. The impact of the 2008 financial crisis on food security and food expenditures in Mexico: a disproportionate effect on the vulnerable. *Public Health Nutrition*, 18(16): 2934–2942.

47. Organisation for Economic Co-operation and Development (OECD). 2020. *Food supply chains and COVID-19: Impacts and policy lessons* [online]. Paris. [Cited 12 July 2021]. https://read.oecd-ilibrary.org/view/?ref=134_134305-ybqvdf0kg9&title=Food-Supply-Chains-and-COVID-19-Impacts-and-policy-lessons

48. FAO. 2020. *How is COVID-19 affecting the fisheries and aquaculture food systems*. Rome. (also available at http://www.fao.org/3/ca8637en/CA8637EN.pdf).

49. Anonymous. 2021. Kenyans are starting to drink their own coffee. *The Economist* [online]. [Cited 5 May 2021]. https://www.economist.com/middle-east-and-africa/2021/04/08/kenyans-are-starting-to-drink-their-own-coffee?frsc=dg%7Ce

50. Béné, C., Bakker, D., Chavarro, M.J., Even, B., Melo, J. & Sonneveld, A. 2021. *Impacts of COVID-19 on people's food security: Foundations for a more resilient food system*. Discussion Paper. Montpellier, France, CGIAR. 81 pp. (also available at https://doi.org/10.2499/p15738coll2.134295).

51. Steffen, W., Richardson, K., Rockström, J., Cornell, S.E., Fetzer, I., Bennett, E.M., Biggs, R. *et al.* 2015. Planetary boundaries: Guiding human development on a changing planet. *Science*, 347(6223): 1259855 [online]. [Cited 12 July 2021]. DOI: 10.1126/science.1259855

52. Aiyar, A. & Pingali, P.L. 2020. Pandemics and food systems – towards a proactive food safety approach to disease prevention and management. *Food Security*, 12(4): 749–756.

53. United Nations. 2019. *World urbanization prospects 2018*. In: United Nations [online]. New York. [Cited 12 July 2021]. https://population.un.org/wup/

54. Anderies, J.M., Folke, C., Walker, B. & Ostrom, E. 2013. Aligning key concepts for global change policy: robustness, resilience, and sustainability. *Ecology and Society*, 18(2): 8 [online]. [Cited 12 July 2021]. http://dx.doi.org/10.5751/ES-05178-180208

55. Brand, F.S. & Jax, K. 2007. Focusing the meaning(s) of resilience: resilience as a descriptive concept and a boundary object. *Ecology and Society*, 12(1): 3 [online]. [Cited 12 July 2021]. http://www.ecologyandsociety.org/vol12/iss1/art23/

56. Rees, W.E. 2010. Thinking resilience. *In* R. Heinberg & D. Lerch, eds. *The Post Carbon Reader: Managing the 21st century's sustainability crises*, ch. 3. Santa Rosa, USA, Post Carbon Institute.

57. Maleksaeidi, H. & Karami, E. 2013. Social-ecological resilience and sustainable agriculture under water scarcity. *Agroecology and Sustainable Food Systems*, 37(3): 262–290.

58. Kummu, M., Kinnunen, P., Lehikoinen, E., Porkka, M., Queiroz, C., Röös, E., Troell, M. & Weil, C. 2020. Interplay of trade and food system resilience: Gains on supply diversity over time at the cost of trade independency. *Global Food Security*, 24: 100360.

59. Kahiluoto, H., Mäkinen, H. & Kaseva, J. 2020. Supplying resilience through assessing diversity of responses to disruption. *International Journal of Operations & Production Management*, 40(3): 271–292.

CHAPTER 2

1. Béné, C. 2020. Resilience of local food systems and links to food security – A review of some important concepts in the context of COVID-19 and other shocks. *Food Security*, 12(4): 805–822.

2. Cardwell, R. & Ghazalian, P.L. 2020. COVID-19 and international food assistance: Policy proposals to keep food flowing. *World Development*, 135: 105059.

3. Laborde, D., Martin, W., Swinnen, J. & Vos, R. 2020. COVID-19 risks to global food security. *Science*, 369(6503): 500–502 [online]. [Cited 12 July 2021]. DOI: 10.1126/science.abc4765

4. Fader, M., Gerten, D., Krause, M., Lucht, W. & Cramer, W. 2013. Spatial decoupling of agricultural production and consumption: quantifying dependences of countries on food imports due to domestic land and water constraints. *Environmental Research Letters*, 8(1): 014046.

5. Anonymous. 2021. Kenyans are starting to drink their own coffee. *The Economist* [online]. [Cited 5 May 2021]. https://www.economist.com/middle-east-and-africa/2021/04/08/kenyans-are-starting-to-drink-their-own-coffee?frsc=dg%7Ce

6. Yu, S. & Goh, B. 2021. As coronavirus sinks global demand, China's exporters go online to tap domestic market. In: *Reuters* [online]. [Cited 12 July 2021]. https://www.reuters.com/article/us-health-coronavirus-china-exporters/as-coronavirus-sinks-global-demand-chinas-exporters-go-online-to-tap-domestic-market-idUSKBN23C0DL

7. Remans, R., Wood, S.A., Saha, N., Anderman, T.L. & DeFries, R.S. 2014. Measuring nutritional diversity of national food supplies. *Global Food Security*, 3(3–4): 174–182.

8. FAO. 2017. *Water for sustainable food and agriculture: A report produced for the G20 Presidency of Germany*. Rome. 27 pp. (also available at www.fao.org/3/a-i7959e.pdf).

9. Zhang, Y., Chen, H.Y.H. & Reich, P.B. 2012. Forest productivity increases with evenness, species richness and trait variation: a global meta-analysis. *Journal of Ecology*, 100(3): 742–749.

10. Hooper, D.U., Adair, E.C., Cardinale, B.J., Byrnes, J.E.K., Hungate, B.A., Matulich, K.L., Gonzalez, A., Duffy, J.E., Gamfeldt, L. & O'Connor, M.I. 2012. A global synthesis reveals biodiversity loss as a major driver of ecosystem change. *Nature*, 486(7401): 105–108.

11. Renard, D. & Tilman, D. 2019. National food production stabilized by crop diversity. *Nature*, 571(7764): 257–260.

12. Sicuro, B. 2021. World aquaculture diversity: origins and perspectives. *Reviews in Aquaculture*, 13(3): 1619–1634.

13. Metian, M., Troell, M., Christensen, V., Steenbeek, J. & Pouil, S. 2020. Mapping diversity of species in global aquaculture. *Reviews in Aquaculture*, 12(2): 1090–1100.

14. Herrero, M., Thornton, P.K., Power, B., Bogard, J.R., Remans, R., Fritz, S., Gerber, J.S. *et al.* 2017. Farming and the geography of nutrient production for human use: a transdisciplinary analysis. *The Lancet Planetary Health*, 1(1): e33–e42 [online]. [Cited 12 July 2021]. https://doi.org/10.1016/S2542-5196(17)30007-4

15. Khoury, C.K., Bjorkman, A.D., Dempewolf, H., Ramirez-Villegas, J., Guarino, L., Jarvis, A., Rieseberg, L.H. & Struik, P.C. 2014. Increasing homogeneity in global food supplies and the implications for food security. *Proceedings of the National Academy of Sciences*, 111(11): 4001–4006 [online]. [Cited 12 July 2021]. https://doi.org/10.1073/pnas.1313490111

REFERENCES

16. Bennett, E., Carpenter, S.R., Gordon, L., Ramankutty, N., Balvanera, P., Campbell, B., Cramer, W. *et al.* 2014. Toward a more resilient agriculture. *Solutions: For a Sustainable and desirable Future*, 5(5): 65–75.

17. Kummu, M., Kinnunen, P., Lehikoinen, E., Porkka, M., Queiroz, C., Röös, E., Troell, M. & Weil, C. 2020. Interplay of trade and food system resilience: Gains on supply diversity over time at the cost of trade independency. *Global Food Security*, 24: 100360.

18. Dolfing, A.G., Leuven, J.R.F.W. & Dermody, B.J. 2019. The effects of network topology, climate variability and shocks on the evolution and resilience of a food trade network. *PLoS ONE*, 14(3): e0213378 [online]. [Cited 12 July 2021]. https://doi.org/10.1371/journal.pone.0213378.

19. Puma, M.J., Bose, S., Chon, S.Y. & Cook, B.I. 2015. Assessing the evolving fragility of the global food system. *Environmental Research Letters*, 10(2): 024007.

20. FAO. 2020. *The State of World Fisheries and Aquaculture 2020. Sustainability in action*. Rome. 244 pp. (also available at http://www.fao.org/documents/card/en/c/ca9229en/).

21. D'Odorico, P., Laio, F. & Ridolfi, L. 2010. Does globalization of water reduce societal resilience to drought? *Geophysical Research Letters*, 31(13): L13403.

22. Suweis, S., Carr, J.A., Maritan, A., Rinaldo, A. & D'Odorico, P. 2015. Resilience and reactivity of global food security. *Proceedings of the National Academy of Sciences*, 112(22): 6902–6907 [online]. [Cited 12 July 2021]. https://doi.org/10.1073/pnas.1507366112

23. FAO & WHO. 2019. *Sustainable healthy diets – Guiding principles*. Rome. 37 pp. (also available at http://www.fao.org/3/ca6640en/ca6640en.pdf).

24. Distefano, T., Laio, F., Ridolfi, L. & Schiavo, S. 2018. Shock transmission in the international food trade network. *PLoS ONE*, 13(8): e0200639 [online]. [Cited 12 July 2021]. https://doi.org/10.1371/journal.pone.0200639

25. Fair, K.R., Bauch, C.T. & Anand, M. 2017. Dynamics of the global wheat trade network and resilience to shocks. *Scientific Reports*, 7(1): 7177 [online]. [Cited 12 July 2021]. https://doi.org/10.1038/s41598-017-07202-y

26. d'Amour, C.B., Wenz, L., Kalkuhl, M., Steckel, J.C. & Creutzig, F. 2016. Teleconnected food supply shocks. *Environmental Research Letters*, 11(3): 035007.

27. Tamea, S., Laio, F. & Ridolfi, L. 2016. Global effects of local food-production crises: a virtual water perspective. *Scientific Reports*, 6(1): 18803 [online]. [Cited 12 July 2021]. https://doi.org/10.1038/srep18803

28. Nelson, A., de By, R., Thomas, T., Girgin, S., Brussel, M., Venus, V. & Ohuru, R. (forthcoming). *The resilience of domestic transport networks in the context of food security – a multi-country analysis*. Background paper for *The State of Food and Agriculture 2021*. FAO Agricultural Development Economics Technical Study No. 14. Rome, FAO.

29. Pyatkova, K., Chen, A.S., Butler, D., Vojinović, Z. & Djordjević, S. 2019. Assessing the knock-on effects of flooding on road transportation. *Journal of Environmental Management*, 244: 48–60.

30. Timmer, C.P. 2000. The macro dimensions of food security: economic growth, equitable distribution, and food price stability. *Food Policy*, 25(3): 283–295.

31. FAO, IFAD, UNICEF, WFP & WHO. 2021. *The State of Food Security and Nutrition in the World 2021. Transforming food systems for food security, improved nutrition and affordable healthy diets for all*. Rome, FAO. 240 pp. (also available at http://www.fao.org/documents/card/en/c/cb4474en).

32. Chao, S. 2012. *Forest peoples – Numbers across the world*. Moreton-in-Marsh, UK, Forest Peoples Programme. (also available at https://www.forestpeoples.org/sites/fpp/files/publication/2012/05/forest-peoples-numbers-across-world-final_0.pdf).

33. FAO & United Nations Environment Programme (UNEP). 2020. *The State of the World's Forests 2020. Forests, biodiversity and people*. Rome, FAO. 188 pp. (also available at http://www.fao.org/3/ca8642en/CA8642EN.pdf).

34. Seekell, D., Carr, J., Dell'Angelo, J., D'Odorico, P., Fader, M., Gephart, J., Kummu, M. *et al.* 2017. Resilience in the global food system. *Environmental Research Letters*, 12(2): 025010.

35. World Bank. 2021. COVID-19 High Frequency Phone Survey of Households 2020-2021, Living Standards Measurement Study Plus. In: *The World Bank* [online]. Washington, DC. [Cited 12 July 2021]. https://microdata.worldbank.org/index.php/catalog/3860

36. BRAC International. 2020. *Rapid food and income security assessment: How are BRAC International volunteers and programme participants coping with COVID-19*. 7 pp. (also available at https://www.bracuk.net/wp-content/uploads/2020/04/Covid-FS-Rapid-Assessment-BI_20200404.pdf).

37. Gomes, C.M., Favorito, L.A., Henriques, J.V.T., Canalini, A.F., Anzolch, K.M.J., Fernandes, R. de C., Bellucci, C.H.S. *et al.* 2020. Impact of COVID-19 on clinical practice, income, health and lifestyle behavior of Brazilian urologists. *International Brazilian Journal of Urology*, 46(6): 1042–1071.

38. World Bank. 2021. PovcalNet: an online analysis tool for global poverty monitoring. In: *World Bank* [online]. Washington, DC. [Cited 12 July 2021]. http://iresearch.worldbank.org/PovcalNet/

39. World Bank. 2021. *World Development Indicators: Population, total* [online]. Washington, DC. [Cited 1 June 2021]. https://data.worldbank.org/indicator/SP.POP.TOTL

40. World Bank. 2020. Global consumption database - food and beverages. In: *World Bank* [online]. Washington, DC. [Cited 12 July 2021]. https://datatopics.worldbank.org/consumption/sector/Food-and-Beverages

41. World Bank. 2021. *The gradual rise and rapid decline of the middle class in Latin America and the Caribbean*. Washington, DC. (also available at https://openknowledge.worldbank.org/handle/10986/35834).

42. FAO, IFAD, UNICEF, WFP & WHO. 2020. *The State of Food Security and Nutrition in the World 2020. Transforming food systems for affordable healthy diets*. Rome, FAO. 320 pp. (also available at https://doi.org/10.4060/ca9692en).

43. Reardon, T. & Swinnen, J. 2020. COVID-19 and resilience innovations in food supply chains. In: *IFPRI Blog* [online]. [Cited 12 July 2021]. https://www.ifpri.org/blog/covid-19-and-resilience-innovations-food-supply-chains

CHAPTER 3

1. FAO. 2021. FAOSTAT. In: *FAO* [online]. Rome. [Cited 12 July 2021]. http://faostat.fao.org

2. Yi, J., Meemken, E.-M., Mazariegos-Anastassiou, V., Liu, J., Kim, E., Gómez, M.I., Canning, P. & Barrett, C.B. 2021. Post-farmgate food value chains make up most of consumer food expenditures globally. *Nature Food*, 2(6): 417–425.

3. Reardon, T. 2015. The hidden middle: the quiet revolution in the midstream of agrifood value chains in developing countries. *Oxford Review of Economic Policy*, 31(1): 45–63.

4. Reardon, T., Echeverria, R., Berdegué, J.A., Minten, B., Liverpool-Tasie, S., Tschirley, D. & Zilberman, D. 2019. Rapid transformation of food systems in developing regions: Highlighting the role of agricultural research and innovations. *Agricultural Systems*, 172: 47–59.

5. Godfray, H.C.J., Crute, I.R., Haddad, L., Lawrence, D., Muir, J.F., Nisbett, N., Pretty, J., Robinson, S., Toulmin, C. & Whiteley, R. 2010. The future of the global food system. *Philosophical Transactions of the Royal Society B: Biological Sciences*, 365(1554): 2769–2777.

6. Stone, J. & Rahimifard, S. 2018. Resilience in agri-food supply chains: a critical analysis of the literature and synthesis of a novel framework. *Supply Chain Management*, 23(3): 207–238.

7. FAO. 2017. *The State of Food and Agriculture 2017. Leveraging food systems for inclusive rural transformation*. Rome. 160 pp. (also available at http://www.fao.org/3/a-i7658e.pdf).

8. Reardon, T. & Zilberman, D. 2021. The economics of food system resilience – conceptual overview and evidence. Background paper for *The State of Food and Agriculture 2021. Making agri-food systems more resilient to shocks and stresses*. Rome, FAO (unpublished).

9. Liverpool-Tasie, S., Omonona, B., Sanou, A., Ogunleye, W., Padilla, S. & Reardon, T. 2017. *Growth and transformation of food systems in Africa: Evidence from the poultry value chain in Nigeria*. Feed the Future Innovation Lab for Food Security Policy Research Brief. Michigan State University. 6 pp.

REFERENCES

10. Reardon, T. & Swinnen, J. 2020. COVID-19 and resilience innovations in food supply chains. In: *IFPRI Blog* [online]. [Cited 12 July 2021]. https://www.ifpri.org/blog/covid-19-and-resilience-innovations-food-supply-chains

11. Reardon, T., Tschirley, D., Liverpool-Tasie, L.S.O., Awokuse, T., Fanzo, J., Minten, B., Vos, R. *et al.* 2021. The processed food revolution in African food systems and the double burden of malnutrition. *Global Food Security*, 28: 100466.

12. Ali, I., Nagalingam, S. & Gurd, B. 2017. Building resilience in SMEs of perishable product supply chains: enablers, barriers and risks. *Production Planning and Control*, 28(15): 1236–1250.

13. Handayati, Y., Simatupang, T.M. & Perdana, T. 2015. Agri-food supply chain coordination: the state-of-the-art and recent developments. *Logistics Research*, 8(1): 5.

14. Ali, I., Nagalingam, S. & Gurd, B. 2018. A resilience model for cold chain logistics of perishable products. *The International Journal of Logistics Management*, 29(3): 922–941.

15. Kelly, S. & Ilie, E.T. 2021. *Engaging with small and medium agrifood enterprises to guide policy making*. Rome, FAO. 78 pp. (also available at https://doi.org/10.4060/cb4179en).

16. Lu, Y., Wu, J., Peng, J. & Lu, L. 2020. The perceived impact of the Covid-19 epidemic: evidence from a sample of 4807 SMEs in Sichuan Province, China. *Environmental Hazards*, 19(4): 323–340.

17. Ali, I. 2021. Risk and resilience in SMEs of agri-food supply chains amid the COVID-19 pandemic: A cross-country comparison. Background paper for *The State of Food and Agriculture 2021. Making agri-food systems more resilient to shocks and stresses*. Melbourne, Australia, School of Business and Law, CQUniversity (unpublished).

18. Global Alliance for Improved Nutrition (GAIN), World Food Programme (WFP), Scaling Up Nutrition (SUN) & Business Network. 2020. *Impacts of COVID-19 on small- and medium-sized enterprises in the food system – Results of an online survey* [online]. [Cited 12 July 2021]. https://www.gainhealth.org/resources/reports-and-publications/impacts-covid-19-small-and-medium-sized-enterprises-food-system-results-of-an-online-survey

19. Jola-Sanchez, A.F. 2020. *Humanitarian response to COVID-19: A discussion of challenges in disaster management for developing countries*. Mosbacher Institute for Trade, Economics and Public Policy. (also available at https://hdl.handle.net/1969.1/187866).

20. Abu Hatab, A., Lagerkvist, C. & Esmat, A. 2021. Risk perception and determinants in small- and medium-sized agri-food enterprises amidst the COVID-19 pandemic: Evidence from Egypt. *Agribusiness*, 37(1): 187–212.

21. Qanti, S.R., Reardon, T. & Iswariyadi, A. 2017. Triangle of linkages among modernising markets, sprayer-traders, and mango farming intensification In Indonesia. *Bulletin of Indonesian Economic Studies*, 53(2): 187–208.

22. Zhang, X., Yang, J. & Reardon, T. 2017. Mechanization outsourcing clusters and division of labor in Chinese agriculture. *China Economic Review*, 43: 184–195.

23. Thulasiraman, V., Nandagopal, M.S.G. & Kothakota, A. 2021. Need for a balance between short food supply chains and integrated food processing sectors: COVID-19 takeaways from India. *Journal of Food Science and Technology* [online]. [Cited 12 July 2021]. https://doi.org/10.1007/s13197-020-04942-0

24. Hobbs, J.E. 2020. Food supply chains during the COVID-19 pandemic. *Canadian Journal of Agricultural Economics*, 68(2): 171–176.

25. Thilmany, D., Canales, E., Low, S.A. & Boys, K. 2021. Local food supply chain dynamics and resilience during COVID-19. *Applied Economic Perspectives and Policy*, 43(1): 86–104.

26. Fei, S., Ni, J. & Santini, G. 2020. Local food systems and COVID-19: an insight from China. *Resources Conservation and Recycling*, 162: 105022.

27. Hobbs, J.E. 2021. Food supply chain resilience and the COVID-19 pandemic: What have we learned? *Canadian Journal of Agricultural Economics*, 69(2): 189–196.

28. Marusak, A., Sadeghiamirshahidi, N., Krejci, C.C., Mittal, A., Beckwith, S., Cantu, J., Morris, M. & Grimm, J. 2021. Resilient regional food supply chains and rethinking the way forward: Key takeaways from the COVID-19 pandemic. *Agricultural Systems*, 190: 103101.

29. FAO, IFAD, UNICEF, WFP & WHO. 2021. *The State of Food Security and Nutrition in the World 2021. Transforming food systems for food security, improved nutrition and affordable healthy diets for all*. Rome, FAO. 240 pp. (also available at http://www.fao.org/documents/card/en/c/cb4474en).

30. Reardon, T., Heiman, A., Lu, L., Nuthalapati, C.S.R., Vos, R. & Zilberman, D. 2021. "Pivoting" by food industry firms to cope with COVID-19 in developing regions: E-commerce and "copivoting" delivery intermediaries. *Agricultural Economics*, 52(3): 459–475.

31. FAO. 2007. *Promises and challenges of the informal food sector in developing countries*. Rome. 34 pp. (also available at http://www.fao.org/3/a1124e/a1124e00.pdf).

32. Béné, C., Bakker, D., Rodriguez, M.C., Even, B., Melo, J. & Sonneveld, A. 2021. *Impacts of COVID-19 on people's food security: Foundations for a more resilient food system*. Discussion Paper. Montpellier, France, CGIAR. 81 pp. (also available at https://doi.org/10.2499/p15738coll2.134295).

33. Conz, E., Denicolai, S. & Zucchella, A. 2017. The resilience strategies of SMEs in mature clusters. *Journal of Enterprising Communities: People and Places in the Global Economy*, 11(1): 186–210.

34. Darnhofer, I. 2020. Farm resilience in the face of the unexpected: lessons from the COVID-19 pandemic. *Agriculture and Human Values*, 37(3): 605–606.

35. Sandmo, A. 1971. On the theory of the competitive firm under price uncertainty. *The American Economic Review*, 61(1): 65–73. (also available at https://www.jstor.org/stable/1910541).

36. Riordan, M.H. & Williamson, O.E. 1985. Asset specificity and economic organization. *International Journal of Industrial Organization*, 3(4): 365–378.

37. Hernandez, R., Belton, B., Reardon, T., Hu, C., Zhang, X. & Ahmed, A. 2018. The "quiet revolution" in the aquaculture value chain in Bangladesh. *Aquaculture*, 493: 456–468.

38. Barrett, C.B., Bachke, M.E., Bellemare, M.F., Michelson, H.C., Narayanan, S. & Walker, T.F. 2012. Smallholder participation in contract farming: Comparative evidence from five countries. *World Development*, 40(4): 715–730.

39. Dolan, C. & Humphrey, J. 2000. Governance and trade in fresh vegetables: The impact of UK supermarkets on the African horticulture industry. *The Journal of Development Studies*, 37(2): 147–176.

40. Ingram, J. 2011. A food systems approach to researching food security and its interactions with global environmental change. *Food Security*, 3(4): 417–431.

41. Jin, H.J., Skripnitchenko, A. & Koo, W.W. 2004. *The effects of the BSE outbreak in the United States on the beef and cattle industry*. Center for Agricultural Policy and Trade Studies, Department of Agribusiness and Applied Economics, North Dakota State University.

42. Meyer, F., Reardon, T., van der Merwe, M., Jordaan, D., Delport, M. & van der Burgh, G. 2021. *Hotspots of vulnerability: Analysis of food value chain disruptions by COVID-19 policies in South Africa*. *Agrekon*, 60(4).

43. Knox, A.J., Bressers, H., Mohlakoana, N. & De Groot, J. 2019. Aspirations to grow: when micro- and informal enterprises in the street food sector speak for themselves. *Journal of Global Entrepreneurship Research*, 9(1): 38.

44. Young, G. & Crush, J. 2019. *Governing the informal food sector in cities of the global south*. Discussion Paper No. 30. Hungry Cities Partnership. 23 pp.

45. Ali, I. & Gölgeci, I. 2020. Managing climate risks through social capital in agrifood supply chains. *Supply Chain Management*, 26(1): 1–16.

46. Gálvez Nogales, E. 2010. *Agro-based clusters in developing countries: staying competitive in a globalized economy.* Agricultural Management, Marketing and Finance Occasional Paper No. 25. Rome, FAO. 105 pp. (also available at http://www.fao.org/3/i1560e/i1560e.pdf).

47. Gálvez Nogales, E. & Webber, M. 2017. *Territorial tools for agro-industry development – A sourcebook*. Rome, FAO. 368 pp. (also available at http://www.fao.org/3/i6862e/i6862e.pdf).

48. Dai, R., Mookherjee, D., Quan, Y. & Zhang, X. 2021. Industrial clusters, networks and resilience to the Covid-19 shock in China. *Journal of Economic Behavior and Organization*, 183: 433–455.

REFERENCES

49. Zambon, I., Cecchini, M., Egidi, G., Saporito, M.G. & Colantoni, A. 2019. Revolution 4.0: Industry vs. Agriculture in a future development for SMEs. *Processes*, 7(1): 36.

50. Barcaccia, G., D'Agostino, V., Zotti, A. & Cozzi, B. 2020. Impact of the SARS-CoV-2 on the Italian agri-food sector: An analysis of the quarter of pandemic lockdown and clues for a socio-economic and territorial restart. *Sustainability*, 12(14): 5651.

51. FAO. 2020. *Enabling sustainable food systems: Innovators' handbook*. Rome. 262 pp. (also available at http://www.fao.org/documents/card/en/c/ca9917en/).

52. United Nations. 2015. *Sendai Framework for Disaster Risk Reduction 2015–2030*. Geneva. 35 pp. (also available at https://www.preventionweb.net/files/43291_sendaiframeworkfordrren.pdf).

53. United Nations. 2020. *UN Common Guidance on Helping Build Resilient Societies. Draft*. New York. 64 pp. (also available at https://www.sparkblue.org/basic-page/un-common-guidance-helping-build-resilient-societies)

CHAPTER 4

1. FAO. 2003. *Enhancing Support for Sustainable Rural Livelihoods*. Committee on Agriculture, 17th Session, Rome. (also available at http://www.fao.org/3/Y8349e/Y8349e.htm).

2. United Nations Development Programme & Oxford Poverty and Human Development Initiative. 2020. *Charting pathways out of multidimensional poverty: Achieving the SDGs*. New York. (also available at http://hdr.undp.org/sites/default/files/2020_mpi_report_en.pdf).

3. Kankwamba, H. 2020. *Economic disruptions, markets and food security*. Bonn, Germany, University of Bonn. (Dissertation) (also available at https://bonndoc.ulb.uni-bonn.de/xmlui/handle/20.500.11811/8870).

4. Pradhan, K.C. & Mukherjee, S. 2018. Covariate and idiosyncratic shocks and coping strategies for poor and non-poor rural households in India. *Journal of Quantitative Economics*, 16(1): 101–127.

5. Dercon, S. & Hoddinott, J. 2005. *Livelihoods, growth, and links to market towns in 15 Ethiopian villages*. FCND Discussion Paper 194. Washington, DC, IFPRI. 34 pp.

6. Bhattamishra, R. & Barrett, C.B. 2008. *Community-based risk management arrangements: an overview and implications for social fund programs*. SP Discussion Paper No. 0830. World Bank. (also available at https://documents1.worldbank.org/curated/en/511011468157517454/pdf/463330NWP0Box334086B01PUBLIC10SP00830.pdf).

7. United Nations Development Programme (UNDP). 2014. *Human Development Report 2014: Sustaining human progress: Reducing vulnerabilities and building resilience*. New York. (also available at http://hdr.undp.org/en/content/human-development-report-2014).

8. Devereux, S. 2007. The impact of droughts and floods on food security and policy options to alleviate negative effects. *Agricultural Economics*, 37(s1): 47–58.

9. Notten, G. & Crombrugghe, D. de. 2012. Consumption smoothing in Russia. *Economics of Transition*, 20(3): 481–519. (also available at https://papers.ssrn.com/abstract=2079408).

10. FAO. 2021. *The impact of disasters and crises on agriculture and food security: 2021*. Rome. 211 pp. (also available at http://www.fao.org/documents/card/en/c/cb3673en).

11. Reardon, T. & Zilberman, D. 2021. The economics of food system resilience – conceptual overview and evidence. Background paper for *The State of Food and Agriculture 2021. Making agri-food systems more resilient to shocks and stresses* (unpublished).

12. d'Errico, M., Pinay, J., Luu, A., & Jumbe, E. 2021. *Drivers and stressors of resilience to food insecurity – Evidence from 35 countries*. Background paper for *The State of Food and Agriculture 2021*. FAO Agricultural Development Economics Working Paper 21-09. Rome, FAO.

13. Harmer, A. & Macrae, J., eds. 2004. *Beyond the continuum: The changing role of aid policy in protracted crises*. HPG Research Report No. 18. London, Overseas Development Institute.

14. Debebe, Z.Y. & Raju, D. 2020. *Covariate shocks and child undernutrition: A review of evidence from low- and middle-income countries*. Policy Research Working Paper No. 9273. Washington, DC, World Bank. (also available at https://openknowledge.worldbank.org/handle/10986/33875).

15. Grantham-McGregor, S., Cheung, Y.B., Cueto, S., Glewwe, P., Richter, L. & Strupp, B. 2007. Developmental potential in the first 5 years for children in developing countries. *The Lancet*, 369(9555): 60–70.

16. Alderman, H., Hoddinott, J. & Kinsey, B. 2006. Long term consequences of early childhood malnutrition. *Oxford Economic Papers*, 58(3): 450–474.

17. Meuwissen, M.P.M., Feindt, P.H., Spiegel, A., Termeer, C.J.A.M., Mathijs, E., Mey, Y. de, Finger, R. *et al.* 2019. A framework to assess the resilience of farming systems. *Agricultural Systems*, 176: 102656.

18. Khalil, C.A., Conforti, P. & Gennari, P. 2017. *Defining smallholders to monitor target 2.3. of the 2030 Agenda for Sustainable Development*. FAO Statistics Working Paper Series. Rome, FAO. 43 pp. (also available at http://www.fao.org/publications/card/en/c/e7f3e6f7-59ee-42e7-9cce-36c18af2daea/).

19. Dixon, J., Tanyeri-Abur, A. & Wattenbach, H. 2004. Framework for analysing impacts of globalization on smallholders. In J. Dixon, K. Taniguchi, H. Wattenbach & A. Tanyeri-Arbur, eds. *Smallholders, globalization and policy analysis.* Rome, FAO. (also available at http://www.fao.org/3/y5784e/y5784e02.htm).

20. Brooks, J., Cervantes-Godoy, D. & Jonasson, E. 2009. Strategies for smallholders in developing countries: Commercialisation, diversification and exit. *European Association of Agricultural Economists, 111th Seminar, June 26–27, 2009, Canterbury, UK*. (also available at https://ideas.repec.org/p/ags/eaa111/52867.html).

21. Watson, J.R., Armerin, F., Klinger, D.H. & Belton, B. 2018. Resilience through risk management: cooperative insurance in small-holder aquaculture systems. *Heliyon*, 4(9): e00799 [online]. [Cited 12 July 2021]. https://doi.org/10.1016/j.heliyon.2018.e00799

22. FAO. 2020. *The State of World Fisheries and Aquaculture 2020: Sustainability in action.* Rome. 244 pp. (also available at http://www.fao.org/documents/card/en/c/ca9229en/).

23. Arthur, R., Bondad-Reantaso, M.G., Campbell, M.I., Hewitt, C.I., Phillips, M.J. & Subasinghe, R.P. 2008. *Understanding and applying risk analysis in aquaculture. A manual for decision-makers*. FAO Fisheries and Aquaculture Technical Paper No. 519/1. Rome, FAO. 113 pp. (also available at http://www.fao.org/3/i1136e/i1136e.pdf).

24. Flaten, O., Lien, G. & Tveterås, R. 2011. A comparative study of risk exposure in agriculture and aquaculture. *Acta Agriculturae Scandinavica, Section C — Food Economics*, 8(1): 20–34.

25. Engle, C.R. 2010. Risk analysis in production aquaculture research. In *Aquaculture economics and financing: Management and analysis*, pp. 197–206. John Wiley & Sons, Ltd. (also available at https://onlinelibrary.wiley.com/doi/abs/10.1002/9780813814346.ch16).

26. Karmakar, K. G., Mehta, G.S., Ghosh, S.K. & Selvaraj, P. 2011. *Review of the development of microfinance services for coastal small scale fisheries and aquaculture for South Asia countries (including India, Bangladesh and Sri Lanka) with special attention to women*. FAO, Rome. (also available at http://www.fao.org/apfic/publications/detail/en/c/419583/).

27. Pomeroy, R., Arango, C.A., Lomboy, C.G. & Box, S. 2020. Financial inclusion to build economic resilience in small-scale fisheries. *Marine Policy*, 118: 103982 [online]. [Cited 12 July 2021]. DOI: 10.1016/j.marpol.2020.103982.

28. Darnhofer, I. 2021. Resilience or how do we enable agricultural systems to ride the waves of unexpected change? *Agricultural Systems*, 187: 102997.

29. FAO. 2020. *Impact of COVID-19 on agriculture, food systems and rural livelihoods in Eastern Africa.* Accra, Ghana. 9 pp. (also available at http://www.fao.org/documents/card/en/c/cb0552en).

30. FAO. 2021. *Impact de la crise covid-19 sur les secteurs de la pêche et de l'aquaculture dans les pays du Maghreb.* Tunis, Tunisia. 8 pp. (also available at http://www.fao.org/documents/card/en/c/cb2991fr).

31. FAO. 2020. *Farmers and agribusinesses at risk under COVID-19: What role for blended finance funds?* Rome. 11 pp. (also available at http://www.fao.org/documents/card/en/c/ca9753en).

REFERENCES

32. Hernandez Lagana, M. & Savino, L. 2018. *Climate resilience assessment of small-scale pastoralists and agro-pastoralists in sub-Saharan Africa. An assessment of pastoral and agro-pastoral communities in Angola, Burkina Faso, Burundi, Gambia, Kenya, Mozambique, Niger, Uganda and South Sudan.* Rome, FAO (unpublished).

33. Diogo, V., Reidsma, P., Schaap, B., Andree, B.P.J. & Koomen, E. 2017. Assessing local and regional economic impacts of climatic extremes and feasibility of adaptation measures in Dutch arable farming systems. *Agricultural Systems*, 157: 216–229.

34. Giller, K.E. 2013. Can we define the term 'farming systems'? A question of scale. *Outlook on Agriculture*, 42(3): 149–153.

35. FAO. 2019. *Dimitra Clubs in action. Special Edition of the Dimitra Newsletter.* Rome. 64 pp. (also available at http://www.fao.org/3/i7865en/i7865en.pdf).

36. FAO and International Institute for Sustainable Development (IISD). 2018. *Model agreement for responsible contract farming - with commentary.* Rome, FAO. 68 pp. (also available at http://www.fao.org/3/ca1772en/CA1772EN.pdf).

37. Murekezi, P., Menezes, A. & Ridler, N. 2018. *Contract farming and public–private partnerships in aquaculture: Lessons learned from East African Countries.* FAO and Fisheries Aquaculture Technical Paper 623. Rome, FAO. 57 pp. (also available at http://www.fao.org/3/ca0134en/ca0134en.pdf).

38. Mottet, A., Bicksler, A., Lucantoni, D., De Rosa, F., Scherf, B., Scopel, E., López-Ridaura, S. *et al.* 2020. Assessing transitions to sustainable agricultural and food systems: A Tool for Agroecology Performance Evaluation (TAPE). *Frontiers in Sustainable Food Systems*, 4: 579154 [online]. [Cited 12 July 2021]. https://bit.ly/35TGbTK

39. FAO. 2019. *Tool for Agroecology Performance Evaluation (TAPE) – Test version: Process of development and guidelines for application.* Rome. 94 pp. (also available at http://www.fao.org/documents/card/en/c/ca7407en/).

40. FAO. 2018. *Livestock and agroecology: How they can support the transition towards sustainable food and agriculture.* Rome. 16 pp. (also available at http://www.fao.org/publications/card/en/c/I8926EN/).

41. Institut de recherche et de promotion des alternatives en développement (IRPAD). (forthcoming). Évaluation des performances de l'agroécologie et cartographie des marches territoriaux dans la region de Kayes au Mali. Report of Letter of Agreement in support a the GEF preparation grant. Eds. Goïta M. & Ouattara O. Bamako, Mali, IRPAD.

42. Lucantoni D., Mottet A., Bicksler A., Sy M.R, Veyret-Picot M., Vicovaro, M. & Goïta M. (forthcoming). *Evidence on the multidimensional performance of agroecology in Mali, using the Tool for Agroecology Performance Evaluation – TAPE*. Rome, FAO.

43. FAO. 2018. *The 10 elements of agroecology: Guiding the transition to sustainable food and agricultural systems*. Rome. 15 pp. (also available at http://www.fao.org/documents/card/en/c/I9037EN/).

44. FAO. 2019. The State of the World's Biodiversity for Food and Agriculture 2019. In: *FAO* [online]. Rome. [Cited 17 June 2021]. http://www.fao.org/state-of-biodiversity-for-food-agriculture/en

45. DuVal, A., Mijatovic, D. & Hodgkin, T. 2019. *The contribution of biodiversity for food and agriculture to the resilience of production systems: Thematic Study for The State of the World's Biodiversity for Food and Agriculture*. Rome, FAO. 88 pp. (also available at http://www.fao.org/documents/card/en/c/ca5008en/).

46. FAO. 2018. *Future Smart Food: Rediscovering hidden treasures of neglected and underutilized species for Zero Hunger in Asia* [online]. Rome. [Cited 17 June 2021]. http://www.fao.org/family-farming/detail/en/c/1154249/

47. Li, X., El Solh, M. & Siddique, K., eds. 2019. *Mountain agriculture: Opportunities for harnessing Zero Hunger in Asia*. Bangkok, FAO. 322 pp. (also available at http://www.fao.org/documents/card/en/c/ca5561en/).

48. Capalbo, S.M., Seavert, C., Antle, J.M., Way, J. & Houston, L. 2018. Understanding tradeoffs in the context of farm-scale impacts: An application of decision-support tools for assessing climate smart agriculture. In L. Lipper, N. McCarthy, D. Zilberman, S. Asfaw & G. Branca, eds. *Climate smart agriculture*, pp. 173–197. Natural Resource Management and Policy, vol. 52. Springer International Publishing. (also available at http://link.springer.com/10.1007/978-3-319-61194-5_9).

49. Steenwerth, K.L., Hodson, A.K., Bloom, A.J., Carter, M.R., Cattaneo, A., Chartres, C.J., Hatfield, J.L. *et al.* 2014. Climate-smart agriculture global research agenda: scientific basis for action. *Agriculture and Food Security*, 3(1): 11.

50. Brohm, K.-A. & Klein, S. 2020. The concept of climate smart agriculture – a classification in sustainable theories. *International Journal for Quality Research*, 14: 291–302.

51. Nyasimi, M., Amwata, D., Hove, L., Kinyangi, J. & Wamukoya, G. 2014. *Evidence of impact: Climate-smart agriculture in Africa*. Working Paper No. 86. Copenhagen, CGIAR. (also available at https://cgspace.cgiar.org/bitstream/handle/10568/51374/WP86.pdf).

52. FAO. 2020. *Building resilient farming communities to boost local economies and promote rural employment*. Thirty-fifth Session of FAO Regional Conference for the Near East. (also available at http://www.fao.org/3/nc214en/nc214en.pdf).

53. FAO. 2015. *The State of Food and Agriculture 2015. Social protection and agriculture: breaking the cycle of rural poverty*. Rome. 129 pp. (also available at http://www.fao.org/3/i4910e/I4910E.pdf).

54. Croppenstedt, A., Knowles, M. & Lowder, S.K. 2018. Social protection and agriculture: Introduction to the special issue. *Global Food Security*, 16: 65–68.

55. Dorward, A., Sabates-Wheeler, R., MacAuslan, I., Buckley, C., Kydd, J & Chirwa, E. 2006. *Promoting agriculture for social protection or social protection for agriculture: strategic policy and research issues.* Discussion Paper. Future Agricultures Consortium

56. Gilligan, D.O., Hoddinott, J. & Taffesse, A.S. 2009. The impact of Ethiopia's productive safety net programme and its linkages. *The Journal of Development Studies*, 45(10): 1684–1706.

57. HLPE. 2012. *Social protection for food security.* A report by the High Level Panel of Experts on Food Security and Nutrition of the Committee on World Food Security. Rome, FAO. 96 pp. (also available at http://www.fao.org/fileadmin/user_upload/hlpe/hlpe_documents/HLPE_Reports/HLPE-Report-4-Social_protection_for_food_security-June_2012.pdf).

58. Devereux, S. 2016. Social protection for enhanced food security in sub-Saharan Africa. *Food Policy*, 60: 52–62.

59. Lowder, S.K., Bertini, R. & Croppenstedt, A. 2017. Poverty, social protection and agriculture: Levels and trends in data. *Global Food Security*, 15: 94–107.

60. Mastrorillo, M., Scognamillo, A., Ginet, C., Pietrelli, R., D'Errico, M. & Ignaciuk, A. (forthcoming). *Evaluating the impacts of cash versus food social transfers on agricultural self-reliance capacity in refugee-hosting districts of Uganda*. FAO Agricultural Development Economics Working Paper. Rome, FAO.

61. Sitko, N.J., Scognamillo, A. & Malevolti, G. 2021. Does receiving food aid influence the adoption of climate-adaptive agricultural practices? Evidence from Ethiopia and Malawi. *Food Policy*: 102041 [online]. [Cited 17 July 2021]. https://doi.org/10.1016/j.foodpol.2021.102041.

62. Ignaciuk, A. & Scognamillo, A., Sitko, N. 2021. *Leveraging social protection to advance climate-smart agriculture: evidence from Malawi.* FAO Agricultural Development Economics Working Paper 21-04. FAO Agricultural Development Economics Working Paper 21–04. Rome, FAO. 40 pp. (also available at http://www.fao.org/documents/card/en/c/cb3649en).

63. Ginet, C., Ignaciuk, A., Pietrelli, R., Scognamillo, A. & Mastrorillo, M. (forthcoming). *Building resilience to weather shock through social protection: evidence from the implementation of PSNP public work programme in Ethiopia*. FAO Agricultural Development Economics Working Paper. Rome, FAO.

64. Carrasco Azzini, G. 2020. *Social assistance and productive support policies implementation in rural areas: Are social protection policies designed to reach the rural poor?* Rome, FAO. 50 pp. (also available at http://www.fao.org/documents/card/en/c/cb1541en).

65. Béné, C., Bakker, D., Rodriguez, M.C., Even, B., Melo, J. & Sonneveld, A. 2021. *Impacts of COVID-19 on people's food security: Foundations for a more resilient food system*. Discussion Paper. Montpellier, France, CGIAR. 81 pp. (also available at https://doi.org/10.2499/p15738coll2.134295).

66. Gentilini, U., Almenfi, M., Orton, I. & Dale, P. 2020. *Social protection and jobs responses to COVID-19 : A real-time review of country measures*. Washington, DC, World Bank. (also available at https://openknowledge.worldbank.org/handle/10986/33635).

REFERENCES

67. International Labour Organization (ILO). 2020. *Social protection responses to the COVID-19 pandemic in developing countries: Strengthening resilience by building universal social protection* [online]. Geneva. [Cited 17 June 2021]. http://www.ilo.org/secsoc/information-resources/publications-and-tools/Brochures/WCMS_744612/lang--en/index.htm

68. Tirivayi, N., Knowles, M. & Davis, B. 2016. The interaction between social protection and agriculture: A review of evidence. *Global Food Security*, 10: 52–62. (also available at https://doi.org/10.1016/j.gfs.2016.08.004).

69. Nesbitt-Ahmed, Z. & Pozarny, P., Z. 2021. *Qualitative research on impacts of the Zambia Home Grown School Feeding and Conservation Agriculture Scale Up Programmes*. Rome, FAO. 80 pp. (also available at https://doi.org/10.4060/cb4442en).

70. Béné, C., Devereux, S., & Roelen, K. 2015. Social protection and sustainable natural resource management: initial findings and good practices from small-scale fisheries. In: *FAO* [online]. Rome. [Cited 17 June 2021]. http://www.fao.org/family-farming/detail/en/c/384497/

71. FAO. 2020. *The contribution of social protection to economic inclusion in rural areas*. Rome. 32 pp. (also available at http://www.fao.org/3/cb2458en/CB2458EN.pdf).

CHAPTER 5

1. FAO, IFAD, UNICEF, WFP & WHO. 2021. *The State of Food Security and Nutrition in the World 2021. Transforming food systems for food security, improved nutrition and affordable healthy diets for all*. Rome, FAO. 240 pp. (also available at http://www.fao.org/documents/card/en/c/cb4474en).

2. Brouwer, I.D., McDermott, J. & Ruben, R. 2020. Food systems everywhere: Improving relevance in practice. *Global Food Security*, 26: 100398.

3. Kahiluoto, H. 2020. Food systems for resilient futures. *Food Security*, 12(4): 853–857.

4. Kummu, M., Kinnunen, P., Lehikoinen, E., Porkka, M., Queiroz, C., Röös, E., Troell, M. & Weil, C. 2020. Interplay of trade and food system resilience: Gains on supply diversity over time at the cost of trade independency. *Global Food Security*, 24: 100360.

5. Kahiluoto, H. & Kaseva, J. 2016. No evidence of trade-off between farm efficiency and resilience: Dependence of resource-use efficiency on land-use diversity. *PLoS ONE*, 11(9): e0162736 [online]. [Cited 13 July 2021]. https://doi.org/10.1371/journal.pone.0162736

6. International Maritime Organization (IMO). 2020. IMO urges keyworker exemptions for crew changes and repatriations. In: *IMO* [online]. London. [Cited 12 April 2021]. https://www.imo.org/en/MediaCentre/PressBriefings/Pages/09-seafarers-COVID19.aspx

7. Pape, M. 2020. *EU shipping and ports facing coronavirus*. At a Glance. European Parliamentary Research Service. European Union. (also available at https://www.europarl.europa.eu/RegData/etudes/ATAG/2020/651907/EPRS_ATA(2020)651907_EN.pdf).

8. Fan, S., Teng, P., Chew, P., Smith, G. & Copeland, L. 2021. Food system resilience and COVID-19 – Lessons from the Asian experience. *Global Food Security*, 28: 100501.

9. Wilcox, B.A. & Colwell, R.R. 2005. Emerging and reemerging infectious diseases: Biocomplexity as an interdisciplinary paradigm. *EcoHealth*, 2(4): 244.

10. Liu, Q., Xu, W., Lu, S., Jiang, J., Zhou, J. Shao, Z., Liu, X. *et al.* 2018. Landscape of emerging and re-emerging infectious diseases in China: impact of ecology, climate, and behavior. *Frontiers of Medicine*, 12(1): 3–22. (also available at https://doi.org/10.1007/s11684-017-0605-9).

11. Weiss, R.A. & McMichael, A.J. 2004. Social and environmental risk factors in the emergence of infectious diseases. *Nature Medicine*, 10(12): S70–S76.

12. Taylor, L.H., Latham, S.M. & Woolhouse, M.E. 2001. Risk factors for human disease emergence. *Philosophical Transactions of the Royal Society of London B Biological Sciences*, 356(1411): 983–989.

13. Orden, D. 2020. Resilience test of the North American food system. *Canadian Journal of Agricultural Economics*, 68(2): 215–217.

14. WHO. 2017. One Health. In: *WHO* [online]. Geneva. [Cited 13 July 2021]. https://www.who.int/news-room/q-a-detail/one-health

15. FAO. 2020. *One Health legislation: Contributing to pandemic prevention through law*. Rome. 10 pp. (also available at https://doi.org/10.4060/ca9729en).

16. FAO. 2020. *Cities and local governments at the forefront in building inclusive and resilient food systems: Key results from the FAO survey "Urban Food Systems and COVID-19"*. Policy Brief. Rome. 16 pp. (also available at http://www.fao.org/3/cb0407en/CB0407EN.pdf).

17. Marusak, A., Sadeghiamirshahidi, N., Krejci, C.C., Mittal, A., Beckwith, S., Cantu, J., Morris, M. & Grimm, J. 2021. Resilient regional food supply chains and rethinking the way forward: Key takeaways from the COVID-19 pandemic. *Agricultural Systems*, 190: 103101.

18. Brunori, G. & Galli, F., eds. 2013. *Short food supply chains as drivers of sustainable development. Evidence Document*. Document developed in the framework of the FP7 project Foodlinks. Laboratorio di studi rurali Sismondi. (also available at https://orgprints.org/id/eprint/28858/1/evidence-document-sfsc-cop.pdf).

19. Ackerman, K., Conard, M., Culligan, P., Plunz, R., Sutto, M.-P. & Whittinghill, L. 2014. Sustainable food systems for future cities: The potential of urban agriculture. *The Economic and Social Review*, 45(2): 189–206. (also available at https://www.esr.ie/article/view/136).

20. Tzachor, A., Richards, C.E. & Holt, L. 2021. Future foods for risk-resilient diets. *Nature Food*, 2(5): 1–4.

21. Meuwissen, M.P.M., Feindt, P.H., Spiegel, A., Termeer, C.J.A.M., Mathijs, E., Mey, Y. de, Finger, R. *et al.* 2019. A framework to assess the resilience of farming systems. *Agricultural Systems*, 176: 102656.

22. Giller, K.E., Hijbeek, R., Andersson, J.A. & Sumberg, J. 2021. Regenerative agriculture: An agronomic perspective. *Outlook on Agriculture*, 50(1): 13–25 [online]. [Cited 13 July 2021]. https://doi.org/10.1177/0030727021998063

23. Alvar-Beltrán, J., Elbaroudi, I., Gialletti, A., Heureux, A., Neretin, L. & Soldan, R. 2021. *Climate resilient practices: Typology and guiding material for climate risk screening*. Rome, FAO. 30 pp. (also available at http://www.fao.org/3/cb3991en/cb3991en.pdf).

24. Bioversity International. 2017. *Mainstreaming agrobiodiversity in sustainable food systems: Scientific foundations for an agrobiodiversity index*. Rome. 157 pp. (also available at https://www.bioversityinternational.org/fileadmin/user_upload/online_library/Mainstreaming_Agrobiodiversity/Mainstreaming_Agrobiodiversity_Sustainable_Food_Systems_WEB.pdf).

25. FAO, World Organisation for Animal Health (OIE) & WHO. 2019. *Taking a multisectoral, One Health approach: A tripartite guide to addressing zoonotic diseases in countries*. Rome, FAO, Paris, OIE and Geneva, WHO. 151 pp. (also available at http://www.fao.org/3/ca2942en/ca2942en.pdf).

26. FAO. 2019. *Disaster risk reduction at farm level: Multiple benefits, no regrets: Results from cost–benefit analyses conducted in a multi-country study, 2016–2018*. Rome. 160 pp. (also available at http://www.fao.org/publications/card/en/c/CA4429EN/).

27. Han, Y., Chong, W.K. & Li, D. 2020. A systematic literature review of the capabilities and performance metrics of supply chain resilience. *International Journal of Production Research*, 58(15): 4541–4566 [online]. [Cited 13 July 2021]. https://doi.org/10.1080/00207543.2020.1785034

28. World Bank. 2017. *ICT in agriculture: Connecting smallholders to knowledge, networks, and institutions*. Washington, DC, World Bank. (also available at https://openknowledge.worldbank.org/handle/10986/27526).

29. Blay-Palmer, A., Santini, G., Halliday, J., Malec, R., Carey, J., Keller, L., Ni, J., Taguchi, M. & van Veenhuizen, R. 2021. City region food systems: Building resilience to COVID-19 and other shocks. *Sustainability*, 13(3): 1325.

30. FAO, IFAD, UNICEF, WFP & WHO. 2018. *The State of Food Security and Nutrition in the World 2018. Building climate resilience for food security and nutrition*. Rome. 183 pp. (also available at http://www.fao.org/3/i9553en/i9553en.pdf).

31. FAO. 2017. *Averting risks to the food chain: A compendium of proven emergency prevention methods and tools*. Rome. 103 pp. (also available at http://www.fao.org/3/i6538e/i6538e.pdf).

REFERENCES

32. FAO. 2019. *UN Climate Resilience – A2R study on 'Tracking progress on climate resilience for agriculture and food systems at national, subnational and local levels'*. Rome. UN Climate Resilience Initiative A2R. 5 pp. (also available at https://static1.squarespace.com/static/5651e0a2e4b0d031533efa3b/t/5dee29d1ce1e084cec9b590e/1575889365403/Summary+of+the+A2R+study+for+DC+days_+final.pdf).

33. FAO. 2021. *The impact of disasters and crises on agriculture and food security: 2021*. Rome. 211 pp. (also available at http://www.fao.org/documents/card/en/c/cb3673en).

34. United Nations. 2016. Report of the open-ended intergovernmental expert working group on indicators and terminology relating to disaster risk reduction. New York. 41 pp. (also available at https://www.undrr.org/publication/report-open-ended-intergovernmental-expert-working-group-indicators-and-terminology).

35. FAO. 2019. Policy support and governance gateway. In: *FAO* [online]. Rome. [Cited 13 July 2021]. http://www.fao.org/policy-support/governance/en/

36. Halloran, A., Wood, A. & Sellberg, M. 2020. *What can the COVID-19 pandemic teach us about resilient Nordic food systems?* [online]. Nordic Council of Ministers. [Cited 13 July 2021]. https://pub.norden.org/nord2020-038

37. FAO. 2021. City region food systems programme: Reinforcing rural–urban linkages for resilient food systems. In: *FAO* [online]. Rome. [Cited 13 July 2021]. http://www.fao.org/in-action/food-for-cities-programme/overview/crfs/en/

38. Lyson, T.A., Stevenson, G.W. & Welsh, R., eds. 2008. *Food and the mid-level farm: Renewing an agriculture of the middle* [online]. The MIT Press. [Cited 13 July 2021]. https://direct.mit.edu/books/book/4212/Food-and-the-Mid-Level-FarmRenewing-an-Agriculture

39. Gebresenbet, G. & Bosona, T. 2012. Logistics and supply chains in agriculture and food. *In* A. Groznik & Y. Xiong, eds. *Pathways to supply chain excellence*, pp. 125–146. (also available at https://www.intechopen.com/books/pathways-to-supply-chain-excellence/logistics-chains-in-food-and-agriculture-sector).

40. Hobbs, J.E. 2020. Food supply chains during the COVID-19 pandemic. *Canadian Journal of Agricultural Economics*, 68(2): 171–176.

41. Shuvaeva, O. & Belova, E. *2019. Contribution of the social protection to reducing poverty and ensuring food security in Kyrgyz Republic. Analysis of cost and benefits, effectiveness of investment in nutrition-sensitive social protection. FAO's pilot programs in Kyrgyzstan* (unpublished).

42. Arslan, A., McCarthy, N., Lipper, L., Asfaw, S., Cattaneo, A. & Kokwe, M. 2015. Climate smart agriculture? Assessing the adaptation implications in Zambia. *Journal of Agricultural Economics*, 66(3): 753–780.

43. Asfaw, S., McCarthy, N., Lipper, L., Arslan, A. & Cattaneo, A. 2016. What determines farmers' adaptive capacity? Empirical evidence from Malawi. *Food Security*, 8(3): 643–664.

44. Mäkinen, H., Kaseva, J., Virkajärvi, P. & Kahiluoto, H. 2015. Managing resilience of forage crops to climate change through response diversity. *Field Crops Research*, 183: 23–30.

45. Notten, G. & Crombrugghe, D. de. 2012. Consumption smoothing in Russia. *Economics of Transition*, 20(3): 481–519. (also available at https://papers.ssrn.com/abstract=2079408).

46. FAO. 2015. *The State of Food and Agriculture 2015. Social protection and agriculture: breaking the cycle of rural poverty.* Rome. 129 pp. (also available at http://www.fao.org/3/i4910e/i4910e.pdf).

47. Carrasco Azzini, G. 2020. *Social assistance and productive support policies implementation in rural areas: Are social protection policies designed to reach the rural poor?* Rome, FAO. 50 pp. (also available at http://www.fao.org/documents/card/en/c/cb1541en).

48. FAO & Red Cross Red Crescent Climate Centre. 2019. *Managing climate risks through social protection – Reducing rural poverty and building resilient agricultural livelihoods*. Rome, FAO. (also available at http://www.fao.org/3/ca6681en/CA6681EN.pdf).

49. Hertel, T., Elouafi, I., Ewert, F. & Tanticharoen, M. 2021. *Building resilience to vulnerabilities, shocks and stresses – Action Track 5*. United Nations Food Systems Summit 2021 Scientific Group. 20 pp. (also available at https://www.un.org/sites/un2.un.org/files/5-action_track-5_scientific_group_draft_paper_8-3-2021.pdf).

50. Tirivayi, N., Knowles, M. & Davis, B. 2016. The interaction between social protection and agriculture: A review of evidence. *Global Food Security*, 10: 52–62. (also available at https://doi.org/10.1016/j.gfs.2016.08.004).

51. Miralles-Wilhelm, F. 2021. *Nature-based solutions in agriculture: Sustainable management and conservation of land, water and biodiversity*. Virginia, USA, FAO and The Nature Conservancy. 68 pp. (also available at http://www.fao.org/documents/card/en/c/cb3140en).

52. International Union for Conservation of Nature (IUCN). 2021. Nature-based solutions. In: *Commission on Ecosystem Management* [online]. [Cited 16 April 2021]. https://www.iucn.org/commissions/commission-ecosystem-management/our-work/nature-based-solutions

53. FAO. 2020. *The State of Food and Agriculture 2020: Overcoming water challenges in agriculture*. Rome. 178 pp. (also available at http://www.fao.org/documents/card/en/c/cb1447en/).

54. Hallstein, E. & Iseman, T. 2021. *Nature-based solutions in agriculture: Project design for securing investment*. Virginia, USA, FAO and The Nature Conservancy. 67 pp. (also available at http://www.fao.org/3/cb3144en/cb3144en.pdf).

55. Iseman, T. & Miralles-Wilhelm, F. 2021. *Nature-based solutions in agriculture: The case and pathway for adoption*. Virginia, USA, FAO and The Nature Conservancy. 52 pp. (also available at http://www.fao.org/3/cb3141en/cb3141en.pdf).

56. Cutter, S.L., Barnes, L., Berry, M., Burton, C., Evans, E., Tate, E. & Webb, J. 2008. A place-based model for understanding community resilience to natural disasters. *Global Environmental Change*, 18(4): 598–606.

57. FAO. 2021. One Health. In: *FAO* [online]. Rome [Cited 10 March 2021]. http://www.fao.org/one-health/en/

58. Sánchez, M.V., Cicowiez, M. & Ortega, A. 2021. *Inversión pública productiva en la agricultura para la recuperación económica con bienestar rural: un análisis de escenarios prospectivos para México*. Economía del desarrollo agrícola de la FAO – Estudio técnico 11. Rome, FAO. 92 pp. (also available at http://www.fao.org/3/cb4562es/cb4562es.pdf)

59. Sadiddin, A. 2013. An assessment of policy impact on agricultural water use in the northeast of Syria. *Environmental Management and Sustainable Development*, 2(2): 2164–7682.

60. Ababsa, M. 2013. Crise agraire, crise foncière et sécheresse en Syrie (2000–2011). *Maghreb - Machrek*, 215(1): 101–122.

61. Office for the Coordination of Humanitarian Affairs (UNOCHA). 2010. *Syria drought response plan 2009–2010. Mid-term review*. New York. (also available at https://reliefweb.int/report/syrian-arab-republic/syria-drought-response-plan-2009-2010-mid-term-review).

62. Weinthal, E., Zawahri, N. & Sowers, J. 2015. Securitizing water, climate, and migration in Israel, Jordan, and Syria. *International Environmental Agreements: Politics, Law and Economics*, 15(3): 293–307.

63. Organisation for Economic Co-operation and Development (OECD). 2020. *Strengthening agricultural resilience in the face of multiple risks*. Paris. 144 pp. (also available at https://www.oecd-ilibrary.org/agriculture-and-food/strengthening-agricultural-resilience-in-the-face-of-multiple-risks_2250453e-en).

ANNEX 1

1. Shannon, C.E. 1948. A mathematical theory of communication. *Bell System Technical Journal*, 27(3): 379–423.

2. FAO. 2021. FAOSTAT. In: *FAO* [online]. Rome [Cited 12 July 2021]. http://faostat.fao.org

3. Agricultural Market Information System. 2021. *Supply and Demand Balance* [online]. [Cited 1 July 2021]. http://statistics.amis-outlook.org/data/index.html#DOWNLOAD_STANDARD

4. FAO. 2021. *GIEWS – Global Information and Early Warning System on Food and Agriculture* [online]. Rome. [Cited 12 July 2021]. http://www.fao.org/giews/data-tools/en/

5. United States Department of Agriculture (USDA). 2021. *Production, Supply and Distribution* [online]. Washington, DC. [Cited 1 June 2021]. https://apps.fas.usda.gov/psdonline/app/index.html#/app/home

6. FAO, IFAD, UNICEF, WFP & WHO. 2021. *The State of Food Security and Nutrition in the World 2021. Transforming food systems for food security, improved nutrition and affordable*

REFERENCES

healthy diets for all. Rome, FAO. 240 pp. (also available at http://www.fao.org/documents/card/en/c/cb4474en).

7. FAO, IFAD, UNICEF, WFP & WHO. 2020. *The State of Food Security and Nutrition in the World 2020. Transforming food systems for affordable healthy diets*. Rome, FAO. 320 pp. (also available at https://doi.org/10.4060/ca9692en).

8. World Bank. 2021. PovcalNet: an online analysis tool for global poverty monitoring. In: *World Bank* [online]. Washington, DC. [Cited 12 July 2021]. http://iresearch.worldbank.org/PovcalNet/

9. INDDEX Project. 2021. Data4Diets: building blocks for diet-related food security analysis. In: *International Dietary Data Expansion Project* [online]. [Cited 12 July 2021]. https://inddex.nutrition.tufts.edu/data4diets

10. Smith, L.C. & Subandoro, A. 2007. *Measuring food security using household expenditure surveys*. Washington, DC, IFPRI. (also available at https://ebrary.ifpri.org/digital/collection/p15738coll2/id/125275).

11. Lele, U., Masters, W.A., Kinabo, J., Meenakshi, J.V., Ramaswami, B., Tagwireyi, J., Bell, W.F.L. & Goswami, S. 2016. *Measuring food and nutrition security: An independent technical assessment and user's guide for existing indicators*. Measuring Food and Nutrition Security Technical Working Group. Rome, WFP. (also available at https://reliefweb.int/sites/reliefweb.int/files/resources/1_FSIN-TWG_UsersGuide_12June2016.compressed.pdf).

12. Moltedo, A., Troubat, N., Lokshin, M. & Sajaia, Z. 2014. *Analyzing food security using household survey data*. Washington, DC, World Bank. (also available at https://openknowledge.worldbank.org/bitstream/handle/10986/18091/9781464801334.pdf;sequence=1).

13. World Bank. 2021. *World Development Indicators: Population, total* [online]. Washington, DC. [Cited 1 June 2021]. https://data.worldbank.org/indicator/SP.POP.TOTL

14. Nelson, A., de By, R., Thomas, T., Girgin, S., Brussel, M., Venus, V. & Ohuru, R. (forthcoming). *The resilience of domestic transport networks in the context of food security – a multi-country analysis*. Background paper for *The State of Food and Agriculture 2021*. FAO Agricultural Development Economics Technical Study No. 14. Rome, FAO.

THE STATE OF THE WORLD

2021

THE STATE OF FOOD AND AGRICULTURE

MAKING AGRIFOOD SYSTEMS MORE RESILIENT TO SHOCKS AND STRESSES

The COVID-19 pandemic exposed the vulnerability of agrifood systems to shocks and stresses and led to increased global food insecurity and malnutrition. Action is needed to make agrifood systems more resilient, efficient, sustainable and inclusive.

The State of Food and Agriculture 2021 presents country-level indicators of the resilience of agrifood systems. The indicators measure the robustness of primary production and food availability, as well as physical and economic access to food. They can thus help assess the capacity of national agrifood systems to absorb shocks and stresses, a key aspect of resilience.

The report analyses the vulnerabilities of food supply chains and how rural households cope with risks and shocks. It discusses options to minimize trade-offs that building resilience may have with efficiency and inclusivity. The aim is to offer guidance on policies to enhance food supply chain resilience, support livelihoods in the agrifood system and, in the face of disruption, ensure sustainable access to sufficient, safe and nutritious food to all.

ISBN 978-92-5-134329-6 ISSN 0081-4539

9 789251 343296

CB4476EN/1/11.21

remote sensing

MDPI

Article

Deep ResU-Net Convolutional Neural Networks Segmentation for Smallholder Paddy Rice Mapping Using Sentinel 1 SA R and Sentinel 2 Optical Imagery

Alex Okiemute Onojeghuo [1,*], Yuxin Miao [2] and George Alan Blackburn [3]

[1] Research and Development Unit, Jolexy Environmental Services Ltd., Edmonton, AB T5T7L1, Canada
[2] Precision Agriculture Center, Department of Soil, Water and Climate, University of Minnesota, 1991 Upper Buford Circle, Saint Paul, MN 55108, USA
[3] Lancaster Environment Centre, Library Avenue, Bailrigg, Lancaster LA1 4YQ, UK
* Correspondence: alex.onojeghuo@jolexyenviro.com or alex.onojeghuo@gmail.com

Abstract: Rice is a globally significant staple food crop. Therefore, it is crucial to have adequate tools for monitoring changes in the extent of rice paddy cultivation. Such a system would require a sustainable and operational workflow that employs open-source medium to high spatial and temporal resolution satellite imagery and efficient classification techniques. This study used similar phenological data from Sentinel-2 (S2) optical and Sentinel-1 (S1) Synthetic Aperture Radar (SAR) satellite imagery to identify paddy rice distribution with deep learning (DL) techniques. Using Google Earth Engine (GEE) and U-Net Convolutional Neural Networks (CNN) segmentation, a workflow that accurately delineates smallholder paddy rice fields using multi-temporal S1 SAR and S2 optical imagery was investigated. The study's accuracy assessment results showed that the optimal dataset for paddy rice mapping was a fusion of S2 multispectral bands (visible and near infra-red (VNIR), red edge (RE) and short-wave infrared (SWIR)), and S1-SAR dual polarization bands (VH and VV) captured within the crop growing season (i.e., vegetative, reproductive, and ripening). Compared to the random forest (RF) classification, the DL model (i.e., ResU-Net) had an overall accuracy of 94% (three percent higher than the RF prediction). The ResU-Net paddy rice prediction had an F1-Score of 0.92 compared to 0.84 for the RF classification generated using 500 trees in the model. Using the optimal U-Net classified paddy rice maps for the dates analyzed (i.e., 2016–2020), a change detection analysis over two epochs (2016 to 2018 and 2018 to 2020) provided a better understanding of the spatial–temporal dynamics of paddy rice agriculture in the study area. The results indicated that 377,895 and 8551 hectares of paddy rice fields were converted to other land-use over the first (2016–2018) and second (2018–2020) epochs. These statistics provided valuable insight into the paddy rice field distribution changes across the selected districts analyzed. The proposed DL framework has the potential to be upscaled and transferred to other regions. The results indicated that the approach could accurately identify paddy rice fields locally, improve decision making, and support food security in the region.

Keywords: Sentinel-1 and 2; random forest; U-Net; Google Earth Engine; rice paddy; change detection

check for updates

Citation: Onojeghuo, A.O.; Miao, Y.; Blackburn, G.A. Deep ResU-Net Convolutional Neural Networks Segmentation for Smallholder Paddy Rice Mapping Using Sentinel 1 SAR and Sentinel 2 Optical Imagery. *Remote Sens.* **2023**, *15*, 1517. https://doi.org/10.3390/rs15061517

Academic Editor: Bingfang Wu

Received: 21 February 2023
Revised: 7 March 2023
Accepted: 8 March 2023
Published: 9 March 2023

Copyright: © 2023 by the authors. Licensee MDPI, Basel, Switzerland. This article is an open access article distributed under the terms and conditions of the Creative Commons Attribution (CC BY) license (https://creativecommons.org/licenses/by/4.0/).

1. Introduction

On a global scale, over 12% of the world's cropland area is assigned to rice agriculture, with South and East Asia being the two central regions for paddy rice production [1]. Paddy rice production accounted for over 212 million metric tons in 2020, making China a significant player in providing a third of the total global paddy rice production [1,2]. A system that adequately monitors paddy rice fields is crucial, providing a staple grain supply to 7.5 billion people globally [3]. Effective monitoring of rice intensification is essential to addressing food security and socioeconomic and sustainable development concerns [4].

It provides valuable information for policy and decision-makers handling critical issues such as food production, climate change mitigation and adaptation, and water and health security.

Advances in remote sensing technology offer the scientific community and stakeholders in the agricultural sector an effective tool for monitoring and mapping the spatial extent of agricultural landscapes. In addition, remote sensing offers smallholder farmers valuable statistics for decision-making and planning, such as crop growth cycles and yield forecasting [5–7]. Smallholder farming areas are typically characterized by small-size plots (usually less than 2 hectares) and heterogeneous with unclear field patterns. This pattern of farming provides over 70% of China's food production [8]. Considering the small sizes of paddy rice fields, utilizing a Moderate Resolution Imaging Spectroradiometer (250 m) would prove ineffective for accurate cropland mapping due to its coarse spatial resolution. However, European Space Agency (ESA) medium to high-spatial-resolution satellite data like Sentinel-1 (S1) Synthetic Aperture Radar (SAR) and Sentinel-2 (S2) optical sensors with 10 m spatial resolution have immense potential for agricultural mapping and diverse applications [9,10]. The Google Earth Engine (GEE) cloud-computing platform offers massive computing power for geospatial analysis on a planetary scale [11] and has vast applications such as landcover mapping and monitoring [12], mapping of paddy rice fields [4,13], and other environmental applications requiring multi-temporal remote sensing data inputs [13–17]. For effective paddy rice field mapping, identifying earth observation (EO) data acquired during the rice crop growth cycle (i.e., vegetative, reproductive and ripening stages) is critical. By adopting a phenological approach, end-users can identify important cyclic and seasonal growing patterns unique to the rice crop and incorporate this valuable information in the mapping process. These phenological characteristics facilitate the accurate mapping of rice paddy fields. The backscatter coefficient values of S1 SAR data change under varying paddy rice stage conditions, making it suitable for tracking the growth stages of paddy rice crops [18,19]. The three distinct paddy rice growing stages (i.e., vegetative, reproductive, and ripening) can serve as valuable input for remote sensing analysis and accurate delineation of paddy rice fields.

The use of optical-derived indices such as the Enhanced Vegetation Index (EVI) [20,21], the Land Surface Water Index (LSWI) [22], and the Normalized Difference Vegetation Index (NDVI) [23], have been explored to extract phenological information as inputs for mapping accurately the spatial extent of rice fields with a combination of field observations [24,25]. Reference [25] explored the use of optical-derived indices to map paddy rice fields using the MODIS sensor onboard the National Aeronautics and Space Administration's (NASA) Earth observation satellite (EOS) Terra satellite MODIS sensor. The vegetation indices explored were EVI, LSWI, and NDVI, respectively. The authors explored time-series indices to identify rice crop growth stages (flooding and transplanting) by identifying the sensitivity of LSWI to surface moisture increase during its phenological stages. Though a logical approach, the limitation of the study was the coarse resolution of the MODIS imagery used for the analysis. The research community and operators can utilize this information for paddy rice field mapping with access to medium and fine-resolution satellite data (like Sentinel and Landsat sensor imagery) through cloud-based platforms such as GEE. Recent studies have demonstrated that Landsat or Sentinel optical sensor-derived indices (such as LSWI, NDVI, and EVI) are effective proxies for discriminating flooding or transplanting signals of paddy rice fields [4,26]. Studies have demonstrated the value of these optically-derived indices in discriminating flooding/transplanting signals [25,26].

Traditional classifiers, such as the Maximum Likelihood Classifier or shallow machine learning classifiers (e.g., Random Forest (RF), Support Vector Machine (SVM), etc.), have become standard algorithms for mapping agricultural fields [19,27]. However, due to technological advances and the availability of high-performance computing machines, Deep Learning (DL) remote sensing applications are gaining ground quickly [9,10,28]. In the study by [10], the authors demonstrated the potential of combining deep learning models and phenological-driven training data and imagery for rice paddy distribution

mapping in the northeastern parts of China. Combining knowledge-based proxies derived from phenological information through combining a suite of vegetation and water indices (such as NDVI and NDWI), the authors could distinguish paddy rice fields from other land cover classes. Other indices explored were EVI and LSWI, all of which served as inputs to generating rice paddy maps subsequently used to generate training data needed in the DL modeling. The DL model, Long Short-Term Memory [29], was used in the study. By exploring Sentinel-2 (S2) optical satellite imagery acquired over the paddy rice crop cycle (i.e., May to October), the authors were able to extract valuable phenological input in the classification process.

Similarly, [30] explored S2 imagery in GEE to map paddy rice fields accurately using an enhanced pixel-based phenological approach. Phenological data were obtained by combining a time series of several indices generated from S2 time acquired during the transplanting, growth and maturity periods of the paddy rice crops [30]. The phenological features used were Plant Senescence Reflectance Index (PSRI), Bare Soil Index (BSI), LSWI, and NDVI. Unlike the previous approach of DL modelling, a one-class classifier approach was adopted in the study. However, both studies illustrate the benefits of phenological information in paddy rice mapping on both small and large scales. A similar approach was developed using a full-resolution DL model for paddy rice mapping with Landsat data for parts of northeastern China [31].

Studies have also explored using SAR time-series data (such as S1) and DL models to map paddy rice fields [9]. Reference [9] proposed using multi-temporal S1 SAR imagery to address intra-class variability resulting from diverse management practices. A modified U-Net model was used for the DL modelling to identify paddy rice fields across Thailand. Studies have explored combining SAR and optical data for paddy rice mapping with shallow ML and DL models [19,28,32]. The existing literature shows that phenological information primarily derived from EO data (such as SAR and optical imagery) further analyzed using DL or non-DL models provides accurate paddy rice map products. However, limited information answers questions about paddy rice mapping in DL modelling.

This study evaluates several singular and multisensor approaches for paddy rice field mapping using a deep residual U-Net (ResU-Net) CNN model. By utilizing GEE and the ResU-Net DL models, this study proposes a workflow that accurately delineates smallholder paddy rice fields using multi-temporal S1 SAR and S2 optical imagery acquired during the crop growth cycle (vegetative, reproductive, and ripening stages). In addition to evaluating DL modelling, this study explored the RF classifier. This study addressed four research questions (RQ). The four RQs (RQ1, RQ2, RQ3, and RQ4) addressed in this study were:

1. Which combination is optimal for paddy rice mapping using GEE-sourced multi-temporal S1 SAR and S2 optical derivatives as inputs in a U-Net DL model?
2. How does the optimal image composite identified in RQ1 compare with RF experiments performed under different model parameters?
3. Based on RQs 1 and 2, what are the implications of these outcomes in building a transferable and operational workflow? The transferability of the optimal model identified in RQs 1 and 2 was tested by upscaling (covering five districts in the southeastern parts of Heilongjiang province) over different years (i.e., 2016, 2018, and 2020).
4. Based on the outcomes of RQ3, a spatial-temporal analysis of paddy rice agriculture between 2016 and 2020 was performed to quantify and better understand the dynamics and challenges associated with paddy rice mapping in the study area.

2. Materials and Methods

2.1. Study Site

The study site is in the southeastern Heilongjiang province and covers five districts: Xiangyang, Qianjin, Jianshan, Taoshan, and Jiguan in Northeast China (Figure 1). The region is characterized by a sub-humid continental monsoon climate with warm summers

and cold winters [33], an annual mean temperature of 2 °C, and annual mean precipitation of 550 mm [34]. Heilongjiang is popularly known as a paddy rice agriculture hub in the region. Other prominent croplands in the study area are soybean, corn, and wheat [35].

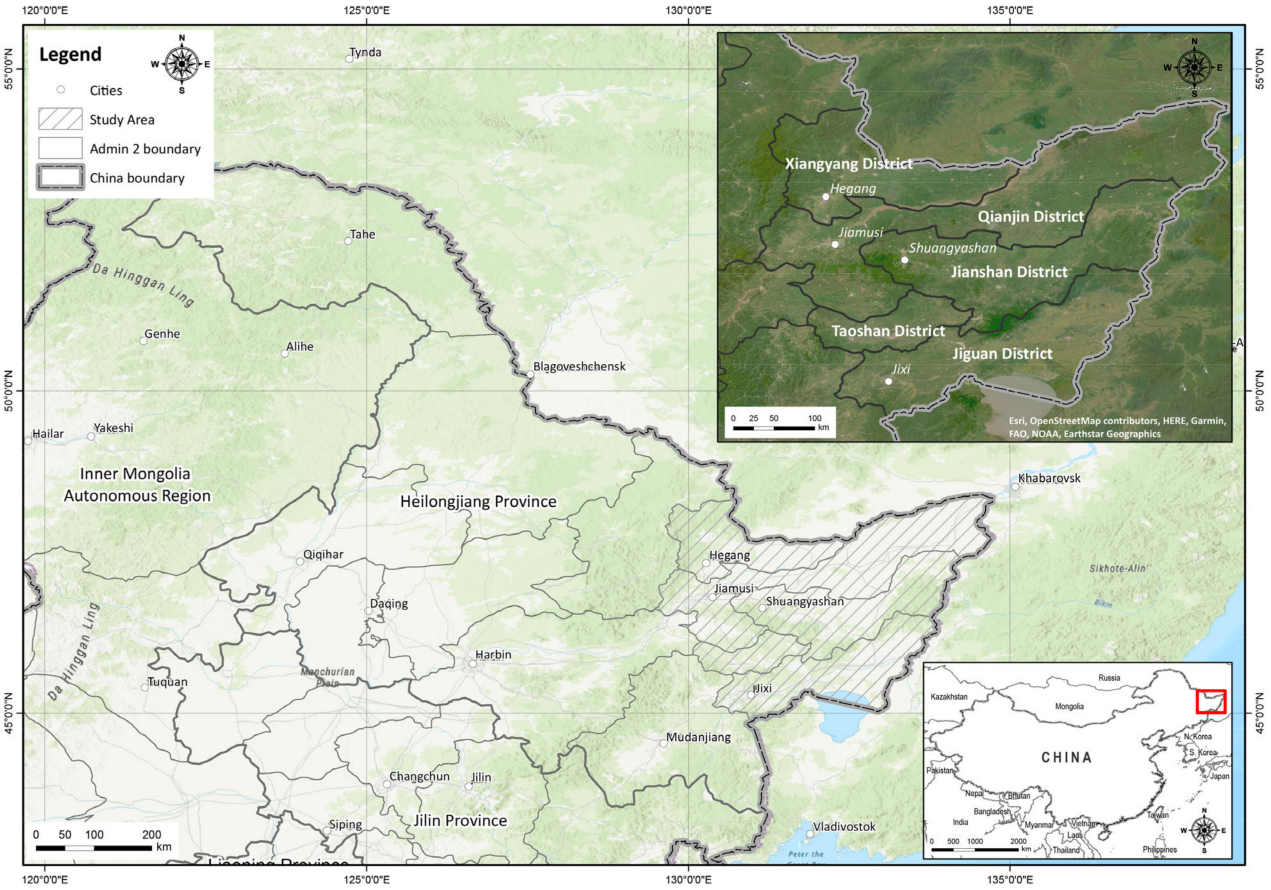


Figure 1. Study area map showing the Xiangyang, Qianjin, Jianshan, Taoshan, and Jiguan Districts in the southeastern Heilongjiang Province of China.

Paddy rice fields in the study area are cultivated yearly and have a growth cycle of 140 to 150 days (between April and October) [13,36]. Previous studies have outlined the different paddy rice fields for the study site [5,19,24,36].

2.2. Description of the Overall Methodology

Figure 2 shows the workflow for paddy rice mapping proposed in this study. As shown in the proposed workflow, the methodology consists of three main stages, (a) data preparation, (b) segmentation and classification, and (c) performance assessment. The final output of this workflow was an optimal paddy rice prediction based on the performance evaluation of the RF and U-Net models. Using the most effective of the evaluated shallow learning and DL models, we generated three upscaled paddy rice maps covering five districts in the Heilongjiang Province of China. The final component of the methodology employed in this study was (d) upscaling of the identified optimal model and change detection analysis. This section of the paper discusses the four work components presented above.

2.2.1. Data Preparation

The satellite imagery employed in this study was multi-temporal S1 SAR and S2 optical data (as described in Section 2.3) downloaded from the GEE platform. The pre-processed satellite images used in the study were acquired during the rice crop growing season (i.e., vegetative, reproductive, and ripening). The optical and SAR-derived inputs

contained valuable phenological information for identifying important cyclic and seasonal growing patterns unique to rice crops. The phenologically driven approach was a vital component of this approach to paddy rice mapping.

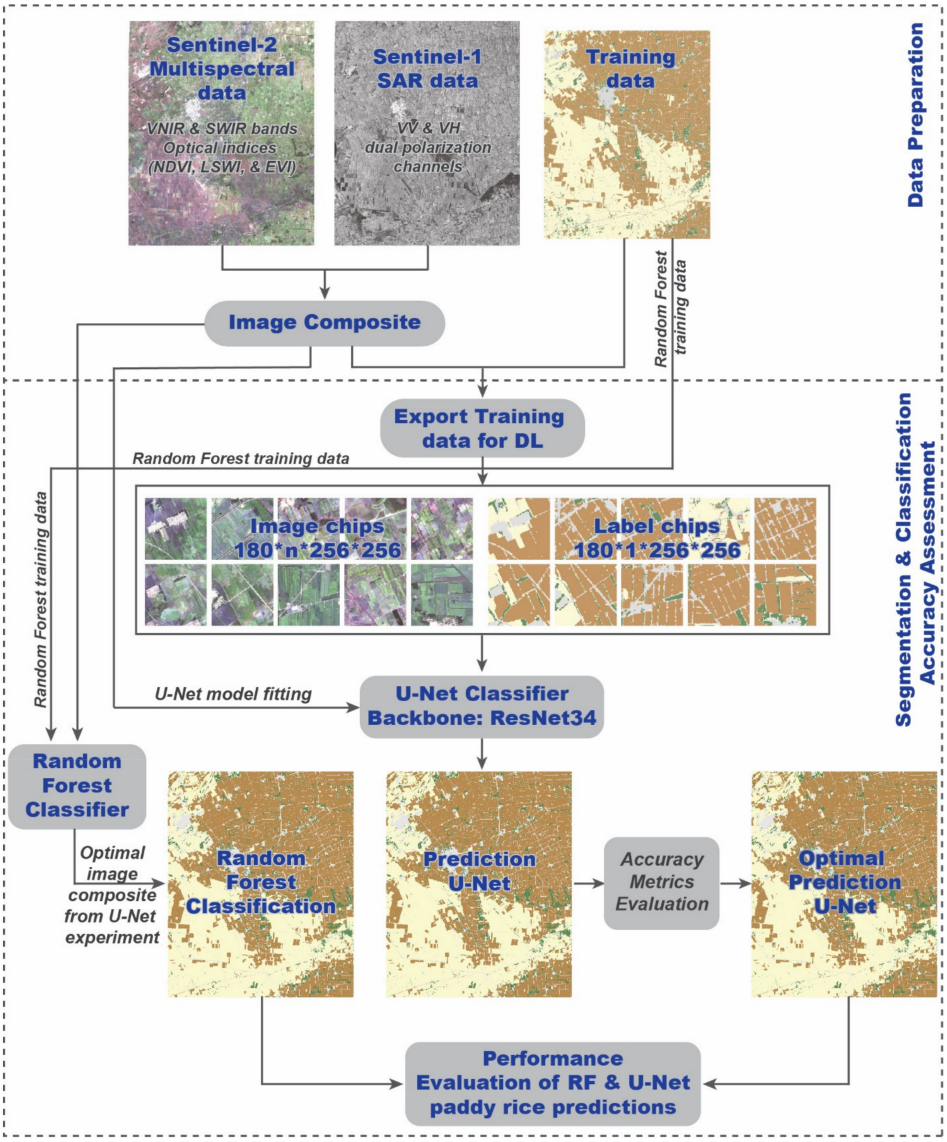


Figure 2. Proposed workflow for paddy rice mapping adapted in this study. The image chip dimensions were 256 × 256 pixels (n = the number of bands of input image composites used for deep learning experiments).

2.2.2. Segmentation and Classification

Several S1 SAR and S2 optical image combinations were used as inputs in a shallow ML model (RF) and a DL model (i.e., ResU-Net). The first step of this component (RQ1) was to determine the optimal image composite using several inputs of GEE-sourced multi-temporal S1 SAR and S2 optical derivatives in a U-Net DL model. Section 2.3.3 describes the image composites evaluated in this component of the study. Details of the U-Net segmentation and the model parameters evaluated are presented in Section 2.3.5. The workflow diagram (Figure 2) presents the components associated with the U-Net modelling (such as exporting the training data for DL and the model fitting backbone–ResNet 34). The second part of the segmentation and classification workflow component was comparing the performance of the RF and U-Net models on the optimal image composite identified in RQ1. The optimal image composite identified from the U-Net experiments was further evaluated

using the RF classifier under different model parameters. Section 2.3.6 presents the details of the RF classifier and the evaluated model parameters. For both models, independent training and validation data sets were employed for developing the models and assessing their performance. Section 2.3.4 details the ground validation and training data used in the study.

2.2.3. Performance Assessment

This study used the same reference training dataset to assess the accuracy of the RF and U-Net predictions. Section 2.3.4 details the ground validation and training data employed in the study. Figure 3 provides the spatial distribution of training polygons used for the RF classification and the validation points used for both models (RF and U-Net). Section 2.3.7 discusses the accuracy assessment metrics used to evaluate the model predictions' performance and establish their accuracies.

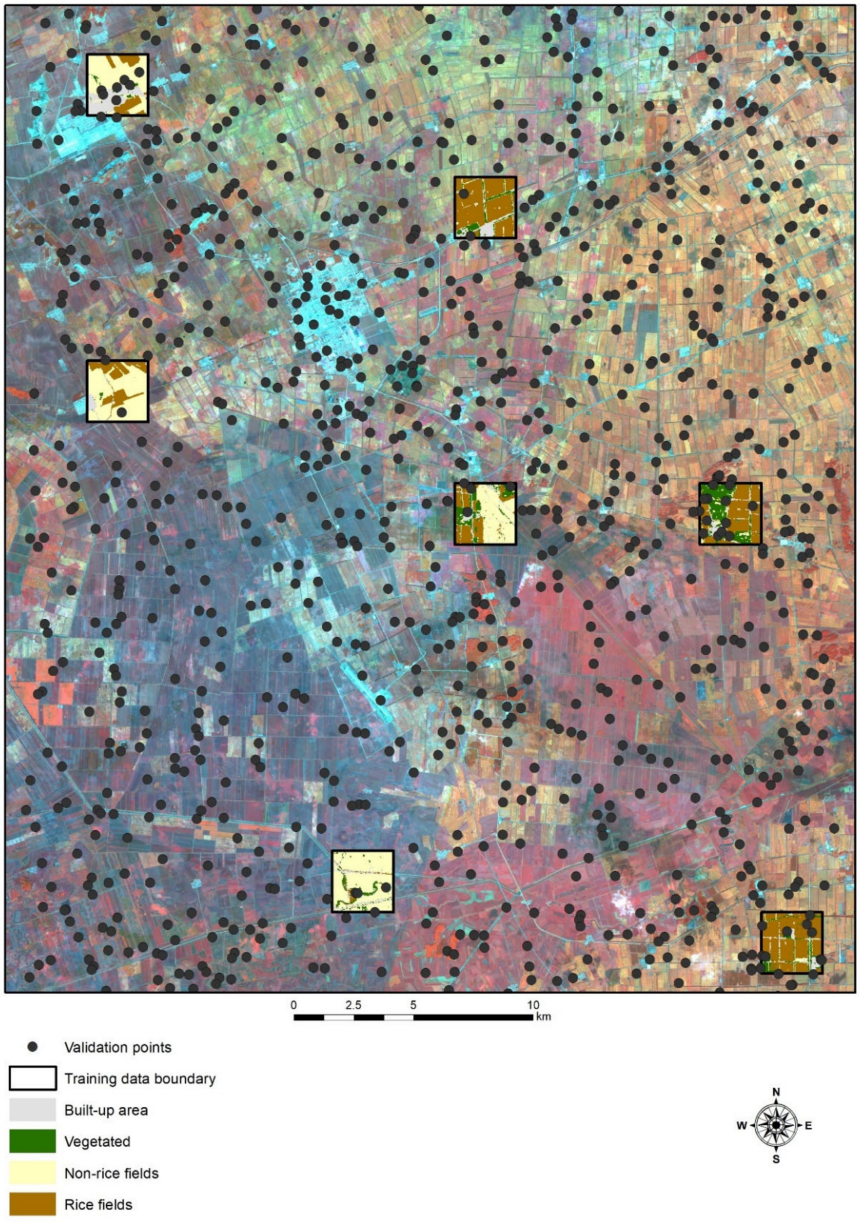


Figure 3. Map showing the distribution of training polygons and validation points used for random forest classification and accuracy assessment. The validation points were also used to assess the accuracy of the DL model.

2.2.4. Upscaling of the Identified Optimal Model and Change Detection Analysis

In this study component, the identified optimal U-Net model was used to generate three upscaled paddy rice maps (dated 2016, 2018 and 2020) covering the five districts investigated. This component addressed RQ3 and RQ4. This component's primary output was testing the model's transferability and operational capacity by upscaling the developed U-Net based on a subset of the study area.

The upscaled paddy rice maps for the three years (2016, 2018, and 2020) were used as inputs in a change detection analysis, quantifying the dynamics of rice agriculture in the study area. Section 3.4 presents the outcomes of the change detection analysis.

2.3. Inventory and Processing of Radar and Optical Satellite Sensor

2.3.1. Sentinel 1 Radar Data

GEE provides a rich repository of pre-processed satellite data, such as S1 SAR imagery. The S1 Image Collection consists of backscatter coefficient (σ°, in decibels) values processed from Level-1 Ground Range Detected scenes. The pre-processing workflow steps were: radiometric calibration, terrain correction, image re-projection, and speckle [11,37]. The S1 imagery was post-processed using standard steps that included the exclusion of pixels affected by wind and speckle filtering.

Finally, the radar image collection's monthly mean composites were calculated and used as inputs for image classification. The monthly average composites for the descending satellite paths were generated using GEE. The S1 Image Collection was reduced to single bands in GEE with a mean *(imageCollection.reduce)* function. This image collection contained S1 images acquired over the paddy rice stages (i.e., from April to October) for 2016, 2018, and 2020 [19]. Table 1 presents details of the Sentinel data used in the study.

Table 1. Description of satellite data (Sentinel-1 SAR and Sentinel-2 optical imagery) used in the study.

SAR Data			
Sensor	Sentinel 1A		
Spatial resolution	10 m		
Wavelength	C band		
Polarization	Dual-polarization bands—vertical transmission/horizontal receiver—VH/VV		
Orbital properties	Descending		
Instrument Mode	Interferometric Wide (IW) swath mode		
# of VH/VV scenes	*2016*	*2018*	*2020*
	2219/2233	2219/2233	2219/2233
Provider	European Space Agency		
Optical Data			
Sensor	Sentinel 2A MSI (Multispectral Instrument)		
Spatial resolution	10/20 m		
Band and wavelength (µm)	Band 2 (Blue)–490 µm		Band 3 (Green)–560 µm
	Band 4 (Red)–665 µm		Band 5 (Red edge 1)–704 µm
	Band 6 (Red edge 2)–740 µm		Band 7 (Red edge 3)–780 µm
	Band 8 (Near-infrared)–842 µm		Band 8A (Red edge 4)–865 µm
	Band 11 (SWIR-1)–1614 µm		Band 12 (SWIR-2)–2202 µm
# of image scenes	*2016*	*2018*	*2020*
	296	634	511
Provider	European Space Agency		
Date Range	Vegetative: 10 April–25 June (2016, 2018 and 2020)		
	Reproductive: 28 June–10 August (2016, 2018, and 2020)		
	Ripening: 10 August–10 October (2016, 2018, and 2020)		

2.3.2. Sentinel 2 Optical Data

The S2 imagery used for this study was downloaded from GEE within the same time frame as the S1 imagery (i.e., April to October 2016, 2018, and 2020). Seventy-eight images covering the study area over the paddy rice stages were acquired using the GEE cloud-computing platform. The GEE platform was used for cloud masking and compositing. The median image reducer was used to calculate the median values of the image collections covering the rice growth stage. All 20 m bands were pan-sharpened to 10 m using the NIR band as performed by [38]. Using the GEE spatial enhancement tool (*hsvToRgb*), two 20 m RGB composites, namely composite 1 (B5, B6, and B7) and composite 2 (B8A, B11, and B12), were pan-sharpened [38]. Using the S2 median reduced bands, the optical indices NDVI, EVI, and LSWI with Equations (1)–(3) below.

$$NDVI = \frac{(B8 - B4)}{(B8 + B4)} \quad (1)$$

$$LSWI = \frac{(B8 - B11)}{(B8 + B11)} \quad (2)$$

$$EVI = 2.5 \times \frac{(B8 - B4)}{(B8 + 6 \times B4 - 7.5 \times B2 + 1)} \quad (3)$$

where *B2, B4, B8*, and *B11* (10 m pan-sharp) are the top of atmospheric reflectance values of the blue, red, NIR, and SWIR bands.

Appendix S1 in the Supplementary Materials presents the GEE codes used to download the S1 and S2 images used in the study.

2.3.3. Description of Image Composites Used for Experiments

Table 2 describes the image composites used for experiments in this study. The image composites had the following combinations: S2 multispectral bands (Dataset 1), S1 SAR bands only (Dataset 2), S2 optical indices only (EVI + NDVI + LSWI)–Dataset 3, S2 multispectral bands, and S1 SAR bands (Dataset 4), S1 SAR bands and optical indices (Dataset 5), S2 multispectral bands and optical indices (Dataset 6) and S2 multispectral bands, optical indices, and S1 SAR bands combination (Dataset 7).

Table 2. Description of image composites used for experiments in this study (where B = bands).

Dataset #	Input Bands	Description	# of Input Bands
Dataset 1	B2, B3, B4 and B8 B5, B6, and B8A B11 and B12	Visible and Near Infrared (VNIR) Red edge Short Wave Infrared (SWIR)	10
Dataset 2	$VH_{VEG+REP+RIP}$ $VV_{VEG+REP+RIP}$	Vertical–Horizontal polarization band Vertical–Vertical polarization band	6
Dataset 3	EVI NDVI LSWI	Enhanced Vegetation Index Normalized Difference Vegetation Index Land Surface Water Index	3
Dataset 4	Datasets (1 + 2)	Multispectral + $SAR_{VEG+REP+RIP}$ bands	16
Dataset 5	Datasets (2 + 3)	$SAR_{VEG+REP+RIP}$ bands + Optical Indices	9
Dataset 6	Datasets (1 + 3)	Multispectral bands + Optical Indices	13
Dataset 7	Datasets (1 + 2 + 3)	Multispectral + SAR + Optical indices	19

Since the study area was prone to cloud cover issues, median composites of the available S2 imagery captured over the rice crop growth period (i.e., 10 April to 10 October) were used. It was a different approach from the S1 SAR bands, where the median values covered individual rice growth stages (i.e., vegetative, reproductive, and ripening).

2.3.4. Ground Validation and Training Data

An independent set of ground validation data was generated using a stratified random approach for accuracy assessment. This data was used to assess the accuracy of the RF classification and the optimal U-Net predictions. This study generated a thousand equally stratified random points (250 points per class) from the reference training dataset for accuracy assessment (Figure 3). These were the same reference training dataset used for assessing the accuracies of the RF and U-Net predictions evaluated in the study.

For the stratified random sampling, the study area was split into strata and random samples within each selected stratum. These strata are based on prior knowledge of the landscape. Using Google Earth imagery, landcover reference data (over 2000 GPS data representing major land-cover classes) were employed in the design of sampling grids across the project area.

Figure 3 shows the spatial distribution of training polygons used for RF classification. The classification schema adopted in this study was similar to that in [19]. Four broad classes were selected: built-up area (comprised of bare surfaces, buildings—commercial and industrial, road surface, and paved surfaces), non-rice fields (water bodies and other croplands), vegetated (forested landscape, wetlands, vegetation with considerable density and height, and shrubs), and paddy rice fields. At some point in the study, these four broad classes were recoded into two broad classes—other land-use and paddy rice fields.

2.3.5. U-Net CNN Segmentation

This study explored the U-Net model with a deep residual U-Net (ResU-Net) network framework for image segmentation. Its architecture comprises two components: namely encoding and decoding, respectively.

The encoder extracts features and labels patterns followed by a downsampling max-pool. The second half of the architecture (i.e., the decoder) spatially learns the information needed for reconstructing the original input data [39]. The decoder architecture semantically discriminates lower-resolution features onto higher-resolution pixel spaces to generate a dense classified output [39,40]. Reference [41] proposed using temporal feature-based segmentation for paddy rice mapping with time-series SAR images. The developed model extracts temporal features and learns the spatial context of extracted features for rice crop mapping [41]. This study used the ArcGIS API for Python to run the U-Net classifier. The U-Ner classifier runs the ResNet34 backbone by default. The ResU-Net network handles problems associated with vanishing gradients by including connections to convolutional layers into the U-Net framework [42–44]. In this study, the number of epochs used for all the U-Net experiments was 200. The training data used for the U-Net CNN segmentation experiments were obtained from the existing land use cover database of paddy rice monitoring plots in the center of Heilongjiang. The land use training data represented the study area's general land use, including paddy rice fields. This raster layer was vectorized and served as input in the DL modelling performed in the study. Table 3 lists the other DL parameters and arguments for the U-Net prediction experiments. The parameters considered in the study included padding, batch size, and tile size.

Table 3. Deep learning parameters used in U-Net prediction experiments.

Input Dataset	Learning Rate	Padding	Batch Size	Tile Size	Predict Background	Test Time Augmentation
Dataset 1	0.00016	54	4	256	False	False
Dataset 2	0.00009	54	4	256	False	False
Dataset 3	0.00008	54	4	256	False	False
Dataset 4	0.00013	54	4	256	False	False
Dataset 5	0.00009	54	4	256	False	False
Dataset 6	0.00033	54	4	256	False	False
Dataset 7	0.00016	54	4	256	False	False

The padding parameter refers to the border area discarded by the model during analysis. An example is the paddy rice field samples truncated from multiple overlapping tiles during inferencing. The padding ensures that areas that lie at the edge of one pass and are ignored in the first pass are captured in the inferencing's second pass.

The batch size refers to the number of image tiles a Graphics Processing Unit (GPU) can process at a go while inferencing. Ideally, during inferencing, the input imagery is clipped to smaller tiles that the GPU can analyze in a single batch. The batch size is usually dependent on the computer system's GPU. This project includes a computer laptop with an Intel i-Core CPU @ 2.60 GHz with 16 GB RAM and an NVIDIA-enabled GeForce GTX, 1650 Ti GPU, with 4 Gigabytes of memory employed. The batch size used for all the experiments was 4.

The tile size refers to the size of the image chips exported for the DL model development. After a series of tests, the tile size of 256 × 256, depicting dimension sizes of 2560 × 2560 m, was selected. The learning rates evaluated in the DL experiments are presented in the Supplementary Materials (see Figure S1). After the optimal dataset for paddy rice segmentation was determined, the model file was saved and applied to the upscaled imagery covering the entire study area.

2.3.6. Random Forest (RF) Classifier

The RF classifier was selected for this study because it is generally less affected by noise and overfitting remotely sensed data [45]. Studies have shown that RF can handle high data dimensionality compared to classifiers like Support Vector Machines, maximum likelihood, and single decision trees [46–49]. RF constructs bootstrapped de-correlated decision trees (DTs) and aggregates these to classify input datasets [50].

For this study, several experiments were conducted using the optimal image dataset determined from the U-Net segmentation. The RF parameters explored included maximum tree depths (250 and 500), maximum tree depth (30) and samples per class (1000). Table 4 presents the samples used for the RF classification experiments performed in the study.

Table 4. Inventory of training polygons used for Random Forest experiments.

Class	# Samples	Pixels (%)
Built-up area	113	12.2
Vegetated	652	11.72
Non-rice fields	1179	37.43
Rice fields	394	38.66

2.3.7. Accuracy Assessment

The accuracy assessment component was performed in two stages: the first evaluated the U-Net CNN segmentation's performance and determined the optimal image. The second stage compared the performance of the optimal U-Net prediction and RF classifications.

The accuracy metrics, namely User's and Producer's Accuracy (UA and PA), Overall Accuracy (OA), and F1-score, were calculated for the optimal U-Net prediction and RF classifications from confusion matrices (see Equations (4)–(7) below).

$$UA = \frac{X_{ij}}{X_j} \times 100\% \quad (4)$$

$$PA = \frac{X_{ij}}{X_i} \times 100\% \quad (5)$$

$$OA = \frac{S_d}{n} \times 100\% \quad (6)$$

$$F1 - score = 2 \times \frac{UA \times PA}{UA \times PA} \quad (7)$$

where X_{ij} = observation in row i column j, X_i = marginal total of row i, X_j = marginal total of row j, S_d is the total number of correctly-classified pixels, and n = the total number of validation pixels.

The classifier's performance on datasets was evaluated using the overall classification accuracy and F1-score of the paddy rice field class, as this was the study's focus.

The mean intersection over union (IoU) was used as an additional metric for the U-Net predictions. Equation (8) shows how the IoU is calculated:

$$IoU = \frac{TP}{FN + TP + FP} \quad (8)$$

where *TP, FN*, and *FP* represent true positives, false negatives, and false positives.

The mean F1 Score of all the classes was considered in explaining the performance evaluation of experiments conducted in the study.

2.3.8. Upscale Optimal U-Net Model for Rice Paddy Spatial–Temporal Analysis

The third RQ investigates the transferability and upscaling of the proposed optimal workflow for operational use. As proposed in the study's objectives, the optimal model based on a subset of the study area was subsequently used to generate three paddy rice maps (dated 2016, 2018 and 2020) covering the five districts described in Section 2.1 of this paper. A change detection analysis was performed to understand better the dynamics of paddy rice field changes over time in this region of Heilongjiang province.

3. Results

The study's uniqueness is in assessing the value of combining radar, multispectral and optical-derived indices with the cloud-based GEE computing platform. Considering the challenges of obtaining cloud-free images, complementary information from radar imagery is of immense value in paddy rice mapping [19,24,51,52]. This all-weather capability of SAR data and its ability to capture the different stages of paddy rice growth, monitor biomass development, and detect other biophysical measures makes it a valuable component of this study [53,54].

3.1. Selection of Optimal Image Composite in the U-Net DL Model Experiments

The first RQ focused on determining the optimal image combination of multi-temporal SAR and optical derivatives while utilizing the U-Net DL model prediction for paddy rice mapping. The U-Net model experiments were done with varying learning rates, the same padding (54), batch size (4), and epoch (200) (Table 3).

The U-Net model segmentation accuracy metrics indicated that the mean IoU, mean F1-Score and Rice F1-Score were highest for Dataset 4 (i.e., MS + SAR bands with 0.82, 0.67, and 0.95) and Dataset 7 (i.e., MS + SAR + Optical indices with 0.82, 0.67, and 0.95), respectively (see Figure S2 in the Supplementary Materials). The other datasets in the order of combined performance were Dataset 6 (MS + optical indices–0.81, 0.65, and 0.94), Dataset 5 (SAR + optical indices–0.80, 0.65, and 0.95), Dataset 1 (MS bands–0.80, 0.64, and 0.93), Dataset 2 (SAR bands–0.77, 0.60, and 0.94) and Dataset 3 (optical indices–0.76, 0.59, and 0.92). The results indicated that the singular use of the optical bands (Dataset 1), optical indices (Dataset 3), or SAR (Dataset 2) data did not outperform the multisensor combinations. Based on the accuracy assessment results, Dataset 4 (i.e., a combination of the multispectral and SAR bands) was selected as the optimal image combination and used for subsequent analysis. A few predictions from the validation dataset were compared with actual ground truth data as part of the validation process. Figure S3 shows a preview of ground truth and prediction chips for one of the optimal datasets from the U-Net DL experiments (i.e., Dataset 4). Table S1 presents the accuracy assessment results of U-Net predictions performed to establish the optimal image combination (see the Supplementary Materials). Figure S4 presents the U-Net predictions of paddy rice fields generated using datasets evaluated in the study.

3.2. Comparison of Random Forest and U-Net Predictions

Based on the results of RQ1, Dataset 4 (i.e., MS + SAR bands) was selected as the optimal dataset and used as input in the RF classification tests. RQ2 aimed to evaluate RF experiments performed under different model parameters using Dataset 4 as its input.

The two RF experiments were performed with varying decision tree numbers (250 and 500), and with the same maximum tree depth of 30 and samples per class (1000). The RF classification experiments were compared with the U-Net segmentation output using an independent set of validation data points. The four class predictions were recoded into two broad classes (other land-use and rice fields). This approach was adopted to allow easy comparison with similar studies on paddy rice mapping. Table S2 presents the RF classification and optimal U-Net prediction error matrices.

The classification accuracy assessment results indicate the optimal U-Net segmentation model had OA, OK, and Mean F1-Scores of 94%, 0.84, and 0.92, respectively (see Figure S5). The RF (500 trees) were 91% (OA), 0.78 (OK), and 0.89 (mean F1-score). In comparison, RF (250 trees) had 91% (OA), 0.77 (OK), and 0.89 (mean F1-score). The Rice F1-score was highest for the U-Net segmentation (0.88), followed by RF (500 trees) predictions with 0.84 and 0.83 for the RF (250 trees) prediction (see Table S2). Figure 4 shows the optimal U-Net segmentation from a combination of S2 multispectral and S1 dual polarization bands (Dataset 4) and a comparison with S2 composites. Figures S6 and S7 present the paddy rice maps generated using the U-Net model and RF classifier (with 500 trees). The U-Net segmentation and Random Forest predictions using Dataset 4 were compared (see Figures S8 and S9).

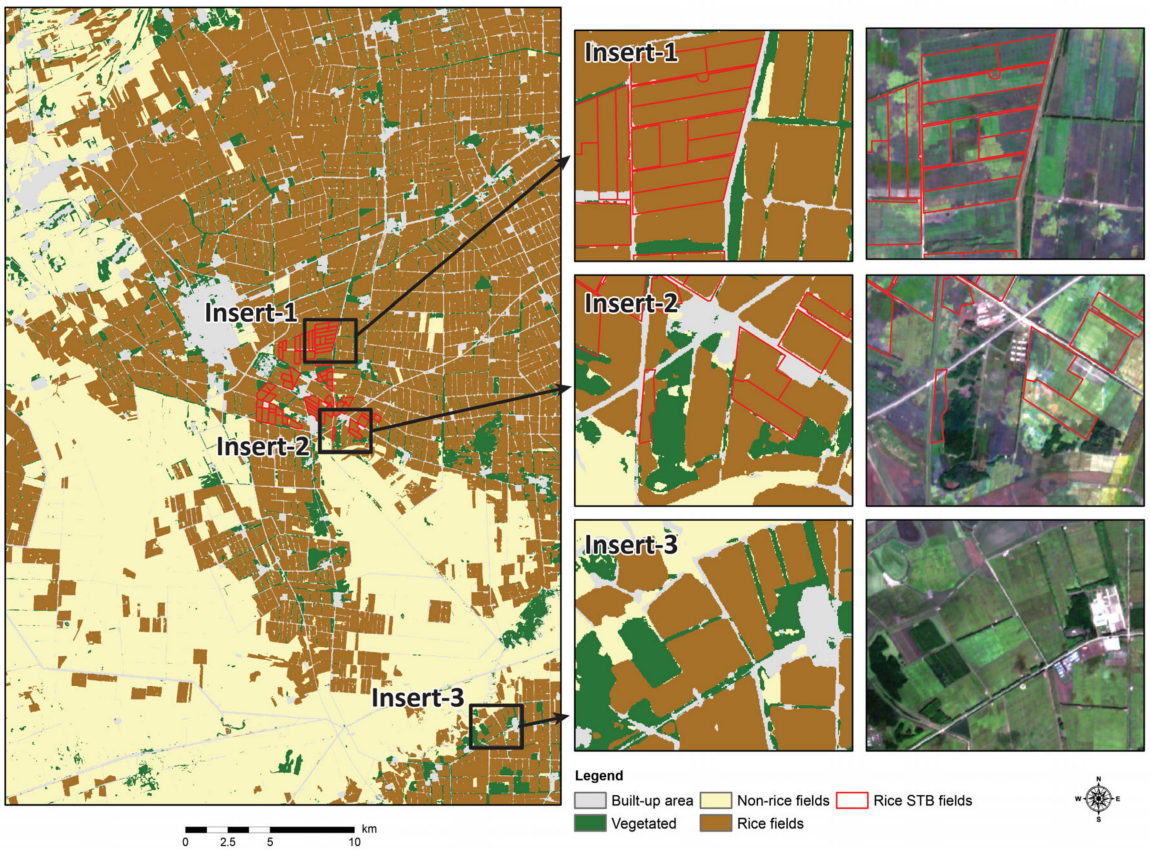


Figure 4. Optimal U-Net segmentation generated from a combination of Sentinel 2 multispectral and Sentinel-1 dual polarization bands (Dataset 4). The three insert maps represent mapped paddy rice fields and their corresponding Sentinel-2 image coverage.

3.3. Transferability of Operational ResU-Net Model

Based on the outcomes of RQs 1 and 2, the proposed operational workflow was evaluated. The optimal paddy rice model (i.e., for Dataset 4) was applied to a more extensive spatial coverage over different years (i.e., 2016, 2018 and 2020). The five districts in the southeastern parts of Heilongjiang province (i.e., Xiangyang, Qianjin, Jianshan, Taoshan, and Jiguan) have similar rice crop practices. They represent the site used in developing the ResU-Net model adopted in the study. This section of the paper outlines the accuracy assessment results of the upscaled ResNet model based on the optimal dataset identified in RQs 1 and 2.

Table S3 presents the accuracy assessment results associated with the upscaled paddy rice mapping on the district scale for 2016, 2018, and 2020, respectively. The ground validation data used to assess the yearly upscaled paddy rice maps (dated 2016, 2018, and 2020) were sourced independently from Google Earth. The results had OK and OA values of 0.86 and 94% (2016), 0.74 and 90% (2018), and 0.73 and 90% (2020). The paddy rice F1-Score for 2016, 2018, and 2020 upscaled predictions were 0.89, 0.81, and 0.80, respectively. Figure 5 presents the paddy rice map fields of selected districts in southeastern Heilongjiang province (i.e., Xiangyang, Taoshan, Jianshan, Jiguan, and Qianjin districts).

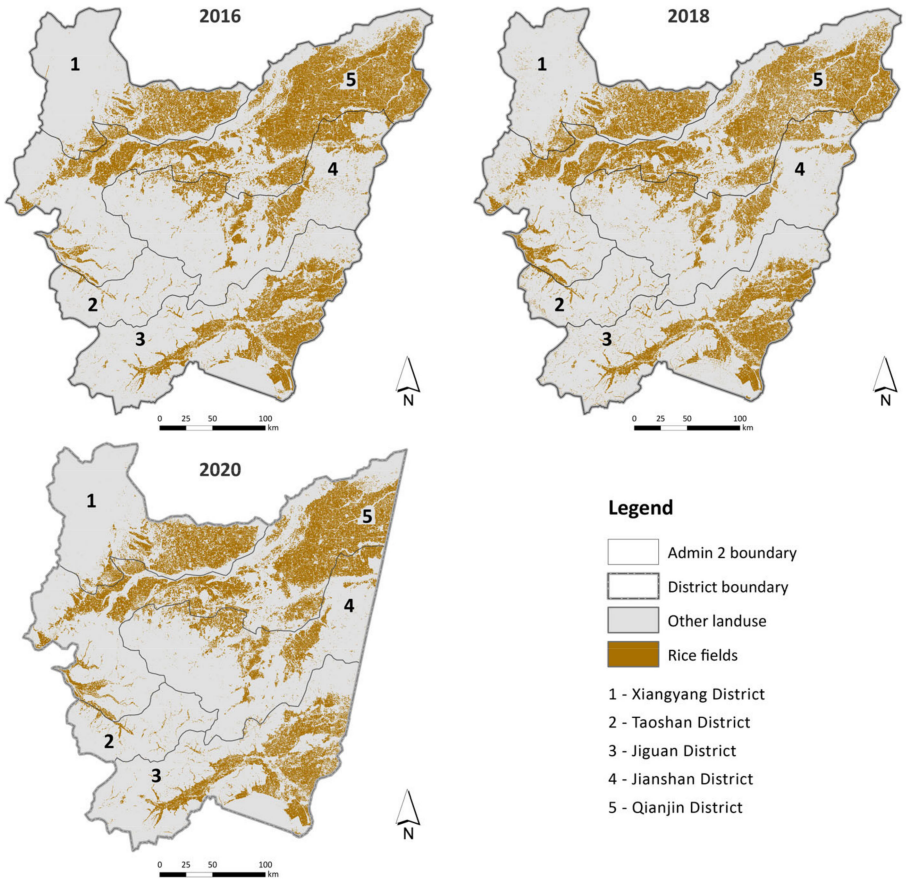


Figure 5. Paddy rice map fields of selected districts in southeastern Heilongjiang province (Xiangyang, Taoshan, Jianshan, Jiguan, and Qianjin). The 2020 boundaries were modified based on the limited Sentinel-1 radar data coverage in Jianshan, Jiguan, and Qianjin districts.

3.4. Spatial–Temporal Dynamics of Paddy Rice Fields from 2016 to 2020

Figure S10A shows the spatial distribution of mapped paddy rice fields for the five districts in Southeast Heilongjiang province. The spatial extent of mapped paddy rice fields over the study area was 2,363,423 hectares (2016), 2,308,506 hectares (2018), and 2,010,532 hectares (2020).

The spatial extent of the study area was modified (for 2018 and 2020) to accommodate the limited availability of S1 SAR data coverage across three districts affected (namely, Jianshan, Jiguan and Qianjin) (Figure 5). This step allowed determining the rates of change in paddy rice distribution over two epochs, namely 2016–2018 and 2018–2020, respectively.

Table 5 presents the change detection analysis results for both epochs, 2016–2018 and 2018–2020. The results indicated that the proportion of paddy rice fields converted to other land-use in the first epoch (i.e., 2016–2018) was 5% (approximately 437,123 hectares). For the second epoch (i.e., 2018–2020), the spatial extent of paddy rice fields converted to other land use was approximately 359,515 hectares (i.e., approximately 4% of the study area). The other land-use classes converted to paddy rice were approximately 378,831 hectares (4% of the total landscape) in 2016–2018 and 328,354 hectares in 2018–2020 (3% of the total landscape) (Figure S10B). Between 2016 and 2018, 71% of the other land-use classes remained unchanged, while 20% of the total study area remained paddy rice fields. These had spatial extents of approximately 6,832,948 and 1,932,610 hectares. Similarly, for the second epoch (i.e., 2018–2020), the spatial extent of unchanged other land-use and paddy rice fields were 6,459,426 (i.e., 67% of the study area) and 1,689,886 hectares (18% of the study area), respectively (Table 5 and Figure S10). Figures S11 and S12 show the change detection maps and sample hotspot locations of paddy rice fields for two epochs, 2016 to 2018 and 2018 to 2020, respectively.

Table 5. Results of change detection analysis for 2016–2018 and 2018–2020 time intervals.

Class Name	Class from	Class to	Land-Use Change Extent (Hectares)	
			2016–2018	2018–2020
Other land-use (unchanged)	Other landuse	Other land-use	6,832,948.43	6,459,425.82
Other land-use to Rice fields	Other landuse	Rice fields	378,830.84	328,353.98
Rice fields Other land-use	Rice fields	Other land-use	437,123.16	359,514.62
Rice fields (unchanged)	Rice fields	Rice fields	1,932,609.97	1,689,886.41
	Total area (ha)		9,581,512.40	8,837,180.83

4. Discussion

4.1. Approach for Effective Paddy Rice Mapping

The availability of accurate and timely land monitoring information, especially for paddy rice fields in China and other parts of the world, is crucial for food security and sustainable development. Satellite remote sensing offers a cost-effective monitoring solution compared to the traditional "*feet on the ground*" approach, requiring time-consuming and costly human resources.

RQs 1 and 2 outputs demonstrate the value of combining SAR and optical data captured over the rice crop growth stages (i.e., vegetative, reproductive, and ripening) as inputs in the ResNet-34 CNN model for mapping paddy rice fields at field scales. The combined use of Sentinel optical and radar derivatives (i.e., Datasets 4, 5, 6, and 7) captured during the rice crop growth cycle in the evaluated ResU-Net models showed immense potential in paddy rice mapping (with the rice F1-Score ranging from 0.94 to 0.95) and overall performance (the mean F-1 Score was between 0.81 and 0.82). The study identified the optimal dataset for paddy rice mapping as Dataset 4, a fusion of S2 multispectral bands (VNIR, red edge, and SWIR) and S1-SAR dual polarization bands (VH and VV) acquired in the crop growing season. These results substantiate existing studies that associate multisensory data fusion techniques with crop-specific phenological data as a practical approach for mapping paddy rice distribution [19,44,55–57]. Compared to exploring only singular sensor inputs, multispectral-derived indices or radar inputs, using the full range of spectral information in the VNIR, red edge, and SWIR regions proved more effective in

paddy rice mapping. The optical sensors′ VNIR, SWIR, and red edge regions of remotely sensed imagery are sensitive in detecting changes in the physiology of rice crops [58,59]. The red-edge region is a valuable input for crop discrimination, crop health assessment, and species identification [60,61]. Studies have evaluated the performance and importance of SAR satellite data (such as RADARSAT-2 or Sentinel-1) for crop and soil moisture monitoring and assessment [62–64].

As demonstrated by Reference [19], the temporal backscatter profile of the VV and VH polarization channels tends to vary over the rice crop growing season. Results of the study showed that for selected rice field training data, the VV polarizations were higher than the VH, a pattern observed in similar studies [65]. The temporal profile of VH polarization over rice fields is known to have a consistent variation in the recorded backscatter. The VH backscatter is known to have a consistent trend of increase in the backscatter during the reproductive and ripening stages of the rice crop growing season [19,65]. A similar trend was observed in the panicle initiation to the early milking phase (i.e., the reproductive stage). The rice crop attains peak growth at this stage and tends toward the maturity phase. For the VV polarization, an early peak at the flowering phase (i.e., the reproductive stage) is a usual occurrence in paddy rice fields in the study area [19]. The sustained VH temporal backscatter profile is attributed to the signal being less affected by changes in waterlogged surfaces [66]. Both VH and VV polarization channels offer valuable information on the temporal changes of backscatter transition for rice fields making this a valuable resource in large-scale mapping studies. As demonstrated in several studies, the singular or combined use of optical and SAR satellite data for paddy rice mapping has become common practice [4,10,19,28,52,66,67]. Combining the S1 SAR and S2 optical inputs has immense benefits in accurately mapping the spatial extent of paddy rice fields in this study.

The multisensor datasets outperformed the singular sensor datasets. The single sensor datasets of multispectral bands alone (Dataset 1), the radar bands alone (Dataset 2), and the MS optical indices (Dataset 3) had a Mean IoU of 0.64, 0.6 and 0.59, respectively. However, the multisensor datasets had mean IoU values ranging from 0.65 to 0.67 (Table S1). Overall, the combination of the mean F1-Score, the mean IoU, and the F1-Score of the paddy rice class showed the combined optical, and radar datasets outperformed the singular use of either optical or radar datasets (Figure S2). When the Sentinel radar and optical data captured during the paddy rice crop cycle were utilized in the DL model, the rice fields were better identified.

In comparison to several studies that have utilized DL techniques (Wei et al. 2021; Xu et al. 2021), the accuracy of this proposed approach has immense potential. Wei et al. (2021) exploited phenological similarity contained in S1 SAR time-series data to identify rice distribution with DL techniques. The overall accuracy of this study was 91% compared to the 94% obtained in this study. Similarly, Reference [9] utilized DL techniques to map rice fields using S1 SAR data as input into the model and obtained an accuracy of 91%. Our approach explores the ResU-Net DL framework allowing the training of multiple layers [68]. Reference [69] developed a U-Net DL model based on multi-temporal S1 SAR imagery (2019–2021) for paddy rice mapping across a similar landscape as this study in northeast China. The producers′ and users′ accuracies of our study were comparable with the results of [69]. Both studies provide a practical approach toward large-scale rice mapping based on multi-temporal satellite imagery. Table S4 in the Supplementary Materials presents the error matrices of the U-Net segmentation experiments.

In addition to the effectiveness of the prediction technique, using open-source S1 SAR and S2 optical data through GEE is a cost-effective and sustainable approach to explore in the long-term. Considering the level of detail required for mapping small-size paddy rice fields in the region, the high temporal and spatial resolution offered by combining S1 SAR and S2 optical imagery is an efficient approach for mapping paddy rice distribution.

However, a limitation of the DL technique is that it heavily depends on a large volume of training information needed for the modelling process. Establishing science and agriculture hubs, like the Science and Technology Backyard [70], would provide valuable

training and validation data for rice mapping, yield estimation and regional fertilizer application studies. As part of the next steps in this study, the authors propose collecting more up-to-date seasonal training data to train further and validate the developed U-Net model. These experimental stations can also train local technicians and farmers on water-saving technology and practical fertilizer usage [19,70].

4.2. Understanding Spatial–Temporal Dynamics of Paddy Rice Agriculture

The change detection analysis revealed the spatial distribution of paddy rice fields across the study area over the two epochs analyzed. The spatial extent of converted paddy rice fields was 377,895 hectares between 2016 and 2018, which subsequently declined by 18,551 hectares in the second epoch (i.e., 2018–2020) (Figure S13A). On a district level, the change detection analysis revealed a similar trend of rise in the percentage of paddy rice fields converted to other land-uses for three districts, namely Xiangyang, Taoshan, and Jiguan (Figure S13B). The other two districts (Jiansahan and Qianjin) experienced declines in the percentage of paddy rice fields converted to other land-use over both epochs (Supplementary Figure S13B). Overall, the percentage of paddy rice fields converted to other land-use for all five districts declined by 0.2% over the two epochs analyzed (2016–2018 = 4.3% and 2018–2020 = 4.1%, see Figure S13B). The dynamics of these variations could be attributed to varied management practices by farmers across the five districts considered in this study. Several studies focused on change detection monitoring in paddy rice fields across parts of northeastern China indicate that rice production areas have experienced a substantial decline since 2015 [71]. The study noted that though the northeast of China is an emerging force in rice production, the region is affected by challenges related to sustainable agricultural practices, over-fertilization, and water degradation [71]. Considering the importance of large volumes of water supply needed for paddy rice production, there are concerns about the unavailability and reliability of its supply to farmers in the northeastern parts of China [72]. Due to the upsurge in paddy rice farming in the region, the pressure from pumping groundwater for irrigation and inter-basin water transfer from rivers negatively affects water availability [71]. This current practice does not offer aquifers sufficient time to recharge.

5. Conclusions

The main objective of this study was to evaluate several singular and multisensor approaches for paddy rice field mapping in a deep residual CNN model. Considering the limitation of cloud cover occurrence associated with optical sensors such as S2, complementary radar data from the S1-SAR sensor is a promising approach for mapping rice. This study explored several combinations of multi-temporal multispectral and radar derivatives as inputs in a deep residual ResU-Net CNN segmentation model for paddy rice field mapping. The study showed the optimal dataset for paddy rice mapping was a fusion of S2 multispectral bands (VNIR, RE and SWIR) and S1-SAR dual polarization bands (VH and VV) acquired in the rice crop growing season (i.e., vegetative, reproductive, and ripening). Compared to the RF classification, the ResU-Net model outperformed the shallow ML algorithm by over 3% with an OA of 94%.

Regarding paddy rice prediction, the F1-Score of the ResU-Net model was 0.92 compared to 0.84 for the RF classification (that used 500 trees in the modelling process). The proposed DL method indicated an immense potential to be upscaled and transferred to a more extensive spatial coverage. The optimal model identified in the study was subsequently used to generate yearly paddy rice maps between 2016 and 2020 (at a 2-year interval) covering five districts in the southeastern parts of Heilongjiang province. These yearly paddy rice maps were used to quantify and better understand the study area's dynamics and challenges associated with paddy rice fields. The change detection analysis revealed the spatial extent of paddy rice fields was 377,895 hectares between 2016 and 2018 and later declined by 18,551 hectares in the second epoch (i.e., 2018–2020).

This proposed framework can accurately identify paddy rice fields locally and better inform decision-making and support. As the next step in this study, a DL approach shall be explored using the identified optimal inputs detailed in this research. The approach would prove beneficial to building a paddy rice monitoring inventory system that assists with decision-making and policy implementation to benefit smallholder farmers in the region.

Supplementary Materials: The following supporting information can be downloaded at: https://www.mdpi.com/article/10.3390/rs15061517/s1. The Supplementary Materials contain a list of figures and tables related to the results obtained in this study. In addition, hyperlinks to the GEE codes and an inventory of the results are presented. Figure S1: Learning rates chart of U-Net segmentation models evaluated in the study. Figure S2: Accuracy assessment of U-Net prediction experiments performed in the study. Figure S3: Preview of ground truth and prediction chips for one of the optimal datasets from the U-Net DL experiments (Dataset 4). Figure S4: U-Net prediction of paddy rice fields generated using datasets evaluated in the study. Figure S5: Accuracy assessment of U-Net prediction and Random Forest classification using optimal dataset. Figure S6: U-Net CNN segmentation paddy rice map produced from a combination of Sentinel 2 multispectral and Sentinel-1 dual polarization bands (Dataset 4). Figure S7: Random Forest (500 trees) paddy rice map produced from a combination of Sentinel 2 multispectral and Sentinel-1 dual polarization bands (Dataset 4). Figure S8: Comparison of U-Net segmentation and Random Forest predictions using Dataset 4. Figure S9: Comparison of U-Net segmentation and Random Forest predictions using Dataset 4 (contd.). Figure S10: Graph showing (A) the spatial distribution of mapped paddy rice fields and (B) the percentages of landuse change relative to the total project area for 2016, 2018, and 2020 respectively. Figure S11: Change detection analysis results of selected sites between 2016 and 2018. Figure S12: Change detection analysis results of selected sites between 2018 and 2020. Figure S13: Graph showing (A): changes in paddy rice distribution and (B): the percentage of paddy rice loss for each district in the study area over two epochs (i.e., 2016–2018 and 2018–2020). Table S1: Accuracy assessment results of U-Net predictions to establish the optimal image combination. Table S2: Error matrix and classification accuracy results of the Random Forest classification and optimal U-Net prediction. Table S3: Accuracy assessment results associated with the upscaled paddy rice mapping on the district scale for 2016, 2018, and 2020. Table S4: Error matrix and classification accuracy results of U-Net predictions.

Author Contributions: Conceptualization, A.O.O., G.A.B. and Y.M.; methodology, A.O.O., G.A.B. and Y.M., software, A.O.O.; validation, A.O.O. and Y.M.; formal analysis, A.O.O., G.A.B. and Y.M.; investigation, A.O.O.; resources, A.O.O.; data curation, A.O.O.; writing—original draft preparation, A.O.O., review and editing, A.O.O. and Y.M.; funding acquisition, A.O.O. All authors have read and agreed to the published version of the manuscript.

Funding: This research received no external funding.

Data Availability Statement: All data generated or analyzed during this study are included in the manuscript. An inventory of the earth observation data and results generated in this study are available as a web app for information dissemination purposes. The web app can be accessed using this link: https://jolexy.maps.arcgis.com/apps/webappviewer/index.html?id=d4d061430bea480eb20ace85919861e5 (accessed on 20 February 2023).

Acknowledgments: The author would like to thank the anonymous reviewers and editors for their valuable comments and inputs to improve the quality of this manuscript. Thanks to Google Earth Engine and Copernicus for making free Sentinel imagery available in the study.

Conflicts of Interest: The author declares that no known competing financial interests or personal relationships could have appeared to influence the work reported in this paper.

References

1. FAOSTAT. FAO Statistical Databases (Food and Agriculture Organization of the United Nations) Databases. UW-Madison Libraries. 2020. Available online: http://digital.library.wisc.edu/1711.web/faostat (accessed on 24 December 2022).
2. Shahbandeh, M. Paddy Rice Production Worldwide 2017–2018, by Country. Statista. Available online: https://www.statista.com/statistics/255937/leading-rice-producers-worldwide/ (accessed on 9 July 2020).
3. Elert, E. Rice by the numbers: A good grain. *Nature* **2014**, *514*, S50–S51. [CrossRef] [PubMed]

4. Singha, M.; Dong, J.; Zhang, G.; Xiao, X. High resolution paddy rice maps in cloud-prone Bangladesh and Northeast India using Sentinel-1 data. *Sci. Data* **2019**, *6*, 26. [CrossRef] [PubMed]
5. Abdelraouf, M.A.; Abouelghar, M.A.; Belal, A.-A.; Saleh, N.; Younes, M.; Selim, A.; Emam, E.M.; Elwesemy, A.; Kucher, D.E.; Magignan, S. Crop Yield Prediction Using Multi Sensors Remote Sensing. *Egypt. J. Remote Sens. Space Sci.* **2022**, *25*, 711–716.
6. Son, N.T.; Chen, C.F.; Chen, C.C. Remote Sensing Time Series Analysis for Early Rice Yield Forecasting Using Random Forest Algorithm. In *Remote Sensing of Agriculture and Land Cover/Land Use Changes in South and Southeast Asian Countries*; Vadrevu, K.P., Toan, T.L., Ray, S.S., Justice, C., Eds.; Springer International Publishing: Cham, Switzerland, 2022; pp. 353–366.
7. Wen, Y.; Li, X.; Mu, H.; Zhong, L.; Chen, H.; Zeng, Y.; Miao, S.; Su, W.; Gong, P.; Li, B.; et al. Mapping corn dynamics using limited but representative samples with adaptive strategies. *ISPRS J. Photogramm. Remote Sens.* **2022**, *190*, 252–266. [CrossRef]
8. Lowder, S.K.; Skoet, J.; Raney, T. The Number, Size, and Distribution of Farms, Smallholder Farms, and Family Farms Worldwide. *World Dev.* **2016**, *87*, 16–29. [CrossRef]
9. Xu, L.; Zhang, H.; Wang, C.; Wei, S.; Zhang, B.; Wu, F.; Tang, Y. Paddy Rice Mapping in Thailand Using Time-Series Sentinel-1 Data and Deep Learning Model. *Remote Sens.* **2021**, *13*, 3994. [CrossRef]
10. Zhu, A.-X.; Zhao, F.-H.; Pan, H.-B.; Liu, J.-Z. Mapping Rice Paddy Distribution Using Remote Sensing by Coupling Deep Learning with Phenological Characteristics. *Remote Sens.* **2021**, *13*, 1360. [CrossRef]
11. Gorelick, N.; Hancher, M.; Dixon, M.; Ilyushchenko, S.; Thau, D.; Moore, R. Google Earth Engine: Planetary-scale geospatial analysis for everyone. *Remote Sens. Environ.* **2017**, *202*, 18–27. [CrossRef]
12. Huang, H.; Chen, Y.; Clinton, N.; Wang, J.; Wang, X.; Liu, C.; Gong, P.; Yang, J.; Bai, Y.; Zheng, Y.; et al. Mapping major land cover dynamics in Beijing using all Landsat images in Google Earth Engine. *Remote Sens. Environ.* **2017**, *202*, 166–176. [CrossRef]
13. Dong, J.; Xiao, X.; Menarguez, M.A.; Zhang, G.; Qin, Y.; Thau, D.; Biradar, C.; Moore, B., III. Mapping paddy rice planting area in northeastern Asia with Landsat 8 images, phenology-based algorithm and Google Earth Engine. *Remote Sens. Environ.* **2016**, *185*, 142–154. [CrossRef]
14. Casu, F.; Manunta, M.; Agram, P.S.; Crippen, R.E. Big Remotely Sensed Data: Tools, applications and experiences. *Remote Sens. Environ.* **2017**, *202*, 1–2. [CrossRef]
15. Gulácsi, A.; Kovács, F. Sentinel-1-imagery-based high-resolution water cover detection on wetlands, Aided by Google Earth Engine. *Remote Sens.* **2020**, *12*, 1614. [CrossRef]
16. Hu, Y.; Dong, Y.; Batunacun. An automatic approach for land-change detection and land updates based on integrated NDVI timing analysis and the CVAPS method with GEE support. *ISPRS J. Photogramm. Remote Sens.* **2018**, *146*, 347–359. [CrossRef]
17. Oliphant, A.J.; Thenkabail, P.S.; Teluguntla, P.; Xiong, J.; Gumma, M.K.; Congalton, R.G.; Yadav, K. Mapping cropland extent of Southeast and Northeast Asia using multi-year time-series Landsat 30-m data using a random forest classifier on the Google Earth Engine cloud. *Int. J.App. Earth Observ. Geoinf.* **2019**, *81*, 110–124. [CrossRef]
18. Le Toan, T.; Ribbes, F.; Wang, L.-F.; Floury, N.; Ding, K.-H.; Kong, J.A.; Fujita, M.; Kurosu, T. Rice crop mapping and monitoring using ERS-1 data based on experiment and modeling results. *IEEE Trans. Geosci. Remote Sens.* **1997**, *35*, 41–56. [CrossRef]
19. Onojeghuo, A.O.; Blackburn, G.A.; Wang, Q.; Atkinson, P.M.; Kindred, D.; Miao, Y. Mapping paddy rice fields by applying machine learning algorithms to multi-temporal Sentinel-1A and Landsat data. *Int. J. Remote Sens.* **2018**, *39*, 1042–1067. [CrossRef]
20. Huete, A.; Didan, K.; Miura, T.; Rodriguez, E.P.; Gao, X.; Ferreira, L.G. Overview of the radiometric and biophysical performance of the MODIS vegetation indices. *Remote Sens. Environ.* **2002**, *83*, 195–213. [CrossRef]
21. Huete, A.R.; Liu, H.Q.; Batchily, K.V.; van Leeuwen, W. A comparison of vegetation indices over a global set of TM images for EOS-MODIS. *Remote Sens. Environ.* **1997**, *59*, 440–451. [CrossRef]
22. Chandrasekar, K.; Sesha Sai, M.V.R.; Roy, P.S.; Dwevedi, R.S. Land Surface Water Index (LSWI) response to rainfall and NDVI using the MODIS Vegetation Index product. *Int. J. Remote Sens.* **2010**, *31*, 3987–4005. [CrossRef]
23. Tucker, C.J. Red and photographic infrared linear combinations for monitoring vegetation. *Remote Sens. Environ.* **1979**, *8*, 127–150. [CrossRef]
24. Onojeghuo, A.O.; Blackburn, G.A.; Wang, Q.; Atkinson, P.; Kindred, D.; Miao, Y. Rice crop phenology mapping at high spatial and temporal resolution using downscaled MODIS time-series. *GIScience Remote Sens.* **2018**, *55*, 659–677. [CrossRef]
25. Xiao, X.; Boles, S.; Liu, J.; Zhuang, D.; Frolking, S.; Li, C.; Salas, W.; Moore, B., III. Mapping paddy rice agriculture in southern China using multi-temporal MODIS images. *Remote Sens. Environ.* **2005**, *95*, 480–492. [CrossRef]
26. Boschetti, M.; Nutini, F.; Manfron, G.; Brivio, P.A.; Nelson, A. Comparative Analysis of Normalised Difference Spectral Indices Derived from MODIS for Detecting Surface Water in Flooded Rice Cropping Systems. *PLoS ONE* **2014**, *9*, e88741. [CrossRef] [PubMed]
27. Zhao, R.; Li, Y.; Ma, M. Mapping Paddy Rice with Satellite Remote Sensing: A Review. *Sustainability* **2021**, *13*, 20503. [CrossRef]
28. Thorp, K.; Drajat, D. Deep machine learning with Sentinel satellite data to map paddy rice production stages across West Java, Indonesia. *Remote Sens. Environ.* **2021**, *265*, 112679. [CrossRef]
29. Sepp, H.; Schmidhuber, J. Long Short-Term Memory. *Neural Comput.* **1997**, *9*, 1735–1780. [CrossRef]
30. Ni, R.; Tian, J.; Li, X.; Yin, D.; Li, J.; Gong, H.; Zhang, J.; Zhu, L.; Wu, D. An enhanced pixel-based phenological feature for accurate paddy rice mapping with Sentinel-2 imagery in Google Earth Engine. *ISPRS J. Photogramm. Remote Sens.* **2021**, *178*, 282–296. [CrossRef]
31. Xia, L.; Zhao, F.; Chen, J.; Yu, L.; Lu, M.; Yu, Q.; Liang, S.; Fan, L.; Sun, X.; Wu, S.; et al. A full resolution deep learning network for paddy rice mapping using Landsat data. *ISPRS J. Photogramm. Remote Sens.* **2022**, *194*, 91–107. [CrossRef]

32. Ranjan, A.K.; Parida, B.R. Paddy acreage mapping and yield prediction using sentinel-based optical and SAR data in Sahibganj district, Jharkhand (India). *Spat. Inf. Res.* **2019**, *27*, 399–410. [CrossRef]
33. Gnyp, M.L.; Miao, Y.; Yuan, F.; Ustin, S.L.; Yu, K.; Yao, Y.; Huang, S.; Bareth, G. Hyperspectral canopy sensing of paddy rice aboveground biomass at different growth stages. *Field Crops Res.* **2014**, *155*, 42–55. [CrossRef]
34. Wang, F.-M.; Huang, J.-F.; Wang, X.-Z. Identification of Optimal Hyperspectral Bands for Estimation of Rice Biophysical Parameters. *J. Integr. Plant Biol.* **2008**, *50*, 291–299. [CrossRef] [PubMed]
35. Liu, J.; Kuang, W.; Zhang, Z.; Xu, X.; Qin, Y.; Ning, J.; Zhou, W.; Zhang, S.; Li, R.; Yan, C.; et al. Spatiotemporal characteristics, patterns, and causes of land-use changes in China since the late 1980s. *J. Geogr. Sci.* **2014**, *24*, 195–210. [CrossRef]
36. Dong, J.; Xiao, X.; Kou, W.; Qin, Y.; Zhang, G.; Li, L.; Jin, C.; Zhou, Y.; Wang, J.; Biradar, C.; et al. Tracking the dynamics of paddy rice planting area in 1986–2010 through time series Landsat images and phenology-based algorithms. *Remote Sens. Environ.* **2015**, *160*, 99–113. [CrossRef]
37. ESA. ESA Step—Science Toolbox Exploitation Platform. *European Space Agency.* 2019. Available online: http://step.esa.int/main/doc/tutorials/ (accessed on 12 July 2020).
38. Kau, L.J.; Lee, T.L. An HSV model-based approach for the sharpening of color images. In Proceedings of the 2013 IEEE International Conference on Systems, Man, and Cybernetics, Manchester, UK, 13–16 October 2013; IEEE: New York, NY, USA, 2013.
39. Ronneberger, O.; Fischer, P.; Brox, T. U-Net: Convolutional networks for biomedical image segmentation. In *Medical Image Computing and Computer-Assisted Intervention 2015*; Navab, N., Hornegger, J., Wells, W.M., Frangi, A.F., Eds.; Springer International Publishing: Cham, Switzerland, 2015; pp. 234–241. [CrossRef]
40. ESRI. How U-Net works? 2022. Available online: https://developers.arcgis.com/python/guide/how-unet-works/?rsource=https%3A%2F%2Flinks.esri.com%2FDevHelp_HowUNetWorks (accessed on 29 December 2022).
41. Yang, L.; Huang, R.; Huang, J.; Lin, T.; Wang, L.; Mijiti, R.; Wei, P.; Tang, C.; Shao, J.; Li, Q.; et al. Semantic Segmentation Based on Temporal Features: Learning of Temporal-Spatial Information from Time-Series SAR Images for Paddy Rice Mapping. *IEEE Trans. Geosci. Remote Sens.* **2021**, *60*, 1–16. [CrossRef]
42. Dang, K.B.; Nguyen, M.H.; Nguyen, D.A.; Phan, T.T.H.; Giang, T.L.; Pham, H.H.; Nguyen, T.N.; Tran, T.T.V.; Bui, D.T. Coastal Wetland Classification with Deep U-Net Convolutional Networks and Sentinel-2 Imagery: A Case Study at the Tien Yen Estuary of Vietnam. *Remote Sens.* **2020**, *12*, 3270. [CrossRef]
43. He, K.; Zhang, X.; Ren, S.; Sun, J. Deep residual learning for image recognition. In Proceedings of the IEEE Conference on Computer Vision and Pattern Recognition, Las Vegas, NV, USA, 26 June–1 July 2016.
44. Zhang, Z.; Liu, Q.; Wang, Y. Road extraction by deep residual u-net. *IEEE Geosci. Remote Sens. Lett.* **2018**, *15*, 749–753. [CrossRef]
45. Teluguntla, P.; Thenkabail, P.S.; Oliphant, A.; Xiong, J.; Gumma, M.K.; Congalton, R.G.; Yadav, K.; Huete, A. A 30-m landsat-derived cropland extent product of Australia and China using random forest machine learning algorithm on Google Earth Engine cloud computing platform. *ISPRS J. Photogramm. Remote Sens.* **2018**, *144*, 325–340. [CrossRef]
46. Belgiu, M.; Drăguţ, L. Random forest in remote sensing: A review of applications and future directions. *ISPRS J. Photogramm. Remote Sens.* **2016**, *114*, 24–31. [CrossRef]
47. Gislason, P.O.; Benediktsson, J.A.; Sveinsson, J.R. Random Forests for land cover classification. *Pattern Recognit. Lett.* **2006**, *27*, 294–300. [CrossRef]
48. Pelletier, C.; Valero, S.; Inglada, J.; Champion, N.; Dedieu, G. Assessing the robustness of Random Forests to map land cover with high resolution satellite image time series over large areas. *Remote Sens. Environ.* **2016**, *187*, 156–168. [CrossRef]
49. Rodriguez-Galiano, V.F.; Ghimire, B.; Rogan, J.; Chica-Olmo, M.; Rigol-Sanchez, J.P. An assessment of the effectiveness of a random forest classifier for land-cover classification. *ISPRS J. Photogramm. Remote Sens.* **2012**, *67*, 93–104. [CrossRef]
50. Breiman, L. Random forests. *Mach. Learn.* **2001**, *45*, 5–32. [CrossRef]
51. Kussul, N.; Skakun, S.; Shelestov, A.; Kussul, O. The use of satellite SAR imagery to crop classification in Ukraine within JECAM project. In Proceedings of the 2014 IEEE Geoscience and Remote Sensing Symposium, Quebec City, QC, Canada, 13–18 July 2014; IEEE: New York, NY, USA, 2014.
52. Park, S.; Im, J.; Park, S.; Yoo, C.; Han, H.; Rhee, J. Classification and Mapping of Paddy Rice by Combining Landsat and SAR Time Series Data. *Remote Sens.* **2018**, *10*, 447. [CrossRef]
53. Bouvet, A.; Le Toan, T.; Lam-Dao, N. Monitoring of the Rice Cropping System in the Mekong Delta Using ENVISAT/ASAR Dual Polarization Data. *IEEE Trans. Geosci. Remote Sens.* **2009**, *47*, 517–526. [CrossRef]
54. Kuenzer, C.; Knauer, K. Remote sensing of rice crop areas. *Int. J. Remote Sens.* **2013**, *34*, 2101–2139. [CrossRef]
55. Saadat, M.; Seydi, S.T.; Hasanlou, M.; Homayouni, S. A Convolutional Neural Network Method for Rice Mapping Using Time-Series of Sentinel-1 and Sentinel-2 Imagery. *Agriculture* **2022**, *12*, 2083. [CrossRef]
56. Zhai, P.; Li, S.; He, Z.; Deng, Y.; Hu, Y. Collaborative mapping rice planting areas using multisource remote sensing data. In Proceedings of the 2021 IEEE International Geoscience and Remote Sensing Symposium IGARSS, Kuala Kumpur, Malaysia, 17–22 July 2021.
57. Zhang, X.; Wu, B.; Ponce-Campos, G.E.; Zhang, M.; Chang, S.; Tian, F. Mapping up-to-Date Paddy Rice Extent at 10 M Resolution in China through the Integration of Optical and Synthetic Aperture Radar Images. *Remote Sens.* **2018**, *10*, 1200. [CrossRef]
58. Du, M.; Huang, J.; Wei, P.; Yang, L.; Chai, D.; Peng, D.; Sha, J.; Sun, W.; Huang, R. Dynamic Mapping of Paddy Rice Using Multi-Temporal Landsat Data Based on a Deep Semantic Segmentation Model. *Agronomy* **2022**, *12*, 1583. [CrossRef]

59. Mandal, N.; Das, D.K.; Sahoo, R.N.; Adak, S.; Kumar, A.; Viswanathan, C.; Mukherjee, J.; Rajashekara, H.; Ranjan, R.; DAS, B. Assessing rice blast disease severity through hyperspectral remote sensing. *J. Agrometeorol.* **2022**, *24*, 241–248. [CrossRef]
60. Forkuor, G.; Dimobe, K.; Serme, I.; Tondoh, J.E. Landsat-8 vs. Sentinel-2: Examining the added value of sentinel-2′s red-edge bands to land-use and land-cover mapping in Burkina Faso. *GIScience Remote Sens.* **2018**, *55*, 331–354. [CrossRef]
61. Jiang, X.; Fang, S.; Huang, X.; Liu, Y.; Guo, L. Rice Mapping and Growth Monitoring Based on Time Series GF-6 Images and Red-Edge Bands. *Remote Sens.* **2021**, *13*, 579. [CrossRef]
62. Khabbazan, S.; Steele-Dunne, S.; Vermunt, P.; Judge, J.; Vreugdenhil, M.; Gao, G. The influence of surface canopy water on the relationship between L-band backscatter and biophysical variables in agricultural monitoring. *Remote Sens. Environ.* **2021**, *268*, 112789. [CrossRef]
63. McNairn, H.; Brisco, B. The application of C-band polarimetric SAR for agriculture: A review. *Can. J. Remote Sens.* **2004**, *30*, 525–542. [CrossRef]
64. Woźniak, E.; Rybicki, M.; Kofman, W.; Aleksandrowicz, S.; Wojtkowski, C.; Lewiński, S.; Bojanowski, J.; Musiał, J.; Milewski, T.; Slesiński, P.; et al. Multi-temporal phenological indices derived from time series Sentinel-1 images to country-wide crop classification. *Int. J. Appl. Earth Obs. Geoinf.* **2022**, *107*, 102683. [CrossRef]
65. Mansaray, L.R.; Huang, W.; Zhang, D.; Huang, J.; Li, J. Mapping Rice Fields in Urban Shanghai, Southeast China, Using Sentinel-1A and Landsat 8 Datasets. *Remote Sens.* **2017**, *9*, 257. [CrossRef]
66. Nguyen, D.B.; Gruber, A.; Wagner, W. Mapping rice extent and cropping scheme in the Mekong Delta using Sentinel-1A data. *Remote Sens. Lett.* **2016**, *7*, 1209–1218. [CrossRef]
67. Xiao, W.; Xu, S.; He, T. Mapping Paddy Rice with Sentinel-1/2 and Phenology-, Object-Based Algorithm—A Implementation in Hangjiahu Plain in China Using GEE Platform. *Remote Sens.* **2021**, *13*, 990. [CrossRef]
68. De Bem, P.P.; Júnior, O.A.D.C.; de Carvalho, O.L.F.; Gomes, R.A.T.; Guimarães, R.F.; Pimentel, C.M.M. Irrigated rice crop identification in Southern Brazil using convolutional neural networks and Sentinel-1 time series. *Remote Sens. Appl. Soc. Environ.* **2021**, *24*, 100627. [CrossRef]
69. Wei, P.; Chai, D.; Lin, T.; Tang, C.; Du, M.; Huang, J. Large-scale rice mapping under different years based on time-series Sentinel-1 images using deep semantic segmentation model. *ISPRS J. Photogramm. Remote Sens.* **2021**, *174*, 198–214. [CrossRef]
70. Jiao, X.-Q.; Zhang, H.-Y.; Ma, W.-Q.; Wang, C.; Li, X.-L.; Zhang, F.-S. Science and Technology Backyard: A novel approach to empower smallholder farmers for sustainable intensification of agriculture in China. *J. Integr. Agric.* **2019**, *18*, 1657–1666. [CrossRef]
71. Xin, F.; Xiao, X.; Dong, J.; Zhang, G.; Zhang, Y.; Wu, X.; Li, X.; Zou, Z.; Ma, J.; Du, G. Large increases of paddy rice area, gross primary production, and grain production in Northeast China during 2000–2017. *Sci. Total Environ.* **2020**, *711*, 135183. [CrossRef] [PubMed]
72. Lu, W.; Cheng, W.; Zhang, Z.; Xin, X.; Wang, X. Differences in rice water consumption and yield under four irrigation schedules in central Jilin Province, China. *Paddy Water Environ.* **2016**, *14*, 473–480. [CrossRef]

Disclaimer/Publisher's Note: The statements, opinions and data contained in all publications are solely those of the individual author(s) and contributor(s) and not of MDPI and/or the editor(s). MDPI and/or the editor(s) disclaim responsibility for any injury to people or property resulting from any ideas, methods, instructions or products referred to in the content.

Yuzuncu Yil University
Journal of Agricultural Sciences
(Yüzüncü Yıl Üniversitesi Tarım Bilimleri Dergisi)
https://dergipark.org.tr/en/pub/yyutbd

ISSN: 1308-7576 e-ISSN: 1308-7584

Research Article

Determination of the Relationship between Rice Suitability Classes and Satellite Images with Different Time Series for Yeşil Küre Farm Lands

Orhan DENGİZ[1], Mert DEDEOĞLU[*2], Nursaç Serda KAYA[3]

[1,3] Ondokuz Mayıs University, Agriculture Faculty, Soil Science and Plant Nutrition Department, 55139, Samsun, Turkey
[2]Selcuk University, Agriculture Faculty, Soil Science and Plant Nutrition, Department, 42100, Konya, Turkey

[1]https://orcid.org/ 0000-0002-0458-6016, [2]https://orcid.org/ 0000-0001-8611-3724, [3]https://orcid.org/ 0000-0001-9814-5651

*Corresponding author e-mail: mertdedeoglu@gmail.com

Article Info

Received: 11.05.2022
Accepted: 20.06.2022
Online published: 15.09.2022
DOI: 10.29133/yyutbd.1114636

Keywords

Land evaluation,
NDVI,
RE-OSAVI,
Rice

Abstract: In this study, rice land designated for agricultural land suitability indices belonging to the enterprise Yeşil Küre Farm Land with different time series Sentinel-2A satellite images calculated utilizing spectral vegetation index, which are Normalized Difference Vegetation Index and Red Edge Optimized Soil Adjusted Vegetation Index values by statistical comparison of the relationship between rice for monitoring and estimation of potential productivity is presented a different perspective. Firstly, according to the rice suitability assessment for the study area, the area of 5488.9 ha was determined to be suitable for rice cultivation at the S1 and S2 levels, whereas the area of 588.9 ha was determined to be unsuitable. In this study, it was determined that the most successful results for each land conformity class were obtained using the NDVI. In particular, it was determined that August received the highest r^2 value (NDVI; 0.8580 and RE-OSAVI; 0.8465) in both vegetation index models at the S1 level, and on the other hand, a higher r^2 value was obtained with NDVI.

To Cite: Dengiz, O, Dedeoğlu, M, Kaya, N S, 2022. Determination of the Relationship between Rice Suitability Classes and Satellite Images with Different Time Series for Yeşil Küre Farm Lands. *Yuzuncu Yil University Journal of Agricultural Sciences*, 32(3): 507-526.
DOI: https://doi.org/10.29133/yyutbd.1114636

1. Introduction

Soil is a limited and non-renewable natural resource for the needs of the increasing human population, as well as being the main element in meeting the nutritional and shelter needs of the terrestrial ecosystem (Blum, 2006). As a matter of fact, it is predicted that the world population will grow by 19.7% until 2050 and reach 9.6 billion. The increase in the world population and the increase in the demand for food that it will bring with it causes the intensification of agricultural activities and an increase in the pressure on the limited land resources (FAO, 2009; Liniger, et al., 2011; Dumanski and Peiretti, 2013). Therefore, food security, demand for energy and water, climate change, and biodiversity in relation to sustainable land use are among the important global problems of the 21st century (Lal, 2008; 2009; Jones, et al., 2009; Lichtfouse, et al., 2009). The continuity of the functionality of the ecosystem depends on using the soil in the best way to get high productivity (Lal, 2009; Walter and Stützel, 2009).

Determination of soil quality is the basis of common and reliable approaches in the evaluation of soil fertility (Mueller et al., 2010; Ahmed et al., 2016; Xue et al., 2019; Dengiz, 2020). Soil quality

is defined as the capacity of soil to perform its functions within the boundaries of natural or managed ecosystems (Larson and Pierce, 1991; Doran and Parkin, 1994; Karlen, et al., 1997). Soil quality, like air and water, has a profound impact on the health and productivity of a particular ecosystem and its associated environments. Soil fertility is also the basic elements of a high input-based agricultural production system. For this reason, it is essential to evaluate soil fertility with parametric approaches in a periodic process (Rogowski and Wolf, 1994; Dengiz and Sağlam, 2012; Askari et al., 2015).

Today, Geographic Information Systems (GIS) and Remote Sensing (RS) technologies are useful tools used in similar monitoring issues encountered in the agricultural sector. Saving time and providing reliable, cost-effective, and repetitive information are among the advantages of GIS and UA to the agricultural sector. GIS and UA technologies are used in many areas, such as monitoring plant development process, evaluation of soil quality, crop yield estimation, and spatial analysis required in modern agriculture. As a matter of fact, the use of visible near infrared (VNIR) spectroscopy and GIS technologies in the evaluation of soil fertility by integrating agricultural practices and expert opinions makes it practical and economical to monitor agricultural areas locally (Moran, et al., 1996; Malczewski, 2006; Vohland, et al., 2014; Askari, et al., 2015). For this purpose, spectral reflections at different wavelengths obtained from earth observation satellites have been used to determine measurable plant vegetation characteristics such as plant biomass and active photosynthetic radiation since the launch of the Landsat-1 satellite in 1972 and to monitor the phenological changes of plants (Jackson, 1986). However, developing spectral sensors and band combination techniques have brought along the concept of vegetation index and have been widely used in the evaluation of cultivars grown in large-scale areas (Shou, et al., 2007; Jia, et al., 2011; Savasli, et al., 2021). It is known that especially the red (Red), red edge (Red-Edge), and near infrared (NIR) bands of the electromagnetic spectrum play an active role in monitoring the agricultural ecosystem (Liu, et al., 2004). Indeed, the relevant spectral regions are closely related to plant biophysical variables (height, density, and percentage of coverage), and it is known that the ratio of near-infrared bands to red edge spectral bands provides a high correlation with crop development in different growth periods. Today, many spectral indices, defined as unitless radiometric measurements, have been developed to obtain information about the biophysical properties of green leafy plants. The working principle of vegetation indices is basically based on the presence of chlorophyll, which is directly related to green leaf area and plant biomass and its response to biotic/abiotic factors (Kokaly and Clark, 1999; Li, et al., 2015). For this purpose, Normalized Difference Vegetation Index (NDVI), Effective Leaf Area Index, Chlorophyll Absorption Index at Modified Reflection Rate (Red-Edge Modified Chlorophyll Absorption in Reflectance Index), Red Edge Optimized Soildable Vegetation Index Red-Edge Optimized Soil Adjusted Vegetation Index, Green Normalized Difference Vegetation Index, Green Normalized Difference Vegetation, Health Index and Leaf Area Index are used (Fitzgerald, et al., 2010; Bagheri, et al., 2012; Wójtowicz, et al., 2016; Demir and Başayiğit, 2021). However, while studies have shown that vegetation indices derived from multi-spectral satellite images give successful results in early yield estimations, similar spectral index approaches that can directly evaluate the yield potential of soils could not evolve with a pragmatic model due to the complex nature of soils (Barnes et al., 2000). For this reason, the vegetation indices of the plants grown in agricultural lands and the biomass ratios determined at varying levels provide an indirect benefit to the researchers in the evaluation of soil fertility. In this way, the productivity of the soil where strategically important crops based on crop yield are grown under an agricultural management can be estimated experimentally (Gupta, et al., 2003; Zand and Matinfar, 2012; Mezera, et al., 2017; Sharabiani, et al., 2019). As a matter of fact, the factors affecting plant spectral reflections and indices values may be due to differences in management practices, as well as related to soil fertility (Zhou, et al., 2018; Dedeoğlu, et al., 2020). With this study, it is aimed to establish the land suitability classes of rice lands of Yeşil Küre Agricultural Enterprise and to reveal the relationship between NDVI and RE-OSAVI vegetation index values produced from Sentinel-2A satellite images with different time series and rice land suitability classes.

2. Material and Methods

Yeşil Küre Agricultural Enterprise (Center) is located at the 40th km on the Samsun-Bafra highway and is between 249000-254000 East and 4599200 - 4602400 North (WGS84, Zone 37, UTM-m) coordinates. Total land asset is 9239.8 da. Düden, which is the other part of the operation area where

the Black Sea is located in the east, Bünyan Mountain in the south, and the Bafra Plain in the west and north, is adjacent to the western shore of Balık Lake in the Kızılırmak Delta.

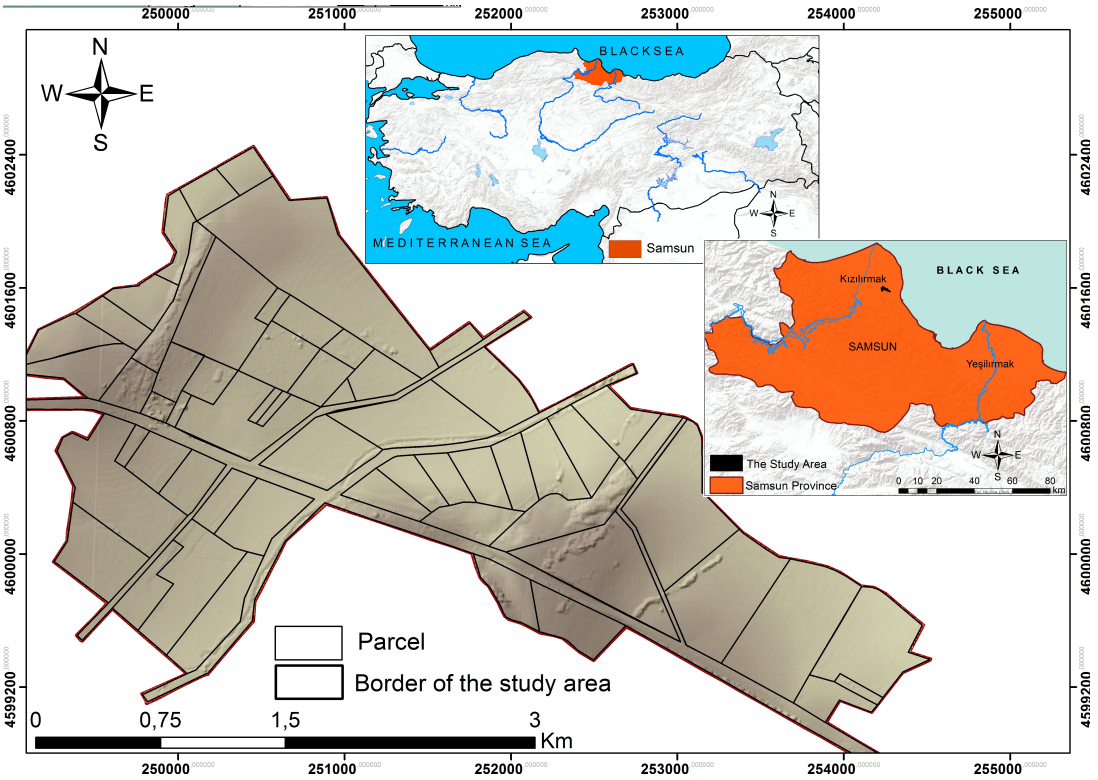


Figure 1. Location map of Yeşil Küre agricultural enterprise.

The height of the operation lands (Center and Düden) above sea level varies between 5 and 74 m. While the northwest and southeast parts of the land are areas where moderately steep and steep slopes are distributed in terms of slope, generally, the middle and northwest parts of the land constitute areas with 0-4%, nearly flat and mild slopes (Figure 2).

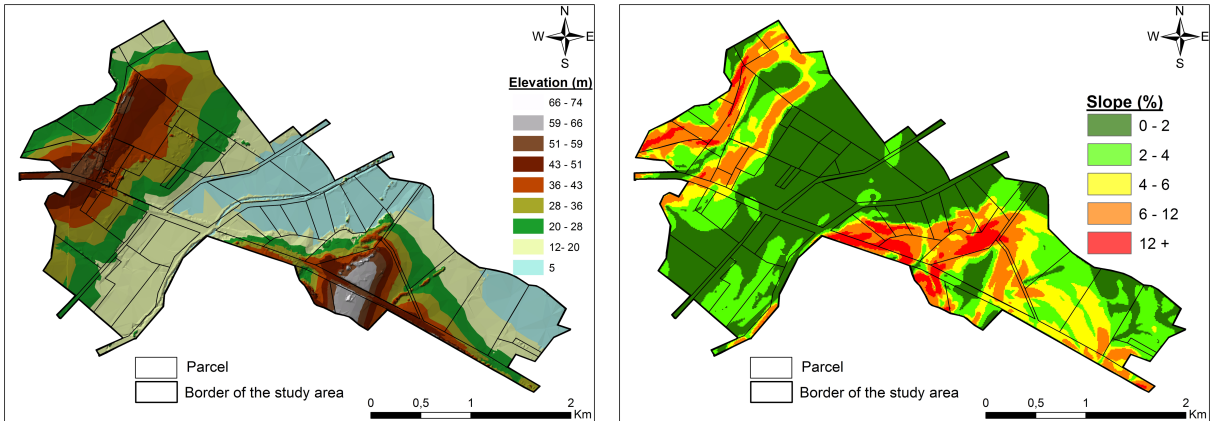


Figure 2. Elevation and slope map of the study area.

The widest coastal plains of the Black Sea Region are Çarşamba and Bafra plains. Yeşil Küre Agricultural Enterprise is also located on the Bafra Plain. The Black Sea climate, which is rainy in all seasons, cool in summers and warm in winters, is active on the coastline of the Black Sea Region. This effect of the climate extends to the inner parts depending on the landforms in the Central Black Sea Region. The annual average temperature of Yeşil Küre Agricultural Enterprise was 14.3˚C, the highest average air temperature was 18˚C and the lowest average temperature was 10.7˚C. The annual

precipitation average of the enterprise is around 710.0 mm. Snowfall in this region is less and does not last long. Snow does not stay for long in the coastal part. The coldest months in Bafra district are January, February and the hottest month is August.

The Bafra Plain, where the Yeşil Küre Agricultural Enterprise lands are located, is a wide delta plain formed by the rich alluvial soils brought by the Kızılırmak river. Bafra Plain is the largest plain of the Black Sea Region. Kızılırmak has formed many lakes near the sea. The area where the Agricultural Enterprise is located is covered by new Holocene alluvial deposits. In the central enterprise, there are high lands that emerged as a result of the erosion of these alluviums and carrying the eroded material (MTA, 1974). In addition, another series was added to the soil profiles in the updated study carried out in 2021 for the series classified as vertisol, mollisol, and entisol in the soil mapping study of the area carried out in 2005 by the General Directorate of Agricultural Enterprises, and the Yörükler series, which was classified as mollisol, was included in the entisol order due to losing its mollic feature as a result of intensive agricultural applications. (Figure 3).

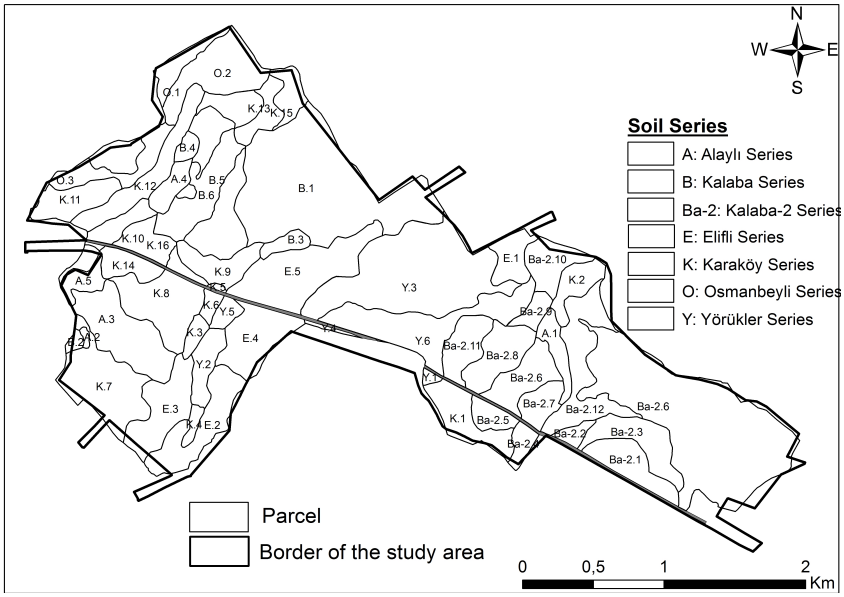


Figure 3. Updated soil map of the study area.

Almost all of the central part of the study area, called "Hara", has been cultured. Corn, wheat, alfalfa, and garlic are grown extensively. In addition, hazelnut and blackberry are planted. Rice farming is carried out in the farm area called Düden, located around Balık Lake in the Bafra delta. There are also oak, pine, poplar, maple, and elm trees, as well as ash, which are naturally found among dense rice fields. In Düden, natural living conditions prevail in the lower parts of the sea, where rice farming is not done. These regions are used as seasonal pastures by the local people. However, in periods when the rainfall is not heavy, cattle can be found in this region for grazing and sheltering.

Table 1. Characteristics of the Sentinel-2 satellite sensor

Band	Name	Wavelength (nm)	Band width (nm)	Spatial Resolution (m)
B1	**Coastal Aerosol**	443	20	60
B2	**Blue**	490	65	10
B3	**Green**	560	35	10
B4	**Red**	665	30	10
B5	**Vegetation Red-Edge**	705	15	20
B6	**Vegetation Red-Edge**	740	15	20
B7	**Vegetation Red-Edge**	783	20	20
B8	**Infrared**	842	115	10
B8A	**Vegetation Red-Edge**	865	20	20
B9	**Water vapor**	945	20	60
B10	**Cirrus**	1380	30	60
B11	**SWIR1**	1610	90	20
B12	**SWIR2**	2190	180	20

In this study, a total of 4 Sentinel-2 satellites images (with WGS84 datum) dated May, June, July and August 2021 of the Yeşil Küre Agricultural Enterprise lands on which various cultural plants are grown were used (Figure 4). Satellite images were obtained from the United States Geological Survey (USGS) open access center (https://earthexplorer.usgs.gov/). Multispectral Sentinel-2 satellite images have a spatial resolution of 10 m in 4 bands, 20 m in 6 bands, and 60 m in the other 3 bands (Table 1).

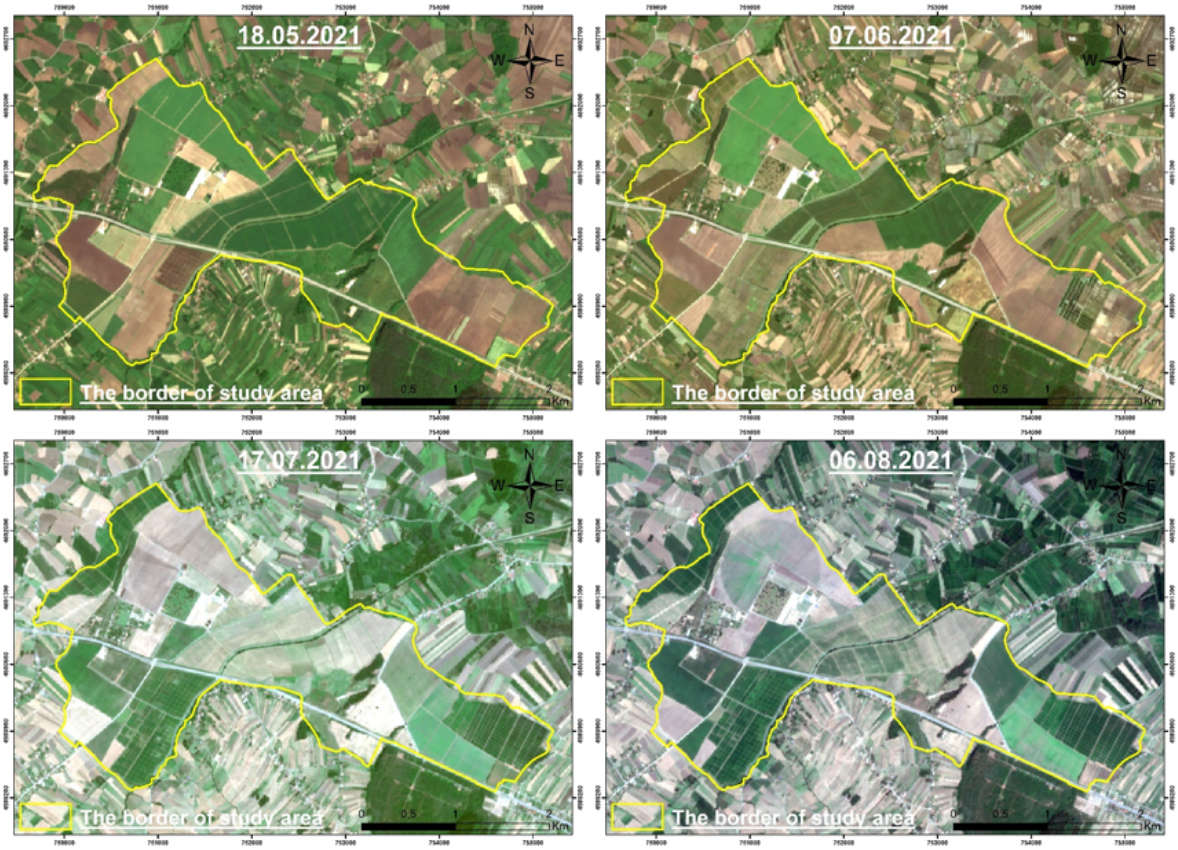


Figure 4. Sentenal-2 satellite images of different months.

2.1. Method

2.1.1. Creation of rice land suitability classes and index values

Soil series and their important phases were used as the mapping unit in the creation of the 1:25,000 scale basic soil map of the Yeşil Küre Agricultural Enterprise. Soil Survey Staff (1962) and Özbek et al., (1974) were used to classify important criteria such as depth, slope, salinity, alkalinity, drainage, and stoniness observed in the separation of soils into phases. Then, these criteria of the study area and topographic data were used to create the rice land suitability classes and index values. The determination of rice land suitability index values in terms of topographic and soil physico-chemical criteria has been handled by many researchers (FAO, 1983 and 1985; Sys et al., 1993; Yamada et al., 1995; Sönmez, 2003; Özcan, 2004; Mongkolsawat et al., 2002; Dengiz, 2013). These criteria used to determine the rice land suitability indices were obtained by multiplying the quality index value (SQI) (Equation 1) of the rice land soils belonging to each soil series with the nutrient availability index value (NAI) (Equation 2) and (Equation 3).

$$SQI: R * T * D * F * Y * P * G * S * K * H \quad (1)$$

R: Drainage, T: Texture, D: Depth, T: Topography, Y: Surface stony, P: Cream layer, G: Hydraulic conductivity, S: Salinity, K: Lime, H: Soil reaction.

$$NAI = N * P * K * Zn \quad (2)$$

NAI: Nutrient availability index.

$$LSC = NAI\ SQI \quad (3)$$

LSC: Land suitability class, NAI: Nutrient availability index, SQI*: Soil quality index.

Table 2. Rice suitability classes and index values

Statement	Suitability Classes	Index Value
Very suitable	S1	1.00-0.250
Moderate Suitable	S2	0.250-0.100
Low Suitable	S3	0.100-0.025
Not Suitable	N	< 0.025

2.1.2. Vegetation indexes

In this study, the vegetation indices of NDVI and RE-OSAVI, which are chlorophyll sensitive indices, were applied on the different time series Sentinel-2 satellite images of the rice fields of the Yeşil Küre Agricultural Enterprise by using the SNAP 8.0 tool and ArcGIS 10.7 environment. Information on both indexes is presented below.

2.1.2.1. Normalized difference vegetation index (NDVI)

There are many methods used in the identification of herbal product phenology. NDVI is the most widely used among these methods (Matton, et al., 2015). There have been many studies emphasizing the importance (Pettorelli et al., 2005a) of the role of satellite images in ecology, especially on the Normalized Difference Vegetation Index (NDVI) (Kerr and Ostrovsky, 2003; Damian, et al., 2019; Vorobiova and Chernov, 2017). As a matter of fact, Sahararini, et al. (2020) reported that the NDVI algorithm can be used as a base for processes such as image processing in Sentinel-2 satellite data, determination of rice phenology, estimation of rice harvest time. NDVI is used by many national and international organizations in many countries as an indicator of product yield. NDVI provides information with values ranging from -1 to +1 on subjects such as the spatial and temporal distribution of plant communities, plant biomass, CO_2 flows, pasture quality, and land degradation in various ecosystems (Salinas-Zavala et al., 2002; Al-Bakri et al., 2004; Pettorelli et al., 2005; Jiang et al., 2021).

NDVI values approaching -1 on the specified scale correspond to water bodies, while values approaching 0 indicate the presence of bare lands, rocky areas, sand, snow, or residential areas. NDVI values ranging from 0.2 to 0.4 correspond to bush or pasture areas, while this value approaching +1 indicates the presence of temperate regions, tropical rainforests, or areas with healthy and dense vegetation. With NDVI, it helps users in subjects such as the absorption of red wavelength energy within the visible region on the electromagnetic spectrum by the chlorophyll of the plant and the reflection of infrared (IR) energy by the plant cell structure, determination of biomass, and monitoring of changes in product development and production. By using NDVI in different time series satellite images, different growth periods of the plant, such as tillering, rooting, and harvesting, can be observed (Hufkens et al., 2019). In the Sentinel-2 satellite image, NDVI is calculated by using the red (B4) and infrared (B8) bands (Equation 4). The NDVI class values used in the estimation of the amount of product to be obtained from rice plants are given in Table 3.

$$NDVI = \frac{NIR - RED}{NIR + RED} \quad (4)$$

Table 3. NDVI values used in the definition of rice phenology (Pradipta, 2012).

NDVI values	Vegetation density	Age of Rice Plant (number of weeks after planting)
-0.096-0.036	No vegetation/bare/water	<3
0.036-0.240	Very low	3 - 4
0.240-0.456	low	4-6
0.456-0.652	Middle	6-8
0.652-0.884	high	8-13

2.1.2.2. Rededge optimized soil adjusted vegetation index (RE-OSAVI)

RE-OSAVI is an updated version of the Soil Vegetation Index (SAVI) family developed by Rondeaux et, al., (1996). The Optimized SAVI (OSAVI) model (RE-OSAVI) has been updated with the addition of the red edge (705 nm) band instead of the red band (670 nm) to minimize the effect of the submass on the red wavelength spectral reflections and make it more sensitive to the green field. It has been reported that this index can be used especially in periods when the vegetation density of plants is low (Wu et al., 2008). RE-OSAVI is calculated using the following formula (Equation 5).

$$\mathrm{RE-OSAVI} = (1 + 0.16) \times [(\mathrm{NIR} - \mathrm{REdge})/(\mathrm{NIR} + \mathrm{REdge} + 0.16)] \quad (5)$$

Vegetation indices (NDVI, RE-OSAVI) were calculated using the ESA-SNAP 8.0 tool in Sentinel-2 satellite images of the rice fields of the Yeşi Küre Farm Land.

2.1.3. Production of thematic maps and spatial statistical analysis in GIS environment

NDVI and RE-OSAVI vegetation index values were derived from each satellite image on a pixel basis, and maximum (S1), average (S2, N), and minimum (S3) NDVI and RE-OSAVI values were obtained for each rice suitability class. Thus, index values representing each parcel belonging to different rice land suitability classes were created. ArcGIS 10.7v was developed by ESRI (2010), for this purpose. Using the Zonal Statistics tool in the Spatial Analysis extension of the software, the index values reserved for different plots were extracted and transferred to MS Excel. Then, all indices' values were statistically compared with rice land suitability index (LSI) values, and regression relations (r^2) were determined.

3. Results and Discussion

3.1. Distribution of rice suitable areas

The areal and proportional distributions of rice suitability classes in the study area are given in Table 4, and its map is given in Figure 5. It was determined that 7205.5 da area, which is more than half of the study area (69.6%), is suitable for rice cultivation (S1 and S2), while 588.9 decares, which corresponds to 7.8% of the area, were found to be unsuitable for rice cultivation. In addition, depending on the limiting factor (slope, soil depth, texture, etc.) and grade of rice cultivation, less suitable (S3) classes cover 23.0% of the area.

Table 4. Spatial-proportional distributions of rice suitability classes

Statement	Suitability Classes	Area (da)	Ratio (%)
Suitable	S1	2964.4	37.6
Moderate Suitable	S2	2524.5	32.0
Low Suitable	S3	1816.3	23.0
Not Suitable	N	588.9	7.4
Total	-	7894.1	100.0

Areas that are not suitable for rice cultivation in the study area are generally the K12 and K11 mapping units of the Karaköy series, located in the northwest of the study area, and the B7, B8, B9, and B11 mapping units of the Kalaba series, which are distributed in the southeastern parts of the study area, especially the height and elevation in the slope grade. It has been determined that unsuitable areas are formed due to factors such as soil shallowness.

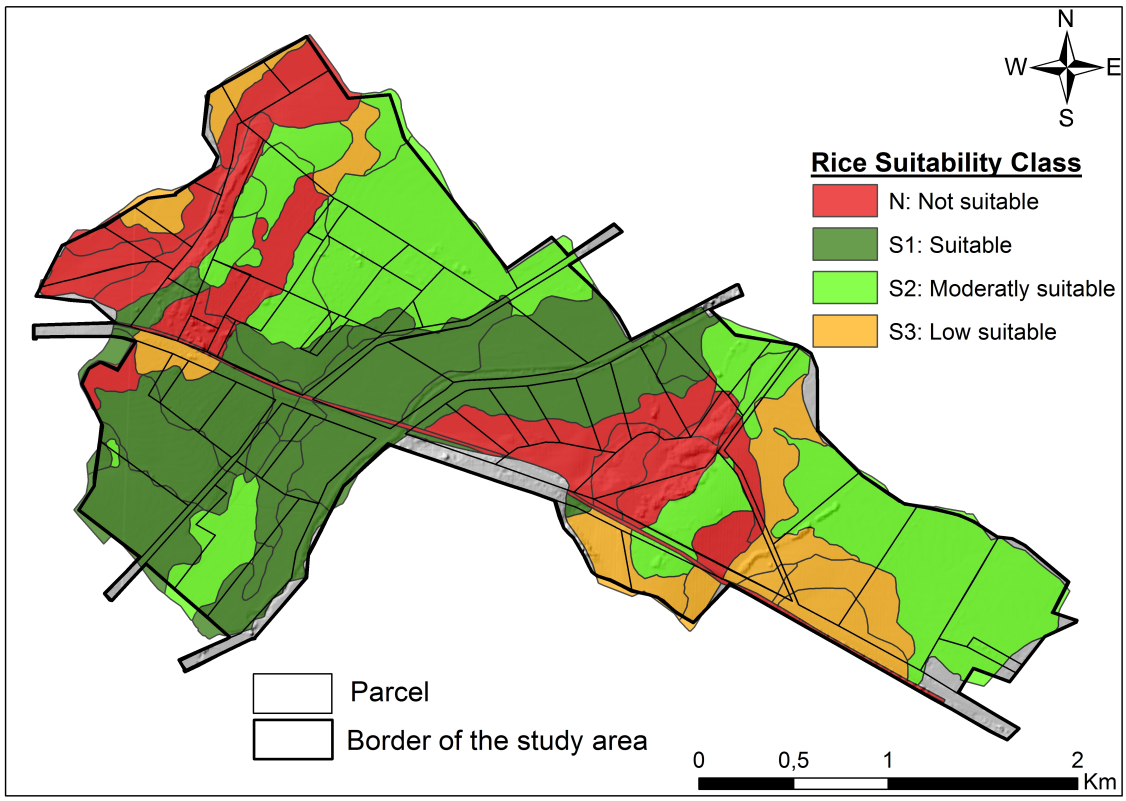


Figure 5. Rice suitability distribution map of the study area.

3.2. The relationship between rice suitability classes and vegetation indices

The land suitability index values for each land suitability class (S1, S2, S3, and N) of the rice fields obtained from the satellite images during May, June, July, and August dated May, June, July, and August of 2021, and the land suitability index values of the Sentinel-2A satellite images with different time series. The NDVI values and the r^2 values between which the statistical relationship was established are given in Table 5 and Figure 6, respectively. When the statistical relationship between the NDVI values obtained from the satellite image of May and the rice suitability index classes (S1, S2, S3, and N) is examined, the r^2 values are 0.7583, 0.8878, 0.8212, and 0.992, respectively; The r^2 values of the statistical relationship between the NDVI values obtained from the satellite image of June and the rice suitability index classes (S1, S2, S3, and N) were determined as 0.795, 0.873, 0.4725 and 0.9274, respectively.

In addition, the r^2 values of the statistical relationship between the NDVI values obtained from the July satellite image and the rice suitability index classes (S1, S2, S3, and N) were determined as 0.8396, 0.8833, 0.8879, and 0.9135, respectively, and finally, obtained from the August satellite image. When the statistical relationship between the obtained NDVI values and the rice suitability index classes (S1, S2, S3, and N) was examined, the r^2 values were found to be 0.858, 0.898, 0.8394, and 0.8924, respectively.

It should not be ignored that data variability may be caused by different cultural practices (fertilization, irrigation, soil cultivation, hoeing, etc.), such as the r^2 values of which the statistical relationship between the individual NDVI values of the land suitability classes and the ones belonging to the S3 suitability class are higher than the r^2 values of the S1 suitability class. (Dedeoğlu, et al., 2020).

Table 5. Each land suitability index values of rice fields and NDVI values of Sentinel-2A satellite images with different time series

Mapping Unit	Land Suitability Index	Land Suitability Class	NDVI Values			
			18.05.2021 Sentinel-2A	07.06.2021 Sentinel-2A	17.07.2021 Sentinel-2A	06.08.2021 Sentinel-2A
B11	0.02	N	0.6305	0.3091	0.2132	0.1530
B7	0.02	N	0.7319	0.5377	0.5690	0.4742
B8	0.016	N	0.6916	0.2862	0.4149	0.4987
B9	0.02	N	0.7359	0.7263	0.3275	0.3910
K11	0.016	N	0.5512	0.4934	0.3717	0.4185
K12	0.02	N	0.7368	0.5280	0.5277	0.4237
YOL	--	--	--	--	--	--
A1	0.4	S1	0.8119	0.8233	0.8135	0.8203
Ba.2	0.32	S1	0.7416	0.7217	0.6324	0.5041
Ba.4-A4	1	S1	0.6086	0.6348	0.7634	0.8094
Ba3	0.64	S1	0.8059	0.7391	0.6923	0.7842
E2	0.64	S1	0.5477	0.5507	0.6835	0.7711
E4-Y3	1	S1	0.7583	0.7677	0.7614	0.7795
E5	0.64	S1	0.7501	0.7662	0.7530	0.7753
K10	0.256	S1	0.7043	0.7114	0.8114	0.8093
K3	0.256	S1	0.7723	0.8009	0.8109	0.8050
K3	0.625	S1	0.7828	0.7541	0.8081	0.8037
K6	0.4	S1	0.8459	0.8108	0.7922	0.7317
K7	0.32	S1	0.7860	0.7860	0.7455	0.7968
K8	0.5	S1	0.7195	0.7766	0.7615	0.7950
K8	0.5	S1	0.8282	0.8011	0.7897	0.8043
K9	0.512	S1	0.8277	0.7542	0.7146	0.7198
Y1-E1	0.25	S1	0.8435	0.8053	0.7691	0.7305
Y2	0.4	S1	0.8481	0.8136	0.7547	0.7351
Y4-A3	0.205	S2	0.2462	0.3331	0.5227	0.6367
Y5	0.16	S2	0.4133	0.3386	0.2319	0.2064
A2	0.18	S2	0.6273	0.4220	0.2983	0.2493
A4	0.2	S2	0.5202	0.2388	0.5191	0.6134
A4	0.16	S2	0.7707	0.5536	0.2460	0.3673
A4	0.18	S2	0.7244	0.7342	0.2395	0.3238
B10	0.22	S2	0.7302	0.6552	0.1863	0.3435
B5-B9	0.16	S2	0.6897	0.5321	0.3012	0.3566
B6	0.25	S2	0.6195	0.5511	0.3192	0.3295
Ba.1	0.18	S2	0.7500	0.7136	0.1442	0.3505
Ba.4	0.2	S2	0.5989	0.5520	0.3741	0.4768
E3	0.14	S2	0.7540	0.7198	0.1325	0.4039
E3	0.25	S2	0.5630	0.5738	0.3178	0.3148
K2	0.128	S2	0.7534	0.7182	0.1519	0.3046
K2	0.1	S3	0.1545	0.1746	0.2079	0.1565
K2	0.08	S3	0.1216	0.1179	0.0786	0.0579
B1	0.08	S3	0.1430	0.1403	0.1470	0.1236
B2	0.054	S3	0.1237	0.1312	0.1880	0.1586
B3	0.042	S3	0.1402	0.1308	0.1027	0.1011
K1	0.05	S3	-0.0218	-0.2451	0.1350	0.1657
O1	0.051	S3	0.1344	0.1119	0.1129	0.1728
O2	0.09	S3	0.1067	0.1851	0.1123	0.1321
B12	0.05	S3	0.1492	0.1322	0.0876	0.0906

A*: Alaylı, B*: Kalaba, E*: Elifli, K*: Karaköy, O*: Osmanbeyli, Y*: Yörükler.

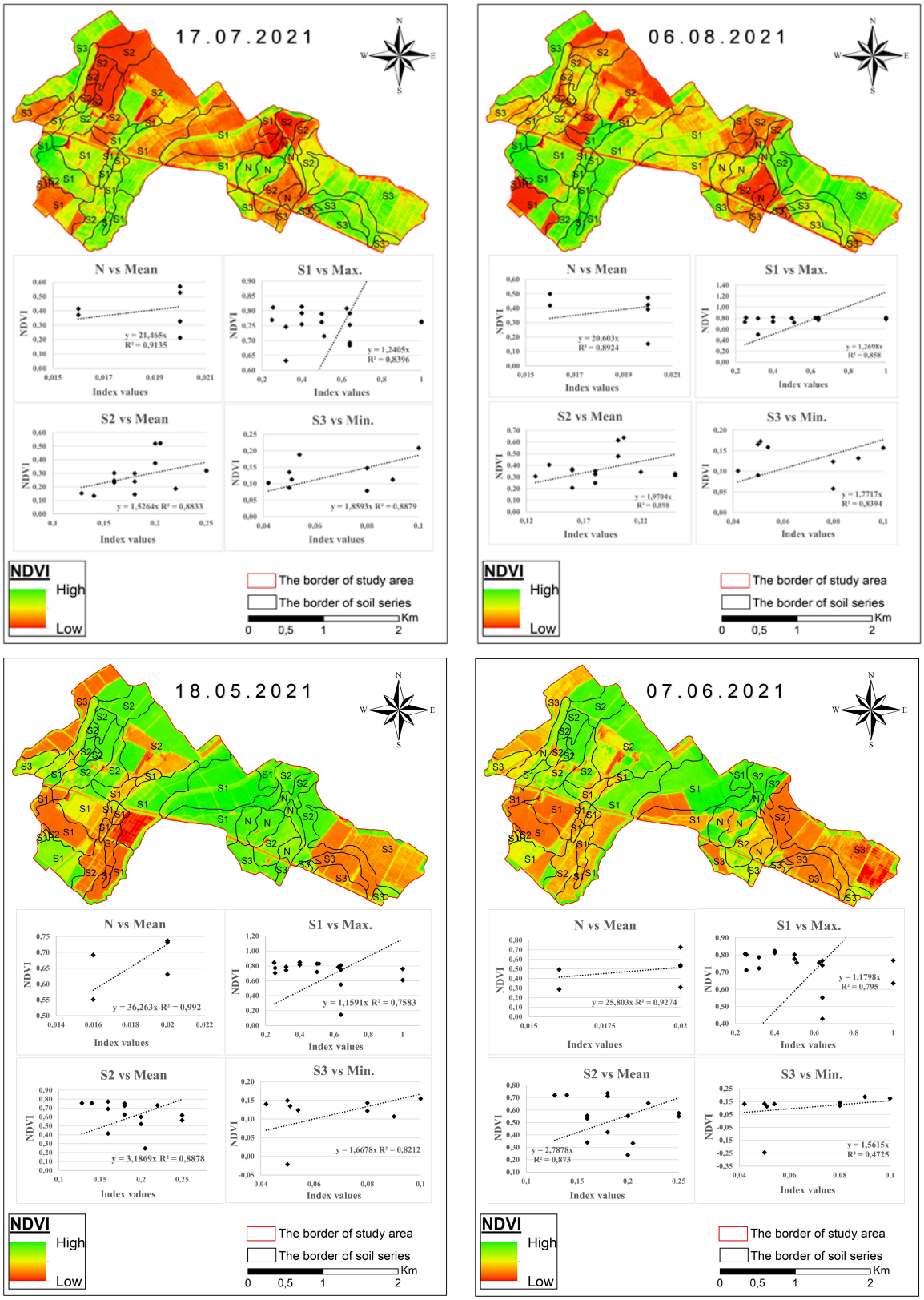


Figure 6. r2 values of each land suitability index value of rice fields and NDVI values obtained from Sentinel-2A satellite images with different time series.

The r^2 values, in which the statistical relationship is established between the NDVI values obtained from the May, June, July, and August satellite images of the Yeşil Küre Farm Land Enterprise, dated 2021, without evaluating the land suitability classes (S1, S2, S3, and N) separately, are shown in

Figure 7 and Table 6, respectively. In the evaluation of the statistical relationship between the land suitability classes (S1, S2, S3, and N) and the NDVI values without evaluating them separately, the r^2 values for July and August, which were determined to be high, were determined as 0.5707 and 0.6321, respectively, according to the r^2 results discussed. According to the r^2 results, which were considered in the evaluation of the statistical relationship between the NDVI values without evaluating the land suitability classes (S1, S2, S3, and N) separately, the r^2 values for the months of May and June, which were determined as low, were determined as 0.3341 and 0.4297, respectively.

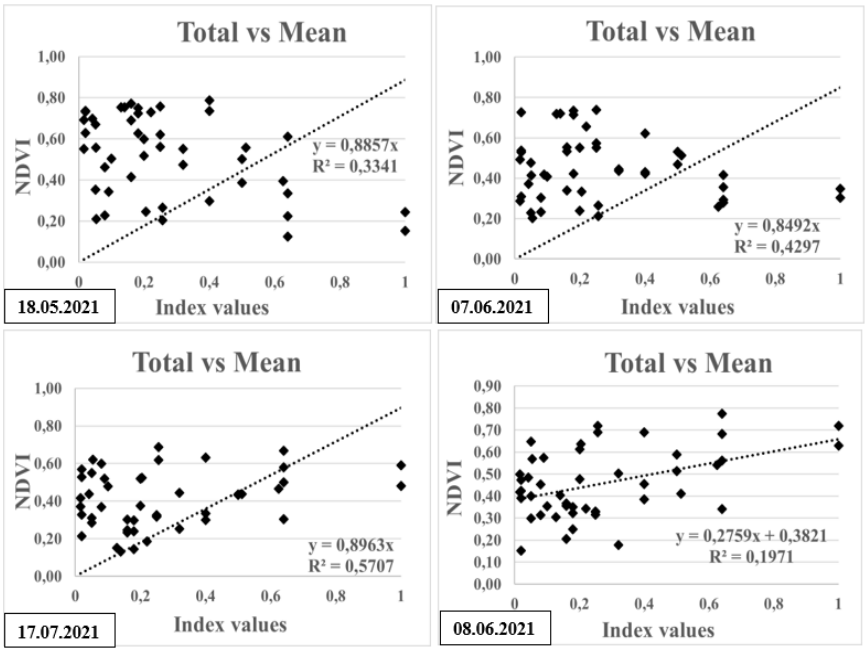


Figure 7. Land suitability index values of rice fields and r^2 values of NDVI values obtained from Sentinel-2A satellite images with different time series.

The highest r^2 values for NDVI were obtained in satellite images of July and August. This situation was associated with the fact that the plant vegetation density of the rice fields reached its maximum value within a month from mid-July. The high NDVI values of the July and August satellite images may also be associated with the shade forming feature of the rice plant (structural or vegetation cover percentage). The abundance of the stem and leaves of the rice plant reduces the reflectance effects of the plant substrate, and thus the enhanced vegetation of the rice allows more reliable estimates of the NDVI reflectance values, an index based on slope (Panda et al., 2010; Mirasi et al., 2019). As a matter of fact, Verhulst et al. (2009) reported that NDVI vegetation indices have a strong correlation with plant physiological parameters, crop yield and biomass.

The lowest r^2 values for NDVI were obtained in satellite images of May and June. In this period (May-June), the rice plant is in tillering period and tillering is one of the basic rice growth stages that determines the final yield. During the first six months after the start of the rice season (until the end of June), it is known that there is almost no correlation between the spectral reflectance values and the AUI values, considering the short height of the rice plant and the fact that it is a plant that grows constantly under water (Franch et al., 2021). This is considered as an important reason why the relationship between NDVI values and AUI values of satellite images in May and June is lower than in July and August.

Table 6. Land suitability index values of rice lands of Yeşil Küre Agricultural Enterprise and NDVI values of different time series satellite images

		NDVI Values			
Mapping Unit	Land Suitability Index	18.05.2021 Sentinel-2A	07.06.2021 Sentinel-2A	17.07.2021 Sentinel-2A	06.08.2021 Sentinel-2A
B11	0.02	0.6305	0.3091	0.2132	0.1530
B7	0.02	0.7319	0.5377	0.5690	0.4742
B8	0.016	0.6916	0.2862	0.4149	0.4987
B9	0.02	0.7359	0.7263	0.3275	0.3910
K11	0.016	0.5512	0.4934	0.3717	0.4185
K12	0.02	0.7368	0.5280	0.5277	0.4237
YOL	--	--	--	--	--
A1	0.4	0.8119	0.8233	0.8135	0.8203
Ba.2	0.32	0.7416	0.7217	0.6324	0.5041
Ba.4-A4	1	0.6086	0.6348	0.7634	0.8094
Ba3	0.64	0.8059	0.7391	0.6923	0.7842
E2	0.64	0.5477	0.5507	0.6835	0.7711
E4-Y3	1	0.7583	0.7677	0.7614	0.7795
E5	0.64	0.7501	0.7662	0.7530	0.7753
K10	0.256	0.7043	0.7114	0.8114	0.8093
K3	0.256	0.7723	0.8009	0.8109	0.8050
K3	0.625	0.7828	0.7541	0.8081	0.8037
K6	0.4	0.8459	0.8108	0.7922	0.7317
K7	0.32	0.7860	0.7860	0.7455	0.7968
K8	0.5	0.7195	0.7766	0.7615	0.7950
K8	0.5	0.8282	0.8011	0.7897	0.8043
K9	0.512	0.8277	0.7542	0.7146	0.7198
Y1-E1	0.25	0.8435	0.8053	0.7691	0.7305
Y2	0.4	0.8481	0.8136	0.7547	0.7351
Y4-A3	0.205	0.2462	0.3331	0.5227	0.6367
Y5	0.16	0.4133	0.3386	0.2319	0.2064
A2	0.18	0.6273	0.4220	0.2983	0.2493
A4	0.2	0.5202	0.2388	0.5191	0.6134
A4	0.16	0.7707	0.5536	0.2460	0.3673
A4	0.18	0.7244	0.7342	0.2395	0.3238
B10	0.22	0.7302	0.6552	0.1863	0.3435
B5-B9	0.16	0.6897	0.5321	0.3012	0.3566
B6	0.25	0.6195	0.5511	0.3192	0.3295
Ba.1	0.18	0.7500	0.7136	0.1442	0.3505
Ba.4-A4	0.2	0.5989	0.5520	0.3741	0.4768
E3	0.14	0.7540	0.7198	0.1325	0.4039
E3	0.25	0.5630	0.5738	0.3178	0.3148
K2	0.128	0.7534	0.7182	0.1519	0.3046
K2	0.1	0.1545	0.1746	0.2079	0.1565
K2	0.08	0.1216	0.1179	0.0786	0.0579
B1	0.08	0.1430	0.1403	0.1470	0.1236
B2	0.054	0.1237	0.1312	0.1880	0.1586
B3	0.042	0.1402	0.1308	0.1027	0.1011
K1	0.05	-0.0218	-0.2451	0.1350	0.1657
O1	0.051	0.1344	0.1119	0.1129	0.1728
O	0.09	0.1067	0.1851	0.1123	0.1321
B	0.05	0.1492	0.1322	0.0876	0.0906

A*: Alaylı, B*: Kalaba, E*: Elifli, K*: Karaköy, O*: Osmanbeyli, Y*: Yörükler.

RE-OSAVI is a plant index that functions with the Red-Edge spectral reflectance band, which is stated to be able to reduce the spectral reflectance values of plants and the substrate reflection effects (Feng et al., 2014), and has a widespread and reliable use in the determination of plant biomass (Fitzgerald et al. et al., 2010). There is a strong correlation between RE-OSAVI and plant chlorophyll content, and the RE-OSAVI index is used in plant yield potential estimation studies (Huang et al., 2017).

The land suitability index values for each land suitability class (S1, S2, S3, and N) of the rice fields obtained from the satellite images of May, June, July, and August dated May, June, July, and August 2021 of Yeşil Küre Agricultural Enterprise and different time series Sentinel-2A satellite images were obtained. The RE-OSAVI values obtained and the r^2 values with which the statistical relationship was established are given in Table 7 and Figure 8, respectively. When the statistical relationship between the RE-OSAVI values obtained from the satellite image of May and the rice suitability index classes (S1, S2, S3, and N) was examined, the r^2 values were found to be 0.7167, 0.9135, 0.0265 and 0.9877, respectively, while the RE-OSAVI values obtained from the satellite image of June were examined. - The r^2 values determined as a result of the statistical relationship between the OSAVI values and the

rice suitability index classes (S1, S2, S3, and N) were determined to be 0.795, 0.873, 0.4725, and 0.9274, respectively.

In addition, the r^2 values obtained as a result of the statistical relationship between the RE-OSAVI values obtained from the satellite image of July and the rice suitability index classes (S1, S2, S3, and N) were 0.8465, 0.915, 0.789, and 0.8872, respectively. When the statistical relationship between the RE-OSAVI values obtained from the satellite image of the rice plant and the rice suitability index classes (S1, S2, S3, and N) was examined, the r^2 values were determined as 0.8162, 0.8907, 0.7987 and 0.9166, respectively.

Table 7. Each land suitability index values of rice fields and RE-OSAVI values of Sentinel-2A satellite images with different time series

Mapping Unit	Land Suitability Index	Land Suitability Class	RE-OSAVI Values			
			18.05.2021 Sentinel-2A	07.06.2021 Sentinel-2A	17.07.2021 Sentinel-2A	06.08.2021 Sentinel-2A
B11	0.02	N	0.5221	0.2285	0.1982	0.1449
B7	0.02	N	0.6483	0.4863	0.5277	0.4361
B8	0.016	N	0.6105	0.2657	0.3853	0.4832
B9	0.02	N	0.6705	0.6843	0.3060	0.3644
K11	0.016	N	0.4682	0.3984	0.3331	0.3746
K12	0.02	N	0.6448	0.4629	0.4619	0.3645
YOL	--	--	--	--	--	--
A1	0.4	S1	0.7384	0.7729	0.7637	0.8375
Ba.2	0.32	S1	0.6684	0.6188	0.6092	0.4404
Ba.4-A4	1	S1	0.5071	0.5591	0.7191	0.8104
Ba3	0.64	S1	0.7445	0.6640	0.6096	0.8017
E2	0.64	S1	0.4385	0.4156	0.5915	0.7111
E4-Y3	1	S1	0.5760	0.6352	0.6285	0.7441
E5	0.64	S1	0.5945	0.6507	0.6071	0.7379
K10	0.256	S1	0.6130	0.5823	0.7785	0.8278
K3	0.256	S1	0.7377	0.7229	0.7868	0.8221
K3	0.625	S1	0.7234	0.6704	0.7734	0.8124
K6	0.4	S1	0.8327	0.7623	0.7033	0.7180
K7	0.32	S1	0.6841	0.7069	0.7229	0.8297
K8	0.5	S1	0.5838	0.7057	0.7466	0.8138
K8	0.5	S1	0.8099	0.7644	0.7675	0.8231
K9	0.512	S1	0.7576	0.6745	0.6849	0.6458
Y1-E1	0.25	S1	0.8308	0.7586	0.7459	0.7176
Y2	0.4	S1	0.8379	0.7521	0.6801	0.7212
Y4-A3	0.205	S2	0.2286	0.2368	0.4463	0.5875
Y5	0.16	S2	0.3517	0.2639	0.1922	0.2002
A2	0.18	S2	0.5489	0.3448	0.2783	0.2354
A4	0.2	S2	0.4573	0.1898	0.4607	0.5657
A4	0.16	S2	0.7066	0.5228	0.2296	0.3397
A4	0.18	S2	0.6465	0.6719	0.2332	0.3003
B10	0.22	S2	0.6243	0.5178	0.1776	0.3186
B5-B9	0.16	S2	0.5771	0.4203	0.2798	0.3265
B6	0.25	S2	0.5282	0.4482	0.2896	0.3067
Ba.1	0.18	S2	0.6251	0.5459	0.1576	0.3322
Ba.4-A4	0.2	S2	0.5132	0.4543	0.3497	0.4378
E3	0.14	S2	0.6186	0.5460	0.1361	0.3606
E3	0.25	S2	0.4915	0.4749	0.2878	0.2954
K2	0.128	S2	0.6493	0.5729	0.1495	0.2804
K2	0.1	S3	0.1098	0.1679	0.1781	0.1727
K2	0.08	S3	-0.0444	0.1081	0.1303	0.1106
B1	0.08	S3	0.1252	0.1149	0.1291	0.1524
B2	0.054	S3	-0.0394	-0.0505	0.1930	0.1510
B3	0.042	S3	0.1322	0.0605	0.0972	0.1057
K1	0.05	S3	-0.0917	-0.3849	0.0779	0.1583
O1	0.051	S3	0.0991	0.0773	0.1214	0.1965
O2	0.09	S3	0.0479	0.0108	0.0840	0.1268
B12	0.05	S3	0.1393	0.1171	0.0863	0.0803

A*: Alaylı, B*: Kalaba, E*: Elifli, K*: Karaköy, O*: Osmanbeyli, Y*: Yörükler.

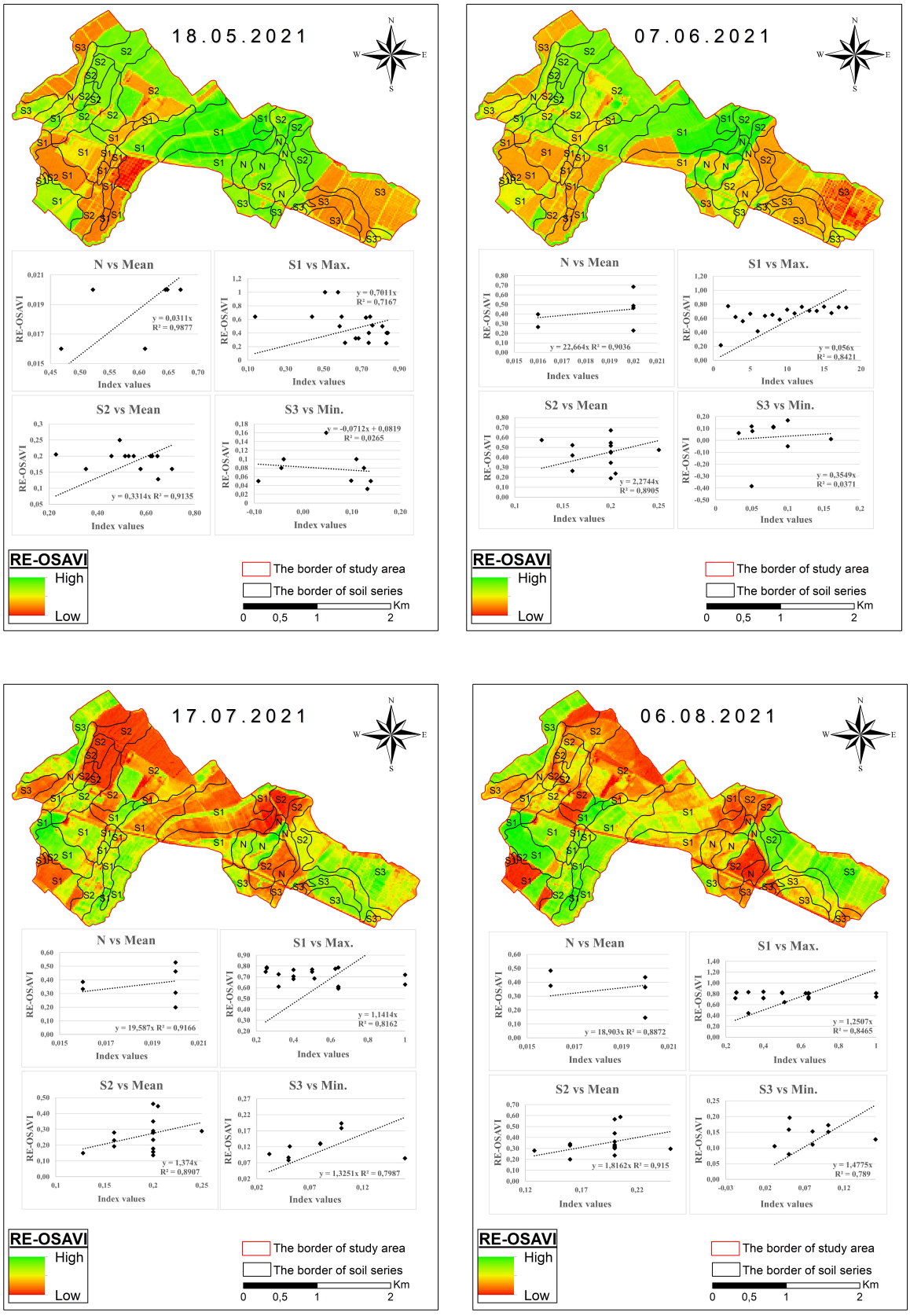


Figure 8. The r^2 values of each land suitability index value of rice fields and RE-OSAVI values obtained from Sentinel-2A satellite images with different time series.

It is thought that the low results of RE-OSAVI values in May and June are due to the fact that this index was calculated to represent the soil series instead of establishing a relationship with the rice land suitability index values. It is also predicted that the effects of climatic and atmospheric conditions may have reduced the vegetation index prediction values. Such problems show the fragile side of using remote sensing for agricultural purposes, especially when the database is limited. For this reason, it is predicted that in future similar studies with spectral vegetation indices, more successful results will be obtained when soil series and reference plant plots of similar size are used (Dedeoğlu et al., 2020).

The r^2 values, in which the statistical relationship is established between the RE-OSAVI values obtained from the satellite images of May, June, July, and August of 2021 dated May, June, July, and August belonging to the Yeşil Küre Farm Land and the land suitability classes (S1, S2, S3, and N) without evaluating them separately, are shown in Figure 9, respectively, and are given in Table 8. According to the r^2 results considered in the statistical evaluation between the RE-OSAVI values without evaluating the land suitability classes separately, the relationship between the RE-OSAVI values obtained from the satellite images of July and August, which were determined to be high, and the suitability index classes (S1, S2, S3, and N). The r^2 values were determined as 0.5732 and 0.6508, respectively. According to the r^2 results, in which the statistical relationship between the land suitability classes (S1, S2, S3, and N) and the RE-OSAVI values was evaluated without evaluating them separately, the r^2 values for the months of May and June, which were determined to be low, were determined as 0.3433 and 0.4012, respectively. According to these results, it was seen that the use of RE-OSAVI index of rice plants in late vegetation periods is suitable for estimating soil fertility potential, but not in early vegetation periods.

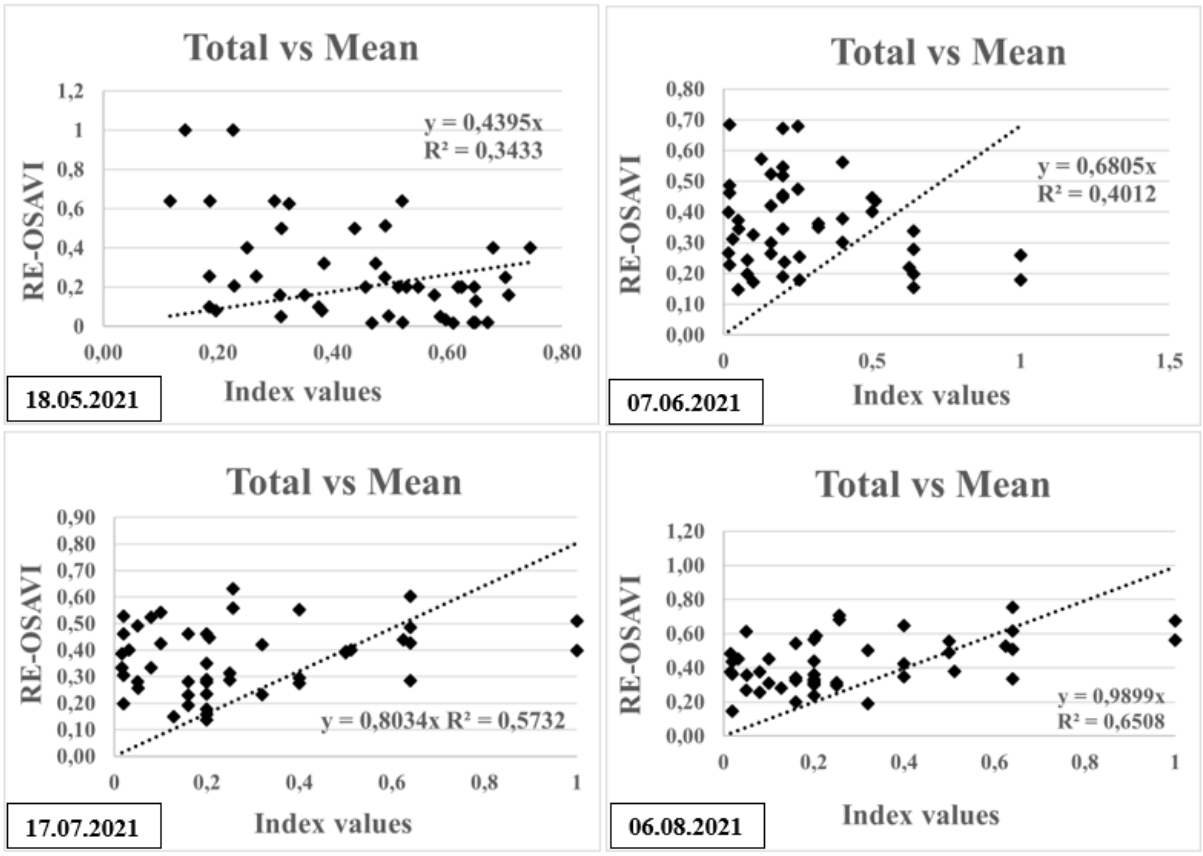


Figure 9. Land suitability index values of rice fields and r^2 values of RE-OSAVI values obtained from Sentinel-2A satellite images with different time series

Table 8. Land suitability index values of rice fields and RE-OSAVI values of different time series satellite images

Mapping Unit	Land Suitability Index	RE-OSAVI Values			
		18.05.2021 Sentinel-2A	07.06.2021 Sentinel-2A	17.07.2021 Sentinel-2A	06.08.2021 Sentinel-2A
B11	0.02	0.5221	0.2285	0.1982	0.1449
B7	0.02	0.6483	0.4863	0.5277	0.4361
B8	0.016	0.6105	0.2657	0.3853	0.4832
B9	0.02	0.6705	0.6843	0.3060	0.3644
K11	0.016	0.4682	0.3984	0.3331	0.3746
K12	0.02	0.6448	0.4629	0.4619	0.3645
YOL	0.64	0.1168	0.1538	0.6020	0.7552
YOL-A1	0.4	0.2509	0.3008	0.5523	0.6456
Ba.2	0.32	0.4750	0.3618	0.2315	0.1909
Ba.4-A4-Ba	1	0.1422	0.1780	0.5091	0.6747
Ba3	0.64	0.5209	0.3372	0.2846	0.3347
E2	0.64	0.1858	0.1985	0.4855	0.6155
E4-Y3	1	0.2269	0.2587	0.3978	0.5633
E5	0.64	0.2985	0.2786	0.4270	0.5084
K10	0.256	0.1849	0.1792	0.5578	0.6803
K3	0.256	0.2660	0.2547	0.6306	0.7064
K3	0.625	0.3239	0.2196	0.4388	0.5260
K6	0.4	0.6785	0.3789	0.2955	0.3482
K7	0.32	0.3849	0.3495	0.4209	0.5028
K8	0.5	0.3114	0.4007	0.3946	0.4903
K8	0.5	0.4389	0.4463	0.3908	0.5557
K9	0.512	0.4920	0.4367	0.3999	0.3794
Y1-E1	0.25	0.7007	0.6792	0.3129	0.3143
Y2	0.4	0.7449	0.5619	0.2740	0.4230
Y4-A3	0.205	0.2286	0.2368	0.4463	0.5875
Y5	0.16	0.3517	0.2639	0.1922	0.2002
A2	0.18	0.5489	0.3448	0.2783	0.2354
A4	0.2	0.4573	0.1898	0.4607	0.5657
A4	0.16	0.7066	0.5228	0.2296	0.3397
A4	0.18	0.6465	0.6719	0.2332	0.3003
B10	0.22	0.6243	0.5178	0.1776	0.3186
B5-B9	0.16	0.5771	0.4203	0.2798	0.3265
B6	0.25	0.5282	0.4482	0.2896	0.3067
Ba.1	0.18	0.6251	0.5459	0.1576	0.3322
Ba.4-A4-Ba	0.2	0.5132	0.4543	0.3497	0.4378
E3	0.14	0.6186	0.5460	0.1361	0.3606
E3	0.25	0.4915	0.4749	0.2878	0.2954
K2	0.128	0.6493	0.5729	0.1495	0.2804
K2	0.1	0.3755	0.3254	0.4239	0.3101
K2	0.08	0.1964	0.1973	0.5238	0.3752
B1	0.08	0.3802	0.2426	0.3338	0.2559
B2	0.054	0.1853	0.1723	0.5429	0.4509
B3	0.042	0.5964	0.3112	0.4003	0.4499
K1	0.05	0.3103	0.1475	0.4905	0.6109
O1	0.051	0.4975	0.3452	0.2557	0.3566
O	0.09	0.3069	0.2999	0.4610	0.5423
B	0.05	0.5876	0.3734	0.2812	0.2685

A*: Alaylı, B*: Kalaba, E*: Elifli, K*: Karaköy, O*: Osmanbeyli, Y*: Yörükler.

Conclusion

In this study, the statistical relationship between the land suitability indices determined for rice lands belonging to Yeşil Küre Agricultural Enterprise and the spectral vegetation index (NDVI and RE-OSAVI) values calculated by using different time series Sentinel-2A satellite images, and the estimation of the rice productivity potential. A different perspective is presented for viewing and monitoring. First of all, according to the rice conformity assessment study of the farm lands, 6488.9 ha area was determined to be suitable for rice cultivation at S1 and S2 levels, while the 588.9 ha area was determined to be unsuitable. In this study, it was observed that the most successful results for each land suitability class were obtained by using the NDVI index. It has been determined that the RE-OSAVI index gives more accurate results in determining the sparse vegetation, and provides a limited opportunity to monitor cultivars grown in water-saturated land conditions.

The r^2 values, in which the statistical relationship between the rice land suitability index values values were revealed without evaluating the land suitability classes separately, showed that both indices

were not suitable for soil fertility potential estimations in early vegetation periods, but were suitable for soil fertility potential estimations in medium to long vegetation periods. It was concluded that the vegetation indices obtained from the satellite images of the different growth stages of the rice plant can be used as an alternative to determine the critical growth stages of the rice plant. With this study, it is predicted that the use of vegetation indices can help to monitor the rice plant at critical time stages and to intervene in time to possible problems, as well as to ensure the continuity of food safety by getting more yield from the rice plant with these interventions. In addition, this study showed that the spectral capabilities of Sentinel-2A satellite images can be used in similar studies to be done in the future with the ESA-SNAP image processing tool. As a result, this study using vegetation index values obtained from different time series satellite images covering different development stages of rice plants has created an awareness for future research in determining the potentials for the relationships between index values and rice soil quality.

References

Ahmed, G. B., Shariff, A.R.M., Balasundram, S.K., & Fikri bin Abdullah, A. (2016). Agriculture land suitability analysis evaluation based multi criteria and GIS approach. IOP Conference series: *Earth and Environmental Science*, 37, 012044.

Al-Bakri, J.T., & Suleiman, A.S. (2004). NDVI response to rainfall in different ecological zones in Jordan. *International Journal of Remote Sensing*, 25(19), 3897-3912.

Askari, M.S., Cui, J., O'Rourke, S.M., & Holden, N.M. (2015). Evaluation of soil structural quality using VIS–NIR spectra. Soil and Tillage Research, 146, 108–117.

Bagheri, N., Ahmadi, H., Alavipanah, S., & Omid, M. (2012). Soil-line vegetation indices for corn nitrogen content prediction. *International Agrophysics*, 26(2), 103–108.

Barnes, E., Clarke, T., Richards, S., Colaizzi, P., Haberland, J., Kostrzewski, M., Waller, P., Choi, C., Riley, E., Thompson, T., Lascano, R. J., Li, H., & Moran, M.S. (2000). *Coincident detection of crop water stress, nitrogen status and canopy density using ground based multispectral data*. In Proceedings of the Fifth International Conference on Precision Agriculture, Bloomington, MN, USA, 2000 (Vol. 1619).

Blum, W.E.H. (2006). *Soil Resources- The basis of human society and the environment*. Bodenkultur 57, 197–202.

Damian, J.M., Pias, O.H.D.C., Cherubin, M.R., Fonseca, A.Z.D., Fornari, E.Z., Santi, A.L., (2020). Applying the NDVI from satellite images in delimiting management zones for annual crops. *Sci. Agric*. 77 (1).

Dedeoğlu, M., Başayiğit, L., Yüksel, M., & Kaya, F. (2020). Assessment of the vegetation indices on Sentinel-2A images for predicting the soil productivity potential in Bursa, Turkey. *Environmental Monitoring and Assessment*, 192(1), 1-16.

Demir, S., & Başayiğit, L. (2021). Kısıtlı sulama uygulamalarının İHA multispektral algılamaya dayalı vejetasyon indekslerine etkisi. *Yuzuncu Yıl University Journal of Agricultural Sciences*, 31(3), 629-643.

Dengiz, O. (2013). Land suitability assessment for rice cultivation based on GIS modeling. *Turkish Journal of Agriculture and Forestry*. 37: 326-334, DOI: 10.3906/tar-1204-36.

Dengiz, O. (2020). Soil quality ındex for paddy fields based on standard scoring functions and weight allocation method. *Archives of Agronomy and Soil Science*, 66(3), 301-315.

Dengiz, O., & Sağlam, M. (2012). Determination of land productivity index based on parametric approach using GIS technique. *Eurasian Journal of Soil Science*, 1, 51–57.

Doran, J.W., & Parkin, T.B. (1994). *Defining and assessing soil quality*. Defining soil quality for a sustainable environment, 35, 1-21.

Dumanski, J., & Peiretti, R. (2013). Modern concepts of soil conservation. *International soil and water conservation research*, 1(1), 19-23.

Explorer, E. (2000). *Geological Survey* (US). Earth observatory NASA. http://earthobservatory.nasa.gov/Features/MeasuringVegetation.

ESRI, (2010). *ArcGIS user's guide*. http://www.esri.com

FAO, (1983). *Land and Water Development Division. Guidelines: land evaluation for rainfed agriculture*. Food and Agriculture Organization of the United Nations.

FAO (1985). *Guideline: land evaluation for irrigated agriculture*. FAO Soils Bulletin, No. 55, Rome

FAO, I., & ISRIC, I. (2009). *Harmonized world soil database (version 1.1)*. FAO, Rome, Italy and IIASA, Laxenburg, Austria. http://www.fao.org/nr/land/soils/harmonized-world-soildatabase/en.

Feng, W., Guo, B.-B., Wang, Z. J., He, L., Song, X., Wang, Y. H., & Guo, T.C. (2014). Measuring leaf nitrogen concentration in winter wheat using double-peak spectral reflection remote sensing data. *Field Crops Research*, 159: 43–52.

Fitzgerald, G., Rodriguez, D., & O'Leary, G. (2010). Measuring and predicting canopy nitrogen nutrition in wheat using a spectral index—the canopy chlorophyll content index (CCCI). *Field Crops Research*, 116(3), 318–324.

Franch, B., Bautista, A.S., Fita, D., Rubio, C., Tarrazó-Serrano, D., Sánchez, A., Skakun, S., Vermote, E., Becker-Reshef, I., & Uris, A. (2021). Within-Field Rice Yield Estimation Based on Sentinel-2 Satellite Data. *Remote Sensing*, 13(20), 4095.

Gupta, R.K., Vijayan, D., & Prasad, T.S. (2003). Comparative analysis of red-edge hyperspectral indices. *Advances in Space Research*, 32(11), 2217–2222.

Huang, S., Miao, Y., Yuan, F., Gnyp, M., Yao, Y., Cao, Q., Wang, H., Lenz-Wiedemann, V., & Bareth, G. (2017). Potential of RapidEye and WorldView-2 satellite data for improving rice nitrogen status monitoring at different growth stages. *Remote Sensing*, 9(3), 227.

Hufkens K., Melaas, E.K., Foster, T., Ceballos, F., Robles, M., & Kramer, B. (2019). Monitoring crop phenology using a smartphone based near-surface remote sensing approach. *Agricultural and Forest Meteorology*, 265: 327-337.

Jackson, R.D. (1986). Remote sensing of biotic and abiotic plant stress. *Annual Review of Phytopathology*, 24(1), 265–287.

Jia, L., Yu, Z., Li, F., Gnyp, M., Koppe, W., Bareth, G., Miao, Y., Chen, X., & Zhang, F. (2011). Nitrogen status estimation of winter wheat by using an Ikonos satellite image in the north china plain. *Computer and computing technologis in agriculture V. 5th IFIP TC5/SIG 5,1 Conference*, CCTA 2011 Beijing, Cina, October 2011 Proceedings, Part II.

Jiang, L., Liu, Y., Wu, S., & Yang, C. (2021). Analyzing ecological environment change and associated driving factors in China based on NDVI time series data. *Ecological Indicators*, 129: 107933.

Jones, A., Stolbovoy, V., Rusco, E., Gentile, A.R., Gardi, C., Marechal, B., & Montanarella, L. (2009). Climate change in Europe. 2. Impact on soil. A review. *Agronomy for sustainable development*, 29(3), 423-432.

Karlen D.L., Mausbach M.J., Doran J.W., Cline R.G., Harris R.F., & Schuman G.E. (1997). Soil quality: a concept, definition and framework for evaluation. *Soil Sci. Soc. Am. J.* 61, 4–10.

Kerr, J.T., & Ostrovsky, M. (2003). From space to species: ecological applications for remote sensing. *Trends in ecology & evolution*, 18(6), 299-305.

Kokaly, R.F., & Clark, R.N. (1999). Spectroscopic determination of leaf biochemistry using band-depth analysis of absorption features and stepwise multiple linear regression. *Remote Sensing of Environment*, 67(3), 267–287.

Kostrzewski, M., Waller, P., Guertin, P., Haberland, J., Colaizzi, P., Barnes, E., Thompson, T., Clarke, T., Riley, E., & Choi, C. (2003). Ground-based remote sensing of water and nitrogen stress. *Transactions of the ASAE*, 46(1), 29.

Lal R. (2008). *Soils and sustainable agriculture*. A review, Agron. Sustain. Dev. 28, 57–64.

Lal R. (2009). *Soils and food sufficiency*. A review, *Agron. Sustain. Dev*. 29, 113–133.

Larson, W. E., & Pierce, F. J. (1991). *Conservation and enhancement of soil quality*. In Evaluation for sustainable land management in the developing world: Proceedings of the International Workshop on Evaluation for Sustainable Land Management in the Developing World, Chiang Rai, Thailand, 15-21 September 1991.

Lichtfouse, E., Navarrete, M., Debaeke, P., Souchère, V., & Alberola, C. (2009). *Sustainable Agriculture*. Springer, 1st ed., 645 p., ISBN: 978-90-481-2665-1.

Liniger, H.P., Studer, R.M., Hauert, C., & Gurtner, M. (2011). Sustainable land management in practice: guidelines and best practices for Sub-Saharan Africa. *FAO*.

Liu, J., Miller, J. R., Haboudane, D., & Pattey, E. (2004). *Exploring the relationship between red edge parameters and crop variables for precision agriculture*. IEEE International Geoscience and Remote Sensing Symposium (Vol. 2, pp. 1276-1279).

Malczewski, J. (2006). Ordered weighted averaging with fuzzy quantifiers: GIS-based multicriteria evaluation for land-use suitability analysis. *International Journal of Applied Earth Observation and Geoinformation*, 8(4), 270–277.

Matton, N., Canto, G.S., Waldner, F., Valero, S., Morin, D., Inglada, J., Arias, M., Bontemps, S., Koetz, B., & Defourny, P. (2015). An automated method for annual cropland mapping along the season for various globally distributed agrosystems using high spatial and temporal resolution time series. *Remote Sensing*, 7(10): 13208-13232.

Mezera, J., Lukas, V., & Elbl, J. (2017). Evaluation of crop yield spatial variability in relation to variable rate application of fertilizers. *MendelNet*, 24(1), 2017.000.

Mirasi, A., Mahmoudi, A., Navid, H., Valizadeh Kamran, K., & Asoodar, M.A. (2019). Evaluation of sum-NDVI values to estimate wheat grain yields using multi-temporal Landsat OLI data. *Geocarto International*, 36(12), 1309–1324.

Mongkolsawat, C.P., Thirangoon, & Kuptawutinan, P. (2002). *A physical evaluation of landsuitability for rice: A methodological study using GIS*. Computer Centre, Khon Kaen University, Thailand. http://www. gisdevelopment.net.

Moran, M.S., Rahman, A.F., Washburne, J.C., Goodrich, D.C., Weltz, M.A., & Kustas, W.P. (1996). Combining the Penman-Monteith equation with measurements of surface temperature and reflectance to estimate evaporation rates of semiarid grassland. *Agricultural and Forest Meteorology*, 80(2), 87–109.

MTA, (1974). *1:500000 scaled Geological Map of Turkey*. General Directorate of Maps Printing House, 1974, Ankara.

Mueller, L., Schindler, U., Mirschel, W., Shepherd, T.G., Ball, B.C., Helming, K., Rogasik J., Eulenstein F., & Wiggering H. (2010). Assessing the productivity function of soils. *In Sustainable Agriculture*, 2:743– 760.

Özbek, H., Dinç, U., & Kapur, S. (1974). *Detailed Survey and Mapping of Çukurova University Settlement Area Soils*. Ankara University Press, Ankara.

Özcan, H. (2004). *The Effect of Zinc Application on Yield and Zinc, Phosphorus and Phytin Acid Concentration in Some Rice Varieties*. A.U. Natural Science Ins., Soil Department, *from PhD thesis*, Ankara.

Panda, S.S., Ames, D.P., & Panigrahi, S. (2010). Application of vegetation indices for agricultural crop yield prediction using neural network techniques. *Remote Sensing*, 2(3), 673–696.

Pettorelli, N., Vik, J.O., Mysterud, A., Gaillard, J.M., Tucker, C.J., & Stenseth, N.C. (2005). Using the satellite-derived NDVI to assess ecological responses to environmental change. *Trends in Ecology & Evolution*, 20(9), 503-510.

Pradipta, D., (2012). *Analisis Data Time Series NDVI-SPOT Vegetation Untuk Tanaman Padi* (Studi Kasus: Kabupaten Karawang). Institut Pertanian Bogor.

Rogowski, A., & Wolf, J. (1994). Incorporating variability into soil map unit delineations. *Soil Science Society of America Journal*, 58(1), 163–174.

Rondeaux, G., Steven, M., & Baret, F. (1996). Optimization of soil-adjusted vegetation indices. *Remote Sensing of Environment*, 55(2), 95–107.

Sahararini, A.F., & Wibowo, A. (2020). *Estimation of rice productivity using Sentinel-2 imagery with NDVI algorithm in Cariu sub-district, Bogor, West Java*. In IOP Conference Series: Earth and Environmental Science (Vol. 481, No. 1, p. 012056). IOP Publishing.

Salinas-Zavala, C.A., Douglas, A.V., & Diaz, H.F. (2002). Interannual variability of NDVI in northwest Mexico. Associated climatic mechanisms and ecological implications. *Remote Sensing of Environment*, 82(2-3), 417-430.

Savaslı, E., Önder, O., Dayıoğlu, R., Didem, Ö., Karaduman, Y., Özdemir, S., & Özsayın, M. (2021). Ekmeklik Buğdayda Optik Sensör ile Azotlu Gübre Tavsiyesi. *Yuzuncu Yıl University Journal of Agricultural Sciences*, 31(2), 453-465.

Sharabıanı, V.R., Nazarloo, A.S., & Taghınezhad, E. (2019). Prediction of protein content of winter wheat by canopy of near infrared spectroscopy (NIRS), using partial least squares regression (PLSR) and artificial neural network (ANN) models. *Yüzüncü Yıl Üniversitesi Tarım Bilimleri Dergisi*, 29(1), 43-51.

Shou, L., Jia, L., Cui, Z., Chen, X., & Zhang, F. (2007). Using high-resolution satellite imaging to evaluate nitrogen status of winter wheat. *Journal of Plant Nutrition*, 30(10), 1669– 1680.

Soil Survey Staff, (1962). *Soil Survey Manuel*. Agriculture Handbook No:18. Washington D.C.

Sönmez, B. (2003). *Türkiye Çoraklık Kontrol Rehberi*. T.C Tarım ve Köyişleri Bakanlığı Köy Hizmetleri Genel Müdürlüğü, Toptak ve Gübre Araştırma Enstitüsü. Teknik Yayın No: 33.

Sys. C., Ranst, V., Debaveye, J., & Beernaert, F. (1993). *Land Evaluation Part III, Crop Requirements*. Agr. Publication No. 7, ITC Ghent.

Verhulst, N., Govaerts, B., Sayre, K. D., Deckers, J., François, I. M., & Dendooven, L. (2009). Using NDVI and soil quality analysis to assess influence of agronomic management on within-plot spatial variability and factors limiting production. *Plant and Soil*, 317(1), 41–59.

Vohland, M., Ludwig, M., Thiele-Bruhn, S., & Ludwig, B. (2014). Determination of soil properties with visible to near- and mid-infrared spectroscopy: effects of spectral variable selection. *Geoderma*, 223-225: 88–96.

Vorobiova, N., & Chernov, A. (2017). Curve fitting of MODIS NDVI time series in the task of early crops identification by satellite images. *Procedia Engineering*, 201: 184-195.

Walter, C., & Stützel, H. (2009). A new method for assessing the sustainability of land-use systems (I): Identifying the relevant issues. *Ecol. Econ*. 68, 1275–1287.

Wójtowicz, M., Wójtowicz, A., & Piekarczyk, J. (2016). Application of remote sensing methods in agriculture. *Communications in Biometry and Crop Science*, 11(1), 31– 50.

Wu, C., Niu, Z., Tang, Q., & Huang, W. (2008). Estimating chlorophyll content from hyperspectral vegetation indices: modeling and validation. *Agricultural and Forest Meteorology*, 148(8), 1230–1241.

Xue, R., Wang, C., Liu, M., Zhang, D., Li, K., & Li, N. (2019). A new method for soil health assessment based on analytic hierarchy process and meta-analysis. *Science of the Total Environment*, 650, 2771–2777.

Yamada, Y., Suzuki, M., Amorndham, W., & Sukjarn, S. (1995). Plan of the construction of GIS for northeast Thailand. *16th Asian Conference on Remote Sensing, Nakhon Ratchasima, Thailand*. (available online at http://www.a-a-r-s.org/acrs/proceeding/ ACRS1995/Papers/WSI95-4.htm).

Zand, F., & Matinfar, H.R. (2012). Winter wheat yield estimation base upon spectral data and ground measurement. *Annals of Biological Research*, 3(11), 5169–5177.

Zhou, C., Chen, S., Zhang, Y., Zhao, J., Song, D., & Liu, D. (2018). Evaluating metal effects on the reflectance spectra of plant leaves during different seasons in post-mining areas, China. *Remote Sensing*, 10(8), 1211.

JURNAL GEOGRAFI
https://journal.unnes.ac.id/nju/index.php/JG

Klasifikasi Berbasis Objek Citra Satelit Sentinel 2 untuk Pemetaan Perubahan Lahan di Kecamatan Parongpong Kabupaten Bandung Barat

Akhmad E Firlli Dimyati, Lili Somantri, Nanin Trianawati Sugito

Departemen Pendidikan Geografi, Universitas Pendidikan Indonesia, Indonesia

Article Info

Article History
Submitted 2021-12-15
Revised 2021-12-30
Accepted 2022-01-30

Keywords
Land Change, Sentinel 2, Parongpong, OBIA

Abstrak

Kecamatan Parongpong merupakan kawasan pinggiran kota dimana wilayah ini menjadi salah satu wilayah favorit dalam pemilihan wilayah pemukiman, di sisi lain wilayah ini masih di dominasi oleh lahan pertanian. Pentingnya monitoring dalam Perubahan lahan di suatu wilayah terutama wilayah pinggiran kota adalah sangat penting. Penggunaan data citra satelit resolusi menengah akan menjadi pilihan yang baik karena aksesnya yang mudah dan ketersediaan data gratis. Sentinel-2 adalah salah satu Citra satelit resolusi menengah yang dapat diakses gratis dimana memiliki resolusi spasial 10 meter dalam saluran tampak. Metode yang digunakan adalah penginderaan jauh dengan pendekatan OBIA (Object-Based Image Analysis) dengan data temporal selama dua tahun pada tahun 2017-2019. Uji akurasi Citra menghasilkan nilai Akurasi Total (*Overal Accuracy)* sebesar 94,8 % dan nilai *Kappa Accuracy* diperoleh sebesar 95,04%. Dari hasil Penelitian menunjukan bahwa Tingkat perubahan Penggunaan lahan yang terjadi di Kecamatan Parongpong pada kurun waktu dua tahun yaitu dimulai pada tahun 2017 sampai dengan tahun 2019 memiliki laju perubahan pada rentang nilai antara -0,21% sampai dengan 0,17 %. Pengurangan penggunaan lahan terbesar pada semak Belukar dan lahan kosong berkurang sebesar -8,9 Ha dan penambahan terbesar pada penggunaan lahan Pemukiman dan Tempat Kegiatan Sebesar 7,27 Ha. Pola Perubahan yang terjadi hanya pada empat jenis Penggunaan lahan Hutan, Semak Belukar ladang dimana pola perubahan yang terjadi adalah penggunaan lahan hutan menjadi pemukiman dan ladang. Sementara semak belukar menjadi ladang dan Pemukiman.

Abstract

Parongpong sub-district is a suburban area where this area is one of the favorite areas in selecting residential areas, on the other hand this area is still dominated by agricultural land. The importance of monitoring in land change in an area, especially in suburban areas is very important. The use of medium resolution satellite imagery data would be a good choice because of the easy access and availability of free data. Sentinel-2 is one of the free medium resolution satellite imagery which has a spatial resolution of 10 meters in the visible channel. The method used is remote sensing with the OBIA (Object-Based Image Analysis) approach with temporal data for two years in 2017-2019. Image accuracy test resulted in an Overal Accuracy value of 94.8% and a Kappa Accuracy value of 95.04%. The results of the study show that the rate of land use change that occurred in Parongpong Subdistrict in a period of two years, starting in 2017 to 2019, has a rate of change in the value range between -0.21% to 0.17%. The largest reduction in land use was in scrub scrub and empty land by -8.9 Ha and the largest increase in land use for Settlements and Activities by 7.27 Ha. Patterns of change that occur are only in four types of forest land use, bush scrub, where the pattern of change that occurs is the use of forest land to settlement and fields. Meanwhile, shrubs become fields and settlements.

* Address: Jl. Dr. Setiabudhi No. 229 Kota Bandung 40154
E-mail: akhmad.firli@student.upi.edu

© 2022. Published by UNNES. This is an open access article under the CC BY license (http://creativecommons.org/licenses/by/4.0/)

DOI 10.15294/jg.v19i1.33958

p-ISSN 2549-3078 e-ISSN 2549-3094

PENDAHULUAN

Konsentrasi kepadatan penduduk di Provinsi Jawa Barat berpusat pada wilayah Bandung raya yang terdiri dari Kota Bandung, Kota Cimahi, Kabupaten Bandung,Kabupaten Bandung barat dan Sebagian wilayah kabupaten Sumedang, dimana secara berurutan wilayah ini memiliki kepadatan penduduk sebanyak 14.832 Jiwa/, 15.478 Jiwa/, 2.103 Jiwa/ dan 1289 Jiwa/ (BPS Jawa Barat, 2020).

Kota Bandung membentuk kawasan Metropolitan Bandung. Kawasan Metropolitan Bandung memiliki hubungan antar satu wilayah dengan wilayah lainnya, sehingga memiliki kemiripan baik karakter fisik kekotaan maupun kondisi sosial ekonomi masyarakatnya. Adapun wilayah yang termasuk kawasan Metropolitan Bandung yaitu Kota Bandung, Kabupaten Bandung, Kota Cimahi, Kabupaten Bandung Barat, dan sebagian Kabupaten Sumedang. Berdasarkan Peraturan Pemerintah No.47 tentang Rencana Tata Ruang Wilayah Provinsi Jawa Barat, Metropolitan Bandung salah satu kawasan unggulan di Jawa Barat dan Nasional.

Konsentrasi penduduk di perkotaan akan berdampak pada daerah atau kota sekitarnya, sehingga mobilitas penduduk dan kebutuhan lahan terutama di permukiman akan semakin tinggi. Mahdiyah (2019) mendukung pernyataan tersebut, yang menyatakan bahwa: pertambahan penduduk di suatu wilayah akan berdampak kompleks pada semua aspek kehidupan, termasuk dampaknya terhadap tata guna lahan atau tata guna lahan yang selalu berubah secara dinamis. Selain itu, Wibisana (2002) berpendapat bahwa tingkat perkembangan fisik kota dan wilayah perbatasan wilayah saat ini dipengaruhi oleh perkembangan wilayah perkotaan, dan perkembangan wilayah perkotaan akan dialihkan ke pinggiran kota.

Kecamatan Parongpong merupakan kawasan pinggiran kota, salah satu kawasan yang sangat strategis ketika memilih kawasan hunian. Pasalnya, lahan di kawasan ini masih didominasi oleh kawasan pertanian dan jumlah penduduk yang tinggal sedikit. Selain itu, kawasan ini juga jauh dari pusat kota, namun dekat dengan pusat keramaian, seperti perguruan tinggi dan aksesibilitas jalan raya, serta tidak terlalu jauh dari akses transportasi yang menghubungkan dari dan ke Kota Bandung dan sekitarnya. Pentingnya monitoring dalam Perubahan lahan di suatu wilayah adalah sangat penting, metode monitoring yang dapat dimonitor secara garis besar dapat melalui pengamatan langsung maupun tidak langsung. Namun, pengamatan langsung bisa mahal dan memakan waktu, sehingga data penginderaan jauh dapat digunakan untuk pemantauan tutupan lahan (Martono, 2008). Zhang et al. (2014) mengemukakan bahwa ada tiga cara atau metode yang dapat mengekstraksi citra penginderaan jauh perkotaan, yaitu: berdasarkan pada indeks spektrum spektral, kombinasi data spektral dan informasi berbasis spasial, serta menggunakan data multi sensor. Satelit Sentinel-2 adalah resolusi spektralnya dapat menghasilkan 13 saluran sinyal multi-spektral, termasuk sensor sinar tampak, inframerah-dekat dan inframerah gelombang pendek, dan resolusi spasialnya dapat dikatakan cukup tinggi, pada pita merah. 10 meter, resolusi spektralnya mudah diperoleh dan gratis digunakan. Berbagai ekstraksi informasi citra satelit sedang dikembangkan saat ini dalam keilmuan Penginderaan jauh, salah satunya adalah OBIA (Object Based Image Analysis), pemilihan metode ini menjadi pilihan karena dalam proses klasifikasinya bukan hanya mempertimbangkan pada aspek spectral namun juga pada aspek spasial objek (S.Wibowo 2013).

METODE

Lokasi penelitian terletak di Kecamatan Parongpong. Lokasi geografis Kecamatan Parongpong terletak pada koordinat 107°33’ 36” LS sampai 107°37’ 12” LS dan 06°43’ 12” BT sampai 06°52’ 48” BT

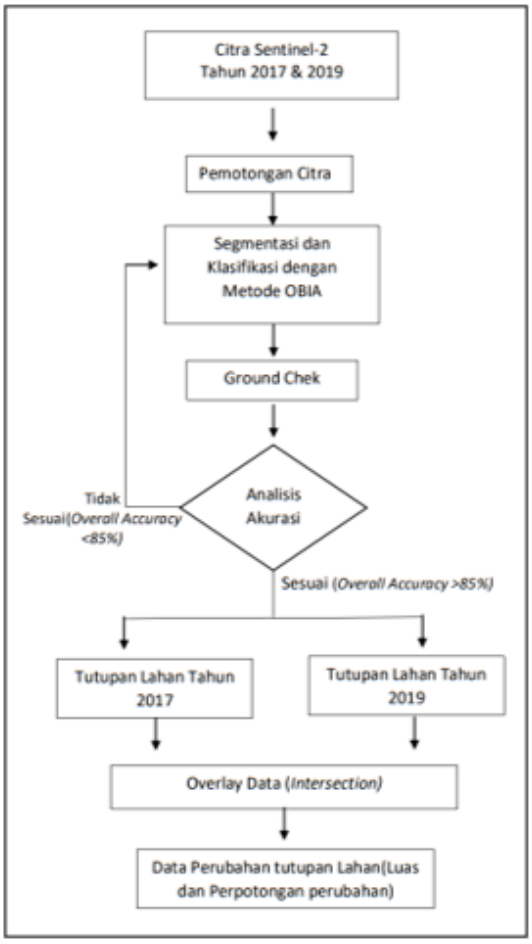
Populasi dalam penelitian kali ini adalah seluruh penggunaan lahan di Kecamatan Parongpong. Variable yang diukur pada penelitian ini adalah perubahan tutupan lahan dengan indikator dua data tutupan lahan tahun 2017 dan tahun 2019 yang dibandingkan. Dalam penelitian ini, metode yang digunakan adalah metode penginderaan jauh dengan pendekatan *OBIA (Klasifikasi Berbasis Objek).* Teknik Interpretasi Citra digital yang digunakan dalam penelitian kali ini adalah metode OBIA terdiri dari dua langkah utama: segmentasi dan klasifikasi. Metode OBIA merupakan langkah semi otomatis yang dapat digunakan untuk mengekstraksi kelas penggunaan / tutupan lahan dari citra satelit. Proses ini dapat dilakukan sebagai hasil dari gambar berbasis objek klasifikasi. Lalu poses selanjutnya adalaha proses klasifikasi dimana hasil segmentasi dikelompokan sesusai kelas masing-masing.

Tabel 1. Parameter Proses Segmentasi *OBIA*

Band with for seed point generation	5
Neoghbourhoud	4 (Neumann)
Distance	Feature space and Position
Number of cluster	6

Sumber: Hasil Penelitian 2020

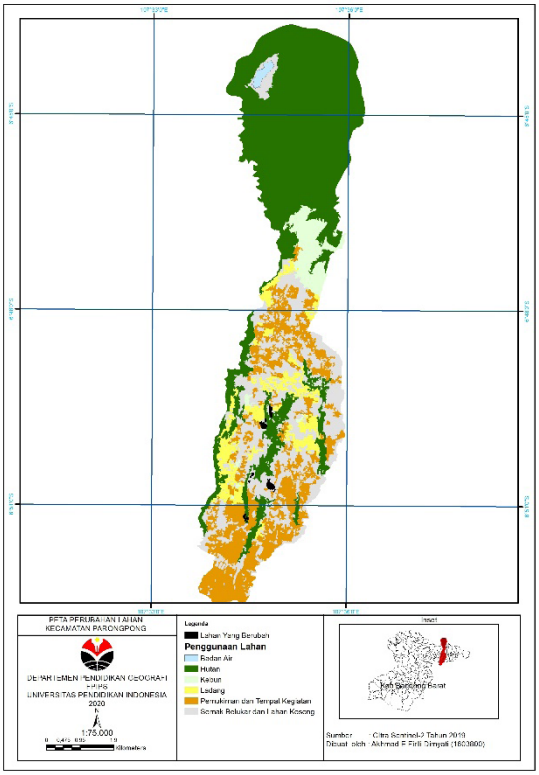
Sebelum melakukan analisis perlu dilakukan uji akurasi terlebih dahulu karena langkah Uji akurasi dalam interpretasi peta sangat krusial karena bisa berdampak signifikan pada hasil penelitian. Menurut Danoedoro (2012: 331), ambang batas presentasi akurasi secara keseluruhan adalah sebesar 85%. Nilai tersebut merupakan ambang batas minimum untuk dapat diterimanya hasil interpretasi citra sebuah penelitian.



Sumber: Penelitian tahun 2020
Gambar 1. Alur Penelitian

HASIL DAN PEMBAHASAN

Nilai ambang diterimanya sebuah hasil interpretasi adalah memiliki nilai >85%. Hasil perhitungan di atas nilai *Overal Accuracy* diperoleh sebesar 94,8% dan *Kappa Accuracy* diperoleh sebesar 95,04% sehingga dapat disimpulkan bahwa hasil interpretasi citra dapat digunakan**.** Tingkat perubahan Penggunaan lahan yang terjadi di Kecamatan Parongpong pada kurun waktu dua tahun yaitu dimulai pada tahun 2017 sampai dengan tahun 2019 memiliki laju perubahan pada rentang nilai antara -0,21% sampai dengan 0,17 %.

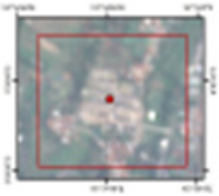
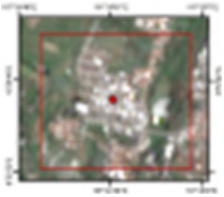
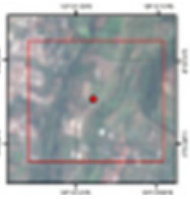
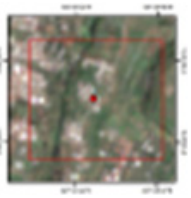
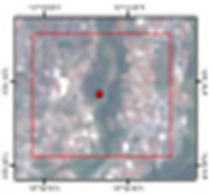
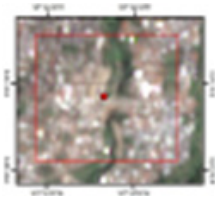
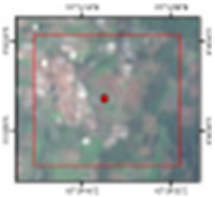
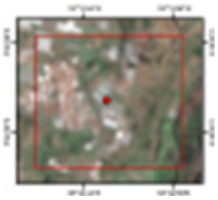
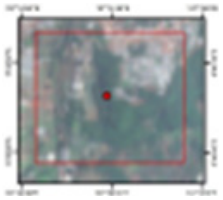
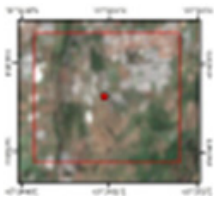


Sumber: Citra Satelit Sentinel 2;Hasil Penelitian Tahun 2020
Gambar 2. Peta Perubahan Penggunaan lahan Kecamatan Parongpong Tahun 2017-2019

Pengurangan penggunaan lahan terbesar pada semak Belukar dan lahan kosong berkurang sebesar -8,9 Ha dan penambahan terbesar pada penggunaan lahan Pemukiman dan Tempat Kegiatan Sebesar 7,27 Ha sementara untuk Jenis Penggunaan Lahan Badan air dan Kebun tidak mengalami perubahan. Jika melihat data dan berasumsi nilai rata-rata kenaikan dan penurunan pertahun pada masing-masing penggunaan lahan adalah sebesar -2,145 Ha/Tahun.

Pola Perubahan yang terjadi hanya pada empat jenis Penggunaan lahan dan lima wilayah Desa yaitu Desa Cihanjuang, Desa Cihanjuang Rahayu, Desa Cigugur Girang, Desa Sariwangi

Tabel 2. *Matriks Perbandingan Perubahan Lahan*

	Data Tahun 2017		Data Tahun 2019	
	Penggunaan Lahan	Tampilan Citra Satelit	Penggunaan Lahan	Tampilan Citra Satelit
107,580426 -6,844921	Semak Belukar dan Lahan Kosong		Pemukiman dan tempat Kegiatan	
107,575289 -6,842676	Semak Belukar dan Lahan Kosong		Pemukiman dan Tempat Kegiatan	
107,573779 -6,852882	Hutan		Pemukiman dan Tempat Kegiatan	
107,578475 -6,829207	Semak Belukar dan Lahan Kosong		Ladang	
107,580329 -6,825982	Hutan		Ladang	

Sumber : Penelitian tahun 2020

dan Desa Karyawangi.

Secara umum citra Sentinel 2 dengan pengolahan metode OBIA dapat mendeteksi perubahan lahan yang terjadi dalam kurun waktu yang singkat dan wilayah yang memiliki penggunaan lahan yang relatif homogen, namun kurang baik dalam mendeteksi wilayah yang memiliki karakteristik wilayah heterogen dan tidak memiliki pola lahan yang beragam karena terdapat pixel campuran, dimana dua jenis tutupan lahan dapat masuk ke dalam satu pixel yang sama karena resolusi spasial yang hanya 10x10 meter atau luasan yang terdeteksi per satu pixel sebesar 100m2. Tingkat perubahan lahan yang terjadi di Kecamatan Parongpong menunjukan bahwa perubahan yang terjadi dalam kurun waktu dua tahun yang paling tinggi adalah adanya areal penggunaan lahan baru berupa hutan menjadi pemukiman dan ladang serta pola perubahan lain adalah berupa semak belukar menjadi Ladang dan Pemukiman. Berdasarkan Penelitian As-syakur (2012) bahwa perubahan penggunaan lahan di sebuah kawasan yang berupa wilayah pertanian dan lahan yang digunanakan untuk hutan akan mengalamai pengurangan luas pada periode waktu tertentu, sementara untuk pemukiman dan lahan kosong/ semak belukar cenderung mengalami kenaikan luas lahan dalam periode waktu yang sama. Dalam penelitian ini Kecamatan Parongpong mengalami perbedaan dalam penambahan dan pengurangan lahan dimana penambahan lahan pertanian berupa ladang dan pemukiman yang

Tabel 3. *Matriks Pola Perubahan Lahan*

		Tahun 2019						
Ba		Ht	Kb	Ld	Pk	Sb	Total	
	Ba	20,11	0	0	0	0	0	20,11
	Ht	0	1966,78	0	2,41	1,88	0	1971,07
	Kb	0	0	192,752	0	0	0	192,752
Tahun 2017	Ld	0	0	0	280,237	0	0	280,237
	Pk	0	0	0	0	801,407	0	801,407
	Sb	0	0	0	3,502	5,398	947,666	956,566
	Total	20,11	1966,78	192,752	286,149	808,685	947,666	4222,142

Sumber : Penelitian tahun 2020

bertambah sementara penggunaan lahan hutan dan semak belukar/lahan kosong yang mengalami penurunan jumlah luasan lahan. Penambahan luas lahan Pemukiman mengindikasikan bahwa kebutuhan akan pemukiman di Kecamatan Parongpong begitu banyak dan juga penambahan wilayah pertanian Konversi lahan .

SIMPULAN

Tingkat perubahan Penggunaan lahan yang terjadi di Kecamatan Parongpong pada kurun waktu dua tahun yaitu dimulai pada tahun 2017 sampai dengan tahun 2019 memiliki laju perubahan pada rentang nilai antara -0,21% sampai dengan 0,17 %. Pengurangan penggunaan lahan terbesar pada semak Belukar dan lahan kosong berkurang sebesar -8,9 Ha dan penambahan terbesar pada penggunaan lahan Pemukiman dan Tempat Kegiatan Sebesar 7,27 Ha.

Pola Perubahan yang terjadi hanya pada empat jenis Penggunaan lahan Hutan, Semak Belukar ladang dimana pola perubahan yang terjadi adalah penggunaan lahan hutan menjadi pemukiman dan ladang. Sementara semak belukar menjadi ladang dan Pemukiman. Perubahan yang terjadi berada pada lima wilayah Desa yaitu Desa Cihanjuang, Desa Cihanjuang Rahayu, Desa Cigugur Girang, Desa Sariwangi dan Desa Karyawangi.

DAFTAR PUSTAKA

Arsyad, S. (1989). *Pengawetan tanah dan air*. Bogor:Departemen Ilmu tanah IPB.

As-syakur, A., Adnyana, I., Arthana, I. W., & Nuarsa, I. W. (2012). Enhanced built-up and bareness index (EBBI) for mapping built-up and bare land in an urban area. *Remote Sensing*, *4*(10), 2957-2970.

Badan Pusat Statistik Jakarta Pusat , (2015). *Statistik Indonesia Tahun 2015*. Jakarta Pusat : Badan Pusat Statistik

Danoedoro, P. (2012). *Pengantar Penginderaan Jauh Digital*.Penerbit Andi: Yogyakarta

Giyarsih, S.R. (2001). Gejala Urban Sprawl sebagai Pemicu Proses Densifikasi Permukiman di Daerah Pinggiran Kota (Urban Fringe Area). [Jurnal]. *Jurnal Pembangunan Wilayah*, vol 12 No. 1/Maret, hal 40-45.

Marangoz, A. M., Sekertekin, A., & Akçin, H. (2017). Analysis of land use land cover classification results derived from Sentinel-2 image. *Proceedings of the 17th International Multidisciplinary Scientific GeoConference Surveying Geology and Mining Ecology Management, SGEM*, 25-32.

Martono, D. N. (2008). Aplikasi teknologi penginderaan jauh dan uji validasinya untuk deteksi penyebaran lahan sawah dan penggunaan/ penutupan lahan. In *Seminar Nasional Aplikasi Teknologi Informasi (SNATI)* (Vol. 1, No. 1).

Phiri, D., Simwanda, M., Salekin, S., R Nyirenda, V., Murayama, Y., & Ranagalage, M. (2020). Sentinel-2 Data for Land Cover/Use Mapping: A Review. *Remote Sensing*, *12*(14), 2291.

Turner, V. B., Shalamzari, M. J. and Farajollahi, A., (2017), Sediment and soil nutrient loss under simulated rainfall, *Journal of the Faculty of Forestry Instanbul University*, 67 (1), 37-48.

Wibowo, T. S., & R Suharyadi, R. S. (2012). Aplikasi Object-Based Image Analysis (OBIA) untuk Deteksi Perubahan Penggunaan Lahan Menggunakan Citra ALOS AVNIR-2. *Jurnal Bumi Indonesia*, *1*(3).

Zhang, J., Li, P., & Wang, J. (2014). Urban built-up area extraction from Landsat TM/ETM+ images using spectral information and multivariate texture. *Remote Sensing*, *6*(8), 7339-7359.

JURNAL GEOGRAFI
https://journal.unnes.ac.id/nju/index.php/JG

Klasifikasi Berbasis Objek Citra Satelit Sentinel 2 untuk Pemetaan Perubahan Lahan di Kecamatan Parongpong Kabupaten Bandung Barat

Akhmad E Firlli Dimyati, Lili Somantri, Nanin Trianawati Sugito

Departemen Pendidikan Geografi, Universitas Pendidikan Indonesia, Indonesia

Article Info

Article History
Submitted 2021-12-15
Revised 2021-12-30
Accepted 2022-01-30

Keywords
Land Change, Sentinel 2, Parongpong, OBIA

Abstrak

Kecamatan Parongpong merupakan kawasan pinggiran kota dimana wilayah ini menjadi salah satu wilayah favorit dalam pemilihan wilayah pemukiman, di sisi lain wilayah ini masih di dominasi oleh lahan pertanian. Pentingnya monitoring dalam Perubahan lahan di suatu wilayah terutama wilayah pinggiran kota adalah sangat penting. Penggunaan data citra satelit resolusi menengah akan menjadi pilihan yang baik karena aksesnya yang mudah dan ketersediaan data gratis. Sentinel-2 adalah salah satu Citra satelit resolusi menengah yang dapat diakses gratis dimana memiliki resolusi spasial 10 meter dalam saluran tampak. Metode yang digunakan adalah penginderaan jauh dengan pendekatan OBIA (Object-Based Image Analysis) dengan data temporal selama dua tahun pada tahun 2017-2019. Uji akurasi Citra menghasilkan nilai Akurasi Total (*Overal Accuracy)* sebesar 94,8 % dan nilai *Kappa Accuracy* diperoleh sebesar 95,04%. Dari hasil Penelitian menunjukan bahwa Tingkat perubahan Penggunaan lahan yang terjadi di Kecamatan Parongpong pada kurun waktu dua tahun yaitu dimulai pada tahun 2017 sampai dengan tahun 2019 memiliki laju perubahan pada rentang nilai antara -0,21% sampai dengan 0,17 %. Pengurangan penggunaan lahan terbesar pada semak Belukar dan lahan kosong berkurang sebesar -8,9 Ha dan penambahan terbesar pada penggunaan lahan Pemukiman dan Tempat Kegiatan Sebesar 7,27 Ha. Pola Perubahan yang terjadi hanya pada empat jenis Penggunaan lahan Hutan, Semak Belukar ladang dimana pola perubahan yang terjadi adalah penggunaan lahan hutan menjadi pemukiman dan ladang. Sementara semak belukar menjadi ladang dan Pemukiman.

Abstract

Parongpong sub-district is a suburban area where this area is one of the favorite areas in selecting residential areas, on the other hand this area is still dominated by agricultural land. The importance of monitoring in land change in an area, especially in suburban areas is very important. The use of medium resolution satellite imagery data would be a good choice because of the easy access and availability of free data. Sentinel-2 is one of the free medium resolution satellite imagery which has a spatial resolution of 10 meters in the visible channel. The method used is remote sensing with the OBIA (Object-Based Image Analysis) approach with temporal data for two years in 2017-2019. Image accuracy test resulted in an Overal Accuracy value of 94.8% and a Kappa Accuracy value of 95.04%. The results of the study show that the rate of land use change that occurred in Parongpong Subdistrict in a period of two years, starting in 2017 to 2019, has a rate of change in the value range between -0.21% to 0.17%. The largest reduction in land use was in scrub scrub and empty land by -8.9 Ha and the largest increase in land use for Settlements and Activities by 7.27 Ha. Patterns of change that occur are only in four types of forest land use, bush scrub, where the pattern of change that occurs is the use of forest land to settlement and fields. Meanwhile, shrubs become fields and settlements.

* Address: Jl. Dr. Setiabudhi No. 229 Kota Bandung 40154
E-mail: akhmad.firli@student.upi.edu

© 2022. Published by UNNES. This is an open access article under the CC BY license (http://creativecommons.org/licenses/by/4.0/)

DOI 10.15294/jg.v19i1.33958

p-ISSN 2549-3078 e-ISSN 2549-3094

PENDAHULUAN

Konsentrasi kepadatan penduduk di Provinsi Jawa Barat berpusat pada wilayah Bandung raya yang terdiri dari Kota Bandung, Kota Cimahi, Kabupaten Bandung,Kabupaten Bandung barat dan Sebagian wilayah kabupaten Sumedang, dimana secara berurutan wilayah ini memiliki kepadatan penduduk sebanyak 14.832 Jiwa/, 15.478 Jiwa/, 2.103 Jiwa/ dan 1289 Jiwa/ (BPS Jawa Barat, 2020).

Kota Bandung membentuk kawasan Metropolitan Bandung. Kawasan Metropolitan Bandung memiliki hubungan antar satu wilayah dengan wilayah lainnya, sehingga memiliki kemiripan baik karakter fisik kekotaan maupun kondisi sosial ekonomi masyarakatnya. Adapun wilayah yang termasuk kawasan Metropolitan Bandung yaitu Kota Bandung, Kabupaten Bandung, Kota Cimahi, Kabupaten Bandung Barat, dan sebagian Kabupaten Sumedang. Berdasarkan Peraturan Pemerintah No.47 tentang Rencana Tata Ruang Wilayah Provinsi Jawa Barat, Metropolitan Bandung salah satu kawasan unggulan di Jawa Barat dan Nasional.

Konsentrasi penduduk di perkotaan akan berdampak pada daerah atau kota sekitarnya, sehingga mobilitas penduduk dan kebutuhan lahan terutama di permukiman akan semakin tinggi. Mahdiyah (2019) mendukung pernyataan tersebut, yang menyatakan bahwa: pertambahan penduduk di suatu wilayah akan berdampak kompleks pada semua aspek kehidupan, termasuk dampaknya terhadap tata guna lahan atau tata guna lahan yang selalu berubah secara dinamis. Selain itu, Wibisana (2002) berpendapat bahwa tingkat perkembangan fisik kota dan wilayah perbatasan wilayah saat ini dipengaruhi oleh perkembangan wilayah perkotaan, dan perkembangan wilayah perkotaan akan dialihkan ke pinggiran kota.

Kecamatan Parongpong merupakan kawasan pinggiran kota, salah satu kawasan yang sangat strategis ketika memilih kawasan hunian. Pasalnya, lahan di kawasan ini masih didominasi oleh kawasan pertanian dan jumlah penduduk yang tinggal sedikit. Selain itu, kawasan ini juga jauh dari pusat kota, namun dekat dengan pusat keramaian, seperti perguruan tinggi dan aksesibilitas jalan raya, serta tidak terlalu jauh dari akses transportasi yang menghubungkan dari dan ke Kota Bandung dan sekitarnya. Pentingnya monitoring dalam Perubahan lahan di suatu wilayah adalah sangat penting, metode monitoring yang dapat dimonitor secara garis besar dapat melalui pengamatan langsung maupun tidak langsung. Namun, pengamatan langsung bisa mahal dan memakan waktu, sehingga data penginderaan jauh dapat digunakan untuk pemantauan tutupan lahan (Martono, 2008). Zhang et al. (2014) mengemukakan bahwa ada tiga cara atau metode yang dapat mengekstraksi citra penginderaan jauh perkotaan, yaitu: berdasarkan pada indeks spektrum spektral, kombinasi data spektral dan informasi berbasis spasial, serta menggunakan data multi sensor. Satelit Sentinel-2 adalah resolusi spektralnya dapat menghasilkan 13 saluran sinyal multi-spektral, termasuk sensor sinar tampak, inframerah-dekat dan inframerah gelombang pendek, dan resolusi spasialnya dapat dikatakan cukup tinggi, pada pita merah. 10 meter, resolusi spektralnya mudah diperoleh dan gratis digunakan. Berbagai ekstraksi informasi citra satelit sedang dikembangkan saat ini dalam keilmuan Penginderaan jauh, salah satunya adalah OBIA (Object Based Image Analysis), pemilihan metode ini menjadi pilihan karena dalam proses klasifikasinya bukan hanya mempertimbangkan pada aspek spectral namun juga pada aspek spasial objek (S.Wibowo 2013).

METODE

Lokasi penelitian terletak di Kecamatan Parongpong. Lokasi geografis Kecamatan Parongpong terletak pada koordinat 107°33’ 36” LS sampai 107°37’ 12” LS dan 06°43’ 12” BT sampai 06°52’ 48” BT

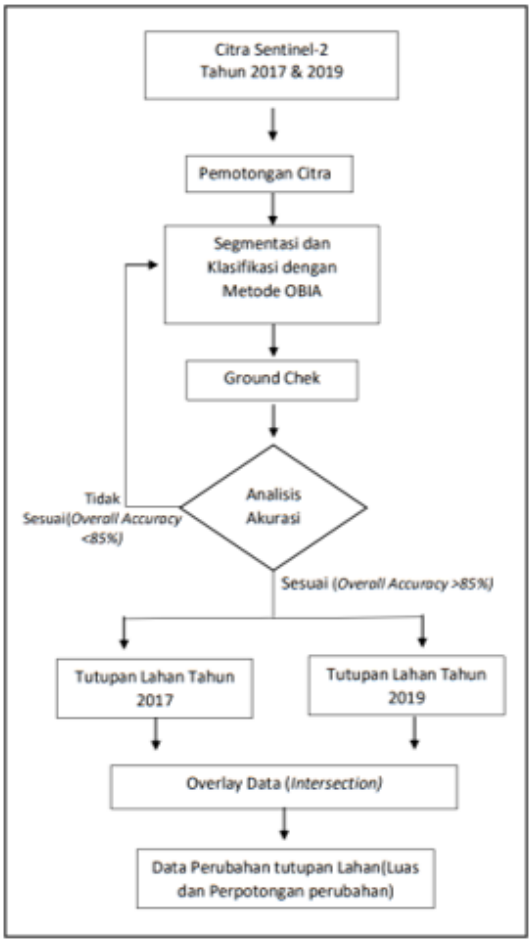
Populasi dalam penelitian kali ini adalah seluruh penggunaan lahan di Kecamatan Parongpong. Variable yang diukur pada penelitian ini adalah perubahan tutupan lahan dengan indikator dua data tutupan lahan tahun 2017 dan tahun 2019 yang dibandingkan. Dalam penelitian ini, metode yang digunakan adalah metode penginderaan jauh dengan pendekatan *OBIA (Klasifikasi Berbasis Objek).* Teknik Interpretasi Citra digital yang digunakan dalam penelitian kali ini adalah metode OBIA terdiri dari dua langkah utama: segmentasi dan klasifikasi. Metode OBIA merupakan langkah semi otomatis yang dapat digunakan untuk mengekstraksi kelas penggunaan / tutupan lahan dari citra satelit. Proses ini dapat dilakukan sebagai hasil dari gambar berbasis objek klasifikasi. Lalu poses selanjutnya adalaha proses klasifikasi dimana hasil segmentasi dikelompokan sesusai kelas masing-masing.

Tabel 1. Parameter Proses Segmentasi *OBIA*

Band with for seed point generation	5
Neoghbourhoud	4 (Neumann)
Distance	Feature space and Position
Number of cluster	6

Sumber: Hasil Penelitian 2020

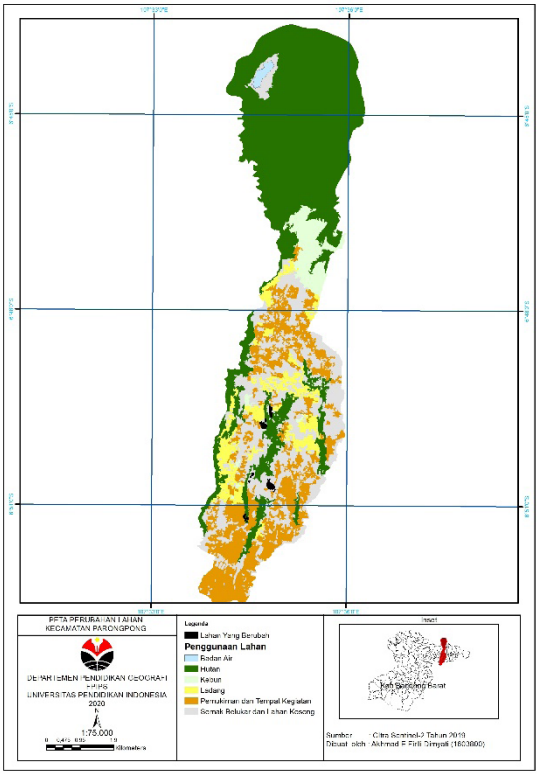
Sebelum melakukan analisis perlu dilakukan uji akurasi terlebih dahulu karena langkah Uji akurasi dalam interpretasi peta sangat krusial karena bisa berdampak signifikan pada hasil penelitian. Menurut Danoedoro (2012: 331), ambang batas presentasi akurasi secara keseluruhan adalah sebesar 85%. Nilai tersebut merupakan ambang batas minimum untuk dapat diterimanya hasil interpretasi citra sebuah penelitian.



Sumber: Penelitian tahun 2020
Gambar 1. Alur Penelitian

HASIL DAN PEMBAHASAN

Nilai ambang diterimanya sebuah hasil interpretasi adalah memiliki nilai >85%. Hasil perhitungan di atas nilai *Overal Accuracy* diperoleh sebesar 94,8% dan *Kappa Accuracy* diperoleh sebesar 95,04% sehingga dapat disimpulkan bahwa hasil interpretasi citra dapat digunakan**.** Tingkat perubahan Penggunaan lahan yang terjadi di Kecamatan Parongpong pada kurun waktu dua tahun yaitu dimulai pada tahun 2017 sampai dengan tahun 2019 memiliki laju perubahan pada rentang nilai antara -0,21% sampai dengan 0,17 %.

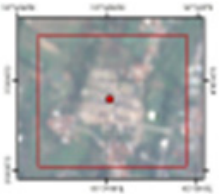
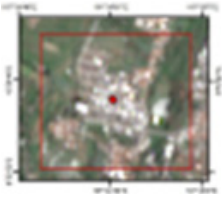
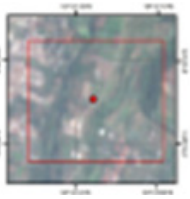
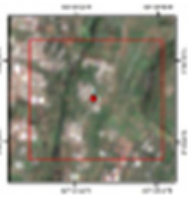
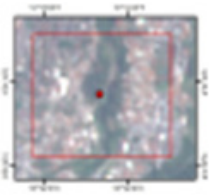
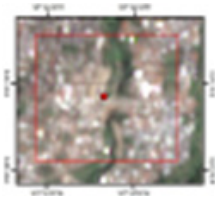
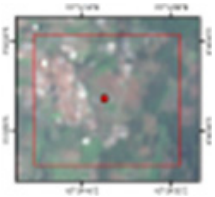
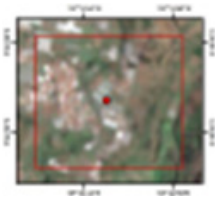
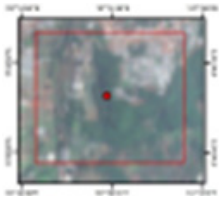
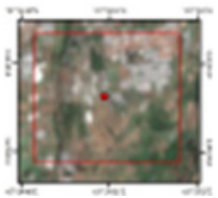


Sumber: Citra Satelit Sentinel 2;Hasil Penelitian Tahun 2020
Gambar 2. Peta Perubahan Penggunaan lahan Kecamatan Parongpong Tahun 2017-2019

Pengurangan penggunaan lahan terbesar pada semak Belukar dan lahan kosong berkurang sebesar -8,9 Ha dan penambahan terbesar pada penggunaan lahan Pemukiman dan Tempat Kegiatan Sebesar 7,27 Ha sementara untuk Jenis Penggunaan Lahan Badan air dan Kebun tidak mengalami perubahan. Jika melihat data dan berasumsi nilai rata-rata kenaikan dan penurunan pertahun pada masing-masing penggunaan lahan adalah sebesar -2,145 Ha/Tahun.

Pola Perubahan yang terjadi hanya pada empat jenis Penggunaan lahan dan lima wilayah Desa yaitu Desa Cihanjuang, Desa Cihanjuang Rahayu, Desa Cigugur Girang, Desa Sariwangi

Tabel 2. *Matriks Perbandingan Perubahan Lahan*

	Data Tahun 2017		Data Tahun 2019	
	Penggunaan Lahan	Tampilan Citra Satelit	Penggunaan Lahan	Tampilan Citra Satelit
107,580426 -6,844921	Semak Belukar dan Lahan Kosong		Pemukiman dan tempat Kegiatan	
107,575289 -6,842676	Semak Belukar dan Lahan Kosong		Pemukiman dan Tempat Kegiatan	
107,573779 -6,852882	Hutan		Pemukiman dan Tempat Kegiatan	
107,578475 -6,829207	Semak Belukar dan Lahan Kosong		Ladang	
107,580329 -6,825982	Hutan		Ladang	

Sumber : Penelitian tahun 2020

dan Desa Karyawangi.

Secara umum citra Sentinel 2 dengan pengolahan metode OBIA dapat mendeteksi perubahan lahan yang terjadi dalam kurun waktu yang singkat dan wilayah yang memiliki penggunaan lahan yang relatif homogen, namun kurang baik dalam mendeteksi wilayah yang memiliki karakteristik wilayah heterogen dan tidak memiliki pola lahan yang beragam karena terdapat pixel campuran, dimana dua jenis tutupan lahan dapat masuk ke dalam satu pixel yang sama karena resolusi spasial yang hanya 10x10 meter atau luasan yang terdeteksi per satu pixel sebesar 100m2. Tingkat perubahan lahan yang terjadi di Kecamatan Parongpong menunjukan bahwa perubahan yang terjadi dalam kurun waktu dua tahun yang paling tinggi adalah adanya areal penggunaan lahan baru berupa hutan menjadi pemukiman dan ladang serta pola perubahan lain adalah berupa semak belukar menjadi Ladang dan Pemukiman. Berdasarkan Penelitian As-syakur (2012) bahwa perubahan penggunaan lahan di sebuah kawasan yang berupa wilayah pertanian dan lahan yang digunanakan untuk hutan akan mengalamai pengurangan luas pada periode waktu tertentu, sementara untuk pemukiman dan lahan kosong/ semak belukar cenderung mengalami kenaikan luas lahan dalam periode waktu yang sama. Dalam penelitian ini Kecamatan Parongpong mengalami perbedaan dalam penambahan dan pengurangan lahan dimana penambahan lahan pertanian berupa ladang dan pemukiman yang

Tabel 3. *Matriks Pola Perubahan Lahan*

		Tahun 2019						
Ba		Ht	Kb	Ld	Pk	Sb	Total	
	Ba	20,11	0	0	0	0	0	20,11
	Ht	0	1966,78	0	2,41	1,88	0	1971,07
	Kb	0	0	192,752	0	0	0	192,752
Tahun 2017	Ld	0	0	0	280,237	0	0	280,237
	Pk	0	0	0	0	801,407	0	801,407
	Sb	0	0	0	3,502	5,398	947,666	956,566
	Total	20,11	1966,78	192,752	286,149	808,685	947,666	4222,142

Sumber : Penelitian tahun 2020

bertambah sementara penggunaan lahan hutan dan semak belukar/lahan kosong yang mengalami penurunan jumlah luasan lahan. Penambahan luas lahan Pemukiman mengindikasikan bahwa kebutuhan akan pemukiman di Kecamatan Parongpong begitu banyak dan juga penambahan wilayah pertanian Konversi lahan .

SIMPULAN

Tingkat perubahan Penggunaan lahan yang terjadi di Kecamatan Parongpong pada kurun waktu dua tahun yaitu dimulai pada tahun 2017 sampai dengan tahun 2019 memiliki laju perubahan pada rentang nilai antara -0,21% sampai dengan 0,17 %. Pengurangan penggunaan lahan terbesar pada semak Belukar dan lahan kosong berkurang sebesar -8,9 Ha dan penambahan terbesar pada penggunaan lahan Pemukiman dan Tempat Kegiatan Sebesar 7,27 Ha.

Pola Perubahan yang terjadi hanya pada empat jenis Penggunaan lahan Hutan, Semak Belukar ladang dimana pola perubahan yang terjadi adalah penggunaan lahan hutan menjadi pemukiman dan ladang. Sementara semak belukar menjadi ladang dan Pemukiman. Perubahan yang terjadi berada pada lima wilayah Desa yaitu Desa Cihanjuang, Desa Cihanjuang Rahayu, Desa Cigugur Girang, Desa Sariwangi dan Desa Karyawangi.

DAFTAR PUSTAKA

Arsyad, S. (1989). *Pengawetan tanah dan air*. Bogor:Departemen Ilmu tanah IPB.

As-syakur, A., Adnyana, I., Arthana, I. W., & Nuarsa, I. W. (2012). Enhanced built-up and bareness index (EBBI) for mapping built-up and bare land in an urban area. *Remote Sensing*, *4*(10), 2957-2970.

Badan Pusat Statistik Jakarta Pusat , (2015). *Statistik Indonesia Tahun 2015*. Jakarta Pusat : Badan Pusat Statistik

Danoedoro, P. (2012). *Pengantar Penginderaan Jauh Digital*.Penerbit Andi: Yogyakarta

Giyarsih, S.R. (2001). Gejala Urban Sprawl sebagai Pemicu Proses Densifikasi Permukiman di Daerah Pinggiran Kota (Urban Fringe Area). [Jurnal]. *Jurnal Pembangunan Wilayah*, vol 12 No. 1/Maret, hal 40-45.

Marangoz, A. M., Sekertekin, A., & Akçin, H. (2017). Analysis of land use land cover classification results derived from Sentinel-2 image. *Proceedings of the 17th International Multidisciplinary Scientific GeoConference Surveying Geology and Mining Ecology Management, SGEM*, 25-32.

Martono, D. N. (2008). Aplikasi teknologi penginderaan jauh dan uji validasinya untuk deteksi penyebaran lahan sawah dan penggunaan/ penutupan lahan. In *Seminar Nasional Aplikasi Teknologi Informasi (SNATI)* (Vol. 1, No. 1).

Phiri, D., Simwanda, M., Salekin, S., R Nyirenda, V., Murayama, Y., & Ranagalage, M. (2020). Sentinel-2 Data for Land Cover/Use Mapping: A Review. *Remote Sensing*, *12*(14), 2291.

Turner, V. B., Shalamzari, M. J. and Farajollahi, A., (2017), Sediment and soil nutrient loss under simulated rainfall, *Journal of the Faculty of Forestry Instanbul University*, 67 (1), 37-48.

Wibowo, T. S., & R Suharyadi, R. S. (2012). Aplikasi Object-Based Image Analysis (OBIA) untuk Deteksi Perubahan Penggunaan Lahan Menggunakan Citra ALOS AVNIR-2. *Jurnal Bumi Indonesia*, *1*(3).

Zhang, J., Li, P., & Wang, J. (2014). Urban built-up area extraction from Landsat TM/ETM+ images using spectral information and multivariate texture. *Remote Sensing*, *6*(8), 7339-7359.

MONITORING MODEL OF LAND COVER CHANGE FOR THE INDICATION OF DEVEGETATION AND REVEGETATION USING SENTINEL-2

Samsul Arifin[1]*,Tatik Kartika[1], Dede Dirgahayu[1], and Gatot Nugroho[1]
[1]Remote Sensing Applications Center – National Institute of Aeronautics and Space (LAPAN)
*e-mail: samsul_lapan@yahoo.com

Received: 11 August 2020; Revised: 17 December 2020; Approved: 21 December 2020

Abstract. Information on land cover change is very important for various purposes, including the monitoring of changes for environmental sustainability. The objective of this study is to create a monitoring model of land cover change for the indication of devegetation and revegetation using data from Sentinel-2 from 2017 to 2018 of the Brantas watershed. This is one of the priority watersheds in Indonesia, so it is necessary to observe changes in its environment, including land cover change. Such change can be detected using remote sensing data. The method used is a hybrid between Normalized Difference Vegetation Index (NDVI) and Normalized Burn Ratio (NBR) which aims to detect land changes with a focus on devegetation and revegetation by determining the threshold value for vegetation index (ΔNDVI) and open land index (ΔNBR). The study found that the best thresholds to detect revegetation were Δ NDVI > 0.0309 and Δ NBR < 0.0176 and to detect devegetation Δ NDVI < - 0.0206 and Δ NBR > 0.0314. It is concluded that Sentinel-2 data can be used to monitor land changes indicating devegetation and revegetation with established NDVI and NBR threshold conditions.

Keywords*: Model, Monitoring. Land Cover, Sentinel-2, devegetation, revegetation*

1 INTRODUCTION

Geobiophysics is one of the parameters for determining the phenomenon of land surface change. It has been applied by several researchers using the vegetation index and open/burned land index from optical satellite data. The vegetation index describes the level of greenness of plants, using a mathematical combination of the red band and NIR (Near-Infrared) band (Lillesand & Kiefe, 1997). According to Ryan (1997), the calculation of the Normalized Difference Vegetation Index (NDVI) is based on the principle that green plants grow very effectively by absorbing radiation in the red spectrum region of Photosynthetic Active Radiation (PAR), and strongly reflect sunlight from the infrared region close to the range value indices -1 to 1. The vegetation index has been used in numerous studies on a global scale of vegetation and to map drought, devegetation and deforestation (Horning **,** Juli. Robinson, Eleanor Sterling, Turner, and Spector, 2010; Kartika et al., 2018). Determination of the extraction of forest identification geobiophysical parameters can be made using the NDVI model with a threshold value with SATELIT LAPAN -3 data (Arifin, S., Kartika, T., & Carolita, I., 2019).

In general, NDVI with a combination of red and infrared specimens is an index that is widely used to identify signs of burning land (Chuvieco, E., Martin, M.P., & Palacios, A ., 2002., 2002). In addition, there have been many developments in the method of identifying burnt land/forests through the single band method (Near IR, Mid IR, Spectral thermal temperature Brightness) and the ratio band vegetation index. Research on the detection of burnt land has been widely conducted globally

http://dx.doi.org/10.30536/j.ijreses.2020.v17.a3385 @National Institute of Aeronautics and Space of Indonesia (LAPAN)

using low to medium resolution remote sensing satellite data, such as that from MODIS (Martín M.P., & Díaz-Delgado R., 2002; Roy, D.P, Boschettm, L., & Triffm, S.N., 2002; Chuvieco et al., 2005); from NOAA-AVHRR (Barbosa, P.M., Pereira, J.M.C., & Grégoire, J. M., 1998); Nielsen, T.T., Mbow, C., & Kane R., 2002);; Nielsen et al., 2002); and from SPOT VEGETATION (Silva, J.M.N, Cadima, J.F.C.L., Pereira, J.M.C. M. Grégoire., 2004). This study aims to map mangrove density in Arakan village and to determine the best NDVI results from the band combination used (Philiani, I, Saputra, L, Harvianto, L., & Muzaki, A.A., 2016). However, it should be noted that low and medium resolution data cannot detect burnt areas of less than 25 ha well (Miettinen, 2007). NDVI, the Normalized Burn Ratio (NBR), Soil-adjusted Vegetation Index (SAVI), Modified Soil-Adjusted Vegetation Index (MSAVI), and multivariate component (Principle Component Analysis, Tasseled Cap-greenness, Tasseled Cap-wetness) (Escuin, 2007) will be compared by the calculation of field data using the Composite Burn Index (CBI) method. The results show that the NBR index using the Near Infrared (NIR) and Shortwave Infrared (SWIR) spectral has a high correlation with the field data (CBI), especially in forest vegetation, in comparison to other indices. NIR and SWIR radiation spectral are exceptionally good at separating burnt and unburned land. Decreases in the tree canopy and water content after changes due to fire can be represented well by the SWIR spectrum, which has increased reflection (Key & Benson 1999; Escuin et al., 2007).NBR can be used to identify burned areas using SPOT-4 (Parwati et al., 2012). According to the index theory, NBR would be optimal in quantifying fire severity. Although previous studies have reported a high correlation between fire severity as measured in the field and satellite-derived NBR, our results provide no evidence for this (Roy et al., 2006). The formula is similar to a NDVI, except that it uses NIR and SWIR portions of the electromagnetic spectrum (Key & Benson, 1999). The TIRS band has a 100-metre spatial resolution but can be resampled to 30 metres for it to be used to identify burned scar areas. SWIR bands (TM bands 5 and 7 in Landsat 5 and 7 systems) as an NBR composite can be used to detect and map burnt areas. The Thermal Infrared Sensor (TIRS) algorithm which was used to detect fires and SWIR, which was used to detect water stress in vegetation and burned vegetation, will be seen in green, and both will become darker when burning takes place. This method modifies the dNBR (pre-NBR-post-NBR) composite (Indratmoko & Rizqihandar, 2019).

Based on several examples of studies on the utilization of NDVI and NBR geobiophysical information extracts, it is necessary to use this geobiophysical combination as a requirement for the devegetation and revegetation of land.

The objective of this study is to create a monitoring model of land cover change for the indication of devegetation and revegetation using Sentinel-2 data from 2017 to 2018. The definition of devegetation used is when there is a decrease in the appearance of the green level in the image (Aldrian & Sucahyono, 2013), while revegetation is shown by an increase in the appearance of the green level in the image at a certain location compared to the previous time.

2 MATERIALS AND METHODOLOGY

The Sentinel-2 satellite uses remote sensing technology that is easily obtained for analysis of spatial information. The satellite is a medium resolution type and has a temporal resolution of 5 days. Sentinel-2 is faster than Landsat, which has temporal resolution of 16 days. The data can be used to monitor land and

coastal cover. The Sentinel-2 Multi-spectral Instrument (MSI) has 13 spectral bands: four bands (Bands 2, 3, 4 and 8) with a resolution of 10m; six (Bands 5, 6, 7, 8a, 11 and 12) with a spatial resolution of 20m; and three (Bands 1, 9 and 10) with a spatial resolution of 60m. Sentinel-2 is complements Landsat-7 and 8 and can also be used for other themes, such as spatial planning, agro/environmental monitoring, water resources, forests and vegetation, carbon resources, and global agricultural products (The European Spance Agency, 2015)

The research location was the Brantas watershed in East Java Province (Figure 2-1). The data used in the study were Sentinel-2A multi-temporal data for 2017 and 2018 (Figure 2-2).

2.3 Sentinel Characteristics

Sentinel-2 is a European wide-swath, high-resolution, multi-spectral imaging mission. The full mission specification of the twin satellites, flying in the same orbit but phased at 180°, is designed to give a high revisit frequency of 5 days at the Equator and with orbital swath width is 290 km.

2.3.1 Sentinel-2 MSI

The Sentinel-2 Multi-spectral Instrument (MSI) measures the earth's reflected radiance in 13 spectral bands consisting of three levels of spatial resolution: four bands at 10 meters , six bands at 20 meters and three bands at 60 meters. Sentinel-2 is supporting Copernicus land monitoring studies with an imaging mission to monitor vegetation, soil and water cover, as well as to observe inland waterways and coastal areas. The data is designed to be modified and adapted by users interested in areas such as spatial planning and the monitoring of the agro-environment, water, forests and vegetation, land carbon and natural resources, and global crops.

The spatial resolution of Sentinel-2 depends on the spectral band, as shown in Table 2.1.

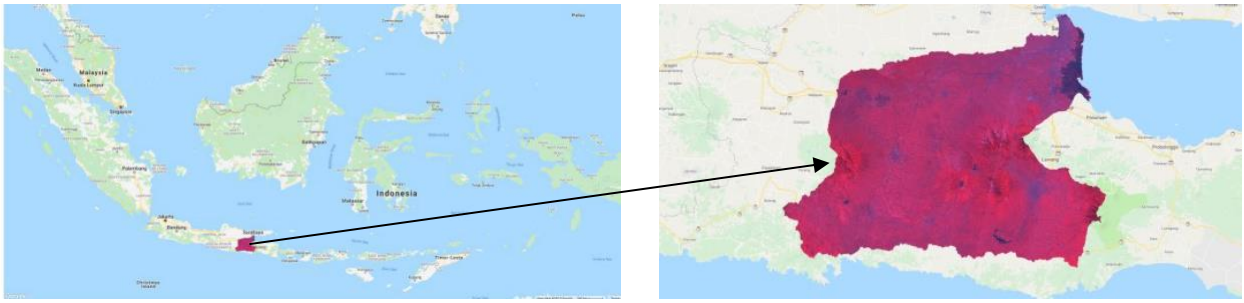


Figure 2-1: Research location: the Brantas Watershed in East Java



Figure 2-2: Sentinel-2 Data 2017-2018

Table 2-1. Spatial Resolution of Sentinel-2

Sentinel-2 Bands	Central Wavelength (μ)	Resolution (m)
Band 1: Coastal Aerosol	0.443	60
Band 2: Blue	0.490	10
Band 3: Green	0.560	10
Band 4: Red	0.665	10
Band 5: Vegetation Red Edge	0.705	20
Band 6: Vegetation Red Edge	0.740	20
Band 7: Vegetation Red Edge	0.783	20
Band 8: NIR	0.842	10
Band 8A: Vegetation Red Edge	0.865	20
Band 9: Water Vapour	0.945	60
Band 10: SWIR-Cirrus	1.375	60
Band 11: SWIR	1.610	20
Band 12: SWIR	2.190	20

2.3.3 Normalized Difference Vegetation Index (NDVI)

The NDVI quantifies vegetation by measuring the difference between near-infrared (which vegetation strongly reflects) and red light (which vegetation absorbs). As shown below, NDVI uses the NIR and red channels in its formula:

$$NDVI = \frac{NIR - Red}{NIR + Red} \quad (2\text{-}1)$$

Healthy vegetation (chlorophyll) reflects more near-infrared (NIR) and green light compared to other wavelengths, but absorbs more red and blue light. Therefore, we see vegetation as green. If it were possible to see near-infrared, this would also show strong vegetation. The satellite sensors of Sentinel-2 both have the necessary NIR and red bands. The result of this formula generates a value between -1 and +1.

$$\Delta NDVI = NDVI_{t1} - NDVI_{t2} \quad (2\text{-}2)$$

where $NDVI_{t1}$ is NDVI at the initial time and $NDVI_{t2}$ is NDVI at the final time.

2.3.4 Normalized Burn Ratio (NBR)

The NBR is used to identify burned areas. The formula is similar to a NDVI, except that it uses near-infrared (NIR) and shortwave-infrared (SWIR) portions of the electromagnetic spectrum (Key & Benson, 1999).

$$NBR = \frac{NIR - SWI}{NIR + SWIR} \quad (2\text{-}3)$$

$$\Delta NBR = NBR_{t1} - NBR_{t2} \quad (2\text{-}4)$$

where NBR_{t1} is NBR at the initial time and NBR_{t2} is NBR at the final time.

The NIR and SWIR parts of the electromagnetic spectrum are a powerful combination of bands for the index to use, given that vegetation is reflected strongly in the NIR region of the electromagnetic spectrum and weakly in the SWIR (see Figure 2-3).

Plants are reflected very strongly on the NIR spectrum, but weak on the SWIR spectrum, the combination of the NIR and SWIR spectra is excellent for identifying areas of burned land (wood / bark burnt) and soil / earth US Forest Service

The NBR index was originally developed for use with Landsat TM and ETM+ bands 4 and 7, but it will work with any multi-spectral sensor with an NIR band between 760-900 nm and a SWIR band between 2080-2350 nm. Therefore, this index can be used with both Landsat-8, MODIS and other multi (and hyper) spectral sensors.

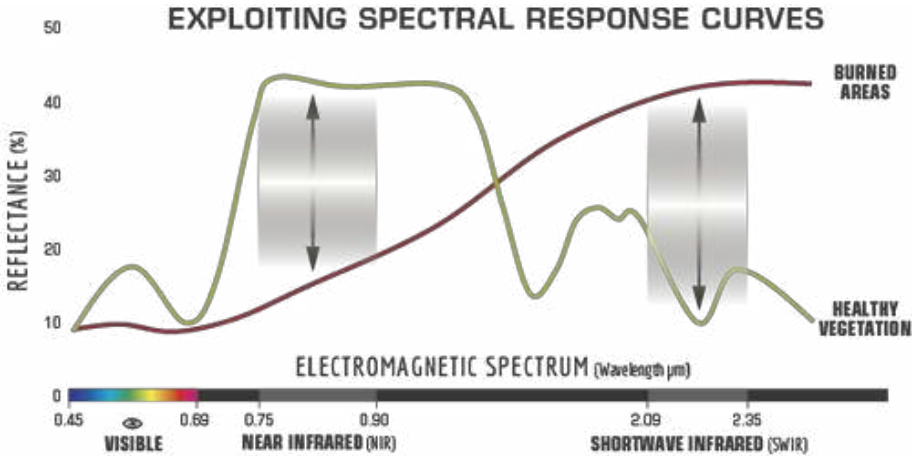


Figure 2-3: Exploiting Spectral Response Curves of Burned Areas with Healthy Vegetation
Source: US Forest Service, 2017

Based on the USGS, NBR succeeded to level 2 derived from Landsat from Landsat 4–5 (TM)), Landsat 7 (ETM +), and Landsat 8 (OLI) / (TIRS), so that it became a Level-2 Surface Reflectance product.

It is calculated as a ratio between the NIR and SWIR values in a traditional fashion (NIR - SWIR) / (NIR + SWIR). In Landsat 4-7, NBR = (Band 4 – Band 7) / (Band 4 + Band 7). In Landsat 8, NBR = (Band 5 – Band 7) / (Band 5 + Band 7).

NBR is delivered as a single band product, specified as shown in the Table 2-2.

Table 2-2: Landsat Surface Reflectance-derived Normalized Burn Ratio (NBR) Specifications

Attribute	Value
Long Name	Normalized Burn Ratio
Short Name	LC8NBR, LE7NBR, LT5NBR, or LT4NBR
File Name	*_sr_nbr.tif
Data Type	Signed 16-bit Integer
Units	Spectral Index (Band Ratio)
Valid Range	-10,000 — 10,000
Fill Value	-9999
Saturate Value	20,000
Scale Factor	*0.0001

Source : USGS Earth Resources Observation and Science (EROS) Center Science Processing Architecture (ESPA) On Demand Interface (ESPA).

2.3.5 Determination of the Threshold

In previous example, the threshold of NDVI and NBR single data was ascertained visually by comparison between 2017 and 2018 using the trial and error

In previous studies that correlated between LAPAN, KLHK and WRI, the NDVI and NBR single data threshold was visually confirmed by comparison between 2017 and 2018 using trial and error. method. However, this research was conducted by observing changes in the vegetation index (NDVI) and in the open land index (NBR). Differences between NDVI and NBR between 2017 and 2018 were minimal as a threshold to identify indications of changes in land cover. This was determined by sampling the difference between the NDVI and NBR points.

To detect revegetation and devegetation, the threshold requirements of each index were used. Revegetation can be expressed using equation 5 and devegetation by equation 6.

$$If\ (NDVI > n\ and\ NBR < m),\ then\ class\ 1 \quad (2\text{-}5)$$

$$If\ (NDVI < n\ and\ NBR > m),\ then\ class\ 2 \quad (2\text{-}6)$$

where n is the NDVI threshold, m is the NBR threshold. The revegetation area (class 1) is based on the result of equation 2-5, and the revegetation area (class 2) is based on the result of equation 2-6.

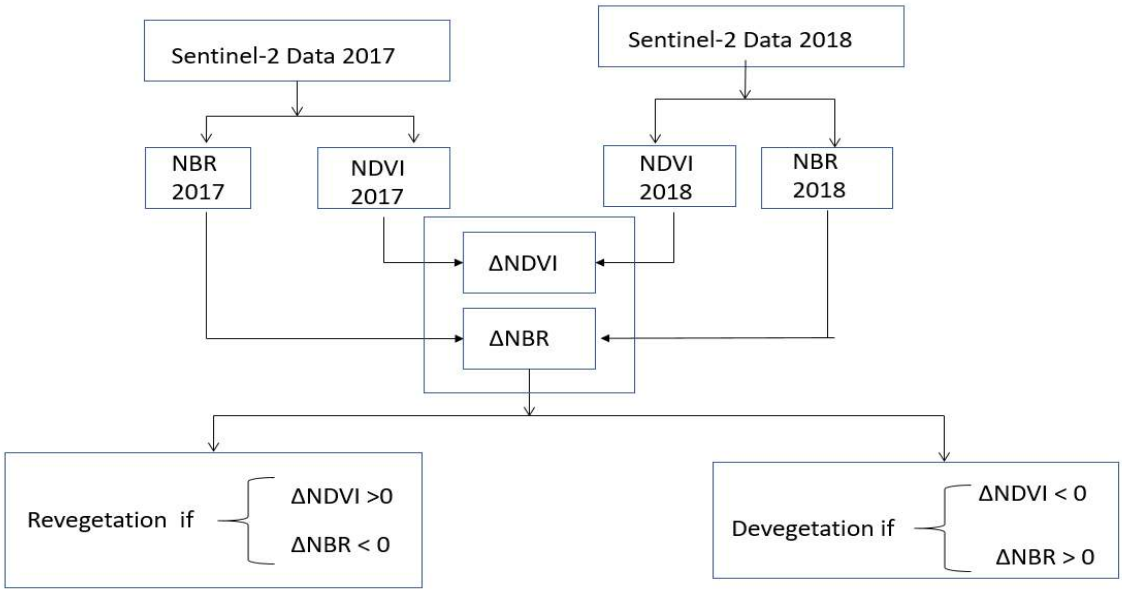


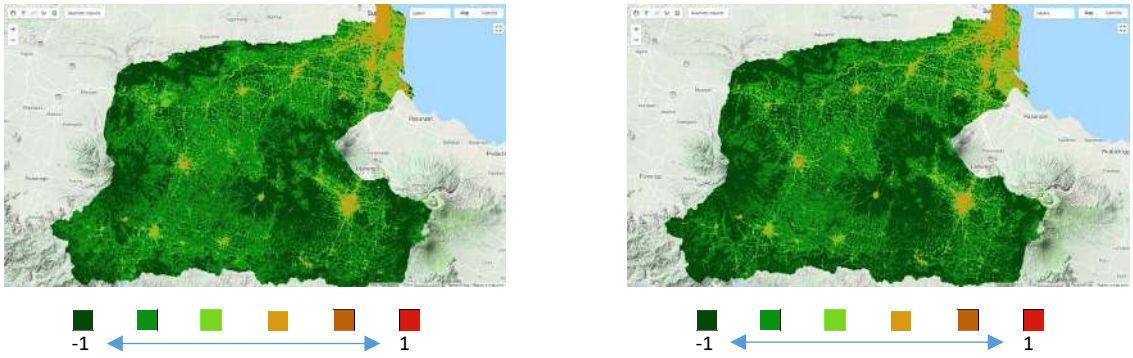
Figure 2-4: Flow diagram of the research development.

3 RESULTS AND DISCUSSION

The results from equations 1 and 3 are shown in Figures 3.1 and 3.2. Figure 3.1(a) shows the annual mean NDVI images for 2017, while 3.1(b) shows those for 2018 for the Brantas watershed. Figure 3.2(a) shows the annual mean NBR images for 2017 and 3.2(b) those for 2018. Visually, the NDVI and NBR imagery from 2017 and 2018 shows no changes in land cover. However, a digital assessment shows there is a change in land cover, indicated by a change in the NDVI and NBR values from 2017 to 2018. If the NDVI in 2018 is lower than that of 2017 and the NBR in 2018 is higher than that of 2017, then land cover is indicated to be devegetated; the sample data are shown in Figure 3.3. Conversely, if the value of NDVI in 2018 is higher than that of 2017 and if the NBR in 2018 is lower than that of 2017, then this indicates land cover revegetation, as shown in Figure 3-4. Figure 3-1 shows images of NDVI in 2017 and 2018, with an index value of -1 to 1. This value is depicted by the gradation of colour from light to dark, namely yellow, green and dark green, which shows the level of green of the vegetation.

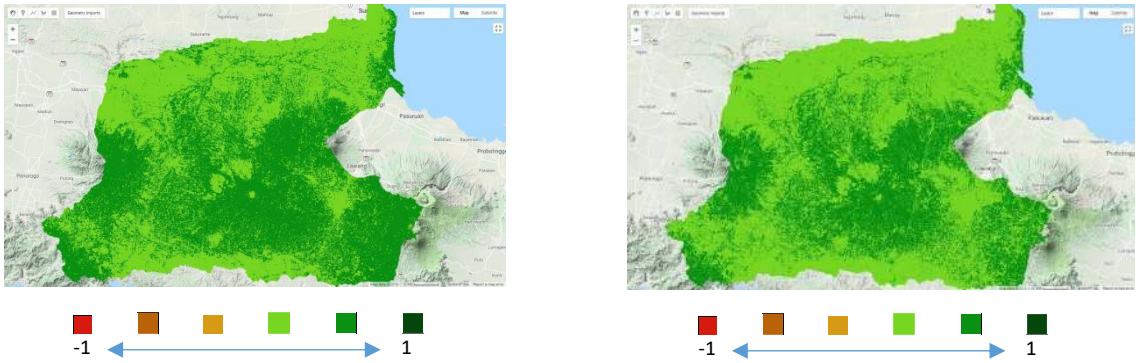
Figure 3-2 shows NBR images from 2017 and 2018, with the NBR index value from -1 to 1, which shows the level of land openness. The light green colour indicates a greater level of land openness than that shown in dark green. Figure 3-3(a) shows an image of the results of the 2017 and 2018 NDVI change analysis. The level of vegetation change is divided into three classes based on the ΔNDVI value interval, as shown in Table 3.2. Figure 3-3(b) shows an image of the results of the analysis of NBR changes in 2017 and 2018. The level of vegetation change is also divided into three classes based on the ΔNBR value interval, as shown in Table 3.3.

http://dx.doi.org/10.30536/j.ijreses.2020.v17.a3385 @National Institute of Aeronautics and Space of Indonesia (LAPAN)



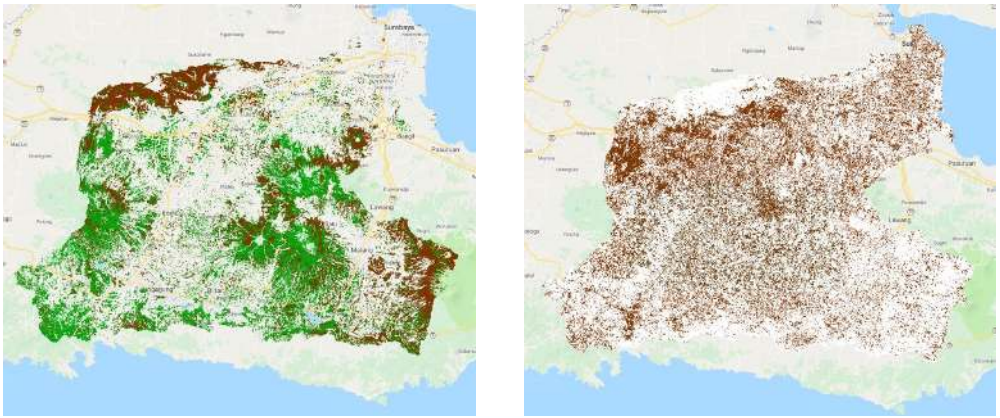
(a) NDVI 2017 (b) NDVI 2018

Figure 3-1: NDVI 2017-2018



NBR 2017 NBR 2018

Figure 3-2: NBR 2017-2018



(a) Change in vegetation in 2017-2018 (b) Change in open land in 2017-2018

Figure 3-3: Change in vegetation and open land 2017-2018.

Table 3-2. NDVI 2017-2018 Changes

No	ΔNDVI (2017-2018)	NDVI Change	Colour
1	>-1	No Change	
2	-1 to 0	Small Change	
3	0 to 1	Large Change	

Table 3-3. NBR 2017-2018 Changes

No	ΔNBR (2017-2018)	NBR Change	Colour
1	>-1	No Change	
2	-1 to 0	Small Change	
3	0 to 1	Large Change	

http://dx.doi.org/10.30536/j.ijreses.2020.v17.a3385
@National Institute of Aeronautics and Space of Indonesia (LAPAN)

Revegetation and devegetation areas were determined by application of the threshold of Δ NDVI and Δ NDVI, obtained from several sample points which were visually experiencing changes, as shown in figures 3-3, 3-4 and 3-5 Example Revegetation and devegetation. The results of the sample points obtained by the threshold for identifying indications of revegetation and devegetation are shown in Figure 3-6.

The threshold obtained to determine the existence of revegetation was ΔNDVI= 0.0309 and ΔNBR= -0.0176, while ΔNDVI= -0.0206 and ΔNBR= 0.0314 was the threshold for devegetation. Based on these calculations, the spatial information of revegetation and devegetation obtained is shown in Figure 3-6.

Spatial revegetation locations can be determined using the equation 5 algorithm, namely if Δ NDVI > 0.0309 and Δ NBR < 0.0176; and the spatial location of devegetation can also be determined using the equation 5 algorithm, namely if Δ NDVI < - 0.0206 and Δ NBR > 0.0314.

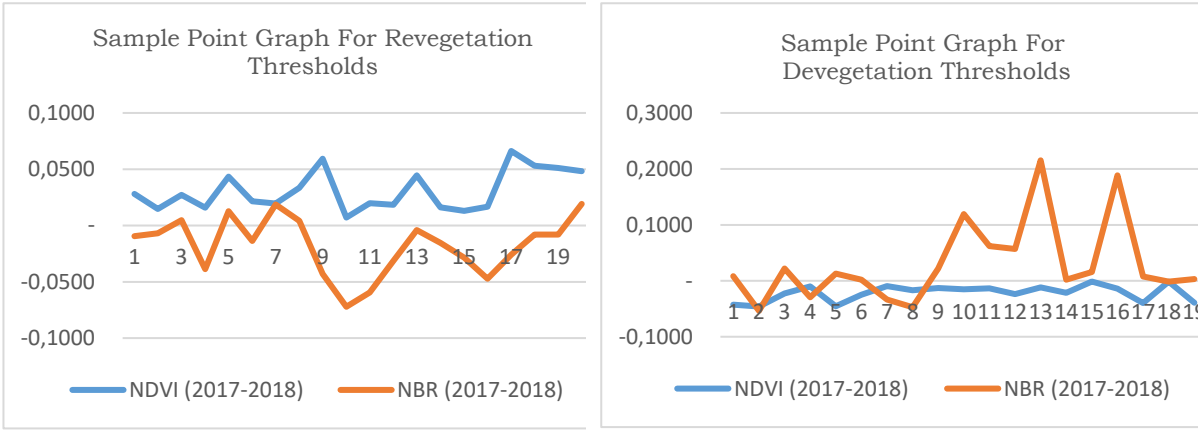
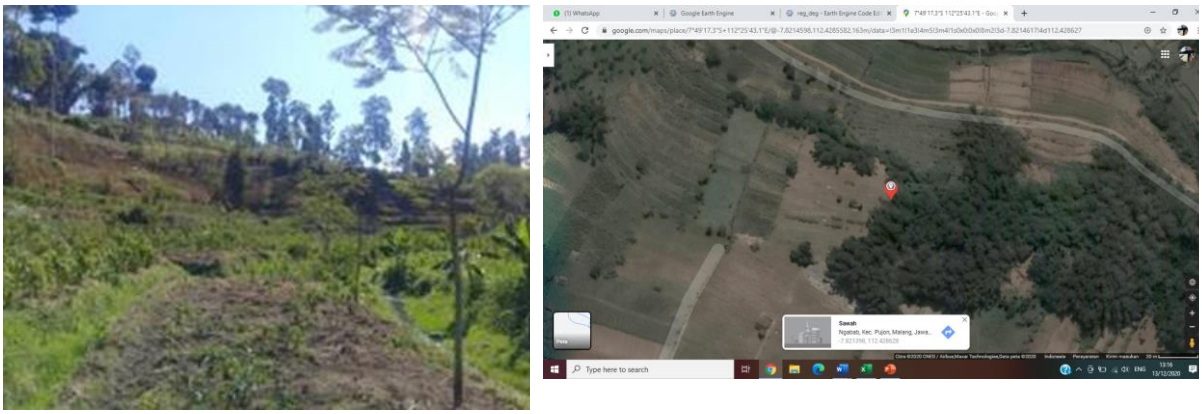
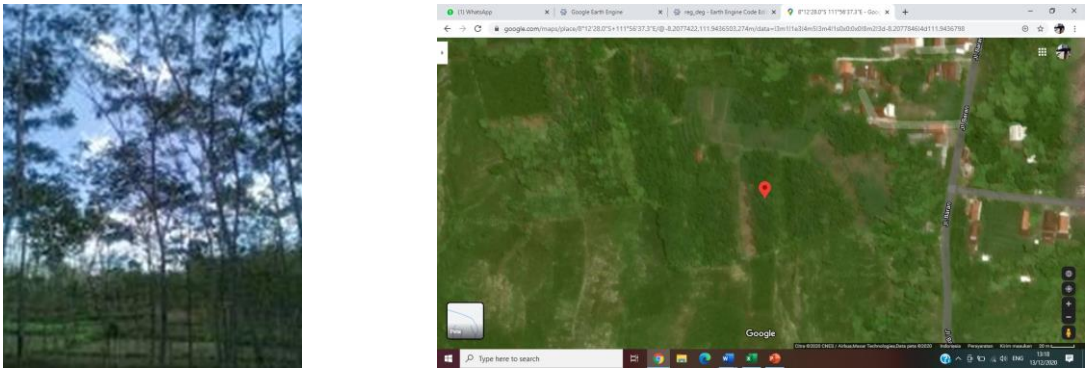


Figure 3-4: Graph of sample points for threshold determination



Devegetation, Malang,Pujon,Ngabab
-7.8214617,112.428627

http://dx.doi.org/10.30536/j.ijreses.2020.v17.a3385
@National Institute of Aeronautics and Space of Indonesia (LAPAN)



Revegetation Tulungagung,Kalidawir,Banyuurip
-8.2077846,111.9436798

Figure 3-5: Revegetation and devegetation spatial information

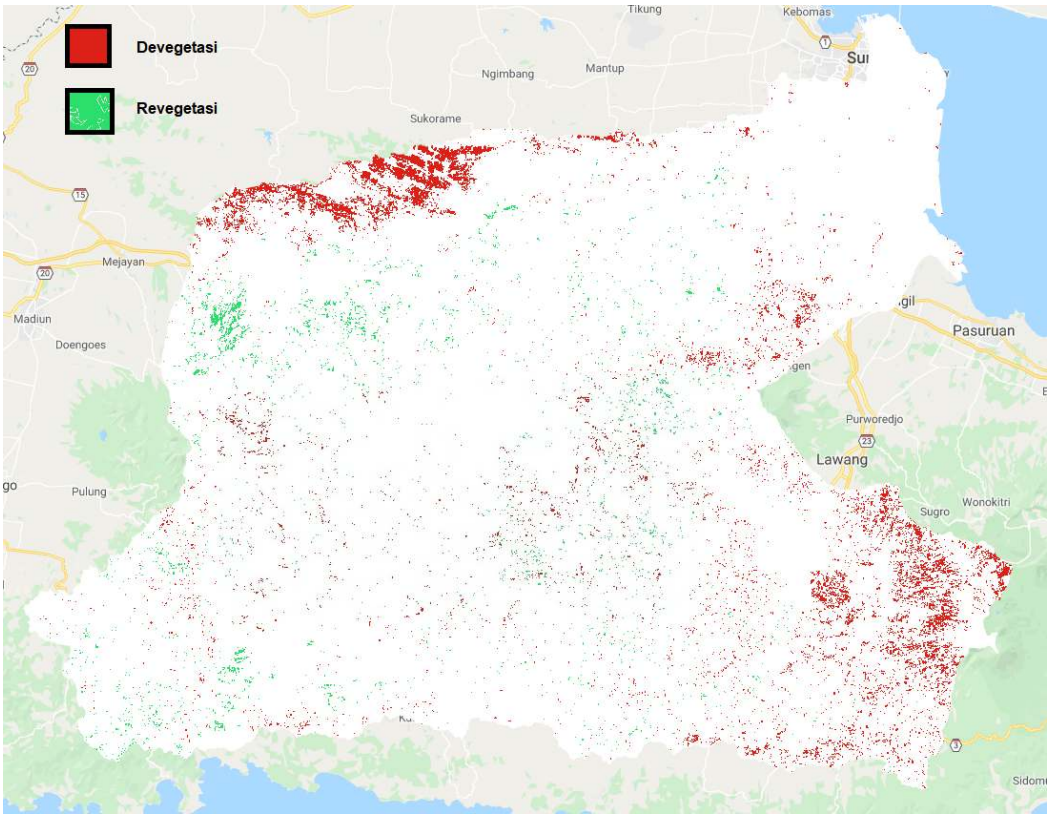


Figure 3-6: Revegetation and devegetation spatial information

In the study area, not all land-cover experienced revegetation or devegetation changes, as it includes cultivation and natural land. For example, rice fields are not considered to be devegated or revegetated due to the growth of the rice plant phase, or changes in teak forests can be due to changes between the rainy season and dry season, so such change in land cannot be said to be devegetation or revegetation.

4 CONCLUSION

Sentinel-2 MSI data with multi-temporal mosaic data can be used for monitoring changes in land cover dynamics, especially for tree cover loss. The results showed that revegetation can be determined by if Δ NDVI > 0.0309 and Δ NBR < 0.0176, and devegetation if Δ NDVI < - 0.0206 and Δ NBR > 0.0314. Based on the NDVI and NBR threshold requirements set in this study, it is shown that devegetation is more widespread

than revegetation. Devegetation generally occurs in the barren highlands and revegetation in the low and high lands/mountains, which often experience rain. The weakness of using the Sentinel satellite is that the method cannot detect land that is narrow or steep.

ACKNOWLEDGMENTS

This research was able to be carried out because of the collaboration of several parties. We would like to thank the INSINAS 2019 Program, the Ministry of Research and Technology/National Agency for Research and Technology and national research program 2020 LPDP for funding the research. Thanks also to the Remote Sensing Application Center and Remote Sensing Technology and Data LAPAN which provided us with facilities and input, as well as suggestions for the research.

AUTHOR CONTRIBUTIONS

The main authors of the scientific work of this research are Samsul Arifin and Tatik Kartika, while Dede Dirgahayu and Gatot Nugroho are contributing members.

REFERENCES

Aldrian and Sucahyono. (2013). Dictionary of climate change terms. BMKG

Arifin, S., Kartika, T., & Carolita, I. (2019) Application of geobiophysics NDVI model for forest identification in Lapan-A3 Satellite data. *Jurnal Penginderaan Jauh dan Pengolahan Data Citra Digital 16*(2), 91-100 http://dx.doi.org/10.30536/j.pjpdcd.2018 .v0.a3109

Barbosa, P.M., Pereira, J.M.C., & Grégoire, J. M. (1998). Compositing criteria for burned area assessment using multi-temporal low resolution satellite data, *Remote Sensing of Environment 65*(1), 38-49.

Chuvieco, E., Martin, M.P., & Palacios A. (2002). Assessment of different spectral indices in the red-near infrared spectral domain for burned land discrimination, *International Journal of Remote Sensing 23*, 5103–5110.

Escuin, S., Navarro, R.M., & Fernandez, P. (2008). Fire severity assessment by using NBR (Normalized Burn Ratio) and NDVI (Normalized Difference Vegetation Index) derived from LANDSAT TM/ETM images. *International Journal of Remote Sensing*, *29*(4), 1053–1073. DOI:10.1080/01431160701281072.

ESA-Sentinel-2. (2015) Mission Sentinel-2, https://sentinel.esa.int/web/sentinel/missions/sentinel-2, Europe.

Garcia, M.J.L., & Caselles, V. (1991). Mapping burns and natural reforestation using Thematic Mapper data. *Geocarto International*, *6*(1), 31–37.

Horning, N., Robinson, J.A., Sterling E.J., Turning, W., Spector, S. (2010). *Remote Sensing for Ecology and Conservation*. New York: Oxford University Press.

Indratmoko S., & Rizqihandar N. (2019). Burn area detection using Landsat 8 OLI TIRS. *Southeast Asian Geography Association (SEAGA) 13th Conference IOP Conf. Series: Earth and Environmental Science* 338 012035 IOP Publishing doi:10.1088/1755-1315/338/1/012035 1 of Geography, Faculty of Mathematic and Natural Science Universitas Indonesia Depok, Indonesia

Kartika, T., Arifin S., Sari I.L., Tosiani, A., Firmansyah, R., Kustiyo, Carolita, I., Adi, K., Daryanto, F., Said, Z. (2018), Analysis of vegetation indices using metric landsat-8 data to identify tree cover change in Riau Province**.** *Earth and Environmental Science 280*, 1-8. doi:10.1088/1755-1315/280/1/ 012013

Key, C.H., & Benson N. (1999). *Measuring and remote sensing of burn severity: the CBI and NBR*. https://www.researchgate.net

Lillesand, T.M., Kiefer R.W., & Chipman J.W. (2008). *Remote sensing and image interpretation* (Sixth Edition). New York: John Wiley & Sons, Inc.

Martín M.P., & Díaz-Delgado R. (2002). Burnedland mapping using NOAA-AVHRR

and TERRA-MODIS. In: Viegas (Ed.). *Conference proceedings: Forest fire research & wildland fire safety*. Millpress, Rotterdam.

Miettinen, J. (2007). *Burnt area mapping in insular Southeast Asia using* medium resolution satellite imagery. Academic dissertation. Department of Forest Resource Management Faculty of Agriculture and Forestry University of Helsinki.

Nielsen, T.T., Mbow, C., & Kane R. (2002). A statistical methodology for burned area estimation using multi-temporal AVHRR data. *International Journal of Remote Sensing 23*(6), 1181-1196.

Parwati, Zubaidah, A., Vetrita, Y., Yulianto, F., Ayu, K. DS, Khomarudin, M.R. (2012), Usage of Spot-4, Normalized Burn Ratio (NBR) and Normalized Difference Vegetation Index (NDVI) to identify burnt area. *Jurnal Ilmiah Geomatika 18*(1), 29-41.

Philiani, I, Saputra, L, Harvianto, L., & Muzaki, A.A. (2016). Mapping of mangrove forest vegetation using method Normalized Difference Vegetation Index (NDVI). *Surya Octagon Interdisciplinary Journal of Technology*, *1*(2), 211-222.

Roy, D.P., Lewis, P.E., & Justice C.O. (2002). Burned area mapping using Multi-temporal moderate spatial resolution data - a bi-directional reflectance model-based expectation approach. *Remote Sensing and Environment 83*, 263- 286.

Roy, D.P, Boschettm, L., & Triffm, S.N. (2006). Remote sensing of fire severity: assessing the performance of the normalized burn ratio. *IEEE Geoscience and Remote Sensing Letters, 3*(1), 112-116.

Ryan, L. (1997). Creating a Normalized Difference Vegetation Index (NDVI) image using multispectral. University of New Hampshire.

Silva, J.M.N, Cadima, J.F.C.L., Pereira, J.M.C. M. Grégoire. (2004), Assessing the feasibility of a global model for multi-temporal burned area mapping using SPOT-VEGETATION data. *International Journal of Remote Sensing 25*(22), 4889-4913. DOI: 10.1080/01431160412331291251.

USGS-EROS. (2017). Comparison-Sentinel-2-And-Landsat, https://www.usgs.gov /centers/eros/science/.

Weier, J, Herring, D, (2000), Measuring Vegetation (NDVI and EVI), NASA, https://earthobservatory.nasa.gov/features.

Jurnal Ilmiah Mahasiswa Pertanian
Volume 4, Nomor 1, Februari 2019
www.jim.unsyiah.ac.id/JFP

Prediksi Ketersediaan Lahan Sawah Menggunakan Metode Forecasting Di Kecamatan Darussalam

(Prediction of Paddy Fields Availability Using Forecasting Method in Darussalam Sub District)

Arif Faisaluddin[1], Yulia Dewi Fazlina[1], Sugianto[1*]
[1]Program Studi Ilmu Tanah, Fakultas Pertanian, Universitas Syiah Kuala

Abstrak. Lahan pertanian di wilayah pinggiran kota besar di Indonesia, sangat rentan mengalami alih fungsi menjadi kawasan non pertanian. Kegiatan pemantauan lahan secara periodik dalam bentuk penelitian terhadap alih fungsi lahan sawah sangat diperlukan untuk menemukan apakah Rencana Tata Ruang Wilayah Kabupaten yang telah ditetapkan tersebut berjalan sesuai dengan perencanaannya atau telah terjadi ketidakselarasan. Penelitian ini bertujuan mengetahui perubahan penggunaan lahan sawah tahun 2007-2016 dan untuk menghitung prediksi ketersediaan lahan sawah dan produksi beras tahun 2017-2026 di Kecamatan Darussalam Kabupaten Aceh Besar. Hasil yang diperoleh dari penelitian ini yaitu luas lahan sawah di Kecamatan Darussalam telah berkurang sebesar 1.068 ha atau 56,9% selama tahun 2007-2016. Sebaran sawah aktual akan mengalami defisit kecukupan lahan sawah terhadap kebutuhan beras di Kecamatan Darussalam di periode tahun 2024-2025.

Kata kunci *:* Lahan sawah, alih fungsi, darussalam

Abstract. The agricultural land at suburban region in Indonesia, is very vurnerable to being converted into non-agricultural sector. The land monitoring activities in study form against paddy fields land conversion is very necessary to figure out whether the District Spatial Plans that had been set goes according to the planed or there have been inconsistencies. This study aims to know the change of paddy fields land use in 2007-2016 and to calculate the predictions of availability of paddy fields and rice productions on 2017-2026 in Darussalam, Aceh Besar Districts. The results obtained from this study are the paddy fields in Darussalam Sub Districts have decreased by 1,068 ha or 56,9% during 2007-2016. The actual paddy fields swill be deficit in the adequacy of paddy fields to the needs of rice in Darussalam Sub Dictricts in 2024-2025.

Keywords: Paddy fields, land conversion, darussalam

PENDAHULUAN

Lahan sawah mempunyai arti yang terpenting dalam menentukan ketahanan pangan nasional. Sekitar 95% dari beras dalam negeri dihasilkan dari lahan sawah (Ginting, 2005). Saat ini permasalahan lahan pertanian di Indonesia adalah maraknya alih fungsi di sektor pertanian menjadi kawasan non pertanian, yang telah menjadi fenomena hampir di seluruh wilayah. Dampak yang ditimbulkan dari alih fungsi lahan antara lain adalah ancaman terhadap ketahanan pangan (Zulfikar et al. 2013).

Konversi lahan padi sawah di Aceh Besar terjadi bervariasi. Di tahun 2014 total luas tanam mencapai 42.234 Hektar (ha), lalu pada 2015 mengalami peningkatan luas sebanyak 7.658 ha yaitu 49.892 ha, namun terjadi penurunan luas tanam di tahun 2016 yang mencapai 6.796 ha yaitu tersisa 43.096 ha.

Sedangkan jumlah penduduk Kabupaten Aceh Besar dari tahun ketahun mengalami peningkatan cukup tinggi. Dari tahun 2009 jumlah penduduk Kabupaten Aceh Besar adalah 342.537 jiwa, pada tahun 2014 jumlah penduduk meningkat menjadi 384.168 dan pada hasil sensus terakhir tahun 2016 jumlah penduduk meningkat menjadi 400.913 jiwa (BPS, 2017).

Kecamatan Darussalam Kabupaten Aceh Besar terletak di daerah pinggiran kota Banda Aceh. Daerah pinggiran kota menurut Rahayu (2009), merupakan wilayah yang sering mengalami perubahan penggunaan lahan terutama pada sektor pertanian yang menjadi bangunan yang disebabkan adanya pengaruh perkembangan kota.

Menurut laporan statistik, pada tahun 2007 jumlah penduduk tetap di Kecamatan Darussalam berjumlah 20.652 Jiwa. Kemudian di tahun 2016 berjumlah 25.853 Jiwa. Dengan

Corresponding author:sugianto@unsyiah.ac.id

adanya peningkatan jumlah penduduk yang mencapai 5.201 jiwa, maka hal tersebut diduga dapat menyebabkan terjadinya alih fungsi lahan sawah.

Kecamatan Darussalam memiliki luas lahan baku padi sawah sebesar 2.483 Hektar (ha) pada tahun 2007. Kemudian hasil laporan statistik menyebutkan luas sawah eksisting 1.415 ha pada tahun 2016. Dengan terjadinya penuruan luas sawah tersebut, maka perlu diteliti mengenai hubungan antara jumlah penduduk terhadap penurunan luas sawah di Kecamatan Darussalam.

Berdasarkan uraian diatas, penelitian tentang prediksi ketersediaan lahan sawah menggunakan metode forecasting diharapkan dapat menjadi sebuah acuan dalam memanejemen penggunaan lahan sawah di Kecamatan Darussalam. Perlunya pengawasan dan evaluasi baik dalam bentuk laporan ilmiah maupun penelitian sebagai upaya pengendalian dan mempertahankan ruang kawasan persawahan. Dan diharapkan lahan sawah di Kecamatan Darussalam dapat tersedia di masa yang akan datang.

METODE PENELITIAN

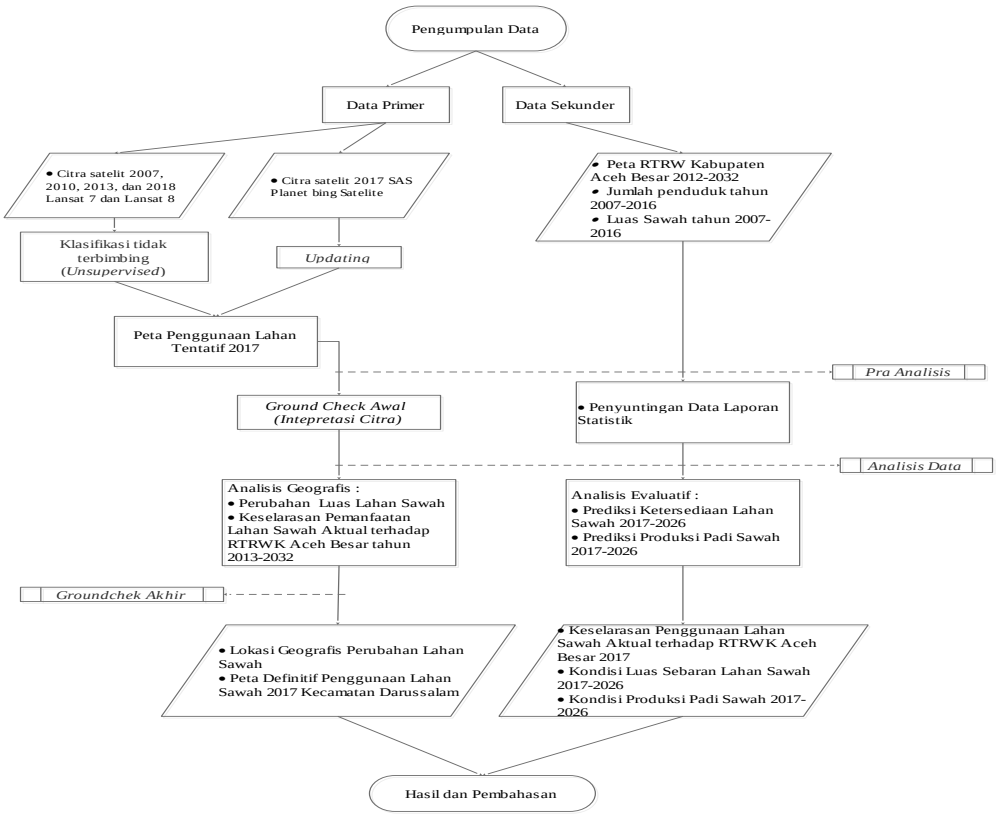
Penelitian ini dilaksanakan di Penelitian ini dilaksanakan di Laboratorium Penginderaan Jauh dan GIS Fakultas Pertanian dengan wilayah kajian di Kecamatan Darussalam, Kabupaten Aceh Besar

MATERI DAN METODE

Alat-alat yang digunakan berupa alat tulis, Global Positioning System (GPS), laptop, printer dan perangkat lunak pengolah data seperti ArcGIS, Erdas Imagine, Microsoft Office (Word, Excel, Power Point), SPSS dan Edraw Max. Adapun data yang dibutuhkan berupa data primer dan data sekunder. Data primer yang digunakan merupakan citra satelit berkala (time series) tahun 2007, 2010, 2013, 2017 dan 2018 diperoleh dari Landsat 7, Landsat 8 dan SAS Planet bing satelite. Data sekunder yang digunakan adalah peta RTRWK Aceh Besar 2013-2032

Penelitian ini menggunakan metode deskriptif dengan pendekatan kuantitatif. Menurut Sugiyono (2012) penelitian deskriptif kuantitatif yaitu, penelitian yang dilakukan untuk mengetahui nilai variabel mandiri, satu variabel atau lebih (independen) tanpa membuat perbandingan, atau menghubungkan dengan variabel yang lain.

Sedangkan untuk prediksi ketersediaan luas lahan sawah menggunakan analisis tren linear sederhana. Notasi (X) pada analisis tren linear adalah deret waktu tahun 1,2,3,4,5...20. berikut urutan pelaksanaan penelitian dapat dilihat pada gambar 1.



Gambar 1. Diagram Alir Penelitian

Tahapan Penelitian

Pengumpulan Data

Dalam penelitian ini data primer diperoleh dengan mengunduh citra Kecamatan Darussalam tahun 2007, 2010, 2013, 2017 dan 2018. Untuk citra tahun 2007 didapatkan melalui satelit Landsat 7 sedangkan untuk tahun 2010, 2013 dan 2018 dari satelit Landsat 8 diunduh melalui website USGS. Untuk citra tahun 2017 menggunakan satelit via Bing dari SAS Planet. Hal ini dikarenakan penampakan citra via satelit Bing cukup jelas hingga skala 1:1.000.

Data primer tersebut kemudian diolah menggunakan metode penginderaan jarak jauh dan sistem informasi geografis agar menghasilkan peta tentatif sebaran sawah di tahun 2007, 2010, dan 2013. Kemudian untuk citra tahun 2017 di lakukan cek lapangan pada pengguaan lahan sawah yang mengalami alih fungsi dengan menyelaraskan pada RTRW Kabupaten Aceh Besar tahun 2013 sebagai peta definitif penggunaan lahan sawah.

Data sekunder yang digunakan diperoleh dari badan/ instansi yang menyediakan data-data yang dipublikasikan, diantaranya Badan Pusat Statitik Aceh Besar, Badan Perencanaan Pembangunan Daerah Kabupaten Aceh Besar, dan Perpustakaan. Data statistik dikumpulkan setiap tahun dimulai dari tahun 2007 sampai 2016. Hal ini dikarenakan semakin banyak data historis yang dikumpulkan maka semakin terlihat kecenderungan tren yang sudah berlangsung.

Tahap Pra Analisis

Tahapan pra analisis pada penelitian ini yaitu penyuntingan data dan observasi visual. Penyuntingan data sekunder dilakukan pada laporan statistik yang dipublikasi oleh BPS. Penyuntingan dilakukan pada beberapa data statistik yang akan digunakan untuk penelitian. Data penginderaan jauh juga di koreksi secara geometrik dengan peta RBI skala 1:50.000.

Citra aktual yang sudah dikoreksi, dilakukan observasi visual pada beberapa penggunaan lahan sawah dan kebun. Hal ini dikarenakan presentasi beberapa objek yang terdapat pada citra mengalami kabur (blur). Identifikasi keselarasan data spasial terhadap kondisi aktual dilakukan observasi dengan mencatat titik koordinat lokasi tersebut melalui GPS dan menangkap gambar (capture) kondisi lingkungan yang di observasi.

Analisis Data

1. Perubahan Luas Penggunaan Lahan Sawah

Data luas sebaran lahan sawah Kecamatan Darussalam dari kurun waktu 2007-2016 yang diperoleh dari data sekunder dirangkum dan ditabulasikan ke dalam perangkat lunak. Lalu data tersebut di persentasekan dengan luas total wilayah di setiap tahunnya. Untuk mempresentasikan sebaran lahan sawah, data primer yang diperoleh dari Landsat 7 dan Landsat 8 dilakukan klasifikasi citra dengan cara penginderaan jarak jauh.

Pada prosesnya, band yang digunakan sebanyak delapan (8) band. Format band yang telah diunduh berjenis gambar raster (*bitmap image*). Kemudian, band 1-8 diproses dengan cara menumpukkan menjadi satu layar (*stacking*). Hasil stacking citra wilayah Aceh Besar di potong dengan cara subset citra untuk di ambil bagian Kecamatan Darussalam. Setelah didapatkan raster Kecamatan Darussalam, maka proses selanjutnya siap untuk dikelompokkan (*clustering*) jenis penggunaan lahan dengan klasifikasi tidak termbimbing (*Unsupervised*).

2. Prediksi Ketersediaan Lahan Sawah dan Kondisi Produksi Beras

Perumusan model untuk mencari persamaan tren regresi linear serupa dengan perumusan model regresi, namun peubah penjelas yang digunakan adalah waktu. Menurut Maryati (2010), setelah persamaan garis tren yang linier tersusun berdasarkan data tahunan, maka dapat diramalkan garis tren linier untuk masa mendatang. Model persamaan regresi linear yang digunakan adalah sebagai berikut :

$$\boldsymbol{Y = a + bX}$$

$$\mathbf{a} = \frac{(\sum \mathbf{y})(\sum \boldsymbol{x^2}) - (\sum \mathbf{x})(\sum \mathbf{xy})}{\mathbf{n}(\sum \mathbf{x^2}) - (\sum \mathbf{x})^2}$$

$$\mathbf{b} = \frac{\mathbf{n}(\sum \boldsymbol{xy}) - (\sum \mathbf{x})(\sum \mathbf{y})}{\mathbf{n}(\sum \mathbf{x^2}) - (\sum \mathbf{x})^2}$$

keterangan :
Y = Besarnya Alih fungsi lahan (Ha)
X = Tahun yang diprediksi
a = Nilai tetap (Konstanta) atau nilai Y' pada X sama dengan nol
b = Kemiringan (slope) atau perubahan nilai Y setiap waktu.
n = Jumlah populasi

Pemeriksaan Lapangan

Kegiatan pemeriksaan di lapangan dilakukan dengan menelusuri lokasi-lokasi pengamatan yang telah ditentukan meliputi pengambilan titik-titik pengamatan, dokumentasi

contoh-contoh alih fungsi atau penggunaan lahan sawah. Hal ini dilakukan untuk memahami serta mengenal kondisi daerah penelitian yang dilakukan.

Setelah hasil pemeriksaan lapangan diinput kembali ke komputer untuk dikoreksi dan difinalisasi, maka imagery tersebut dilakukan layout untuk menghasilkan peta penggunaan lahan sawah 2017 di Kecamatan Darussalam.

HASIL DAN PEMBAHASAN

Perubahan Luas Lahan Sawah

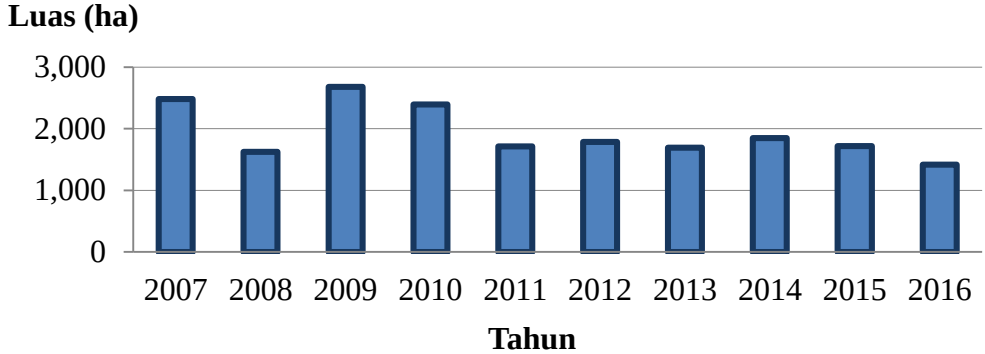
Perubahan luas eksisting lahan sawah di Kecamatan Darussalam, Kabupaten Aceh Besar tahun 2007-2016 dapat dilihat pada Tabel 1.

Tabel 1. Perubahan Luas Lahan Sawah Kecamatan Darussalam 2007-2016

No.	Tahun	Luas Sawah (Hektar)	Perubahaan Luas Lahan Sawah	
			Luas (Hektar)	Persentase (%)
1	2007	2.483		
2	2008	1.627	-856	-34,4
3	2009	2.678	1.051	64,6
4	2010	2.392	286	10,7
5	2011	1.714	-678	-28,3
6	2012	1.787	73	4,2
7	2013	1.690	-97	-5,4
8	2014	1.850	160	9,5
9	2015	1.718	-132	-7,1
10	2016	1.415	-303	-17,6
Jumlah			1.068	56,9
Rerata			119	6,31

Sumber : Data Analisis

Pada tahun 2007 luas sawah mencapai 2.483 ha, namun luas sawah di Kecamatan Darussalam terus mengalami perubahan hingga tahun 2016 tersisa 1.415 ha. Grafik tren perubahaan luas lahan sawah dapat dilihat pada Gambar 2.



Gambar 2. Grafik Luas Lahan Sawah

Luas lahan sawah di Kecamatan Darussalam dalam kurun waktu 2007-2016 telah berkurang sebesar 1.068 ha atau 56,9% yang mana jika dirata-rata setiap tahunnya terjadi penurunan luas lahan sawah sekitar 119 ha atau 6,3%. Penurunan luas lahan sawah terbesar

terjadi pada periode 2007-2008, yaitu sebesar 865 ha atau sekitar 34,4% lahan sawah berkurang.

Prediksi Perubahan Luas Lahan Sawah dan Kondisi Produksi Beras 2017-2026

Prediksi Perubahan Luas Lahan Sawah 2017-2026

Dengan terjadinya perubahaan luas lahan sawah sebesar 56% selama tahun 2007-2016 dan jika tren tersebut dilanjutkan dengan analisis tren linear untuk tahun 2017-2026, maka dapat dilihat proyeksinya pada Tabel 2. Sehingga hasil analisis tren linear untuk perubahaan luas lahan sawah :

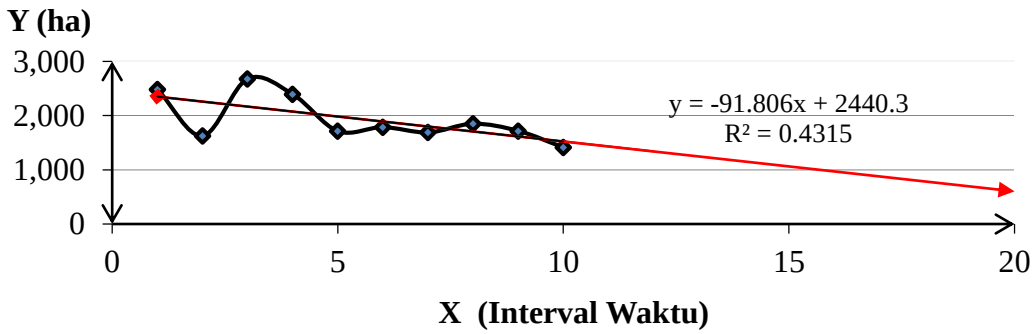
$$\hat{Y} = 2.440 + -99{,}80\ X$$

Tabel 2. Prediksi Perubahan Luas Lahan Sawah 2017-2026

No	Tahun	X	Y(ha)
1	2017	11	1.430
2	2018	12	1.339
3	2019	13	1.247
4	2020	14	1.155
5	2021	15	1.063
6	2022	16	971
7	2023	17	880
8	2024	18	788
9	2025	19	694
10	2026	20	604

Sumber : Hasil Analisis 2018

Melalui persamaan tren regresi linear tersebut, maka bisa diperoleh gambaran perubahan luas lahan sawah dari tahun 2017 hingga tahun 2026. Tabel 2 menunjukan jika luas lahan sawah terus mengalami penurunan hingga tahun 2026. Pada tahun 2017 diperkiran jumlah luas lahan sawah sekitar 1.430 ha. Dan jika tren tersebut tetap berlangsung hingga tahun 2026, maka prediksi luas sebaran sawah aktual (eksisting) di Kecamatan Darussalam sekitar 604 ha. Grafik tren linear sebaran lahan sawah dapat dilihat pada Gambar 3.



Gambar 3. Grafik Tren Linear Luas Lahan Sawah 2007-2026 Kecamatan Darussalam

Berdasarkan Gambar 3, tren linear yang terjadi selama 2007-2016 berdampak pada prediksi tren linear untuk 2017-2026 kedepan. Tren linear cinderung menuju ke arah tren negatif. Hal ini juga dipengaruhi dengan besarnya selisih luas sebaran sawah di tahun 2007 dengan tahun 2016. Diketahui jika luas sawah pada tahun 2007 seluas 2.483 ha sedangkan di

tahun 2016 tersisa 1.415 ha. Dengan besarnya selisih tersebut maka tren yang tercipta akan cenderung terus mengurangi jumlah luas sawah di Kecamatan Darussalam.

Prediksi Kondisi Produksi Beras 2017-2026

Dari persamaan yang diperoleh maka dapat diketahui prediksi produksi padi sawah untuk tahun 2017–2026 dengan memasukkan nilai X di persamaan Y=a+bX dengan nilai X yang telah ditentukan untuk tahun (Tabel 3) tersebut. Sehingga didapatkan hasil analisis tren linear untuk produksi padi :

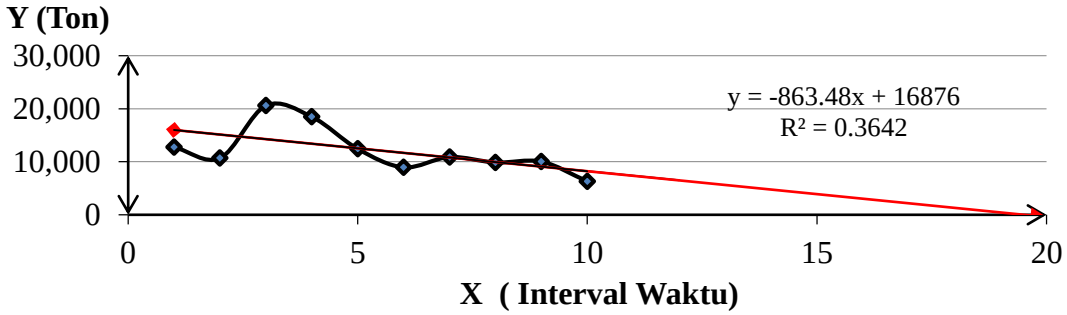
$\hat{Y}$ = 16.876+-863,4 X

Tabel 3. Prediksi Produksi Beras Kecamatan Darussalam tahun 2017-2026

No	Tahun	X	Y(Ton)
1	2017	11	7.378
2	2018	12	6.514
3	2019	13	5.651
4	2020	14	4.787
5	2021	15	3.924
6	2022	16	3.060
7	2023	17	2.197
8	2024	18	1.333
9	2025	19	470
10	2026	20	-394

Sumber : Hasil Analisis 2018

Melalui hasil prediksi tren linear tersebut, maka bisa diperoleh prediksi informasi produksi padi dari tahun 2017 hingga tahun 2026. Tabel 3 menunjukan jika produktivitas padi akan terus mengalami penurunan hingga tahun 2026. Pada tahun 2017 diperkiran jumlah produksi padi sawah sekitar 7.378 Ton. Dan jika tren tersebut tetap berlangsung 2017-2026, maka kondisi produksi beras di Kecamatan Darussalam tidak akan tersedia lagi di periode tahun 2026-2027. Grafik tren linear produktivitas lahan sawah dapat dilihat pada Gambar 4.



Gambar 4. Grafik Tren Linear Produksi Padi Sawah 2007-2026 Kecamatan Darussalam

Berdasarkan Gambar 4, tren linear yang terjadi selama tahun 2007-2016 berdampak pada prediksi tren linear untuk tahun 2017-2026. Tren linear cinderung menujuke arah tren negatif. Tren negatif tersebut juga sama halnya dengan trem perubahaan lahan sawah yang mengarah kearah negatif. Hal ini diduga karena tidak adanya produksi yang mampu mencapai atau lebih ke angka 20.000 ton pada tahun 2009. Sedangkan data produksi selanjutnya cenderung menurun hingga ke angka 6.348 ton pada tahun 2016.

Prediksi Kebutuhan Sebaran Lahan dan Produksi Beras 2017-2026

Jumlah produktivitas lahan sawah di Kecamatan Darussalam hingga tahun 2016 terus mengalami penurunan. Hingga tahun 2016 kebutuhan beras di Kecamatan Darussalam mencapai 6.348 Ton dengan luas lahan sawah 1.415 ha. Sedangkan hasil analisis kebutuhan produksi berasuntuk tahun 2017-2026 yang akan datang di Kecamatan Darussalam dibutuhkan 3.955 Ton untuk dikonsumsi penduduk sekita 31.671 Jiwa. Berikut Tabel 6 hasil analisis kebutuhan beras dan kebutuhan luas lahan sawah di Kecamatan Darussalam 2017-2026.

Tabel 4. Prediksi Kebutuhan Beras dan Luas Lahan Sawah Kecamatan Darussalam 2017-2026

No	Tahun	Prediksi Jumlah Penduduk (Jiwa)	Nilai Konsumsi Beras (Kg/Kap/Thn)	Kebutuhan Beras (Ton)	Kebutuhan Luas Sawah (ha)	Prediksi Luas Sawah (ha)	Keterangan
1	2017	26.592	124,89	3.321	664	1.430	Baik
2	2018	27.156	124,89	3.392	678	1.339	Baik
3	2019	27.721	124,89	3.462	692	1.247	Baik
4	2020	28.285	124,89	3.533	707	1.155	Baik
5	2021	28.849	124,89	3.603	721	1.063	Baik
6	2022	29.414	124,89	3.673	735	971	Baik
7	2023	29.978	124,89	3.744	749	880	Baik
8	2024	30.543	124,89	3.814	763	788	Baik
9	2025	31.107	124,89	3.885	777	694	Defisit
10	2026	31.671	124,89	3.955	791	604	Defisit

Sumber : *Hasil Analisis 2018*

Keterangan : Nilai konsumsi beras berdasarkan Permentan Nomor 16/Permentan/HK.140/4/2014. Rerata produktivitas sawahdari 2007-2016adalah 1 ton = 0,2 Hektar atau 1 ha = 6,16 Ton.

Katagori keterangan :

i. Baik, apabila nilai kebutuhan luas sawah lebih rendah daripada nilai prediksi luas sawah.
ii. Defisit, apabila nilai kebutuhan luas sawah lebih tinggi daripada nilai prediksi luas sawah.

Dari Tabel 4. diperoleh jika luas sawah di Kecamatan Darussalam saat ini masih bisa mencukupi konsumsi penduduk hingga tahun 2024. Namun jika merujuk pada hasil analisis tren linear, luas lahan sawah tersedia diprediksi akan mengalami defisit terhadap kemampuan sebaran sawah dalam menghadapi konsumsi penduduk pada tahun 2025-seterusnya.

SIMPULAN DAN SARAN

Luas lahan sawah di Kecamatan Darussalam tahun 2007-2016 telah berkurang sebesar 1.068 Hektar atau 56,9% yang mana jika dirata-ratakan setiap tahunnya terjadi penurunan luas lahan sawah sekitar 119 Hektar atau 6,3%. Jika tren tersebut tetap berlangsung hingga tahun 2026, maka sebaran sawah aktual (eksisting) akan mengalami defisit kecukupan lahan sawah terhadap kebutuhan beras di Kecamatan Darussalam di periode tahun 2025-2026. Maka perlu dilakukannya penelitian lanjutan mengenai deviasi penggunaan lahan sawah aktual terhadap RTRW Kabupaten Aceh Besar di sektor peri urban Kota Banda Aceh

DAFTAR PUSTAKA

Badan Pusat Statistik. 2016. *Kabupaten Aceh Besar dalam Angka 2017*. Badan Pusat Statistik Kabupaten Aceh Besar, Aceh.

Ginting, M. 2005. *Faktor-Faktor yang Mempengaruhi Alih Fungsi Lahan Pertanian Padi Sawah Terhadap Pendapatan Petani*. Tesis. Universitas Sumatera Utara.

Rahayu, Sri. 2009. Kajian Konversi Lahan Pertanian di Daerah Pinggiran Kota Yogyakarta Bagian Selatan (Studi Kasus di Sebagian Daerah Kecamatan Umbulharjo). Jurnal *Pembangunan Wilayah dan Kota*. Universitas Diponegoro, Semarang. 5(01): 365-372.

Zulfikar, M., Barus B., Atang S. Pemetaan Lahan Sawah Dan Potensinya Untuk Perlindungan Lahan Pertanian Pangan Berkelanjutan di Kabupaten Pasaman Barat, Sumatera Barat. *Jurnal Tanah Lingk*. Vol 15: 20-28.

IOP Conference Series:
Earth and
Environmental Science

PURPOSE-LED PUBLISHING™

PAPER • **OPEN ACCESS**

Application of NDVI Sentinel-2Ac Imagery for Agricultural Land Development in Food Buffer Area of New Capital City Indonesia

To cite this article: D. Ramadhani *et al* 2024 *IOP Conf. Ser.: Earth Environ. Sci.* **1290** 012016

View the article online for updates and enhancements.

You may also like

- Projection of Electric Ships as Sustainable Transportation in the Capital City of Indonesia "Nusantara"
Z.H.A. Syahr, D.H. Syaifullah, M.R. Hakim et al.
- Challenges in Realizing the Protected Green Area in Ibu Kota Nusantara
Endra Wijaya, Cipta Indralestari Rachman, Neisya Azzahra et al.
- Comparison of the Naïve Bayes and the Nearest Neighbor method to detect vegetation in some of the New Capital of Indonesia (IKN)
J T Nugroho, N M Sari, K I N Rahmi et al.



This content was downloaded from IP address 140.213.218.151 on 27/08/2025 at 17:54

Application of NDVI Sentinel-2Ac Imagery for Agricultural Land Development in Food Buffer Area of New Capital City Indonesia

D. Ramadhani, S. Susanto*, C. Setyawan, M. Khoiruzaki, M. R. W. Abdilah
Department of Agricultural and Biosystems Engineering, Faculty of Agricultural Technology, Universitas Gadjah Mada, Yogyakarta 55281, Indonesia

*Email: *s_susanto@ugm.ac.id*

Abstract. Paser Regency is one of the food buffer areas for the New Capital City (IKN) of Indonesia in East Kalimantan Province. The relocation of the capital to IKN increases the number of populations and food demand as well. To meet food needs in IKN in the future, the development of agricultural land is needed. This study aimed to identify the type and direction of land use in Paser Regency to ensure food self-sufficiency. Sentinel-2 satellite Imagery with the Maximum Likelihood Classification (MLC) method was used in this study. The sentinel data from 2018 to 2022 was analyzed to identify the existing land use types over the past five years. The land use direction was determined based on the existing land use type, soil type, and land slope class. The results with an accuracy value for the overall test of 91.68% and kappa accuracy of 0.86 showed a change in land use from 2018 to 2022. Eight types of main land used were identified such as non-swamp rice fields, swamp rice fields, oil palm plantations, moors, shrubs, forests, settlements, and water bodies. The application of NDVI Sentinel-2Ac Imagery can identify a potential area of 13,249.7 hectares for rice field development and can significantly increase rice production to ensure food self-sufficiency in IKN.

1. Introduction

Food needs are one of the primary requirements of humans. Meeting the food needs in a region becomes a challenge for a country in order to fulfill the basic needs of its people. The relocation of Indonesia's capital city from Jakarta, originally located in the Special Capital Region of Jakarta, to the New Capital City (IKN) in East Kalimantan Province, will certainly impact the increase in population. The increase in population will lead to a higher demand for food. One of the areas that serves as a food buffer for the New Capital City (IKN) in Indonesia is Paser Regency. As a food buffer area for IKN, the development of agricultural land is necessary to meet future food needs. Land development necessitates the consideration of various factors, including land use. This will be an important factor in determining suitable land development locations to enhance food crop commodities. Furthermore, land use planning needs to be further examined, both historically and in determining land development locations. The extension of agricultural land from less productive land is a significant aspect of this research. The development of agricultural land poses a challenge due to Indonesia's topographic diversity, which results in a variety of land uses. The utilization of spatial technology can aid in land development, especially in regions with diverse topography, such as Indonesia.

Content from this work may be used under the terms of the Creative Commons Attribution 3.0 licence. Any further distribution of this work must maintain attribution to the author(s) and the title of the work, journal citation and DOI.
Published under licence by IOP Publishing Ltd

Remote sensing has become one of the effective methods in monitoring land cover due to its capability to provide information about spatial diversity on the Earth's surface quickly and easily [1]. Satellite imagery is a component of remote sensing that provides geographic information through aerial photographs and is periodically available. Spatial resolution poses a challenge in satellite imagery for further analysis, especially in the field of agriculture. Sentinel-2 is one of the satellite images with high resolution, specifically with a 10-meter resolution. Spatial resolution will affect the accuracy level in the analysis of satellite images; higher resolution leads to a greater number of pixels. The utilization of Sentinel-2 can be employed to detect land cover in a region, resulting in various land use classifications. [2].

The analysis of Sentinel-2 imagery for land cover classification using unsupervised classification methods has been widely conducted. The unsupervised method for land cover classification is considered less accurate because certain classes with similar colour spectra might be considered the same. Therefore, in this study, a supervised classification method was utilized to reduce errors in classification. One of the supervised classification methods is the Maximum Likelihood Classification (MLC). This method (MLC) can compare and calculate the average values of diversity between classes and bands. MLC is a classification that categorizes parameters by assuming a normal or near-normal spectral distribution for each distinct characteristic. Equal likelihood among classes is also assumed. [3]. The results of the classification analysis can be used as one of the indicators in decision support for agricultural land development.

2. Materials and methods

2.1. Study Area

The present study was conducted in Paser Regency, one of the supporting areas for the New Capital City. Paser Regency is situated in the southernmost part of East Kalimantan Province. To the north, it shares a border with Kutai Barat Regency, while to the east, it borders Penajam Paser Utara Regency and the Makassar Strait. To the south, it is adjacent to Kota Baru Regency in South Kalimantan Province, and to the west, it shares a border with Tabalong Regency in South Kalimantan Province. The current area of Paser Regency is 11,603.94 km^2, with most of its land consisting of green areas including forests, gardens, plantations, shrubs, and rice fields. The geographical overview of Paser Regency was described in Figure 1.

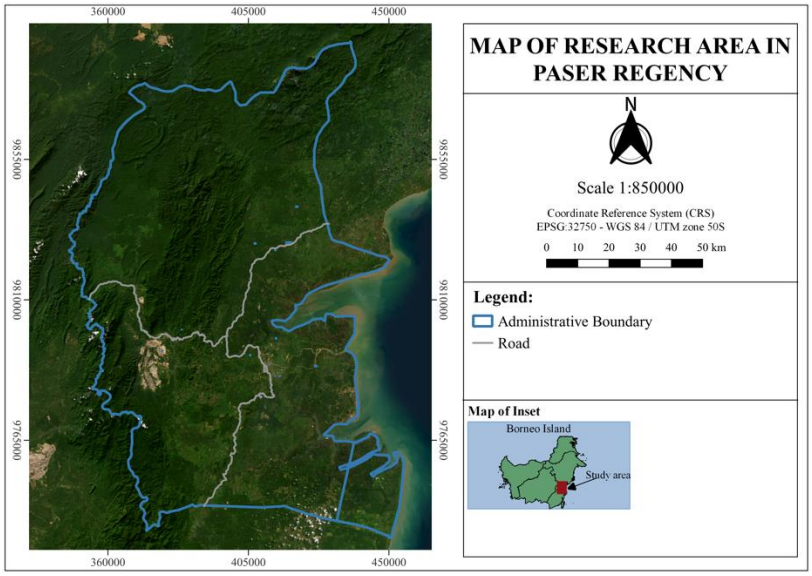


Figure 1. Map of research area in Paser Regency.

Generally, the eastern area has flatter land compared to the western area. This indicates that the eastern area is more suitable for the development of food crops. Additionally, the slope of the terrain also affects water availability and nutrient availability for crops. The land slope distribution of Paser Regency is presented in Figure 2.

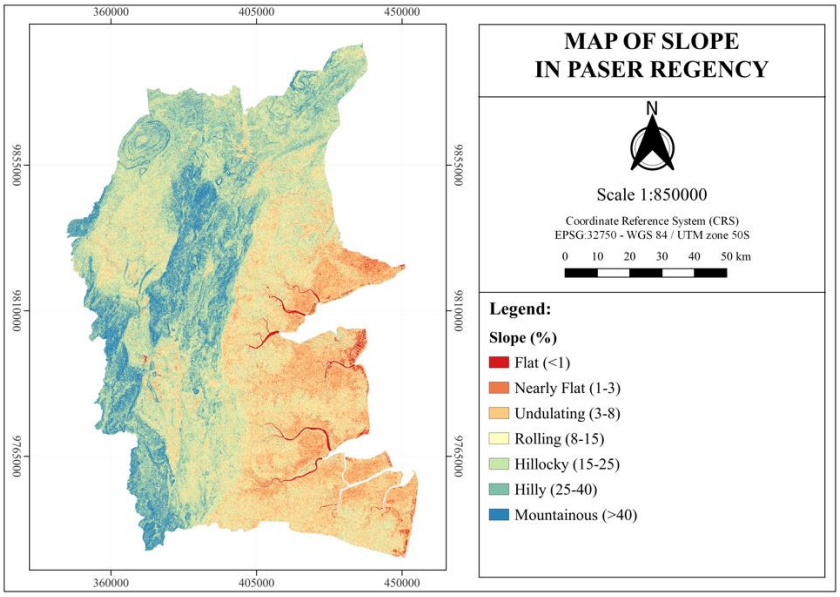


Figure 2. Map of slope in Paser Regency

The study area has 5 soil types that influence the vegetation types and agricultural crop commodities cultivated (Figure 3). In the eastern area, there are 3 types of soil such as Ferralic Cambisols (Bf), Ferric Acrisols (Af), and Dystric Fluvisols (Jd). Based on land use classification, all three soil types are suitable for agricultural cultivation.

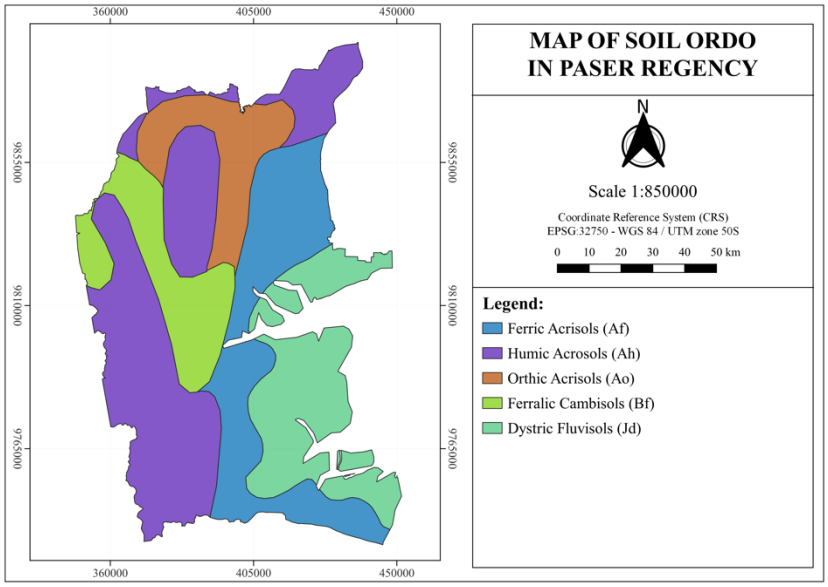


Figure 3. Map of soil ordo in Paser Regency.

Ferric Acrisols are utilized for crop and plantation cultivation. This type of soil has an appropriate acidity level for agricultural crops and provides nutrients that support plant growth and development

[4]. In this area, Ferric Acrisols are primarily dominated by oil palm plantations. While this soil type is less suitable for cultivating food crops, it can be managed for such cultivation with specific treatments. Ferric Acrisols are suitable for production of rainfed and irrigated crops only after liming and full fertilization. Most of the food crop areas in this region are found on Dystric Fluvisols soil types (1950. 66 km^2). It indicates that this soil type has sufficient nutrient availability for crops, although certain specific measures are needed to address soil acidity issues in the region. Two other types of soil i.e., Humic Acrosol (Ah) and Orthic Acrisols (Ao) are found in the western and northern part of the study site. Coverage area of soil types in Paser Regency is described in Table 1.

Table 1. Area of Soil Ordo in Paser Regency

Soil Ordo	Symbol	Area (Km^2)
Ferric Acrisols	Af	2,215.12
Humic Acrosols	Ah	3,512.21
Orthic Acrisols	Ao	1,080.75
Ferralic Cambisols	Bf	1,285.33
Dystric Fluvisols	Jd	1,950.66

2.2. Tools and Materials

Maps from the Indonesian Geospatial Information Agency and Google Earth were used as training areas for data preprocessing, data processing, accuracy assessment, and result analysis in a QGIS. The data used in this study consisted of Sentinel-2 satellite imagery captured between 2018 and 2022, obtained from the website https://earthexplorer.usgs.gov/ , specifically within the geographical boundaries of Paser Regency. The imagery used in this research was sourced from the Sentinel-2 satellite which is designed for monitoring land cover, environmental conditions, and the physical state of the Earth's surface. Land cover classification was adjusted based on both the spectral and spatial resolution of the imagery, ensuring that the results of land cover classification have high accuracy [5].

2.3. Supervised Classification

Guided classification was used as a classification method in this research. Guided classification is a process of identifying and grouping pixels found in training areas using pixel samples with pre-defined class information to classify pixels whose class is unknown. Determining samples for various objects/features in relatively homogenous areas needs to be performed before the classification process. The determination of these areas is a crucial step in the process [6].

2.4. Maximum Likelihood (MLC)

Maximum Likelihood Classification (MLC) is one of the most widely used guided classification methods for remote sensing data processing. Before conducting the classification, the initial step involves determining training areas to examine the statistical characteristics of each object that will be classified. This process is undertaken to establish a statistical representation of the various classes or objects present in the image [7].

MLC classifies specific objects based on their shape and size using the algorithmic representation of statistical values, such as the mean, standard deviation, variance, and covariance. Generally, MLC is used for land cover classification and urban area monitoring. Additionally, MLC can provide high accuracy values, often reaching around 84%. This method is effective in distinguishing different land cover types based on the statistical properties of their spectral signatures, thus enabling accurate classification results[8].

2.5. Accuracy Assessment

Accuracy testing is conducted to assess the precision of the algorithm used in the classification process. This method compares the results of multispectral classification in the imagery with the actual

conditions. In this study, the actual conditions were obtained from the latest maps published by the Indonesian Geospatial Information Agency, supplemented by data from Google Earth. The method used for accuracy testing involves utilizing a confusion matrix to calculate accuracy values such as Kappa and Overall accuracy. The equations to calculate Kappa and Overall accuracy values can be seen in equations 1 to 3.

$$User\ Accuracy = \frac{Xii}{X+i} \times 100\ \% \quad (1)$$

$$Accuracy\ Metrics = \frac{Xii}{Xi+} \times 100\ \% \quad (2)$$

$$Overall\ Accuration = \frac{\sum_{i=1}^{r} Xii}{N} \times 100\ \% \quad (3)$$

For systematic assessment, Kappa and Overall accuracy values can be calculated using equations 4 to 5.

$$Kappa\ Accuration = \frac{N\ \sum_{i=1}^{r} \times Xii - \sum_{i=1}^{r} \times Xi + X_{i+}}{N^2 - \sum Xi + X_{i+}} \times 100\ \% \quad (4)$$

$$Overall\ Accuration = \frac{(\sum_{i}^{r} Xii\ )}{N} \times 100\% \quad (5)$$

Where:
Xii = The diagonal values of the contingency matrix for row i and column i.,
X+1 = The total number of pixels in column i.
Xi + = The total number of pixels in row i.
N = The total number of pixels in the sample.

2.6. Procedures

2.6.1. *Pre Data Processing.* In the pre-processing stage, there are several processes, including atmospheric correction to eliminate errors in the image data caused by atmospheric factors. To mitigate these errors, the Dark Object Subtraction (DOS) method provided by the Semi-Automatic Classification Plugin (SCP) in the QGIS software is employed. Subsequently, a composite band is created to obtain digital numbers that will distinguish objects. The next step involves the mosaic process, which aimed to merge several satellite images into a single scene covering the study area.

2.6.2. Data Processing. The data processing stage involves several processes, as follows:

a. Determination of Training Area
   In this stage, the identification and determination of training areas were conducted, which adequately represent and provide numerical descriptions of the spectral attributes for each land use type that will undergo classification. These Training Areas are created in accordance with the thirteen pre-defined land cover classes.
b. Classification using MLC Algorithm
c. Accuracy Assessment with Confusion Matrix and Calculation of Kappa and Overall Accuracy.

2.7. Results Analysis

The calculated accuracy assessment results provide insights into land use classification outcomes and their respective areas. This information can offer an understanding of the potential of certain land areas to be used as productive green spaces for food production.

3. Results and discussion

3.1 Land Use Change

Land use in Paser Regency has experienced spatial changes from 2018 to 2022 (Figure 4). Spatial changes in land use are more predominant in the eastern region, mainly due to the presence of residential areas in the east. Notably significant changes occurred from 2021 to 2022. Spatial analysis indicates 13 types of land uses in the study area such as wetland rice fields, non-wetland rice fields, oil palm plantations, gardens, shrubs, Imperata grasslands, mangroves, forests, open land, settlements, water bodies, ponds, and mining areas.

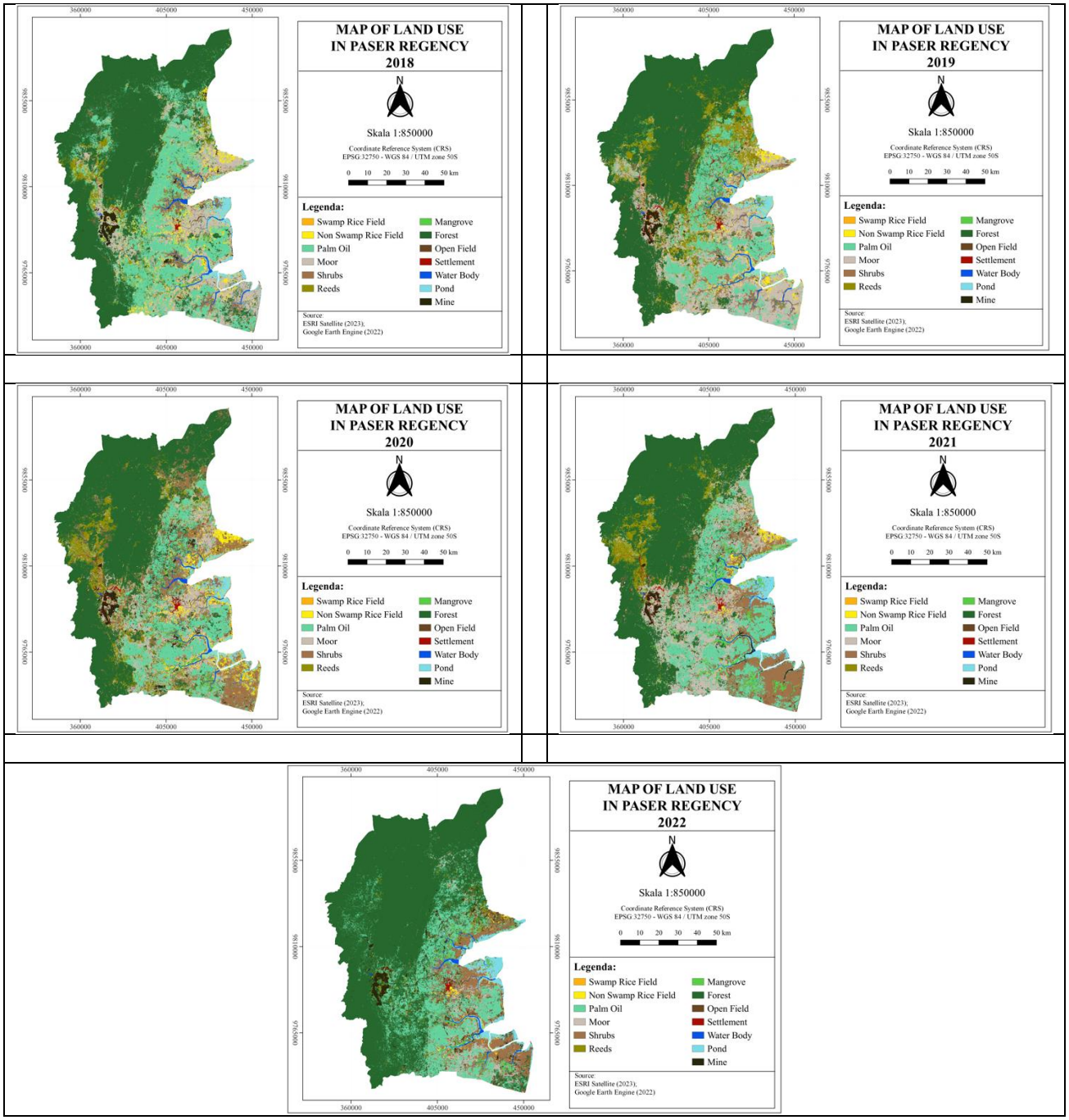


Figure 4. Map of Land Use in Paser Regency from 2018 to 2022

The land use classification results in Paser Regency demonstrate changes in land use across all categories each year from 2018 to 2022. While most of the land is still categorized as forest, it experiences a gradual reduction each year. Following the forests, agricultural classifications are widespread, with oil palm plantations covering most agricultural areas. In contrast, paddy fields, while not extensive, are still present, primarily in the eastern parts of Paser Regency. Other prevalent classifications include garden areas, shrubs, and Imperata grasslands, which are areas where land use changes are possible. Additionally, open land areas are distributed in the southeast and undergo changes each year. These changes, in general, are a result of human efforts to meet their needs.

These classifications require accuracy testing to assess the precision of the satellite image classification. The accuracy of the classification results is determined using the Kappa method, as presented in Table 2. The accuracy assessment results for the years 2018 to 2022 are displayed.

Table 2. Adjusted error matrix by the proportion of area

Classification	1	2	3	4	5	6	7	8	9	10	11	12	13	Total	User's (%)
1	0.0005	0	0	0	0	0	0	0	0	0	0	0	0	0.0005	100
2	0	0.0025	0	0.0009	0.0014	0	0	0	0	0	0	0.0009	0	0.0057	43.8667
3	0	0	0.1682	0.0001	0.0009	0	0	0.0069	0	0	0	0	0.0001	0.1762	95.4372
4	0	0	0.0035	0.0026	0.0254	0	0.0001	0.0002	0.0003	0	0	0	0	0.0321	8.0967
5	0	0	0	0.0001	0.0755	0	0.0001	0.003	0	0	0	0	0	0.0787	95.9012
6	0	0	0	0	0.0058	0.0035	0	0.0005	0	0	0	0	0.0032	0.013	26.5766
7	0	0	0	0	0.0007	0	0.0152	0	0	0	0	0	0	0.0159	95.7201
8	0	0	0.0003	0	0.0003	0	0	0.5836	0	0	0	0	0	0.5842	99.8964
9	0	0	0.0065	0.0002	0.0178	0	0	0.0003	0.0008	0	0	0	0.0006	0.0262	2.9941
10	0	0	0	0	0	0	0	0	0	0.0034	0	0	0	0.0034	99.5089
11	0	0	0	0	0	0	0	0	0	0	0.008	0	0	0.008	100
12	0	0	0	0	0.0004	0	0	0.0001	0	0	0	0.033	0	0.0335	98.6439
13	0	0	0.0003	0	0.0007	0	0	0.0016	0	0	0	0	0.0203	0.0229	88.9427
Total	0.0005	0.0025	0.1788	0.0039	0.1288	0.0035	0.0153	0.5962	0.0011	0.0034	0.008	0.0339	0.0241	1	
Producer's (%)	99.9254	99.92	94.0442	65.9957	58.6531	97.9531	98.9177	97.8859	72.1454	99.9744	99.9248	97.4218	83.9368		
95 % CI area	5294	1527227	3681236	1904676	4484473	2446758	916658	2994254	868962	65461	27611	1199501	2527184		
Overall accuracy [%]	91.686														
Kappa hat classification	0.8632														

Where: 1 = swamp rice field; 2 = non-swamp rice field; 3 = palm oil; 4 = moor; 5 = shrubs; 6 = reeds; 7 = mangrove; 8 = forest; 9 = open field; 10 = settlement; 11 = water body; 12 = pond; 13 = mine; CL = confidence interval

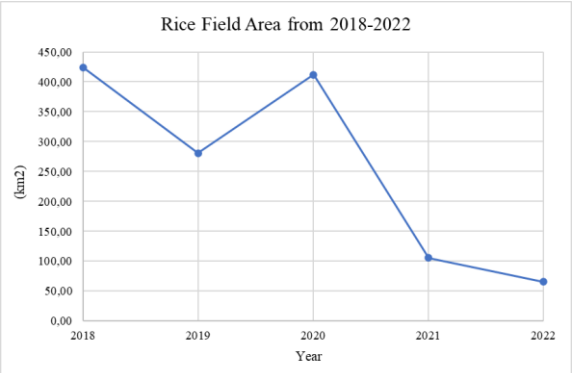
The error matrix in land use classification using Card's method adjusts both user and producer accuracy for each classification, based on the reference interval shown in the specific table (please provide the table number). The overall accuracy of the land use classification is 91.68%. In 2022, there were overestimations for forest, oil palm plantations, and shrubs due to commission errors, while non-wetland rice fields, wetland rice fields, settlements, and water bodies were underestimated due to omission errors. Despite these overestimations and underestimations, the classified land use areas fall within the upper and lower bounds of the actual regions with a confidence level of 95%. Errors in land use classification stem from spectral value similarities among categories, primarily observed in forest areas with shrubs, rice fields with Imperata grasslands, open land, and water bodies with ponds. After conducting the accuracy assessment, percentages and area calculations are derived from the land classification performed. The results of these calculations are presented in Table 3.

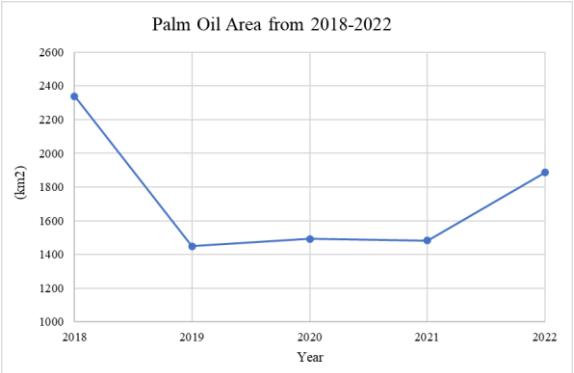
Table 3. Area of land use classes from 2018 to 2022

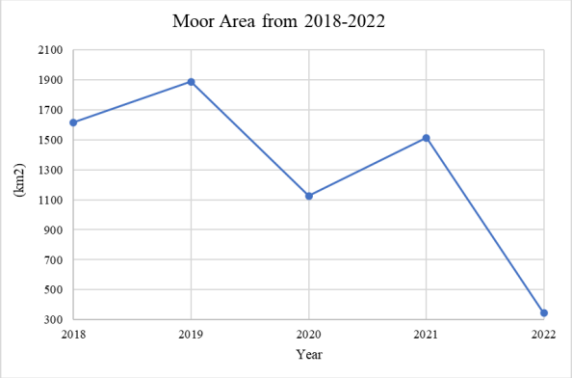
Land Use Classification	2018		2019		2020		2021		2022	
	Area (Km^2)	Precentage (%)	Area (Km^2)	Precentage (%)	Area (Km^2)	Precentage (%)	Area (Km^2)	Precentage (%)	Area (Km^2)	Precentage (%)
Swamp Rice Field	1.83	0.02	10.80	0.10	11.61	0.11	7.89	0.07	5.12	0.05
Non-Swamp Rice Field	422.27	3.95	270.01	2.52	400.18	3.74	98.02	0.92	60.77	0.57
Palm Oil	2338.88	21.85	1448.21	13.53	1493.38	13.95	1482.23	13.85	1886.03	17.62
Moor	1617.52	15.11	1889.45	17.66	1126.71	10.53	1513.78	14.14	342.84	3.20
Shrubs	375.83	3.51	489.69	4.58	1398.67	13.07	1165.52	10.89	843.15	7.88
Reeds	313.97	2.93	946.21	8.84	681.56	6.37	537.24	5.02	138.98	1.30
Mangrove	76.66	0.72	75.69	0.71	133.39	1.25	378.63	3.54	169.73	1.59
Forest	4998.20	46.70	4980.02	46.54	4742.68	44.31	4829.17	45.12	6253.22	58.42
Open Field	0.25	0.00	11.02	0.10	0.03	0.00	20.89	0.20	280.77	2.62
Settlement	24.42	0.23	110.28	1.03	95.01	0.89	87.71	0.82	36.24	0.34
Water Body	106.12	0.99	105.90	0.99	93.79	0.88	54.70	0.51	85.81	0.80
Pond	216.53	2.02	255.55	2.39	263.13	2.46	344.13	3.22	357.90	3.34
Mine	209.65	1.96	108.45	1.01	262.12	2.45	183.04	1.71	243.85	2.28
Total	10702.13547	100	10701.28307	100	10702.25562	100	10702.93966	100	10704.39437	100

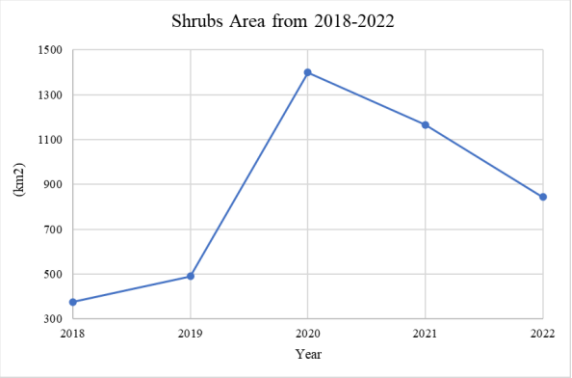
The data from Table 3 indicates that forests remain the largest land classification among others. It consistently maintains the highest percentage each year, and its expansive area demonstrates that forests still constitute the majority of land use in Paser Regency. Following forests, agricultural land becomes the second-largest classification in terms of percentage each year. Agricultural land in the form of oil palm plantations holds a significant share. Paddy fields, on the other hand, occupy a relatively smaller area. Meanwhile, classifications like gardens, Imperata grasslands, and shrubs have higher percentages compared to settlements. This presents an opportunity for their utilization as agricultural land, particularly for paddy fields, although their percentages are not as substantial as other classifications.

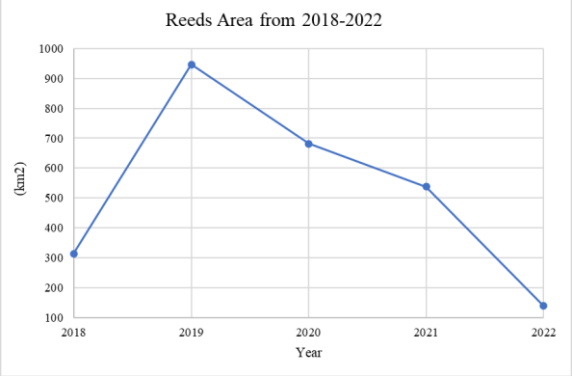
Between 2021 and 2022, all land classifications on the mainland, except for forests, oil palm plantations, open land, and mining, experienced a decrease in area. Agricultural land classifications in the form of paddy fields also decreased during this period. Similarly, classifications with the potential for conversion to paddy fields, such as gardens, shrubs, and Imperata grasslands, also saw a decrease. However, during the same period, the areas of oil palm plantations and open land increased. These changes indicate shifts in land use across various classifications, with conversions primarily occurring to either oil palm plantations or open land as part of the land use transition. The land area graphs for each classification in each year from 2018 to 2022 are presented in Figure 5.

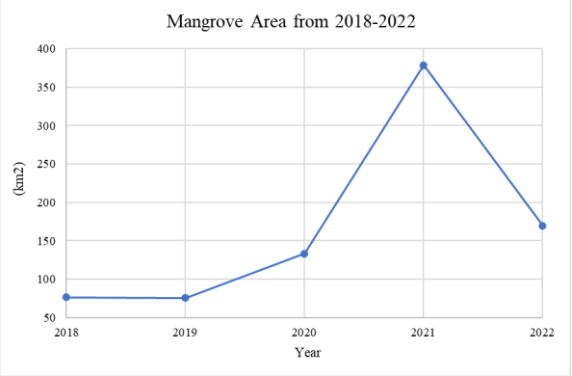


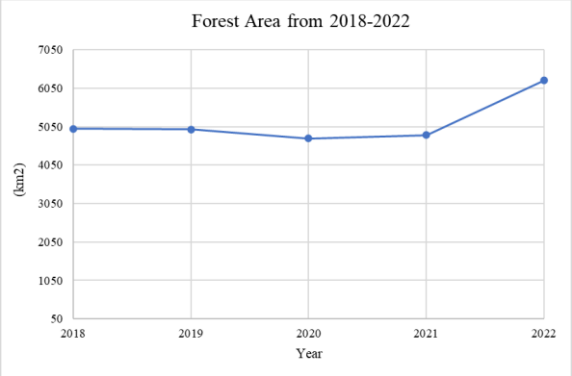


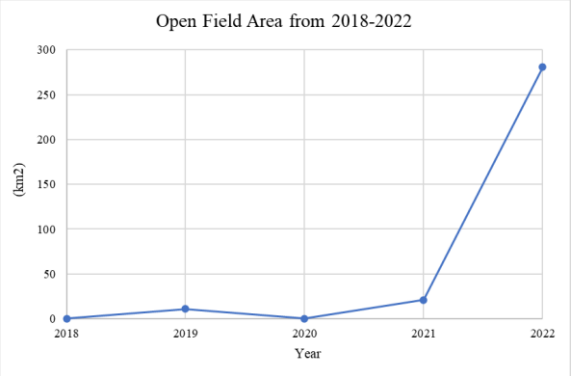

Moor Area from 2018-2022
(km2)
Year

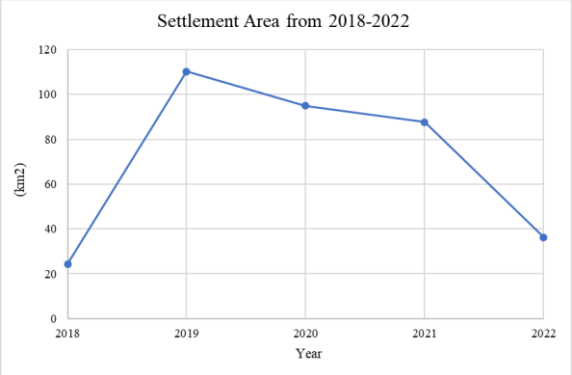

Shrubs Area from 2018-2022
(km2)
Year

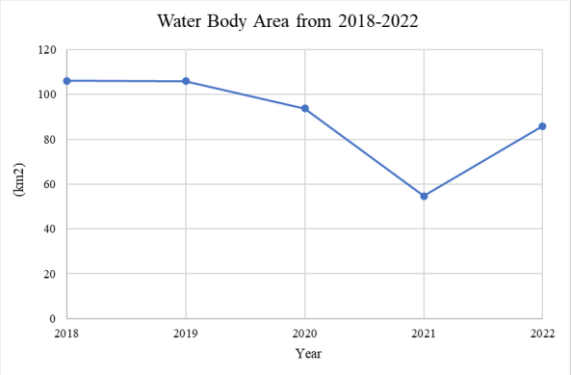

Reeds Area from 2018-2022
(km2)
Year


Mangrove Area from 2018-2022
(km2)
Year


Forest Area from 2018-2022
(km2)
Year


Open Field Area from 2018-2022
(km2)
Year


Settlement Area from 2018-2022
(km2)
Year


Water Body Area from 2018-2022
(km2)
Year

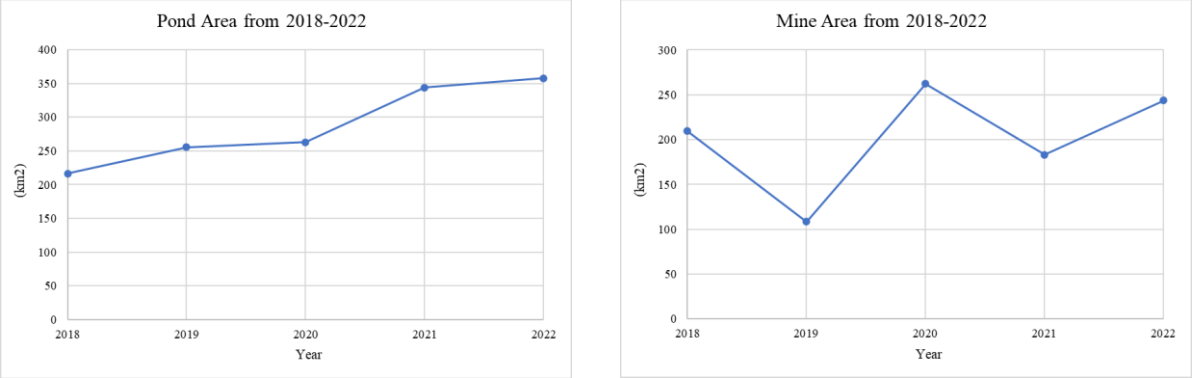


Figure 5. Graph of land use from 2018 to 2022

The land classifications of oil palm plantations, mining areas, and open land, as observed in the graph, tend to show an increasing trend. There was a decrease in 2019, but in the subsequent years, the area of these three land classifications consistently increased. The most significant increase for these land classifications occurred between 2021 and 2022, with oil palm plantations increasing by 3.77% and adding an area of 403.79 km², mining areas increasing by 0.56% and adding an area of 60.81 km², and open land increasing by 2.43% and adding an area of 259.88 km².

In the agricultural land classification, specifically paddy fields, there's a noticeable decrease in area. While there was an increase in 2020, the area of paddy fields decreased annually thereafter. Between 2021 and 2022, the paddy field area decreased by 0.37%, equating to a reduction of 40.02 km². For garden areas, there is a consistent trend of decreasing areas each year. Similarly, both shrubs and Imperata grasslands also exhibit a decreasing trend. The combined decrease in area for these three classifications amounts to 19.29%, covering 189.157 km². This highlights the susceptibility of these three classifications to land use changes.

3.2 Potential for Development of Agricultural Land for Food Crops

The development of agricultural land for food crops in Paser Regency should consider terrain conditions and soil types. Considering both slope and soil type is essential for expanding agricultural land. In this context, classifications such as gardens, shrubs, and Imperata grasslands emerge as potential candidates for conversion into agricultural land for food crops.

Based on the spatial analysis of land use in Paser Regency, the combined percentage of land occupied by garden areas, shrubs, and Imperata grasslands accounts for 12.38% of the total land area in Paser Regency. This percentage corresponds to an area of 132.497 km² or 13,249.7 hectares.

3.3 Potential for rice field land development

With an average rice crop production of 4 tons per hectare per year in Paser Regency, and considering this average production along with the potential land area for rice cultivation, the 132,497 hectares of land have the potential to yield approximately 5,299.88 tons of rice per year.

4. Conclusion

Spatially, there is a potential area of approximately 1,324.97 hectares in Paser Regency that can be developed into rice fields. However, land condition factors, particularly the characteristics of peat soil, which is naturally acidic, require special attention for the land to achieve optimal productivity. The use of NDVI Sentinel-2Ac Imagery enables accurate spatial land development analysis.

Acknowledgments
We would like to express my gratitude to the Directorate of Research at Universitas Gadjah Mada for providing research funding through the Final Project Recognition (RTA) Grant, Universitas Gadjah Mada, Number 5075/UN1.P.II/Dit-Lit/PT.01.01/2023.

References
[1] Rwanga S S and Ndambuki J M 2017 Accuracy Assessment of Land Use/Land Cover Classification Using Remote Sensing and GIS *Int. J. Geosci.* **08** 611–22
[2] Putri D R, Sukmono A and Sudarsono B 2018 Analisis Kombinasi Citra Sentinel-1a Dan Citra Sentinel-2a Untuk Klasifikasi Tutupan Lahan (Studi Kasus: Kabupaten Demak, Jawa Tengah) *J. Geod. Undip* **7** 85–96
[3] Lu D, Mausel P, Batistella M and Moran E 2004 Comparison of land-cover classification methods in the Brazilian Amazon basin *Photogramm. Eng. Remote Sensing* **70** 723–31
[4] Food and Agriculture Organization of the United Nations 2015 *The International Soil Classification System WRB, Third Edition, 2014*
[5] Nadzirah R, Indarto I and Brillyansyah D F 2022 Studi Pendahuluan Aplikasi Citra Sentinel Untuk Deteksi Luas Sawah Irigasi Di Kabupaten Jember *J. Ilm. Rekayasa Pertan. dan Biosist.* **10** 24–38
[6] Indarto I and Arif Faisol 2009 Identifikasi Dan Klasifikasi Peruntukan Lahan Menggunakan Citra Aster **IX**
[7] Kanata B, Iqbal M S and Ramdayanti R 2021 Analisis Citra Satelit Menggunakan Metode Supervised Classification Maximum Likelihood Pada Pemetaan Tutupan Lahan Di Taman Nasional Bukit Barisan Selatan (Tnbbs) *Dielektrika* **8** 44
[8] Rimal B, Rijal S and Kunwar R 2020 Comparing Support Vector Machines and Maximum Likelihood Classifiers for Mapping of Urbanization *J. Indian Soc. Remote Sens.* **48** 71–9

remote sensing

MDPI

Article

Detection of Leek Rust Disease under Field Conditions Using Hyperspectral Proximal Sensing and Machine Learning

Simon Appeltans [1], Jan G. Pieters [2] and Abdul M. Mouazen [1,*]

[1] Department of Environment, Faculty of Bioscience Engineering, Ghent University, 9000 Ghent, Belgium; Simon.Appeltans@UGent.be
[2] Department of Plants and Crops, Faculty of Bioscience Engineering, Ghent University, 9000 Ghent, Belgium; Jan.Pieters@UGent.be
* Correspondence: Abdul.Mouazen@UGent.be

Abstract: Rust disease is an important problem for leek cultivation worldwide. It reduces market value and in extreme cases destroys the entire harvest. Farmers have to resort to periodical full-field fungicide applications to prevent the spread of disease, once every 1 to 5 weeks, depending on the cultivar and weather conditions. This implies an economic cost for the farmer and an environmental cost for society. Hyperspectral sensors have been extensively used to address this issue in research, but their application in the field has been limited to a relatively low number of crops, excluding leek, due to the high investment costs and complex data gathering and analysis associated with these sensors. To fill this gap, a methodology was developed for detecting leek rust disease using hyperspectral proximal sensing data combined with supervised machine learning. First, a hyperspectral library was constructed containing 43,416 spectra with a waveband range of 400–1000 nm, measured under field conditions. Then, an extensive evaluation of 11 common classifiers was performed using the scikit-learn machine learning library in Python, combined with a variety of wavelength selection techniques and preprocessing strategies. The best performing model was a (linear) logistic regression model that was able to correctly classify rust disease with an accuracy of 98.14%, using reflectance values at 556 and 661 nm, combined with the value of the first derivative at 511 nm. This model was used to classify unlabelled hyperspectral images, confirming that the model was able to accurately classify leek rust disease symptoms. It can be concluded that the results in this work are an important step towards the mapping of leek rust disease, and that future research is needed to overcome certain challenges before variable rate fungicide applications can be adopted against leek rust disease.

Keywords: hyperspectral; proximal sensing; disease detection; leek; rust; machine learning

check for updates

Citation: Appeltans, S.; Pieters, J.G.; Mouazen, A.M. Detection of Leek Rust Disease under Field Conditions Using Hyperspectral Proximal Sensing and Machine Learning. *Remote Sens.* **2021**, *13*, 1341. https://doi.org/10.3390/rs13071341

Academic Editor: Mario Cunha

Received: 5 March 2021
Accepted: 30 March 2021
Published: 1 April 2021

Publisher's Note: MDPI stays neutral with regard to jurisdictional claims in published maps and institutional affiliations.

Copyright: © 2021 by the authors. Licensee MDPI, Basel, Switzerland. This article is an open access article distributed under the terms and conditions of the Creative Commons Attribution (CC BY) license (https://creativecommons.org/licenses/by/4.0/).

1. Introduction

Agricultural production systems are under increasing pressure to produce qualitative products in a complex economic system while adhering to strict environmental guidelines [1]. These environmental and economic constraints stimulate farmers to reduce the amount of agrochemical inputs as much as possible. At the same time, crop diseases have been one of the most important yield limiting factors since the dawn of agriculture and require a constant input of crop protection compounds [2]. With advances in smart farming made in the last decade, sustainable crop protection using site-specific technology has advanced enough to start being brought into practice. However, the use of crop sensing tools to provide accurate data on specific diseases is still challenging for the majority of crops, especially at the field level [1,3,4].

Leek (*Allium ampeloprasum* var. *porrum*) is a high value vegetable crop grown all over the world [5–7]. One of the most important yield limiting factors in commercial leek cultivation is rust disease, caused by the pathogen *Puccinia allii* Rud. [8–10]. The pathogen damages the crop by forming small, orange pustules, which reduce its market value. In extreme cases, this disease can completely destroy the harvest. This happens when enough

inoculum is present in the field combined with the presence of free moisture on the crop surface and temperatures ranging from 12 to 20 °C. Leek cultivation is performed year-round in most cultivation systems, making it likely that at some point in the cultivation process favourable climatic conditions for the pathogen occur in temperate climates. The threat presented by this pathogen therefore causes the need for regular full-field fungicide treatments, at intervals between once a week to once every five weeks depending on the cultivar and the weather conditions [10]. This represents a significant economic cost for the farmer and puts a strain on the environment [11]. Moreover, constant full-field application of a small range of fungicides can have detrimental effects due to the build-up of fungicide resistance in the pathogen population [10]. It has further been shown that rust disease inoculum mainly stems from existing leek infection sites, with only minor significance of alternate hosts and survival spores [12]. This means that despite regular fungicide treatments, there is still a self-propagating presence of rust disease in leek growing areas. This continuous infection cycle, together with the high environmental and economic costs, show the need for more advanced crop protection strategies.

Precision agriculture has the potential to help solve this problem (not only the disease itself, but also the environmental and economic costs of its control) by applying the correct dose at the correct place at the correct time [13–15]. Even though precision agriculture has risen in popularity with the development of new sensing technologies, its core principles have been in practice for a much longer time. The first records of detection and variable rate fungicide treatment of leek rust disease can be traced back as far as 1995 [12]. Farmers at that time are reported to already have experimented with waiting to apply crop protection measures until first symptoms were visible and with spraying only the infected sites in the field. However, these disease detection strategies relied on visual inspection of the crop by either the farmer or a specialist trained in the diagnosis of disease symptoms [4]. This is an extremely labour-intensive process, which is not feasible for an entire field, except in dedicated experimental trials. Modern crop protection strategies aim to replace visual inspection by employing cutting-edge sensors to detect crop diseases in the field [16]. This information provided at high sampling density both in space and time can then be used to apply variable rate fungicide treatments [14]. Of these cutting-edge sensors, hyperspectral sensors have been put forward as valuable tools for disease detection, especially for diseases with pigment changes such as leek rust disease [3,4,14,17,18]. These authors reported that the visible region is interesting regarding changes in pigmentation, with an increase in the orange and red spectral region (600–680), while the NIR-region (near-infrared) reflectance reduces due to cell structural damage. However, despite an extensive literature search, no published work was found regarding the detection of leek rust disease using hyperspectral sensing, even though leek rust disease has been described in the literature for the past 40 years [12,19–28]. Instead, the rust disease control strategies cited here focus on searching for resistant cultivars and effective control strategies using fungicides. This could be explained by the fact that most of these articles were situated between 1978 and 2000, before hyperspectral sensors became commonplace in research.

Several authors have used hyperspectral sensing for detecting rust disease in other arable crops such as wheat and sugarcane [1,3,18,29–35]. Looking at recent findings in the literature regarding variable rate crop protection with hyperspectral sensors, it is clear that one of the biggest remaining challenges is disease detection under field conditions. [1,3,4]. This is because the analysis of hyperspectral data often involves the use of complex algorithms, such as machine learning techniques, which are often trained on data gathered in laboratory conditions that is not necessarily representative for field conditions. A summary of such techniques may be found in the recent review by Paulus and Mahlein (2020) [36]. In the field, more unknown biotic and abiotic factors influence measurements compared to highly controlled laboratory conditions, making it difficult to scale conclusions reached in laboratory studies to the field. [1,16,37]. A recent review specifically aimed at close-range hyperspectral imaging confirms that there has been a lot of progress under controlled conditions (laboratory or greenhouse), but that a lot of challenges remain for field appli-

cations at close range [38]. The main challenges are (a) the variability of reflectance due to within-crop shading and the complex geometry of the crop canopy, (b) the extremely large amount of data provided by these techniques, and (c) the high cost of commercially available hyperspectral sensors. Regarding this last point, it is important to realize that for research, the ability to study the entire spectrum can be a valuable asset, because it allows the researcher to determine which wavebands are important features. It further allows the researcher to use preprocessing techniques such as smoothing, with large smoothing windows, to reduce noise. For practical/commercial applications, it would however be better to employ multispectral or RGB cameras (red-green-blue cameras) where possible, because they are cheaper and simpler. The possibility of being able to use simpler sensors is one of the outcomes of hyperspectral crop sensing studies.

The aim of this work was to develop a novel method for detecting leek rust disease under field conditions using a linescan hyperspectral sensor. The objectives to reach this goal were: (a) construction of a labelled hyperspectral library containing field data corresponding to four classes (healthy leek crops, leek rust disease symptoms, weeds, and soil); (b) training a machine learning disease detection model based on this dataset; (c) validation of this model on completely new, unlabelled hyperspectral images

2. Materials and Methods

2.1. Test Field

Due to weather conditions, there was limited availability of naturally occurring leek rust disease in commercial farmers' fields, and artificial inoculation proved difficult. For this reason, and to increase the variability in the hyperspectral training dataset, two data collection sites were selected. Because the aim was to develop an in-situ disease detection methodology, both measurement locations were subjected to standard farming procedures for leek cultivation.

Data was first collected from leek plot trials at two locations. The first measurement site was the experimental field of the 'Provinciaal Proefcentrum voor de Groenteteelt Oost-Vlaanderen' (PCG), Kruishoutem (Kruisem), Belgium, with coordinates of 50°56′40.3404″ N, 3°31′26.4108″ E. This field was used by the experimental centre to conduct a leek rust disease fungicide trial, whereby the Lucretius cultivar was cultivated under normal farming conditions and the efficacy of a range of fungicides was assessed by comparing levels of naturally occurring infection under different spraying regimes. Leek plants were planted in ridges with a width of 0.65 m and a within row distance of 0.10 m, with four ridges per crop row. Plots were delineated with a length of 2.5 m per plot (Figure 1). Measurements were taken in December 2018 and in February 2019. Data was measured at 6 points along the crop row (Figure 1), scanning in the direction perpendicular to the crop row (Figure 1A). The soil type in this field was loamy sand, with a relatively dark colour. The second data collection site was a dedicated disease detection experimental field at the Bottelare experimental farm (Merelbeke, Belgium) of Ghent University and Ghent University College with coordinates of 50°57′45.2″ N, 3°45′36.3″ E. The soil type in Bottelare consisted of a sandy loam, with a reddish-brown colour. Leek plants of cultivar Pluston were pre-germinated and grown in pots, after which they were transplanted to the field in ridges with a width of 0.75 m and a height of 0.30 m, at a within-row distance of 0.12 m. The field was then divided into plots of 3 by 3 m, to match the width of the measurement frame in both directions (making it possible to measure along the crop row), and artificially inoculated on 18 March 2019. The inoculation consisted of four treatments: inoculation with rust disease, with leek white tip disease (*Phytophthora porri* Foister), with both diseases at the same time, on the same plants, and finally a control without artificial inoculation. Four plots were treated for each of these four treatments, leading to a total of 16 plots. Inoculation followed a randomized block design. Since the first inoculation proved unsuccessful, a second inoculation attempt was performed on 4 April 2019, which was relatively successful. However, disease pressure in the Bottelare experimental field never grew to more than a few plants infected per plot, for either disease. Measurements were taken at approximately one-week intervals

between March 2019 and May 2019 (Table 1), with concurrent measurements of % leaf area infected by rust disease (Figure 2). These measurements were performed along the crop row (Figure 1B). Only the middle two rows of each plot were measured, to avoid edge effects. Results for white tip disease are not shown in this work.

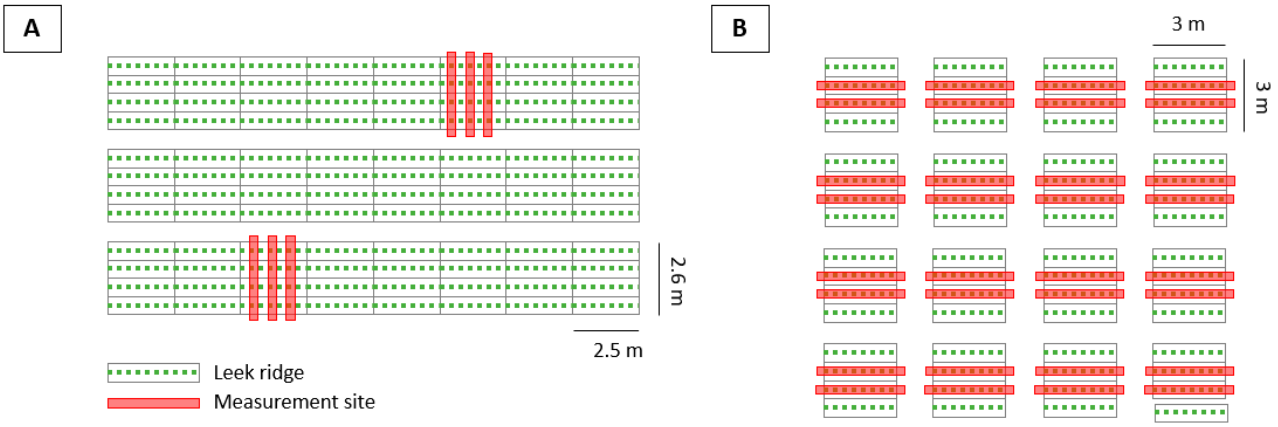


Figure 1. (**A**) Layout of the leek field at the experimental centre, 'Provinciaal Proefcentrum voor de Groenteteelt Oost-Vlaanderen' (PCG) in Kruishoutem, cultivated under normal farming conditions. Lines indicate the delineation of plots, each representing a different fungicide used in the fungicide trial of the experimental centre in Kruishoutem. PCG plots had a dimension of 2.5 by 2.6 m. The direction of measurement is perpendicular to the crop row. (**B**) Layout of the leek test plots at Bottelare. Direction of measurement is along the crop row. Each plot represents a site that received one of four inoculation treatments (leek rust disease, leek white tip disease, both diseases, no disease). Results for white tip disease are not shown in this work. Bottelare plots had dimensions of 3 by 3 m.

Table 1. Measurement scheme of the PCG and Bottelare data acquisition campaigns. Each 'plot' contained 4 rows of leek, but only the middle 2 rows were measured to avoid edge effects.

Measurement Description	Bottelare	PCG
Measurement days	12 days: weekly from March 2019–May 2019	2 days: 19 December 2018 and 14 February 2019
#plots scanned	16	2
Total # scans	384: 2 scans per plot, taken at 12 timepoints	12: 3 scans per plot, taken at two timepoints
Total # of plants scanned	8640: 20 plants per scan	120: 10 plants per scan
Disease pressure at the time of measurement, scored following the EPPO PP 1/120(2) Guideline	Disease pressure too low to measure (only a few plants per plot showing mild symptoms)	One plot at 10.32 % leaf surface area infected (highly diseased) One plot at 0.84 % leaf surface area infected (early disease)

Infection Statistics	Bottelare	PCG (Low Infection)	PCG (High Infection)
Mean leaf are infected (%)	Under detection limit	0.84	10.32
Standard deviation of infected leaf area	Under detection limit	0.62	4.60

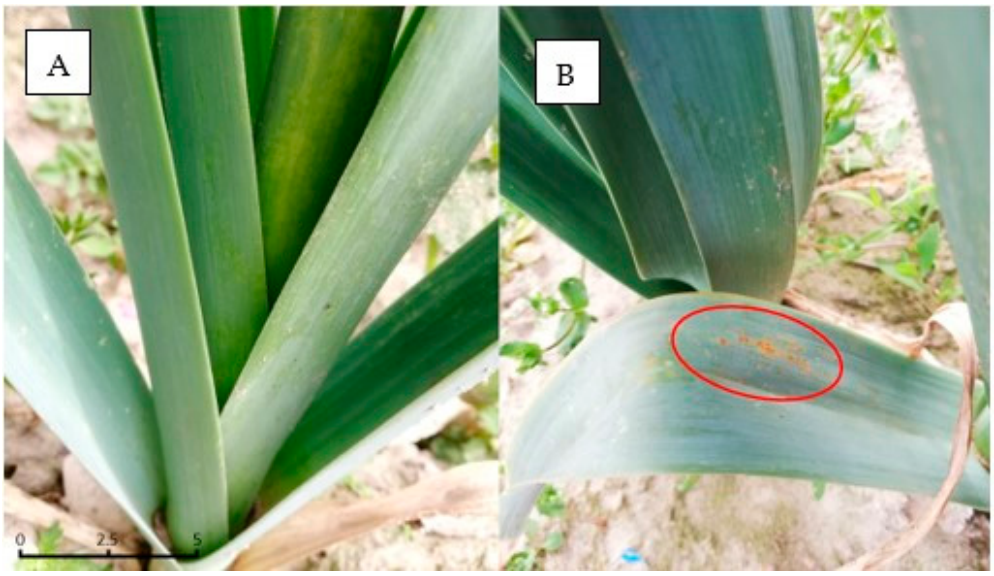


Figure 2. (**A**) Healthy leek crop with 0% leaf area infected. (**B**) leek plant infected with rust disease, showing orange pustules on approximately 3% of leaf area infected. Scale in cm.

2.2. Visual Assessment of Rust Disease Severity

During the first measurement campaign at PCG, 6 sites were selected in the crop row for scanning based on the visual presence of rust disease. During the second scanning campaign, the same 6 sites were scanned again (Table 1; Figure 1). The average infection was measured over 25 plants for both plots, using the percentage of area covered with rust symptoms per plant as a measure for disease intensity, which conforms with the EPPO PP 1/120(2)—Guideline for the efficacy evaluation of fungicides on foliage diseases of Allium crops. The intensity of infection was only available from the experimental centre for the first measurement day in December. The first plot contained low rust infection with an average of 0.84% of the leaf area infected, while the second plot showed high rust infection, with an average of 10.32%. This gave two datasets, one with relatively low disease pressure and one with high disease pressure.

Since the Bottelare test plots showed very low levels of infection, a different disease severity assessment was used, based on the methodology described in Clarkson et al. (1997) [19]. The low amount of pustules per plant measured at the Bottelare experimental facility were likely due to the weather, which was extremely dry for the time of year, limiting spread of infection [8]. The data gathered at the Bottelare experimental farm contained mostly plants with zero rust pustules and a small amount of plants with 0–10 rust pustules per plant on average, representing an early stage of leek rust infection.

2.3. Sensor Setup

Measurements were performed with a hyperspectral pushbroom sensor with a range of 400 to 1000 nm (Specim, Oulu, Finland) and a full width at half maximum value of 5.5 nm, which is the distance between the centre and the edge of the band. Data was collected following a previously determined optimal scanning configuration, with an exposure time of 1 ms, a measurement height of 0.30 m, and a scanning angle of 17° [39]. The sensor was moved over the crop canopy with a customised aluminium frame (Figure 3). The aluminium frame formed an upturned U-shaped structure, which rested on four wheels. Between the supports of the frame, an aluminium bar with a length of 3 m was positioned at adjustable height. The sensor box was attached to this bar by a wheels-and-rail system. The aluminium frame pieces and the aluminium bar could be dismounted and broken up into several smaller pieces for transport. An electric motor powered by a 12 V battery moved the sensor box along the length of the bar at a pre-set constant speed, using a rubber driver belt. Two 500 W tungsten halogen lamps (Powerplus, Ah Joure, The Netherlands) were attached

on both sides of the sensor box to provide additional illumination for the hyperspectral camera, following the setup of Whetton et al. (2018) [35]. It was essential that these lamps were halogen, to ensure they emitted radiation with a continuous spectrum [3]. A generator was used to power the sensor and artificial lamps. A battery-powered pyranometer (Skye Instruments, Llandrindod Wells, UK) was used to measure incoming solar radiation. Two reference values, a 'dark' reference and a 'white' or 'bright' reference, were measured at the start of each measurement, and repeatedly during measurements if the incoming solar radiation (measured with the pyranometer) varied more than 75 W/m^2. The value of 75 W/m^2 was empirically observed to be greater than the natural fluctuations of incident light when cloud conditions remained stable. The dark reference was the signal measured while the camera shutter or lens cap was closed, representing the background signal caused by electrical currents in the sensor. The white reference value was measured by scanning a white reference target (SphereOptics, Germany, Alucore reflectance target, 500 × 500 mm, 95% reflectance, calibrated) with the hyperspectral camera. All data storage was done on external solid state drives.

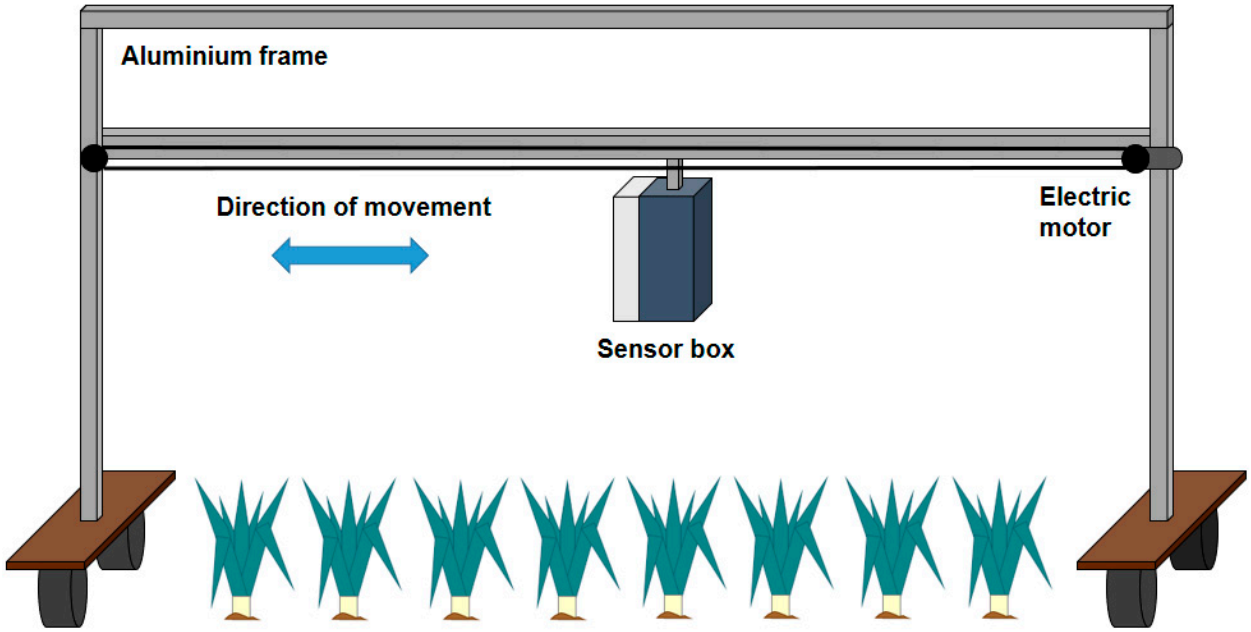


Figure 3. Aluminium measurement frame with sensor box containing a pushbroom hyperspectral sensor, which is propelled by an electric motor at constant speeds over a lateral aluminium bar. The entire frame is then moved to measurement sites, over the crop row.

2.4. Hyperspectral Library Building

Since the pixel resolution was on the sub-millimetre scale, it was possible to visually select representative regions of interest (ROI) from hyperspectral images (belonging to both the PCG and Bottelare datasets) for each of the four classes (healthy, rust, weeds, soil), using ENVI software (Harris Geospatial, Boulder, CO, USA). Images were selected based on the clear visual presence of pure pixels for each of the four training classes, needed for ROI delineation. Each ROI consisted of an area of image pixels (spatial resolution 0.38 mm) with underlying spectra. This selection was done manually in ENVI, with the mouse button, defining the regions in the image that were clearly visible as soil, healthy leek, rust disease or weeds. The spectra belonging to these pixels were then exported from ENVI to the final hyperspectral training library (in '.csv' format). This method of extracting spectra from a ROI and treating each spectrum as a sample is concurrent to the work of Xie et al. (2015), where hyperspectral data was used to detect early and late blight disease on tomato leaves [40]. The dataset resulting from these visually selected regions is referred to as the hyperspectral library.

Since the Bottelare dataset contained relatively few infection sites that were clearly visible to the naked eye on the hyperspectral images, the hyperspectral library was based solely on rust spectra measured at PCG (Table 2). More than 10,000 spectra were selected that clearly belonged to rust pustules, both shaded and unshaded. For healthy leek spectra, it was decided to only incorporate the Bottelare dataset, since it was impossible to clearly delineate fully healthy ROIs in the hyperspectral images measured at PCG, because the infection was so severe. ROIs were selected from different leaves of different plants until again more than 10,000 healthy spectra were gathered. Because the PCG dataset showed extremely low weed presence, only weed spectra from the Bottelare dataset were incorporated in the hyperspectral library. Here, weed pressure was extremely high, with dozens of weed species on the crop ridge. Again, more than 10,000 weed spectra were selected and incorporated into the hyperspectral library. These spectra were obtained from pixels that were evenly spread over the weed mass present in a representative scan taken before disease pressure was present in the field. Because weed coverage was so intense in Bottelare, it was difficult to clearly delineate ROIs that contained only soil and no plant matter with relative certainty. It was therefore necessary to select and incorporate soil spectra based on the PCG measurements. The size of each individual ROI varied, from 2 by 2 pixels for individual leek rust symptoms to several dozens by dozens of pixels for soil, healthy leek, and weeds. However, the final number of training spectra for each training class was made identical at 10,854, leading to a hyperspectral library containing 43,416 spectra.

Table 2. Sampling location of the regions of interest used in the construction of the hyperspectral library, for each of the four classes.

	Training Dataset
Rust	PCG experimental field, 3 locations from the heavy disease pressure plot, measured in December
Healthy	Bottelare, 1 plot, measured PI 50 *
Weeds	Bottelare,1 plot, measured PI 30
Soil	PCG experimental field, 1 plot, measured in December

* PI is Post Infection, signifying the number of days after initial inoculation of the crop.

2.5. Preprocessing and Model Selection

The hyperspectral library was used to optimize preprocessing and modelling, following the flow outlined in Figure 4. The square box with marked 'Final workflow' outlines the final workflow for detecting leek rust disease, including the steps: preprocessing 1, soil model, differentiation non-soil from soil pixels in the hyperspectral image, preprocessing 2, and finally the rust model that determines the pixels representing leek rust diseased areas of the crop. The steps that are not outlined in this box represent the steps taken to achieve the final workflow, including the following steps: initial preprocessing, data exploration, followed by an iteration of: selection of disease detection models, their evaluation on unlabelled data, and improved preprocessing. First, the process used to determine the final workflow is discussed in this section. Then, the final workflow is summarized in the next section.

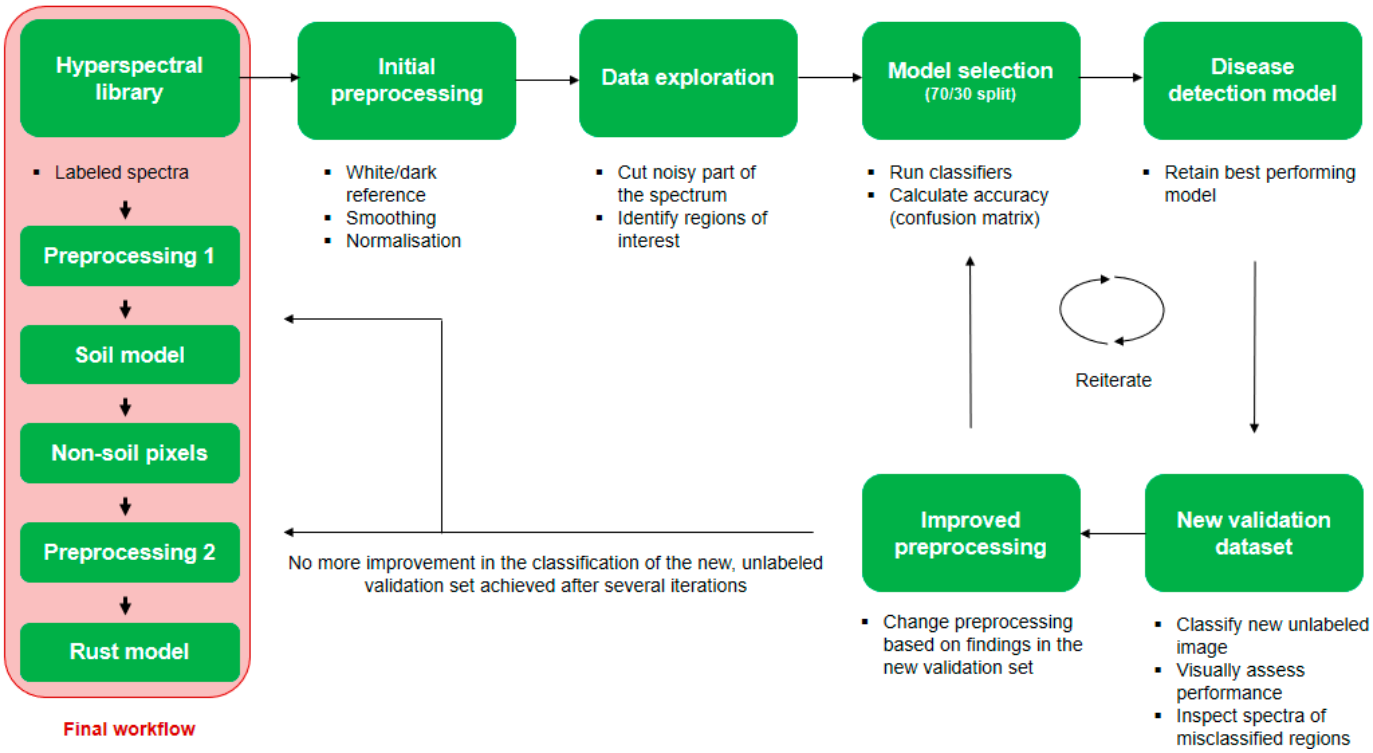


Figure 4. Preprocessing and model selection cycle. The area highlighted in the leftmost square box with wording 'Final workflow' represents the final workflow. The rest of the chart represents the steps taken to determine this final workflow.

The first part of the initial preprocessing step was the pixel per pixel correction of the raw hyperspectral image from the sensor using following formula:

$$R_cor = (R_raw - R_dr)/(R_wr - R_dr) \quad (1)$$

where R_cor is the corrected reflectance spectrum of the measured sample at a certain pixel, R_wr is the averaged white reference reflectance spectrum, representing the 'maximum' reflectance spectrum, measured on a calibrated white reference target (SphereOptics, Herrsching, Germany, Alucore reflectance target, 500 × 500 mm, 95% reflectance, calibrated), R_raw is the raw reflectance of the sample measured and R_dr is the averaged dark, or minimum, reflectance spectrum, measured with a closed camera shutter.

Initial results showed that there was a lot of noise and variability in the spectral dataset. The second step therefore was to apply a Savitsky-Golay smoothing algorithm (window 33, polyorder 2), followed by a min/max normalisation that scaled the reflectance measurements between 0 and 1 [41]. The smoothing window was determined by trial and error, by iteratively changing the smoothing window from 1 to 55 (after which a greater window had no further effect) and assessing the classification accuracy. Part of the spectrum before 445 nm and after 914 nm were cut from the dataset because they appeared to contain more noise than the rest of the spectrum during data exploration (Figure 5). The presence of noise is a common issue in hyperspectral sensing, especially in field conditions, and can be caused by a variety of environmental and sensor-specific parameters [42]. Data exploration further involved the visual identification of regions in the spectrum that appeared to contain differences between the four classes of the model (healthy leek, rust disease, weeds, and soil).

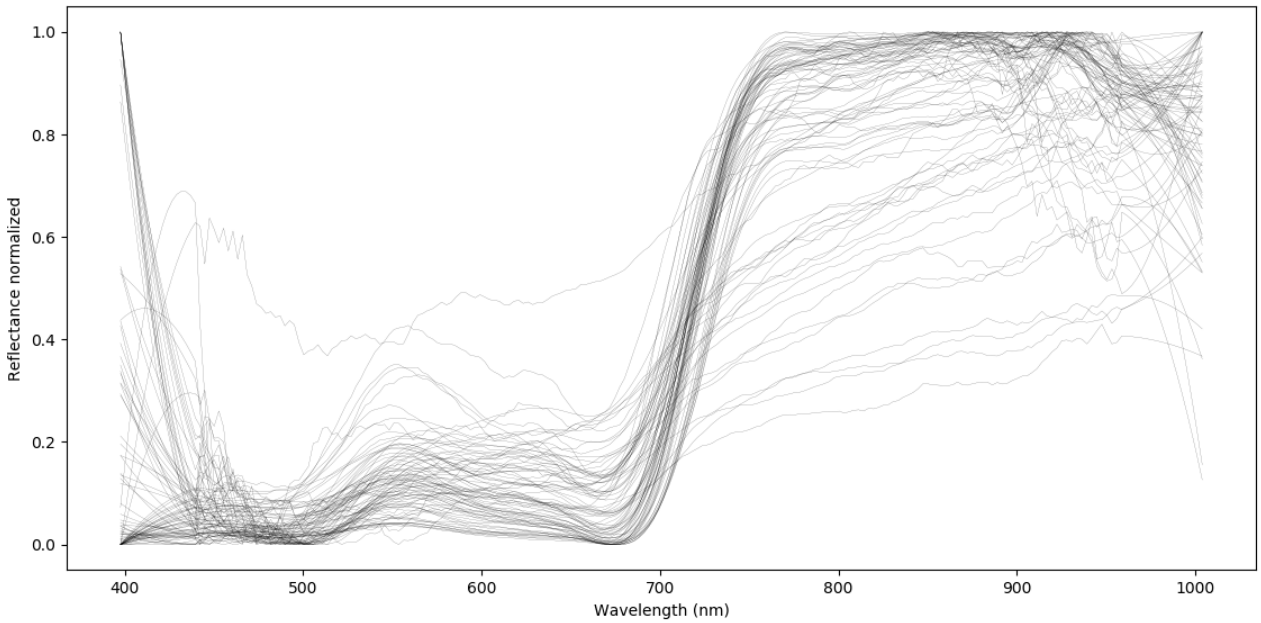


Figure 5. Random selection of spectra from the hyperspectral library after Savitsky-Golay smoothing and normalisation, showing high amounts of noise at the beginning and end of the spectrum.

These initial preprocessed spectra (after white/dark reference correction, smoothing and normalisation) were then tested for classification using the scikit-learn library of the Python programming environment (Python Software Foundation, Wilmington, DE, USA), with a selection of common classifiers, including: K nearest neighbors classifier, support vector machine classifier, gaussian process classifier, decision tree classifier, random forest classifier, multilinear perceptron classifier, AdaBoost classifier, gaussianNB classifier, logistic regression classifier, Linear Discriminant Analysis classification, and quadratic discriminant analysis classification [43]. The classifiers were tested with both the default model parameters and variations concerning for example kernel or solver type.

To assess the performance of each classifier, the hyperspectral library was split into two datasets: 70% of the data was used for model training, and 30% was used as an independent validation set, also known as the 'hold-out' set [44]. The quality of this validation was assessed by computing the accuracy of classification (obtained from the confusion matrix) on the labelled validation set. The best performing model, or models in case results were close, was retained and used to classify a new, unlabelled hyperspectral image, referred to as the 'new validation set' in the workflow of Figure 4. The quality of this classification was then assessed by visually comparing the RGB image obtained from the hypercube to the classified image. The spectra of misclassified areas were studied, and the preprocessing or modelling strategy was adapted based on these misclassifications. These adaptations included combinations of several commonly used techniques [45–49]:

1. Changing the wavebands used as model input based on (a) manual selection of wavebands and (b) applying wavelength selection algorithms
2. Changing the smoothing window
3. Changing and combining classifiers
4. Including first and/or second derivative data in the model input
5. Including ratios and indices in the model input
6. Performing principle component analysis (PCA) and/or linear discriminant analysis as a dimensionality reduction step
7. Training label manipulation by changing labels in the hyperspectral library of problematic spectra, intentionally feeding 'falsely' labelled data to the model to increase model performance (see Section 2.6, Final Disease Detection Workflow) [49]

After changing the preprocessing strategy following the steps mentioned above, the cycle started anew by running each classifier with this new preprocessing strategy and again calculating the accuracy. During this iterative process, some classifiers were excluded from the analysis because they consistently underperformed. This process was repeated until no apparent improvement was observed in the confusion matrix and in the unlabelled classification.

The waveband selection algorithms tested were the standard algorithms provided by the scikit-learn package, namely 'SelectKBest' and 'SelectFromModel' [43]. These algorithms suffered from the high correlation between neighbouring bands and often resulted in the selection of a group of neighbouring bands from a single spectral region as being 'optimal'. This might not represent the true optimal combination, since it does not contain information for each region. We therefore adopted a strategy to use these waveband selection algorithms to select the optimal waveband per region of the spectrum. This then lead for example to 1 band for the first 10 bands measured, and another for each consecutive group of 10 bands. Then, the waveband selection algorithm was run again on this new group of 17 'optimal' bands, resulting in a small group of 3–5 bands. Other dimensionality reduction strategies were tested as well, including LDA and PCA.

2.6. Final Disease Detection Workflow

The final workflow consisted of two classification steps: soil classification and leek rust disease classification. These two classification steps each have respective preprocessing steps, represented by 'Preprocessing 1' and 'Preprocessing 2' in Figure 4.

Preprocessing 1. First, white/dark reference correction was performed on the raw data coming from the hyperspectral camera. A Savitsky-Golay smoothing algorithm (window 33, polyorder 2) was then applied to this data. Then, reflectance values for wavelengths below 445 or higher than 914 nm were cut, retaining only the 174 bands in between. Finally, the first derivative of the reflectance curve was taken.

Soil classification model. Soil classification was achieved by using the value of the 702 nm waveband of this 'first derivative spectrum', combined with a standard LDA algorithm from the scikit-learn Python library. No normalisation was applied to this data during this step. This resulted in a matrix containing the location of soil and non-soil pixels. The non-soil pixel indices were then used to isolate non-soil spectra from the (non-preprocessed) hyperspectral library, which were then submitted to the 'Preprocessing 2' step. Note that the non-soil spectra were extracted from the non-preprocessed hyperspectral library, meaning that the spectra used in the disease detection model only received the 'Preprocessing 2' treatment at the time they are used as model inputs. The 'Preprocessing 1' and 'Soil model' steps were used exclusively to differentiate between soil and non-soil pixels.

Preprocessing 2. First, white/dark reference correction was performed on the raw data acquired by the hyperspectral camera. A Savitsky-Golay smoothing algorithm (window 33, polyorder 2) was then applied to this data. Then, reflectance values before 445 and after 914 nm were cut, retaining only the 174 bands in between. A normalisation step was added after this, transforming the data to a range between 0 and 1, to reduce effects of within crop shading and differences due to solar radiation. The first derivative was also taken, but after normalisation (contrary to the 'Preprocessing 1' step for soil classification, where the first derivative was taken before normalisation because the distinction between soil and non-soil first derivative spectra was more clear prior to normalisation). The normalisation step was necessary to reduce effects of differences in absolute reflectance, such as within crop shading. Using this data, a large amount of false positives occurred due to the misclassification of weed spectra as 'rust', even in scans without rust disease present in the field. Analysis of these misclassified spectra showed that these weed spectra showed a relatively high reflectance in and near the 661 nm band (reflectance of up to 0.1 after preprocessing). Rust spectra typically show a much higher reflectance in this band, up to 0.35, which is not surprising given the orange/red appearance of rust pustules. However, some rust spectra in the hyperspectral library showed a reflectance in this band lower than

0.1, making these spectra more similar to the misclassified weed spectra. It is possible that these particular rust spectra were selected (during the construction of the hyperspectral library, see Section 2.4, Hyperspectral Library Building) from pixels located at the edge of the rust pustule, where the rust spectrum is mixed with that of the surrounding plant tissue. It appeared that the similarity between certain rust spectra in the training data with relatively low reflectance (for being rust spectra) in the 661 nm band and certain weed spectra in the training data with relatively high reflectance (for being weed spectra) in the 661 nm band contributed to misclassification.

To solve this issue, the training labels of rust spectra in the hyperspectral library with a reflection in the 661 nm waveband lower than 0.13 (after preprocessing) were changed from 'rust' to 'weed', essentially performing a form of training label manipulation by intentionally feeding altered information to the training step of the model to increase model performance [49]. By changing the labels from 'rust' to 'weed' of these specific rust spectra with low reflectance in the 661 nm band, a new training dataset was created, where all rust-labelled spectra have a reflectance in the 661 nm higher than 0.13. As a result, the model learned that spectra with low reflectance in this waveband (below 0.13) should be classified as 'non-rust spectra', since all training spectra with a 'rust' label showed high reflectance (above 0.13) in this waveband. This step solved the misclassification issue and proved essential to increase model performance.

Rust classification model. The preprocessed dataset was fed to a logistic regression model using only three values: the reflectance values at 556 and 661 nm, combined with the value of the first derivative at 511 nm (see Results section for feature selection process). The class weights were set to 0.4 for rust, 1 for healthy plant parts, and 1 for weeds. The general form of a linear logistic regression model and further details on its structure can be found in the Scikit-learn documentation and in Serneels and Lambin (2001) [43,50].

3. Results

3.1. Data Exploration

Figure 6 shows a plot of the average reflectance spectrum for each of the four classes in the training dataset after normalisation and smoothing. Error bars represent the standard deviation for each wavelength. It can be observed that the healthy leek spectra appeared most 'stable', showing lower standard deviation values throughout the spectrum. Note that the minimum was around the 680 nm wavelength, which represents the photosystem II absorption band, which typically shows low reflectance (i.e. high absorbance) in healthy crops [51]. Weed spectra generally showed higher standard deviations, with also low reflection around the 680 nm band but with a larger standard deviation compared to the healthy leek spectra. It is interesting to note the apparent decrease in reflection at wavelengths higher than 880 nm in the weed spectrum. The difference is relatively small however, with a quite high standard deviation in this region. The rust spectrum showed both a high reflectance and a high standard deviation around the 680 nm waveband. Higher reflection in the entire red colour region of the spectrum was clearly visible, even though standard deviation values were high. It is worth noting that the red edge region appeared to start around 680–690 nm. This work therefore adopts the spectral range nomenclature proposed by Malacara (2003), but makes the distinction that the red region is defined from 625 to 690 nm and the red edge region from 690 to 750 nm [52]. The soil reflectance curve appeared more flattened compared to that of the leek, rust, and weed spectra, with less of a steep curve in the red edge region of the spectrum. The 480 nm absorption band (associated with carotenoids in leaves and soil) and the 670 nm chlorophyll absorption band showed clear minima in both the weed and healthy reflectance curves, which is in line with observation by other scientists [53]. The rust and soil reflectance curves showed no minimum at the chlorophyll band, only at the 480 nm band.

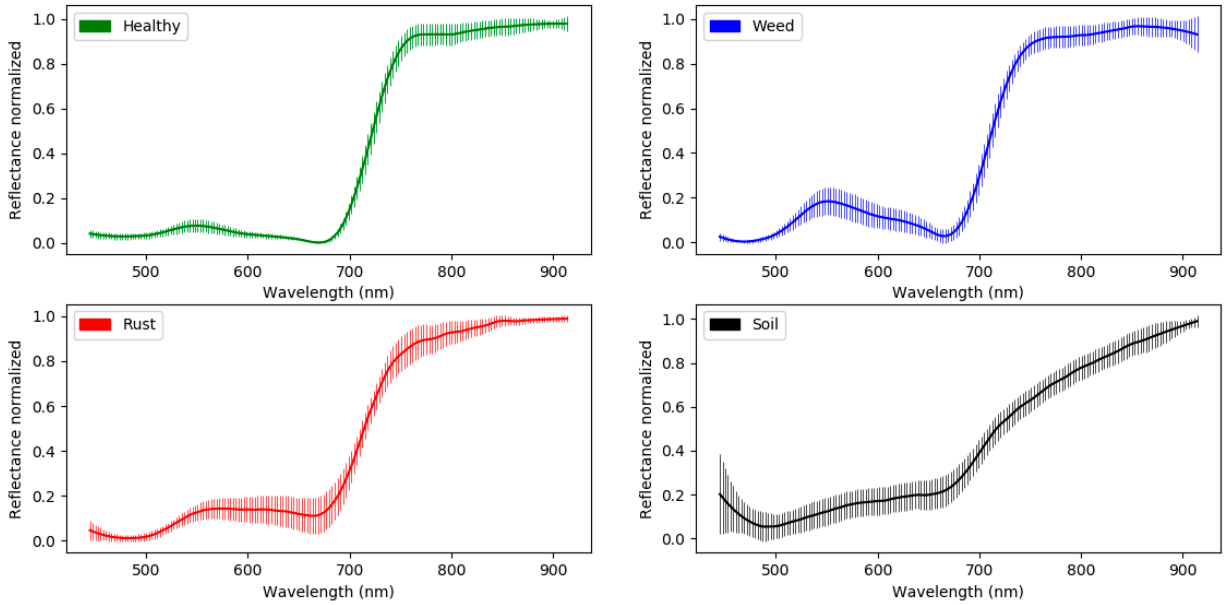


Figure 6. Average reflectance curve for each of the four data classes included in the hyperspectral training library, after preprocessing. Error bars show standard deviation, giving an indication of the variability of the data per waveband and per class.

To compare the shape of the spectra of each of the four classes, the average reflectance curves from Figure 6 were plotted in one figure (Figure 7). The first important region to examine is the red edge region. The healthy leek spectrum showed relatively low reflectance in the visible region compared to the NIR region, resulting in a large 'jump' from the visible to the NIR part of the spectrum. This difference was less pronounced in the spectrum of the weed class, and even less in that of the rust class. The soil class showed an almost continuous incline, which is typical of soil, with only a mild rise in reflectance near the red edge [54]. Comparing the rest of the spectrum, there was little difference after preprocessing in the NIR region between all non-soil classes. The visible region seemed most likely to result in good classification performance, especially the spectral range between 450 and 680 nm, based on visible differences.

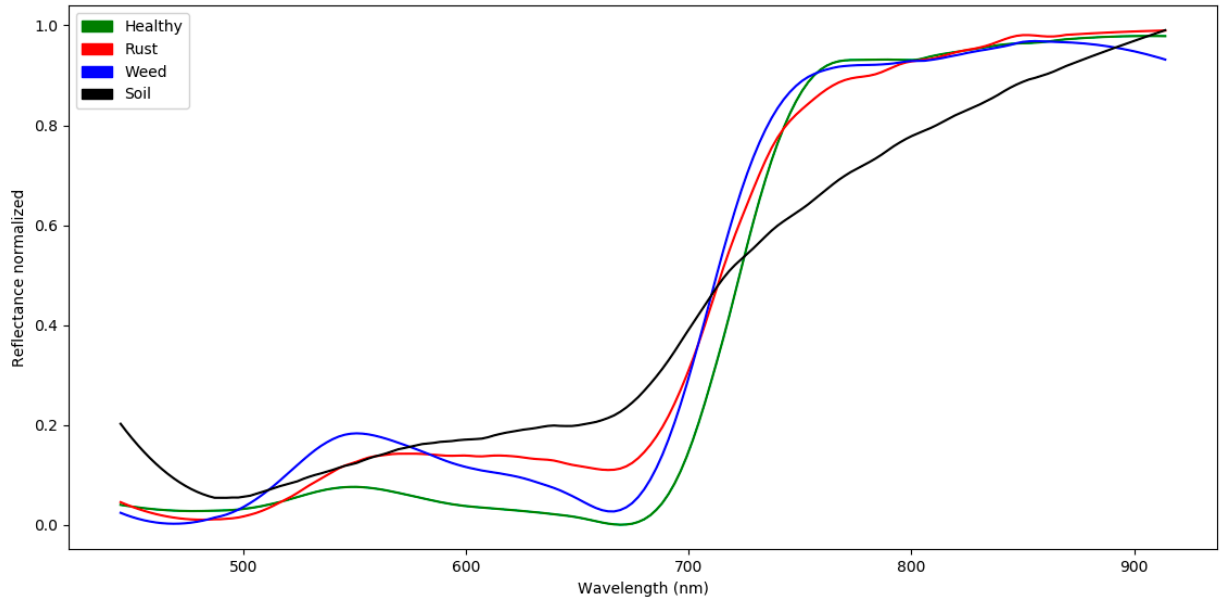


Figure 7. Comparative plot of the average reflectance spectra of each data class of the hyperspectral training library, after normalisation and initial preprocessing steps.

3.2. Preprocessing and Model Selection

3.2.1. Preprocessing

Of the preprocessing steps listed in the materials and methods section, the following steps proved to have negligible effect on classification accuracy:

1. Feature selection: feature selection algorithms did not yield better modelling results, due to the high correlation between neighbouring bands. However, the adapted feature selection strategy where the algorithm was used to select the best waveband for each region of the spectrum, and then the best wavebands overall, also did not yield better results than visual waveband selection based on the spectra in Figures 5 and 6.
2. Changing the smoothing window: the smoothing window was important, but did not greatly affect model performance within a given range. During the iterations of the preprocessing optimization (Figure 4), it became clear that any change in smoothing window within the range of 21 to 55 did not greatly alter the classification results.
3. Including ratios and indices in the model input: several indices were tested, including normalized difference vegetation index, the red edge position index and variations on the ratio vegetation index [55,56]. None of these indices seemed to significantly improve model classification compared to the use of single wavebands, even when these indices were combined with other indices or with individual wavebands.
4. Performing PCA and/or LDA as a dimensionality reduction step.

The steps that were effective for increasing model performance include:

1. Changing the wavebands used as model input based on manual selection of wavebands.
2. Including first and/or second derivative data in the model input.
3. Training label manipulation by changing labels in the hyperspectral library of problematic spectra, intentionally feeding 'falsely' labelled data to the model.
4. Changing and combining classifiers.

Due to the high correlation of neighbouring bands, traditional feature selection methods did not prove useful. An effort was made to counteract this correlation issue by using such feature selection on each region of the spectrum separately (e.g. for each consecutive 10 bands, determine the most important band, and then out of the resulting 17 bands determine the best 3–5 bands, see Section 2.5). It was observed that these methods did not outperform visual waveband selection based on the plots of the spectral signatures (Figure 7). The most effective waveband selection tool for increasing model performance proved to be the plotting of spectra belonging to misclassified pixels, and observing differences between those spectra and the target spectra. The addition of certain bands of the first derivative spectrum using this strategy also benefited classification. During the iterations, the number of wavebands used in the model was varied from only one or two bands to the full 348 band spectrum, which is the normal spectrum followed by the first derivative. It became clear that too many wavebands (more than 10), containing redundant information, deteriorated classification, while too little information (less than 3 wavebands) was not enough to accurately classify the data (assed using confusion matrix calculation). Furthermore, changing the label of certain input spectra was essential to achieve accurate classification of leek rust disease. The combination of two classifiers, one for soil and one for leek rust disease also greatly improved classification accuracy. From this point on, we therefore distinguish between the soil classification model and the crop classification model.

3.2.2. Model Diagnostics

Soil classification model. Soil classification was achieved with a linear discriminant analysis model, using the value of the first derivative spectrum in the 702 nm band. As seen in Figure 8, the first derivative value of the 702 nm band was 10 times smaller for soil samples compared to the other classes. The accuracy of classification was assessed using 30% of the dataset that was set aside for independent validation, with a corresponding confusion matrix shown in Table 3. A classification accuracy of 94.3% was achieved. However, it is important to note that all soil spectra were correctly classified, with a true

positive rate of 1 and a subsequent false negative rate of 0. The 5.7% accuracy loss was due to misclassification of non-soil spectra. The false positive rate was low, at 7.5%, with a subsequent true negative rate of 92.4%, meaning less than 8% of the non-soil samples were misclassified as being soil. Note that the total amount of rust labelled samples in this dataset appears relatively low, while the amount of weed labelled samples appears relatively high. This is the result of the training label manipulation step, in which certain rust spectra were re-labelled as 'weed' (see Materials and Methods).

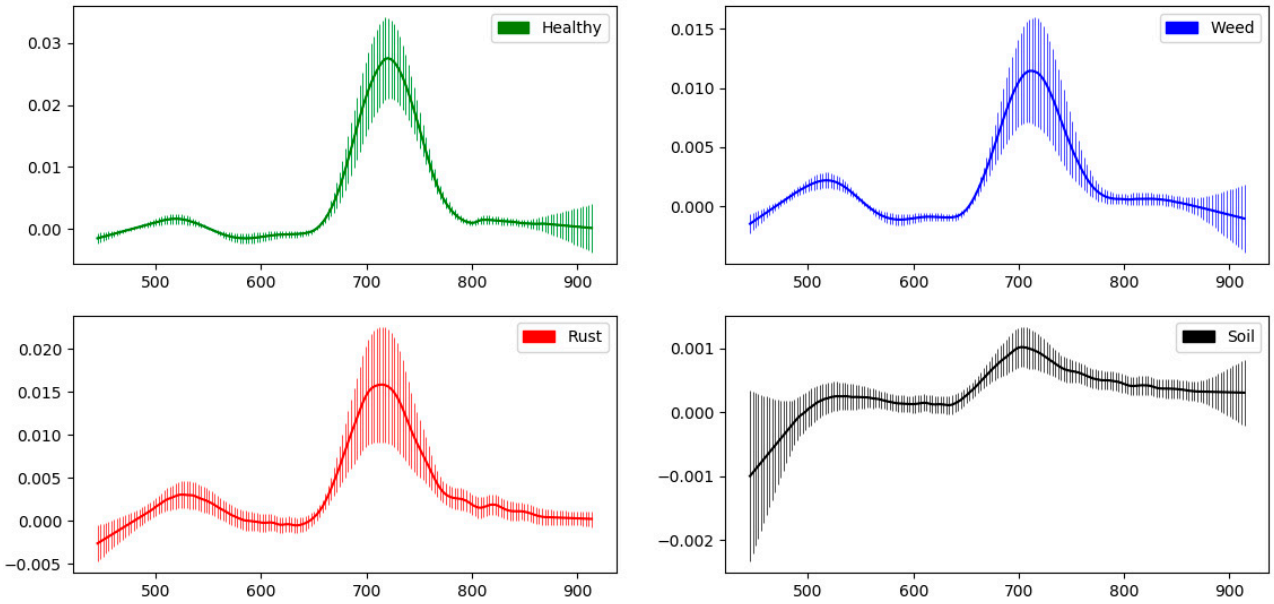


Figure 8. First derivative of the average reflectance spectrum, after preprocessing, shown for each of the classes included in the hyperspectral training library. Error bars indicate standard deviation of the values of the first derivative, per waveband and per class.

Table 3. Confusion matrix corresponding to the soil classification model. This model used a linear discriminant analysis classifier trained on the value of the first derivative spectrum at the 702 nm band, of the hyperspectral library (see the Section 2.4). The hyperspectral library was randomly split with a 70/30 ratio for training/validation. Columns represent the actual condition in the population (R). Rows represent the condition predicted by the model (P).

	Healthy (R)	**Rust (R)**	**Weeds (R)**	**Soil (R)**
Healthy (P)	2091	150	662	0
Rust (P)	0	0	0	0
Weeds (P)	1183	892	4085	0
Soil (P)	0	68	668	3226
Precision	81.4%		**True pos. rate**	100%
Accuracy	94.3%		**False pos. rate**	7.5%
PLR *	13.3138		**False neg. rate**	0%
F1 score	0.8976		**True neg. rate**	92.5%

* PLR = Positive Likelihood Ratio.

Leek rust classification model. As discussed in the methodology section, leek rust classification was achieved using the reflectance values at 556 and 661 nm, combined with the value of the first derivative at 511 nm in a logistic regression model. The results of the confusion matrix calculations are shown in Table 4. Precision and accuracy of leek rust disease classification were 99% and 98.1%, respectively. The true positive rate was 84.4%,

with a subsequent false negative rate of 15.6%, meaning 84.4% of condition positives were correctly classified. The true negative rate was 99.9%, with a subsequent false positive rate of 0.1%, meaning 99.9% of the negative condition was correctly classified.

Table 4. Confusion matrix with corresponding indices for the leek rust detection model. This model used a logistic regression classifier trained the hyperspectral library (see the Section 2.4), using the reflectance value at 556 and 661 nm, combined with the value of the first derivative at 511 nm. The class weights were set to 0.4 for rust, 1 for healthy and 1 for weeds. The hyperspectral library was randomly split with a 70/30 ratio for training/validation. Columns represent the actual condition in the population (R). Rows represent the condition predicted by the model (P).

	Healthy (R)	**Rust (R)**	**Weeds (R)**
Healthy (P)	3163	0	1127
Rust (P)	0	932	9
Weeds (P)	62	172	4304
Precision (%)	99%	**True pos. rate**	84.4%
Accuracy (%)	98.1%	**False pos. rate**	0.10%
PLR *	812.780	**False neg. rate**	15.58%
F1 score	0.9115	**True neg. rate**	99.90%

* PLR = Positive Likelihood Ratio.

3.2.3. Classification of Unlabelled Data

Results of the unlabelled classification still showed some misclassification of weeds in certain situations, even after the training label manipulation step described in the Materials and Methods section. Figure 9 shows a selection of these misclassified (false positive) weed spectra in green, together with rust spectra of confirmed rust pixels (red) and spectra of correctly classified weed spectra (blue). Both the green and blue spectra were selected from the leaves of one grassy weed plant, with one leaf that was classified correctly and one that was classified as a false positive. It is clear that some weed spectra (green) deviated strongly from the normal weed spectrum (blue), causing misclassification.

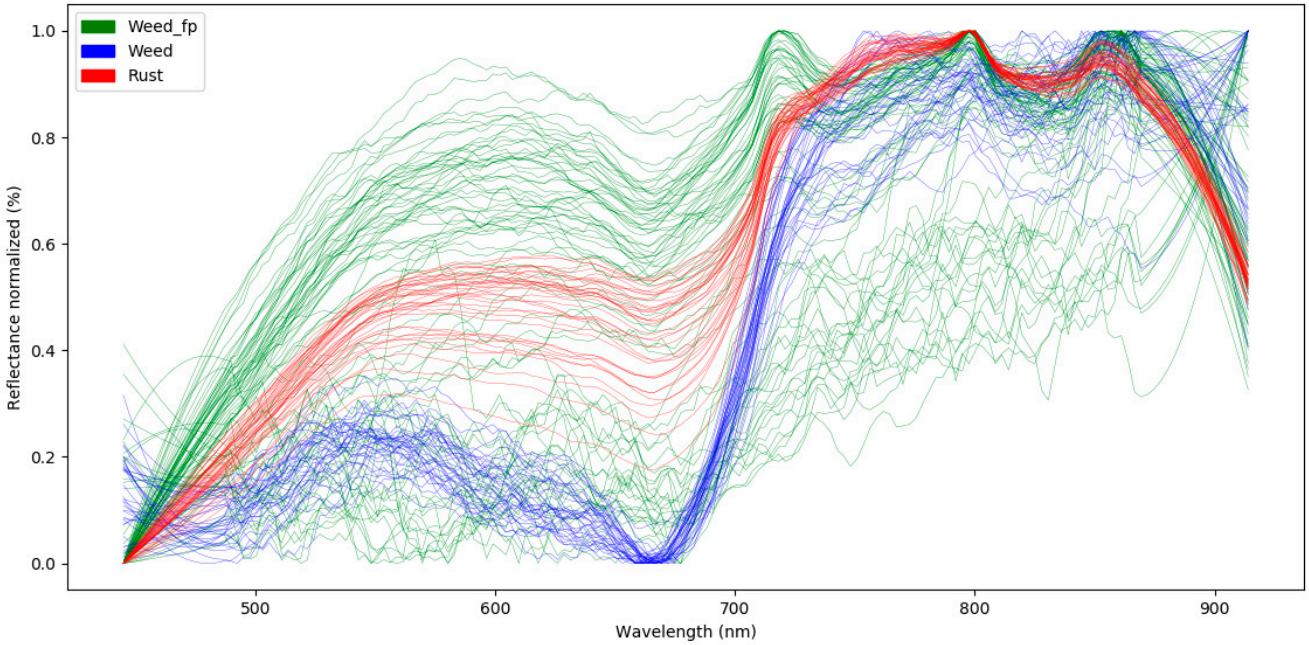


Figure 9. Example of reflectance spectra of rust pixels (red), correctly classified weed pixels (blue) and weed pixels, which were misclassified by the rust disease classification model as rust (false positives—green).

Two representative images of these unlabelled classifications are shown in Figures 10 and 11. Figure 10 shows the classification of an image from the PCG dataset, measured in February, at a different growing stage and different weather conditions compared to the data used for model building. This image contains leek plants with relatively high rust infection, but low weed pressure. Figure 10A. shows the RGB image, with circles indicating the areas magnified in Figure 10C,D, and an area containing weed pixels (rectangle) that were misclassified as rust disease. Figure 10C,D show a close-up of an area with clear rust symptoms in RGB (Figure 10D) and the classified image (Figure 10C).

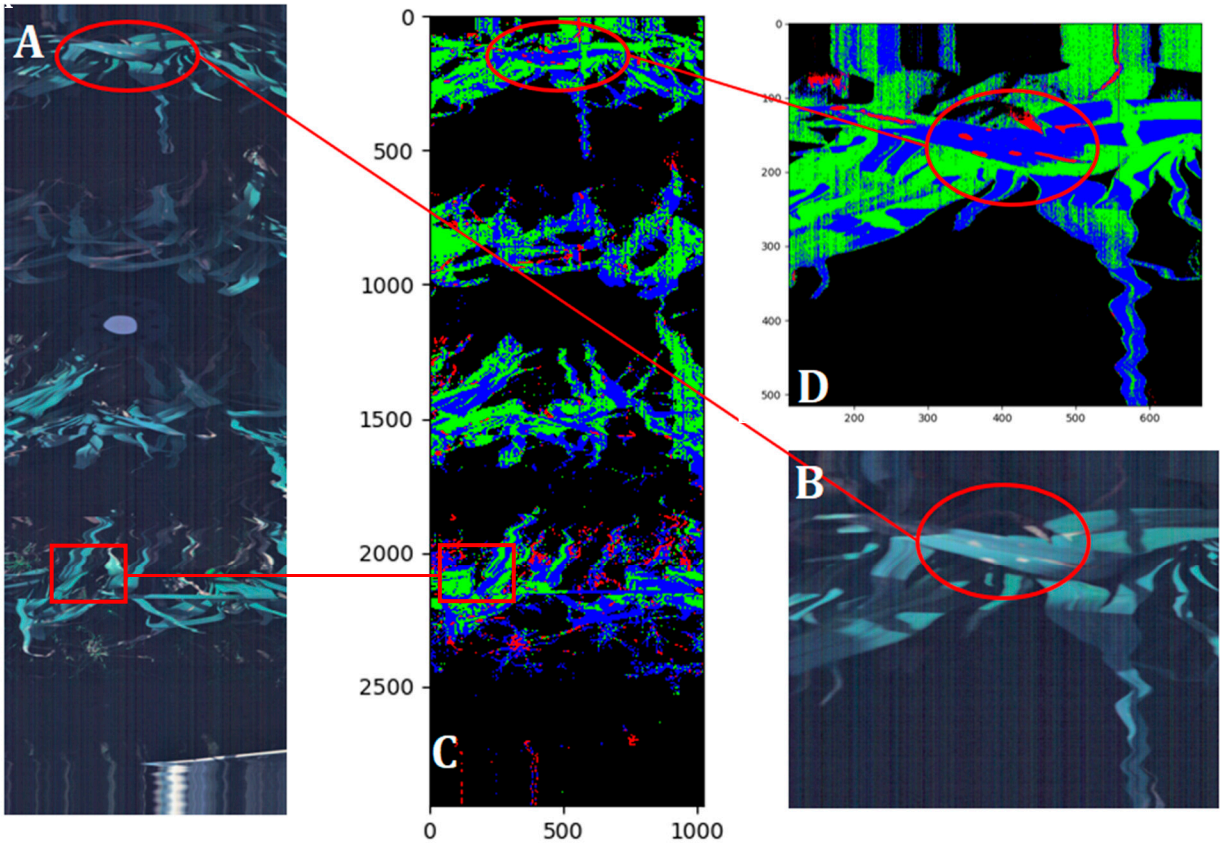


Figure 10. Classification of a new, unlabelled validation dataset using the soil and leek rust classification models. RGB images shown (**A**,**D**) corresponding to the full classified image (**B**) and a close-up (**C**). Circles indicate a typical rust infected leaf. Rectangle corresponds to a weed plant that appeared to contain rust disease after classification.

Figure 11 shows a representative scan for the Bottelare dataset, measured 43 days after the initial infection. It is representative of the Bottelare measurements because it shows no disease scores above zero (contrary to the PCG), with high weed coverage and a different soil type. It also represents a scan taken much later in the season, on 30 April 2019, thus for different weather conditions and a different growing stage compared to the images used in model building. Figure 11A shows the classified image. Figure 11B shows an RGB image taken from the hyperspectral datacube, which has been slightly enhanced using Microsoft Office Powerpoint software (Microsoft, Redmond, WA, USA) to make it clearer. There was no rust disease visibly present in the field. However, during classification of this dataset, a large number of false positives was encountered during the initial preprocessing and model selection steps. As seen in Figure 11, the final classification workflow was able to fully avoid false positives. Note that certain areas of the leek leaf are miscoloured blue, which is the result of the rust classification model being focused on accurately detecting leek rust disease, rather than accuracy concerning weeds versus healthy leek.

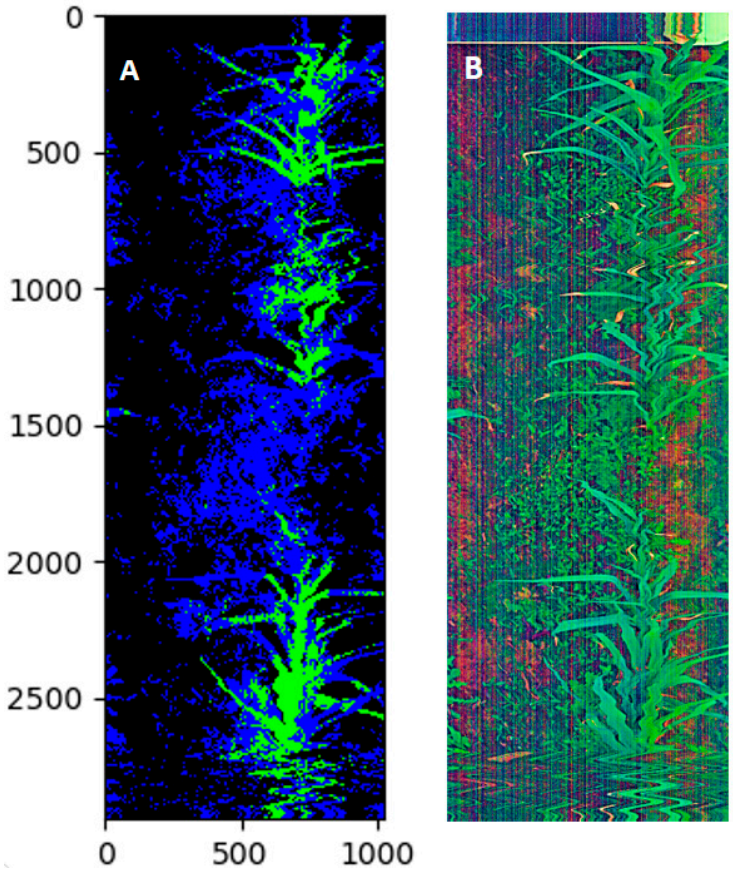


Figure 11. Classification of a new, unlabelled validation dataset using the soil and leek rust classification models. The infection score for this image is zero, an indication that no (or negligible) rust infection was present. Black pixels represent the soil, green represents healthy leek, and blue pixels represent weeds. (**A**) classified image and (**B**) RGB image taken from the hyperspectral datacube.

4. Discussion

4.1. Measurement Setup

Comparing the leek rust disease detection protocol in this work to that of wheat rust disease reported in the literature, some key differences become apparent [29,35]. First, one of the major constraints in wheat experiments was the absence of a measurement setup that could move the hyperspectral pushbroom sensor over the crop canopy at a continuous pace. The measurement setup in the current work made it possible to measure relatively large areas of the field from a proximal distance that gives a high pixel resolution. This resulted in a dataset with the high spatial variability and large sample size normally associated with field trials, e.g. with drone equipment, while maintaining a pixel resolution normally associated with laboratory trials [3,29,35,40,44,53,57,58]. The ability to select ROIs directly from field data and build a hyperspectral library with 'pure' spectra for each class is important, because one of the biggest challenges in disease detection is the translation of results from lab to field scale [1,3,4]. The results shown in Figure 7 seemed promising because there appeared to be a clear difference between healthy, rust, weed and soil spectra. However, it became apparent during modelling that the variability and the noisiness of field data was high, leading to considerable misclassification (Figure 9). A downside of this method of pixel-wise classification compared to the method of using averages over all image pixels, as used in wheat rust disease, is that the averaging of spectra removes a certain amount of noise from the data [29,35]. Since non-averaged spectra were used, a more vigorous smoothing algorithm was needed to compensate for the large amount of noise of some spectra, as seen in Figure 9, where even after vigorous smoothing considerable noise remained. This type of highly variable reflectance spectra

could be caused by a number of reasons, for example the overlap of different types of classes in one pixel, creating a hybrid spectrum. Another possible explanation is that due to the low exposure time of the sensor (1 ms), some areas of the crop showed very low, noisy reflectance spectra. This effect would then be magnified by the normalisation preprocessing step. The low exposure time was necessary, however, to avoid saturation under field conditions and to allow sufficiently high scanning frequency to match the speed of the electric motor sliding the hyperspectral camera over the crop canopy, so a sharp image could be produced.

Some other practical difficulties associated with field measurements include windiness, varying solar radiation due to cloud movement, rain and dust damaging the sensor setup, and higher variability in growing conditions and stresses compared to the laboratory environment. During detection of wheat rust disease (using average reflectance measurements over a certain area over the crop), this made it difficult to assess whether any change in the average reflectance curve was caused by disease or by other stress factors or different growing conditions [3]. It was therefore an important advantage to be able to visually select ROIs containing leek rust infection on field data at within-leaf spatial resolution, rather than take average values measured over several plants, because it allowed the comparison of reflectance spectra coming from non-averaged pixels belonging specifically to diseased or healthy leek tissue on the same plant/leaf.

To apply this leek rust disease detection measurement setup in practice, it could be interesting to employ multispectral sensors that specifically focus on the wavebands used by the soil and leek rust disease detection model. Then, multiple sensors could be placed on the sprayer to map the spread of disease throughout the field. This could then be used to either immediately apply variable rate spraying (if data processing occurs fast enough), to adapt future disease management strategies, or even perform selective harvesting based on disease incidence. However, the high cost for buying multiple sensors is an issue, especially if these sensors are specific for one disease. It would be a significant improvement if certain bands could be found that can be used to detect a range of diseases, increasing the profitability of each sensor.

4.2. Preprocessing and Model Selection

Results of the preprocessing optimization (Figure 4) showed that despite the clear differences in the average spectra of Figure 7, several steps were needed to achieve acceptable model performance. The first step involved the development of a dedicated soil classification model. This was necessary, because the use of strategies such as soil pixel deletion based on the Normalized Difference Vegetation Index (NDVI) proved unreliable after normalisation and Savitsky-Golay smoothing, leading to soil NDVI values of over 0.8, as opposed to values of less than 0.3 for soil spectra reported by other authors [30,58,59]. A method was developed that, to the best of our knowledge, is new for the deletion of soil spectra. Exploration of the data showed that the difference between soil spectra and rust/healthy/weed spectra was most distinct when the dataset was subjected to first order derivation and smoothing, without normalisation. Using only the 702 nm wavelength reflectance value, it was possible to correctly classify and isolate soil spectra in the validation set, leading to a true positive rate of 1 (Table 3). With a false positive rate of 0.075, only around 8% of the non-soil pixels were misclassified as soil. Given that 91% of these misclassifications were weed spectra and 9% rust spectra, the chance of rust pixels being misclassified by the soil classification model was 0.7%. Looking at the validation of a completely new, unlabelled hyperspectral image, the performance of the soil classification model was high, giving a clear separation between soil and crop pixels (Figure 10). Even the small white reference target in the centre of the image and the black plastic pot supporting it were classified as soil (or non-plant material). The bottom of the image shows a section where the hyperspectral imager scanned the edge of the aluminium plate that affixes the aluminium frame to the wheel base. In addition, these pixels were classified as soil and excluded from further analysis.

Following soil pixel classification, the remaining non-soil pixels were used to train a model dedicated to distinguishing rust disease symptoms from weeds and healthy leek crops. The goal of this model is the mapping of the spread of leek rust disease throughout the field. Given that disease typically occurs in patches, especially for windborne diseases such as rust, it is not necessary for the model to be able to detect all rust pustules on the crop. If only a certain percentage of rust spots in a certain area are detected, it is enough indication to have to apply fungicides in that area of the field because it is likely the wider area is also infected. Moreover, the economic threshold for leek rust disease is zero, meaning fungicides are to be applied whether one or fifty rust pustules are present [12]. In the context of reducing fungicide usage, it is therefore more important that rust pustules detected are effectively rust, and not a false positive, than to detect every rust pustule present, with the risk of increasing the amount of false positives. This differs from other diseases that are tolerable at mild infection rates, in which case it is important to know exactly how much infection occurs because this affects the decision to spray or not. In the case of leek rust disease, fungicides have to be applied as soon as one pustule is detected, meaning it is not necessary to know the exact number of rust pustules as long as their presence is detected with relative certainty. The focus was therefore on reducing the amount of false positives during modelling.

It was observed during model building iterations that large amounts of false positives stemmed from the misclassification of weed pixels as rust, also in images taken before disease was present in the field. To account for this problem, two extra preprocessing steps were introduced. First, training label manipulation was performed by altering the label from 'rust to 'weed' of all rust training samples with a reflectance (after preprocessing) lower than 0.13 in the 661 nm band. This step greatly reduced the amount of false positives due to weed misclassification. The second step was to shift the model weights to give less weight to the rust class, and more weight to the healthy and weed classes. This further reduced the amount of weed pixel misclassification, to the point where even images with heavy weed infection showed no misclassification (Figure 11).

As seen in Table 4, the final model succeeded in avoiding a large number of false positives, even though this comes at a price of more false negatives. A true positive rate of 84.42% was achieved, meaning 84.42% of the condition positives in the population were detected (Table 4), leading to a relatively large sensitivity to detect the presence of rust disease pustules. Moreover, even though the accuracy of this model was relatively low at 84%, the precision was high at 99%. This again indicates that the model performance focuses on detecting rust disease and accurately classifying these pixels, with less importance given to the correct classification of weeds or healthy leek pixels.

In the model presented in this work, the false positive rate was 0.1%, meaning that 1 out of 1000 non-rust pixels was misclassified. This seems like an acceptably low ratio, but in field conditions, it could be a problem. Given that the sensor has a scanning width of 1024 pixels, this 1 in 1000 false positive ratio is significant. Two important remarks have to be made. First, out of these 1024 pixels, a relatively large amount will be soil pixels (depending on the growing stage). Looking at the confusion matrix of the soil classification model, not a single soil pixel was misclassified as rust (Table 3). Secondly, the 1/1000 false positive ratio is most problematic if the false positives appear randomly. Looking at Figures 9–11, it is clear that the false positive values did not appear randomly. Specific weed or healthy leek spectra were misclassified as rust, based on their reflectance spectrum (Figure 9). Moreover, the classification shown in Figure 11 shows that there is no problem of false positives appearing in approximately 3 million classified pixels.

In the final model, the largest amount of misclassifications came from misclassifying healthy plant pixels as 'weed' (Figures 10 and 11). It makes sense that spectra of healthy leek crops and healthy weed plants appear more similar and require models that specialize in making this distinction (which is not the purpose of this study). However, as seen in the square at the bottom of Figure 10, there were also some incidents of false rust detection due to misclassification of weed pixels. The spectra in Figure 9 show that these

persistently misclassified weed spectra (green) strongly deviate from the normal weed spectrum (blue). We can further see that there is a similarity between the reflectance spectra of misclassified weeds and rust pustules (red). Both curves show an elevation in the amount of reflectance measured in the red region of the spectrum, which is typical of fully developed rust pustules. It could be possible that there is an effect due to low reflectance or shading, causing a low intensity signal in the sensor that gives a distorted spectrum after normalisation. However, the fact that both the correctly classified (blue) and the misclassified (green) spectra were obtained from the same plant does not support this assumption. Another possible explanation is that the misclassified weeds were infected either by rust disease or another pathogen or stress factor, leading to spectra similar to rust disease spectra on leek. This assumption is supported by the fact that this type of misclassification was only observed on hyperspectral images of leek rows showing a high degree of rust infection (Figure 10), and not on images taken before rust disease was present in the crop (Figure 11). Looking at Figure 11, there are no false positives, even though there is ample weed cover, with certain areas showing low reflectance signals due to for example the angle between the sensor and the weed leaf. This supports the assumption that these misclassified spectra indicate rust disease or a different stress in the weed plant, rather than being caused by the measurement conditions or random noise.

Note that due to the lateral movement of the hyperspectral sensor during measurement, there was a distortion (wobble-effect) in the hyperspectral image. However, due to the fact that the data analysis uses spectral information on a pixel-by-pixel basis (rather than on a full plant level), this did not affect data analysis. The presence of vertical stripe noise, which is typical for pushbroom hyperspectral sensors [60], also did not affect the classification in these bands (Figures 10 and 11).

Due to the focus on a low number of false positives, the amount of rust pustules missed during classification increased. In practice, this would mean that the farmer would falsely assume an area of the field is infected and waste fungicides, leading to an increased cost and a pressure on the environment. It is therefore necessary to further research the trade-off between (a) the risk of missing an infected area when the model focus is on reducing false positives, and (b) wasting more fungicides on an increased number false positives, when the focus is on missing as few rust pustules as possible. As stated before, the economic threshold for rust disease is essentially zero, meaning fungicides are applied even at low infection rates due to cosmetic damage. Looking at the confusion matrix (Table 4), the leek rust detection model showed a miss rate of only 15.6%. This means that there is a roughly one in six chance of not detecting a rust pixel, which is relatively low for practical purposes given that as soon as one rust pixel is detected, the immediate surrounding area is treated with fungicides. This could however be an issue if the amount of linescans decreases for practical applications, leading to for example one scan every 0.10 m. The validity of this disease detection model in practice must therefore be tested under field conditions with variable rust disease pressure. Moreover, the spread of rust disease depends highly on the weather, meaning some conditions are worse for 'missing' an infected site compared to others. This information also needs to be taken into account for practical applications. Lastly, it needs to be tested whether the reduction in fungicides used outweighs any potentially missed infection sites, which in turn spread infection to the rest of the field.

4.3. Optimal Wavebands for Detecting Leek Rust Disease

The selection of the optimal combination of features is important to remove wavebands with low discriminative power between classes from model training, thus increasing model performance [54]. The optimum waveband combination for leek rust disease detection consisted of 1 band at 702 nm for the soil classification model and three bands, namely the 556 and 661 nm band, combined with the value of the first derivative at 511 nm, for the disease classification model. The 702 band lies at the start of the red edge region, which signifies the 'jump' in the reflectance curve typically seen in plant spectra (where

chlorophyll absorption takes place), but not as prominently in soil spectra (Figure 7). The 511 nm band lies in the cyan colour part of the spectrum, the 556nm band in the green part, and 661 nm band in the red part [52]. This result is not surprising, given that leek leaves are normally blue-greenish in colour, while rust pustules appear a bright orange-red. It is important to note that three bands is a relatively low amount of wavebands to include in a rust detection model, compared to a recent study reporting six selected bands for wheat rust detection [29]. These researchers found the 538, 598, 689, 702, 751, and 895 nm bands to be optimal for detection of wheat rust disease, highlighting the importance of the visual region, which includes all of the bands used in the leek rust detection model presented in this work, but also of the NIR region. The importance of the visual region of the spectrum for rust detection on wheat has already been suggested in 2004 by Moshou et al. [34], and has later been confirmed by numerous authors for rust disease of wheat and sugarcane, and for other diseases such as Fusarium disease on wheat [31,35,61,62]. It can be noted that contrary to the results found for leek rust disease, many of the authors above included the NIR region into their rust disease model. The addition of NIR bands was found to not increase model performance compared to the current rust disease detection model setup. However, as indicated by other authors, this region also contains discriminative information and could be used in addition to the information presented in the visible region, if needed. It can be further observed that in all studies mentioned above, no two works conclude on the same optimal waveband selection. It is for this reason that authors often mention optimal waveband ranges, since there is a large correlation between neighbouring bands when the spectral resolution of the sensor is high enough. This was also observed during model training, where waveband selection algorithms often resulted in the selection of a group of directly adjacent bands as being 'optimal'. The fact that a relatively simple logistic regression model (compared to more complex deep learning structures) with relatively few bands could be used to detect the pathogen is beneficial for practical applications. This because it is less challenging to implement these models in small processors on farm equipment, and the low number of bands suggest it might be possible to replace the hyperspectral sensor with cheaper, easier to use sensors (RGB, multispectral).

4.4. Challenges and Future Perspective

As mentioned in the introduction, three key problems remain in close-range hyperspectral imaging under field conditions: (a) the variability of reflectance due to within-crop shading and the complex geometry of the crop canopy, (b) the extremely large amount of data provided by these techniques, and (c) the high cost of commercially available hyperspectral sensors [38]. The latter can partially be addressed by the fact that more and more researchers are using these sensors, increasing demand and therefore production, which is gradually decreasing prices. Additionally, the fact that only a few wavebands were needed for leek rust disease detection gives the opportunity to replace the expensive hyperspectral sensor with a much cheaper multispectral sensor that is dedicated to measuring these specific wavebands.

As shown in Figure 10, the disease detection model suffers from the problem of a complex reflectance pattern caused by the crop canopy structure and within-crop shading, leading to a misclassification of weeds and healthy crops. Even after normalisation, this issue could not be resolved. However, this problem did not affect the ability of the model to detect rust symptoms. Even in the shaded areas of the crop canopy, the classification of rust disease is accurate to a pixel level. The ability to detect single rust pustules opens up possibilities for variable rate fungicide applications, since it is suggested in the literature that it is possible to curatively treat early rust infection [10].

Another problem of close-range hyperspectral imaging is the large amount of data to be processed. If this model is to be used in variable rate applications, a sufficiently high sampling density needs to be achieved to ensure the detection of any disease present with high enough certainty. The mapping of an entire field would require storage capacity easily exceeding the terabyte level, even for small fields. To solve this issue, two possible modes

of action are proposed. First, reducing the sampling resolution, either by increasing pixel size (measuring from a greater altitude), or by reducing the amount of lines scanned per m^2 of the crop. An increase in altitude would mean that pixel size increases to be larger than individual rust pustules, which could greatly decrease disease detection potential. However, a greater measuring height also increases the width of the scanned area, so that fewer scans are needed to map a certain area. In this work, a scanning height of 0.30 m resulted in a sub-millimetre pixel size, while maintaining a scanning width larger than the width of the canopy of a single leek row. The reduction of the amount of samples per m^2 would also increase the chance of missing an infected area of the crop canopy. This reduction can be divided into two options: (a) reducing the amount of lines scanned in the field, where one line consists of a measurement across the entire length of the field, and (b) reducing the amount of samples taken per line scanned. Future experiments have to clarify to which extent either of these options are viable, and what the optimal sampling resolution and distribution is.

Besides the issue of data storage, another important downside of map-based variable rate fungicide applications is the increase in time and fuel needed to first scan the field, then produce maps, and finally return to the field to apply fungicides. This cost could outweigh the gains achieved by variable rate fungicide treatments. A possible solution for this problem would be to use a faster, less fuel intensive vehicle (rover, robot or drone) to produce a disease map. Another strategy to reduce fuel use could be immediate, real-time processing of sensor data measured on the front of a sprayer, directly followed by variable rate fungicide application at the back. This could for example be done with multiple cheaper, multispectral sensors specifically aimed at the wavebands needed for the model. If the sensor signal is immediately processed and this result (diseased or not diseased) is immediately sent to a sprayer, there is no need for data storage, as sensor-based variable rate application can be implemented. However, this would require high computing power and multiple sensors, mounted far enough in front of the spray nozzles to allow time for computation. The speed at which the sprayer could be driven would then depend on both the desired sampling density and the speed at which the signal can be processed. If this means the vehicle needs to move at a low velocity, the fuel and labour costs of the operation could again outweigh the benefits of variable rate fungicide treatments. A possible solution would be the combination of disease detection with other cultivation practices such as weeding. Note that also for these automated (non-map based) methods, it could be useful to map the spread of disease in the field for later use. An important downside of these specialised multispectral sensors would be that they are focused on just one disease. It would therefore be interesting to test whether certain combinations of wavebands can be used to detect more than one disease.

Based on literature on wheat rust detection, the most promising method for variable rate leek rust treatment could be the use of a mapping method but with a lower sample resolution (for example one sample per 0.10 m) [3]. However, the canopy structure in wheat is much more uniform compared to leek. This makes it more likely for a single line to contain relatively large amounts of soil pixels in scans of a leek canopy compared to a wheat canopy, which is denser. Additionally, the difference in canopy structure could potentially mean that rust symptoms are more easily concealed in lower parts of the leek canopy. Dedicated experiments in leek crops are therefore needed to validate this methodology used in wheat [3].

5. Conclusions

Based on the hyperspectral sensing experiments on rust disease in leek canopies carried out in two experimental sites, the developed methodology shows promising results for detection of rust pustules under field conditions. The capacity to differentiate weeds from healthy leek plants can be further improved to increase the usefulness of this system for the farmer. Further development is also necessary to integrate data acquisition and analysis in an automatic framework for immediate analyses after scanning. This would

allow for sensor-based variable rate fungicide application by means of real-time on-line measurement of leek disease pressure, by setting up the hyperspectral sensor on a sprayer, followed immediately by automatic data analysis and fungicide treatment if necessary. A first step towards this goal is the scanning and mapping of an entire field and producing management zone maps. Even if it is not possible to implement sensor-based fungicides application, it would be interesting to investigate the use of disease maps for future farm management. The hypothesis that this model could be used to curatively treat rust infections should also be investigated. It would further be useful to explore the use of fast, fuel efficient modes of transportation, such as drones, to map the disease pressure in the field before fungicide application. Lastly, it could prove interesting to try to expand the methodology used in this work to a new leek disease and see if it is possible to distinguish between several diseases present in the same crop.

Author Contributions: Conceptualization, S.A., J.G.P. and A.M.M.; data curation, A.M.M.; formal analysis, S.A.; funding acquisition, A.M.M.; investigation, S.A.; methodology, S.A., J.G.P. and A.M.M.; project administration, J.G.P. and A.M.M.; resources, A.M.M.; software, S.A.; supervision, J.G.P. and A.M.M.; validation, S.A., J.G.P. and A.M.M.; visualization, S.A.; writing—original draft, S.A.; writing—review & editing, S.A., J.G.P. and A.M.M. All authors have read and agreed to the published version of the manuscript.

Funding: The author(s) disclosed receipt of the following financial support for the research, authorship, and/or publication of this article: This work was supported by the Research Foundation—Flanders (FWO) for Odysseus I SiTeMan Project [Nr. G0F9216N].

Data Availability Statement: Data available from Ghent University data server upon reasonable request.

Acknowledgments: Apart from the people listed on this paper, a big thanks to the people at Bottelare experimental farm, UGent mechanical workshop, the people from the 'Provinciaal Proefcentrum voor de Groenteteelt Oost-Vlaanderen', and the colleagues of our research group who helped me in the field.

Conflicts of Interest: The authors declare no conflict of interest.

References

1. Bohnenkamp, D.; Behmann, J.; Mahlein, A.-K. In-Field Detection of Yellow Rust in Wheat on the Ground Canopy and UAV Scale. *Remote Sens.* **2019**, *11*, 2495. [CrossRef]
2. Agrios, G. *Plant Pathology*, 5th ed.; Academic Press: San Diego, CA, USA, 2005. [CrossRef]
3. Whetton, R.L.; Waine, T.W.; Mouazen, A.M. Hyperspectral measurements of yellow rust and fusarium head blight in cereal crops: Part 2: On-line field measurement. *Biosyst. Eng.* **2018**, *167*, 144–158. [CrossRef]
4. Zhang, J.; Huang, Y.; Pu, R.; Gonzalez-Moreno, P.; Yuan, L.; Wu, K.; Huang, W. Monitoring plant diseases and pests through remote sensing technology: A review. *Comput. Electron. Agric.* **2019**, *165*, 104943. [CrossRef]
5. De Clercq, H.; Peusens, D.; Roldan-Ruiz, I.; Van Bockstaele, E. Causal relationships between inbreeding, seed characteristics and plant performance in leek (*Allium porrum* L.). *Euphytica* **2003**, *134*, 103–115. [CrossRef]
6. Smilde, W.; Van Nes, M.; Reinink, K.; Kik, C. Genetical studies of resistance to Phytophthora porri in Allium porrum, using a new early screening method. *Euphytica* **1997**, *93*, 345–352. [CrossRef]
7. Declercq, B.; Van Buyten, E.; Claeys, S.; Cap, N.; De Nies, J.; Pollet, S.; Höfte, M. Molecular characterization of Phytophthora porri and closely related species and their pathogenicity on leek (*Allium porrum*). *Eur. J. Plant Pathol.* **2010**, *127*, 341–350. [CrossRef]
8. Gilles, T.; Kennedy, R. Effects of an Interaction Between Inoculum Density and Temperature on Germination of Puccinia allii Urediniospores and Leek Rust Progress. *Phytopathology* **2003**, *93*, 413–420. [CrossRef] [PubMed]
9. Bruycker, E.D.; Reyke, L.D.; Plovie, N.; Callens, D.; Roosterd, L.D.; Cardoen, I.; Delobelle, I.; Tierry, L.; van de Steene, F.; Hofte, M. *Ziekten En Plagen in Prei*; 2004; p. 23.
10. Cap, N.; De Rooster, L.; Darwich, S. Roestbestrijding in Prei. *Proeftuin Nieuws*, 3 July 2014; 32–35.
11. Geiger, F.; Bengtsson, J.; Berendse, F.; Weisser, W.W.; Emmerson, M.; Morales, M.B.; Ceryngier, P.; Liira, J.; Tscharntke, T.; Winqvist, C.; et al. Persistent negative effects of pesticides on biodiversity and biological control potential on European farmland. *Basic Appl. Ecol.* **2010**, *11*, 97–105. [CrossRef]
12. de Jong, P.D.; Daamen, R.A.; Rabbinge, R. The reduction of chemical control of leek rust, a simulation study. *Eur. J. Plant Pathol.* **1995**, *101*, 687–693. [CrossRef]
13. Taylor, G.A.; Torres, H.B.; Ruiz, F.; Marin, M.N.; Chaves, D.M.; Arboleda, L.T.; Parra, C.; Carrillo, H.; Mouazen, A.M. pH Measurement IoT System for Precision Agriculture Applications. *IEEE Lat. Am. Trans.* **2019**, *17*, 823–832. [CrossRef]

14. Mahlein, A.-K. Plant Disease Detection by Imaging Sensors—Parallels and Specific Demands for Precision Agriculture and Plant Phenotyping. *Plant Dis.* **2016**, *100*, 241–251. [CrossRef]
15. Nawar, S.; Corstanje, R.; Halcro, G.; Mulla, D.; Mouazen, A.M. Delineation of Soil Management Zones for Variable-Rate Fertilization. *Adv. Agron.* **2017**, *143*, 175–245. [CrossRef]
16. Behmann, J.; Mahlein, A.-K.; Rumpf, T.; Römer, C.; Plümer, L. A review of advanced machine learning methods for the detection of biotic stress in precision crop protection. *Precis. Agric.* **2015**, *16*, 239–260. [CrossRef]
17. Grisham, M.P.; Johnson, R.M.; Zimba, P.V. Detecting Sugarcane yellow leaf virus infection in asymptomatic leaves with hyperspectral remote sensing and associated leaf pigment changes. *J. Virol. Methods* **2010**, *167*, 140–145. [CrossRef] [PubMed]
18. Zhang, J.; Pu, R.; Huang, W.; Yuan, L.; Luo, J.; Wang, J. Using in-situ hyperspectral data for detecting and discriminating yellow rust disease from nutrient stresses. *Field Crop. Res.* **2012**, *134*, 165–174. [CrossRef]
19. Clarkson, J.P.; Kennedy, R.; Phelps, K.; Davies, J.; Bowtell, J. Quantifying the effect of reduced doses of propiconazole (Tilt) and initial disease incidence on leek rust development. *Plant Pathol.* **1997**, *46*, 952–963. [CrossRef]
20. De Jong, P. Disease Management of Leek Rust, a Study at Field, Farm and Regional Level. 1995. Available online: https://edepot.wur.nl/206535 (accessed on 31 March 2021).
21. Doherty, M.A.; Preece, T. Bacillus cereus prevents germination of uredospores of Puccinia allii and the development of rust disease of leek, Allium porrum, in controlled environments. *Physiol. Plant Pathol.* **1978**, *12*, 123–132. [CrossRef]
22. Huang, J.W. Control of Chinese Leek Rust with a Plant Nutrient Formulation. *Plant Pathol. Bull.* **1994**, *3*, 9–17.
23. Jennings, D.M.; Ford-Lloyd, B.; Butler, G.M. Effect of plant age, leaf position and leaf segment on infection of leek by leek rust, Puccinia allii. *Plant Pathol.* **1990**, *39*, 591–597. [CrossRef]
24. Jong, P.D.; Bree, J. Analysis of the spatial distribution of rust-infected leek plants with the Black-White join-count statistic. *Eur. J. Plant Pathol.* **1995**, *101*, 133–137. [CrossRef]
25. Roberts, A.M.; Walters, D.R. Nitrogen assimilation and metabolism in rusted leek leaves. *Physiol. Mol. Plant Pathol.* **1988**, *32*, 229–235. [CrossRef]
26. Roberts, A.M.; Walters, D.R. Shoot: Root interrelationships in leeks infected with the rust, *Puccinia allii* Rud.: Growth and nutrient relations. *New Phytol.* **1989**, *111*, 223–228. [CrossRef]
27. Smith, B.M.; Crowther, T.C.; Clarkson, J.P.; Trueman, L. Partial resistance to rust (*Puccinia allii*) in cultivated leek (*Allium ampeloprasum* ssp. porrum): Estimation and improvement. *Ann. Appl. Biol.* **2000**, *137*, 43–51. [CrossRef]
28. Theunissen, J.; Schelling, G. Pest and disease management by intercropping: Suppression of thrips and rust in leek. *Int. J. Pest Manag.* **1996**, *42*, 227–234. [CrossRef]
29. Guo, A.; Huang, W.; Ye, H.; Dong, Y.; Ma, H.; Ren, Y.; Ruan, C. Identification of Wheat Yellow Rust Using Spectral and Texture Features of Hyperspectral Images. *Remote Sens.* **2020**, *12*, 1419. [CrossRef]
30. Whetton, R.L.; Waine, T.W.; Mouazen, A.M. Optimising configuration of a hyperspectral imager for on-line field measurement of wheat canopy. *Biosyst. Eng.* **2017**, *155*, 84–95. [CrossRef]
31. Apan, A.; Held, A.; Phinn, S.; Markley, J. Detecting sugarcane 'orange rust' disease using EO-1 Hyperion hyperspectral imagery. *Int. J. Remote Sens.* **2004**, *25*, 489–498. [CrossRef]
32. Huang, W.; Lamb, D.W.; Niu, Z.; Zhang, Y.; Liu, L.; Wang, J. Identification of yellow rust in wheat using in-situ spectral reflectance measurements and airborne hyperspectral imaging. *Precis. Agric.* **2007**, *8*, 187–197. [CrossRef]
33. Zhang, J.; Yuan, L.; Pu, R.; Loraamm, R.W.; Yang, G.; Wang, J. Comparison between wavelet spectral features and conventional spectral features in detecting yellow rust for winter wheat. *Comput. Electron. Agric.* **2014**, *100*, 79–87. [CrossRef]
34. Moshou, D.; Bravo, C.; West, J.; Wahlen, S.; McCartney, A.; Ramon, H. Automatic detection of 'yellow rust' in wheat using reflectance measurements and neural networks. *Comput. Electron. Agric.* **2004**, *44*, 173–188. [CrossRef]
35. Whetton, R.L.; Hassall, K.L.; Waine, T.W.; Mouazen, A.M. Hyperspectral measurements of yellow rust and fusarium head blight in cereal crops: Part 1: Laboratory study. *Biosyst. Eng.* **2018**, *166*, 101–115. [CrossRef]
36. Paulus, S.; Mahlein, A.-K. Technical workflows for hyperspectral plant image assessment and processing on the greenhouse and laboratory scale. *GigaScience* **2020**, *9*. [CrossRef] [PubMed]
37. Mahlein, A.-K.; Kuska, M.; Behmann, J.; Polder, G.; Walter, A. Hyperspectral Sensors and Imaging Technologies in Phytopathology: State of the Art. *Annu. Rev. Phytopathol.* **2018**, *56*, 535–558. [CrossRef]
38. Mishra, P.; Asaari, M.S.M.; Herrero-Langreo, A.; Lohumi, S.; Diezma, B.; Scheunders, P. Close range hyperspectral imaging of plants: A review. *Biosyst. Eng.* **2017**, *164*, 49–67. [CrossRef]
39. Appeltans, S.; Guerrero, A.; Nawar, S.; Pieters, J.; Mouazen, A. Practical Recommendations for Hyperspectral and Thermal Proximal Disease Sensing in Potato and Leek Fields. *Remote. Sens.* **2020**, *12*, 1939. [CrossRef]
40. Xie, C.; Shao, Y.; Li, X.; He, Y. Detection of early blight and late blight diseases on tomato leaves using hyperspectral imaging. *Sci. Rep.* **2015**, *5*, 16564. [CrossRef]
41. Virtanen, P.; Gommers, R.; Oliphant, T.E.; Haberland, M.; Reddy, T.; Cournapeau, D.; Burovski, E.; Peterson, P.; Weckesser, W.; Bright, J.; et al. SciPy 1.0: Fundamental algorithms for scientific computing in Python. *Nat. Methods* **2020**, *17*, 261–272. [CrossRef]
42. Rasti, B.; Scheunders, P.; Ghamisi, P.; Licciardi, G.; Chanussot, J. Noise Reduction in Hyperspectral Imagery: Overview and Application. *Remote Sens.* **2018**, *10*, 482. [CrossRef]
43. Pedregosa, F.; Varoquaux, G.; Gramfort, A.; Michel, V.; Thirion, B.; Grisel, O.; Blondel, M.; Prettenhofer, P.; Weiss, R.; Dubourg, V.; et al. Scikit-Learn: Machine Learning in Python. *JMLR* **2011**, *12*, 2825–2830.

44. Abdulridha, J.; Ehsani, R.; De Castro, A. Detection and Differentiation between Laurel Wilt Disease, Phytophthora Disease, and Salinity Damage Using a Hyperspectral Sensing Technique. *Agriculture* **2016**, *6*, 56. [CrossRef]
45. Rinnan, Å.; Berg, F.V.D.; Engelsen, S.B. Review of the most common pre-processing techniques for near-infrared spectra. *TrAC Trends Anal. Chem.* **2009**, *28*, 1201–1222. [CrossRef]
46. Caporaso, N.; Whitworth, M.B.; Fisk, I.D. Near-Infrared spectroscopy and hyperspectral imaging for non-destructive quality assessment of cereal grains. *Appl. Spectrosc. Rev.* **2018**, *53*, 667–687. [CrossRef]
47. Lowe, A.; Harrison, N.; French, A.P. Hyperspectral image analysis techniques for the detection and classification of the early onset of plant disease and stress. *Plant Methods* **2017**, *13*, 1–12. [CrossRef] [PubMed]
48. Sankaran, S.; Mishra, A.; Ehsani, R.; Davis, C. A review of advanced techniques for detecting plant diseases. *Comput. Electron. Agric.* **2010**, *72*, 1–13. [CrossRef]
49. Heaton, J. An Empirical Analysis of Feature Engineering for Predictive Modeling. In Proceedings of the Conference Proceedings-IEEE SOUTH-EASTCON, Norfolk, VA, USA, 30 March–3 April 2016. [CrossRef]
50. Serneels, S.; Lambin, E.F. Proximate causes of land-use change in Narok District, Kenya: A spatial statistical model. *Agric. Ecosyst. Environ.* **2001**, *85*, 65–81. [CrossRef]
51. Murchie, E.; Lawson, T. Chlorophyll fluorescence analysis: A guide to good practice and understanding some new applications. *J. Exp. Bot.* **2013**, *64*, 3983–3998. [CrossRef] [PubMed]
52. Malacara, D. Color vision and colorimetry: Theory and applications. *Color Res. Appl.* **2002**, *28*, 77–78. [CrossRef]
53. Hunt, E.R.; Doraiswamy, P.C.; McMurtrey, J.E.; Daughtry, C.S.; Perry, E.M.; Akhmedov, B. A visible band index for remote sensing leaf chlorophyll content at the canopy scale. *Int. J. Appl. Earth Obs. Geoinf.* **2013**, *21*, 103–112. [CrossRef]
54. Hong, Y.; Guo, L.; Chen, S.; Linderman, M.; Mouazen, A.M.; Yu, L.; Chen, Y.; Liu, Y.; Liu, Y.; Cheng, H.; et al. Exploring the potential of airborne hyperspectral image for estimating topsoil organic carbon: Effects of fractional-order derivative and optimal band combination algorithm. *Geoderma* **2020**, *365*. [CrossRef]
55. Curran, P.J.; Dungan, J.L.; Gholz, H.L. Exploring the relationship between reflectance red edge and chlorophyll content in slash pine. *Tree Physiol.* **1990**, *7*, 33–48. [CrossRef]
56. Xue, J.; Su, B. Significant Remote Sensing Vegetation Indices: A Review of Developments and Applications. *J. Sens.* **2017**, *2017*, 1–17. [CrossRef]
57. Sugiura, R.; Tsuda, S.; Tamiya, S.; Itoh, A.; Nishiwaki, K.; Murakami, N.; Shibuya, Y.; Hirafuji, M.; Nuske, S. Field phenotyping system for the assessment of potato late blight resistance using RGB imagery from an unmanned aerial vehicle. *Biosyst. Eng.* **2016**, *148*, 1–10. [CrossRef]
58. Bravo, C.; Moshou, D.; Oberti, R.; West, J.S.; McCartney, A.; Bodria, L.; Ramon, H.; Orberti, R.; West, J.S.; McCartney, A.; et al. Foliar Disease Detection in the Field Using Optical Sensor Fusion. *Agric. Eng. Int. CIGR J.* **2004**, *VI*, 8.
59. Rouse, J.W.; Haas, R.H.; Schell, J.A.; Deering, D.W. Monitoring the Vernal Advancement and Retrogradation (Green Wave Effect) of Natural Vegetation. 1974; NASA/GSFC Type III Final Report, Greenbelt, Md, 371.
60. Gómez-Chova, L.; Alonso, L.; Guanter, L.; Valls, G.C.-; Calpe, J.; Moreno, J. Correction of systematic spatial noise in push-broom hyperspectral sensors: Application to CHRIS/PROBA images. *Appl. Opt.* **2008**, *47*, F46–F60. [CrossRef] [PubMed]
61. Bauriegel, E.; Giebel, A.; Geyer, M.; Schmidt, U.; Herppich, W. Early detection of Fusarium infection in wheat using hyper-spectral imaging. *Comput. Electron. Agric.* **2011**, *75*, 304–312. [CrossRef]
62. Krishna, G.; Sahoo, R.N.; Pargal, S.; Gupta, V.K.; Sinha, P.; Bhagat, S.; Saharan, M.; Singh, R.; Chattopadhyay, C. Assessing Wheat Yellow Rust Disease through Hyperspectral Remote Sensing. *Int. Arch. Photogramm. Remote Sens. Spatial Inf. Sci.* **2014**, *XL8*, 1413–1416. [CrossRef]

Estimation Of Productivity Based On Rice Growth Phenology Using Sentinel-2 Image (Case Study In Karawang And Malang District)

Gilang Aulia Herlambang[1], Ike Sari Astuti[1][0000-0002-6455-3697], Bagus Setiabudi Wiwoho[1][0000-0002-1246-561X] and Dede Dirgahayu Domiri[2]

[1] Dept. of Geography, State University of Malang, Malang City, 65145, East Java, Indonesia
[2] Remote Sensing Application Center, BRIN, Central Jakarta, 10340, DKI Jakarta, Indonesia
ike.sari.fis@um.ac.id

Abstract. Estimation and monitoring of rice plants using satellite imagery must be to provide information on rice growth and predict the yields efficiently. Utilization of remote sensing using the Sentinel-2 satellite is expected to be able to analyze agriculture at a detailed scale. The research was conducted in Karawang and Malang to compare rice plants' phenology, harvested areas, and productivity. The Enhanced Vegetation Index (EVI) parameter of Sentinel-2 multitemporal 10-day images in 2019-2021 was used to produce regional rice data information. Based on the analysis of maximum EVI values, 7 classes of rice fields were identified, namely 0.40-0.45; 0.45-0.50; 0.50-0.55; 0.55-0.60; 0.60-0.65; 0.65-0.70; and > 0.70. The days (age) after planting, locally termed as Days After Planting (DAP) based on the EVI value in Karawang is 0.91, while Malang is 0.90. The identified harvested area in Karawang Regency in 2019 is 174.95 thousand hectares and in 2020 is 185.80 thousand hectares, the average ratio is 0.94 slightly smaller than the statistics agency BPS data. While in Malang, the the average ratio was 0.87. Based on productivity, production in Karawang in 2019 was 73.87 qwintals/Ha, and in 2020 it was 72.91 qwintals/Ha. The estimated production in Malang Regency 2019 and 2020 was 74.59 qwintals/Ha, and 74.87 qwintals/Ha respectively. This result shows the potential of remote sensing for rice growth monitoring.

Keywords: Sentinel-2; EVI; rice; phenology, productivity.

1 Introduction

Rice is one of the most important grain crops cultivated and it is primary food for almost half of the world's population [1]. Around 969 million tonnes of rice were produced worldwide in 2010 [2]. The Asian continent produces almost 90% of the world's total rice production [3]. Indonesia is ranked 3rd in the world with the highest rice production after China and India, with a production level of 70.8 tons in 2015 [4]. Two of the regions in Indonesia having high rice production are Karawang Regency and Malang Regency. Karawang Regency is the second largest rice producer in Indonesia after In-

© The Author(s) 2023
A. Nugroho Widiadi et al. (eds.), *Proceeding of the 3rd International Conference on Social Knowledge Sciences and Education (ICSKSE) 2023 "Change and Continuity in Southeast Asia"*, Advances in Social Science, Education and Humanities Research 800, https://doi.org/10.2991/978-2-38476-168-5_7

dramayu Regency. Rice productivity in Karawang Regency is 77.67 tons/ha with a production of 1,101,076.56 tons in 2018 [5]. In contrast to Malang Regency, which has a productivity of 71.07 tons/ha with a total rice production of 312,544 tons [6].

It is necessary to estimate and monitor the phenology of a wide range of rice plants in order to provide information on rice growth. Monitoring plant phenology over a large area can estimate net primary production spatially [7]. Monitoring using conventional approaches like surveys requ ires large costs, time, money, and manpower [8]. Remote sensing has been increasingly used as a monitoring tool due to its efficiency. Haw et al. [9] used photo spectral color vision to detect rice ripeness, but only covered a small (limited) area. Pei et al. [10] used an integrated sensor system to monitor rice growing conditions based on the UAV (Unmanned Aerial Vehicle) system. However, field observations are difficult to extrapolate data to a large area [11, 12]. This problem can be overcome by using remote sensing technology combined with field parameterization. Remote sensing imagery is useful in many applications, especially to obtain land cover information at a lower cost and shorter time [13, 14].

Remote sensing techniques for precisely mapping agriculture can be carried out by the use of Sentinel-2. The Sentinel-2 constellation, with its enhanced spatial, spectral, and temporal resolution, was specifically designed to meet the needs of semi-detailed agriculture [15]. Sentinel-2 features a multispectral (MSI) instrument holding an anastigmatic telescope that minimizes thermo-elastic distortion, and an optimized optical design to achieve cutting-edge imaging quality across a 290 km field of view [16]. MSI displays 13 spectral bands with a spatial resolution ranging from 10 m to 60 m (depending on the band) and a current temporal resolution of about 5-10 days (depending on latitude). [16]. The spatial, temporal resolution and free image availability make Sentinel-2 suitable for agricultural monitoring [17].

Several remote sensing approaches using sentinel imagery for agricultural applications have been widely used. Research [18] evaluated several methodologies that automatically delineate cropland boundaries from Sentinel-2 imagery with image segmentation to delineate farmland, orchards, and vineyards. Promising results were achieved by applying Canny edge to Sentinel-2. In [19] the Sentinel 2 imageries were used to design the pre-operational service for rice farming systems, based on the assimilation of EO products and in-situ data into crop modeling solutions. The research of Son et al [20] developed a methodology to create a map of rice plants using S2 data and plant phenological information. The [21], proposed a method to create rice cultivation maps using Random Forest and time-series data S1 and S2.

Most of the analysis of satellite imagery is carried out on the observation of rice fields, namely by observing the density of vegetation [22]. Detection of vegetation density commonly uses a spectral index such as the Enhanced Vegetation Index (EVI). EVI is sensitive to changes in water and vegetation which can help differentiating normal plants or rice plants [23, 24, 25, 26]. EVI also is sensitivity to the greenness of plants due to the influence of soil background and canopy signals and reduces the influence of atmospheric conditions by adding information on the blue channel [27]. The research of [28] used the multitemporal MODIS EVI to determine the growth model of rice plants in Sumatra. Another example is [29] with the use of time series of vegetation indices (EVI, NDWI, and NDBI) derived from Landsat images to develop a method for

classifying paddy and non-rice paddy fields in Indramayu. Later, the [30] used the EVI Landsat 8-OLI index to estimate the harvested area and productivity of rice crops in Bekasi Regency.

Based on the background that has been prepared regarding the study of rice phenology using remote sensing, the purpose of this study is (a) Identifying the trend of rice growth from the beginning of planting to harvesting in the period 2019-2021 in Karawang Regency and Malang Regency. (b) Estimation of harvested area and estimation of rice crop productivity using the 2019-2021 remote sensing approach in Karawang Regency and Malang Regency.

2 Methods

2.1 Research Location

The location of this research study is in Karawang Regency, West Java and Malang Regency, East Java (Figure 1). Geographically, Karawang Regency is located between 107º02'-107º40'BT and 5º562'-6º34'LS. Meanwhile, Malang Regency is located 112º17' - 112º57' east longitude and 7º44' - 8º26' south latitude. The area of Karawang Regency is 1,753.27 km^2, most of the land is used for agriculture. Meanwhile, Malang Regency has an area of 3,530.35 km^2. This research was conducted by using Sentinel-2 satellite imagery in a time series 2019-2021.

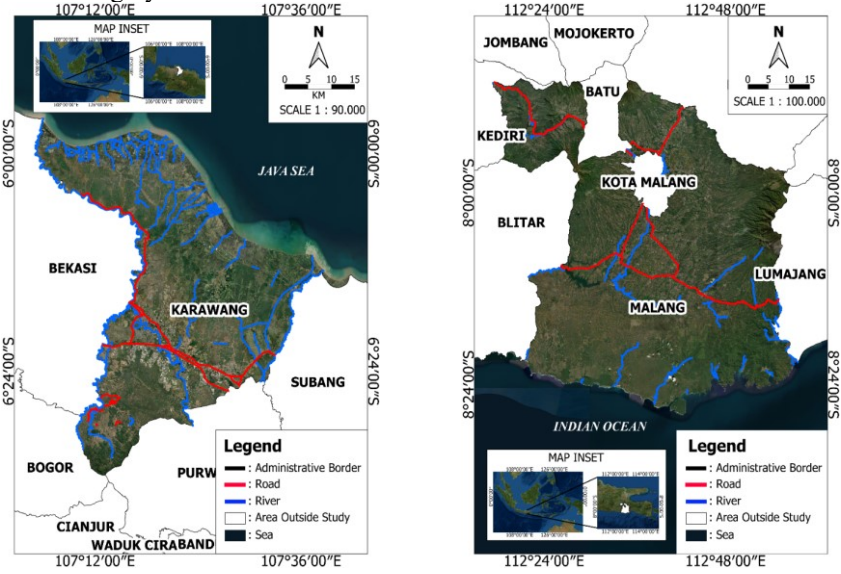


Fig. 1. (a) Image Map of Karawang Regency, West Java and (b) Image Map of Malang Regency, East Java

In this study, Sentinel-2 imagery with a spatial resolution of 10 meters was used to determine the EVI value in Karawang Regency and Malang Regency. Sentinel-2 imagery provides better spatial resolution than MODIS and Landsat images as in previous studies. Therefore, to determine the level of accuracy, a validation was carried out on rice productivity data issued from the local statistical agency "Badan Pusat Statistik (BPS)". The results were evaluated using the coefficient determination (R^2). If the results show the standard error values between 0.0–1.0 can be said to be small, thus the EVI method on the Sentinel-2A image can be considered reliable in estimating rice productivity [31].

2.2 Trend Analysis of Rice Phenology in Karawang Regency and Malang Regency

The stages of rice phenology management derived from satellite imagery vegetation index and the management and planting data from field were used for validation. The tools used to run the analysis are Google Earth Engine, Qgis, and ArcGis, with additional tools are rulers and cameras to measure height, leaf width, number of tillers and age of rice plants. Besides Sentinel-2 for 2019-2021, the ancillary data collected are Sentinel-2 Image for 2019-2021, administrative boundary vectors, productivity data for 2019-2021, raw land data for rice fields at a scale of 1:10,000 in 2019, field data on rice crop variability in Karawang Regency in 2019 and Malang Regency in year 2021.

Detection of paddy fields is using a combination of EVI, NDBI, and NDWI vegetation indices data as shown in Table 1. Meanwhile, prior to statistical analysis, all blank or missing pixels were interpolated using the Savitzky-Golay method, which is also to reduce time series image noise [32] and to do Smoothing 3x3 [28]. All was performed using Google Earth Engine (GEE).

Table 1. Vegetation Index Algorithm for Rice Plants

No	Vegetation Index	Algorithm	Source
1	EVI (Enhanced Vegetation Index)	$\text{EVI} = 2.5\text{x}\frac{NIR-Red}{(NIR+6xRed-7{,}5xBlue+1)}$	[33]
2	NDWI (Normalized Difference Water Index)	$\text{NDWI} = \frac{Green-SWIR2}{Green+SWIR2}$	[34]
3	NDBI (Normalized Difference Build-up. Index)	$\text{NDBI} = \frac{SWIR1-NIR}{SWIR1+NIR}$	[35]

The value that has been extracted is determined by a threshold to determine paddy fields with IV Max > 0.45; IV Range (IV Min – IV Max) > 0.3; and IV Early Planting (NDWI > 0.226 and EVI < 0.188) and IV Harvest (NDBI > 0), other than this value, it is not a rice crop area [36]. The total area of rice fields was assessed for the overall accuracy and Kappa accuracy using observation data on raw rice fields with a scale of 1:10,000 [37, 38]. Extraction of the vegetation index that has been smoothed, was carried out by applying the density slicing for rice grades based on the Maximum EVI and cut into 5-7 classes from the EVI max range of 0.40-0.45 as class 1 [28]. The maximum

EVI was assumed to occur when the rice is 60 DAP (Days After Planting). Thus, early planting (AT) and harvest time (WP) on Sentinel 10 daily data can be seen in equations (1) and (2) below

$$AT = LM - 60/P \quad (1)$$

$$WP = LM + 60/P \quad (2)$$

Where, AT = Early Planting; WP = Harvest Time, LM = Maximum Place, P = Daily Period (Sentinel Daily Period-2 Basis (10 days))

To be able to distinguish the vegetative and generative phases, two images with different dates (t and t-1) are needed. Rice plant growth phase conditions can be detected from changes in the value of EVI (dEVI). Determination of the rice growth phase according to the following formula (3) [39]:

$$dEVI = EVIt - EVI\ t\text{-}1 \quad (3)$$

Where: dEVI = Values change (+/-); EVIt = EVI; EVIt-1 = EVI previously

Training area of EVI time series plotting based on the same planting date was analyzed by regression to obtain a rice plant growth model. Sampling used purposive random sampling based on the EVI Maximum class. Image sampling is done with a buffer of 30 x 30 meters. The form of the regression equation is a polynomial of order 3 or Spline Qubic [28] with the following equation (4)

$$Y = b0 + b1*X + b2*X2 + b3*X3 \quad (4)$$

Where, X = Rice Crop time/age (HST); Y = maximum EVI growth parameter; b0 = intercept; b1, b2, b3 = coeficient

2.3 Estimation of Harvest Area and Rice Crop Productivity Using Remote Sensing Approach in Karawang Regency and Malang Regency

The rice plant growth profile that has been made is extracted based on the same harvest time polygon to determine the harvested area. The harvested area is divided into 3 periods, namely January-April, May-August, and September-December which are then added up to get the harvest area for 1 year. The harvested area for 1 year will be compared with BPS data using a ratio to find out the comparison.

Estimation of lowland rice productivity is based on the formula (5) resulting from the dissertation [40] which explains the productivity value derived from the Maximum EVI value. Then the results of a simple linear regression in the formula (6) are used to determine the relationship between productivity and Maximum EVI [30]. Random sampling was conducted to obtain the relationship between productivity and Maximum EVI. From this equation, the coefficient of determination (R^2) is obtained which explains the closeness between the productivity of Rice Plants and the maximum EVI value

$$Productivity = log\ (EVI_Max/0{,}103)\ x\ (38{,}46154\ x\ 1{,}11) \quad (5)$$

$$Productivity\ (qwintals/ha) = b0 + b1\ x\ EVI_Max \quad (6)$$

Where, EVI_Max = EVI_ Maximum, b0 = constanta; b1 = n parameters; EVI_Max = EVI Maximum.

As a validation step, the model was applied in the research area by estimating the average productivity for 1 year and then compared with BPS data. The results will calculate the ratio and coefficient of variance to determine the comparison and spatial diversity of productivity in the two study areas [41].

3 Results and Discussion

3.1 Rice Phenological Trend Analysis in Karawang Regency and Malang Regency

The extraction results of the threshold data for fields classification from Sentinel 2 images for a period of 2 years (2019-2020) was 89,723.51 Ha for Kerawang Regency, while in Malang Regency it was 32,902.20 Ha (Figure 2). The results of the rice field classification using the threshold method are smaller than the classification of Raw Rice Fields in 2019, namely for Karawang Regency 97,541 Ha and Malang Regency 45,851 Ha [42, 43]. The results of the classification of rice fields were tested with detailed data of Rice Raw Land in 2019 from BPN using the error matrix method, namely Overall Accuracy and Kappa. The results are presented in table 2.

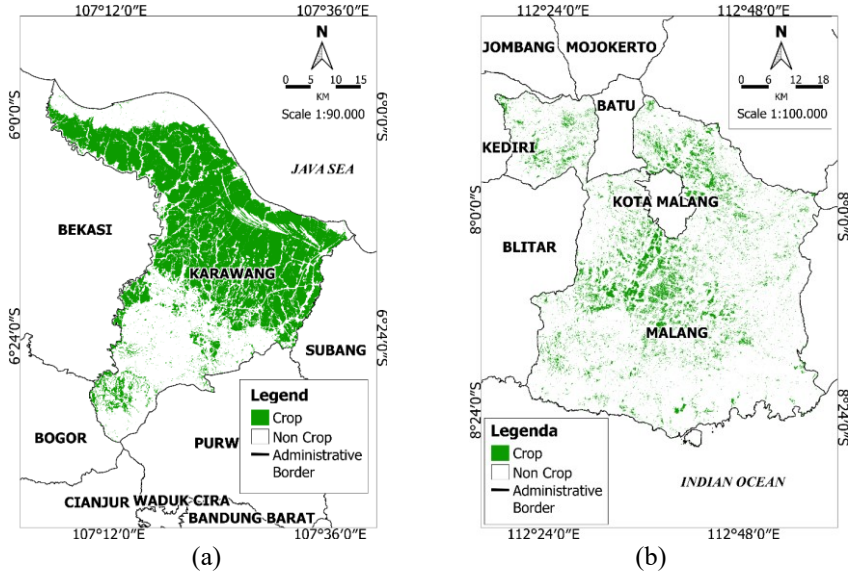


Fig. 2. Classification of Rice Fields based on Image Sentinel 2 years 2019-2020 (a) Rice fields in Karawang Regency and (b) Rice fields in Malang Regency

Table 2. Rice Field Accuracy Test in Karawang Regency (Left) and Malang Regency (Right)

Class	Crop	Non Crop
Crop	1967	72
Non Crop	176	2105
Overall Accuracy: 0.94	*Kappa*: 0.87	

Class	Crop	Non Crop
Crop	5001	251
Non Crop	461	266
Overall Accuracy: 0.87	*Kappa*: 0.36	

The classification accuracy of the threshold index method has a fairly good accuracy value in Karawang Regency and Malang Regency. Overall accuracy for each region has a value above 0.8, so it can be categorized as good enough and can be used [44]. The Kappa value in Karawang Regency is 0.874 and Malang Regency is 0.363, this indicates that the distribution element of the data sample is less balanced in Malang Regency. However, this classification can be used as a reference to analyze the growth phenology of rice plants.

The results of the spatial distribution show that the spectral value of the Rice Plant object in the study area is different. Rice field area based on Maximum EVI in Karawang Regency is dominantly high in class 0.60-0.65 with an area of 18758.49 Ha and class 0.40-0.45 with the lowest area of 4263.50 Ha. Meanwhile, in Malang Regency, the class > 0.70 was at most 16149.04 Ha and the class 0.40 to 0.45 was at least 58.85 Ha. The percentage of paddy fields based on the Maximum EVI class can be seen in Figure 3 and Figure 4.

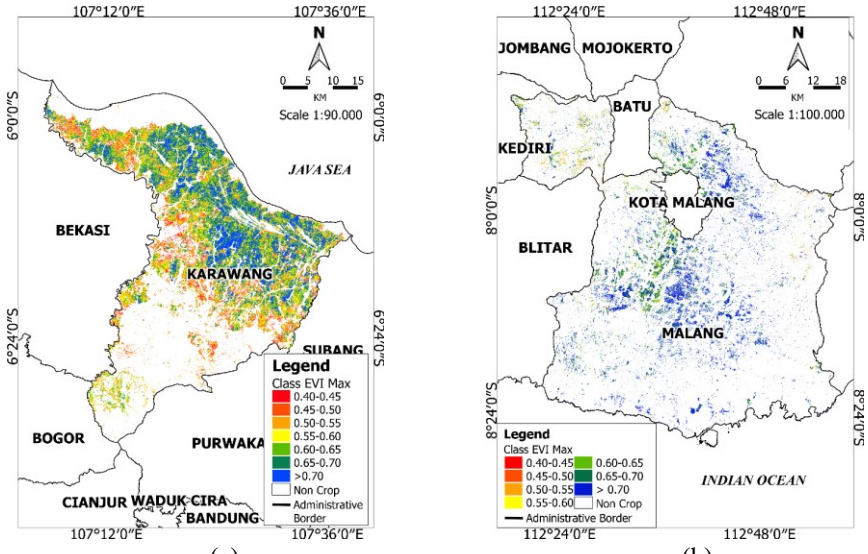


Fig. 3. Rice Field Classification Map based on Maximum EVI (a) Karawang Regency and (b) Malang Regency

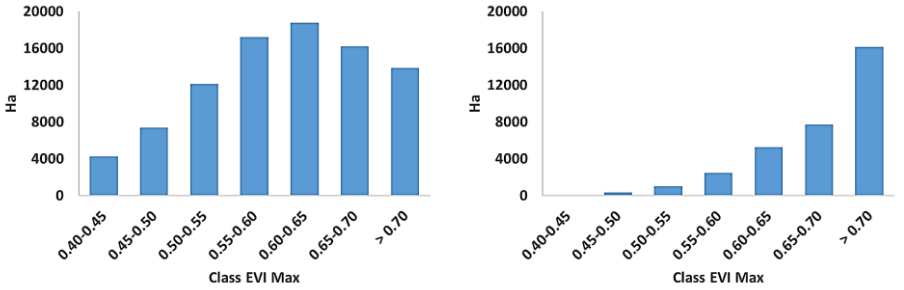
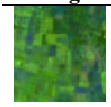
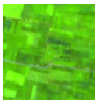
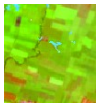


Fig. 4. Rice Field Area according to Class EVI Maximum (a) Karawang Regency and (b) Malang Regency

Based on the Maximum EVI class, the rice field class in Karawang Regency is more evenly distributed when compared to the rice field class in Malang Regency. It indicates that in Karawang Regency there are many classes of Rice Plants that can grow, while in Malang Regency only certain classes are dominant. This can occur due to several factors such as rainfall, soil, topography, water requirements, rice crop patterns, and types of rice plants in the area [45].

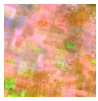
Visually, the growth phase of the Rice Plant can be seen from the Sentinel-2 RGB bands 11, 8, and 3. The appearance of the rice field will be in the form of an irregular square with certain colors according to its growth stages as can be seen in table 3. If detected through the EVI spectral values, the beginning of planting was < 0.2, fallow with a value of 0.2-0.1 and each vegetative/generative phase was worth > 0.2 (Figure 5). The vegetative phase is characterized by a positive change in the value (dEVI) and the generative phase is characterized by a negative change in the value (dEVI) (Figure 6) [41]. By identifying this, it is easy to detect the beginning of planting and harvesting rice plants.

Table 3. Rice Plant Phase seen from Sentinel 2 RGB Images (11, 8, 3) in Malang areas.

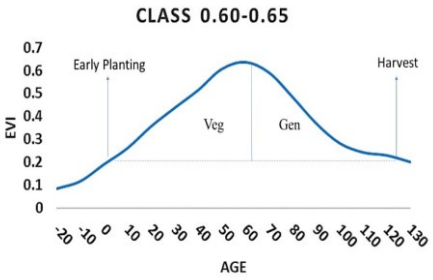
Image	Photo	Phase	Age	Image	Photo	Phase	Age
		Early Planting	0-10			Gen 1	60-90
		Veg 1	10-30			Gen 2	90-110



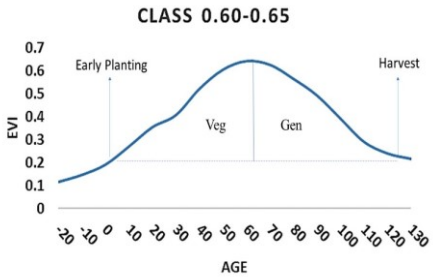

Veg 2 30-60




Harvest 110-120

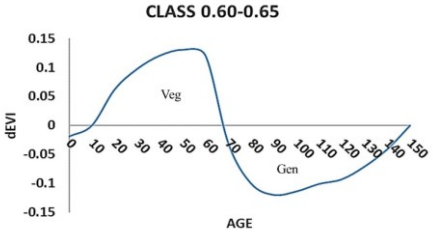


(a)

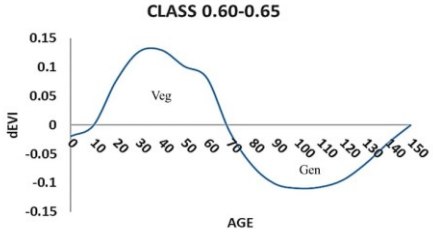


(b)

Fig. 5. Profile of Days After Planting (DAT) of Rice Plants based on Maximum EVI Class 0.60-0.65 (a) Karawang Regency and (b) Malang Regency



(a)



(b)

Fig. 6. dEVI of Rice Plants (a) Karawang Regency and (b) Malang Regency Class 0.60-0.65

The results of statistical analysis of the polynomial 3 or spline qubic regression model in each research area were shown. Regression was applied to 7 classes of rice fields in the two research areas. The regression model parameters obtained can be seen in tables 4 and 5.

Table 4. 3rd order polynomial regression test based on rice class in Karawang Regency

EVIMax	0,40-0.45	0,45-0,50	0,50-0,55	0,55-0,60	0,60-0,65	0,65-0,70	> 0,70
b0	2E-07	3E-07	-3E-08	2E-08	-4E-08	-8E-08	2E-07
b1	-9E-05	-0,0001	-7E-05	-9E-05	-9E-05	-9E-05	-0,0001
b2	0,0087	0,011	0,0097	0,0118	0,0126	0,0127	0,017
b3	0,1506	0,1267	0,1563	0,1408	0,1336	0,1408	0,1111
R^2	90,07%	90,72%	90,06%	90,89%	90,25%	91,27%	92,66%

Table 5. 3rd order polynomial regression test based on rice class in Malang Regency

EVIMax	0,40-0.45	0,45-0,50	0,50-0,55	0,55-0,60	0,60-0,65	0,65-0,70	> 0,70
b0	-5E-08	1E-07	8E-08	3E-07	2E-07	3E-07	2E-07
b1	-6E-05	-8E-05	-1E-04	-0,0001	-0,0002	-0,0002	-0,0002
b2	0,0072	0,0089	0,011	0,0139	0,016	0,0178	0,0183
b3	0,1737	0,1544	0,1513	0,1481	0,1202	0,1292	0,1357
R^2	91,02%	87,61%	89,21%	89,25%	90,36%	91,83%	91,44

The regression test of the two research areas throughout the Maximum EVI class resulted in the coefficient of determination (R2) > 0.8 or 80% indicating it was good [46]. Karawang Regency has an average R2 = 0.91 or 91% and for Malang Regency an average R2 = 0.90 or 90.1%. This indicates that the two regions have a significant relationship between the EVI value and the age of the rice plants. Therefore, the phenology of rice growth can be applied in the research area.

3.2 Estimation of Harvest Area and Productivity of Rice Crops Using Remote Sensing Approach in Karawang Regency and Malang Regency.

Based on multitemporal analysis of Sentinel-2 satellite imagery, the estimated rice harvested area seen from May-August 2020 images in Karawang Regency is 78,002.79 Ha while for Malang Regency it is 27,964.28 Ha. The spatial distribution of rice crop yield estimates from satellite imagery analysis is presented in Figure 7.

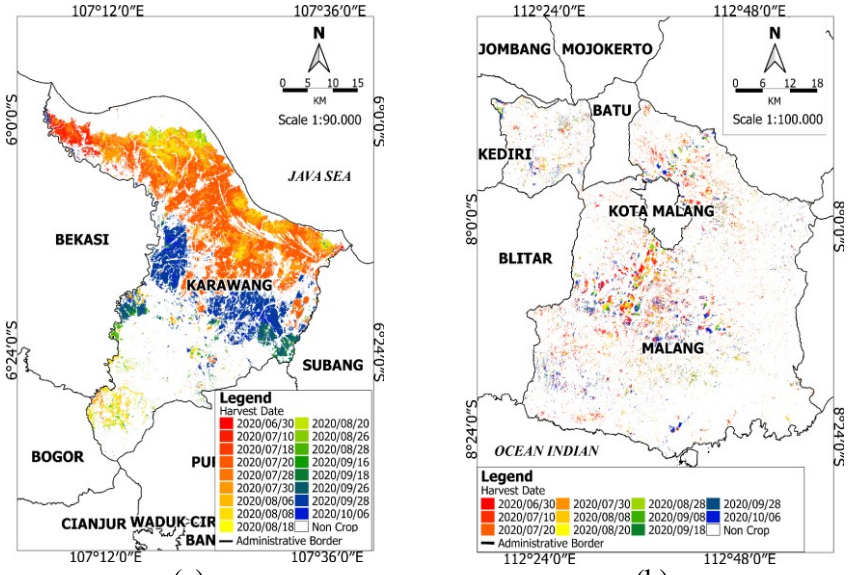


Fig. 7. Image Harvest Dates May-August 2020 (a) Karawang Regency and (b) Malang Regency

The harvested area yields are accumulated for 1 year so that in general the harvested area data generated from the analysis of Sentinel 2 satellite imagery is relatively smaller than the harvested area data released by BPS in the same period. The total harvested area for lowland rice in Karawang Regency based on Sentinel-2 images in the 2019 period is 174,955 Ha and for 2020 it is 185,806 Ha, while in Malang Regency in 2019 it is 55,318 and in 2020 it is 38,192. The results of the comparison of image data with BPS data can be seen in Figure 8.

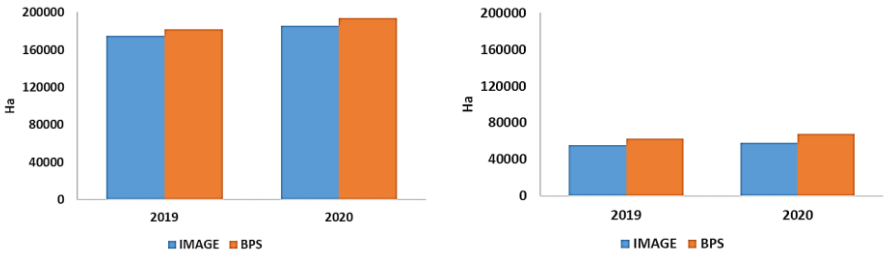


Fig. 8. Comparison Graph of Harvest Area (a) Karawang Regency and (b) Malang Regency

Table 6. Comparison of Harvested Area on Image and BPS data

Area	2019			2020		
	Image (Ha)	BPS (Ha)	Rasio	Image (Ha)	BPS (Ha)	Rasio
Kab Karawang	174.955,79	181.737,09	0,96	185.806,99	193.976,07	0,91
Kab Malang	55.318,23	62.773	0,88	58.192,33	67.833	0,86

The difference between the harvested area in the Image and the BPS data can be seen from the ratio value. The average Karawang Regency has a ratio of 0.935 while in Malang Regency it is 0.87. If the ratio value is close to 1, it means that the harvested area of Image Sentinel-2 data with BPS data tends to be the same. If the ratio value is more than 1, it means that the Image harvested area is larger than the BPS data. On the other hand, if the ratio value is less than 1, it means that the harvested area according to BPS data is greater than the harvested area based on Image [41]. Thus, the harvest area based on images in Karawang is better than in Malang areas.

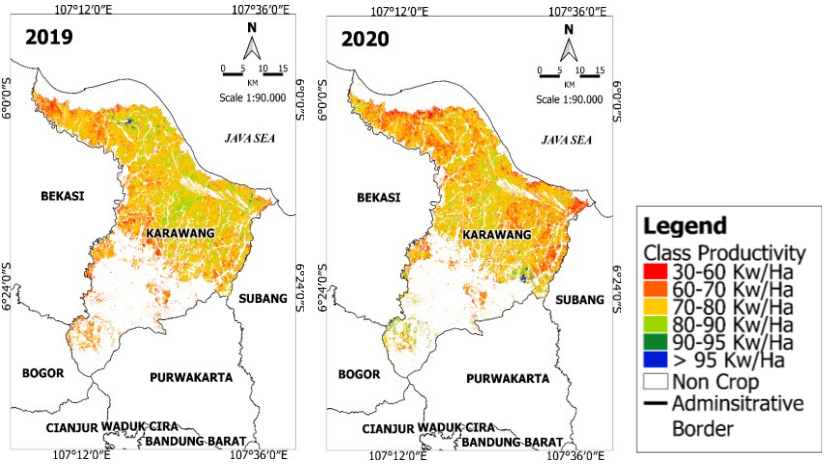


Fig. 9. Rice Crop Productivity in Karawang Regency

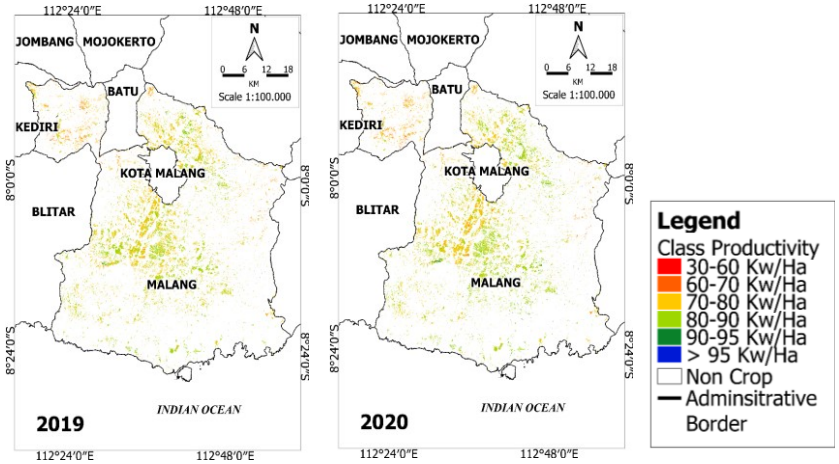


Fig. 10. Rice Crop Productivity in Malang Regency

The average productivity of paddy fields as a result of the analysis of Image Sentinel-2 (Figure 3.9) in Karawang Regency in the 2019 period was 73.87 and in 2020 it was 72.91 Qwintals/Ha, then for Malang Regency, in the 2019 period it was 74,59 Qwintals/Ha and in 2020 as much as 74.87 Qwintals/Ha. When compared with BPS data, in general, the average productivity of lowland rice resulting from Image analysis has a greater value than BPS data. For more clarity, a comparison of the estimated data for lowland rice productivity from Image and BPS analysis is presented in table 7 and table 8.

Table 7. Comparison of 2019 productivity estimates

Area	2019				
	Image (Qwintals/Ha)	BPS (Qwintals/Ha)	Rasio	Std Dev	Coef Varians (%)
Karawang	73,87	60,14	1,23	5,30	4,31
Malang	74,59	70,91	1,05	5,32	5,06

Table 8. Comparison of 2020 productivity estimates

Area	2020				
	Image (Qwintals/Ha)	BPS (Qwintals/Ha)	Rasio	Std Dev	Coef Varians (%)
Karawang	72,91	61,49	1,19	6,12	5,16
Malang	74,87	70,91	1,06	5,37	5,09

Based on tables 7 and 8, the ratio of Image to BPS data in Karawang Regency in 2019 is 1.23 and Malang Regency is 1.05 while in 2020 Karawang Regency has a ratio of 1.19 and Malang Regency 1.06. If the ratio value is close to 1, then the productivity of Image data with BPS data tends to be the same. If the ratio value is more than 1, it means that Image productivity is greater than the BPS data. On the other hand, if the ratio value is less than 1, it means that productivity according to BPS data is greater than Image [41]. This indicates that the productivity results based on Image Sentinel-2 in both Karawang Regency and Malang Regency have greater results than BPS data in 2019-2020.

Furthermore, the results of the coefficient of variance in Karawang Regency in 2019 were 4.73% and Malang Regency 5.06%. Meanwhile, in 2020, Karawang Regency has a coefficient of variance of 5.16% and Malang Regency is 5.09%. If the percentage of the coefficient of variance is small, it means that the distribution of productivity on the Image tends to be homogeneous (same). If the percentage coefficient is high, it means that productivity differences tend to be heterogeneous (various) [41]. Apparently that rice farmings'productivity in 2019 in Karawang Regency are more homogeneous, and for 2020 Malang Regency has a more homogeneous productivity than Karawang Regency.

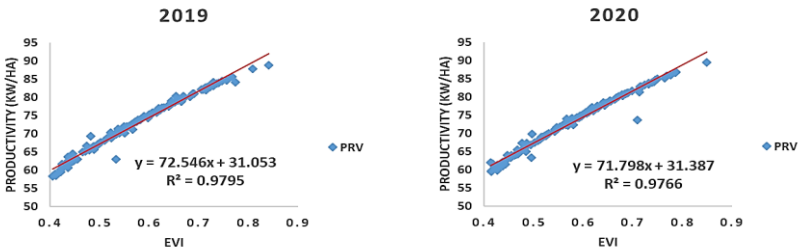


Fig. 11. Relationship of Maximum EVI with Rice Productivity in Karawang Regency

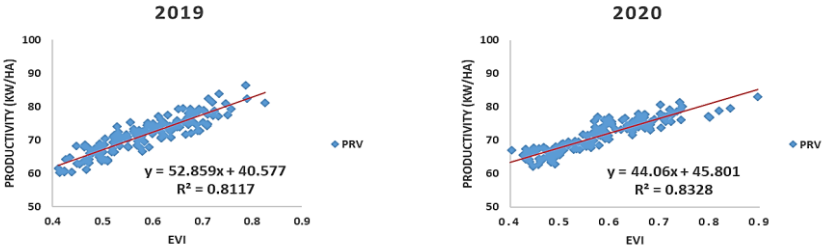


Fig. 12. The Relationship of Maximum EVI with Rice Crop Productivity in Malang Regency

Figures 11 and 12 explain the relationship between the maximum EVI value and rice productivity in different areas, namely Malang Regency and Karawang Regency. Based on the statistical analysis carried out, the regression value for Karawang Regency in 2019 was R2 = 0.98 and in 2020 it was R2 = 0.97. While in Malang Regency in 2019 it was R2 = 0.82 and in 2020 the R2 = 0.83. The two areas indicate that there is a positive relationship between the maximum EVI value and the productivity of rice plants. The correlation between the two variables is also interpreted as a strong relationship. Interpretation with R2 value close to 1 as a strong variable relationship, indicating its high potential for application [46].

4 Conclusions

The results of the identification of the Multitemporal Sentinel-2 Image in 2019-2021 in each research area has a maximum EVI class of rice fields from 0.40 to > 0.70. Karawang Regency has a dominant EVI class of 0.60-0.65 while in Malang Regency the EVI Maximum class is dominant > 0.70. The accuracy of the relationship between age and the EVI value in each rice field class is quite significant or related, namely in Karawang Regency an average of $R^2 = 0.9084$ and Malang Regency with an average of $R^2 = 0.9010$.

Based on Image Sentinel-2, the estimated harvested area in 2019-2020 is smaller than BPS data, while productivity is greater than BPS data. Harvested area is measured by the ratio value, namely in Karawang Regency it has a ratio of 0.93 and Malang Regency has a ratio of 0.86, which is smaller than BPS data. While productivity is measured by the coefficient of variance, Karawang Regency has an average of 4.73% and Malang Regency has an average of 5.07%.

References

1. Chen, C., Son, N.T., Chang, L. Monitoring of rice cropping intensity in the upper Mekong Delta, Vietnamu sing time-series MODIS data. *Adv. Space Res*, 49, pp 292–301 (2012).

2. McLean, J., Hardy, B., Hettel, G. Rice Almanac, 4th ed. Philippines: International Rice Research Institute (2013).
3. Qwintalsenzer, C.; Knauer, K. Remote sensing of rice crop areas. Int J Remote Sens, 34, pp 2101–2139 (2013).
4. FAO & WWC. Towards a Water and Food Secure Future: Critical Perspectives for Policy-makers. Rome: Food and Agriculture Organization of The United Nation (2015).
5. BPS Kabupaten Karawang. Kabupaten Karawang Dalam Angka 2019. Karawang: Badan Pusat Statistik. (2019).
6. BPS Kabupaten Malang. Kabupaten Malang Dalam Angka 2019. Malang: Badan Pusat Statistik (2019).
7. Qwintalsrnianto, M., Ariffin, dan Azizah Nur. Pendugaan Produktivitas Padi (Oryza Sativa) Berdasarkan Curah hujan Di Kabupaten Malang. Jurnal Produksi Tanaman, 6(8), pp 1859–1867 (2018).
8. Corcione, V.; Nunziata, F.; Mascolo, L.; Migliaccio, M. A study of the use of COSMO-Sky Med SAR Ping Pong polarimetric mode for rice growth monitoring. Journal Remote Sensing, 37, pp 633–647 (2016).
9. Haw C L, Ismail W I W, Kairunniza-Bejo S, Putih A, Shamshiri R. Colour vision to determine paddy maturity. J. Agric. & Biol. Eng., 7(5), 55–63 (2014).
10. Pei W, Lan Y B, Luo X W, Zhou Z Y, Wang Z, Wang Y. Integrated sensor system for monitoring rice growth conditions based on unmanned ground vehicle system. Int. J. Agric. & Biol. Eng., 7(2), 75–81 (2014).
11. Dash J, Jeganathan C, Atkinson P M. The use of MERIS Terrestrial Chlorophyll Index to study spatio-temporal variation in vegetation phenology over India. Remote Sens. Environment., 114(7), 1388–1402 2010.
12. Li B, Li L, Qin Y, Liang L, Li J, Liu Y. Impacts of climate variability on streamflow in the upper and middle reaches of the Taoer River based on the Budyko Hypothesis. Resources Science, 33(1): 70–76 (2011).
13. Shidiq, I. P. A., & Ismail, M. H. Stand Age Model for Mapping Spatial Distribution of Rubber Tree Using Remotely Sensed Data in Kedah, Malaysia. Jurnal Teknologi, 78(5), pp 239-244 (2016).
14. Shidiq, I. P. A., Ismail, M. H., Ramli, M. F., & Kamarudin, N. Combination of ALOS PALSAR and Landsat 5 Imagery for Rubber Tree mapping. The Malaysian Forester, 80(1), pp 55-72 (2017).
15. Segarra, J., Buchaillot, Maria, L., Araus, Jose, L., Kefauver, Shawn, C. Remote sensing for precision agriculture: Sentinel-2 improved features and applications. Journal Agronomy, 10(641), pp 1-18 (2020).
16. Drusch, M., Del Bello, U., Carlier, S., Colin, O., Fernandez, V., Gascon, F., Bargellini, P. Sentinel-2: ESA's Optical High-Resolution Mission for GMES Operational Services. Remote Sensing of Environment, 120, pp 25–36 (2012).

17. Escola, A., Badia, N., Arnó, J., & Martínez-Casasnovas, J. A. Using Sentinel-2 images to implement Precision Agriculture techniques in large arable fields: First results of a case study. Advances in Animal Biosciences, 8(2), 377–382 (2017).
18. Zhan, P.; Zhu, W.; Li, N. An automated rice mapping method based on flooding signals in synthetic aperture radar time series. Remote Sens Environment, 252, 112112 (2021).
19. Campos-Taberner, M.; García-Haro, F.J.; Busetto, L.; Ranghetti, L.; Martínez, B.; Gilabert, M.A.; Camps-Valls, G.; Camacho, F.; Boschetti, M. A critical comparison of remote sensing leaf area index estimates over rice-cultivated areas: From Sentinel-2 and Landsat-7/8 to MODIS, GEOV1 and EUMETSAT Polar system. Remote Sensing, 10, 763 (2018).
20. Son, N.T.; Chen, C.F.; Chen, C.R.; Duc, H.N.; Chang, L.Y. A phenology-based classification of time-series MODIS data for rice crop monitoring in Mekong Delta, Vietnam. Remote Sensing, 6, 135–156 (2012).
21. Cai, Y.; Lin, H.; Zhang, M. Mapping paddy rice by the object-based random forest method using time series Sentinel-1/Sentinel-2 data. Adv. Space Res, 64, 2233–2244 (2019).
22. Noureldin N A, Aboelghar M A, Saudy H S, and Ali A M. Rice yield forecasting models using satellite imagery in Egypt. Egyptian Journal of Remote Sensing and Space Science, 16(1), pp 125-31 (2018).
23. Li, S.; Xiao, J.T.; Ni, P.; Zhang, J.; Wang, H.S.; Wang, J.X. Monitoring paddy rice phenology using time series MODIS data over Jiangxi Province, China. J. Agric. Biol. Eng, 7, pp 28–36 (2014).
24. Meier, M.S., Stoessel, F., Jungbluth, N., Juraske, R., Schader, C., Stolze, M. Environmental impacts of organic and conventional agricultural products we are the differences captured by life cycle assessment. J. Environ. Manag, 149, pp 193-208 (2015).
25. Wu,C.,Hou,X.,Peng,D.,Gonsamo,A.,Xu, S. Land surface phenology of China's temperate ecosystems over 1999–2013 : Spatial–temporal patterns ,interactioneffects, covariation with climate and implications for productivity. Agric. For. Meteorol. 216, pp 177–187 (2016).
26. Liu, Q., Fu, Y. H., Zhu, Z., Liu, Y., Liu, Z., Huang, M., Piao, S. Delayed autumn phenology in the Northern Hemisphere is related to change in both climate and spring phenology. Global Change Biology, 22, pp 3702–3711 (2016).
27. Lonita Bahtiar Ibnu, Prasetyo Yudo, Hani'ah. Analisis Perubahan Luas Dan Kerapatan Hutan Menggunakan Algoritma Ndvi (Normalized Difference Vegetation Index) Dan Evi (Enhanced Vegetation Index) Pada Image landsat 7 Etm+ Tahun 2006, 2009, Dan 2012. Jurnal Geodesi Undip, 4(3), pp 122-120 (2015).

28. Dirgahayu, Dede., Noviar, H., & Anwar, S. Model pertumbuhan tanaman padi di pulau Sumatera menggunakan data EVI MODIS multitemporal. Proceedings, Seminar Nasional Penginderaan Jauh 2014, pp. 333–343 (2014).
29. Parsa, M., Dirgahayu, D., & Harini, S. Pengembangan Metode Klasifikasi Lahan Sawah Berbasis Indek Image Landsat Multiwaktu. Jurnal Penginderaan Jauh Dan Pengolahan Data Image Digital, 16(1), pp 35–44 (2019).
30. Rudiana, E., Rustiadi, E., Firdaus, M., & Dirgahayu, D. Pengembangan Penggunaan Penginderaan Jauh Untuk Estimasi Produksi Padi (Studi Kasus Kabupaten Bekasi). Jurnal Ilmu Tanah Dan Lingkungan, 19(1), pp 6–12 (2019).
31. Khoirunnisa, Supriatna and A Wibowo. Using NDVI algorithm in Sentinel-2A imagery for rice productivity estimation (Case study: Compreng sub-district, Subang Regency, West Java). IOP Conf. Series: Earth and Environmental Science, 481, pp 012-064 (2020).
32. Li Shihua , Xiao Jiangtao , Ni Ping, Zhang Jing , Wang Hongshu, Wang Jingxian. Monitoring paddy rice phenology using time series MODIS data over Jiangxi Province, China. J Agric & Biol Eng, 7(6), 28－36 (2014).
33. Liu, H.Q.; Huete, A.R. A feedback based modification of the NDV I to minimize canopy background and atmospheric noise. IEEE Transactions on Geoscience and Remote Sensing (1995).
34. Gao, B. NDWI – A normalized difference water index for remote sensing of vegetation liquid water from space. Remote Sensing of Environment, 58(3), pp 257–266 (1995).
35. Guo, G. et al. Impacts of urban biophysical composition on land surfacetemperature in urban heat island clusters. Landscape and Urban Planning, 135, pp 1–10 (2015).
36. Dirgahayu, Dede. The New Method for Detecting Early Planting and Bare Land Condition in Paddy Field by Using Vegetation-Bare-Water Index. The 2nd International Conference of Indonesian Society for a Better Govermance, pp 331-342 (2016).
37. Qwintalsshardono, D. Klasifikasi Digital Pada Penginderaan Jauh (Cetakan 1). Bogor: IPB Press (2017).
38. Hestie, T., Tibshirani, R. & Fridman, J. The Elements of Statistical Learning Data Mining, Inference, and Prediction. Second Edition. Stanford. California: Springer (2017).
39. Pusfatja Lapan. Pedoman Pemantauan Fase Pertumbuhan Tanaman Padi Menggunakan Data Satelit Penginderaan Jauh. Jakarta: Pusat Pemanfaatan Penginderaan Jauh Lembaga Penerbangan dan Antariksa Nasional. (2015).

40. Dirgahayu, Dede. Spatial modelling of rice production vulnerability using remote sensing and GIS technology (case studies in Indramayu Regency, West Java). Disertation. Bogor: IPB University (2012).
41. Octora, Wilona. Analisis Luas Lahan Sawah Berbasis Image MODIS di Provinsi Jawa Barat Tahun 2002-2012. Skripsi. Bogor: IPB (2014).
42. BPS Kabupaten Karawang. Kabupaten Karawang Dalam Angka 2020. Karawang: Badan Pusat Statistik (2020).
43. BPS Kabupaten Malang. Kabupaten Malang Dalam Angka 2020. Malang: Badan Pusat Statistik (2020).
44. Rini, Meliana Swatika. Kajian kemampuan metode neural network untuk klasifikasi penutup lahan dengan menggunakan Image Landsat-8 OLI (kasus di Kota Yogyakarta dan sekitarnya). Geomedia, 16(1), pp 1-12 (2018).
45. Avicienna, Muya. Teknik Pemilihan Lahan Pertanian Padi Sawah Berkelanjutan. Thesis. Bogor: Sekolah Pascasarjan IPB (2011).
46. Ndruru, R. E., Situmorang, M., & Tarigan, G. Analisa faktor-faktor yang mempengaruhi hasil produksi padi di deli serdang. Saintia Matematika, 2 (1), pp: 71-83 (2014).

Open Access This chapter is licensed under the terms of the Creative Commons Attribution-NonCommercial 4.0 International License (http://creativecommons.org/licenses/by-nc/4.0/), which permits any noncommercial use, sharing, adaptation, distribution and reproduction in any medium or format, as long as you give appropriate credit to the original author(s) and the source, provide a link to the Creative Commons license and indicate if changes were made.

The images or other third party material in this chapter are included in the chapter's Creative Commons license, unless indicated otherwise in a credit line to the material. If material is not included in the chapter's Creative Commons license and your intended use is not permitted by statutory regulation or exceeds the permitted use, you will need to obtain permission directly from the copyright holder.



Jurnal Ilmu Pertanian Indonesia (JIPI), April 2022
ISSN 0853-4217
EISSN 2443-3462

Vol. 27 (2) 226–236
http://journal.ipb.ac.id/index.php/JIPI
DOI: 10.18343/jipi.27.2.226

Deteksi Alih Fungsi Lahan Padi Sawah Menggunakan Sentinel-2 dan *Google Earth Engine* di Kota Serang, Provinsi Banten

(Rice Fields Change Detection Using Sentinel-2 and *Google Earth Engine* In Serang City, Banten Province)

Tian Mulyaqin[1]*, Kardiyono[1], Ismatul Hidayah[1], Fadhlullah Ramadhani[2], Muchamad Yusron[3]

(Diterima Juni 2021/Disetujui Maret 2022)

ABSTRAK

Lahan merupakan salah satu faktor utama dalam produksi padi, tetapi alih fungsi lahan pertanian ke sektor lain terus berlanjut dan menjadi tantangan dalam penyediaan pangan di Indonesia. Kota Serang merupakan salah satu daerah penghasil beras di Provinsi Banten. Kajian ini bertujuan menganalisis perubahan alih fungsi lahan sawah ke sektor lain dengan memetakan tutupan lahan sawah menggunakan citra satelit Sentinel-2 tahun 2021 dibandingkan tahun 2019 dengan metode *Random Forest* dengan mendayagunakan aplikasi *Google Earth Engine* (GEE) dan dukungan komputasi awan (*cloud computing*). Hasil kajian menunjukkan bahwa tutupan lahan sawah di Kota Serang pada tahun 2021 berkurang 602,87 ha (–7,20%) dibandingkan tahun 2019 dari total tutupan lahan; tutupan lahan berupa vegetasi lain juga berkurang 242 ha (–2,45%), sementara tutupan lahan wilayah perkotaan pada tahun 2021 meningkat 781,82 ha (10,89%). Kajian ini menunjukkan telah terjadi perubahan alih fungsi lahan di Kota Serang akibat ekspansi perkotaan dalam rentang waktu 3 tahun, sekaligus juga bahwa penggunaan GEE dapat mengefisienkan pemantauan perubahan alih fungsi lahan dan tutupan penggunaan lahan.

Kata kunci: *Google Earth Engine*, padi, Sentinel-2

ABSTRACT

Land availability is one of the main factors in rice production. However, the agricultural land-use change to other sectors continues and becomes a challenge in the food supply in Indonesia. Serang City is one of the rice-producing areas in Banten Province. This study aims to analyze changes in the land use of rice field functions to other sectors by mapping rice field cover using Sentinel-2 satellite imagery in 2021 compared to 2019 with the Random Forest method by using Google Earth Engine (GEE) applications and cloud computing approach. The study results showed that the cover of rice fields in Serang City in 2021 decreased by 602.87 ha (–7.20%) compared to 2019 from the total land cover. Land cover in other vegetation was also reduced by 242 ha (–2.45%), while urban land cover in 2021 increased by 781.82 ha (10.89%). This study shows that there has been a change in land transfer in Serang City due to urban expansion in 3 years, as well as that the use of GEE can streamline monitoring of land-use change and land use cover.

Keywords: Google Earth Engine, rice field, Sentinel-2

PENDAHULUAN

Produksi padi di Indonesia khususnya Provinsi Banten merupakan salah satu kunci ketahanan pangan di Indonesia. Kota Serang sebagai ibukota Provinsi Banten juga mengalami kontraksi produksi. Walaupun berstatus kota, Serang masih merupakan kontributor produksi padi bagi Banten. BPS Banten mencatat produksi padi Kota Serang pada tahun 2019 mencapai 67,34 ribu ton atau 4,48% dari total produksi padi Banten (BPS Banten 2021). Konsumsi beras sebagai bahan makanan pokok akan seiring dengan jumlah penduduk yang ada di Kota Serang, yaitu 688.603 jiwa dengan tingkat kepadatan penduduk 2582 jiwa/km^2 dan laju pertumbuhan penduduk 1,59% pada tahun 2019 (BPS Kota Serang 2020). Lahan pertanian untuk produksi beras harus bersaing juga dengan kebutuhan lahan untuk pemukiman dan sektor lain yang juga semakin tinggi. Peningkatan jumlah penduduk dan peningkatan aktivitas ekonomi dari sektor lainnya menyebabkan upaya mencapai ketahanan pangan di masa mendatang menjadi semakin berat. Peningkatan tersebut menyebabkan meningkatnya kebutuhan lahan termasuk mengakibatkan alih fungsi lahan pertanian menjadi permukiman, pembangunan infrastruktur (jalan, bendungan, dan sebagainya), atau industri. Pembangunan yang terus dilaksanakan menyebabkan banyak lahan pertanian yang harus beralih fungsi menjadi non-pertanian. Harga lahan yang cukup tinggi menjadi salah satu faktor pemicu para petani untuk melepas kepemilikan lahannya ke

[1] Balai Pengkajian Teknologi Pertanian Provinsi Banten Jl. Ciptayasa KM 01 Ciruas Serang Banten 42182
[2] Balai Penelitian Agroklimat dan Hidrologi, Jl. Tentara Pelajar No. 1A Bogor 16114
[3] Balai Besar Pengkajian dan Pengembangan Teknologi Pertanian, Jl. Tentara Pelajar No. 10 Bogor 16114
* Penulis Korespondensi:
E-mail: tianmulyaqin@pertanian.go.id

investor untuk dialihfungsikan. Artinya, motif ekonomi menjadi salah satu penyebab utama dari alih fungsi lahan (Ridwan 2016; Janah *et al*. 2017). Selain itu, pendapatan petani, luas kepemilikkan lahan, sistem waris, pengaruh tetangga yang mengalihfungsikan lahannya, pengaruh pengusaha/investor, keadaan lingkungan, kebijakan pemerintah dan pendidikan petani juga ikut berperan dalam pengambilan keputusan untuk mengalihfungsikan lahan (Martunisa & Noor 2018).

Alih fungsi lahan semakin masif terjadi di wilayah perkotaan dan kadang terjadi gejala penjalaran kota yang tidak teratur atau sering disebut dengan *urban sprawl*. Gejala ini terjadi dalam bentuk pembangunan kota dengan kepadatan rendah atau tersebar tidak teratur dan sering kali juga berimbas pada terjadinya alih fungsi lahan dari sektor pertanian ke pemukiman atau bangunan untuk pemanfaatan sektor lain (Prasetyo 2017). Untuk mengatasi penjalaran kota yang tidak teratur, pemerintah menerbitkan Undang-Undang No. 26 Tahun 2007 tentang Penataan Ruang yang telah mengamanatkan asas penyelenggaraan penataan ruang, yaitu keterpaduan, keserasian, keselarasan dan keseimbangan, keberlanjutan, keberdayagunaan dan keberhasilgunaan, keterbukaan, kebersamaan dan kemitraan, perlindungan kepentingan umum, kepastian hukum dan keadilan, serta akuntabilitas. Asas tersebut tentunya ditetapkan demi mencapai dan mewujudkan harmonisasi antara lingkungan alam dan buatan, keterpaduan dalam penggunaan sumber daya alam dan sumber daya buatan dengan memperhatikan sumber daya manusia, serta perlindungan fungsi ruang dan pencegahan dampak negatif pada lingkungan akibat pemanfaatan ruang. Hal ini sesuai dengan tujuan penyelenggaraan penataan ruang, yaitu mewujudkan ruang wilayah nasional yang aman, nyaman, produktif, dan berkelanjutan berlandaskan wawasan nusantara dan ketahanan nasional.

Diharapkan penataan ruang di daerah selaras juga dengan Undang-undang No. 41 Tahun 2009 tentang Perlindungan Lahan Pertanian Pangan Berkelanjutan untuk mewujudkan ketahanan, kemandirian dan kedaulatan pangan. Agar cita-cita tersebut terwujud, diperlukan lahan pertanian eksisting dan tidak dialihfungsikan untuk keperluan di luar pertanian pangan. Ekspansi perkotaan sudah berlangsung cukup lama dan tidak terelakkan, sehingga pemerintah daerah perlu memantau kondisi eksisting lahan sawah untuk melihat status ketahanan pangan di daerahnya secara cepat dan akurat.

Salah satu metode yang yang dapat digunakan untuk mendeteksi perubahan tutupan lahan untuk penggunaan tanaman padi sawah dan ekspansi perkotaan dengan cepat ialah menggunakan penginderaan jauh. Satelit-satelit yang membawa sensor optik dan radar telah diluncurkan oleh berbagai badan antariksa di dunia seperti NASA-Amerika Serikat dan ESA-Eropa. Satelit Sentinel-2 adalah bagian dari program *Copernicus* dari *European Commission* (EC), *European Space Agency* (ESA) yang telah mengembangkan dan mengoperasikan misi Sentinel-2 untuk memperoleh citra optik resolusi spasial tinggi. Sentinel-2 merupakan misi pencitraan multispektral lebar, resolusi tinggi dengan konstelasi dua satelit yaitu Sentinel-2A dan Sentinel-2B yang diluncurkan tahun 2015 dan 2017. Konstelasi satelit ini memungkinkan dengan frekuensi kunjungan ulang 5 hari di skala global. Instrumen Multispektral S2 (MSI) mengambil sampel 13 *band spectral* (Tabel 1): *visible* (terlihat), dan NIR (*near infrared*) dengan ketinggian 10, *Red Edge* (tepi merah), dan SWIR (*Short Wave Infrared*) pada ketinggian 20 m, dan pita atmosfer pada resolusi spasial 60 m. Fitur tersebut memberikan data yang sesuai untuk menilai keadaan dan perubahan vegetasi, tanah, dan tutupan air (Gascon *et al.* 2016).

Era *big data* saat ini memungkinkan tutupan lahan sawah dapat dideteksi dengan sangat mudah dan terbuka. Salah satu *platform open source* yang sudah memanfaatkan *big data* berupa data citra satelit dan sudah sering dimanfaatkan untuk memetakan dan memantau tutupan lahan, vegetasi, ekspansi perkotaan, dan kepentingan lainnya ialah aplikasi *Google Earth Engine* (GEE) (Mutanga & Kumar 2019). Aplikasi GEE ini merupakan platform komputasi awan yang dirancang untuk menyimpan dan memproses kumpulan data yang sangat besar (pada skala *petabyte*) untuk analisis dan pengambilan keputusan akhir. Selain itu juga GEE dilengkapi bahasa pemrograman yang memungkinkan pengguna menginvestigasi perubahan lahan secara cepat dan akurat.

Google Earth Engine (GEE)

Koleksi data penginderaan jauh geospasial yang disediakan di GEE telah banyak dimanfaatkan dalam berbagai studi mengenai stadia tanaman padi (Ramadhani *et al.* 2020), perkebunan kelapa sawit (Shaharum *et al.* 2020), deteksi perubahan (Miettinen *et al*. 2019), klasifikasi perkotaan (Nguyen 2020), bahkan digunakan untuk mengkaji kondisi sosial ekonomi di suatu wilayah (Jean *et al.* 2016). Platform GEE merupakan platform *open-source*, tidak berbayar, dan menggunakan *Application Programming Interface* (API) atau *Interactive Development Environtment* (IDE) berbasis web (Gambar 1). Pengguna dapat mendaftar dan login melalui tautan https://earthengine.google.com dan mengakses antarmuka pengguna, serta panduan penggunaan, bahkan menyediakan kurikulum pendidikannya. Katalog data publik *Earth Engine* adalah kumpulan multi-*petabyte*, yakni kumpulan data geospasial yang banyak digunakan. Sebagian besar katalog terdiri atas citra penginderaan jauh pengamatan bumi, termasuk seluruh arsip Landsat serta arsip lengkap data dari Sentinel-1 dan Sentinel-2, bahkan mencakup prakiraan iklim, data tutupan lahan, dan lainnya (Gorelick *et al.* 2017).

Kajian ini mendeteksi dan memetakan tutupan penggunaan lahan dan alih fungsi lahan padi sawah menggunakan koleksi citra satelit Sentinel-2 pada

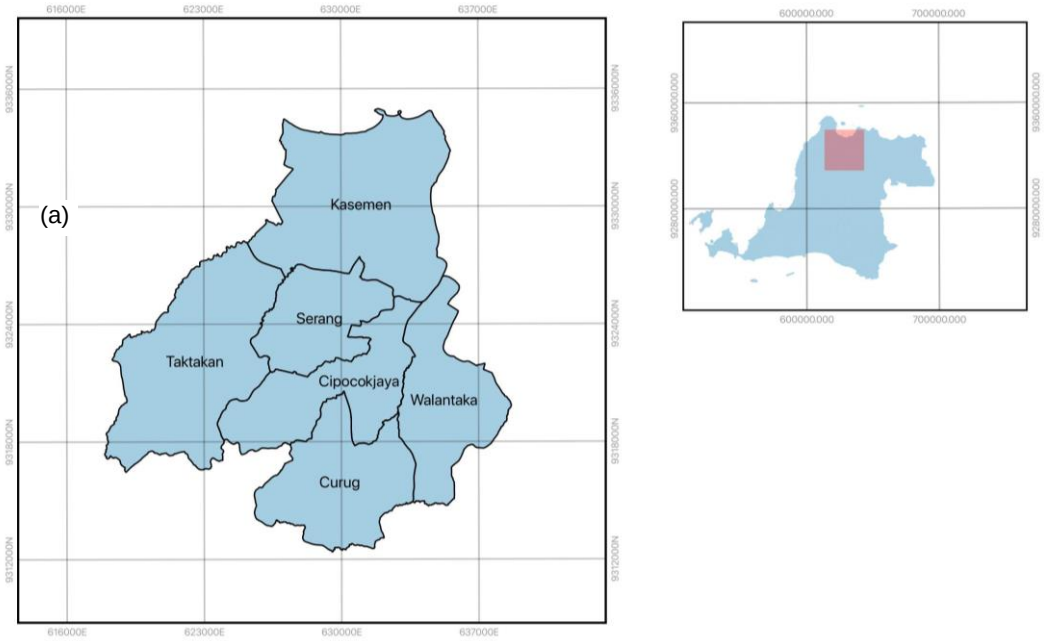
aplikasi GEE di Kota Serang pada tahun 2019 dan tahun 2021 guna mendukung pemantauan ketahanan pangan di Provinsi Banten.

METODE PENELITIAN

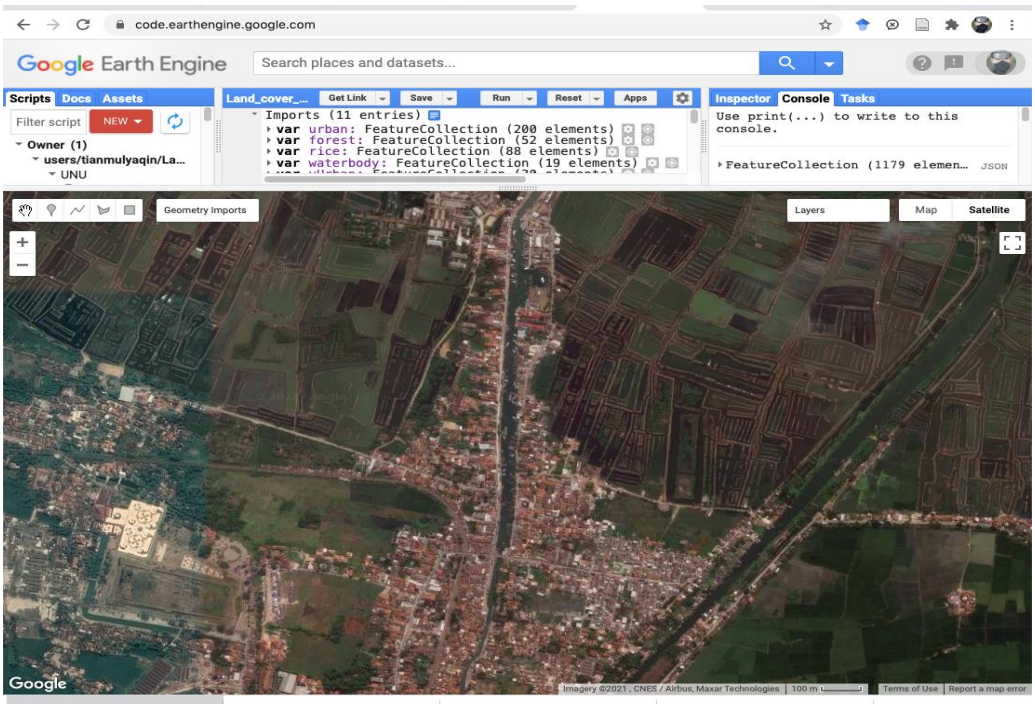
Lokasi Penelitian

Kota Serang terletak di sebelah utara Provinsi Banten; di sebelah utara berbatasan dengan Laut Jawa, dan sebelah timur, selatan, serta barat berbatasan dengan Kabupaten Serang. Secara astronomis, kota ini terletak pada 5°99'–6°22' Lintang Selatan dan 106°07'–106°25' Bujur Timur (Gambar 2). Luasnya 266,74 km^2 atau 26674 ha dan sebagian besar wilayahnya terletak di dataran rendah dengan ketinggian kurang dari 500 mdpl (BPS Kota Serang 2020).

Kota Serang memiliki potensi lahan sawah 8.474 ha (4,26%) dari total luas baku sawah Provinsi Banten, yaitu 198.520 ha. Sawah di Kota Serang yang luasnya 4.945 ha (53,04%) merupakan sawah irigasi dan sisanya, 3.979 ha (46,94%), merupakan sawah tadah hujan. Hal ini akan memengaruhi frekuensi tanam padi sebab di sawah irigasi padi



Gambar 1 Lokasi penelitian: (a) Kota Serang Provinsi Banten dan (b) Letak Kota Serang di Provinsi Banten.



Gambar 2 Tampilan platform *Google Earth Engine* (GEE) berbasis web.

dapat ditanam sedikitnya dua kali dalam setahun, sementara sawah tadah hujan dapat ditanami padi tidak lebih dari dua kali dali dalam setahun (BPS Banten 2020).

Metode

Penelitian ini sepenuhnya menggunakan aplikasi GEE (koleksi dan analisis data) dan aplikasi ArcMap 10.4 untuk membantu membuat *layout* peta. Data yang digunakan dalam penelitian ini ialah dataset Sentinel-2A pada rentang waktu 1 Januari 2019 sampai 31 Desember 2019 dibandingkan dengan dataset Sentinel-2A pada rentang waktu 1 Januari 2021 sampai 31 Desember 2021 untuk menghasilkan peta tutupan lahan di Kota Serang. Untuk mengetahui alih fungsi lahan sawah ke sektor lain sebagai akibat ekspansi perkotaan dilakukan analisis lanjutan dengan menumpang-susun (*overlay*) peta tutupan lahan wilayah perkotaan dengan lahan baku sawah Kota Serang tahun 2019 dan citra satelit *Google Earth* resolusi tinggi.

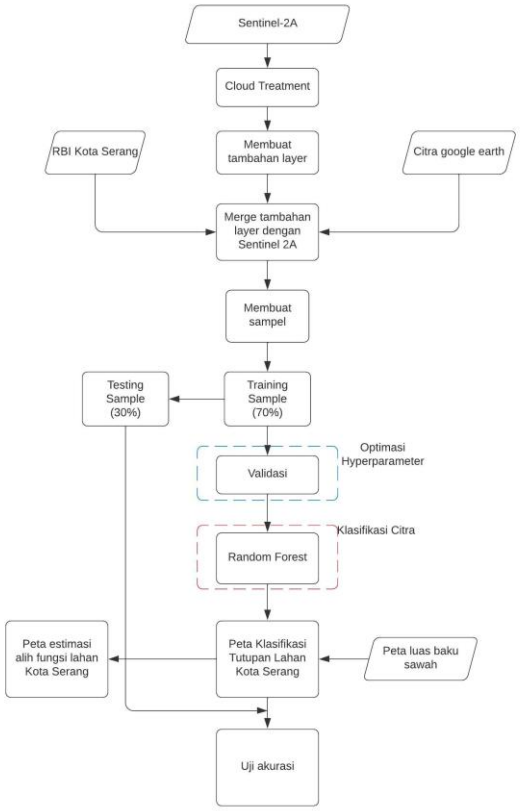
Pada tahap pertama, dipilih citra Sentinel-2 yang bebas awan pada rentang waktu studi, kemudian dibuat *region of interest* (ROI) dengan menumpang-susun citra Sentinel-2 dengan Peta Rupa Bumi Indonesia (RBI) Kota Serang, membuat titik sampel analisis dengan melihat citra satelit resolusi tinggi *Google Earth*, dan menganalisis titik sampel menggunakan algoritma mesin pembelajaran (*machine learning*) Random Forest (RF) pada aplikasi GEE. Klasifikasi menggunakan RF sudah digunakan untuk mengklasifikasi tanaman skala luas (Shelestov *et al.* 2017), tutupan lahan tanaman sawit (Descals *et al.* 2019), dan deteksi penebangan-habis hutan (Johansen *et al*. 2015).

Klasifikasi tutupan lahan pada kajian ini dibagi menjadi empat kelas, yaitu sawah, urban (pemukiman, lahan terbangun, jalan dan atau wilayah perkotaan), vegetasi lain, dan air (sungai, kolam, empang, rawa, tambak). Kerangka kerja penelitian diberikan pada Gambar 3.

Data untuk Klasifikasi

Studi ini memanfaatkan data katalog dari Sentinel-2A dan B melalui aplikasi GEE. Data yang digunakan merupakan data Sentinel-2A Bottom of Atmosphere (BOA) yang sudah dilakukan *cloud treatment*. Sentinel-2 sangat baik digunakan untuk memantau, mengklasifikasi, atau mendeteksi perubahan ter-utama untuk kegiatan pertanian (Zhang *et al.* 2017; Van der Werff & Van der Meer 2016).

Citra satelit Sentinel-2 untuk mengklasifikasi lahan memanfaatkan data 13 pita yang ada pada citra tersebut (Tabel 1). Namun, dari 13 pita, kajian ini hanya memanfaatkan tiga jenis pita, yaitu NIR, *Red,* dan *Green*. Selain itu juga digunakan data beberapa indeks untuk mengklasifikasi tutupan lahan, yaitu menggunakan *Normalised Difference Vegetation Index* (NDVI), *Normalised Difference Water Index* (NDWI), dan *Soil Adjusted Vegetation Index* (SAVI). Data pita ini dimaksudkan untuk menghasilkan data tambahan (Tabel 2). Sejumlah persamaan digunakan untuk menghasilkan data tambahan yang digunakan pada tahap klasifikasi citra. Lapisan pada Tabel 2 ditumpang-susun bersama dengan pita Sentinel-2 (Tabel 1) untuk digunakan dalam proses klasifikasi. Lapisan tambahan ini mampu mengekstraksi informasi tertentu dengan cara yang lebih efisien.



Gambar 3 Kerangka kerja penelitian.

Sampel

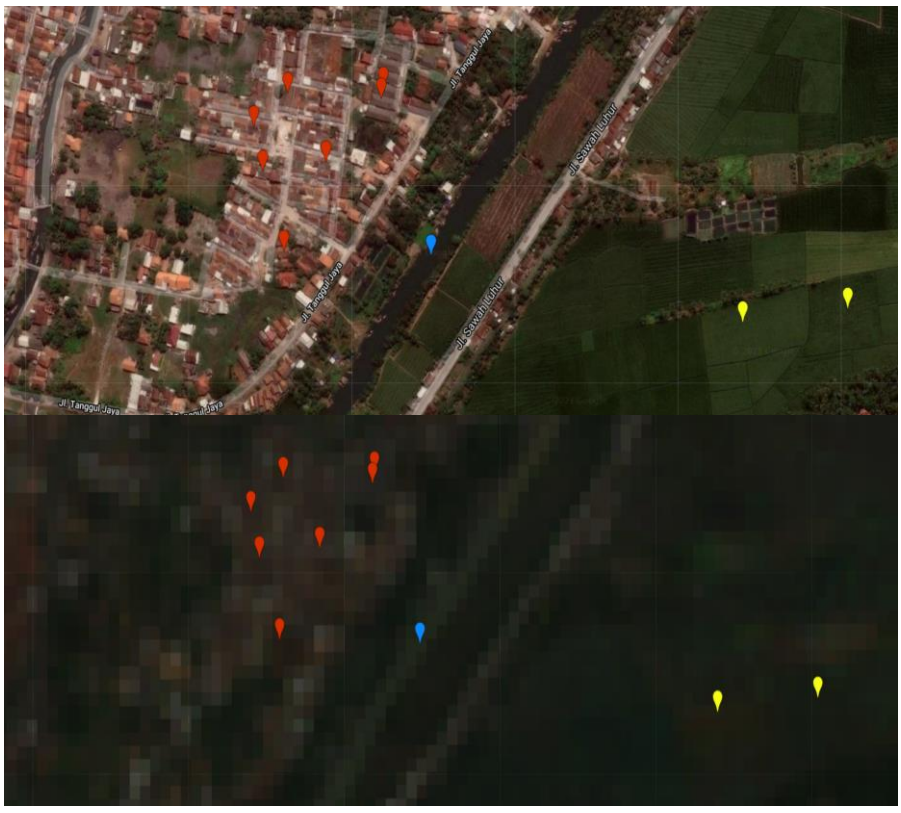
Sampel dibuat pada platform GEE dengan total 4 kelas diidentifikasi: sawah, urban, vegetasi lain, dan air. Sampel dibuat menggunakan format poin yang tersebar di wilayah administrasi Kota Serang, dengan bantuan peta RBI dari Badan Informasi Geospasial guna menentukan batas lokasi penelitian dan citra Google Earth resolusi tinggi dibandingkan dengan citra Sentinel-2 seperti yang ditunjukkan pada Gambar 4. Sampel kemudian dibagi menjadi dua komponen: pelatihan (*training*) dan validasi. *Training* terdiri atas 70% dari semua sampel yang dibuat (510 titik), yang terdiri atas sawah (200 titik), urban (200 titik), vegetasi lain (60 titik), dan air (50 titik), yang digunakan untuk mengklasifikasikan citra Sentinel 2-A. Sementara validasi merupakan 30% dari semua sampel (153 buah poligon), yang terdiri atas sawah (60 buah), urban (60 buah), vegetasi lain (20 buah), dan air (15 buah) untuk divalidasi dan dinilai akurasinya menggunakan RF. Semua sampel ini menjadi hiperparameter yang dipakai oleh mesin pembelajaran dalam pengklasifikasian. Hiperparameter adalah parameter yang nilainya mengendalikan proses pembelajaran dan menen-tukan nilai parameter model yang akhirnya dipelajari oleh algoritma pembelajaran. Awalan *'hiper_*' menunjukkan parameter 'tingkat atas' yang

Tabel 1 Informasi Pita pada Sentinel- 2

Nama pita	Deskripsi	Ukuran piksel (m)	Panjang gelombang (nm)
Pita 1	Aerosols	60	443,9 nm (S2A)/442,3 nm (S2B)
Pita 2	Blue	10	496,6 nm (S2A)/492,1 nm (S2B)
Pita 3	Green	10	560 nm (S2A)/559 nm (S2B)
Pita 4	Red	10	664,5 nm (S2A)/665 nm (S2B)
Pita 5	Red Edge 1	20	703,9 nm (S2A)/703,8 nm (S2B)
Pita 6	Red Edge 2	20	740,2 nm (S2A)/739,1 nm (S2B)
Pita 7	Red Edge 3	20	782,5 nm (S2A)/779,7 nm (S2B)
Pita 8	NIR	10	835,1 nm (S2A)/833 nm (S2B)
Pita 8A	Red Edge 4	20	864,8 nm (S2A)/864 nm (S2B)
Pita 9	Water vapor	60	945 nm (S2A)/943,2 nm (S2B)
Pita 11	SWIR 1	20	1613,7 nm (S2A)/1610,4 nm (S2B)
Pita 12	SWIR 2	20	2202,4 nm (S2A)/2185,7 nm (S2B)

Tabel 2 Lapisan tambahan yang digunakan untuk klasifikasi tutupan lahan

Lapisan	Rumus	Sumber
NDVI	$NDVI = \frac{NIR - Red}{NIR + Red}$	(Piragnolo *et al.* 2018)
NDWI	$NDWI = \frac{Green - NIR}{Green + NIR}$	
SAVI	$SAVI = \frac{NIR - Red}{NIR + Red + 0.5} * (0.5 + 1)$	



Gambar 4 (a) Citra satelit Google Earth resolusi tinggi, (b) Citra satelit Sentinel-2: titik kuning menunjukkan sampe sawah, titik merah menunjukkan sampel urban (terbangun), dan titik biru menunjukkan sampel air.

mengendalikan proses pembelajaran dan parameter model yang dihasilkannya. Klasifikasi dan validasi dilakukan pada aplikasi GEE dan penilaian akurasi dihitung menggunakan metode matriks konfusi.

Uji Akurasi

Pengujian akurasi bertujuan menilai galat klasifikasi sehingga dapat diketahui persentase ketepatannya (akurasi). Akurasi hasil klasifikasi diuji dengan cara membuat matriks kontingensi yang sering disebut dengan matriks galat *(error matrix*) atau matriks konfusi (*confusion matrix*). Matriks ini dihitung menggunakan fungsi matriks konfusi pada pengkodean di GEE. Dari matriks ini, akurasi suatu klasifikasi dapat dihitung dari akurasi keseluruhan (*overall accuracy*), pembuat akurasi (*producer's accuracy*), akurasi pengguna (*user's accuracy*), dan akurasi kappa (*kappa accuracy*) (Tabel 3). Semakin tinggi nilai akurasinya semakin tinggi pula tingkat kebenaran citra hasil klasifikasi. Pedoman pengolahan data satelit multispektral secara *digital supervised* untuk klasifikasi menetapkan akurasi klasifikasi tutupan lahan adalah rata-rata di atas 75% (LAPAN 2015).

Tingkat akurasi suatu klasifikasi dapat dinilai dari akurasi keseluruhan, pembuat akurasi, dan akurasi pengguna. Menurut (Jensen 2015) untuk mencari nilai ketiga-tiganya digunakan formula sebagai berikut:

Akurasi keseluruhan (OA) merupakan jumlah nilai akurasi keseluruhan dari klasifikasi, yang merupakan perbandingan jumlah total area (piksel) yang diklasifikasikan dengan benar terhadap total area (piksel) observasi; ini menunjukkan tingkat kebenaran citra hasil klasifikasi:

$$\text{Akurasi keseluruhan} = D/N \times 100\% \quad .....(1)$$

Keterangan:
D = Total nilai baris yang benar yang telah ditambah secara diagonal
N = Total nilai yang benar di dalam matriks galat

Nilai akurasi pembuat (PA) menunjukkan persentase peluang rata-rata suatu piksel akan diklasifikasikan dengan benar dan secara rata-rata menunjukkan seberapa baik setiap kelas di lapangan telah diklasifikasi. Semakin tinggi nilai PA semakin tinggi pula piksel dari kelas tersebut tidak masuk ke kelas yang lain:

$$\text{Akurasi pembuat} = x_{ii} / x_{+i} \times 100\% \quad .....(2)$$

Keterangan:
x_{ii} = Total nilai sel yang benar di dalam kelas
x_{+i} = Jumlah nilai sel di dalam baris

Nilai Akurasi Pengguna (UA) mengindikasikan persentase peluang rata-rata suatu piksel dari citra yang telah terklasifikasi secara aktual mewakili kelas-kelas tersebut di lapangan. Apabila semua kelas mempunyai nilai akurasi pengguna 100%, ini menunjukkan bahwa pada kelas-kelas tersebut tidak terjadi galat klasifikasi dengan tidak mengambil piksel dari kelas lain:

$$\text{Akurasi pengguna} = x_{ii}/x_{i+} \times 100\% \quad ....(3)$$

Keterangan:
x_{ii} = Total nilai sel yang benar di dalam kelas
x_{i+} = Jumlah nilai sel di dalam baris

HASIL DAN PEMBAHASAN

Klasifikasi Tutupan Lahan

Dalam kajian ini tutupan lahan kota Serang berhasil dibagi menjadi 4 kelas yaitu sawah, urban, vegetasi lain, dan air. Namun, tujuan utama kajian ini ialah untuk mendeteksi perubahan sebaran lahan yang digunakan untuk padi sawah yang ada di Kota Serang pada tahun 2019 dan tahun 2021. Kelas lahan sawah mengklasifikasikan tutupan lahan yang selalu atau sering digunakan untuk budi daya padi sawah. Kelas urban mengklasifikasikan tutupan lahan berupa bangunan, perumahan, jalan, dan lahan non-pertanian. Adapun kelas vegetasi lain mengklasifikasikan tutupan lahan berupa vegetasi lain selain padi berupa vegetasi besar seperti pohon atau wilayah dapat berupa kebun atau hutan yang terdapat banyak pohon. Kelas air merupakan tutupan lahan yang diklasifikasikan sebagai air seperti kolam/empang, sungai, atau tambak. Seperti diketahui, Kota Serang berbatasan langsung dengan Laut Jawa; masyarakat di sekitar pantai utara banyak membudidayakan ikan pada tambak. Hasil klasifikasi tutupan lahan yang dihasilkan oleh GEE ditunjukkan pada Tabel 4 dan Gambar 5.

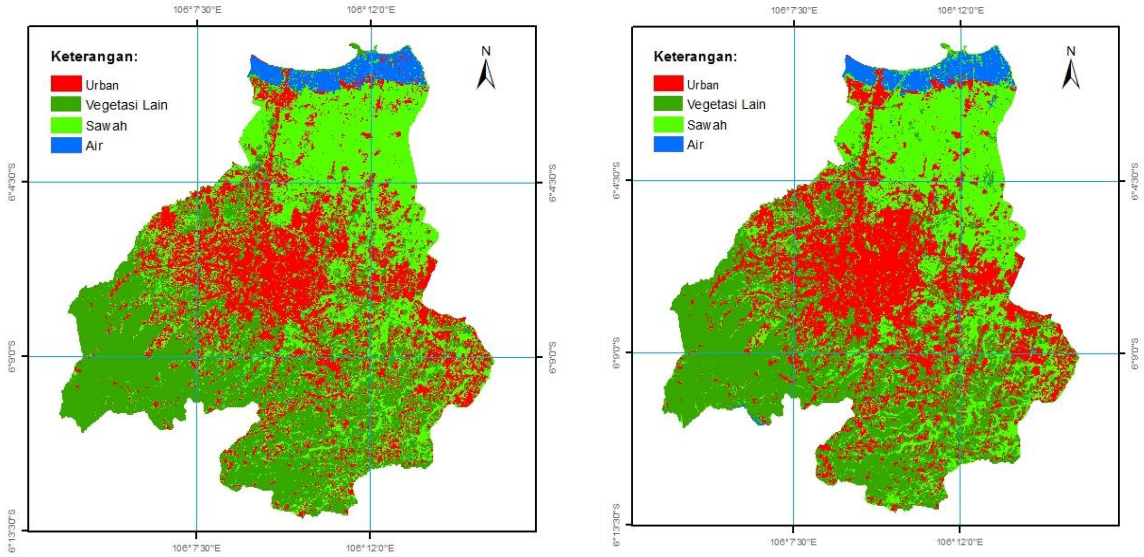
Hasil klasifikasi tutupan lahan menggunakan data Sentinel-2A pada aplikasi GEE menunjukkan bahwa tutupan lahan di Kota Serang didominasi oleh kelas vegetasi lain 9.899,39 ha (37,65%) pada tahun 2019 dan seluas 9.657,22 ha (36,73%) pada tahun 2021.

Tabel 3 Hasil uji akurasi klasifikasi tutupan lahan di Kota Serang

Uraian	Tahun 2019			Tahun 2021		
	Akurasi Pembuat (%)	Akurasi Pengguna (%)	Akurasi Keseluruhan (%)	Akurasi Pembuat (%)	Akurasi Pengguna (%)	Akurasi Keseluruhan
Urban	93,36	94,69	96,56	98,39	91,40	95,59
Vegetasi Lain	100,00	99,60		99,73	97,23	
Sawah	94,88	93,68		88,30	96,79	
Air	96,41	98,17		92,81	98,10	

Tabel 4 Luas tutupan lahan berdasarkan klasifikasi di Kota Serang

Kelas	Tahun 2019		Tahun 2021		Selisih	
	Luas (ha)	%	Luas (ha)	%	Luas (ha)	%
Urban	7.180,63	27,31	7.962,45	30,28	781,82	10,89
Vegetasi Lain	9.899,39	37,65	9.657,22	36,73	–242,17	–2,45
Sawah	8.376,36	31,86	7.773,49	29,56	–602,87	–7,20
Air	838,34	3,19	901,56	3,43	63,22	7,54
Total	26.294,72	100,00	26.294,72	100,00		



Gambar 5 Hasil klasifikasi tutupan lahan oleh *Google Earth Engine* (GEE) di Kota Serang (a) tahun 2019 dan (b) tahun 2021.

Vegetasi lain ini dapat berupa tanaman atau pohon di hutan dan atau di kebun, semak, dan lainnya selain tanaman padi. Tutupan lahan kedua didominasi oleh sawah seluas 8.376,36 ha (31,86%) pada tahun 2019, tetapi pada tahun 2021 urutan kedua didominasi oleh kelas urban 7.962,45 ha (30,28%). Data ini memperlihatkan perubahan alih fungsi lahan sawah ke sektor lain berupa kelas urban. Tutupan lahan ketiga, pada tahun 2019 didominasi oleh kelas urban 7.189,63 ha (27,31%), sementara pada tahun 2021 didominasi oleh kelas sawah 7.773,49 ha (29,56%). Tutupan lahan keempat, pada tahun 2019 dan 2021 sama-sama didominasi oleh tutupan lahan berupa kelas air, berturut-turut 838,34 ha (3,19%) dan 901,56 ha (3,43%) dari total tutupan lahan (Gambar 6).

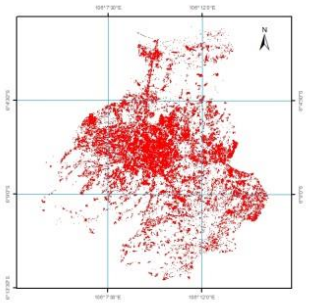
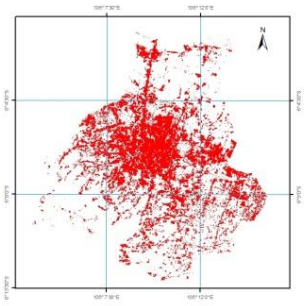
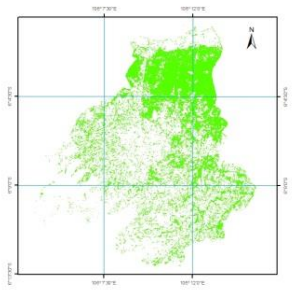
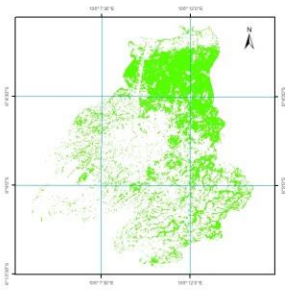
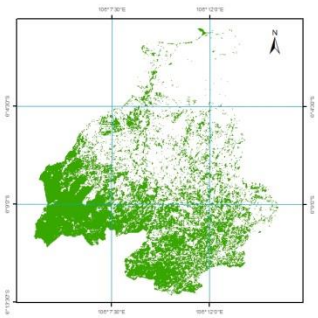
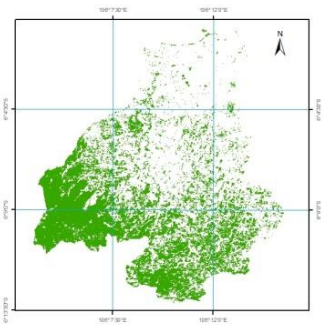
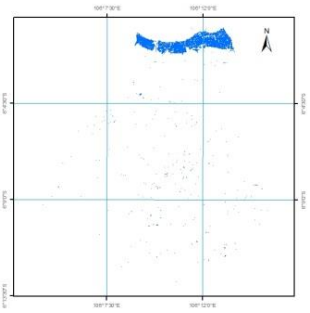
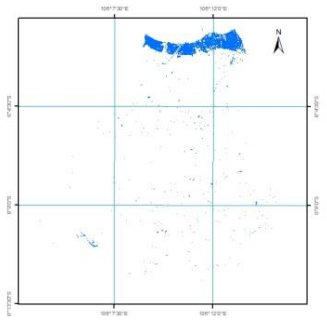
Hasil Uji Akurasi

Tingkat akurasi klasifikasi dan pemetaan lahan sawah menggunakan GEE dapat dinilai dari nilai akurasi keseluruhan, akurasi pembuat, dan akurasi pengguna yang dihasilkan dari matriks konfusi pada aplikasi GEE (Tabel 4). Perhitungan matriks dan hasil analisis GEE menunjukkan akurasi keseluruhan dari citra yang diklasifikasikan ke dalam 4 kelas memiliki tingkat akurasi keseluruhan 96,56% (tahun 2019) dan 95,59% (tahun 2021). Nilai akurasi pembuat dan akurasi pengguna pada klasifikasi kajian ini pun menunjukkan akurasi yang baik, dengan nilai di atas 90% untuk semua kelas baik untuk tahun 2019, kecuali untuk kelas sawah sebesar 88,30% pada tahun 2021.

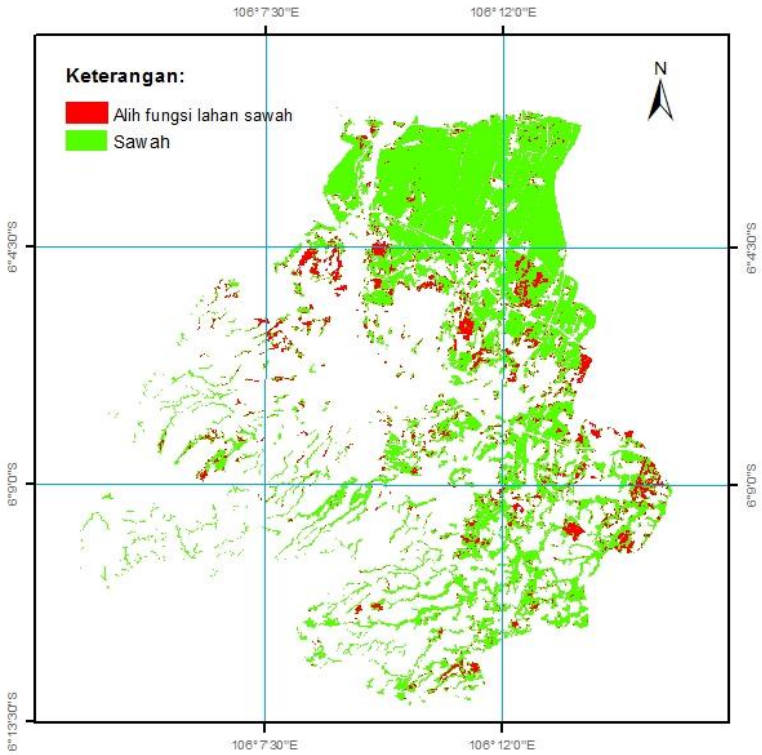
Estimasi Alih Fungsi Lahan Sawah

Hasil klasifikasi tutupan lahan menggunakan data Sentinel-2A pada aplikasi GEE (Tabel 4) juga menunjukkan bahwa tutupan lahan sawah menurun 7,20% (602,87 ha) pada tahun 2021 dibandingkan tahun 2019. Hal sama juga terjadi pada tutupan lahan untuk vegetasi lain, menurun 2,45% (242,17 ha). Penurunan ini diduga karena ekspansi dari tutupan lahan berupa kelas lain, yaitu urban dan atau tutupan lahan berupa air. Hal ini dibuktikan dengan meningkatnya tutupan lahan untuk kelas urban 10,89% (781,82 ha) pada tahun 2021 dibandingkan tahun 2019. Selain itu, tutupan lahan untuk kelas air juga meningkat 7,54% (63,22 ha).

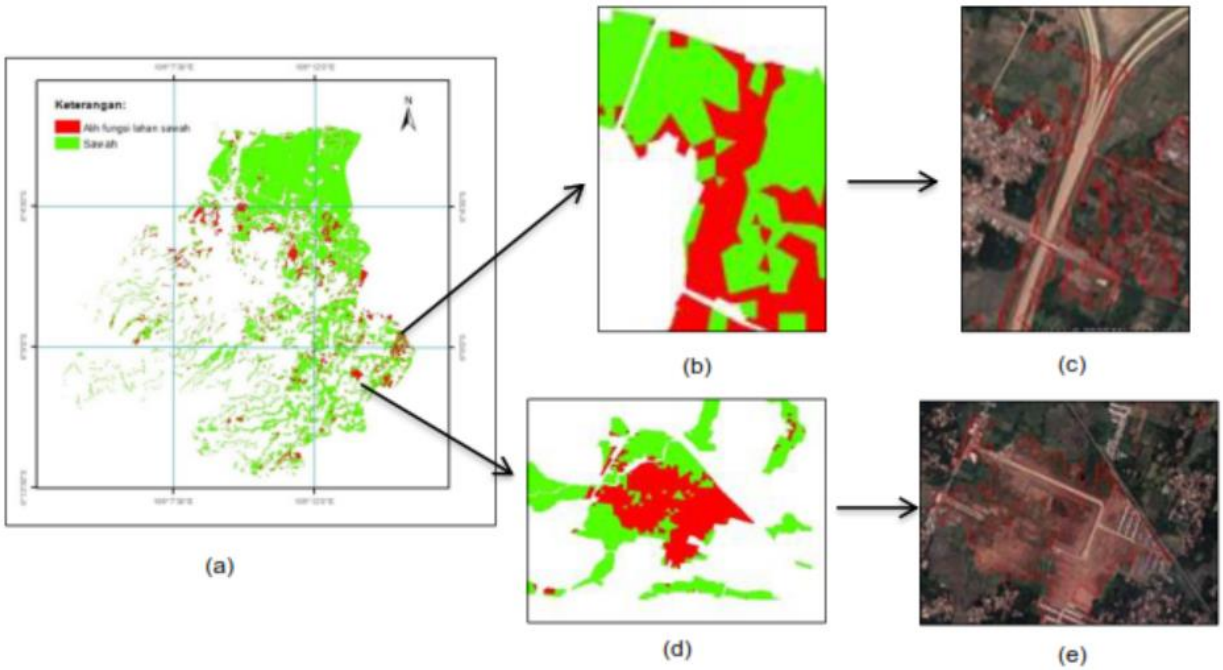
Berdasarkan kajian ini, lokasi atau titik yang mengalami alih fungsi lahan sawah ke sektor lain dideteksi dengan menganalisis peta lebih lanjut. Peta dianalisis lebih lanjut dengan menumpang-susun peta hasil klasifikasi kelas urban dengan luas baku sawah dan citra satelit *Google Earth* yang beresolusi tinggi. Hasil estimasi ekspansi urban ke lahan sawah dapat dilihat pada peta estimasi alih fungsi lahan (Gambar 7). Ekspansi urban terjadi hampir di seluruh wilayah Kota Serang. Dengan membandingkan peta hasil estimasi alih fungsi lahan dengan citra satelit resolusi tinggi *Google Earth*, diduga beberapa jenis ekspansi perkotaan yang terjadi dapat berupa perumahan/pemukiman, jalan, dan lahan kosong

Tahun 2019	Tahun 2021
	
(a)	
	
(b)	
	
(c)	
	
(d)	

Gambar 6 Peta hasil klasifikasi citra Sentinel-2 menggunakan GEE pada tahun 2019 dan tahun 2021 (a) Peta tutupan lahan berupa urban area; (b) Peta tutupan lahan berupa sawah; (c) Peta tutupan lahan berupa vegetasi lain; (d) Peta tutupan lahan berupa air.



Gambar 7 Peta estimasi alih fungsi lahan sawah pada tahun 2021 dibandingkan tahun 2019.



Gambar 8 Deteksi alih fungsi lahan sawah sentinel-2 divalidasi dengan citra google earth (a) Peta estimasi alih fungsi lahan sawah; (b) titik diduga lokasi alih fungsi lahan sawah; (c) terjadi alih fungsi lahan sawah ke jalan dan lainnya; (d) titik diduga lokasi allih fungsi lahan sawah; (e) terjadi alih fungsi lahan sawah menjadi perumahan atau pemukiman

untuk kegiatan sektor lain. Kelebihan dari Sentinel-2 adalah resolusi yang tinggi sehingga memungkinkan lokasi dan bentuk perubahan lahan pertanian ke non-pertanian secara akurat dapat diketahui. Gambar 8 memperlihatkan hasil deteksi alih fungsi lahan sawah divalidasi dengan citra satelit *Google Earth* sehingga terlihat bahwa di Kota Serang terjadi perubahan lahan sawah ke perumahan atau pemukiman, jalan tol, dan sektor lain.

Peta hasil estimasi alih fungsi lahan sawah ini dapat dimanfaatkan oleh pemangku kepentingan untuk memantau dan mendeteksi dini ekspansi

perkotaan yang tidak teratur atau tidak sesuai dengan Rencana Tata Ruang Wilayah di Kota Serang. Perhatian ditujukan terutama berkaitan dengan alih fungsi lahan sawah, sebab sawah merupakan salah satu faktor utama dalam penyediaan pangan di Kota Serang.

KESIMPULAN

Pemanfaatan citra satelit Sentinel-2 menggunakan aplikasi *Google Earth Engine* dapat memetakan tutupan lahan sawah dan mendeteksi perubahan alih fungsi lahan sawah ke sektor lain. Kota Serang memiliki tutupan lahan berupa sawah seluas 29,56% (7.773,49 ha) dari total luas Kota Serang pada tahun 2021. Perubahan alih fungsi lahan terdeteksi mencapai 7,20% (602,87 ha) pada tahun 2021 dibandingkan tahun 2019. Alih fungsi lahan sawah ke sektor lain diakibatkan oleh ekspansi perkotaan berupa pembangunan perumahan atau pemukiman, jalan tol, serta perubahan ke sektor lainnya. Tutupan lahan menggunakan citra satelit Sentinel-2 dan aplikasi GEE dapat dipetakan dengan cepat dan cukup akurat, sebagaimana ditunjukkan dengan tingkat akurasi keseluruhan yang melebihi 90%. Informasi tutupan lahan berupa lahan sawah akan sangat bermanfaat bagi para pemangku kepentingan untuk menentukan kebijakan yang berkaitan dengan produksi pangan dan status ketahanan pangan di wilayahnya.

DAFTAR PUSTAKA

[BPS] Badan Pusat Statistik Banten. 2020. *Luas Lahan Menurut Penggunaanya Provinsi Banten Tahun 2020*. Serang (ID): BPS Provinsi Banten.

[BPS] Badan Pusat Statistik Banten. 2021. *Provinsi Banten Dalam Angka 2020*. Serang (ID): BPS Provinsi Banten.

[BPS] Badan Pusat Statistik Kota Serang. 2020. *Kota Serang Dalam Angka 2020*. Serang (ID): BPS Kota Serang.

Descals A, Szantoi Z, Meijaard E, Sutikno H, Rindanata G, Wich S. 2019. “Oil Palm (Elaeis Guineensis) Mapping with Details: Smallholder versus Industrial Plantations and Their Extent in Riau, Sumatra.” *Remote Sensing* 11(21). https://doi.org/10.3390/rs11212590

Gascon F, Thépaut O, Jung M, Francesconi B, Louis J, Lonjou V, Lafrance B, Massera S, Vacaresse AG, Languille F, Alhammoud B, Viallefont F, Pflug B, Vieniarz J, Clerc S, Pessiot L, Tremas T, Cadau E, Bonis RD, Isola C, Martimort P, Fernandez v. 2016. “Copernicus Sentinel-2 Calibration and Products Validation Status.” *Remote Sensing* 9(6): 1–81. https://doi.org/10.20944/preprints201610.0078.v1

Gorelick N, Hancher M, Dixon M, Ilyuschenko S, Thau D, Moore R. 2017. “*Google Earth Engine*: Planetary-Scale Geospatial Analysis for Everyone.” *Remote Sensing of Environment* 202: 18–27. https://doi.org/10.1016/j.rse.2017.06.031

Janah, R, B.T Eddy, and T Dalmiyatun. 2017. “Alih Fungsi Lahan Pertanian Dan Dampaknya Terhadap Kehidupan Penduduk Di Kecamatan Sayung Kabupaten Demak (Changes In Agricultural Land Use And Its Impacts On The Lives Of Farmers At Sayung Subdistrict, Demak Regency).” *Agrisocionomics* 1(1): 1–10. https://doi.org/10.14710/agrisocionomics.v1i1.1629

Jean N, Burke M, Xie M, Davis WM, Lobel DB, Ermon S. 2016. “Combining Satellite Imagery and Machine Learning to Predict Poverty.” *Science* 353(6301): 790–794. https://doi.org/10.1126/science.aaf7894

Jensen, John R. 2015. *Introductory Digital Image Processing: A Remote Sensing Perspective*. 4th editio. United State of America: Pearson. www.pearsonhighere.com.

Johansen, Kasper, Stuart Phinn, and Martin Taylor. 2015. “Mapping Woody Vegetation Clearing in Queensland, Australia from Landsat Imagery Using the *Google Earth Engine*.” *Remote Sensing Applications: Society and Environment* 1(October 2017): 36–49. https://doi.org/10.1016/j.rsase.2015.06.002

LAPAN. 2015. “Pedoman Pengolahan Data Satelit Multispektral Secara Digital Supervised Untuk Klasifikasi.” : 1–8. http://pusfatja.lapan.go.id/files_uploads_ebook/pedoman/000_Buku_Pedoman_Klasifikasi_final.pdf.

Martunisa, Prilly, and Trisna Insan Noor. 2018. “Faktor-Faktor Yang Memengaruhi Proses Alih Fungsi Lahan Padi Sawah Di Kelurahan Kersanegara, Kecamatan Cibeureum, Kota Tasikmalaya, Provinsi Jawa Barat.” *Jurnal Rekayasa Hijau*. 2(1). https://doi.org/10.26760/jrh.v2i1.2038

Miettinen, Jukka, David L.A. Gaveau, and Soo Chin Liew. 2019. “Comparison of Visual and Automated Oil Palm Mapping in Borneo.” *International Journal of Remote Sensing* 40(21): 8174–85. https://doi.org/10.1080/01431161.2018.1479799

Mutanga, Onisimo, and Lalit Kumar. 2019. “*Google Earth Engine* Applications.” *Remote Sensing* 11(591): 11–14. https://doi.org/10.3390/rs11050591

Nguyen, Luong B. 2020. “Land Cover Change Detection in Northwestern Vietnam Using Landsat Images and *Google Earth Engine*.” *Journal of Water and Land Development* 46(October): 162–69.

Piragnolo, M., G. Lusiani, and F. Pirotti. 2018. "Comparison of Vegetation Indices from RPAS and Sentinel-2 Imagery for Detecting Permanent Pastures." *International Archives of the Photogrammetry, Remote Sensing and Spatial Information Sciences - ISPRS Archives* 42(3): 1381–87. https://doi.org/10.5194/isprs-archives-XLII-3-1381-2018

Prasetyo, Arief. 2017. "Pola Spasial Penjalaran Perkotaan Bodetabek: Studi Aplikasi Model Shannon'S Entropy." *Jurnal Geografi Gea* 16(2): 144. https://doi.org/10.17509/gea.v16i2.2439

Ramadhani, Fadhlullah, Reddy Pullanagari, Gabor Kereszturi, and Jonathan Procter. 2020. "Automatic Mapping of Rice Growth Stages Using the Integration of Sentinel-2, Mod13q1, and Sentinel-1." *Remote Sensing* 12(21): 1–21. https://doi.org/10.3390/rs12213613

Ridwan, Ita Rustiati. 2016. "Faktor-Faktor Penyebab Dan Dampak Konversi Lahan Pertanian." *Jurnal Geografi Gea.* 9(2). https://doi.org/10.17509/gea.v9i2.2448

Shaharum N, Shafri H, Ghani W, Samsatli S, Al-Habshi M, Yusuf B. 2020. "Oil Palm Mapping over Peninsular Malaysia Using *Google Earth Engine* and Machine Learning Algorithms." *Remote Sensing Applications: Society and Environment* 17(January): 100287. https://doi.org/10.1016/j.rsase.2020.100287

Shelestov, Andrii, Mykola Lavreniuk, Nataliia Kussul, and Alexei Novikov. 2017. "Exploring *Google Earth Engine* Platform for Big Data Processing : Classification of Multi-Temporal Satellite Imagery for Crop Mapping." 5(February): 1–10. https://doi.org/10.3389/feart.2017.00017

DOI: 10.24114/jg.v12i02.16970
e-ISSN: 2549–7057 | p-ISSN: 2085–8167

APLIKASI CITRA SENTINEL-2 UNTUK PEMETAAN TUTUPAN DAN PERUNTUKAN LAHAN PADA TINGKAT DESA

Marga Mandala[1], Indarto Indarto*[1], Fery Febrian Arifin[2], Farid Lukman Hakim[2]
[1]Keris P-LSO (Pengembangan Lahan Sub-Optimal), Universitas Jember
[2]PS Teknik Pertanian, Fakultas Teknologi Pertanian, Universitas Jember
Jalan Kalimantan No 37, Kampus Bumi Tegalboto, Krajan Timur, Kecamatan Sumbersari, Kabupaten Jember, Jawa Timut, 68121, Indonesia
e-mail: indarto.ftp@unej.ac.id

Diterima: 05 Februari 2020, Direvisi: 18 Juni 2020, Disetujui: 22 Juni 2020

Abstrak

Sentinel-2 menjanjikan citra yang gratis, pada ketelitian spasial sedang dan ketelitian spektral tinggi. Data citra ini mungkin dapat digunakan sebagai dasar pemetaan tutupan lahan (land cover) dan pruntukan lahan (land use) sampai dengan level Desa. Artikel ini bertujuan untuk membandingkan dan mengevaluasi peta tematik yang dihasilkan dari: (1) Klasifikasi dari citra Sentinel-2A, (b) digitasi manual dari Google Earth Image, (c) dan peta RBI (Rupa Bumi Indonesia). Citra Sentinel-2A, citra google earth dan peta RBI digital digunakan sebagai input utama. Pengolahan citra Sentinel-2A mencakup: atmosferic correction, image composite, klasifikasi terbimbing, koleksi training area, dan uji-akurasi. Selanjutnya, ke tiga jenis peta tematik yang dihasilkan digunakan untuk membandingkan luasan per jenis tutupan lahan yang dipetakan dan interpretasi perubahan peruntukan lahan yang terjadi. Selanjutnya, wilayah empat desa digunakan sebagai sampel pengukuran. Penelitian menghasilkan peta tematik tutupan dan peruntukan lahan pada level Desa. Perbandingan peta tematik menunjukkan bahwa citra Sentinel mampu untuk menangkap fitur tutupan lahan yang utama (yaitu: Lahan-sub-optimal kering, lahan irigasi, lahan non-irigasi, area terbangun, hutan-perkebunan, dan badan air) pada level desa. Lebih lanjut peta yang dihasilkan dari citra Sentinel dapat digunakan untuk memperbaharui, perencanaan dan evaluasi kegiatan pembangunan di Desa.

Kata Kunci: *Sentinel-2A, Pemetaan, Tutupan Lahan, peruntukan lahan, desa.*

Abstract

Sentinel-2 provide a free of cost imagery in medium spatial and high spectral resolutions. These data promise a rapid, low-cost and easy to apply imagery for the end-user. These free data may produce a rationale thematic land cover and land use (LCLU) map at the village level. This paper aims to compare and to evaluate the thematics maps created by (a) Sentinel-2, (b) digitalisation from Google Earth and (c) RBI (Rupa Bumi Indonesia) Digital Map. Sentinel-2 image, google earth image, and RBI digital map used as the primary input. The treatment of sentinel 2A imagery consists of atmospheric correction, image composite, supervised classification, collecting training areas, and accuracy assessment. The three types of maps use to compare area extent mapped for each type of land cover (LC), and the interpretation of land-use change occurred. Four villages used as samples of measurement. The research produces thematic LCLU maps at the village level. Comparison of maps shows that Sentinel capable of capturing major LC (i.e., Dry-marginal land, non-irrigated area, irrigated area, pavement areas, forest - plantation, and water

DOI: 10.24114/jg.v12i02.16970
e-ISSN: 2549–7057 | p-ISSN: 2085–8167

body) at the village level. Moreover, Sentinel-2A produce more detail of land cover type. Finally, the maps derived from Sentinel data provide data for up-dating, planning and evaluation of village development.

Keywords : *Sentinel-2A, mapping, land cover, land use, village.*

PENDAHULUAN

Pada tulisan ini definisi tutupan lahan atau *Land cover (LC)* dan peruntukan lahan atau *Land use (LU)* mengacu pada publikasi oleh EUROSTAT (2001) sebagai berikut : tutupan lahan (LC) menyatakan deskripsi fisik dari suatu ruang di permukaan bumi kita dan dengan deskripsi ini memungkinkan berbagai macam kategori sifat bio-fisik dapat dibedakan. Pengamatan tutupan lahan dapat dilakukan melalui berbagai metode, mencakup: pengamatan langsung, fotografi udara dan sensor satelit.

Peruntukan lahan atau *land use (LU)* mengacu pada dimensi fungsi dari suatu luasan terkait dengan tujuan ekonomi (misal: luasan untuk pemukiman, industri, pusat komersial, pertanian atau hutan, tempat rekreasi atau konservasi alam (EUROSTAT, 2001). Selanjutnya, (Parece and Campbell, 2015) mengadopsi definisi yang sama dan menyatakan bahwa pada prakteknya istilah tutupan-lahan *(LC)* dan peruntukan-lahan *(LU)* dapat saling dipertukarkan. Citra satelit menawarkan alternatif solusi untuk berbagai malasah terkait dengan perubahan *LCLU* dan dampaknya terhadap masyarakat dan lingkungan.

Ketersedian data citra yang gratis dengan ketelitian spasial sedang dan ketelitian spektral tinggi, seperti citra satelit Sentinel-2, menawarkan metode pemetaan yang cepat, murah dan mudah untuk diterapkan. Peta tematik yang dihasilkan dari citra Sentinel-2 dapat menyediakan informasi yang lebih terbaharui. Informasi tersebut selanjutnya dapat digunakan sebagai dasar perencanaan dan aplikasi peta lainya.

Sentinel-2 merupakan salah satu satelit penginderaan jauh dengan sensor pasif. Sentinel-2 memiliki 13-band spektral yaitu band 2,3,4 dan 8 dengan ketelitian spasial 10 m, band 5,6,7, 8a, 11 dan 12 mempunyai ketelitian spasial 20 m dan band 1, 9, dan 10 memiliki ketelitian spasial 60 m (Esa, 2013). Citra sentinel-2 banyak digunakan untuk identifikasi dan analisis permasalahan terkait dengan lingkungan, perencanaan perkotaan, deteksi perubahan tutupan lahan, pemetaan resiko bencana dan beragam aplikasi lainnya (Clerici, Valbuena Calderón & Posada, 2017; Tavares *et al.*, 2019; Lopes *et al.*, 2020).

Peta tematik *LCLU* dapat dihasilkan dari peta konvensional yang ada atau diturunkan melalui citra satelit. Ke dua jenis peta tersebut dapat digunakan untuk mempelajari *LCLU* dan perubahannya, seperti pada penelitian yang dilakukan oleh (Eremiasova & Skokanova 2009) dan (Ptak & Ławniczak, 2012).

Selanjutnya Lambin *et al.* (2001); Martínez & Mollicone (2012); Efroymson *et al.* (2016); dan Song *et al.* (2018) memberi contoh bagaimana eksplorasi lebih lanjut hubungan sebab-akibat antara perubahan *LCLU* dan kosenkuensinya terhadap masyarakat dan lingkungan. Pada kasus yang lain, beberapa penelitian mencoba mengintegrasikan berbagai macam data citra melalui teknik fusi citra *(image fusion)* untuk mempelajari fenomena *LCLU* dengan lebih komprehensif (Moran, 2010; Li, Lu, Moran, Dutra, & Batistella, 2012; Wężyk, Hawryło, Szostak, Pierzchalski, & Kok, 2016; Tavares *et al.*, 2019).

Penggunaan citra Sentinel-2A untuk interpretasi *LCLU*, perubahan dan konsekuensinya telah menjadi subjek penelitian yang cukup populer pada 5 tahun terakhir. Beberapa contoh aplikasi citra Sentinel-2A untuk identifikasi dan pemetaan pada bidang terkait dengan

DOI: 10.24114/jg.v12i02.16970
e-ISSN: 2549–7057 | p-ISSN: 2085–8167

pertanian, misalnya dijumpai dalam tulisan (Rujoiu-Mare *et al.*, 2017; Tavares *et al.*, 2019 ; Abdi, 2019). Penelitian tersebut menunjukkan potensi aplikasi citra sentinel-2A untuk pemetaan *LCLU* dan fenomena terkait.

Interval waktu pemotretan dengan frekuensi yang cukup tinggi, yang ditawarkan oleh Landsat-8 (Operational Land Imager) dan citra Sentinel 2A atau 2B MSI (*Multi Spekctral imaging*) memberikan peluang baru untuk memetakan dan mengidentifikasi karakteristik dinamika perubahan permu-kaan bumi kita dari waktu ke waktu dengan mengkombinasikan ke dua citra tersebut (Bolton *et al.*, 2020). Memetakan menggunakan citra satelit pada prinsipnya adalah mengklasifikasikan piksel menjadi sekelompok piksel berdasar-kan logika tertentu, sehingga objek atau fitur yang ada di alam dapat digambarkan semirip mungkin. Hal ini dapat dilakukan dengan berbagai metode, misalnya: klasifikasi, segmentasi, *machine-learning* atau algoritma yang lain.

Metode klasifikasi sudah sangat umum digunakan. Khorram *et al.*, (2013) menyatakan bahwa kebanyakan metode klasifikasi citra didasarkan pada "*hard-logic*", menggunakan baik infomasi spektral dan pola temporal-spasial. Klasifikasi berbasis "*hard-logic*" ini secara umum dibedakan menjadi dua, yaitu klasifikasi terbimbing *(supervised classification)* dan klasifikasi tidak terbimbing *(un-supervised classification)*.

Secara prinsip ke dua jenis teknik klasifi-kasi tersebut dapat menggunakan berbagai macam algoritma yang ada. Pada klasifikasi terbimbing, titik kritis metode ada pada jenis dan jumlah training area yang digunakan untuk proses klasifikasi. Kombinasi kanal yang dipilih juga akan menentukan hasil klasifikasi (Richards, 2013).

Klasifikasi tidak terbimbing dapat menggunakan berbagai algoritma pengelom-pokan *(clustering-algorithm)*. Klasifikasi tidak terbimbing menggabungkan piksel hanya berdasarkan kemiripan karaktertisik piksel dan dilambangkan oleh nilai digital (DN value)(Richards, 2013). Lebih lanjut, Khorram *et al.* (2013) menyatakan bahwa algoritma yang paling umum digunakan pada proses klasifikasi terbimbing adalah *Maximum Likelihood Classification (MLC).*

Ketelitian hasil klasifikasi dapat diukur dengan berbagai metode (Foody, 2002, 2004). Metode yang paling umum digunakan untuk mengukur ketelitian hasil kaslifikasi adalah matrik kesalahan atau *confusion-matrix* (Foody, 2004). Konsep matrik kesalahan umumnya telah ditulis pada buku teks tentang penginderaan jauh (Lillesand, Kiefer & Chipman, 2008; Campbell & Wynne, 2011).

Ada perbedaan tingkat penerimaan dari hasil matrik kesalahan. USGS, (2019) menyatakan minimal 85% tingkat kesalahan cukup untuk menyatakan hasil klasifikasi yang baik. Sementara, LAPAN (2015) mensyaratkan tingkat ketelitian lebih dari 75% untuk menyatakan bahwa hasil klasifikasi memadai. Selanjutnya Foody (2008) merekomendasikan tingkat ketelitian 89% ± 5% interval konfidensi untuk menyatakan hasil klasifikasi yang baik.

Di Indonesia, sumber utama untuk interpretasi *LCLU* pada wilayah pedesaan adalah Peta Rupa bumi Indonesia (RBI). Peta ini dapat didownload secara gratis untuk semua wilayah NKRI, melalui laman resmi portal BIG. Peta RBI dapat didownload dalam format raster (*.Jpeg) dari hasil scan lembar peta atau dalam format shapefile (*.shp) (format vektor)(BIG, 2019).

Pada kebanyakan wilayah pedesaan di Indonesia, peta RBI yang tersedia adalah peta RBI produksi tahun 1999 sd 2001. Artinya peta RBI yang ada menggambarkan tutupan dan peruntukan lahan wilayah pada sekitar tahun 2000 (atau 20 tahun yang lalu). Dan pada kebanyakan wilayah peta RBI yang ada masih belum terbaharui. Tetapi pada kenyataannya, peta RBI juga masih digunakan sebagai dasar kajian dan

DOI: 10.24114/jg.v12i02.16970
e-ISSN: 2549–7057 | p-ISSN: 2085–8167

interpretasi (Riadi & Makmuriyanto, 2014; Susetyo, 2015).

Pada beberapa kasus peta RBI masih dapat dan layak digunakan. Pada kasus dimana fenomena yang akan dibahas adalah masalah terkait kekinian, peta detail perkotaan, maka peta RBI perlu diperbaharui dengan interpretasi citra satelit yang memiliki ketelitian spasial tinggi, hasil survei, foto udara atau drone (Hakim, Riqqi & Harto, 2014; Riadi & Rachma, 2017; Sudarman, Sadikin & Prijatna, 2020).

Salah satu cara sederhana membuat peta adalah dengan digitasi manual dari peta Google Earth. Namun demikian, proses digitasi manual tidak disarankan untuk wilayah yang luas, karena beresiko pada banyak-nya kesalahan digitasi yang mungkin dilakukan, disamping proses lebih lama, hasil kurang teliti dan biaya mahal. Alternatif lain adalah menggunakan Citra satelit resolusi tinggi, *Unmanned Aerial Vehicle (UAV)* atau drone. Drone sangat bagus untuk digunakan pada wilayah yang relatif sempit dan membutuhkan ketelitian yang cukup tinggi. Namun demikian, penggunaan citra resolusi tinggi dan drone untuk pemetaan wilayah yang luas, akan membutuhkan banyak biaya, proses rendering, penggabungan *(mozaick)* dan interpretasi menjadi lebih lama, dan membutuhkan teknologi hardware dan software dengan kapasitas memadai.

Ketersediaan data citra Sentinel yang gratis dan mencakup setiap wilayah di permukaan bumi kita, menjanjikan alternatif solusi bagi proses pemetaan yang cukup akurat, biaya murah, dan mudah diterapkan.

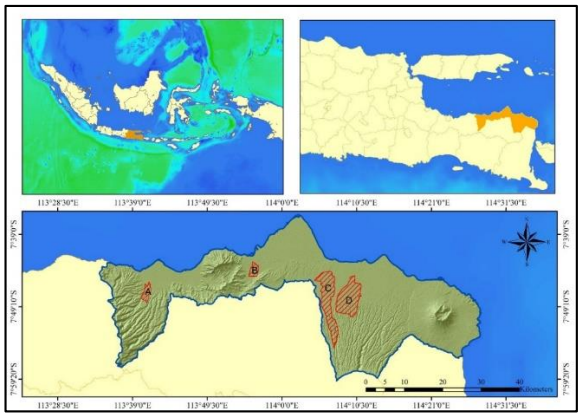
Penelitian ini bertujuan untuk: (1) menghasilkan peta tematik *LCLU* dari interpretasi Sentinel, (2) membandingkan peta tematik yang dihasilkan dari interpretasi citra sentinel, digitasi manual dan peta RBI, (3) menginterpretasikan peta tutupan dan peruntukan lahan pada level desa. Desa merupakan wilayah administrasi paling kecil. Perencanaan wilayah, perubahan *LCLU* dan aspek pembangunan lainnya dimulai dari level Desa, sehingga pemetaan status dan perubahan *LCLU* pada level desa sangat pentin untuk dilakukan. Apa jenis LCLU utama pada level desa yang dapat dideteksi melaluai Sentinel? Apakah hasil pemetaan rasional dan dapat dibandingkan dengan RBI, dan dengan digitasi manual.

METODE PENELITIAN

Lokasi Penelitian

Kabupaten Situbondo (Gambar 1) terletak di bagian timur wilayah Jawa Timur memiliki luas wilayah total = 1651,33 km^2. Jumlah penduduk per Kabupaten = 691622 orang. Kepadatan populasi = 422 per km^2 dan pertumbuhan penduduk tahunan dihitung selama periode 2018–2019 is 0,46 (%)(BPS, 2019).

Wilayah kabupaten situbondo relatif kering dibanding wilayah lain di Jawa Timur. Hujan tahunan rerata berkisar antara 500 sd 1500 mm/tahun. Umumnya di Jawa timur hujan tahunan berkisar antara 1000 sd 3500 mm/tahun. Bulan kering (hujan < 100mm/bln) , lamanya antara 7 sd 9 bulan per tahun. Penelitian ini dilaksanakan antara bulan Maret sampai November 2019.



Gambar 1. Lokasi Penelitian

Alat dan Bahan

1. Perangkat lunak *multispec Versi* 9 (Landgrebe, 2005) digunakan untuk klasifikasi dan interpretasi citra sentinel-2A.

DOI: 10.24114/jg.v12i02.16970
e-ISSN: 2549–7057 | p-ISSN: 2085–8167

2. Q-GIS 3.2.0 diunduh dari website https://qgis.org (QGIS Development Team, 2019) dan digunakan untuk *reclass dan koreksi atmosferik.*
4. GPS digunakan untuk mengambil titik GCP *(Ground check point)* dan *Google earth* image (digunakan untuk melihat kecocokan keadaan yang ada dilapang.
5. Camera untuk mengambil gambar GCp.

Input Data

1. Input utama pada penelitin ini adalah citra Sentinel-2A yang mencakup seluas wilayah Kabupaten Situbondo. Citra diunduh dengan kriteria penutupan awan *(cloud coverage)* yang paling minimal. Citra didownload dari web site USGS (USGS, 2019). Karena fokus penelitian ini adalah pemetaan jenis *LCLU* maka citra yang paling baik untuk diunduh adalah citra dengan tutupan awan yang minimal. Dua scene citra dari tanggal 25 bulan Juni 2019 diunduh dan digabung.

Tabel 1. *Raw image metadata*

Cloud cover(%)	Data type	orbit
0,0179	S2A_MSIL1C	Descending
0,1016	S2A_MSIL1C	Descending

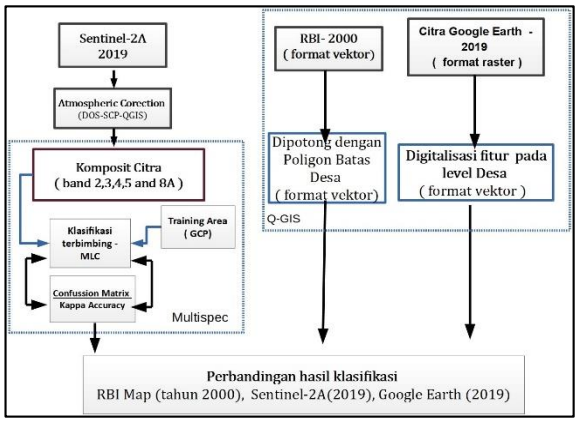
Sumber: Pemrosesan Data, 2019

2. Peta RBI diunduh dari laman resmi website BIG (BIG, 2019). Peta RBI skala 1:25000 (skala sedang) diunduh seluas wilayah Kab. Situbondo. Peta RBI selanjutnya di potong seluas wilayah 4 desa sebagai sampel evaluasi.
3. Google Earth image diunduh hanya seluas 4 wilayah desa yang dijadikan sample. Baik RBI maupun google erath image dignakan sebagai pembanding dapam penelitian ini.

Prosedur Pemrosesan Data

Gambar (2) menampilkan prosedur penelitian. Blok kiri merinci urutan langkah pengolahan citra sentinel-2A, yang mencakup: koreksi atmosferik *(atmospheric correction),* komposit citra, klasifikasi terbimbing, survey lapang, dan *accuracy assessment*.

Koreksi atmospheric menggunakan algo-ritma DOS *(Dark Object Sub-traction)* yang ada pada tool SCP *(semi automatic plugin)* dan mengikuti prosedur yang telah dipubikasi oleh (Congedo, 2016). Koreksi atmosferik dilakukan menggunakan QGIS. Citra Sentinel-2A yang tersedia adalah Level-1C artinya telah terkoreksi secara geometrik. Komposit citra dibuat dengan kombinasi 5 kanal yaitu (kanal 2,3,4,5 dan 8A).



Gambar 2. Prosedur Pemrosesan Data

Beberapa kali kegiatan survey lapang dilakukan antar bulan Mei sd November 2019 untuk mengoleksi GCP dan memotret wilayah kajian. Sejumlah 771 GCP dibuat untuk membantu proses klasifikasi terbimbing (Tabel 2).

Tabel 2. Ringkasan GCP

LCLU class	Jumlah GCP	Luas ukuran GCP (ha)		
		Total	Min	Mak
Water body	40	553,9	1,23	54,3
Forest-plantation	184	12.366,5	1,78	209
DryMAL	165	4.280,2	1,21	93,5
Non-Irrigated	92	2.169,5	1,40	46,8
Built- up area	140	3.425,6	2,38	56,7
Irrigated paddy field	150	3.222,6	1,14	56,8
Total	771	26.018,3		

Sumber: Pemrosesan Data, 2019

DOI: 10.24114/jg.v12i02.16970
e-ISSN: 2549–7057 | p-ISSN: 2085–8167

Klasifikasi dilakukan dengan algoritma *maximul likelihood classification (MLC) (Landgrebe and Biehl, 2011)*. *MLC* dijalankan dengan menggunakan lima kanal untuk komposit citra dan 771 GCP. Proses kasifikasi mengikuti prosedur pada tutorial (Landgrebe, 2015).

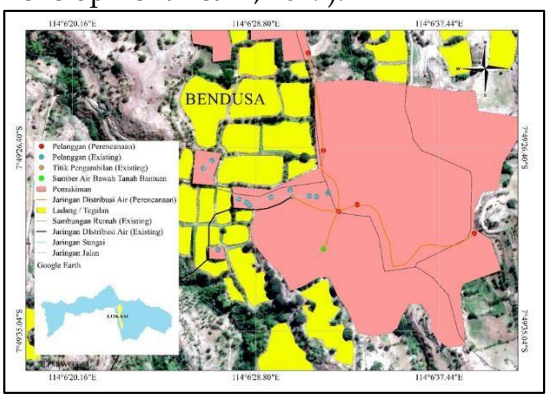
Selanjutnya digunakan, matrik kesalahan berbasis indek *overall* dan *kappa accuracy*, untuk menilai kualitas hasil klasifikasi. Kriteria ketelitian menggunakan 89% (Foody, 2008).

Langkah berikutnya, Empat (4) wilayah Desa digunakan sebagai sampel untuk mengevaluasi hasil klasifikasi, yaitu desa: Jatisari, Sopet, Kendit, dan Jatibanteng. Pemilihan desa berdasarkan lokasi dan karakteristik LCLU yang ada pada tiap desa. Selanjutnya peta tematik hasil klasifikasi dipotong *(clip)* seluas batas Desa untuk dibandingkan dengan peta RBI dan hasil digitasi manual.

Peta RBI yang diunduh dari laman BIG, se batas wilayah kabupaten Situbondo (dalam format vector), selanjutnya dipotong dengan poligon batas desa (Blok tengah dari gambar 2). Hasilnya berupa peta LCLU desa versi RBI tahun 2000, sebagai bahan perbandingan. Proses dilakukan pada software QGIS.

Selanjutnya, pada blok kanan, google earth image diunduh dengan Easy Google Map downloader dan digabung seluas batas Desa. Selanjutnya , citra *Google Earth* (dalam format raster) tersebut, dijadikan sebagai background map-file untuk proses digitalisasi. Hasil digitalisasi adalah peta raster.

Selanjutnya, (1) peta RBI dan (2) peta hasil digitasi manual dari Google Earth digunakan untuk Evaluasi. Peta RBI dipotong *(clip)* sebatas desa Jatisari dan dihitung luas tiap jenis peruntukan lahan. Kemudian, Citra Google Earth di mosaick dan dipotong dengan batas Desa Jatisari. Selanjutnya, dilakukan pembuatan peta LCLU desa secara manual dengan melakukan digitalisasi. Dalam hal ini citra google tidak diolah, tetapi hanya digunakan sebagai back- ground map file untuk melakukan digitalisasi (gambar 3). Metode ini sudah sangat umum dipraktekkan. Proses digitalisasi dilakukan menggunakan QGIS (QGIS Development Team, 2019).



Gambar 3. Ilustrasi Proses Digitasi

Selanjutnya, evaluasi dilakukan dengan membandingkan jenis fitur yang dapat dipetakan dan prosentase luas. Interpretasi dilakukan dengan membandingkan ke tiga peta tematik *LCLU*, yaitu: (1) dari RBI, (2) hasil klasifikasi terbimbing metode *MLC*, (3) Digitasi dari google earth. Interpretasi juga dilakukan dengan membandingkan kenya-taan yang ada di Lapang.

HASIL DAN PEMBAHASAN

Interpretasi Umum

Klasifikasi terbimbing menggunakan *MLC* menghasilkan indek overall dan kappa accuracy = 95,6% dan 93%. Menurut Foody (2008) hasil ini cukup memadai dan memenuhi kriteria standar klasifikasi. Tabel 3 menampilkan perbandingan hasil klasifi-kasi dengan peta RBI tahun 2000.

Table 3. Perbandingan RBI dan Sentinel

LULC Class	RBI-2000		Sentinel - 2019	
	km²	%	km²	%
Area terbangun	90	5,45	174	10,53
LSO-kering	859	52,0	439,1	26,6
Lahan irigasi	207	12,5	170,9	10,35
Lahan non-irigasi	109	6,6	33,4	2,02
Hutan-perkebunan	363,3	22,0	821,7	49,8
Badan air	23,0	1,39	12,18	0,74
Total	1651,3	100	1651,3	100

Sumber: Pengolahan Data, 2019

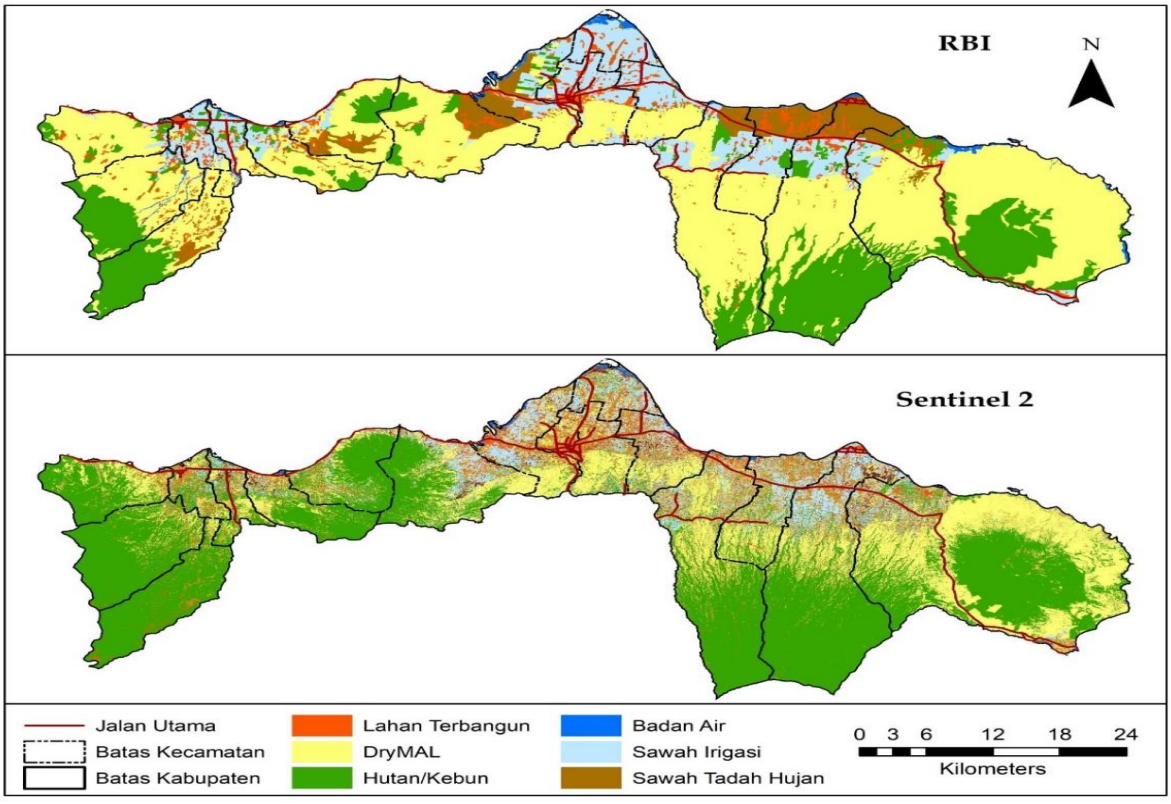
DOI: 10.24114/jg.v12i02.16970
e-ISSN: 2549–7057 | p-ISSN: 2085–8167

Gambar (4) menampilkan peta hasil klasifikasi Sentinel dibandingkan dengan peta RBI. RBI dibuat pada tahun 2000-an, sementara sentinel berdasarkan citra tahun 2019. Perubahan *LCLU* dapat diamati dengan membandingkan 3 kelas, yaitu: LSO-kering, kebun-hutan, dan lahan non-irigasi. Asal dari ke tiga kelas ini pada hakekatnya sama yaitu Lahan Sub-optimal kering (LSO-Kering). Definisi LSO-kering merujuk pada publikasi (Mulyani & Sarwani, (2013) ; Mulyani, Priyono & Agus, (2013).

Luas total ke tiga kelas pada RBI = (859 + 109 + 363,3) = 1331,3 km^2 = 80,62% dari total luas wilayah Situbondo. Sedangkan pada citra Sentinel luas total = 439,1 + 33,4 + 821,7 1294,2 km^2= 78.37%. Hal ini menunjukan telah terjadi perubahan peruntukan lahan (LU) dari LSO-kering menjadi peruntukan lainnya. LSO-kering berkurang karena dimanfaatkan untuk peruntukan lainnya, menjadi hutan dan sebagian besar LSO-Kering telah dimanfaatkan untuk kebun, pemukiman dan sawah atau ladang.

Peruntukan lahan untuk area terbangun (berupa pemukiman warga, infrastruktur jalan, kawan pertokoan, dll) telah meningkat secara signifikan selama dua dekade. Pada peta RBI (tahun 2000) luas total area terbangun = 90 km^2 , hanya mencakup 5,45% dari luas total wilayah Kabupaten Situbondo. Pada tahun 2019 (sentinel), area terbangun sudah mencapai = 174 km^2 = 10,53% luas total wilayah. Jadi dari tahun 2000 sd 2019 telah terjadi peningkatan luas pemukiman di Kabupaten Situbondo menjadi 2x lipat.

Perubahan terjadi dan dapat disebabkan karena urbanisasi dan peningkatan jumlah penduduk di wilayah perkotaan Situbondo. Misalnya terjadi di kecamatan Besuki, Bungatan, Panarukan, Mangaran, Situbondo, Panji, Kapongan, Jangkar, Arjasa dan Asembagus. Umumnya wilayah kecamatan yang berada di sepanjang Pantai utara Jawa. Perkembangan industri dan lokasi wisata di sepanjang pantai Situbondo juga meningkatkan konversi lahan ke pemukiman dan fasilitas perkotaan terkait.



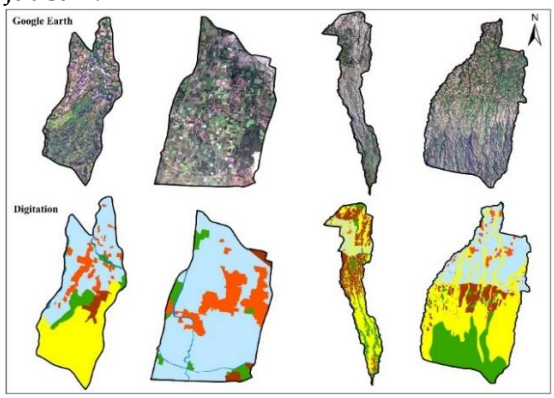
Gambar 4. Perbandingan hasil klasifikasi dengan peta RBI.

DOI: 10.24114/jg.v12i02.16970
e-ISSN: 2549–7057 | p-ISSN: 2085–8167

Konversi lahan sawah dan tegalan menjadi pemukiman (lahan terbangun) juga terjadi. Fenomena ini teramati pada wilayah perkotaan (bagian tengah dari Peta), di kecamatan Mangaran, Situbondo, Panarukan, Panji, dan Kapongan. Lahan Irigasi di wilayah tersebut telah terkonversi sebagian menjadi area-terbangun untuk pemukiman atau fasilitas kota lainnya (infrastruktur jalan, mall, dll). Lahan irigasi pada peta RBI tampak sebagai blok-luasan berwarna biru-muda, dan telah berubah menjadi lahan campuran yang terdiri dari pemukiman dan lahan sawah (terlihat pada peta hasil klasifikasi Sentinel).

Peta Hasil Digitalisasi

Gambar (5) menampilkan perbandingan antara citra Google Earth dan hasil digitalisasi pada ke empat (4) desa sampel. Ketelitian proses digitalisasi sangat tergantung pada konsistenti dan ketelitian operator dalam melakukan digitasi. Terlihat bahwa hasil digitalisasi yang baik dan paling detail adalah desa Jatisari.



Gambar 5. Peta Hasil Digitasi

Luas wilayah ke empat desa juga berbeda, yaitu : Jatibanteng (6.78 km²), Kendit (6.45 km²), Jatisari (45.97 km²), and Sopet (43.51 km²).

Pada wilayah desa Jatibanteng, Kendit dan Sopet relatif hanya fitur utama yang didigitasi. Artinya, seharusnya pada penelitian ini, peta hasil digitasi dari Google Earth dapat menjadi acuan utama, tetapi faktor operator dapat menyebabkan hasil digitasi atau perhitungan luas menjadi kurang tepat, sehingga digitasi menjadi pertimbangan dalam interpretasi tetapi tidak dapat menjadi tolok ukur utama.

Interpretasi LCLU Desa Jatisari

Tabel (4) menampilkan perbandingan *LCLU* di desa Jatisari (45.97 km²). Luasan yang sama dipetakan dengan cara yang berbeda akan menghasilkan detail yang berbeda.

Table 4. Perbandingan LCLU Jatisari

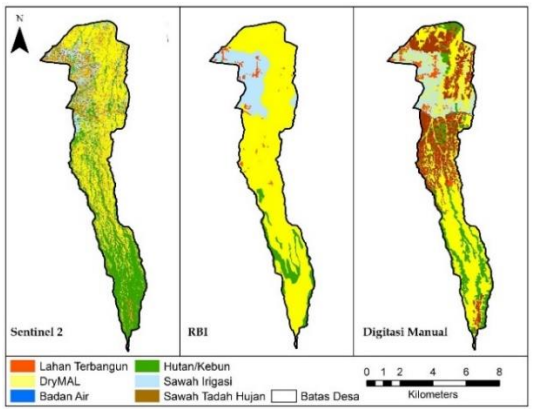
Kelas LCLU	RBI-2000		Google Earth - 2019		Sentinel 2A-2019	
	km²	%	km²	%	km²	%
Area terbangun	1,03	2,24	1,79	3,90	1,83	3,99
LSO-kering	34,9	76,0	23,3	50,6	23,7	51,6
Lahan irigasi	6,57	14,3	6,89	15,0	4,65	10,1
Lahan non-irigasi	0,00	0,00	8,12	17,7	0,49	1,08
Hutan-kebun	3,42	7,44	5,83	12,6	15,3	33,2
Badan air	0,00	0,00	0,05	0,12	0,00	0,01
Luas total	45,9	100	45,9	100	45,9	100

Sumber: Pengolahan Data, 2019

Area terbangun yang pada tahun 2000 hanya seluas 1,03 km² atau (2,24%) dari luas Desa Jatisari. Pada tahun 2019 telah berkembang menjadi hampir 2x lipat (1,83 km²) atau (±3,90%) pada tahun 2019. Hasil klasifikasi relatif identik dengan hasil digitasi manual. Perbedaan hanya sekitar = 1.83 – 1.79 = 0.04 km².

Kemiripan hasil juga terlihat untuk kelas LSO-kering. Sentinel dapat memisahkan dengan jelas pemukiman dan LSO. Proses digitasi sawah irigasi lebih luas dari yang seharusnya, karena mungkin ada lahan non-irigasi yang dianggap sebagai lahan irigasi. Pada citra Google Earth kenampakan ke dua-nya hampir mirip. Lahan irigasi pada wilayah Jatisari relatif tidak bertambah, sejak dibangun-nya Jaringan Irigasi. Daerah irigasi (warna biru muda) hanya ada diujung sebelah kiri atas dari peta RBI (Gambar 6).

DOI: 10.24114/jg.v12i02.16970
e-ISSN: 2549–7057 | p-ISSN: 2085–8167



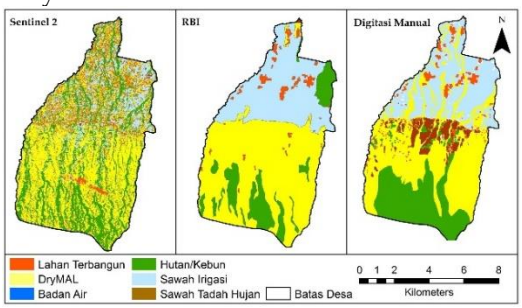
Gambar 6. LCLU Desa Jatisari

Pada proses digitasi, karena dilakukan secara manual, maka lahan non-irigasi dapat dipisahkan dari Kebun. Proses digitasi mengindentifikasi kebun mangga warga dengan baik. Dimana area berpohon dianggap kebun, sedangkan area kosong didigit lahan non-irigasi. Pada Sentinel tutupan lahan (LC) dipisahkan menjadi 2, area yang tidak bervegatasi dimasukan sebagai LSO (ladang/tegalan) dan area berpohon (termasuk tanah kosong di sekitar kebun atau tanaman) diklasifikan sebagai hutan-kebun. Dalam hal ini, sentinel melihat hutan dan kebun sama sebagai kelas tanaman tahunan. Pohon besar yang hijau sepanjang tahun. Sementara, RBI mengidentifikasi lahan berbasis land use (fungsi kebun dan fungsi hutan).

Lahan irigasi yang pada peta RBI digambarkan sebagai blok-area (*Land-use*) berwarna biru muda, telah berubah karena sebagian dikonversi untuk pemukiman warga. Sehingga, tampak di peta Sentinel sebagai campuran warna biru-merah-kuning yang menunjukan kondisi tutupan lahan *(LC)* yang lebih terfragmentasi berupa campuran antara pemukiman vegetasi dan lahan irigasi.

LCLU Desa Sopet

Peruntukan lahan (LU) di peta RBI terbagi ke dalam : area-terbangun, lahan-irigasi, LSO-kering, hutan dan perkebunan (gambar 7). Saluran irigasi Sampeanbaru melintas dari Barat ke Timur dan membagi wilayah Sopet menjadi dua bagian yang kontras (Gambar 7). Di bawah saluran adalah lahan irigasi. Pada peta RBI, lahan irigasi berupa blok-area berwarna biru-muda, mencakup ± 30% wilayah desa dan terletak di sebelah utara saluran. Sebagian lahan irigasi telah terkonversi menjadi pemukiman. Di atas saluran adalah LSO-kering, perkebunan dan hutan mencakup seluas ±30 km² atau 67,7% dari total wilayah desa.



Gambar 7. LCLU Desa Sopet

Proses digitasi dilakukan dengan mengikuti fitur utama dari google earth sehingga hasilnya menyerupai RBI. Sentinel dapat mengklasifikasikan konsidi *penutupan lahan (LC)* di Sopet dengan lebih detail. Dimana terlihat bahwa area yang awalnya diperuntukan untuk lahan irigasi, telah terkonversi sebagian menjadi area terbangun dan vegetasi tahunan. Demikian juga di bagian selatan dari saluran. LSO-kering (pada RBI 2000) diklasifikasikan menjadi LSO-kering dan vegatsi tahunan (hutan –perkebunan) dalam bentuk yang lebih terfragmentasi. Hal ini karena sentinel mengelompokan pixel ke dalam kelas berdasarkan penutupan lahan (*land cover*).

Table 5. LCLU desa Sopet

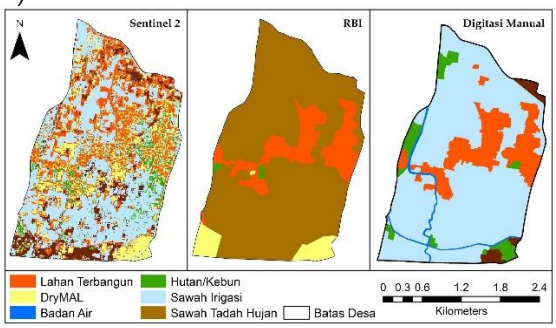
Kelas LCLU	RBI 2000		Google Earth- 2019		Sentinel 2A - 2019	
	km²	%	km²	%	km²	%
Area terbangun	1,15	2,64	1,42	3,3	5,6	12,9
LSO-kering	23,5	54,1	17,42	40,1	18,7	43,0
Lahan irigasi	12,9	29,7	11,09	25,5	6,31	14,5
Lahan non irigasi	0,04	0,09	3,07	7,07	0,54	1,24
Hutan - perkebunan	5,9	13,5	9,11	20,9	12,3	28,4
Badan air	0,00	0,00	1,39	3,19	0,00	0,00
Total	43,5	0,00	43,51	100	43,5	100

DOI: 10.24114/jg.v12i02.16970
e-ISSN: 2549–7057 | p-ISSN: 2085–8167

Selama 19 tahun, area terbangun meningkat 4,86 kali lebih luas. LSO-kering berkurang – 20% dari luas sebelumnya. Lahan irigasi telah berkurang hampir 50%. Luas area untuk perkebunan dan hutan menjadi 2 kali lipat (Tabel 5).

LCLU Desa Kendit

Desa kendit terletak di wilayah bawah, dekat dengan pantai dan pada topografi yang relatif datar. Pada tahun 2000 (peta RBI), hampir 80% wilayah di Kendit adalah lahan non-irigasi atau sawah tadah hujan. Pengembangan jaringan irigasi (dalam hal ini, saluran Induk Panarukan) telah mampu mengairi lahan tersebut menjadi sawah irigasi. Saluran irigasi pada proses digitalisasi digambarkan sebagai badan air (Gambar 8).



Gambar 8. LCLU Desa Kendit

Lahan irigasi didigitasi seluas 75%. Selama 19 tahun, area terbangun hanya bertambah = 1,07 – 0,99 = 0,08 km², sesuatu yang sulit untuk dipahami untuk suatu wilayah perkotaan. Hal ini karena proses digitasi dilakukan hanya mengambil secara umum (berupa zona). Ini salah satu kelemahan dari operator dalam proses digitasi. Dalam hal ini, Sentinel dapat menggambarkan proses perubahan dari lahan non-irigasi ke lahan-irigasi, area terbangun dan vegetasi tahunan dengan lebih baik. Luas area terbangun selama 19 tahun telah meningkat menjadi 1,6 x dari sebelumnya (tabel 6). Lahan irigasi tinggal 45% dari luas total. Lahan non-irigasi (tegalan/ladang) seluas 10% berada di utara saluran dan merupakan wilayah yang lebih tinggi dari saluran induk, sehingga tidak terairi. Hutan-perkebunan seluas 4,34% hakekat-nya adalah tanaman tahunan, seperti pohon mangga, tanaman di sekitar jalan atau pohon di sekitar pekarangan rumah.

Table 6. LCLU at Kendit

Kelas LCLU	RBI 2000		Google Earth - 2019		Sentinel 2A - 2019	
	km²	%	km²	%	km²	%
Area terbangun	0,99	15,4	1,07	16,6	1,58	24,5
LSO-kering	0,34	5,26	0,00	0,00	0,96	14,9
Lahan irigasi	0,00	0,00	4,81	74,6	2,92	45,2
Lahan non-irigasi	5,07	78,6	0,15	2,33	0,70	10,9
Hutan - perkebunan	0,04	0,69	0,31	4,75	0,28	4,34
Badan air	0,00	0,00	0,11	1,72	0,01	0,12
Total	6,45	100	6,45	100	6,45	100

Sumber: Pengolahan Data, 2019

LULC Desa JatiBanteng

Desa Jatibanteng merupakan pusat dari Kecamatan Jatibanteng. Dalam hal ini area terbangun relatif tidak berubah selama 19 tahun. LSO-kering berkurang dai 36% menjadi 24% (Tabel 7).

Tabel 7. LCLU Jatibanteng

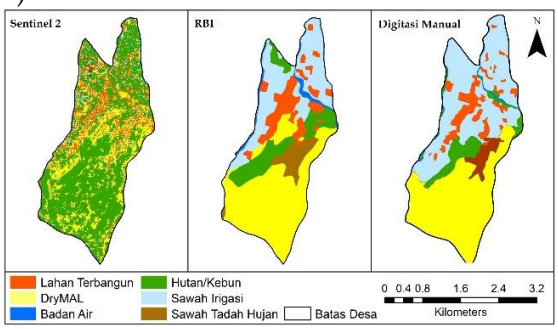
LCLU class	RBI 2000		Google Earth- 2019		Sentinel 2019	
	km²	%	km²	%	km²	%
Area terbangun	0,79	11,7	0,59	8,7	0,80	11,9
LSO-kering	2,43	35,9	2,69	39,6	1,60	23,6
Lahan irigasi	1,72	25,4	2,70	39,9	0,27	4,0
Lahan non-irigasi	0,41	6,00	0,25	3,68	0,06	0,88
Hutan-perkebunan	1,18	17,4	0,49	7,17	4,05	59,7
Badan air	0,24	3,57	0,07	1,00	0,00	0,00
Total	6,78	100	6,78	100	6,78	100

Sumber: Pengolahan Data, 2019

Sebaliknya wilayah hutan-perkebunan digambarkan oleh Sentinel lebih besar. Hal ini karena, citra yang digunakan adalah hasil pemotretan pada akhir musim penghujan (juni 2019). Lahan di wilayah Jati Banteng masih banyak tertutup oleh vegetasi. Vegetasi yang dominan, diklasifikasikan lebih ke

DOI: 10.24114/jg.v12i02.16970
e-ISSN: 2549–7057 | p-ISSN: 2085–8167

dalam kelas hutan-perkebunan (Gambar 9).



Gambar 9. LCLU Desa Jatibanteng

KESIMPULAN

Artikel ini membahas perbandingan peta hasil klasifikasi dari citra-Sentinel 2A, peta hasil digitasi manual dari Google Earth dan peta RBI Digital untuk menggambarkan tutupan dan peruntukan lahan (*LCLU*) pada level desa. Perbandingan hasil klasifikasi, dengan digitasi manual dan RBI dapat digunakan sebagai dasar interpretasi *LCLU* di wilayah empat desa tersebut dan identifikasi perubahan *LCLU* yang utama selama 19 tahun terakhir.

Hasil evaluasi juga menunjukan kemampuan Sentinel 2A untuk memetakan tutupan lahan sampai dengan level desa. Digitasi secara manual dari goole earth beresiko pada terjadinya kesalahan interpre-tasi. Secara umum citra sentinel dapat digunakan untuk mengambarkan fitur utama *LCLU* suatu Desa. Citra juga dapat digunakan untuk memperbaharuai peta RBI dan perencanaan pembangunan di tingkat Desa

UCAPAN TERIMA KASIH

Penelitian dan publikasi terkait LSO di wilayah Jatisari merupakan bagian dari skema Hibah Pendamping IDB LP2M UNEJ tahun anggaran 2019, No SK rektor: 13455/UN25/LT/2019 (Tanggal 9 Agustus 2019) dan contract no: 3200 /UN25.3.1/LT/2019 (tanggal 16 Agustus 2019). A.n Indarto, berjudul : "Pengembangan Jaringan Distribusi Air dan Desain Irigasi Mikro Berbasis Sumur Tanah dalam pada Lahan Sub-Optimal di Desa Jatisari, Kec Arjasa, Kab Situbondo", di bawah koordinasi keris LSO. Kepada LP2M UNEJ, pemkab Situbondo dan semua pihak yang telah membantu kelancaran proses penelitian ini disampaikan banyak terima kasih.

DAFTAR PUSTAKA

Abdi, A. M. (2019) 'Land cover and land use classification performance of machine learning algorithms in a boreal landscape using Sentinel-2 data', *GIScience & Remote Sensing*. Taylor & Francis, pp. 1–20. doi: 10.1080/15481603.2019.1650447.

BIG (2019) *Indonesia Geospatial Portal*. Available at: http://tanahair.indonesia.go.id/portal-web (Accessed: 15 December 2019).

Bolton, D. K. *et al.* (2020) 'Continental-scale land surface phenology from harmonized Landsat 8 and Sentinel-2 imagery', *Remote Sensing of Environment*. Elsevier Inc., 240. doi: 10.1016/j.rse.2020.111685.

BPS, S. (2019) *Kabupaten Situbondo dalam angka tahun 2019 (Regency Situbondo in number)*. Situbondo. Available at: https://situbondokab.bps.go.id/publication/2019/12/26/ee20f467bae2040464413b80/statistik-daerah-kabupaten-situbondo-2019.html (Accessed: 25 May 2020).

Campbell, J. B. and Wynne, R. H. (2011) *Introduction to remote sensing*. Guilford Press.

Clerici, N., Valbuena Calderón, C. A. and Posada, J. M. (2017) 'Fusion of sentinel-1a and sentinel-2A data for land cover mapping: A case study in the lower Magdalena region, Colombia', *Journal of Maps*. doi: 10.1080/17445647.2017.1372316.

Congedo, L. (2016) *Semi-Automatic Classification Plugin Documentation*. doi: 10.13140/RG.2.2.29474.02242/1.

Efroymson, R. A. *et al.* (2016) 'A causal analysis framework for land-use change and the potential role of bioenergy

policy', *Land Use Policy*. Elsevier Ltd, 59, pp. 516–527. doi: 10.1016/j.landusepol.2016.09.009.

Eremiášová, R. and Skokanová, H. (2009) 'Land Use Changes (Recorded in Old Maps) and Delimitation of the Most Stable Areas from the Perspective of Land Use in the Kašperské Hory Region', *Journal of Landscape Ecology*. Berlin: Sciendo, 2(1), pp. 20–34. doi: https://doi.org/10.2478/v10285-012-0012-5.

Esa (2013) *SENTINEL-2 User Handbook Sentinel-2 User Handbook SENTINEL-2 User Handbook Title Sentinel-2 User Handbook Issue 1 Revision 1 SENTINEL-2 User Handbook*.

EUROSTAT (2001) *Manual of concepts on land cover and land use information systems*. Available at: http://europa.eu.int (Accessed: 17 May 2020).

Foody, G. (2008) 'Harshness in image classification accuracy assessment', *International Journal of Remote Sensing*. Taylor and Francis Ltd., 29(11), pp. 3137–3158. doi: 10.1080/01431160701442120.

Foody, G. M. (2002) 'Status of land cover classification accuracy assessment', *Remote Sensing of Environment*. Elsevier Inc., pp. 185–201. doi: 10.1016/S0034-4257(01)00295-4.

Foody, G. M. (2004) 'Thematic map comparison: Evaluating the statistical significance of differences in classification accuracy', *Photogrammetric Engineering and Remote Sensing*. American Society for Photogrammetry and Remote Sensing, pp. 627–633. doi: 10.14358/PERS.70.5.627.

Hakim, Y. F., Riqqi, A. and Harto, A. B. (2014) 'Kontrol Kualitas Dalam Alur Produksi Kartografi Peta RBI di Badan Informasi Geospasial', *GEOMATIKA*, 20(1).

Hariyono, M. I. (no date) 'Kajian Perubahan Penutup Lahan Peta Rupabumi pada Skala yang Berbeda'.

Khorram, S. *et al.* (2013) 'Digital Image Acquisition: Preprocessing and Data Reduction BT - Handbook of Satellite Applications', in Pelton, J. N., Madry, S., and Camacho-Lara, S. (eds). New York, NY: Springer New York, pp. 809–837. doi: 10.1007/978-1-4419-7671-0_46.

Lambin, E. F. *et al.* (2001) 'The causes of land-use and land-cover change: Moving beyond the myths', *Global Environmental Change*. Elsevier Ltd, pp. 261–269. doi: 10.1016/S0959-3780(01)00007-3.

Landgrebe, D. (2015) *MultiSpec Tutorial: Supervised Classification-Select Training Fields*. Available at: https://engineering.purdue.edu/~biehl/MultiSpec/documentation.html (Accessed: 26 November 2019).

LAPAN (2015) 'LAPAN Pedoman Pengolahan Data Penginderaan Jauh Landsat 8 untuk MPT'. Available at: file:///F:/BISMILLAH/Ris/000_Buku_Pedoman_TSM_final.pdf.

Li, G. *et al.* (2012) 'A comparative analysis of ALOS PALSAR L-band and RADARSAT-2 C-band data for land-cover classification in a tropical moist region', *ISPRS Journal of Photogrammetry and Remote Sensing*, 70, pp. 26–38. doi: 10.1016/j.isprsjprs.2012.03.010.

Lillesand, T. M., Kiefer, R. W. and Chipman, J. W. (2008) *Remote Sensing and Image Interpretation*. 6th edn. New Jersey.

Lopes, M. *et al.* (2020) 'Combining optical and radar satellite image time series to map natural vegetation: savannas as an example', *Remote Sensing in Ecology and Conservation*. Wiley-Blackwell. doi: 10.1002/rse2.139.

Martínez, S. and Mollicone, D. (2012) 'From Land Cover to Land Use: A Methodology to Assess Land Use from Remote Sensing Data', *Remote Sensing*. MDPI AG, 4(4), pp. 1024–1045. doi: 10.3390/rs4041024.

Moran, E. F. (2010) 'Land Cover Classification in a Complex Urban-Rural Landscape with Quickbird Imagery', *Photogrammetric engineering and remote sensing*. NIH Public Access, 76(10), p. 1159.

DOI: 10.24114/jg.v12i02.16970
e-ISSN: 2549–7057 | p-ISSN: 2085–8167

Mulyani, A., Priyono, A. and Agus, F. (2013) 'Semiarid Soils of Eastern Indonesia: Soil Classification and Land Uses', in, pp. 449–466. doi: 10.1007/978-94-007-5332-7_24.

Mulyani, A. and Sarwani, M. (2013) 'Karakteristik dan Potensi Lahan Sub Optimal untuk Pengembangan Pertanian di Indonesia | Mulyani | Jurnal Sumberdaya Lahan', *Jurnal Sumberdaya Lahan*, 7(1), pp. 47–55. Available at: http://ejurnal.litbang.pertanian.go.id/index.php/jsl/article/view/6429 (Accessed: 26 November 2019).

Parece, T. E. and Campbell, J. B. (2015) 'Land use/land cover monitoring and geospatial technologies: An overview', in *Handbook of Environmental Chemistry*. Springer Verlag, pp. 1–32. doi: 10.1007/978-3-319-14212-8_1.

Ptak, M. and Ławniczak, A. E. (2012) 'Changes in land use in the buffer zone of lake of the Mała Wełna catchment', *Limnological Review*. Berlin: Sciendo, 12(1), pp. 35–44. doi: https://doi.org/10.2478/v10194-011-0043-z.

Putri Abdi. Sudarsono, Bambang., D. R. S. (2018) 'Analisis Kombinasi Citra Sentinel-1a Dan Citra Sentinel-2a Untuk Klasifikasi Tutupan Lahan (Studi Kasus: Kabupaten Demak, Jawa Tengah)', *Jurnal Geodesi Undip*, 7(2), pp. 85–96. doi: 10.1016/j.cirp.2008.03.009.

Riadi, B. and Makmuriyanto, A. (2014) 'Kajian Percepatan Penetapan dan Penegasan Batas Kecamatan/Distrik, Desa/Kelurahan Secara Kartometris', *Majalah Ilmiah Globe*, 16(2).

Riadi, B. and Rachma, T. R. N. (2017) 'Kajian Prototipe Peta Desa Menggunakan Citra Satelit Resolusi Tinggi', *Majalah Ilmiah Globe*, 19(2), pp. 147–156.

Richards, J. A. (2013) *Remote Sensing Digital Image Analysis*. 5th edn. Heidelberg: Springer-Verlag. Available at: file:///D:/KULIAH/SKRIPSI/05_Jurnal Penunjang/Remote_Sensing_Digital_Image_Analysis_www.GISman.ir.pdf.

Rujoiu-Mare, M.-R. *et al.* (2017) 'Land cover classification in Romanian Carpathians and Subcarpathians using multi-date Sentinel-2 remote sensing imagery', *European Journal of Remote Sensing*. Taylor & Francis, 50(1), pp. 496–508. doi: 10.1080/22797254.2017.1365570.

Song, X. P. *et al.* (2018) 'Global land change from 1982 to 2016', *Nature*. Nature Publishing Group, 560(7720), pp. 639–643. doi: 10.1038/s41586-018-0411-9.

Sudarman, S., Sadikin, H. and Prijatna, K. (2020) 'Desain Alternatif Lembar Peta Rupabumi Indonesia (RBI) Skala Besar', *GEOMATIKA*, 26(1), pp. 35–44.

Susetyo, D. B. (2015) 'Generalisasi kartografis pada peta Rupabumi Indonesia (RBI) skala 1: 25.000 menjadi 1: 50.000', *Proceeding of Simposium Sains Geoinformasi*, pp. 217–225.

Tavares, P. A. *et al.* (2019) 'Integration of sentinel-1 and sentinel-2 for classification and LULC mapping in the urban area of Belém, eastern Brazilian Amazon', *Sensors (Switzerland)*. MDPI AG, 19(5). doi: 10.3390/s19051140.

USGS (2019) 'EarthExplorer - Home', *U.S. Geological Survey*. Available at: https://earthexplorer.usgs.gov/ (Accessed: 15 December 2019).

USGS, U. S. G. (2019) 'Landsat 8 (L8) Data Users Hanbook Version 4.0', *Department of the Interior, U.S. Geological Survey*, 4(April), p. 106. Available at: https://prd-wret.s3-us-west-2.amazonaws.com/assets/palladium/production/atoms/files/LSDS-1574_L8_Data_Users_Handbook_v4.0.pdf.

Wężyk, P. *et al.* (2016) 'Using Geobia and Data Fusion Approach for Land use and Land Cover Mapping', *Quaestiones Geographicae*. Berlin: Sciendo, 35(1), pp. 93–104. doi: https://doi.org/10.1515/quageo-2016-0009.

environmental sciences proceedings

MDPI

Proceeding Paper

Rice Crop Yield Prediction from Sentinel-2 Imagery Using Phenological Metric †

Javier A. Quille-Mamani [1,*], Luis A. Ruiz [1] and Lía Ramos-Fernández [2]

[1] Grupo de Cartografía GeoAmbiental y Teledetección, Universitat Politècnica de València, Camí de Vera s/n, 46022 Valencia, Spain; laruiz@upv.es
[2] Departamento de Recursos Hídricos, Universidad Nacional Agraria La Molina, Lima 15024, Peru; liarf@lamolina.edu.pe
* Correspondence: jaquille@upv.es
† Presented at the IV Conference on Geomatics Engineering, Madrid, Spain, 6–7 July 2023.

Abstract: Crop yield prediction at plot scale is a vitally important magnitude for farmers at the socio-economic level. This study aims to quantify rice yield using phenological metrics from a normalized difference vegetation index (NDVI) time series derived from Sentinel-2 imagery, with yield data collected from 32 plots with an area of 36 ha in the Ferreñafe District of the Lambayeque region, Peru. Three different rice yield models were obtained, the best linear regression models were obtained for the SVM classification, with R^2 of 0.69, MAE = 1.01 and RMSE = 1.23 t ha^{-1}; and MRL with R^2 of 0.61, MAE = 1.10 and RMSE = 1.38 t ha^{-1}; RF with R^2 of 0.44, MAE = 1.23 and RMSE = 1.66 t ha^{-1}. The models obtained open the possibility to generate more robust models using a larger number of samples, which would be useful for farmers as well as for management and planning decisions for food and economic security.

Keywords: NDVI; multispectral imaging; machine learning; time series; precision agriculture

check for updates

Citation: Quille-Mamani, J.A.; Ruiz, L.A.; Ramos-Fernández, L. Rice Crop Yield Prediction from Sentinel-2 Imagery Using Phenological Metric. *Environ. Sci. Proc.* **2023**, *28*, 16. https://doi.org/10.3390/environsciproc2023028016

Academic Editors: María Belén Benito Oterino, José Fernández Torres, Rosa María García Blanco, Jorge Miguel Gaspar Escribano, Miguel Ángel Manso Callejo and Antonio Vázquez Hoehne

Published: 2 January 2024

Copyright: © 2024 by the authors. Licensee MDPI, Basel, Switzerland. This article is an open access article distributed under the terms and conditions of the Creative Commons Attribution (CC BY) license (https://creativecommons.org/licenses/by/4.0/).

1. Introduction

One of the world's major cereal crops is rice [1], which meets the nutritional demand and food security of 50% of the world's population [2]. The importance of yield knowledge has been a challenge for future food production due to climatic factors and water scarcity. Remote sensing tools allow yield prediction using satellite imagery (MODIS, LandSat, Sentinel) [3]. However, being Sentinel-2 optical imagery, with higher spatial and temporal resolution it allows to decrease cloud-induced noise. Therefore, it allows the use of different methodologies, including Machine Learning for yield prediction [4].

Northern Peru's contribution to national rice production is distributed in three regions: San Martin with 24%, Piura with 15% and Lambayeque with 13% of the national production. In the Lambayeque region, with a per capita consumption of 63.5 kg, approximately 417,597 ha are planted, representing 40% of the total sown area [5,6], playing a fundamental role from an economic and food security point of view for its inhabitants.

Therefore, and in line with similar studies [3,4,7], this study aims to quantify rice yield using phenological metrics from a Normalized Difference Vegetation Index (NDVI) time series derived from Sentinel-2 images.

2. Materials and Methods

2.1. Study Area

The study area of this work is the district of Ferreñafe, located in the region of Lambayeque, Peru (79°47′09.73″ W; 6°35′36.68″ S; 46 m above sea level); with a mean annual rainfall of 22 mm and mean annual temperatures with a minimum average of 15.4 °C and a maximum average of 28.8 °C, with clay soils. The tests were carried out on a total area

of 36 ha in 5 different zones of approximately 5–12 ha each, with a total of 32 plots of rice (Tinajones variety) (Figure 1). Yield samples were taken from each study plot at the end of the growing season. See Table 1.

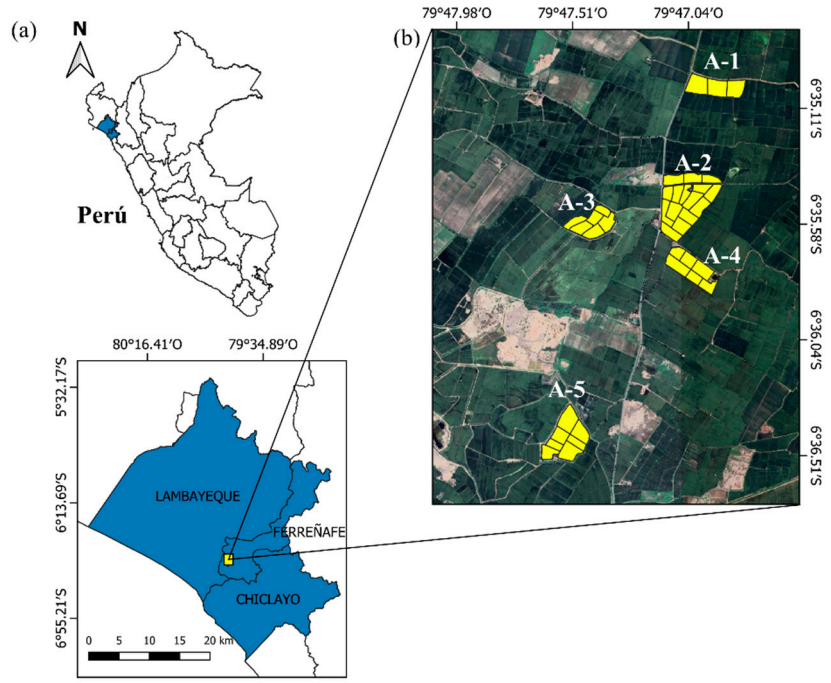


Figure 1. Rice cultivation map of the study region (**a**) and study rice growing areas (**b**).

Table 1. Information rice fields.

A-1		A-2		A-3		A-4		A-5	
Area (Ha)	**Yield (t ha^{-1})**	**Area (Ha)**	**Yield (t ha^{-1})**	**Area (Ha)**	**Yield (t ha^{-1})**	**Area (Ha)**	**Yield (t ha^{-1})**	**Area (Ha)**	**Yield (t ha^{-1})**
1.98	10.41	1.11	10.45	0.64	11.63	0.77	11.91	1.99	8.81
1.74	9.66	0.96	10.51	1.14	8.11	0.99	13.26	1.42	7.36
1.58	9.72	0.76	10.90	1.11	10.00	1.38	14.31	1.11	7.87
		0.75	10.75	1.03	12.04	1.49	12.29	0.80	6.28
		1.16	9.91	0.85	10.21	0.95	13.88	1.58	4.98
		1.13	11.06					0.66	5.06
		0.90	10.18					0.99	7.57
		0.78	11.53						
		1.13	10.71						
		1.03	10.81						
		1.02	10.61						
		1.15	8.69						

2.2. Data Processing

The Google Earth Engine (GEE) platform was used to extract the NDVI time series from ten Sentinel-2 images, with a spatial resolution of 10 m, considering a filtering of <30% cloud cover. In addition, the mean and maximum NDVI value at a 15-day interval was extracted for the entire rice growing season (December 2021 to June 2022). Subsequently, the extracted values of the NDVI time series were input to generate the phenological metrics in the R programming language with the "CropPhenology" library [8]. In addition, "Weka" software [9] was used for variable selection, model generation and cross-validation, as shown in Figure 2.

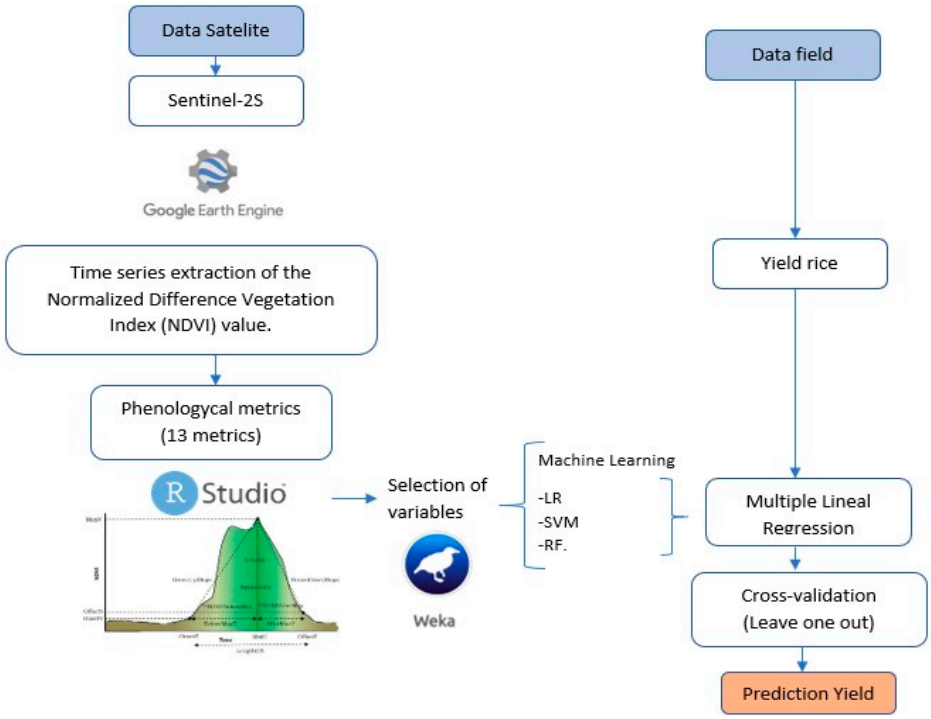


Figure 2. Methodological Working Procedure.

2.3. Phenological Metrics

The phenological metrics were extracted considering studies conducted by Araya et al. [8]. They are defined as shown in Figure 3.

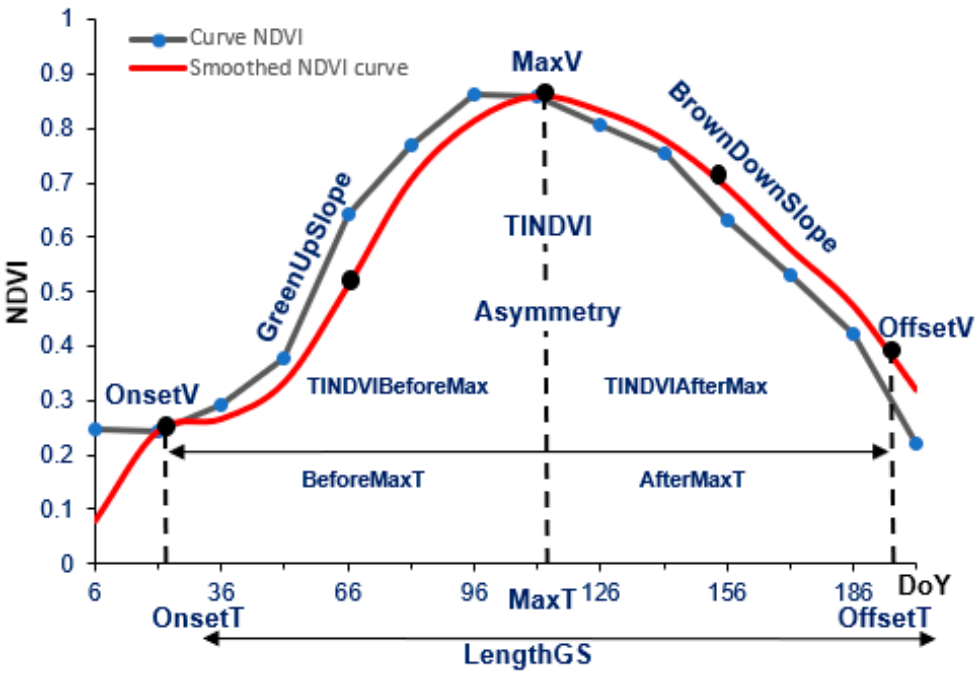


Figure 3. NDVI curve with representation of phenological metrics of rice.

2.4. Statistical Analysis

Data analysis was performed by applying Support Vector Machine (SVM), Linear Regression (LR) and Random Forest (RF) for the selection of the metrics, and Multiple Linear Regression (MRL) to obtain rice yield models, which were evaluated by Leave-One-Out Cross-Validation (LOOCV) [10], obtaining the coefficients of determination (R^2), the root mean square error (RMSE) and the Mean Absolute Error (MAE).

3. Results and Discussion

Figure 4 shows the r-Pearson correlation coefficients between the phenological metric variables extracted from the NDVI time series of the rice crop. Presenting collinearity between the variables "GreenUpSolpe" and "MaxV", and in the other hand, between "TINDVI" and "TINDVIAfterMax", withan r-Pearson correlation ≥ 0.90.

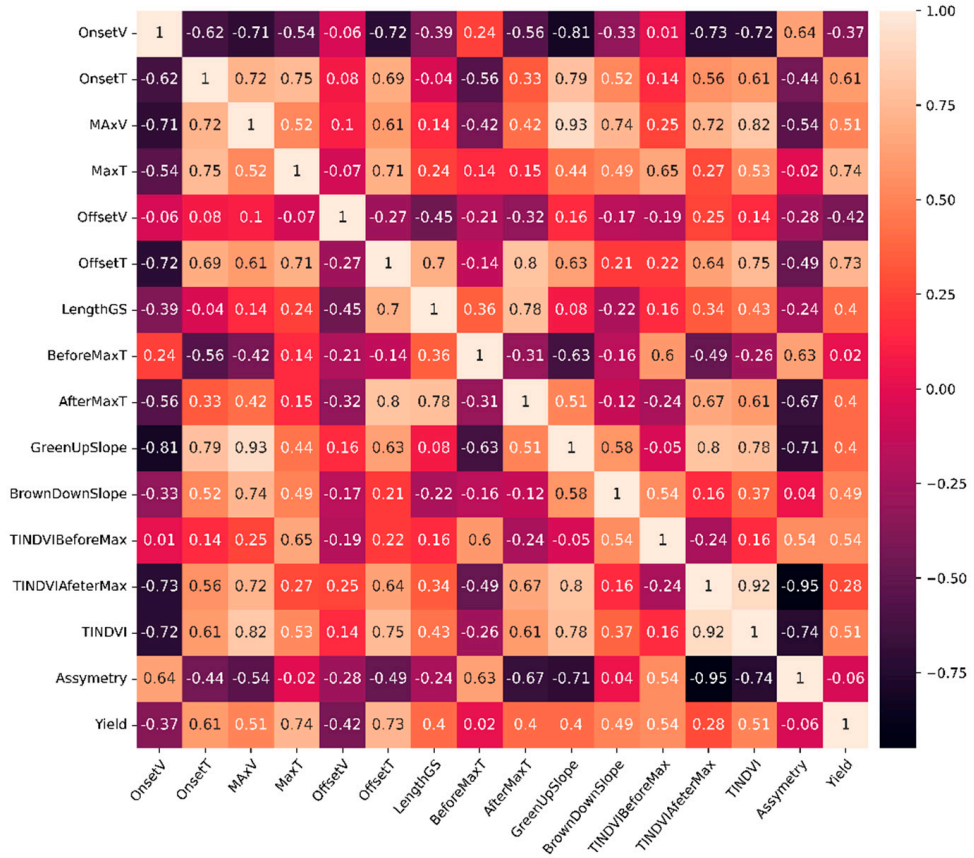


Figure 4. r-Pearson correlation of rice yield and phenological metrics.

Normally, rice yield models are based on NDVI analysis during different phenological stages of the crop, which are reflected in the phenological metrics according to [8]. This allows to generate models by automatic learning, thus obtaining reasonable errors even with few images available due to weather conditions. Therefore, a higher frequency of images could potentially allow a better accuracy in determining the key date for model creation.

The machine learning models selected the following metrics: LR (OffsetT and TINDVIBeforeMax), SVM (OnsetV, MaxT, OffsetT and BrownDownSolpe) and RF (MaxT, TINDVIAfterMax and TINDVI). Table 2 shows the summary statistics of the models generated by the multiple linear regression of the variables selected for each automatic selection method. The best result was obtained using SVM for metrics selection, with R^2 of 0.69, MAE = 1.01 and RMSE = 1.23 t ha^{-1}; and LR with R^2 of 0.61, MAE = 1.10 and RMSE = 1.38 t ha^{-1}; RF with R^2 of 0.44, MAE = 1.23 and RMSE = 1.66 t ha^{-1}.

Table 2. Statistical summary of yield prediction models evaluated using cross-validation (leave-one-out), coefficient of determination, root mean square error and mean absolute error.

Method of Selection		Models	R^2	RMSE (t ha^{-1})	MAE	N-Value
LR	Multiple Linear Regression	2.3369 × OffsetT + 8.6715 × TINDVIBeforeMax − 21.0089	0.61	1.38	1.10	32
SVM		36.4304 × OnsetV + 1.4759 × MaxT + 3.0196 × OffsetT + 74.65 × BrownDownSlope − 34.6315	0.69	1.23	1.01	32
RF		2.8828 × MaxT − 4.9856 × TINDVIAfeterMax + 7.2392 × TINDVI − 15.0098	0.44	1.66	1.23	32

4. Conclusions

The present study evaluated three rice yield models, based on the analysis of sentinel-2 NDVI time series, with the extraction of 15 phenological metrics. Three machine learning methods (LR, SVM and RF) were used for variable selection, then multiple linear regressions were generated for each machine learning model. The best models were generated using the following phenological metrics of OnsetV, MaxT, OffsetT, brownDownSlopw, TINDVIBeforeMax, TINDVIAfterMax and TINDVI. It is expected to obtain data from future seasons at the same points in order to develop a more robust model applicable to plots without yield information.

Author Contributions: Conceptualization, J.A.Q.-M., L.R.-F. and L.A.R.; methodology, J.A.Q.-M., L.R.-F. and L.A.R.; software, J.A.Q.-M. and L.A.R.; validation, J.A.Q.-M., L.R.-F. and L.A.R.; writing—original draft preparation, J.A.Q.-M., L.R.-F. and L.A.R.; writing—review and editing, J.A.Q.-M., L.R.-F. and L.A.R. All authors have read and agreed to the published version of the manuscript.

Funding: This research has been funded by the projects AGENCIA ESPAÑOLA DE COOPERACION INTERNACIONAL/2020/ACDE/000307 and the scholarship (Generación del Bicentenario) of the Peruvian government for the completion of the thesis (Programa Nacional de Becas y Crédito Educativo (Pronabec) of the Peruvian Ministry of Education (Minedu)).

Institutional Review Board Statement: Not applicable.

Informed Consent Statement: Not applicable.

Data Availability Statement: All data generated during this study are included in this published article.

Conflicts of Interest: The authors declare no conflict of interest.

References

1. Rahman, M.M.; Hasan, S.; Ahmed, R.; Adham, A.K.M. Recycling deep percolated water in continuously flooding irrigated rice fields to mitigate water scarcity. *Paddy Water Environ.* **2022**, *20*, 449–466. [CrossRef]
2. Jiang, Y.; Carrijo, D.; Huang, S.; Chen, J.; Balaine, N.; Zhang, W.; van Groenigen, K.J.; Linquist, B. Water management to mitigate the global warming potential of rice systems: A global meta-analysis. *Field Crop. Res.* **2019**, *234*, 47–54. [CrossRef]
3. Tornos, L.; Domínguez, J.A.; Moyano, M.C.; Recuero, L.; Cicuéndez, V.; García-García, M.J.; Palacios-Orueta, A. Assessment of the SASI Spectral Shape Index Time Series for Mapping Rice Ecosystems in the Mediterranean Region. *Agronomy* **2021**, *11*, 1365. [CrossRef]
4. López-Andreu, F.J.; Erena, M.; Dominguez-Gómez, J.A.; López-Morales, J.A. Sentinel-2 Images and Machine Learning as Tool for Monitoring of the Common Agricultural Policy: Calasparra Rice as a Case Study. *Agronomy* **2021**, *11*, 621. [CrossRef]
5. Aguilar, E.H.; Pando, L.G.; Sosa, G. Utilización de los índices de selección en la identificación de genotipos de arroz (*Oryza sativa* L.) tolerantes a sequía. *Producción Agropecuaria y Desarrollo Sostenible* **2017**, *2*, 11–31. [CrossRef]
6. Porras-Jorge, R.; Ramos-Fernández, L.; Ojeda-Bustamante, W.; Ontiveros-Capurata, R. Performance assessment of the AquaCrop model to estimate rice yields under alternate wetting and drying irrigation in the coast of Peru. *Sci. Agropecu.* **2020**, *11*, 309–321. [CrossRef]

7. Kucuk, C.; Taskin, G.; Erten, E. Paddy-Rice Phenology Classification Based on Machine-Learning Methods Using Multitemporal Co-Polar X-Band SAR Images. *IEEE J. Sel. Top. Appl. Earth Obs. Remote. Sens.* **2016**, *9*, 2509–2519. [CrossRef]
8. Araya, S.; Ostendorf, B.; Lyle, G.; Lewis, M. CropPhenology: An R package for extracting crop phenology from time series remotely sensed vegetation index imagery. *Ecol. Informatics* **2018**, *46*, 45–56. [CrossRef]
9. Hall, M.; Frank, E.; Holmes, G.; Pfahringer, B.; Reutemann, P.; Witten, I.H. The WEKA data mining software: An update. *SIGKDD Explor. Newsl.* **2009**, *11*, 10–18. [CrossRef]
10. Stone, M. Cross-Validatory Choice and Assessment of Statistical Predictions. *J. R. Stat. Soc. Ser. B (Methodol.)* **1974**, *36*, 111–133. [CrossRef]

Disclaimer/Publisher's Note: The statements, opinions and data contained in all publications are solely those of the individual author(s) and contributor(s) and not of MDPI and/or the editor(s). MDPI and/or the editor(s) disclaim responsibility for any injury to people or property resulting from any ideas, methods, instructions or products referred to in the content.

remote sensing

MDPI

Article

Within-Field Rice Yield Estimation Based on Sentinel-2 Satellite Data

Belen Franch [1,2,*,†], Alberto San Bautista [3,†], David Fita [3], Constanza Rubio [4], Daniel Tarrazó-Serrano [4], Antonio Sánchez [2], Sergii Skakun [2], Eric Vermote [2,5], Inbal Becker-Reshef [2] and Antonio Uris [4]

1 Global Change Unit, Image Processing Laboratory, Universitat de València, Paterna, 46980 Valencia, Spain
2 Department of Geographical Sciences, University of Maryland, College Park, MD 20742, USA; asgalve@umd.edu (A.S.); skakun@umd.edu (S.S.); eric.f.vermote@nasa.gov (E.V.); ireshef@umd.edu (I.B.-R.)
3 Departamento de Producción Vegetal, Universitat Politécnica de València, 46022 Valencia, Spain; asanbau@prv.upv.es (A.S.B.); dafisil@etsiamn.upv.es (D.F.)
4 Centro de Tecnologías Físicas, Universitat Politécnica de València, 46022 Valencia, Spain; crubiom@fis.upv.es (C.R.); dtarrazo@fis.upv.es (D.T.-S.); Auris@fis.UPV.es (A.U.)
5 NASA Goddard Space Flight Center Code 619, 8800 Greenbelt Road, Greenbelt, MD 20771, USA
* Correspondence: belen.franch@uv.es
† Both authors contributed equally to this work and should be considered co-first authors.

Abstract: Rice is considered one of the most important crops in the world. According to the Food and Agriculture Organization of the United Nations (FAO), rice production has increased significantly (156%) during the last 50 years, with a limited increase in cultivated area (24%). With the recent advances in remote sensing technologies, it is now possible to monitor rice crop production for a better understanding of its management at field scale to ultimately improve rice yields. In this work, we monitor within-field rice production of the two main rice varieties grown in Valencia (Spain) *JSendra* and *Bomba* during the 2020 season. The sowing date of both varieties was May 22–25, while the harvesting date was September 15–17 for *Bomba* and October 5–8 for *JSendra*. Rice yield data was collected over 66.03 ha (52 fields) by harvesting machines equipped with onboard sensors that determine the dry grain yield within irregular polygons of 3–7 m width. This dataset was split in two, selecting 70% of fields for training and 30% for validation purposes. Sentinel-2 surface reflectance spectral data acquired from May until September 2020 was considered over the test area at the two different spatial resolutions of 10 and 20 m. These two datasets were combined assessing the best combination of spectral reflectance bands (SR) or vegetation indices (VIs) as well as the best timing to infer final within-field yields. The results show that SR improves the performance of models with VIs. Furthermore, the correlation of each spectral band and VIs with the final yield changes with the dates and varieties. Considering the training data, the best correlation with the yields is obtained on July 4, with R^2 for *JSendra* of 0.72 at 10 m and 0.76 at 20 m resolution, while the R^2 for *Bomba* is 0.87 at 10 m and 0.92 at 20 m resolution. Based on the validation dataset, the proposed models provide within-field yield modelling Mean Absolute Error (MAE) of 0.254 t·ha^{-1} (Mean Absolute Percentage Error, MAPE, of 3.73%) for *JSendra* at 10 m (0.240 t·ha^{-1}; 3.48% at 20 m) and 0.218 t·ha^{-1} (MAPE 5.82%) for *Bomba* (0.223 t·ha^{-1}; 5.78% at 20 m) on July 4, that is three months before harvest. At parcel level the model's MAE is 0.176 t·ha^{-1} (MAPE 2.61%) for *JSendra* and 0.142 t·ha^{-1} (MAPE 4.51%) for *Bomba*. These results confirm the close correlation between the rice yield and the spectral information from satellite imagery. Additionally, these models provide a timeliness overview of underperforming areas within the field three months before the harvest where farmers can improve their management practices. Furthermore, it highlights the importance of optimum agronomic management of rice plants during the first weeks of rice cultivation (40–50 days after sowing) to achieve high yields.

Keywords: agriculture; yield; within-field; rice; remote sensing; Sentinel-2; surface reflectance

check for updates

Citation: Franch, B.; Bautista, A.S.; Fita, D.; Rubio, C.; Tarrazó-Serrano, D.; Sánchez, A.; Skakun, S.; Vermote, E.; Becker-Reshef, I.; Uris, A. Within-Field Rice Yield Estimation Based on Sentinel-2 Satellite Data. *Remote Sens.* **2021**, *13*, 4095. https://doi.org/10.3390/rs13204095

Academic Editors: Kuniaki Uto, Nicola Falco and Mauro Dalla Mura

Received: 10 September 2021
Accepted: 9 October 2021
Published: 13 October 2021

Publisher's Note: MDPI stays neutral with regard to jurisdictional claims in published maps and institutional affiliations.

Copyright: © 2021 by the authors. Licensee MDPI, Basel, Switzerland. This article is an open access article distributed under the terms and conditions of the Creative Commons Attribution (CC BY) license (https://creativecommons.org/licenses/by/4.0/).

1. Introduction

Rice (*Oryza sativa* L.) is one of the three most important crops in the world, being vital for the world's food supply. Rice is grown in Asia, America, Australia, Europe, and Africa, following diverse production practices. In 2019, the global rice production was close to 755 million tons, covering an area of 162 million hectares. In Europe, its production is mostly located in the southern countries, Spain being one of the major producers and representing approximately 28% of the total production across the European Union in 2019 [1]. The Valencian Community produces 16% (125 thousand tons) of the national rice, covering an area of approximately 15 thousand hectares in 2019 [2]. During the last 50 years, world rice production has increased by 156%, while the cultivated area has only increased by 24%, resulting in a 107% increase in yield. The evolution of world population growth and the increase in rice production have been closely connected over the last 50 years [1]. According to the latest United Nations' forecasts for the next 50 years, the world population could increase by 35% [3], which means that rice production must continue increasing. Given that the statistics of the last five decades show that the cultivated area has hardly changed, the required increase in rice production must imply an increase in yield [4].

Earth observation (EO) data allow efficient monitoring of crop growth at field scale owning to its high spatial (~10 m) and temporal (each 5 days) resolutions (e.g., [5–7]). The launch of the ESA optical high-resolution missions Sentinel-2A in 2015 and Sentinel-2B in 2017 and their fusion with Landsat providing free high-frequency and high-resolution data, along with the significant advances in big data analytics and high-performance computing, have revolutionized the EO uptake for agriculture applications. Recent works have shown that satellite data can be used to infer crop yields both within-field and at field scales. For instance, Skakun [8] showed that corn and soybean yield variability could be explained using Planet 3 m spatial resolution while the coarser resolution of Sentinel-2 (10 m) reduces the explained yield variability by 14%. The same study also concluded that the most important spectral bands explaining the yield variability are green, red edge and Near Infrared (NIR) but the lower correlation obtained for high yields suggested saturation of multi-spectral optical data. Kayad [9] investigated different Vegetation Indices (VI) from Sentinel-2 and machine learning techniques to assess corn yield within the field scale. Their study selected as the best VI the Green Normalized Difference Vegetation Index (GNDVI), which integrated into a Random Forest provided an R^2 of 0.60 over an independent validation test. Zhao [10] tested a set of VI from Sentinel-2 to estimate wheat yield at the field scale. Deines [11] applied the Scalable Crop Yield Mapper (SCYM) [12] to over one million corn fields yield observations spanning nine states in the US Corn Belt and based on Landsat observations. Their results showed that remote sensing technology at within-field scale show coefficients of determination of 0.40 and increase to 0.45 and 0.69 when aggregated to field level and county level scales, respectively.

Focusing on rice crops, the Asia-RiCE initiative [13] is the rice monitoring component of the Group on Earth Observations Global Agricultural Monitoring initiative (GEOGLAM) [14]. Its main goal is to foster the use of EO, leveraging existing agricultural monitoring programs and initiatives for rice monitoring at national, regional and global scales as an input to the GEOGLAM Crop Monitor [15] and the Agricultural Market Information System (AMIS) Market Monitor [16]. EO technologies have proven to be useful in monitoring rice crops biophysical and biochemical properties pushing towards a more efficient farming management. The implementation of remote sensing technologies in rice farming has evident advantages in monitoring rice growth, soil fertility evaluation, detection of diseases, and yield estimation, among others. Previous works have shown that the growth of the rice crops, as well as the nitrogen content, can be inferred based on the spectral reflectance from EO sensors. For instance, Cai [17] showed that the Normalized Difference Vegetation Index (NDVI) or the Green NDVI (GDVI) can be used to monitor the nitrogen content of rice crops. Shi [18] studied the use of different VIs to map the distribution of rice diseases such as rice blast. In fact, several studies (e.g. [19–21]) show that the NIR spectral region is sensitive enough to detect the first symptoms produced by rice

blast, and other studies show how remote sensing data can be used to monitor the nitrogen deficit in rice (e.g., [22,23]). Regarding rice yield monitoring, Gilardelli [24] assimilated Leaf Area Index (LAI) data from Landsat and Sentinel-2 at 30 m spatial resolution into the WARM rice model [25] to derive within-field rice yields in Italy with a Mean Absolute Error (MAE) of 0.66 t·ha^{-1} and Relative Root Mean Square Error (RRMSE) of 13.8%. Finally, an extensive overview on rice yield estimation or forecasting based on EO can be found in Mosleh [26]. One of the major challenges in rice monitoring over Asia is the high frequency of cloud coverage. Therefore, most of the works based on this area use synthetic aperture radar (SAR) for rice yield monitoring (e.g. [27–29]). Other works use optical data based on VI that are then related to forecast rice yields mostly at regional level using coarse resolution data (MODIS [30,31], SPOT-4 [32] or AVHRR [33]) or medium resolution (Landsat [34]). However, most works or rice yield monitoring are applied at regional scale or at parcel level and there are essentially no works on rice yield estimation at within-field scale. Additionally, VIs are widely used as inputs for the yield models, and Skakun [8] showed that surface reflectance-based models outperformed VI-based models highlighting the importance of incorporating surface reflectance (SR) values directly into the yield models. Therefore, in this work we aim to expand the science of rice yield monitoring at within-field scale, testing all spectral information retrieved by Sentinel-2. Particularly, the main science questions that we aim to answer in this study are: To what degree can EO data in the optical spectral region explain the rice within-field yield variability? Which spectral band or combination of bands is better correlated with the final yield? When is the most critical timing of the rice growing season when satellite imagery can explain the final yields?

In this work we present a study to monitor rice within-field yield variability. It is based on multi-spectral SR data retrieved by Sentinel-2 and rice yield maps acquired with harvesting machines over 52 fields covering a total area of 66ha in Valencia (Spain) during the 2020 season.

2. Materials and Methods

2.1. Study Area

The coastal wetland Albufera is located at the Mediterranean Spanish coast and south of Valencia city (39°20′ N, 0°21′ W). The wetland has an area of 211.2 km^2 and is bordered by the Turia (north) and Jucar (south) rivers. The Albufera is the second largest lake in the Iberian Peninsula with an area of 23.2 km^2. It is shallow (1.2 m of mean depth) and has a mean salinity of 1–2%. The European Commission [35] considers the Albufera a special protected area in the Natura 2000 network and restricts agriculture practices in the area to only rice crops. This area has a typical Mediterranean climate, with an annual mean air temperature and humidity of 18.3 ± 0.1 °C and 65.0 ± 0.5%, respectively [36]. Annual rainfall is usually concentrated in the spring and autumn seasons. The water level of the lake is regulated by a large network of irrigation channels that connect it to the rice fields and to the Mediterranean Sea. This area can be considered a homogeneous rice planting area of approximately 10 × 20 km^2 extension.

JSendra and *Bomba* common japonica-type Spanish rice varieties (*Oryza sativa* var.*japonica*), were used in the experiment. The most commercial cultivar in East Spain (Valencia) is *JSendra* (cross between *M202* and *Senia* in 2005 by Instituto Valenciano de Investigaciones Agrarias, IVIA), characterized by high yields (typically 7.5–8.0 t·ha^{-1}) and good culinary quality. *Bomba* is a traditional rice variety, obtained by selection in 1929 in Valencia, and it is characterized by low yields (typically 3.5–4.0 t·ha^{-1}) and excellent culinary quality. The differences in performance between the two varieties are significant: *JSendra* plants have a greater number of tillers, a lower height, and a longer season than *Bomba* plants. The planted area of *JSendra* in 2020 was 6716 ha (44%), while in *Bomba*'s planted area was 1777 ha (12%). Table 1 shows the timing of the main stages of both varieties in Valencia.

Table 1. Timing of the main phenological stages of rice in Valencia.

No Cultivation				Sowing		Growing			Harvest		No Cultivation	
						Vegetative	Reproductive	Ripening				
Flooded		Dry		Flooded					Dry		Flooded	
Jan	Feb	Mar	Apr	May	Jun	Jul	Aug		Sep	Oct	Nov	Dec

2.2. Field Data Pre-Processing

Field data was collected by harvesting machines and provide dry volumetric yield in irregular polygons as shown in Figure 1A. These data were preprocessed to remove errors in the software acquisition such as turns, overlaps (keeping the first overpass) and extreme values (*JSendra*: >11.0 t·ha^{-1}; *Bomba*: >7.0 t·ha^{-1}) that had no biological meaning [37]. Additionally, we removed small sized polygons with extreme values compared to the neighbors [38]. Given the noise observed in the dataset, these data were aggregated to an intermediate 5 m resolution (Figure 1B) to apply a grid moving average filter of 7 × 7 pixels (Figure 1C). Finally, this dataset was aggregated to 10 m resolution removing the edge pixels (Figure 1D).

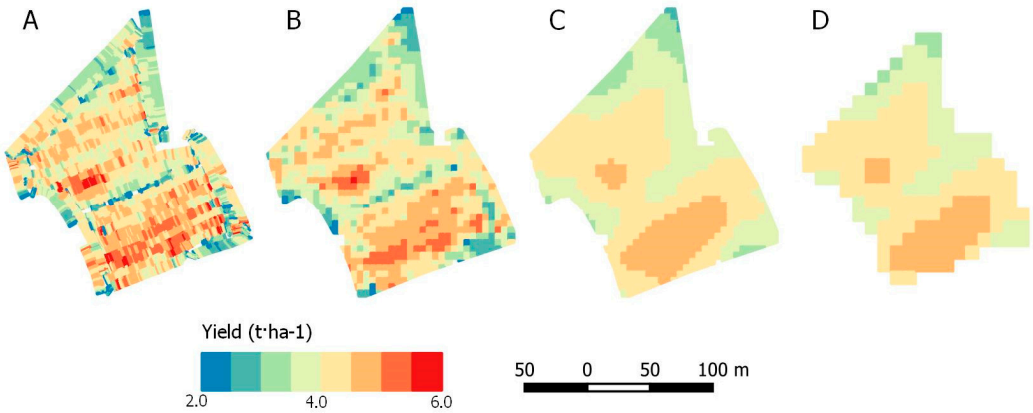


Figure 1. Example of the harvester data curation of a *Bomba* rice field within the training samples being (**A**) the original harvester machine data, (**B**) the 5 m aggregated data, (**C**) the 5 m aggregated data after applying the grid moving average filter and (**D**) picture C aggregated to 10 m.

2.3. Satellite Data

We downloaded Sentinel-2A and Sentinel-2B data covering the main rice area in Valencia, that is using the tiles 30SYJ and 31SBD, from May until September 2020 and we applied the atmospheric correction algorithm LaSRC [39]. All the Sentinel-2 spectral bands at 10 m and 20 m spatial resolution were analyzed to select the best combination to infer rice crop yield. Table 2 shows the spectral response and spatial resolution of the considered bands.

2.4. Methods

The two rice varieties were treated separately. For each variety, 70% of the data was randomly selected as training data and 30% of data was kept for validation purposes (Table 3). Additionally, Figure 2 shows the spatial distribution of the datasets.

Table 2. Sentinel-2 bands analyzed in this study.

Band Name	Central Wavelength (nm)	Spatial Resolution (m)
B02-Blue	490	10
B03-Green	560	10
B04-Red	665	10
B05-Vegetation Red Edge 1	705	20
B06-Vegetation Red Edge 2	740	20
B07-Vegetation Red Edge 3	783	20
B08-NIR	842	10
B8A-NIR 2	865	20
B11-SWIR 1	1610	20
B12-SWIR 2	2190	20

Table 3. Field data dissemination to build and evaluate the algorithms (the number of pixels was obtained at 10 m (20 m in parenthesis)).

	Training			Validation		
Variety	**Area (ha)**	**Number of Pixels**	**Number of Fields**	**Area (ha)**	**Number of Pixels**	**Number of Fields**
JSendra	34.93	2439 (531)	25	15.48	980 (205)	13
Bomba	10.74	801 (163)	8	4.88	328 (64)	6

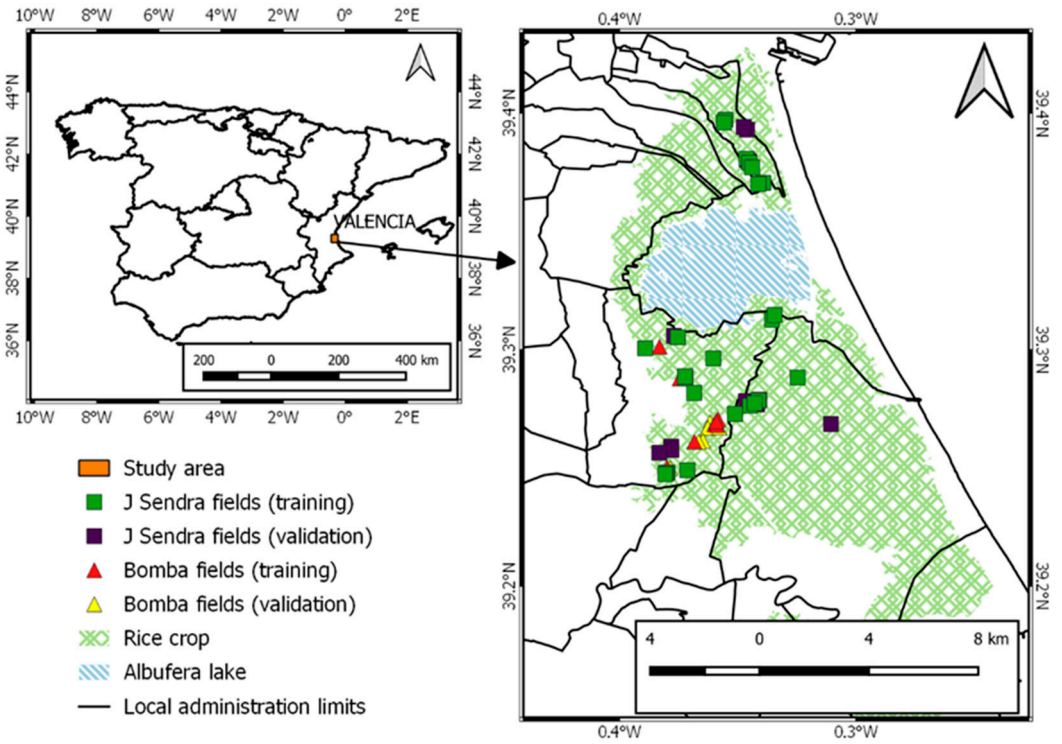


Figure 2. Location of the rice fields analyzed in this study.

Each date and spatial resolution were analyzed independently, looking for the best combination that provided the best performance metrics against the yield values. Additionally, multivariable linear regressions were built between yields at pixel level and their corresponding surface reflectance values of a given band, interactions between bands and vegetation indices (Appendix C). Specifically, when combining all bands at each spatial resolution, the following equation was tested to derive the yield of pixel i:

$$y_{est} = a_0 + a_1 \cdot x_1 + a_2 \cdot x_2 + a_3 \cdot x_3 + \cdots + a_n \cdot x_n \quad (1)$$

where y_{est} is the estimated yield; a_0, a_1, a_2, a_3, a_n are the model coefficients; and x_1, x_2, x_3, x_n are the surface reflectance (SR) spectral bands, vegetation index (VI) or the interaction between the different SR for a given date of the growing season.

The software StatGraphics Centurion XVII (v.17.2.00) [40] was implemented to determine the best combination of SR on equation 1, using a stepwise regression method, for each date, spatial resolution, and variety.

Finally, the following performance metrics were derived based on the validation data: the coefficient of determination (R^2); the Mean Absolute Error (MAE); and the Mean Absolute Percentage Error (MAPE).

$$R^2 = 1 - \frac{\sum_{i=1}^{n}\left(y_{est} - y_{ref}\right)^2}{\sum_{i=1}^{n}\left(\overline{y}_{ref} - y_{ref}\right)^2} \quad (2)$$

$$MAE = \frac{\sum_{i=1}^{n}\left|y_{est} - y_{ref}\right|}{n} \quad (3)$$

$$MAPE = \frac{100}{n}\sum_{i=1}^{n}\left|\frac{y_{est} - y_{ref}}{y_{ref}}\right| \quad (4)$$

These performance metrics of each model based on a spectral band or combination of bands. Finally, each of the variables were validated with a linear regression analysis to test the statistical significance of each factor with a probability $p < 0.05$, according to the Student's *t*-test. The linear model was validated with the Snedecor statistical *F*-test ($p < 0.05$).

The processing of the yield maps and the satellite images, as well as the validation, was carried out with the QGIS 3.10.14 software [41].

3. Results

3.1. Evaluation at Within-Field Level in JSendra Rice

The *JSendra* fields' coefficient of determination evolution for each Sentinel-2 spectral band at 10 m (Figure A1a) and at 20 m (Figure A1b) spatial resolution is analyzed in Appendix A. These results include the R^2 temporal evolution of three simple linear regression models combining the different spectral bands (M1S in Figure A1a and M2S and M3S in Figure A1b). Note that the R^2 values studied represent all within-field pixels of the *JSendra* training data. The models can be written as:

$$M1S: \; y_{est} = a_0 + a_1 \cdot B2 + a_2 \cdot B3 + a_3 \cdot B4 + a_4 \cdot B8 \; (10\text{ m})$$

$$M2S: \; y_{est} = a_0 + a_1 \cdot B2 + a_2 \cdot B3 + a_3 \cdot B4 + a_4 \cdot B8 \; (20\text{ m})$$

$$M3S: \; y_{est} = a_0 + a_1 \cdot B2 + a_2 \cdot B3 + a_3 \cdot B4 + a_4 \cdot B5 + a_5 \cdot B6 + a_6 \cdot B7 + a_7 \cdot B8 + a_8 \cdot B8A + a_9 \cdot B11 + a_{10} \cdot B12 \; (20\text{ m})$$

where the spatial resolution is specified in parenthesis and the model coefficients are different for each equation and for each date.

Figure A1a shows that at 10 m, the band that shows the highest correlation with the yield is B8 (NIR), followed by B2 (Blue) and B3 (Green), while B4 (Red) shows the lowest correlation. At 20 m (Figure A1b), B8A shows the highest correlation, followed by B8 and B7 (Red edge) whose evolution is very close to B6 (Red edge), but has a minor peak at the beginning of the season. Other bands, such B11 and B12 (SWIR), show some lower peaks of correlation, having only one significant peak on July 4. Visible bands show a similar tendency compared to 10 m resolution and B5 (Red edge) is very close to B4 (Red). The linear models combining spectral bands (M1S, M2S and M3S) show the best correlation, which is consistent with previous works utilizing remote sensing data to infer within-field maize and soybean yields [8]. The best performance (based on the coefficient

of determination evolution) happens on July 4 for both spatial resolutions, that is when rice is in the tillering phase. Comparing the performance at 10 m and 20 m the coefficient of determination remains almost the same and shows an equivalent evolution.

Focusing on July 4, Figure 3 shows the average spectral response of each band, splitting all training data into nine yield ranges. Note that we preserved the spatial resolution of each band. B6, B7, B8A and specially B8 show the largest differences amongst yield ranges by increasing their reflectance values with the yield.

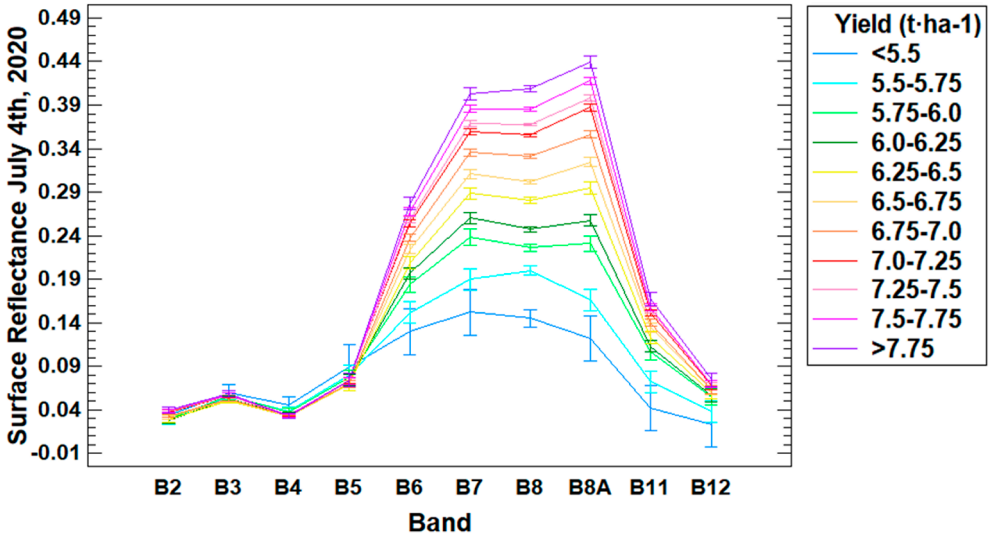


Figure 3. Surface reflectance average values for each Sentinel-2 band grouping all pixels of the *JSendra* training data within the yield range specified in the legend (the vertical bars indicate the LSD interval ($p < 0.05$) for the separation of means).

Next, Tables A1 and A2 (Appendix B) show the performance metrics of each model at 10 m and 20 m spatial resolution, respectively, focusing on the tillering phase and based on the training data. This phenological stage has been determined in the previous results as critical to monitor rice yield. Three Sentinel-2 acquisition dates were selected to analyze the performance metrics of each model: the date of the R^2 peak (July 4), the previous date (June 29) and the next one (July 19). Note that in these tables, models consisting in bands are built based on a linear regression of said band or combination of band. Additionally, the tables show the performance metrics of three models (M1S+, M2S+ and M3S+) whose definition is based on a stepwise regression program (StatGraphics). These models are written as:

$$\text{M1S+}: \; y_{est} = a_0 + a_1 \cdot B4 + a_2 \cdot \frac{B3}{B4} + a_3 \cdot \frac{B2}{B8} + a_4 \cdot \frac{B3}{B2} \; (10 \text{ m})$$

$$\text{M2S+}: \; y_{est} = a_0 + a_1 \cdot B4 + a_2 \cdot \frac{B3}{B4} + a_3 \cdot \frac{B2}{B8} + a_4 \cdot \frac{B3}{B2} \; (20 \text{ m})$$

$$\text{M3S+}: \; y_{est} = a_0 + a_1 \cdot B4 + a_2 \cdot \frac{B3}{B4} + a_3 \cdot \frac{B2}{B8} + a_4 \cdot \frac{B3}{B2} + a_5 \cdot B6 + a_6 \cdot B7 \; (20 \text{ m})$$

where the spatial resolution is specified in parenthesis and the model coefficients are different for each equation and for each date. As a summary of the results, Table 4 shows the evaluation of the best performing models for each date and spatial resolution.

The best performing models at 10 m are M1S and M1S+, which combine the four bands (B2, B3, B4 and B8). In relation to 20 m, the best performing models are M3S, M2S+ and M3S+. Comparing the dates, July 4 observations provide the best performance metrics, showing R^2 greater than 0.70, MAPEs lower than 4% (<3% at 20 m) and MAEs ranging from 0.20–0.25 t·ha^{-1}. In relation to the VIs (based on visible, NIR, Red edge and SWIR regions), they do not improve considerably the spectral bands or linear combinations of bands with higher R^2 (data, equations and references are shown in Appendix C). The best

results for VIs are obtained with the Rice Growth Vegetation Index (RGVI) (R^2 = 0.66). Appendix D shows an example at 10 m and 20 m of a reference yield map, each spectral band, and the modeled yield.

Table 4. *JSendra* best model evaluation for each date and spatial resolution with training data.

		29 June 2020			04 July 2020			19 July 2020		
Model	**Spatial Resolution (m)**	**R^2**	**MAE (t·ha^{-1})**	**MAPE (%)**	**R^2**	**MAE (t·ha^{-1})**	**MAPE (%)**	**R^2**	**MAE (t·ha^{-1})**	**MAPE (%)**
M1S+	10	0.64	0.258	3.75	0.72	0.234	3.36	0.63	0.263	3.81
M3S+	20	0.69	0.237	3.41	0.76	0.204	2.92	0.70	0.232	3.35

Finally, Figure 4 shows the evaluation of the best performing models (M1S and M1S+ at 10 m and M3S and M3S+ at 20 m) for the *JSendra* variety on July 4 considering all data from the validation fields for each spatial resolution. M1S+ and M3S+ provide a yield modelling error (MAE) of 0.254 t·ha^{-1} (3.73%) and 0.240 t·ha^{-1} (3.48%), respectively, which is aligned with the statistics shown on the training data. In fact, 60% of all pixels evaluated presented a difference between modelled and referenced yield lower than the MAE value, with a maximum difference of 1.0 t·ha^{-1} and with only 10% of data exceeding a difference of 0.50 t·ha^{-1}. Additionally, Figure 4 (right) shows the performance metrics of the models without interactions at a spatial resolution of 10 m (M1S) and 20 m (M3S). The performance metrics (MAE of 0.318 t·ha^{-1} (4.71%) at 10 m and 0.305 t·ha^{-1} (4.50%) at 20 m) show worse results than on the training data modelling, which suggests that the interactions proposed in M1S+ and M3S+ models provide a better consistency and applicability. Finally, we tested a Random Forest model considering all bands from the training data as inputs and evaluating its performance with the validation data. This model provides an R^2 of 0.79 and MAE of 0.292 t·ha^{-1} (4.33%) at 10 m and R^2 of 0.78 and MAE of 0.302 t·ha^{-1} (4.46%) at 20 m. These statistics are equivalent to M1S+ and M3S+.

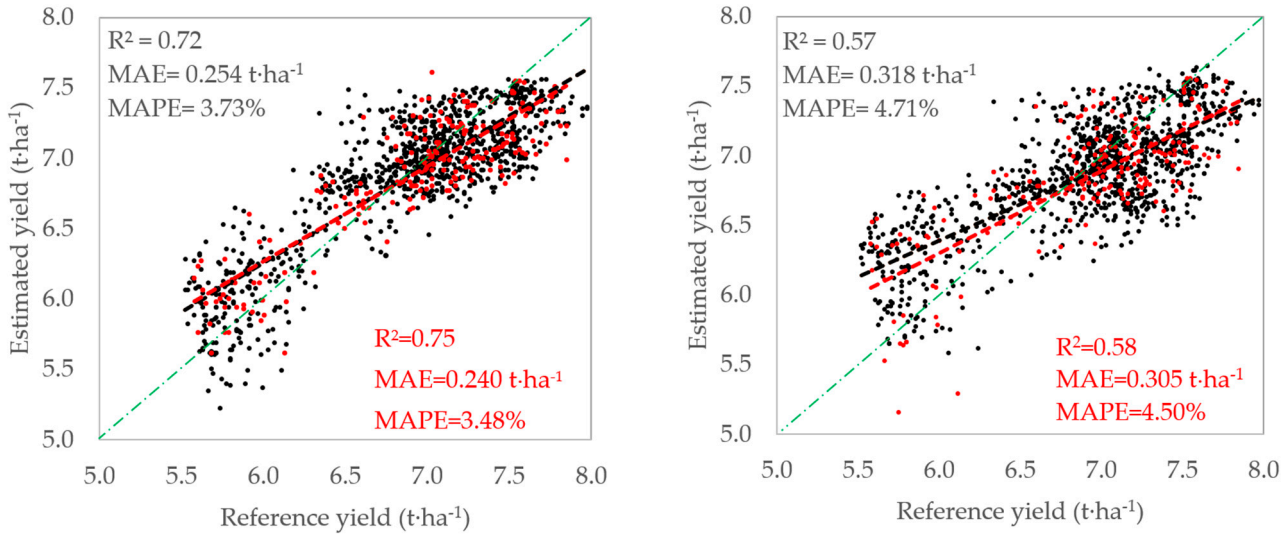


Figure 4. Validation of the *JSendra* models on July 4 at validation area: M1S+ (black) and M3S+ (red) (**left**); M1S (black) and M3S (red) (**right**).

3.2. Evaluation at Within-Field Level in Bomba Rice

Focusing now on the *Bomba* variety, Figure A2 (Appendix A) shows the coefficient of determination evolution along the rice season for each Sentinel-2 band acquisition at 10 m (Figure A2a) and at 20 m (Figure A2b) spatial resolution considering the training data. Additionally, the figures include the R^2 for three models which linearly combine all bands, following the same structure than the models described in *JSendra* (M1S, M2S and M3S)

but changing the model coefficients. Thus, for *Bomba* these equations are named M1B, M2B and M3B (M1B in Figure A2a and M2B and M3B in Figure A2b). Note that *Bomba* rice was harvested by mid-September, thus latter dates are excluded in the plot.

In this case, there are two dates with the maximum correlation at 10 m and 20 m, July 4 and August 28, although the latter includes half the number of pixels than the former. Analogously to *JSendra*, the results are similar at both spatial resolutions. However, in *Bomba* rice the visible bands (B2, B3, B4) show the best correlation with the final yields on July 4. B5 shows a very similar performance to the visible bands, and even improves and anticipates the correlation peak with the final yield on June 29. Furthermore, these bands keep a high R^2 throughout July and decrease in August (when the flowering stage happens). Additionally, B3 (Green) and B5 show an acceptable value of R^2 on August 28. On the contrary, the NIR bands show poor correlation on July 4, which is improved by mid-season (end of July), and finally shows an R^2 peak on August 28. Analogously to *JSendra*, B8, B8A and B7 present very similar results. B6 shows an equivalent evolution to these bands but with a poor correlation during mid-season. Regarding the SWIR bands, at the beginning of the season they show a small correlation peak which decreases until reaching a minimum by the end of June and then improves again, reaching a peak by the end of July which is comparable to the visible bands' correlation. Finally, the models M1B, M2B and M3B show the best performance.

Focusing on July 4, Figure 5 shows the average spectral surface reflectance for all pixels within the training fields splitting them by yield ranges. In this variety and date, the visible bands (specially B3) have a larger separability showing lower SR values for higher yields. Otherwise, the NIR, Red edge and SWIR reflectance do not show a clear dependency with the yield.

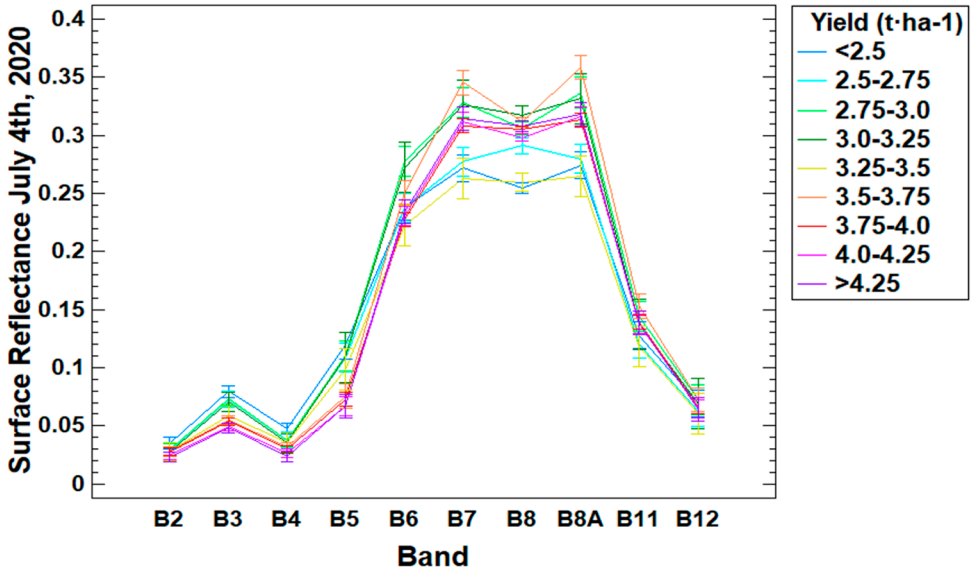


Figure 5. Surface reflectance average values for each Sentinel-2 band grouping all pixels of the *Bomba* training data within the yield range specified in the legend (the vertical bars indicate the LSD interval ($p < 0.05$) for the separation of means).

Next, Tables A3 and A4 (Appendix B) show the performance metrics of each model at 10 m and 20 m spatial resolution respectively, focusing on the same dates as in *JSendra*. These three dates are essential for a forecast, since tillering is still being defined and it is still possible to modify crop management to improve final yields. Models are built and shown based on the same principles as in the *JSendra* variety. The resulting models of the stepwise regression program (StatGraphics), M1B+, M2B+ and M3B+ are defined as:

$$\text{M1B+}: \; y_{est} = a_0 + a_1 \cdot B2 + a_2 \cdot \frac{B3}{B4} + a_3 \cdot B2 \cdot B3 \; (10\text{ m})$$

$$\text{M2B+}: \; y_{est} = a_0 + a_1 \cdot B2 + a_2 \cdot \frac{B3}{B4} + a_3 \cdot B2 \cdot B3 \; (20 \text{ m})$$

$$\text{M3B+}: \; y_{est} = a_0 + a_1 \cdot B2 + a_2 \cdot \frac{B3}{B4} + a_3 \cdot B2 \cdot B3 + a_4 \cdot B12 + a_5 \cdot B11 \cdot B12 \; (20 \text{ m})$$

where the spatial resolution is specified in parenthesis and the model coefficients are different for each equation and for each date. As a summary of the results, the Table 5 shows the evaluation of the best models for each date and spatial resolution.

Table 5. *Bomba* best model evaluation for each date and spatial resolution with training data.

		29 June 2020			04 July 2020			19 July 2020		
Model	**Spatial Resolution (m)**	**R^2**	**MAE (t·ha^{-1})**	**MAPE (%)**	**R^2**	**MAE (t·ha^{-1})**	**MAPE (%)**	**R^2**	**MAE (t·ha^{-1})**	**MAPE (%)**
M1B+	10	0.75	0.288	10.08	0.87	0.229	7.37	0.8	0.266	9.59
M3B+	20	0.87	0.223	7.67	0.92	0.175	5.74	0.88	0.222	7.77

Comparing the dates, July 4 observations provide the best performance metrics, showing an R^2 greater than 0.85, MAPEs lower than 8% (<6% at 20 m) and MAEs ranging from 0.18–0.23 t·ha^{-1}. The best model at 10 m is M1B+, that is the model including B2, B3, B4 and their interactions. Note that this model does not include the NIR band. Additionally, model M1B shows similar results to the simple linear model without the NIR band ($a_0 + a_1 \cdot B2 + a_2 \cdot B3 + a_3 \cdot B4$). At 20 m, M2B+ and M3B+ show the best performance metrics. Note that M2B+, which depends only on B2 and B3, shows similar performance metrics to M3B+ (that depends on B2, B3, B11 and B12) and M3B (that includes all bands). Additionally, it is important to note that B3 (Green) and B5 individually show excellent results. Regarding VIs, the best performance is obtained using the Normalized Difference Red Edge 2 (NDRE2) (R^2 = 0.59). All the performance metrics of the VIs tested, their equations and references can be found in Appendix C. Analogously to the *JSendra* section, Appendix D shows an example at 10 m and 20 m of a reference yield map, each spectral band, and the modeled yield.

Figure 6 (left) shows the validation of the best performance models (M1B+ and M3B+) for the *Bomba* variety on July 4 considering the validation fields. These results show that the proposed models M1B+ and M3B+ provide a MAE of 0.218 t·ha^{-1} (5.82%) and 0.223 t·ha^{-1} (5.78%), respectively. A total of 60% of pixels presented a difference between modelled and referenced yield lower than the MAE, being the maximum difference around 0.80 t·ha^{-1}, with only 9% of data exceeding a difference of 0.50 t·ha^{-1}. Note that the differences in MAPE between varieties were due to their corresponding average yields, being 3.8 t·ha^{-1} for *Bomba* and 7.0 t·ha^{-1} for *JSendra* in the studied area. The validation results of M1B and M3B are shown in Figure 6 (right) (MAE of 0.261 t·ha^{-1} (6.93%) at 10 m and 0.273 t·ha^{-1} (7.17%) at 20 m) and are slightly worse than M1B+ and M3B+, respectively. The decrease in R^2 when compared to the training data evaluation is caused by the limited yield variability in the validation pixels (between 2.5 and 5.0 t·ha^{-1}) compared to the training pixels (between 0.8 and 5.0 t·ha^{-1}). Note that this is not the case in *JSendra*, where the training and validation pixels show similar variability (5.5–8.0 t·ha^{-1}). Finally, a Random Forest algorithm based on the same dataset provides a R^2 of 0.71 and MAE of 0.287 t·ha^{-1} (7.67%) at 10 m and R^2 of 0.67 and MAE of 0.297 t·ha^{-1} (7.69%) at 20 m. These performance metrics are worse than the previous models based on linear regressions (M1B+, M3B+, M1B and M3B).

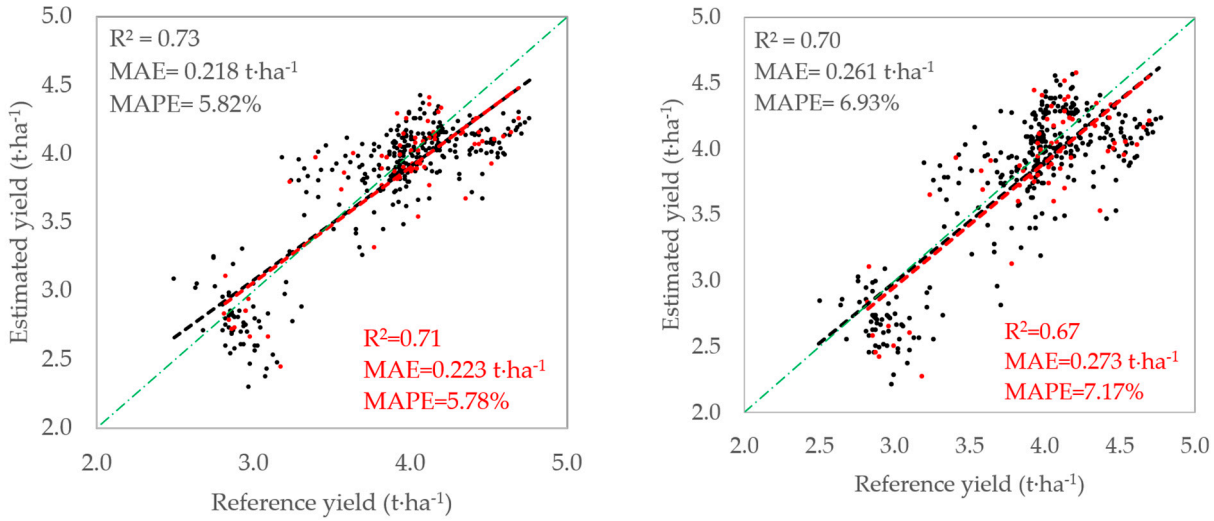


Figure 6. Validation of the *Bomba* models on July 4 at validation area: M1B+ (black) and M3B+ (red) (**left**); M1B (black) and M3B (red) (**right**).

3.3. Evaluation at Parcel Level

Finally, Figure 7 shows the evaluation of the model at parcel level by aggregating at this scale the pixel level estimations at 10 m based on models M1S+ for *JSendra* (left) and M1B+ for *Bomba* (right) on July 4, and the harvester machine measurements through all validation fields. These plots show a very good agreement with a MAE of 0.176 t·ha^{-1} and 2.61% MAPE for *JSendra*; and a MAE of 0.142 t·ha^{-1} and 4.51% MAPE for *Bomba*.

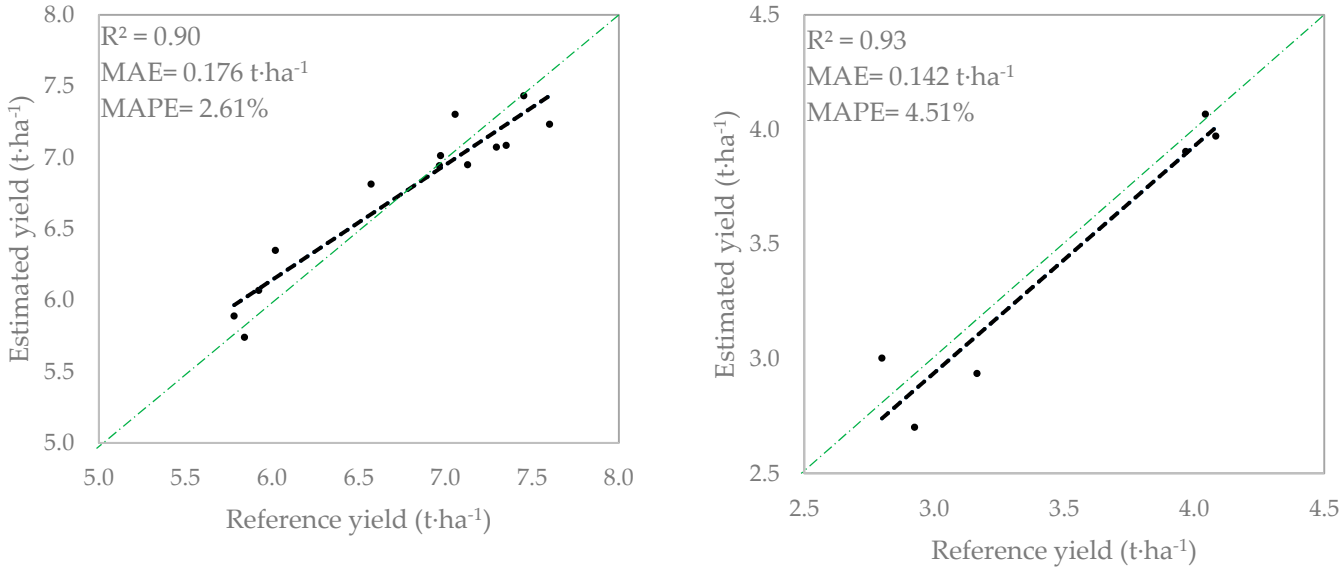


Figure 7. Validation at parcel level of the *JSendra* fields (**left**) and *Bomba* fields (**right**).

4. Discussion

In this work we analyze the rice yield dependency on the spectral information provided by Sentinel-2 satellite image acquisitions prior to harvest. To do so, an extensive dataset of harvester machine measurements of within-field yield during the 2020 campaign is preprocessed and linked to the pixel level surface reflectance retrievals considering all Sentinel-2 spectral bands. The two major rice varieties planted in the Albufera region have been analyzed: *JSendra* and *Bomba*.

First of all, it is worth noting the high variability of within-field yields despite the limited size of the Valencian fields (areas around 1 ha). In the few examples that we show

in this work, even at 10 m resolution and after applying the grid moving average filter to the harvester machine data, the variability of yields can get up to 2.5 t·ha^{-1}, highlighting underperforming areas within the field. Given that all areas within a field are managed in the same manner, empirical models are the only feasible solution to model such variability. Looking at the plots of the coefficient of determination's seasonal evolution of each band against the final yield, two periods with maximum values of R^2 can be identified in both varieties. There is a first period, when the crop is ending the vegetation stage and a second period, when the crop is ending the maturity stage. Both periods are preceded and followed by a decrease of R^2. During the first month after the start of season (until end of June) there is barely correlation of the spectral information with the final yield given the reduced size of the rice plants and their signal mixture with water (we need to keep in mind that Valencian rice remains flooded during most of the season). By the beginning of July, the highest correlation is achieved in both varieties. This might be a consequence of the higher density of vegetation and the minimization of the water background signal. During this period, rice plants are in the tillering stage. Tillering is one of the fundamental rice stages defining the final yield since it determines the number of productive tillers per plant which in turn determine the number of grains and their weight. During this phase, the importance of each spectral region is very different among both varieties. *JSendra* shows a stronger correlation of NIR bands with the yield while *Bomba* shows a larger R^2 with visible bands and band 5 (red edge). This might be a consequence of the agronomic characteristics of each variety. While *JSendra* plants are denser but smaller in size, *Bomba* plants are thinner and have a lighter green color. The higher NIR importance in *JSendra* during this stage might be linked to the positive impact in the final yield of denser fields or areas within the field. Besides, when monitoring vegetation, visible band spectral response is linked to the leaf pigments performance. In particular, Feng [42] showed that band 5 (red edge) is correlated with the chlorophyll-a content during the rice tillering stage. Therefore, the higher importance of this spectral region in *Bomba* final yields might highlight the dependency of the yield with the chlorophyll-a content during tillering. From mid-July until mid-August the NDVI reaches its maximum in both varieties and remains high and stable. During this period the plant remains in the reproductive stage. By mid-August, the coefficient of determination that decreases during the reproductive stage reaches a minimum value. This could be caused by mixing different fields with different phenological stages, where some areas remain in the reproductive stage while others enter the ripening stage. It could also be a consequence of the mixing signal from the springs. By the end of August there is another R^2 peak for both varieties. The *JSendra* variety shows a stronger correlation of visible bands (and specially the green band) with the final yield. The importance of the visible bands at the ripening stage might differ in those fields that enter the senescence phase earlier compared to those that remain green longer, which may enhance final yields. Regarding *Bomba*, NIR bands are predominant during this stage. However, looking at the number of pixels covered during this second peak of correlation, which is reduced to 20% in *JSendra* and 50% in *Bomba*, and considering its proximity to harvest, this second date has not been considered to build the forecast model. Finally, comparing the performance metrics of modeled rice yield with different VIs and SR data supports the findings in Skakun [8] in corn and soybean, that is SR-based models outperform VI-based models to monitor rice yields.

We also studied different models to correlate yield with the spectral surface reflectance. The simplest model is the linear regression of all bands both at 10 m and at 20 m spatial resolution. Besides, the models proposed by a stepwise regression model (StatGraphics), linearly combine the spectral bands but add some multiplicative terms or band ratios. The results show a similar performance by both models on the training samples, but when applied to the validation samples, the StatGraphics model outperform the linear regression models. Overall, and based on the available dataset and the particular year analyzed, the best statistics can be achieved on July 4 with an error of 0.254 t·ha^{-1} (3.73%) for *JSendra* and 0.218 t·ha^{-1} (5.82%) for *Bomba* rice based on the 10 m spatial resolution

data. The 20 m resolution analysis, despite adding more spectral information, shows very similar performance metrics. At parcel level the proposed models provide a MAE of 0.176 t·ha^{-1} (2.61% MAPE) for *JSendra* and a MAE of 0.142 t·ha^{-1} (4.51% MAPE) for *Bomba*. More complex relationships were also tested using a Random Forest algorithm, providing equivalent results to the linear regression models in *JSendra* rice and worse results in *Bomba* rice (given the lower number of samples). Therefore, given the simplicity of linear models, which allow a better interpretation of the inputs considered, we propose using linear models to monitor within-field rice yield.

Finally, we need to highlight that despite the good performance metrics obtained, Figures 4 and 6 (validation plots) and the examples in Appendix D, show that extreme yield values are smoothed out by the models, that is overestimation of low yields and underestimation of high yields. This might be a consequence of the uncertainties of the harvester machine. This is consistent with previous studies [8–10].

As a summary and addressing the science questions stated in the Introduction Section, the most critical timing when EO data is better correlated with the final rice yield for both varieties is the beginning of July during the rice tillering stage. The best bands that explain the within-field yield variability are the NIR bands for *JSendra* and visible and red edge (B5) for *Bomba*. The proposed models based uniquely on EO data provide accuracies of 0.22–0.25 t·ha^{-1} at within-field scale and 0.14–0.17 t·ha^{-1} at parcel level.

These models were developed considering as a reference yields from a particular year (2020) and a limited sized area where meteorological conditions can be considered constant so no meteorological data could be integrated. Therefore, these models are expected to work on those years with similar meteorological conditions. To solve this limitation, future works will integrate both EO and meteorological data of forthcoming seasons.

5. Conclusions

In this work we analyzed the use of remote sensing data to monitor rice yield. To do so we leveraged an extensive within-field rice yield dataset covering 66 ha of the two major rice varieties planted in Valencia, *JSendra* and *Bomba*. The results showed very different correlation of the spectral bands with the final yields, depending on the variety and phenology. During the vegetation stage, the NIR bands showed a stronger correlation in *JSendra*, whereas the visible bands showed a higher importance in *Bomba* rice. On the contrary, during the maturity stage, *JSendra* yield is better correlated with the visible bands while *Bomba* yields show higher R^2 with the NIR bands. These results highlight the need for discriminating between the two varieties to generate EO-based yield models. The proposed model allows a within-field yield forecast error with a MAE of 0.254 t·ha^{-1} (3.73%) for *JSendra* and 0.218 t·ha^{-1} (5.82%) for *Bomba* on July 4th and parcel level MAE of 0.176 t·ha^{-1} (2.61% MAPE) for *JSendra* and a MAE of 0.142 t·ha^{-1} (4.51% MAPE) for *Bomba*. This date coincides with the rice tillering stage and underlines the importance of achieving a good performance of the plants during this stage. Therefore, agronomic decisions in crop management before this stage are critical to improve rice yield. Additionally, these estimations are about three months prior to harvest and provide enough time for improving the rice management towards more direct interventions of those areas that already show any underperformance in plant nutrition (or diseases control) during the tillering stage, thus advancing the science of precision agriculture.

Author Contributions: Conceptualization and methodology, B.F., A.S.B. and C.R.; formal analysis and investigation, D.F., D.T.-S., A.S.; resources, B.F., A.S.B.; data curation, B.F., A.S.B., C.R., S.S., E.V.; writing—original draft preparation, B.F.; writing—review and editing, B.F., A.S.B., D.F., C.R., D.T.-S., A.S., S.S., E.V., I.B.-R., A.U.; supervision, B.F., C.R. All authors have read and agreed to the published version of the manuscript.

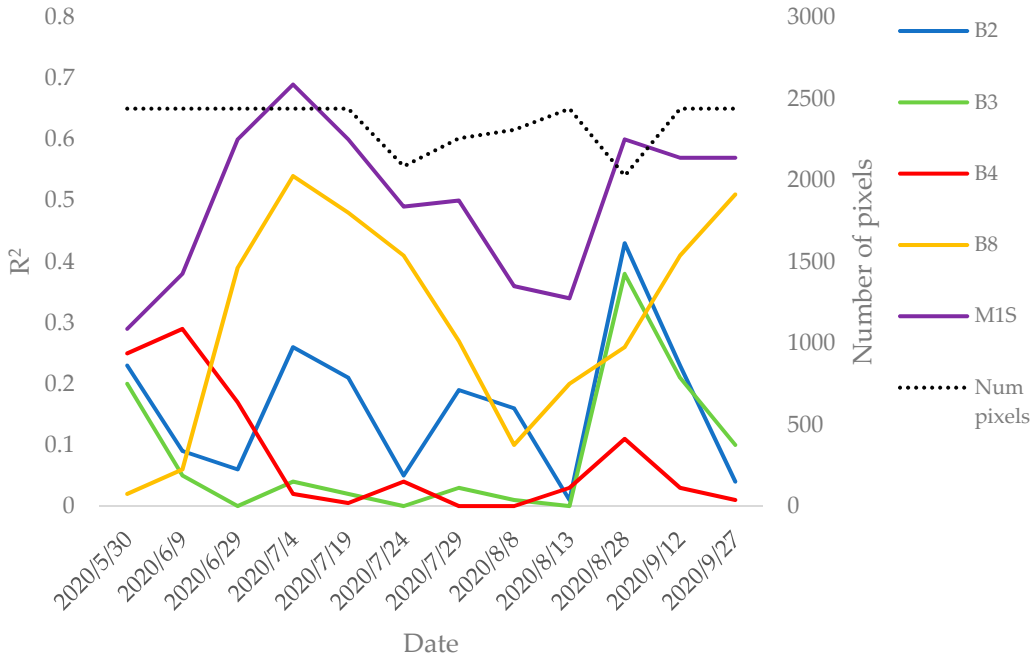
Funding: This research was partially funded by the program Generacio Talent of Generalitat Valenciana (CIDEGENT/2018/009).

Informed Consent Statement: Not applicable.

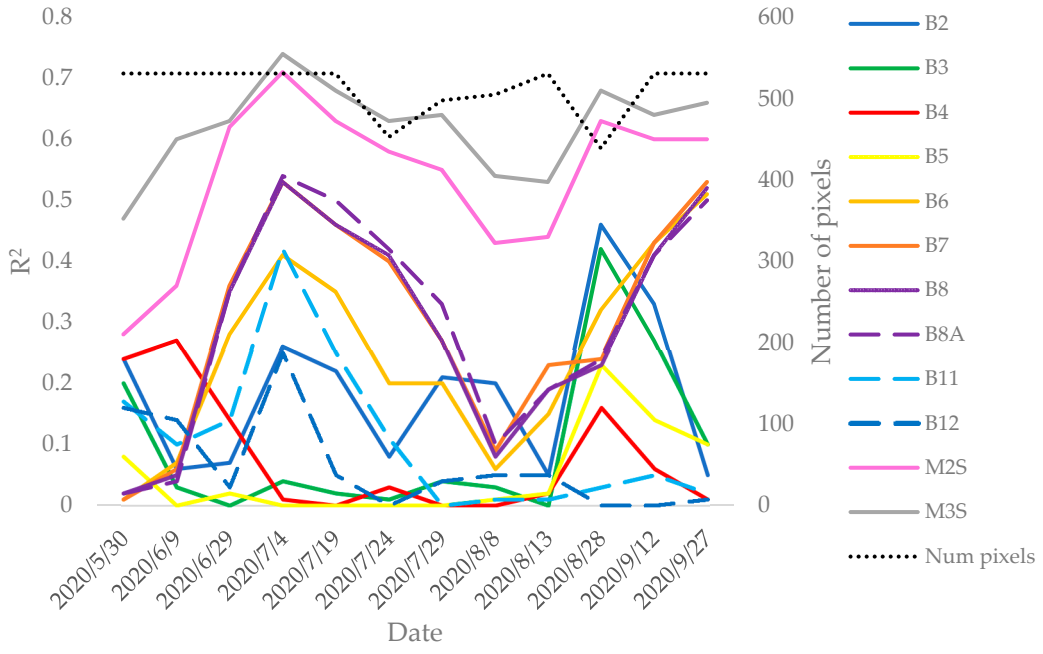
Acknowledgments: We acknowledge the program Generacio Talent of Generalitat Valenciana (CIDEGENT/2018/009).

Conflicts of Interest: The authors declare no conflict of interest.

Appendix A

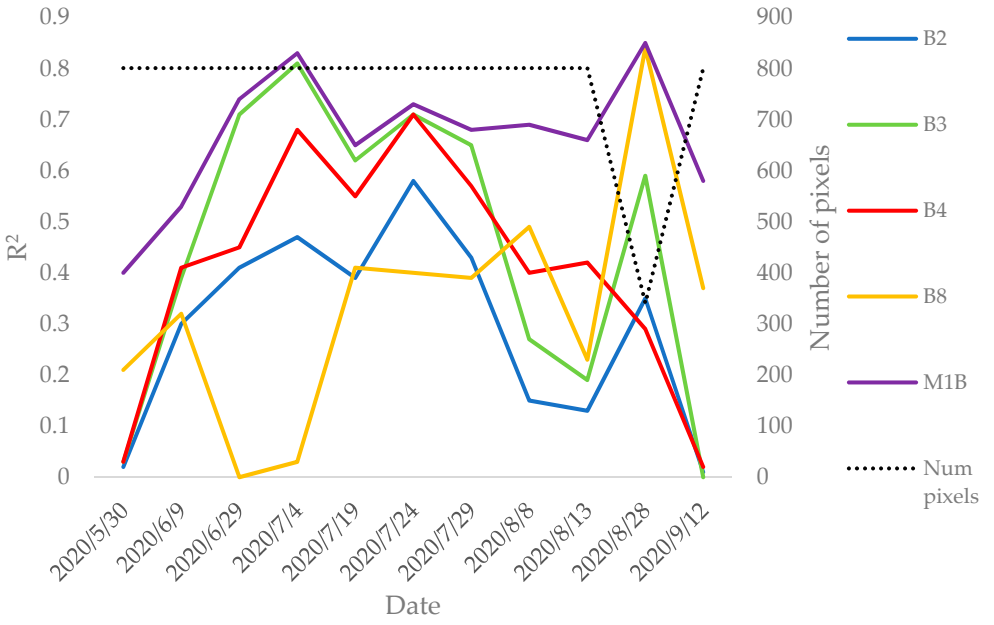


(**a**)

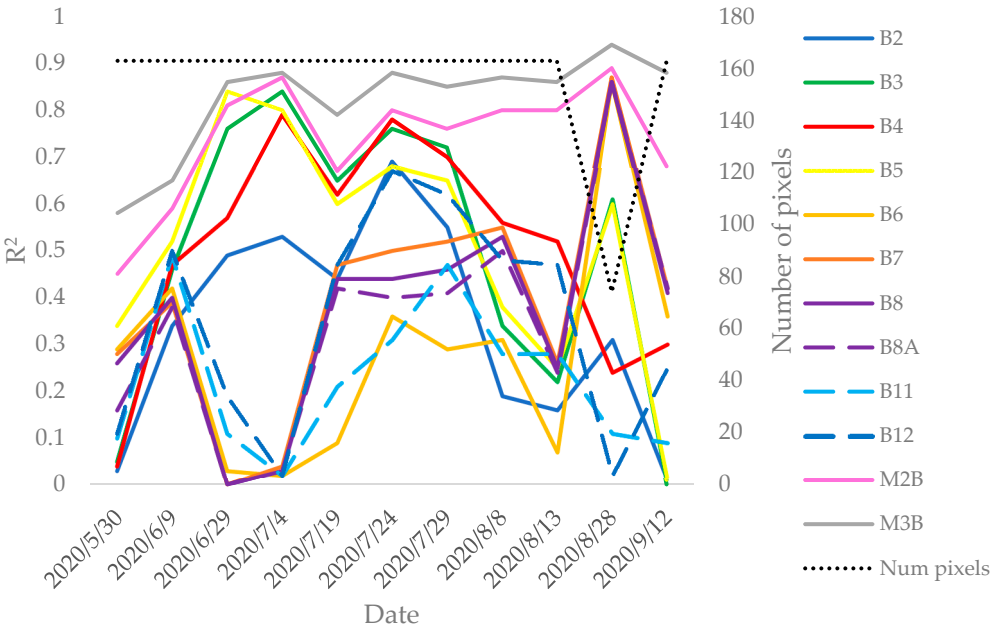


(**b**)

Figure A1. Coefficient of determination timeseries evolution focusing on *JSendra* training data of each band at 10 m (**a**) and at 20 m (**b**) spatial resolution and the linear combination of all of them against the final yield at pixel level (M1S, M2S and M3S). Additionally, the number of pixels is added as a reference of the cloud situation.



(**a**)



(**b**)

Figure A2. Coefficient of determination timeseries evolution focusing on *Bomba* training data of each band at 10 m (**a**) and at 20 m (**b**) spatial resolution and the linear combination of all of them against the final yield at pixel level (M1B, M2B and M3B). Additionally, the number of pixels is added as a reference of the cloud situation.

Appendix B

Table A1. *JSendra* 10 m spatial resolution model evaluation with training data (model coefficients are different for each equation).

10 m	29 June 2020			04 July 2020			19 July 2020		
Model	**R^2**	**MAE ($t \cdot ha^{-1}$)**	**MAPE (%)**	**R^2**	**MAE ($t \cdot ha^{-1}$)**	**MAPE (%)**	**R^2**	**MAE ($t \cdot ha^{-1}$)**	**MAPE (%)**
$a_0 + a_1 \cdot B2$	0.06	0.419	6.20	0.26	0.359	5.29	0.21	0.374	5.51
$a_0 + a_1 \cdot B3$	0.00	0.437	6.45	0.04	0.419	6.20	0.02	0.428	6.32
$a_0 + a_1 \cdot B4$	0.17	0.387	5.68	0.02	0.439	6.47	0.01	0.438	6.46
$a_0 + a_1 \cdot B8$	0.39	0.355	5.16	0.54	0.295	4.28	0.48	0.310	4.50
$a_0 + a_1 \cdot B2 + a_2 \cdot B3$	0.29	0.351	5.19	0.51	0.309	4.49	0.43	0.324	4.75
$a_0 + a_1 \cdot B2 + a_2 \cdot B4$	0.54	0.285	4.18	0.61	0.269	3.90	0.46	0.320	4.69
$a_0 + a_1 \cdot B2 + a_2 \cdot B8$	0.39	0.355	5.16	0.55	0.292	4.23	0.54	0.292	4.23
$a_0 + a_1 \cdot B3 + a_2 \cdot B4$	0.41	0.322	4.73	0.31	0.352	5.18	0.15	0.399	5.88
$a_0 + a_1 \cdot B3 + a_2 \cdot B8$	0.44	0.336	4.88	0.55	0.292	4.24	0.49	0.308	4.47
$a_0 + a_1 \cdot B4 + a_2 \cdot B8$	0.47	0.320	4.66	0.55	0.291	4.22	0.49	0.308	4.48
$a_0 + a_1 \cdot B2 + a_2 \cdot B3 + a_3 \cdot B4$	0.54	0.285	4.17	0.62	0.269	3.90	0.48	0.312	4.56
$a_0 + a_1 \cdot B2 + a_2 \cdot B3 + a_3 \cdot B8$	0.58	0.288	4.17	0.68	0.257	3.71	0.60	0.273	3.96
$a_0 + a_1 \cdot B2 + a_2 \cdot B4 + a_3 \cdot B8$	0.57	0.281	4.10	0.66	0.254	3.68	0.57	0.283	4.10
$a_0 + a_1 \cdot B3 + a_2 \cdot B4 + a_3 \cdot B8$	0.47	0.315	4.59	0.55	0.291	4.21	0.49	0.308	4.47
M1S	0.60	0.277	4.02	0.69	0.251	3.63	0.60	0.274	3.96
M1S+	0.64	0.258	3.75	0.72	0.234	3.36	0.63	0.263	3.81

Table A2. JSendra 20 m spatial resolution model evaluation with training data (model coefficients are different for each equation).

20 m	29 June 2020			04 July 2020			19 July 2020		
Model	**R^2**	**MAE ($t \cdot ha^{-1}$)**	**MAPE (%)**	**R^2**	**MAE ($t \cdot ha^{-1}$)**	**MAPE (%)**	**R^2**	**MAE ($t \cdot ha^{-1}$)**	**MAPE (%)**
$a_0 + a_1 \cdot B2$	0.07	0.401	5.90	0.26	0.346	5.07	0.22	0.355	5.22
$a_0 + a_1 \cdot B3$	0.00	0.421	6.20	0.04	0.403	5.94	0.02	0.410	6.03
$a_0 + a_1 \cdot B4$	0.14	0.382	5.60	0.01	0.424	6.23	0.00	0.422	6.21
$a_0 + a_1 \cdot B5$	0.02	0.415	6.11	0.00	0.422	6.21	0.00	0.421	6.20
$a_0 + a_1 \cdot B6$	0.28	0.374	5.44	0.41	0.330	4.79	0.35	0.338	4.91
$a_0 + a_1 \cdot B7$	0.36	0.353	5.13	0.53	0.294	4.25	0.46	0.312	4.51
$a_0 + a_1 \cdot B8$	0.35	0.357	5.19	0.53	0.293	4.24	0.46	0.310	4.48
$a_0 + a_1 \cdot B8A$	0.35	0.358	5.21	0.54	0.291	4.19	0.50	0.297	4.29
$a_0 + a_1 \cdot B11$	0.14	0.392	5.76	0.42	0.328	4.75	0.25	0.372	5.40
$a_0 + a_1 \cdot B12$	0.03	0.414	6.10	0.25	0.373	5.43	0.05	0.417	6.11
M2S	0.62	0.261	3.78	0.71	0.232	3.33	0.63	0.261	3.77
M2S+	0.66	0.240	3.47	0.74	0.216	3.09	0.66	0.246	3.53
M3S	0.63	0.259	3.75	0.74	0.221	3.18	0.66	0.247	3.57
M3S+	0.69	0.237	3.41	0.76	0.204	2.92	0.70	0.232	3.35

Table A3. Bomba 10 m spatial resolution model evaluation with training data (model coefficients are different for each equation).

10 m	29 June 2020			04 July 2020			19 July 2020		
Model	**R^2**	**MAE ($t \cdot ha^{-1}$)**	**MAPE (%)**	**R^2**	**MAE ($t \cdot ha^{-1}$)**	**MAPE (%)**	**R^2**	**MAE ($t \cdot ha^{-1}$)**	**MAPE (%)**
$a_0 + a_1 \cdot B2$	0.41	0.476	17.91	0.47	0.443	16.08	0.39	0.463	17.64
$a_0 + a_1 \cdot B3$	0.71	0.317	11.63	0.81	0.274	9.87	0.62	0.365	14.47
$a_0 + a_1 \cdot B4$	0.45	0.458	16.47	0.68	0.336	12.12	0.55	0.385	15.83

Table A3. *Cont.*

10 m	29 June 2020			04 July 2020			19 July 2020		
Model	**R^2**	**MAE ($t \cdot ha^{-1}$)**	**MAPE (%)**	**R^2**	**MAE ($t \cdot ha^{-1}$)**	**MAPE (%)**	**R^2**	**MAE ($t \cdot ha^{-1}$)**	**MAPE (%)**
$a_0 + a_1 \cdot B8$	0.00	0.584	24.49	0.03	0.587	24.28	0.41	0.452	18.32
$a_0 + a_1 \cdot B2 + a_2 \cdot B3$	0.72	0.312	11.67	0.81	0.274	9.84	0.62	0.357	14.39
$a_0 + a_1 \cdot B2 + a_2 \cdot B4$	0.46	0.448	16.26	0.68	0.336	12.19	0.55	0.372	15.69
$a_0 + a_1 \cdot B2 + a_2 \cdot B8$	0.41	0.473	17.79	0.47	0.443	16.05	0.54	0.420	15.63
$a_0 + a_1 \cdot B3 + a_2 \cdot B4$	0.71	0.314	11.43	0.82	0.261	9.27	0.62	0.365	14.36
$a_0 + a_1 \cdot B3 + a_2 \cdot B8$	0.71	0.310	11.4	0.82	0.267	9.64	0.64	0.359	14.07
$a_0 + a_1 \cdot B4 + a_2 \cdot B8$	0.51	0.414	14.73	0.72	0.319	11.32	0.59	0.378	15.16
$a_0 + a_1 \cdot B2 + a_2 \cdot B3 + a_3 \cdot B4$	0.74	0.293	10.61	0.83	0.255	9.24	0.63	0.360	14.36
$a_0 + a_1 \cdot B2 + a_2 \cdot B3 + a_3 \cdot B8$	0.73	0.298	11.21	0.82	0.268	9.63	0.64	0.355	14.04
$a_0 + a_1 \cdot B2 + a_2 \cdot B4 + a_3 \cdot B8$	0.51	0.416	14.81	0.74	0.304	11.07	0.59	0.378	15.16
$a_0 + a_1 \cdot B3 + a_2 \cdot B4 + a_3 \cdot B8$	0.71	0.311	11.37	0.82	0.262	9.28	0.65	0.358	13.87
M1B	0.74	0.293	10.61	0.83	0.253	9.19	0.65	0.359	13.86
M1B+	0.75	0.288	10.08	0.87	0.229	7.37	0.8	0.266	9.59

Table A4. Bomba 20 m spatial resolution model evaluation with training data (model coefficients are different for each equation).

20 m	29 June 2020			04 July 2020			19 July 2020		
Model	**R^2**	**MAE ($t \cdot ha^{-1}$)**	**MAPE (%)**	**R^2**	**MAE ($t \cdot ha^{-1}$)**	**MAPE (%)**	**R^2**	**MAE ($t \cdot ha^{-1}$)**	**MAPE (%)**
$a_0 + a_1 \cdot B2$	0.49	0.464	17.20	0.53	0.419	14.93	0.44	0.470	17.72
$a_0 + a_1 \cdot B3$	0.76	0.296	11.10	0.84	0.263	9.72	0.65	0.367	14.82
$a_0 + a_1 \cdot B4$	0.57	0.423	14.59	0.79	0.265	9.24	0.62	0.361	15.23
$a_0 + a_1 \cdot B5$	0.84	0.244	8.92	0.80	0.267	10.65	0.60	0.360	15.54
$a_0 + a_1 \cdot B6$	0.03	0.591	25.42	0.02	0.590	25.46	0.09	0.558	24.28
$a_0 + a_1 \cdot B7$	0.00	0.603	25.89	0.04	0.605	25.51	0.47	0.429	18.06
$a_0 + a_1 \cdot B8$	0.00	0.603	25.89	0.03	0.604	25.57	0.44	0.442	18.62
$a_0 + a_1 \cdot B8A$	0.00	0.603	25.89	0.03	0.604	25.57	0.42	0.453	19.02
$a_0 + a_1 \cdot B11$	0.11	0.612	24.18	0.02	0.594	25.49	0.21	0.528	21.22
$a_0 + a_1 \cdot B12$	0.19	0.596	22.65	0.02	0.602	25.65	0.47	0.437	17.17
M2B	0.81	0.256	9.10	0.87	0.215	7.93	0.67	0.362	14.16
M2B+	0.83	0.251	8.49	0.90	0.201	6.48	0.84	0.247	8.98
M3B	0.86	0.228	7.89	0.88	0.213	7.74	0.79	0.285	10.52
M3B+	0.87	0.223	7.67	0.92	0.175	5.74	0.88	0.222	7.77

Appendix C

Table A5 provides detailed information about the vegetation indices, and their mathematical formula according to [8,10,26], that have been tested in the yield models. Table A6 shows the performance metrics of these VIs on July 4 for each variety.

Table A5. Vegetation indices used in the study.

Vegetation Index	Formula
Normalized difference vegetation index (NDVI)	$\frac{B8-B4}{B8+B4}$
Difference vegetation index (DVI)	$B8 - B4$
Enhanced vegetation index (EVI)	$2.5 \times \frac{B8-B4}{B8+6\times B4-7.5\times B2+1}$
Enhanced vegetation index 2 (EVI2)	$2.5 \times \frac{B8-B4}{B8+2.4\times B4+1}$
Green NDVI (GNDVI)	$\frac{B8-B3}{B8+B3}$
Green difference vegetation index (GDVI)	$B8 - B3$
Green chlorophyll vegetation index (GCVI)	$\frac{B8}{B3} - 1$

Table A5. *Cont.*

Vegetation Index	Formula
Wide dynamic range vegetation index (WDRVI)	$\frac{0.1\times B8-B4}{0.1\times B8+B4}$
Soil-adjusted vegetation index (SAVI)	$\frac{B8-B4}{B8+B4+L}(1+L), \quad L=0.33$
Ratio vegetation index (RVI)	$\frac{B8}{B4}$
Land surface water index (LSWI)	$\frac{B8-B11}{B8+B11}$
Normalized difference built-up index (NDBI)	$\frac{B11-B8}{B11+B8}$
Triangular vegetation index (TVI)	$\sqrt{\frac{B8-B4}{B8+B4}+0.5}$
Infrared percentage vegetation index (IPVI)	$\frac{B8}{B8+B4}$
Rice growth vegetation index (RGVI)	$1-\frac{B2-B4}{B8+B11+B12}$
Red edge chlorophyll index 1 (CIre1)	$\frac{B7}{B5}-1$
Normalized difference red edge 1 (NDRE1)	$\frac{B6-B5}{B6+B5}$
Normalized difference red edge 2 (NDRE2)	$\frac{B7-B5}{B7+B5}$

Table A6. Performance metrics of the VIs-based models considering the training dataset at 20 m spatial resolution.

	***JSendra* Rice**			***Bomba* Rice**		
	R^2	**MAE (t·ha^{-1})**	**MAPE (%)**	**R^2**	**MAE (t·ha^{-1})**	**MAPE (%)**
a_0+a_1·NDVI	0.40	0.331	4.82	0.36	0.485	18.86
a_0+a_1·DVI	0.55	0.292	4.23	0.07	0.590	23.98
a_0+a_1·EVI	0.60	0.274	3.97	0.11	0.585	23.59
a_0+a_1·EVI2	0.56	0.287	4.17	0.11	0.585	23.56
a_0+a_1·GNDVI	0.42	0.322	4.68	0.49	0.436	16.63
a_0+a_1·GDVI	0.55	0.292	4.24	0.11	0.587	23.57
a_0+a_1·GCVI	0.35	0.349	5.09	0.41	0.475	18.48
a_0+a_1·WDRVI	0.40	0.329	4.78	0.36	0.494	19.28
a_0+a_1·SAVI	0.56	0.286	4.15	0.14	0.578	23.17
a_0+a_1·RVI	0.37	0.339	4.95	0.33	0.511	20.11
a_0+a_1·LSWI	0.07	0.397	5.85	0.02	0.613	25.85
a_0+a_1·NDBI	0.07	0.397	5.85	0.02	0.613	25.85
a_0+a_1·TVI	0.40	0.334	4.86	0.36	0.484	18.85
a_0+a_1·IPVI	0.40	0.331	4.82	0.36	0.485	18.86
a_0+a_1·RGVI	0.66	0.245	3.54	0.57	0.394	16.3
a_0+a_1·CIre1	0.40	0.325	4.71	0.48	0.446	17.77
a_0+a_1·NDRE1	0.45	0.307	4.44	0.54	0.414	16.34
a_0+a_1·NDRE2	0.43	0.313	4.52	0.59	0.393	15.29

Appendix D

Figure A3 shows the reference yield maps from the harvester machine (D1A and D1H) over a *JSendra* training field and the corresponding surface reflectance and DVI values from Sentinel-2 on July 4 (B-F at 10 m, I-M at 20 m). Furthermore, Figure A3G,N show the resulting yield estimations based on the M1S+ (left) and M3S+ model (right). Looking at the spatial distribution of the yield measurements, there are two areas with larger yield in the center of the field while the left and right edges show lower yield values. This pattern is very close to the NIR (B8) and DVI distribution across the parcel whereas the other bands hardly show any similarity. This provides a visual idea of how each spectral band or VI intervenes and how it affects the change of spatial resolution (10 m, left and 20 m, right). The models can identify high and low yield zones. However, extreme values are smoothed.

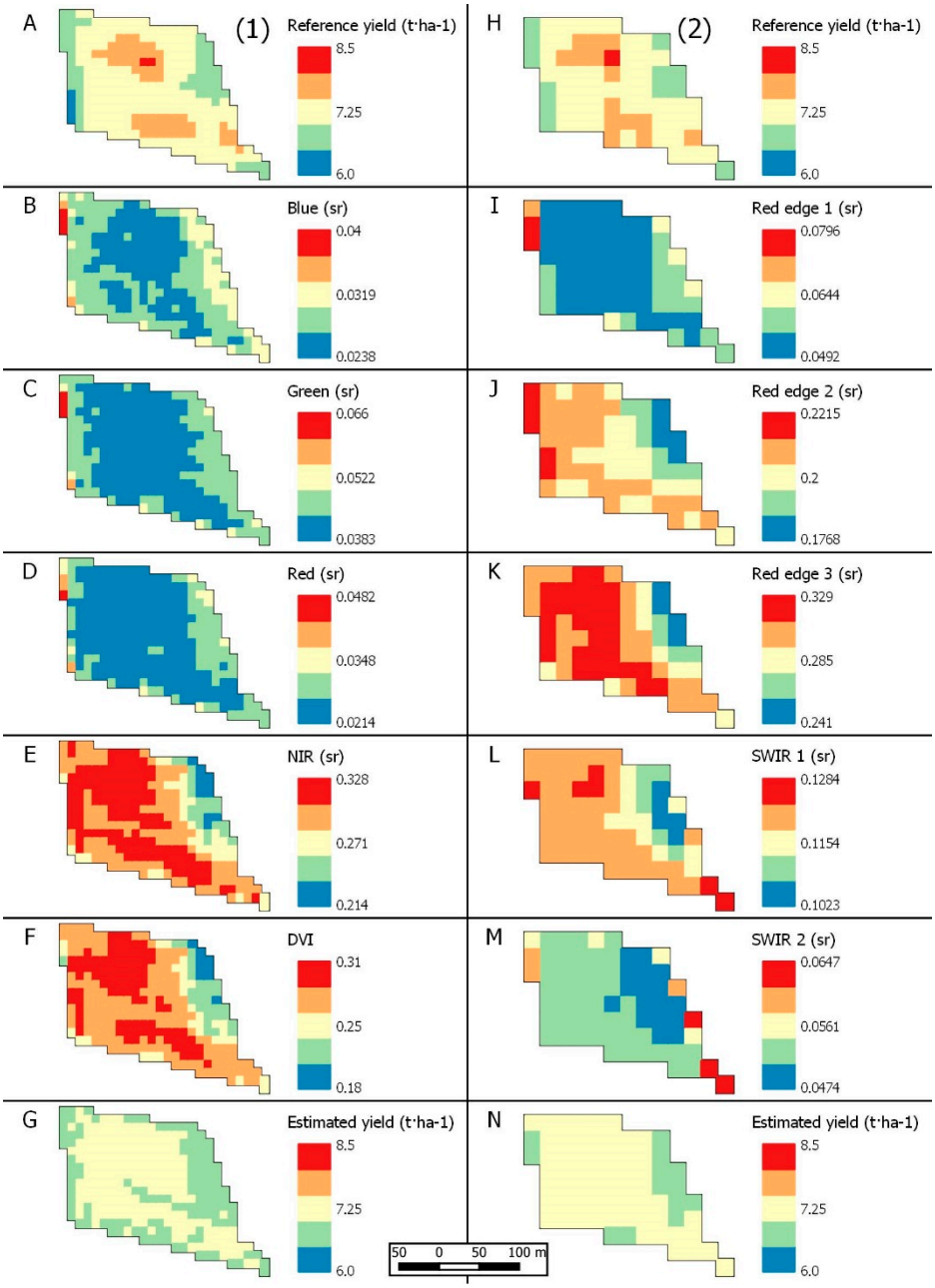


Figure A3. Example of one training *JSendra* field at 10 m (left, (1)) and 20 m (right, (2)) spatial resolution, being: (**A**,**H**) the reference yield map; (**B**–**F**) and (**I**–**M**) the SR or VI indicated at legend; (**G**,**N**) the modelling result (M1S+ for G and M3S+ for N).

Figure A4 shows an example of a *Bomba* training field where D2A and D2H show the reference yields at 10 m and 20 m, respectively, other images show the corresponding pixel level reflectance and DVI values (D2B-F at 10 m, D2I-M at 20 m). D2G and D2N show the yield resulting maps after implementing M1B+ and M3B+ respectively. The yield maps show two clusters with high within-field yields, while the top edge shows the lowest yields. Looking at the surface reflectance and the DVI images, the green (B3) and red (B4) bands show the highest correspondence with said distribution. Moreover, the maps give a visual validation of the effect of spatial resolution. From these figures, NIR, Red edge and SWIR should have better results in the modelling. However, those bands do not explain the yield variability between fields well. Finally, the estimated yield maps present a good agreement with the reference yield map identifying high and low yield zones, although extreme values are smoothed out.

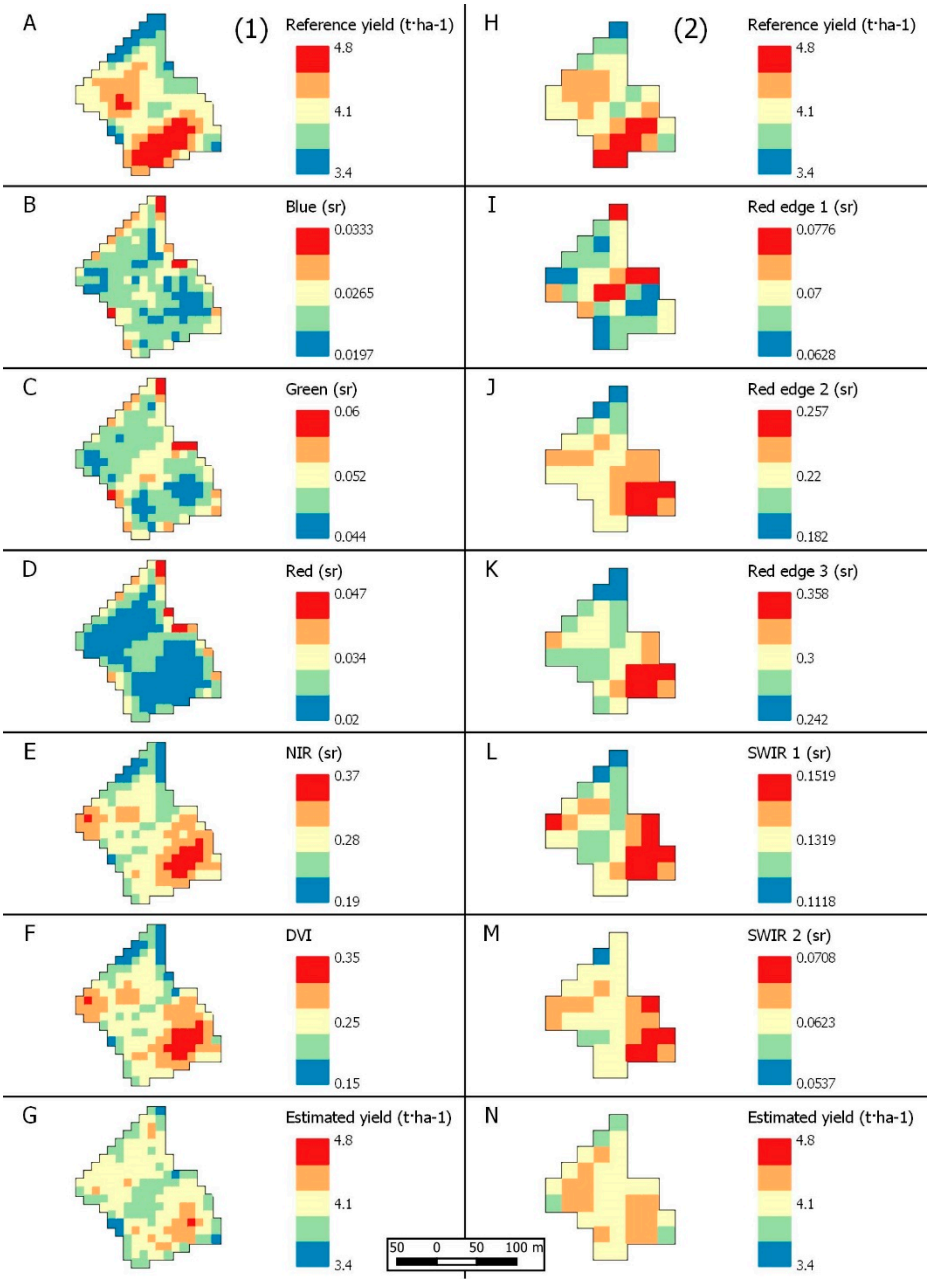


Figure A4. Example of one training *Bomba* field at 10 m (left, (1)) and 20 m (right, (2)) spatial resolution, being: (**A**,**H**) the reference yield map; (**B**–**F**) and (**I**–**M**) the SR or VI indicated at legend; (**G**,**N**) the modelling result (M1B+ for G and M3B+ for N).

References

1. FAOSTAT. Food and Agriculture Statistics. Available online: htttp://www.fao.org/faostat (accessed on 15 June 2021).
2. MAPA. Ministerio de Agricultura, Pesca y Alimentación. Available online: https://www.mapa.gob.es (accessed on 15 June 2021).
3. United Nations. Available online: https://www.un.org/en (accessed on 15 June 2021).
4. La Agricultura Mundial en la Perspectiva del Año 2050. Available online: http://www.fao.org/fileadmin/templates/wsfs/docs/Issues_papers/Issues_papers_SP/La_agricultura_mundial.pdf (accessed on 15 June 2021).
5. Johnson, D.M. A comprehensive assessment of the correlations between field crop yields and commonly used MODIS products. *Int. J. Appl. Earth Obs. Geoinf.* **2016**, *52*, 65–81. [CrossRef]
6. Franch, B.; Vermote, E.F.; Skakun, S.; Roger, J.C.; Becker-Reshef, I.; Murphy, E.; Justice, C. Remote sensing based yield monitoring: Application to winter wheat in United States and Ukraine. *Int. J. Appl. Earth Obs. Geoinf.* **2019**, *76*, 112–127. [CrossRef]

7. Skakun, S.; Vermote, E.; Franch, B.; Roger, J.C.; Kussul, N.; Ju, J.; Masek, J. Winter wheat yield assessment from Landsat 8 and Sentinel-2 data: Incorporating surface reflectance, through phenological fitting, into regression yield models. *Remote Sens.* **2019**, *11*, 1768. [CrossRef]
8. Skakun, S.; Kalecinski, N.I.; Brown, M.G.; Johnson, D.M.; Vermote, E.F.; Roger, J.C.; Franch, B. Assessing within-Field Corn and Soybean Yield Variability from WorldView-3, Planet, Sentinel-2, and Landsat 8 Satellite Imagery. *Remote Sens.* **2021**, *130*, 872. [CrossRef]
9. Kayad, A.; Sozzi, M.; Gatto, S.; Marinello, F.; Pirotti, F. Monitoring within-field variability of corn yield using Sentinel-2 and machine learning techniques. *Remote Sens.* **2019**, *11*, 2873. [CrossRef]
10. Zhao, Y.; Potgieter, A.B.; Zhang, M.; Bingfang, W.; Hammer, G.L. Predicting wheat yield at the field scale by combining high-resolution Sentinel-2 satellite imagery and crop modelling. *Remote Sens.* **2020**, *12*, 1024. [CrossRef]
11. Deines, J.M.; Patel, R.; Liang, S.Z.; Dado, W.; Lobell, D.B. A million kernels of truth: Insights into scalable satellite maize yield mapping and yield gap analysis from an extensive ground dataset in the US Corn Belt. *Remote Sens. Environ.* **2021**, *253*, 112174. [CrossRef]
12. Lobell, D.B.; Thau, D.; Seifert, C.; Engle, E.; Little, B. A scalable satellite-based crop yield mapper. *Remote Sens. Environ.* **2015**, *164*, 324–333. [CrossRef]
13. RICA: A Rice Crop Calendar for Asia Based on MODIS Multi-Year Data. Available online: http://asia-rice.org (accessed on 1 June 2021).
14. GEOGLAM. Available online: https://www.earthobservations.org/geoglam.php (accessed on 3 June 2021).
15. Open, Timely, and Science-Driven Information on Crop Conditions in Support of Market Transparency and Early Warning of Production Shortfalls. Available online: https://cropmonitor.org (accessed on 3 June 2021).
16. Agricultural Market Information System. Available online: http://www.amis-outlook.org// (accessed on 3 June 2021).
17. Cai, Y.; Guan, K.; Nafziger, E.; Chowdhary, G.; Peng, B.; Jin, Z.; Wang, S.; Wang, S. Detecting in-season crop nitrogen stress of corn for field trials using UAV-and CubeSat-based multispectral sensing. *IEEE J. Sel. Top. Appl. Earth Obs. Remote Sens.* **2019**, *12*, 5153–5166. [CrossRef]
18. Shi, Y.; Huang, W.; Ye, H.; Ruan, C.; Xing, N.; Geng, Y.; Dong, Y.; Peng, D. Partial least square discriminant analysis based on normalized two-stage vegetation indices for mapping damage from rice diseases using PlanetScope datasets. *Sensors* **2018**, *18*, 1901. [CrossRef]
19. Kobayashi, T.; Sasahara, M.; Kanda, E.; Ishiguro, K.; Hase, S.; Torigoe, Y. Assessment of rice panicle blast disease using airborne hyperspectral imagery. *Open Agric. J.* **2016**, *10*, 28–34. [CrossRef]
20. Yang, Y.; Chai, R.; He, Y. Early detection of rice blast (Pyricularia) at seedling stage in Nipponbare rice variety using near-infrared hyper-spectral image. *Afr. J. Biotechnol.* **2012**, *11*, 6809–6817. [CrossRef]
21. Zhang, G.; Xu, T.; Tian, Y.; Xu, H.; Song, J.; Lan, Y. Assessment of rice leaf blast severity using hyperspectral imaging during late vegetative growth. *Australas. Plant Pathol.* **2020**, *49*, 571–578. [CrossRef]
22. Bacenetti, J.; Paleari, L.; Tartarini, S.; Vesely, F.M.; Foi, M.; Movedi, E.; Ravasi, R.A.; Bellopede, V.; Durello, S.; Ceravolo, C.; et al. May smart technologies reduce the environmental impact of nitrogen fertilization? A case study for paddy rice. *Sci. Total Environ.* **2020**, *715*, 136956. [CrossRef] [PubMed]
23. Moreno-Garcia, B.; Casterad, M.; Guillén, M.; Quílez, D. Agronomic and Economic Potential of Vegetation Indices for Rice N Recommendations under Organic and Mineral Fertilization in Mediterranean Regions. *Remote Sens.* **2018**, *10*, 1908. [CrossRef]
24. Gilardelli, C.; Stella, T.; Confalonieri, R.; Ranghetti, L.; Campos-Taberner, M.; García-Haro, F.J.; Boschetti, M. Downscaling rice yield simulation at sub-field scale using remotely sensed LAI data. *Eur. J. Agron.* **2019**, *103*, 108–116. [CrossRef]
25. Confalonieri, R.; Rosenmund, A.S.; Baruth, B. An improved model to simulate rice yield. *Agron. Sustain. Dev.* **2009**, *29*, 463–474.
26. Mosleh, M.K.; Hassan, Q.K.; Chowdhury, E.H. Application of remote sensors in mapping rice area and forecasting its production: A review. *Sensors* **2015**, *15*, 769–791. [CrossRef]
27. Shao, Y.; Fan, X.; Liu, H.; Xiao, J.; Ross, S.; Brisco, B.; Brown, R.; Staples, G. Rice monitoring and production estimation using multi-temporal RADARSAT. *Remote Sens. Environ.* **2001**, *76*, 310–325. [CrossRef]
28. Li, Y.; Liao, Q.; Li, X.; Liao, S.; Chi, G.; Peng, S. Towards an operational system for regional-scale rice yield estimation using a time-series of RADARSAT ScanSAR images. *Int. J. Remote Sens.* **2003**, *24*, 4207–4220. [CrossRef]
29. Chen, C.; McNairn, H. A neural network integrated approach for rice crop monitoring. *Int. J. Remote Sens.* **2006**, *27*, 1367–1393. [CrossRef]
30. Nuarsa, I.W.; Nishio, F.; Hongo, C. Relationship between rice spectral and rice yield using MODIS data. *J. Agric. Sci.* **2011**, *2*, 80–88. [CrossRef]
31. Son, N.T.; Chen, C.F.; Chen, C.R.; Chang, L.Y.; Due, H.N.; Nguyen, L.D. Prediction of rice crop yield using MODIS EVI-LAI data in the Mekong Delta, Vietnam. *Int. J. Remote Sens.* **2013**, *34*, 7275–7292. [CrossRef]
32. Noureldin, N.A.; Aboelghar, M.A.; Saudy, H.S.; Ali, A.M. Rice yield forecasting models using satellite imagery in Egypt. *Egypt. J. Remote Sens. Space Sci.* **2013**, *16*, 125–131. [CrossRef]
33. Rahman, A.; Khan, K.; Krakauer, N.Y.; Roytman, L.; Kogan, F. Use of remote sensing data for estimation of Aman rice yield. *Int. J. Agric. For.* **2012**, *2*, 101–107. [CrossRef]
34. Nuarsa, I.W.; Nishio, F.; Hongo, C. Rice yield estimation using Landsat ETM+ data and field observation. *J. Agric. Sci.* **2012**, *3*, 45–56. [CrossRef]

35. Natura 2000. Available online: https://ec.europa.eu/environment/nature/natura2000/index_en.htm (accessed on 4 June 2021).
36. Romo, S.; Soria, J.; Fernandez, F.; Ouahid, Y.; Barón-Solá, Á. Water residence time and the dynamics of toxiccyanobacteria. *Freshw. Biol.* **2013**, *58*, 513–522. [CrossRef]
37. Kharel, T.P.; Swink, S.N.; Maresma, A.; Youngerman, C.; Kharel, D.; Czymmek, K.J.; Ketterings, Q.M. Yield monitor data cleaning is essential for accurate corn grain and silage yield determination. *Agron. J.* **2019**, *111*, 509–516. [CrossRef]
38. Dobermann, A.; Ping, J.L. Geostatistical integration of yield monitor data and remote sensing improves yield maps. *Agron. J.* **2004**, *96*, 285–297. [CrossRef]
39. Vermote, E.; Justice, C.; Claverie, M.; Franch, B. Preliminary analysis of the performance of the Landsat 8/OLI land surface reflectance product. *Remote Sens. Environ.* **2016**, *185*, 46–56. [CrossRef] [PubMed]
40. Statgraphics 19® Centurion. Available online: https://www.statgraphics.com/centurion-overview (accessed on 10 June 2021).
41. Un Sistema de Información Geográfica Libre y de Código Abierto. Available online: https://www.qgis.org/es/site/ (accessed on 10 June 2021).
42. Feng, H.; Chen, G.; Xiong, L.; Liu, Q.; Yang, W. Accurate digitization of the chlorophyll distribution of individual rice leaves using hyperspectral imaging and an integrated image analysis pipeline. *Front. Plant Sci.* **2017**, *8*, 1238. [CrossRef]

HIGH-LEVEL POLITICAL FORUM
ON SUSTAINABLE DEVELOPMENT

2024

SDG 2: ZERO HUNGER



End hunger, achieve food security and improved nutrition and promote sustainable agriculture

2 ZERO HUNGER

To learn more about global progress on the 17 SDGs, click here to read the latest Sustainable Development Goals Report 2024.

FACTS AND FIGURES

- **Between 691 million and 783 million** people faced hunger in 2022. Considering the midrange (735 million), **122 million more** people faced hunger in 2022 than in 2019.
- Globally in 2022, an estimated **148 million (22.3%) children** were affected by stunting, **37 million (5.6%)** were overweight, while **45 million (6.8%)** experienced wasting.
- **Record-high food prices** in 2022 worsened **purchasing power and access to food**, negatively impacting food security and nutritional outcomes.
- Globally, the proportion of countries facing moderately to abnormally high food prices rose sharply in 2022, reaching a **new record high of 58.1%.** This represented a **nearly fourfold** increase from the 2015-2019 average level of 15.2%.
- In 95% of countries with available data, the average annual income of **small-scale producers** is **less than half** that of larger-scale producers. Small-scale food producers **headed by men** typically generate higher incomes than those headed by women.
- Between 2015 and 2022, global **government spending on agriculture** increased steadily, reaching a **record high of $749 billion** in 2022. However, government expenditure on agriculture **relative to the sector's GDP contribution declined** from 0.5 in 2015 to 0.43 in 2021 **before rebounding** to 0.48 in 2022.
- From 2015 to 2022, the **volume of aid** for agriculture provided to developing countries increased **by 47.2%**, from $12.3 billion **to $18.1 billion** (in constant 2022 prices).
- Data from 2021 showed that the world was **at a moderate distance** from achieving productive and sustainable agriculture (**with a score of 3.4 out of 5**), with the highest score of 4.1 in Europe and Northern American compared to the lowest score of 2.6 in the LDCs.

WHERE WE STAND

- Nearly **1 in 10 people** globally face hunger. In 2022, **2.4 billion** people experienced **moderate to severe food insecurity**.
- Despite progress, **148 million children under age 5** suffered from stunting in 2022. If current trends persist, **1 in 5 children under age 5** will be affected by stunting in 2030.
- In 2022, almost **60% of countries** worldwide faced **moderately to abnormally high food prices** due to the spillover effects of conflicts.
- Achieving zero hunger requires intensified efforts to **transform food systems** so they are sustainable, resilient and equitable. Moreover, accelerating improvements in **diets, nutrition, health and hygiene** is crucial to meeting the SDG target of halving the number of children suffering from chronic undernutrition.

SPOTLIGHT

FOOD SYSTEMS TRANSFORMATION

The High Impact Initiative on Food Systems Transformation aims mobilize commitments from Member States to prioritize their journey of food systems transformation to ensure food security and healthy diets for all. The initiative calls on UN Agencies, international financial institutions (IFIs), the private sector, civil society partners and all relevant stakeholders to assist countries in this journey. Further, academia will help assure state of the art science and innovation is part of this process. Building on the outcomes of the Food Systems Summit 2021 and the UNFSS+2 Stocktaking Moment, and ongoing means of implementation that will help to accelerate national processes (such as **Hand-in-Hand Initiative**, **School Meals Coalition**, **Food is Never Waste Coalition**, **Coalition of Action on Healthy Diets**, **Zero Hunger Coalition**, among others). The initiative will achieve its objectives through three key pillars:

- The development and provision of **tools, methods, models, and analyses** that leverage the best results obtained from the implementation of the FSS recommendations, including the advantages of applying a territorial approach and data resources of the Hand-in-Hand Geospatial Platform.
- A **flexible and innovative approach to partnership** based on identifying technical and programmatic challenges and supporting the design and implementation of innovative solutions.
- The pooling of existing investments and, where appropriate, the deployment of **new financial instruments** as well as **risk-reducing or risk-sharing financial structures**, as investment is an indispensable driver of transformative change.

For more information about the high impact initiative, please visit here.



UN DESA, FAO, *with the support of interested UN entities, organized an* ***Expert Group Meeting on SDG 2 and its interlinkages with other SDGs*** *in Rome, Italy on 26-27 March 2024 to inform the thematic review at 2024 HLPF.* *>>> LEARN MORE*

UN SYSTEM IN ACTION

- Led by an Oversight Steering Group comprising the Principals of **FAO, WFP, IFAD, UN-DCO** and the UN "Food Systems Task Force" Leads (**WHO and UNDP**), the **United Nations Food Systems Coordination Hub** serves countries through systemic, country-driven, customized support in translating their commitments into effective actions to reach sustainable food systems by 2030, leveraging the wider UN system's capacities. (see its 2024-2026 work plan)

- **The State of Food Security and Nutrition in the World** report, co-published by **FAO, IFAD, UNICEF, WFP and WHO**, provides an annual update on global progress towards the targets of ending hunger (SDG Target 2.1) and all forms of malnutrition (SDG Target 2.2).

- With **UNIDO and FAO** leading at the global level, **ILO and UNFPA** at the country-level, the **Agrifood Systems Transformation Accelerator (ASTA)** assists countries in transforming their agrifood systems by facilitating innovative partnership and SDG-compliant investments in selected value chains. It designs and implements catalytic systems-based projects that create new opportunities and partnership at the interface between the public, private and civil society sectors.

- The **Humanitarian-Development-Peace (HDP) Nexus Coalition**, co-led by the Stockholm International Peace Research Institue (SIPRI), Group of 7+, **FAO and WFP**, funded by the EU and hosted by the Global Network Against Food Crises, aims to contribute to ending hunger through pursuing peace and unleashing the potential of sustainable food systems to enhance the prospects for peace.

- The **Sustainable Rice Landscapes Initiative**, a collaborative initiative of WBCSD, SRP, **FAO, UNEP**, IRRI, GIZ, brings together diverse stakeholder to promote more sustainable rice production practices and products to deliver a range of local and global environmental benefits.

- Working with relevant government ministries and local stakeholders, **FAO**'s **Global Network of Digital Agriculture Innovation Hubs** initiative aims to establish a global network of interconnected national Digital Agriculture Innovation Hubs to share knowledge, experience and expertise.

- The Thirteen Replenishment of **IFAD Resources** (IFAD13) aims to deliver a programme of work of USD10 billion and generate a significant impact for over 100 million rural people, including the endorsement of the **Additional Climate Contribution (ACC)** as a new instrument to attract new climate finance to small-scale agriculture.

- **UNICEF** continue to implement nutrition programmes in **140 countries** including in development and humanitarian settings, and in fragile contexts to reach **over 430 million children and caregivers** with policies, programmes and services for the prevention of malnutrition in early childhood.

* This is not an exhaustive list of UN system actions to implement the Sustainable Development Goals. For more information, please visit

UN SYSTEM SDG IMPLEMENTATION DATABASE

Version of Record: https://www.sciencedirect.com/science/article/pii/S2352938519303465
Manuscript_f1ce01ed6043ee836098ac1a688757b1

Spatio-temporal landscape changes and the impacts of climate change in mountainous Bhutan: a case of Punatsang Chhu Basin

Abstract

Agro-ecological landscape changes along the Punatsang Chhu (River) Basin of Bhutan was assessed using Geographic Information System (GIS) and Remote Sensing techniques. The study used satellite data (Landsat imageries) of three periods (1996, 2010 and 2017). The result showed a 51% reduction in the snow and glacial area over the last 20 years. Further, the area under rock outcrops and bare land almost doubled (8% in 1996 to 15% in 2017) during the same period. These changes could be directly related to the impacts of climate change since the study site showed increases in both maximum and minimum temperatures by about 1 ^{o} C and 0.5^{o} C, respectively based on 1997 to 2017 data. The rainfall during the same period also showed a decreasing trend, which might have affected snow and glacier cover in the higher mountains. Thus, this research further confirms the existing knowledge that climate change impacts are more severely felt in the high altitudes and mountainous locations, such as the Himalayas. The study highlights land cover changes due to climate change and anthropogenic factors which could be used for suitable policy interventions and management of natural resources.

Keywords: Climate, environment, GIS, landscape, sustainability

1 Introduction

Bhutan is a small and mountainous country with a geographical area of 38,394 km^2. Due to its size and rugged topography there is limited cultivable area and makes land the most precious natural resource in the country. While the country has a forest coverage of about 70% (NSB, 2016), land resources are increasingly getting stressed by both natural and human modifications. Information on such changes are crucial from the view point of bio-diversity conservation (Turner et al., 2003), climate change (Liu et al., 2016), and sustainable resource use and planning (Karunakaran, 2011). Since the land cover and land use (LC-LU) changes are influenced by the changes in bio-physical conditions of the environment, it has been widely used as an indicator of environmental changes and is considered as an important discipline of climate studies (Mahmood et al., 2010; Liu et al., 2016). Turner et al. (2007), further mentioned that spatially explicit information on land cover are important for determining anthropogenic, bio-geographical and eco-climatic diversity of a particular location on the earth's surface. As the earth warms up through the twenty first century and beyond, the environment and natural resources are likely to experience unrelenting stress.

© 2020 published by Elsevier. This manuscript is made available under the Elsevier user license
https://www.elsevier.com/open-access/userlicense/1.0/

Such environmental stresses could have large ramifications on sustainability of natural resources, which not only affect farming but also biodiversity and ecosystem functions.

Literature mentions that there exists an explicit relationship between climate change and land cover changes (Mahmood et al., 2010). Different land cover and land use systems have the potential to change micro-climate of a region through changes in spatio-temporal heat fluxes (Tölle et al., 2017) and albedo (Cao et al., 2015). Based on a systematic review, Deng et al. (2013) explicitly reported that the climate of a region could be largely influenced by the changes in LC-LU. Studies have indicated that LC-LU were affected by climate variables, such as changes in precipitation (Dong et al., 2015) and changing patterns of rainfall and temperature rises (Ménégoz et al., 2013; Viste and Sorteberg, 2015). In the case of Bhutan, Dorji et al. (2016) reported a temperature lapse rate of 0.42-0.58^{o} C per 100 m rise. This report also showed that the land cover was affected by topography and temperature. This means that studies reporting upward trends in temperature over the years, and future projections (Beldring and Vokso, 2011; NEC, 2011) could bring about changes in agro-ecological landscape in the country. Studies undertaken in similar environments of the Himalayas provide conclusive evidence of the impacts of climate change on farming, vegetation and land use systems over a period of time (ICIMOD, 2010; Komori et al., 2012). Thus, it warrants similar studies across different geographical regions of the world where conditions are dissimilar. Bhutan is one of the least studied countries of the world and by virtue of its location in the Himalayas, environmental changes due to the impacts of climate change are reported to be happening at a very fast rate (Singh et al., 2011). The country is located within the Hindukush regions of the Himalayas which is highly fragile and prone to changes. The region is reported to be one of the fastest changing environments of the world with fast retreating snows and glaciers, shift in vegetation, increased glacial lake outburst floods and increased erosive activities. A country-specific study would be highly imperative for the country to come up with LC-LU trends over twenty years (1996-2017) and link them to climatic variables. Many studies examine changes on yearly basis for specific purpose investigations, however, for synoptic view and landscape monitoring reasons, a window period is useful (Rawat and Kumar, 2015; Langat et al., 2019). Though Bhutan is a small country, its high variability in climate (due to high variability in elevation and terrain) makes it an interesting focus of research. Of particular concern for Bhutan is changes in agro-ecology in terms of location and magnitude, area loss to flash floods, bareness, desertification and changes in the glacierized areas which could be linked to climate change. Studies

capturing broader perspective of landscape changes are crucial for a country that has been grappling with issues of climate change impacts.

Advances in the Geographic Information System (GIS) and Remote sensing technologies have made environmental monitoring and landscape change detection studies more efficient (Chen and Wang, 2010; Jensen, 2015; Wulder et al., 2018). The application of GIS and Remote sensing in monitoring of environmental changes has helped in understanding the agro-ecological modifications resulting from both natural processes and anthropogenic causes (Saidi et al., 2018; Saleh and Becker, 2018). Hence, the aim of the current study was to assess spatio-temporal land cover changes along ecological landscapes of Punatsang Chhu Basin over a three window periods (1996, 2010 and 2017), with specific objectives: (1) to quantify spatial land cover changes and (2) to discuss and link the land cover changes to the impacts of climate change. Thus, the current study would bridge the existing knowledge gap on spatio-temporal land cover dynamics and would serve as baseline information for better understanding of the status of ecosystem health, sustainability and functions. These information are crucially important for designing interventions and response mechanisms for environmental protection and farming system resilience.

2 Methodology

2.1 Study area

The study area comprised of five districts (Gasa, Punakha, Wangdue, Tsirang and Dagana) in Bhutan that form the Punatsang Chhu River Basin and its sub-basins (**Fig. 1**). It lies between the geographic coordinates 26^0 42' 2.36"N -$28^0$14' 51.64"N latitudes and 89^0 46' 5.7"E-90^0 32' 3.29" E longitudes. The total area of the study site is 10,655 km^2, and is about one third of the country. Punatsang Chhu is one of the most important rivers of Bhutan and it starts from the glaciers in the north western district of Gasa, moves southwards through the districts of Punakha, Wangdue, Tsirang and Dagana before entering the West Bengal state of India. The river, finally becomes one of the three major tributaries of Brahmaputra in India (Rahaman and Varis, 2009). The study area extends from subtropical region in the south to the alpine areas in the north, thus covering the main agro-ecological zones of Bhutan. In terms of altitudinal variation, the highest point of the river basin is above 7000 m over mean sea level (msl), which gradually falls to about 1000-1500m in the mid-altitude districts of Wangdue, Punakha, Tsirang and parts of Dagana. Vegetation in these areas is characterized

by broad leaved conifer and mixed conifer forests (NSSC and PPD, 2011). As the river meanders down to the southern foothills, the altitude drastically falls to about 100 m in the lower subtropical zone of Dagana district (adjoining the West Bengal state of India). Here, vegetation is mostly evergreen broadleaved forests (NBSAP, 2014).

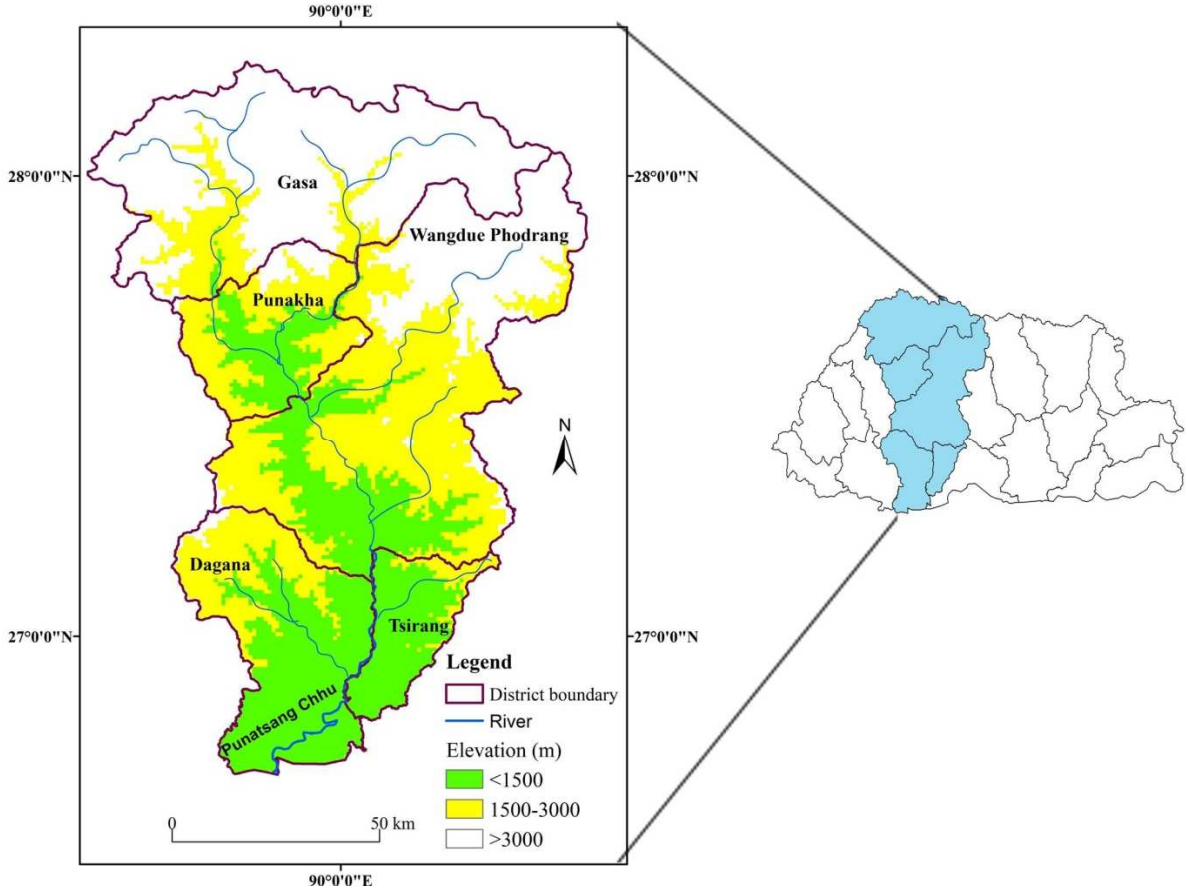


Fig. 1 Map of Bhutan showing the study area

2.2 Characteristics of study area

In all the five districts of the study area, farming is the main occupation and the land use categories, in general, are agricultural land and government reserve forest. It also includes snow covered lands and glaciers in the high altitude areas of Gasa and Wangduephodrang districts. A major portion of the study area is forested and agricultural land occupies only about 3% of the total area (~ 31,000 ha). In high altitude regions, alpine meadows and natural grasslands are quite abundant, thus making it favourable for pastoralism. Yak and cattle herding is the most common form of livestock farming in the pastoral communities of northern Bhutan (Wangdi and Norbu, 2018). This is also the case in other temperate and alpine zones of the Himalayas (Ning et al., 2016). Except for the northern district of Gasa

where livestock dominates, the four other districts (Punakha, Wangduephodrang, Dagana and Tsirang) cultivate crops with integration of some livestock components. The dominant crops in high altitude zones are wheat, barley, buckwheat, potatoes and cole crops, whereas in the lower areas the major crops are paddy, maize, wheat, chillies, and potatoes (DoA, 2016). The topography of the study area is highly rugged and farming is limited to the narrow valleys and mountain slopes.

2.3 Weather and climate

Due to large variations in elevation and topography, climate in Bhutan varies substantially from one place to another even over smaller distances. The southern part of the country is characterized by a sub-tropical type of climate with high humidity and heavy rainfall while the central flat valleys experience cool winters and hot summers with moderate rainfall. The high altitude valleys are characterized by cold winters and cool summers. Much of the areas above 5000 m elevation remain permanently covered in snow and glaciers. The monsoon rains are influenced by the southern circulation from the Bay of Bengal in the Indian Ocean, while winter showers are brought by northerly winds originating from the Arabian sea which enters via the western part of the Himalayas that brings cold waves and snowfall in the higher ridges of the country (NEC, 2006). Although a small country, temperature and precipitation in Bhutan varies significantly with rising altitude from south to north and between east to west. Shahnawaz and Strobl (2015) reported that due to paucity of data, coupled with stronger influence by dramatic changes in elevation over a smaller distance at different locations, it is quite difficult to generalize average values of temperature and precipitations for Bhutan. However, this report indicated that minimum and maximum temperatures in Bhutan over 1996-2013 varied between 0-15^0 C and 28-31^0 C, respectively. The same report also indicated that the mean minimum and maximum precipitation varied between 0-80mm and 840-1360 mm, respectively over the same period.

In order to relate the findings of the current study to the impacts of climate change, temperature and rainfall trends for the study period (1997-2017) were also analysed and presented for discussion. The 20-year meteorological data of the study site might be too short, but we wanted to present whatever is possible from the existing climate data which potentially affects the land cover changes overtime. Bhutan has four seasons: spring, summer, autumn and winter. The spring months comprise of March, April and May, whereas summer months are June, July and August. September, October and November fall under

autumn and cold winter months are December, January and February. In general, temperatures were low in winter months with low rainfall (~80mm) whereas, the hottest months were of summer and are often accompanied by heavy rainfall (Dorji et al., 2016). The two terminologies, rainfall and precipitation, have been synonymously used throughout the manuscript since rainfall in the lower elevation would mean snowfall in the higher mountainous areas. The weather data was obtained from the National Centre for Hydrology and Meteorology, Royal Government of Bhutan.

2.4 Data sourcing and pre-processing

The satellite imageries of the study sites in Bhutan were obtained from the website of the United States Geological Survey (USGS) earth pro-resources observation system (https://earthexplorer.usgs.Gov/). Imageries of Landsat Thematic Mapper (Landsat TM) 4-5 and Landsat 8 OLl were downloaded from the satellite path and row number 138 and 041 respectively, for the years 1996, 2010 and 2017 **(Table 1**). The three sets of imageries were acquired in same season (winter) when the sky is clear and mountains are usually covered with snow to get representative land cover. Clear images of the study area with less than 10% cloud cover were selected and pre-processed for the classification and analysis. Pre-processing and analysis of satellite imageries were done using remote sensing software ENVI (version 5.4.1) and ArcGIS (ArcMap 10.4) was also used for the enhancement of mapping functions.

Image pre-processing involved radiometric correction of the satellite imageries through dark object subtraction and atmospheric calibration **(Fig. 2**). ArcGIS was used for sub-setting the radio-metrically corrected images to get the areas of interest, the study area before the actual classification processes.

Table 1. Information about the satellite imageries used for the classification of land cover classes

Data Type	Row/path	Date of Acquisition	Source
Landsat TM 4-5	138/41	01/03/1996	USGS (https://earthexplorer.usgs.Gov/)
Landsat TM 4-5	138/41	06/02/2010	USGS (https://earthexplorer.usgs.Gov/)
landsat 8 OLI	138/41	24/01/2017	USGS (https://earthexplorer.usgs.Gov/)

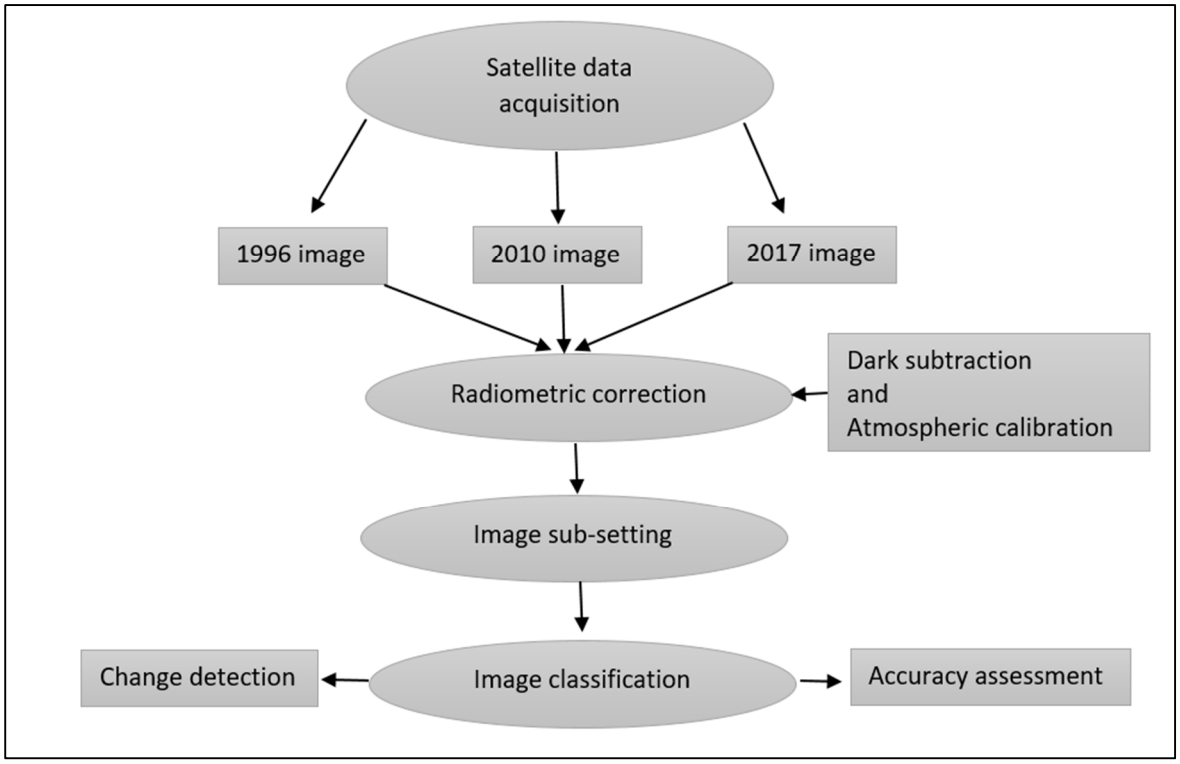


Fig. 2 Illustration of satellite image pre-processing and classification process

2.5 Image classification and accuracy assessment

Image classification was done using supervised method, which used maximum likelihood principles for pixel class algorithm clustering of training sites. Six broad land cover classes were identified. The training of sites, as well as the preparations of ground truth regions of interest (ROI) were guided by the online version of the google earth pro historical images *(https://earth.google.com)*. The six land cover classes used for the analysis included is presented in **Table 2**. The classified images underwent accuracy assessment which is an important tool to obtain kappa statistics, including producer's and user's accuracies for classified products. Kappa statistics, or the Kappa coefficient indicate the probability of a reference pixels being correctly classified and is also a measure of omission error which is the producer's accuracy of classification. It is a measure of agreement, and is known as KHAT ($\hat{k}$) (Congalton et al., 1983; Cohen, 2016), and calculated using the following equation:

$$\hat{k} = \frac{\sum_{i=1}^{r} x_{ii+} - \sum_{i=1}^{r}(x_{i+} * x_{+i})}{N^2 - \sum_{i=1}^{r}(x_{i+} * x_{+i})} \quad (1)$$

Where r is the number of rows in the matrix, x_{ii} is the number of observations in rows *i* and column *i* (i.e., the i^{th} diagonal element), x_{i+} and x_{+i} are the marginal totals of row *i* and column *i*, respectively, and N is the total number of observations. Accuracy assessment was done to ensure the integrity of the products developed and for gaining the confidence of the end users (Wulder et al., 2018). General range of ($\hat{k}$) for reference is as follows:

- $\hat{k}$<0.4 : poor
- 0.4<$\hat{k}$<0.75 : good, and
- $\hat{k}$>0.75 : excellent

Temporal images of 1996, 2010 and 2017 were classified separately and post classification change detection technique was applied for detecting image differences and change statistics. Despite having low resolution, Landsat TM imageries have been widely used for land cover and change detection studies with reasonably good level of accuracies (Sinha et al., 2012; Chalise et al., 2018). During change detection analysis, the classified image of 1996 was compared with 2010 and 2017, and similar comparison made between 2010 and 2017 images.

Table 2. Land cover classes used for the classification of remotely sensed images.

Sl.No	Land cover classes	Description
1	Snow and glaciers	Includes glaciers, snow and ice covered areas, including water bodies and marshes
2	Rock outcrops and bare land	Includes all rocky and barren lands including eroded bare river/stream beds
3	Grassland and pastures	Includes all grasslands, alpine meadows and pastures
4	Forest	Includes all forested areas, including areas covered under shrubs
5	Agricultural land	Includes all cultivated land (dryland, wetland and orchards)
6	Others	Includes areas that could not fit into any of the land cover classes (eg. Mixtures of green patches and built ups, rocks and barelands, etc.) and represents small fraction of land cover

3 Results and discussion

3.1 *Classification of land cover*

The study area was classified into six broad land cover classes for the year 1996, 2010 and 2017 (**Fig. 3**). The estimated area occupied by each category of land cover for the three temporal images is presented in **Table 4**. The classification results of the three images of 1996, 2010 and 2017 showed that the forest cover occupied the largest area of 6301 km^2 (59.22%), 6904 km^2 (64.08%) and 6711 km^2 (62.99%), respectively. The least area was under

227 the "others" land cover class. In 1996, about one-fourth of the study area was under snow and
228 glacier cover (2534 km^2) (23.78%) and the area under rock outcrops and bare lands was much
229 less. In the same year, agricultural land was 359 km^2 (3.37%), grassland 497 km^2 (4.67%)
230 and others occupied 20 km^2 (0.19%). In 2010, the area under snow and glacier cover
231 decreased to 1597 km^2 (14.99%), which corresponded to 37% reduction as compared to the
232 base year of 1996. In the same year, agricultural land, rock outcrops and bare land, grassland
233 and others were 159 km^2 (2.43%), 1221 km^2 (11.46%), 638 km^2 (5.99%) and 35 km^2
234 (0.33%), respectively. However, the analysis of 2017 land cover showed that the rock
235 outcrops and bare land had drastically increased to 1589 km^2 (11.91%), making it the highest
236 after forest cover in comparison to 1996 or 2010. Area under snow and glacier had further
237 declined to 1,238 km^2 (11.62%) in comparison to 1996 or 2010. The grassland and pasture
238 coverage was 710 km^2, which is nearly the same at 6.66%.

239 Land cover classification of Punatsang Chhu Basin, covering five districts in the current
240 study was done at a reasonably good accuracy levels of 93.55%, 97.74% and 97.54% with
241 kappa statistics of 0.91, 0.97 and 0.96 for 1996, 2010 and 2017, respectively (**Table 3**).

242 The highest forest cover in the three study periods could be attributed to the country's sound
243 natural environment conservation laws. Bhutan is considered to have one of the most
244 stringent natural environment protection rules and regulations in the region (NEC, 2000;
245 Dorji, 2008). The constitution of the Kingdom of Bhutan mandates a minimum forest cover
246 of 60% at all times (NC, 2008), thus the country continues to strive at maintaining a major
247 area under forest cover for both present and future generations by focussing on sustainable
248 development policies. Bhutan is largely a forested country and currently the forest cover
249 stands at 70.20% (NSB, 2016).

250 Much of the country's high altitude areas remain covered with snow in winter and early
251 spring. In 1996 the study area under snow and glacier cover was roughly one fourth of the
252 total (23.79%), whereas rock outcrops and bare lands made up about 8%. Areas below
253 snowline in the alpine regions mostly constitute grassland and meadows, including glacial
254 moraines which form grazing lands for yaks owned by pastoral nomads (Wangdi and Norbu,
255 2018). However, in the mid-and low altitude regions, agricultural land was 3.40%, grassland
256 6.70% and others was 0.20% in 1996. The current analysis does not deviate much from those
257 available figures and reports maintained with the Department of Agriculture (DoA) under the
258 Ministry of Agriculture and Forests in Bhutan (NSSC and PPD, 2011). In all the three study

periods, agricultural land continued to be low at about 3% which corroborates well with the statistics of the Department of Agriculture (DoA, 2016). Agriculture is the mainstay of Bhutan's economy, with 57% of the country's population depending on farming (MoLHR, 2016). It has been reported that agriculture contributes 16.52% to the national economy (NSB, 2017), and will most likely continue to be one of the most important sectors for the next couple of decades. On the other hand, limited cultivable land is considered to be one of the limiting factors mainly due to topographic challenges (Chhogyel and Ghimiray, 2018). .

The overall accuracy of ≥ 93.55% and the kappa statistics of ≥ 0.91 indicates that there exists almost perfect agreement between the classification and actual ground cover categories presented in **Table 3**. The producer's and user's accuracies were generally around 90-100%, except for a few classes that were lower due to commission and omission errors (Kiage et al., 2007; Chen and Wang, 2010). Slightly higher percentages of omission and commission errors in "others" could be attributed to overlap in land cover classes such as lawn grasses, greeneries and built up areas and sometimes barrenness getting depicted as agricultural land and pastures. However, the land cover category depicted as "others" in the current study is too small and does not have any significant contribution to the overall changes.

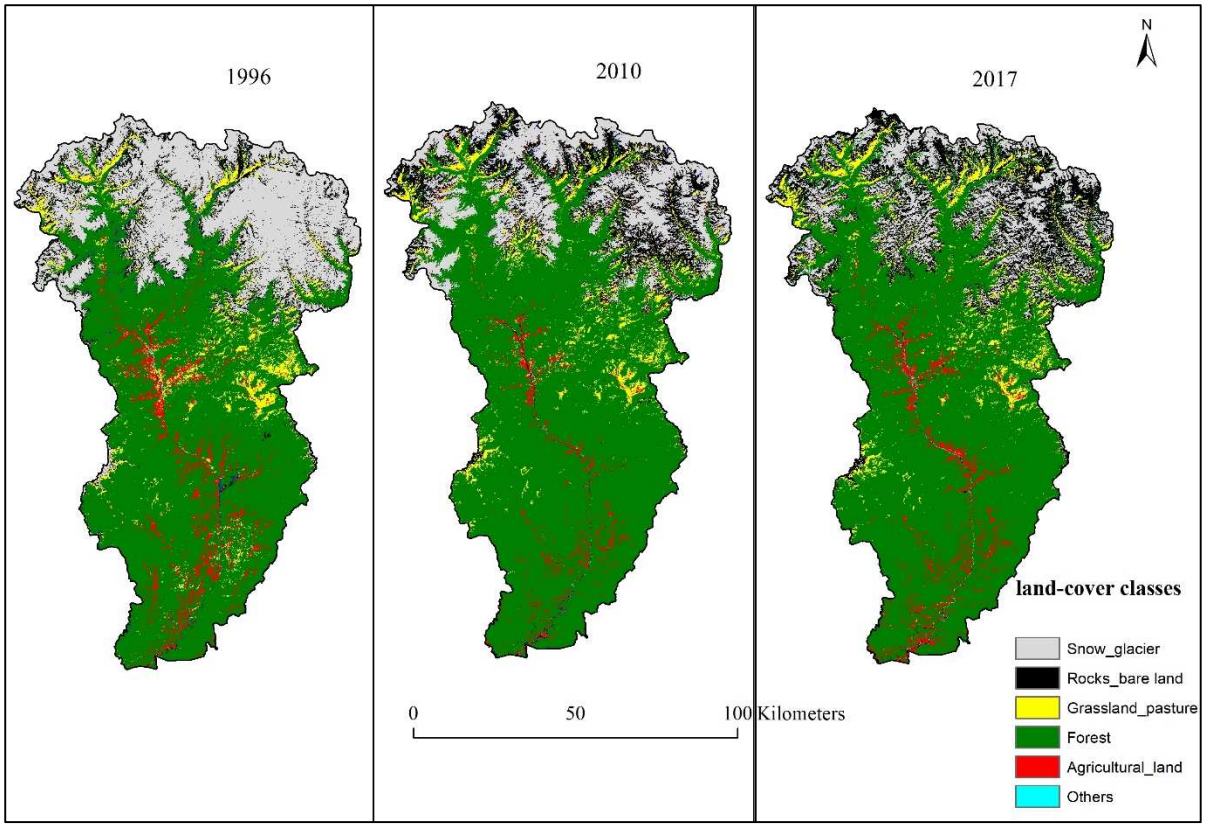


Fig. 3 Spatio-temporal images of land use and land cover for 1996, 2010 and 2017

Table 3. Information on accuracy assessment and kappa statistics

Classes	1996		2010		2017	
	Producer's accuracy	User's accuracy	Producer's accuracy	User's accuracy	Producer's accuracy	User's accuracy
Snow_glaciers	99.59	94.16	97.96	100.00	96.30	100.00
Rocks_bare land	88.89	99.05	96.19	94.39	93.91	96.35
Grassland_pasture	97.56	76.19	100.00	90.91	100.00	96.67
Forest	94.21	100.00	99.32	98.66	100.00	99.44
Agricultural land	81.63	95.24	97.89	100.00	95.41	99.05
Others	75.00	50.00	76.92	100.00	100.00	80.36
Overall accuracy	93.55		97.74		97.54	
Kappa coefficient ($\hat{k}$)	0.91		0.97		0.96	

3.2 Change detection

In terms of altitudinal landscape, our change detection analysis showed large changes in the higher elevation areas, which are mainly in the form of increases or decreases in extents of snow and glacier cover, rock outcrops and bare land (**Fig. 3**). Though there were some changes in grassland, pastures and forest cover in both high and mid-altitude regions, the changes in mid and low altitude areas were exclusively in agricultural land and others (built up areas). Since agricultural and others were just about 3% and <1%, respectively, the changes in these two land cover classes were too small to show visible changes at the current resolution of coarse Landsat image analysis (**Fig. 5**). Moreover, the greenery of forest cover showed a continuous spatial coverage right from the sub-tropical lower belt to the snow-clad mountains of greater Himalayas. Thus, the landscape changes were not clearly visible in the mid-and lower altitude areas. In terms of changes in agricultural land, the average changes in three window period corresponded to less than 100 km^2, thus making it invisible on the map obtained through change detection analysis.

The area under snow and glaciers had drastically reduced from 2534 km^2 to 1597 km^2 over 1996-2010 and to 1238 km^2 in 2017 (**Table 4**). This is a large reduction of 51% in a matter of 20 years (1996-2017). However, there was a slight increase in areas under rock outcrops and bare land from 935 km^2 (8.77%) to 1588 km^2 (14.91%) in the same period. Grasslands and pastures have also showed slight increase in area from 497 km^2 (4.67%) to 710 km^2 (6.66%) over the same period. The forest cover stood at 59.22% in 1996, 64.80% in 2010 and 62.99% in 2017 indicating a slight rise in later years. These changes could be attributed largely to the extent of snow cover when the images were taken as change detection images did not show

visible changes in the lower altitudes. It has been observed and reported that the glaciers and snows in the mountains of Bhutan have been receding at a faster rate in the last couple of decades (Karma et al., 2003; Rupper et al., 2012). **Fig. 4** depicts large changes in snow and glacier area in the northern zone of the study area which forms the watershed and source of water running Bhutan's hydro-electricity plants downstream (Hoy et al., 2015). One immediate impact could be on the reduction in supply of water to the Punatsang Chhu (river) and its tributaries which may affect hydro-electricity generation. The effect in future could be felt by two major hydropower projects of Punatsang Chhu I and II. There were also similar reports in the neighbouring countries of the Himalayas (Immerzeel et al., 2009; Gurung et al., 2011).

3.3 Attribution of changes to climatic factors

Increase in rock outcrops and bare lands could be an effect of snow and glacial melt and mass loss in the high mountains, thus leading to exposure of rocks underneath. A climate change vulnerability study of Eastern Himalayas by ICIMOD (2010) has also highlighted decreasing trend in snow cover, grassland and forest area with increasing bare rocks. These changes could also be attributed to increased erosive activities of rivers and streams caused by high intensity rains and GLOF, which were of frequent occurrence in the country (NEC, 2011). Bhutan has recorded some devastating incidences of GLOF in the last couple of decades and it is predicted that more events are likely in the near future due to the impacts of climate change (Komori et al., 2012). A series of devastating impacts of climate change on the country's farming was highlighted in the review of Chhogyel and Kumar (2018). Thus, the pressure on already limited cultivable land resources is likely to intensify in the near future. Lesser snow could also mean lesser quantity of water fed to rivers and streams which ultimately reduce irrigation water for farming. As we tread along, it is highly likely that the area under rocks and barren land in the current study would further increase which would also potentially affect the micro-climate of the particular area (Liu et al., 2016). On the other hand, as snow and glaciers recede further due to rise in temperature, the high altitude pastures and meadows would become more favourable for livestock farming. Slight increases in areas under grasslands and pastures over 1996-2017 indicates possibility of expanding pastoral farming areas in the high altitude areas of the country, which is a positive outcome of climate

change impact. Under the impact of climate change scenario in the high altitude areas, there will be likely gain in farming area due to warming (Maracchi et al., 2005).

Much of the changes in forest cover and pasture lands in the high altitude areas could be attributed to reduction in the frequency and amount of snow fall. Though Bhutan lacks in-depth research data on both snowfall pattern and frequency, a survey which assessed people's perception across the country showed that snowfall during the winters have become quite irregular in the recent years (NBC, 2011). Farmers in high altitude zones of the country opined that the depth of snowfall had decreased by about 61% in the last 10 years. Palazzi et al. (2013), also reported that total winter precipitation, as well as number of wet days in the Himalayas has decreased. The temperature and rainfall records of the study site for the study period 1997-2017 also support the findings of current research (**Fig. 6 and 7**). The six study districts received 90% of rainfall (480mm) in summer, followed by autumn (142mm) and winter months were usually drier (<20mm) (**Fig. 7**). Overall, the rainfall showed a decreasing trend, which might have largely affected snow cover and glacial area in higher elevation areas. Such a decreasing trend in winter precipitation, which falls mostly as snow in the high mountains, could contribute to the reduction in snow cover. Furthermore, a decreasing trend in snowfall was also reported in the western Himalayan region and was attributed to increasing trends in maximum, minimum and annual temperatures (Mir et al., 2015). The maximum temperatures in all four seasons showed rising trends with overall increase of 1^{o}C over a span of 20 years. While the minimum temperature fluctuated without discernible changes, it had risen by about 0.5^{o} C in the same period, thus indicating that the mountains are getting warmer. The summer months (June, July and August) were hotter with mean maximum temperature (Tmax) of 27.22^{o} C, whereas the Tmax for winter months (December, January and February) was 19.16^{o} C (**Fig. 6**). Likewise, the means of minimum temperatures (Tmin) for summer and winter months were 20.21^{o}C and 8.31^{o}C, respectively. These show that the weather in the study districts, in general, are hot and humid summers with driy cold winters. Generally, temperature rises in the spring and peaks in summer months, and gradually falls towards the later part of autumn before the onset of winter. The rising spring and summer temperatures were reported to substantially contribute to snow and glacial mass loss (Beniston et al., 2018), hence increasing bare rocks and grassland cover in the high elevations. Therefore, the landscape cover changes in the study area could be attributed to the rising temperature and decreasing precipitation. A research involving the use of T-index models in the Italian Alps revealed that snow ablation showed a Degree Day Factor (DDF) values of 2.3 mm D^{-1} ^{o} C^{-1} when a temperature threshold of +0.5^{o} C was applied (Senese et

al., 2014). This shows rising temperature is responsible for the ablation of glacier and snows in the high mountains. Also, the work of Madhura et al. (2015) indicated mid-tropospheric warming trend in the recent decades over western and central Asia that greatly increased baroclinic instability of the mean westerly wind that brings most of snow fall in the region. These changes could be directly correlated with the decreasing snow and glacier cover, thus leading to increased area under rock outcrop in the study site. Other studies undertaken within the regions of Himalayas also supports the findings of the current study (Shrestha et al., 1999; Miller et al., 2012).

Further, an ensemble of the present day estimation and future projections of temperature and snowfall through extensive bias corrected re-analysis by Viste and Sorteberg (2015) showed large reduction in snowfall in the basins of Ganga and Brahmaputra (which includes Bhutan) that forms main part of the Himalayan glacier (**Table 5**). The paper presented an extensive analysis of climate models which projected large changes in snowfall in the river basins of Ganga, Indus and Brahmaputra, indicating an upward shift in snowline by about 400-500m. The models also showed that these changes were mainly driven by temperature rise. It highlighted that the countries, such as Nepal and Bhutan, including parts of India are highly vulnerable to the temperature changes. The major highlights of their findings were all negative values in snow fraction with a positive change in rain (precipitation) (ΔP) in both MERRA and APHRODITE data, thus indicating that the annual reduction for all the river basins were due to the change in temperature (**Table 5**). Under the anthropogenic forcing of RCP 8.5, relative percent reduction in snowfall projected in the Indus, Ganges and Brahmaputra basins ranged between 34 to 71%. Similar findings have been reported by Ménégoz et al. (2013) whose simulations showed pronounced effects of temperature rise and precipitation changes in the Himalayas, leading to drastic reduction in snow and increased glacier melt. Thus, it is highly likely that land cover changes in Bhutan was driven by increase in temperature leading to changes in the pattern of precipitation.

The area under forest also increased slightly in 2010 as compared to 1996 due to lesser snow as evidenced from the temporal images (**Fig. 4 and 5**). However, in 2017, the forest cover decreased (-2.79%) which could represent area loss due to the combined factors of human and natural forces. Like elsewhere in the world, forest cover is reported to be declining despite interventions to curb indiscriminate use of forestry resources and logging operations (Wijaya et al., 2015; FAO, 2016). Although small in terms of area, there was also decline in agricultural land between 1996 and 2010 by about 27%. This decline could have been

brought about by fallowing of land which has become an important national issue in the country (Rinzin et al., 2016). According to agriculture statistics, 20,939.57 ha of agricultural land was left fallow across the country (DoA, 2012). The other factor, responsible for changes in the agricultural land cover was reported to be the impacts of agriculture as perceived by the farmers (Chhogyel et al., 2020). However, in most recent years, the DoA has been able to intensify crop cultivation through various plans, programs and projects to improve the country's food security status (Chhogyel and Ghimiray, 2018). This could have helped in bringing fallow land back to cultivation at 3.48% in 2017.

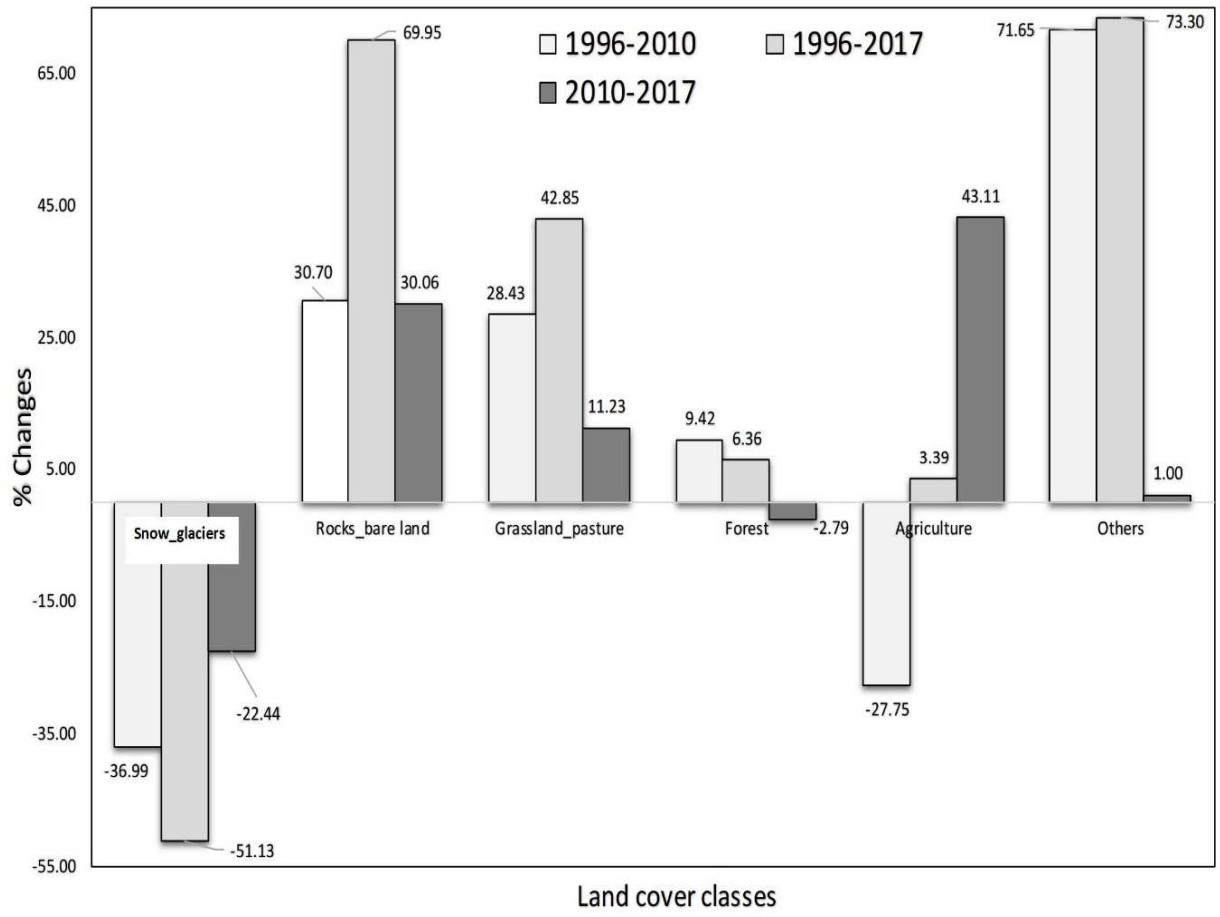
Table 4. Land cover and land use classes for the year 1996, 2010 and 2017 as derived through change detection analysis.

Land cover classes	1996		2010		2017	
	Area (km^2)	%	Area (km^2)	%	Area (km^2)	%
Snow_glaciers	2534	23.79	1598	14.99	1238	11.62
Rocks_bare land	935	8.77	1221	11.46	1589	14.91
Grassland_pasture	497	4.67	638	5.99	710	6.66
Forest	6310	59.22	6904	64.80	6711	62.99
Agricultural land	359	3.37	259	2.43	371	3.48
Others	20	0.19	35	0.33	36	0.33
Total	10,655	100.00	10,655	100.00	10,655	100.00

Table 5. MERRA and APHRODITE estimations of current percentages of snowfall and its relative percent changes in the projections of snow under the anthropogenic forcing of RCP8.5

Input data	Indus basin	Ganga basin	Brahmaputra basin
	%S	%S	%S
MERRA T2m	104	77	92
P APHRODITE	44	42	30
P,T APHRODITE	33	22	17
MERRA, ΔT	-34	-28	-71
MERRA, ΔP	4	12	17
MERRA, ΔTP	-33	-27	-64
APHRODITE, ΔT	-52	-57	-71
APHRODITE, ΔP	1	6	16
APHRODITE, ΔTP	-51	-56	-67

(Adapted from Viste and Sorteberg, 2015)



422

423 **Fig. 4 Changes in land cover classes between 1996, 2010 and 2017**

424

425

426

427

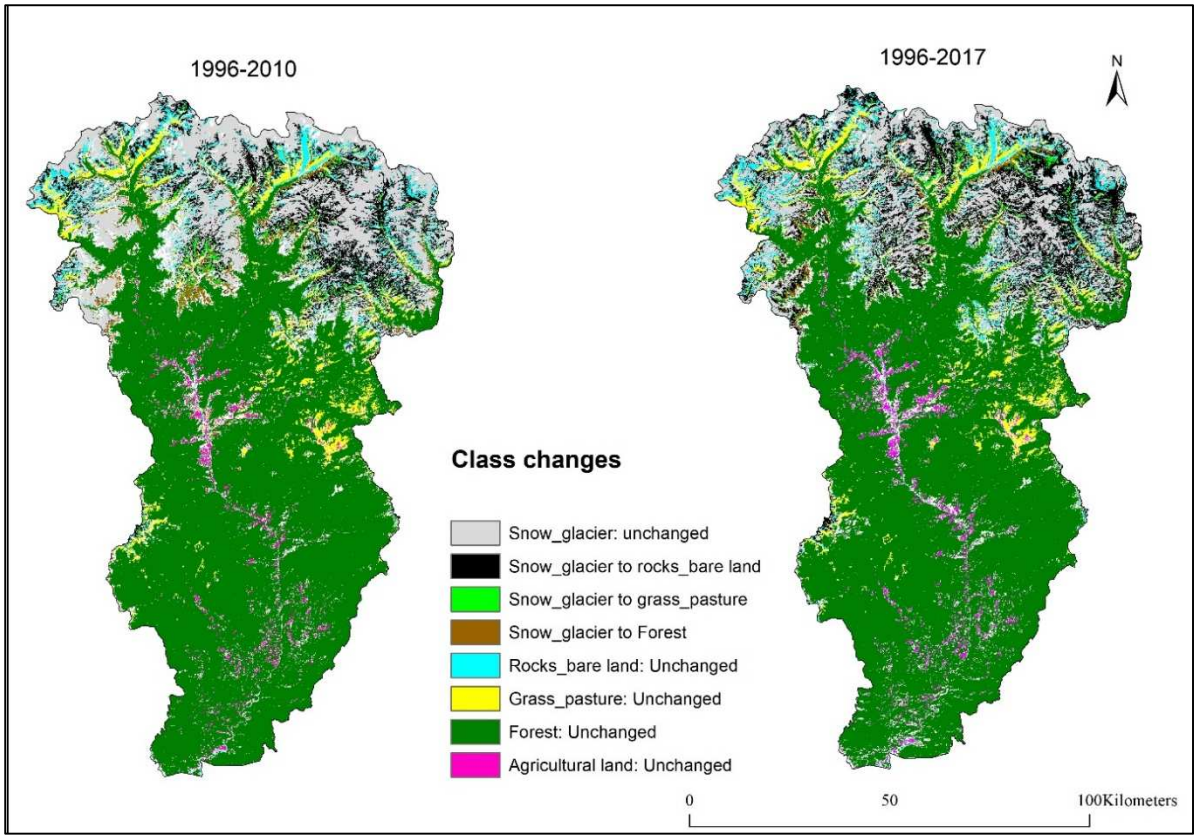
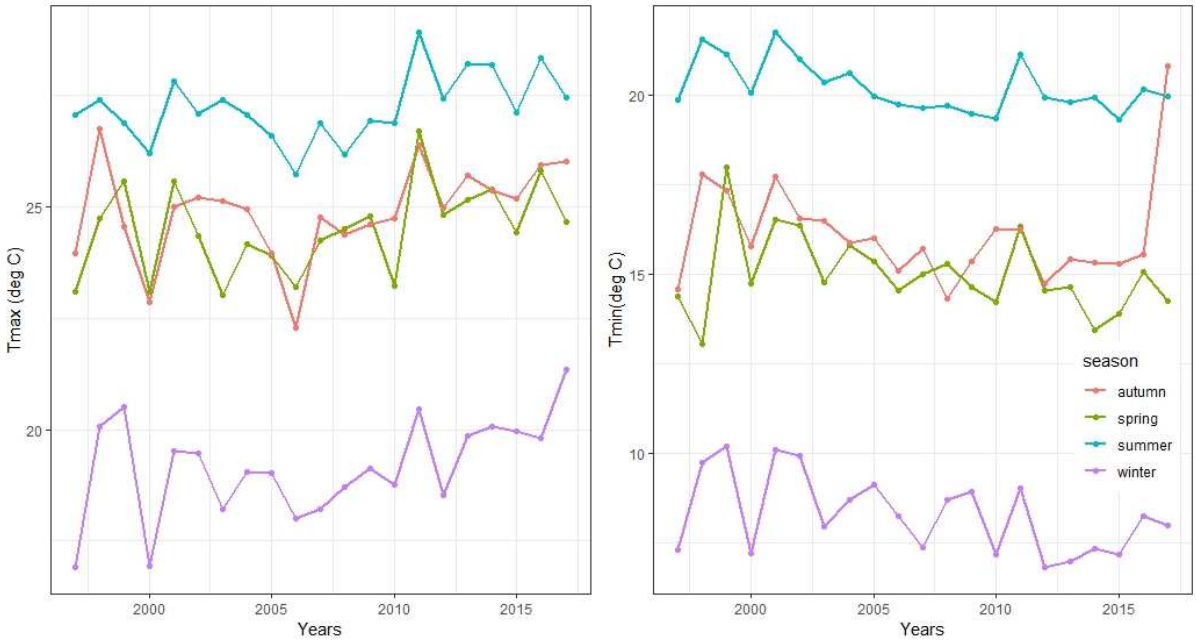


Fig. 5 Map of the study site depicting largest land cover class changes in snow and glacial areas.

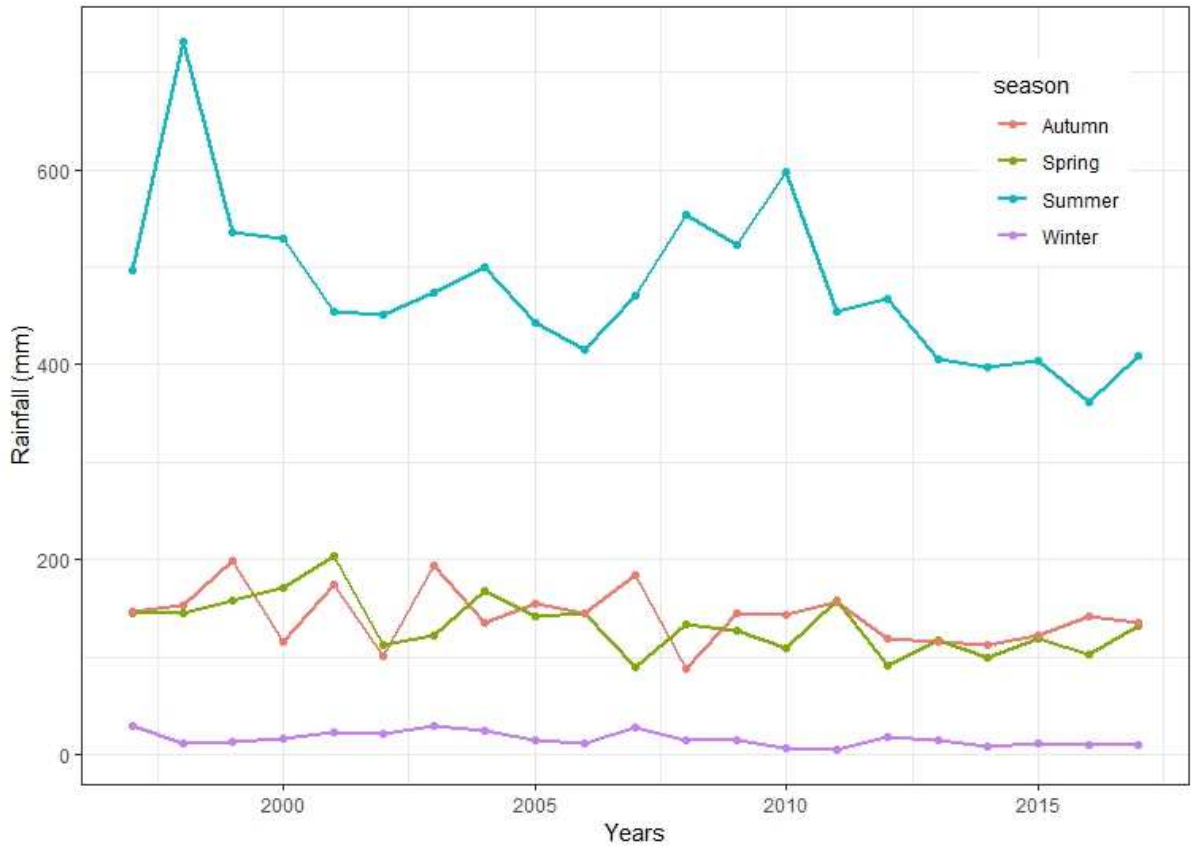


442

443 **Fig. 6 Seasonal fluctuations in maximum and minimum temperature (Tmax and Tmin)**
444 **trends for the study period 1996-2017.**

445

446



447

448 **Fig. 7 Seasonal rainfall trend of the study site (1997-2017)**

4 Conclusion

The study shows that major land cover changes have occurred over the three window periods (1996, 2010 and 2017) and these are possibly due to changes in climatic factors, especially temperature and precipitation. The temperature and rainfall trends for the same period shows a slight increase in mean temperature with fluctuating but decreasing rainfall, thus supporting the findings of this research. Reduction of snow and glacerized area by 51% in a span of about 20 years is a warning sign for Bhutan. This indicates that the impacts of global warming are being felt more in the high altitude mountains which are also supposed to be one of the most fragile landscapes of the world. The other attributes of land cover changes linked to climate change are increasing area under rock outcrops and barren land which could be attributed not only to the receding of snows and glaciers, but also to erratic patterns of rains, GLOF induced flash floods and drying of irrigation water sources. On the whole, there has been changes in agro-ecological landscape during the three window periods spanning over 20 years. Thus, this study provides an important scientific input for guiding socio-economic development policies, especially in the context of climate change and sustainability of natural resources. Additionally, it presents valuable information on the sustainability of hydro-power plants in the country. Though this research did not investigate yearly land cover changes, it does provide a synoptic view of the landscape changes which is very important for monitoring as well as management of natural resources for development and ecosystem sustainability.

Conflict of interest: The authors declare that they have no conflict of interest

References

Beldring, S., Vokso, A., 2011. Climate change impacts on the flow regimes of river in Bhutan and possible conssequences for hydropower development. In: Beldring, S. (Ed.). Norwegian Water Resources and Energy Directorate, Middelthunsgate, Norway, p. 156.

Beniston, M., Farinotti, D., Stoffel, M., Andreassen, L.M., Coppola, E., Eckert, N., Fantini, A., Giacona, F., Hauck, C., Huss, M., Huwald, H., Lehning, M., López-Moreno, J.-I., Magnusson, J., Marty, C., Morán-Tejéda, E., Morin, S., Naaim, M., Provenzale, A., Rabatel, A., Six, D., Stötter, J., Strasser, U., Terzago, S., Vincent, C., 2018. The European mountain cryosphere: a review of its current state, trends, and future challenges. The Cryosphere 12, 759-794.

Cao, Q., Yu, D., Georgescu, M., Han, Z., Wu, J., 2015. Impacts of land use and land cover change on regional climate: a case study in the agro-pastoral transitional zone of China. Environ. Res. Lett. 10, 124025.

Chalise, D., Kumar, L., Shriwastav, C.P., Lamichhane, S., 2018. Spatial assessment of soil erosion in a hilly watershed of Western Nepal. Environ. Earth Sci. 77.

Chen, Z., Wang, J., 2010. Land use and land cover change detection using satellite remote sensing techniques in the mountainous Three Gorges Area, China. Int. J. Remote Sens. 31, 1519-1542.

Chhogyel, N., Ghimiray, M., 2018. Food Policy in Bhutan. Reference module in food science. Elsevier, pp. 1-11.

Chhogyel, N., Kumar, L., 2018. Climate change and potential impacts on agriculture in Bhutan: a discussion of pertinent issues. Agric. Food Secur. 7, 7-79.

Chhogyel N, Kumar L, Bajgai Y, Hasan MK (2020) Perception of farmers on climate change and its impacts on agriculture across various altitudinal zones of Bhutan Himalayas International Journal of Environmental Science and Technology doi:10.1007/s13762-020-02662-8

Cohen, J., 2016. A Coefficient of Agreement for Nominal Scales. Educational and Psychological Measurement 20, 37-46.

Congalton, R.G., Oderwald, R.G., Mead, R.A., 1983. Assessing landsat classification accuracy using discrete multivariate analysis statistical techniques. Photogramm. Engg. Remote Sens. 49, 1671-1678.

Deng, X., Zhao, C., Yan, H., 2013. Systematic Modeling of Impacts of Land Use and Land Cover Changes on Regional Climate: A Review. Adv. Meteorol. 2013, 1-11.

DoA, 2012. Agriculture statistics 2012. Department of Agriculture (DoA), Ministry of Agriculture and Forests, Royal Government of Bhutan, Thimphu Bhutan.

DoA, 2016. Agriculture Statistics 2016. Department of Agriculture (DoA), Ministry of Agriculture and Forests, Royal Government of Bhutan, Thimphu Bhutan.

Dong, L., Xiong, L., Lall, U., Wang, J., 2015. The effects of land use change and precipitation change on direct runoff in Wei River watershed, China. Water Sci Technol. 71, 289-295.

Dorji, K., 2008. Water security: Leadership and committment. In: Secretarait (Ed.), 1st Asia Pacific water submit. World scientific publishing Co. Pte.Ltd, Beppu, Japan, pp. 74-77.

Dorji, U., Olesen, J.E., Bøcher, P.K., Seidenkrantz, M.S., 2016. Spatial Variation of Temperature and Precipitation in Bhutan and Links to Vegetation and Land Cover. Mt. Res. Dev. 36, 66-79.

FAO, 2016. State of the world's forests 2016. Forests and agriculture: landuse challenges and opportunities. Food and Agriculture Organization (FAO) of the United Nations, Rome, Italy.

Gurung, D.R., Kulkarni, A.V., Girraj, A., Aung, K.S., Shrestha, B., 2011. Monitoring of seasonal snow cover in Bhutan using remote sensing techniques. Curr. Sci. 101, 1364-1370.

Hoy, A., Katel, O., Thapa, P., Dendup, N., Matschullat, J., 2015. Climatic changes and their impact on socio-economic sectors in the Bhutan Himalayas: an implementation strategy. Reg. Environ. Change 16, 1401-1415.

ICIMOD, 2010. Climate change vulnerability of mountain ecosystems inthe Eastern Himalayas: Climate change impact and vulnerability in the Eastern Himalayas-Synthesis report. International Centre for Integrated Mountain Development (ICIMOD), kathmandu, Nepal.

Immerzeel, W.W., Droogers, P., de Jong, S.M., Bierkens, M.F.P., 2009. Large-scale monitoring of snow cover and runoff simulation in Himalayan river basins using remote sensing. Remote Sens. Environ. 113, 40-49.

Jensen, J.R., 2015. Introductory Digital Image Processing: a remote sensing perspective. Pearson Education, University of South Carolina, United States of America.

Karma, Ageta, Y., Naito, N., Iwata, S., Yabuki, H., 2003. Galcier distribution in the Himalayas and glacier shrinkage from 1963 to 1993 in the Bhutan Himalayas. Bulletin of glaciol. Res. 20, 29-40.

Karunakaran, S., 2011. Land use planning in the Jaffna peninsula of Northern Srilanka. LAP LAMBERT Academic publishing GmbH and Co.KG, Germany.

Kiage, L.M., Liu, K.B., Walker, N.D., Lam, N., Huh, O.K., 2007. Recent land-cover/use change associated with land degradation in the Lake Baringo catchment, Kenya, East Africa: evidence from Landsat TM and ETM+. Int. J. Remote Sens. 28, 4285-4309.

Komori, J., Koike, T., Yamanokuchi, T., Tshering, P., 2012. Glacial lake outburst events in the Bhutan Himalayas. Global Environ. Res. 16, 59-70.

Langat, P.K., Kumar, L., Koech, R., Ghosh, M.K., 2019. Monitoring of land use/land-cover dynamics using remote sensing: a case of Tana River Basin, Kenya. Geocarto Int. 1-19.

Liu, J., Shao, Q., Yan, X., Fan, J., Zhan, J., Deng, X., Kuang, W., Huang, L., 2016. The climatic impacts of land use and land cover change compared among countries. J. Geogr. Sci. 26, 889-903.

Madhura, R., Krishnan, R., Revadekar, J., Mujumdar, M., Gosami, B., 2015. Changes in western distrubances over the Western Himalayas in a warming environment. Clim. Dyn. 44, 1157-1168.

Mahmood, R., Pielke Sr, R.A., Hubbard, K.G., Niyogi, D., Bonan, G., Lawrence, P., McNider, R., McAlpine, C., Etter, A., Gameda, S., 2010. Impacts of land use/land cover change on climate and future research priorities. Bull. Am. Meteorol. Soc. 91, 37-46.

582 Maracchi, G., Sirotenko, O., Bindi, M., 2005. Impacts of present and future climate
583 variability on agriculture and forestry in the temperate regions: Europe. Clim. Change 70,
584 117-135.
585
586 Ménégoz, M., Gallée, H., Jacobi, H.W., 2013. Precipitation and snow cover in the Himalaya:
587 from reanalysis to regional climate simulations. Hydrol. Earth Syst. Sci. 17, 3921-3936.
588
589 Miller, J.D., Immerzeel, W.W., Rees, G., 2012. Climate Change Impacts on Glacier
590 Hydrology and River Discharge in the Hindu Kush–Himalayas. Mt. Res. Dev. 32, 461-467.
591
592 Mir, R.A., Jain, S.K., Saraf, A.K., Goswami, A., 2015. Decline in snowfal in response to
593 temperature in Satluj basin, Western Himalaya. J. Earth Syst. Sci 24, 365-382.
594
595 MoLHR, 2016. Labour force survey report 2016. Labour Market Information and Research
596 Division, Department of Employment and Human Resources, Ministry of Labour and Human
597 Resoruces (MoLHR), Thimphu Bhutan.
598
599 NBC, 2011. National action plan. Biodiversity persistence and climate change, Bhutan.
600 National Biodiversity Centre (NBC), Ministry of Agriculture and forests, Royal Government
601 of Bhutan, Thimphu Bhutan.
602
603 NBSAP, 2014. National biodiversity strategies and action plan (NBSAP) of Bhutan 2014.
604 National Biodiversity Centre (NBC), under the Ministry of Agriculture and Forests, Royal
605 Government of Bhutan, Thimphu Bhutan.
606
607 NC, 2008. The constitution of the kingdom of Bhutan. National Council (NC), the Partiament
608 of Bhutan, Thimphu.
609
610 NEC, 2000. Environment Assessment Act, 2000. National Environment Commission (NEC),
611 Royal Government of Bhutan, Thimphu Bhutan.
612
613 NEC, 2006. Bhutan National Adaptation Programme of Action. National Environment
614 Commission (NEC), Royal Government of Bhutan, Thimphu Bhutan.
615
616 NEC, 2011. Second national communication to the UNFCCC. National Environment
617 Commission (NEC), Ministry of Agriculture, Royal Government of Bhutan, Thimphu
618 Bhutan.
619
620 Ning, W., Shaoliang, Y., Joshi, S., Bisht, N., 2016. Yaks on the move. Transboundary
621 challenges and opportunities for yak raising in a changing Hindu Kush Himalayan region.
622 International Centre for Integrated Mountain Development (ICIMOD), Kathmandu, Nepal.
623
624 NSB, 2016. Statistical year book of Bhutan 2016. National statistical Bureau (NSB), Royal
625 Government of Bhutan, Thimphu Bhutan.
626
627 NSB, 2017. National Accounts Statistics 2017. National Statistics Bureau (NSB), Royal
628 Government of Bhutan, Thimphu Bhutan.
629

NSSC, PPD, 2011. Bhutan land cover assessment 2010 (LCMP-2010). National Soil Service Centre (NSSC) and Policy and Planning Division (PPD), Ministry of Agriculture and Forests, Royal Government of Bhutan, Thimphu Bhutan.

Palazzi, E., von Hardenberg, J., Provenzale, A., 2013. Precipitation in the Hindu-Kush Karakoram Himalaya: Observations and future scenarios. J. Geophy. Res. : Atmos. 118, 85-100.

Rahaman, M.M., Varis, O., 2009. Integrated water management of the Brahmaputra basin: Perspectives and hope for regional development. Natural Resources Forum 33, 60-75.

Rawat, J.S., Kumar, M., 2015. Monitoring land use/cover change using remote sensing and GIS techniques: A case study of Hawalbagh block, district Almora, Uttarakhand, India. Egypt. J. Remote Sens. Sp. Sci. 18, 77-84.

Rinzin, J., Gyeltshen, N., Dorji, T., Tenzin, P., Dorji, R., Dakpa, p., Tshering, S., Karma, 2016. Review of agriculture policy by the Natural Resources and Environment Committee (NREC). Parliament of Bhutan, Thimphu Bhutan, p. 29.

Rupper, S., Schaefer, J.M., Burgener, L.K., Koenig, L.S., Tsering, K., Cook, E.R., 2012. Sensitivity and response of Bhutanese glaciers to atmospheric warming. Geophy. Res. Lett. 39, n/a-n/a.

Saidi, H., Dresti, C., Manca, D., Ciampittiello, M., 2018. Quantifying impacts of climate variability and human activities on the streamflow of an Alpine river. Environ. Earth Sci. 77.

Saleh, M., Becker, M., 2018. New estimation of Nile Delta subsidence rates from InSAR and GPS analysis. Environ. Earth Sci. 78.

Senese, A., Maugeri, M., Vuillermoz, E., Smiraglia, C., Diolaiuti, G., 2014. Using daily air temperature thresholds to evaluate snow melting occurrence and amount on Alpine glaciers by T-index models: the case study of the Forni Glacier (Italy). The Cryosphere 8, 1921-1933.

Shahnawaz, S., Strobl, J., 2015. A zonal analysis of the climatic conditions in Bhutan. In: Shahnawaz, S., Thinley, U. (Eds.), Climate change, environment and development in Bhutan. College of Natural Resources (CNR), Royal University of Bhutan, Thimphu Bhutan, pp. 1-22.

Shrestha, A.B., Wake, C.P., Mayewski, P.A., Deibb, J., 1999. maximum temperature trends in the Himalaya and its vicinity: An analysis based ontemperature records from Nepal for the peroid 1971-94. Am.Meteorol. Soc. 12, 2775-2786.

Singh, S.P., Singh, V., Skutsch, M., 2011. Rapid warming in the Himalayas: Ecosystem responses and development options. Clim. Dev. 2, 221-232.

Sinha, P., Kumar, L., Reid, N., 2012. Three-date landsat thematic mapper composite in seasonal land-cover change identification in a mid-latitudinal region of diverse climate and land use. J. Appl. Remote Sens. 6, 063595.

679 Tölle, M.H., Engler, S., Panitz, H.-J., 2017. Impact of Abrupt Land Cover Changes by
680 Tropical Deforestation on Southeast Asian Climate and Agriculture. J. Clim. 30, 2587-2600.
681
682 Turner, B.L., Lampin, E.F., Reenbery, A., 2007. The emergence of land change science for
683 global environmental change and sustainability. Proc. Natl. Acad. Sci. 104, 20666-20671.
684
685 Turner, W., Spector, S., Gardiner, N., Fladeland, M., Sterling, E., Steininger, M., 2003.
686 Remote sensing for biodiversity science and conservation. Trends in Ecol. Evol. 18, 306-314.
687
688 Viste, E., Sorteberg, A., 2015. Snowfall in the Himalayas: an uncertain future from a little-
689 known past. The Cryosphere 9, 1147-1167.
690
691 Wangdi, S., Norbu, N., 2018. Good fences are key to sustainable pasture management and
692 harmonious pastoral society of Merak and Sakteng in Bhutan. Pastoralism 8.
693
694 Wijaya, A., Sugardiman Budiharto, R.A., Tosiani, A., Murdiyarso, D., Verchot, L.V., 2015.
695 Assessment of Large Scale Land Cover Change Classifications and Drivers of Deforestation
696 in Indonesia. ISPRS - International Archives of the Photogrammetry, Remote Sensing and
697 Spatial Information Sciences XL-7/W3, 557-562.
698
699 Wulder, M.A., Coops, N.C., Roy, D.P., White, J.C., Hermosilla, T., 2018. Land cover 2.0.
700 Int. J. Remote Sens. 39, 4254-4284.

701

702

Jurnal Pengabdian Kolaborasi dan Inovasi IPTEKS
Volume 1, No 4 – Agustus 2023
e-ISSN : 29863104

PEMETAAN PENGGUNAAN LAHAN DI KOTA PALU MENGGUNAKAN CITRA SENTINEL 2-A

Muhammad Adam Suni[1*], Andre Kurniawan Borman[2], Mohammad Fahrul Himalaya Umar[2], Agung Dwi Kurniawan[3],
[1] Balai Besar Taman Nasional Lore Lindu, Palu
[2,3] Fakultas Kehutanan, Universitas Tadulako, Palu

muhammadadamsuni@gmail.com*

Received: 12-08- 2023	Revised: 20-08-2023	Approved: 25-08-2023

ABSTRAK

Pembuatan peta dalam pengabdian masyarakat ini dilatarbelakangi kebutuhan data akan luas areal penggunaan lahan oleh berbagai pihak baik dari instansi pemerintah, kebutuhan penelitian dan pendidikan, maupun instansi non pemerintah. Kebutuhan data ini cukup tinggi sementara ketersediaan data terbatas dan tidak ada pembaharuan data setiap tahun. Sementara perubahan luasan areal penggunaan sangat dinamis. Untuk mengetahui luas areal penggunaan lahan secara efektif dan efisien, dapat dilakukan pemetaan dengan menggunakan penginderaan jauh. Tujuan pengabdian Masyarakat ini adalah untuk mengetahui luas dan kelas penggunaan lahan di Kota Palu. Pengabdian ini merupakan penelitian secara deskriptif. Luas penggunaan lahan didapatkan melalui penginderaan jauh dengan metode digitasi visualisasi (on screen) menggunakan citra sentinel 2-A dan survey langsung dilapangan. Kombinasi band yang digunakan pada citra sentinel 2-A adalah kombinasi band 4-3-2. Hasil pengabdian masyarakat menunjukkan bahwa terdapat 12 (dua belas) kelas penggunaan lahan di Kota Palu yang didominasi oleh kelas tutupan lahan semak belukar 14.185,91 Ha (37,36%), hutan 6.669,53 Ha (17,57%) dan pemukiman6.431,04 Ha (16,94%).

Kata Kunci : *Pemetaan, Citra Sentinel 2A, Sistem Informasi Geografis*

PENDAHULUAN

Kota Palu dengan wilayah seluas 395,06 Km^2 adalah Ibu Kota Provinsi Sulawesi Tengah. Terdiri atas 8 kecamatan pada tahun 2018. Wilayah ini terbentang dari Palu Selatan (Kecamatan paling selatan) sampai di tawaeli (Kecamatan paling utara. Kecamatan yang terluas adalah Kecamatan Mantikulore yaitu 206,8 Km^2 dan yang terkecil adalah Kecamatan Palu Timur yaitu sebesar 7,7 Km^2. Implikasi pertumbuhan penduduk berdapak pada kebutuhan lahan antara lain: pertanian, pemukiman, jasa dan sarana transportasi. Desakan lahan terpakai akan berdampak pada penggunaan lahan yang menimbulkan terjadinya konversi lahan. Di sisi lain, penggunaan lahan adalah aktivitas manusia yang dilakukan di atas lahan untuk memenuhi tujuan tertentu. Tutupan dan penggunaan lahan dalam beberapa kasus dapat memiliki sebutan yang sama (Van Noordwijk *et al*. 2008).

Permasalahan lahan di perkotaan secara umum berkisar pada persoalan kepemilikan, alih fungsi lahan bervegetasi menjadi kawasan terbangun, kerusakan

lahan akibat kegiatan penambangan sumberdaya alam secara terbuka dan merusak lingkungan yang dapat mengakibatkan bencana alam seperti banjir dan tanah longsor. Tutupan lahan yang tergerus merupakan persoalan serius yang terdapat pada pengelolaan lahan perkotaan yang terus mengalami perubahan signifikan dari tahun ke tahun. Perubahan penggunaan lahan terutama terjadi pada alih fungsi lahan pertanian sawah dan bukan sawah yang mengalami penurunan serta peningkatan lahan yang dibangun (Hidayat dan Noor, 2020). Kepadatan penduduk dapat mempengaruhi kualitas hidup penduduknya. Pada daerah dengan kepadatan yang tinggi, usaha peningkatan kualitas penduduk akan lebih sulit dilakukan. Hal ini menimbulkan permasalahan sosial ekonomi, kesejahteraan, Keamanan, ketersediaan lahan, air bersih dan kebutuhan pangan (Suni *et al,* 2023).

Penginderaan jauh didefinisikan sebagai perolehan informasi suatu objek tanpa adanya kontak fisik dengan objek tersebut. Informasi dalam penginderan jauh diperoleh dengan mendeteksi dan mengukur perubahan dari objek yang digeneralisasikan dengan kondisi optic disekitarnya, meliputi elektromagnetik, akustik dan potensial. Medan Elektromagnetik yang dipancarkan lalu dipantulkan oleh objek, gelombang akustik dipantulkan atau dihamburkan oleh objek (Rahmatsyah, Juliani, dan Tampubolon, 2020). Satelit Sentinel 2 MSI adalah satelit milik *Europe Space Agency* (ESA) yang diluncurkan pada 23 Juni 2015. Sentinel 2 MSI memiliki sudut inklinasi 98,62^{o} dengan periode rotasi selama 40 menit dan merekam permukaan bumi pada 10:30 pagi waktu setempat dengan tujuan untuk memperoleh hasil dengan tutupan awan minimal serta penyinaran matahari yang sesuai (Suhet, 2014).

Perkembangan perubahan tutupan lahan suatu wilayah dapat dianalisis dengan memanfaatkan data penginderaan jauh (remote sensing) berupa citra satelit multitemporal. Pemanfaatan teknologi penginderaan jauh merupakan salah satu cara untuk mengetahui secara cepat alih fungsi lahan. Alih fungsi lahan juga dapat diartikan sebagai perubahan untuk penggunaan lain disebabkan oleh faktor–faktor yang secara garis besar meliputi keperluan untuk memenuhi kebutuhan penduduk yang makin bertambah jumlahnya dan meningkatnya tuntutan akan mutu kehidupan yang lebih baik (Suni, dan Baharuddin, 2023).

Perkembangan perubahan tutupan lahan suatu wilayah dapat dianalisis dengan memanfaatkan data penginderaan jauh (*remote sensing*) berupa citra satelit *multitemporal*. Pemanfaatan teknologi penginderaan jauh merupakan salah satu cara untuk mengetahui secara cepat alih fungsi lahan. (Suni *et al,* 2023). Citra penginderaan jauh, dapat memberikan gambaran keruangan dan ukuran yang merupakan data yang bermanfaat dalam mempelajari fenomena atau kenampakan muka bumi, yang selanjutnya dapat digunakan sebagai dasar rencana dan pemanfaatan praktis (Feri, 2007).

Penginderaan jauh dapat memberikan informasi mengenai karakteristik tutupan vegetasi suatu hutan yang di teliti. Maullana dan Darmawan (2014) mengungkapkan bahwa penginderaan jauh adalah suatu metode untuk mengidentifikasi objek di permukaan bumi tanpa kontak langsung dengan objek. Klasifikasi *supervised* melibatkan interaksi analis secara intensif, dimana analis menuntun proses klasifikasi dengan identifikasi objek pada citra (training area). Sehingga pengambilan sampel perlu dilakukan dengan mempertimbangkan pola spektral pada setiap panjang gelombang tertentu, sehingga diperoleh daerah acuan

yang baik untuk mewakili suatu objek tertentu. Metode *supervised* (dengan bimbingan), pada metode ini, analis terlebih dahulu menentukan beberapa training area (daerah contoh) pada citra sebagai kelas kenampakan objek tertentu. Penetapan ini berdasarkan pengetahuan analis terhadap wilayah dalam citra mengenai daerah-daerah tutupan lahan. Nilai-nilai piksel dalam daerah contoh kemudian digunakan oleh perangkat lunak komputer sebagai kunci untuk mengenali piksel lain. Daerah yang memiliki nilai-nilai piksel sejenis akan dimasukkan ke dalam kelas yang telah ditentukan sebelumnya.

Suni *et al* (2023) melakukan penelitian dengan menggunakan citra satelit Landsat 8 OLI untuk mengetahui kelas dan perubahan luasan tutupan lahan pada sub DAS Toili di Kabupaten Banggai. Hasil penelitian menunjukan bahwa terdapat 9 (Sembilan) kelas tutupan lahan yaitu, hutan lahan kering sekunder, pemukiman, perkebunan, pertanian lahan kering, sawah, semak belukar, tanah terbuka, tubuh air, dan awan yang didominasi oleh kelas tutupan lahan perkebunan, pertanian lahan kering, sawah dan semak belukar. Terjadi perubahan luasan terbesar terdapat pada kelas tutupan lahan perkebunan yang mengalami perubahan luasan di tahun 2022 menjadi 6.342,54 Ha atau bertambah luasannya sebanyak 2.392,35 Ha. Sedangkan perubahan tutupan lahan terkecil terdapat pada kelas tutupan lahan berupa tutupan lahan berupa hutan lahan kering sekunder mengalami perubahan luasan di tahun 2022 menjadi 255,07 Ha atau berkurang luasannya sebanyak 103,48 Ha.

Tablaseray, Pairin, Fakdawer, dan Hamuna, (2018) melakukan penelitian dengan menggunakan citra satelit Landsat 8 OLI untuk mengetahui kerapatan dan sebaran mangrove di pesisir Pulau Biak, Papua. Pada penelitian tersebut dilakukan analisis kerapatan mangrove dengan menggunakan formula Normalized Differece Vegetation Index (NDVI). Hasil penelitian menunjukan bahwa luasan mangrove di wilayah pesisir timur Pulau Biak sebesar 144,81 ha, dimana kerapatan jarang 89,64 ha, kerapatan sedang 26,19 ha dan kerapatan padat 28,98 ha. Rendahnya luasan mangrove umumnya diakibatkan oleh faktor antropogenik seperti penebangan, perubahan alih fungsi mangrove dan akibat tsunami yang terjadi pada tahun 1996.

Gifari, Kusrini, dan Yuana, (2023) Melakukan penelitian dengan hasil identifikasi jenis tutupan lahan di Kota Samarinda menggunakan metode terbimbing MLC pada tahun 1994 menghasilkan luasan tutupan lahan vegetasi alami dengan persentase 53,81% seluas 38.868 ha, vegetasi sekunder dengan persentase 32,66% seluas 23.591 ha, pemukiman dengan persentase 10,24% seluas 7401 ha, water body dengan persentase 3,29% seluas 2368 ha. Sedangkan pada tahun 2022 menghasilkan luasan tutupan lahan vegetasi alami dengan persentase 47,43% seluas 34.077 ha, vegetasi sekunder dengan persentase 27,14% seluas 19.503 ha, pemukiman dengan persentase 19,75% seluas 14.172 ha, water body dengan persentase 5,68% seluas 4086 ha.

Hasil penelitian Dimyati, Somantri, dan Sugito, (2022) menunjukan tingkat perubahan Penggunaan lahan yang terjadi di Kecamatan Parongpong pada kurun waktu dua tahun yaitu dimulai pada tahun 2017 sampai dengan tahun 2019 memiliki laju perubahan pada rentang nilai antara -0,21% sampai dengan 0,17 %. Pengurangan penggunaan lahan terbesar pada semak Belukar dan lahan kosong berkurang sebesar 8,9 Ha dan penambahan terbesar pada penggunaan lahan

Pemukiman dan Tempat Kegiatan Sebesar 7,27 Ha. Pola Perubahan yang terjadi hanya pada empat jenis Penggunaan lahan Hutan, Semak Belukar, ladang dan pemukiman.

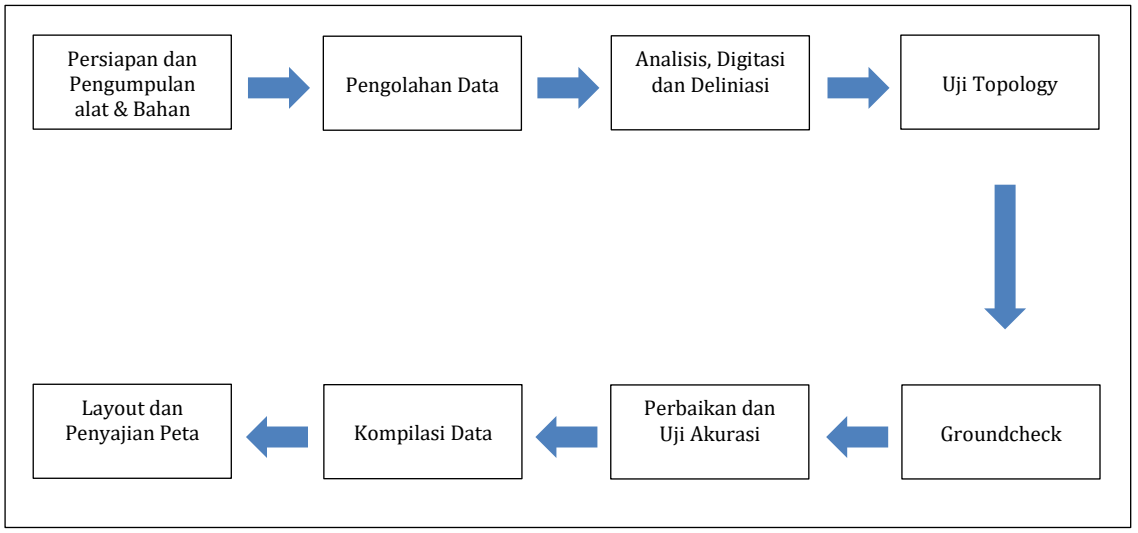
Salah satu upaya untuk mengetahui kelas penggunaan lahan dan luasan terkini adalah dengan sistem penginderaan jauh. Teknologi penginderaan jauh adalah teknologi yang mudah, murah, dan cepat sebagai alternatif yang cukup baik untuk melakukan pemetaan ekosistem mangrove. Citra yang sering digunakan dalam penginderaan jauh diantaranya foto udara menggunakan drone, citra SPOT, Landsat, Google Earth, Sentinel, dan lainnya.

Melalui sistem penginderaan jauh dapat mempermudah penyajian informasi spasial khususnya yang terkait dengan kondisi lahan serta dapat menganalisis dan memperoleh informasi terbaru kondisi suatu lingkup wilayah tertentu. Mengingat pentingnya data luasan dan areal kelas penggunaan lahan di Kota Palu, perlu dilakukan pengabdian masyarakat yang merupakan hilirisasi penelitian pemetaan areal penggunaan lahan dengan metode penginderaan jauh menggunakan citra satelit yang memiliki resolusi cukup baik dan mudah didapatkan. Pengabdian masyakat ini bertujuan untuk mengetahui kondisi terkini penggunaan lahan dan luas areal di kota Palu. Batasan masalah dalam pengabdian masyarakat ini adalah :

1) Daerah pelaksanaan ini berada di wilayah administrasi Kota Palu Provinsi Sulawesi Tengah yang secara geografis terletak di koordinat 119°45 - 121°15 BT dan 0°36 - 0°56 LS.
2) Data spasial yang digunakan adalah citra sentinel level 2-A liputan bulan 28 Juli 2021 dan 18 Juni 2022, citra satelit google earth, dan peta rupa bumi Indonesia.

METODE KEGIATAN

Pengabdian masyarakat ini dilaksanakan pada bulan Oktober sampai Desember 2022 yang meliputi studi literatur, pengumpulan dan pengolahan data, pengecekan lapangan, analisis data, dan penyusunan naskah. Lokasi pengabdian masyarakat berada di Kota Palu. Bahan yang digunakan adalah data sekunder berupa citra sentinel 2-A liputan tanggal 28 Juli 2021 dan 18 Juni 2022, citra satelit google earth, peta Rupa Bumi Indonesia skala 1: 50.000 tahun 2019. Alat yang digunakan adalah laptop dengan spesifikasi RAM 8 Gb, Software ArcGIS 10.8, Software SAS Planet, dan Google Chrome. Peta penggunaan lahan didapatkan dengan metode *digitasi on screen* mengunakan citra satelit google earth dan citra sentinel level 2A dengan kombinasi band 4-3-2. Sesuai SNI 7645-2010 *Klasifikasi Penutup Lahan*, luas dinyatakan dalam bilangan bulat dengan satuan hektar. Kelas penutupan lahan ditentukan dengan interpretasi berdasarkan kenampakan visual pada citra satelit. Tahapan pelaksanaan pengabdian masyarakat pembuatan peta mangrove iniadalah sebagai berikut:



Gambar 1.
Diagram alur pelaksanaan pengabdian masyarakat

(a) Persiapan dan pengumpulan alat bahan
Komputer yang digunakan diinstal aplikasi ArcGIS 10.8.1 dan SAS Planet. Buka software SAS Planet dan buat polygon pada kota Palu Provinsi Sulawesi Tengah, kemudian unduh citra dengan resolusi pada *zoom* 19. Buka website https://scihub.copernicus.eu/pada lalu buat akun dan unduh citra sentinel level 2-A pada lokasi kota Palu Provinsi Sulawesi Tengah. Buka website https://tanahair.indonesia.go.id/ lalu buat akun dan unduh peta Rupa Bumi Indonesia kota Palu Provinsi Sulawesi Tengah. Buka software ArcGIS 10.8.1 kemudian buat shapefile polygon baru dan tambahkan atribut kelas lahan, luas, keterangan. Simpan semua data yang akan digunakan pada lokasi penyimpanan yang sama.

(b) Pengolahan data
Buka aplikasi ArcGIS 10.8.1, sambungkan folder lokasi penyimpanan data spasial yang digunakan. Tambahkan data *shapefile* wilayah administrasi seluruh kota, gabungkan dengan perintah *Union* atau *Intersect* pada tab *Geoprocessing*. Tambahkan data citra sentinel 2-A, buka Composit Band pada *ArcToolbox* lalu *composite* semua citra sentinel 2-A yang ada. Simpan hasil *Composit Band* pada lokasi penyimpanan yang sama.

(c) Proses analisis, digitasi dan deliniasi
Ubah sistem koordinat pada layer menjadi *Universal Transverse Mercator* Zona 50 S. Tambahkan shapefile polygon, citra satelit google earth, citra sentinel 2-A ke layer ArcGIS. Lakukan tumpang susun (overlay) data-data tersebut. Ubah band (pita) pada citra sentinel 2-A menjadi 4-3-2 untuk memudahkan proses analisis. Aktifkan editor, digitasi dan deliniasi pada lokasi kota Palu. Tentukan kelas penggunaan lahan berdasarkan kenampakan visual dan tuliskan kategori kelas pada *attribute table*. Hitung luas dengan *calculate geometry*. Tambahkan *shapefile* administrasi yang telah di *union* kemudian *overlay* dengan *shapefile* penggunaan lahan yang telah dibuat.

(d) Uji topology dan perbaikan data

Lakukan *uji topology* pada *shapefile* batas admistrasi dan penggunaan lahan yang telah digabungkan untuk melihat *polygon* yang tumpang tindih dan terdapat celah diantara polygon yang ada. Perbaiki apabila *terdapat topology error*. Periksa *atribute table* dan isi atribut pada kolom yang masih kosong dengan disesuaikan pada *polygon* terdekat.

(e) Penentuan lokasi dan *Groundcheck*
Lokasi pengecekan lapangan ditentukan dengan mempertimbangkan akses menuju lokasi dan diutamakan pada lokasi yang yang terdapat keraguan saat interpretasi citra. Dokumentasikan kondisi lokasi pengecekan lapangan. Catat koordinat, dan catatan lain apabila terdapat informasi penting lainnya.

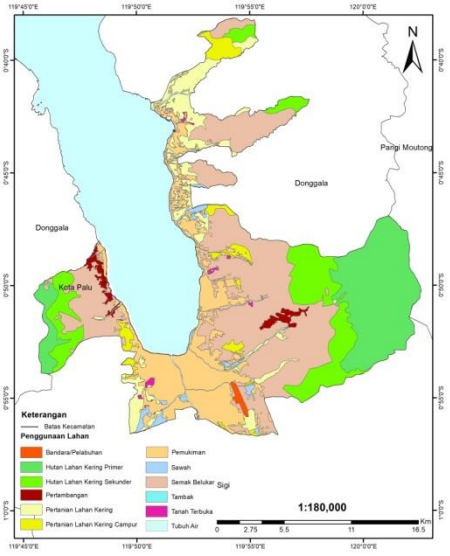
(f) Uji Akurasi
Perbaiki peta pada lokasi yang tidak sesuai antara kondisi lapangan dengan hasil analisis peta. Uji akurasi hasil pengolahan citra diperlukan untuk menghasilkan informasi yang sesuai dengan kondisi yang seharusnya.

(g) Kompilasi Data
Kompilasi data digunakan untuk menghitung jumlah kategori kelas penggunaan lahan dan seluruh luasan dari hasil akhir.

(h) *Layout* dan Penyajian peta
Buat layout pada ukuran kertas A4 dan cetak peta menggunakan skala 1:180.000.

HASIL DAN PEMBAHASAN

Hasil pengolahan dan analisis data dari pengabdian masyarakat didapatkan kelas dan luas penggunaan lahan di Kota Palu tahun 2022 diperoleh dari hasil *digitasi on screen* menggunakan citra satelit *google earth* dan citra Sentinel level 2A. Dari hasil analisis ini, diperoleh 12 (dua belas) tipe/kelas penggunaan lahan di Kota Palu dapat dilihat pada gambar 2.



Gambar 2.
Peta Penggunaan Lahan Kota Palu

Dari hasil pengolahan data citra Sentinel 2A tahun 2022 menunjukan bahwa

kawasan hutan lahan kering primer memiliki luas 6.669,53 Ha atau (17,57%), hutan lahan kering sekunder memiliki luas 4.842,32 Ha atau (12,75%), permukiman memiliki luas 6.431,04 Ha atau (16,94%), pertambangan memiliki luas 543,48 Ha atau (1,43%), pertanian lahan kering memiliki luas 3.024,21 Ha atau (7,96%), pertanian lahan kering campuran memiliki luas 1.187,57 Ha atau (3,13), sawah memiliki luas 396,17 Ha atau (1,04%), semak belukar memiliki 14.185,91 Ha atau (37,36%), tambak memiliki luas 7,48 Ha atau (0,02%) tanah terbuka memiliki luas 192,41 Ha atau (0,51%), tubuh air memiliki luas 250,94 Ha atau (0,66%) dan bandara/pelabuhan memiliki luas 239,18 Ha atau (0,63%) dari luas total. Pada tabel tersebut diketahui penggunaan lahan terluas yaitu semak belukar seluas 14.185,91 Ha, sedangkan penggunaan lahan terendah yaitu bandara/Pelabuhan dengan luas 7,48 Ha, dapat dilihat pada tabel 1.

Tabel 1. Kelas dan Luas Penggunaan Lahan Kota Palu tahun 2022

Penggunaan Lahan 2022	Luas (Ha)	Persen (%)
Hutan lahan kering primer	6.669,53	17,57
Hutan lahan kering sekunder	4.842,32	12,75
Permukiman	6.431,04	16,94
Pertambangan	543,48	1,43
Pertanian Lahan Kering	3.024,21	7,96
Pertanian Lahan Kering Campuran	1.187,57	3,13
Sawah	396,17	1,04
Semak Belukar	14.185,91	37,36
Tambak	7,48	0,02
Tanah Tebuka	192,41	0,51
Tubuh Air	250,94	0,66
Bandara/Pelabuhan	239,18	0,63
Jumlah	**37.970,26**	**100**

KESIMPULAN

Berdasarkan hasil pengabdian kepada masyarakat yang telah dilakukan, dapat diperoleh kesimpulan terdapat 12 (dua belas) tipe/kelas penggunaan lahan di Kota Palu yaitu, hutan lahan kering primer, hutan lahan kering sekunder, pemukiman, pertambangan, pertanian lahan kering, pertanian lahan kering campuran, sawah, semak belukar, tambak, tanah terbuka, tubuh air, dan bandara yang didominasi oleh kelas tutupan lahan semak belukar 14.185,91 Ha (37,36%), hutan 6.669,53 Ha (17,57%) dan pemukiman6.431,04 Ha (16,94%).

DAFTAR PUSTAKA

Dimyati, A. E. F., Somantri, L., dan Sugito, N. T. (2022). Klasifikasi Berbasis Objek Citra Satelit Sentinel 2 untuk Pemetaan Perubahan Lahan di Kecamatan Parongpong Kabupaten Bandung Barat. Jurnal Geografi: Media Informasi Pengembangan dan Profesi Kegeografian, 19(1), 24-28.

Feri, T. 2007. Analisis Perubahan Penggunaan Lahan dan Keterkaitannya Dengan Fluktuasi Debit Sungai Di DAS Antokan Provinsi Sumatera Barat. Tesis. Institut Pertanian Bogor. Bogor. 124.

Gifari, O. I., Kusrini, K., dan Yuana, K. A. (2023). Analisis Perubahan Tutupan Lahan Menggunakan Metode Klasifikasi Terbimbing Pada Data Citra Penginderaan

Jauh Kota Samarinda-Kalimantan Timur. Informatika Mulawarman: Jurnal Ilmiah Ilmu Komputer, 18(2), 71-77. http://dx.doi.org/10.30872/jim.v18i2.5716

Hidayat, M. A., dan Noor, A. (2020). Pengaruh pertumbuhan ekonomi terhadap alih fungsi lahan di kota samarinda. Inovasi, 16(2), 299-308. https://doi.org/10.30872/jinv.v16i2.8256

Maullana, D. A., dan Darmawan, A. (2014). Perubahan penutupan lahan di taman nasional way kambas. Jurnal Sylva Lestari, 2(1), 87-94.

Rahmatsyah, M. S., Juliani, R., dan Tampubolon, T. (2020). Fisika Kelautan. Media Sains Indonesia.

Suhet. (2014). Sentinel-2 User Handbook. Paris. ESA Standard Document : European Space Agency.

Suni, M. A., Muis, H., Arianingsih, I., Misra, M., dan Baharuddin, R. F. (2023). Analisis dan Permodelan Spasial Perubahan Tutupan Lahan Di Hutan Produksi Terbatas Kecamatan Kulawi Kabupaten Sigi. Jurnal Tanah dan Sumberdaya Lahan, 10(2), 273-284. https://doi.org/10.21776/ub.jtsl.2023.010.2.11

Suni, M. A., Asa, S., Umar, F. H., dan Baharuddin, R. F. (2023). Analisis Perubahan Tutupan Lahan Di Sub DAS Toili Kabupaten Banggai. Nusantara Hasana Journal, 2(10), 28-37.

Suni, M. A., dan Baharuddin, R. F. (2023). Analisis Perubahan Tutupan Lahan di Hutan Produksi Terbatas Kecamatan Kulawi Kabupaten Sigi. BULLET: Jurnal Multidisiplin Ilmu, 2(1), 77-84.

Tablaseray, V.E., Pairin, M., Fakdawer, N., dan Hamuna, B. (2018). Pemetaan Sebaran dan Kerapatan Mangrove di Pesisir Timur Pulau Biak, Papua Menggunakan Citra Satelit Landsat 8. Jurnal Perikanan dan Kelautan Universitas Cenderawasih, Vol.VIII, hlm. 31-39.

Van Noordwijk, M., Mulyoutami, E., Sakuntaladewi, N. and Agus, F. 2008. Swiddens in transition: shifted perceptions on shifting cultivators in Indonesia. Occasional Paper no.9. World Agroforestry Centre. Bogor. 49 p.

BADAN INFORMASI GEOSPASIAL

PERATURAN BADAN INFORMASI GEOSPASIAL
REPUBLIK INDONESIA
NOMOR 12 TAHUN 2018
TENTANG
STANDAR PEMETAAN LAHAN GAMBUT SKALA 1:50.000

DENGAN RAHMAT TUHAN YANG MAHA ESA

KEPALA BADAN INFORMASI GEOSPASIAL REPUBLIK INDONESIA,

Menimbang : a. bahwa untuk mendukung penyelenggaraan pemetaan lahan gambut skala 1:50.000, diperlukan standar pemetaan untuk menghasilkan peta lahan gambut skala 1:50.000 yang akurat, terintegrasi, dan dapat dipertanggungjawabkan;

b. bahwa sesuai ketentuan Pasal 57 Undang-Undang Nomor 4 Tahun 2011 tentang Informasi Geospasial, Badan Informasi Geospasial melakukan pembinaan kepada penyelenggara Informasi Geospasial Tematik berupa penerbitan peraturan perundang-undangan, pedoman, standar dan spesifikasi teknis;

c. bahwa berdasarkan pertimbangan sebagaimana dimaksud dalam huruf a dan huruf b, perlu menetapkan Peraturan Badan Informasi Geospasial tentang Standar Pemetaan Lahan Gambut 1:50.000;

Mengingat : 1. Undang-Undang Nomor 5 Tahun 1990 tentang Konservasi Sumber Daya Alam Hayati dan Ekosistemnya (Lembaran Negara Tahun 1990 Nomor 49, Tambahan Lembaran Negara Nomor 3419);

2. Undang-Undang Nomor 32 Tahun 2009 tentang Perlindungan dan Pengelolaan Lingkungan Hidup (Lembaran Negara Republik Indonesia Tahun 2009 Nomor 140, Tambahan Lembaran Negara Republik Indonesia Nomor 5059);
3. Undang-Undang Nomor 4 Tahun 2011 tentang Informasi Geospasial (Lembaran Negara Republik Indonesia Tahun 2011 Nomor 49, Tambahan Lembaran Negara Republik Indonesia Nomor 5214);
4. Peraturan Pemerintah Nomor 9 Tahun 2014 tentang Pelaksanaan Undang-Undang Nomor 4 Tahun 2011 tentang Informasi Geospasial (Lembaran Negara Republik Indonesia Tahun 2014 Nomor 31, Tambahan Lembaran Negara Republik Indonesia Nomor 5502);
5. Peraturan Presiden Nomor 94 Tahun 2011 tentang Badan Informasi Geospasial (Lembaran Negara Republik Indonesia Tahun 2011 Nomor 144) sebagaimana telah diubah dengan Peraturan Presiden Nomor 127 Tahun 2015 tentang Perubahan atas Peraturan Presiden Nomor 94 Tahun 2011 tentang Badan Informasi Geospasial (Lembaran Negara Republik Indonesia Tahun 2015 Nomor 255);

MEMUTUSKAN:

Menetapkan : PERATURAN BADAN INFORMASI GEOSPASIAL TENTANG STANDAR PEMETAAN LAHAN GAMBUT SKALA 1:50.000.

BADAN INFORMASI GEOSPASIAL

Pasal 1

Standar Pemetaan Lahan Gambut 1:50.000 merupakan acuan bagi kementerian, lembaga, pemerintah daerah, dan setiap orang dalam melaksanakan pemetaan lahan gambut skala 1:50.000.

Pasal 2

Standar Pemetaan Lahan Gambut 1:50.000 sebagaimana dimaksud dalam Pasal 1 tercantum dalam Lampiran yang merupakan bagian yang tidak terpisahkan dari Peraturan Badan ini.

Pasal 3

Pada saat Peraturan Badan ini mulai berlaku, Peraturan Kepala Badan Informasi Geospasial Nomor 2 Tahun 2015 tentang pemberlakuan wajib Standar Nasional Indonesia tentang Pemetaan Lahan Gambut Skala 1:50.000 Berbasis Citra Penginderaan Jauh, dicabut dan dinyatakan tidak berlaku.

Pasal 4

Peraturan Badan ini mulai berlaku pada tanggal ditetapkan.

BADAN INFORMASI GEOSPASIAL

Ditetapkan di Cibinong
pada tanggal 28 Desember 2018

KEPALA BADAN INFORMASI GEOSPASIAL
REPUBLIK INDONESIA,

ttd

HASANUDDIN Z. ABIDIN

Salinan sesuai dengan aslinya,
Kepala Bagian Hukum,

Ida Suryani

LAMPIRAN
PERATURAN BADAN INFORMASI GEOSPASIAL
NOMOR 12 TAHUN 2018
TENTANG
STANDAR PEMETAAN LAHAN GAMBUT SKALA 1:50.000

DAFTAR ISI

DAFTAR ISI ..... - 4 -
PENDAHULUAN ..... - 5 -
STANDAR PEMETAAN LAHAN GAMBUT SKALA 1:50.000 ..... - 6 -
1 Ruang Lingkup ..... - 6 -
2 Acuan Normatif ..... - 6 -
3 Istilah dan Definisi ..... - 6 -
4 Metode Pemetaan Lahan Gambut ..... - 8 -

BADAN INFORMASI GEOSPASIAL

PENDAHULUAN

Standar pemetaan lahan gambut skala 1:50.000 berisi rangkaian proses yang digunakan dalam pemetaan lahan gambut di Indonesia. Standar ini menjadi acuan bagi pemangku kepentingan dalam melakukan pemetaan lahan gambut sehingga menghasilkan informasi yang akurat dan berkualitas.

Standar ini mengatur sumber data yang digunakan dan proses pemetaan lahan gambut skala 1:50.000 yang meliputi penyiapan (pengumpulan dan kompilasi) data, interpretasi citra satelit, survei lapangan, penyusunan basis data, dan penyajian peta lahan gambut.

Keluaran dari standar ini adalah peta lahan gambut skala 1:50.000 dengan keterangan meliputi keberadaan lahan gambut dan tanah mineral sekitarnya, informasi tipologi yang meliputi luas, tingkat kematangan, dan ketebalan gambut.

Penyusunan standar mengacu SNI 7925:2013, SNI 8473:2018, SNI 7645:1:2014, laporan akhir finalis *Indonesian Peat Prize,* dan masukan dari tim kerja penyusunan standar pemetaan gambut yang terdiri atas regulator, produsen, konsumen, dan pakar.

BADAN INFORMASI GEOSPASIAL

STANDAR PEMETAAN LAHAN GAMBUT SKALA 1:50.000

1 Ruang Lingkup

Standar ini menetapkan sumber data dan proses pemetaan lahan gambut skala 1:50.000 yang meliputi penyiapan (pengumpulan dan kompilasi) data, interpretasi lahan gambut, survei lapangan, penyusunan basis data, dan penyajian peta lahan gambut. Keluaran dari standar ini adalah peta lahan gambut skala 1:50.000. Standar ini menetapkan kebutuhan minimal parameter yang diambil secara in-situ dalam pemetaan lahan gambut skala menengah. Jumlah parameter dapat ditambahkan sesuai kebutuhan pemetaan.

2 Acuan Normatif

SNI 8473 Survei dan Pemetaan Tanah Semidetail Skala 1:50.000.
SNI 7645-1 Klasifikasi Penutup Lahan Bagian 1: Skala Kecil/Menengah.

3 Istilah dan Definisi

3.1

Lahan Gambut

lahan dengan tanah jenuh air, terbentuk dari endapan yang berasal dari penumpukan sisa-sisa (residu) jaringan tumbuhan masa lampau yang melapuk dengan ketebalan lebih dari 50cm.

3.2

Gambut Fibris (Mentah)

gambut yang belum melapuk, bahan asalnya masih dapat dikenali, berwarna coklat, dan jika diremas kandungan seratnya lebih dari >75%.

3.3

Gambut Hemis (Setengah Matang)

gambut setengah lapuk, sebagian bahan asalnya masih bisa dikenali, berwarna coklat dan jika diremas kandungan seratnya berkisar 15% sampai dengan 75%.

BADAN INFORMASI GEOSPASIAL

3.4

Gambut Sapris (Matang)

gambut yang sudah melapuk lanjut dan bahan asalnya tidak dikenali, berwarna coklat tua sampai hitam, dan jika diremas kandungan seratnya kurang dari 15% (lima belas persen).

3.5

Tipologi Lahan Gambut

satuan pemetaan lahan gambut yang mencirikan kesamaan tipe pemanfaatan, ketebalan, dan tingkat kematangan.

3.6

Model Medan Digital

Digital Terrain Model

DTM

model yang merepresentasikan titik ketinggian permukan tanah yang dapat digunakan sebagai data masukan untuk membentuk model elevasi digital (DEM), garis kontur, dan sebagai data masukan untuk pembuatan citra tegak.

3.7

Ketebalan (gambut)

ukuran tebal tipisnya gambut yang diukur dari permukaan paling atas hingga lapisan material dasar gambut yang ditandai dengan adanya tanah mineral dalam satuan tebal

BADAN INFORMASI GEOSPASIAL

3.8

Luasan (gambut)

Cakupan area lahan gambut dalam satuan luas.

3.9

Elevasi

Ketinggian sebuah titik dari muka air laut rata-rata.

3.10

Penutup Lahan

Tutupan biofisik pada permukaan bumi yang dapat diamati dan merupakan suatu hasil pengaturan, aktivitas, dan perlakuan manusia yang dilakukan pada jenis penutup lahan tertentu untuk melakukan kegiatan produksi, perubahan, ataupun perawatan pada penutup lahan tersebut.

3.12

Bentuk Lahan

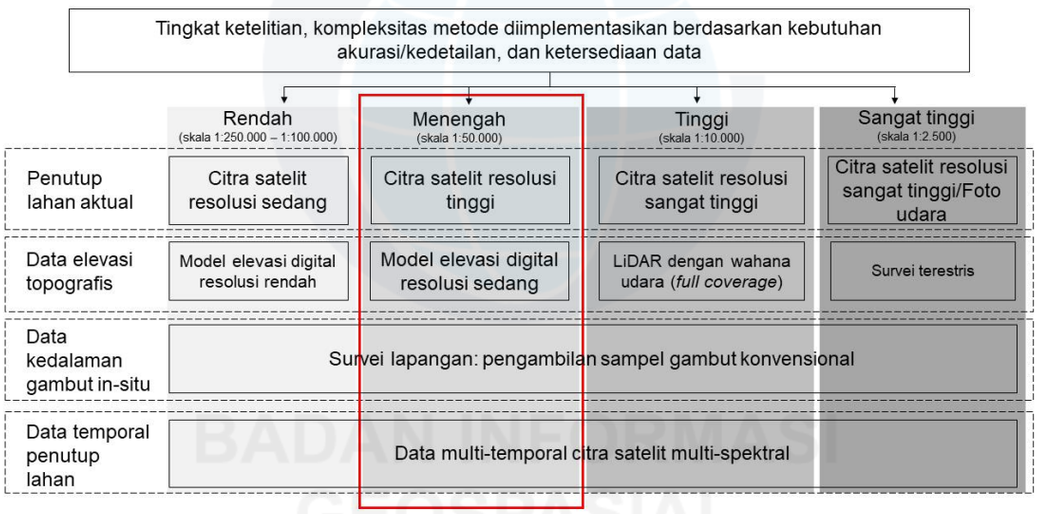
Bentukan alam di permukaan bumi akibat proses pembentukan secara geologi dan evolusinya, yang sangat erat kaitannya dengan iklim, litologi, stratigrafi dan topografi

4 Metode Pemetaan Lahan Gambut

Lahan gambut menyimpan jumlah karbon yang sangat besar, yang tersimpan dalam material tanaman yang belum terurai dengan sempurna, dan terakumulasi di lingkungan jenuh air dalam waktu lebih dari ribuan tahun. Lahan gambut umumnya berkembang di lingkungan bentang lahan yang memiliki ketersedian air yang besar. Beberapa bentang lahan yang berasosiasi dengan adanya lahan gambut di wilayah tropis antara lain: (1) dataran rendah pesisir, (2) daratan yang dipengaruhi oleh aktivitas marin (delta sungai, rawa garam/*salt marsh*, laguna, dll.), (3) dataran banjir (danau tapal kuda, rawa belakang, dan cekungan), (4) tepian danau, dan (5) lingkungan pegunungan (lahan gambut dataran tinggi/lembah). Untuk itu dalam memetakan lahan gambut diperlukan pemahaman akan bentang lahan yang terkait dengan proses pembentukan lahan gambut tersebut. Pemetaan informasi tematik, yang berasosiasi dengan proses pembentukan elemen fisik di permukaan bumi, seperti halnya dalam bentang lahan, secara umum juga sudah melalui penelitian yang intensif untuk mendapatkan hasil berupa konsep dan metode yang dianggap mewakili proses yang terjadi di alam.

BADAN INFORMASI GEOSPASIAL

Di bidang pemetaan tanah, aplikasi data penginderaan jauh sudah semakin mengemuka sebagai salah satu data utama untuk menurunkan informasi spasial proses "*soil-landscape*" (bentang lahan tanah). Konsep "bentang lahan tanah" ini dianggap sebagai satuan pemetaan *(mapping unit)* yang paling mewakili karakteristik fisik tanah yang ada di dalam lingkungan tertentu termasuk di lingkungan lahan gambut. Selanjutnya dalam pemetaan skala 1:50.000 ini, "bentang lahan" merupakan sebuah satuan pemetaan utama yang harus diturunkan sebelum diperinci ke satuan pemetaan yang lebih detil menyesuaikan tujuan dan skala pemetaan seperti yang disajikan pada Gambar 1. Untuk skala/tingkat kedetilan menengah (skala 1:50.000), bentang lahan disusun oleh berbagai macam bentuk lahan *(landform)* atau faset lahan (*land facet*) dalam konteks hierarki satuan medan, oleh karena itu pemetaan bentang lahan skala 1:50.000 disebut sebagai pemetaan bentuk lahan atau faset lahan.



Gambar 1. Skema Tingkat Kedetilan Pemetaan Lahan Gambut Skala 1:50.000 (Dalam Kotak Merah), Serta Perbandingannya dengan Skala yang Lain, Mencakup Tingkat Ketelitian, Metode, dan Data yang Diperlukan.

Metode pemetaan lahan gambut ini dijelaskan pada Gambar 2. Garis besar metode pemetaan lahan gambut ini mencakup:

1. Penyiapan (pengumpulan dan kompilasi) data,

   Tahapan penyiapan dilakukan untuk mengumpulkan data dan informasi yang akan digunakan untuk pemetaan lahan gambut. Data dan informasi yang dikumpulkan meliputi data peta Rupa Bumi Indonesia (RBI), data DTM, data tanah, data geologi, data iklim, dan data citra satelit.

2. Interpretasi lahan gambut,

   Tahapan interpretasi lahan gambut dilakukan dengan menggunakan teknik pemetaan bentuk lahan dan interpretasi penutup lahan. Penyusunan peta bentuk lahan yang berasosiasi lahan gambut menggunakan metode interpretasi citra penginderaan jauh untuk mendapatkan *synoptic overview* wilayah kajian, termasuk informasi posisi relatif bentang lahan. Data DTM digunakan untuk identifikasi bentuk permukaan bumi sebagai analisis dasar pemetaan bentuk lahan. Data tanah dan data geologi digunakan untuk mengidentifikasi material penyusun bentuk lahan dalam pemetaan bentuk lahan. Data iklim digunakan untuk membantu analisis proses pembentukan tanah yang menjadi salah satu unsur penyusun bentuk lahan.

   Interpretasi penutup lahan yang berasosiasi dengan lahan gambut dilakukan menggunakan citra multi-temporal untuk mendapatkan perbedaan kondisi penutup lahan saat ini dan masa lampau. Penutup lahan masa lampau digunakan untuk mengidentifikasi lahan gambut saat dalam kondisi alami dan belum ada pemanfaatan oleh kegiatan manusia. Kondisi gambut yang masih alami digunakan sebagai *baseline* dalam penyusunan peta tentatif lahan gambut.

3. Survei lapangan,

   Tahapan survei lapangan dibagi menjadi tiga kegiatan yaitu survei lapangan 1, penyusunan peta tentatif lahan gambut, dan survei lapangan 2. Survei lapangan 1 merupakan survei pendahuluan. Survei ini menghasilkan kunci interpretasi lahan gambut. Selanjutnya, disusun peta tentatif lahan gambut yang akan digunakan pada survei lapangan 2. Penyusunan peta ini merupakan penyusunan satuan lahan (satuan pemetaan) dilakukan dengan menggunakan metode *superimposed* antara hasil interpretasi bentuk lahan dan hasil interpretasi penutup lahan. Hasil dari interpretasi bentuk lahan yang berasosiasi dengan lahan gambut (lihat tabel 3) dikombinasikan dengan hasil interpretasi penutup lahan yang berasosiasi dengan gambut dan hasil kunci interpretasi yang dilakukan pada survei lapangan 1 maka dapat dihasilkan peta lahan gambut tentatif.

   Survei lapangan 2 untuk melakukan pengukuran in-situ dan validasi batas lahan gambut. Keluaran proses ini adalah data tipologi lahan gambut.

BADAN INFORMASI GEOSPASIAL

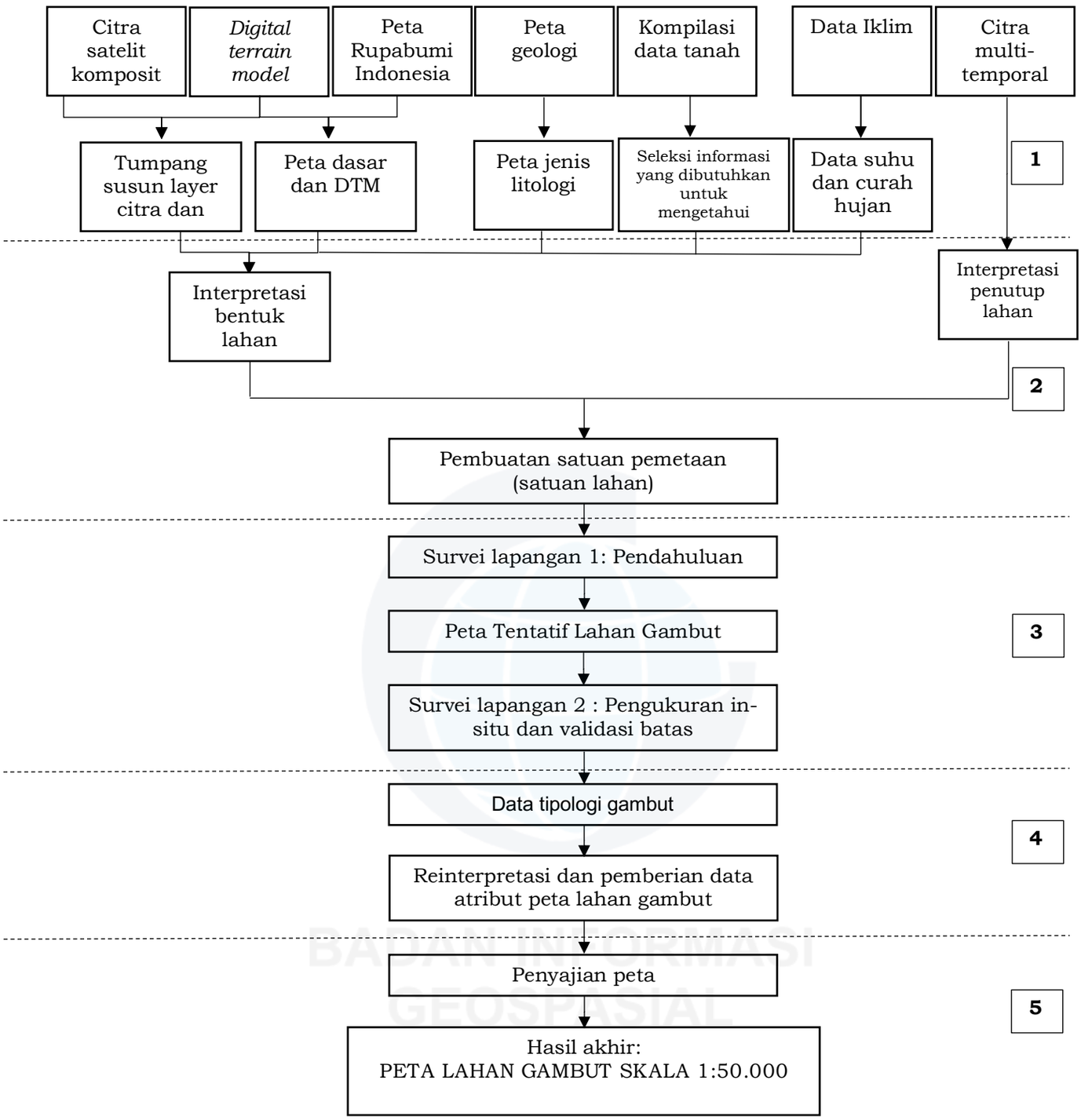
4. Penyusunan basis data,

   Tahapan penyusunan basis data meliputi penyusunan basis data tipologi lahan gambut, reinterpretasi lahan gambut dan pemberian data atribut peta lahan gambut. Penyusunan basis data tipologi lahan gambut dilakukan untuk mengisi atribut lahan gambut. Reinterpretasi dan pemberian data atribut peta lahan gambut, hasil dari pengukuran in-situ dan validasi batas lahan gambut digunakan untuk panduan melakukan perbaikan interpretasi batas gambut dan pengisian atribut peta lahan gambut yang meliputi kedalaman gambut serta tingkat kematangan gambut.

5. Penyajian peta lahan gambut.

   Tahapan penyajian peta lahan gambut meliputi penyusunan layout peta lahan gambut. Informasi utama yang disajikan dari peta lahan gambut yaitu tipologi lahan gambut.

BADAN INFORMASI GEOSPASIAL



Gambar 2. Diagram Alir Pemetaan Lahan Gambut

BADAN INFORMASI GEOSPASIAL

4.1 Penyiapan (pengumpulan dan kompilasi) data

4.1.1 Data Penginderaan Jauh, Sumber Data Pendukung dan Satuan Pemetaan Minimal

Data citra penginderaan jauh yang digunakan mengacu pada SNI 8473:2018 Survei dan pemetaan tanah semidetail skala 1:50.000. Namun untuk kepentingan pemetaan ini ada beberapa tambahan data dan metode untuk mendapatkan informasi yang akurat, seperti pemanfaatan citra penginderaan jauh multi-temporal dan metode transformasi spektral.

Sebelum dilakukan interpretasi objek dalam penginderaan jauh, perlu diketahui tujuan pemetaan dan satuan pemetaan terkecil supaya pernurunan informasi (delineasi objek bentuk lahan) tidak mengalami generalisasi atau sebaliknya terlalu detail (*over-detail*). Ukuran satuan pemetaan terkecil untuk pemetaan bentuk lahan 1:50.000 adalah 1 atau (1x1) cm^2 atau 500x500 m^2, untuk area kajian dengan keberagaman bentuk lahan rendah/sedang, dan 0,25 atau (0,5x0,5) cm^2 atau 250x250 m^2 hingga 125x125 m^2 jika diperlukan untuk wilayah dengan keberagaman bentuk lahan tinggi (Tabel 1).

Untuk keluaran peta lahan gambut skala menengah, satuan pemetaan yang digunakan adalah bentuk lahan (*landform*), dengan ukuran satuan pemetaan terkecil seluas 125 m x 125 m, untuk skala 1:50.000; dan 62,5 m x 62,5 m untuk skala 1:25.000. Satuan pemetaan ini yang akan digunakan sebagai dasar penentuan sampel (percontoh) di lapangan, menggunakan metode *stratified random sampling*. Jumlah dan lokasi percontoh tanah ditentukan berdasarkan luasan wilayah kajian dan keberagaman satuan pemetaan.

BADAN INFORMASI GEOSPASIAL

Tabel 1. Jenis Data Penginderaan Jauh dan Pendukung, serta Satuan Pemetaan Terkecil untuk Pemetaan Bentuk Lahan di Lingkungan Lahan Gambut Skala 1:50.000

Kedetilan bentuk lahan	**Data pendukung**	**Satuan pemetaan minimal**	
		pada citra (cm^2)	**di lapangan (m^2)**
Rendah/sedang	- Peta Rupa Bumi Skala 1:50.000 atau yang lebih besar - Citra penginderaan jauh multi-temporal resolusi spasial minimal 30 m untuk kepentingan *synoptic overview;* - Citra penginderaan jauh multi-temporal resolusi spasial 5-10 m; - Data DEM resolusi spasial 5-10 m; - Peta geologi 1:50.000 dan satu tingkat diatasnya. - Peta tanah umum skala 1:50.000 dan satu tingkat diatasnya. - Survei lapangan	1x1	500x500
Tinggi	- Peta Rupa Bumi Skala 1:50.000 atau yang lebih besar; - Citra penginderaan jauh multi-temporal resolusi spasial minimal 30 m untuk kepentingan *synoptic overview;* - Citra penginderaan jauh multi-temporal resolusi spasial 5-10 m; - Data DEM resolusi spasial 5-10 m; - Peta geologi 1:50.000 dan satu tingkat diatasnya.	0,5x0,5 0,25x0,25	250x250 125x125

Kedetilan bentuk lahan	Data pendukung	Satuan pemetaan minimal	
		pada citra (cm^2)	di lapangan (m^2)
	- Peta tanah umum skala 1:50.000 dan satu tingkat diatasnya. - Peta hidro-geologi - Data pasang surut - Survei lapangan		

4.2 Interpretasi lahan gambut

4.2.1 Interpretasi Bentuk Lahan

4.2.1.1 Informasi Elevasi dari Model Medan Digital (DTM) atau Peta Kontur

Data Model Medan Digital digunakan dengan resolusi horizontal minimal 12 meter dan resolusi vertikal minimal 1 meter serta akurasi vertikal minimal 10 m. DTM digunakan untuk memperoleh data elevasi dan kesan bentuk permukaan bumi yang dijadikan acuan sebagai delineasi bentuk lahan termasuk lahan gambut dan bukan gambut. Penentuan lahan gambut dan bukan gambut berdasarkan kriteria pembeda elevasi untuk lahan gambut mengacu pada Tabel 2. Uji akurasi citra model elevasi digital ini dilakukan menggunakan survei elevasi lapangan.

Tabel 2. Klasifikasi Kriteria Elevasi Permukaan Tanah untuk Dasar Interpretasi dan Delineasi Lahan Gambut

Kelas Kriteria	**Beda Tinggi Dari Permukaan Lahan Non Gambut**		
	Lahan gambut	**Lahan transisi (lahan gambut yang sudah terexploitasi/bagian tepi dome gambut)**	**Bukan lahan gambut**
Untuk "*peat dome*"	Ketinggian naik secara gradual dari 0,5 m hingga mencapai lebih dari 10 m pada puncak dome, dan kembali turun secara gradual mencapai titik ketinggian 0.5 m dan akhirnya sama dengan titik awal lahan non-gambut.	Gradasi elevasi naik dari ketinggian lahan non-gambut hingga ketinggian 0,5m.	0 m
Untuk lahan gambut tipe lain (datar, pesisir)	<1 m	<0.5 m	0 m

BADAN INFORMASI GEOSPASIAL

4.2.1.2 Pengabungan Informasi Jenis Litologi dan Kompilasi Data Tanah

Informasi dan delineasi jenis litologi diperoleh dari peta geologi. Setiap jenis litologi diberi simbol huruf kecil. Apabila dalam satuan formasi geologi memiliki lebih dari satu jenis litologi, dipilih 2 jenis batuan yang pertama. Hasil interpretasi litologi harus diverifikasi dengan kondisi aktual di lapangan. Pengelompokan jenis litologi untuk penyusunan peta bentuk lahan mengacu pada pengelompokan jenis litologi dan bahan induk. Sebagai contoh, dalam satu satuan formasi geologi disebutkan jenis litologi yang komposisinya terdiri dari batu pasir, batu lanau, napal, batu gamping, dan konglomerat, maka dipilih 2 jenis yang pertama, yaitu batu pasir (kasar) dan batu lanau (halus), dan diberi simbol fq.

Informasi data tanah digunakan untuk analisis material permukaan penyusun bentuk lahan. Informasi material permukaan penyusun bentuk lahan dapat membantu dalam interpretasi lahan gambut dan bukan gambut.

4.2.2 Delineasi Objek Bentuk Lahan

Hasil kompilasi data sekunder dan peta citra hasil beberapa analisis data penginderaan jauh yang telah dijelaskan sebelumnya, digunakan sebagai panduan interpretasi batas area lahan gambut. Tahapan interpretasi menggunakan metode interpretasi multi-tingkat, dengan memperhatikan fitur kunci identifikasi lahan gambut dari penelitian teruji yang ada sebelumnya, dan didampingi ahli yang memiliki pengalaman di bidang pemetaan lahan gambut.

Kriteria yang digunakan dalam analisis bentuk lahan melalui pendekatan pengelompokan grup fisiografi/landform berdasarkan: relief/topografi, drainase permukaan, pola drainase, kondisi geologi/litologi dan kondisi tanah. Umumnya terdapat hubungan antara grup fisiografi *(landform)* dan penyebaran sifat-sifat lahan gambut. Satuan bentuk lahan tersebut digunakan sebagai wadah satuan pemetaan (*mapping unit*) lahan gambut.

Langkah awal untuk melakukan analisis bentuk lahan dengan pendekatan fisiografis adalah dengan melakukan tumpang susun data kontur dari peta RBI (atau DTM), citra penginderaan jauh, data litologi dari peta geologi, dan data tanah.

Proses interpretasi bentuk lahan secara fisiografis dilakukan melalui dua tahap, yaitu pertama, mengggunakan klasifikasi group bentuk lahan yang umumnya dijumpai di daerah lahan rawa dan lahan gambut antara lain grup: Aluvial (A), Marin (M), Fluvio-Marin (B), Gambut (G).Tabel 3 dan Tabel 4 menunjukkan satuan bentuk lahan yang berasosiasi dengan keberadaan lahan gambut. Selanjutnya, jika terdapat informasi lebih detail, tahap kedua dilakukan, dengan membedakan grup bentuk lahan menjadi subgrup bentuk lahan. Grup bentuk lahan diberi simbol berupa huruf besar, sedangkan subgrup bentuk lahan diberi simbol berupa angka Arab di belakang huruf besar. Pedoman klasifikasi bentuk lahan Indonesia dengan menggunakan pendekatan fisiografis dapat dilihat pada SNI 8473 Survei dan pemetaan tanah semidetail skala 1:50.000.

Pedoman ini mencakup informasi tentang hierarki dan struktur legenda bentuk lahan, klasifikasi grup bentuk lahan, cara mengindentifikasi grup bentuk lahan, serta pembagian bentuk lahan menjadi subgrup, unit, dan subunit bentuk lahan.

BADAN INFORMASI GEOSPASIAL

Tabel 3. Klasifikasi Beberapa Bentuk Lahan Umum yang Berada di Lingkungan/Berasosiasi dengan Lahan Gambut

Kode	Grup	Sub-kode 1	Subgrup	Sub-kode 2	Unit bentuk lahan
A	Aluvial	1	Lahan Aluvial	1	Dataran banjir
				2	Teras sungai
				3	Dataran aluvial
				5	Jalur aliran
				6	Delta danau
		2	Lahan aluvio-koluvial	1	Kipas aluvial
		3	Basin/rawa aluvial	1	Dataran danau
				2	Basin tertutup
				3	Depresi alluvial

Kode	Grup	Sub-kode 1	Subgrup	Sub-kode 2	Unit bentuk lahan
B	Fluvio Marin	1	Delta laut	1	Delta estuarine
				2	Delta arkuit
				3	Delta kaki burung
		2	Dataran estuarin		
		3	Dataran fluvio-marin		
M	Marin	1	Pesisir	1	Punggung dan cekungan pesisir
				2	Pesisir pasir
				3	Pesisir lumpur
				4	Beting pantai penghalang
				5	Laguna
		2	Dataran pasang surut (tidal flat)	1	Dataran pasang surut pasir
				2	Dataran pasang surut lumpur (mud flat)
				3	Dataran pasang surut *marshy*
				4	Dataran pasang surut mangrove
				5	Rawa belakang pasang surut
		3	Teras marin	1	Teras marin subresen
G	Gambut	1	Kubah gambut (dome)	1	Tepi/kaki kubah gambut
				2	Kubah gambut
		2	Gambut topogen	1	Gambut topogen air tawar
				2	Gambut topogen air payau
CATATAN Informasi lebih detil tersedia dalam SNI 8473:2018 survei pemetaan tanah					

Tabel 4. Persentase kemungkinan ditemukan lahan gambut pada beberapa bentuk lahan

No	Unit Bentuk Lahan	Persentase Kemungkinan Diketemukan Di Lahan Gambut
1.	Dataran aluvial	Sempit *(minor)*: 10-25%
2.	Depresi aluvial *(closed basin)*	Luas *(dominant)*: 50-75%
3.	Dataran estuarin	Sempit *(minor)*: 10-25%
4.	Rawa belakang sungai *(Back swamp)*	Sedang-luas *(fair-dominant)*: 25-75%
5.	Rawa belakang pantai *(Swalle/lagoon)*	Sedang-luas *(fair-dominant)*: 25-75%

BADAN INFORMASI GEOSPASIAL

No	Unit Bentuk Lahan	Persentase Kemungkinan Diketemukan Di Lahan Gambut
6.	Dataran pantai	Sempit *(minor)*: 10-25%
7.	Gambut topogen air tawar	Sangat luas *(predominant)*: > 75%
8.	Gambut topogen pasang surut	Sangat luas *(predominant)*: > 75%
10.	Kubah gambut	Sangat luas *(predominant)*: >75%

Peta bentuk lahan hasil interpretasi perlu dilengkapi dengan keterangan legenda peta. Legenda peta disusun berdasarkan urutan berikut: Nomor urut, simbol satuan lahan, uraian satuan bentuk lahan, satuan litologi, satuan bentuk wilayah/kelas lereng dan luas masing-masing satuan lahan dalam hektar dan persentasenya. Legenda peta ini selanjutnya diperbaiki berdasarkan hasil pengamatan lapangan untuk penyusunan tipologi lahan gambut. Kelas bentuk lahan pada tahapan ini digunakan untuk mengidentifikasi bentuk lahan gambut dan non-gambut yang mengacu pada Tabel 3 dan 4.

4.2.3 Delineasi Penutup Lahan untuk Identifikasi Lahan Gambut dan Non-gambut

Tahapan kedua adalah interpretasi penutup lahan untuk analisis batas lahan gambut dan tipe pemanfaatan lahan gambut. Pemanfaatan lahan yang sudah berkembang pesat di atas lahan gambut, menyulitkan proses penentuan batas lahan gambut yang sebenarnya serta perkembangan tipe lahan gambut yang digunakan untuk analisis tipologi lahan gambut. Untuk itu, pada tahapan kedua, penarikan garis batas lahan gambut ditentukan menggunakan pendekatan citra multi-temporal untuk mendapatkan batas asli luasan lahan gambut tersebut serta tipe pemanfaatan lahan gambut.

BADAN INFORMASI GEOSPASIAL

Empat fitur kunci yang digunakan untuk mengidentifikasi lahan gambut dan dapat dideteksi dengan bantuan data penginderaan jauh meliputi:

a. keberagaman vegetasi yang rendah
   Lahan gambut pada daerah tropis umumnya ditutupi oleh penutup lahan berupa hutan, semak, semak belukar, padang rumput, padang alang-alang, herba atau vegetasi herba lainnya dengan keberagaman vegetasi yang rendah.
b. struktur vegetasi yang khas
   Struktur vegetasi pada lahan gambut umumnya memiliki karakteristik kanopi yang nampak seragam karena keragaman vegetasi yang rendah.
c. topografi atau elevasi yang khas
   Lahan gambut pada daerah tropis umumnya berbentuk kubah sehingga dapat dideteksi dengan menggunakan data DTM. Kubah gambut dapat diidentifikasi dari data DTM jika memiliki kenampakan permukaan yang cembung.
d. tingkat kebasahan
   Lahan gambut pada umumnya memiliki tinggi muka airtanah yang rendah sehingga lahan gambut keberadaanya dapat dicirikan yaitu terletak pada area yang basah.

Berdasarkan fitur kunci itulah, metode pemetaan lahan gambut ini disusun, terutama mengenai bagaimana menurunkan informasi batas satuan bentuk lahan tersebut dari data penginderaan jauh untuk berbagai skala pemetaan. Namun tidak semua fitur kunci harus digunakan sebagai dasar interpretasi, jika minimal dua dari fitur kunci tersebut sudah dapat digunakan untuk mengidentifikasi lahan gambut.

Gambar 3 menunjukkan contoh peta citra multi-temporal yang menggambarkan kondisi lahan gambut sebelum dan sesudah dimanfaatkan oleh manusia. Pemrosesan citra multi-temporal digunakan untuk mengidentifikasi tingkat keberagaman dan kerapatan vegetasi pada peta penutup lahan pada waktu yang berbeda di sebuah wilayah. Pemilihan citra ditentukan berdasarkan pada ketersediaan citra perekaman terlama dan terbaru, waktu perekaman (musim), serta maksimal tutupan awan 25% yang tidak terdistribusi rata.



Gambar 3. Contoh Citra Komposit Warna Semu dan Multi-Temporal untuk Mengetahui Perubahan Penutup Lahan atau Penutup Lahan Historis Sebagai Dasar Penarikan Batas Delineasi Lahan Gambut.

Informasi penutup lahan bisa didapatkan melalui interpretasi visual citra multi-temporal. Klasifikasi penutup lahan mengacu SNI 7645-1 dengan modifikasi (seleksi dan penyederhanaan) berdasarkan jenis penutup lahan yang sering muncul di lingkungan lahan gambut. Klasifikasi jenis penutup lahan tersebut disajikan dalam Tabel 5.

Tabel 5. Klasifikasi Penutup Lahan untuk Pemetaan Lahan Gambut Skala Menengah, Berdasarkan Tipe yang Umum Ditemui di Lahan Gambut dan Sekitarnya

No.	Skala 1:250.000 (sebagai panduan hierarki)	Kode	Skala 1:50.000/25.000
1.	Semak dan belukar	I	Semak belukar
		II	Semak
2.	Herba dan rumput	III	Padang rumput
		IV	Padang alang-alang
		V	Herba
		VI	Vegetasi herba lainnya
3.	Hutan rawa/gambut	VII	Hutan rawa/gambut primer kerapatan tinggi
		VIII	Hutan rawa/gambut primer kerapatan sedang
		IX	Hutan rawa/gambut primer kerapatan rendah

		X	Hutan rawa/gambut sekunder kerapatan tinggi
		XI	Hutan rawa/gambut sekunder kerapatan sedang
		XII	Hutan rawa/gambut sekunder kerapatan rendah
4.	Hutan lahan rendah	XIII	Hutan lahan rendah primer kerapatan tinggi
		XIV	Hutan lahan rendah primer kerapatan sedang
		XV	Hutan lahan rendah primer kerapatan rendah
		XVI	Hutan lahan rendah sekunder kerapatan tinggi
		XVII	Hutan lahan rendah sekunder kerapatan sedang
		XVIII	Hutan lahan rendah sekunder kerapatan rendah
5.	Hutan mangrove	XIX	Hutan mangrove primer kerapatan tinggi
		XX	Hutan mangrove primer kerapatan sedang
		XXI	Hutan mangrove primer kerapatan rendah
		XXII	Hutan mangrove sekunder kerapatan tinggi
		XXIII	Hutan mangrove sekunder kerapatan sedang
		XXIV	Hutan mangrove sekunder kerapatan rendah
6.	Perkebunan dengan tanaman berkayu keras	XXV	Perkebunan sawit
		XXVI	Perkebunan lainnya (jenis perkebunan lain tidak didetilkan)
7.	Tanaman semusim lahan basah	XXVII	Sawah dengan padi terus menerus

BADAN INFORMASI GEOSPASIAL

		XXVIII	Sawah dengan padi diselingi tanaman lain/bera
		XXIX	Tanaman semusim lahan basah lainnya
8.	Bangunan permukiman/campuran	XXX	Bangunan permukiman kota
		XXXI	Bangunan permukiman desa (berasosiasi dengan vegetasi pekarangan)
9.	Tubuh air	XXXII	Tubuh air (tidak didetailkan)
10.	Penutup lahan lain	XXXIII	Penutup lahan lain yang tidak ada di SNI 7645-1.

4.2.4 Penyusunan Satuan Pemetaan

Tahap pertama yang harus dipersiapkan adalah pemetaan bentang lahan (yang terdiri atas beberapa informasi bentuk lahan) dari wilayah yang akan dipetakan. Bentang lahan gambut yang berada di wilayah pesisir, di antara dua sungai, atau posisi aluvial (jarak dari sungai, estuari, serta laut) dengan luasan gambut yang berbeda, memiliki karakteristik proses pembentukan dan latar belakang material penyusun yang berbeda juga, sehingga tahapan ini akan memberikan informasi awal kondisi wilayah secara menyeluruh (*synoptic overview*).

Tujuan dari tahapan ini adalah untuk memberikan justifikasi dan informasi yang komprehensif dalam menentukan wilayah yang akan dipetakan sehingga tujuan pemetaan dapat tercapai dan akurat. Prosedur pemetaan bentuk lahan ini mengacu pada SNI 8473 Survei dan pemetaan tanah semidetail skala 1:50.000. Tahapan pertama ini memanfaatkan unsur interpretasi umum dalam ilmu penginderaan jauh untuk mendapatkan kunci interpretasi lahan gambut, seperti: tekstur, warna, pola, asosiasi, bentuk, ukuran dan relief dan topografi. Data penginderaan jauh dan informasi pendukung yang digunakan, serta metode delineasi dan klasifikasi bentuk lahan utama mengacu SNI 8473:2018 Survei dan pemetaan tanah semidetail skala 1:50.000. Keluaran dari tahapan ini kemudian digunakan sebagai input dalam proses survei pendahuluan sehingga menghasilkan peta tentatif lahan gambut.

BADAN INFORMASI GEOSPASIAL

Peta satuan lahan, mengacu SNI 8473 Survei dan pemetaan tanah semidetail skala 1:50.000, disusun dengan menggunakan pendekatan fisiografis, dengan mempertimbangkan aspek fisik yang didapatkan dari genesis dan evolusi bentuk lahan, kondisi batuan induk/litologi, relief, iklim dan penutup lahan. Pendekatan fisiografis mencakup informasi grup/subgrup bentuk lahan, jenis litologi, bentuk wilayah/lereng, dan/atau tingkat kebasahan lahan yang diturunkan dari data iklim dan/atau citra. Data-data yang digunakan adalah citra penginderaan jauh, DTM atau kontur, data litologi, data tanah, data iklim dan data penutup lahan hasil interpretasi.

Hasil dari delineasi bentuk lahan dan penutup lahan menghasilkan peta satuan pemetaan. Peta satuan pemetaan berisi informasi bentuk lahan, litologi, bentuk wilyah dan penutup lahan. Contoh satuan pemetaan tertera pada Tabel 6.

Tabel 6. Contoh Tabel Satuan Pemetaan

Satuan Pemetaan	**Uraian**			
	Bentuk Lahan	**Litologi**	**Bentuk Wilayah**	**Penutup Lahan**
A1.f.11.n.II	Dataran Banjir	Endapan halus	Agak datar	Semak belukar

BADAN INFORMASI GEOSPASIAL

4.3 Survei lapangan

4.3.1 Peralatan

Peralatan yang digunakan dalam kegiatan persiapan survei dan survei lapangan meliputi:

1. peta rencana transek dan pengambilan sampel;
2. satu unit GPS; dan
3. satu set bor gambut yang terdiri atas 50 cm auger (volume 500 cm3), pemutar dengan tangkai bentuk T (50 cm), batang besi 100 cm (jumlah sesuai kebutuhan dan kedalaman gambut), dan satu alat bantu pengungkit, dan 2 set spana (Gambar 4).



Gambar 4. Alat Bor Gambut (Sumber : Eijkelkamp.Com)

4.3.2 Survei Lapangan 1 (Pendahuluan)

Survei pendahuluan bertujuan melakukan konsultasi dengan Pemerintah Daerah setempat untuk menggali (*explore*) informasi sumber daya lahan gambut yang akan dipetakan, pengumpulan data dukung yang relevan terkait pelaksanaan survei lapangan, seperti jaringan jalan, sarana transportasi, tenaga daerah pendamping tim, penyelesaian administrasi dan untuk melakukan cek kunci interpretasi. Informasi yang diperoleh dari hasil survei pendahuluan digunakan untuk perencanaan dan memperlancar pelaksanaan survei lapangan. Kunci interpretasi digunakan untuk membantu dalam analisis penyusunan peta bentuk lahan dan peta penutup lahan yang akan digunakan sebagai satuan pemetaan dalam peta tentatif lahan gambut.

4.3.3 Penyusunan Peta Tentatif Lahan Gambut

Peta satuan pemetaan lahan gambut tentatif perlu disajikan dengan informasi satuan pemetaan yaitu bentuk lahan, litologi, bentuk wilayah dan penutup lahan. Peta tentatif lahan gambut yang digunakan untuk survei lapangan juga memuat rencana titik pengamatan dan pengukuran lahan gambut serta validasi batas lahan gambut di lapangan.

Penentuan titik pengambilan percontoh lahan gambut dilakukan secara *stratified sampling* dengan memperhatikan keterwakilan satuan pemetaan. Pengambilan percontoh tanah di lapangan dilakukan dengan membuat garis transek di atas peta satuan pemetaan.

Penentuan lokasi titik percontoh tipologi dilakukan dengan mempertimbangkan:

1. proporsi jumlah populasi satuan pemetaan;
2. mewakili daerah yang luas dari satu satuan pemetaan (tipologi dan bentuk lahan);
3. tidak berada di perbatasan antara dua poligon; dan
4. aksesibilitas dapat terjangkau.

Penentuan lokasi titik percontoh validasi batas dilakukan dengan mempertimbangkan:

1. proporsi jumlah pengambilan percontoh pada lahan gambut yang dimanfaatkan lebih banyak daripada lahan gambut alami ;
2. harus berada di perbatasan antara dua poligon ;
3. aksesibilitas dapat terjangkau; dan
4. jika masih menemukan batas yang meragukan di lapangan dan tidak menjadi titik percontoh maka percontoh validasi bisa ditambah.

4.3.4 Survei Lapangan 2

BADAN INFORMASI GEOSPASIAL

Survei lapangan 2 dilakukan untuk pengecekan dan perbaikan peta satuan pemetaan hasil interpretasi, pengamatan tipologi gambut di lapangan dan validasi batas lahan gambut.

4.3.4.1 Pengecekan dan Perbaikan Peta Satuan Pemetaan Hasil Interpretasi

Pengecekan satuan pemetaan bertujuan untuk mengecek apakah satuan pemetaan hasil interpretasi sudah sesuai dengan kondisi di lapangan baik itu dari karakteristik bentuk lahan, litologi, bentuk wilayah dan penutup lahan.

4.3.4.2 Pengamatan Tipologi Gambut

Pengamatan tipologi gambut di lapangan dilakukan untuk mengetahui karakteristik lahan gambut. Jalur transek yang dibuat digunakan untuk melakukan pengamatan tipologi gambut yang mencakup:

1. Lokasi
   Koordinat lokasi titik percontoh ditentukan meggunakan GNSS;
2. Tipe Pemanfaatan Gambut
   Dilakukan melalui pengamatan penutup lahan dan penggunaan lahan di lapangan;
3. Ketebalan Gambut
   Dilakukan melalui pengeboran sesuai titik percontoh yang telah ditentukan; dan
4. Tingkat Kematangan Gambut (Fibris, Hemis, dan Sapris)
   Identifikasi tingkat kematangan dilakukan melalui pengamatan di lapangan.

Ketebalan gambut diklasifikasikan seperti pada Tabel 7. Ketebalan gambut <300 cm dikelaskan dengan interval 50 cm, sedangkan ketebalan gambut ≥300 cm dikelaskan dengan interval 200 cm.

Tabel 7. Klasifikasi Ketebalan Gambut

Kode	Ketebalan (cm)
1	50—100
2	101—150
3	151—200
4	201—250
5	251—300
6	301—500
7	501—700
8	701—900
…	dan seterusnya kelipatan 200 meter

4.3.3.3 Validasi Batas Lahan Gambut

Informasi batas lahan gambut dihasilkan melalui survei validasi batas terhadap peta tentatif lahan gambut. Validasi dilakukan melalui survei lapangan yang dilaksanakan bersama-sama dengan pengukuran in-situ tipologi lahan gambut.

4.4 Penyusunan Basis Data

4.4.1 Penyusunan Basis Data Tipologi Lahan Gambut

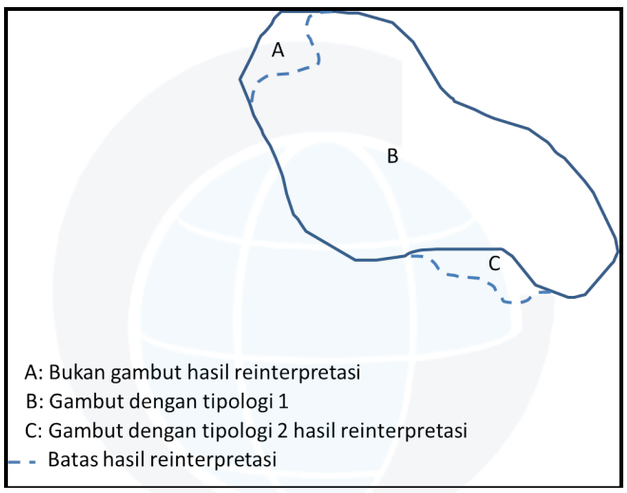
Tipologi lahan gambut setiap kelas didelineasi berdasarkan peta tentatif lahan gambut yang telah diverifikasi saat survei lapangan. Informasi tipologi dijabarkan dalam data atribut yang meliputi tipe pemanfaatan, ketebalan dan tingkat kematangan. Data atribut ini harus diisikan dalam setiap polygon satuan pemetaan. Tipologi lahan gambut skala menengah menggunakan klasifikasi satuan lahan berdasarkan Tabel 8.

Tabel 8. Klasifikasi Tipologi Lahan Gambut Skala 1:50.000

Kode	**Tipe pemanfaatan**	**Deskripsi**			
Utama		**Sub-Kode 1**	**Ketebalan (cm)**	**Sub-Kode 2**	**Tingkat Kematangan**
G1	Lahan gambut dimanfaatkan *(utilized)*	1	50-100	1	Sapris
		2	101-150	2	Hemik
		3	151-200	3	Fibrik
		4	201-250		
		5	251-300		
		6	301-500		
		7	501-700		
		8	>700		
G2	Lahan gambut alami *(unutilized)*	1	50-100	1	Sapris
		2	101-150	2	Hemik
		3	151-200	3	Fibrik
		4	201-250		
		5	251-300		
		6	301-500		
		7	501-700 dst (per 200)		
TG	Tanah bergambut	1	0-25	0	N/a
		2	26-49	0	N/a
NG	Lahan non-gambut	NG	-	-	-

4.4.2 Reinterpretasi dan Pemberian Data Atribut

Hasil dari survei lapangan digunakan untuk reinterpretasi batas lahan gambut dan tipologi lahan gambut serta pemberian data atribut tipologi lahan gambut. Reinterpretasi dilakukan dengan cara menarik batas baru hasil dari survei lapangan (Gambar 5). Pemberian data atribut tipologi lahan gambut hasil survei lapangan mengacu pada tabel 8 diantaranya tipe pemanfaatan, ketebalan dan tingkat kematangan. Basis data peta lahan gambut skala menengah mengikuti ketentuan pada Katalog Unsur Geografi Indonesia versi terbaru.



Gambar 5. Penarikan Batas Baru dan Validasi Tipologi Lahan Gambut Hasil Interpretasi

BADAN INFORMASI GEOSPASIAL

4.5 Penyajian Peta Lahan Gambut

Peta lahan gambut disusun berdasarkan hasil analisis dan hasil pengamatan lapangan. Informasi utama yang disajikan dalam peta lahan gambut berupa tipologi. Dalam penyusunan peta lahan gambut, sebaran setiap satuan tipologi gambut diberi kode tersendiri. Informasi tipe pemanfaatan lahan gambut menjadi label utama, sedangkan kedalaman gambut dan tingkat kematangan disimpan dalam bentuk atribut dan bisa ditampilkan dalam simbologi yang berbeda.

Peta lahan gambut di*overlay*kan dengan peta RBI skala 1:50.000 dengan desain tata letak dan format peta yang akan dicetak dilengkapi dengan informasi:

1. Judul;
2. Legenda peta, yang terdiri atas informasi satuan pemetaan, tipologi lahan gambut yang mencakup tipe pemanfaatan, ketebalan gambut dan tingkat kematangan, dan luas dalam hektar (ha) dan persentase (%);
3. Peta indeks lokasi bersangkutan;
4. Koordinat geografis/UTM;
5. Institusi pelaksana; dan
6. Institusi penerbit peta.

KEPALA BADAN INFORMASI GEOSPASIAL
REPUBLIK INDONESIA,

ttd

HASANUDDIN Z. ABIDIN

Salinan sesuai dengan aslinya,
Kepala Bagian Hukum,

Ida Suryani

UNIVERSITAS
GADJAH MADA
**Analisis Pengaruh Alih Fungsi Lahan Pertanian terhadap Produksi Padi di Kabupaten/Kota Provinsi Jawa
Timur Tahun 2016-2021**
Intam Tiwi Utami, Prof. Dr. Catur Sugiyanto, M.A.; Gigih Fitrianto, S.E., M.Sc., Ph.D.
Universitas Gadjah Mada, 2023 | Diunduh dari http://etd.repository.ugm.ac.id/

Daftar Isi

Halaman Judul i

Halaman Pengesahan ii

Pernyataan Keaslian Karya Tulis iii

Kata Pengantar iv

Daftar Isi vi

Daftar Tabel viii

Daftar Grafik ix

Daftar Gambar x

Daftar Diagram xi

Daftar Lampiran xii

Daftar Singkatan xiii

Intisari xv

Abstract xvi

BAB I PENDAHULUAN

1.1 Latar Belakang 1
1.2 Rumusan Masalah 6
1.3 Pertanyaan Penelitian 6
1.4 Tujuan Penelitian 6
1.5 Motivasi Penelitian 7
1.6 Manfaat Penelitian 7
1.7 Kontribusi Penelitian 8
1.8 Ruang Lingkup dan Batasan Penelitian 8
1.9 Sistematika Penulisan 8

BAB II LANDASAN TEORI DAN TINJAUAN PUSTAKA

2.1 Landasan Teori 10
2.1.1 Teori Produksi 10
2.1.2 Lahan Pertanian/Sawah 11
2.1.3 Alih Fungsi Lahan Pertanian 13
2.1.4 *Normalized Difference Vegetation Index* (NDVI) 14

UNIVERSITAS
GADJAH MADA
**Analisis Pengaruh Alih Fungsi Lahan Pertanian terhadap Produksi Padi di Kabupaten/Kota Provinsi Jawa
Timur Tahun 2016-2021**
Intam Tiwi Utami, Prof. Dr. Catur Sugiyanto, M.A.; Gigih Fitrianto, S.E., M.Sc., Ph.D.
Universitas Gadjah Mada, 2023 | Diunduh dari http://etd.repository.ugm.ac.id/

2.1.5 Curah Hujan 15
2.1.6 Dana Alokasi Khusus Fisik Bidang Pertanian (DAKFP) 16
2.1.7 Tenaga Kerja Pertanian (TKP) 17
2.2 Penelitian Terdahulu dan Keaslian Penelitian 18

BAB III METODE PENELITIAN
3.1 Desain Penelitian 27
3.2 Teknik Pengumpulan Data 27
3.3 Definisi Operasional Variabel 29
3.4 Metode Analisis Data 33
3.4.1 Pemilihan Model Estimasi 34
3.4.2 Analisis Regresi Data Panel 35
3.4.3 Uji Analisis Statistik 36
3.5 Model Penelitian 38

BAB IV HASIL DAN PEMBAHASAN
4.1 Deskripsi Data 39
4.1.1 Produksi Padi 40
4.1.2 Luas Sawah 42
4.1.3 NDVI 43
4.1.4 Curah Hujan 46
4.1.5 DAFKP 47
4.1.6 TKP 48
4.2 Hasil Penelitian 51
4.2.1 Pemilihan Model Terbaik 51
4.2.2 Uji Analisis Statistik 53
4.3 Pembahasan 56
4.3.1 Pengaruh Luas Sawah Terhadap Produksi Padi 56
4.3.2 Pengaruh NDVI Terhadap Produksi Padi 57
4.3.3 Pengaruh Curah Hujan Terhadap Produksi Padi 57
4.3.4 Pengaruh DAFKP Terhadap Produksi Padi 58
4.3.5 Pengaruh TKP Terhadap Produksi Padi 58

BAB V SIMPULAN
5.1 Simpulan 61
5.2 Keterbatasan Penelitian 61
5.3 Implikasi 62

Daftar Pustaka 63

Lampiran 69

STANDARDISASI KLASIFIKASI DAN INFORMASI SPASIAL PENUTUP LAHAN BERBASIS DATA SATELIT PENGINDERAAN JAUH OPTIS

Standardization Information Classification and Land Cover-Based Spatial Data Optical Satellite Remote Sensing

Wiweka, Surlan, dan Siti Hawariyah

Kantor Kedeputian Penginderaan Jauh LAPAN
Jl. Lapan 70 Pekayon Pasar Rebo Jakarta Timur 13710
e-mail: wiweka@lapan.go.id

Diajukan: 2 Januari 2012, Dinilaikan: 4 Januari 2012, Diterima: 23 April 2012

Abstrak

Makalah ini mengusulkan sebuah standar untuk terminologi kelas penutup lahan dari hasil klasifikasi citra digital dalam skala 1:100.000, sebagai jalan untuk memfasilitasi pandangan sinoptik sumber daya alam Indonesia. Karena belum adanya instansi yang berwenang serta bertanggungjawab menghasilkan standardisasi nasional definisi kelas penutup lahan, maka diharapkan agar tidak terjadi konflik dalam inventarisasi, analisis pemetaan, dan pelaporan data penggunaan tanah. Agar terjadi konsistensi dalam menurunkan kelas penutup lahan, pendekatan delineasi yang digunakan adalah segmentasi orientasi beorientasi obyek dengan dibantu interpretasi visual dan kombinasi warna. Hasil proses ekstraksi citra dalam skala 1:100.000 menghasilkan standardisasi kelas penutup lahan 8 kelas jenis penutup lahan, yaitu: hutan, semak/belukar, sawah, perkebunan, permukiman kota, permukiman desa, tubuh air, dan lahan terbuka.

Kata kunci: citra, klasifikasi, penutup lahan, segmentasi, skala

Abstract

This paper proposes a standard terminology for classes of land cover of classification results 1:100,000-scale digital image, as a way to facilitate the synoptic view of Indonesia's natural resources. Due to the absence of the competent authority responsible for producing national standardization and definition of land cover classes, therefore hopefully to avoid conflicts in the inventory, mapping analysis, and reporting of data on land use. To enable the consistency of the lower classes of land cover, delineation approach used is an object-oriented segmentation of orientation with the help of visual interpretation and color combinations. Image extraction process results in a scale of 1:100,000 produce standardized grade 8 class of land cover types, namely: forest, scrub / shrub, fields, plantations, urban settlements, rural settlements, water bodies, and open land.

***Keywords**: image, classification, land cover, segmentation, scale*

1. PENDAHULUAN

1.1 Latar Belakang

Peta penutup lahan (*land cover*) merupakan salah satu jenis informasi spasial yang dapat diekstraksi berdasarkan data satelit penginderaan jauh. Peta penutup lahan banyak dibuat dan digunakan untuk berbagai jenis tujuan. Oleh karena itu, banyak dijumpai peta penutup lahan dengan versi yang berlainan sesuai dengan tujuan penggunaan dan skala peta yang digunakan. Tingkat kerincian informasi pada peta penutup lahan semakin tinggi jika menggunakan skala peta yang besar, demikian pula sebaliknya. Sebagai contoh, tingkat kerincian informasi pada peta penutup lahan skala 1:100.000 jauh lebih rendah dibandingkan dengan yang menggunakan skala 1: 10.000.

Apabila peta penutup lahan dibuat berbasis data satelit penginderaan jauh, tingkat kerinciannya dipengaruhi oleh jenis data yang digunakan. Secara lebih spesifik, tingkat kerinciannya dipengaruhi oleh resolusi spasial data satelit penginderaan jauh yang digunakan. Sebagi contoh, peta penutup lahan berbasis data landsat lebih tinggi tingkat kerinciannya daripada peta penutup lahan yang berbasis data MODIS.

Peta penutup lahan merupakan salah satu produk informasi berbasis data satelit penginderaan jauh di lingkungan Kedeputian Penginderaan Jauh LAPAN. Peta tersebut banyak dibuat untuk kepentingan riset *in-house* dan juga untuk diserahkan kepada para pengguna informasi berbasis data satelit penginderaan jauh. Sampai saat ini peta penutup lahan di lingkungan Kedeputian Penginderaan

Jauh LAPAN dibuat dengan versi yang berlainan, baik jumlah kelas dan jenis penutup lahannya, maupun *lay out* petanya. Versi-versi penutup lahan tersebut tergantung kepada tim pembuatnya karena belum adanya acuan standar peta penutup lahan berbasis data satelit penginderaan jauh.

1.2 Permasalahan

Peta penutup lahan, yang merupakan salah satu produk informasi berbasis data satelit penginderaan jauh, sampai saat ini dibuat dengan versi yang berlainan, baik jumlah kelas dan jenis penutup lahannya, maupun *lay out* petanya. Versi-versi penutup lahan tersebut tergantung kepada tim pembuatnya karena belum adanya acuan standar peta penutup lahan berbasis data satelit penginderaan jauh. Agar diperoleh keseragaman dalam pembuatan peta penutup lahan berbasis data satelit penginderaan jauh diperlukan adanya acuan standar, baik jumlah kelas dan jenis penutup lahannya, maupun layout petanya.

1.3 Tujuan, Sasaran dan Indikator Kinerja

Tujuan penelitian ini adalah melakukan kajian terhadap: a. Jumlah kelas dan jenis penutup lahan berdasarkan hasil interpretasi citra satelit landsat untuk pembuatan peta penutup lahan dengan skala 1:100.000, dan b. *Lay out* peta penutup lahan skala 1:100.000 berbasis citra satelit landsat. Sasaran penelitian ini adalah tersedianya peta penutup lahan skala 1:100.000 berbasis citra satelit landsat yang dapat diusulkan sebagai peta penutup lahan yang standar, baik jumlah kelas dan jenis penutup lahannya maupun layout petanya.

Indikator Kinerja (IK) output penelitian ini adalah sistem klasifikasi penutup lahan dan *lay out* peta penutup lahan yang standar berbasis data satelit penginderaan jauh optis, dibatasi pada citra satelit landsat dan skala peta 1:100.000.

1.4 Lingkup Penelitian

- Standardisasi jumlah kelas dan jenis penutup lahan untuk skala peta 1:100.000 berdasarkan citra satelit landsat.
- Standardisasi simbol (warna dan/atau tekstur) untuk masing-masing kelas penutup lahan.
- Standardisasi *lay out* peta penutup lahan skala 1:100.000.

1.5 Manfaat

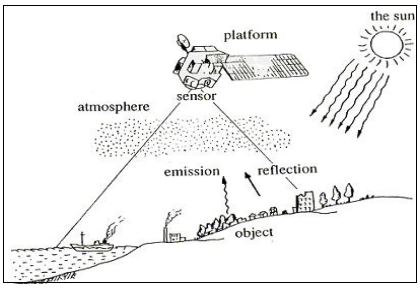
Hasil penelitian ini dapat dijadikan acuan standar dalam pembuatan peta penutup lahan skala 1:100.000 berbasis interpretasi citra landsat TM/ETM+, sehingga ada keseragaman produk informasi (peta penutup lahan) yang dihasilkan di Kedeputian Penginderaan Jauh LAPAN.

2. STUDI PUSTAKA

2.1 Penginderaan Jauh

Penginderaan jauh adalah ilmu dan seni untuk memperoleh informasi tentang suatu objek, area, atau fenomena melalui analisis data yang diperoleh dengan suatu alat tanpa kontak dengan objek, area, atau fenomena yang dikaji (Lillesand, Kiefer, dan Chipman, 2004). Konsep penginderaan jauh untuk satelit sensor optik diilustrasikan pada Gambar 1.

Matahari memancarkan energi yang berupa gelombang radiasi elektromagnetik (*electromagnetic radiation*). Energi radiasi tersebut mengenai berbagai jenis objek yang terdapat di permukaan bumi. Secara alami, jika energi radiasi tersebut mengenai permukaan suatu objek akan terjadi tiga kemungkinan proses fisis, yaitu terjadi pemantulan (*reflection*), penyerapan (*absorption*) dan diteruskan (*transmission*) sesuai dengan keunikan atau kondisi objek yang bersangkutan. Parameter yang menjadi indikator keunikan atau kondisi suatu objek dalam proses fisis disebut koefisien pemantulan, koefisien penyerapan, dan koefisien penerusan. Di samping ketiga proses fisis tersebut, terjadi juga proses pemancaran (*emission*), yaitu pemancaran energi radiasi yang terdapat pada suatu objek ke lingkungan di sekitarnya.

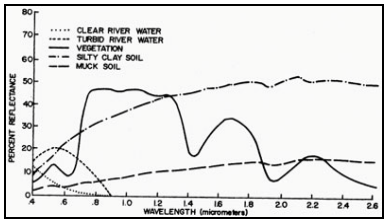


Gambar 1 Ilustrasi Sistem Penginderaan Jauh

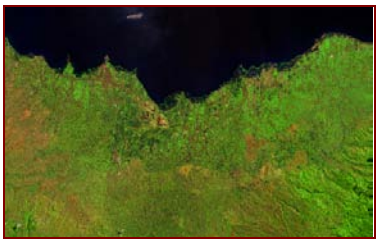
Gelombang elektromagnetik adalah tenaga elektrisitas dan magnetisme yang bergerak dengan kecepatan sinar, pada frekuensi dan panjang gelombang yang sangat bervariasi. Semakin tinggi frekuensi gelombang sinar tersebut, maka semakin tinggi pula tenaganya (Purwadi et al., 2007). Perbedaan karakteristik pemantulan dari objek tanah, air

dan vegetasi untuk setiap panjang gelombang elektromagnetik diperlihatkan pada Gambar 2.

Pada tahap selanjutnya, sensor yang dipasang pada wahana yang berada di angkasa, seperti balon udara, pesawat terbang dan satelit akan merekam energi pantulan dari objek-objek dipermukaan bumi, untuk selanjutnya menampilkan dalam bentuk data citra. Perbedaan karakteristik pemantulan dari objek mengakibatkan perbedaan kenampakan pada objek di data citra (Gambar 3.). Data penginderaan jauh akan diproses secara otomatis oleh komputer dan/atau diinterpretasi secara manual oleh manusia, dan akhirnya berguna untuk pertanian, penggunaan lahan, kehutanan, geologi, hidrologi, oseanografi, meteorologi, lingkungan dan lain sebagainya.



Gambar 2 Perbedaan Karakteristik Pemantulan Tanah, Air dan Vegetasi

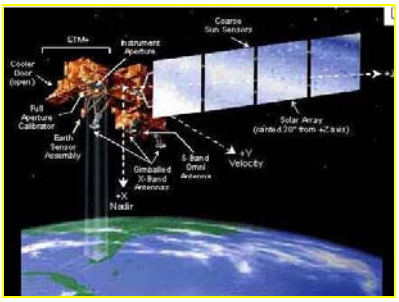


Gambar 3 Perbedaan Kenampakan Berbagai Jenis Objek pada Citra Landsat

2.2 Data Satelit Landsat

Dewasa ini terdapat banyak data satelit penginderaan jauh yang dapat digunakan di berbagai sektor. Data satelit penginderaan jauh tersebut memiliki spesifikasi yang berbeda-beda, salah satu di antaranya adalah data satelit Landsat (*Land Satellite*).

Landsat merupakan contoh satelit sumberdaya milik Amerika Serikat yang diluncurkan sejak tahun 1972. Landsat 5 dengan sensor TM (*Thematic Mapper*) dan Landsat 7 dengan sensor ETM+ (*Enhanched Tematic Mapper plus*) adalah satelit generasi kelima dan ketujuh yang diluncurkan. Landsat 7 ETM+ diluncurkan pada Bulan April 1999 (Gambar 4). Pada Landsat 7 ETM+ terdapat delapan kanal dengan resolusi spasial 30 meter, kecuali pada kanal 8 yang memiliki resolusi spasialnya 15 meter. Panjang gelombang dan manfaat dari masing-masing kanal dapat lilihat pada Tabel 1.



**Sumber: http://www.innoter.com/eng/remote_sensing/*
Gambar 4. Satelit Landsat 7 ETM+

Tabel 1 Panjang Gelombang dan Manfaat Satelit Landsat 7 ETM+

Kanal	Panjang Gelombang (µm)	Manfaat
1	0,450 – 0,515	Penetrasi tubuh air dan studi sumber daya alam perairan
2	0,525 - 0,605	Studi diskriminasi berbagai jenis vegetasi
3	0,630 - 0,690	Diskriminasi objek vegetasi
4	0,750 - 0,900	Identifikasi objek vegetasi, kontras antara tanah dan vegetasi
5	1,550 – 1,750	Studi jenis-jenis tanah dan kandungan air tanah
6	10,400 - 12,500	Diskriminasi kelembaban tanah, studi kandungan air tanah, dan fenomena termal
7	2,080 – 2,350	Identifikasi formasi batu-batuan
8	0,520 - 0,900	*(Kanal Spektral Pankromatik)*

2.3 Sistem Klasifikasi Penutup Lahan

Beberapa sistem klasifikasi penutup lahan yang umumnya digunakan oleh LAPAN dalam memproduksi informasi spasial penutup lahan berbasis data satelit penginderaan jauh adalah sebagai berikut:

a. Sistem Klasifikasi (kelas dan warna) yang digunakan dalam penelitian pelayanan untuk membantu pemerintah daerah (contoh: kerjasama dengan Kabupaten Sampang), seperti ditunjukkan pada Tabel 2

Tabel 2 Sistem Klasifikasi yang Digunakan dalam Penelitian Pelayanan Terhadap Pemerintah Daerah

No	Nama Kelas	Warna	Komposisi		
			R	G	B
1	Hutan Sekunder		2	219	0

No	Nama Kelas	Warna	Komposisi		
			R	G	B
2	Hutan Darat		38	115	0
3	Awan/Tdk ada data		210	210	210
4	Rawa		0	77	168
5	Mangrove		0	150	148
6	Tubuh Air		0	112	255
7	Tambak				
8	Industri		20	164	171
9	Hutan Gambut		247	180	103
10	Perkebunan		168	112	0
11	Kebun campur		205	175	102
13	Semak Belukar		255	255	0
14	Ladang/Tegalan		255	255	190
15	Tanah Terbuka		255	190	132
16	Permukiman kota		230	0	169
17	Permukiman Kampung		255	115	223
18	Bandara		254	0	208
19	Pelabuhan		202	0	219
20	Sawah		0	112	255

b. Sistem Klasifikasi (kelas dan warna) yang digunakan oleh bidang Inslahta Pusbangja dalam memproduksi informasi spasial penutup lahan, seperti ditunjukkan pada Tabel 3.

Tabel 3 Sistem Klasifikasi yang Digunakan Bidang Inslahta Pusbangja dalam Memproduksi Informasi Penutup Lahan

No	Symbol	Keterangan	Warna	R (0-255)	G (0-255)	B (0-255)
1	Aw	Awan / tak ada data		210	210	210
2	B	Belukar / semak		146	174	47
3	Hp	Hutan primer		76	115	0
4	Hg	Hutan gambut		247	180	103
5	Hr	Hutan rawa		173	164	254
6	Hs	Hutan sekunder		2	219	0
7	Hv	Mangrove		0	208	219
8	Kd	Permukiman / kampung		217	198	0
9	Kk	Permukiman / kota		255	199	174
10	L	Ladang / tegalan		183	223	134
11	P	Perkebunan		170	255	0
12	S	Sawah		255	255	115
13	T	Lahan terbuka		255	127	127
14	W	Air / danau / waduk / sungai		0	0	255
15	Wi	Tambak		0	255	255
16	Wr	Rawa		246	164	254
17	Bn	Bandara		254	0	208
18	I	Industri		20	164	171
19	Pl	Pelabuhan		202	0	219

c. Sistem Klasifikasi (kelas dan warna) berdasarkan Peraturan Pemerintah (PP) No. 10 mengenai produksi informasi spasial penutup lahan, seperti dapat dilihat pada Tabel 4.

Tabel 4 Sistem Klasifikasi yang Digunakan Berdasarkan PP-10 Mengenai Produksi Informasi Penutup Lahan

No	Kelas	Warna/simbol	Yellow (1-100%)	Magenta (1-100%)	Cyan (1-100%)	Blue (1-100%)	Bis/ Outline
1.	Kawasan Lindung						
2.	Kawasan Hutan lindung	HL	70	0	30	0	

No	Kelas	Warna/simbol	Yellow (1-100%)	Magenta (1-100%)	Cyan (1-100%)	Blue (1-100%)	Bis/ Outline
3.	Kawasan Bergambut	Gb	70	0	30	0	
4.	Kawasan Cagar Alam	CA	10	70	40	0	
5.	Kawasan Budidaya						
6.	Kawasan Hutan Produksi	Hp	0	0	30	0	
7.	Kawasan Hutan Produksi Terbatas	HPT	0	0	30	0	
8.	Pertanian Lahan Basah		0	0	100	0	
9.	Pertanian lahan kering	LK	40	40	0	0	Hitam 0,1 mm
10.	Perkebunan	TT	40	40	0	0	
11.	Pertambangan		0	0	100	0	Warna Simbol 1mm
12.	Kawasan Industr		100	70	0	0	
13.	Kawasan Permukiman Perkotaan		20	40	0	0	
14.	Pusat permukiman Kota		0	100	0	0	
15.	Pusat permukiman desa		0	100	0	0	

d. Sistem Klasifikasi (kelas dan warna) yang merupakan hasil perumusan oleh Tim Kedeputian Penginderaan Jauh mengenai produksi informasi spasial penutup lahan skala 1:100.000 dan 1:250.000, ditunjukkan pada Tabel 5.

Tabel 5 Sistem Klasifikasi Hasil Perumusan oleh Tim Kedeputian Penginderaan Jauh

Kelas Penutup Lahan	Kelas Penutup Lahan 1:250.000	Kelas Penutup Lahan 1:100.000
1. Daerah bervegetasi (Hijau–kuning–coklat muda)	1.1. Hutan (Hijau = H)	▪ Hutan primer lahan kering, lahan basah, + ketinggian (H+T) ▪ Hutan sekunder/tanaman industri (H+T) ▪ Belukar (H+T) ▪ Mangrove (mix dgn hutan lahan basah, pemilahan dgn ketinggian). (H+T) (T= Tekstur)
	1.2. Sawah (Kuning = K)	▪ Sawah irigasi (dekat DAM, teknis; non teknis: multi temporal) (K+T) ▪ Sawah lahan kering. (K+T) ▪ Ladang/palawija. (K+T) ▪ Tebu. (K+T) Keterangan: ▪ Informasi dari data multi temporal ▪ ”objek” musiman

Kelas Penutup Lahan	Kelas Penutup Lahan 1:250.000	Kelas Penutup Lahan 1:100.000
	1.3. Kebun (Coklat muda = CM)	▪ Perkebunan sawit (CM +T) ▪ Perkebunan teh (CM +T) ▪ Perkebunan karet (CM +T) ▪ Perkebunan (Campur) (CM +T) ▪ Perkebunan lainnya (CM +T)*
2. Area terbangun (ungu - merah hati – merah muda	1.1. Permukiman (ungu)	▪ Permukiman padat (ungu) ▪ Permukiman jarang(merah)
	1.2. Sarana / pra sarana (Merah Muda = MM)	▪ Bandar udara/Lanud->lapangan terbang (MM+T) ▪ Pelabuhan (MM+T) ▪ Jalan (MM+T) ▪ Kawasan industri(gudang) (MM+T) ▪ Kawasan kantor* (MM+T)
3. Perairan (biru)	3.1. Perairan darat (biru tua – hitam)	▪ Sungai (biru tua) ▪ Waduk/danau (biru tua+T) ▪ Rawa (hitam) ▪ Tambak (hitam + T)
	3.2. Laut (biru muda)	▪ Laut (biru muda) ▪ Sedimentasi pantai (cyan) ▪ Terumbu karang)**(cyan +T) ▪ Pasir pantai/beting (Cyan+T)
4. Lahan terbuka (coklat – abu2)	4.1. Lahan terbuka hijau (coklat)	▪ Lahan kosong (padang rumput) (+T) ▪ Taman kota *(coklat) ▪ Lapangan golf (+T)
	4.2. Lahan terbuka (abu2)	▪ Pasir (+T) ▪ Bekas galian tambang (abu2) ▪ Lahar/endapan lahar (+T) ▪ Tanah timbul* (+T) ▪ Batuan* (+T) ▪ Salju abadi (abu2 muda)
5. Tidak terkelaskan (putih)	Mis: Awan, bayangan awan, bayangan gunung, dll	Tidak terkelaskan (putih)

3. METODOLOGI

3.1 Daerah Kajian

Penelitian Standardisasi Klasifikasi dan Informasi Spasial Penutup Lahan Berbasis Data Satelit Penginderaan Jauh Optis ini dilaksanakan dengan mengambil sampel lokasi di wilayah Kabupaten Tuban, Provinsi Jawa Timur.

3.2 Data

Data yang digunakan adalah data satelit Landsat, sedangkan data pendukungnya terdiri dari: vektor batas wilayah administrasi, jaringan jalan raya, dan sungai.

3.3 Metode Penelitian

Metode yang dipakai untuk menentukan kajian standardisasi klasifikasi informasi spasial penutup lahan berbasis data satelit penginderaan jauh, terdiri dari lima tahap, yaitu:

- Melakukan inventarisasi terhadap berbagai sistem klasifikasi penutup lahan berbasis data satelit penginderaan jauh yang digunakan di lingkungan LAPAN.
- Mengkaji sistem klasifikasi penutup lahan yang telah diinvetarisasi. Kajian yang dilakukan terkait dengan jumlah kelas dan jenis penutup lahan yang disesuaikan dengan kemampuan spektral kanal-kanal pada data Landsat untuk output peta skala 1:100.000, dan kajian tentang format layout peta penutup lahan. Kajian dilakukan dengan melakukan perbandingan antara beberapa sistem klasifikasi yang telah ada.
- Melakukan identifikasi objek-objek penutup lahan pada citra Landsat sehingga diperoleh sistem klasifikasi (jumlah kelas dan jenis penutup lahan) yang sesuai untuk informasi spasial penutup lahan skala 1:100.000 berbasis citra Landsat komposit warna (RGB, Red Green Blue) 542.
- Menetapkan sistem klasifikasi penutup lahan untuk skala 1:100.000 berbasis citra Landsat komposit warna (RGB) 542.

- Melakukan klasifikasi penutup lahan dengan menggunakan sistem klasifikasi yang telah ditetapkan pada langkah terdahulu. Klasifikasi dilakukan dengan menggunakan metode interpretasi visual dan deliniasi pada layar (*On Screen Digitation*), dengan tahapan sebagai berikut:
  a) Melakukan koreksi data citra Landsat yang akan digunakan terhadap data referensi.
  b) Memanggil dan menampilkan data raster pada layar monitor.
  c) Memilih kombinasi kanal untuk RGB 542, dan melakukan zooming maksimal 2 kali lebih besar dari skala yang dipilih (untuk data Landsat dengan skala 1:100.000, dilakukan perbesaran pada layar monitor dengan skala 1:50.000).
  d) Melakukan interpretasi citra secara visual berdasarkan 8 kunci interpretasi (rona, warna, pola, bentuk, tekstur, ukuran, bayangan, dan asosiasi).
  e) Melakukan proses delimitasi untuk melihat batas antara dua atau lebih obyek yang berbeda.
  f) Melakukan deliniasi pada setiap kelas obyek hasil interpretasi.
  g) Melakukan layout hasil klasifikasi.

4. HASIL DAN PEMBAHASAN

4.1 Identifikasi Penutup Lahan Secara Visual Berbasis Data Landsat

Berdasarkan hasil kajian sistem klasifikasi penutup lahan yang telah digunakan terdapat sekitar 15-21 kelas penutup lahan untuk pemetaan skala 1:100.000 berbasis data Landsat. Kemudian sistem tata nama dan warna untuk setiap kelas masih berlainan antara satu sistem dengan sistem lainnya, oleh karena perlu upaya untuk menetapkan sistem klasifikasi standar untuk informasi penutup lahan skala 1:100.000 berbasis data Landsat.

Jenis penutup lahan skala 1:100.000 yang dapat diturunkan dengan data Landsat dilakukan dengan melakukan identifikasi setiap jenis objek penutup lahan dengan menggunakan citra komposit warna (RGB) 542. Penggunan komposit warna (RGB) 542 didasarkan karena komposit warna ini dapat menampilkan pewarnaan alam yang natural (mirip dengan aslinya), sehingga biasa digunakan dalam interpretasi visual. Saat melakukan identifikasi setiap kelas penutup lahan pembesaran (*zooming*) maksimal yang dapat dilakukan adalah sampai skala 1:50.000, kemudian melakukan interpretasi secara visual sehingga dipastikan setiap jenis penutup lahan tersebut dapat dikenali.

4.2 Identifikasi Lahan Sawah

Masa tanam padi memiliki 3 fase, yaitu: fase air (fase pada masa pertumbuhan vegetatif awal dimana air mendominasi), fase pertumbuhan lanjut dan perkembangan tanaman padi (fase vegetatif dan generatif), dan fase bera (kondisi lahan sawah setelah panen sampai sebelum masa tanam berikutnya).

Pada setiap fase pertumbuhan tanaman padi, akan memiliki kemiripan warna dengan penggunaan lahan yang lain sehingga dalam interpretasi dapat terjadi kekeliruan dalam penentuan objek. Misalnya: sawah memiliki kemiripan dengan tambak pada saat fase air (kondisi sawah yang didominasi air), sawah memiliki kemiripan dengan perkebunan, semak belukar pada fase vegetatif (kondisi pertumbuhan), dan sawah memiliki kemiripan dengan lahan terbuka/tegalan pada fase bera. Cara yang paling baik untuk mengidentifikasi sawah adalah menggunakan citra multitemporal (berlainan waktu) yang dapat memantau perubahan fase. Akan tetapi bila digunakan data satu waktu, maka kesalahan interpretasi dapat dikurangi dengan memahami pengetahuan mengenai definisi dan ciri-ciri lahan sawah.

Sawah adalah suatu bentuk lahan pertanian yang secara fisik memiliki permukaan yang rata, dilakukan di lahan basah dan memerlukan banyak air. Dari pengertian tersebut, maka ciri-ciri sawah antara lain: dibatasi oleh pematang, memiliki permukaan yang rata, dan memerlukan air, hingga diperlukan sistem irigasi. Berdasarkan ciri-ciri tersebut maka keberadaan sawah dapat diidentifikasi dengan kondisi penampakan pada citra seperti:

1. Ada pembatas, hingga akan membentuk pola (kotak-kotak).
2. Memiliki permukaan yang rata, sehingga tekstur akan tampak halus.
3. Memerlukan air, sehingga akan memerlukan sistem irigasi (adanya jalur irigasi, dekat dengan badan air).



Gambar 5 Objek Sawah Berdasarkan Citra Komposit Warna (RGB) 542 Data Landsat dengan Pembesaran Skala 1:50.000.

Gambar 5 memperlihatkan penampakan objek sawah berdasarkan citra komposit warna (RGB) 542 dari data Landsat dengan pembesaran skala 1:50.000. Dengan pembesaran 1:50.000, sawah masih dapat diidentifikasi menggunakan data Landsat, sawah terlihat dengan warna hijau (fase vegetatif/generatif) dan biru (fase air), terlihat bahwa sawah mempunyai tekstur halus dengan pola kotak-kotak yang dibentuk oleh pematang sawah. Sebagai pembanding, Gambar 6 memperlihatkan sawah pada citra resolusi tinggi *Quick Bird* yang jelas terlihat pola kotak-kotak yang dibentuk oleh pematang sawah.



Gambar 6 Objek Sawah Berdasarkan Citra *Quick Bird.*

4.3 Identifikasi Lahan Permukiman (Permukiman Kota dan Permukiman Desa)

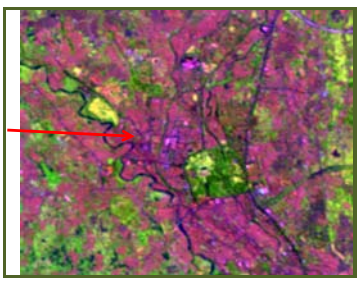
Permukiman adalah kumpulan perumahan dengan segala unsur serta penelitian yang berkaitan dengan yang ada di dalam permukiman. Syarat-syarat permukiman antara lain:

1. Wisma: Tempat Tinggal.
2. Karya: Tempat berkarya dan usaha.
3. Marga: Jaringan tempat mobilitas masyarakat dan barang berlangsung.
4. Suka: Tempat masyarakat berekreasi, bersantai, hiburan.
5. Penyempurna/Fasilitas Umum: Pelayanan penunjang bagi masyarakat (pendidikan, peribadatan, fasilitas umum).

Oleh karena itu, dilihat dari unsur dan syarat-syarat permukiman, maka permukiman akan dapat dilihat dari segi warna, pola, tekstur, dan asosiasi. Hal-hal yang dapat dijadikan patokan dalam interpretasi permukiman antara lain:

1. Dekat dengan akses transportasi (sungai, jalan).
2. Memiliki bentuk terpadu yang sejenis (bangunan).
3. Pola perkembangan selalu kontinyu pada posisi topografi datar.
4. Cenderung dekat dengan tempat usaha (pabrik, ladang, perkebunan, pertanian dan sebagainya).
5. Cenderung dengan lokasi sumberdaya alam yang mempunyai tingkat kebutuhan hidup (air, udara yang segar, tingkat kesuburan dan sebagainya).
6. Memiliki warna yang lebih kontras dibandingkan dengan objek yang lain.
7. Penutupan awan yang cenderung sedikit.
8. Dapat dilihat berdasarkan perkembangan kultur wilayah (Sosial-Ekonomi budaya).
9. Karakteristik warna yang cenderung sama dalam satu region.
10. Terdapat titik warna yang terpusat berkembang meluas dengan gradasi semakin merendah.

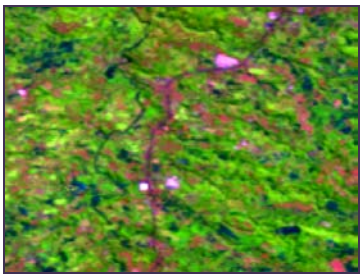
Terdapat dua tipe permukiman, yaitu permukiman kota dan permukiman desa. Permukiman kota adalah permukiman yang berlokasi di dalam kota, biasanya mempunyai pola perumahan teratur, rapat, adanya jaringan jalan dan memiliki warna yang lebih terang. Sedangkan permukiman desa mempunyai pola yang kurang teratur, terpisah-pisah dan bercampur dengan kenampakan vegetasi. Gambar 7 memperlihatkan penampakan objek permukiman kota dan Gambar 8 memperlihatkan penampakan objek permukiman desa berdasarkan citra komposit warna (RGB) 542 dari data Landsat dengan pembesaran skala 1:50.000. Pada citra komposit warna (RGB) 542, objek permukiman berwarna merah muda (pink), dimana pada permukiman kota terlihat warna pink yang mengelompok dengan jaringan jalan yang banyak dan teratur, sedangkan pada permukiman desa terlihat warna pink yang agak menyebar di sepanjang jalan. Gambar 9 memperlihatkan contoh objek permukiman kota pada citra resolusi tinggi *Quick Bird*.



Gambar 7 Objek Permukiman Kota Berdasarkan Citra Komposit Warna (RGB) 542 Data Landsat dengan Pembesaran Skala 1:50.000

Seperti yang telah dijelaskan terdahulu, adanya fasilitas umum merupakan salah satu dari syarat-syarat permukiman. Beberapa contoh

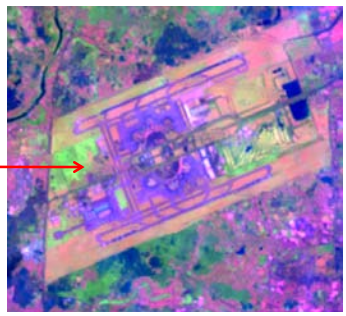
fasilitas umum yang dapat diindentifikasi oleh data Landsat adalah bandara, pelabuhan, kawasan Industri, kawasan perkantoran dan lain-lain. Pada umumnya fasilitas umum terdapat di wilayah perkotaan sehingga dapat dimasukkan dalam kelas permukiman kota. Gambar 10 memperlihatkan penampakan objek Bandara (Bandar Udara) berdasarkan citra komposit warna (RGB) 542 dari data Landsat dengan pembesaran skala 1:50.000.



Gambar 8 Objek Permukiman Desa Berdasarkan Citra Komposit Warna (RGB) 542 Data Landsat dengan Pembesaran Skala 1:50.000



Gambar 9 Objek Permukiman Kota Berdasarkan Citra *Quick Bird*



Gambar 10 Objek Bandara Berdasarkan Citra Komposit Warna (RGB) 542 Data Landsat dengan Pembesaran Skala 1:50.000

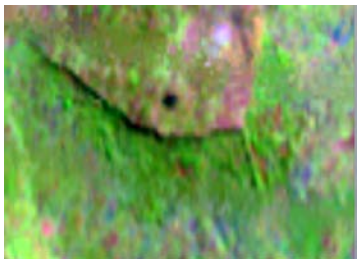
4.4 Identifikasi Lahan Semak/Belukar

Semak/belukar adalah kawasan bekas hutan lahan kering yang telah tumbuh kembali, didominasi oleh tanaman rendah dan tidak menampakkan lagi bekas alur bercak penebangan. Semak/belukar merupakan lahan bervegetasi rendah yang tidak ditujukan untuk tujuan komersil (seperti perkebunan, tegalan, sawah dan sebagainya). Semak/belukar sering tertukar oleh penggunaan lahan bervegetasi yang lain seperti perkebunan, dan sawah fase vegetatif, karena mempunyai tekstur yang relatif sama sehingga menyebabkan terjadinya kekeliruan dalam interpretasi.

Berdasarkan definisi tersebut, maka dapat disimpulkan bahwa semak/belukar mempunyai ciri-ciri sebagai berikut:

1. Memiliki vegetasi yang rendah dan tekstur yang halus.
2. Lahan tidak ditujukan untuk tujuan komersil (mungkin cenderung di area yang sulit dilakukan pengelolaan dalam segi pertanian).
3. Merupakan tanaman bekas hutan lahan kering (umumnya pada wilayah hutan).
4. Tidak memiliki pola (tidak ada tanda batas kepemilikan).
5. Tidak memerlukan irigasi (tidak ada saluran irigasi).

Gambar 11 memperlihatkan penampakan objek semak/belukar berdasarkan citra komposit warna (RGB) 542 dari data Landsat dengan pembesaran skala 1:50.000. Pada citra komposit warna (RGB) 542, objek semak/belukar berwarna hijau, dengan vegetasi rendah dan tekstur halus tanpa memiliki pola. Gambar 12 memperlihatkan penampakan semak/belukar pada citra resolusi tinggi *QuickBird*.



Gambar 11 Objek Semak/Belukar Berdasarkan Citra Komposit Warna (RGB) 542 Data Landsat dengan Pembesaran Skala 1:50.000



Gambar 12 Objek Semak/Belukar pada Citra Resolusi Spasial Tinggi *Quick Bird*

4.5 Identifikasi Lahan Ladang/ Tegalan

Ladang/Tegalan adalah suatu daerah lahan kering yang bergantung pada pengairan air hujan, ditanami tanaman musiman atau tahunan dan terpisah dari lingkungan dalam sekitar rumah dan perkampungan. Tanaman yang tumbuh pada tegalan umumnya berupa tanaman hortikultura (tanaman hias dan sayuran). Pada umumnya tegalan tidak mempunyai sistem irigasi karena permukaannya yang tidak rata, oleh karena itu pada musim kemarau akan lebih mudah kering.

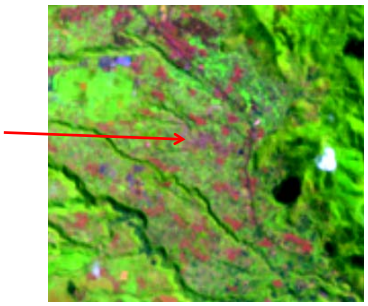
Dilihat dari definisi ladang/tegalan, maka ada beberapa spesifikasi yang dapat dijadikan patokan dalam penentuan areal tegalan antara lain:

1. Pola aliran irigasi yang tidak teratur.
2. Dilihat dari citra temporal, pada musim kering daerah, akan tampak kering.
3. Ada pada dataran menengah-curam dan tinggi.
4. Pola memiliki batas tanaman pagar untuk setiap lahan tegalan.
5. Vegetasi yang berbeda dalam satu batas lahan tegalan.
6. Warna akan cenderung mirip dengan sawah pada fase bera.

Dalam penampakan pada citra Landsat skala 1:100.000, objek lahan ladang/tegalan cukup sulit dibedakan dengan objek sawah, karena:

1. Warna dan pola pada citra Landsat sangat mirip dengan sawah fase bera.
2. Sulit membedakan kelas bila sudah bercampur dengan penggunaan lahan lain seperti sawah.

Dengan alasan tersebut, maka objek ladang/tegalan dimasukan dalam kelas sawah. Gambar 13 memperlihatkan penampakan objek ladang/tegalan berdasarkan citra komposit warna (RGB) 542 dari data Landsat dengan pembesaran skala 1:50.000. Pada citra komposit warna (RGB) 542, objek ladang tegalan berwarna merah keunguan (mirip sawah bera atau permukiman) bercampur warna hijau yang merupakan vegetasi pembatas antara lahan tegalan.



Gambar 13 Objek Ladang/Tegalan Berdasarkan Citra Komposit Warna (RGB) 542 Dari Data Landsat dengan Pembesaran Skala 1:50.000

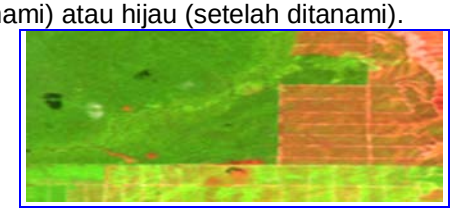
4.6 Identifikasi Lahan Perkebunan

Perkebunan adalah tegakan hutan yang di buat dengan menanam atau pembenihan dalam proses penghijauan/reboisasi. Biasanya untuk tujuan komersil dan hanya dalam bentuk vegetasi saja. Untuk beberapa wilayah tertentu seperti di Sumatera dan Kalimantan, sering terjadi konversi lahan hutan menjadi perkebunan dengan melakukan penggundulan hutan terlebih dahulu sehingga penampakan awal dari perkebunan adalah berupa lahan kosong.

Berdasarkan definisi tersebut, maka lahan perkebunan dapat menggunakan beberapa patokan di bawah ini:

1. Adanya warna vegetasi yang luas dan rata.
2. Warna vegetasi cenderung lebih terang (karena kehijaun tinggi).
3. Berwarna seperti lahan terbuka saat belum ditanami.
4. Adanya batasan-batasan yang tegas dalam suatu areal yang luas.
5. Tidak terpaku pada topografi (tergantung jenis tanamannya).
6. Tanaman untuk tujuan komersil, maka dekat dengan permukiman.

Gambar 14 memperlihatkan penampakan objek perkebunan berdasarkan citra komposit warna (RGB) 542 dari data Landsat dengan pembesaran skala 1:50.000. Perkebunan mempunyai bentuk dan batasan yang teratur, dengan warna merah (dalam kondisi belum ditanami) atau hijau (setelah ditanami).

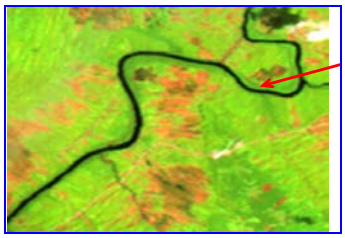


Gambar 14 Objek Perkebunan Berdasarkan Citra Komposit Warna (RGB) 542 Data Landsat dengan Pembesaran Skala 1:50.000

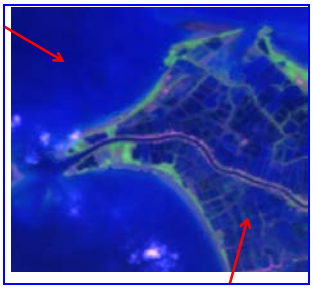
4.7 Identifikasi Tubuh Air

Beberapa objek penutup seperti sungai, waduk, danau, kolam, rawa dan tambak mempunyai dominasi penampakan permukaan berupa air. Hal ini mengakibatkan objek-objek tersebut mempunyai karateristik yang hampir mirip yaitu karateristik air yang menyerap energi gelombang, sehingga penampakannya pada citra menjadi lebih gelap dibandingkan penutup lahan lainnya. Pada pemetaan skala 1:100.000 dengan menggunakan data Landsat, objek-objek tersebut dapat digolongkan ke dalam satu kelas yaitu tubuh air.

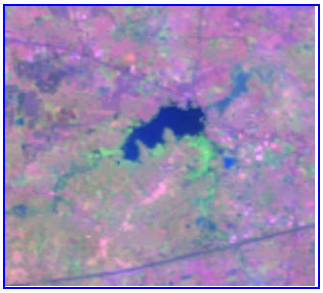
Gambar 15 - 17 memperlihatkan penampakan objek-objek yang merupakan kelas tubuh air (sungai, laut, tambak, dan kolam penampungan) berdasarkan citra komposit warna (RGB) 542 dari data Landsat dengan pembesaran skala 1:50.000. Tubuh air mempunyai warna gelap dibandingkan sekelilingnya. Perbedaan untuk setiap objek dapat teramati dengan menggunakan bentuk atau asosiasi okasi.



Gambar 15 Objek Sungai Berdasarkan Citra Komposit Warna (RGB) 542 Data Landsat dengan Pembesaran Skala 1:50.000



Gambar 16 Objek Laut dan Tambak Berdasarkan Citra Komposit Warna (RGB) 542 Data Landsat dengan Pembesaran Skala 1:50.000



Gambar 17 Objek Kolam Penampungan Berdasarkan Citra Komposit Warna (RGB) 542 Data Landsat dengan Pembesaran Skala 1:50.000

4.8 Identifikasi Lahan Hutan

Hutan adalah sebuah kawasan yang ditumbuhi dengan lebat oleh pepohonan dan tumbuhan lainnya. Kawasan-kawasan semacam ini terdapat di wilayah-wilayah yang luas di dunia dan berfungsi sebagai penampung karbon dioksida (*carbon dioxide sink*), habitat hewan, modulator arus hidrologika, serta pelestari tanah, dan merupakan salah satu aspek biosfera bumi yang paling penting.

Definisi Hutan secara konsepsional yuridis dirumuskan di dalam Pasal 1 Ayat (1) Undang-Undang Nomor 41 Tahun 1999 tentang Kehutanan. Menurut Undang-Undang tersebut, hutan adalah suatu kesatuan ekosistem berupa hamparan lahan berisi sumberdaya alam hayati yang didominasi pepohonan dalam persekutuan alam lingkungan, yang satu dengan yang lainnya tidak dapat dipisahkan. Dari definisi hutan yang disebutkan, terdapat unsur-unsur yang meliputi :

a. Suatu kesatuan ekosistem.
b. Berupa hamparan lahan.
c. Berisi sumberdaya alam hayati beserta alam lingkungannya yang tidak dapat dipisahkan satu dengan yang lainnya.
d. Mampu memberi manfaat secara lestari.

Keempat ciri pokok dimiliki suatu wilayah yang dinamakan hutan, merupakan rangkaian kesatuan komponen yang utuh dan saling ketergantungan terhadap fungsi ekosistem di bumi. Eksistensi hutan sebagai sub ekosistem global menempati posisi penting sebagai paru-paru dunia (Zain, 1996).

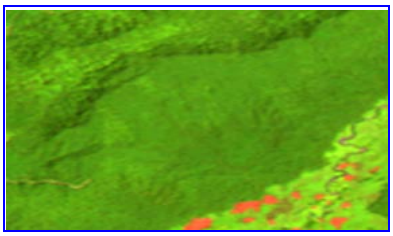
Sedangkan kawasan hutan lebih lanjut dijabarkan dalam Keputusan Menteri Kehutanan No. 70/Kpts-II/2001 tentang Penetapan Kawasan Hutan, perubahan status dan fungsi kawasan hutan, yaitu wilayah tertentu yang ditunjuk dan atau ditetapkan oleh pemerintah untuk dipertahankan keberadaannya sebagai hutan tetap. Dari definisi dan penjelasan tentang

kawasan hutan, terdapat unsur-unsur yang meliputi :

a. Suatu wilayah tertentu.
b. Terdapat hutan atau tidak terdapat hutan.
c. Ditetapkan pemerintah (menteri) sebagai kawasan hutan.
d. Didasarkan pada kebutuhan serta kepentingan masyarakat.

Dari unsur pokok yang terkandung di dalam definisi kawasan hutan, dijadikan dasar pertimbangan ditetapkannya wilayah-wilayah tertentu sebagai kawasan hutan. Kemudian, untuk menjamin diperolehnya manfaat yang sebesar-besarnya dari hutan dan berdasarkan kebutuhan sosial ekonomi masyarakat serta berbagai faktor pertimbangan fisik, hidrologi dan ekosistem, maka luas wilayah yang minimal harus dipertahankan sebagai kawasan hutan adalah 30% dari luas daratan.

Gambar 18 memperlihatkan penampakan objek hutan berdasarkan citra komposit warna (RGB) 542 dari data Landsat dengan pembesaran skala 1:50.000. Hutan didominasi oleh vegetasi yang tinggi sehingga mempunyai warna hijau dan agak gelap dibandingkan sekelilingnya. Hutan yang homogen mempunyai tekstur yang halus sedangkan hutan yang heterogen mempunyai tekstur yang agak kasar. Gambar 19 memperlihatkan penampakan hutan pada citra resolusi tinggi *Quick Bird*.



Gambar 18 Objek Hutan Berdasarkan Citra Komposit Warna (RGB) 542 Data Landsat dengan Pembesaran Skala 1:50.000

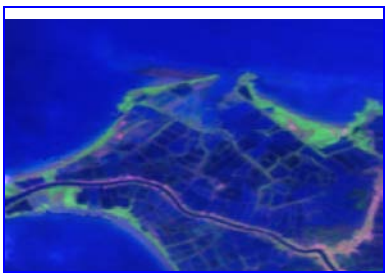


Gambar 19 Objek Hutan pada Citra Resolusi Spasial Tinggi *Quick Bird*

Hutan mangrove adalah hutan yang tumbuh di atas rawa-rawa berair payau yang terletak pada garis pantai dan dipengaruhi oleh pasang surut air laut. Hutan ini tumbuh khususnya di tempat-tempat dimana terjadi pelumpuran dan akumulasi bahan organik. Baik di teluk-teluk yang terlindung dari gempuran ombak, maupun di sekitar muara sungai dimana air melambat dan mengendapkan lumpur yang dibawa dari hulu.

Hutan mangrove dapat diidentifikasi dengan menggunakan komposit warna khusus (RGB 453) dari citra landsat karena mangrove mempunyai karakteristik pantulan yang berbeda dari objek-objek lainnya. Pantulan mangrove merupakan gabungan antara pantulan vegetasi dan serapan air, sehingga hutan mangrove mempunyai warna yang lebih tua dibandingkan hutan pada umumnya. Tetapi bila menggunakan citra komposit warna (RGB) 542 maka penampakan warna mangrove sulit dibedakan dengan hutan-hutan lainnya, oleh karena itu pada mangrove dimasukan dalam kelas hutan.

Gambar 20 memperlihatkan penampakan objek hutan mangrove berdasarkan citra komposit warna (RGB) 542 dari data Landsat dengan pembesaran skala 1:50.000. Mangorve teridentifikasi berwarna hijau seperti halnya warna hutan, tetapi mangrove mempunyai asosiasi dengan lokasi yang basah dan berlumpur, seperti di muara sungai, rawa dan tambak**.**



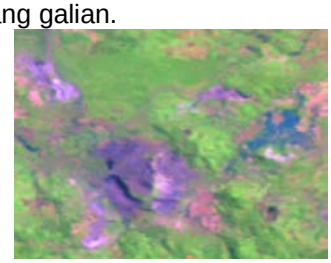
Gambar 20 Objek Hutan Mangrove Berdasarkan Citra Komposit Warna (RGB) 542 Data Landsat dengan Pembesaran Skala 1:50.000

4.9 Identifikasi Lahan Terbuka

Berdasarkan hasil kajian secara visual maka pada pemetaan skala 1:100.000 menggunakan data Landsat, kelas lahan terbuka merupakan kelas lahan tanpa vegetasi yang terdiri dari beberapa objek penutup lahan, seperti: lahan kosong, pasir, bekas galian tambang, endapan lahar, tanah timbul, batuan dan salju abadi.

Gambar 21 memperlihatkan penampakan kelas lahan terbuka (bekas galian tambang) berdasarkan citra komposit warna (RGB) 542 dari data Landsat dengan pembesaran skala 1:50.000. Galiang tambang berwarna merah keunguan yang menandakan tidak adanya

tutupan vegetasi selain itu terdapat genangan yang diperkirakan karena air hujan yang masuk kedalam lubang galian.



Gambar 21 Objek Lahan Terbuka Berdasarkan Citra Komposit Warna (RGB) 542 Data Landsat dengan Pembesaran Skala 1:50.000

4.10 Usulan Standar Klasifikasi Penutup Lahan Skala 1:100.000 Menggunakan Citra Landsat Komposit Warna (RGB) 542

Berdasarkan hasil identifikasi jenis penutup lahan untuk skala 1:100.000 dengan menggunakan citra Landsat komposit warna (RGB) 542, maka ditetapkan bahwa kelas penutup lahan dibagi menjadi 8 kelas yaitu: hutan, semak/belukar, sawah, perkebunan, permukiman kota, permukiman desa, tubuh air dan lahan terbuka.

Nama dan warna kelas dipilih dengan merujuk kepada tata nama dan warna kelas yang digunakan pada sistem klasifikasi yang telah digunakan oleh sebelumnya di lingkungan LAPAN (Tabel 2 s.d. 5). Pemilihan tata nama dan warna didasarkan pada tata nama dan warna yang paling banyak digunakan dalam sistem klasifikasi terdahulu. Bila setiap sistem klasifikasi menggunakan tata nama dan warna yang berbeda maka digunakan tata nama dan warna yang telah umum digunakan dalam proses klasifikasi. Standar jumlah kelas, jenis penutup lahan dan warna untuk simbol kelas penutup lahan yang diusulkan dari penelitian ini diperlihatkan pada Tabel 7.

Tabel 7 Usulan Standar Klasifikasi Penutup Lahan Skala 1:100 000 Menggunakan Citra Landsat Komposit Warna (RGB) 542

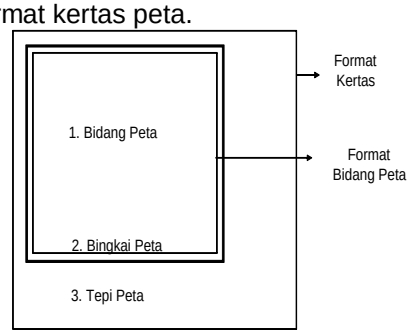
No	Simbol	Kelas	Warna	R (0-255)	G (0-255)	B (0-255)	Generalisasi Penutup Lahan
1	H	Hutan		146	174	47	Hutan primer, hutan sekunder dan mangrove
2	SB	Semak/ Belukar		76	155	0	Semak/belukar
3	S	Sawah		0	254	253	Sawah berbagai fase, Ladang/tegalan
4	P	Perkebunan		170	255	0	Perkebunan, kebun campur
5	PK	Permukiman Kota		230	0	169	Permukiman kota, fasilitas umum: bandara, pelabuhan, perkantoran, industri dll
6	PD	Permukiman Desa		255	199	174	Permukiman desa
7	TA	Tubuh Air		0	0	255	Sungai, danau, laut, kolam, tambak, rawa dll
8	LT	Lahan Terbuka		246	164	254	Lahan kosong, pasir, bekas galian tambang, endapan lahar, tanah timbul, batuan dan salju abadi

4.11 Usulan *Lay out* Peta Penutup Lahan

Informasi penutup lahan skala 1:100.000 yang dihasilkan berbasis data Landsat diberikan kepada pengguna dalam bentuk peta penutup lahan. Pembuatan peta penutup lahan yang baik dan mudah dimengerti membutuhkan layout yang baik dan standar.

Secara umum komponen utama dari peta terdiri dari (Gambar 22):

1. Bidang peta, yaitu bidang yang menggambarkan kandungan informasi peta.
2. Bingkai peta (Prim peta), yaitu garis yang membatasi bidang peta.
3. Tepi peta, yaitu bagian peta yang berada diluar prim peta, dalam hal ini dibatasi oleh format kertas peta.



Gambar 22 Komponen Utama Peta

Bidang peta terdiri dari kandungan peta dan grid peta, sedangkan tepi peta terdiri dari berbagai informasi seperti skala, pentunjuk lokasi, keterangan kelas, sumber data dan lain-lain. Tepi peta dapat terletak di bagian bawah, bagian kiri atau bagian kanan dari peta. Tetapi pada umumnya terletak di bagian bawah atau kanan peta (Gambar 23).



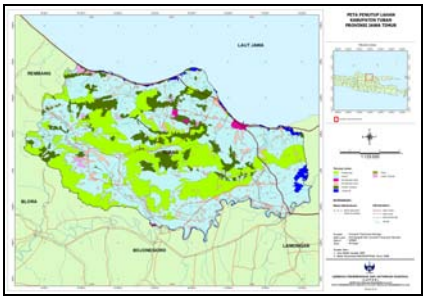
Gambar 23 Format dan Isi Peta

Dengan merujuk pada format peta tersebut dan mempertimbangkan format peta penutup lahan yang umum digunakan selama ini maka diusulkan untuk membuat standar *lay out* peta yang terdiri dari:

1. Bidang peta, yang terdiri dari kandungan peta (informasi spasial dan toponim) dan grid.
2. Bingkai peta, yang terdiri dari garis *frame* koordinat dan garis *frame* pembatas.
3. Tepi peta, yang terdiri dari judul peta, petunjuk lokasi, mata angin, skala, keterangan kelas penutup lahan, keterangan pendukung, proyeksi peta, sumber data, logo dan nama institusi pembuat, tahun pembuatan.

4.12 Penerapan Standar KIsifikasi Penutup Lahan

Standar klasifikasi penutup lahan yang telah ditetapkan (jumlah kelas, jenis kelas dan format *lay out*), selanjutnya diterapkan pada untuk membuat peta penutup lahan wilayah Kabupaten Tuban. Gambar 24 memperlihatkan peta penutup lahan wilayah Kabupaten Tuban skala 1:100.000 berbasis citra Landsat komposit warna (RGB) 542.



Gambar 24 Peta Penutup Lahan Wilayah Kabupaten Tuban Skala 1:100.000 Berbasis Citra Landsat Komposit Warna (RGB) 542

5. KESIMPULAN DAN SARAN

5.1 Kesimpulan

Kajian pembuatan standardisasi sistem klasifikasi penutup lahan berbasis data penginderaan jauh telah dilakukan, dan hasil yang diperoleh adalah sebagai berikut:

1. Informasi spasial penutup lahan berbasis komposit warna (RGB) 542 citra Landsat untuk skala peta 1:100.000 memiliki 8 kelas jenis penutup lahan, yaitu: hutan, semak/belukar, sawah, perkebunan, permukiman kota, permukiman desa, tubuh air, dan lahan terbuka.
2. Hasil akhir sistem klasifikasi penutup lahan untuk skala 1:100.000 dengan menggunakan citra Landsat komposit warna (RGB) 542 dirangkum dalam Tabel 6, sedangkan *lay out* peta penggunaan lahan yang dihasilkan ditampilkan pada Gambar 23.
3. Keseragaman standardisasi terminologi dan visualisasi kelas obyek lahan dapat memberikan pengertian tunggal dalam mengeksplorasi dan kedalaman informasi spasial untuk tujuan aplikasi pemanfaatan.

5.2 Saran

Hasil kajian standardisasi klasifikasi penutup lahan ini masih perlu ditingkatkan dengan cara

melakukan konsultasi, evaluasi, dan verifikasi sehingga dapat diperoleh standar klasifikasi yang sesuai dengan kemampuan data penginderaan jauh dan dapat diterima oleh berbagai pihak.

DAFTAR PUSTAKA

Anderson, J. 1976. A Land Use and Land Cover Classification System for Use with Remote Sensor Data. USGS.

Benz, U. et al., 2004: Multi-resolution, object-oriented fuzzy analysis of remote sensing data for GIS-ready information. In: *ISPRS Journal of Photogrammetry & Remote Sensing* 58 (2004), pp. 239-258.

Gerard W. Hazeu And Allard J. W. De Wit, Corine Land Cover Database Of The Netherlands: Monitoring Land Cover Changes Between 1986 And 2000, Earsel Eproceedings 3, 3/2004

Hay, G. and Castilla, G., 2006: Object-Based Image Analysis: Strengths, Weaknesses, Opportunities and Threats (SWOT). In: *The International Archives of the Photogrammetry, Remote Sensing and Spatial Information Sciences*, Vol XXXVI-4/C42.

Kaufman R K & K C Seto, 2001. Change detection, accuracy, and bias in a sequential analysis of Landsat Imagery in the Pearl River Delta, China: econometric techniques. Agriculture, Ecosystems and Environment*,* 85, 95-105

Lillesand, T.M., Kiefer, R.W., dan Chipman, J.W. 2004. Remote Sensing and Image Interpretation. *Edisi ke-5.* John Wiley & Sons. New York. 763 hal.

Paimin, Priyono. C. N. S., 2004. *"Optimalisasi Pengelolaan Sumber Daya Lahan Secara Terpadu dan Berkelanjutan dalam Menunjang Peningkatan Pendapatan Asli Daerah"*. Prosiding Ekspose BP2TPDAS-IBB Surakarta, Kebumen, 3 Agustus 2004. Hal 102-107.

Peraturan Pemerintah Republik Indonesia, Nomor 10 Tahun 2000, Tentang Ketelitian Peta untuk Penataan Ruang Wilayah.

Purwadhi, S.H., dan Tjaturahono, B.S. 2010. Pengantar Interpretasi Citra Penginderaan Jauh. LAPAN. Hal. 31-32. Jakarta.

----------, TentangTingkat Ketelitian Peta Untuk Penataan Ruang Wilayah, Peraturan Pemerintah Republik Indonesia (PP), Nomor 10 Tahun 2000 (10/2000)